PHD

Pin dynamics and impact in revolute joints with clearance

Ghazavi, M. R.

Award date:
1990

Awarding institution:
University of Bath

PIN DYNAMICS AND IMPACT IN REVOLUTE JOINTS WITH CLEARANCE

submitted by M.R. Ghazavi

for the degree of Ph.D

of the University of Bath

1990

ProQuest LLC
789 East Eisenhower Parkway
P.O. Box 1346
Ann Arbor, MI 48106-1346

SUMMARY

An experimental and theoretical study has been made of a four bar chain having clearance in the coupler-follower bearing.

An electrical circuit method has been used to establish contact loss at the bearing, with care being taken that pin misalignment did not produce spurious results.

Pin path was monitored by two eddy current transducers, recording motion in perpendicular directions. Follower acceleration was also monitored by means of an accelerometer.

Contact loss correlates with rapid changes of pin motion. Runs with the bearing chemically cleaned and with bearing lightly greased indicated that more pin oscillation occurred in the former case than the latter.

The theoretical predictions of pin motion agreed quite well with the experimental results when damping of pin motion was introduced into the model.

The impact pattern around the bush was predicted and it was compared with the recorded wear pattern for a range of speeds.

The predicted wear pattern is roughly a normal distribution.

Acknowledgements

I am greatly indebted to Dr. Stammers, for his continuous supervision, guidance and constructive comments during the course of this study.

I would like to express my gratitude to the Ministry of Higher education of Islamic Republic of Iran for financial support during this work.

I wish to thank Mr Peter Prest for his valuable help in experimental matters, to Mr David Tallin for his diligence in constructing the apparatus, and to Dr. Rahimi, Dr. Rezaeian , Dr. Tehrani, Dr. Mohammadi,Dr. Baseer and Ramazan who were involved in this work in computing.

SUMMARY

An experimental and theoretical study has been made of a four bar chain having clearance in the coupler-follower bearing.

An electrical circuit method has been used to establish contact loss at the bearing, with care being taken that pin misalignment did not produce spurious results.

Pin path was monitored by two eddy current transducers, recording motion in perpendicular directions. Follower acceleration was also monitored by means of an accelerometer.

Contact loss correlates with rapid changes of pin motion. Runs with the bearing chemically cleaned and with bearing lightly greased indicated that more pin oscillation occured in the former case than the latter.

The theoretical predictions of pin motion agreed quite well with the experimental results when damping of pin motion was introduced into the model.

The impact pattern around the bush was predicted and it was compared with the recorded wear pattern for a range of speeds.

The predicted wear pattern is roughly a normal distribution.

Acknowledgements

I am greatly indebted to Dr. Stammers, for his continuous supervision, guidance and constructive comments during the course of this study.

I would like to express my gratitude to the Ministery of Higher education of Islamic Republic of Iran for financial support during this work.

I wish to thank Mr Peter Prest for his valuable help in experimental matters, to Mr David Tallin for his diligence in constructing the apparatus, and to Dr. Rahimi, Dr. Rezaeian , Dr. Tehrani, Dr. Mohammadi,Dr. Baseer and Ramazan who were involved in this work in computing.

CONTENTS

NOTATION

a crank length

b coupler length

c follower length

c_i damping coefficient of joint i

d base length

D_c dissipation energy

e coefficient of restitution

e_i center of mass the links from one end (i=1,3)

F_{a1},F_{b1} lateral forces at A,B

F_{a2},F_{b2} longitudinal forces at A and B

F_n normal force at bearing B

f_t tangential force at bearing B

g gravitational constant

h_i elevation of the c.g. of the link i

H_b normal impulse at bearing B

H_a horizontal impulse at bearing A

I moment of inertia

I_e equivalent inertia

J_b tangential impulse at bearing B

J_a vertical impulse at bearing A

k_p coefficient of proportional control

k_d coefficient of derivative control

k_i coefficient of integral control

m mass

r radial clearance

R_A contact force at crank-coupler joint

R_B contact force at coupler-follower joint

T kinetic energy

T_m motor torque

T input torque

u_x tangential motion of pin relative to follower

u_y longitudinal motion of pin relative to follower

U potential energy

x horizontal

X_{2A}, X_{2B} horizontal forces at A and B

Y_{2A}, Y_{2B} vertical forces at A and B

y vertical

β follower angle

γ contact force angle

α clearance link angle

θ coupler angle

ϕ crank angle

η_p velocities after impact ($\eta=\phi,\theta,\psi$)

CHAPTER 1

INTRODUCTION

1.1 Linkages

Linkages play a major role in all branches of engineering. In most mechanical systems where the rotating motion is converted to reciprocal motion or vica versa, a linkage is used. The joints which connect links together have some clearance.

The presence of clearance in the joints of mechanisms is inevitable to allow relative movement at the connections of the mechanism. However this clearance may allow the paired element to lose contact and subsequently impact occurs. The impact may cause a number of problems such as wear, vibration, noise and impaired performance. Therefore many studies have been made of the dynamic motion of these mechanisms. In spite of that, there is lack of comprehensive work(theoretical and experimental work together) which is recognised by some workers.

Haines(7) , at the end of his survey , considered "the greatest need in this field of study is for deliberately discriminating experimental studies ". Soong and Thompson(19) in their recent work declared that the lack of experimental investigation in this field was a significant void in the literature. Workers have studied the effect of pin motion (mainly vibration and impact) but the actual motion itself has not received detailed examination.

1.2 Clearance effect in linkage joints

In general the displacement of a mechanism with bearing clearance has only a very small deviation from those developed by a system without clearance. However , the velocity and acceleration characteristics and also other related dynamical effects are generally

dramatically different from the zero clearance case , including large impulsive forces which result in wear on the bearing. The vibrational response of the mechanism, which can result in noise, is the other consequence of the clearance. This vibration may excite the mechanism at a resonant frequency. The links are exposed to a more severe fatigue environment. In order to reduce impacts, noise, wear and vibration the clearance should kept as small as possible. This would however increase the manufacturing cost. It is necessary to make a compromise between manufacturing cost and required performance.

1.2.1 Vibration

In many calculations it is assumed that the links are rigid and both pin and bush surfaces are rigid also. Actually there is a small elasticity both in the links and surfaces; this causes vibration in the linkages. A model has been presented by Dubowsky et al (1) in which the elasticity of links and surface friction respectively are assumed as a spring and damper. He has also developed a dynamic response of a linkage with clearance. The vibration may begin with one impact and it may intensify with successive impacts. It has notable effects on performance of the linkages.

1.2.2 Noise

Usually the bearings generate a range of sound frequency which depends on the material lubrication and kinematic of the linkages. The presence of clearance and as a result of that impact vibration increases this range. This increases the level of noise.

1.2.3 Wear

The relative motion between two rigid bodies often causes wear which is reduced in the presence of lubrication. In some circumstances in which lubricant can not be used, the impact causes wear and the wear causes irregular shaping of the bearing. The irregular bearing produces a disturbance in the motion and therefore impact. This generates an increasing cycle of wear and impact.

1.2.4 Out of plane motion

In a linkage with realistic clearance the links with two joints do not necessarily move in a plane. This motion may have an important effect on contact loss and impact. Haines(7) declared that small departures from the above assumption may conceivably have a large effect on likelihood or severity of contact loss.

1.3 Review of previous work

Considerable attention has been paid in recent years to increasing the realism of engineering models. In the case of mechanisms,as explained in previous section, an important factor is the allowance for clearance at the bearings due to manufacturing tolerance. Studies have been undertaken by several workers,principally Earles(2,6), Haines(7-11). The prediction of contact loss has been of key interest, although methods of preventing this phenomenon appear to be highly desirable. The work of Fawcett and Burdess(12)and Perera and Seering(13) are two of the few publications in this area.

The analysis of a mechanism with clearance is complicated by the fact that the orientation of the clearance link(the distance between the centres of pin and bush)depends on the forces at the bearing, which in turn depend on clearance link orientation. One approach, adopted by

Baghat et al (16) is an iterative procedure at a given crank angle. The other approach is a perturbation method adopted by Osman et al(15). Another approach is to assume an initial configuration for starting integration. Because the differential equations of motion are non linear and therefore an analytical solution is not possible, it is necessary to proceed by numerical integration of the equations of motion.

In using theoretical models admitting clearance, a number of workers have reported oscillations of the clearance link (and accordingly the other links) in regions which include those where contact is observed experimentally to be lost (2). Perera(28)does not report oscillations, but refers to a sharp increase in $\dot{\gamma}$ at or near contact loss.

Such predicted oscillations might be simply due to numerical instability , which would indicate a breakdown of the theoretical model(which is based on contact). However,Morita and Furahashi(23,24)recorded input torque fluctuations in an experimental study.

During free flight , the chain moves as two separate pendulum systems. Following contact loss, a free flight of the pin occurs(10,17). Although for free flight to occur the contact force must fall to zero, theoretical models rarely predict this condition(3). Instead the contact force plot passes through a number of local minima, termed a flypast by Haines(8). Where contact loss is observed it is at or soon after a flypast. Another approach declares that at contact loss the force between the pin and journal becomes tensile(14,19).

On the basis of some criterion, the contact force may be set to zero, which is equivalent to applying an impulse,albeit small, to the mechanism.

Following the free flight phase, impact occurs(18,19). A coefficient of restitution may be employed. Mansour and Townsand (18) used a figure of unity. Herbert and McWhannel

(29)used a velocity dependent e, which would indicate values close to unity for the velocities used. Soong and Thompson(19)estimated a value of 0.46 from experimental work. This estimate of e may be low due to the presence of damping (due perhaps to a grease film or deformation of the material) for otherwise far more rebounds are predicted even for a low value of e than experimental work indicates. Material damping may be accommodated via a Kelvin-Voigt model or by a damping force dependent on the product of velocity and spring force(32).

A proximity perturbation method for the kinematic analysis of mechanisms was presented by Osman at el(15). The case of a six-bar linkage was considered to illustrate the procedure and the feasibility of the model. They concluded that the method can be used for linkages with more than one degree of freedom . The authors also mentioned that because of the rapid convergence of each iteration cycle which is an inherent characteristic of the algorithm method the computing time is relatively small.

A dynamic analysis of a four bar mechanism in contact mode was presented by Earles. and Wu.(2) in which they studied the effects of bearing clearance. The clearance was considered as a mass less link, the friction was neglected and by the use of Lagrangian multipliers and adapted mesh constraints a set of time dependent, non linear differential equations with variable coefficients was developed. Since the equations were non linear for a particular set of initial conditions , a numerical solution of the equations is given up to the point at which contact between the bearing surfaces is lost. There was little difference between the displacement response so predicted and that found assuming no clearance. However they found small cyclic fluctuations in the angular acceleration of the links, over and above their mean variations as a result of clearance. They were in doubt if this was real or due to the numerical method used.

Earles and Wu do not mention this cyclic motion in their later work(3). They have examined bearing force polar plots from a zero-clearance analysis,and they have shown that contact loss, leading to impact, is predictable from the empirical ratio $\frac{\dot{\gamma}}{R}$, where R is the reaction force on the bearing and $\dot{\gamma}$ the rate of change of direction of R. From an extensive series of tests on a four-bar mechanism with a single predominating clearance bearing and subject to an oscillatory input, it was shown that the general trend of the actual impact acceleration is predictable from the parametric group, $(B^8)\ln(\frac{\dot{\gamma}}{R})$ where B is a system constant which varies with bearing material and lubrication. The sign of the impact depends on $\frac{\dot{\gamma}}{R}$. If $\frac{\dot{\gamma}}{R}$<1 rad/s/N the impact is negative. Therefor contact-loss would not occur.

No attempt to test this criterion against the actual contact loss was made. Their simulation was restricted to only predicting when contact between the pin and the bearing was terminated.

Fawcett and Burdess(12) have studied the bearing force loci of the crank coupler of a four bar chain. They have declared that is possible to predict the points at which contact is likely to be lost by determining those regions in the cycle where the bearing force vector underwent a decrease in magnitude and rapid reversal of direction.

They concluded that since the form of force loci depends upon the mass distribution of the mechanism and the load transmitted it should be possible to reduce the effect of impact by designing for a more uniform loading within the bearing.

For a four bar mechanism having a rotary input with a bearing clearance at follower-coupler,Grant and Fawcett (14) found the Earles and Wu criterion a useful and simple method for predicting contact loss in a revolving joint. They did not compare the criterion with

actual contact loss results. They assumed that the end of the free flight would be on the other side of the bush in line with γ at $R=R_{min}$, but offered no justification for this. They recorded the pin loci photographically. They obtained a crude polar plot but they did not record the components so some difficulties of interpretation arise. Radial oscillations appear to be significant, but as the displacement transducers are only mounted on one side of the joint it is not possible to eliminate the effect of misalignment angular oscillations which could produce similar measurements. In their theoretical model they did not have a complete picture of the displacement components.

In other reference (33) the same authors have suggested a method for preventing contact loss in the bearing. In this method they use suitable linear springs in such a direction as to move the polar plot of the pin force from the origin, without increasing the maximum pin force . The spring should be attached to the pin and bearing and its direction is assumed constant relative to one of the links. The size of the spring and direction of its line of action to prevent contact loss is established using a no clearance analysis together with Earles and Wu contact loss criterion. The Earles and Wu parameter is kept less than 1 throughout the whole cycle.

Earles and Kilicay(5) have suggested the above criterion $\frac{\dot{\gamma}}{R}$ may be generally applied to determine the operating conditions necessary for contact to be maintained at a plain bearing having clearance . They did not observe significant interactive effects of the impact at one bearing influencing another bearing. They suggested that $\frac{\dot{\gamma}}{R}$ when it is greater than 1 gives an indication of the impact severity. They have also compared polar force plots of a bearing for various driving speeds and that of two different bearing with the same speed for zero clearance.

A general theory of dynamics of a four-bar linkage with clearance at all turning pairs, using continuous contact model ,has been presented by Nobuyoshi Morita,et al (23). This theory has been adapted for analysing the dynamics of crank lever mechanism with a clearance at the joint of coupler and follower and also a mechanism with a clearance at crank and coupler. The results for these two cases have been compared. The effect of the amount of clearance , driving speed and mass of link on the forces acting at the joints and input torque have been investigated. The direction of the force acting at the joint have been compared with the contact angle .

All the results are based on the assumption of constant driving speed. They did not compare their result with the experimental result. Morita et al measured experimentally the input torque only. They have used Lagrangian mechanics and numerical method in their model. They also assumed some damping in the system, but did not consider contact loss in their model . However they declared that there is contact loss in practice.

A different model was developed by Townsend and Mansour (18) in which they did not assume continuous contact at all. It was built around the momentum exchange principles for impacting bodies with an assumed coefficient of restitution,e. In the momentum-exchange model, the system is visualised as being in either the free-flight mode (when contact is lost between the pin and the bush),or the impact mode(when contact is reestablished for very short time). In that model it was assumed that rebound followed the impact mode. The work reported here shows that this assumption can be incorrect. The coefficient of restitution was assumed to be unity. The model was applied to find spectrum of the impacts in a four bar mechanism with clearance in one of the joints. They applied their model for three different cases from the point of view of contact nature. They called those cases Smooth (no friction) , Rough (no relative tangential slip) and Stick-slip (coulomb-type firiction in the tangential direction). The authors presented their model as a proper design tool for

investigating wear, life-expectancy, and noise characteristics of high speed mechanism with clearances.

The crank was assumed to be driven at a constant speed by a source which is capable of meeting the demands of the driving torque at any time. A clearance was assumed between a bush, which forms the terminal end of the follower arm ,and a pin ,which is at the end of coupler. The authors assumed that as the driving crank rotates, torque is transmitted to the follower arm in a succession of impacts which are applied at different angles of the bush. They did not supply experimental support for their model.

Midema and Mansour (34) developed a model to describe the dynamic performance of mechanisms with clearance using the momentum exchange approach. The model was improved to account for the case when contact is maintained between the pin and the bush while they move relative to each other. The coefficient of restitution was assumed to be 0.8. The regions of occurrence of three modes for a crank slider mechanism were discussed using the geometric constraint of clearance link and the sign of contact force. They assume the force to be along the clearance link. The authors found that the distribution of the contact forces as well as zones of contact on the socket are compatible. In consequence of that they concluded that the three-mode-momentum exchange model is valid. No direct experimental support was provided.

A dynamic model for analysing plane multilink mechanisms with clearance was developed by Funabashi et al (35). They have considered the elasticity of pairing elements with coulomb and viscous friction. Using this model, they derived the equations of a four bar and slider crank mechanisms . They studied the influence of clearance and the crank speed upon the relative motions between the pairing elements , input torque and output displacement theoretically and experimentally for a slider crank mechanism with a clearance. The authors

used stroboscopic photographs for detecting the displacement of the pin relative to the bush and recorded the electric current between bush and pin to indicate the contact and separation modes. The theoretical and experimental driving torque were compared and the polar plots of forces for different speeds presented in their model.

This model was used for analysing the plane four bar mechanisms with the same experimental procedure in their later work(36). They studied the effects of the numbers and positions of clearance-connections, the magnitudes of clearances and the crank-speed upon the relative motions of pairing element , the dynamic deviations of rocker angle and the input torque.

They concluded that separations and collisions of pairing elements occur and pulsatory torques are caused in the input-shaft just after the instant when a large force acting at the crank-pin rapidly changes its direction.

They assumed the mechanism rotates in a vertical plane and the input speed of the mechanism is constant . However they attempted to get a general view of pin path by means of stroboscopic pictures. But obviously it is not as clear as a direct polar plot of the pin path . The authors measured the relative displacement on one side of the bearing only. Therefor it was not possible to eliminate the misalignment errors in the traces. The clearance was high (1mm). The friction force was comparable to the inertia force , so the results may be impractical.

The loss of contact in bearings of four bar linkages,and the avoidance of impact within a bearing through prevention of contact loss are both investigated by Perera and Seering (13). They recommended that a properly sized torsional spring be fitted to a joint of mechanism for eliminating impacts within joints. The authors presented two methods for establishing the

spring constant and its free angle. Their method was based on the statement, i.e if the lateral component of reaction force at the coupler follower bearing maintained high and as constant as possible in the zero clearance case , impact at this bearing will be prevented in the clearance case. They have compared pin forces of original mechanism with the same mechanism but with the spring. They have compared their force versus of input angle and their polar plots for different joints at different speeds. They assumed constant input speed in their model. The same authors in another reference(28) declared the need for the experimental work to check their results.

Dubowsky and Freudenstein (37) formulated an impact pair model to predict dynamic response of an elastic mechanical joint with clearance. They have assumed a linear viscous damping law for Kelvin-Voigt model with a coefficient obtained by analogy with non impactive vibration. The surface elasticity, k ,was derived from the Hertzian surface contact theory. The surface compliance so derived is a function of bearing elements and the geometrical properties of the bearing elements. Their results predicted an increase in the joint force above the zero clearance value which is due to impact resulting from contact loss.

Dubowsky and Young(1) developed a one dimensional model(a simple model pin connection with clearances) and subjected it to a sinusoidal input motion. They find out that maximum impact acceleration occur on alternative sides of the connection shortly after the input acceleration changes sign.

Dubowsky and Gardener(46) in an analytical model predicted that the link elasticity would considerably reduce the impact acceleration predicted by the impact pair model. Dubowsky and Moening(49)confirmed that experimentally.

An analytical treatment of dynamic effects of clearance in planar mechanisms was described by Bahgat, Osman and Sankar(16). They developed a mathematical model, using an iteration method, with four modes of contact with multiple clearance, in which the pin forces were calculated and compared with the case of zero clearance . They showed that there are significant changes in acceleration, torque and pin forces as compared with the case without clearances. However minimal changes were detected in displacement and velocity . They attempted to provide a design method for investigating separation occurrence. The authors neglected gravity effect and assumed constant input speed. Their results were for a relatively high clearance (1,2mm).

The same authors in another reference (38) developed a continuous contact model using Lagrangian method. They claimed that the continuous contact assumption is valid, since a separation at any revolute occurs in an infinitesimally small period of time ($dt \rightarrow 0$). They compared displacements velocities ,acceleration and pin forces of slider-crank for two theoretical cases with and without clearance . They concluded that although the difference between computed displacements are minimal , sudden changes in velocities occur in two different region in the cycle. This result in the considerable changes in the torques within this two regions. Oscillation of forces and torques within this two regions indicates that separation has occurred at this instant. The magnifications of forces and torques in the mechanism due to clearances essentially depend on the clearance sizes and operating speed of the mechanism. Linkage dimensions have small effect compared to that of clearance size. However the magnification factor of forces and torques due to the existence of revolute clearance is reduced by bearing and link elasticity.

They assumed constant driving speed in their model. There was no experimental support for their work.

A theoretical analysis of contact loss in a general revolute joint was given by Haines(8). He obtained equation of motion for a typical revolute joint using the principal of virtual work. He constructed a design chart, from the numerical solution of the equations of motion, in which contact-loss was predicted using performance contours. He provided a theoretical explanation for a zero clearance criterion for prediction of contact loss. His solution was based on some assumptions. One of his assumption is that the locus of the contact force is straight line during free flight mode. However as it was reported by Bengisu et al(25) this is not the case. No direct experimental evidence was provided by Haines.

Further investigation in this field was achieved by Bengisu et al (25). They developed a continuous contact model using iterative procedure to solve four bar chain with clearance. Taylor series were used to calculate the clearance angular velocity and acceleration. The authors developed a contact loss criteria in which the clearance size is involved but it was on zero clearance basis. They predict two different regions of contact loss. The authors reported they did not observe rebounds following the impact in the experimental results. They declared that during the free flight mode the motion of the pin relative to the bearing is not necessarily a straight line . They attempted to detect clearance angle by the use of a stroboscope and compared impact position with different criteria. But they did not have any experimental contact loss traces. The input speed was assumed constant in their model .

Vjaters et al(6)compared two different assumed conditions during the impact mode ie.

1-constant input speed but varying input torque,

2-constant driving torque but varying crank speed.

They found significant differences between the two sets of derived result.

A recent investigation on the dynamic performance of linkages with clearance was performed by Soong and Thompson(19) on a slider crank mechanism with clearance in the gudgeon-pin joint. They declared that it should be four (contact, free flight , impact, transient) mode motion and presented in a schematic diagram the phenological behaviour of a revolute joint with clearance (pin motion). However they did not present any experimental record of pin motion. The authors detected impact effect in some acceleration ,velocity and force traces only.

Earles and Seneveiratne(39) in a dynamic model with clearance attempted to investigate the suitability of the mass less link model as a tool design; they declared that the zero clearance method is insufficient to predict contact loss on the basis that it will occur when the joint reaction force approaches zero. The authors concluded that the predicted response shows high frequency oscillations,superimposed on the main zero clearance motion of the links. The extent of the high frequency oscillation is dependent on the assumed initial condition.

The same authors in their later work (40) attempt to find some guidelines for predicting contact loss. They tried to calculate the pin forces for the clearance case versus of system physical and kinematic parameters. Then equating the joint force to zero they defined a contact loss criteria. They admitted that some experimental support is necessary to prove the criteria. They attempted to develop a model, by assuming continuous contact , and found the predicted responses aperiodic and highly dependent on the initial value. Because of the large oscillation in the dynamic responses , they were suspicious about its applicability as a design tool.

1.4 The object of the work described here

The factors which appear to have little attention are as follows

1. The unsteady running of the chain

2. A comprehensive record of pin path(components and polar)

3. Wear pattern

4. Three mode model in four bar chain

5. Out of plane motion of the links

The intent here is to address points 1,2 and 3 by developing a model considering speed fluctuation in input speed of a four bar linkage. The input speed is controlled either by input inertia or a three term control circuit. The dynamic performance of the model is compared with that of constant input speed.

Some clearance is assumed in the coupler the coupler follower joint .

A model with clearance is developed by two different methods

a: iteration method

b: integration method

Assuming continuous contact, plots of parameters concerned with the dynamic performance of the system are obtained. These predictions are compared with the experimental results. Using the experimental results a contact loss procedure is developed. Free flight and an impact mode are added to the model . At this stage the theoretical & experimental results are compared.

A contact loss signal is recorded which detects the exact crank angle position of the starting and end of pin flight. The effect of speed , input inertia and the size of the clearance on the dynamic performance of the system will be investigated . Runs were made with dry , greasy and normal(notionally unlubricated) bearings. The pin locus is recorded and its relation to the other performance traces highlighted.

The effect of the consequent impact on bushes and pin which is wear is recorded by surface roundness measurements and compared with the impact pattern obtained from multi cycle simulations.

The presence of misalignment in the system is highlighted by a set of contact-loss traces.

CHAPTER 2

DYNAMIC ANALYSIS (ZERO CLEARANCE)

2.1 Introduction

This chapter deals with the simple four-bar chain with zero clearance linkages analysed kineticaly by Grosjean (41) to calculate angular velocities and acceleration. The analysis was used to calculate pin forces and required torque at the driving crank. The analysis is given here

(a) for completeness

(b) because the pin forces both in frame and body fixed axes are obtained.

The model which is analysed is an idealized four bar chain. The links are assumed to be rigid . It is assumed that the motor torque T_m just overcomes the load and friction in the joints.

The closure equations are used to define the chain geometry - see sec.(2.2). The equations are differentiated twice to obtain the velocity and acceleration of the links.

The acceleration are calculated in order to obtain the joint forces (see sec.(2.3)). In sec.(2.4) a fly wheel is assumed connected to the crank and then, assuming a known input torque, input acceleration is calculated.

The input speed is assumed constant and the input torque is obtained (see sec.(2.5)). In sec.(2.6). the input speed is not assumed constant. The input torque is generated via a controller which is fitted to produce constant mean crank speed but which also attempts to maintain speed constant within the cycle.

The lateral and longitudinal force components(see sec.(2.7))at the follower are obtained by solution of the equations of motion.

In sec. 2.8 method of solution by computer is discussed.

2.2 Kinematics

Consider the four bar linkage shown in Fig 2.2.1 . The frame of reference is A_0X,A_0Y and the angular positions of the links are measured positively from the A_0X axis It may be assumed as being made of four Vectors A_0A,AB,BB_0,A_0B_0 joined at A,B,B_0 and A_0 of magnitude a,b,c,d respectively; d is the fixed link.

In this case ϕ or link A_0A is the input and ψ or link B_0B the output. The linkage can be solved for a given input angle (ϕ) by projection on the x and y axes

Projection on the x axis gives:

$$a\cos\phi + b\cos\theta - c\cos(\psi - 180) - d = 0 \qquad (2.2.1)$$

And projection on the y axis gives:

$$a\sin\phi + b\sin\theta - c\sin(\psi - 180) = 0 \qquad (2.2.2)$$

2.2.1 Angular position,velocity and acceleration of coupler

One can eliminate ψ from equation 2.2.1 and 2.2.2

$$c\cos\psi = d - (a\cos\phi + b\cos\theta) \qquad (2.2.3)$$

$$c\sin\psi = -(a\sin\phi + b\sin\theta) \tag{2.2.4}$$

giving

$$(\sin\phi)\sin\theta + (\cos\phi - \frac{d}{a})\cos\theta = \frac{c^2 - (a^2+b^2+d^2)}{2ab} + \frac{d}{b}\cos\phi \tag{2.2.5}$$

a Angular position

For a given ϕ as an input, one can solve for θ . Hence by differentiating with respect to time one obtains the velocity and acceleration in terms of the input velocity and acceleration.

To obtain an expression for the output θ as a function of the input ϕ it is more convenient to rewrite as follows:

$$A\sin\theta + B\cos\theta = C \tag{2.2.6}$$

where A ,B and C are as follows:

$$A = \sin\phi$$

$$B = \cos\phi - \frac{d}{a}$$

$$C = \frac{c^2 - (a^2 + b^2 + d^2)}{2ab} + \frac{d}{b}\cos\phi$$

To solve for θ we recall from trigonometry that

$$\sin\theta = \frac{2s}{1+s^2} \quad , \quad \cos\theta = \frac{1-s^2}{1+s^2}$$

where

$$s=\tan\frac{\theta}{2}$$

Hence equation 2.2.6 becomes:

$$(B+C)s^2-2As+(C-B)=0 \qquad (2.2.7)$$

This is a quadratic in s whose solution is

$$\theta=2arctan\frac{A\pm\sqrt{A^2+B^2-C^2}}{(B+C)} \qquad (2.2.8)$$

There are two roots: θ^+ corresponds to the positive sign and θ^- corresponds to the negative sign

The two values correspond to two possible position of the mechanism as shown in figure 2.2.2 ; for given values of a,b,c,d and ϕ

b Coupler angular velocity

To obtain expression for the angular velocity and acceleration of the coupler one can differentiate eq (2.2.4) as follows:

$$A\dot{\theta}\cos\theta+\dot{A}\sin\theta-B\dot{\theta}\sin\theta+\dot{B}\cos\theta=\dot{C} \qquad (2.2.9)$$

Where $\dot{A},\dot{B}$ and $\dot{C}$ are as follows:

$$\dot{A}=\dot{\phi}\cos\phi$$

$$\dot{B}=-\phi\sin\phi$$

$$\dot{C}=-\frac{d}{b}\phi\sin\phi$$

Therefor θ is calculated as follows

$$\theta=\frac{\dot{C}-\dot{A}\sin\theta-\dot{B}\cos\theta}{A\cos\theta-B\sin\theta}$$

i.e

$$\theta=(\frac{Y_1}{Y_2})\phi \qquad (2.2.10)$$

where:

$$Y_1=-\frac{d}{b}\sin\phi+\sin(\phi-\theta)$$

$$Y_2=\sin(\phi-\theta)+\frac{d}{a}\sin\theta$$

c Coupler angular acceleration

By differentiating the above equation we obtain the angular acceleration of the coupler as follows:

$$\ddot{\theta}=\frac{Y_2DY_1-Y_1DY_2}{Y_2^2}\phi+\frac{Y_1}{Y_2}\ddot{\phi} \qquad (2.2.11)$$

where DY_i is the derivative of Y_i with respect to time.

$$DY_1=-\frac{d}{b}\dot{\phi}\cos\phi+(\dot{\phi}-\dot{\theta})\cos(\phi-\theta)$$

$$DY_2=(\dot{\phi}-\dot{\theta})\cos(\phi-\theta)+\frac{d}{a}\dot{\theta}\cos\theta$$

$$\dot{\theta}=G_c\dot{\phi}$$

where

$$G_c=\frac{Y_1}{Y_2},$$

Therefore the components of coupler angular acceleration maybe summarized as follows:

$$\ddot{\theta}=DG_c\dot{\phi}+G_c\ddot{\phi}$$

where DG_c is the derivative of G_c with respect to time.

$$DG_c=\frac{Y_2DY_1-Y_1DY_2}{{Y_2}^2}$$

2.2.2 - Angular position,velocity and acceleration of follower

a . Angular Position

From equations (2.2.1) and (2.2.2) by calculating the functions of coupler angle we will get the following equations.

$b\cos\theta=d-(a\cos\phi+c\cos\psi)$

$b\sin\theta=-(a\sin\phi+c\sin\psi)$

Squaring and adding the above equations yields

$$\sin\psi(\sin\phi)+\cos\psi(\cos\phi-\frac{d}{a})=\frac{b^2-(a^2+c^2+d^2)}{2ac}+\frac{d}{c}\cos\phi$$

which may be written as follows

$$H\sin\psi+E\cos\psi=F \qquad (2.2.12)$$

where H , E, F are as follows

$H=\sin\phi$

$$E=\cos\phi-\frac{d}{a}$$

$$F=\frac{b^2-(a^2+c^2+d^2)}{2ac}+\frac{d}{c}\cos\phi$$

To solve for follower angle , from trigonometry we have the following relations

if $s=\tan(\frac{\psi}{2})$

$$\sin\psi=\frac{2s}{1+s^2}$$

$$\cos\psi=\frac{1-s^2}{1+s^2}$$

$$(E+F)s^2-2Hs+(F-E)=0$$

$$s=\frac{H\pm\sqrt{H^2+E^2-F^2}}{E+F}$$

$$\psi^+=2arctan\frac{H+\sqrt{H^2+E^2-F^2}}{E+F}$$

$$\psi^-=2arctan\frac{H-\sqrt{H^2+E^2-F^2}}{E+F}$$

The two values correspond to the two possible position of the mechanism

b- Calculating angular velocity of the follower:

Let us recall eq.(2.2.12)

$$H\sin\psi+E\cos\psi=F$$

To obtain velocity one can differentiate this equation with respect to time:

$$\dot{H}\sin\psi+H\dot{\psi}\cos\psi+\dot{E}\cos\psi-E\dot{\psi}\sin\psi=\dot{F} \qquad (2.2.13)$$

Solving for the output angular velocity one will have

$$\dot{\psi}=\frac{\dot{F}-\dot{H}\sin\psi-\dot{E}\cos\psi}{H\cos\psi-E\sin\psi}$$

where

$\dot{H},\dot{E}$ and $\dot{F}$ *are as follows*:

$$\dot{H}=\dot{\phi}\cos\phi$$

$$\dot{E}=-\dot{\phi}\sin\phi$$

$$\dot{F}=-\frac{d}{c}\dot{\phi}\sin\phi$$

Therefore follower angular velocity can be summarized as follows:

$$\dot{\psi}=(\frac{Z_1}{Z_2})\dot{\phi}$$

where

$$Z_1=-(\frac{d}{c})\sin\phi+\sin(\phi-\psi)$$

$$Z_2=\sin(\phi-\psi)+(\frac{d}{a})\sin\psi$$

The angular velocity equation may be written as follows:

$$\dot{\psi}=G_f\dot{\phi} \qquad (2.2.14)$$

where

$$G_f=\frac{Z_1}{Z_2}$$

c Follower angular acceleration

By differentiating the above equation one obtains the follower angular acceleration

$$\ddot{\psi}=DG_f\ddot{\phi}+G_f\dddot{\phi} \qquad (2.2.15)$$

where

$$DG_f=\frac{DZ_1Z_2-DZ_2Z_1}{Z_2^2}$$

and

$$DZ_1=-(\frac{d}{c})\dot{\phi}\cos\phi+(\ddot{\phi}-\ddot{\psi})\cos(\phi-\psi)$$

$$DZ_2=(\phi-\dot{\psi})\cos(\phi-\psi)+(\frac{d}{a})\dot{\psi}\cos\psi$$

2.3 DYNAMIC ANALYSIS (fixed co-ordinates)

The joint forces can be found by solution of the equations of motion of moving elements. Because the major part of this investigation is concerned with the joints A and B we attempt to calculate the forces at these two joints and input angular acceleration fig(2.3.1). A total of four component of forces together with input angular acceleration remain to be determined from the five equations of motion , which are

$$X_{2A}+X_{2B}=m_2\ddot{x}_2 \qquad (2.3.1)$$

$$Y_{2A}+Y_{2B}-m_2g=m_2\ddot{y}_2 \qquad (2.3.2)$$

$$X_{2A}e_2\sin\theta-X_{2B}(b-e_2)\sin\theta-Y_{2A}e_2\cos\theta+Y_{2B}(b-e_2)\cos\theta=I_{2c.g.}\ddot{\theta} \qquad (2.3.3)$$

For link A_0A one can write $\sum M_{A_0}=I_{1A_0}\ddot{\phi}$

i.e

$$T-Y_{2A}a\cos\phi+X_{2A}a\sin\phi-m_1ge_1\cos\phi=I_{1A_0}\ddot{\phi} \qquad (2.3.4)$$

For link B_0B one can write $\sum M_{B_0}=I_{3B_0}\ddot{\psi}$

i.e

$$-Y_{2B}c\cos(\psi-\pi)+X_{2B}c\sin(\psi-\pi)-m_3ge_3\cos(\psi-\pi)=I_{3B0}\ddot{\psi} \quad (2.3.5)$$

The linear acceleration $\ddot{x}_2$ and $\ddot{y}_2$ can be calculated in terms of input angular speed and acceleration as follows:

$$x_2=a\cos\phi+e_2\cos\theta \quad (2.3.6)$$

$$y_2=a\sin\phi+e_2\sin\theta \quad (2.3.7)$$

The linear acceleration of c.g. of link 2 are obtained by differentiating equations 2.3.6 and 2.3.7 twice.

$$\dot{x}_2=-a\dot{\phi}\sin\phi-e_2G_c\dot{\phi}\sin\theta \quad (2.3.8)$$

$$\ddot{x}_2=-\ddot{\phi}(a\sin\phi+e_2G_c\sin\theta)-\dot{\phi}^2(a\cos\phi+e_2G_c^2\cos\theta+e_2DG_c\sin\theta) \quad (2.3.9)$$

$$\dot{y}_2=a\dot{\phi}\cos\phi+e_2G_c\dot{\phi}\cos\theta \quad (2.3.10)$$

$$\ddot{y}_2=\ddot{\phi}(a\cos\phi+e_2G_c\cos\theta)-\dot{\phi}^2(a\sin\phi+e_2G_c^2\sin\theta-e_2DG_c\cos\theta) \quad (2.3.11)$$

where $\ddot{\phi}$ is not in general zero.

2.4 Model with flywheel

In this model the input speed(not necessarily constant) is calculated at each step. Then this speed is used in calculating the joint forces. There are five unknowns $X_A,Y_A,X_B,Y_B,\ddot{\phi}$. The equation can be written in matrix form as follows:

$$AX=B \quad (2.4.1)$$

where:

$$A=\begin{bmatrix} 1 & 1 & 0 & 0 & (a\sin\phi+e_2G_c\sin\theta) \\ 0 & 0 & 1 & 1 & -(a\cos\phi+e_2G_c\cos\theta) \\ e_2\sin\theta & -(b-e_2)\sin\theta & -e_2\cos\theta & +(b-e_2)\cos\theta & -I_{2c.g.}G_c \\ a\sin\phi & 0 & -a\cos\phi & 0 & -I_{1A_0} \\ 0 & -c\sin\psi & 0 & c\cos\psi & I_{3B_0}G_f \end{bmatrix} \quad (2.4.2)$$

$$X=\left[X_A,X_B,Y_A,Y_B,\ddot{\phi}\right]^T \quad (2.4.3)$$

$$B = \Big[\, b(1), b(2), b(3), b(4), b(5) \,\Big]^T \tag{2.4.4}$$

$$-m_2[\dot{\phi}^2(a\cos\phi + e_2 G_c^2 \cos theta) - \dot{\phi}(e_2 D G_c \sin\theta)]$$

$$-m_2[\dot{\phi}^2(a\sin\phi + e_2 {G_c}^2 \sin\theta) + \dot{\phi}(e_2 D G_c \cos\theta) - g]$$

$$I_{2c.g.} D G_c \dot{\phi}^2 \qquad \theta)]$$

$$B = \begin{bmatrix} -m_2[\dot{\phi}^2(a\sin\phi + e_2 {G_c}^2 \sin\theta) + \dot{\phi}(e_2 D G_c \cos\theta) - g] \\ I_{2c.g.} D G_c \dot{\phi}^2 \\ m_1 g e_1 \cos\phi - T \\ I_{3B0} D G_f \dot{\phi}^2 - m_3 g e_3 \cos\psi \end{bmatrix} \tag{2.4.5}$$

The crank rotational speed $\dot{\phi}$ can be calculated from the work-energy equation and substituted in the above equations. Then by assuming some value for input torque T, the equations of motion can be solved as a set of 5 equations in 5 unknowns.

Crank speed $\dot{\phi}$ is calculated as follows:

$$U = \Delta K.E. + \Delta V_g + \Delta V_e \tag{2.4.6}$$

Where

U = the total work done on the system by external forces

$\Delta K.E.$ = change in the kinetic energy of the system

ΔV_g = change in potential energy of position in the gravitational field

ΔV_e = change in the stored elastic energy in the connections.

Assuming all the links in the system are rigid , the term ΔV_e disappears in the above equation. Given two crank angle ϕ_1, ϕ_2 kinetic energy ,potential energy and the work done on the system are calculated as follows:

$$\Delta K.E. = \left(\frac{1}{2}\right)(I_{e(2)} \dot{\phi}_2^2 - I_{e(1)} \dot{\phi}_1^2) \tag{2.4.7}$$

where I_e is the equivalent or effective inertia of the system

The total kinetic energy can be expressed as

$$\left(\frac{1}{2}\right) I_e \dot{\phi}^2 = \left(\frac{1}{2}\right)(I_{1A_0} \dot{\phi}^2 + I_{2c.g.} \dot{\theta}^2 + I_{3B_0} \dot{\psi}^2 + m_2(\dot{x}_2^2 + \dot{y}_2^2)) \tag{2.4.8}$$

After substituting and summarizing

$$I_e=I_{1A_0}+G_c^2 I_{2c.g.}+G_f^2 I_{3B0}+m_2(a^2+e_2^2 G_c^2+2ae_2 G_c\cos(\phi-\theta)) \quad (2.4.9)$$

The potential energy V_g is calculated as follows:

$$V_g=m_1 g e_1\cos\phi+m_2 g y_2-m_3 g e_3\cos\psi \quad (2.4.10)$$

U is the work which is done on the linkage is mainly the work of input and output torque where

$$U=\int(T_i d\phi-T_o d\psi) \quad (2.4.11)$$

If T is constant and load is zero it will be in the form of

$$U=T\Delta\phi \quad (2.4.12)$$

By substituting the terms of kinetic and potential energy and the work in the work-energy equation the crank rotational velocity is obtained.

$$\phi_2^2=\frac{-2\Delta V_g+I_{e(1)}\dot{\phi}_1^2+2T\Delta\phi}{I_{e(2)}} \quad (2.4.13)$$

The net input torque is the difference of motor torque and load tcrque average. In this model the mean motor torque is assumed in each instance to overcome the mean load.

2.5 Constant input speed

Assuming constant input speed, then the equations are solved by setting $\ddot{\phi}=0$; input torque T is an unknown in the equations, to be solved for.

2.6 Model with 3 term controller

For driving a four bar linkage an electric motor is used which supplies a constant torque at a certain speed. However the torque which is required to run the linkage at a constant speed varies during the cycle. In the three term model this is carried out by arranging a control circuit using speed error signal = $\dot{\phi}_d-\dot{\phi}$ and its output is the required torque . Then the input torque can be calculated from the following relationship.

$$T_m=k_p(\dot{\phi}_d-\dot{\phi})+k_d(\frac{d}{dt})(\dot{\phi}_d-\dot{\phi})+k_i\int(\dot{\phi}_d-\dot{\phi})dt \quad (2.6.1)$$

where

k_p = coefficient of proportional control

k_d = coefficient of derivative control

k_i = coefficient of integral control

the work which is done on the system is

$$U=\int T_m d\phi \tag{2.6.2}$$

By substituting

$$\Delta t=\frac{\Delta\phi}{\dot{\phi}_{av}} \tag{2.6.3}$$

and

$$\dot{\phi}_{av}=\frac{(\dot{\phi}_1+\dot{\phi}_2)}{2} \tag{2.6.4}$$

we will have the following relationship:

$$U=k_p(\dot{\phi}_d-\dot{\phi}_{av})\Delta\phi-\frac{k_d}{2}(\dot{\phi}_2^{\,2}-\dot{\phi}_1^{\,2})+k_i(\frac{\dot{\phi}_d}{\dot{\phi}_{av}}-1)\Delta\phi \tag{2.6.5}$$

where $\Delta\phi=\phi_2-\phi_1$ By substituting U and Δ K.E in eq.(2.4.6) and assuming some initial value for $\dot{\phi}_{av}$ the equation could be solved for a new $\dot{\phi}$ as follows :

$$\dot{\phi}_2^{\,2}=\frac{k_p(\dot{\phi}_d-\dot{\phi}_{av})\Delta\phi+(k_d+I_{e\,(1)})\dot{\phi}_1^{\,2}+k_i(\frac{\dot{\phi}_d}{\dot{\phi}_{av}}-1)\Delta\phi}{I_{e\,(2)}+k_d} \tag{2.6.6}$$

The new $\dot{\phi}$ will give the new $\dot{\phi}_{av}$ and this is repeated for several iterations. Then the torque may be calculated from equation (2.6.1) . So the same set of dynamic equations which was used for flywheel control could be used to solve the linkage for forces.

Damping friction in the model

Considering some viscous friction in the joints of the model we will have the following relationship :

$$U=T\Delta\phi-W_d \tag{2.6.7}$$

where:

$$W_d=\int c_1(\dot{\phi}-\dot{\theta})d(\phi-\theta)+\int c_2(\dot{\theta}-\dot{\beta})d(\theta-\beta)+\int c_3\dot{\beta}d\beta \tag{2.6.8}$$

W_d is the work absorbed by the dampers c_1, c_2, c_3 are respectively the damping coefficients of the joints A, B and B_0 .

2.7 Body fixed co-ordinates For simplicity a body fixed co-ordinate model can be developed. The work-energy equation is written in the form of

$$\int T^*=I_e\frac{\dot{\phi}^2}{2}-(KE)_0 \tag{2.7.1}$$

where

$$T^*=T+g\sum m_i\frac{dh_i}{d\phi} \tag{2.7.2}$$

T= input torque h_i elevation of the c.g. of the link i

$$g\sum m_i\frac{dh_i}{d\phi}=-dV \tag{2.7.3}$$

differential of potential energy

I_e = equivalent inertia

Differentiating eq (2.7.1) with respect to ϕ ,

$$T^*=I_e\dot{\phi}\frac{d\dot{\phi}}{d\phi}+\frac{dI_e}{2d\phi}\dot{\phi}^2=I_e\ddot{\phi}+\frac{1}{2}\frac{dI_e}{d\phi}\dot{\phi}^2 \tag{2.7.4}$$

The second term in eq (2.7.4) involves the rate of change of the equivalent moment of inertia I_e with respect to the position of the mechanism. $\frac{dI_e}{d\phi}$ is a purely geometric quantity.

Solving eq (2.7.4) , one may obtain the second order nonlinear differential equation in the form

$$\ddot{\phi}=\frac{T^*-\frac{dI_e}{2d\phi}\dot{\phi}^2}{I_e} \tag{2.7.5}$$

substituting T^* from eq (2.7.4) in eq (2.7.5) one may get.

$$\ddot{\phi}=\frac{T+\frac{dV}{d\phi}-\frac{dI_e}{2d\phi}\dot{\phi}^2}{I_e} \qquad (2.7.6)$$

Then for link 1 (see fig 2.7.1) the equation of motion is in the form

of $\sum T_{A_0}=0$

which means that

$$T+F_{a1}.a-m_1.g.e_1\cos\phi=I_1\ddot{\phi}$$

Using $\ddot{\phi}$ from eq (2.7.6) the above equation can be solved as follows:

$$F_{a1}=\frac{T-I_1\ddot{\phi}-m_1ge_1\cos\phi}{-a_1} \qquad (2.7.7)$$

The equation of motion for link 3 can be written as follows:

$\sum M_{B_0}=0$ which means that $cF_{b1}-m_3ge_3\cos\beta=I_{3B_0}\ddot{\psi}$

where $\beta=\psi-\pi$

$$F_{b1}=\frac{I_{3B_0}\ddot{\psi}+m_3ge_3\cos\beta}{c} \qquad (2.7.8)$$

For link 2, for motion along x and y axes one may write

$$\sum F_x=m_2\ddot{x}_2$$

and

$$\sum F_y=m_2\ddot{y}_2$$

$$F_{a1}\begin{bmatrix}\sin\phi\\-\cos\phi\end{bmatrix}+F_{a2}\begin{bmatrix}\cos\phi\\\sin\phi\end{bmatrix}+F_{b1}\begin{bmatrix}+\sin(\frac{\pi}{2}-\beta)\\-\cos(\frac{\pi}{2}-\beta)\end{bmatrix}+F_{b2}\begin{bmatrix}\cos\beta\\\sin\beta\end{bmatrix}+m_2\begin{bmatrix}0\\g\end{bmatrix}=bm\begin{bmatrix}\ddot{x}_2\\\ddot{y}_2\end{bmatrix} \qquad (2.7.9)$$

The eq 2.7.9 is a set of two linear simultaneous equations with F_{a2} and F_{b2} unknowns. It

can be solved by Cramer's rule as follows:

set

$$F_{a2}\cos\phi - F_{b2}\cos\psi = m_2\ddot{x} - F_{a1}\sin\phi + F_{b1}\sin\psi = c_{11} \tag{2.7.10}$$

$$F_{a2}\sin\phi - F_{b2}\sin\psi = m_2(\ddot{y}+g) + F_{a1}\cos\phi - F_{b1}\cos\psi = c_{22} \tag{2.7.11}$$

Then

$$F_{a2} = \frac{-c_{11}\sin\psi + c_{22}\cos\psi}{\sin(\phi-\psi)} \tag{2.7.12}$$

$$F_{b2} = \frac{c_{22}\cos\phi - c_{11}\sin\phi}{\sin(\phi-\psi)} \tag{2.7.13}$$

Then the pin forces can be calculated from the above equations.

2.8 Method of solution

Universal co-ordinates

The dimensions , masses ,inertia , the input angle at starting point and the initial value of input speed are input.

As it is illustrated in the flowchart (fig 2.8.1) first of all the kinematic characteristics of the linkage are calculated (2.2). Then from the equations of motion dynamic characteristics (joint forces and input angular acceleration) are calculated(2.3).

The 5 equations of motion constitute a set of 5 simultaneous linear equations. The forces and angular acceleration are calculated. A NAG routine called fo4aef is used for solving this set of linear simultaneous equations. The routine calculates the solution with multiple righthand sides by Crout's factorisation method. Given a set of linear equations AX=B , the routine first decomposes A using Crout's factorisation with partial pivoting ,PA=LU , where P is a permutation matrix,L is lower triangular and U is unit upper triangular. An approximation to X is found by back-substitution . The residual matrix$R=B-AX$ is then calculated and a correction D , to X , is found by back substitution in $AD=RX$ is replaced by (X+D) and the process repeated until

full machine accuracy has been obtained . Additional accumulation of innerproducts is used throughout . (42)

These parameters can be used to get the contact angle γ and can be used to calculate Earles and Wu criterion $(\frac{\dot{\gamma}}{R})$.

The input speed also can be calculated using the work and energy equation. Then the output of one step is printed out. If the cycle is unfinished the programme will increase one step and start the kinematic calculation again. Before terminating it will write the general results of the cycle (see fig 2.8.1). For flywheel control it is assumed that the input torque is as much as is necessary to compensate the friction during the cycle. Therefor both friction and input torque were set to zero.

When a 3 term controller is used to control the input speed; the torque is calculated from equation(2.6.1) and is used in the equation (2.4.1).

For constant input speed the input acceleration is zero and the required input torque is calculated.

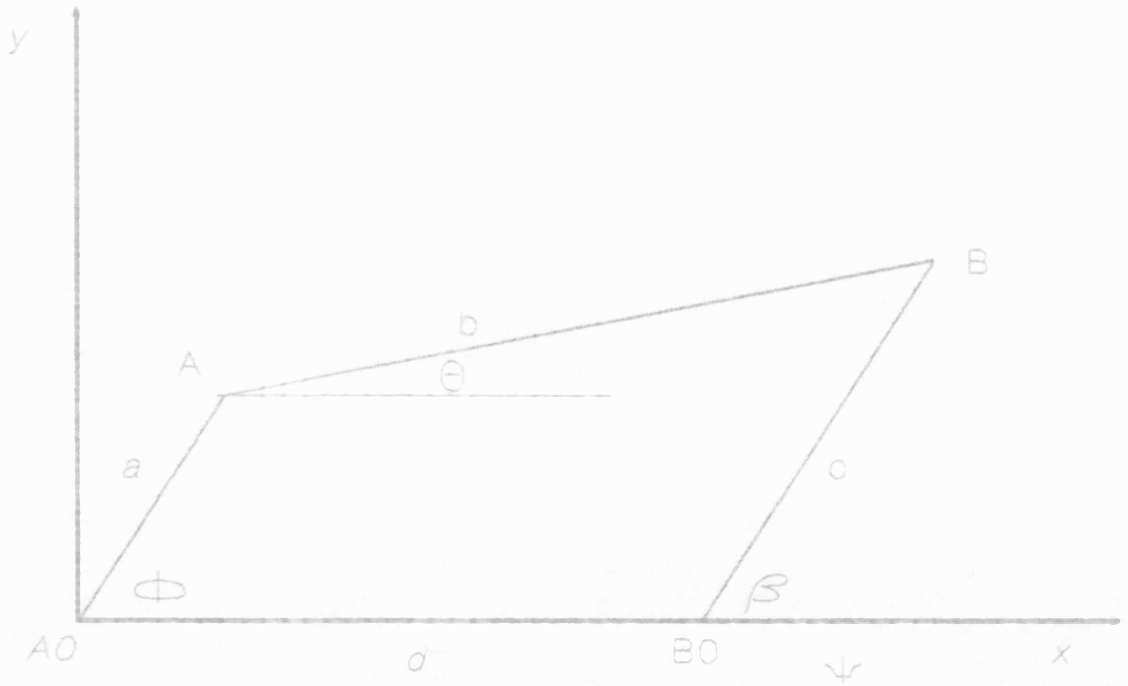

Fig 2.2.1 Four bar chain diagram

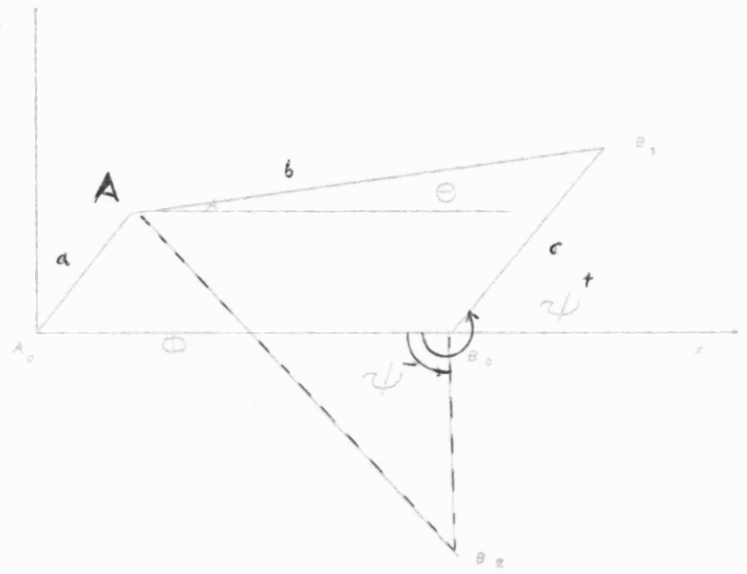

Fig 2.2.2 Four bar chain diagram showing open(B_1)and crossed (B_2) configuration

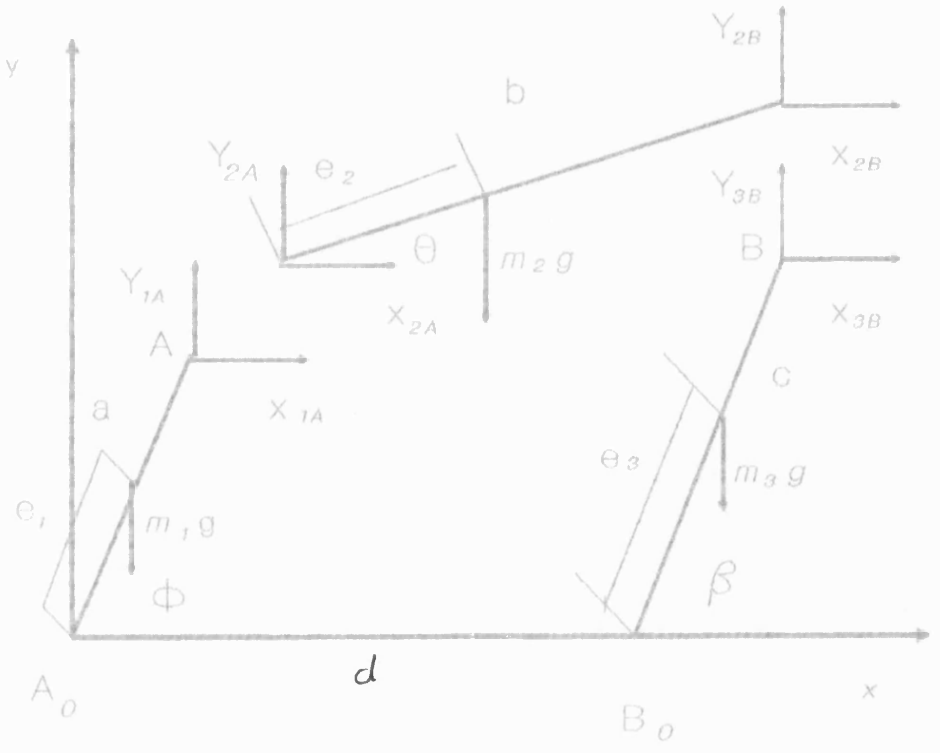

Fig 2.3.1 Free body diagram for fixed co-ordinate

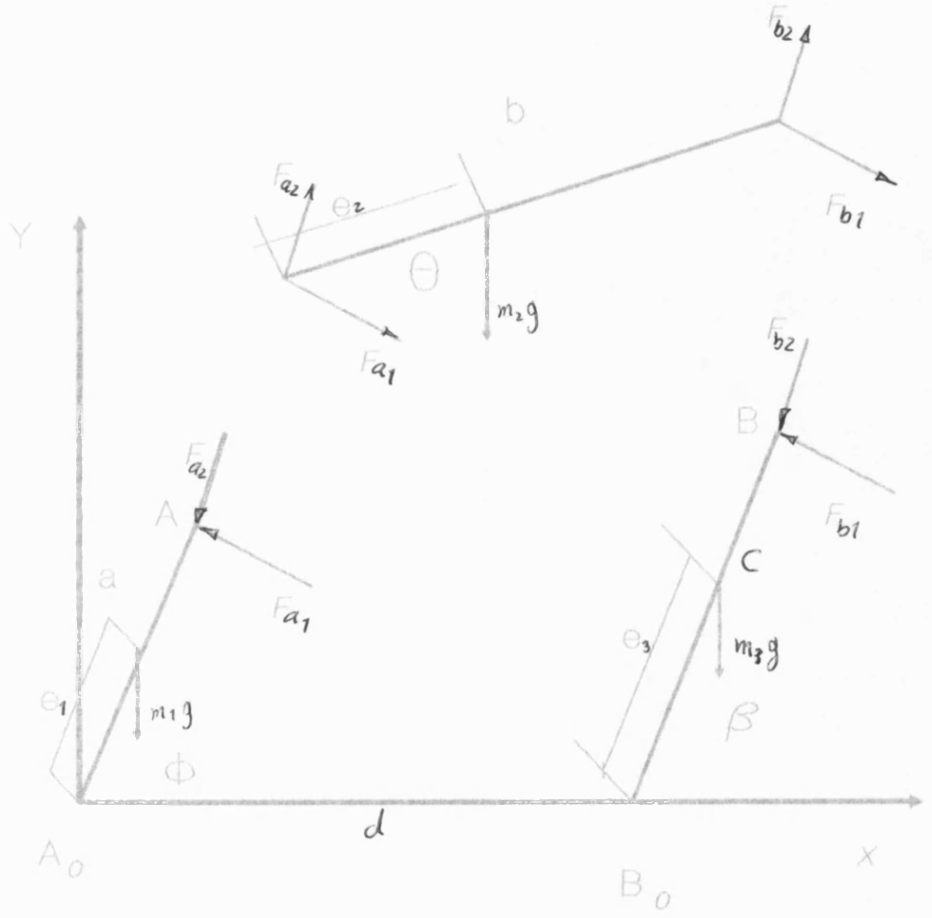

Fig 2.7.1 Free body diagram with body fixed co-ordinates

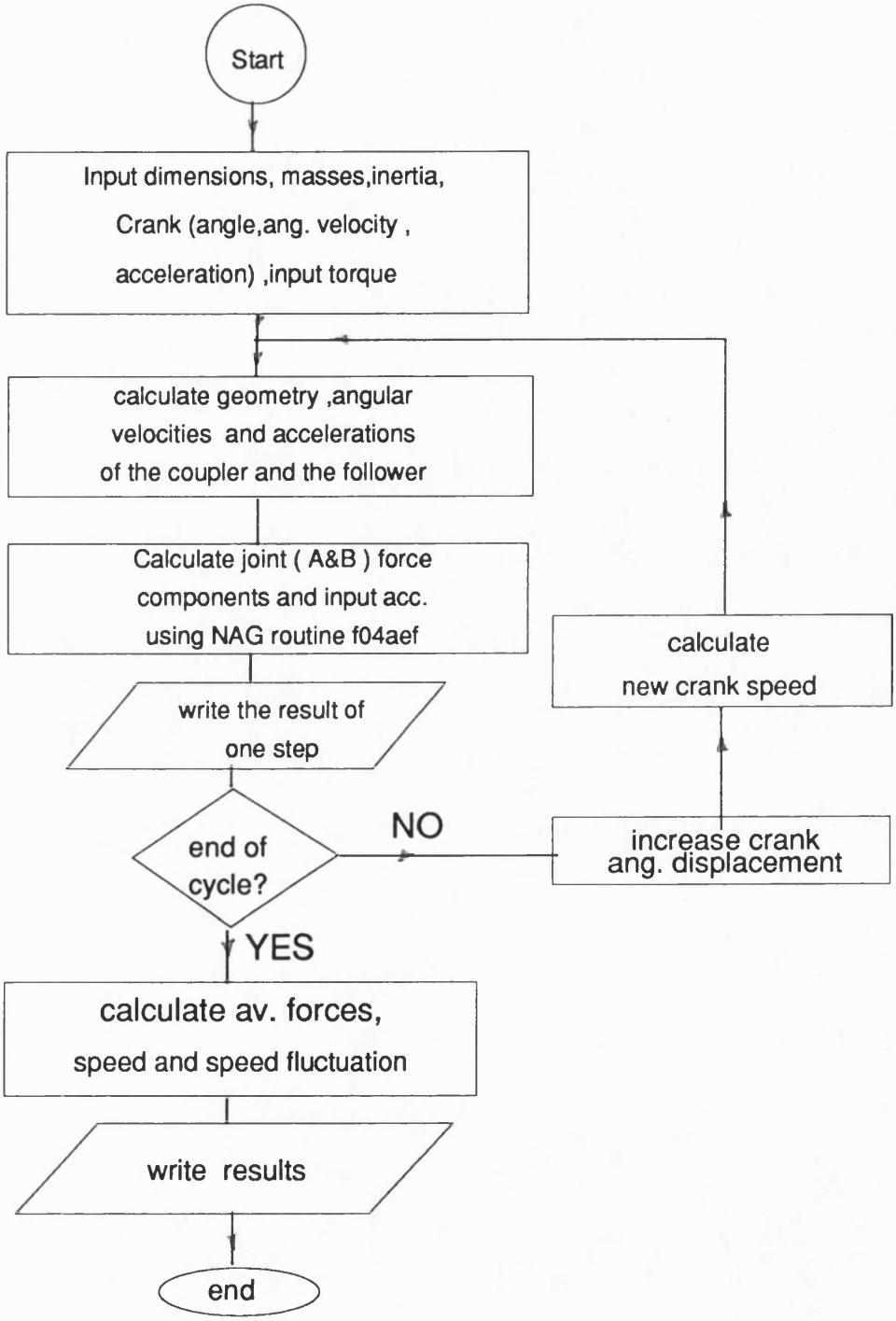

Fig 2.8.1 Computing flowchart for zero clearance model

CHAPTER 3

DYNAMIC ANALYSIS WITH CLEARANCE

3.1 Introduction

Consider the four bar chain with clearance in the coupler-follower joint , which is effectively a five bar chain. The system is a two degree of freedom mechanism , the freedoms being the crank angle ϕ and the clearance angle α . There are two ways to solve the above mechanism.

a. iteration

b. integration

These methods are explained in sub sections(3.2.1,3.2.2)respectively. Assuming the pin and bush are in contact continuously, the method is called continuous contact which is discussed in sec.(3.3).

In practice the pin is not necessarily in contact all the time. Then contact may be broken somewhere. A criterion is required to detect the contact loss position(see sec.(3.4)). When contact is broken the pin goes into free flight inside the bush(see sec.(3.5)). In this mode the chain is treated as two pendulums.

The free flight is terminated by impact(see sec.(3.6)). There will be a momentum exchange between the pin and bush because of the relative radial speed.

The governing equations,which are nonlinear, must be solved numerically. The method is discussed in sec.(3.7).

3.2 mathematical models

3.2.1 iteration method

In the iteration method the equations of motion of the system can be solved for a crank angle and a clearance angle. At a given crank angle one may get an approximation to clearance angle α from the contact angle γ at zero clearance, using $\tan\alpha=\frac{Y_B}{X_B}$ where Y_B and X_B are the vertical and horizontal component of pin force at B respectively (see fig(3.2.2)). Using this angle and the input crank angle the initial configuration of the mechanism can be defined. Using these geometric parameters the forces are calculated. The clearance angle can be calculated again. The iteration continues up to a point where both α and $\dot{\alpha}$ converge within some suitable tolerance. Then the procedure is repeated at the next crank angle.

Kinematic with clearance

Consider the clearance link to be massless . Then we will have a five bar chain (fig3.2.1).with two degrees of freedom. It may be represented by five vectors $\vec{A_0A},\vec{AB},\vec{r},\vec{BB_0}$ and $\vec{A_0B_0}$ with magnitude a,b,r(clearance link) ,c and d respectively.

Projection on x axis gives:

$$a\cos\phi+b\cos\theta+r\cos\alpha-c\cos(\psi-180)-d=0 \qquad (3.2.1)$$

Projection on y axis gives:

$$a\sin\phi+b\sin\theta+r\sin\alpha-c\sin(\psi-180)=0 \qquad (3.2.2)$$

One may eliminate ψ from equations (3.2.1) and (3.2.2)

$$c\cos\psi=d-(a\cos\phi+b\cos\theta+r\cos\alpha) \qquad (3.2.3)$$

$$c\sin(\psi)=-a\sin\phi-b\sin\theta-r\sin\alpha \qquad (3.2.4)$$

Squaring and adding one may get the equation

$$[\sin\phi+(\frac{r}{a})\sin\alpha]\sin\theta+[\cos\phi+(\frac{r}{a})\cos\alpha-\frac{d}{a}]\cos\theta=\frac{c^2-(a^2+b^2+d^2+r^2)}{2ab}+\frac{d}{b}\cos\phi$$
$$-\frac{r}{b}\cos(\phi-\alpha)+\frac{rd}{ab}\cos\alpha$$

It may be written more simply as follows:

$$A\sin\theta + B\cos\theta = C \tag{3.2.5}$$

where:

$$A = \sin\phi + \frac{r}{a}\sin\alpha$$

$$B = \cos\phi + \frac{r}{a}\cos\alpha - \frac{d}{a} \tag{3.2.6}$$

$$C = \frac{c^2 - (a^2 + b^2 + d^2 + r^2}{2ab} + \frac{d}{b}\cos\phi - \frac{r}{b}\cos(\phi - \alpha) + \frac{rd}{ab}\cos\alpha$$

Substituting

$$\sin\theta = \frac{2s}{1+s^2} \quad , \quad \cos\theta = \frac{1-s^2}{1+s^2} \tag{3.2.7}$$

where

$$s = \tan\frac{\theta}{2}$$

$$(B + C)s^2 - 2As + (C - B) = 0 \tag{3.2.8}$$

Substituting

$$\theta = 2arctan\frac{A \pm \sqrt{A^2 + B^2 - C^2}}{(B+C)} \tag{3.2.9}$$

which is similar to zero clearance case

There are two roots namely θ^+ corresponding to the positive sign and θ^- corresponding to the negative sign.

To obtain expression for the angular velocity and acceleration of the coupler we differentiate eq (3.2.5) implicitly with respect to time to give

$$A\dot{\theta}\cos\theta + \dot{A}\sin\theta - B\dot{\theta}\sin\theta + \dot{B}\cos\theta = \dot{C}$$

where $\dot{A}, \dot{B}$ and $\dot{C}$ are as follows:

$$\dot{A} = \dot{\phi}\cos\phi + \frac{r}{a}\dot{\alpha}\cos\alpha$$

$$\dot{B} = -\dot{\phi}\sin\phi - \frac{r}{a}\dot{\alpha}\sin\alpha$$

$$\dot{C} = -\frac{d}{b}\dot{\phi}\sin\phi + \frac{r}{d}(\dot{\phi} - \dot{\alpha})\sin(\phi - \alpha) - \frac{rd}{ab}\dot{\alpha}\sin\alpha$$

Therefor $\dot{\theta}$ is found to be

$$\dot{\theta}=\frac{\dot{C}-\dot{A}\sin\theta-\dot{B}\cos\theta}{A\cos\theta-B\sin\theta}$$

Substitution in the above equations yields the angular velocity of the coupler.

$$\dot{\theta}=(\frac{Y_1}{Y_2})\dot{\phi}+(\frac{Y_3}{Y_2})\dot{\alpha} \qquad (3.2.10)$$

where:

$$Y_1=-\frac{d}{b}\sin\phi+\frac{r}{b}\sin(\phi-\alpha)+\sin(\phi-\theta)$$

$$Y_2=\sin(\phi-\theta)+\frac{r}{a}\sin(\alpha-\theta)+\frac{d}{a}\sin\theta$$

$$Y_3=-\frac{rd}{ab}\sin\alpha-\frac{r}{b}\sin(\phi-\alpha)+\frac{r}{a}\sin(\alpha-\theta)$$

Differentiating the above equation the angular acceleration of the coupler is obtained as

$$\ddot{\theta}=[\frac{Y_2DY_1-Y_1DY_2}{Y_2^2}]\dot{\phi}+\frac{Y_1}{Y_2}\ddot{\phi}+[\frac{Y_2DY_3-Y_3DY_2}{Y_2^2}]\dot{\alpha}+[\frac{Y_3}{Y_2}]\ddot{\alpha} \qquad (3.2.11)$$

and DY signifies $\dot{Y}$

Differentiating the parameters Y_i, i=1 to 3 yields:

$$DY_1=-\frac{d}{b}\dot{\phi}\cos\phi+\frac{r}{b}(\dot{\phi}-\dot{\alpha})\cos(\phi-\alpha)+(\dot{\phi}-\dot{\theta})\cos(\phi-\theta)$$

$$DY_2=(\dot{\phi}-\dot{\theta})\cos(\phi-\theta)+\frac{r}{a}(\dot{\alpha}-\dot{\theta})\cos(\alpha-\theta)+\frac{d}{a}\dot{\theta}\cos\theta$$

$$DY_3=-\frac{rd}{ab}\dot{\alpha}\cos\alpha-\frac{r}{b}(\dot{\phi}-\dot{\alpha})\cos(\phi-\alpha)+\frac{r}{a}(\dot{\alpha}-\dot{\theta})\cos(\alpha-\theta)$$

$$\dot{\theta}=G_c\dot{\phi}+G_{c1}\dot{\alpha} \qquad (3.2.12)$$

$$\ddot{\theta}=DG_c\dot{\phi}+G_c\ddot{\phi}+DG_{c1}\dot{\alpha}+G_{c1}\ddot{\alpha} \qquad (3.2.13)$$

where

$$G_c=\frac{Y_1}{Y_2},\quad G_{c1}=\frac{Y_3}{Y_2}$$

and DG_c is the derivation of G_c with respect to time.

$$DG_c=\frac{Y_2DY_1-Y_1DY_2}{Y_2^2}$$

$$DG_{c1}=\frac{Y_2DY_3-Y_3DY_2}{Y_2^2}$$

Angular position , velocity and acceleration of the follower

a . Angular Position

Expressing equations (3.2.1) and (3.2.2) in terms of the coupler angle.

$$b\cos\theta=d-(a\cos\phi+c\cos\psi+r\cos\alpha) \tag{3.2.14}$$

$$b\sin\theta=-(a\sin\phi+c\sin\psi+r\sin\alpha) \tag{3.2.15}$$

Squaring and adding the above equations yields

$$\sin\psi(\sin\phi+\frac{r}{a}\sin\alpha)+\cos\psi(\cos\phi+\frac{r}{a}\cos\alpha-\frac{d}{a})=\frac{b^2-(a^2+c^2+d^2+r^2)}{2ac}+\frac{d}{c}\cos\phi-\frac{r}{c}\cos(\phi-\alpha)+\frac{rd}{ac}\cos\alpha$$

which may be written as follows

$$H\sin\psi+E\cos\psi=F \tag{3.2.16}$$

where

$$H=\sin\phi+\frac{r}{a}\sin\alpha$$

$$E=\cos\phi+\frac{r}{a}\cos\alpha-\frac{d}{a}$$

$$F=\frac{b^2-(a^2+c^2+d^2+r^2)}{2ac}+\frac{d}{c}\cos\phi-\frac{r}{c}\cos(\phi-\alpha)+\frac{rd}{ac}\cos\alpha$$

To solve for follower angle , substitution

$$\sin\psi=2\frac{s}{1+s^2} \quad where \quad s=\tan(\frac{\psi}{2})$$

$$\cos\psi=\frac{1-s^2}{1+s^2}$$

Substituting ψ and re-arranging the above equation yields:

$$(E+F)s^2-2Hs+(F-E)=0 \qquad (3.2.17)$$

Solving for ψ yields :

$$s=\frac{H\pm\sqrt{H^2+E^2-F^2}}{E+F}$$

There are two roots

$$\psi^+=2arctan\frac{H+\sqrt{H^2+E^2-F^2}}{E+F}$$

$$\psi^-=2arctan\frac{H-\sqrt{H^2+E^2-F^2}}{E+F}$$

The two values correspond to the two possible positions(fig 2.2.2) of the mechanism

as discussed in the zero clearance case (see sec 2.2).

b. Angular velocity of the follower:

Consider eq (3.2.16), namely

$$H\sin\psi+E\cos\psi=F$$

To obtain velocity one can differentiate this eqution implicitly with respect to time:

$$\dot{H}\sin\psi+H\dot{\psi}\cos\psi+\dot{E}\cos\psi-E\dot{\psi}\sin\psi=\dot{F} \qquad (3.2.18)$$

Solving for the output angular velocity

$$\dot{\psi}=\frac{\dot{F}-\dot{H}\sin\psi-\dot{E}\cos\psi}{H\cos\psi-E\sin\psi}$$

where

$\dot{H},\dot{E}$ and $\dot{F}$ are as follows:

$$\dot{H}=\dot{\phi}\cos\phi+(\frac{r}{a})\dot{\alpha}\cos\alpha$$

$$\dot{E}=-\dot{\phi}\sin\phi-(\frac{r}{a})\dot{\alpha}\sin\alpha$$

$$\dot{F}=-\frac{d}{c}\dot{\phi}\sin\phi+\frac{r}{c}(\dot{\phi}-\dot{\alpha})\sin(\phi-\alpha)-\frac{rd}{ac}\dot{\alpha}\sin\alpha$$

Therefore the follower angular velocity equation can be sumarized as follows:

$$\dot{\psi}=(\frac{Z_1}{Z_2})\dot{\phi}+(\frac{Z_3}{Z_2})\dot{\alpha} \qquad (3.2.19)$$

where

$$Z_1=-(\frac{d}{c})\sin\phi+(\frac{r}{c})\sin(\phi-\alpha)+\sin(\phi-\psi)$$

$$Z_2=\sin(\phi-\psi)+(\frac{r}{a})\sin(\alpha-\psi)+(\frac{d}{a})\sin\psi$$

$$Z_3=-(\frac{r}{c})\sin(\phi-\alpha)-(\frac{r}{a})\sin(\psi-\alpha)-(\frac{rd}{ac})\sin\alpha$$

The angular velocity equation may be written versus of two different component $\dot{\alpha},\dot{\phi}$

as follows:

$$\dot{\psi}=G_f\dot{\phi}+G_{f1}\dot{\alpha} \qquad (3.2.20)$$

where

$$G_f=\frac{Z_1}{Z_2} \quad \text{and} \quad G_{f1}=\frac{Z_3}{Z_2}$$

By diffrentiating the above equation one obtains the follower angular acceleration

$$\ddot{\psi}=DG_f\dot{\phi}+G_f\ddot{\phi}+DG_{f1}\dot{\alpha}+G_{f1}\ddot{\alpha} \qquad (3.2.21)$$

$$DG_f=\frac{DZ_1Z_2-DZ_2Z_1}{Z_2^2}$$

$$DG_{f1}=\frac{DZ_3Z_2-Z_3DZ_2}{Z_2^2}$$

where

$$DZ_1=-(\frac{d}{c})\phi\cos\phi+(\frac{r}{c})(\dot{\phi}-\dot{\alpha})\cos(\phi-\alpha)+(\dot{\phi}-\dot{\psi})\cos(\phi-\psi)$$

$$DZ_2=(\dot{\phi}-\dot{\psi})\cos(\phi-\psi)+(\frac{r}{a})(\dot{\alpha}-\dot{\psi})\cos(\alpha-\psi)+(\frac{d}{a})\dot{\psi}\cos\psi$$

$$DZ_3=-(\frac{r}{c})(\dot{\phi}-\dot{\alpha})\cos(\phi-\alpha)-(\frac{r}{a})(\dot{\psi}-\dot{\alpha})\cos(\psi-\alpha)-(\frac{rd}{ac})\dot{\alpha}\cos\alpha$$

Angular velocity and acceleration of clearance link.

Rewriting eq (3.2.2) and differentiating twice one obtains the angular velocity and

acceleration of the clearance link as follows:

$r\sin\alpha=-(a\sin\phi+b\sin\theta+c\sin\psi)$

$$\dot{\alpha}=-\frac{1}{r\cos\alpha}(a\dot{\phi}\cos\phi+b\dot{\theta}\cos\theta+c\dot{\psi}\cos\psi) \tag{3.2.22}$$

$$\ddot{\alpha}=-\frac{1}{r\cos\alpha}(a\ddot{\phi}\cos\phi+b\ddot{\theta}\cos\theta+c\ddot{\psi}\cos\psi-a\dot{\phi}^2\sin\phi-b\dot{\theta}^2\sin\theta-c\dot{\psi}^2\sin\psi+r\dot{\alpha}^2\sin\alpha) \tag{3.2.23}$$

3.2.2 Model using integration

In this model the joint forces, crank,follower and coupler acceleration, linear acceleration of the gravity centre of the coupler and the acceleration of clearance link are calculated at each crank position. Then these accelerations are integrated numerically to obtain velocities and displacements at the next crank step. These displacements and speeds are used in calculating the joint forces and acceleration.The joint forces can be found by solution of the equations of motion. Forces at joints A & B (Fig 3.2.2) are obtained from the acceleleration of the links. The forces at A_0 and B_0 follow from the above calculation. A total of four components of forces , together with linear and angular acceleration of the coupler and the follower remain to be determined from the five equations of motion , two closure and two linear acceleration equations and one Lagrange equation for the massless clearance link. Therefore there are 10 equations in ten unknowns which are obtained from

horizontal forces acting on the coupler,

$$X_{2A}+X_{2B}=m_2\ddot{x}_2 \tag{3.2.24}$$

vertical forces acting on the coupler,

$$Y_{2A}+Y_{2B}-m_2g=m_2\ddot{y}_2 \tag{3.2.25}$$

moment on the coupler relative to its center of mass

$$X_{2A}e_2\sin\theta-X_{2B}(b-e_2)\sin\theta-Y_{2A}e_2\cos\theta+Y_{2B}(b-e_2)\cos\theta=I_{2c.g.}\ddot{\theta}+c_{23}(\dot{\alpha}-\dot{\psi})-c_{12}(\dot{\phi}-\dot{\theta}) \tag{3.2.26}$$

$$X_{2A}e_2\sin\theta-X_{2B}(b-e_2)\sin\theta-Y_{2A}e_2\cos\theta+Y_{2B}(b-e_2)\cos\theta=I_{2c.g.}\ddot{\theta}+c_{23}(\dot{\alpha}-\dot{\psi})-c_{12}(\dot{\phi}-\dot{\theta}) \quad (3.2.26)$$

For crank A_0A one can write $\sum M_{A_0}=I_{1A_0}\ddot{\phi}$

$$T-Y_{2A}a\cos\phi+X_{2A}a\sin\phi-m_1ge_1\cos\phi=I_{1A0}\ddot{\phi}+c_{41}\dot{\phi}+c_{12}(\dot{\phi}-\dot{\theta}) \quad (3.2.27)$$

For link B_0B one may write

$$\sum M_{B_0}=I_{3B_0}\ddot{\psi}$$

$$-Y_{2B}c\cos(\psi-\pi)+X_{2B}c\sin(\psi-\pi)-m_3ge_3\cos(\psi-\pi)=I_{3B0}\ddot{\psi}+c_{34}\dot{\psi}-c_{23}(\dot{\alpha}-\dot{\psi}) \quad (3.2.28)$$

where c_{ij} is the coefficient of viscous friction in the joint between link i and j.

The linear acceleration $\ddot{x}_2$ and $\ddot{y}_2$ can be calculated in terms of angular speeds and accelerations as follows:

$$x_2=a\cos\phi+e_2\cos\theta \quad (3.2.29)$$

$$y_2=a\sin\phi+e_2\sin\theta \quad (3.2.30)$$

$$\dot{x}_2=-a\dot{\phi}\sin\phi-e_2\dot{\theta}\sin\theta \quad (3.2.31)$$

$$\dot{y}_2=a\dot{\phi}\cos\phi+e_2\dot{\theta}\cos\theta \quad (3.2.32)$$

$$\begin{bmatrix}\ddot{x}_2\\ \ddot{y}_2\end{bmatrix}=a\ddot{\phi}\begin{bmatrix}-\sin\phi\\ \cos\phi\end{bmatrix}+e_2\ddot{\theta}\begin{bmatrix}-\sin\theta\\ \cos\theta\end{bmatrix}+a\dot{\phi}^2\begin{bmatrix}-\cos\phi\\ -\sin\phi\end{bmatrix}+e_2\dot{\theta}^2\begin{bmatrix}-\cos\theta\\ -\sin\theta\end{bmatrix} \quad (3.2.33)$$

Differentiating the closure equations (3.2.1) and (3.2.2) twice

$$a\ddot{\phi}\begin{bmatrix}-\sin\phi\\ \cos\phi\end{bmatrix}-r\dot{\alpha}^2\begin{bmatrix}-\cos\alpha\\ -\sin\alpha\end{bmatrix}+b\ddot{\theta}\begin{bmatrix}-\sin\theta\\ \cos\theta\end{bmatrix}+c\ddot{\psi}\begin{bmatrix}-\sin\psi\\ \cos\psi\end{bmatrix}+a\dot{\phi}^2\begin{bmatrix}-\cos\phi\\ -\sin\phi\end{bmatrix}+b\dot{\theta}^2\begin{bmatrix}-\cos\theta\\ -\sin\theta\end{bmatrix}$$
$$+c\dot{\psi}^2\begin{bmatrix}-\cos\psi\\ -\sin\psi\end{bmatrix}-r\ddot{\alpha}\begin{bmatrix}-\sin\alpha\\ \cos\alpha\end{bmatrix}=\begin{bmatrix}0\\ 0\end{bmatrix} \quad (3.2.34)$$

There are 10 unknown variables. The tenth equation is obtained by applying lagrange equation for the clearance link angle α

$$\frac{d}{dt}\left(\frac{\partial T}{\partial\dot{\alpha}}\right)-\frac{\partial T}{\partial\alpha}+\frac{\partial U}{\partial\alpha}+\frac{\partial D_c}{\partial\dot{\alpha}}=0 \quad (3.2.35)$$

where

T = kinetic energy

U = potential energy

D_c = dissipation energy

α = clearance link angle

The relation for kinetic energy and potential energy and dissipation energy can be written as follows:

$$T=(I_{1A_0}\dot{\phi}^2+I_{2c.g.}\dot{\theta}^2+I_{3B_0}\dot{\psi}^2+m_2\dot{x}_2^{\,2}+m_2\dot{y}_2^{\,2})/2 \qquad (3.2.35a)$$

$$U=m_1gy_1+m_2gy_2+m_3gy_3$$

where y_i is the vertical distance of c.m of link i for i=1,2,3

$$D_c=(c_{41}\dot{\phi}^2+c_{12}(\dot{\phi}-\dot{\theta})^2+c_{23}(\dot{\alpha}-\dot{\psi})^2+c_{34}\dot{\psi}^2)/2$$

Because the system has two degrees of freedom ϕ can be specified independent of α which means that

$$\frac{\partial\phi}{\partial\alpha}=0 \rightarrow \frac{\partial y_1}{\partial\alpha}=0$$

Differentiating the equation (3.2.35a) with respect to $\dot{\alpha}$

$$\frac{\partial T}{\partial\dot{\alpha}}=I_{2c.g}\left(\frac{\partial\dot{\theta}}{\partial\dot{\alpha}}\right)\dot{\theta}+I_{3B_0}\left(\frac{\partial\dot{\psi}}{\partial\dot{\alpha}}\right)\dot{\psi}+m_2\left(\frac{\partial\dot{x}_2}{\partial\dot{\alpha}}\right)\dot{x}_2+m_2\left(\frac{\partial\dot{y}_2}{\partial\dot{\alpha}}\right)\dot{y}_2 \qquad (3.2.36)$$

$$\frac{\partial T}{\partial\dot{\alpha}}=I_{2c.g}\left(\frac{\partial\dot{\theta}}{\partial\dot{\alpha}}\right)\dot{\theta}+I_{3B_0}\left(\frac{\partial\dot{\psi}}{\partial\dot{\alpha}}\right)\dot{\psi}+m_2\left(\frac{\partial\dot{x}_2}{\partial\dot{\alpha}}\right)\dot{x}_2+m_2\left(\frac{\partial\dot{y}_2}{\partial\dot{\alpha}}\right)\dot{y}_2$$

Differentiating eq (3.2.36) and substituting $\frac{\partial\eta}{\partial\dot{\alpha}}=\frac{\partial\eta}{\partial\alpha}$ where $\eta=\theta,\psi,x_2,y_2$

$$\frac{d}{dt}\left(\frac{\partial T}{\partial\dot{\alpha}}\right)=I_{2c.g.}\left(\frac{\partial\ddot{\theta}}{\partial\alpha}\right)\dot{\theta}+I_{2c.g.}\left(\frac{\partial\theta}{\partial\alpha}\right)\ddot{\theta}+I_{3B_0}\left(\frac{\partial\dot{\psi}}{\partial\alpha}\right)\dot{\psi}+I_{3B_0}\left(\frac{\partial\psi}{\partial\alpha}\right)\ddot{\psi}+m_2\left(\frac{\partial\dot{x}}{\partial\alpha}\right)\dot{x}$$

$$+m_2\left(\frac{\partial x}{\partial\alpha}\right)\ddot{x}+m_2\left(\frac{\partial\dot{y}}{\partial\alpha}\right)\dot{y}+m_2\left(\frac{\partial y}{\partial\alpha}\right)\ddot{y} \qquad (3.2.37)$$

$$\frac{d}{dt}\left(\frac{\partial T}{\partial\alpha}\right)=I_{2c.g.}\left(\frac{\partial\dot{\theta}}{\partial\alpha}\right)\dot{\theta}+I_{3B_0}\left(\frac{\partial\dot{\psi}}{\partial\alpha}\right)\dot{\psi}+m_2\left(\frac{\partial\dot{x}_2}{\partial\alpha}\right)\dot{x}_2+m_2\left(\frac{\partial\dot{y}_2}{\partial\alpha}\right)\dot{y} \qquad (3.2.38)$$

$$\frac{\partial U}{\partial\alpha}=g\left(m_1\frac{\partial y_1}{\partial\alpha}+m_2\frac{\partial y_2}{\partial\alpha}+m_3\frac{\partial y_3}{\partial\alpha}\right) \qquad (3.2.39)$$

$$\frac{\partial D_c}{\partial \dot{\alpha}}=c_{12}(\dot{\phi}-\dot{\theta})(\frac{-\partial\theta}{\partial\alpha})+c_{23}(\dot{\alpha}-\dot{\psi})(1-\frac{\partial\psi}{\partial\alpha})+c_{34}\dot{\psi}(\frac{\partial\psi}{\partial\alpha}) \qquad (3.2.40)$$

where:

$$y_3=e_3\sin\beta=e_3\sin(\psi-\pi) \qquad (3.2.41)$$

$$\frac{\partial y_3}{\partial\alpha}=(\frac{\partial\psi}{\partial\alpha})e_3\cos(\psi-\pi)=-(\frac{\partial\psi}{\partial\alpha})e_3\cos\psi \qquad (3.2.42)$$

$$\frac{\partial y_1}{\partial\alpha}=0$$

Substituting eq (3.2.37 - 3.2.42) in eq (3.2.34) one may get the following equation

$$I_{2c.g.}(\frac{\partial\theta}{\partial\alpha})\ddot{\theta}+I_{3B0}(\frac{\partial\psi}{\partial\alpha})\ddot{\psi}+m_2(\frac{\partial x}{\partial\alpha})\ddot{x}+m_2(\frac{\partial y}{\partial\alpha})\ddot{y}+g(m_2\frac{\partial y_2}{\partial\alpha}+m_3\frac{\partial y_3}{\partial\alpha})+\frac{\partial D_c}{\partial\dot{\alpha}}=0 \qquad (3.2.43)$$

To evaluate the terms $\frac{\partial\eta}{\partial\alpha},\eta=\theta,\psi,x_i,y_i,\ i=2,3$ in the above equation one may use the closure equations(3.2.1,3.2.2) for the x and y directions and then differentiate with respect to α. There will be two equations and two unknowns i.e. $\frac{\partial\theta}{\partial\alpha},\frac{\partial\psi}{\partial\alpha}$ which can be solved by an elimination method. For $\frac{\partial x_2}{\partial\alpha},\frac{\partial y_2}{\partial\alpha}$ the same procedure can be followed.

$$a\frac{\partial\phi}{\partial\alpha}\begin{bmatrix}-\sin\phi\\ \cos\phi\end{bmatrix}-r\begin{bmatrix}-\sin\alpha\\ +\cos\alpha\end{bmatrix}+b\frac{\partial\theta}{\partial\alpha}\begin{bmatrix}-\sin\theta\\ \cos\theta\end{bmatrix}+c\frac{\partial\psi}{\partial\alpha}\begin{bmatrix}-\sin\psi\\ \cos\psi\end{bmatrix}=0 \qquad (3.2.44)$$

By solving the above equations one may get the following results

$$b\frac{\partial\theta}{\partial\alpha}\sin(\psi-\theta)-r\sin(\psi-\alpha)=0$$

$$c\frac{\partial\psi}{\partial\alpha}\sin(\theta-\psi)-r\sin(\theta-\alpha)=0$$

$$\frac{\partial\theta}{\partial\alpha}=\frac{r\sin(\psi-\alpha)}{b\sin(\psi-\theta)}$$

$$\frac{\partial\psi}{\partial\alpha}=\frac{r\sin(\theta-\alpha)}{c\sin(\theta-\psi)} \qquad (3.2.45)$$

$$\begin{bmatrix} x_2 \\ y_2 \end{bmatrix} = a\begin{bmatrix} \cos\phi \\ \sin\phi \end{bmatrix} + e_2\begin{bmatrix} \cos\theta \\ \sin\theta \end{bmatrix} \tag{3.2.46}$$

$$\begin{bmatrix} \frac{\partial x_2}{\partial \alpha} \\ \frac{\partial y_2}{\partial \alpha} \end{bmatrix} = e_2\frac{\partial\theta}{\partial\alpha}\begin{bmatrix} -\sin\theta \\ \cos\theta \end{bmatrix} = \frac{e_2 r\sin(\psi-\alpha)}{b\sin(\psi-\theta)}\begin{bmatrix} -\sin\theta \\ \cos\theta \end{bmatrix} \tag{3.2.47}$$

By substitution for $\frac{\partial\eta}{\partial\alpha}$ $where \eta=\theta,\psi,x_2,y_2$ from equation (3.2.45,3.2.47) in equation (3.2.43) one may get

$$I_{2.c.g}\left(-\frac{r\sin(\psi-\alpha)}{b\sin(\psi-\theta)}\right)\ddot{\theta} + I_{3B0}\left(-\frac{r\sin(\theta-\alpha)}{c\sin(\psi-\theta)}\right)\ddot{\psi} + m_2 r\frac{e_2}{b}\left(\frac{\sin\theta\sin(\psi-\alpha)}{\sin(\psi-\theta)}\right)\ddot{x} + m_2 e_2\frac{r}{b}\left(-\frac{\cos(\theta)\sin(\psi-\alpha)}{\sin(\psi-\theta)}\right)\ddot{y} +$$

$$\frac{m_2 e_2 g}{b}\left(-\frac{r\cos\theta\sin(\psi-\alpha)}{\sin(\psi-\theta)}\right) + m_3 g e_3\left(\frac{r\sin(\theta-\alpha)}{c\sin(\theta-\psi)}\right)\cos\psi + c_{12}(\dot{\phi}-\dot{\theta})\left(-\frac{r\sin(\psi-\alpha)}{b\sin(\psi-\theta)}\right) +$$

$$c_{23}(\dot{\alpha}-\dot{\psi}) + (c_{34}\dot{\psi} - c_{23}(\dot{\alpha}-\dot{\psi}))\left(\frac{r\sin(\theta-\alpha)}{c\sin(\theta-\psi)}\right) = 0 \tag{3.2.48}$$

By rearrangement of eq. (3.2.48) one may get the following equation

$$\frac{r\sin(\psi-\alpha)}{\sin(\theta-\psi)}\left[\left(\frac{I_2}{b}\right)\ddot{\theta} - \frac{I_3\sin(\theta-\alpha)}{c\sin(\psi-\alpha)}\ddot{\psi} - \left(\frac{m_2 e_2}{b}\right)\sin\theta\ddot{x}_2 + \left(\frac{m_2 e_2}{b}\right)\cos(\theta)\ddot{y}_2\right.$$

$$\left. + \left(\frac{m_2 g e_2}{b}\right)\cos\theta - \frac{m_3 g e_3\sin(\theta-\alpha)\cos\psi}{\sin(\psi-\alpha)}\right] + \frac{\partial D_c}{\partial\dot{\alpha}} = 0 \tag{3.2.49}$$

There are ten unknown $X_A, Y_A, X_B, Y_B, \ddot{\phi}, \ddot{\theta}, \ddot{\psi}, \ddot{\alpha}, \ddot{x}_2, \ddot{y}_2$. A set of equations can be written in matrix form as follows:

$$AX = B \tag{3.2.50}$$

where:

$$A = \begin{bmatrix}
1 & 0 & 1 & 0 & -m_2 & 0 & 0 & 0 & 0 & 0 \\
0 & 1 & 0 & 1 & 0 & -m_2 & 0 & 0 & 0 & 0 \\
a\sin\phi & -a\cos\phi & 0 & 0 & 0 & 0 & -I_{1A_0} & 0 & 0 & 0 \\
e_2\sin\theta & -e_2\cos\theta & -(b-e_2)\sin\theta & +(b-e_2)\cos\theta & 0 & 0 & 0 & -I_{2.c.g} & 0 & 0 \\
0 & 0 & -c\sin\psi & c\cos\psi & 0 & 0 & 0 & 0 & -I_{3B_0} & 0 \\
0 & 0 & 0 & 0 & 0 & 0 & -a\sin\phi & -b\sin\theta & -c\sin\psi & r\sin\alpha \\
0 & 0 & 0 & 0 & 0 & 0 & a\cos\phi & b\cos\theta & c\cos\psi & -\cos\alpha \\
0 & 0 & 0 & 0 & 1 & 0 & a\sin\phi & e_2\sin\theta & 0 & 0 \\
0 & 0 & 0 & 0 & 0 & 1 & -a\cos\phi & -e_2\cos\theta & 0 & 0 \\
0 & 0 & 0 & 0 & m_2\frac{\partial x_2}{\partial\alpha} & m_2\frac{\partial y_2}{\partial\alpha} & 0 & I_{2.c.g}\partial\frac{\theta}{\partial\alpha} & I_{3B_0}\partial\frac{\psi}{\partial\alpha} & 0
\end{bmatrix}$$

$$X = \left[X_{2A}, Y_{2A}, X_{2B}, Y_{2B}, \ddot{x}_2, \ddot{y}_2, \ddot{\phi}, \ddot{\theta}, \ddot{\psi}, \ddot{\alpha} \right]^T$$

$$B = \begin{bmatrix} 0 \\ m_2 g \\ m_1 g e_1 \cos\phi - T + c_{41}\dot{\phi} + c_{12}(\dot{\phi} - \dot{\theta}) \\ c_{23}(\dot{\alpha} - \dot{\psi}) - c_{12}(\dot{\phi} - \dot{\theta}) \\ m_3 g e_3 \cos\psi + c_{34}\dot{\psi} - c_{23}(\dot{\alpha} - \dot{\psi}) \\ a\dot{\phi}^2 \cos\phi + b\dot{\theta}^2 \cos\theta - r\dot{\alpha}^2 \cos\alpha + c\dot{\psi}^2 \cos\psi \\ a\dot{\phi}^2 \sin\phi + b\dot{\theta}^2 \sin\theta - r\dot{\alpha}^2 \sin\alpha + c\dot{\psi}^2 \sin\psi \\ -a\dot{\phi}^2 \cos\phi - e_2\dot{\theta}^2 \cos\theta \\ -a\dot{\phi}^2 \sin\phi - e_2\dot{\theta}^2 \sin\theta \\ -m_2 g \dfrac{\partial y}{\partial \alpha} + m_3 g e_3 \dfrac{\partial \psi}{\partial \alpha} \cos\psi - \dfrac{\partial D_c}{\partial \dot{\alpha}} \end{bmatrix}$$

3.3 continuous contact mode

It is assumed that pin is in contact with the bush during the entire cycle.

The pin forces and angular and linear acceleration are calculated by solving the above simultaneous linear equations. The initial values for displacement and velocities are derived from zero clearance analysis. The solution is calculated from the top dead centre position ($\theta=\phi$) . By integration of acceleration the velocities in the clearance case at the start point of next crank angle are calculated . By integration of the velocities the displacements are derived.

When there is some clearance in at least one of the joints, depending on the relation between pin and bearing different modes of motion can happen. They are

1-contact mode

2- free flight mode

3- impact mode.

All the above equations which were developed in this chapter so far refer to the contact mode . In the case of free flight and impact mode the governing equations are discussed in the next sections:

3- impact mode.

All the above equations which were developed in this chapter so far refer to the contact mode . In the case of free flight and impact mode the governing equations are discussed in the next sections:

3.4 Contact loss criterion

As is observed from the experimental results (section 8.2) in practice there are some contact loss regions. These can be predicted in theoretical model using some criterion. There are several criteria which will be discussed in sec.(6.6). The criterion which was used in this model is $\frac{\ddot{\alpha}}{R_b}$. where

$\ddot{\alpha}$ = angular acceleration of clearance link in rad/s.s

R_b = pin force at B in Newtons

As this parameter was plotted against crank angle for continuous contact model and was compared with the experimental results the value of 6000 $(rads^{-2})/N$ was chosen for integration method . That means when the criterion reaches this value the free flight mode is invoked. If flight starts to occur it will go to the free flight mode otherwise it returns to the following mode.

3.5 Free flight mode

The mechanism is now visualized as being composed composed of two systems of pendulums, as shown in fig(3.5.1). The governing equations for this mode are obtained by considering the systems of forces and torques acting on each link.

The equation of motion for the follower when it is separated from the coupler is given by:

$m_3 g e_3 \cos(\psi-\pi)=I_{3B_0}\ddot{\psi}$

i.e

$$\ddot{\psi}=[\frac{m_3 e_3}{I_{3B0}}]g\cos\psi \tag{3.5.1}$$

The governing equations of the coupler can be written as follows:

$$e_2(X_{2A}\sin\theta-Y_{2A}\cos\theta)=I_{2c.g.}\ddot{\theta} \tag{3.5.2}$$

$X_{2A}=m_2 a_{2x}$

$Y_{2A}=m_2 a_{2y}+m_2 g$

where $(a_{2x},a_{2y})=(\ddot{x}_2,\ddot{y}_2)$ are the (x_2,y_2) components of acceleration at the C.G. of the coupler. Eliminating X_{2A} and Y_{2A} from the first relation in equations (3.5.2) and by using the remaining two one obtains:

$$I_2\frac{\ddot{\theta}}{m_2 e_2}+g\cos\theta=a_{2x}\sin\theta-(a_{2y})\cos\theta=-a_{2t} \tag{3.5.3}$$

where a_{2t} denotes the tangential component of the acceleration at the C.G. of the coupler (normal to its direction). a_{2t} is given as

$$a_{2t}=e_2\ddot{\theta}-a\dot{\phi}^2\sin(\phi-\theta)+a\ddot{\phi}\cos(\phi-\theta) \tag{3.5.4}$$

Eliminating a_{2t} from the last two relations ,the governing equation of the coupler is obtained as

$$\ddot{\theta}=\frac{m_2 e_2}{I_{2c.g.}+m_2{}^2 e_2{}^2}[a\dot{\phi}^2\sin(\phi-\theta)-a\ddot{\phi}\cos(\phi-\theta)-g\cos\theta] \tag{3.5.5}$$

The equation of motion of the crank can be written as follows:

$$X_{2A}a\sin\phi-(Y_{2A}a+m_1 g e_1)\cos\phi=I_1\ddot{\phi} \tag{3.5.6}$$

or

$$\ddot{\phi}=(X_{2A}a\sin\phi-(Y_{2A}a+m_1 g e_1)\cos\phi)/I_1 \tag{3.5.7}$$

By substituting X_{2A} and Y_{2A} from equation (3.5.2) one may get

$$\ddot{\phi}=[m_2 a_{2x}a\sin\phi-(m_2 a(a_{2y}+g)+m_1 g e_1)\cos\phi]/I_1 \tag{3.5.8}$$

If the variation of $\dot{\phi}$ and θ during the free flight mode is not considerable, we may have the following relations:

$$\dot{\theta}=\ddot{\theta}t+\dot{\theta}_1 \tag{3.5.9}$$

$$\theta=\frac{1}{2}\ddot{\theta}t^2+\dot{\theta}_1 t+\theta_1 \tag{3.5.10}$$

$$\dot{\psi}=\ddot{\psi}t+\dot{\psi}_1 \tag{3.5.11}$$

$$\psi=\frac{\ddot{\psi}}{2}t^2+\dot{\psi}t+\psi_1 \tag{3.5.12}$$

where $\dot{\theta}_1, \dot{\psi}_1$ are initial values.

However this is not the case, experimental work shows free flight occures over perhaps 20 degree of crank angle, and therefore there are three second order differential equation for free flight mode .

The equations are non linear and therefore they must be solved numerically.

Given angular displacement,velocity and acceleration ,the other parameters can be calculated. At the end of the free flight mode the pin impacts the bush.

3.6 Impact mode

The impact at the end of the free flight mode may have an important role in the dynamic performance of the linkage .According to the notations of fig.(3.6.1) the impulses are given by

$$H_b=\int F_n dt$$

$$J_b=\int f_t dt$$

$$\begin{aligned} H_a&=\int X_{2A} dt \\ J_a&=\int Y_{2A} dt \end{aligned} \tag{3.6.1}$$

H_b and J_b are normal and tangential impulse at bearing B and also H_a and J_a are horizontal and vertical impulses at bearing A . The equations of momentum exchange for

and for the coupler

$$(I_{2c.g.})(\dot{\theta}_p-\dot{\theta})=(b-e_2)[-H_b\sin(\alpha-\theta)-J_b\cos(\alpha-\theta)]+e_2(H_a\sin\theta-J_a\cos\theta) \quad (3.6.3)$$

$$m_2(\dot{x}_{2p}-\dot{x}_2)=H_a-H_b\cos\alpha+J_b\sin\alpha \quad (3.6.4)$$

$$m_2(\dot{y}_{2p}-\dot{y}_2)=H_a-H_b\sin\alpha-J_b\cos\alpha \quad (3.6.5)$$

Quantities with no suffix are those immediatly before impact. The linear velocity components of the mass centre of the coupler $\dot{x}_{2p},\dot{y}_{2p}$ immediately after the impact are given by :

$$\dot{x}_{2p}=-a\dot{\phi}_p\sin\phi-e_2\dot{\theta}_p\sin\theta \quad (3.6.6)$$

$$\dot{y}_{2p}=a\dot{\phi}_p\cos\phi+e_2\dot{\theta}p\cos\theta \quad (3.6.7)$$

The momentum exchange equation of the follower can be written as follows:

$$I_{3B0}(\dot{\psi}_p-\dot{\psi})=Fc\sin(\alpha-\psi+\pi)+f[c\cos(\alpha-\psi+\pi)] \quad (3.6.8)$$

From the definition of the coefficient of restitution ,e, one can write

$$\dot{\psi}_pc\sin(\alpha-\psi+\pi)-\dot{\phi}_pa\sin(\alpha-\phi)-\dot{\theta}_pb\sin(\alpha-\theta)=e[-\dot{\psi}c\sin(\alpha-\psi+\pi)+\dot{\phi}a\sin(\alpha-\phi)+\dot{\theta}b\sin(\alpha-\theta)] \quad (3.6.9)$$

Therefore there are nine equations containing nine unknowns $\dot{\phi}_p$,$\dot{\theta}_p$,$\dot{\psi}_p$,$\dot{x}_p$,$\dot{y}_p$,H_a,J_a,H_b and J_b .

Considering damping during the impact, it is assumed that there is a grease film on the bearing surface . Before impact the pin is moving through the grease. The reduction of the speed in the grease depends on the grease film thickness. The thickness is assumed constant.

From Cameron(43) F is proportional to v (relative radial velocity of pin in the bush). The speed reduction through grease film is proportional to the grease film thickness and therefore is independent of arrival velocity.

According to the above assumption the speed just before impact is reduced by some constant.

3.7 Computing

As is illustrated in the flowchart fig (3.7.1) first of all the kinematic characteristics of the linkage are calculated for zero clearance in d.c.p (dead centre point ϕ=30°). Then from the equations of motion joint forces and input angular acceleration $\ddot{\phi}$ are calculated. These parameters are used to get the angular accelerations; γ is calculated and can be used as an initial value for the integration routine, which is a NAG routine for integrating a stiff system of first order differential equations over a range with suitable initial conditions , using a variable order variable step Gear method. Initial value of α, clearance angle is taken to be γ, contact angle in zero clearance case.

The 5 equations of motion and two differentiated constrained equations , the two kinematic equations and one Lagrange equation for the clearance link together constitute a set of 10 simultaneous linear equations from which the forces , angular and linear accelerations are calculated.

A NAG routine called fo4aef solves this set of linear simultaneous equations. The routine calculates the solution with multiple right hand side by Crout's factorisation method which was described in section (2.8).

Using these accelerations and integrating them the angular velocities are calculated. Integrating these angular velocities one may get ang. displacement. After starting the first step , clearance angle α also is obtained in this way. Clearance angle for the first step is calculated using the joint forces which are calculated from the linear equation in the routine for zero clearance.

For numerical solution using most of the routines a system of ordinary differential equation must be written in first order form.

In this case there is a set of 2nd-order differential equations. They can be reduced to first order form by introducing new variables.

$$zz=\left[x,\dot{x},y,\dot{y},\phi,\dot{\phi},\theta,\dot{\theta},\psi,\dot{\psi},\gamma,\dot{\gamma}\right]^T$$

As described at the start of this section the acceleration may be calculated from a set

of linear simultaneous equation by Crout's factorisation method. One may set

$\ddot{x}=z(5)$

$\ddot{y}=z(6)$

$\ddot{\phi}=z(7)$

$\ddot{\theta}=z(8)$

$\ddot{\psi}=z(9)$

$\ddot{\gamma}=z(10)$

Defining the above auxilary variables one may get a set of first order differential equation.

F(1)=zz(2) $=\dot{x}$

F(2) =z(5) $=\ddot{x}$

F(3)=zz(4) $=\dot{y}$

F(4) =z(6) $=\ddot{y}$

F(5) =zz(6) $=\dot{\phi}$

F(6) =z(7) $=\ddot{\phi}$

F(7) =zz(8) $=\dot{\theta}$

F(8) =z(8) $=\ddot{\theta}$

F(9) =zz(10)= $\dot{\psi}$

F(10)= z(9)= $\ddot{\psi}$

F(11)=zz(12)= $\dot{\gamma}$

F(12)=z(10) $=\ddot{\gamma}$

The above set can be solved by a NAG routine (do2eaf) using Gear method for integration.

do2eaf integrates a stiff system of first-order ordinary differential equations over a range with suitable initial conditions, using a variable order, variable-step method implementing the backward differentiation formulae.

At each step the contact loss criterion $\frac{\ddot{\alpha}}{R_b}>6000(rad/s)/N$ will be checked; the following mode is selected if $\frac{\ddot{\alpha}}{R_b}$ is smaller than the criterion value. Otherwise the

The above set can be solved by a NAG routine (do2eaf) using Gear method for integration.

do2eaf integrates a stiff system of first-order ordinary differential equations over a range with suitable initial conditions, using a variable order, variable-step method implementing the backward differentiation formulae.

At each step the contact loss criterion $\frac{\ddot{\alpha}}{R_b}>6000(rad/s)/N$ will be checked; the following mode is selected if $\frac{\ddot{\alpha}}{R_b}$ is smaller than the criterion value. Otherwise the free flight mode is selected. In the free flight mode also the same method is used to solve the appropriate differential equations.

At the end of free flight mode there is the impact mode. As was discussed in the previous section(3.6) there are a set of nine linear simultaneous equations for the impact case. There are several ways to solve this set of equations as follows:

1 NAG routine fo4aef can be used for all 9 equations.

2. It can be solved for 4 impulse and 3 angular velocities (see sec.(3.6)); then the set will be 7 equations and then the NAG routine is used. The linear velocities can be calculated independently afterwards.

3. Reducing the above equations to two equations and then using Cramer's rule to solve those equations. This can be achieved by substituting impulses and the follower angular velocity in equations (3.6.2, 3.6.3). Then θ_p and ϕ_p are calculated from these two equations. The other variables can be calculated afterward. This calculation is lengthy but avoids inversion of matrices and hence is quicker.

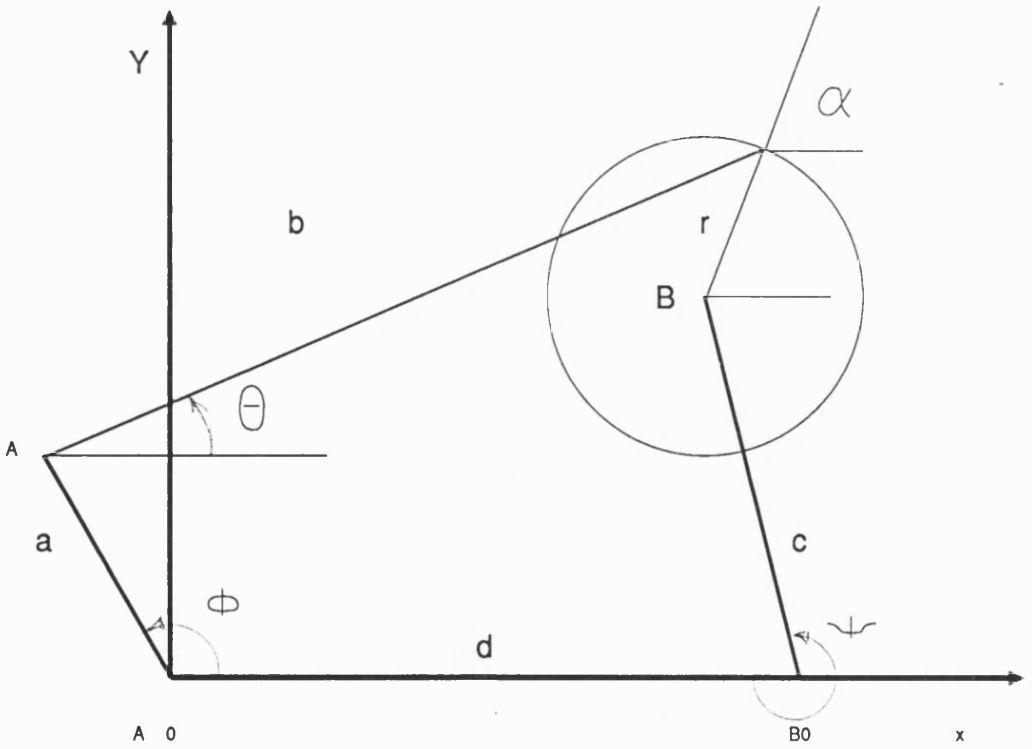

Fig 3.2.1 diagram of four bar chain with clearance

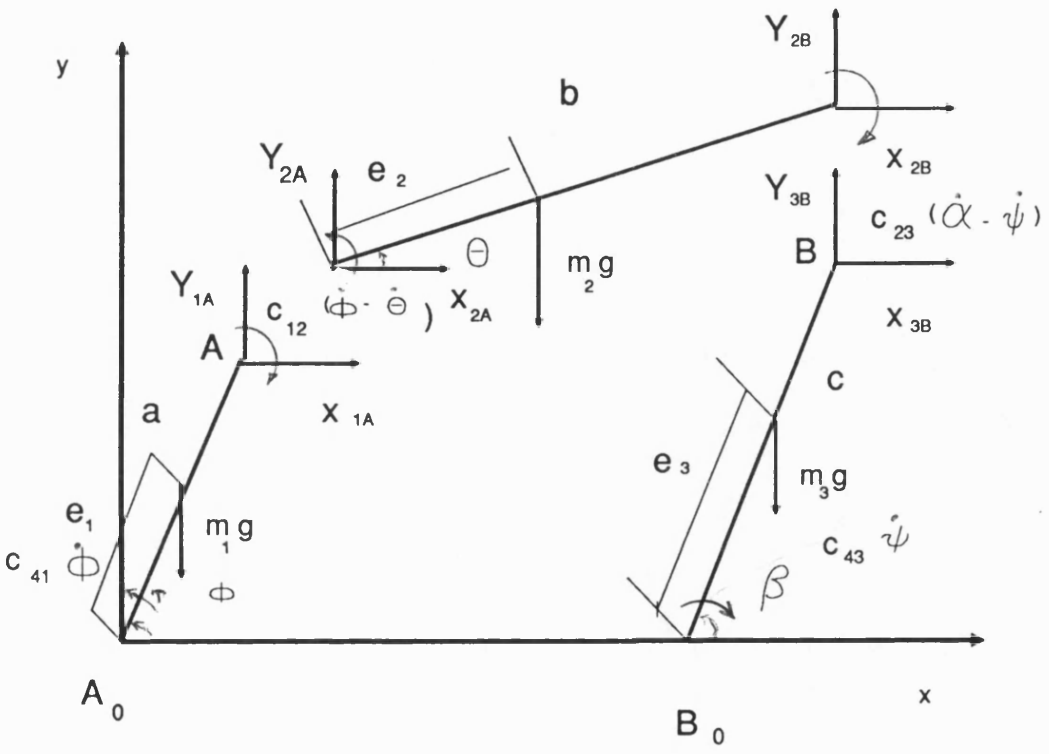

Fig 3.2.2 Free body diagram of four bar chain
In following mode

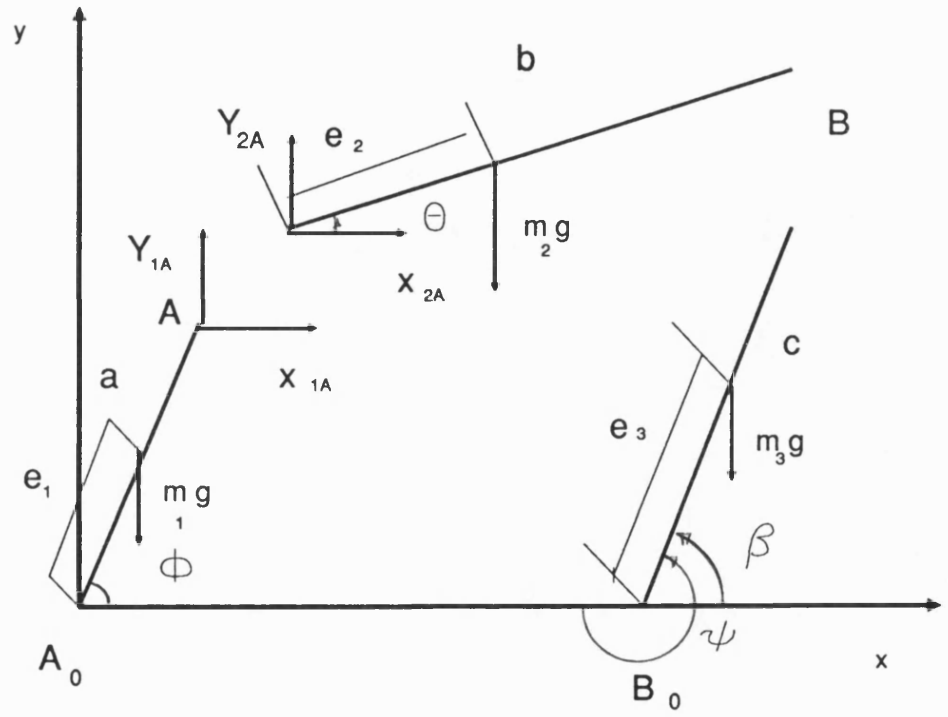

Fig 3.5.1 Free body diagram of four bar chain
In free flight mode

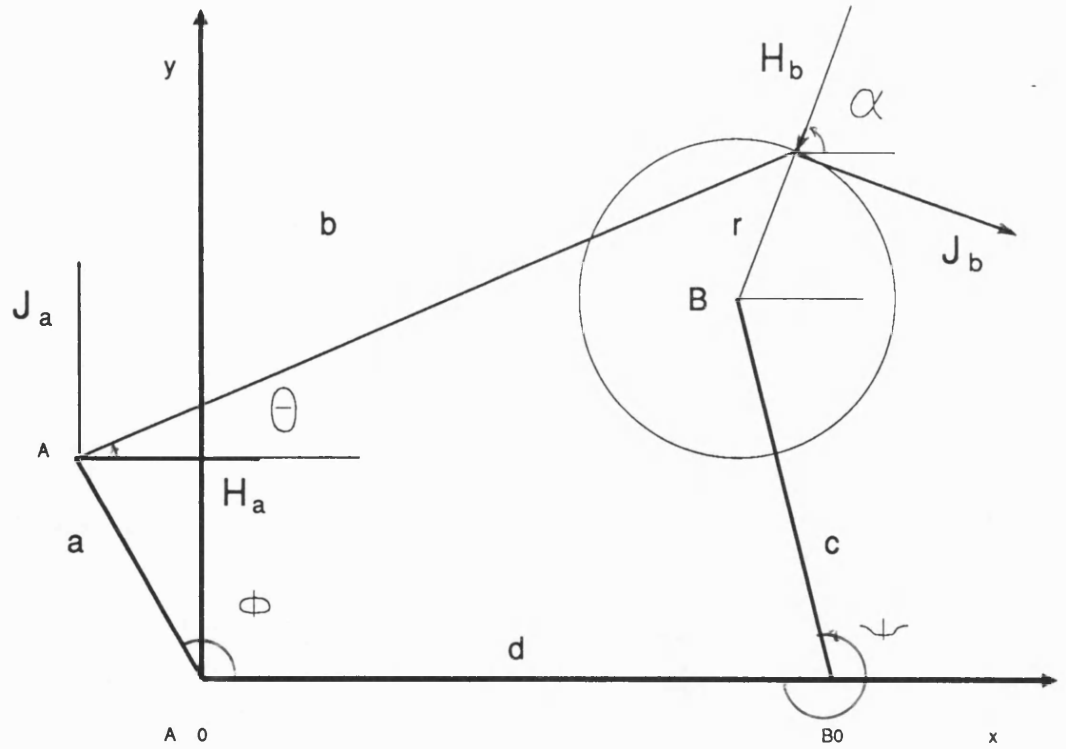

Fig 3.6.1 diagram of four bar chain with clearance
In impact mode

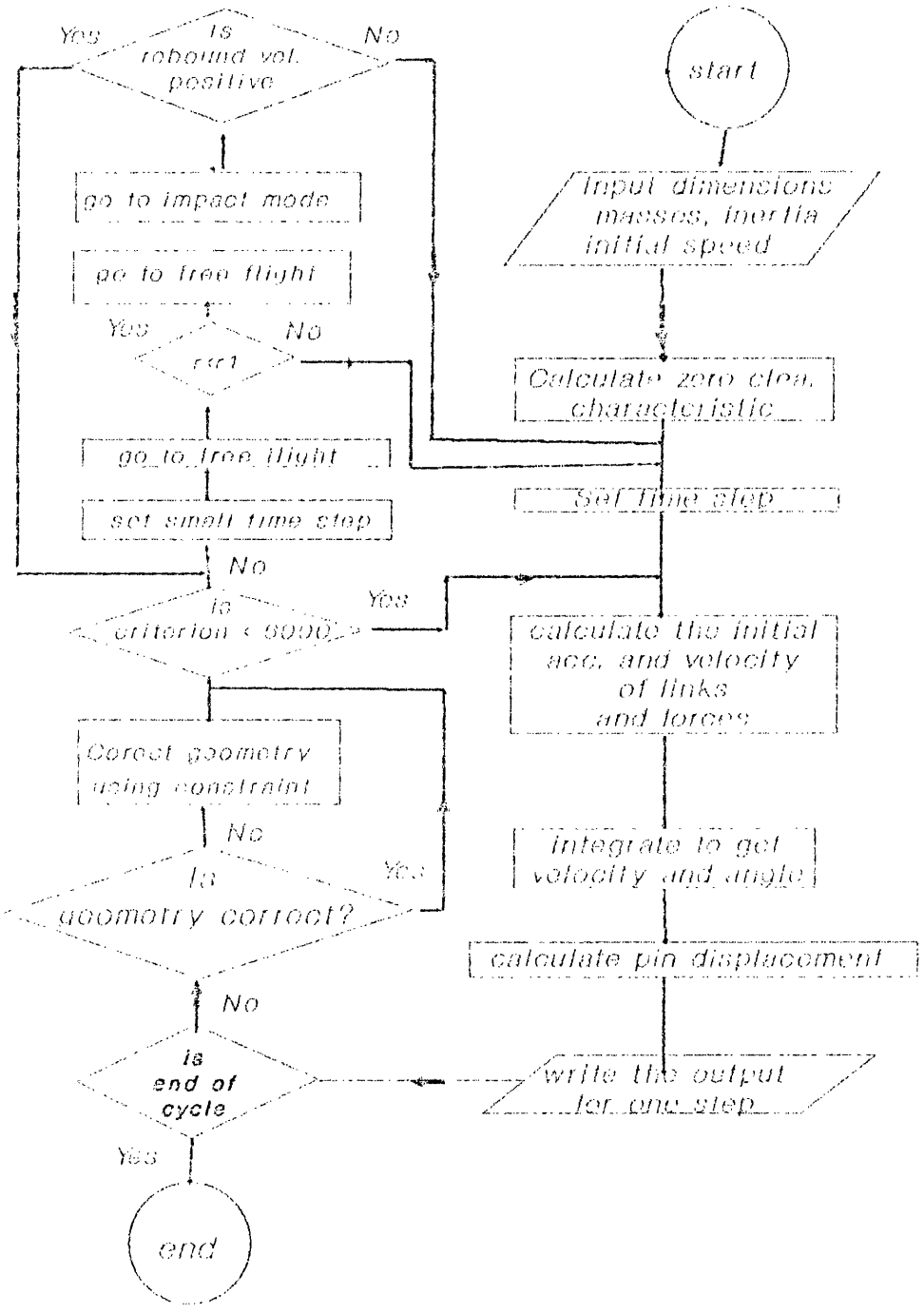

Fig 3.7.1 Flow chart of model with clearance

CHAPTER 4

EXPERIMENTAL APPARATUS

4.1 Design of rig

The rig layout is shown in fig (4.1.1). Detailed discussion of the instrumentation is given in the next sections(see sec.4.1 to 4.12). A four bar chain is used. The data of the chain is tabulated in table (4.1.1).

1. A dc controller enables mean speed to be varied in the range of (100, 1000 rev/min).

2. To the motor and crank inertia can be added a fly wheel. When used a flywheel of inertia 0.23 $kg\text{-}m^2$.

3. Input angular displacement and speed can be measured by an optical encoder connected to the crank. The signal is taken to an spectrum analyser, storage scope or data acquisition system.

4.The follower and coupler acceleration can be measured by use of accelerometer.

5.The pin between the coupler and the follower can be easily removed and some other pin with a different clearance substituted.

6.A circuit is provided for monitoring contact loss in the case of clearance in the joint between the coupler and the follower.

7. A DC motor of 1.25 hp(kw) at 1000 rev/min is used driving the input shaft via pulley and vee belt.

8. The displacement of the coupler follower pin relative to the bearing is measured by two eddy current displacement transducers which are mounted in the follower in longitudinal and lateral directions of the follower(see fig 4.6). They are fitted on the longitudinal and lateral centre lines passing through the centre of pin and bush.

9. The output of the above transducers are fed to a low pass variable frequency "Kemo" filter VBF/14 type to remove noise. It was set at 100 Hz frequency and 6db octave.

4.1.1 Sizing fly wheel

In a four bar chain the fly wheel inertia can be calculated from the work and energy equation as follows:

$$U=\Delta K.E.+\Delta V_g+\Delta V_e \qquad (4.1.1)$$

Where

U = the total work done on the system by external forces

$\Delta K.E.$ = the corresponding change in the kinetic energy of the system

ΔV_g = the change in its potential energy of position in the gravitational field

ΔV_e = the change in the stored elastic energy in the connections.

Assuming all the links in the system are rigid , the term ΔV_e disappears in the above equation. Potential energy and the kinetic energy calculated as follows:

$$\Delta V_g=Mg\,(h_2-h_1) \qquad (4.1.2)$$

where M is the mass of all the elements of the system and h is the height of the system centre of mass from a datum.

$$\Delta K.E.=(\frac{1}{2})\times(I_{e(2)}\dot{\phi}^2{}_2-I_{e(1)}\dot{\phi}_1^2) \qquad (4.1.3)$$

where I_e is the equivalent inertia system that is dynamically equivalent to the actual

system in the sense that the response of the hypothetical equivalent single inertia system to an input torque would be identical to the actual 4-bar linkage. At any instant, assuming the angular velocity of the mass I_e to be ϕ, one may equate the kinetic energies of the equivalent systems

$$(\frac{1}{2})I_e\dot{\phi}^2=(\frac{1}{2})(I_{1A_0}\dot{\phi}^2+I_{2c.g.}\dot{\theta}^2+I_{3B_0}\dot{\psi}^2+m_2(\dot{x}_2^2+\dot{y}_2^2)) \quad (4.1.4)$$

After substituting and summarizing

$$I_e=I_{1A_0}+G_c^2I_{2c.g.}+G_f^2I_{3B_0}+m_2(a^2+e_2^2G_c^2+2ae_2G_c\cos(\phi-\theta)) \quad (4.1.5)$$

Assuming friction in bearings and load torque are just compensated by the motor torque the work done on the system is zero. The work and energy equation will be in the following form.

$$\Delta K.E.+\Delta V_g=0 \quad (4.1.6)$$

$$(\frac{1}{2})\times(I_{e(2)}\dot{\phi}_2^2-I_{e(1)}\dot{\phi}_2^2)=Mg(h_1-h_2) \quad (4.1.7)$$

Looking at the above equation (4.1.7) one may find that there are two factors which causes input speed to fluctuate.

1) variation of effective inertia
2) variation of potential energy

For calculating fly wheel inertia, both must be studied but it is helpful to consider each factor separately.

a Weight effect (neglecting fluctuating Inertia)

In equation (4.1.4) the first term I_{1A0} is the fly wheel inertia and is the main part of the effective inertia. Since the other terms are relatively small - see sec.(6.2) the effective inertia is approximated by the fly wheel inertia and it is represented as I in the following equations.

then

$$\frac{1}{2}I(\omega_2^2-\omega_1^2)=Mg(h_1-h_2) \quad (4.1.8)$$

It is convenient to define a coefficient of speed fluctuation as

$C_s=\frac{\omega_2-\omega_1}{\omega_m}$ where ω_m is the mean angular velocity given by $\omega_m=\frac{\omega_2+\omega_1}{2}$

Then the above equation will be in the form

$$\frac{1}{2}I(2\omega_m)(C_s\omega_m)=Mg(h_1-h_2)$$

Then I can be calculated to be

$$I=\frac{2Mg(h_1-h_2)}{C_s\omega_m{}^2} \qquad (4.1.9)$$

b Assuming weight is neglected

The work and energy equation will be in the following form

$$\frac{1}{2}(I_{e(2)}\omega_2{}^2-I_{e(1)}\omega_1{}^2)=0 \qquad (4.1.10)$$

for any two speeds. In particular if ω_1,ω_2 are min and max speeds.

$I_{e(2)}=I+I_{\min}$

$I_{e(1)}=I+I_{\max}$

$I_{\min},I_{\max}$ are minimum and maximum inertia of the system without fly wheel respectively.

By substituting the effective inertia and summarizing equation (4.1.10), I (fly wheel inertia) can be calculated from

$$(\frac{\omega_2}{\omega_1})^2=\frac{I+I_{\max}}{I+I_{\min}}; \qquad (4.1.11)$$

$$\frac{\omega_2}{\omega_1}=\frac{2+C_s}{2-C_s}$$

The larger of the two flywheel inertia can be chosen. The first one eq.(4.1.9) is speed dependent in principle but the second eq.(4.1.11) dominates.

A better way of fly wheel calculation is to develop a simulation program for the system. Plot of the speed fluctuation versus input inertia can be used for selecting

the required fly wheel size. This procedure was used in this work. A computing model was developed to simulate a zero clearance four bar chain. Then the variation of the speed fluctuation versus input inertia was plotted (see fig 4.1.2). The fly wheel inertia of 0.23 kg-m^2 was chosen to reduce the speed fluctuation from 0.095 to 0.014.

4.2 Electric motor

For a DC motor an increase in load torque will normally tend to cause a reduction in speed; this will reduce the motor back emf and the armature current will increase. Since motor torque is approximately proportional to armature current this effect helps to reduce the drop in speed. However by applying additional feedback proportional to armature current further improvement in speed stability can be achieved.

4.3 Speed controller

In this system speed control is provided by means of a phase control thyristor circuit incorporating armature current feedback. Fig(4.3.2) shows a simplified diagram of the controller. The field winding is supplied with a constant DC voltage derived from the 240 volts AC mains by means of a full wave silicon rectifier bridge. The armature is also supplied by a full wave bridge but in this case two of the rectifiers are silicon controlled rectifiers (thyristor). At the start of each half cycle the thyristors are OFF and no armature current is supplied, after a certain delay the thyristors are turned on and the remainder of the half cycle is completed (fig 4.3.1) In this way the mean voltage supplied to the armature, and hence the speed, can be controlled by the length of the delay period.

At the start of each half cycle V_1 rises until it reaches 12 volts limited by zener diode z_1 (see fig 4.3.2 and 4.3.3) . The speed demand potentiometer P_1 then sets an input voltage to the amplifier A_1. The amplifier output is used to charge C_1

exponentially via R_1 until the voltage V_c reaches the threshold of the unijunction U_{J1} with a delay of d_1. At this point C_1 is discharged into the primary of the transformer T_1 . T_1 Then supplies the resulting pulse to the thyristor gates. This turns on the thyristors and they remain conducting until the end of the half cycle. The sequence above repeats itself.

Although it used to provide a range of mean speed only, the speed controller attempts to control speed fluctuation within the cycle caused by variation in effective inertia, gravitational potential energy or load.

The armature current is sensed by the voltage drop across resistor R_s , amplified by A_2 and applied as a feedback through the potentiometer P_2 . Careful adjustment of P_2 can provide significant compensation although it is not as effective as tachometer feedback.

One important problem in Silicon Controlled Rectifier "SCR" is so called transportation lag in the system , caused by the discrete firing angle conduction. In attempting to control fractional horsepowers motors over a wide range with SCR controls the result is often momentary instability, especially at low speeds(27). In such a situations the system is operating at very small firing angle (see fig 4.3.4) and if a sudden torque disturbance occurs, the resulting change in speed causes the error signal to switch on the output stage, sometimes an early firing angle, as shown in the diagram.

4.4 Speed measurement

The angular velocity of the crank-shaft is measured by means of an incremental optical encoder feeding into a frequency to voltage (F-V) convertor. The higher the encoder frequency the better the dynamic response of the system . The encoder selected provides 2000 pulses per revolution (higher number of counts were

available but only with extended delivery times and at higher cost.) However the number of pulses per revs is multiplied by 4 by means of a circuit which fires monostables off the rising and falling edges of both phases of the encoder output. The flow chart of the above system is illustrated in Fig(4.4.1). The F-V converter choice was based upon the following assumptions:

1) Maximum speed of crank shaft = 500 rev/min

2) A 2 phase encoder would be used with 2000 lines/rev.

3) The full scale output of the F-V converter at 500 rev/min should be 5 Volts.

4-The basic encoder frequency would be multiplied by 4 .

Using the above assumptions the max input frequency of the converter F_{in} is calculated as follows:

$$F_{in}=(500\times2000\times4)/60 \qquad (4.4.1)$$

$$F_{in}=66.666kHz$$

Given the max input frequency,the required resistance R_g for the F-V converter (fig 4.4.2) can be calculated from equation (4.4.2)as follows:

$$V_{out}=F_{in}.C_{ref}.V_{ref}.R_g \qquad (4.4.2)$$

where:

V_{out}= the max required output voltage

F_{in}= the max input frequency in Hz

C_{ref}= the internal reference capacitor for the particular F-V , in farads.

V_{ref}= the F-V refrence voltage (5.6 volts.)

The model of the converter chosen is the Ancom 15FV-3

C_{ref} which is taken from the manufacturers tables, is 220 pf. Then the following

relationship can be written:

$R_g=V_{out}/(F_{in}.C_{ref}.V_{ref})$

$R_g=5/(66666\times220\times10^{(-12)}\times5.6)$ (4.4.3)

Therefore R_g=60876.593 ohm

- The integrating capacitor , C_{rip} , that is in parallel with Rg , determines both the compromise between the ripple amplitude and the overall response speed. The output is given by the relationship:

output ripple,volts peak to peak $=V_{ref}.\frac{C_{ref}}{C_{rip}}$ (4.4.4)

Designing for an output ripple peak to peak of 0.01 V_{out} we will have peak to peak of output ripple = 5×0.01=0.05 volt

Therefore

$C_{ripple}=5.6\times220\times\frac{10^{(-12)}}{0.05}=24640pf=0.025$ micro farad

The 3dB response frequency of F-V is then given by the relationship:

$F_{response}=\frac{1}{(2\pi R_g C_{rip})}=\frac{1}{(2\pi\times60876.593\times0.024\times10^{(-6)})}$

$F_{resp}=108.9Hz$

The calculated value of C_{rip} seems to give a reasonable compromise between ripple and response.The converter and its associated components(fig 4.4.2) are mounted on a Eurocard circuit board. Two variable resistors are provided ,one to trim the zero level and the other to trim the scale factor.

multiplier

A multiplier is a device used to multiply the input signal frequency by some

number. In this case it multiplies the encoder signal frequency by four. It is composed of two 74HC123 chips , one 74HC and one 74HC14 (fig 4.4.3).

The interconnections between the circuit board and the encoder are shown in Fig(4.4.4).

An index pulse can be used for starting the measurement point. Triggering of a measurement can be initiated by an input signal(index signal) on channel A of the spectrum analyser ,using slope and level controls.

Level control : Determines the signal level at which the collection of data should begin. In the detended Free Run position triggering is initiated by the completion of the previous measurement . While the level can be varied over the entire A/D converter range.

Slope : sets the slope of the signal , positive or negative at which triggering occurs.

4.5 Accelerometer

Piezoelectric accelerometers operate on the principle that a mass moves and stresses a piezoelectric disc. This produces an electrical output signal proportional to compression. Since this stress is itself directly related to acceleration, such a signal is proportional to the vibratory acceleration of the surface on which it is mounted.

The accelerometers on the rig were Bruel and Kjaer type No 4366 and 4343. They were calibrated by the manufacturer at $3.99 mV/ms^{-2}$ and $8.78 mV/g$ respectively. The first one was fixed at the end of the follower by means of a screw . The second one was fixed at the gravity centre of the coupler. The signals are amplified in preamplifier by 10. An H.P. spectrum analyzer was used for the accelerometers as an output device which was connected to a plotter.

4.6 Displacement transducers (probes)

Two probes are used to monitor the relative displacement of the pin in the bush (see fig(4.6.1)). These are non-contacting transducer systems which can be used to measure the static and dynamic distance between a probe and an observed target.

The principle of operation is ''Eddy current '' , wherein a low energy RF signal is generated at the probe , which induces an eddy current in the metallic target . Changes in the distance between probe and target change the sensor impedance , and a DC voltage output is given which is linearly proportional to the gap over a defined distance .

The probes A&B are mounted on the bush which is on the follower . Their directions are perpendicular to each other.

Probe A is in the longitudinal direction and probe B in lateral relative to the follower (fig 4.6.3).

In order to get better results more space was provided around the probe tip by removal of the needle bearings(fig 4.6.3). They were replaced by two small brass bushes as plain bearings . Therefore there was enough room between the bushes around the probe tip. In addition a hole was made about 14 mm dia. coaxial with the probe tip effect the probes.

4.7 Monitoring circuit for contact loss

In a " four bar linkage " the links are connected together with pins and bearing (pin and socket). In the absence of the clearance there is a continuous contact between pin and bearing during rotation of the crank. Inevitably there is some clearance in the joints, which may produce contact loss. It is difficult to observe or photograph the contact loss because of smallness of the clearance, but it can be detected by passing an electrical current through a circuit including pin and bearing(Fig 4.7.1)

When the pairing elements (joint between the coupler and the follower) are in contact , two ends of the source are connected together through a short circuit because there is no resistance across the bearing and pin. When both ends of the pin are separated from the bearing the short circuit is broken. The storage oscilloscope displays the voltage jump in the circuit. The record of this voltage can be used for detecting contact loss in the cycle . The fixed joint of the follower must be electrically isolated to prevent passage of the electricity through the frame. Both ends of the pin which runs in the bearing are isolated from the effect coupler by two P.V.C. bushes.

4.8 Data Acquisition system

A data acquisition system is normally used to monitor the variation of physical parameters such as displacement , velocity , acceleration , pressure and temperature with respect to time. The parameters are first converted into analogue voltages by means of transducers such as accelerometers, encoder probes and monitoring circuit. These voltages are sampled at known time intervals and converted into digital form. The time can be defined by a clock signal like encoder output. The clock signal may be a parameter other than time , displacement for example. The digital values are then stored in a computer or on a floppy disc where they can be processed. The information is finally presented in a suitable format such as printed data , graphs or display.

A multiplexer is used to sample the channels in sequence . A circuit known as a Sample and Hold is generally used between the multiplexer and A-D converter to prevent errors developing.

It is often necessary to filter the signals before carrying out the conversion. The filters,one per channel have to be fitted before the multiplexer(see sec. 4.9).

Most transducers provide voltages in the mV range whereas A-D converters operate

with full scale ranges of several volts. An amplifier is therefore generally required. In some systems a single amplifier is fitted between the multiplexer and sample and hold circuit ; in others a separate amplifier is used. A block diagram is shown in Fig (4.8.1)

4.9 Filters

The use of filters in digital instrumentation and data acquisition is important, since noise from external sources and transfer lines, quantisation will inevitably degrade the signal quality . The filter is used also to prevent alias frequency effect . In some applications where critical relative timing of several transients may be required , the step response of the filter should also be considered (fig 4.9.1). There are different type of filters including active and passive. In the rig an active VBF Kemo filter is used to filter the displacement signals

4.10 Amplifiers

Most transducers supply a low level voltage. In order to reduce different form of errors an amplifier should be fitted between the transducer and output device. Small input current can flow into or out of amplifiers and it is possible for these to cause significant errors reading from high impedance particularly at low level .

4.11 Divider circuit

Direct output files of the data acquisition system are in binary form and can be stored on disc. However, the direct output plot lacks definition.

Using a conversion program these binary files can be converted to ASCII form . These ASCII files may be used by plotting packages to produce graphs with better definition.

These files are long and need considerable capacity . In addition the handling of

these files is time consuming and therefore difficult . To resolve the above problem the output of the encoder which is used as an external clock for the system should be divided by some number, to reduce the volume of data.

Therefore a count down divider circuit was made using a BCD counter chips E74ls90 . Its diagram is in fig (4.11.1).

The output of the encoder which is 2000 pulses/rev is used as input for the divider(see page 83). The divider will divide this by 5 . The output of the divider becomes 400 pulse/rev which still gives reasonable definition.

4.12 Profile measurement (Talyrond)

To get a clear profile of surface roughness and roundness of the pin and inside the bush a Talyrond 50 was used.

The principle of the operation of the 'Talyrond' is shown in fig 4.12.1 .

The workpiece to be measured is mounted, with its axis vertical , on the turntable. It remains stationary during the measurement.

The spindle is slowly rotated by a geared motor in the head so that the stylus can trace the variations in the radius of the part.

The pick-up is connected via the amplifier to an indicating meter , and also a recorder , a pen with radial marking on a circular chart. The chart is geared to run in synchronism with the spindle.

The output from the amplifier is then switched to the recorder and a graphical representation of the variations in the radius of the part is obtained.

4.13 PID control circuit components

In the case of system with flywheel the speed fluctuations can be limited with the choice of flywheel inertia. The higher the flywheel inertia the lower the speed fluctuation. But a three term controller can also be used to limit the input speed fluctuation.Before going further it is necessary to get familier with the controller characteristic.

The control circuit is designed to produce a stable, reasonable demand. It should also be accurate within specified limits which means that it must reduce the steady state error to a tolerable value. There are different controllers with different characteristic including proportional(P),integral(I),(P+I),(P+D)and (P+I+D).

1- Proportional control(P)

The simplest form of controller is one in which the output is directly proportional to the input. The proportional control systems have an inherent steady state error. This error is reduced as the proportional gain is increased. Motor torque T_m can be set at

$T_m=k_p\varepsilon_i$

where

$\varepsilon=\phi_d-\phi$ is the speed error.

2- Integral control(I)

$T_m=k_i\int\varepsilon_i dt$ The output is proportional to the integral of the input. With the integral control, the steady state error will be zero . Nevertheless , it tends to produce a less stable response than proportional controllers.

3- Proportional plus derivative control(P+D)

In this case the output is proportional to the input and its integral. It has a more immediate effect than P or I, since it anticipates disturbance and react accordingly. It must be used cautiously since it enhances the instability problem.

$$T_m=k_p\varepsilon_i+k_i\int\varepsilon_i dt$$

4- Three Term controllers (P+I+D)

These controllers includes all three terms and produce stable response with a small steady state error.

$$T_m=k_p\varepsilon_i+k_i\int\varepsilon_i dt+k_d\frac{d}{dt}\varepsilon_i$$

5- Using 3 Term controller to control the speed of a DC motor.

The motor is simplified as an impedance which is connected to a DC voltage as follows - see fig(4.13.1):

$$Z=R+L\frac{di}{dt}=R+sL$$

$$I=\frac{E_t-E}{Z}=\frac{E_t-E}{Z}$$

where

$s=\frac{di}{dt}$

E_t = tacho meter voltage

E = reference voltage

$\tau=\frac{L}{R}$ time constant of the system

$$I=\frac{E_t-E}{R(1-\tau s)}$$

By definition $\omega_a=\frac{R}{L}$

$$I=\frac{E_t-E}{R(1+s/\omega_a)}$$

$$I=(E_t-E)[\frac{1/R}{(1+s/\omega_a)}]$$

In SI system of units $\frac{T_m(N-m)}{I_a(Amp.)}=\frac{E(volts)}{\omega(rad/s)}=K_a$

$$T_m=\frac{EI}{\omega}=K_aI$$

The above equation shows that motor torque is proportional to the motor voltage E and armature current I . By changing E and I via tree term controller and tacho meter, T_m is adjusted to meet the required torque to keep speed constant.

Table 4.1.1

Data of the four bar chain which was used as rig					
link	length (mm)	link centre of mass distance e_i (mm)	mass of link kg	inertia from base joint $10^{-3}kg-m^2$	inertia from c.g $10^{-3}kg-m^2$
Crank (a)	63	31.5	0.721	230	
Coupler (b)	328	176	1.94		10.7
Follower (c)	201	100	1.194	8.94	
Base (d)	300				

Fig 4.1.1 Photograph of the rig which is connected to the data acquisition system

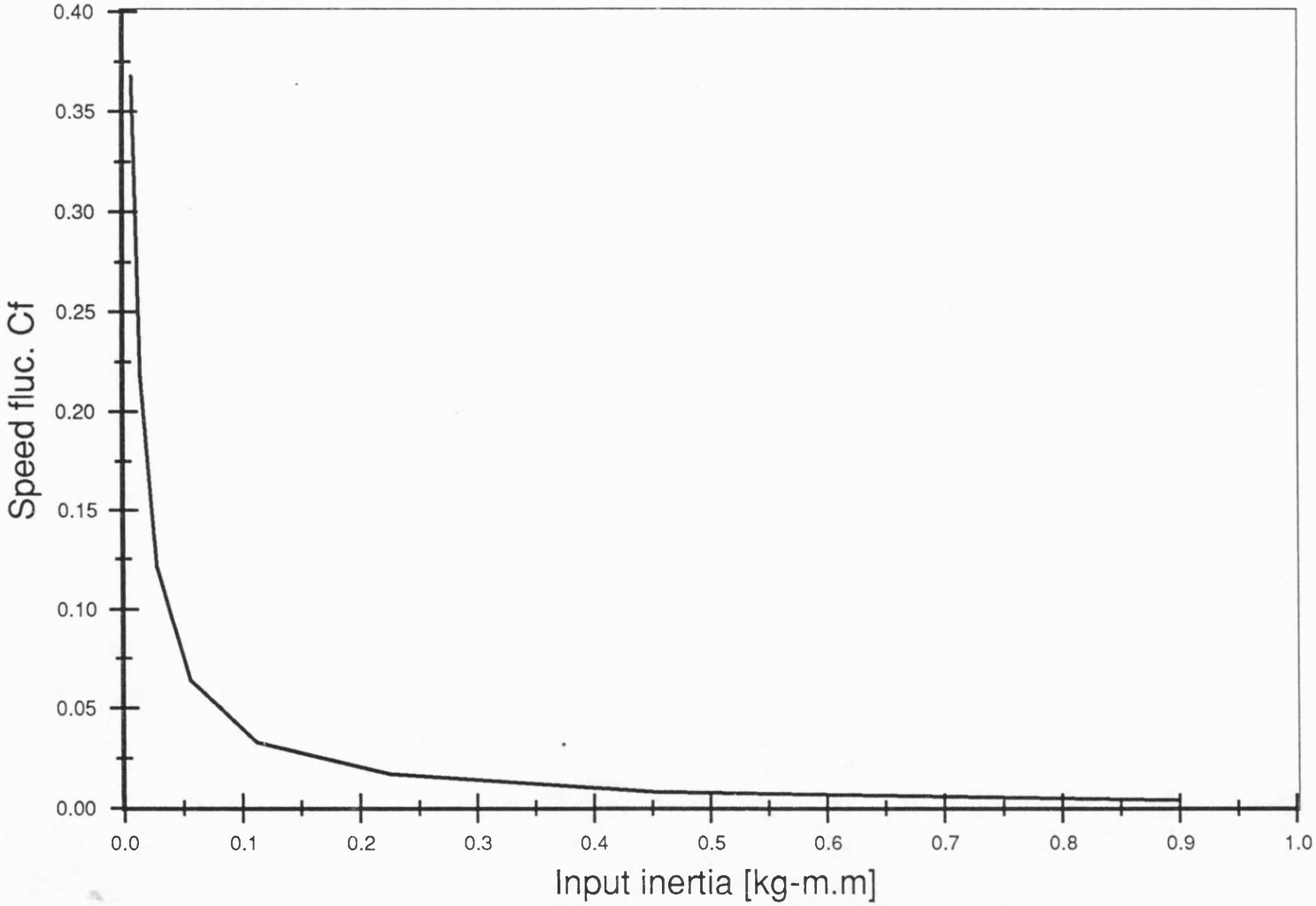

Fig(4.1.2)Speed fluctuation versus of crank input inertia
mean speed=263 rev/min

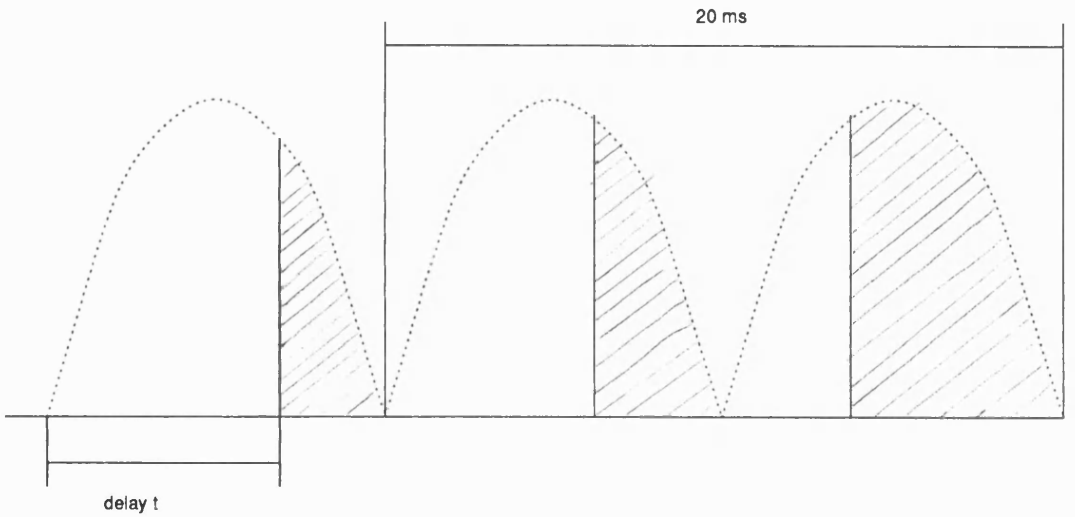

Fig (4.3.1) Voltage waveform in switching amplifiers
of "SCR" control system

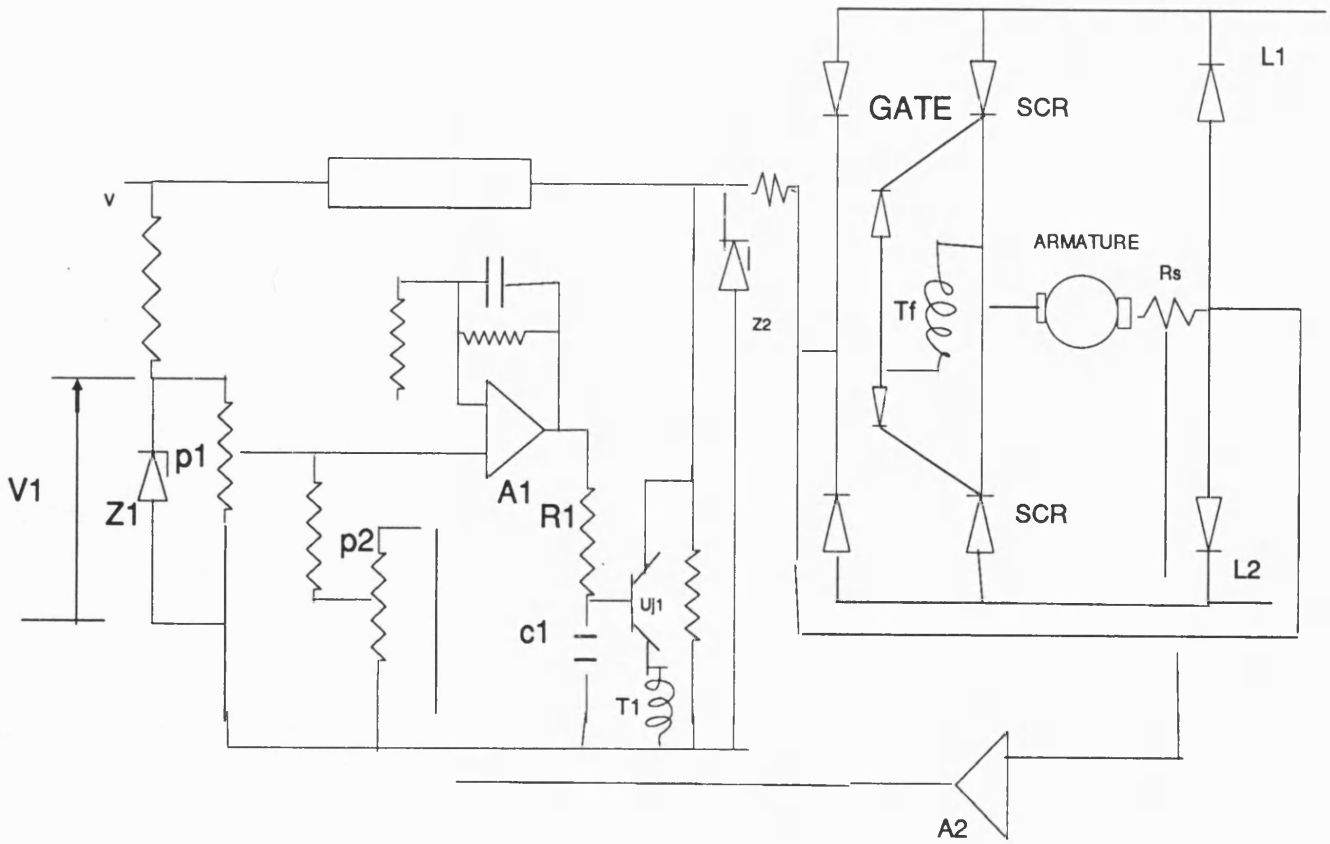

Fig 4.3.2 Simplified diagram of controller circuit

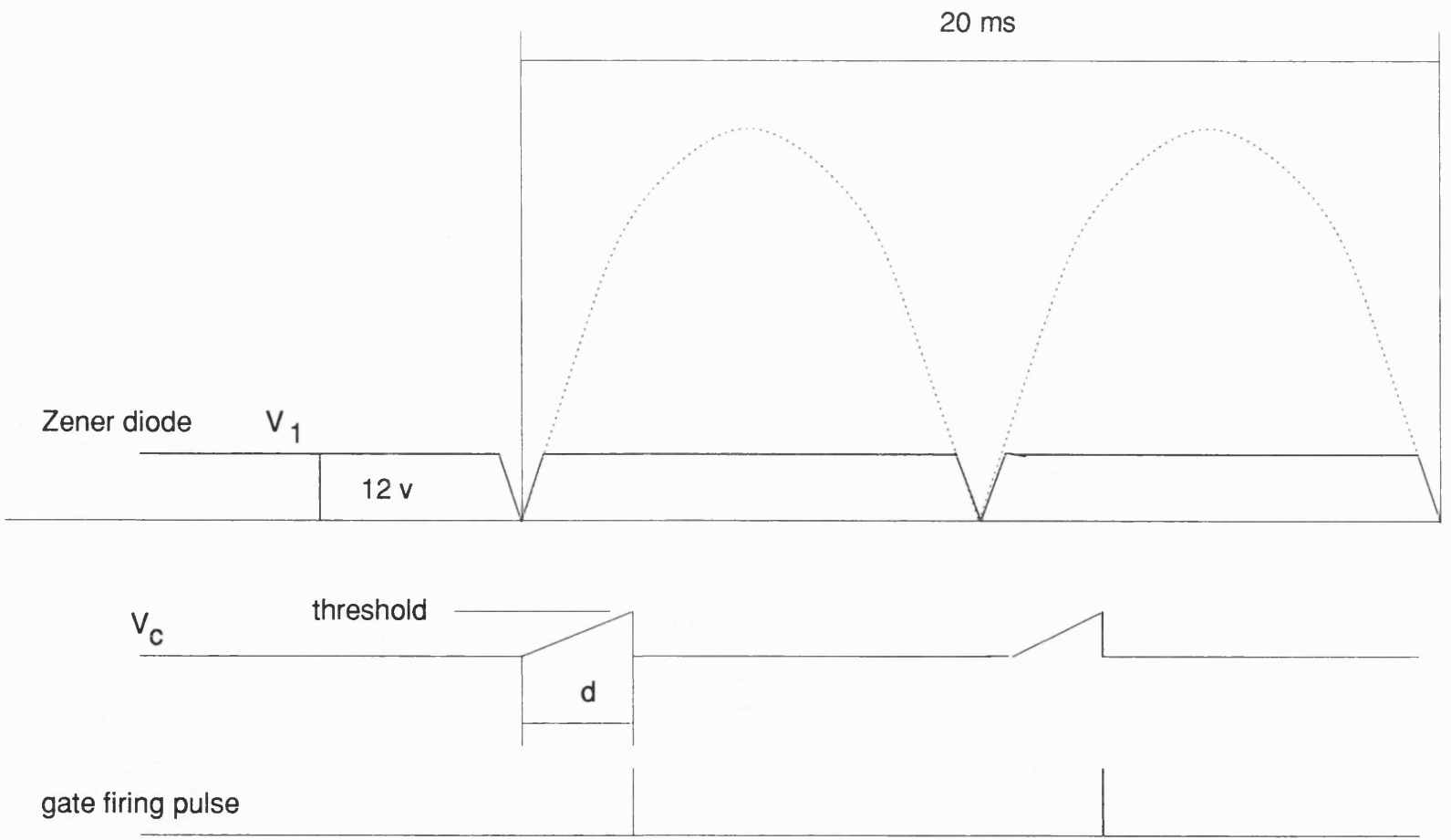

Fig (4.3.3) voltage of Zener diode and gate firing pulse

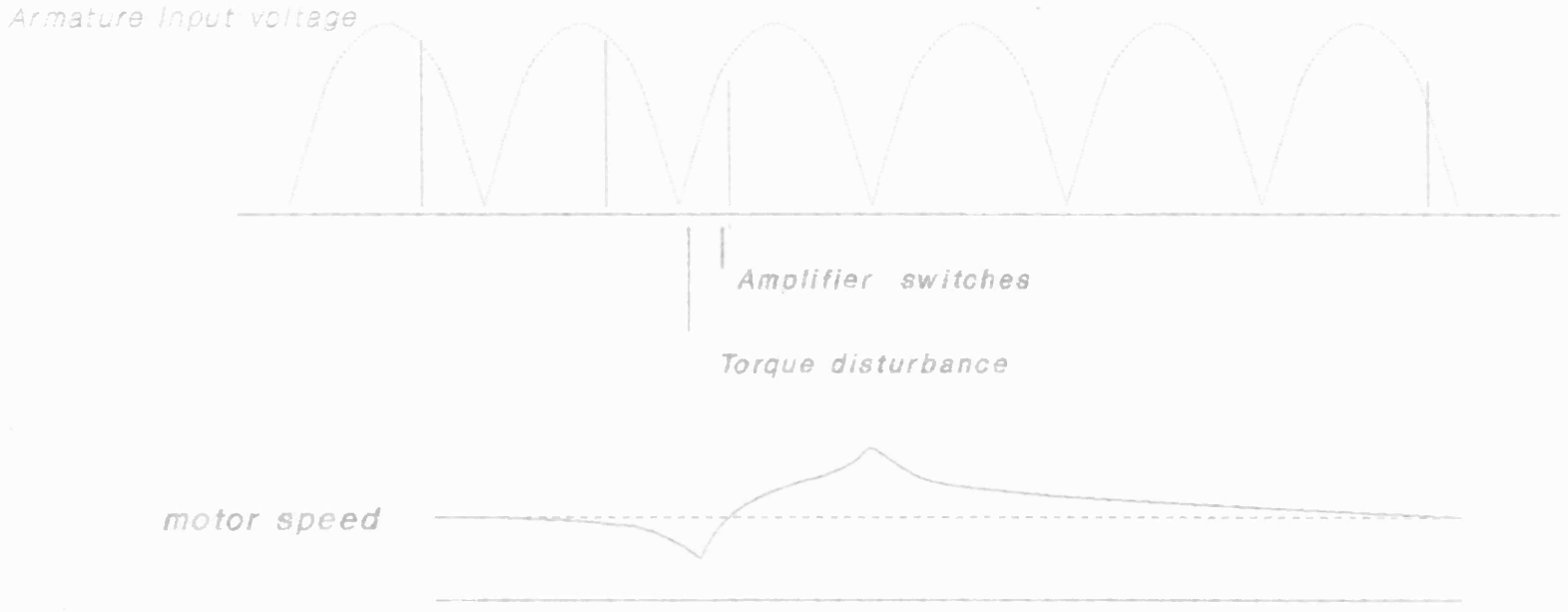

Fig(4.3.4) Result of a sudden torque disturbance in a 'SCR' speed control system

Fig (4.4.1) Block diagram of speed measurement system

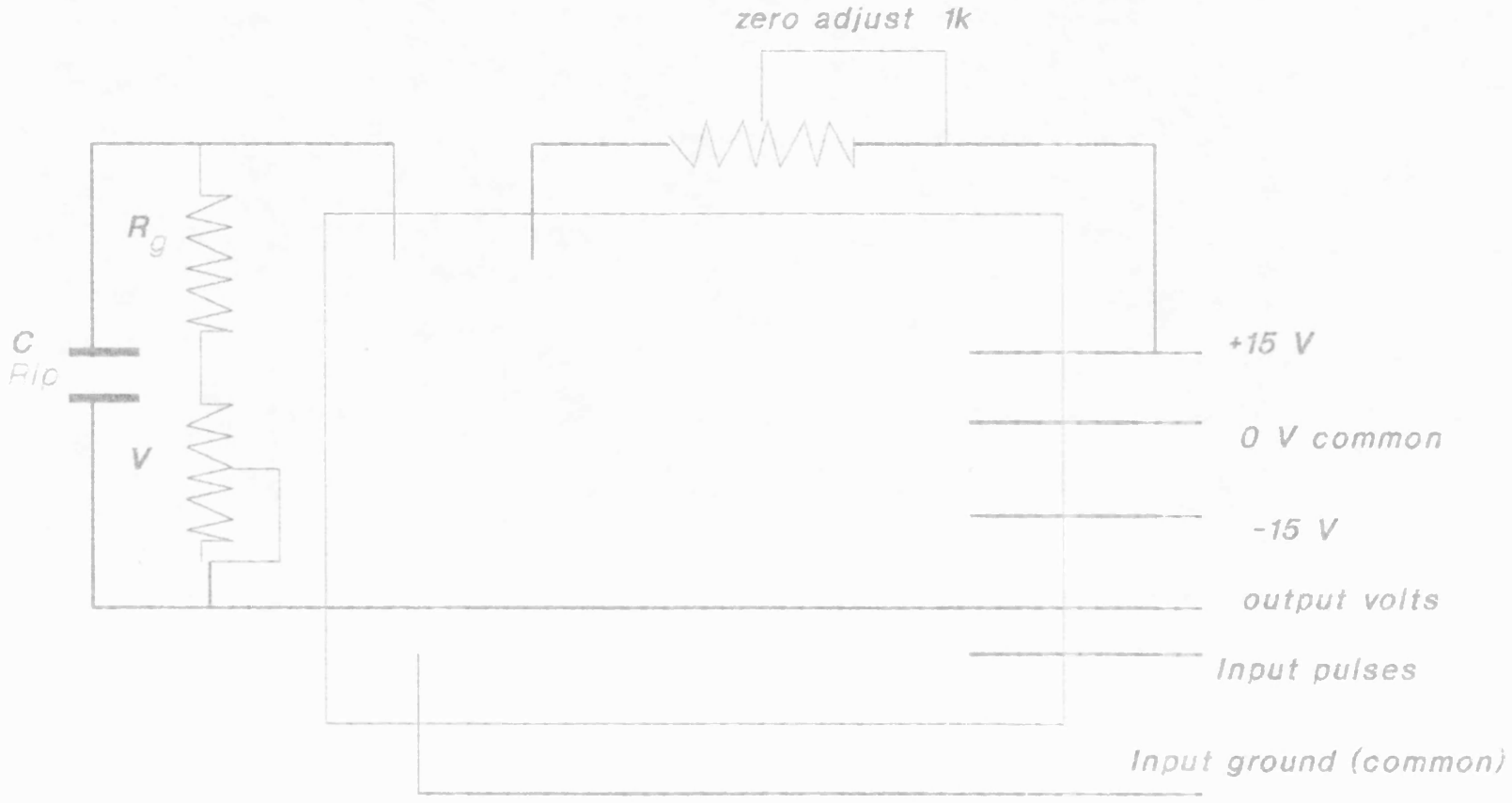

Fig (4.4.2) Diagram of Frequency to Voltage converter(F-v)

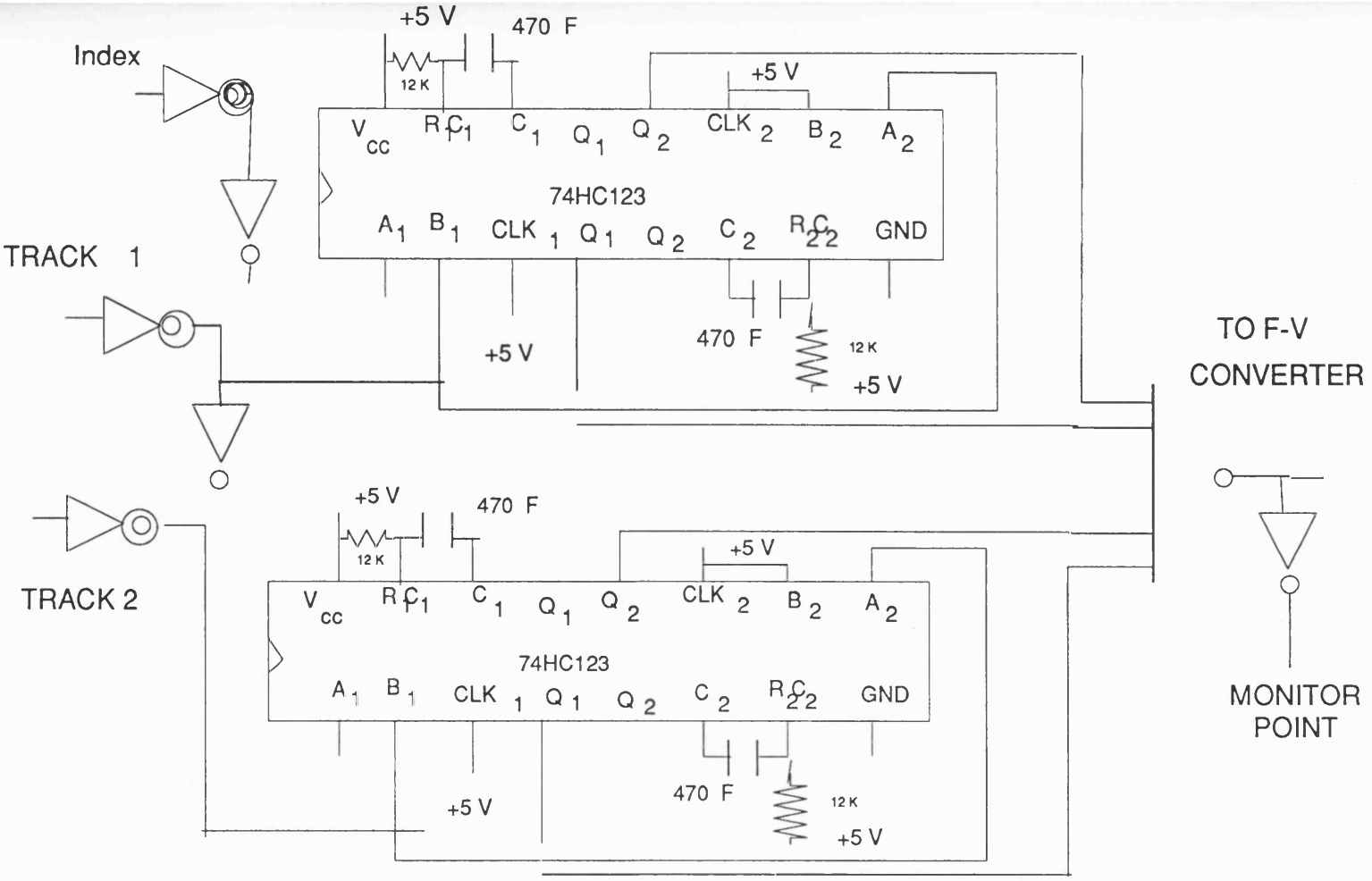

Fig 4.4.3 Cirrcuit diagram of multiplier

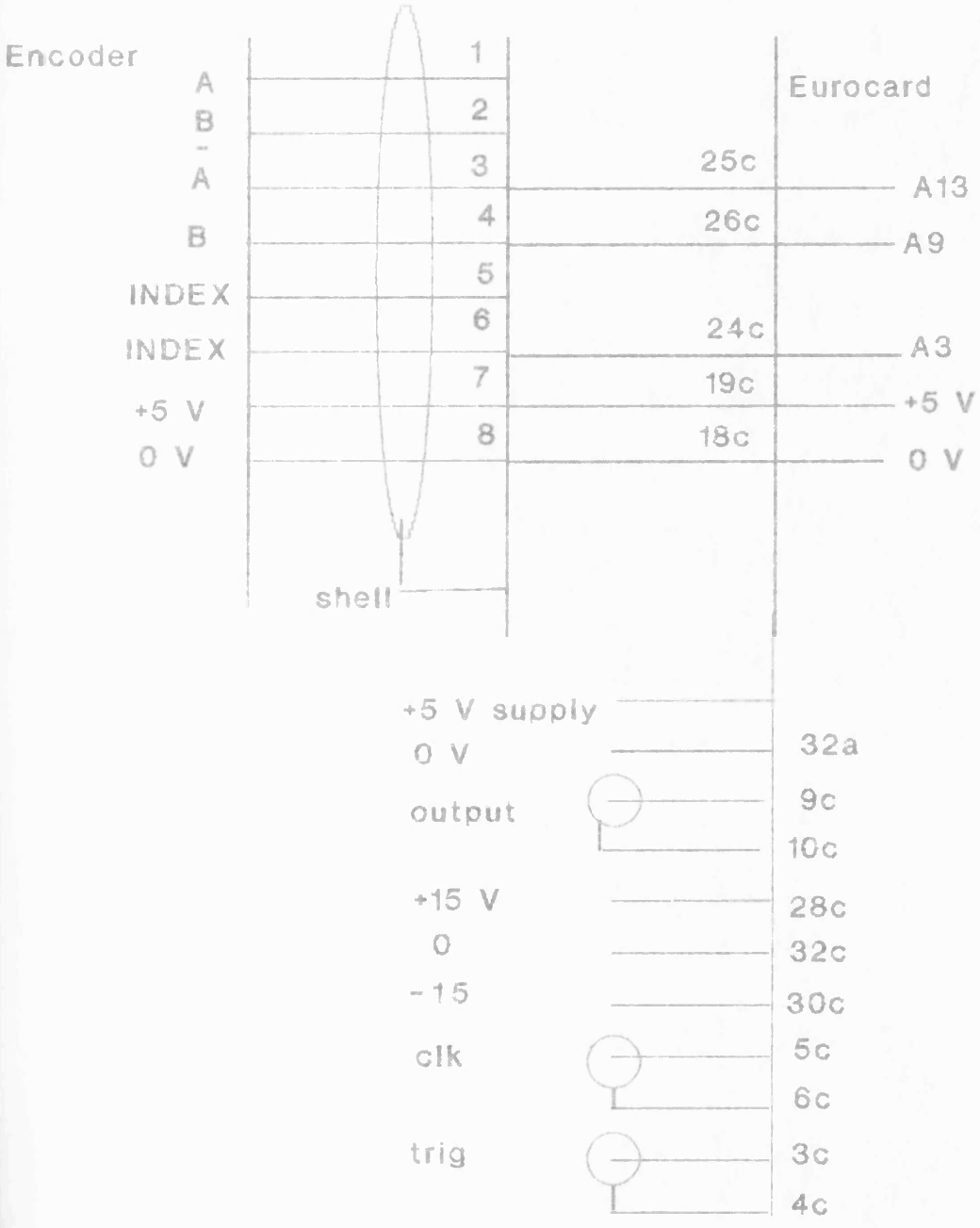

Fig 4.4.4 Interconnection between encoder and circuit board

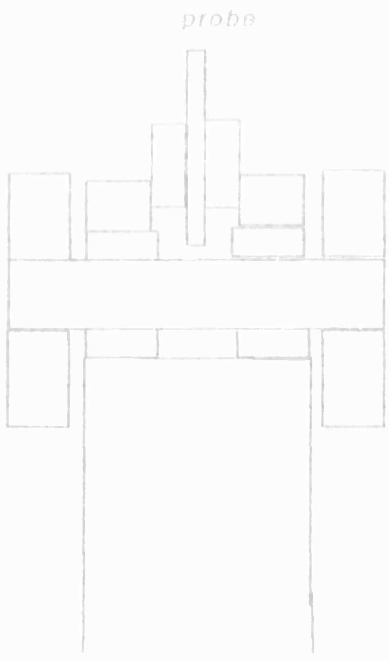

Fig 4.6.1 Position of the probe relative to the pin and bush

Fig 4.6.2 Cross section of pvc ring on pin ends

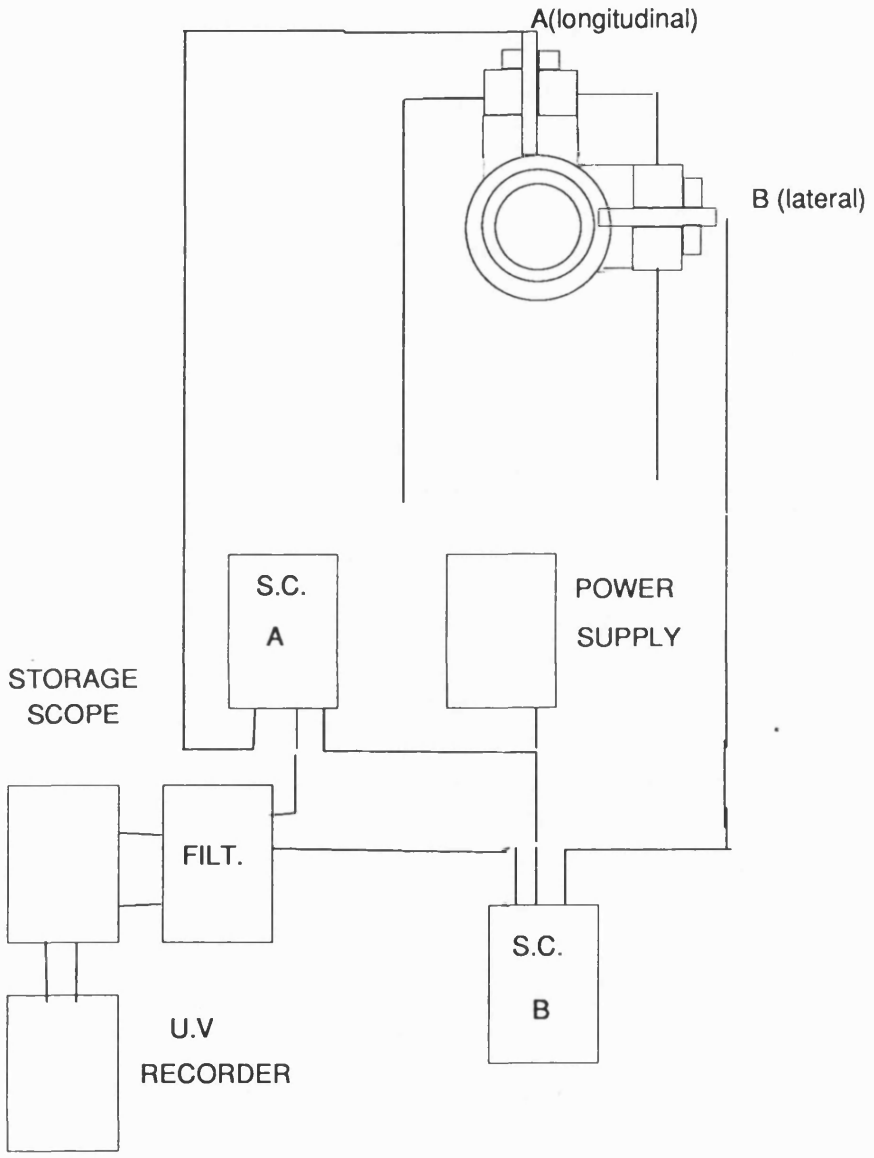

FIG 4.6.3 Pin loci monitoring circuit

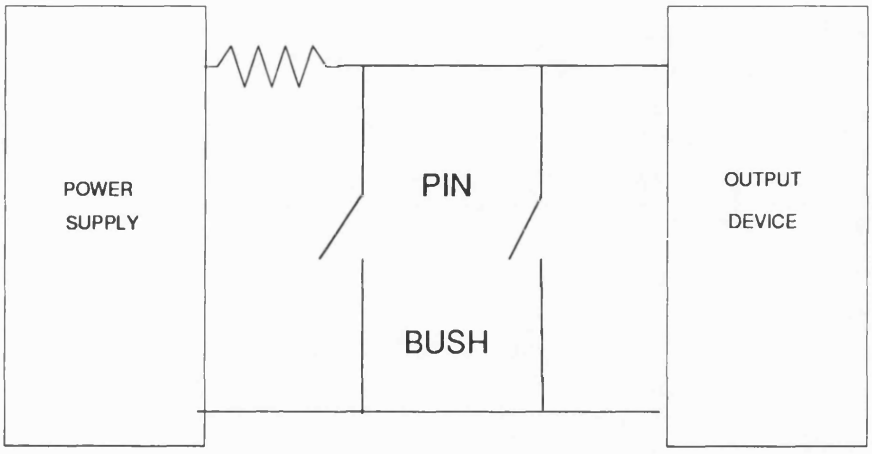

Fig 4.7.1 Contact loss monitoring circuit

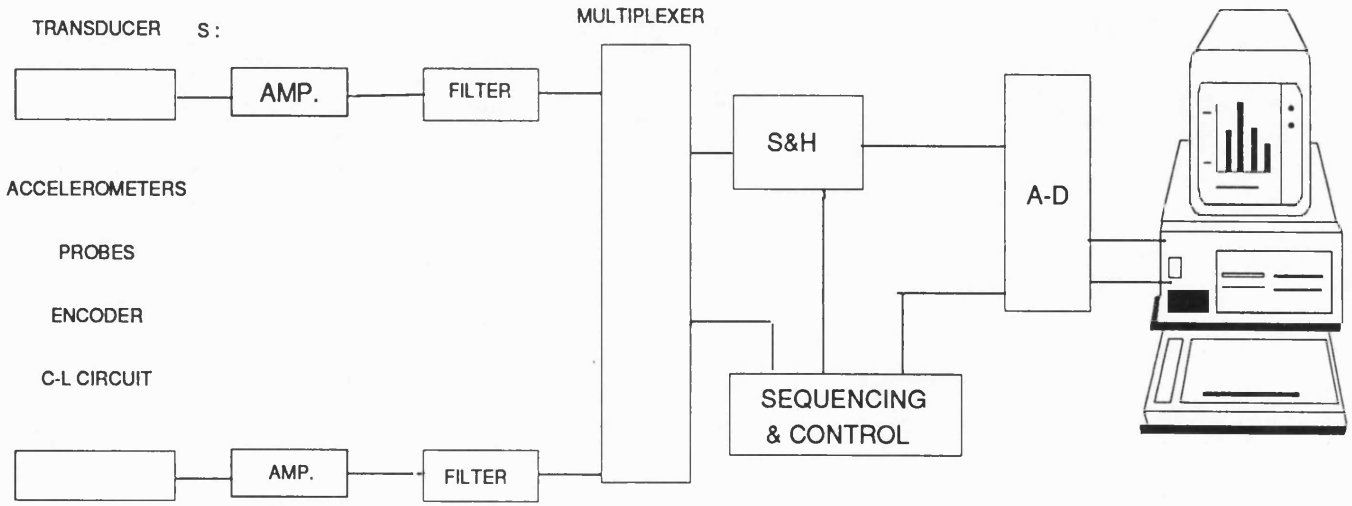

Fig 4.8.1 Data Aquisition system block diagram

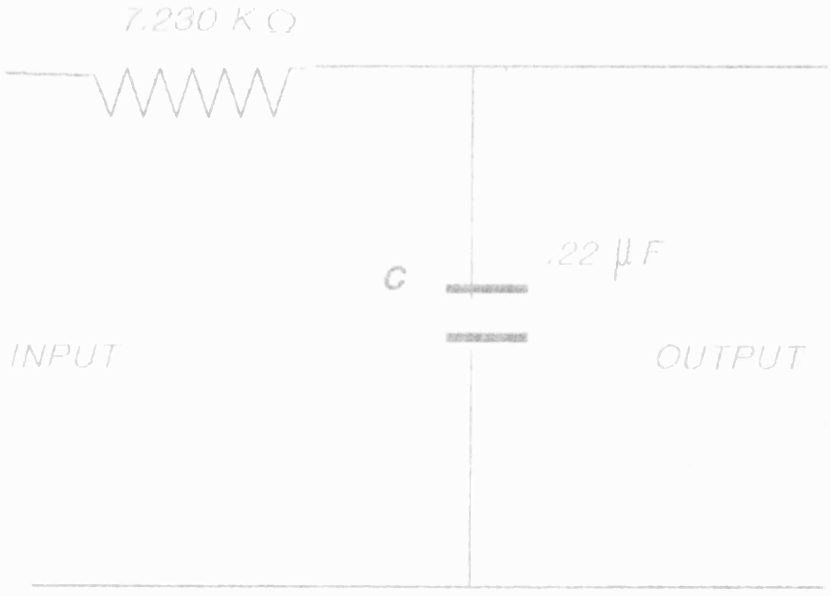

Fig 4.9.1 Circuit diagram of a simple filter

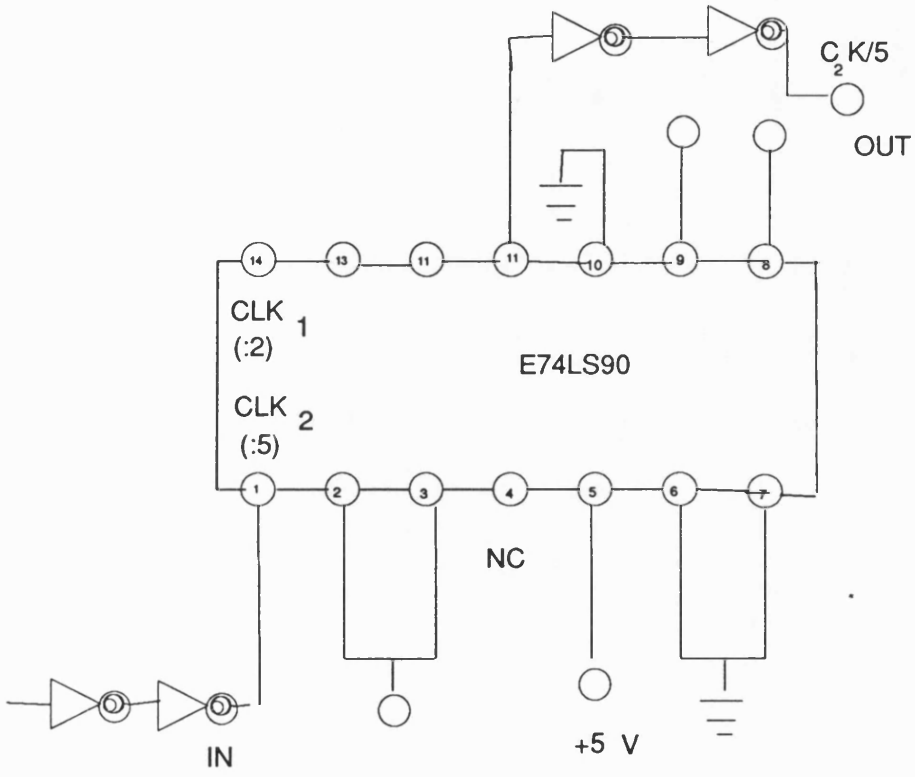

Fig 4.11.1 Divider circuit diagram

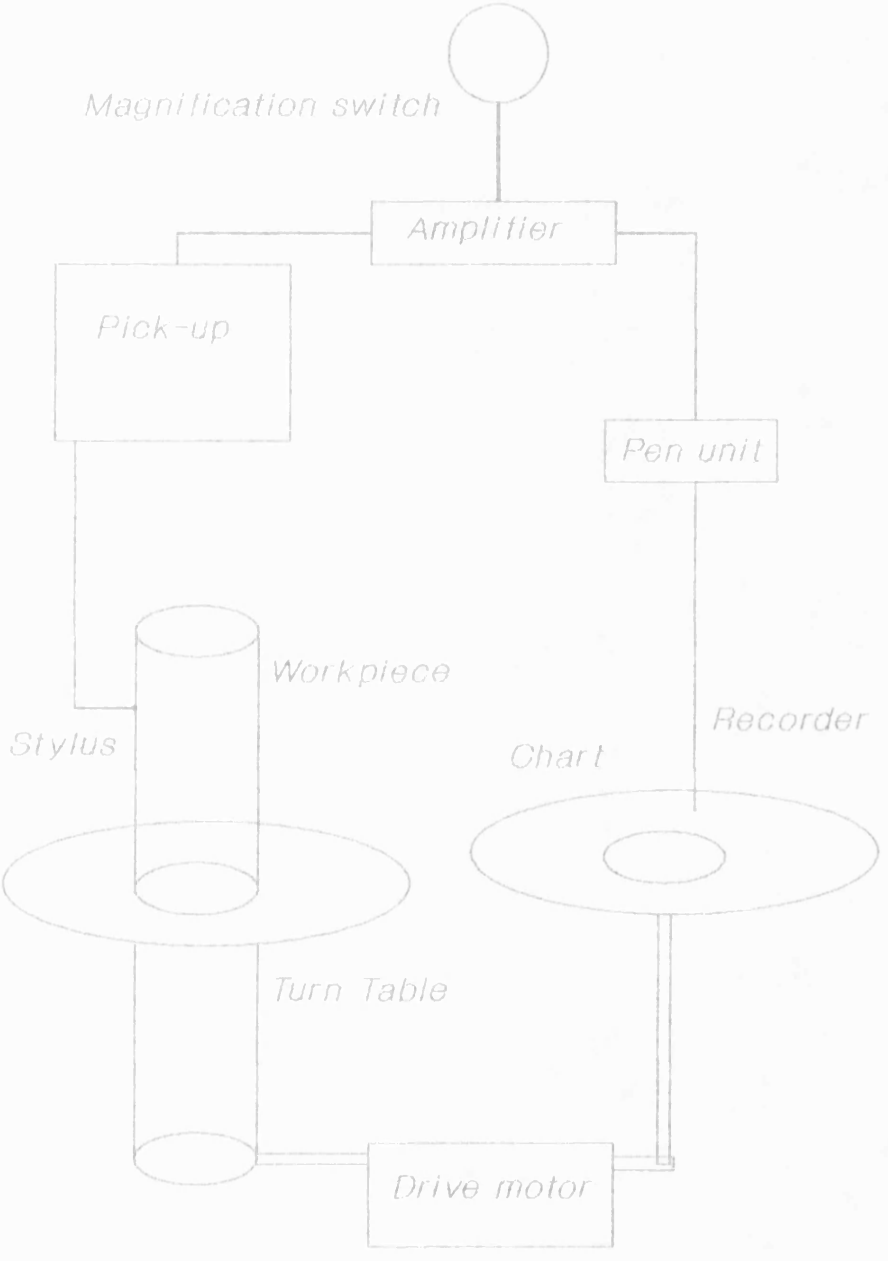

Fig(4.12.1) Diagram showing operation of Talyrond

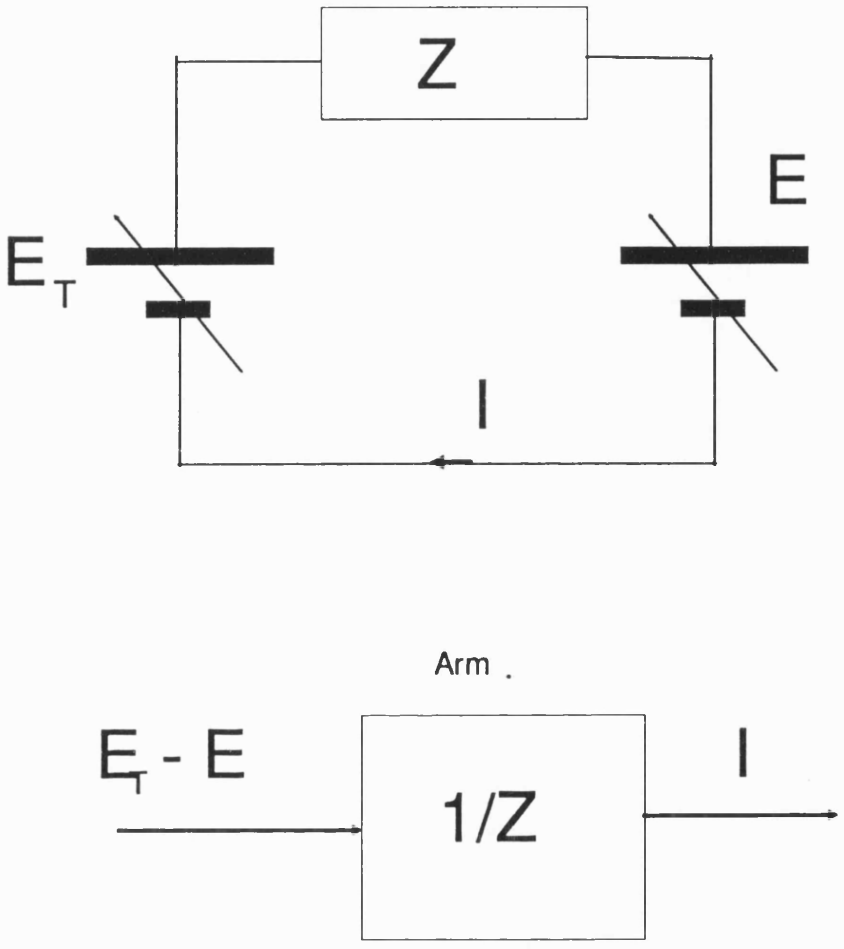

Fig 4.13.1 Symplified motor connection to DC power supply and its block diagram

CHAPTER 5

CALIBRATION

5.1 Frequency to voltage converter(F-V)

A F-V converter is used to convert the encoder frequency to voltage ; the signal can then be observed on the storage scope. Using a plotter the trace of input velocity during the cycle can be obtained. Before using the converter must be calibrated. The calibration procedure is explained in section 5.2.

5.2 Input speed

The following procedure is used to calibrate the speed measurement system:

1- The link between the multiplier and the converter is disconnected.

2- A test circuit is established Fig(5.2.1).

3-The output for zero input is checked .

4-The output for max input is checked .

After disconnecting the link between the multiplier and the converter and arranging the test circuit , when there is no input the zero variable resistor which is indicated in fig (5.2.2) is adjusted so that the output voltage becomes zero. Then the function generator is set to max Fin which is 66.66 k Hz (see sec.(4.4). The corresponding

variable resistor is adjusted to produce an output of 5 volts.

This is chosen to produce a calibration of 500 rev/min =5 volts - see sec.(4.4).

The converter is specified as providing a departure from linearity of less than 0.05 of full scale over its calibration range.

5.3 Accelerometer:

The accelerometer on the follower was a Bruel and Kjaer type number 4365; it was fixed to the end of the follower by means of a screw . It was calibrated by the manufacturer at $3.99 mV/ms^{-2}$. The signal is amplified by 10 in the pre amp. stage. An H.P. spectrum analyzer was calibrated for the accelerometer by the following procedure

1-A function generator was connected to a Nicolet storage oscilloscope

2- Two separate a.c. voltages corresponding to the different settings(3V and 10V)used were chosen and fed to the storage oscilloscope

3- The above sinusoidal voltages were fed to the frequency analyzer . It was plotted and used as a reference for measurement of the accelerometer signal(see fig(5.3.1)).

A second accelerometer was used to measure the lateral acceleration. of center of mass of the coupler. This accelerometer was also Bruel and Kjar type number 4343. It was calibrated by manufacturer at 8.78 mV/g where $g=0.9806 ms^{-2}$.

5.4 Displacement transducer

5.4.1 Calibration with flat target

The inductive displacement transducers (probes) are used to monitor the displacement of the pin inside the bearing . Since the output of the two probes should be the same for the same input , a test was carried out to see if there was any difference .

The probes were mounted on a piece of angle steel. The angle-piece was fixed on an angle block with two screws . The position of the probes were adjusted to a known distance which was measured by feelers and slip gauges (as illustrated in the fig (5.4.1)) .

The instructions of the manufacturers catalogue were carried out . Then the output signal of the probes were fed into a voltmeter and by adjusting the gain. The same output voltage was obtained for both probes.

Probes A & B were then calibrated by the following procedure . While the probes were touching the target the output was adjusted to zero volts. The distance of the probes from the target was increased to 0.5mm. The output voltage was adjusted to obtain -8.0 volts output from both. This adjustment was repeated several times to get the desired output. Then the output was recorded for two other distances(0.25mm,0.35mm). The calibration distances and voltages were recorded in the tables (5.4.1) & (5.4.2).

It seems from the above tables there is slight non linearity in probe output signal in this range but it is acceptable for our purpose.

5.4.2 Calibration of the probes with a pin target

After calibration with the flat slipper target , the actual round pin was used. The output voltage readings were very different from the first case in which flat target was used . The difference was due to target shape.

The probes were fixed on a piece of angle steel which was fitted on an angle block(see fig 5.4.2) . The pin was fixed in a vice on the table of a milling machine directly beneath the probe. The distance of the probe tip and the target was adjusted to 0.25 mm by feeler gauges. Then the table was moved horizontally to get a minimum reading . The signal conditioner controls were adjusted to produce 4 volts output for this condition . Then the table was moved 0.25mm left and right . It was observed that the two readings were very similar. The same procedure was carried out for vertical distances of 0(contact) and 0.5 mm . The same calibration factor was obtained (table 5.4.3).

5.4.3 Calibration on the rig

The follower was separated from the coupler . The probes were mounted in their seats on the follower (Fig 4.6.3). The zero clearance pin was fitted in the bearing , and the probes adjusted to touch the pin. Then the zero clearance pin was taken out and a pin with 0.25 mm diametral clearance was fitted in the bearing. The pin was moved inside the bearing by hand. When it was closest to the transducer, output voltage was set to zero. Then the pin was moved to the opposite side of the bearing and the output was adjusted to -4 volts. The pin was returned to first position ,the output checked again, adjusted to zero. This procedure was repeated several times to get the output between 0 and -4 volts. This procedure was carried out for both probes. Then the pin was placed in contact with the probe. The probes were moved

back (to prevent damage) to get -4 volts output. Then the output is between -4 and -8 volts.

The follower was connected to the coupler . The probes output was passed through a Kemo low pass filter(VBF/14). The filter was adjusted to 100 Hz . The filter output and the other signals of the rig performance were connected to a multiplexor . The multiplexor was explained in data acquisition system (sec 4.8).

5.5 Setting trigger point

After mounting the encoder and connecting the multiplier and F-V converter to it (supplying the required sources) a reference point should be set for the encoder. This was carried out using the following procedure:

1-The crank was set to zero degrees using a spirit level.

2-There are three Allen head screws which lock the rotation of the body of the encoder to the frame. These were loosened.;

3- The output pulse O ,which is high once per revolution, of the encoder was connected to an oscilloscope.

4- The body of the encoder was rotated until the index pulse was appeared on the oscilloscope .

5- The Allen screws securing the encoder were tightened and the body of the encoder locked to the frame. The index pulse is used for starting the measurement point. The triggering of a measurement is initiated by an input signal(index signal).

5.6 Experimental procedure

As is illustrated in the flow chart (fig 5.5.1) first of all the power supply of the transducer is turned on. To allow the transducers to warm up the one should wait for 15 minutes. Then the motor is turned on and set for a percentage of its full speed. A 60 seconds delay is used to ensure steady speed. Then the output is saved for processing or recorded directly.

The same procedure is carried out for other speeds.

After obtaining results for a number of speeds for a typical pin with a certain clearance, a pin with another clearance is inserted and the above procedure repeated.

5.7 Conversion of binary files to ASCII

A program was written to convert the data acquisition output files , which are in binary form, to ASCII form, as the ASCII files can be used in plotting packages . Since the information is in the form of voltage , a conversion factor is required for each parameter . The conversion factor may be calculated as follows :

5.7.1 Conversion factor

A&B displacement probes are calibrated so that an input displacement of 0.25 mm gives 4 volts output. Therefore the conversion factor will be

$$C_{f1}=(0.25mm)/(4V)=0.0625mm/V$$

Input velocity

The frequency to voltage converter ,which has as input the encoder output , was so

calibrated to have an output of 5 volts for 500 rev/min . Therefore the conversion factor Cf2 may be calculated as follows :

$$C_{f2}=(500rev/min)/(5V)=100rev/min/V$$

$$C_{f2}=((100rev/min/V)\times 2)/(60s)$$

$$C_{f2}=10.47197rev/s/V$$

Follower angular acceleration

According to the manufacturer literature the output of the accelerometer is $3.99mV/(ms^{-2})$ the follower length from frame bearing to the accelerometer seat is 0.185 m . The output voltage is amplified by a pre amplifier, of gain 10. Therefore the conversion factor C_{f3} can be calculated as follows :

$$C_{f3}=(1V)/(3.99\times(10^{-3})\times 0.185)=135.473rads^{-2}V^{-1}$$

Coupler c.m lateral acceleration

The output of the accelerometer is 8.78 mv/g where

$$g=0.9806ms^{-2}$$

the conversion factor C_{f4} will be

$$C_{f4}=(1V)/((8.78mV/0.9806m/s^2)\times(10^{-3}))$$

$$=111.68565ms^{-2}V^{-1}$$

Crank angular displacement

The encoder has 2000 lines/rev. When the encoder output is used directly as an external clock, the conversion factor C_{f5} can be calculated as follows :

$$C_{f5}=(360 degrees)/(2000 pulses)$$
$$=0.18 \text{ deg./pulse}$$

In the case which a divider is used to divide the encoder output pulses by 5 the conversion factor is calculated as follows :

$$C_{f5}=(360 degrees)/(2000 pulses/5)$$
$$=0.9 \text{ degree/pulse}$$

Table 5.4.1

Probe A displacement (longitudinal) calibration with flat target		
no	displacement and voltage	
	input(mm)	output(v)
1	0.00	0.00
2	0.25	-3.7
3	0.35	-5.4
4	0.5	-8.0

Table 5.4.2

Probe B displacement (lateral) calibration with flat target		
no	diplacement and voltage	
	input(mm)	output(v)
1	0.00	0.00
2	0.25	-4.3
3	0.375	-6.3
4	0.5	-8.0

Table 5.4.3

Probe A displacement (longitudinal) calibration with pin target(centre)		
no	diplacement and voltage	
	input(mm)	output(v)
1	0.00	-0.05
2	0.25	-4.12
3	0.5	-8.22

Table 5.4.4

Probe B displacement (lateral) calibration with pin target (centre)		
no	diplacement and voltage	
	input(mm)	output(v)
1	0.00	-0.05
2	0.25	-3.0
3	0.5	-8.42

Table 5.4.5

Prob A displacement (longitudinal) calibration with pin target (0.25 mm out of centre)		
position	diplacement and voltage	
	input(mm)	output(v)
left	0.25	-4.23
right	0.25	-4.19
left	0.5	-8.3
right	0.5	-8.25

Table 5.4.6

Probe B displacement (lateral) calibration with pin target (0.25mm out of centre)		
no	diplacement and voltage	
	input(mm)	output(v)
left	0.25	-4.03
right	0.25	-4.06
left	0.5	-8.40
right	0.5	-8.42

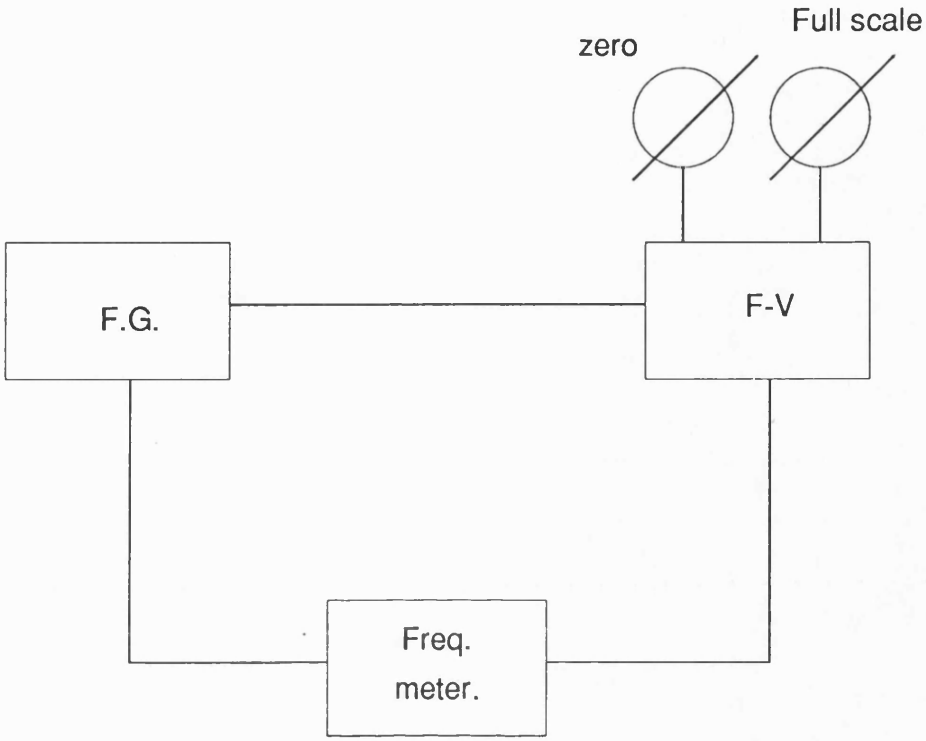

Fig(5.2.1)Test circuit of F-V convertor for calibration.

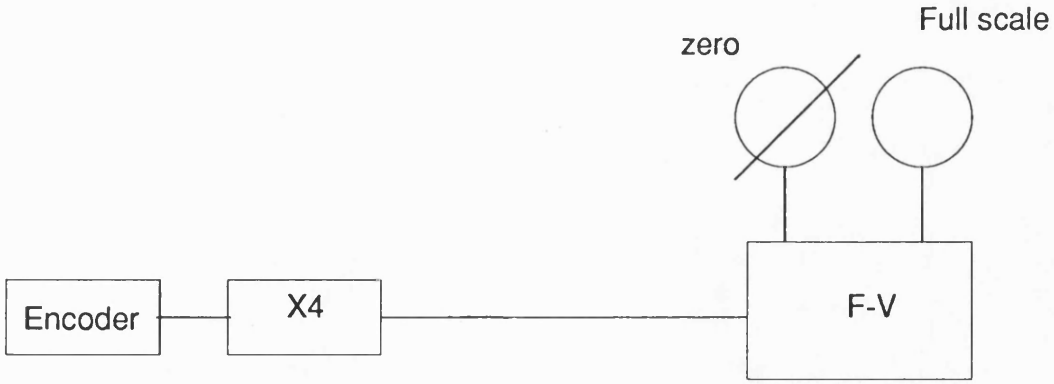

Fig (5.2.2) Position of F-V in the circuit

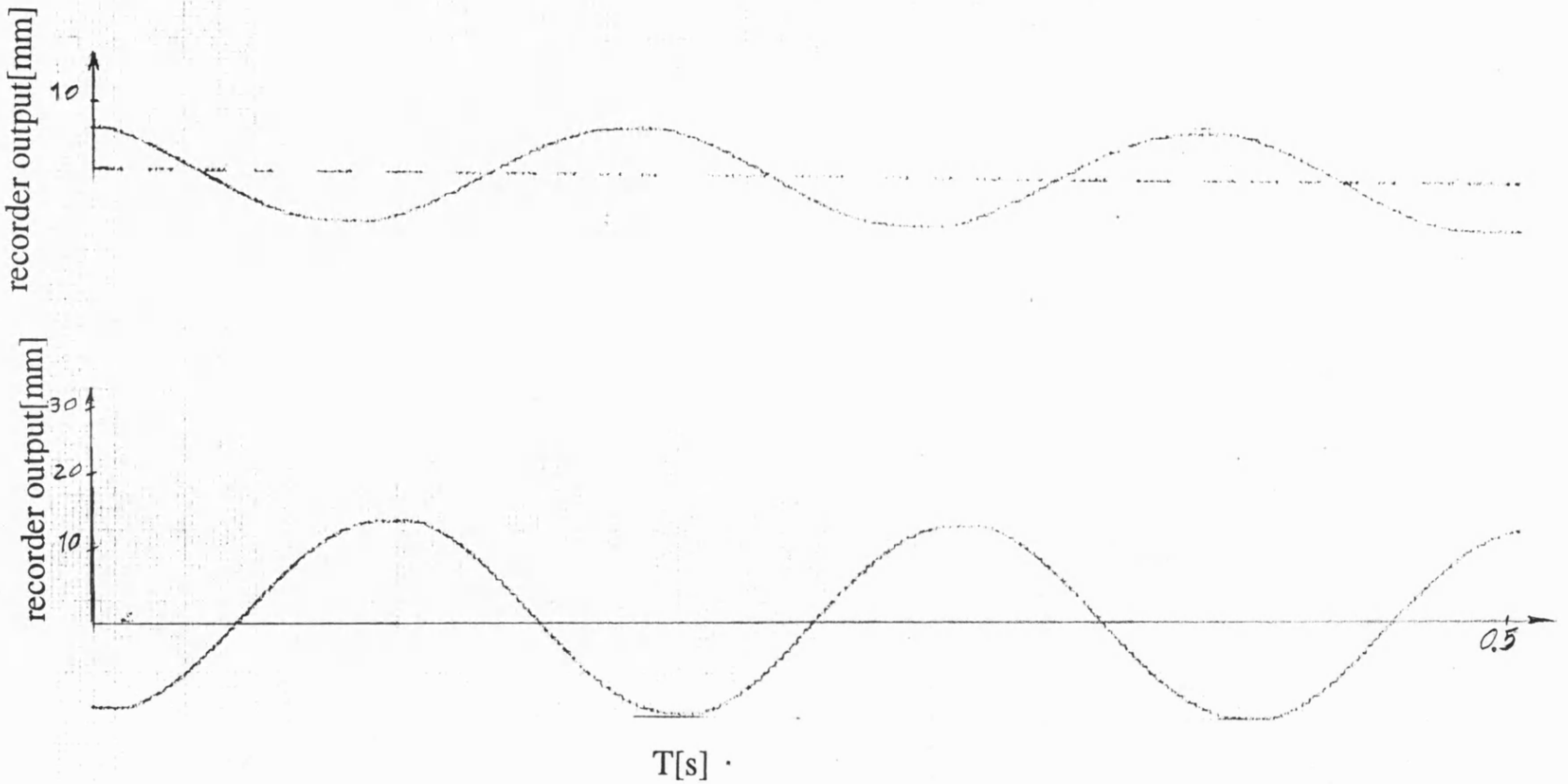

Fig 5.3.1 Recorder output for 10.06 volt(top) on 10 volt setting,

for 6.17 volt(bottom) on 3 volt setting

Fig(5.4.1) Calibration of probes with flat target

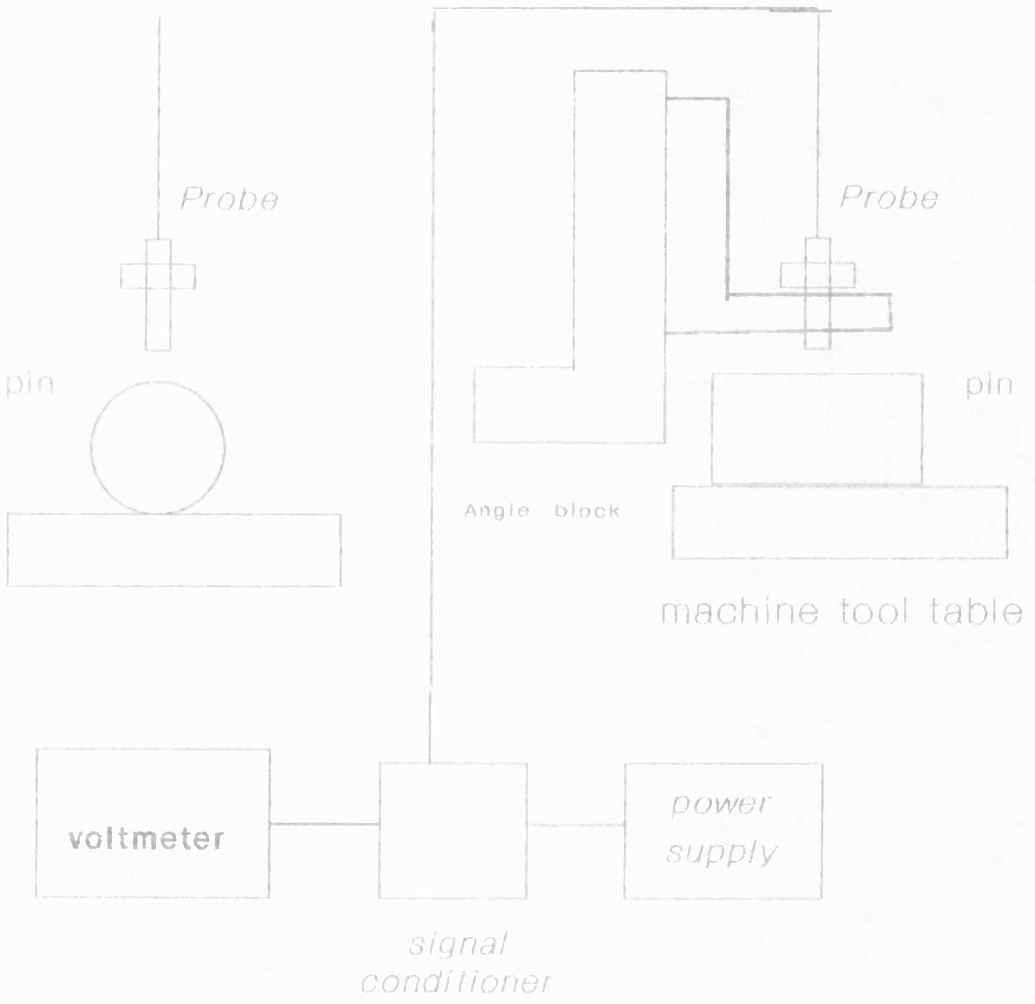

Fig(5.4.2) Calibration of probes with pin target

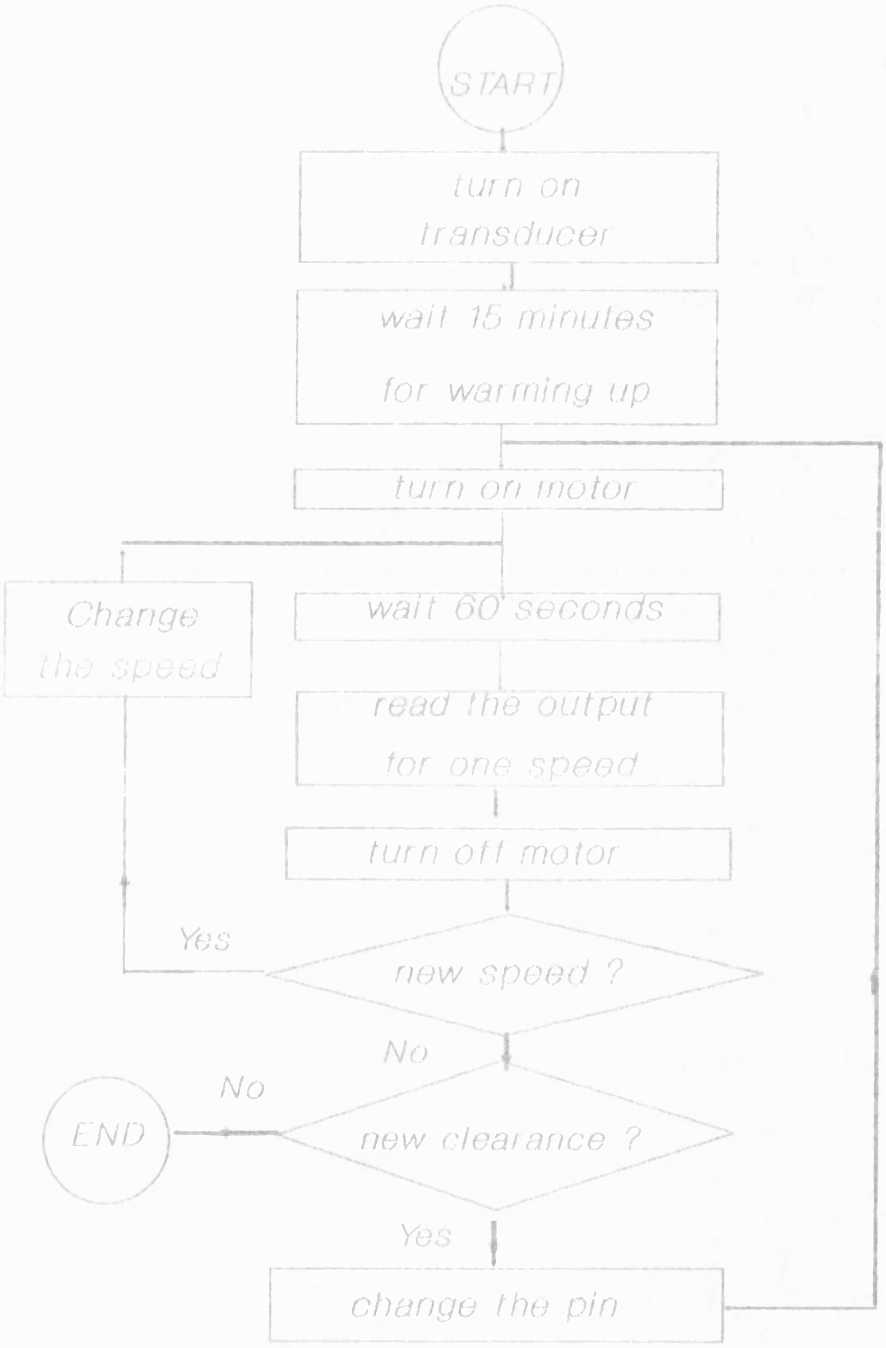

Fig(5.6.1)Experimental procedure

CHAPTER 6

ZERO CLEARANCE RESULTS

6.1 Introduction

In this chapter the zero clearance results are studied. The kinematics predicted by the theoretical model checked with some unpublished results(48)using the plot of the fundamental parameters in sec. (6.2).

The follower angular acceleration and input speed traces were compared with their experimental counterpart in sec. (6.3). Different assumption over input speed were discussed in sec. (6.4). In sec. (6.5) pin force and its components are described by an alternate method. Wear factor and its variation during the cycle are studied in sec. (6.6). In sec 6.7 the variation of system potential energy was discussed. Finally some zero clearance criteria are evaluated in sec. (6.8).

6.2 Configuration checking

Several parameters were plotted against crank angle. The parameters are follower angular displacement, velocity ratio , acceleration ratio and effective inertia (fig 6.2.1 ,6.2.3). They were in agreement with results quoted by Grosjean (48).

6.3 Experimental results

A comparison of predicted and recorded traces is given in fig 6.3.1 for a mean speed of 260 rev/min. No flywheel was fitted; a speed fluctuation twice per revolution

resulted but with superimposed higher harmonics which are not predicted. This is probably due to the speed controller. Although introduced to give a range of mean speeds, it has its own transient response, typical of SCR controllers (see (sec. 4.3)).

The effect of the speed undershoot is to produce a secondary peak on the primary follower acceleration(see fig(6.3.1 and 6.3.2)). This could be predicted by the theoretical model when the transient speed response was allowed for.

A rundown test was carried out to evaluate the viscous friction coefficient. The motor was taken to a speed of 280 rev/min and then switched off. Shaft input speed and follower acceleration were recorded over four cycles of the rundown. Shaft deceleration enabled the friction coefficient (assumed to be the same for all bearings) to be evaluated. The value obtained was 0.09 Nms.

In tests at constant mean speed , input speed and follower angular acceleration were recorded at seven different speeds in the range 100-370 rev/min. Then the peak to peak follower acceleration was compared with the theoretical result Fig(6.3.3). The agreement is quite satisfactory in the range studied.

6.4 Input speed

In most theoretical work on linkages ,especially crank slider and four bar chains, there are two assumptions.

a. The crank is driven with a constant speed. In practice it would require an input device which is capable of meeting the required driving torque at any time for steady motion.

b. The input torque is assumed to overcome friction and load. The average input speed should remain constant from cycle to cycle.

In practice true steady running cannot be achieved. However unsteady running has received little attention. Obviously the dynamic performance of the system is effected by speed fluctuation including pin forces and wear factor.

The effect on pin forces and wear factor is worthy of study.

6.5 Pin forces and input torque

Variation of pin forces during the cycle , specially the regions where the force is minimum , is important from the point of view of wear and contact loss prediction. To study the variation of the force, steady running and running with speed fluctuations, were considered.

In practice there are two ways of controlling the input speed.

1. flywheel control

2. motor control

For the latter a PID controller with the following parameters(see sec.(2.6)).

$$k_p k_d = 26 s^{-1}$$

$$\frac{k_i}{k_d} = 100 s^{-2}$$

were used.

where k_p,$k_i$andk_d are proportional , integration and derivative coefficients respectively.

For the first method flywheel inertia was varied in the range 0.007-0.9 kgm^2 to achieve a given coefficient of fluctuation , and in the commercial controller method (PID) k_d was varied in the range

$$0.0035<k_d<0.45kgm^2$$

The average force at pin B (coupler - follower) is given in fig 6.5.1 for the two control methods(flywheel and PID motor control). The constant speed case is also considered.Speed fluctuation has virtually no effect on the average force compared with the steady speed case. The actual force predicted at B with C_f=0.05 is compared in fig 6.5.2 as a function of crank angle with that for steady speed case. The general similarity of the force in the two cases is apparent. The actual force predicted at A with C_f = 0.05 is compared in fig 6.5.3 as a function of crank angle with that for the steady speed case. The flywheel control plot slightly lags that in the steady speed case. This may be due the fact in modelling flywheel control the speed at each step is calculated at the end of previous step.

The corresponding result for pin A (crank-coupler bearing) is given in fig 6.5.4. When a flywheel is used, allowing speed fluctuations reduces the average force somewhat, while three term control increases it slightly: dF/dC_f is around 10N.

The average force tends to the steady speed case when C_f tend to zero. The pin forces will be influenced by $I_1\ddot{\phi}$. To reduce input angular acceleration calls for a large

flywheel inertia in the fly wheel case and increased gain in

the motor control case. In the case of three term control, as k_d is increased the system eventually becomes unstable.

The pin forces depend on different parameters. To study the pin force it is easier to resolve them to different parameters including inertia and gravity components. The forces R_a and R_b refer to bearing A and B respectively(see fig(6.5.11,6.5.12).

$$R_a=\frac{I_1\ddot{\phi}}{a\sin(\varepsilon-\phi)}+\frac{m_1ge_1\cos\phi}{a\sin(\varepsilon-\phi)} \tag{6.5.1}$$

$$R_b=\frac{I_3\ddot{\psi}}{c\sin(\gamma-\beta)}+\frac{m_3ge_3\cos\beta}{c\sin(\gamma-\beta)} \tag{6.5.2}$$

where ε is the direction of A pin force.

pin force R_a

For R_a these components were plotted against crank angle for different input inertia (fig 6.5.5,6.5.7). Second term depends on g, changes little, i.e ϕ,ε are not affected significantly by increasing I_1.

It might be expected that an increase in input inertia will lead to an increase in the inertia component. However it does not, because by increasing inertia, input acceleration will decrease.

The other point is that at high speed the gravity component is small relative to the inertia component. However at low speed gravity component may be significant.

The common parameter in both components of R_a (eq. 6.5.1) is $\frac{1}{\sin(\phi-\varepsilon)}$.

It is plotted against crank angle ϕ (fig 6.5.8). There are four points which the sign of this term changes; one is around 30° the other is around 240° these are the top and bottom dead centre points. Two others are around 110° and 330°. These are the points which the direction of the force reverses from 'pin toward bush' to or vica versa. This change sometimes has been used by some authors as contact-loss criteria (Soong and Thompson (19)).

Pin force R_b

Writing the motion equation of the follower one may calculate the pin force at B in terms of the follower acceleration.(inertia force) and the gravity component. At low speed the gravity component in force R_b is dominant. However at high speed the inertia component is dominant.

One may express the force R_b as in terms of unsteady and approximately steady components. The first depends on $\ddot{\phi}$; the second depends on $\dot{\phi}^2$ which does not change greatly.

$$\ddot{\psi}=G_f\ddot{\phi}+DG_f\dot{\phi}^2 \qquad (6.5.3)$$

where G_f is the velocity ratio $\frac{\dot{\psi}}{\dot{\phi}}$ and $DG_f=\frac{dG_f}{d\Phi}$

Therefore one may write

$$R_b=\frac{I_3G_f\ddot{\phi}}{c\sin(\gamma-\beta)}+\frac{I_3DG_f\dot{\phi}^2+m_3ge_3\cos\beta}{c\sin(\gamma-\beta)} \qquad (6.5.4)$$

The first component, which depends on the input angular acceleration, is an unsteady component and the second one ,which depends on the follower weight and input speed, is the approximately steady component. It is observed from fig (6.5.9) that the unsteady component is small compared with the ϕ^2 term which is approximately constant. The largest values of G_f and hence unsteady component occurs in the regions (100–150 ° and 320–350 ° of crank angle). DG_f passes through zero in these regions(fig 6.2.2) ie. unsteady effect most important near these regions. As it discussed later these two regions are contact loss regions.

Input torque

The input torque predicted for the steady speed case is compared in fig 6.5.10 as a function of crank angle with the motor (three term) control case. The motor torque lags that required for steady(constant) speed. In the steady speed case the required torque is assumed to be supplied instantaneously to keep the input speed constant. However in motor control there is a time constant between the demanded and supplied torque. The delay in the above traces depends on this time constant.

6.6 Wear factor

For unlubricated surfaces the basic law of wear is(20)

$$V=KLR/P \qquad (6.6.1)$$

where

V = the volume of material removed,

L = the sliding distance,

R= the load,

P = the flow pressure of the material

and

K = coefficient for the particular materials in contact.

At the crank-coupler bearing, the relative angle turned through during a rotation $\Delta\phi$ of the crank is $\Delta\phi(1-G_c)$ where G_c is the velocity ratio $\frac{\dot{\theta}}{\dot{\phi}}$ of coupler to crank.

The wear over a cycle is related to the wear factor

$$R_a(1-G_c)d\phi \qquad (6.6.2)$$

where $R_a(\phi)$ is the normal force at the pin , which is the total force in practice when friction is low , as in this work. The average value over the cycle of the wear factor is proportional to the wear experienced.

For the coupler-follower bearing B the wear factor is

$$R_b \mid G_c-G_f \mid d\phi \qquad (6.6.3)$$

The variation of wear factor at pin A during a cycle is plotted against crank angle (see fig 6.6.1). The wear factor has a similar pattern to the pin force variation. The minima and the maxima occur in the same region. The region between 150° and 300° crank angle the pin force is approximately flat. However in those regions the wear factor is approximately sinusoidal. Its maximum is at around 40° and the minima points are at around 110° and 330°.

For pin B the maximum of wear factor is at around 40° and its minimum is at around

190° (fig 6.6.1a).This is for zero clearance. However when clearance is involved, because of impact, the distribution will be different. As will discussed later in the next chapters (see sec.(8.7)) major wear of the bush occurs when the crank angle is around 130° and 330°.

In fig (6.6.2) is shown the average wear factor at pin B. The motor inertia limits C_f to 0.095. Both with flywheel and motor control there is very little variation of wear with speed fluctuation coefficient for this particular chain. There is a phase difference between the generated torque and that required for steady running. As gain is increased all three terms are magnified, so that the phase difference is maintained.

A coulomb friction load of 20 Nm was assumed and the average wear factor of pin B was plotted (fig 6.6.3). The general patterns are similar. For both cases the average wear factor slightly decreases with speed fluctuation coefficient. The average wear factor for the case of with friction load is greater.

The results for pin A are similar to those for pin B.

For both flywheel and three term motor control there is a modest fall in wear as the speed fluctuation coefficient is increased.

6.7 Variation of potential energy

Since during the crank rotation cycle the system mass is constant the variation of the potential energy is the same as variation of the center of mass(c.m.) height from a datum. The variation of the system c.m. elevation is plotted against crank angle in fig 6.7.1.

As is observed from the graph the potential energy is increasing at the starting point of the cycle. It continues to increase up to a maximum around 100°. Then it decreases and passes through a minimum around 250°. It seems that the variation of the potential energy of the system follows approximately the same pattern as that of centre of mass of the crank itself. At low speed gravitational force is dominant in pin forces. The variation of the potential energy is just opposite to the variation of input speed. i.e the position with minimum input speed is the same as the position with maximum potential energy(see fig 6.7.1). This is only true if gravitational forces are dominant at higher speeds inertia dominants and the max input speed is at minimum effective inertia. Then this is also another criteria to check the model.

The importance of the above variation and its role at contact loss regions in the case with clearance will be discussed in chapter 8.

6.8 Contact-loss criteria

The loss of contact is associated with reduction in contact force and a rapid change in its direction. The empirical contact-loss criterion of Earles and Wu (3) uses a zero clearance model and is of the form $\frac{\dot{\gamma}}{R_b} > 1(rad/s)/N$ where R_b is contact force and γ is angle of the force relative to an axis fixed in the frame , here taken to be horizontal.

Another criterion was developed by Bengisu et al(25). They defined a separation parameter $SP=\frac{M_e r_1 \ddot{\gamma}}{R_b}$ Where $M_e=\frac{m_i+m_j}{2}$ and r_1 is clearance. m_i and m_j are the masses of link i and j respectively.

Evaluation of the criteria

The variation of contact angle (γ) of the bearing force against crank angle is shown in fig 6.8.1 for the four bar chain used by the author. Except around 250°,γ falls continuously with crank angle with two sharp falls at around 100° and 330°. Most of the time $\dot{\gamma}$ is negative(see fig(6.8.2)). There may be a spurious jump in the contact angle due to the use of the atan function when computing. This function maintains γ in the range (-90°,+90°). When γ attempts to exceed the range a jump from -90° to +90° (or vica versa) occurs.

It is therefore possible to get a large value of $\dot{\gamma}$ at $\gamma=\pm 90°$ which is where the Earles and Wu criterion indicates contact loss. When $\gamma=\pm 90°$ the horizontal component of the force is zero. In body fixed coordinates (fixed to the follower fig (6.5.12)) The follower equation can be written as follows:

$$-m_3 g e_3 \cos\beta - cF_{b1} = I_3 \ddot{\psi} \qquad (6.8.1)$$

where F_{b1} is the lateral force component

F_{b2} is the longitudinal force component; when $\gamma=\pm 90°$ F_{b1} becomes zero(see fig (6.5.12)). In coordinates fixed with respect to the follower:

$$\gamma = atan\left(\frac{F_{b2}}{F_{b1}}\right) + \left(\beta - \frac{\pi}{2}\right) \qquad (6.8.2)$$

In the above equation when there is no lateral force $\gamma=\beta or \gamma=\beta\pm\pi$. When there is no lateral force on the follower β is close to 90 and $\gamma\approx 90°,270°$.

If follower weight is neglected $\ddot{\psi}=0$. The experimental results indicate contact-loss when $\ddot{\psi}$ is close to zero. Dubowsky(45) observed $\ddot{\psi}\approx 0$ at impact.

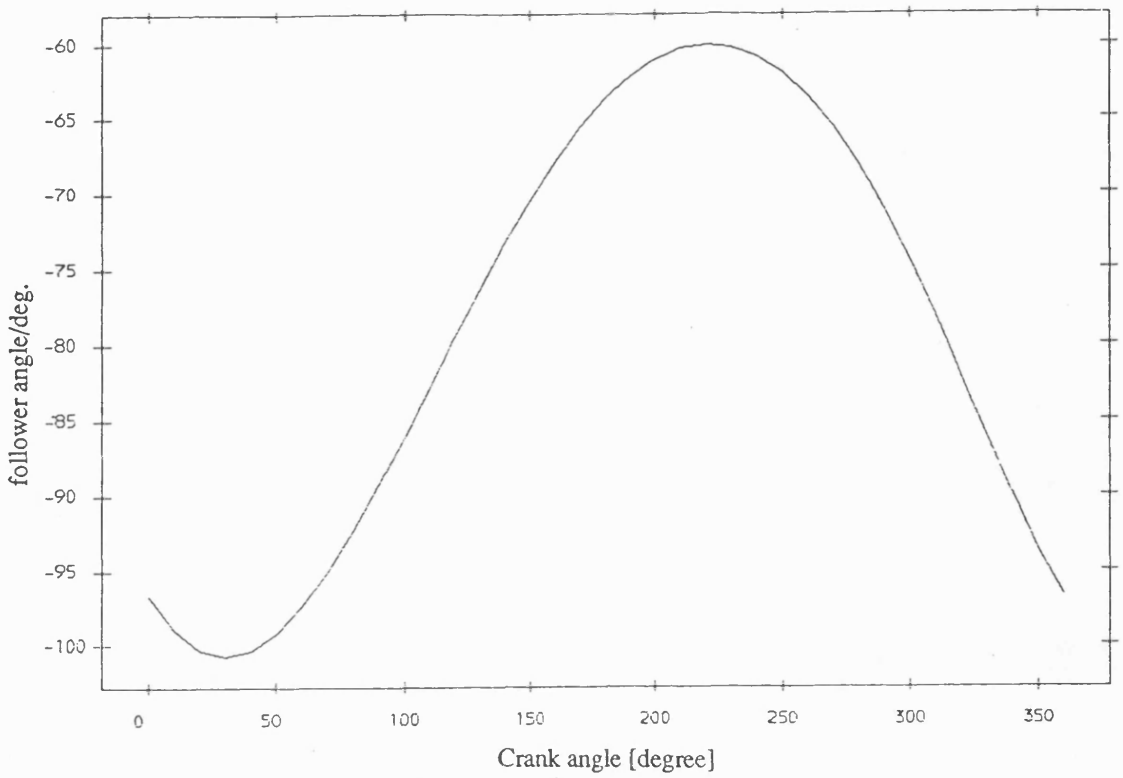

Fig 6.2.1 Follower angle, zero clearance

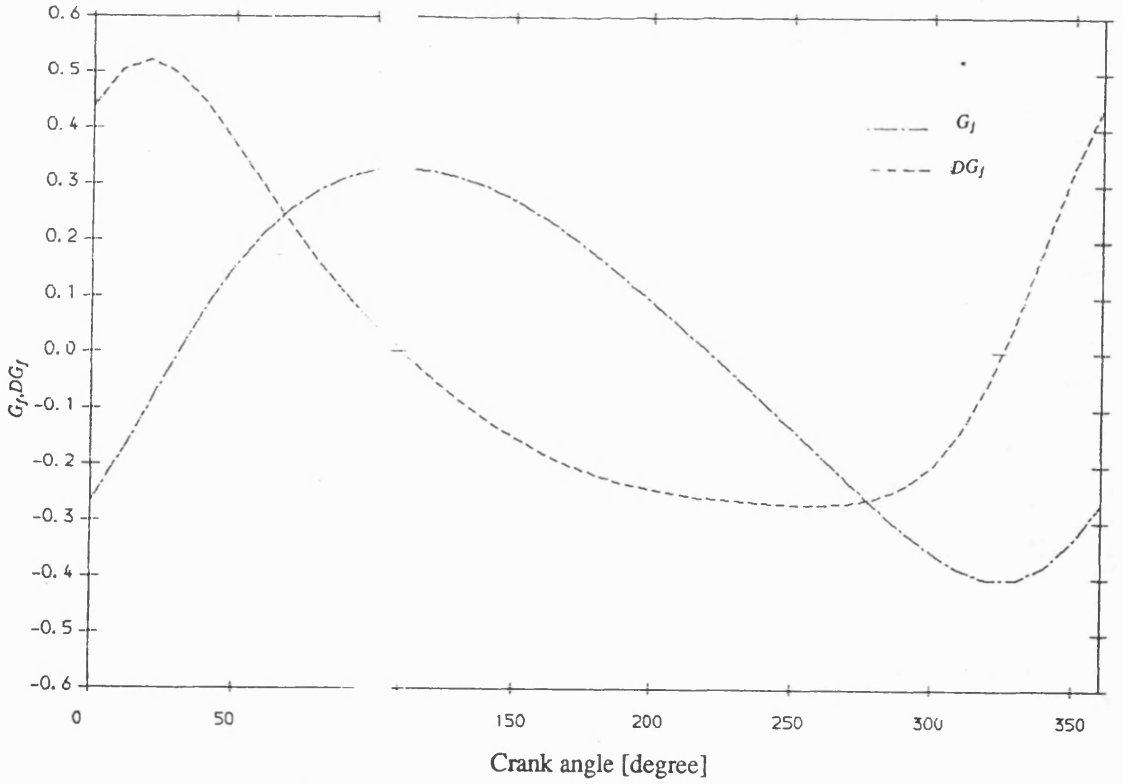

Fig 6.2.2 Follower velocity ratio G_f and its derivative DG_f

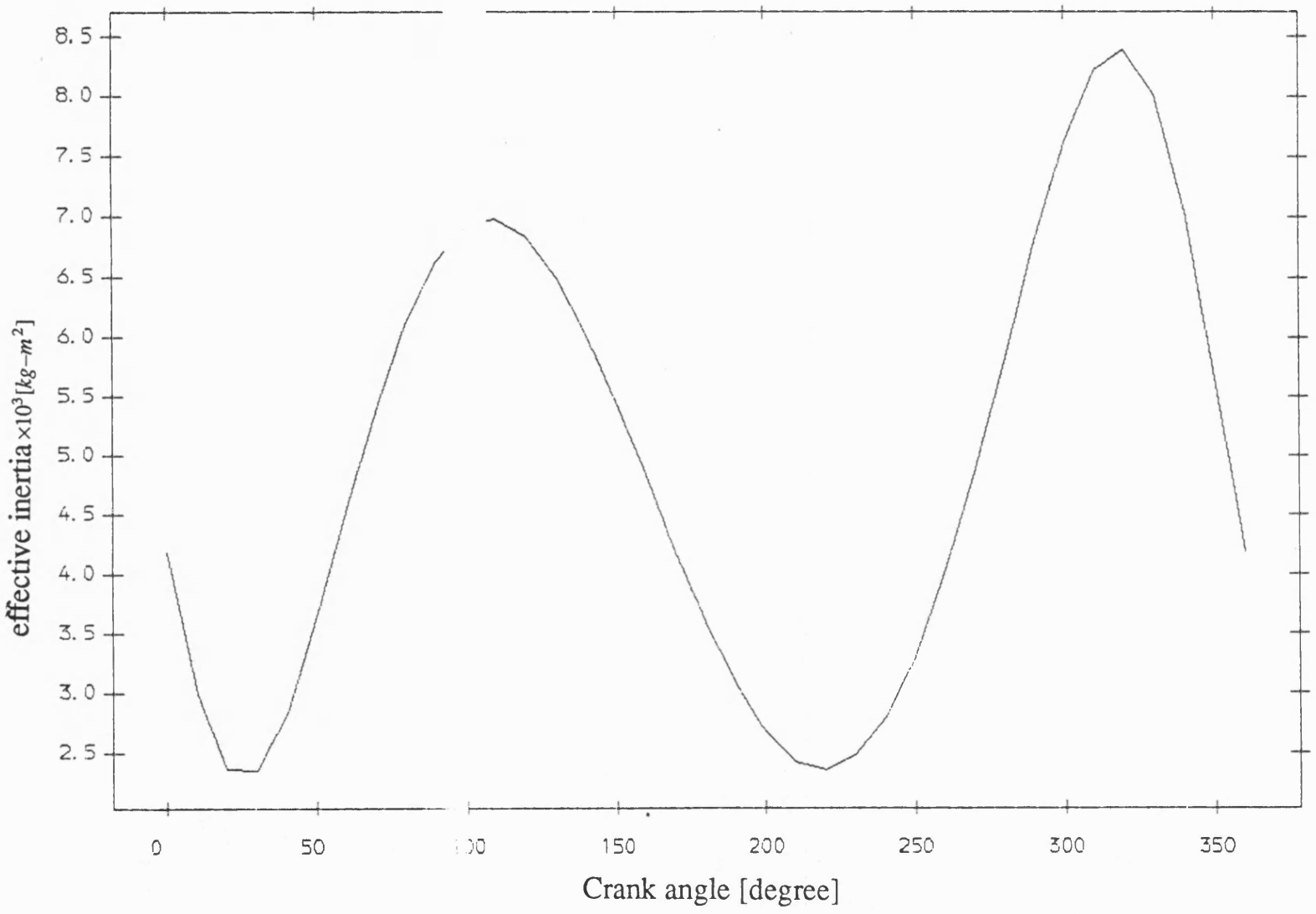

Fig 6.2.3 Effective inertia, zero clearance

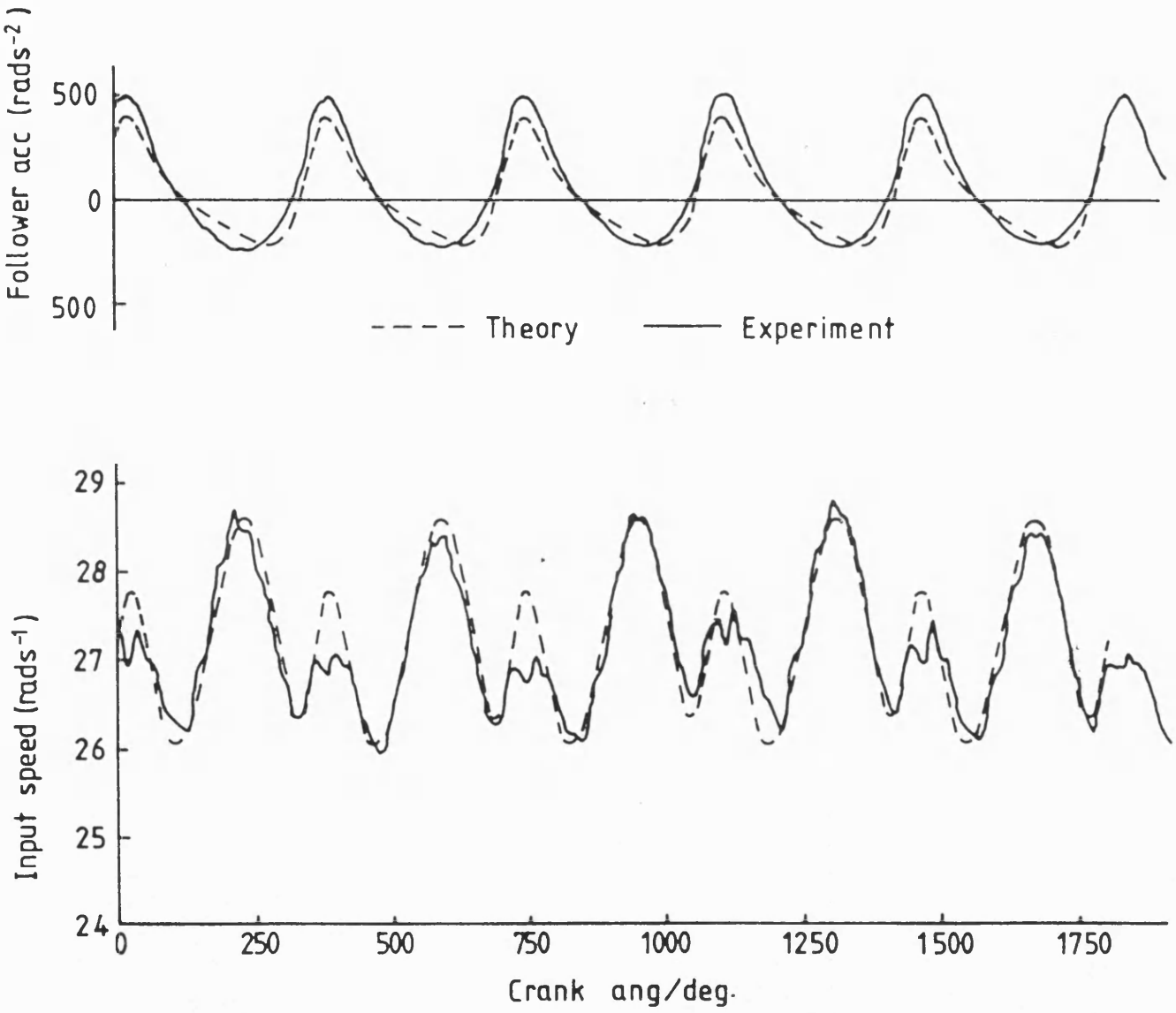

Fig 6.3.1 Without flywheel ($I1 = 0{\cdot}036 kg-m^2$) mean speed= 260 rev/min zero clearance Simulation version experiment.

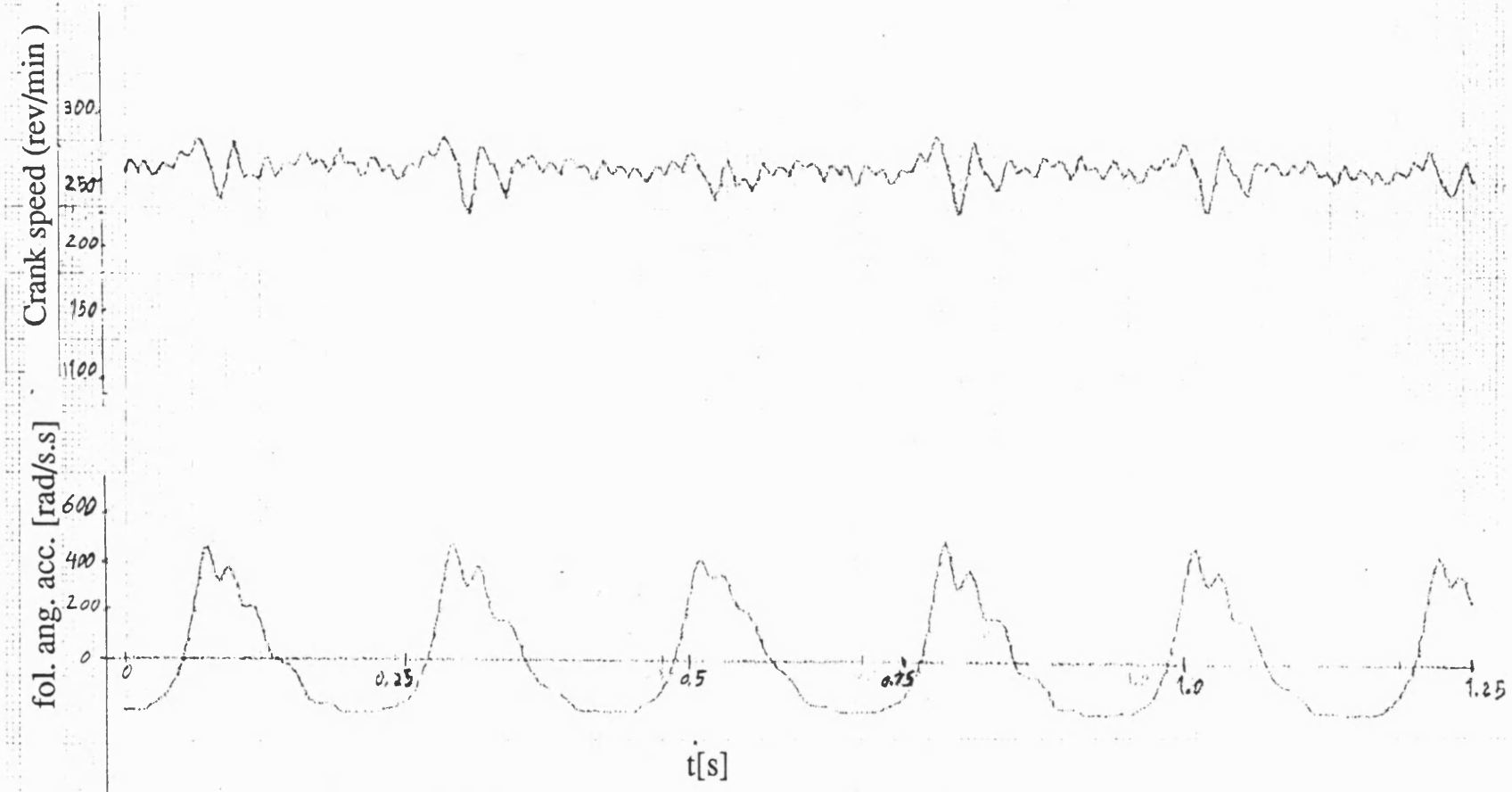

Fig 6.3.2 Crank speed and follower acceleration , experimental with fly wheel; zero clearance

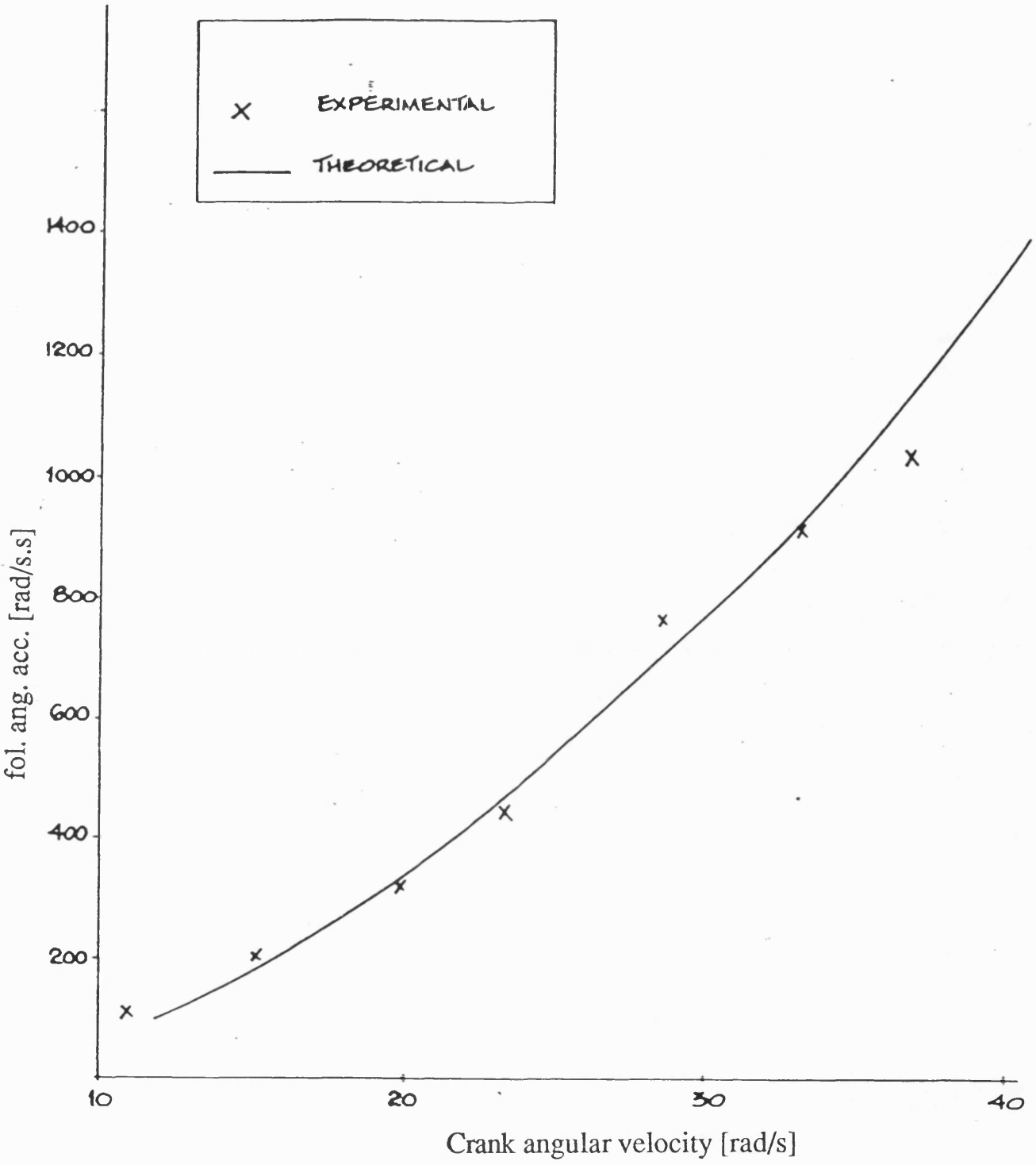

Fig 6.3.3 Follower pk-pk acceleration , zero clearance

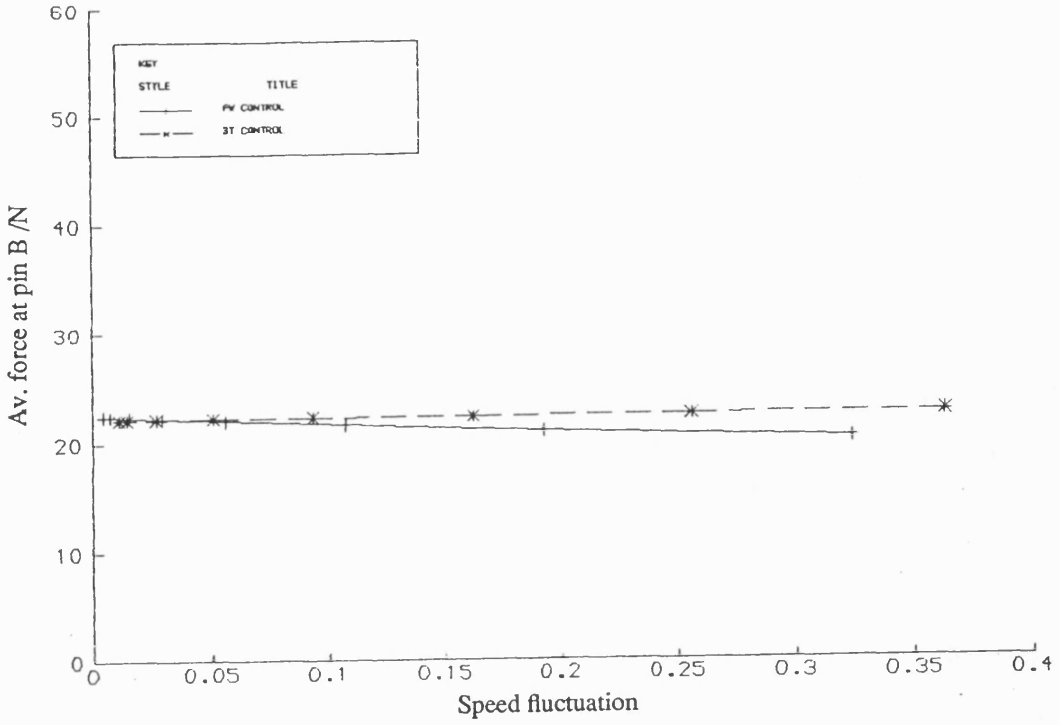

Fig 6.5.1 Av. force at pin B v speed fluctuation
mean speed 290 rev/min

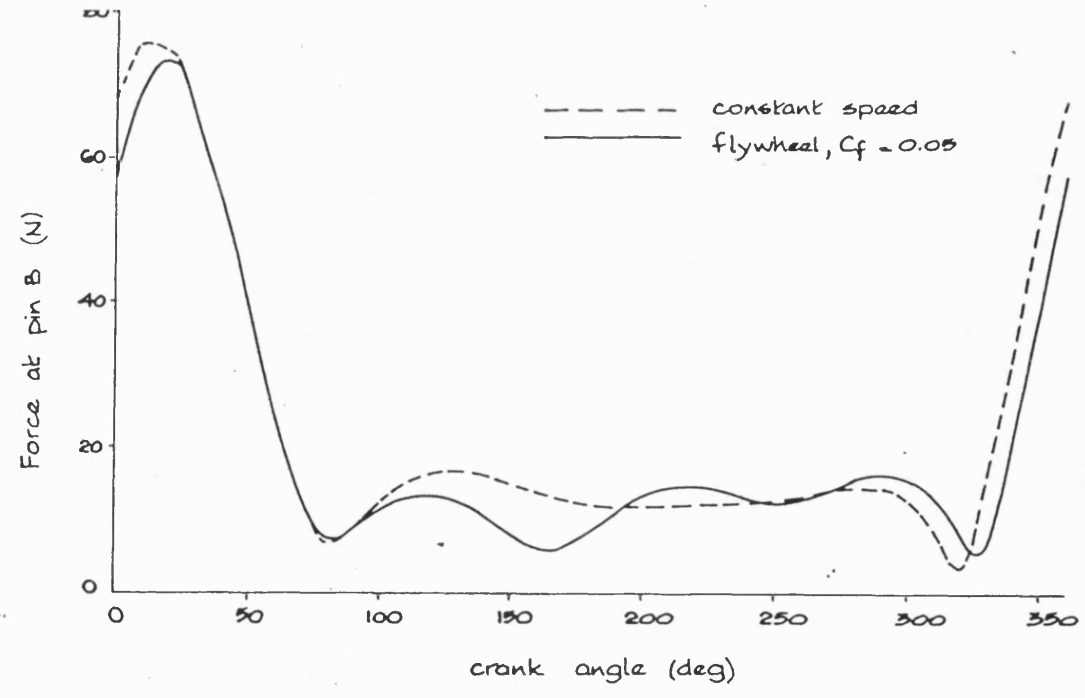

FIG. 6.5.2 Force at pin B, mean speed 290 rev/min.

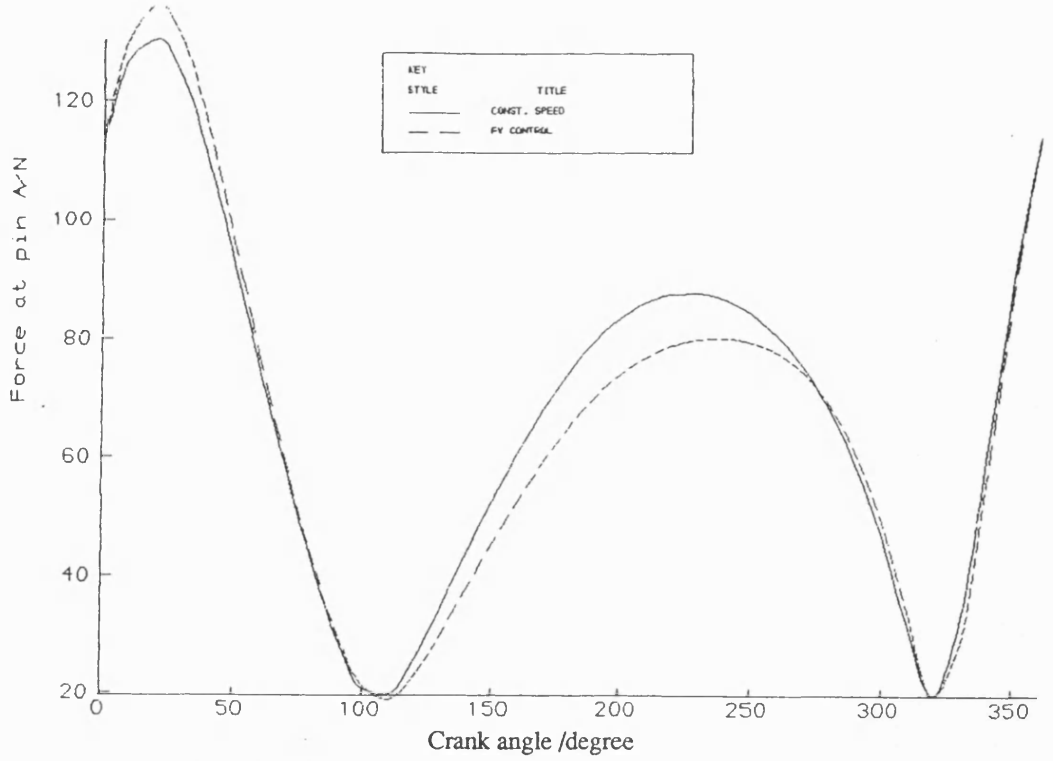

Fig 6.5.3 Force at pin A , speed fluctuation = 0.05
mean speed 290 rev/min

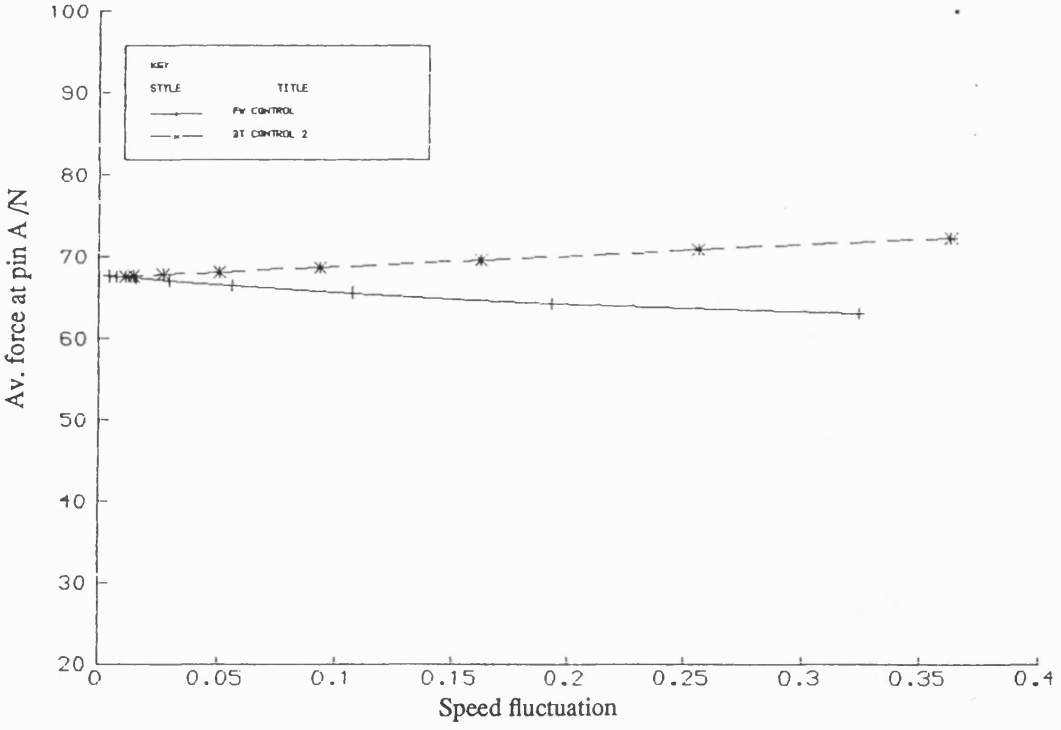

Fig 6.5.4 Av. force at pin A v speed fluctuation
mean speed 290 rev/min

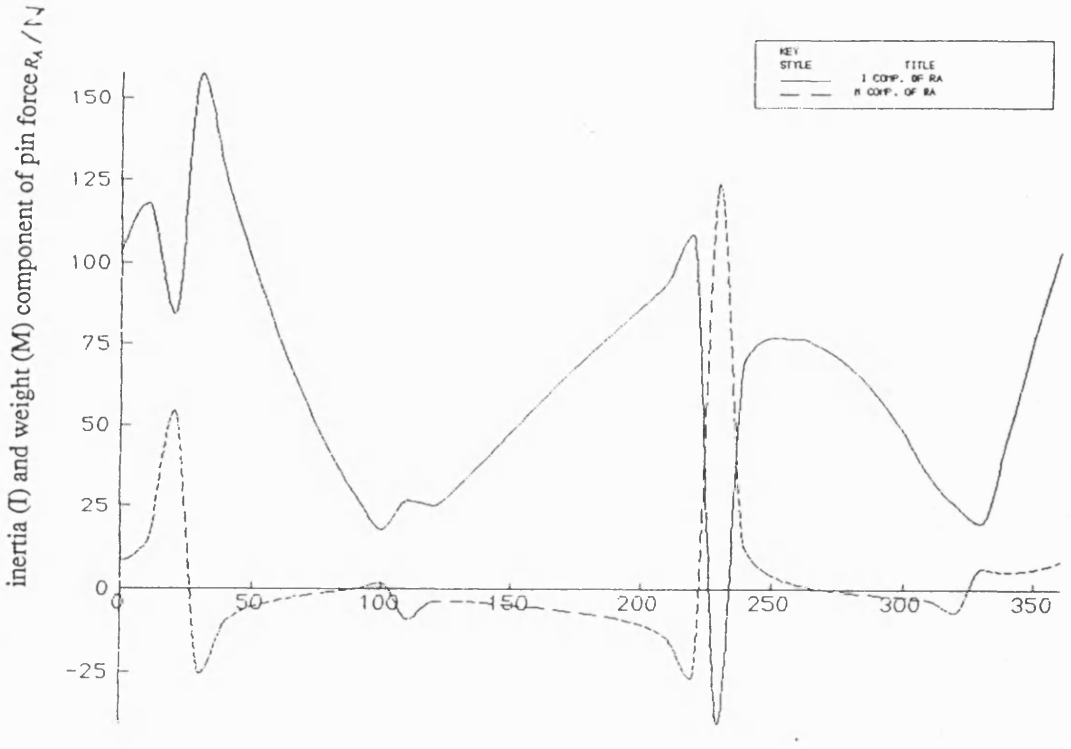

Crank angle/degree

Fig 6.5.5 Pin force components , flywheel 0.0575 kgm^2
mean speed 290 rev/min

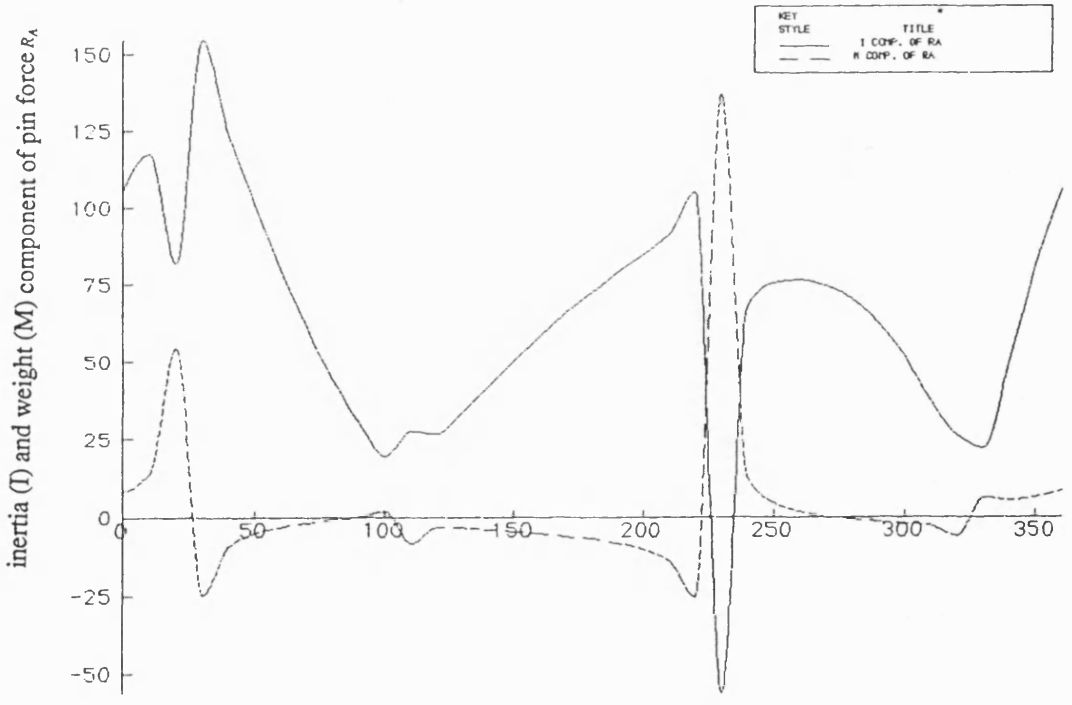

Crank angle/degree

Fig 6.5.6 Pin force components , flywheel 0.23 kgm^2
mean speed 290 rev/min

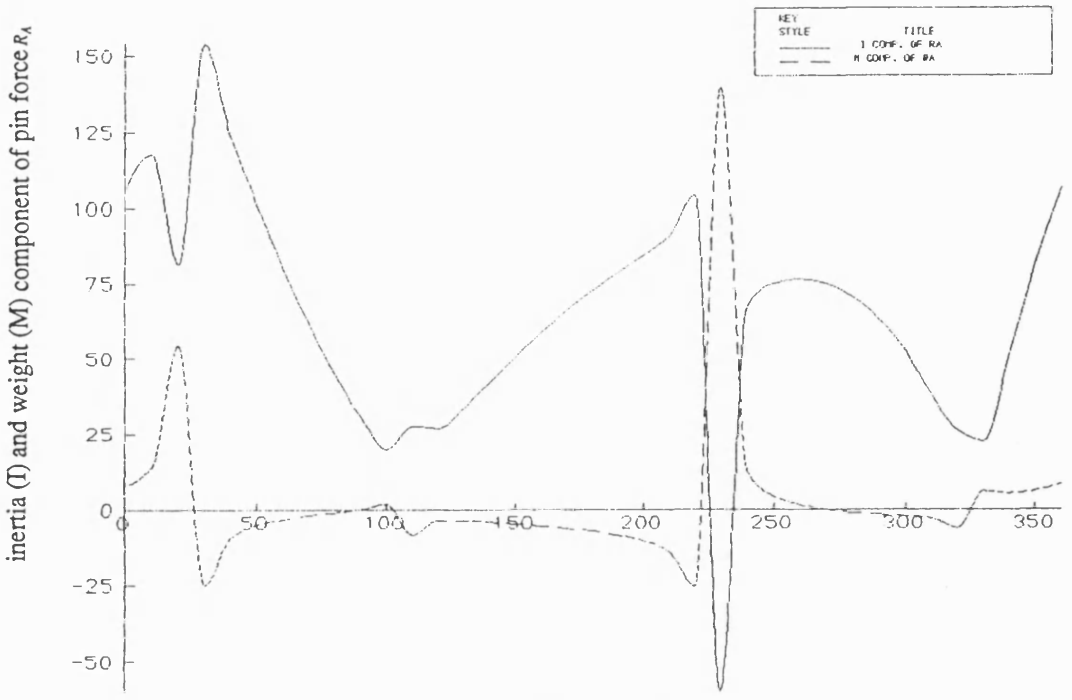

Fig 6.5.7 Pin force components , flywheel 0.46 kgm^2
mean speed 290 rev/min

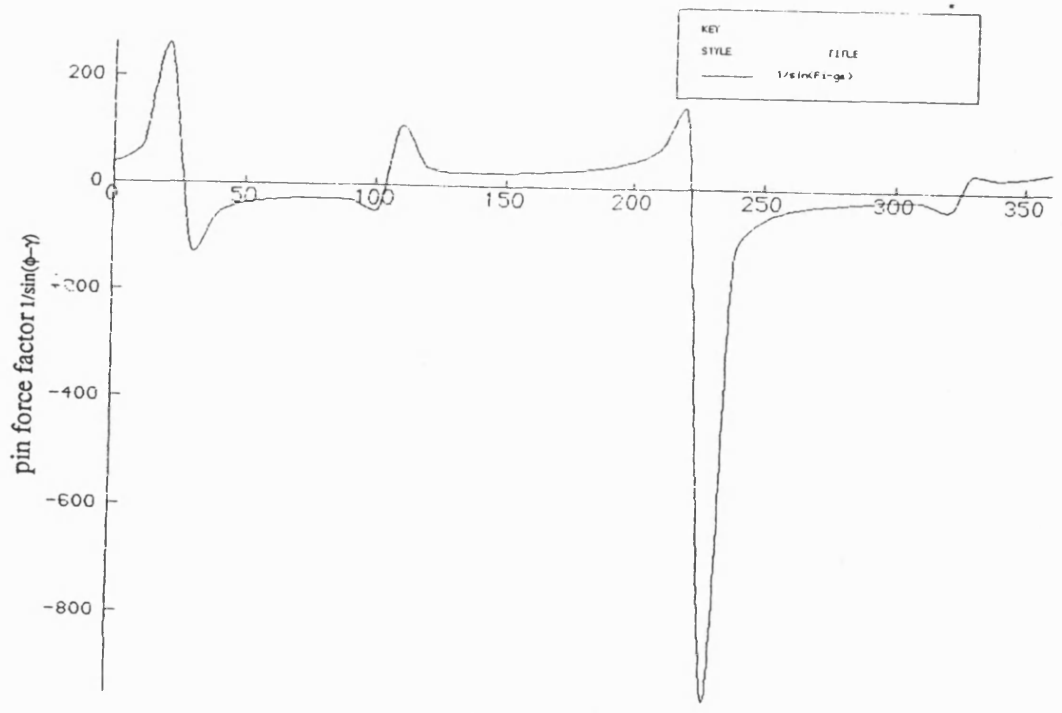

Fig 6.5.8 Pin force factor, fly wheel 0.23 kgm^2
mean speed 290 rev/min

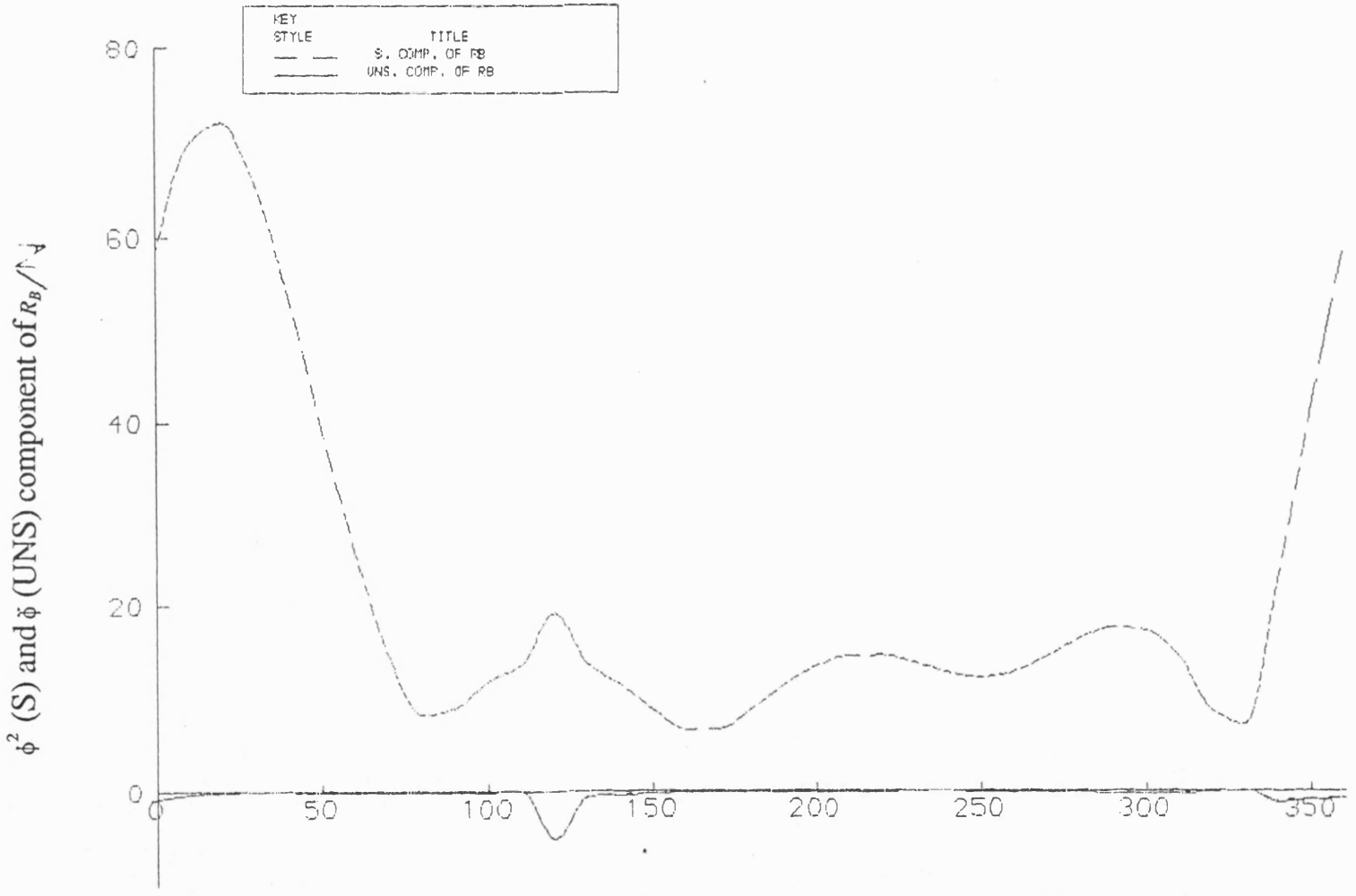

Fig 6.5.9 Components of pin force R_B (S=steady, UNS=unsteady)
fly wheel inertia 0.23 kgm^2 , mean speed 290 rev/min

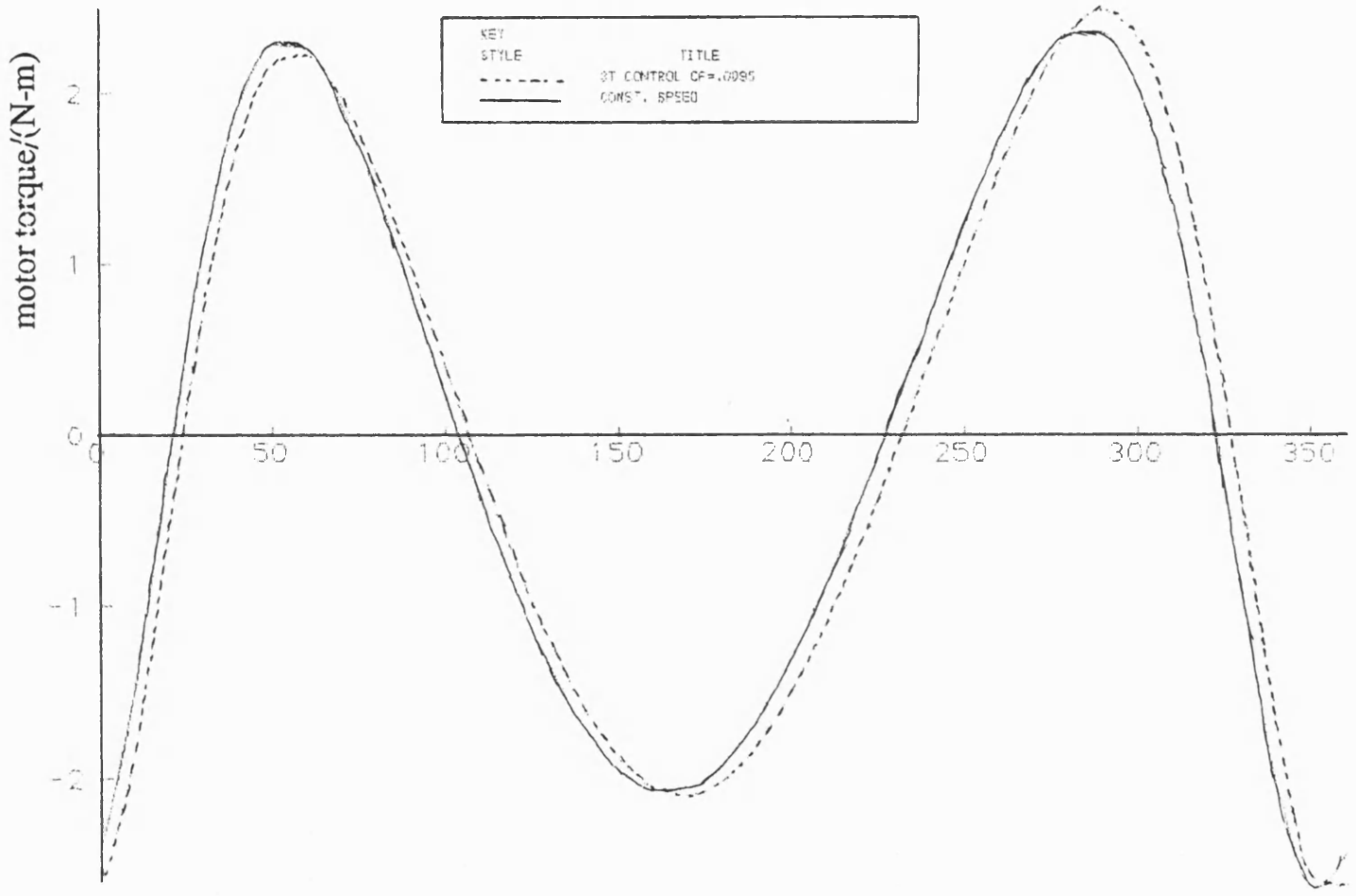

Crank angle/degree

Fig 6.5.10 Torque v crank angle, (a) high gain 3T control (b) constant speed fly wheel $0.036 kgm^2$, mean speed 263 rev/min

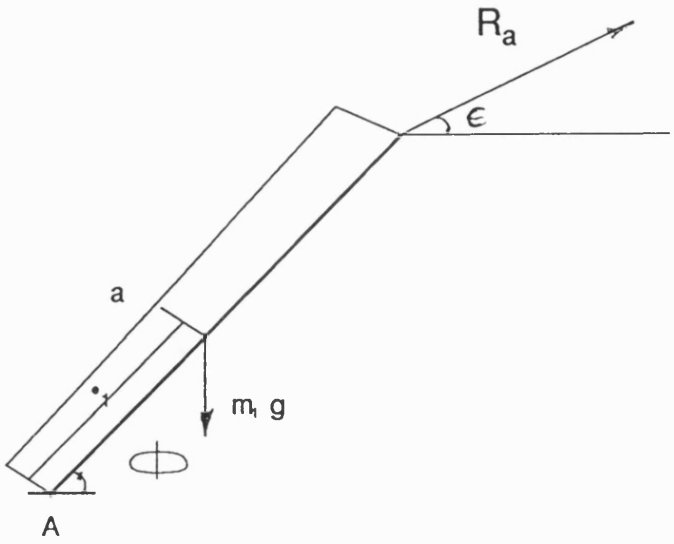

Fig 6.5.11 Crank free body diagram

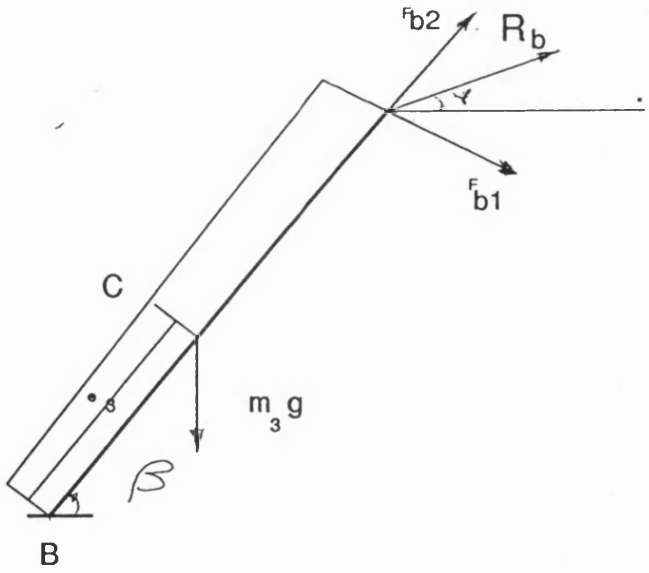

Fig 6.5.12 Follower free body diagram

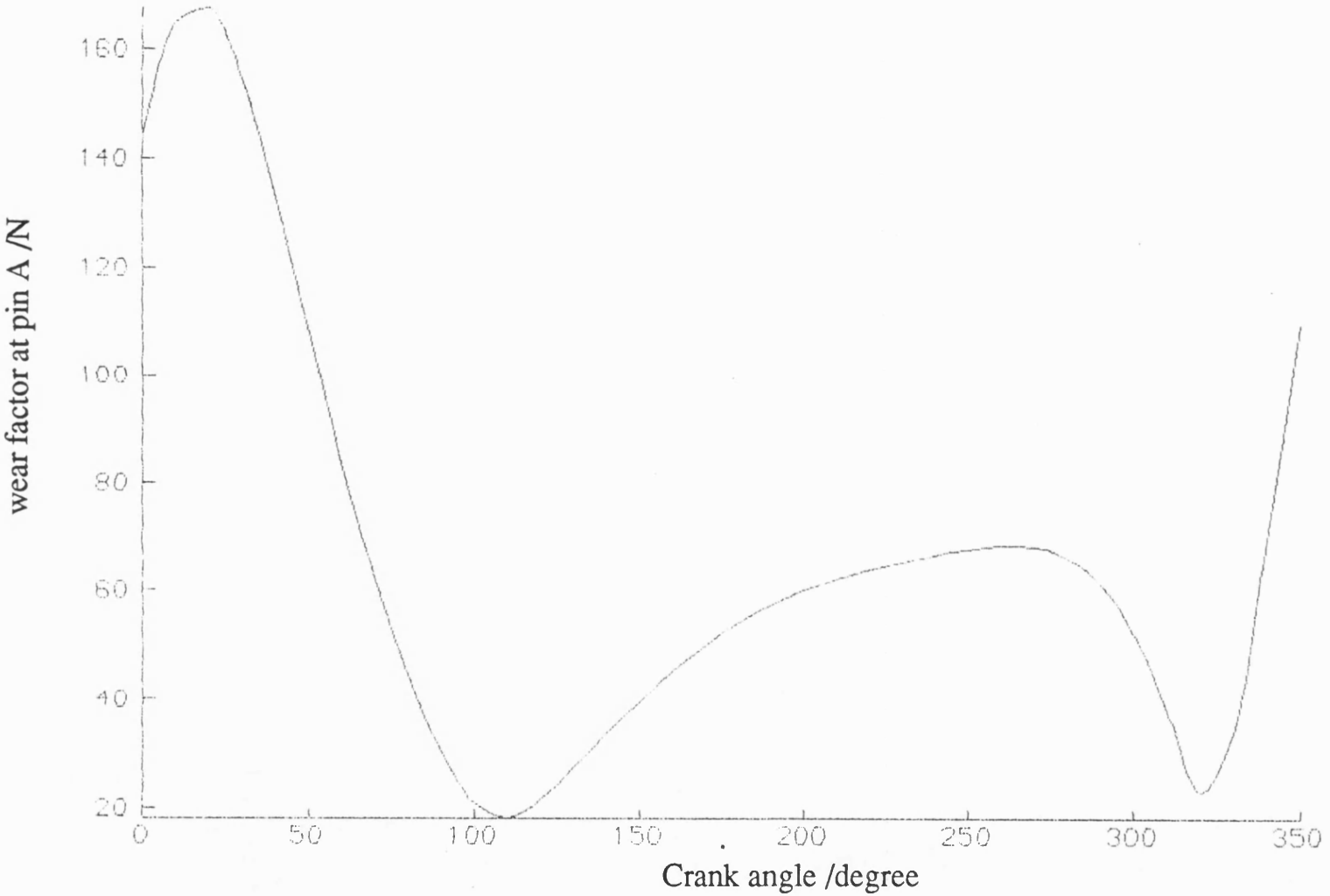

Fig 6.6.1 Wear factor at pin A , mean speed 290 rev/min

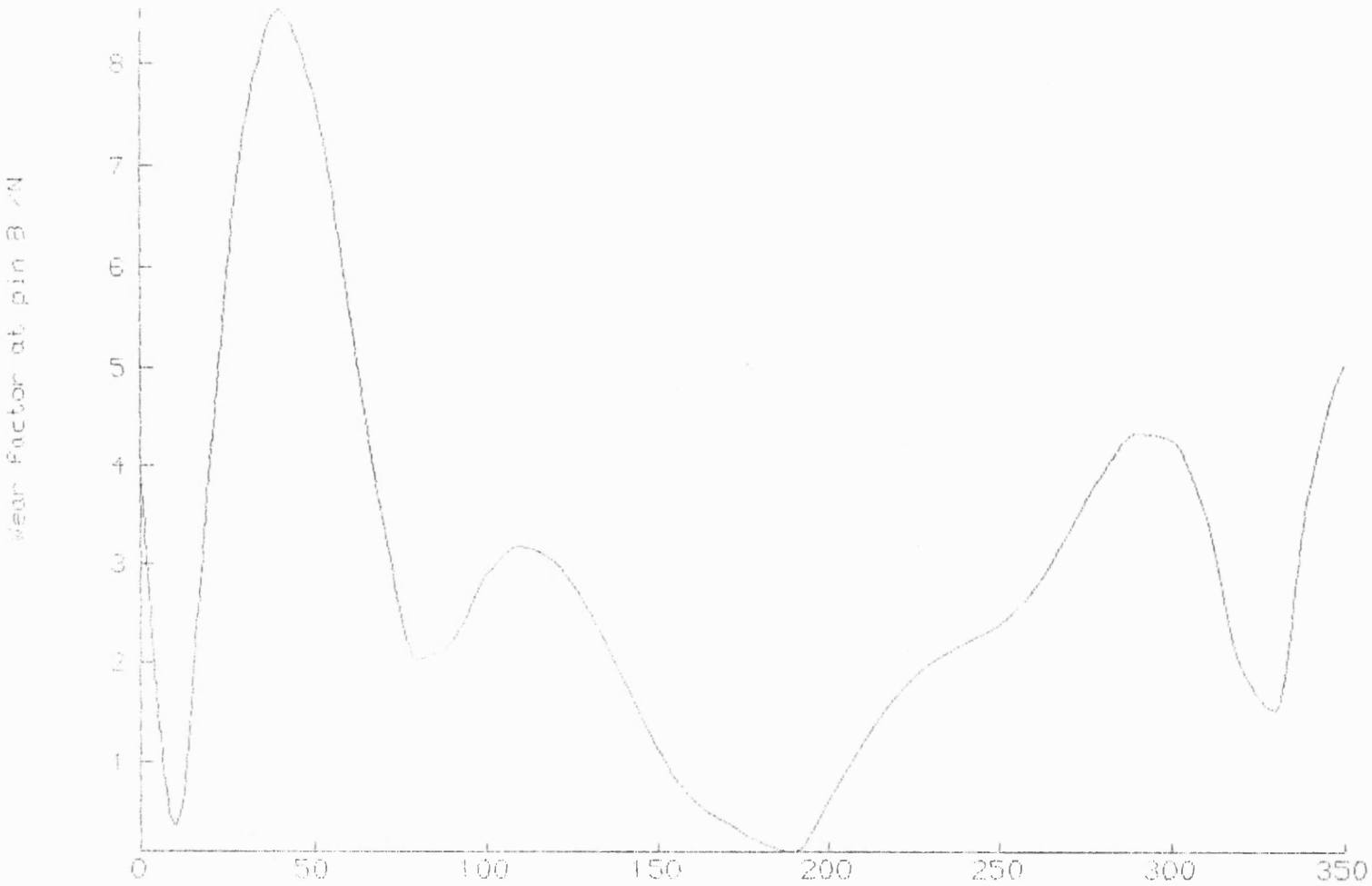

Fig 6.6.1a wear factor at B, mean speed 290 rev/min

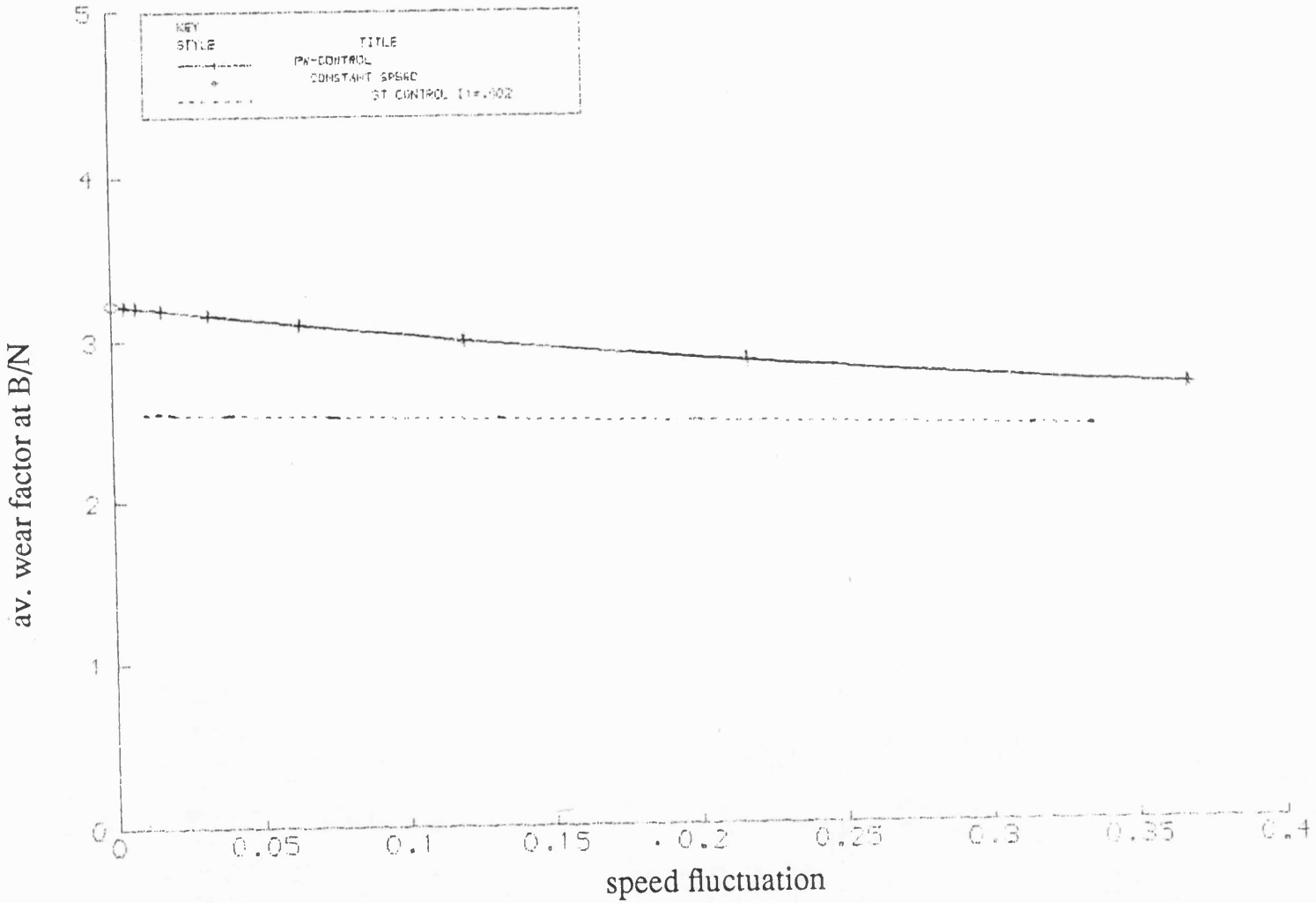

Fig 6.6.2 Av. wear factor at B , mean speed 263.5 rev/min

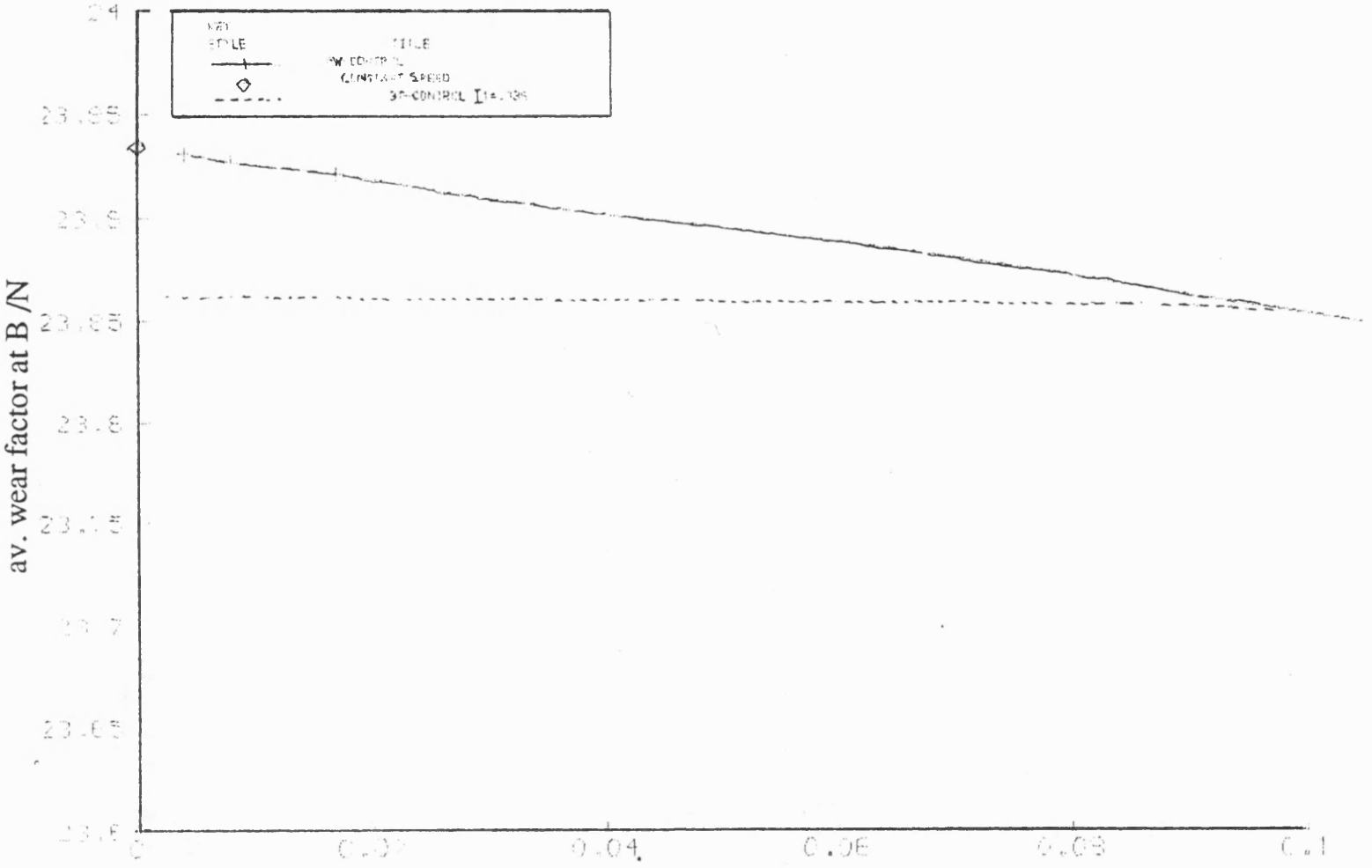

Fig 6.6.3 Av. wear factor at B, mean speed 263.5 rev/min

friction load 20 N-m

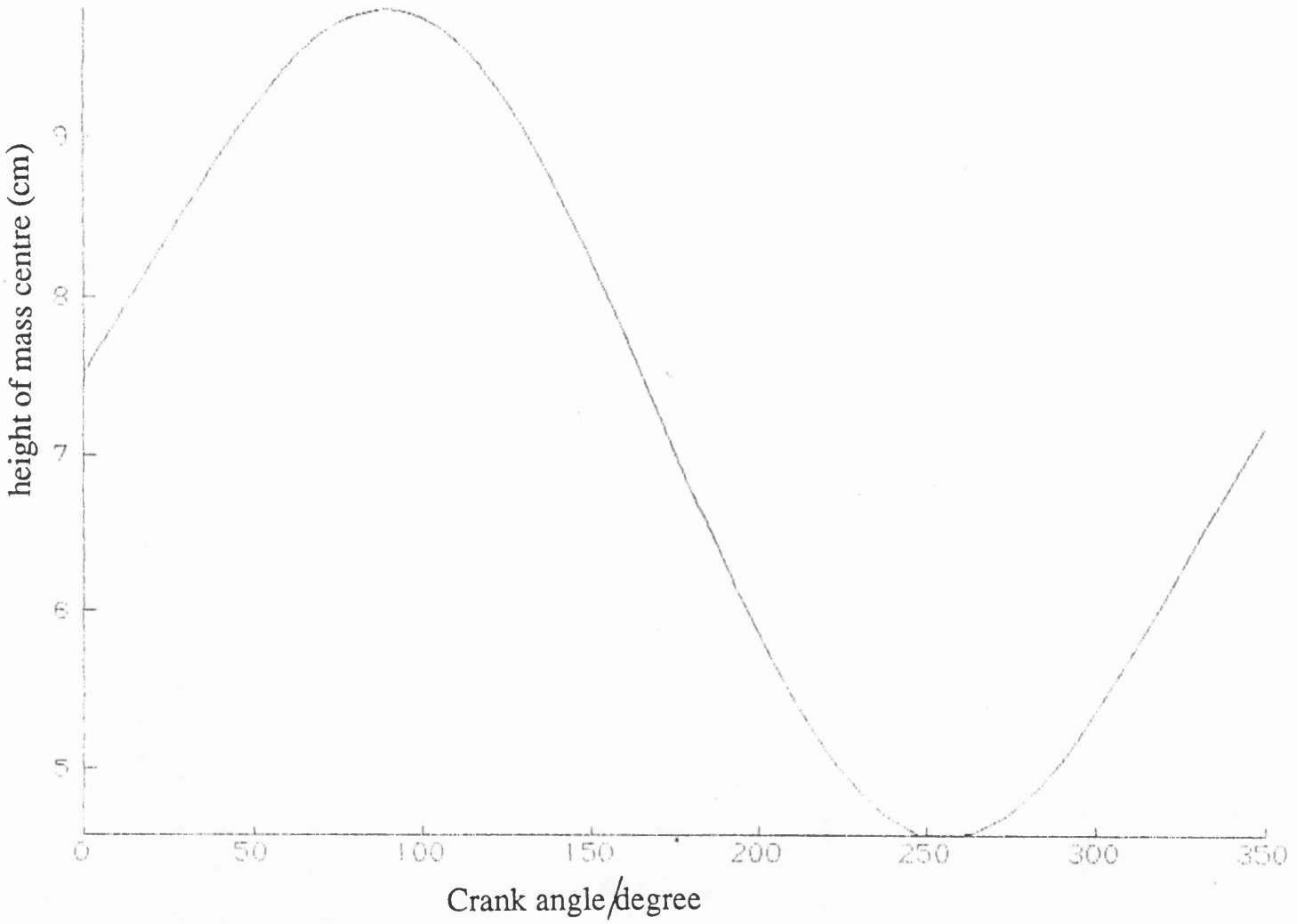

Fig 6.7.1 Height of mass centre

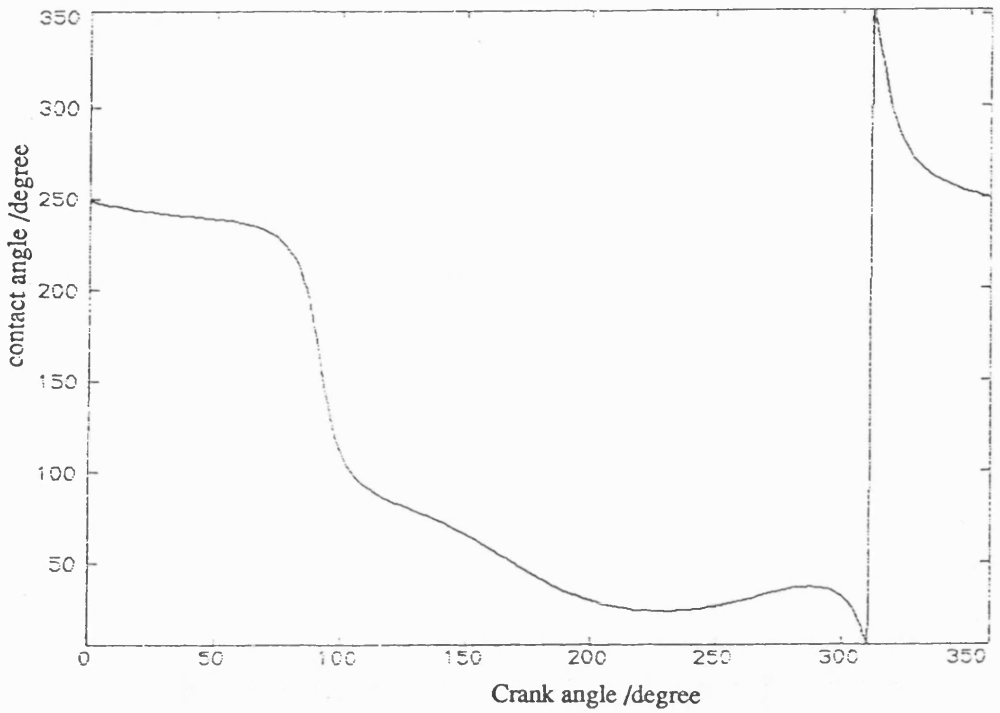

Fig 6.8.1 Contact angle γ, mean speed 206 rev/min
fly wheel inertia $0.036 kgm^2$

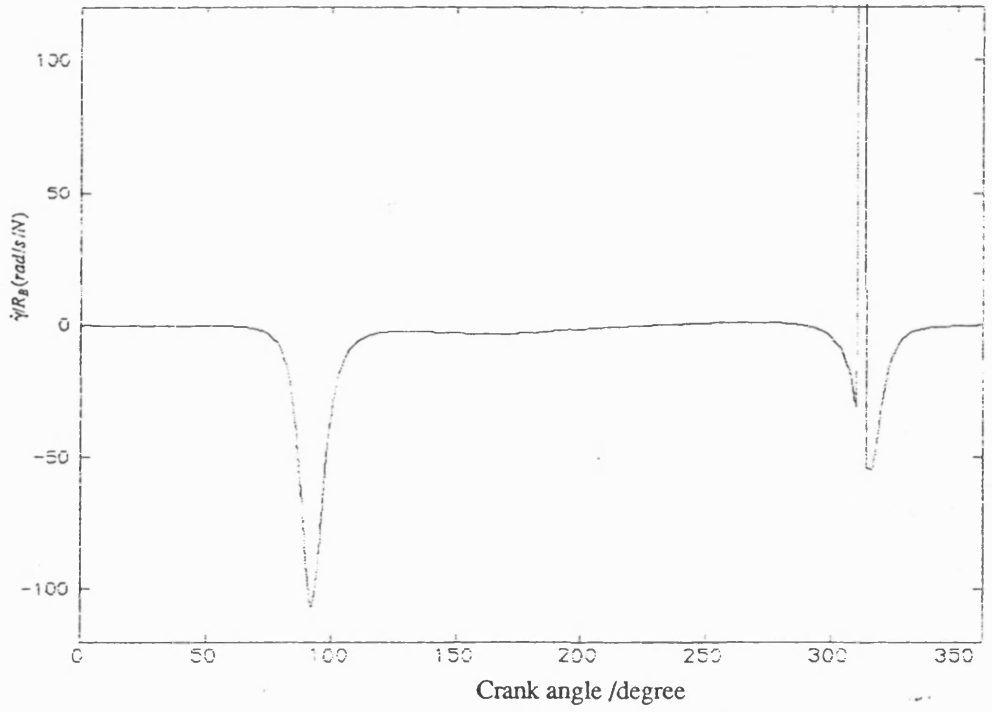

Fig 6.8.2 E&W contact loss criteria , mean speed 206 rev/min
fly wheel inertia $0.036 kgm^2$

CHAPTER 7

THEORETICAL AND EXPERIMENTAL RESULTS

7.1 Introduction

This chapter is mostly concerned with theoretical results and comparison with the experimental counterpart.

The comparison made for case of a joint with diametral clearance of 0.25mm is between coupler and follower.

In sec 7.2 pin forces for the continuous contact theoretical model were studied. The lateral and longitudinal of the clearance joint force components and also its polar form were plotted. The force oscillation is in the region where it is known from experimental work that contact loss occurs. The continuous contact model and the model with free flight and impact are compared in sec. (7.3).

In sec.(7.4) the predicted pin motion with fly wheel(wfw) and no fly wheel are compared.

Several contact loss criteria , generated from continuous contact model, were plotted against crank angle. They are compared with the experimental contact loss results in sec. (7.5).

In sec 7.6 the lateral and longitudinal displacement of the pin relative to the bush were plotted against crank angle for one and half cycles. The follower angular acceleration , coupler c.g. linear lateral acceleration and crank speed also were calculated. They were compared with the experimental result for speeds of 168, 244, and 327 rev/min.

7.2 Pin forces , continuous contact model

This model assumes contact between bush and pin at all time i.e. no contact loss.

Looking at the variation of force at pin B , the following points can be highlighted(fig7.2.1-7.2.3).

1. The general pattern is similar to that of zero clearance pin force traces(fig 7.2.10-7.2.15).

2. The crank angle at which the first local minima occurs reduces with increasing speed. However the crank angle at the second increases with speed.

3. There is an oscillatory region after each local minimum. The Oscillation amplitude and duration depend on the input speed. For example, at low speed(168 rev/min) the oscillation amplitude and duration of the first region is higher than the second region.

4. With increasing speed(244 rev/min) the oscillation in the first region decreases and that in the second increases. At higher speed (327 rev/min) the oscillation in the second region is greater than that in the first.

5. The oscillation in the longitudinal (Y) component of the force at B is greater than in the lateral(X) component.

6. The general pattern of the B pin force component is similar to that of the follower angular acceleration - see fig(7.2.16 to 7.2.18).

7. At low speed the first local minima of pin forces is smaller than the second. However the second one is smaller than the first at high speed.

It can be seen from the pin force polar plots fig(7.2.4 to 7.2.9)) that the pin force tends toward zero but does not pass through the origin. At those 'flypast' points contact can in fact be lost. If contact is to exist, the model fluctuating indicates that force must exist at the pin with corresponding fluctuating coupler and follower acceleration.

The oscillations in the first region are greater at low speed. The pin force in that region is smaller than that in the second region. However at high speed the oscillations in the second region are greater and also the pin force is smaller than that in the first region.

7.3 Continuous contact and free flight

Comparing continuous contact model with a general model considering free flight the following points are highlighted.

-There is a set of oscillations in pin displacement in the continuous contact model ,

particularly at lower speed(see fig 7.3.1). The greatest oscillation amplitude is around the regions where impact occurs in the general model. In the general model with free flight and impact these oscillation are restricted to the contact loss region(see fig 7.3.2).

-The coupler angular velocity traces in the case when free flight is admitted are not much different from the continuous contact case(fig7.3.3,7.3.4). However the acceleration traces are different in the region where impact occurs in the general model. The impacts in the model with free flight mode are greater than the oscillation amplitude in the continuous contact model(7.3.5 , 7.3.6). In the general model the coupler acceleration oscillation passes through zero in the impact region. However in the continous contact model in the area corresponding to those region the coupler acceleration oscillation tends toward zero by oscillation but does not pass through.

The oscillatory region occurs somewhere close to the area which the coupler acceleration is around max. or min. This means the coupler angulur velocity is close to zero in those regions. The criterion that contact loss is at the point where the follower angular acceleration is zero will discussed in sec(7.5). This means the follower angular velocity is maximum or minimum. In relative displacement of pin in the bush, the pin jump occurs at these region. Because the angular velocity of the coupler is around zero, however that of the follower is around max.

It was also observed from experimental traces that between contact loss and impact there is a region where the follower acceleration is approximately constant and close to zero (see sec.(8.2)).

7.4 Comparison of wfw and nfw pin motion in theoretical model

At low speed (168rev/min) the rising edge in wfw slightly leads that at nfw however its falling edge lags that at nfw case(see fig(7.4.1,7.4.2). This may be due to greater input speed in wfw case ,relative to nfw, around rising and falling edges. However the mean input speed for both cases are the same(see fig(7.4.3). The pin jump at rising edge in wfw case is greater than at nfw. This is possibly due to greater inertia . Greater input inertia means input velocity is nearly constant in wfw case. However in nfw case input speed drops it causes decreasing of the coupler angular velocity at rising edge region. This leads to smaller pin jump in nfw case.

Since the speed fluctuation decreases with speed, the nfw input speed at nfw case tend to that at wfw. Therefore at greater speeds(244, 327 rev/min) the rising and falling edges in the nfw and wfw cases occur at the same crank angle position(see fig(7.4.4 to 7.4.7)). However in the experimental traces (see sec.(8.2)) those at wfw case lag that at nfw case. The reason is that in the theoretical model the net input torque is assumed constant. It is assumed that the motor can deliver at any instant the torque required to maintain constant mean speed. However in practice the input torque is supplied via speed contoller. The controller response to a demand torque variation has some delay which depends on the system(controller+ linkage) time constant. The delay of wfw case relative to the nfw depends on the difference in the time constants of the two cases.

7.5 Comparison of criteria with the experimental results

As discussed in section 4.7 a monitoring contact-loss circuit was made and the crank angular position was recorded with a high resolution encoder. Using a data

acquisition system the contact-loss signal was plotted against the crank angle for different input speeds. The signals after processing and scaling define exactly the starting point of the experimental contact-loss (as well as its duration).

The criteria which were discussed earlier can be compared with the above experimental results as follows: Each criteria is obtained using continuous contact model.

The Earles and Wu criterion was explained in section 6.8 , is $\frac{\dot{\gamma}}{R_b}$ for zero clearance.

A similar criterion for the clearance case was considered as $\frac{\dot{\alpha}}{R_b} > 1$ where

γ = direction of pin force in zero clearance case(radian)

α = clearance link angle(radian)

R_b = B pin force at clearance case (N)

$\dot{\alpha}$ = clearance link angular velocity (rad/s)

Earles and Wu criterion for the clearance case and also $\frac{\ddot{\alpha}}{R_b}$, which is the major part of the Bengisu criterion ,assuming continuous contact, were plotted for three different speeds(fig 7.5.1a to 7.5.6a). The clearance angle also was plotted(see fig 7.5.13 to 7.5.15). There are two sharp falls in each cycle. These are appeared in the criteria plots as two distinguishable regions corresponding to the contact loss regions.

They were compared with the experimental results (fig 7.5.7 to 7.5.12). The comparison is summarized in table 7.5.1 (where the numbers in the parenthesis in the tables refer to crank angle position) which may be explained as follows:

For the first region the E&W criterion lags the crank angle of observed contact loss . At low speed the lag is considerable . At high speed the predicted start to the second region also lags the experimental trace.

The criterion was also compared with the experimental greasy bearing contact loss results(table 7.5.2). It was observed that the E&W criterion lags the experimental result. In the first region the lag is greater at low speed than at higher speed.

The criterion $\frac{\ddot{\alpha}}{R_b} > 6000(rad/s^2)/N$ is in fair agreement with the experimental results at high speed. However at low speed it slightly leads the experimental results in the second region and for the first contact loss region slightly lags .

For the greasy bearing case it is in fair agreement in the second region. In the first region it also agrees at high speed. However it lags the experimental trace at low speed.

A similar criterion in the form of $\frac{|\ddot{\alpha}|}{R_b} > 6000$, with the same units as before, was compared with the experimental results.

This criterion most of the time has a small lead with respect to the experimental results. However at high speed it agrees with the experimental contact loss in the first region.

With the greasy bearing case the criterion leads the first contact loss region at low speed. However it agrees in the second region.

At high speed the criterion predicts well at the first region. However the second region leads the experimental results. The lead in this case is longer than that of ungreased bearing case.

In the third method when $\frac{|\ddot{\alpha}|}{R_b} > 6000 rad/s^2/N$ the programme goes into the free flight mode. If free flight does not actually occur, i.e. even with considering the chain as two separate pendulum in the model the pin will not leave the bush, the model returns to the following mode (contact). In this way the actual contact loss criterion is determined by the programme. The criterion could be employed at all crank angles but this would be a waste of computing time. The method is invoked just before expected contact loss.

7.6 Comparison theoretical and experimental results (d. clea.=0.25 mm)

7.6.1 Mean speed = 168 rev/min

Input speed

The experimental input speed trace has some small oscillation at the start of each cycle, but varies little with crank angle often - see fig(7.6.1). Agreement between theory and experiment is fairly good. The oscillation is believed to be due to "SCR" speed controller characteristic - see sec(4.3). The effect of this oscillation appears in acceleration and displacement traces as will discussed in this section.

A (longitudinal) displacement traces

The rising and falling edges of the experimental trace lag those of the theoretical trace (see fig(7.6.2)) . There is some discrepancy before the falling edge . That may

be due to misalignment or to the fact that the pin is very close to both probes at this region(the manufacturer's recommendation is that the minimum distance to prevent interference is twice probe tip diameter i.e 16mm. The pin path is close to that recorded for a dry bearing case(see sec.(8.4)). The lag may be partly due to assumption of the theoretical model. This assumption requires a source to meet the demand torque fluctuation instantaneously. However in practice the speed controller supplies the torque, but with some delay which depends on its time constant. The filter which was used to filter the experimental signal, also caused slightly delay. Assuming friction there will be less oscillation in the theoretical trace(see fig (7.6.3)).

B (lateral) displacement trace

Both rising and falling edges lag those of the theoretical results (fig(7.6.4)). The reason is the same as discussed in this section earlier for A traces. There is some oscillation in the region between falling and rising edges in the experimental which is due to fluctuation in input speed . There are some oscillation immediately after falling edges in both experimental and theoretical result which is due to contact-loss at this region . Assuming friction in the theoretical model the oscillation amplitude after falling edge will be reduced (see fig(7.6.5).

Follower angular acceleration traces

The general pattern of the experimental and theoretical traces are the same (fig(7.6.6)) . However the experimental impact regions lag the theoretical ones. That may be due to speed controller response and partly due to amplification of the experimental signal. The impacts in the experimental traces are greater than that of theoretical There is some noise in the experimental trace .

Coupler c.m. (lateral) acc.

Experimental impact regions lag the theoretical (see fig(7.6.7 ,7.6.8)). This is the same as other traces which discussed in this section However the general patterns are the same and the variations are similar. Because the signal voltages are small , results are prone to errors including the amplifier error(see sec.(4.2)).

7.6.2 mean speed = 244 rev/min

Input speed

In general the theoretical input speed fluctuation is roughly sinusoidal with small amplitude(see fig(7.6.9)). The experimental trace has some oscillation at the start of each cycle which is greater than at lower speed . That is due to "SCR" speed controller characteristic (sec. 4-2) . The effect of this oscillation appears in acceleration and displacement traces as will discussed later .

A (longitudinal) displacement traces

As was discussed in the 168 rev/min case the experimental rising and falling edges lag those of the theoretical trace(see fig(7.6.10)) . However the lag is greater than that at lower speed. The discrepancy before the falling edge (around 225 ° crank angle) is smaller than that at lower speed. That may be due to misalignment which give rise to a force component perpendicular to the four bar plane. Agreement between theory and experiment is closer at higher speeds(see fig (7.6.10,7.6.2)). When a dry(cleaned) bearing is used, agreement is fair at all speeds considered. The lag between predicted and recorded pin jumps increases with speed. This may be due to speed controller and filter time constant. The rising and falling edges are followed by some oscillations in both experimental and theoretical traces. The frequency of

oscillation is predicted correctly but amplitude after rising edge is greater than recorded. The oscillation amplitude decreases by assuming friction in the theoretical model (see fig(7.6.11)).

Lateral pin displacement (B) traces

As before,the rising and falling edges lag those of the theoretical result(see fig(7.6.12)). However the lag of the rising edge is smaller than at lower speed, which cannot be due to filter time constant. In both traces the pin jump length (flight length) at the rising edge is greater than at the lower speed; however at falling edge the jump is smaller. The oscillation in the region between falling and rising edges in the experimental trace, due to input speed fluctuation, is greater than at lower speed. There are some oscillations immediately after the falling edges in both experimental and theoretical results, with approximately the same frequency. occurs at the end of free flight and beginning of contact. After the falling edge, the oscillation amplitude of the experimental trace is less than in the theoretical model. That may be due to the friction in the system or flexibility of the links, ignored in the theoretical model. There is some high amplitude oscillation just after the rising edge. This has approximately the same frequency and amplitude in the experimental and theoretical traces. The oscillation amplitude in the theoretical model with friction is smaller than the case without friction(see fig(7.6.13)).

Follower angular acceleration traces

This is similar to the lower speed case. However the following points should be noted (fig(7.6.14)) .

The experimental lag of the second impact region relative to the theoretical

prediction is greater than at lower speed. That may be due to the speed controller and the amplifier time constant. The second impact (around 330 °) in both traces is considerably greater than the first . The impacts in the experimental traces are in fair agreement with that of the theoretical model. The peak value of the recorded acceleration is slightly greater than predicted and it is a double peak . This is due to a disturbance in input speed . There is some high frequency oscillation in the experimental trace which is due to noise, the amplitude is greater than that at lower speed.

Coupler c.m. (lateral) acc .

Experimental impact regions lag those of the theoretical model(fig(7.6.15 ,7.6.16)) . The lag of the second region is greater than that of the first. The general patterns are the same and the range of variation is close to each other . There is some discrepancy around the starting of each cycle which is due to input speed disturbance at this region .

7.6.3 Mean speed = 327 rev/min

Input speed

As it was discussed earlier the theoretical input speed is roughly sinusoidal with small amplitude(see fig(7.6.17)). The disturbances in the experimental traces at 25 ° and 385 ° are considerable. It is followed by some further oscillation with approximately the same frequency but of smaller amplitude. The disturbance lags its counterpart at lower speed. This is due to speed controller response to torque variation (see sec.(4.3)).

A (longitudinal) displacement traces

As it was discussed earlier, the experimental rising and falling edges lag those of the theoretical trace - see fig(7.6.18). However the lag of the falling edge is greater than at lower speed. The lag of the rising edge is smaller at the starting point but greater at the ending point. The discrepancy between theory and experiment evident around 225 °; which is probably due to misalignment, is considerably smaller than at lower speed. The oscillation before the rising edge in the experimental trace, which is due to disturbance in input speed , is greater than at lower speed. The rising edge of both experimental and theoretical traces lead their counterpart at lower speed . However their falling edge lag those of their counterpart lower speed . The rising and falling edges are followed by some oscillations in both experimental and theoretical traces . The amplitude of oscillation of the theoretical is greater than that of the experimental, specially around the falling edge. Assuming friction in the theoretical model the oscillation amplitude will be smaller (see fig(7.6.19).

Lateral pin displacement(B) trace

It is similar to lower speed with some differences as follows:

The lag of rising edge relative to theory is greater than at lower speed(see fig(7.6.20 , 7.6.21)). The oscillation in the region between falling and rising edges in the experimental results, which is due to fluctuation in input speed , is greater than at lower speed. The oscillation amplitude of the theoretical trace after the rising and falling edges is greater than the experimental trace . This may be due to assumption of the rigidity of the links in the theoretical model(46).

In both experimental and theoretical cases the rising edges lead and falling edges lag their corresponding position at lower speed (i.e first pin jump occurs earlier, the second later).

Follower angular acceleration traces

These are similar to the traces at lower speed(see fig(7.6.22)). However the lag of the first experimental impact region relative to theoretical is greater than at lower speed. That may be due to the preamplifier time constant . The first impact in the experimental trace is greater than at the predicted value. The peak value of the recorded is greater than predicted. It is a double peak. This is due to a disturbance in input speed which in this region is considerably greater than at lower speed. There is some high frequency oscillation in the experimental trace which is due to noise impact in both traces is considerably greater than the first. The second region lags its counterpart at lower speeds .

Coupler c.m. (lateral) acceleration

As was discussed earlier the experimental impact regions lag those of the theoretical model(fig(7.6.23)) , but the lag is considerably greater than at lower speed. The first impact of experimental is smaller than that of theoretical However the second impact is considerably greater. There is fair agreement between recorded and predicted results. The discrepancy around the starting of each cycle, which is due to input speed disturbance in this region, is greater than at lower speed. Because the values are small, the result is influenced by errors including the amplifier error(sec.(4.10)). Therefore there is some discrepancy before second impact region.

In both theoretical and experimental the first impact region starts earlier than that at lower speeds. However the second impact region starts later than that at lower speeds.

Table 7.5.1 Comparison of the criteria with experimental contact loss

Ungreased bearing with 0.25 mm dia. clearance						
criterion speed(rev/min)	$\frac{\dot{\alpha}}{R_b}$		$\frac{\lvert\ddot{\alpha}\rvert}{R_b}$		$\frac{\ddot{\alpha}}{R_b}$	
	region 1	region 2	region 1	region 2	region 1	region 2
168	lag(25)	=	lead(5)	lead(5)	lag(5)	lead(1)
244		=		lead(5)		lead(1)
327	lag(2)	lag(5)	=	lead(5)	=	=

Table 7.5.2

Greasy bearing with 0.25 mm dia. clearance						
criterion speed(rev/min)	$\frac{\dot{\alpha}}{R_b}$		$\frac{\lvert\ddot{\alpha}\rvert}{R_b}$		$\frac{\dddot{\alpha}}{R_b}$	
	region 1	region 2	region 1	region 2	region 1	region 2
168	lag(20)	lag(8)	lead(10)	=	lag(3)	=
244	lag(12)	lag(3)	lag(3)	lead(8)	lead(10)	=
327	lag(10)	lag(5)	=	lead(10)	=	=

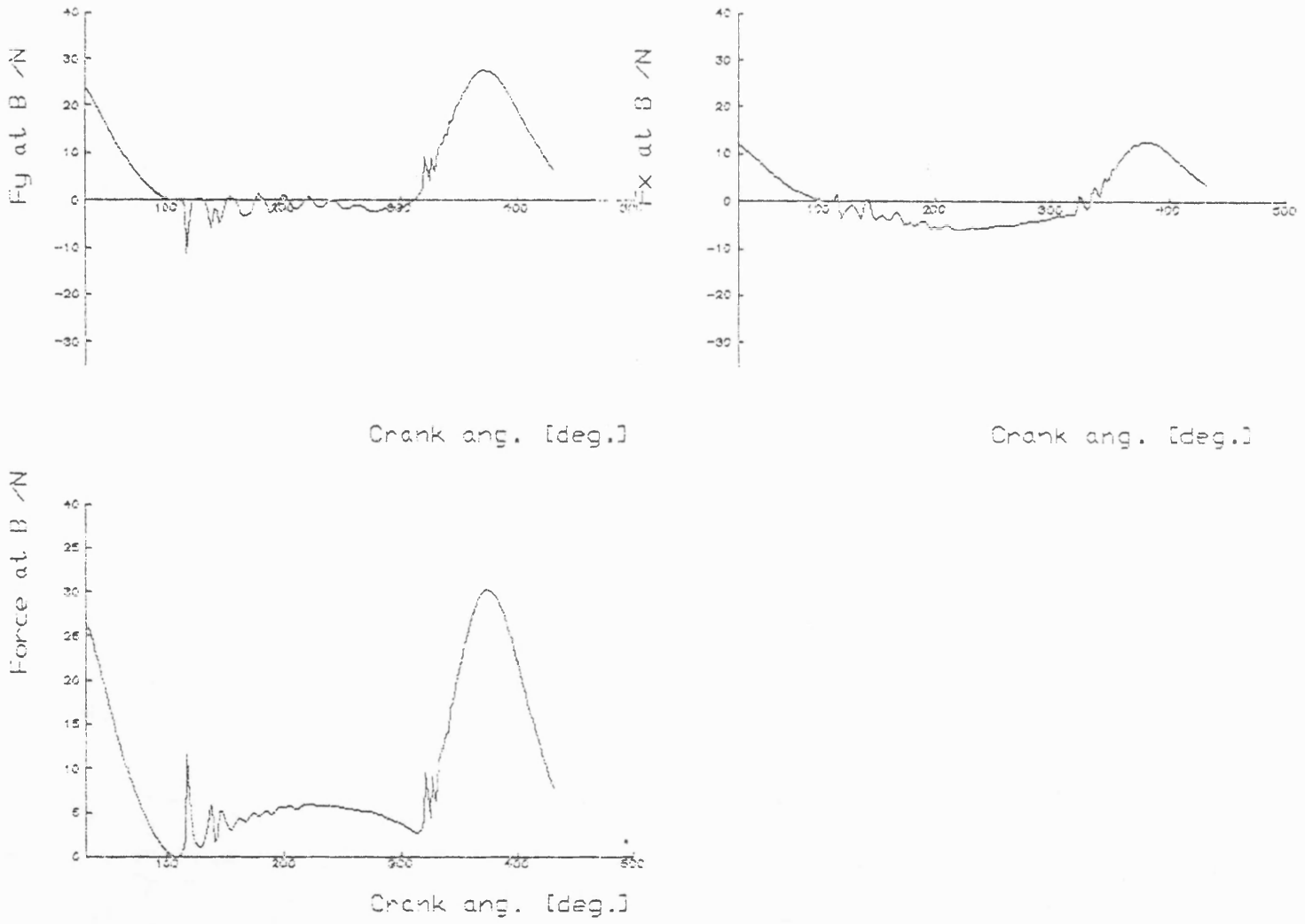

Fig 7.2.1 Pin Force, dia. clearance 0.25 mm,fly wheel inertia 0.23 kg-m.m
mean speed=168 rev/min (continuous contact model)

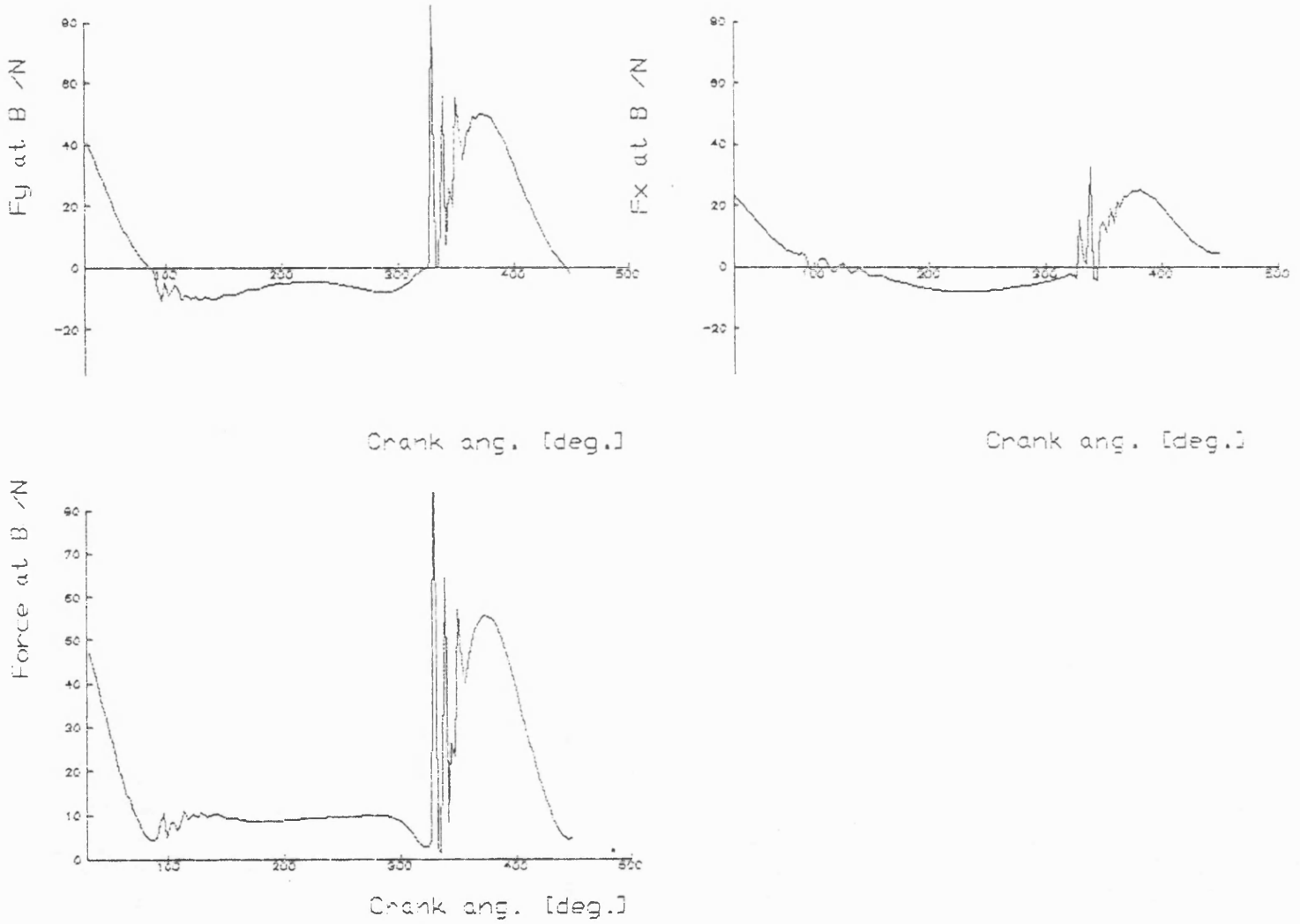

Fig 7.2.2 Pin Force, dia. clearance 0.25 mm, fly wheel inertia 0.23 kg-m.m
mean speed=244 rev/min (continuous contact model)

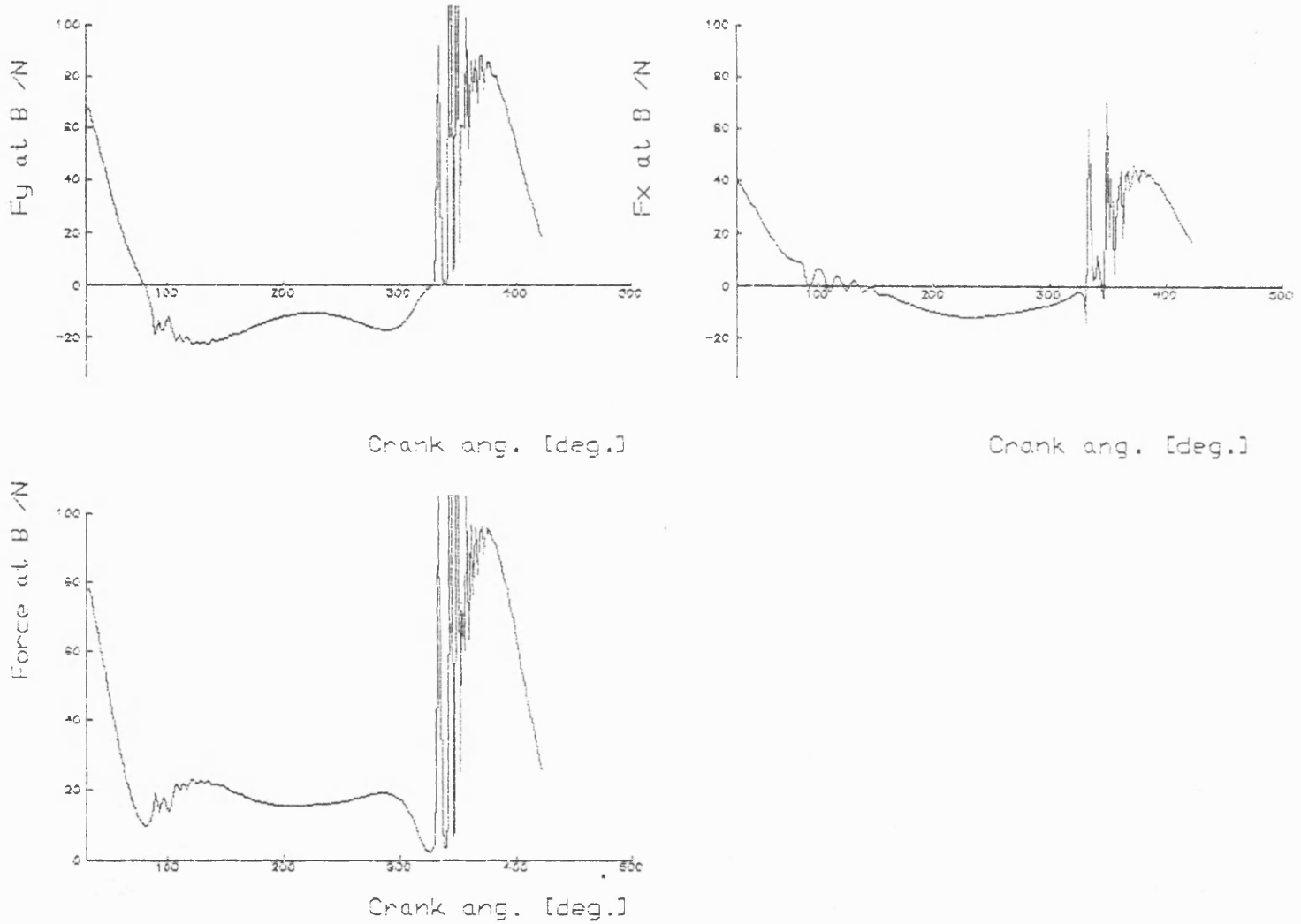

Fig 7.2.3 Pin force, dia. clearance 0.25 mm, fly wheel inertia 0.23 kg-mm
mean speed=327 rev/min (continuous contact model)

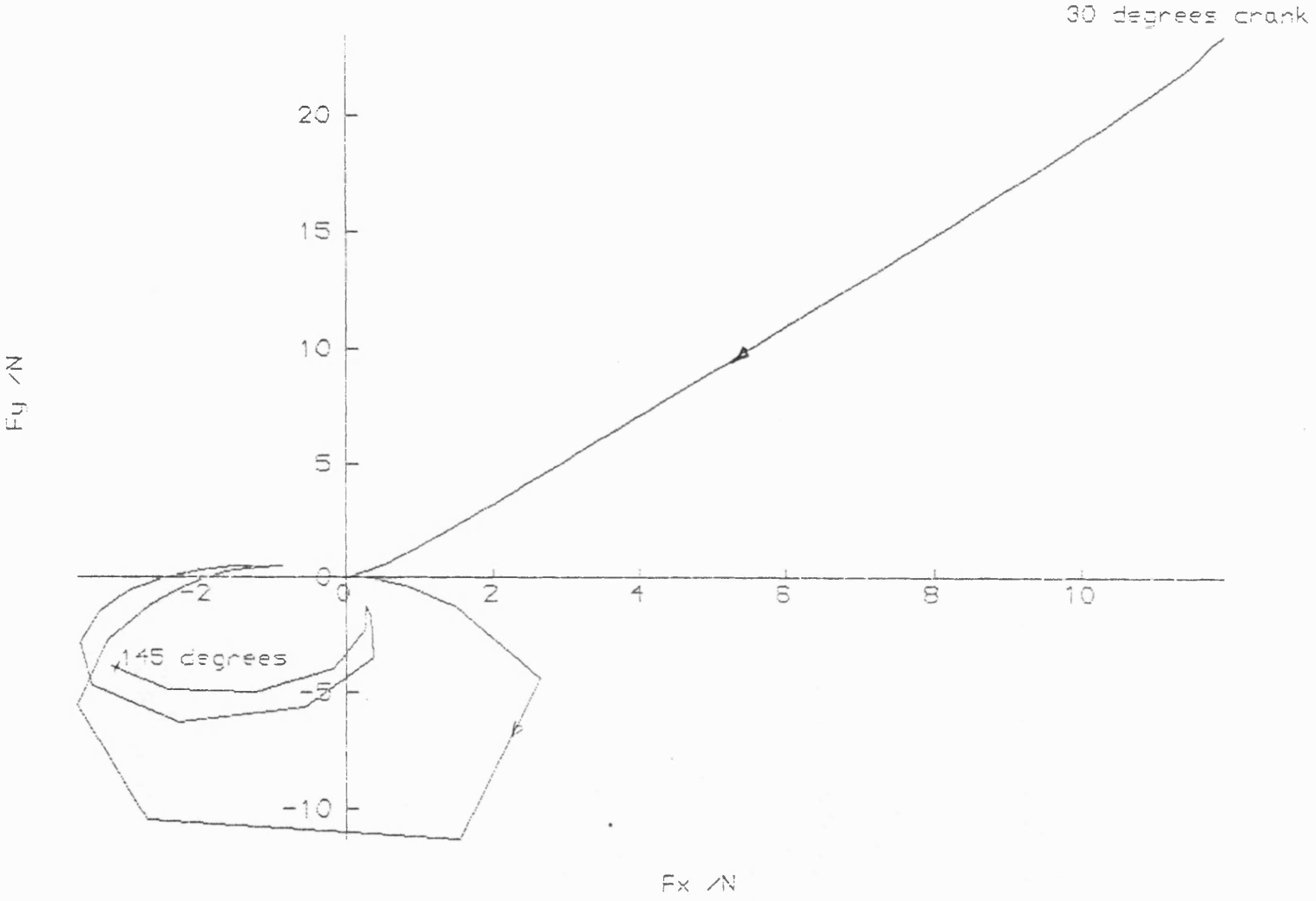

Fig 7.2.4 Pin force(polar plot), dia.clearance 0.25 mm,Fly wheel inertia .23 kg-m.m mean speed=168 rev/min; 30-145,(continuoues contact model)

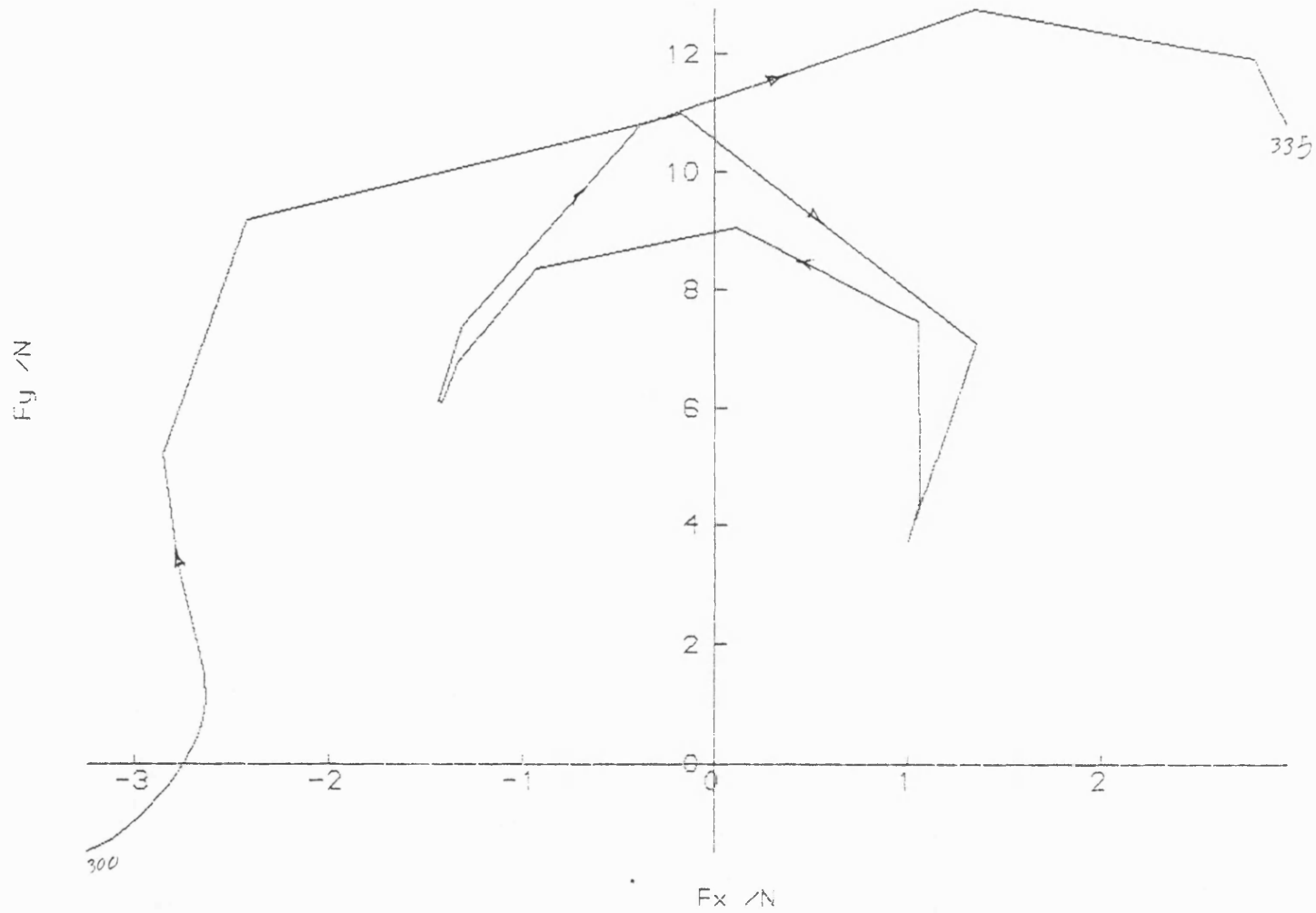

Fig 7.2.5 Pin force(polar plot), dia.clearance .25 mm,fly wheel inertia 0.23 kg-m.m mean speed=168 rev/min; 300-335 (continuoues contact model)

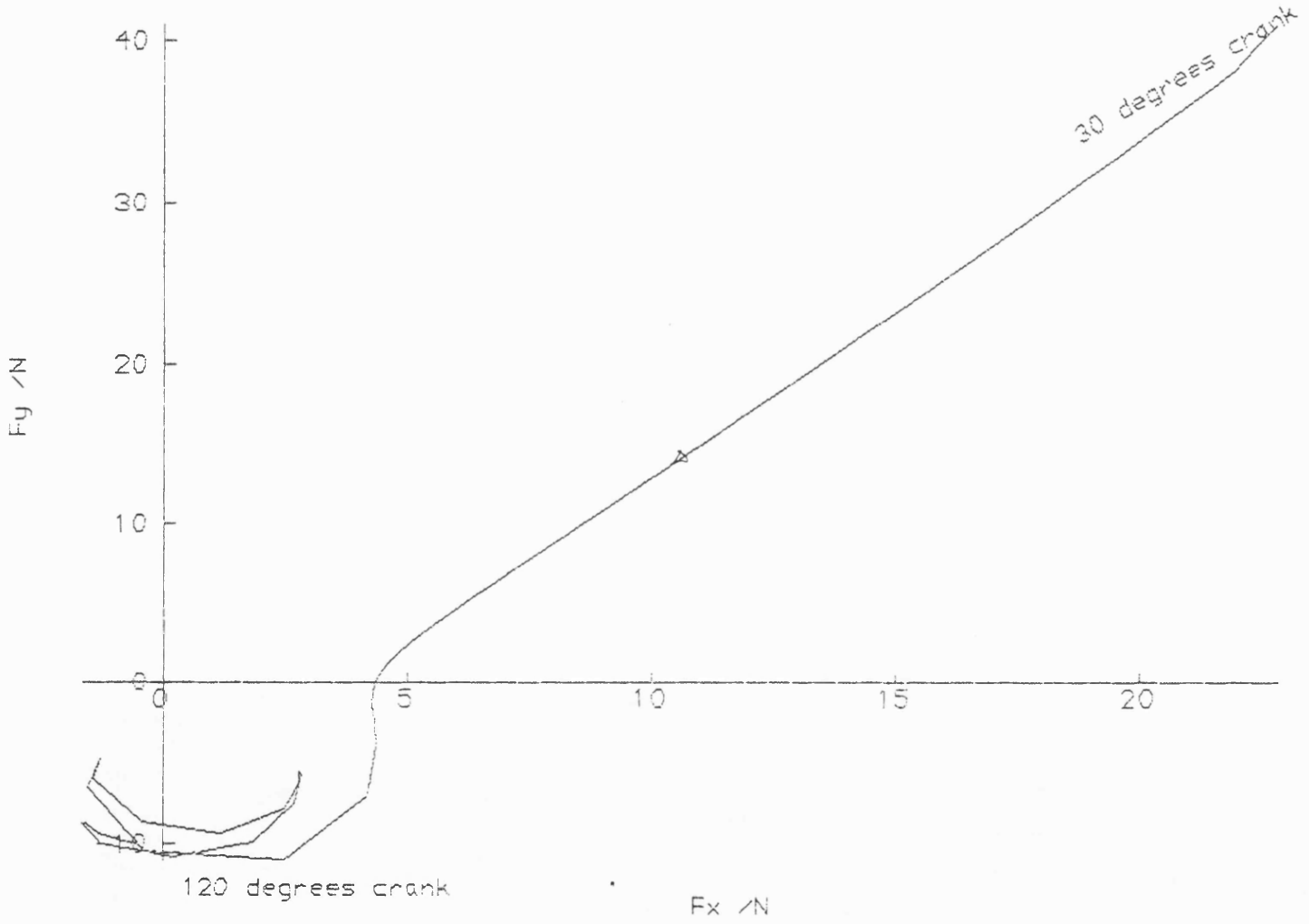

Fig 7.2.6 Pin force(polar plot), dia.clearance 0.25 mm,Fly wheel inertia .23 kg-mm mean speed=244 rev/min; 30-120 ,(continuous contact model)

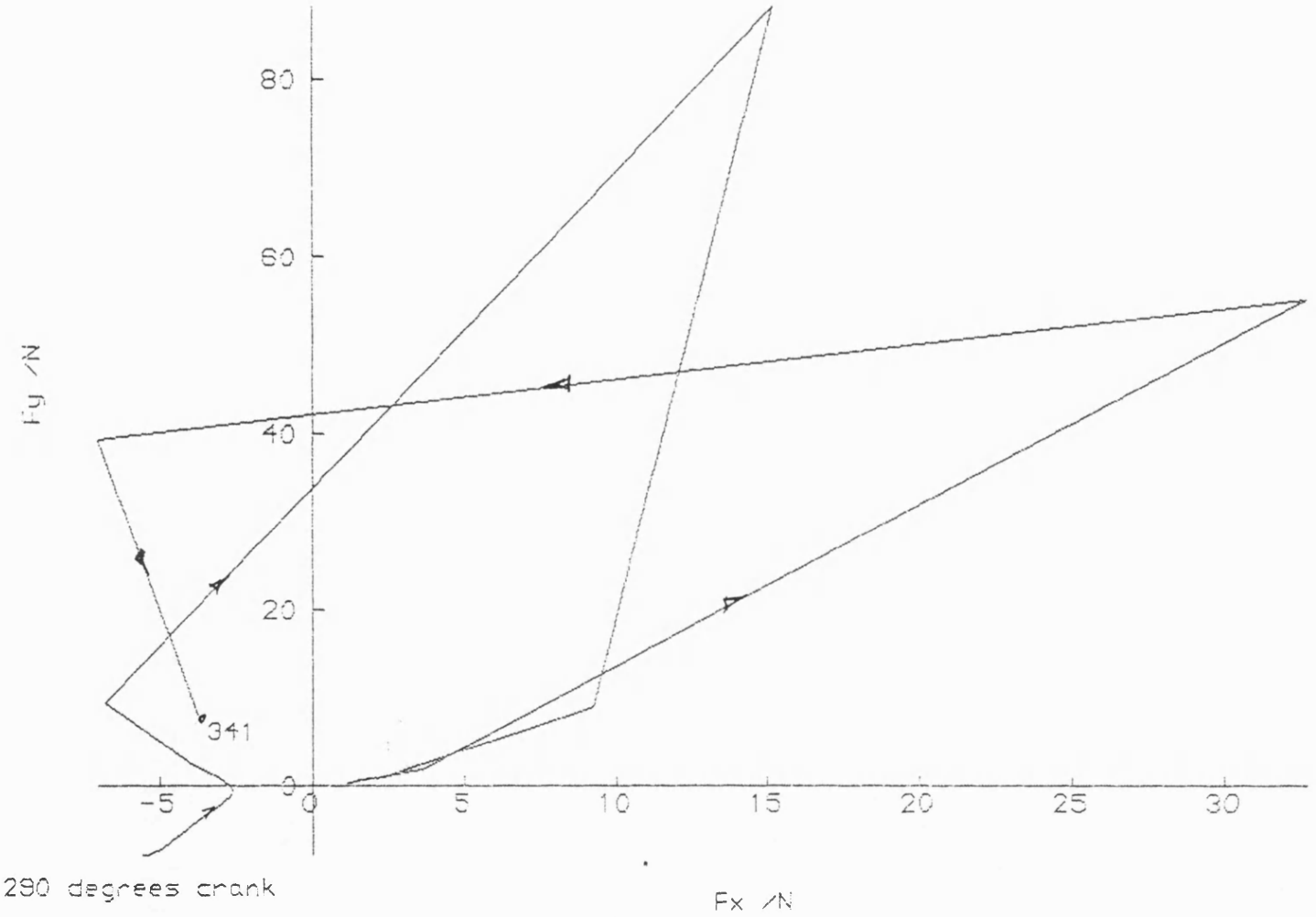

Fig 7.2.7 Pin force(polar plot), dia.clearance 0.25 mm,Fly wheel inertia .23 kg-mm
mean speed=244 rev/min; 290-340,(continuous contact model)

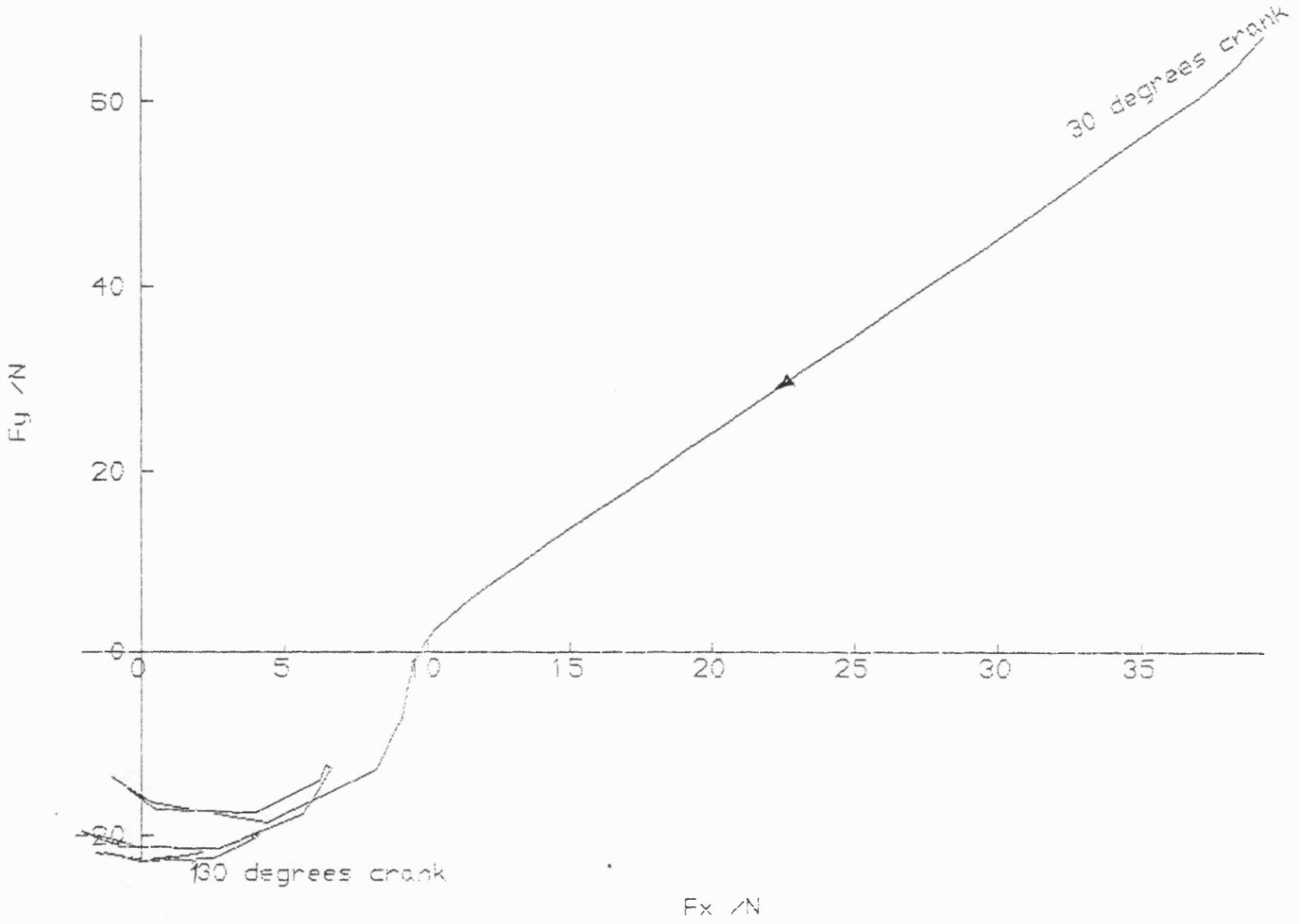

Fig 7.2.8 Pin force(polar plot), dia.clearance 0.25 mm,Fly wheel inertia .23 kg-mm mean speed=327 rev/min; 30-130,(continuous contact model)

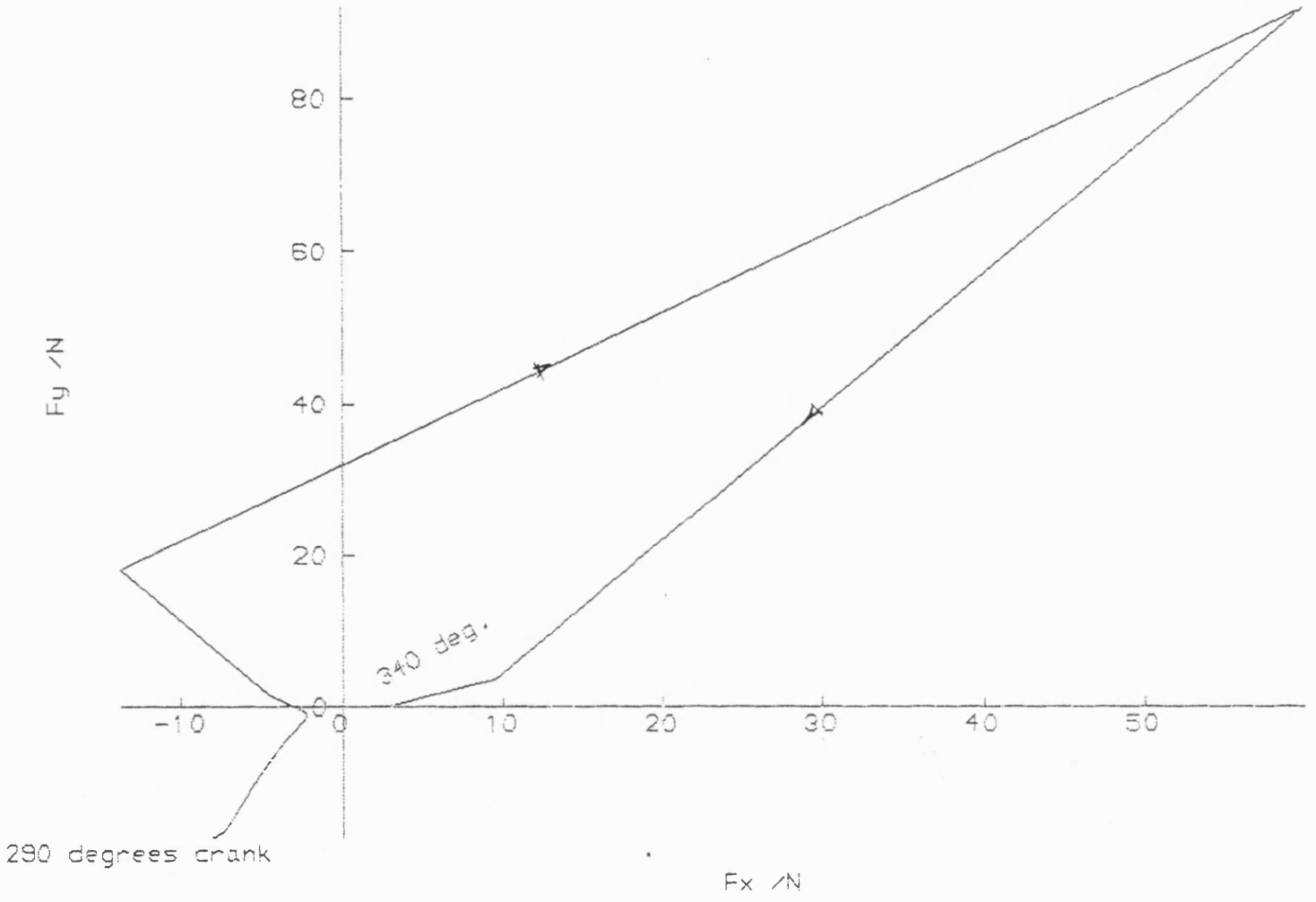

Fig 7.2.9 Pin force(polar plot), dia.clearance 0.25 mm,Fly wheel inertia .23 kg-mm mean speed=327 rev/min; 290-340,(continuous contact model)

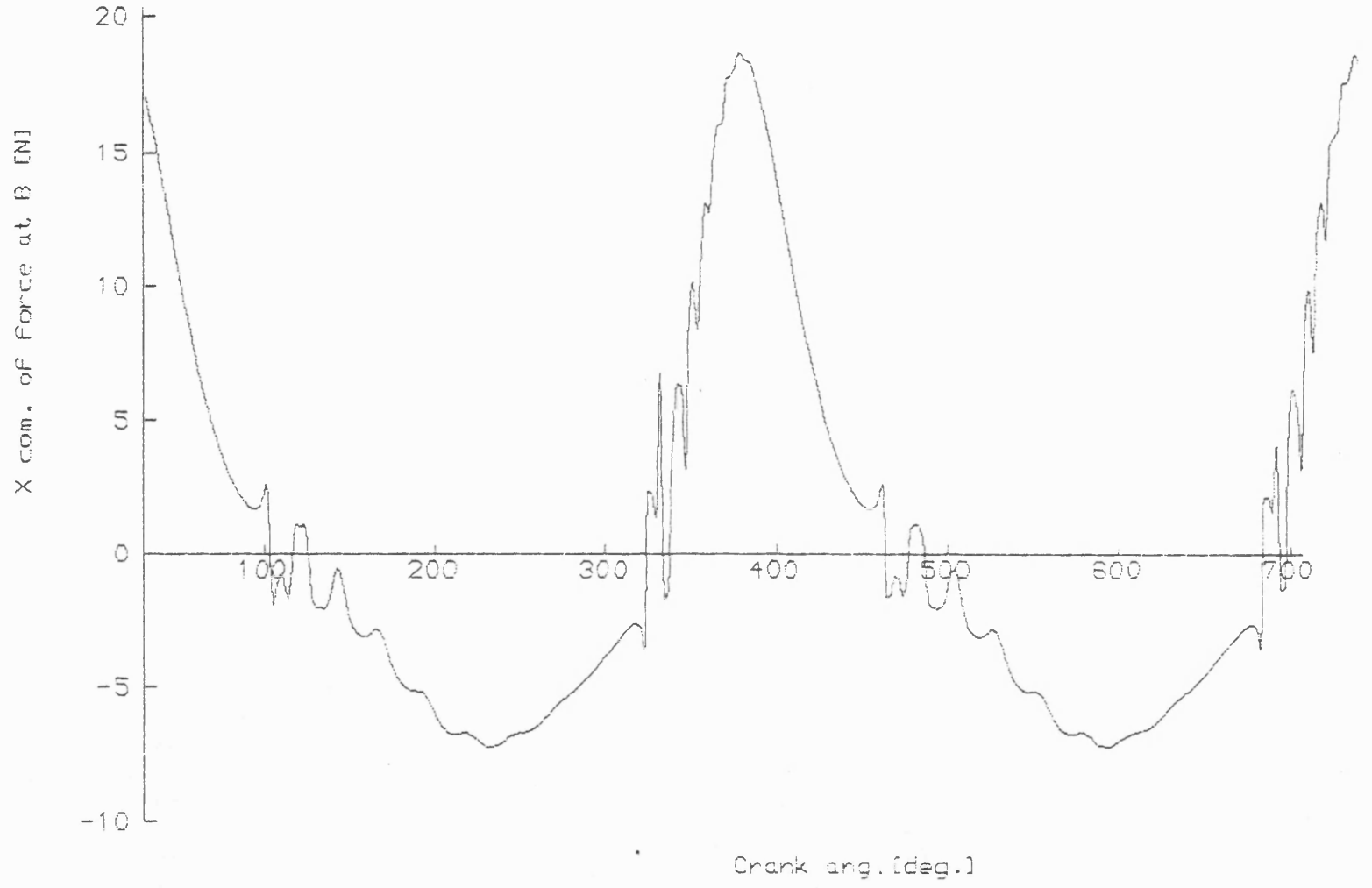

Fig 7.2.10 X component of pin force at B(N), dia. cleance=0.25mm
mean speed 206 rev/min, inertia 0.036 kg-m.m, contivous contact model

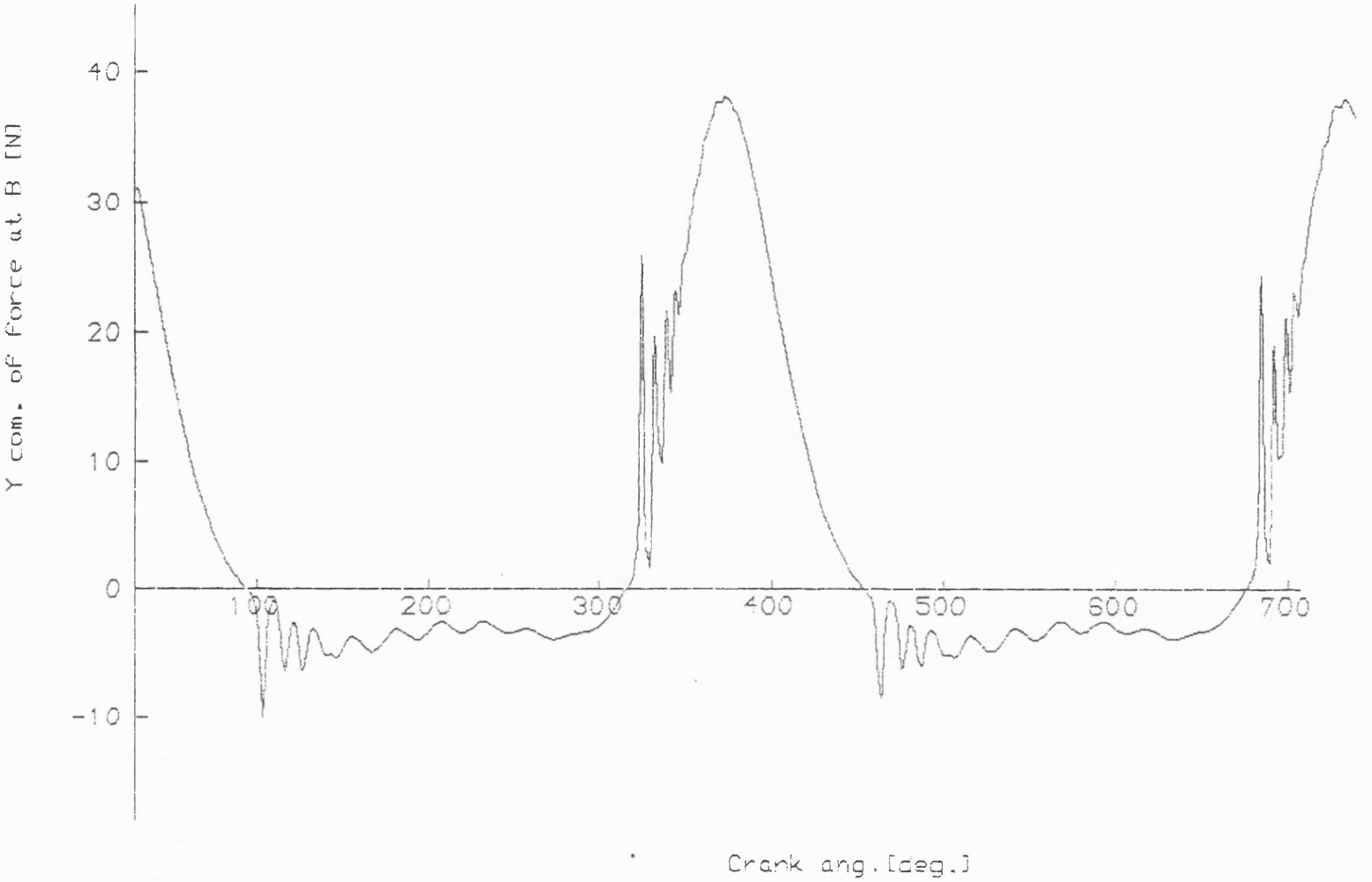

Fig 7.2.11 Y component of pin force at B(N), dia. cleance=0.25mm
mean speed 206 rev/min, inertia 0.036 kg-m.m, contiuous contact model

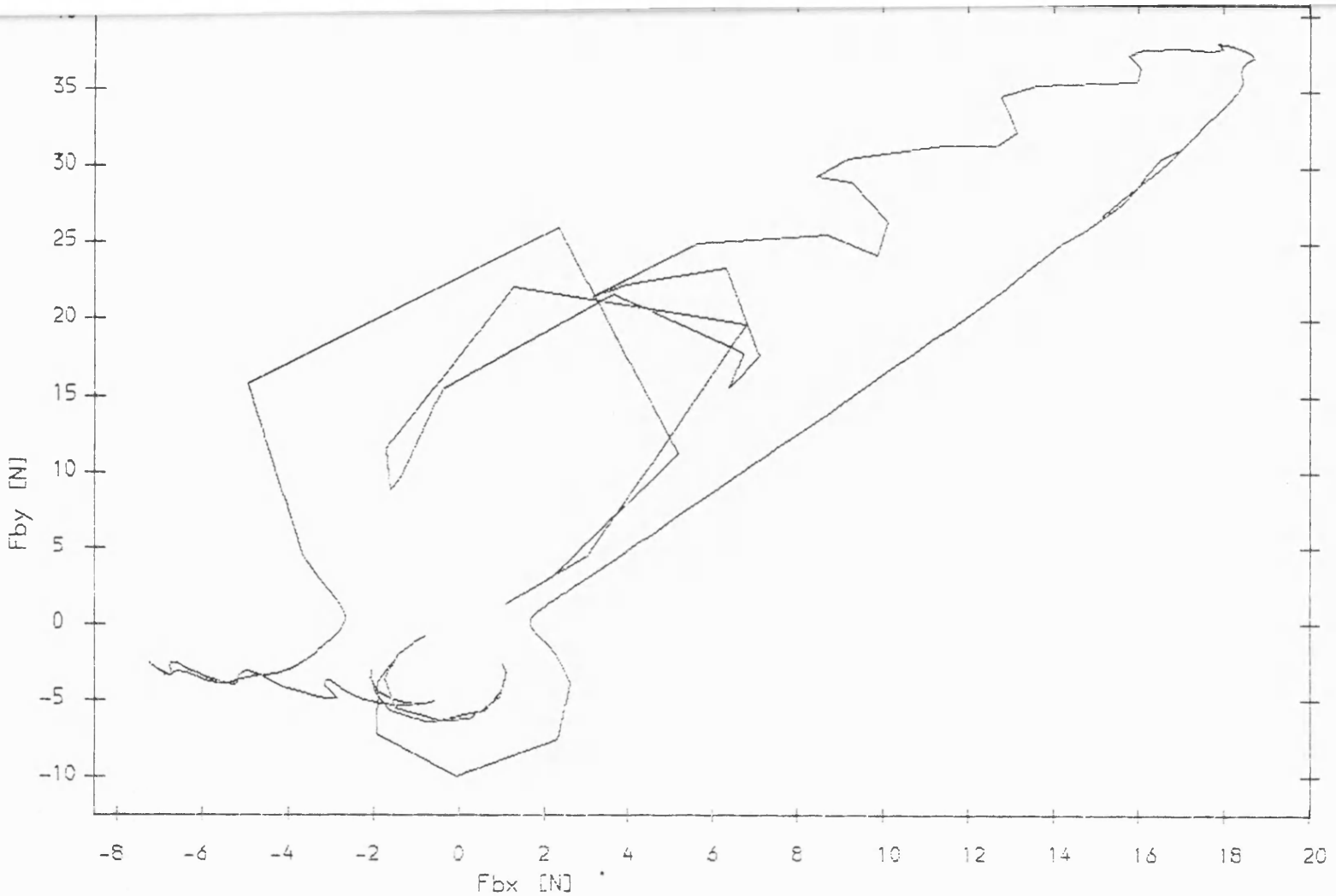

Fig 7.2.12 Polar plot of pin force B body C. CONTATC MODEL
I1=0.036 mean speed=206.0 rev/min clearance=0.25mm

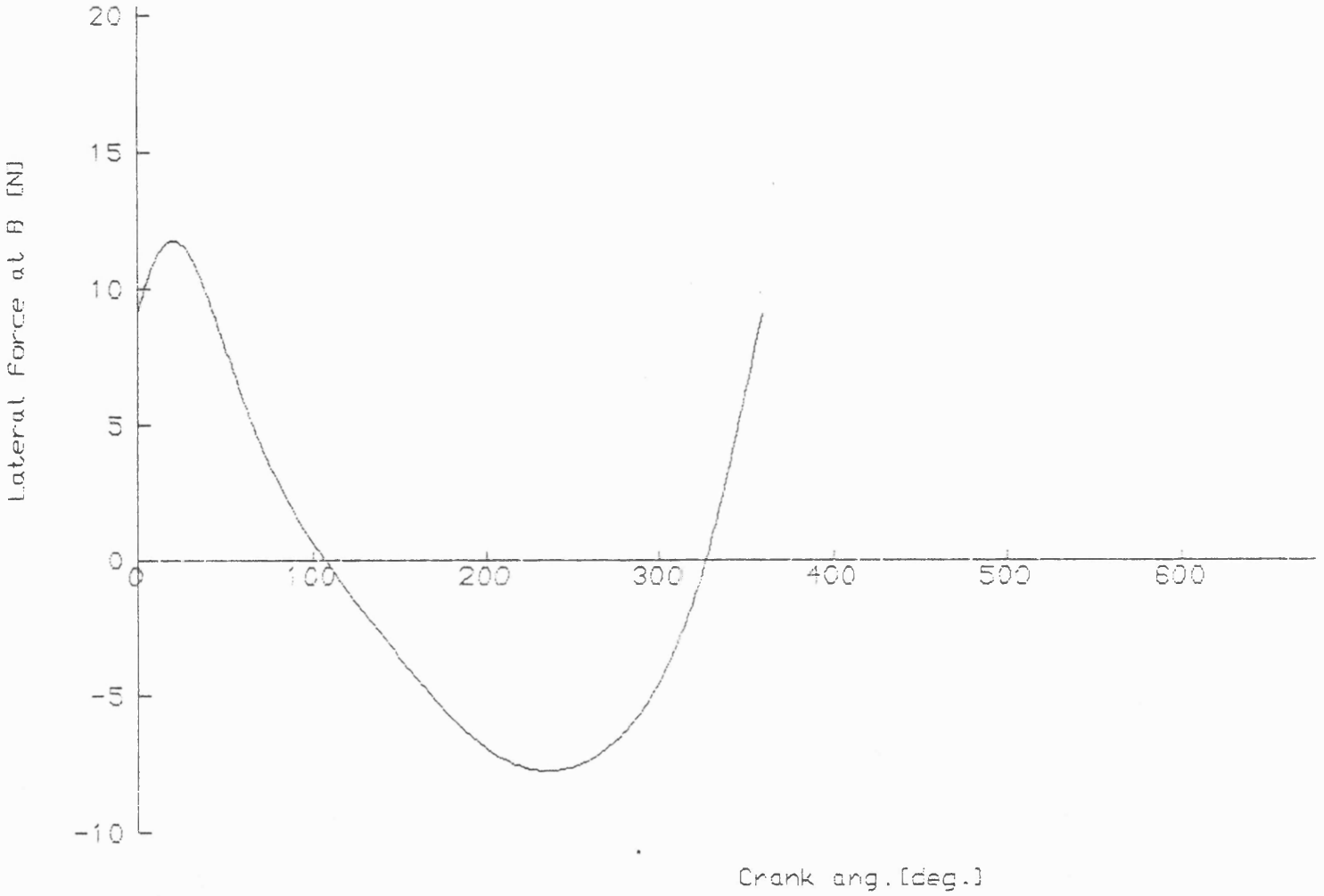

Fig 7.2.13 Lateral component of pin force at B , zero cleance
body fixed axes, mean speed=206 [rev/min], inertia 0.036 kg-m.m

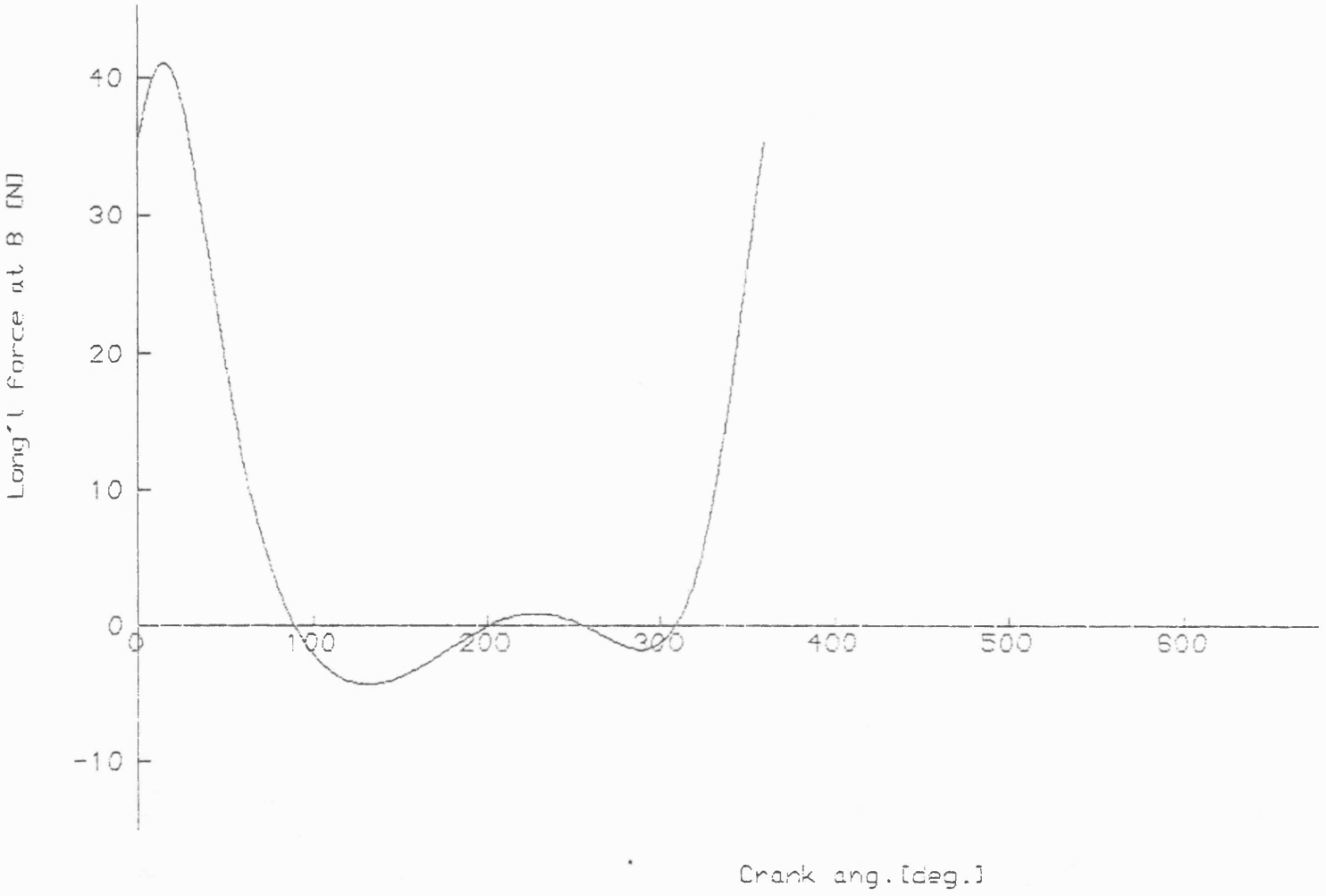

Fig 7.2 14 Long'l component of pin force at B , zero cleance
body fixed axes, mean speed=206 [rev/min], inertia 0.036 kg-m.m

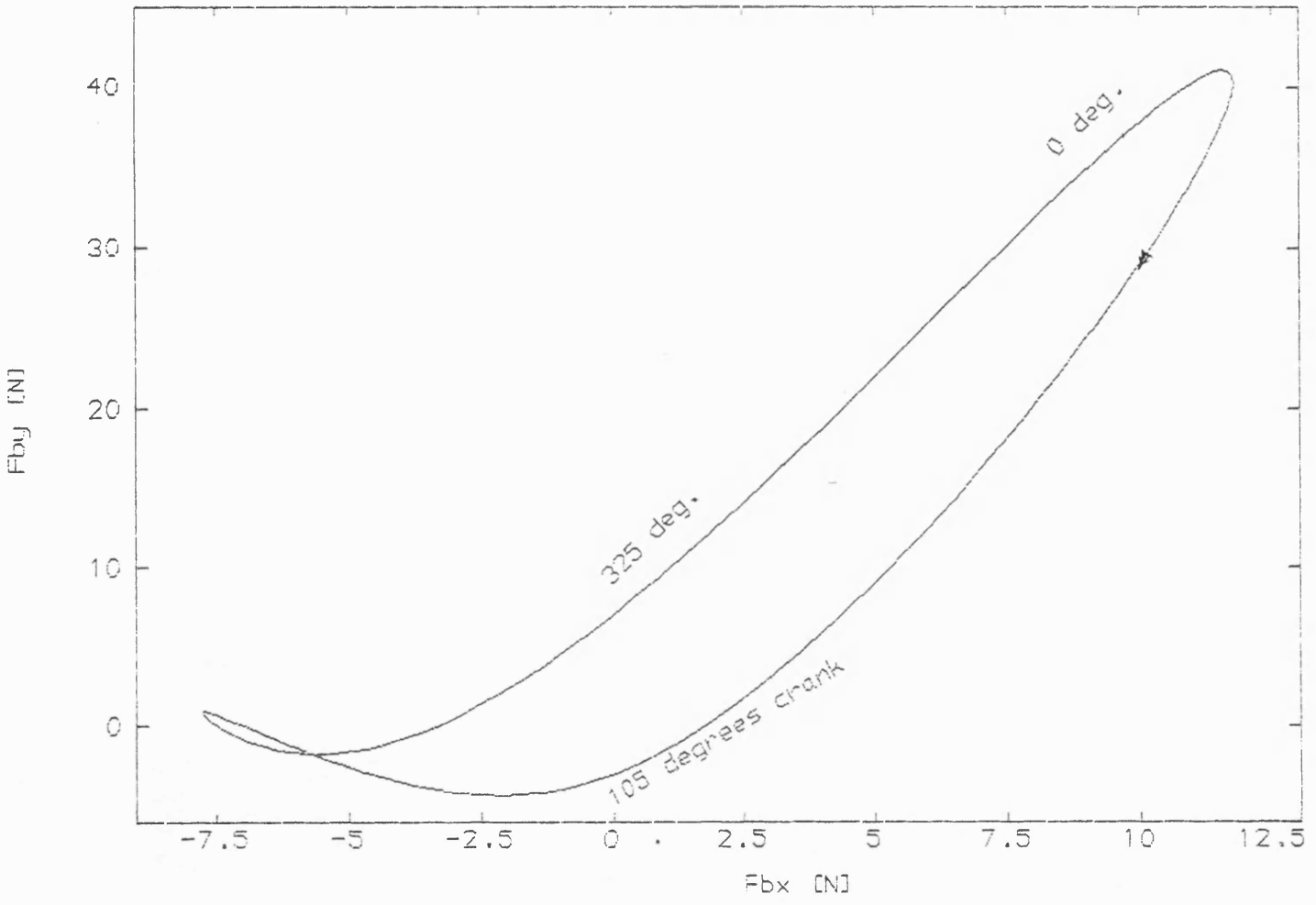

Fig 7.2.15 Polar plot force at B(N) , zero clearance,body fixed axes
mean speed=206 [rev/min], inertia 0.036 kg-m.m

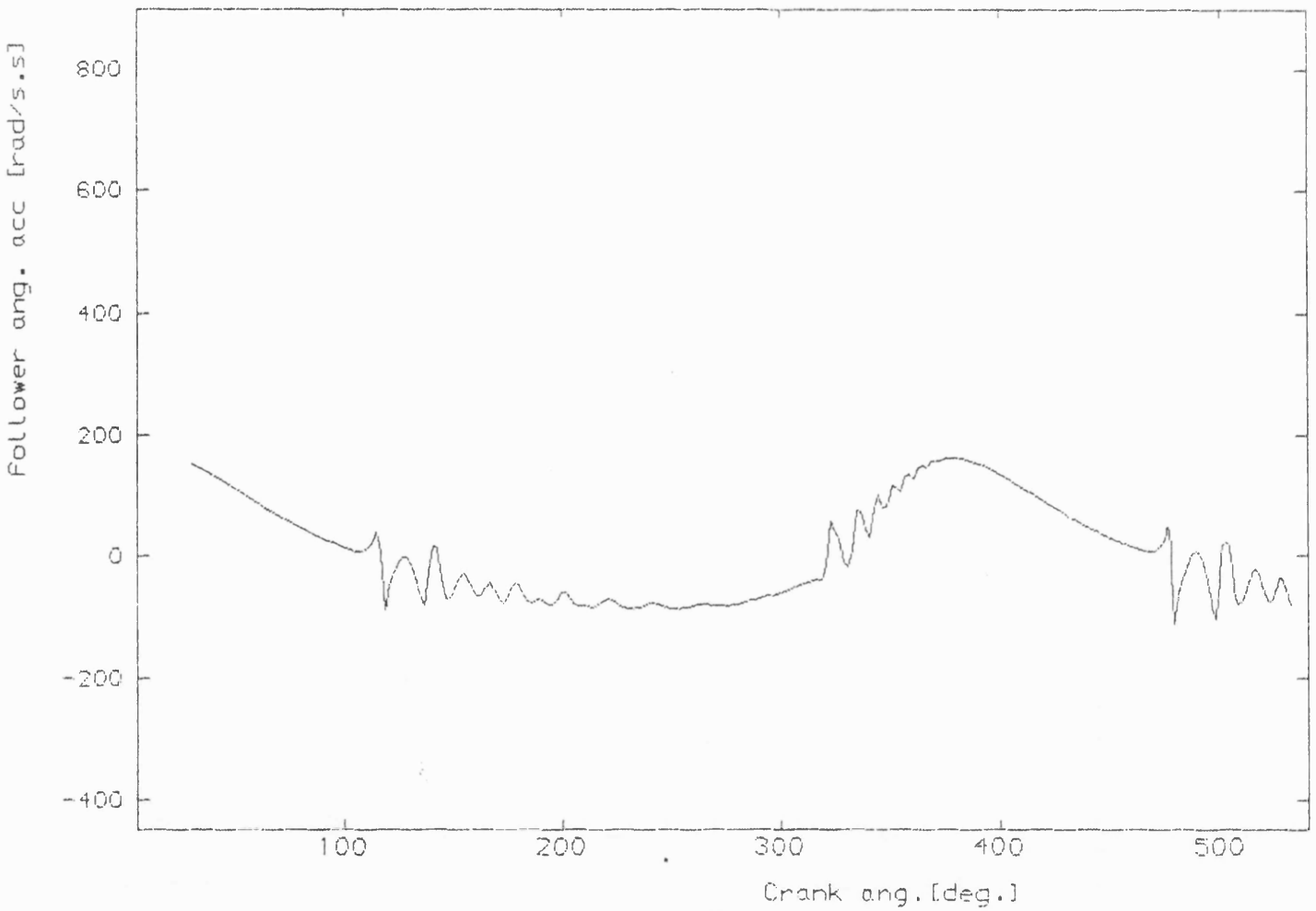

Fig 7.2.16 Follower angular acceleration continuous contact model
mean speed=168 [rev/min] I1=0.23 kg-m.m;d.clearance=0.25mm

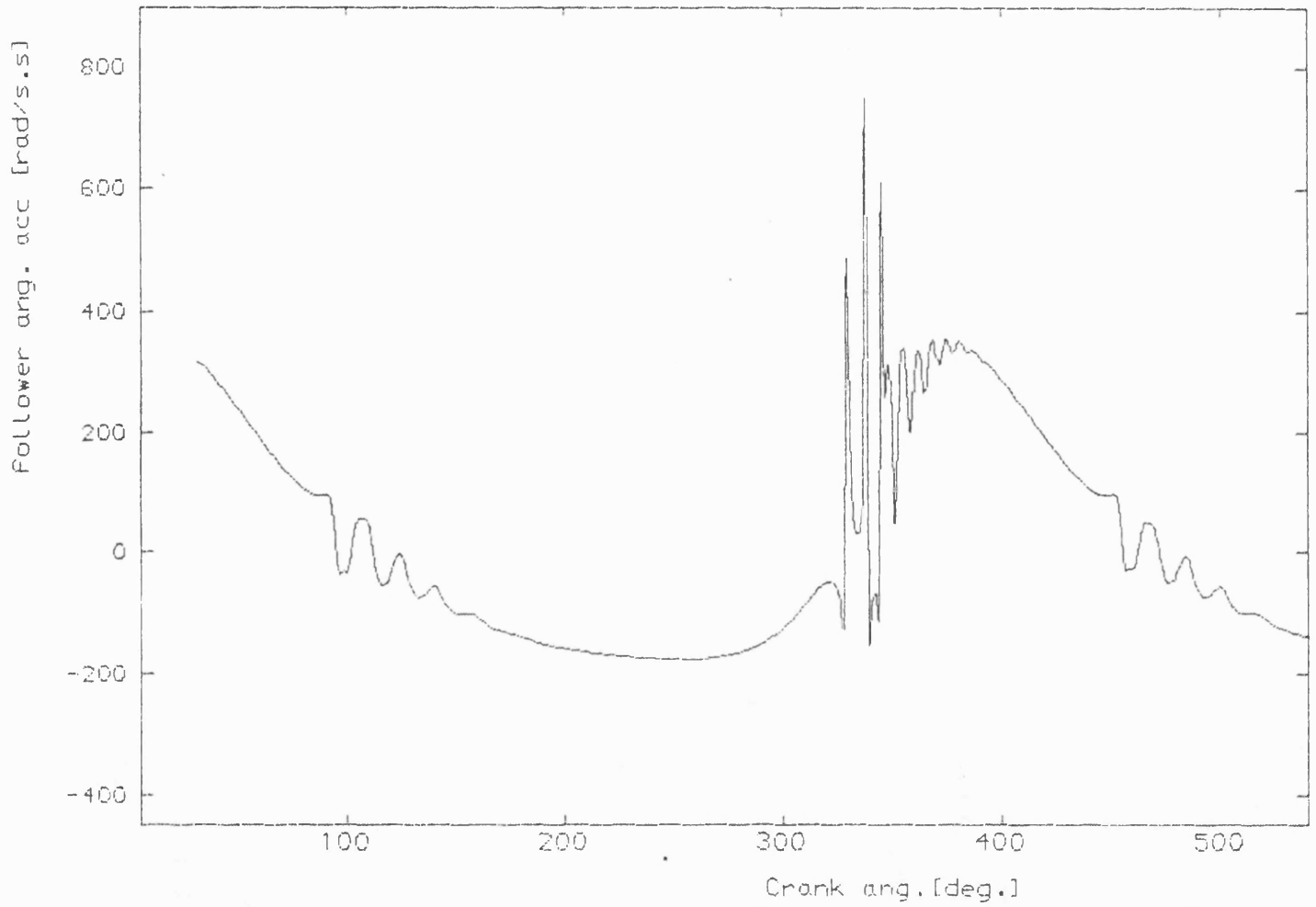

Fig 7.2.17 Follower angular acceleration continuous contact model
mean speed=244 [rev/min] I1=0.23 kg-m.m;d.clearance=0.25mm

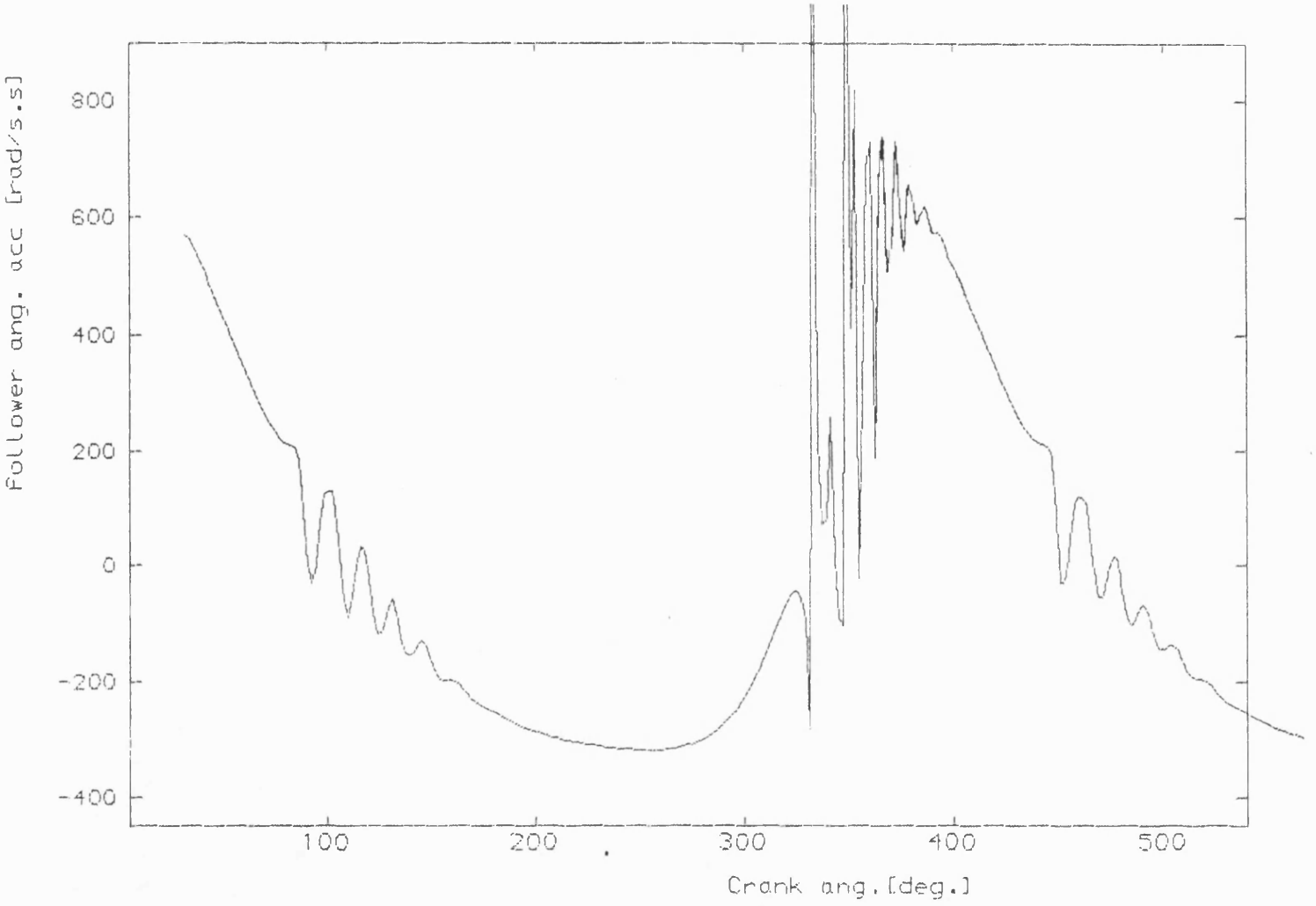

Fig 7.2.18 Follower angular acceleration continuous contact model
mean speed=327 [rev/min] I1=0.23 kg-m.m;d.clearance=0.25mm

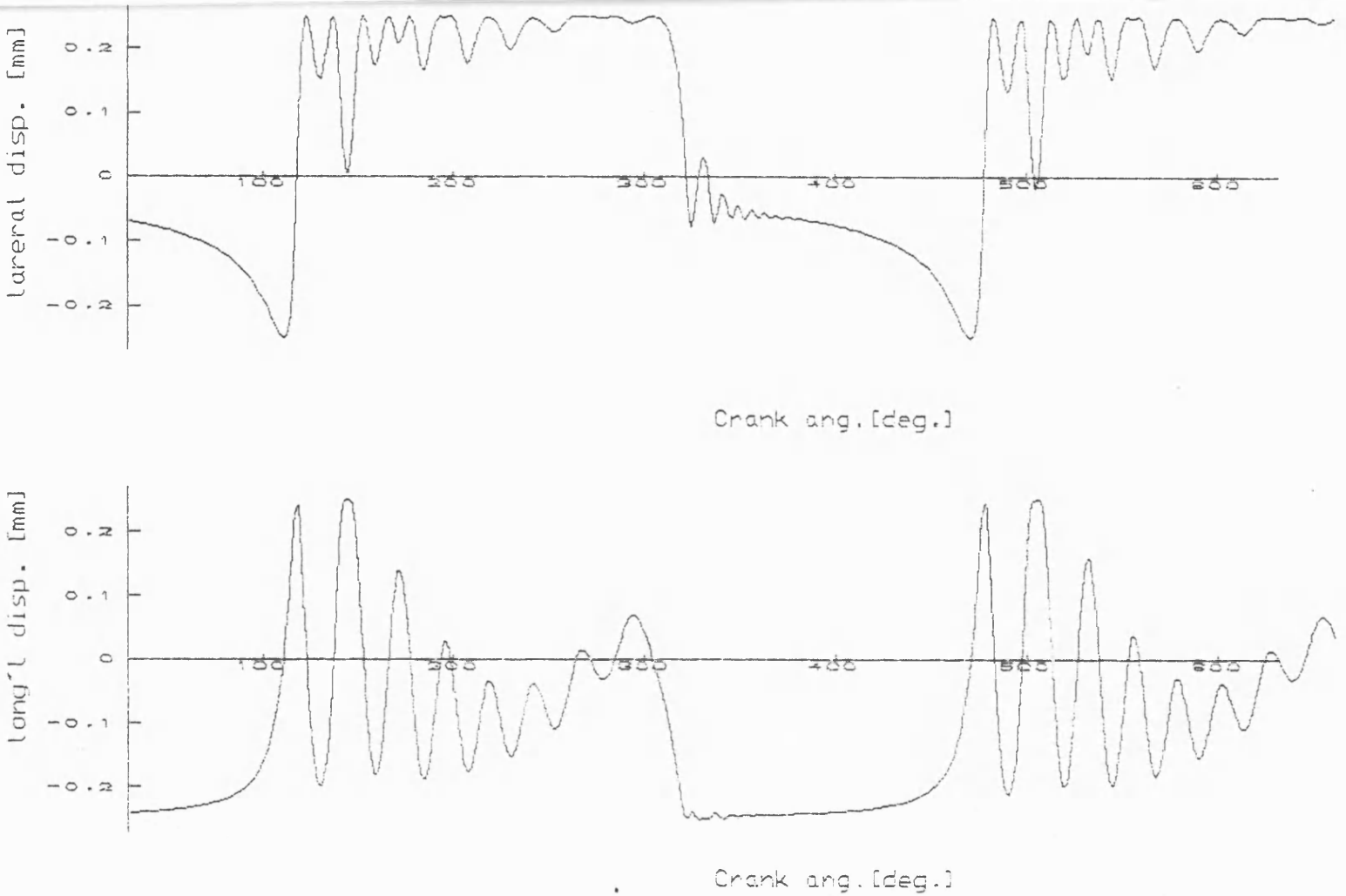

Fig 7.3.1 Components of disp. of pin relative to bush (continuous contact)
mean speed=168 [rev/min] I1=0.23 kg-m.m ;dia. clearance=0.25mm

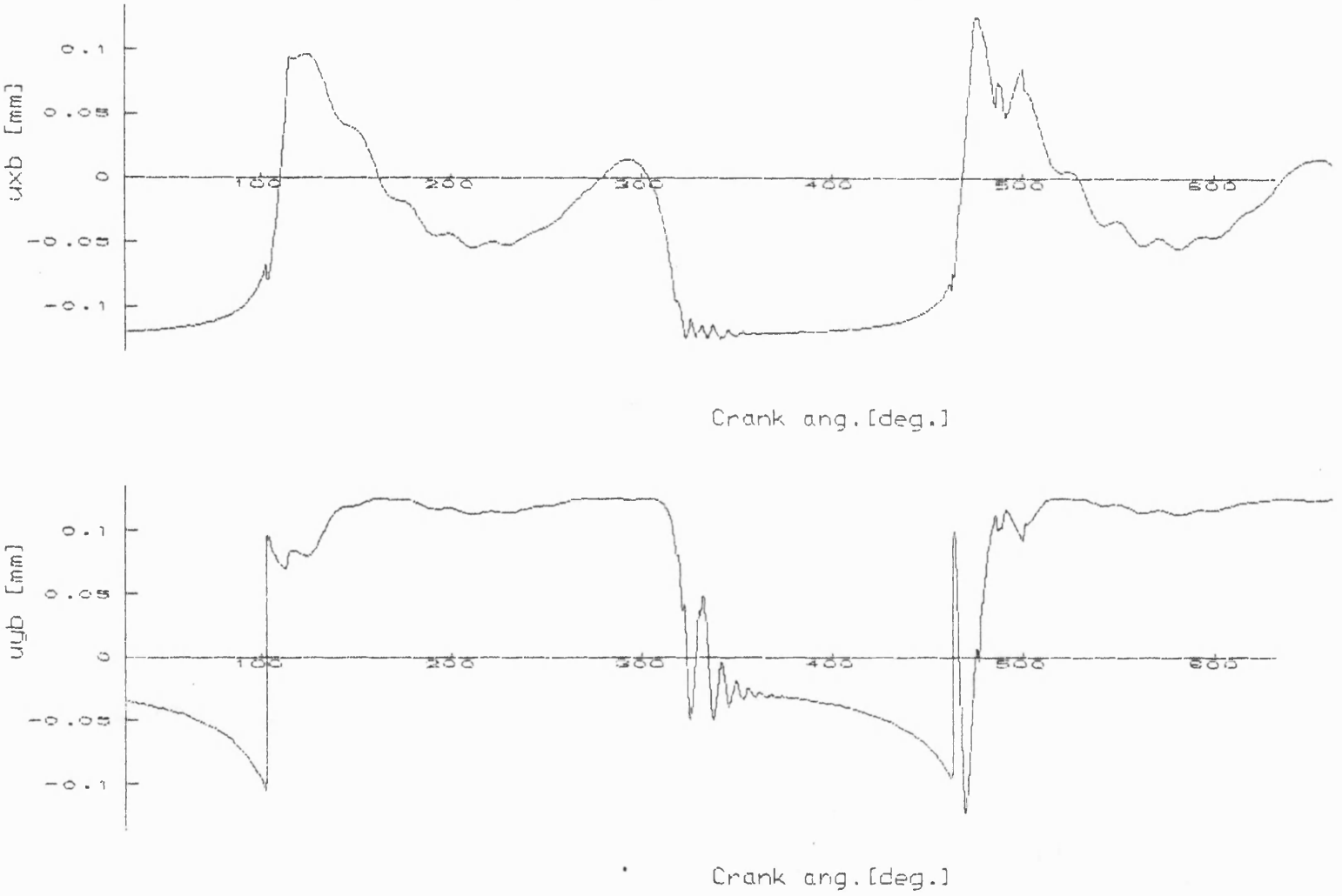

Fig 7.3.2 x&Y components of disp. of pin relative to bush ; (contact loss model)
mean speed=168 [rev/min] I1=0.23 kg-m.m ; dia. clearance=0.25mm

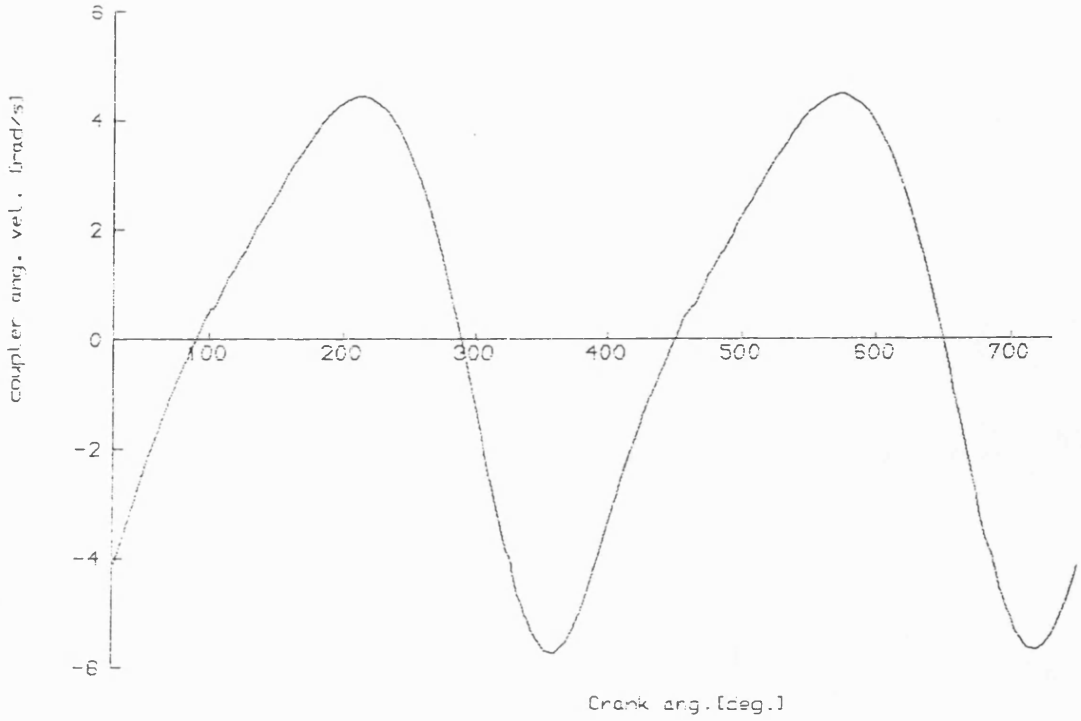

Fig 7.3.3 Coupler angular velocity (continuous contact model)
mean speed=206 rev/min ; I1=0.036 kg-m.m; dia. clearance=0.25mm

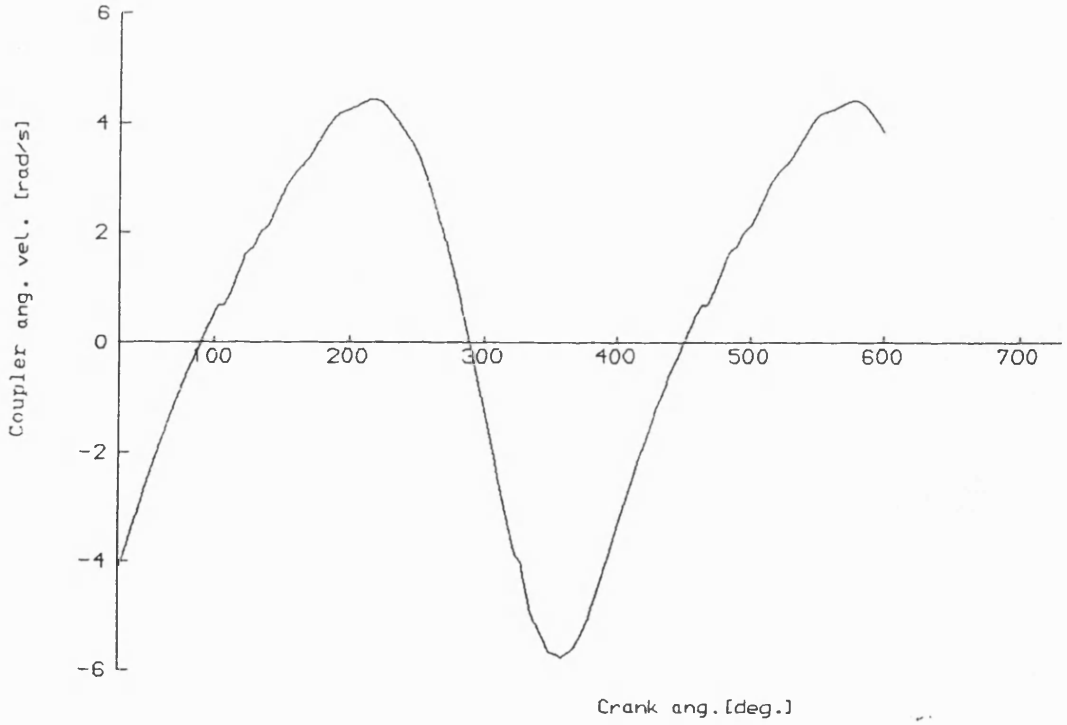

Fig 7.3.4 Coupler angular velocity (contact loss model)
mean speed=206 [rev/min] I1=0.036 ; dia. clearance = 0.25mm

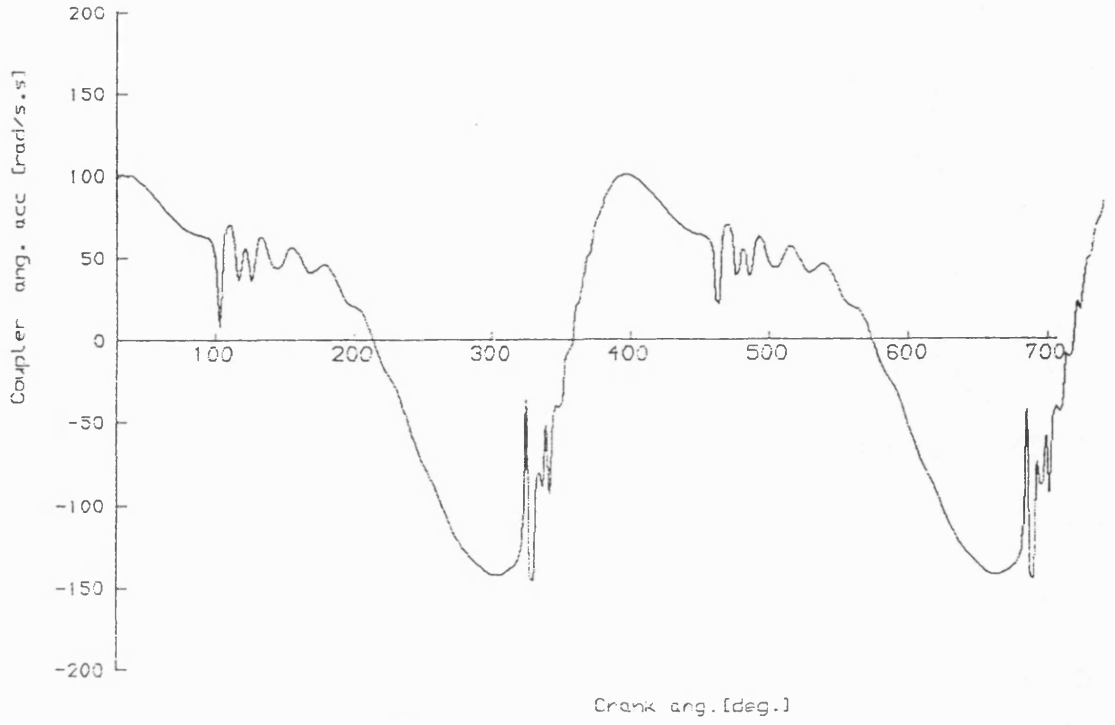

Fig 7.3.5 Coupler angular acceleration (continuous contact model)
mean speed=206 rev/min; I1=0.036 kg-m.m ;dia. cleance=0.25mm

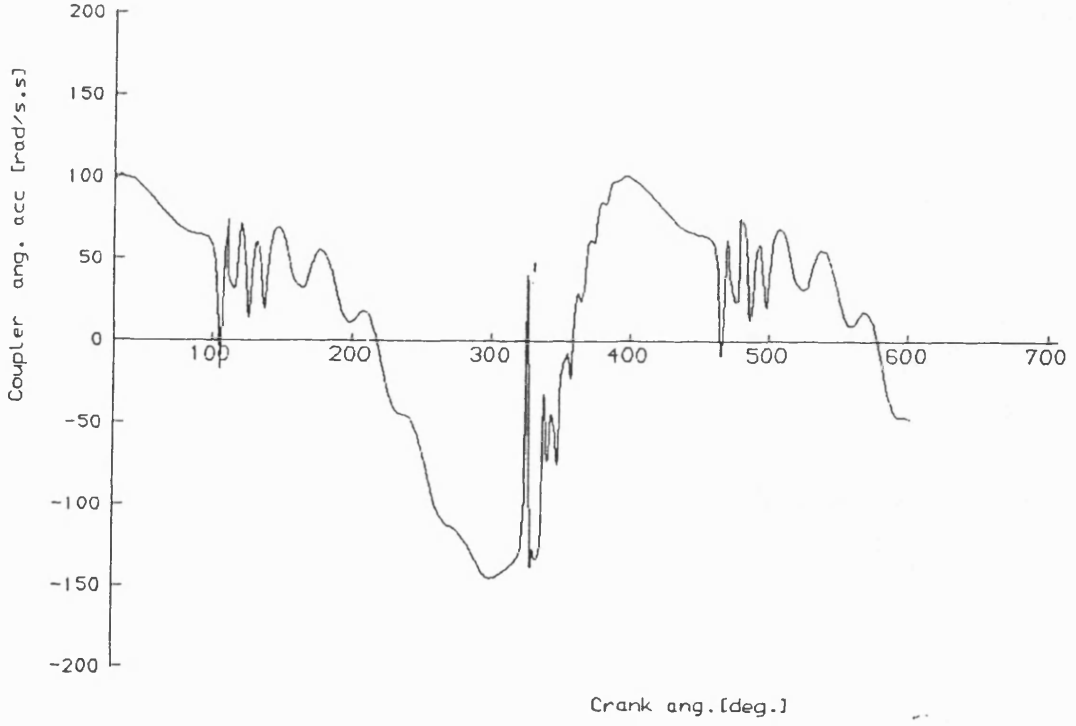

Fig 7.3.6 Coupler angular acceleration (contact loss model)
mean speed=206 [rev/min] I1=0.036 ; dia. clearance = 0.25mm

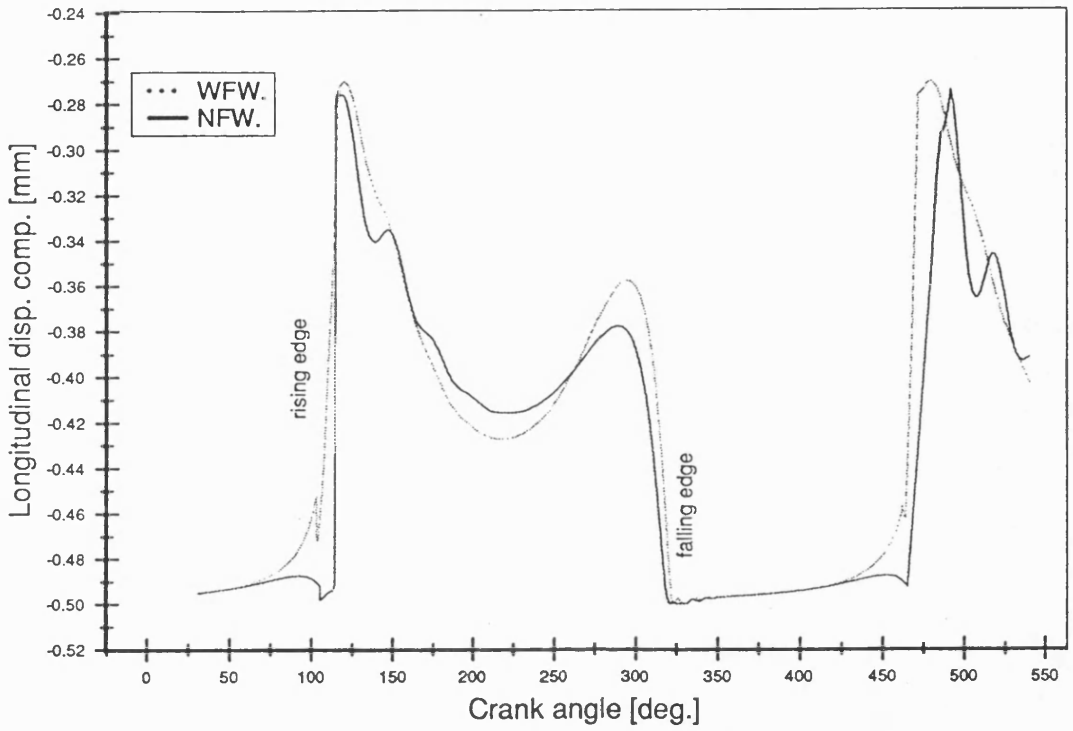

Fig 7.4.1 Theo. longitudinal pin disp. relative to bush, d. cle a.=.25mm
mean speed 168 rev/min ; with viscous friction

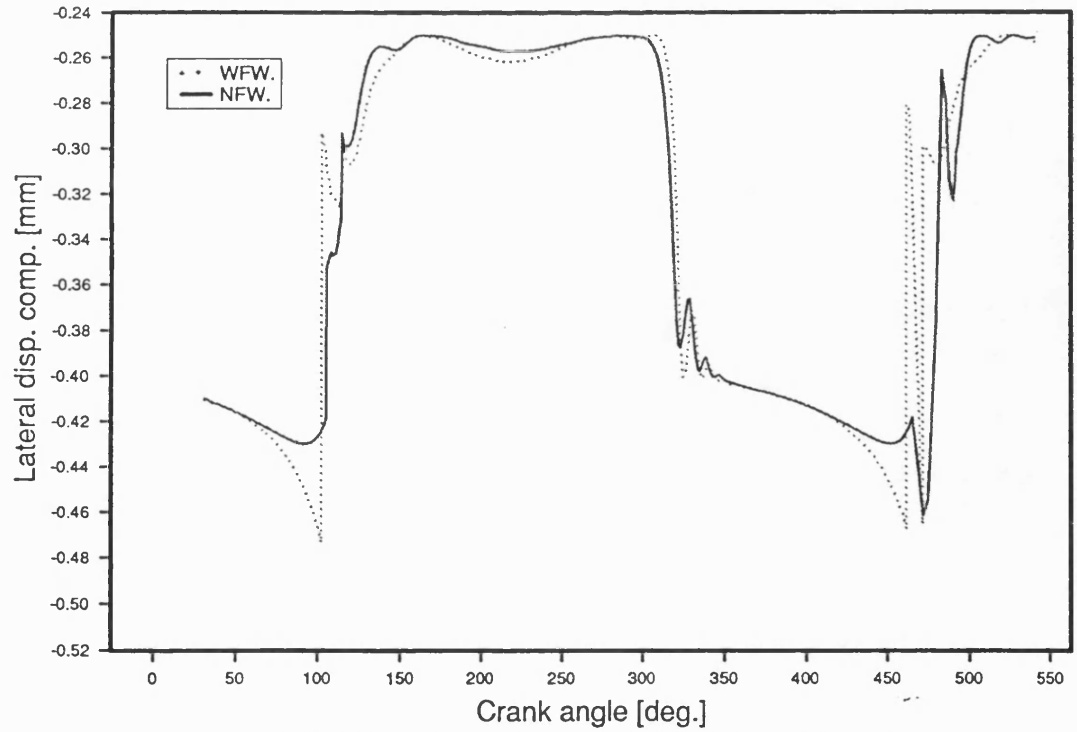

Fig 7.4.2 Theo. lateral pin displacement relative to bush, d.cl ea.=.25mm
mean speed 168 rev/min ; with viscous friction

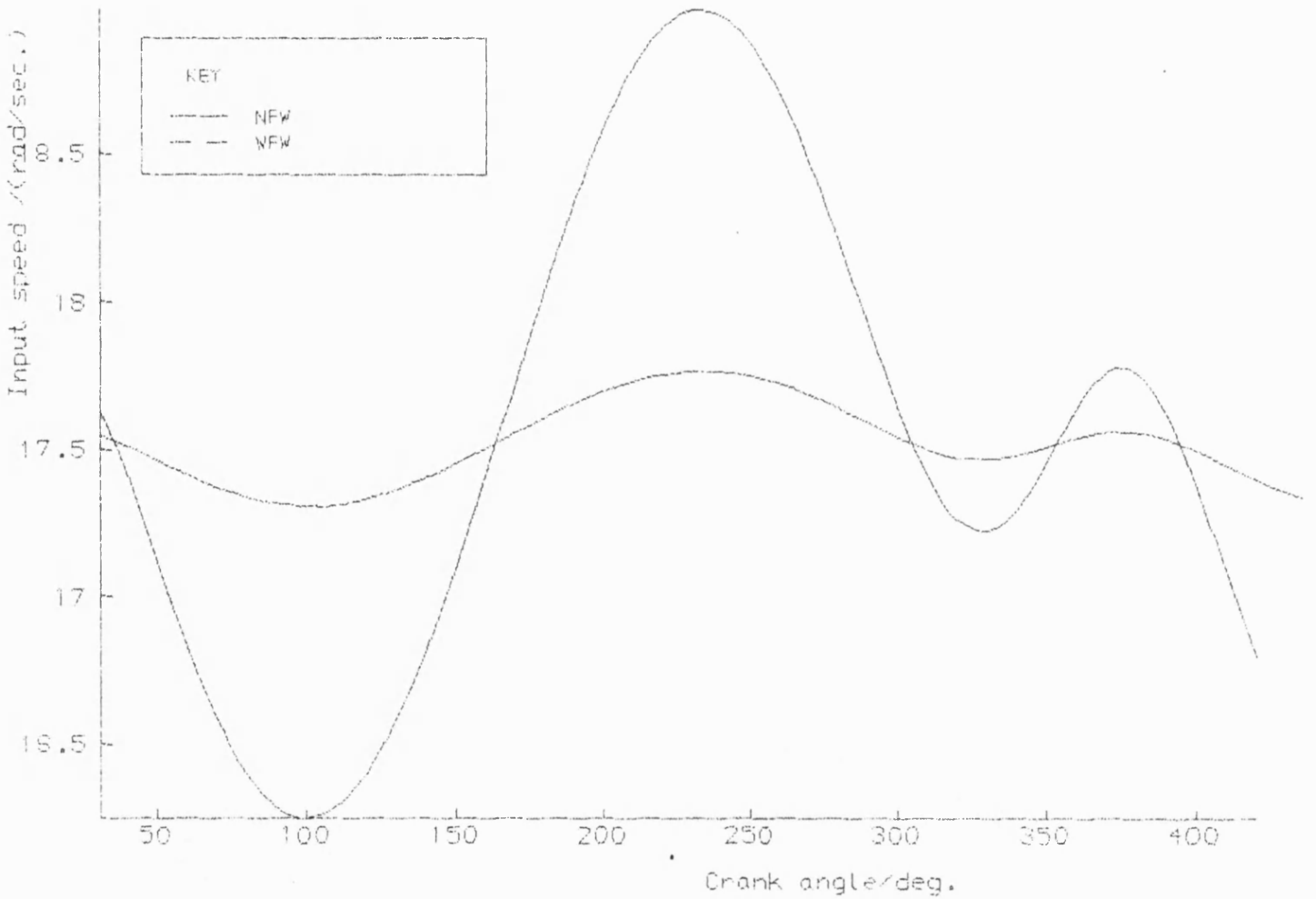

Fig(7.4.3) Input speed for wFw and nFw in theoretical model
mean speed = 168 rev/min ; d. clea.=0.25mm ; Cij=4.0d-7

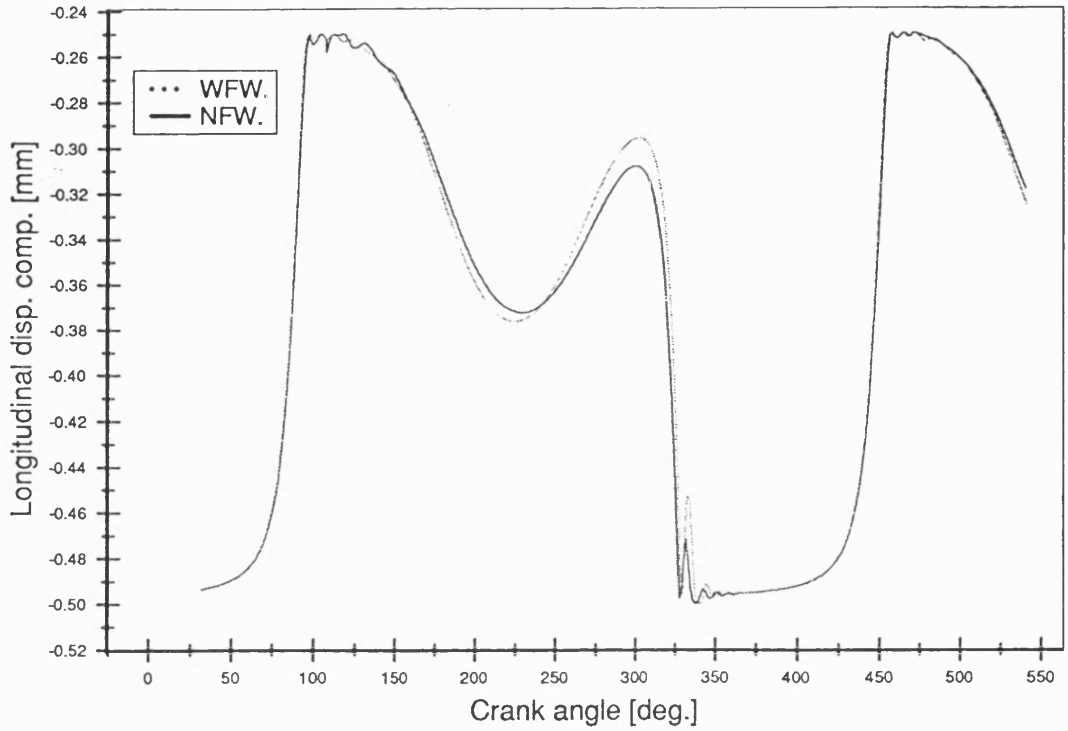

Fig 7.4.4 Theo. longitudinal pin disp. relative to bush, d.clea .=.25mm
mean speed 244 rev/min ; with viscous friction

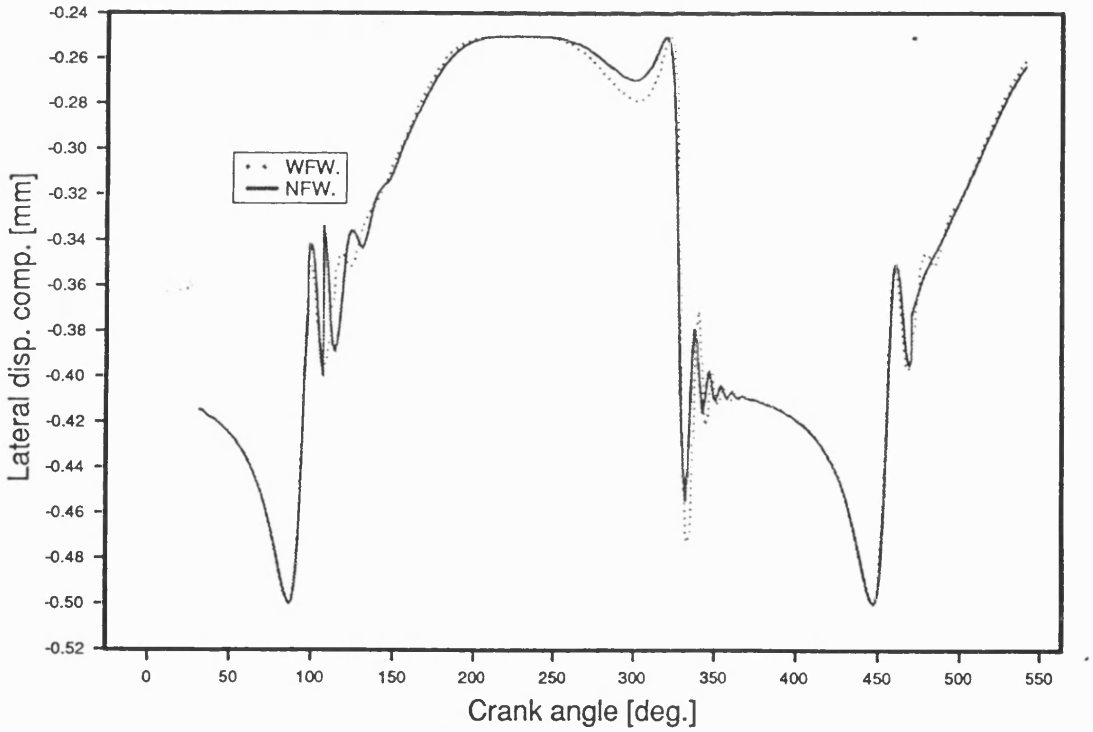

Fig 7.4.5 Theo. lateral pin displacement to bush, d.clea.=0.25m m
mean speed 244 rev/min , with viscous friction

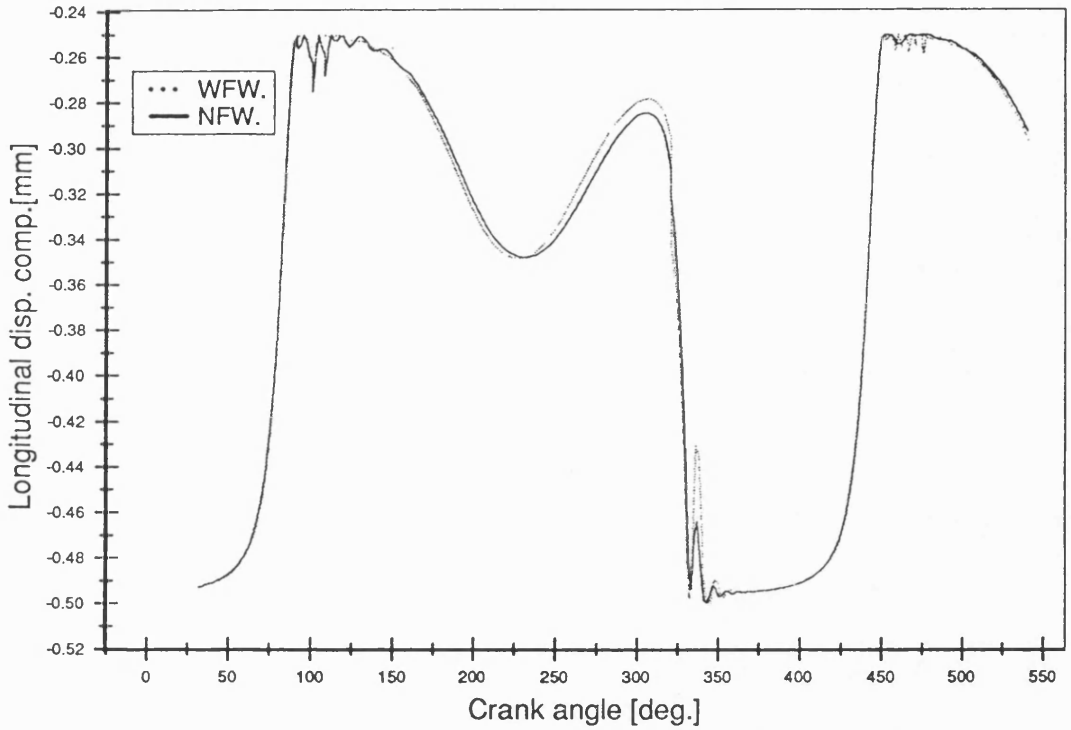

Fig 7.4.6 Theo. longitudinal pin disp. relative to bush, d.clea .=.25mm
mean speed 327 rev/min ; with viscous friction

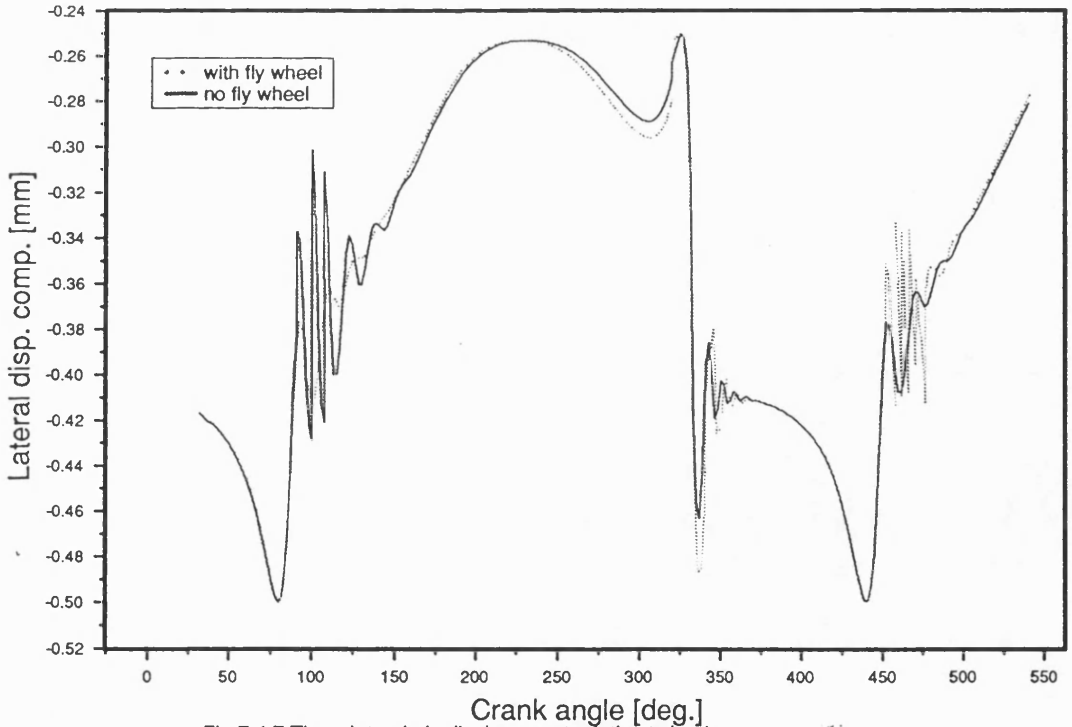

Fig 7.4.7 Theo. lateral pin displacement relative to bush
dia. clearance 0.25mm; mean speed 327 rev/min ; with viscous fr iction

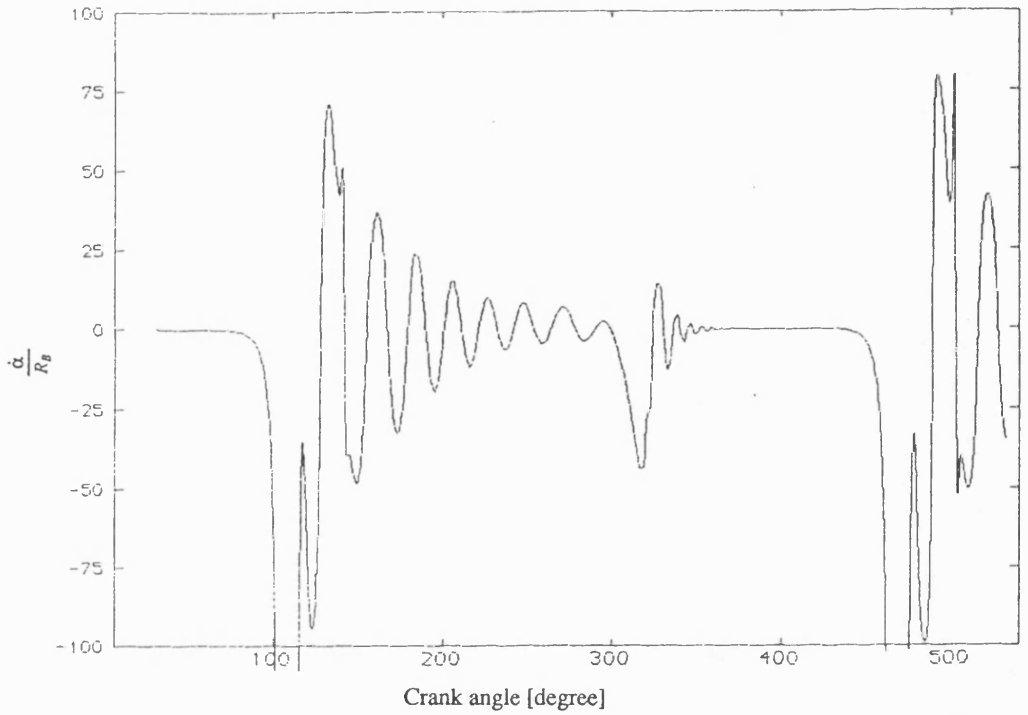

Fig 7.5.1a Contact criterion(E&W) (continuous contact model)
mean speed 168 rev/min ; I1=0.23kgm.m; dia. clearance 0.25mm

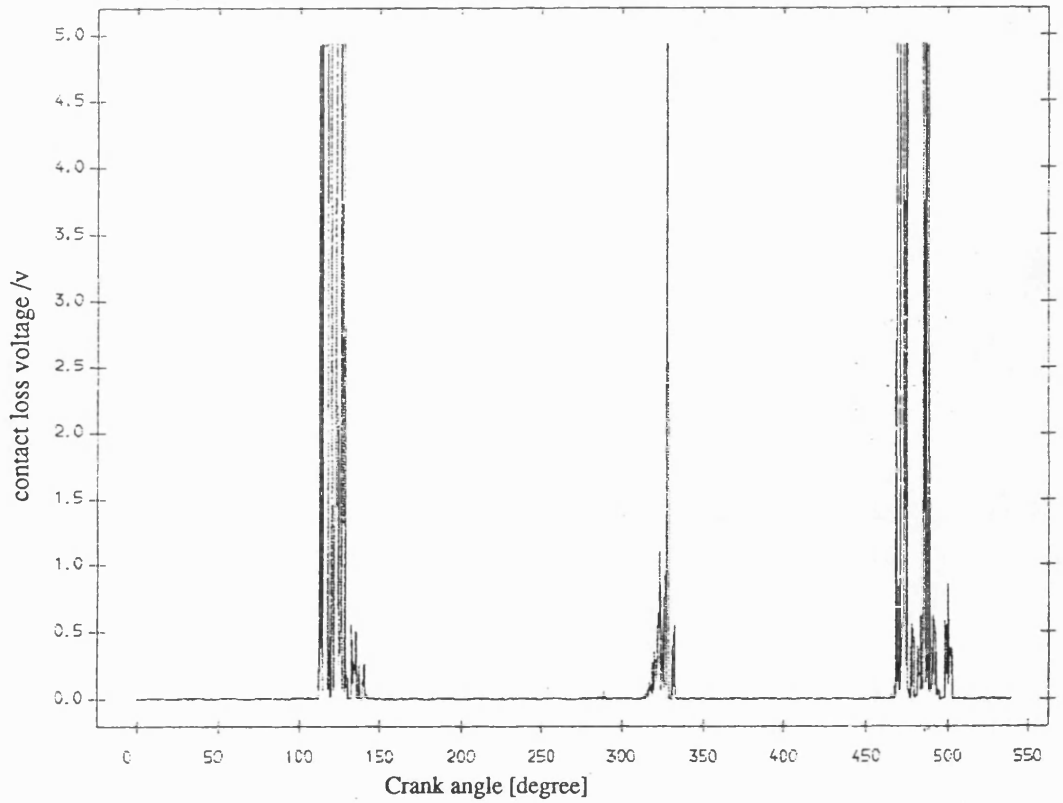

Fig 7.5.1b Exp. result contact loss of pin and greasy bearing
with fly wheel; mean speed 168 rev/min; dia.clearance 0.25mm

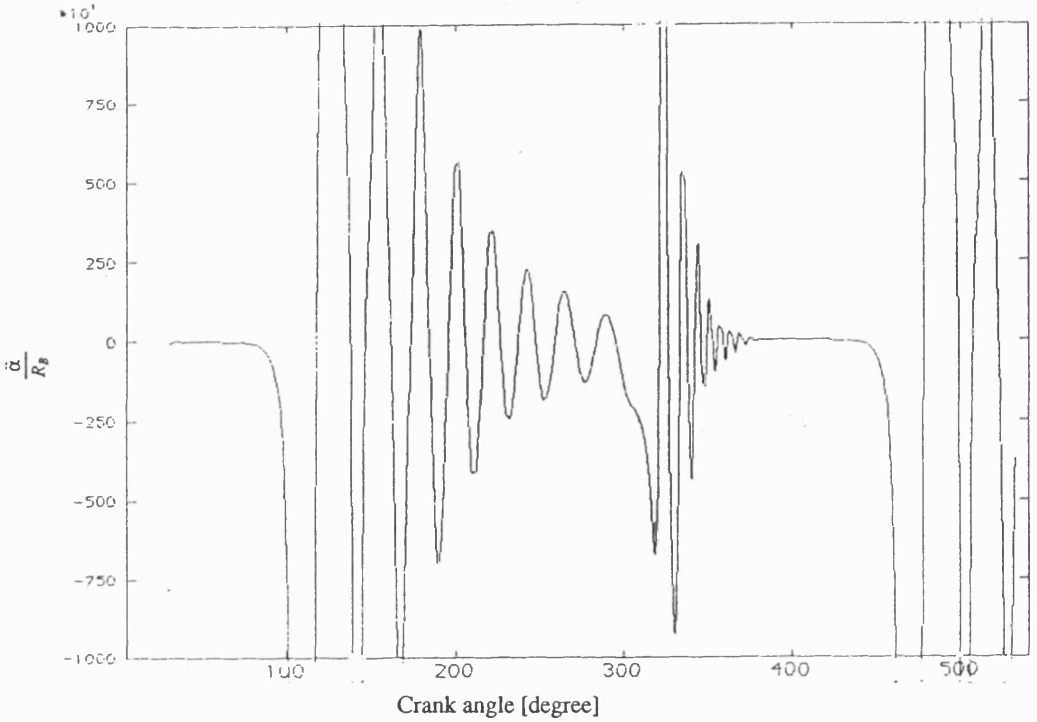

Fig 7.5.2a Contact criterion 2 (continuous contact model)

mean speed 168 rev/min ; I1=0.23kgm.m; dia. clearance 0.25mm

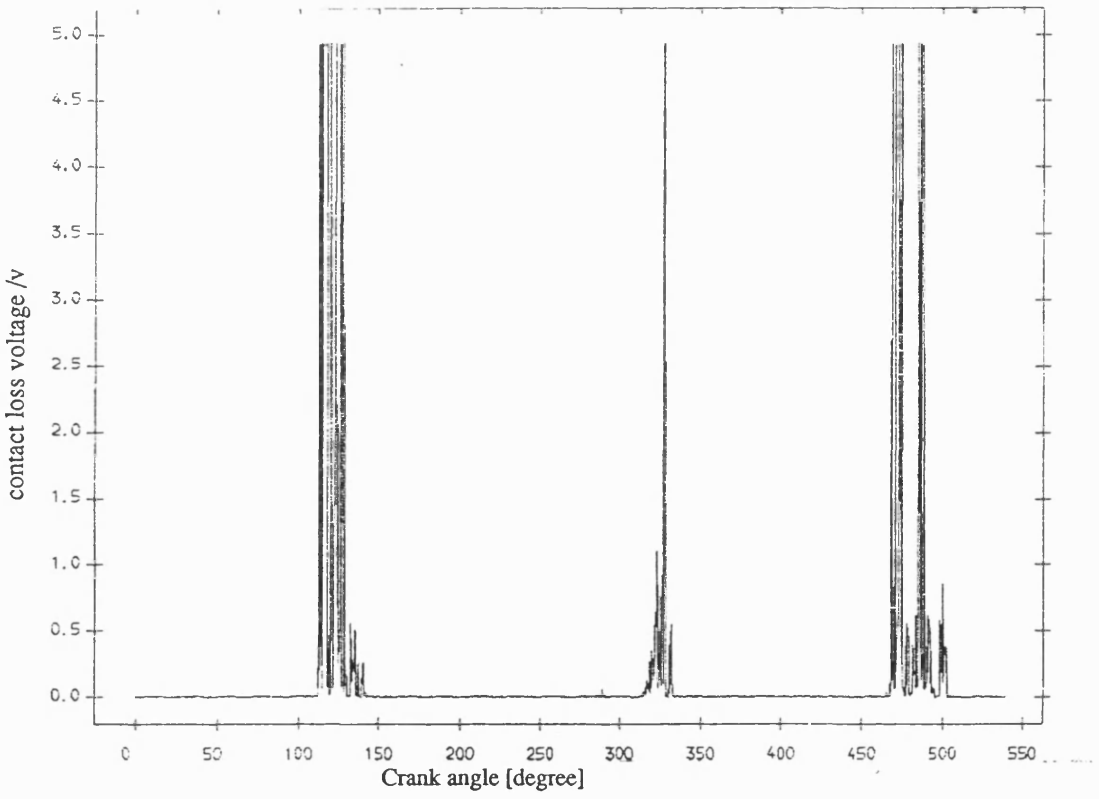

Fig 7.5.2b Exp. result contact loss of pin and greasy bearing

with fly wheel; mean speed 168 rev/min; dia.clearance 0.25mm

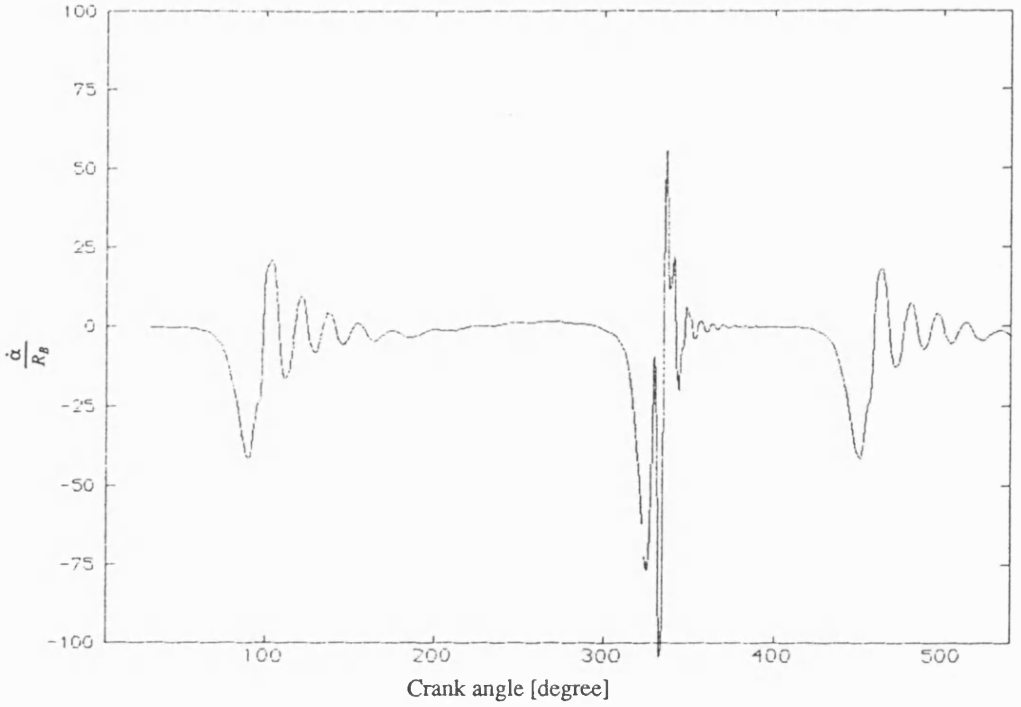

Fig 7.5.3a Contact criterion(E&W) (continuous contact model)
mean speed 244 rev/min ; I1=0.23kgm.m; dia. clearance 0.25mm

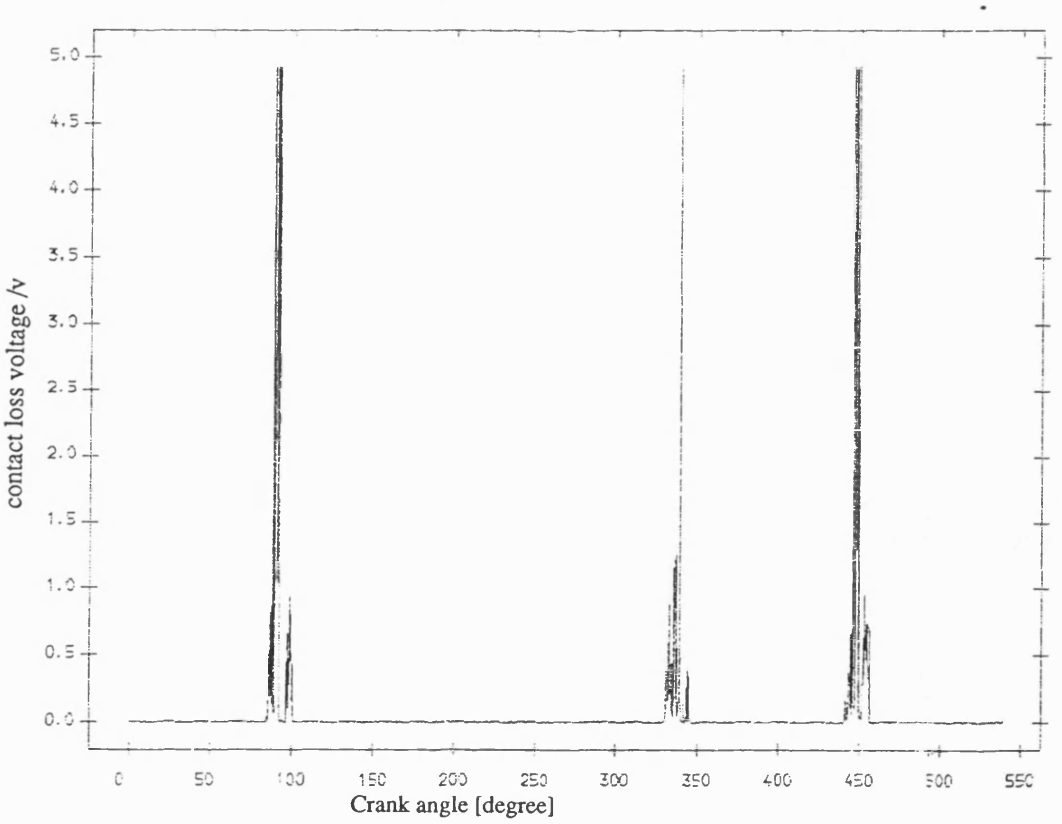

Fig 7.5.3b Exp. result contact loss of pin and greasy bearing
with fly wheel; mean speed 244 rev/min; dia.clearance 0.25mm

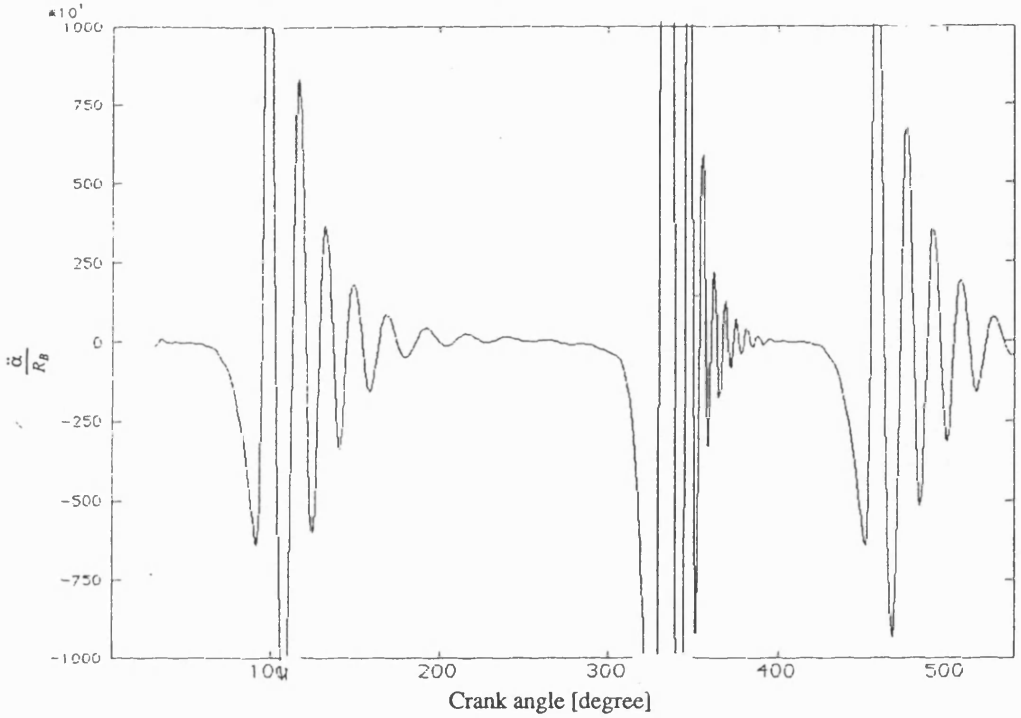

Fig 7.5.4a Contact criterion 2 (continuous contact model)

mean speed 244 rev/min ; I1=0.23kgm.m; dia. clearance 0.25mm

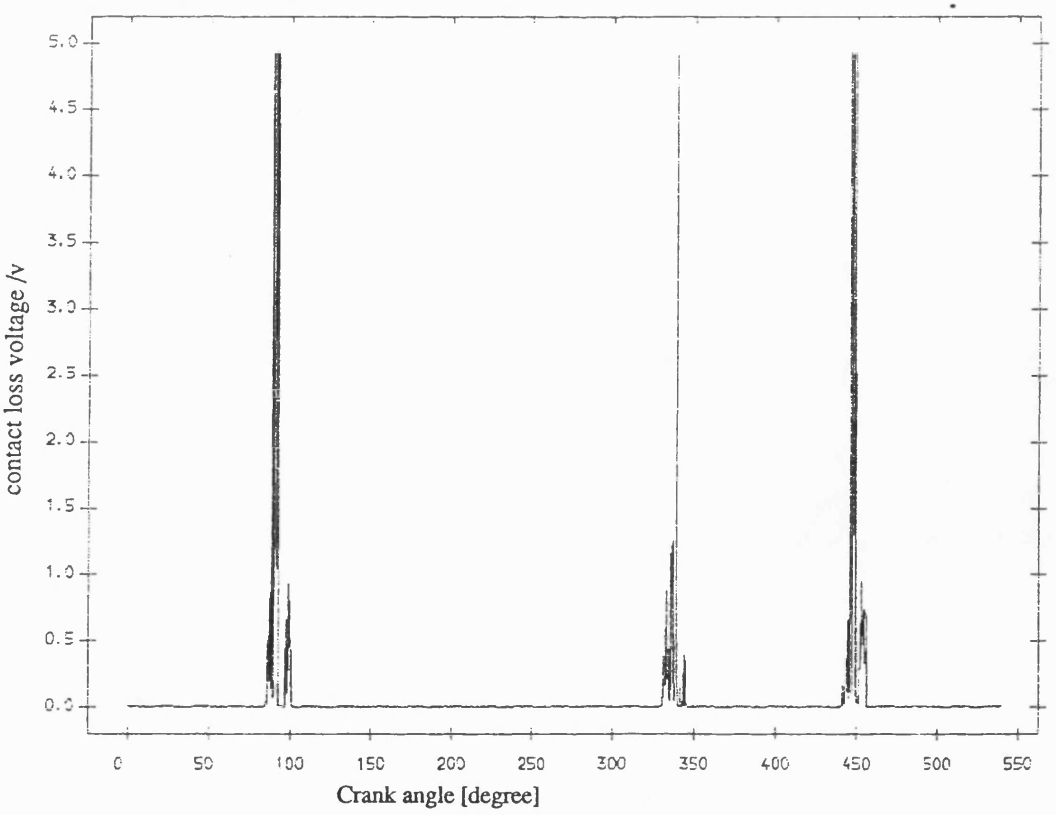

Fig 7.5.4b Exp. result contact loss of pin and greasy bearing

with fly wheel; mean speed 244 rev/min; dia.clearance 0.25mm

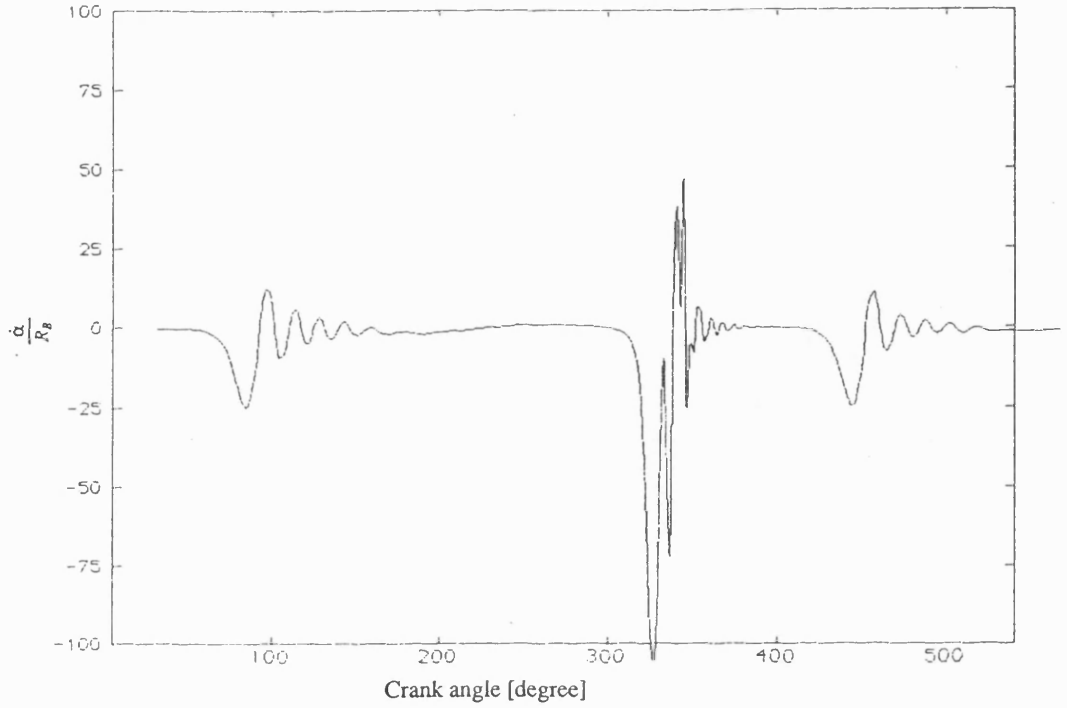

Fig 7.5.5a Contact criterion(E&W) (continuous contact model)
mean speed 327 rev/min ; I1=0.23kgm.m; dia. clearance 0.25mm

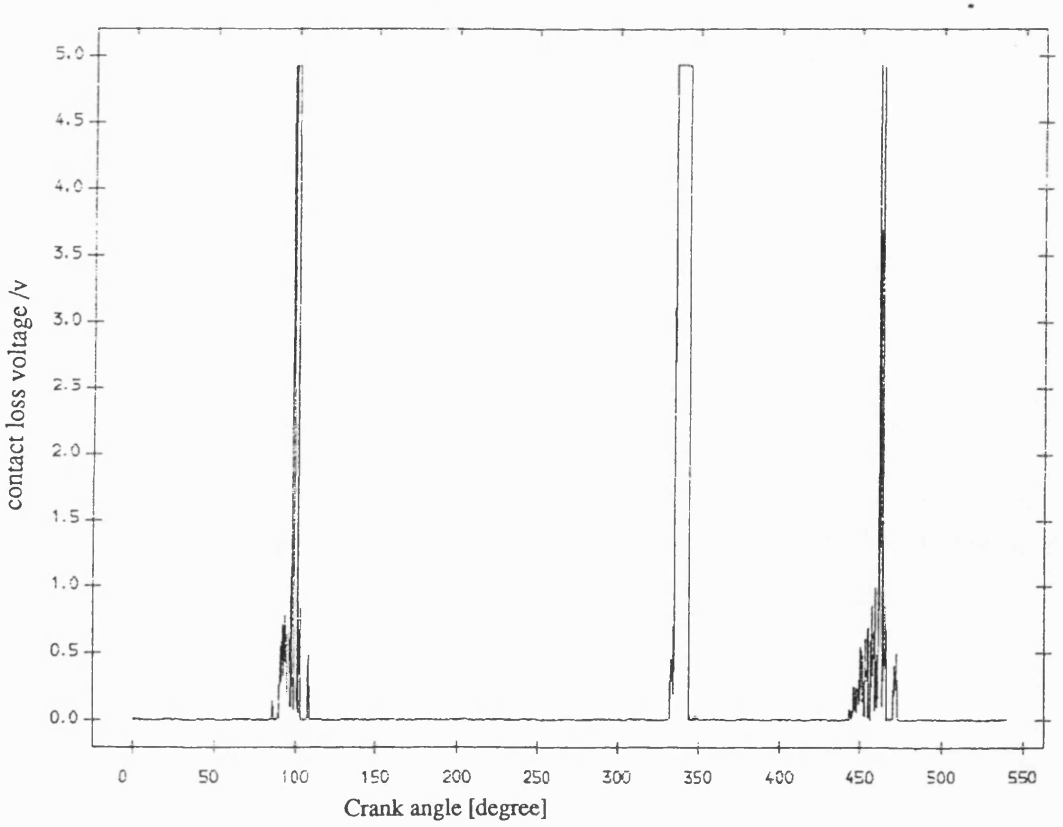

Fig 7.5.5b Exp. result contact loss of pin and greasy bearing
with fly wheel; mean speed 327 rev/min; dia.clearance 0.25mm

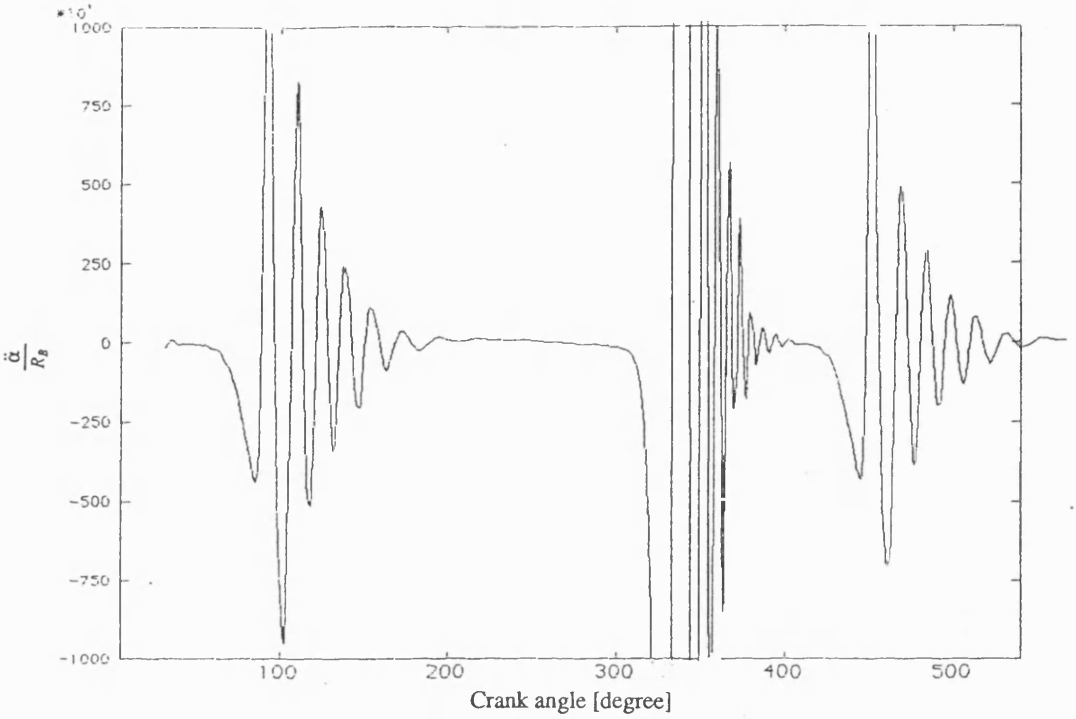

Fig 7.5.6a Contact criterion 2 (continuous contact model)

mean speed 327 rev/min ; I1=0.23kgm.m; dia. clearance 0.25mm

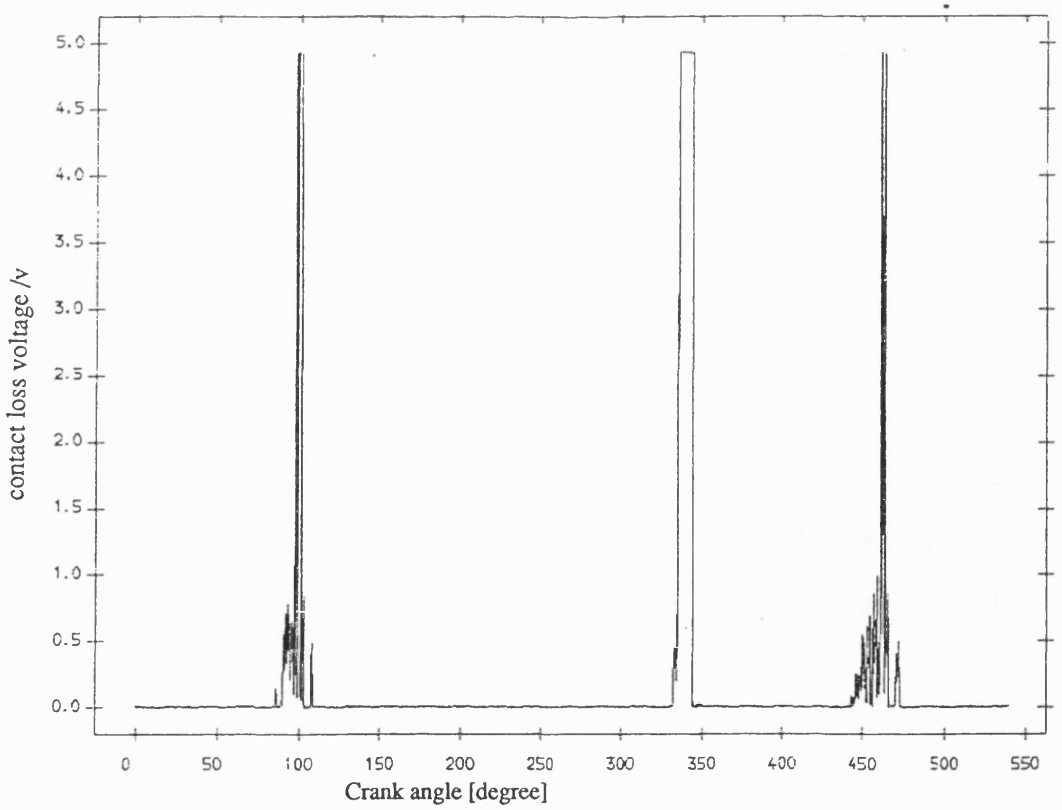

Fig 7.5.6b Exp. result contact loss of pin and greasy bearing

with fly wheel; mean speed 327 rev/min; dia.clearance 0.25mm

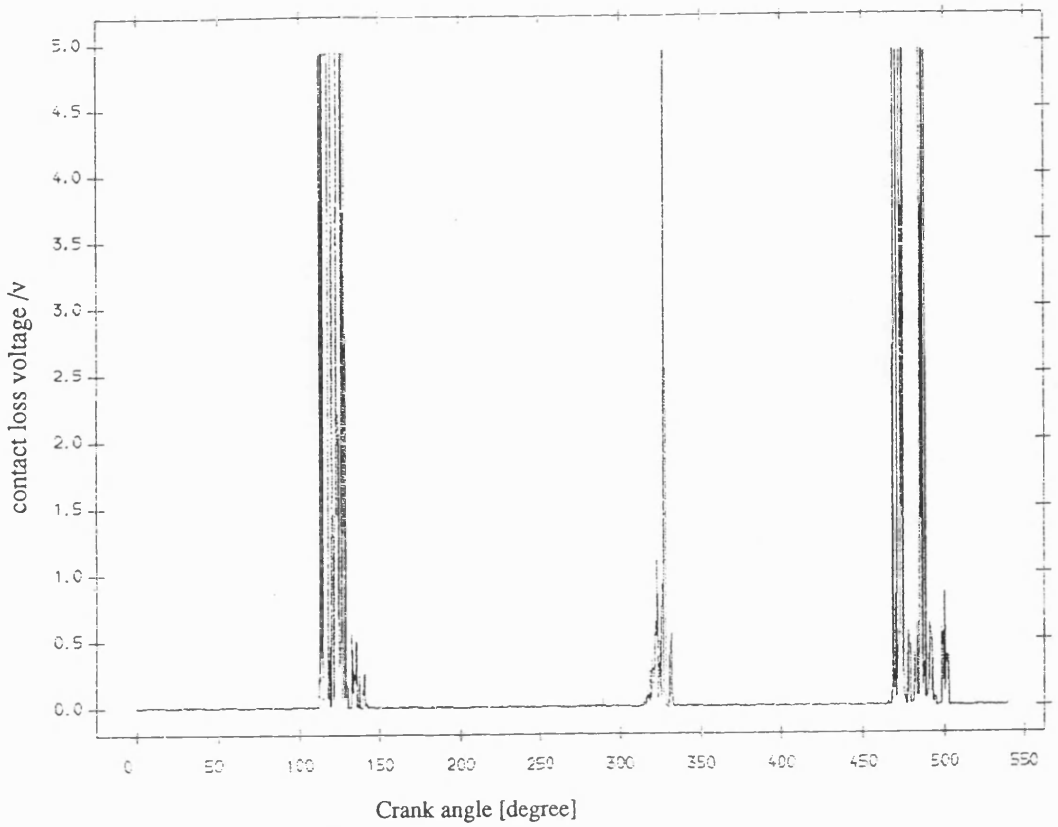

Fig 7.5.7 Exp. result contact loss of pin and greasy bearing
with fly wheel; mean speed 168 rev/min; dia.clearance 0.25mm

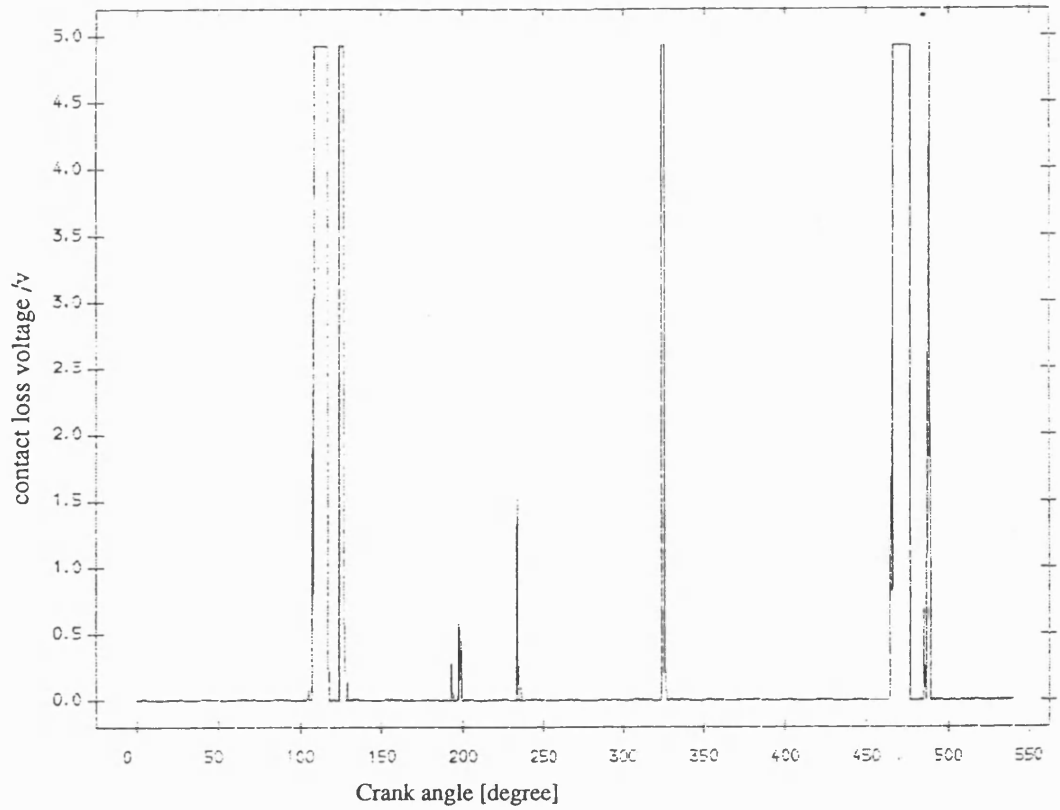

Fig 7.5.8 Exp. result contact loss of pin and normal bearing
with fly wheel; mean speed 168 rev/min; dia.clearance 0.25mm

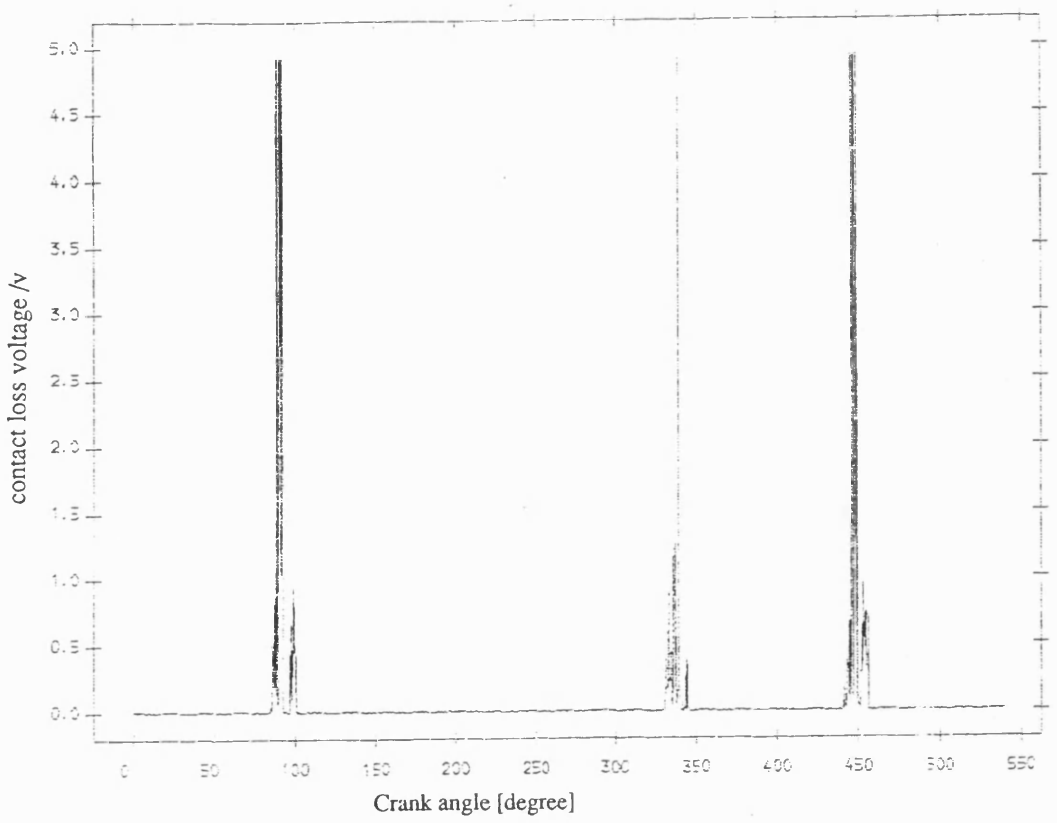

Fig 7.5.9 Exp. result contact loss of pin and greasy bearing
with fly wheel; mean speed 244 rev/min; dia.clearance 0.25mm

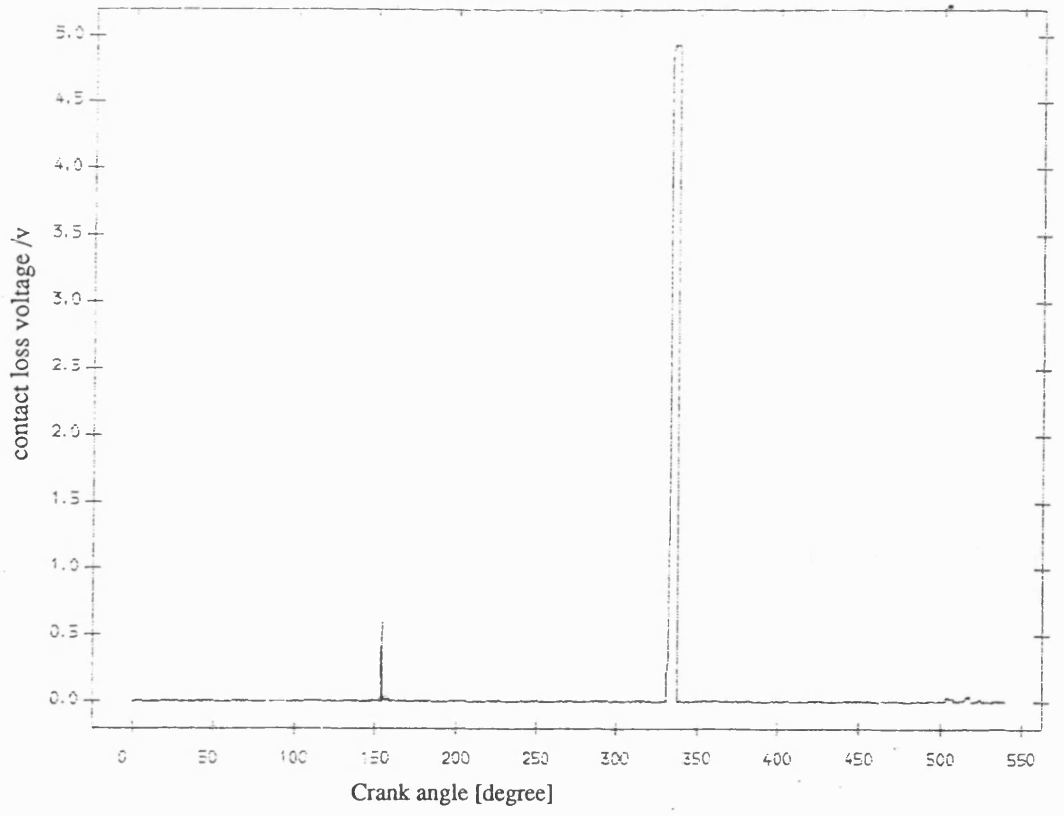

Fig 7.5.10 Exp. result contact loss of pin and normal bearing
with fly wheel; mean speed 244 rev/min; dia.clearance 0.25mm

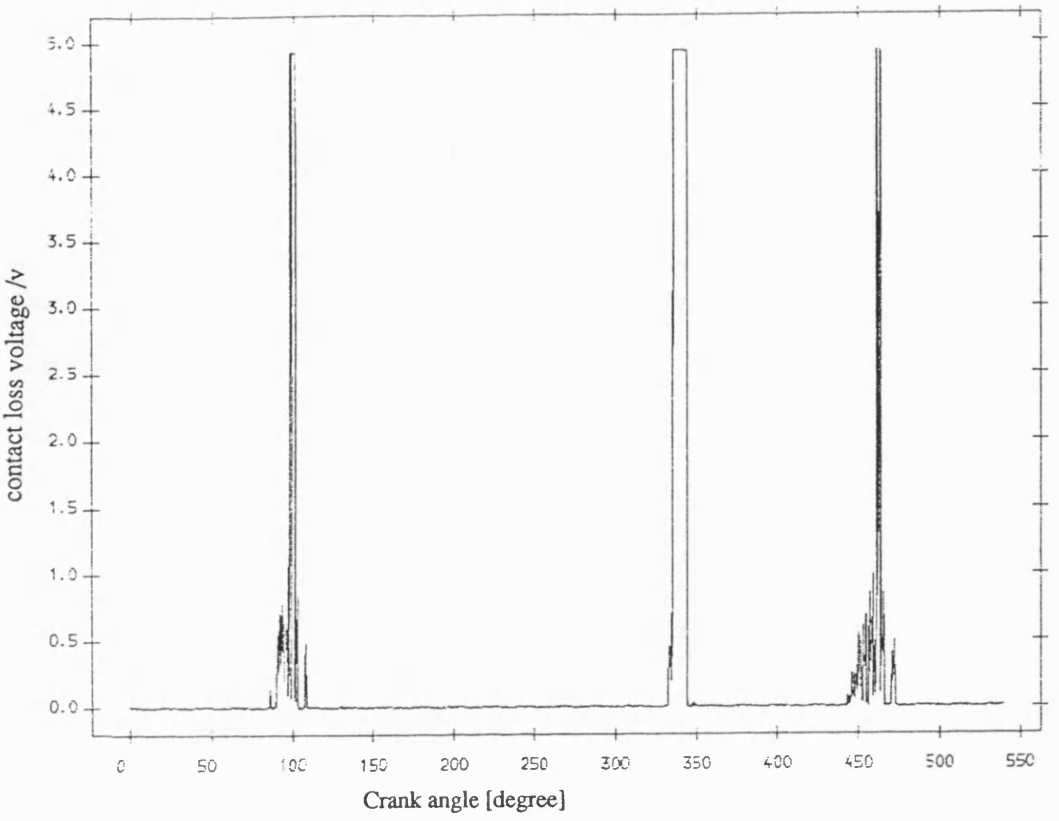

Fig 7.5.11 Exp. result contact loss of pin and greasy bearing
with fly wheel; mean speed 327 rev/min; dia.clearance 0.25mm

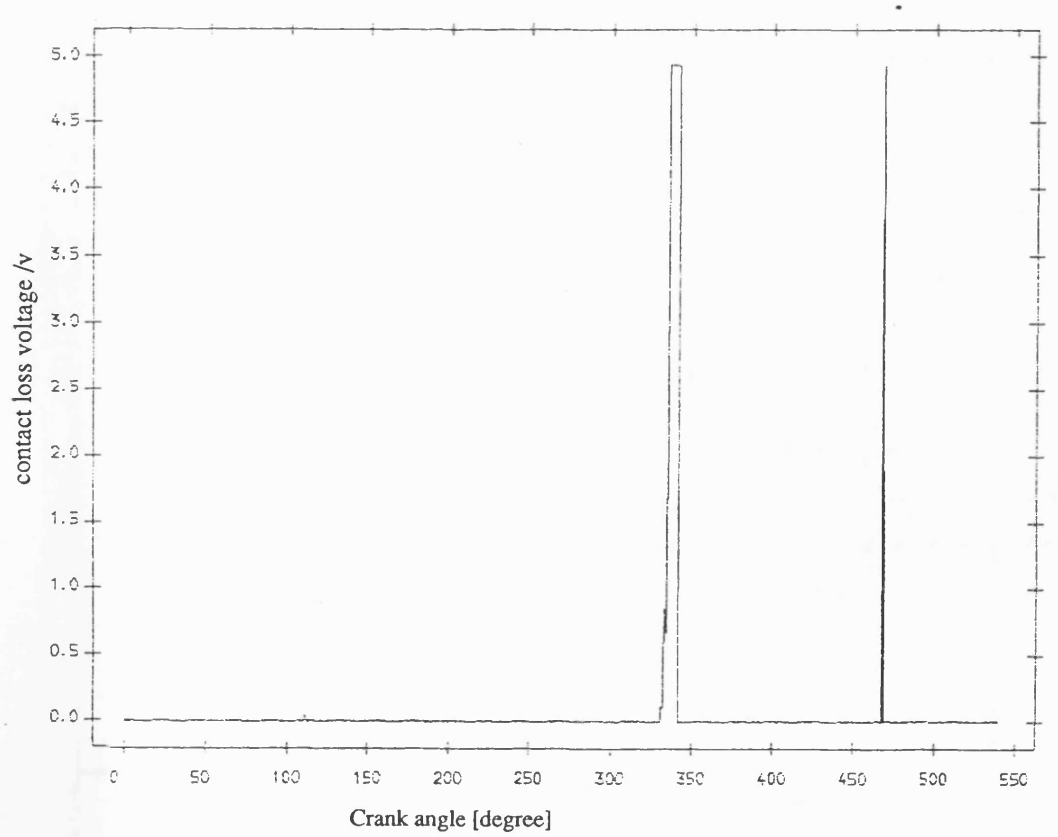

Fig 7.5.12 Exp. result contact loss of pin and normal bearing
with fly wheel; mean speed 327 rev/min; dia.clearance 0.25mm

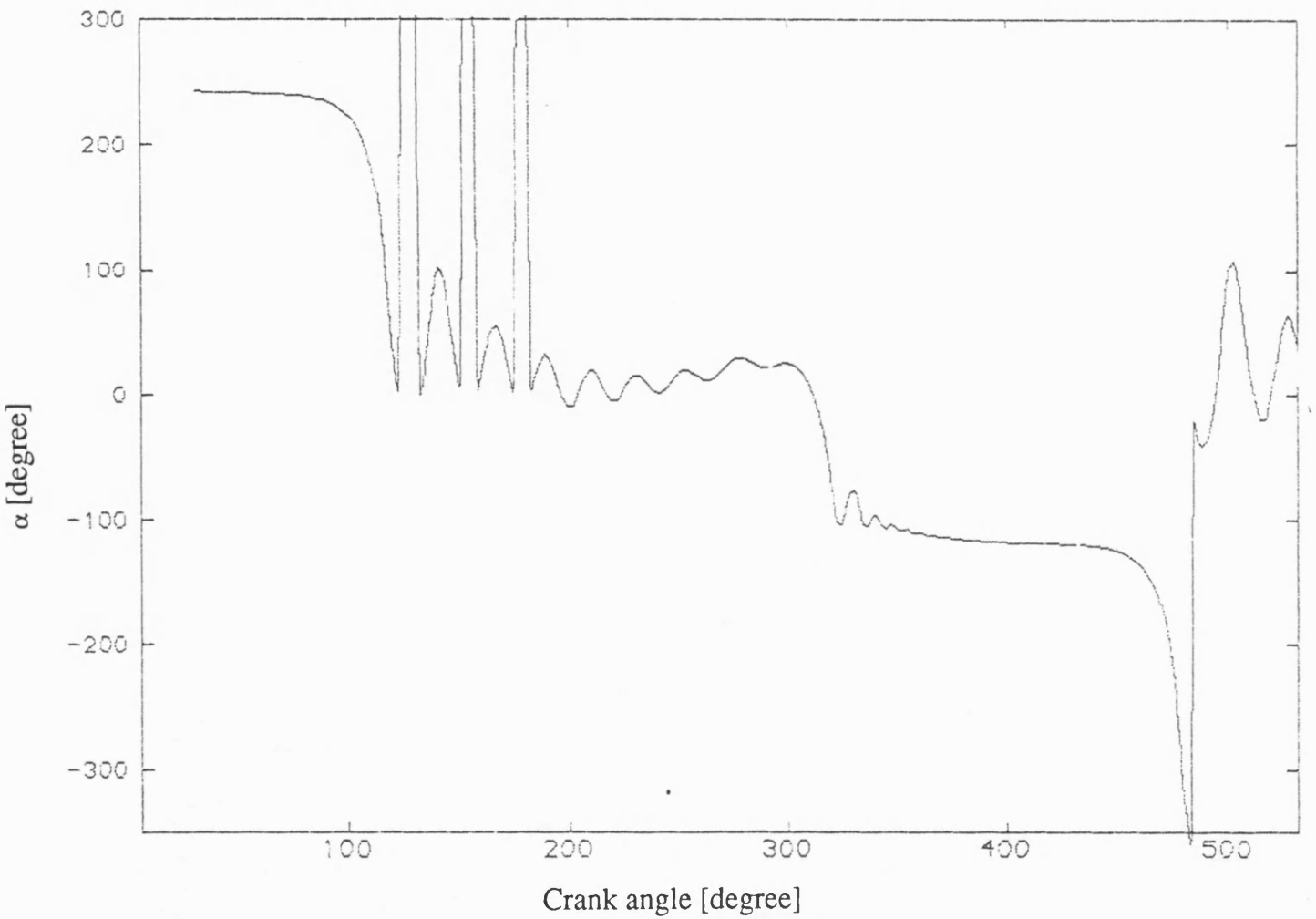

Fig 7.5.13 Angle of clearance link (continuous contact model)

mean speed 168 rev/min ; I1=0.23kgm.m; dia. clearance 0.25mm

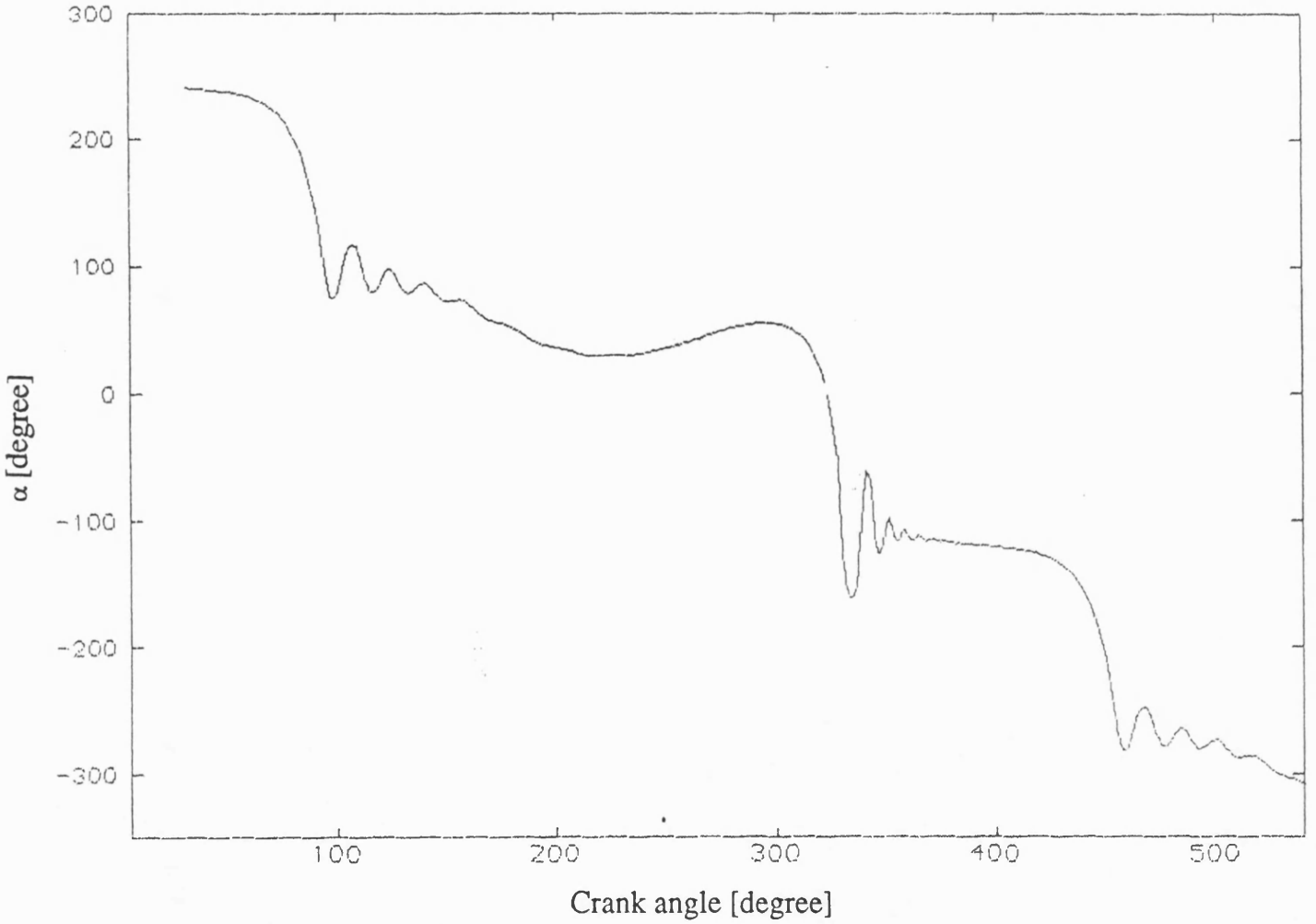

Fig 7.5.14 Angle of clearance link (continuous contact model)

mean speed 244 rev/min ; I_1 =0.23kgm.m; dia. clearance 0.25mm

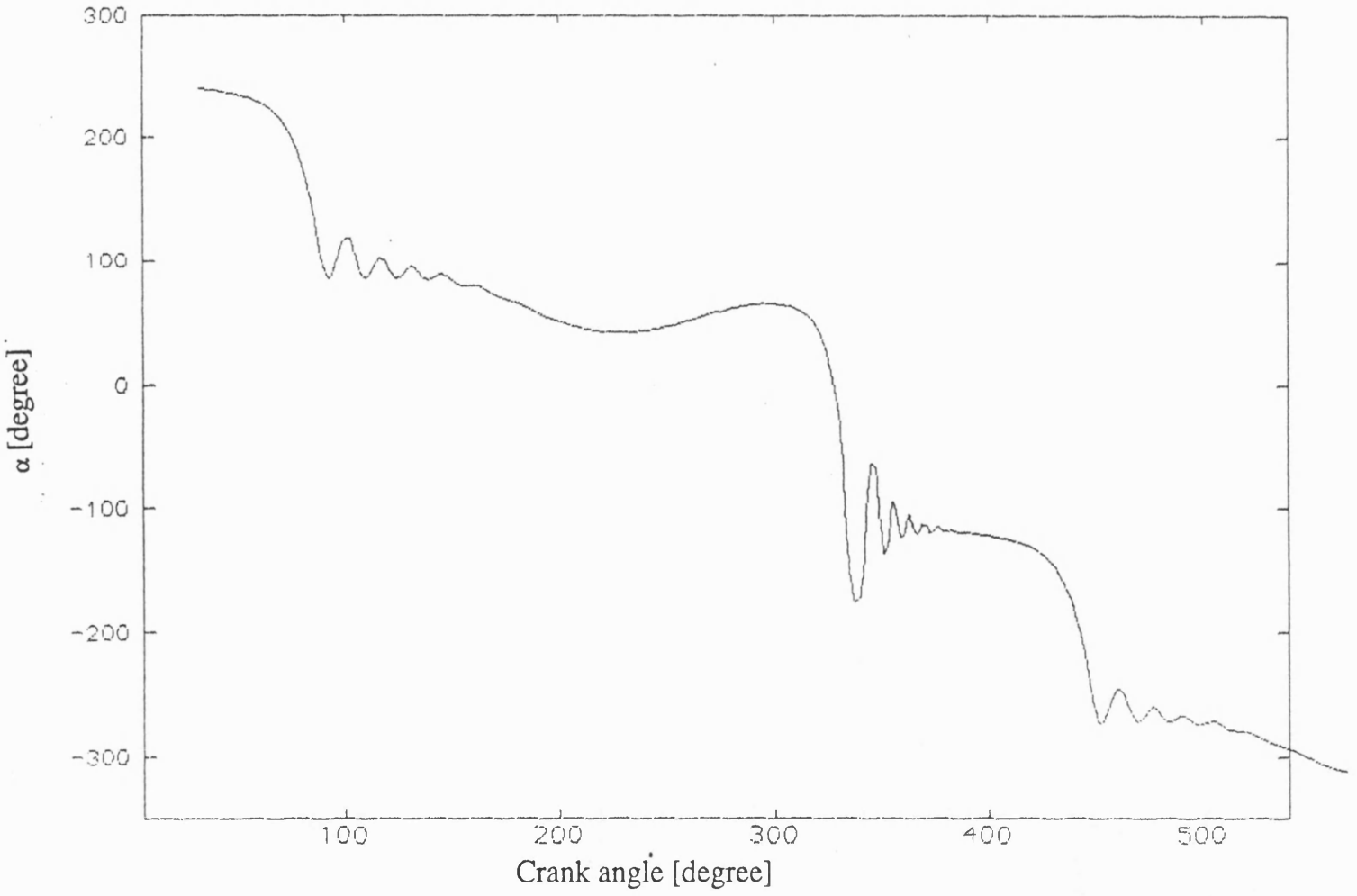

Fig 7.5.15 Angle of clearance link (continuous contact model)

mean speed 327 rev/min, I_1=0.23kgm.m; dia. clearance 0.25mm

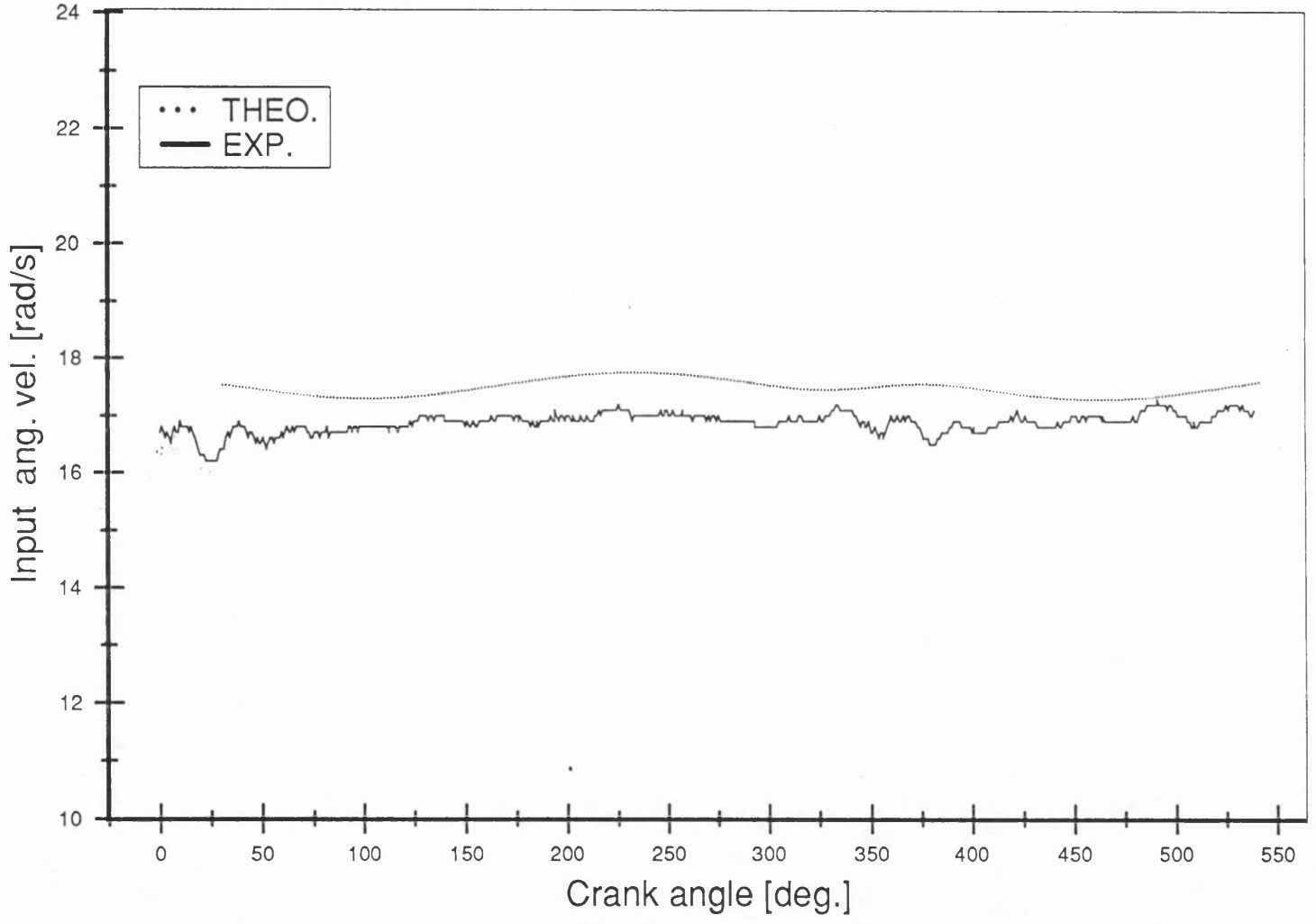

Fig 7.6.1 Input speed , dia. clearance = 0.25 mm
with fly wheel mean speed= 168 rev/min , with friction

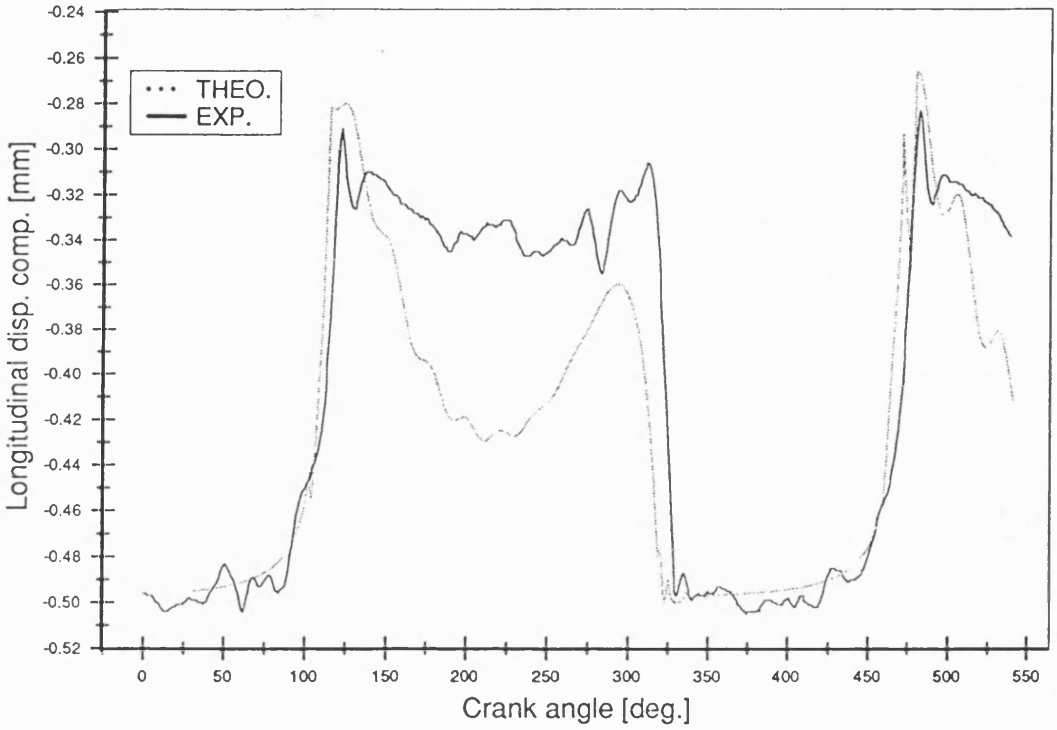

Fig 7.6.2 Longitudinal disp. of pin relative to bearing; d.clea =0.25mm
with fly wheel ; mean speed=168 rev/min ; no friction

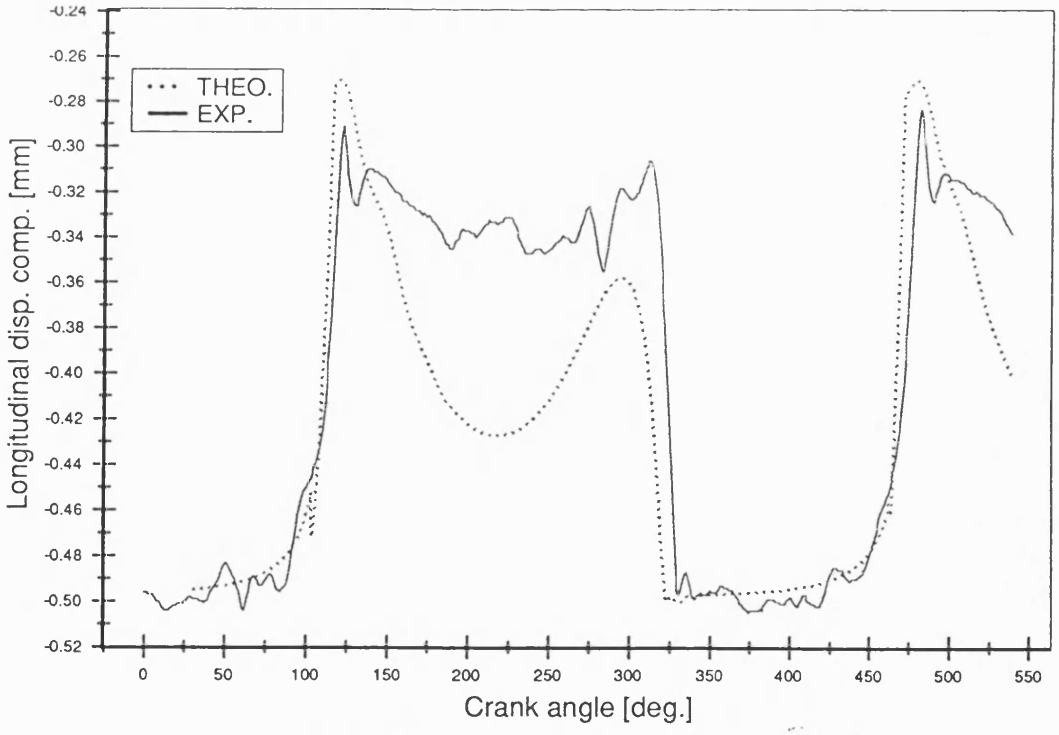

Fig 7.6.3 Longitudinal disp. of pin relative to bearing , d. cl ea=0.25mm
with fly wheel mean speed= 168 rev/min , with friction

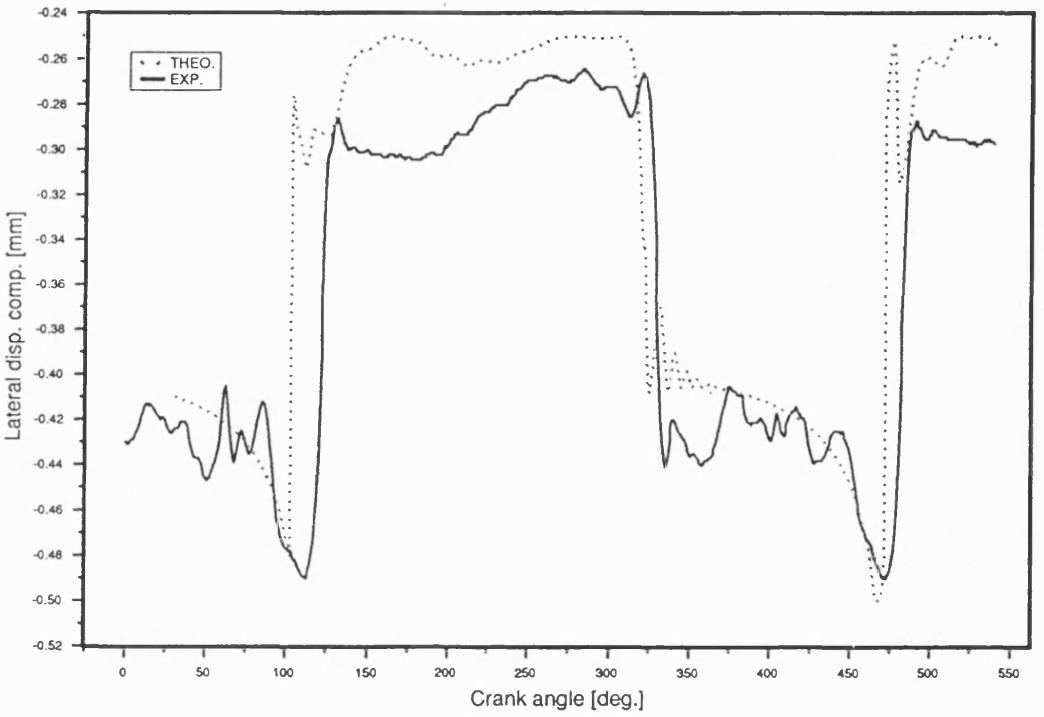

Fig 7.6.4 Lateral pin disp. relative to bearing , d.clea =0.25m m
with fly wheel , mean speed = 168 rev/min , no friction

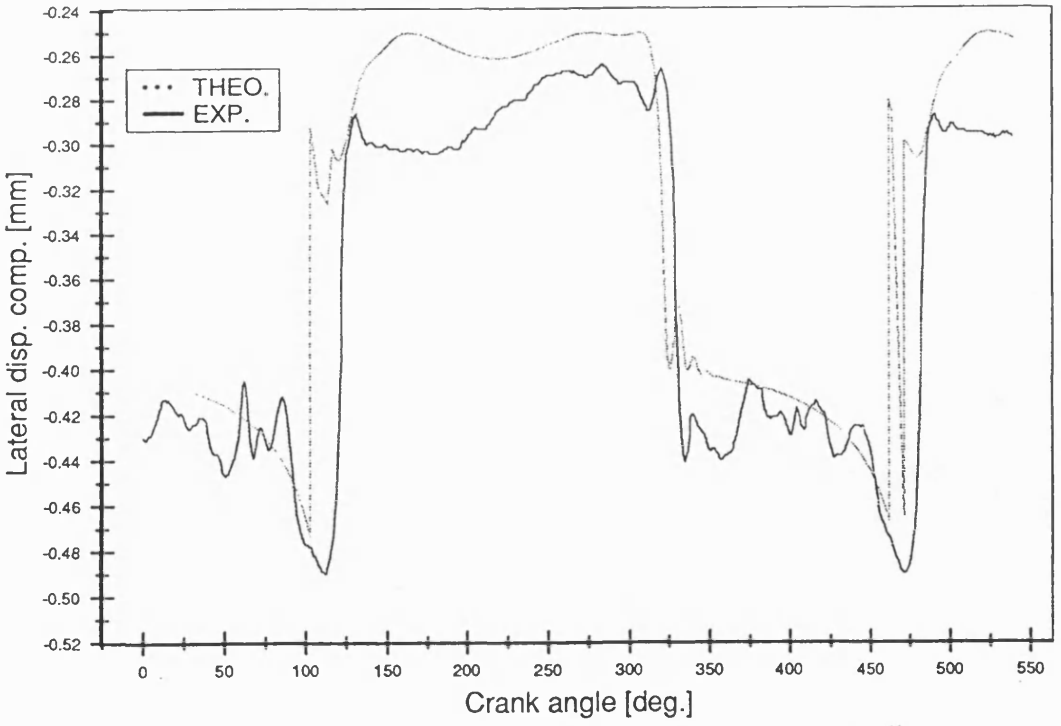

Fig 7.6.5 Lateral pin disp. relative to bush d. clea=0.25mm
with flywheel mean speed=168 rev/min ; with friction

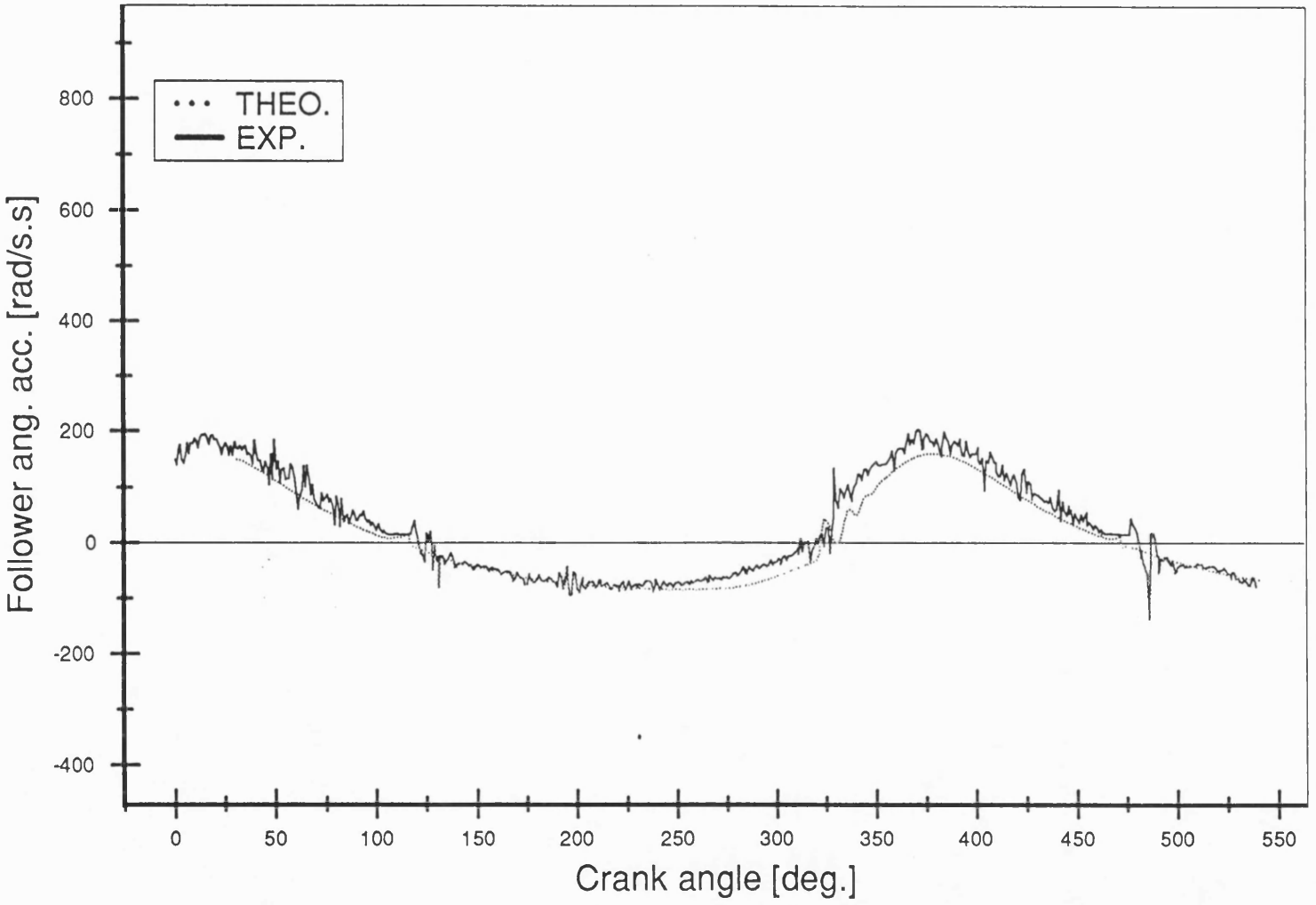

Fig 7.6.6 Follower angular acceleration , dia. clearance = 0.2 5mm
with fly wheel ; mean speed = 168 rev/min ; with friction

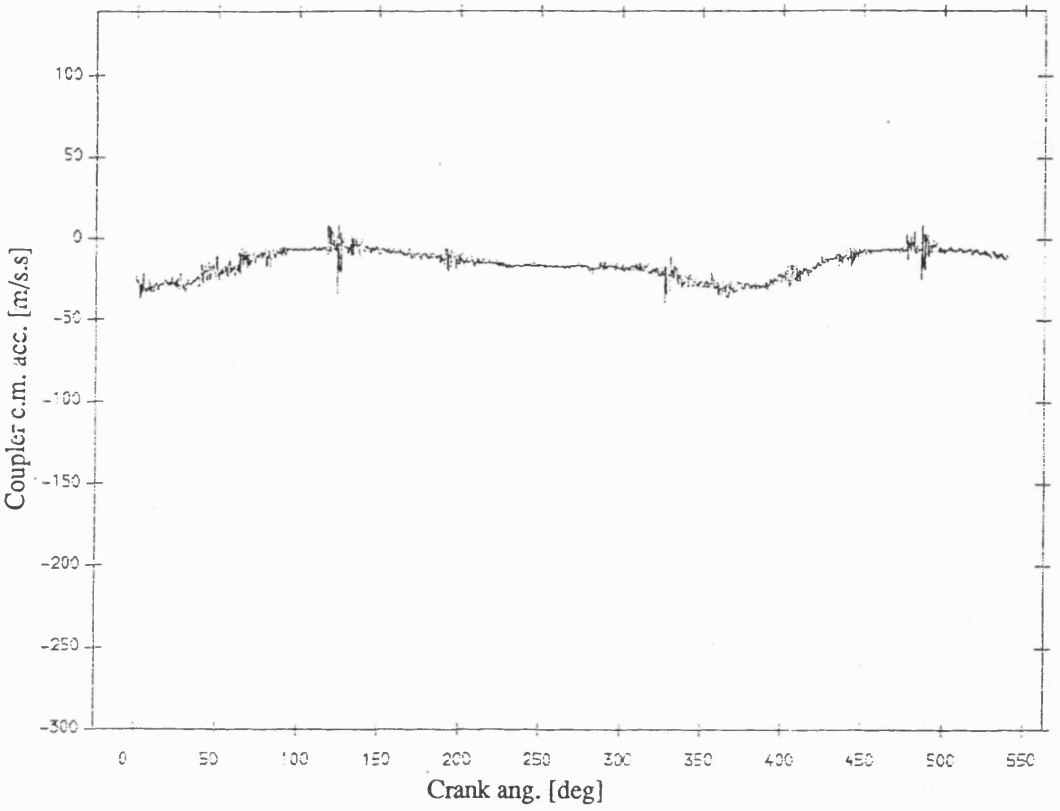

Fig 7.6.7 Exp. result coupler acceleration , normal bearing
with fly wheel ;mean speed=168 rev/min ; dia. clearance=.25mm

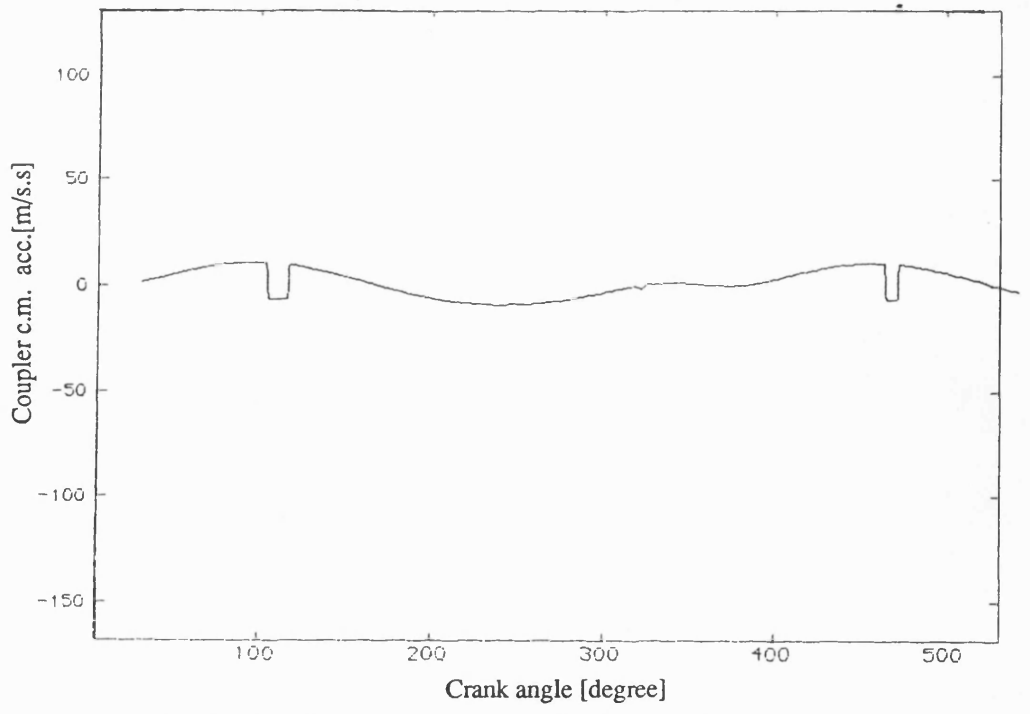

Fig 7.6.8 Coupler c.m. lateral acceleration (theoretical)
d.clea=.25mm , mean speed 168 rev/min ; I1=0.23 kg-m.m

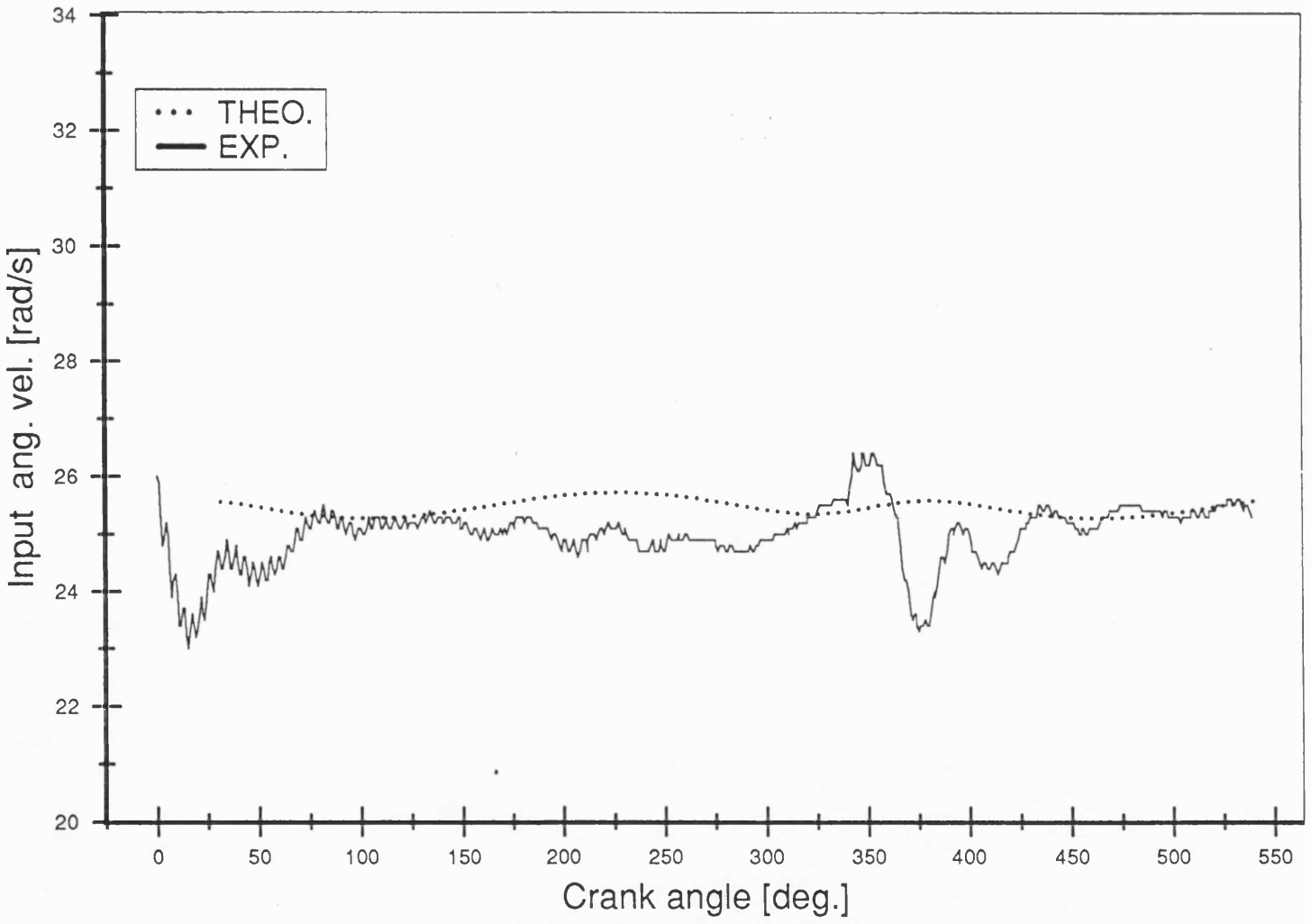

FIG 7.6.9 Input speed , dia. clearance=0.25mm
with fly wheel mean speed=244 rev/min , with friction

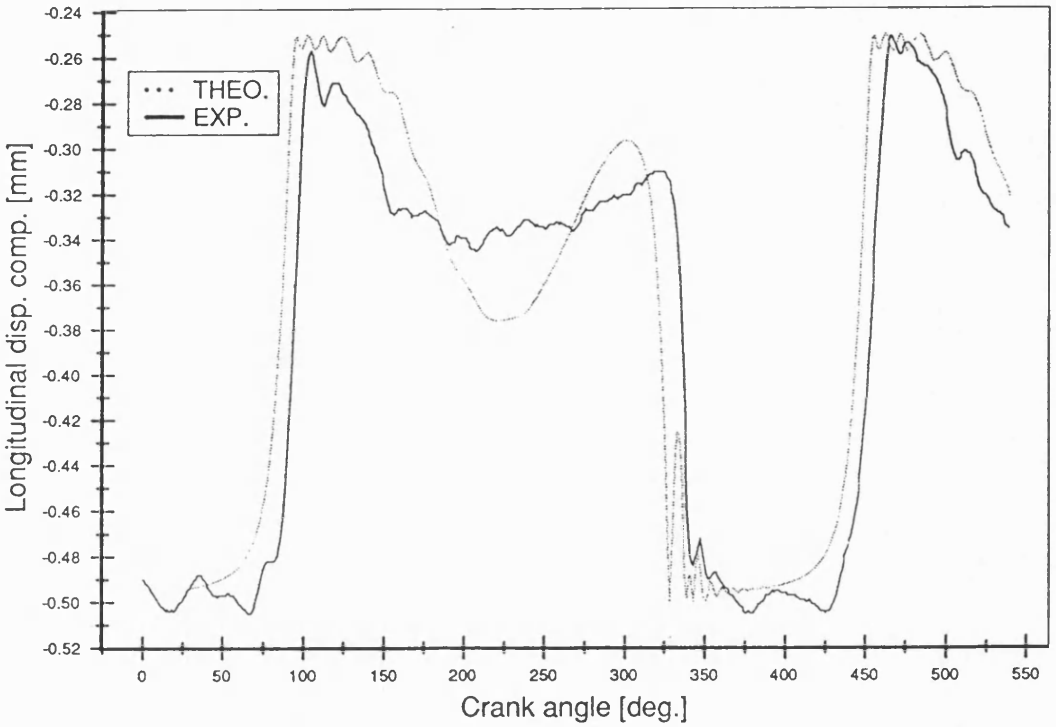

Fig 7.6.10 Longitudinal disp. of pin relative to bearing, d.cle a=0.25mm
with fly wheel ; mean speed = 244 rev/min ; no friction

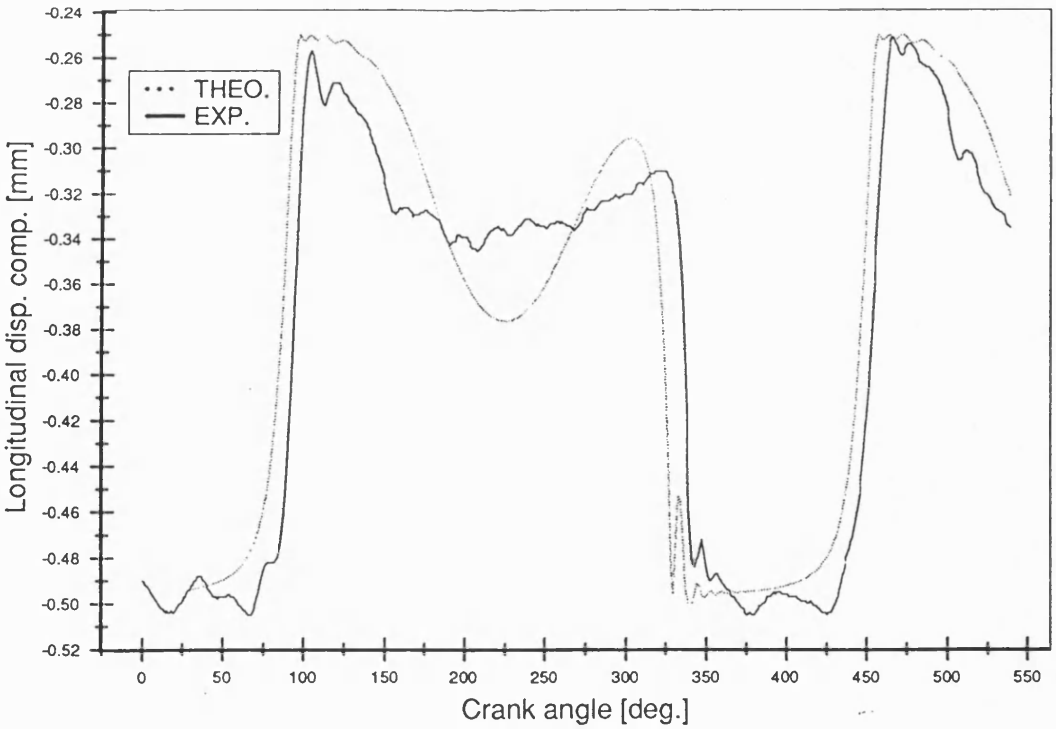

Fig 7.6.11 Longitudinal disp. of pin relative to bearing d. cle a =0.25mm
with fly wheel mean speed=244 rev/min Cij=4.d-7

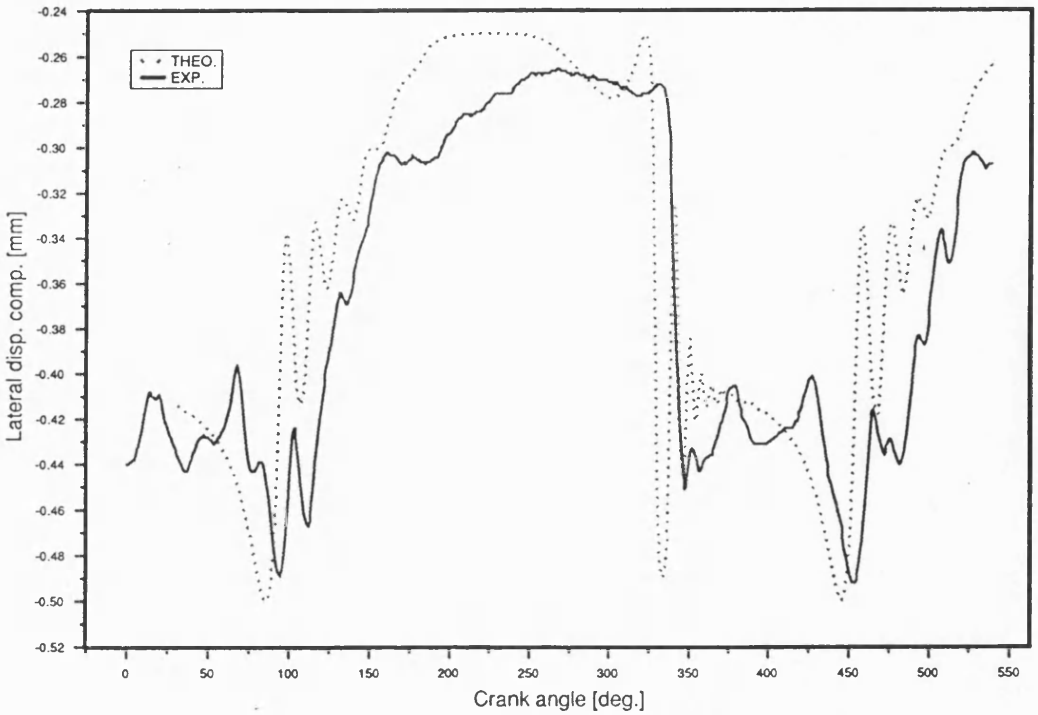

Fig 7.6.12 Lateral pin disp. relative to bearing , d.clea=0.25m m
with fly wheel mean speed = 244 rev/min , no friction

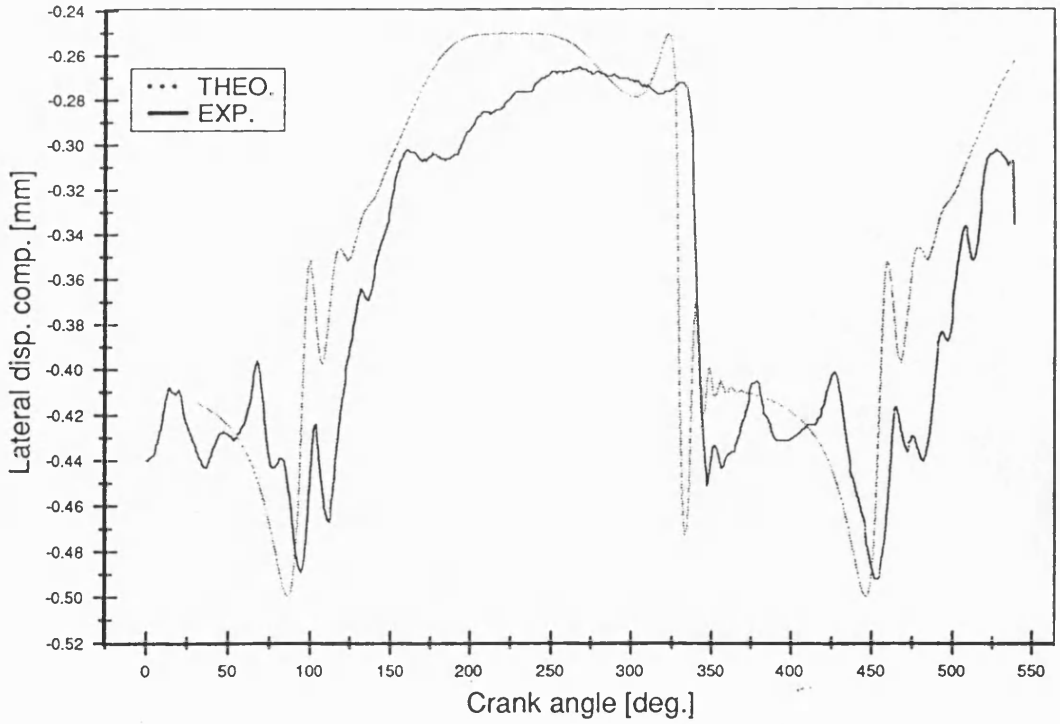

Fig7.6.13 Lateral comp. of pin disp. relative to bearing d.clea =.25mm
with fly wheel mean speed=244 rev/min ; with friction

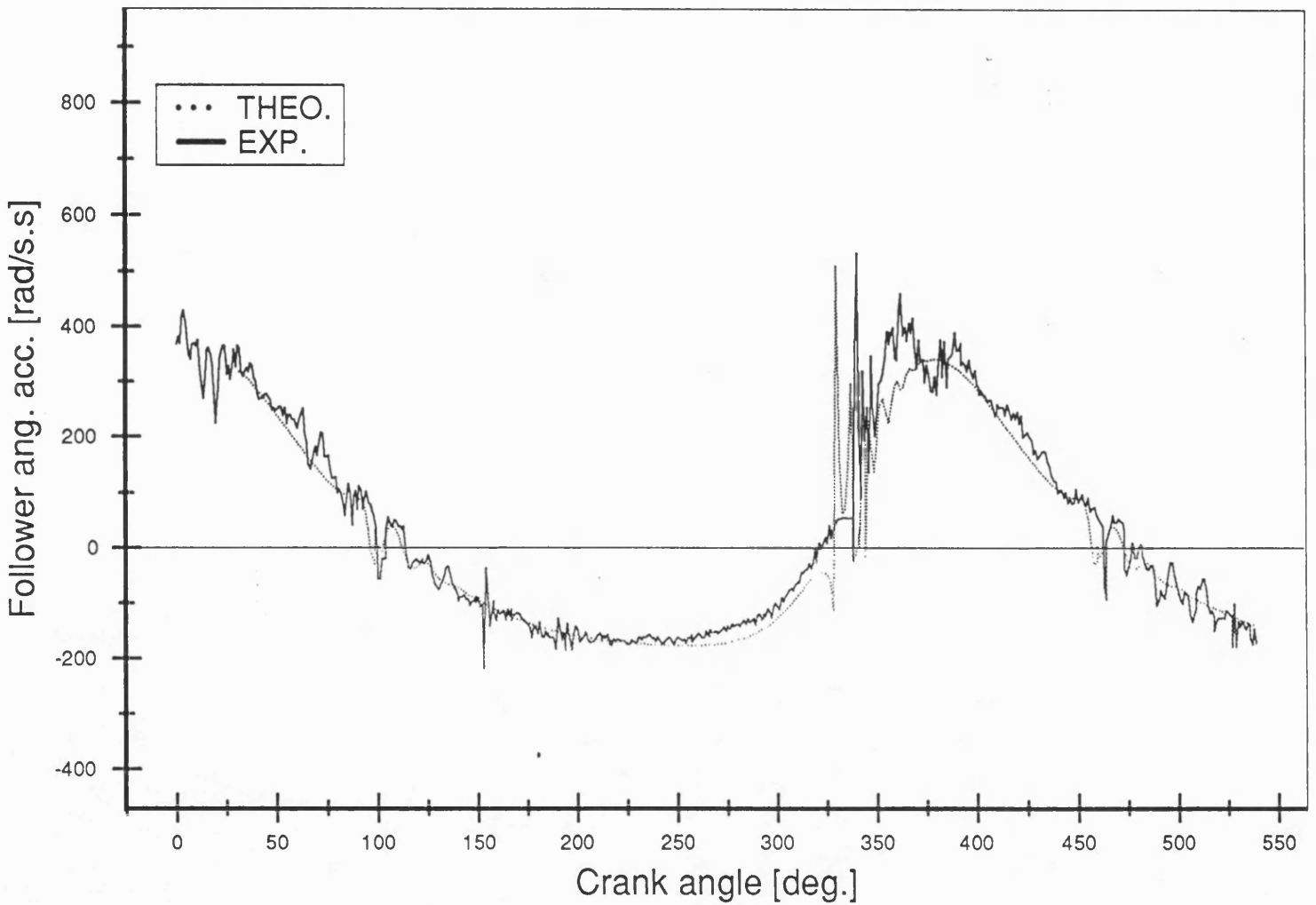

Fig 7.6.14 Follower angular acceleration , dia. clearance=0.25m m
with fly wheel ; mean speed = 244 rev/min ; with friction

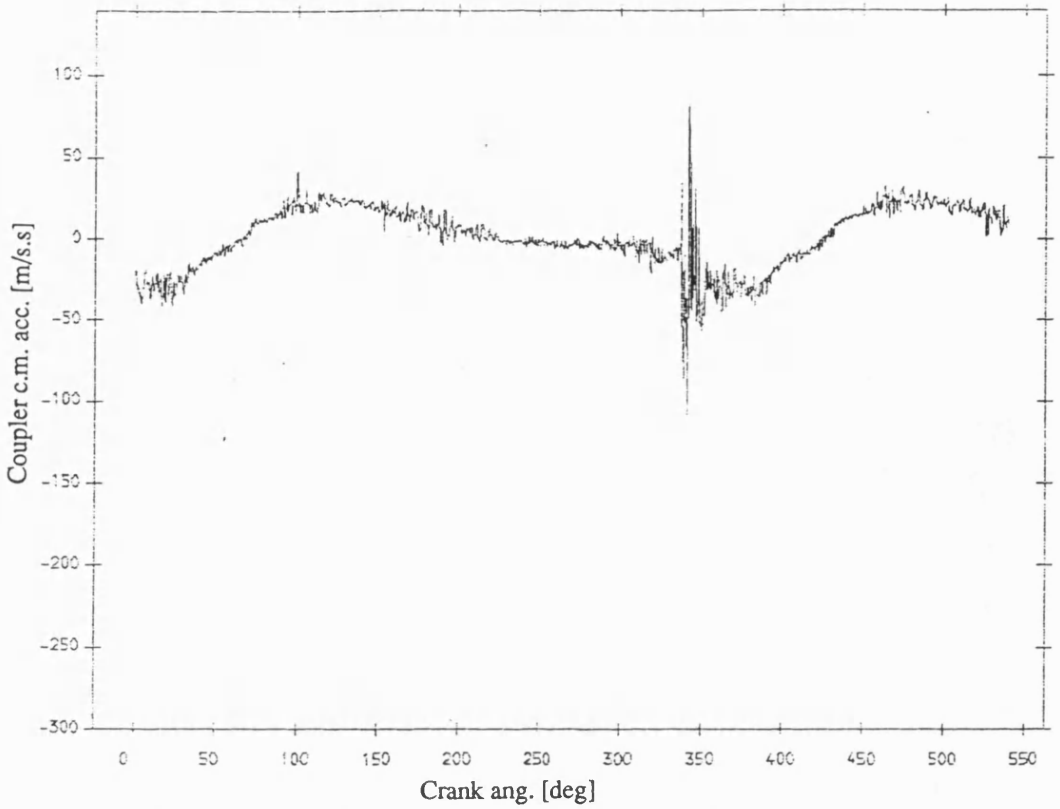

Fig 7.6.15 Exp. result coupler acceleration , normal bearing
with fly wheel ;mean speed=244 rev/min ; dia. clearance=.25mm

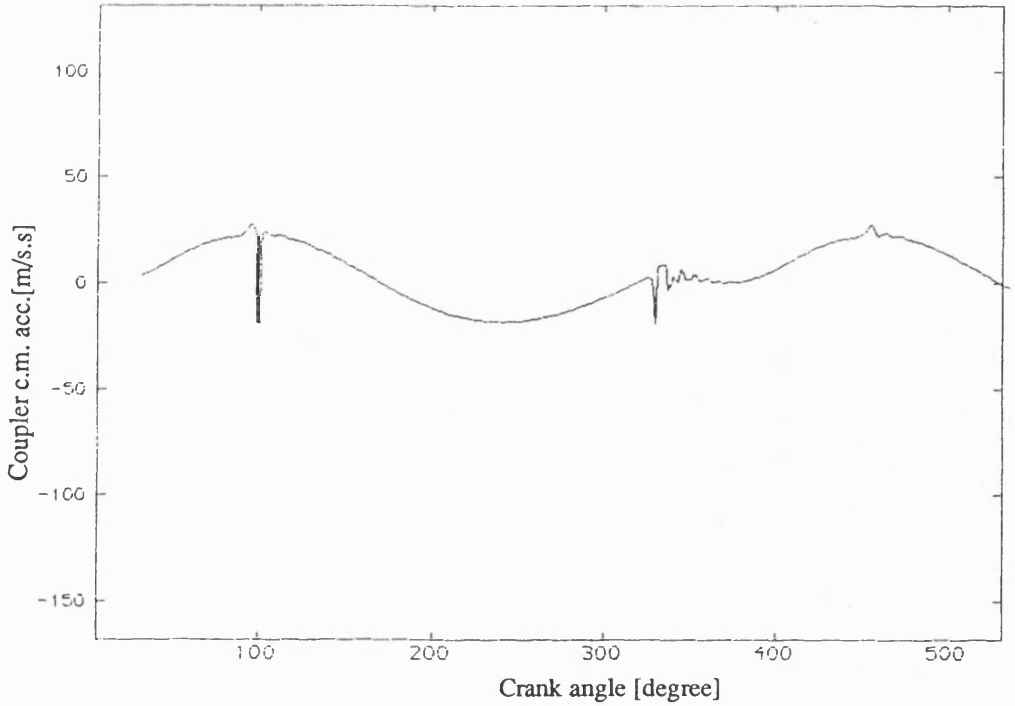

Fig 7.6.16 Coupler c.m. lateral acceleration (theoretical)
d.clea=.25mm , mean speed 244 rev/min ; I1=0.23 kg-m.m

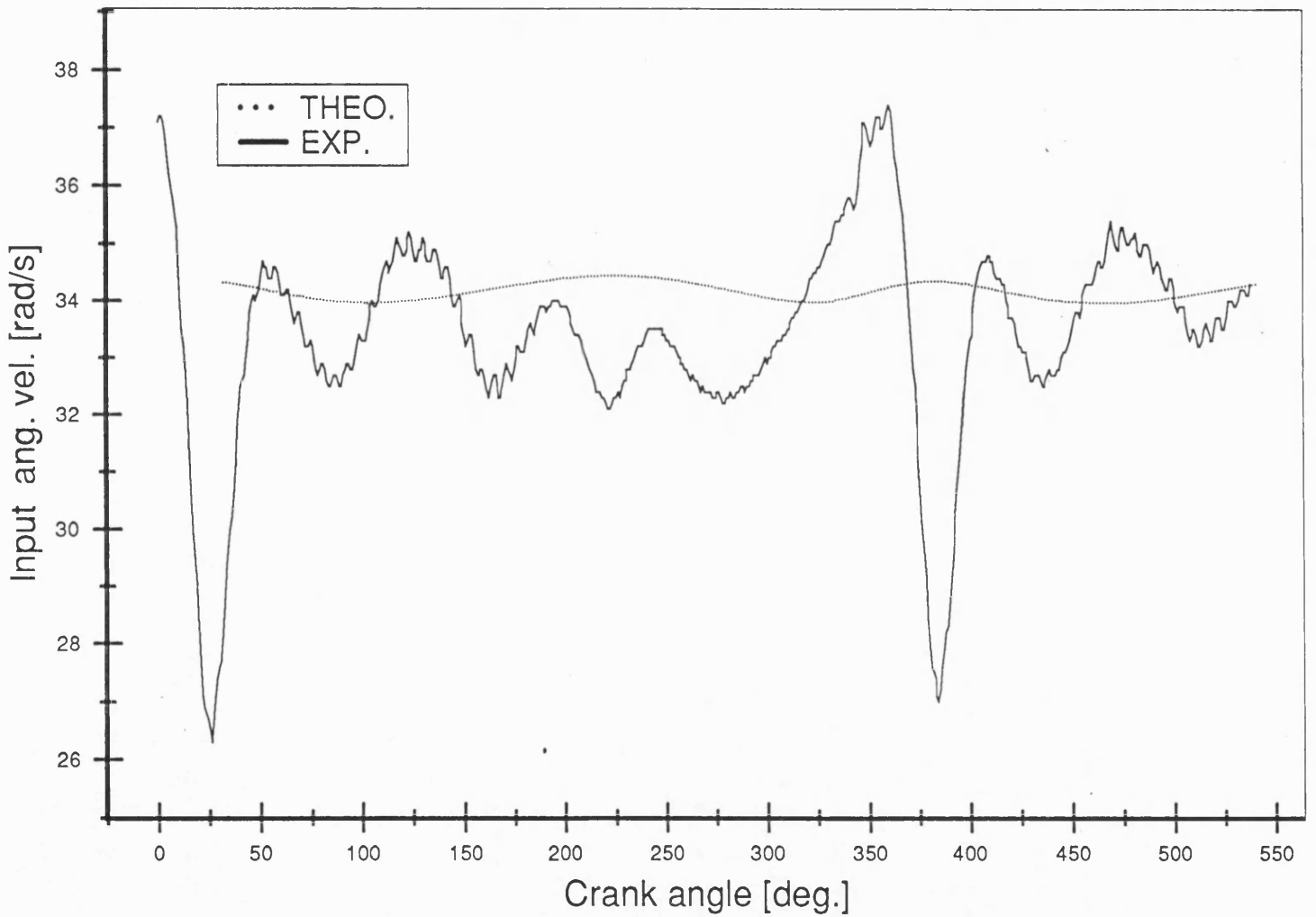

Fig 7.6.17 Input speed , dia. clearance = 0.25 mm

with fly wheel; mean speed 327 rev/min , with friction

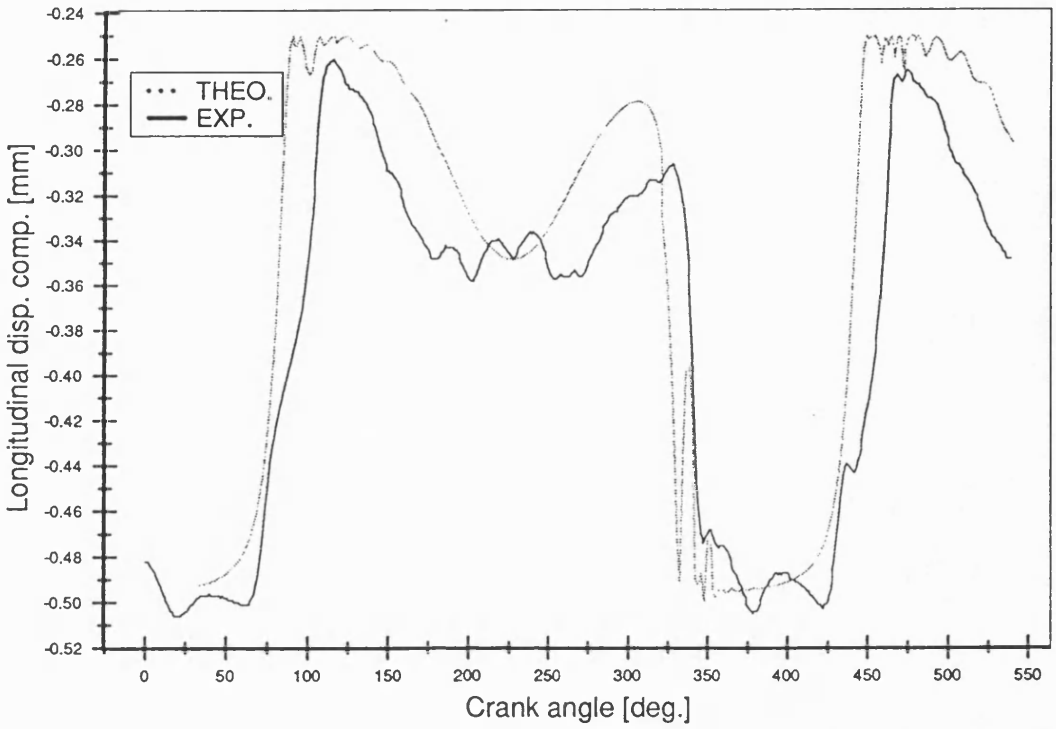

Fig 7.6.18 Longitudinal disp. of pin relative to bearing, d.cle a=0.25mm
with fly wheel ; mean speed = 327rev/min ; no friction

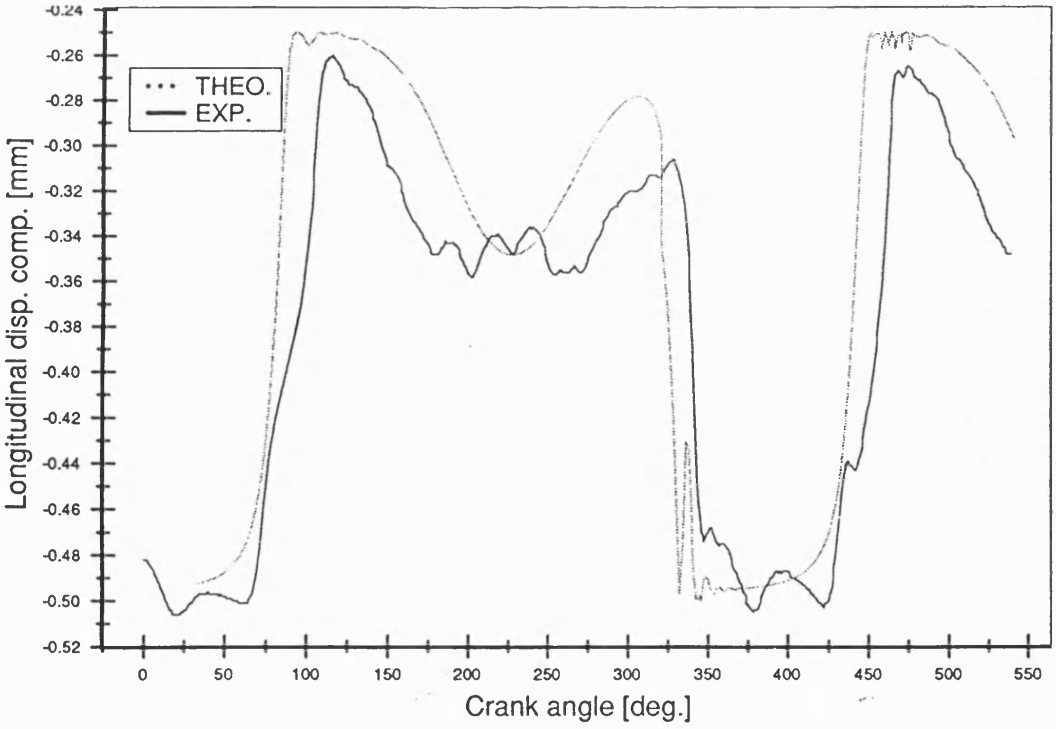

Fig 7.6.19 Longitudinal disp. of pin relative to bearing, d.cle a=0.25mm
with fly wheel; mean speed = 327 rev/min with friction

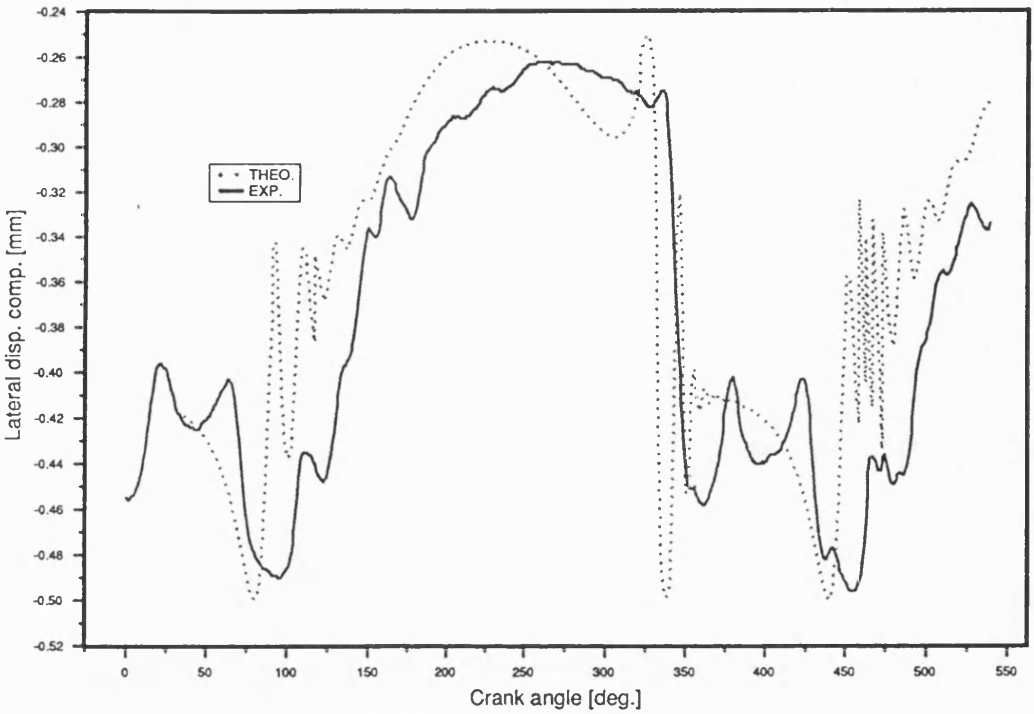

Fig 7.6.20 Lateral pin disp. relative to bearing , d. clea =0.2 5mm
with fly wheel;mean speed = 327 rev/min ; no friction

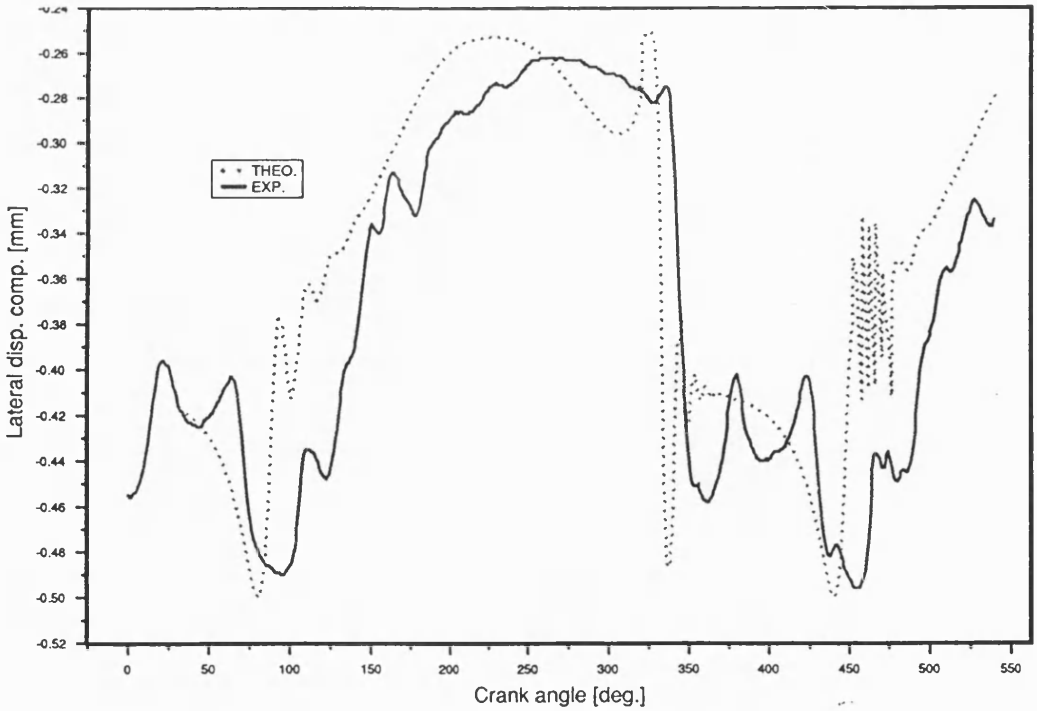

Fig 7.6.21 Lateral pin disp. relative to bearing , d. clea = 0. 25mm
with fly wheel;mean speed = 327 rev/min ; with friction

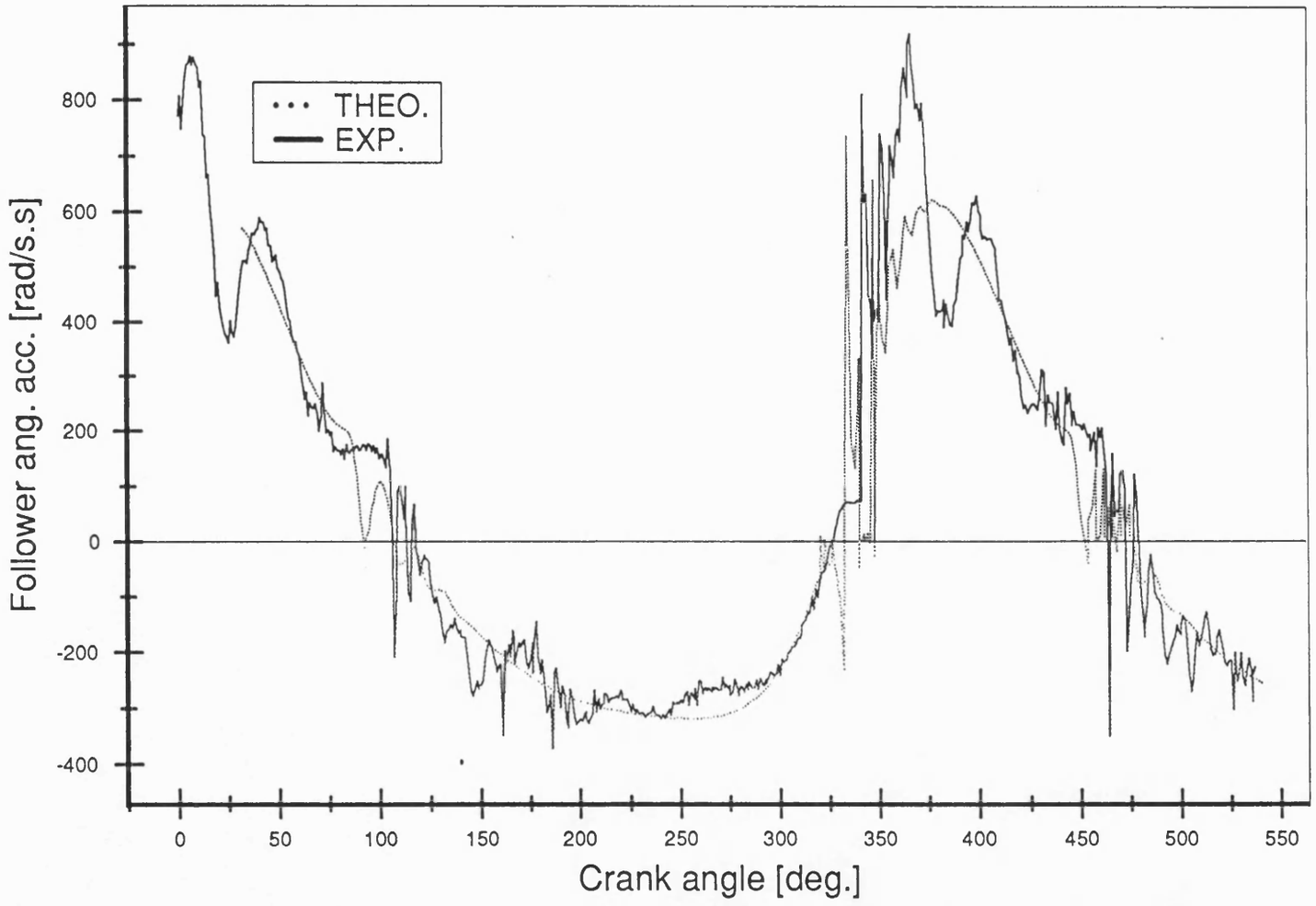

Fig 7.6.22 Follower angular acceleration , dia. clearance=0.25m m
with fly wheel ; mean speed = 327 rev/min ; with friction

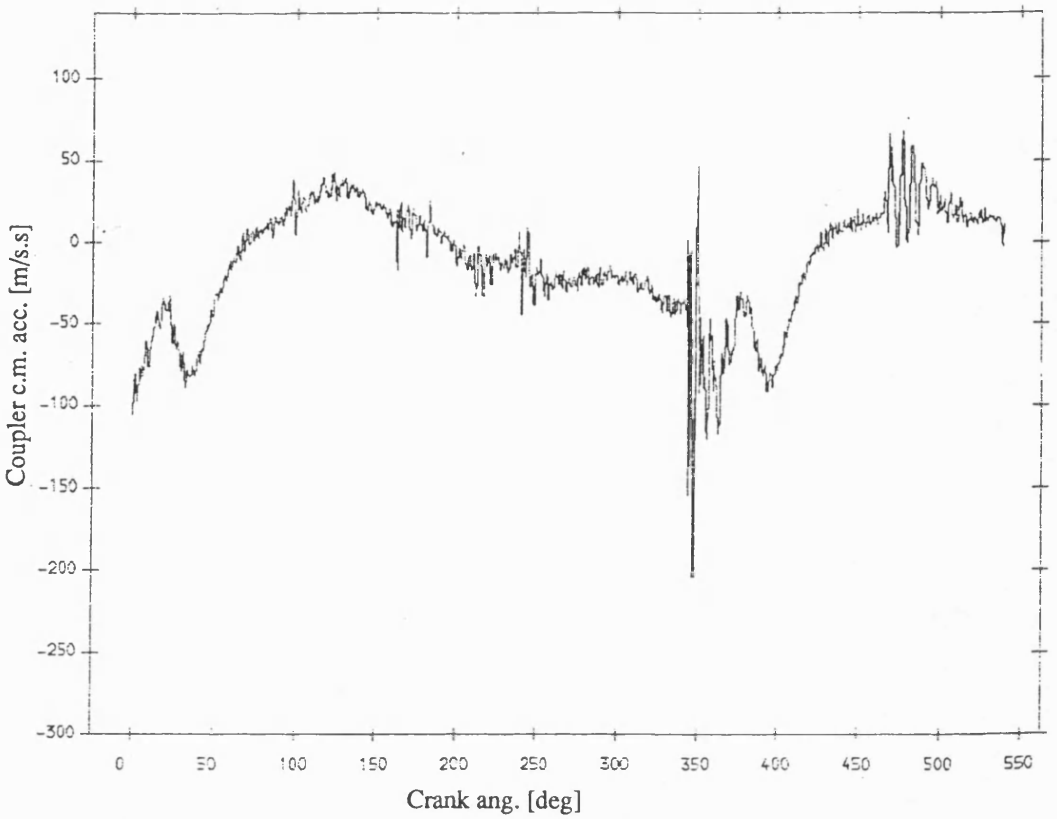

Fig 7.6.23 Exp. result coupler acceleration , dry bearing
with fly wheel ;mean speed=327 rev/min ; dia. clearance=.25mm

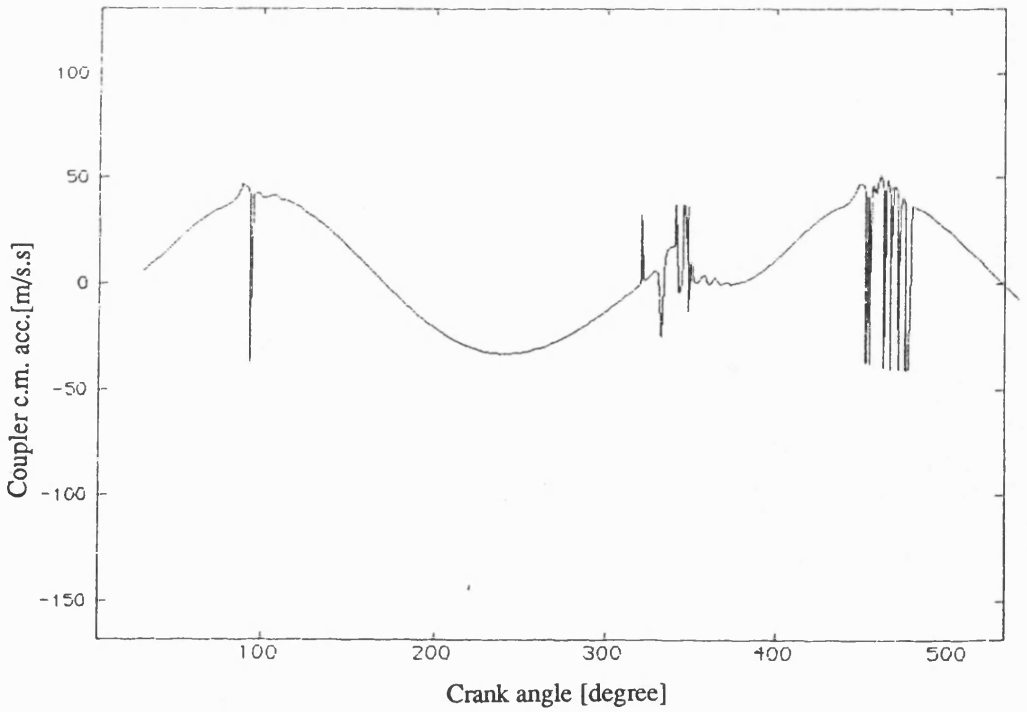

Fig 7.6.24 Coupler c.m. lateral acceleration (theoretical)
d.clea=.25mm , mean speed 327 rev/min ; I1=0.23 kg-m.m

CHAPTER 8
EXPERIMENTAL RESULTS

8.1 Introduction

In this chapter the experimental traces for longitudinal and lateral components of pin displacement relative to bush and , pin path in polar plot form, the follower angular acceleration , c.g. linear lateral coupler acceleration ,input speed and contact-loss traces are presented.

The above traces were generated for different cases as follows:

(a) a range of input speed (168,206,244,290,327 rev/min),

(b) clearances(0.15,0.20,0.25,0.30mm).

(c) with fly wheel, without fly wheel,

(d) greasy, normal and dry(degreased) bearing,

(e) one end of the pin isolated, neither end isolated, from the bush.

Among the results 3 speeds(168,244,327 rev/min) were chosen to be compared in the cases 'with fly wheel' and 'no fly wheel' for diametral clearance of 0.25mm - see sec. (8.2). The results for other clearances (0.15,0.2,0.3mm) are summarized and tabulated in sec. (8.3) for five different speed (168 , 206 , 244 , 290 , 327 rev/min).

The clearance joint was fully greased and for the case with fly wheel traces were

generated for different speeds with a diametral clearance of 0.25mm. Then the pin and bush were washed by 'Glenclean' (tri-chloro-ethane $C_2H_5CL_3$). Similar results were then generated. Later on this case is called 'dry bearing'. The results for the dry and greasy cases are compared in sec.(8.4) for 3 different speeds. For other clearances (0.15 ,0.20 ,0.30mm) similar experiments were carried out for a range of speeds (168, 206, 244 , 290 , 327 rev/min). The result for the dry and the greasy bearing for the above cases were compared. The comparison was summarized into 5 tables for each clearance. They are presented with discussion in sec.(8.5).

The figures in sec. 8.2 to 8.5 had been already numbered when it was decided to present the results in different order. It was decided to put more relevant traces together. In order that the pin displacement and contact loss traces were put together in one page in the following order. One of the contact loss traces was followed by the longitudinal displacement trace. Their fig. numbers are two consecutive odd numbers. The other contact loss trace was followed by the lateral displacement trace. Their fig numbers are two consecutive even numbers. This was carried out for different speeds and clearances ,normal,dry and greasy bearing results which are presented in sec. 8.2 to 8.5.

In order to study the out of plane pin motion or misalignment in the experimental rig one end of the pin was insulated from the bush and similar results were taken. Then the other end of the pin was isolated and a set of traces were recorded. These two cases are discussed in sec. (8.6). The wear pattern of the bushes are discussed in sec.(8.7) using Talyrond charts.

Notation used for brevity in the following sections is

wfw = with fly wheel

nfw = no fly wheel

c-l = contact loss

c.m. = centre of mass

8.2 Comparison of wfw & nfw diametral clearance=0.25mm

8.2.1 Low input speed (mean speed=168 rev/min)

a Input speed traces

The traces have different patterns for wfw and nfw cases - see fig(8.2.1). The input speed of wfw is steady with a small fluctuation. However the trace of nfw case is roughly sinusoidal with a greater speed fluctuation. These traces highlight the role of the fly wheel in the system. There is small decrease and increase at about 20 ° of the crank angle which in nfw case is smaller than wfw case. This is due to 'SCR' speed controller characteristic - see sec(4.3).

b Contact loss traces

The first c-l region in the contact loss traces of both cases is wider than the second one - see fig(8.2.2,8.2.3). The minimum pin force in zero clearance case in the first region is smaller than the second. The chain has greater potential energy at this region than in the second one. Since the input speed is relatively low the potential energy is important. When fly wheel added contact loss occurs slightly later. This is possibly due to higher input inertia.

c Longitudinal pin displacement (A traces)

In the longitudinal displacement trace there is a lag of both rising and falling edges for wfw case relative to nfw - see fig(8.2.4). This is possibly due to higher input inertia which causes slower response. The pin jump for wfw at rising edge is smaller than in the nfw case. The pin jump in this component is mostly depends on the coupler velocity. Since coupler is connected to the crank and fly wheel, the pin jump in wfw case should be smaller than in the nfw case.

d Lateral pin displacement (B traces)

In lateral displacement trace there is a lag in rising and falling edge for the wfw case relative to the nfw - see fig(8.2.5). That is possibly due to greater input inertia. The pin jump of wfw is larger than in the nfw case. This is predicted in the theoretical results - see sec.(7.4). The pin jump in this component depends on the relative velocity of the follower to the crank. The relative velocity in wfw case is greater than that at nfw during the free flight.

e Polar plots

Polar plots of both cases are close to circular shape - see fig(8.2.6, 8.2.7). However that of wfw is closer to the clearance circle. That is due to greater inertia which results in more stability of the input speed in wfw case. Since the inertia force depends on the acceleration and acceleration depends on input speed which is more stable in the wfw case. Therefore the pin force will be more stable and the pin path will be closer to the clearance circle.

f Follower angular acceleration traces

There is more high frequency oscillation for the case of nfw - see fig(8.2.8,8.2.9). Both first and second impact region of wfw case lag those in the nfw case. This is possibly due to greater input inertia. The first impact is higher than the second. This is predicted in the theoretical results - see sec.(7.4). Both impacts in the first and the second regions in the case of wfw are greater than that of nfw case. That may be due to greater inertia, which prevents a fall in input speed around the impact region - see sec.(7.4).

g Coupler c.m. lateral acceleration traces

Both wfw and nfw cases have similar pattern - see fig(8.2.10 , 8.2.11). The impact in the first region is greater than that in the second. This is predicted in the theoretical results - see sec.(7.6). The impact in the first region in the nfw case is greater than that in wfw. This may be due to the fact that the coupler is associated with a greater inertia in the flywheel case so velocity is maintained more stable. The impact region of the wfw case lags that in nfw case. There is less oscillation in the wfw trace. This is possibly due to greater input inertia.

8.2.2 medium speed (mean speed=244 rev/min)

The results are similar to those at low speed. Only the differences are highlighted here.

a Input speed traces

Input speed is steady over all the cycle except in one region for a disturbance (around

20° crank angle) which in the nfw case is smaller than in the wfw case - see fig(8.2.12). This is due to 'SCR' speed controller characteristic - see sec.(4.3). The input speed of the nfw is smaller than that of wfw during the first half of the cycle. However it is greater during the second half of the cycle. That means during the second half of the cycle the fly wheel stores some kinetic energy. However during the first half it releases its stored kinetic energy.

b Contact loss(c-l) traces

The second c-l region in both wfw and nfw cases are wider than the first one - see fig(8.2.13,8.2.14). The first c-l region in the wfw case lags the nfw case. However the second region leads slightly that in the nfw case. This is because in the wfw case the first contact loss region is not quite consistent with the pin jump; also in the second region the input speed is slightly greater than the nfw case.

Both the nfw and wfw cases at both c-l regions lag those at lower speed.

c Longitudinal pin displacement (trace A)

In the displacement trace A there is a lag for both rising and falling edges for wfw case relative to nfw - see fig(8.2.15). The lag is greater than at low speed, because the input inertia has more influence at greater input speed. In other worlds the lag is due to the difference between the time constant of the two cases which results in the displacement increases with speed. For both cases the rising edges lead those at lower speed. However the falling edges lag those at lower speed. There is more oscillation in the nfw trace.

The pin jump for wfw is smaller than nfw case. The reason is discussed earlier - see

sec(8.2.1).

d Lateral pin displacement (trace B)

In the lateral displacement component there is a lead for wfw case in rising edge relative to nfw - see fig(8.2.16) . However there is a lag in the falling edge for wfw case. This is possibly due to slightly greater input speed of wfw case in the impact regions(8.2.2a). The lag is greater than at low speed. For both cases the rising edges lead those at lower speed. However the falling edges lag those at lower speed.

The displacement in the wfw case is larger than in the nfw case.

e Polar plots

Polar plots of both cases are close to circular shape - see fig(8.2.17 ,8.2.18). However that of the nfw case is closer to the clearance circle in the first half cycle. At some point which is around the impact region, the pin path of the wfw comes slightly outside the clearance circle which is only possible if there is bush or pin flexibility. The deviation is greater than at lower speed due to greater input speed and greater impact in those regions.

f Follower angular acceleration traces

There is much more high frequency oscillation for the case of nfw. The oscillation is greater than at low speed - see fig(8.2.19,8.2.20). The first impact region of wfw case leads that in the nfw case. However the second region lags that in nfw case. This may be due to slightly greater input speed of the wfw case in those regions - see sec. (8.2.2a). As is predicted in the theoretical results the impact in the second region is

in the nfw case. This is because of slightly greater input speed in that region. For both cases the first impact region leads those at lower speed. However the second impact regions lags those at lower speed. There is a small fall and rise just after the maximum region which is due to the "SCR" speed controller characteristic - see sec. (8.2.2.a).

g Coupler c.m. lateral acceleration traces

Both wfw and nfw cases have the similar pattern - see fig(8.2.21, 8.2.22). The impact in the second region in both cases is greater than that in the first region. The impact in the second region in the wfw case is greater than that in the nfw case. This may be due to greater input speed in the wfw case in that region. The first impact region at the wfw case leads that at nfw case . However the second impact region lags that of nfw case. That is possibly due to slightly greater input speed in the wfw case in those regions (see sec.(7.2.2.a). There is more oscillation in the nfw trace. The first impact region of both cases leads that at lower speed. However the second impact region lags that at lower speed.

8.2.3 High input speed (mean speed=327 rev/min)

a Input speed traces

Both the wfw and nfw cases have similar pattern - see fig(8.2.23). There is a disturbance in the cycle around 20 ° of the crank angle which in the nfw case is smaller than in the wfw case. The disturbance in the wfw case slightly lags that in the nfw case. This is due to 'SCR' speed controller characteristic - see sec.(4.3). The input speed of the nfw case is slightly smaller than that of the wfw at around impact regions.

around impact regions.

b Contact loss traces

The width of the second contact loss region in c-l traces of both cases is considerable - see fig(8.2.24 , 8.2.25). However the first regions are so narrow they are hardly detected. The minimum pin force in the zero clearance case in the second region is smaller than the first. The chain has greater kinetic energy at this region, than in the first one. Both regions in the wfw case lag those in the nfw case. That may be due to greater input inertia at wfw case which causes smaller input acceleration. The c-l regions at the wfw case lag those at lower input speed. The first c-l region at the nfw case lead that at lower speed. However the second region lags that at lower speed.

The greater input inertia reduces the fall of speed in the wfw case. It results slightly greater input speed in the wfw case in the impact regions. The greater input speed causes lag at the second region for the wfw case relative to the nfw case.

c Longitudinal pin displacement (trace A)

In the longitudinal pin displacement trace there is slightly lag at rising edge in the wfw case relative to the nfw - see fig (8.2.26). This may be due to greater input inertia. For both cases the rising edges lead those at lower speed. However the falling edges lag those at lower speed.

The pin jump for wfw is slightly smaller than nfw case. It is slightly greater at the falling edge than that at low speed.

In lateral displacement there is a lag for wfw case in the rising and falling edge relative to the nfw - see fig(8.2.27). That may be due to greater input inertia.

For both cases the rising edges lead those at lower speed. However the falling edges lag those at lower speed.

The pin jump in the wfw case is greater than in the nfw case. This is predicted in the theoretical model - see fig(7.4.7). The disturbance between the falling and rising edges is due to input speed disturbance which is greater in wfw case.

e Polar plots

Polar plots of both cases are close to circular shape - see fig(8.2.28,8.2.29). However that of the nfw case is closer to the clearance circle in the first half cycle . At some point which is around the impact region, the pin path of the wfw case goes closer to the clearance circle. That is due to slightly greater input speed in those regions, which results greater inertia force. The polar plots are generally semicircular. However the arc which follows clearance circle in nfw is longer and the distance of the second flight of the pin path from the clearance circle centre is smaller in nfw case. The second flight path of the nfw case is closer to straight line.

At medium speed the polar plots are roughly circular in shape. However at this speed which is relatively high the polar plot is semicircular in shape and is at the top of the bush. This is because at low speed the gravity force is comparable with the inertia force. Therefore both forces contribute to the contact force and as a result in the relative displacement of pin in the bush. By increasing the input speed the inertia force predominates. Therefor the inertia force has a greater contribution to the relative displacement of the pin in the bearing. The polar plot of zero clearance case

shows that the longitudinal force at this speed is mostly positive i.e from pin toward the top of the bush - see fig(9.2.2).

f Follower angular acceleration traces

The first impact region in the wfw case lags the nfw case - see fig(8.2.30,8.2.31). This is due to greater input inertia. The first impact in the case of wfw case is greater than that at nfw case. However the second impact is slightly smaller. For both cases , as predicted, the second impact is greater than the first. For both cases the first impact region leads that at lower speed. However the second impact regions lag those of lower speed. These are predicted in the theoretical plots - see sec.(7.4) There is a small disturbance just after the maximum region which is due to the "SCR" speed controller characteristic - see sec.(4.3). The acceleration of the wfw case is slightly greater than that of nfw case. It is clearly detected from the traces that before the impact acceleration is constant. That is due to free flight which results from the separation of the follower from the coupler. Then the follower will move as a pendulum. Since the follower is around vertical position its weight also does not have much effect. This probability is confirmed by matching this region with contact loss region - see fig(8.2.24,8.2.25).

g Coupler c.m. lateral acceleration traces

For both cases the second impact is considerable and greater than the first - see fig(8.2.32 , 8.2.33). Both wfw and nfw cases have similar pattern. The second impact of the nfw case is greater than that of the wfw case. However the first impact of the wfw is greater than that of the nfw. This is because the input speed in wfw case is slightly greater than in the nfw case in the first region. The first impact region of the wfw case lags that of the nfw case . That may be due to greater input inertia.

case is slightly greater than in the nfw case in the first region. The first impact region of the wfw case lags that of the nfw case . That may be due to greater input inertia. There is a disturbance slightly after the second impact region. This is because of the disturbance in input speed at this region, which is greater in the wfw case. The oscillation amplitude in the nfw case is slightly greater than in the wfw case. The first impact regions in both cases lead those at lower speed. However the second impacts lag those at lower speed.

8.3 Comparison of wfw with nfw for diametral clearance=0.15,0.2 and 0.3mm fig(8.3.1 to 8.3.143)

The displacement components and the polar plot of pin path follow the same pattern as for 0.25mm clearance case. However there is some minor differences which are summarized in tables (8.3.1 to 8.3.15). A general discussion will be in section (9.5).

The position of rising and falling edges of pin displacement components relative to bush which is in contact loss region were compared in the tables(8.3.1 to 8.3.15).

The crank position at impact deduced from the
acceleration traces are also tabulated. The impacts were plotted against speed for different cases and clearances - see sec.(9.3 to 9.5).

There are some notations which are used in the tables;

fw = with fly wheel

nfw = without fly wheel

L.S.= lower speed

8.4 Comparison of greasy and dry bearing cases d.clea=0.25mm

8.4.1 Low speed (mean speed=168rev/min)

8.4.1a Input speed

With the same set number on the speed controller the input speed in the greasy case is smaller than that in the dry case see fig(8.4.1). This is presumably due to viscous friction torque in the greasy case. There is small disturbance around the starting of each cycle in both cases. That is due to speed controller characteristic (see sec. 4.2)

8.4.1b Contact loss traces

For both dry and greasy cases the first c-l region is greater than the second one (see fig 8.4.2,8.4.3). The first c-l region starts earlier in the dry bearing case. This may be due to slightly greater input speed.(see sec. 8.4.1a)

Both c-l regions are wider in the greasy case. Apparent contact loss occurs frequently in the c-l regions in the greasy bearing case . This may be due to the insulating property of the grease which acts as an insulator when the contact force is very small. One gets a clearer contact loss trace from the greasy bearing case.

8.4.1c Longitudinal pin displacement (A traces)

The rising edge of the pin displacement at the greased bearing starts later than that in the dry case(see fig 8.4.4). However its falling edge starts earlier than the dry case. That may be due to slightly smaller input speed(see 8.4.1.g). The amplitude of pin displacement in the greasy bearing case is smaller than the dry case. There are two peaks in the displacement signal, of which the second one is relatively smaller than

the first. These occur in the regions of contact loss. This means the duration of first flight is greater than the second. This is predicted in the theoretical trace(see sec.(7.3)).

8.4.1d Lateral pin displacement (B traces)

The rising and falling edges of the pin displacement in the greasy bearing start earlier than those at the dry bearing case see fig(8.4.5). The range of variation in the greasy case is smaller than at the dry case and the frequency of oscillation is lower . There is a small sharp fall just after the rising edge which may represent the duration of contact loss.

8.4.1e Polar plot of pin motion

The polar plot in the dry bearing case is roughly circular and is close to the clearance circle see fig(8.4.6 , 8.4.7). However that of the greasy case is confined to a lower quadrant of the clearance circle.

8.4.1f Follower angular acceleration

The peak value at the dry case is slightly greater than that in the greasy case see fig(8.4.8 , 8.4.9). The first impact region in the dry case starts earlier than that in the greasy case. However the second region starts later than that in the greasy case. That may be due to the slightly greater input speed(see 8.4.1a). The impact in the second region at the greasy case is lower than the dry case. This is possibly due to damping of the grease. This damping is evidence for the squeeze film damping model - see sec.(3.6).

8.4.1.g Coupler c.m. lateral acceleration

The first impact region in the dry case starts earlier than that in the greasy case see fig(8.4.10 , 8.4.11). However the second one starts later. The first impact in the greasy case is smaller than in the dry bearing case. There is some disturbance around 200 deg. on the traces which may be due to misalignment of the pin.

8.4.2 medium speed (mean speed=244 rev/min)

At this speed there are some points which are similar to those at low speed. There are some differences to be noted.

8.4.2a Input speed

There is some disturbance around the start of each cycle in both cases see fig(8.4.12). Its amplitude is considerable. That is due to speed controller characteristic. In the greasy bearing case the oscillation leads that in the dry bearing case. The lead is due to viscous friction which causes earlier drop of the input speed in the greasy case .

8.4.2b Contact loss traces

For the dry case the first c-l region is smaller than the second one - see fig(8.4.13 , 8.4.14). The first c-l region starts later in the dry case .

8.4.2c Longitudinal pin displacement (A traces)

The rising edge of the greasy bearing case starts slightly earlier than that in the dry case see fig(8.4.15). However the falling edge starts slightly later. The range of variation of the greasy is slightly smaller than in the dry case. There are two local

max. in A displacement trace at c-l regions ; the second one is slightly smaller than the first. There is less oscillation in the greasy bearing case than that in the dry. That is possibly due to grease damping.

8.4.2d Lateral pin displacement (B traces)

The rising edge in the greasy starts earlier than that in the dry case - see fig(8.4.16). However its falling edge start later. The range of variation in the greasy bearing case is the same as that in the dry. There is more oscillation in the dry case. There is a small sharp fall just after rising edge in the greasy bearing case which is greater than that at lower speed.

8.4.2e Polar plot

The polar plots of the dry and greasy bearing case are close to circular in shape and are close to the clearance circle see fig(8.4.17 , 8.4.18). However that in dry case is closer to the clearance circle. That is possibly due to grease thickness in the greasy case. There is a small closed loop during the first c-l region for the dry case which is not recorded in the greasy case. It is similar to shaft path in the hydraulic bearing due to impact(44).

8.4.2f Follower angular acceleration

The first impact region in the dry case starts later than that in the greasy case - see fig(8.4.19 , 8.4.20). However the second region starts earlier than that in the greasy. That may be due to decreasing damping in the greasy case caused by reduction of the film thickness because of the increased force due to higher running speeds. In the dry

case coulomb friction occurs which is greater than viscous friction The 2nd impact in the dry case is greater than that in the first.

8.4.2g Coupler c.m. lateral acceleration.

The first and the second impact regions in the dry case start earlier than those in the greasy case - see fig(8.4.21 , 8.4.22). The second impact in the greasy case is smaller than the dry. The oscillation amplitude in the dry case is slightly greater than in the greasy case.

8.4.3 High speed (m speed=327 rev/min)

8.4.3a Input speed

There is some large disturbance in the speed trace around the start of each cycle in both cases see fig(8.4.23). This causes a set of oscillations in input speed. This oscillation has higher amplitude than that at lower speed. That is due to the speed controller characteristic. The oscillation in the greasy case leads that in the dry case.

8.4.3b Contact loss traces

For the greasy case the first c-l region is smaller than the second one - see fig(8.4.24 , 8.4.25). The first c-l region is detected only in the greasy case. The first region starts earlier than at lower speed. However the second c-l regions start later than the lower speed in both cases.

8.4.3c Longitudinal pin displacement (A traces)

The rising and falling edge in the greasy bearing case starts slightly later than that in the dry case see fig(8.4.26). The pin jump in the greasy bearing is slightly smaller than the dry case. There are two peaks in the displacement trace ; the second one is slightly smaller than the first.

8.4.3d B (lateral) displacement. traces

The rising edge pin jump in the greasy bearing starts earlier than that in the dry case - see fig(8.4.27). However its falling edge starts later. There are some modest oscillations after the rising edge in the greasy case. This is puzzling. Since one will expect less oscillation in the greasy than in the dry bearing case. In free flight the pin is close to the bush see sec.(8.4.3d). Therefore when the pin enters the grease film the tangential relative velocity(the sliding speed) of the pin is high this apparently causes some oscillations. At the falling edge they do not appear because the pin is not close to the bush therefore the tangential component is small but the radial component of the relative velocity is considerable. The relative velocity is damped during the impact.

The rising edge of both cases lead those at lower speed. However their falling edges lag.

8.4.3e Polar plot

In both cases at the second flight the distance of the pin from the bush is relatively large see fig(8.4.28 , 8.4.29). However the first flight is short specially in the dry

case. The polar plots in the dry and greasy bearing case are close to circular and are close to the clearance circle. However that of the dry is closer than the greasy to the clearance circle. There is a small closed loop during the first c-l region for the dry case. The arc of the pin path which is close to the clearance circle is greater in the greasy case.

8.4.3f Follower angular acceleration

The second impact in the dry and the greasy cases is greater than that in the first - see fig(8.4.30 , 8.4.31). The second impact region in the dry case starts earlier than that in the greasy case. The first impact in the dry case is smaller than that in the greasy case.

8.4.3g Coupler c.m. lateral acceleration

The first and the second impact regions in the dry case start earlier than those in the greasy case - see fig(8.4.32 , 8.4.33). The second impact in the greasy case is greater than the dry. There is more oscillation in the dry case than the greasy.

8.5 Comparison of greasy and dry for d.clea.=0.15,0.2 and 0.3mm fig(8.5.1 to 8.5.143).

The same as section (8.3) for wfw and nfw , in this section the results for greasy and dry cases are tabulated (tables 8.5.1 to 8.5.15). The discussion of the results is in chapter (9),where the effects of the speeds, inertia ,grease and clearance are discussed. The acceleration impacts are plotted against speed. They are also

discussed. The acceleration impacts are plotted against speed. They are also discussed in the next chapter.

Notation used in the table which should be explained.

lags or leads = the crank position lags or leads

G = Greasy bearing case

D = Dry bearing case

8.6 The results of one end isolated pin :

To detect misalignment between pin and the bushes a special pin was made. The pin was constructed with an isolated ring at one end only. In this case one sees a c-l region in the c-l trace if the non isolated end is separated from the bearing.

A set of traces was derived from experimental results. For different speeds(168, 244, 327 rev/min) one is called ISL1(left hand side) and the other ISL2(right hand side) (Fig (8.6.1 to 8.6.6)).

The c-l trace of each set was compared with its corresponding member from the other set at the same speed. It was observed that there is overlap of contact loss regions ; these are the regions in which the pin is separated from both bushes. However there are some c-l regions in one trace not observed in the other trace. Those regions

correspond to the regions where pin was separated from one of the bushes only. That indicates misalignment.

There are some points which should be highlighted when one end of the pin is isolated. The elasticity of the p.v.c insulator is relatively higher than the steel of which the pin is made. In the c-l regions, particularly where only one plastic end is in contact, there is some oscillation in the displacement and acceleration traces - see fig (8.6.7 to 8.6.12) .

The effect of the plastic elasticity is also observable in the displacement polar plots. When the pin is in contact it presses onto the plastic part of the pin. Therefore pin path apparently goes outside the clearance circle (fig 8.6.7 to 8.6.12).

The elastic deformation of the plastic depends on the contact force. The contact force increases with speed. As a result the elastic deformation increases and the deviation of the pin path outside the clearance circle increases - see fig (8.6.7 to 8.6.12).

The polar plot at low speed (168 rev/min) is circular. By increasing the speed to 244rev/min the max. distance of pin from bush during the second flight increases. At high speed (327rev/min) the polar plot has a semicircular shape and is at the top part of the bush(fig 8.6.7 to 8.6.12).

8.7 Wear in bush and pin of clearance joint

The out of roundness of bushes and pins were measured before and after experiment. Since the pin is made of steel and the bush is of brass it is natural that wear mostly occurs on the bush. The roundness charts confirmed,that as expected, the pin does not wear very much. The range of out of roundness is 4 to 8 micron for the pin.

The result for bush wear is summarized in table (8.7.1). First two samples are profiles after extensive experimental work. The other two are for a shorter time of experimental operation.

Comparing Talyrond charts of the old and new bushes; it was observed that the wear occurs mainly in two regions. One is around 80 deg. bush angle and the other around 250 deg. bush angle. The regions of wear on the bush are concentrated around the contact points after flights indicated by polar plot of the pin motion. This gives confirmation in the performance of the instruments particularly eddy current transducers (fig 8.7.1,8.7.2). There is less wear on the bush in the free flight region. That is because the wear is mostly due to impact and only partly due to sliding during the following mode.

The Talyrond charts of left and right bushes are slightly different in pattern. This may be due to misalignement.

The bush wear can be detected while the rig is running. This can be carried out by comparison of the recorded and the original(unworn)pin motion which should be close to the predicted motion. It was carried out for the present rig - see fig(8.7.3). The difference in longitudinal pin motion pin fall(falling edge) is due to wear. Just after recording this pin motion the bush was taken out, and a roundness measurement chart(Talyrond) made of the internal surface of the bush. It was observed that there is a worn region at the bottom of the bush which agrees with the pin fall recorded - see fig(8.7.4).

This procedure can be used in fault monitoring with a computer on line. When the experimental signal deviates from the predicted by more then a permitted value(wear

This procedure can be used in fault monitoring with a computer on line. When the experimental signal deviates from the predicted by more then a permitted value(wear is more than permitted) the fault monitoring system may send an alarm or some other output.(eg computer print out).

In the absence of a computer the pin motion can be recorded periodically and then compared with a template made from the predicted pin motion or the original record. When the deviation exceeds a predicted limit the bush should be changed.

Table 8.3.1

A displacement (longitudinal) fw & nfw d. clearance= 0.3 mm		
speed (rev/min)	with fly wheel	
	rising edge	falling edge
168	in phase with nfw	in phase with nfw
208	leads nfw	in phase with nfw
244	lags nfw	lags nfw
	leads L.S.	lags L.S.
290	lags nfw	lags nfw
327	lags nfw	lags nfw
	leads L.S.	lags L.S.

Table 8.3.2

B displacement (lateral) fw & nfw d. clearance= 0.3 mm		
speed (rev/min)	with fly wheel	
	rising edge	falling edge
168	lags nfw	in phase with nfw
208	lags nfw	lags nfw
244	lags nfw	lags nfw
	lags L.S.	lags L.S.
290	lags nfw	lags nfw
327	lags nfw	in phase with nfw
	lags L.S.	lags L.S.

Table 8.3.3

Follower angular acceleration fw & nfw d. clearance= 0.3 mm		
speed (rev/min)	with fly wheel	
	first impact	second impact
168	leads nfw	lags nfw
208	in phase with nfw	in phase with nfw
244	leads nfw	in phase with nfw
	leads L.S.	lags L.S.
290	lags nfw	lags nfw
327	lags nfw	lags nfw
	leads L.S.	lags L.S.

Table 8.3.4

contact loss traces fw & nfw d. clearance= 0.3 mm		
speed (rev/min)	with fly wheel	
	first cl region	second cl region
168	leads nfw	lags nfw
208	leads nfw	lags nfw
244	lags nfw	in phase with nfw
	leads L.S.	lags L.S.
290	lags nfw	lags nfw
327		leads nfw
	leads L.S.	lags L.S.

Table 8.3.5

Coupler c.m. lateral acceleration impact fw & nfw d. clearance= 0.3 mm		
speed (rev/min)	with fly wheel	
	first impact	second impact
168	in phase with nfw	in phase with nfw
208	in phase with nfw	in phase with nfw
244	lags nfw	lags nfw
	leads L.S.	lags L.S.
290	lags nfw	lags nfw
327	lags nfw	lags nfw
	leads L.S.	lags L.S.

Table 8.3.6

A displacement (longitudinal) fw & nfw d. clearance= 0.2 mm		
speed (rev/min)	with fly wheel	
	rising edge	falling edge
168	lags nfw	lags nfw
208	leads nfw	lags nfw
244	lags nfw	leads nfw
	leads L.S.	lags L.S.
290	lags nfw	lags nfw
327	lags nfw	leads nfw
	leads L.S.	lags L.S.

Table 8.3.7

B displacement (lateral) fw & nfw d. clearance= 0.2 mm		
speed (rev/min)	with fly wheel	
	rising edge	falling edge
168	leads nfw	leads nfw
208	leads nfw	leads nfw
244	leads nfw	leads nfw
	lags L.S.	lags L.S.
290	lags nfw	in phase with nfw
327	lags nfw	lags nfw
	lags L.S.	lags L.S.

Table 8.3.8

Follower angular acceleration fw & nfw d. clearance= 0.2 mm		
speed (rev/min)	with fly wheel	
	first impact	second impact
168	in phase with nfw	in phase with nfw
208	leads nfw	in phase with nfw
244	leads nfw	leads nfw
	leads L.S.	lags L.S.
290	in phase with nfw	in phase with nfw
327	lags nfw	in phase with nfw
	leads L.S.	lags L.S.

Table 8.3.9

contact loss traces fw & nfw d. clearance= 0.2 mm		
speed (rev/min)	with fly wheel	
	first cl region	second cl region
168	lags nfw	leads nfw
208	lags nfw	leads nfw
244	lags nfw	leads nfw
	leads L.S.	lags L.S.
290	lags nfw	lags nfw
327		lags nfw
	leads L.S.	lags L.S.

Table 8.3.10

Coupler c.m. lateral acceleration impact fw & nfw d. clearance= 0.2 mm		
speed (rev/min)	with fly wheel	
	first impact	second impact
168	in phase with nfw	in phase with nfw
208	lags nfw	leads nfw
244	in phase with nfw	leads nfw
	leads L.S.	lags L.S.
290	lags nfw	lags nfw
327	lags nfw	in phase with nfw
	leads L.S.	lags L.S.

Table 8.3.11

A displacement (longitudinal) fw & nfw d. clearance= 0.15 mm		
speed	with fly wheel	
	rising edge	falling edge
168	leads nfw	lags nfw
244	leads nfw	leads nfw
	leads L.S.	lags L.S.
327	lags nfw	lags nfw
	leads L.S.	lags L.S.

Table 8.3.12

B displacement (lateral) fw & nfw d. clearance= 0.15 mm		
speed	with fly wheel	
	rising edge	falling edge
168	leads nfw	lags nfw
244	leads nfw	in phase with nfw
	lags L.S.	lags L.S.
327	lags nfw	leads nfw
	lags L.S.	lags L.S.

Table 8.3.13

Follower angular acceleration fw & nfw d. clearance= 0.15 mm		
speed	with fly wheel	
	first impact	second impact
168	lags nfw	lags nfw
244	lags nfw	lags nfw
	leads L.S.	lags L.S.
327	lags nfw	in phase with nfw
	leads L.S.	lags L.S.

Table 8.3.14

contact loss traces fw & nfw d. clearance= 0.15 mm		
speed	with fly wheel	
	first cl region	second cl region
168	leads nfw	leads nfw
244	leads nfw	leads nfw
	leads L.S.	lags L.S.
327		in phase with nfw
		lags L.S.

Table 8.3.15

Coupler c.m. lateral acceleration impact fw & nfw d. clearance= 0.15 mm		
speed	with fly wheel	
	first impact	second impact
168	lags nfw	lags nfw
244.nf	lags nfw	leads nfw
	leads L.S.	lags L.S.
327	lags nfw	= nfw
	leads L.S.	lags L.S.

Table 8.5.1

A displacement (longitudinal) dry(D) & Greasy (G) d. clearance= 0.3 mm		
speed (rev/min)	with dry bearing	
	rising edge	falling edge
168	in phase with G	leads G
208	in phase with G	leads G
244	lags G	in phase with G
	leads L.S.	lags L.S.
290	lags G	in phase with G
327	leads G	in phase with G
	leads L.S.	lags L.S.

Table 8.5.2

B displacement (lateral) dry (D) & greasy(G) d. clearance= 0.3 mm		
speed rev/min	with dry bearing	
	rising edge	falling edge
168	lags G	leads G
208	leads G	leads G
244	in phase with G	in phase with G
	lags L.S.	lags L.S.
290	lags G	in phase with G
327	lags G	lags G
	lags L.S.	lags L.S.

Table 8.5.3

Follower angular acceleration dry(D) & greasy(G) d. clearance= 0.3 mm		
speed (rev/min)	with dry bearing	
	first impact	second impact
168	leads G	leads G
208	leads G	in phase with G
244	in phase with G	in phase with G
	leads L.S.	lags L.S.
290	in phase with G	in phase with G
327	in phase with G	in phase with G
	leads L.S.	lags L.S.

Table 8.5.4

contact loss traces dry(D) & greasy(G) d. clearance= 0.30 mm		
speed (rev/min)	with dry bearing	
	first cl region	second cl region
168	lags G	
208	lags G	
244	lags G	lags G
	leads L.S.	lags L.S.
290	lags G	in phase with G
327	in phase with G	in phase with G
	leads L.S.	lags L.S.

Table 8.5.5

Coupler c.m. lateral acceleration impact dry(D)& greasy(G) d. clearance= 0.3 mm		
speed (rev/min)	with dry bearing	
	first impact	second impact
168	in phase with G	leads G
208	in phase with G	in phase with G
244	in phase with G	in phase with G
	leads L.S.	lags L.S.
290	in phase with G	in phase with G
327	leads G	leads G
	leads L.S.	lags L.S.

Table 8.5.6

A displacement (longitudinal) dry(D) & Greasy (G) d. clearance= 0.2 mm		
speed (rev/min)	with dry bearing	
	rising edge	falling edge
168	leads G	in phase with G
208	leads G	in phase with G
244	leads G	in phase with G
	leads L.S.	lags L.S.
290	leads G	lags G
327	leads G	leads G
	leads L.S.	lags L.S.

Table 8.5.7

B displacement (lateral) dry (D) & greasy(G) d. clearance= 0.2 mm		
speed rev/min	with dry bearing	
	rising edge	falling edge
168	lags G	lags G
208	lags G	lags G
244	lags G	lags G
	lags L.S.	lags L.S.
290	lags G	leads G
327	lags G	leads G
	lags L.S.	lags L.S.

Table 8.5.8

Follower angular acceleration dry(D) & greasy(G d. clearance= 0.2 mm		
speed (rev/min)	with dry bearing	
	first impact	second impact
168	leads G	in phase with G
208	leads G	in phase with G
244	leads G	leads G
	leads L.S.	lags L.S.
290	leads G	in phase with G
327	leads G	leads G
	leads L.S.	lags L.S.

Table 8.5.9

contact loss traces dry(D) & greasy(G) d. clearance= 0.20 mm		
speed (rev/min)	with dry bearing	
	first cl region	second cl region
168	leads G	in phase with G
208	lags G	lags G
244	lags G	in phase with G
	leads L.S.	lags L.S.
290	lags G	in phase with G
327		in phase with G
		lags L.S.

Table 8.5.10

Coupler c.m. lateral acceleration impact dry(D)& d. clearance= 0.2 mm		
speed (rev/min)	with dry bearing	
	first impact	second impact
168	leads G	in phase with G
208	leads G	in phase with G
244	leads G	leads G
	leads L.S.	lags L.S.
290	leads G	in phase with G
327	leads G	leads G
	leads L.S.	lags L.S.

Table 8.5.11

A displacement (longitudinal) dry(D) & Greasy (G) d. clearance= 0.15 mm		
speed	with dry bearing	
	rising edge	falling edge
168	lags G	in phase with G
244	lags G	in phase with G
	lags L.S.	lags L.S.
327	lags G	lags G
	leads L.S.	lags L.S.

Table 8.5.12

B displacement (lateral) dry (D) & greasy(G) d. clearance= 0.15 mm		
speed	with dry bearing	
	rising edge	falling edge
168	leads G	leads G
244	leads G	in phase with G
	lags L.S.	lags L.S.
327	leads G	leads G
	lags L.S.	lags L.S.

Table 8.5.13

Follower angular acceleration dry(D) & greasy(G) d. clearance= 0.15 mm		
speed	with dry bearing	
	first impact	second impact
168	in phase with G	in phase with G
244	lags G	in phase with G
	leads L.S.	lags L.S.
327	in phase with G	in phase with G
	leads L.S.	lags L.S.

Table 8.5.14

contact loss traces dry(D) & greasy(G) d. clearance= 0.15 mm		
speed	with dry bearing	
	first cl region	second cl region
168	lags G	in phase with G
244		leads G
	leads L.S.	lags L.S.
327	lags G	leads G
		lags L.S.

Table 8.5.15

Coupler c.m. lateral acceleration impact dry(D)& greasy(G) d. clearance= 0.15 mm		
speed	with dry bearing	
	first impact	second impact
168	in phase with G	in phase with G
244.nf	lags G	lags G
	leads L.S.	lags L.S.
327	in phase with G	in phase with G
	leads L.S.	lags L.S.

Table 8.7.1

Out of roundness of the bushes (micrometers)				
NO.	new bush		old bush	
	left	right	left	right
1	6	3	50	45
2	6	6	35	40
3	6	6	16	17
4	6	7	25	25

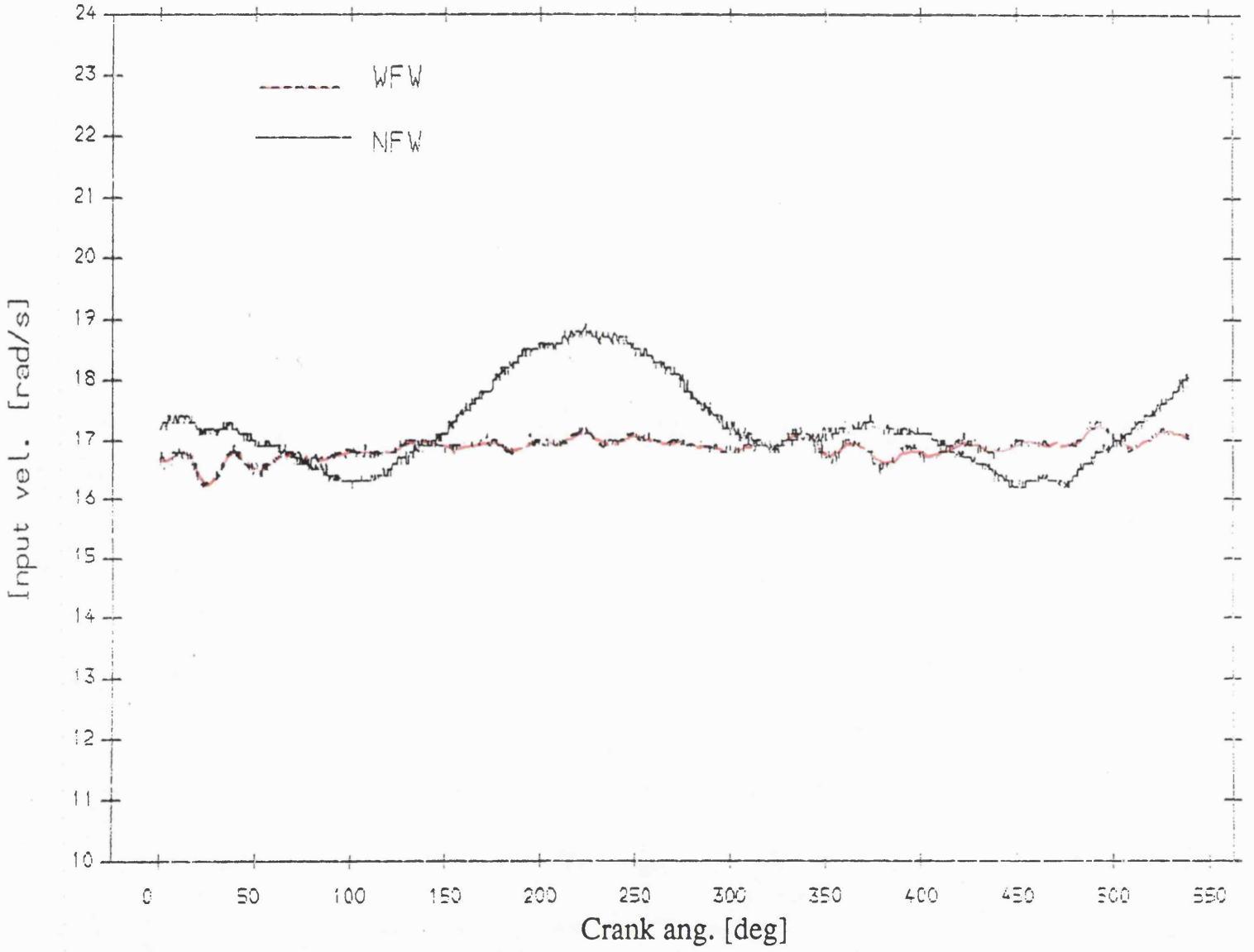

Fig 8.2.1 Exp. result input velocity , normal bearing
mean speed=168 rev/min; dia. clearance=.25mm

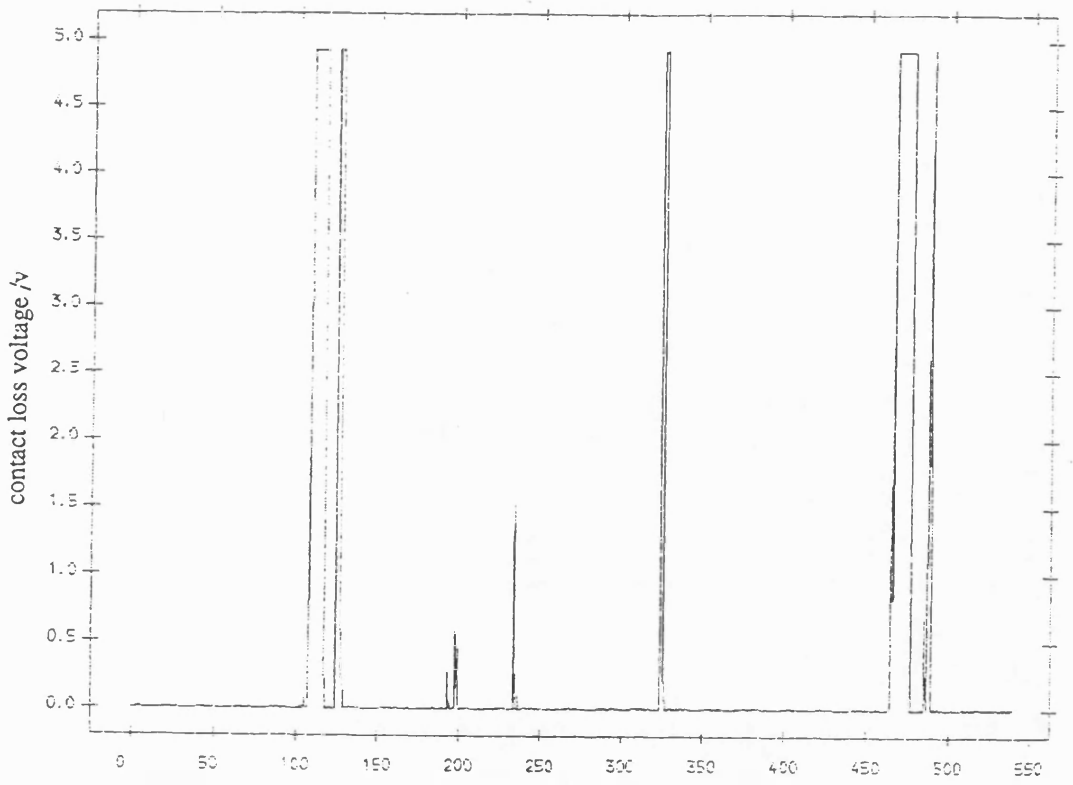

Fig 8.2.2 Exp. result contact loss of pin and normal bearing
with flywheel ;mean speed=168 rev/min ;dia. clearance=0.25mm

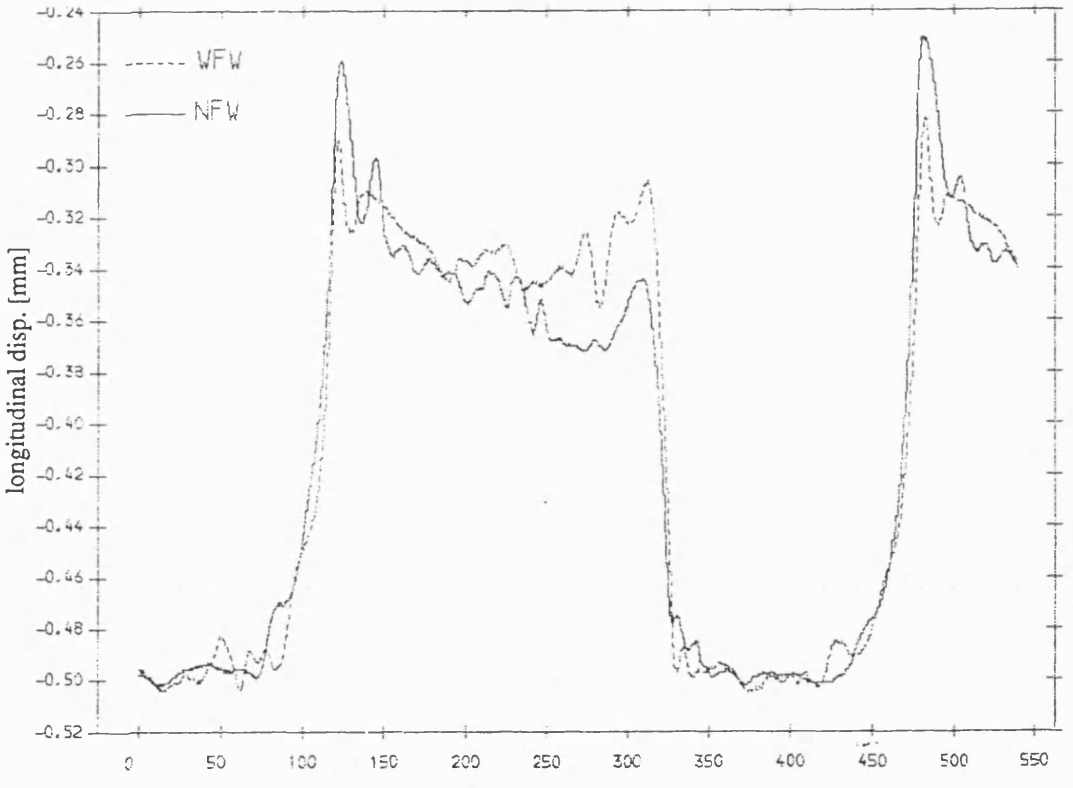

Fig 8.2.4 Exp. result longitudinal disp. of pin , normal bearing
mean speed=168 rev/min; dia. clearance=.25mm

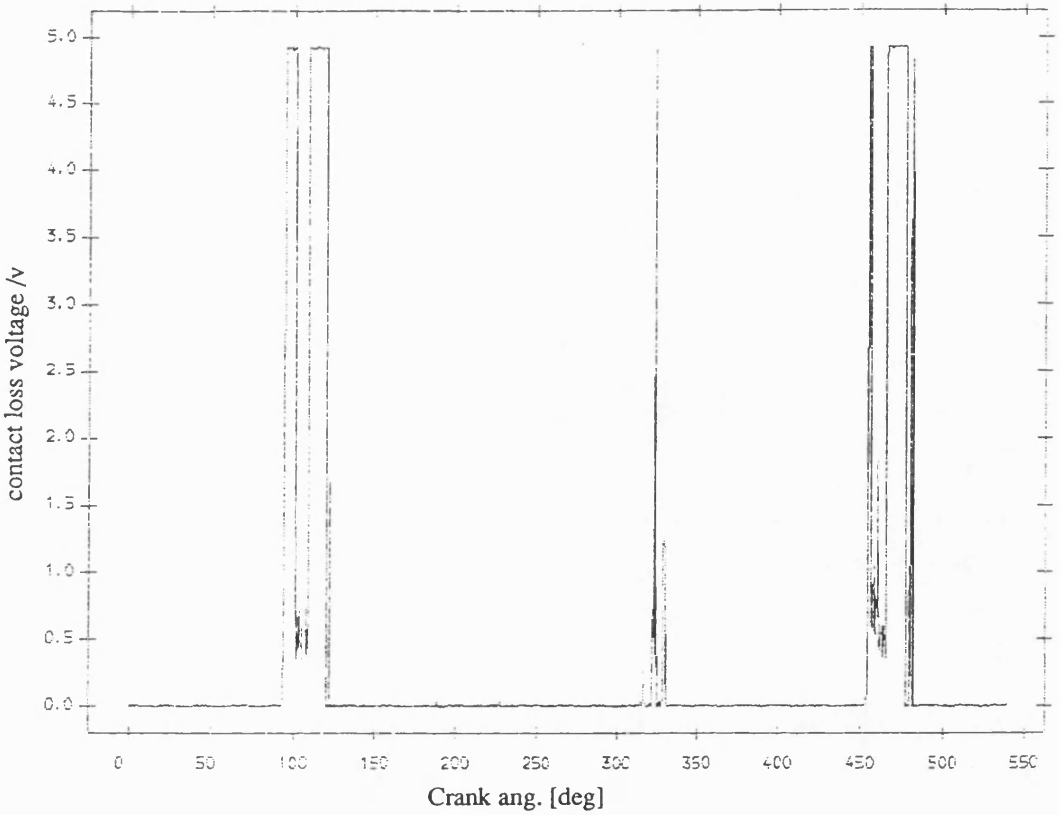

Fig 8.2.3 Exp. result contact loss of pin and normal bearing
no flywheel ;mean speed=168 rev/min ;dia. clearance=0.25mm

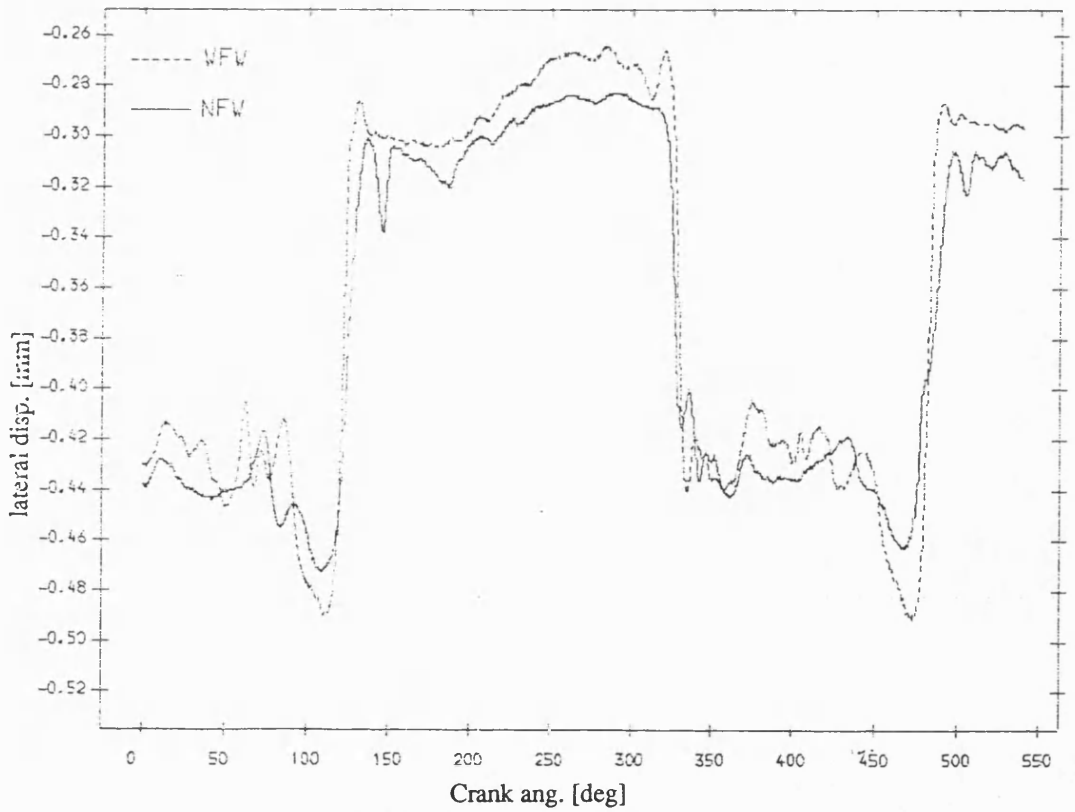

Fig 8.2.5 Exp. result lateral disp. of pin , normal bearing
mean speed=168 rev/min; dia. clearance=.25mm

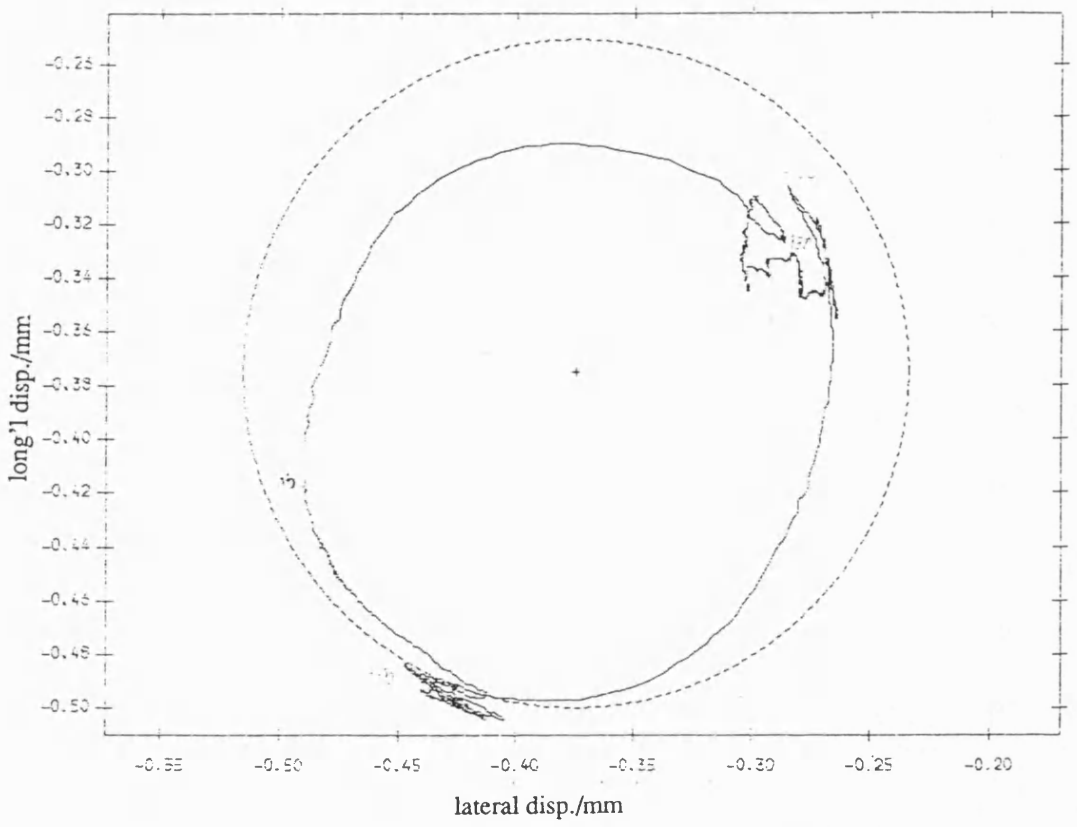

Fig 8.2.6 Exp. result polar plot of relative disp. of pin in normal bearing with fly wheel ;mean speed=168 rev/min ; dia. clearance=.25mm

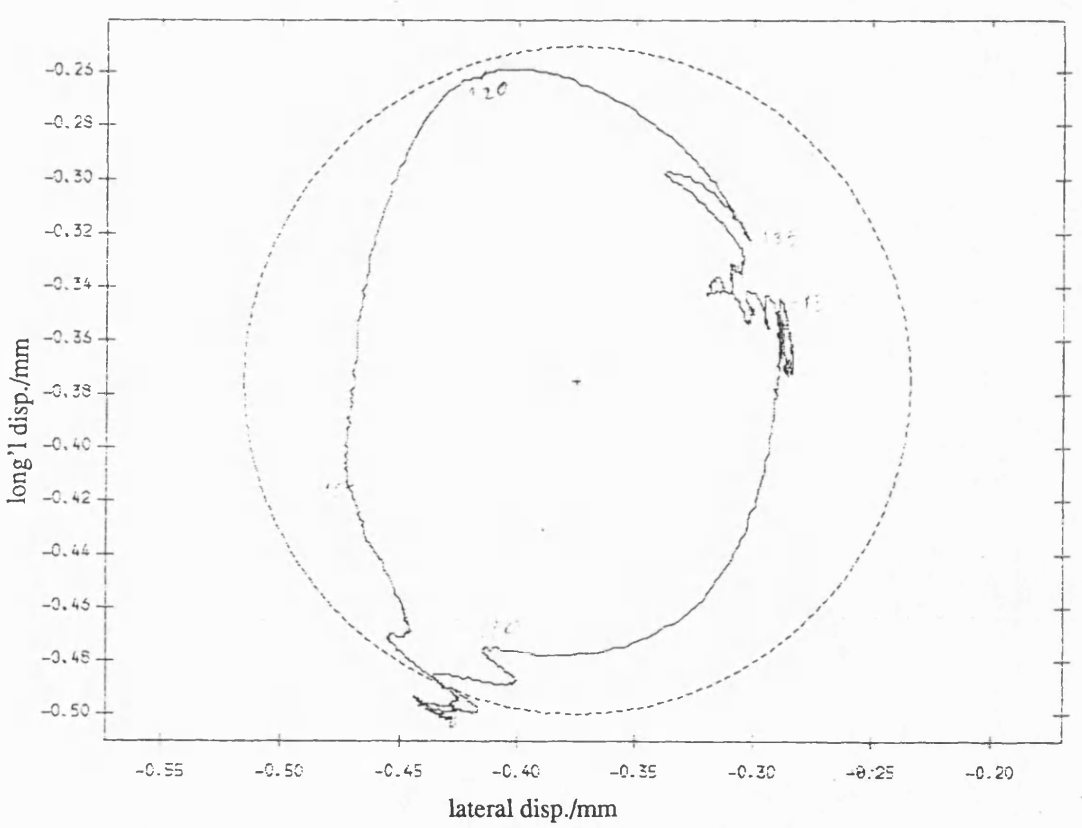

Fig 8.2.7 Exp. result polar plot of relative disp. of pin in normal bearing no fly wheel ;mean speed=168 rev/min ; dia. clearance=.25mm

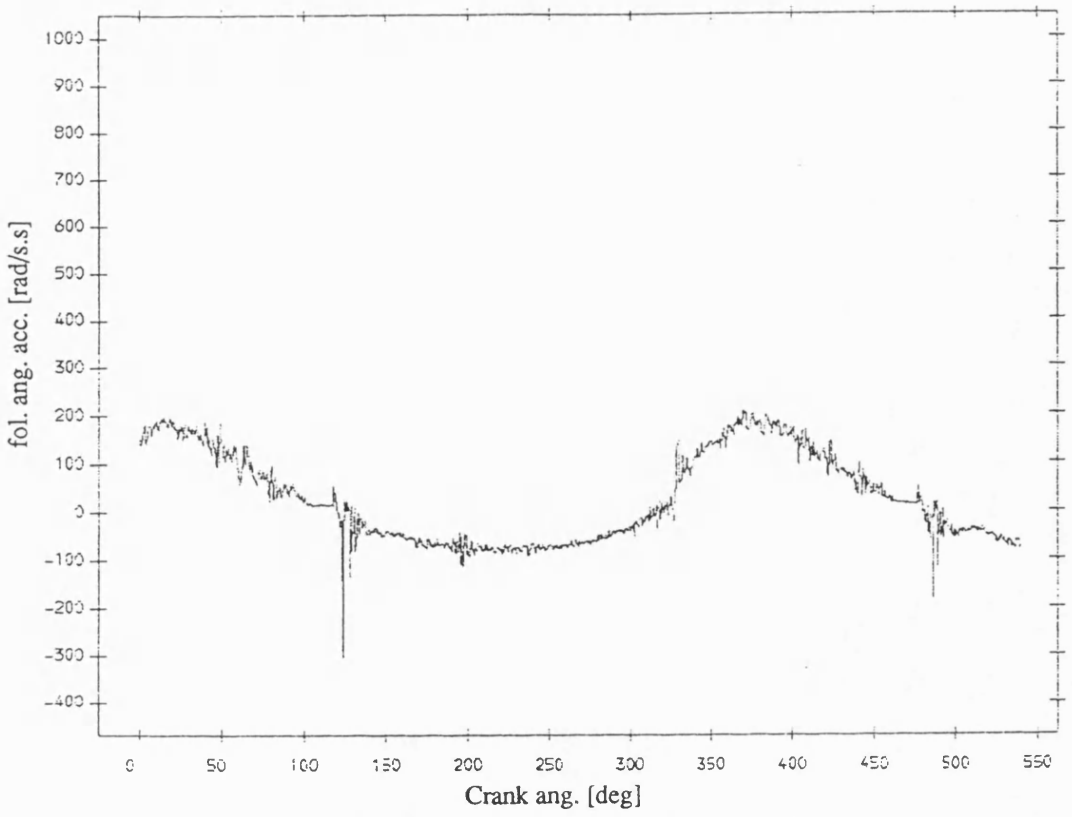

Fig 8.2.8 Exp. result follower ang. acceleration , normal bearing
with fly wheel ;mean speed=168 rev/min ; dia. clearance=.25mm

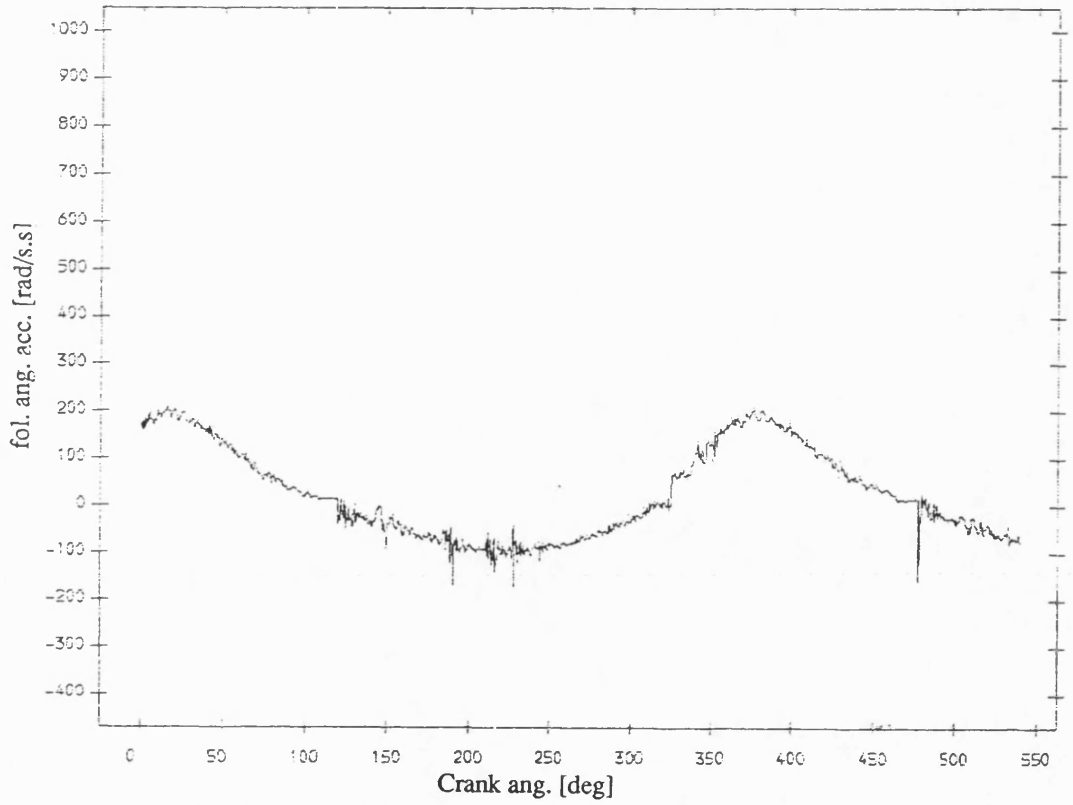

Fig 8.2.9 Exp. result follower ang. acceleration ,normal bearing
no fly wheel ;mean speed=168 rev/min ; dia. clearance=.25mm

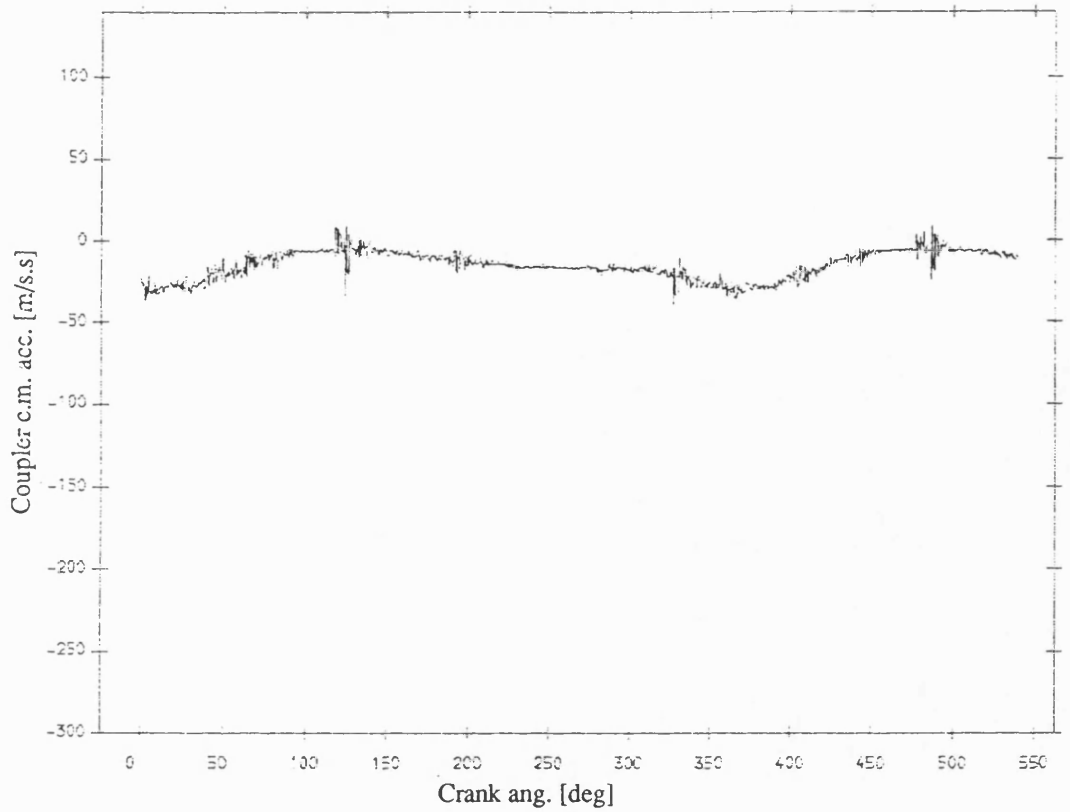

Fig 8.2.10 Exp. result coupler acceleration , normal bearing
with fly wheel ;mean speed=168 rev/min ; dia. clearance=.25mm

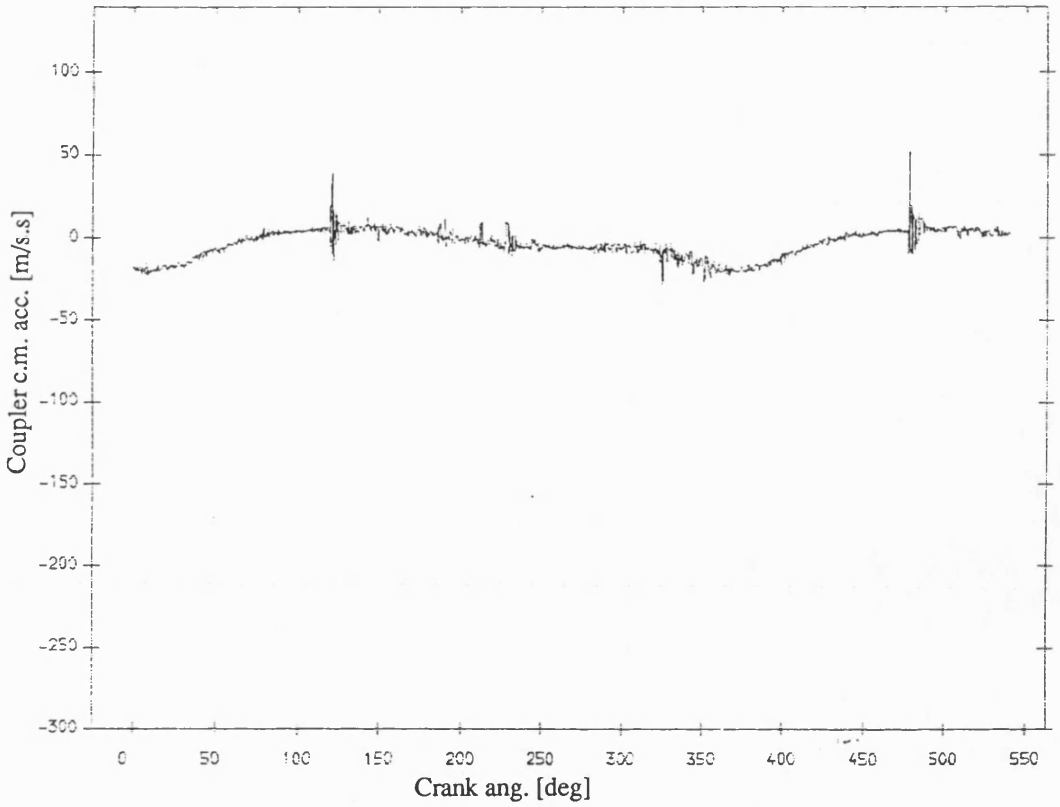

Fig 8.2.11 Exp. result coupler acceleration , normal bearing
no fly wheel ;mean speed=168 rev/min ; dia. clearance=.25mm

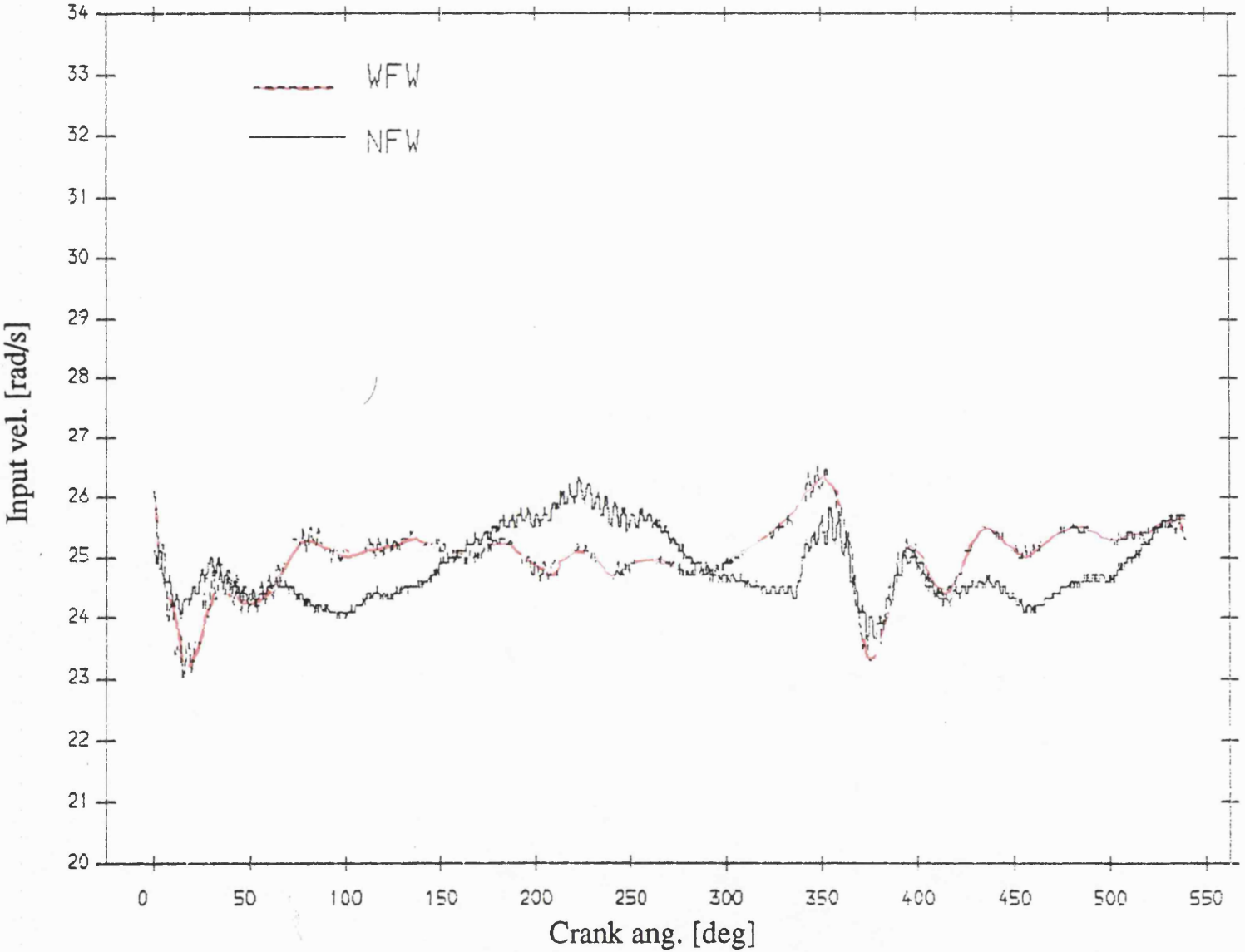

Fig 8.2.12 Exp. result input velocity , normal bearing
mean speed=244 rev/min; dia. clearance=.25mm

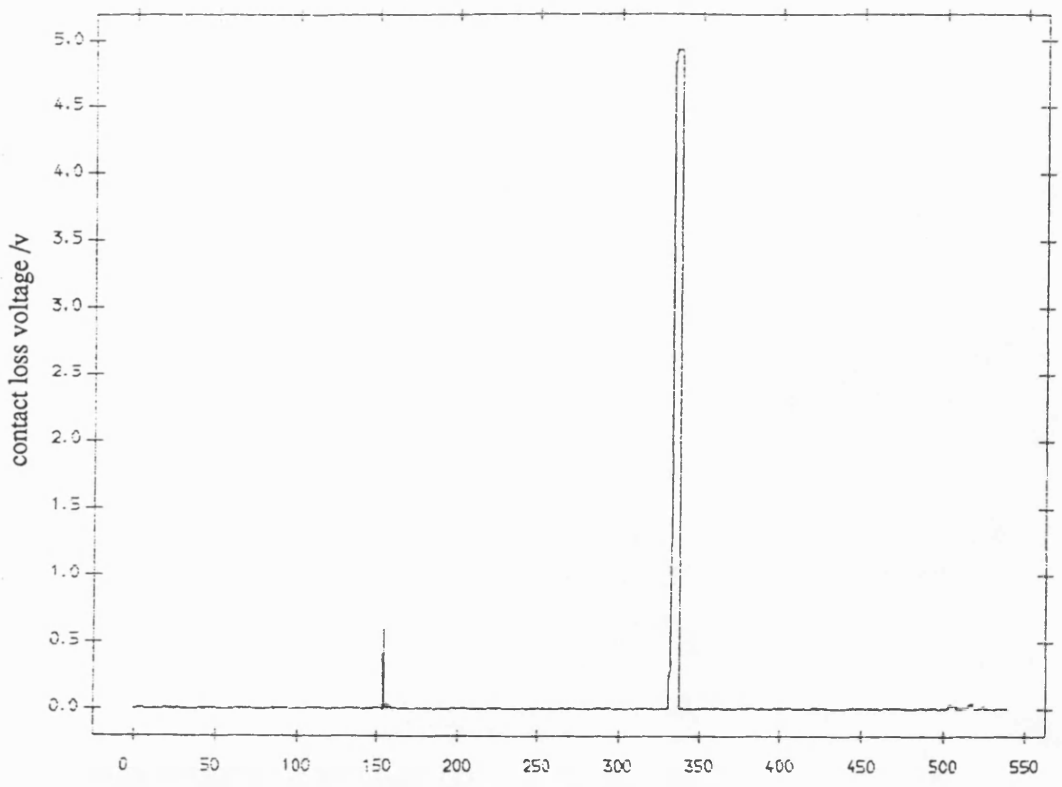

Fig 8.2.13 Exp. result contact loss of pin and normal bearing
with flywheel ;mean speed=244 rev/min ;dia. clearance=0.25mm

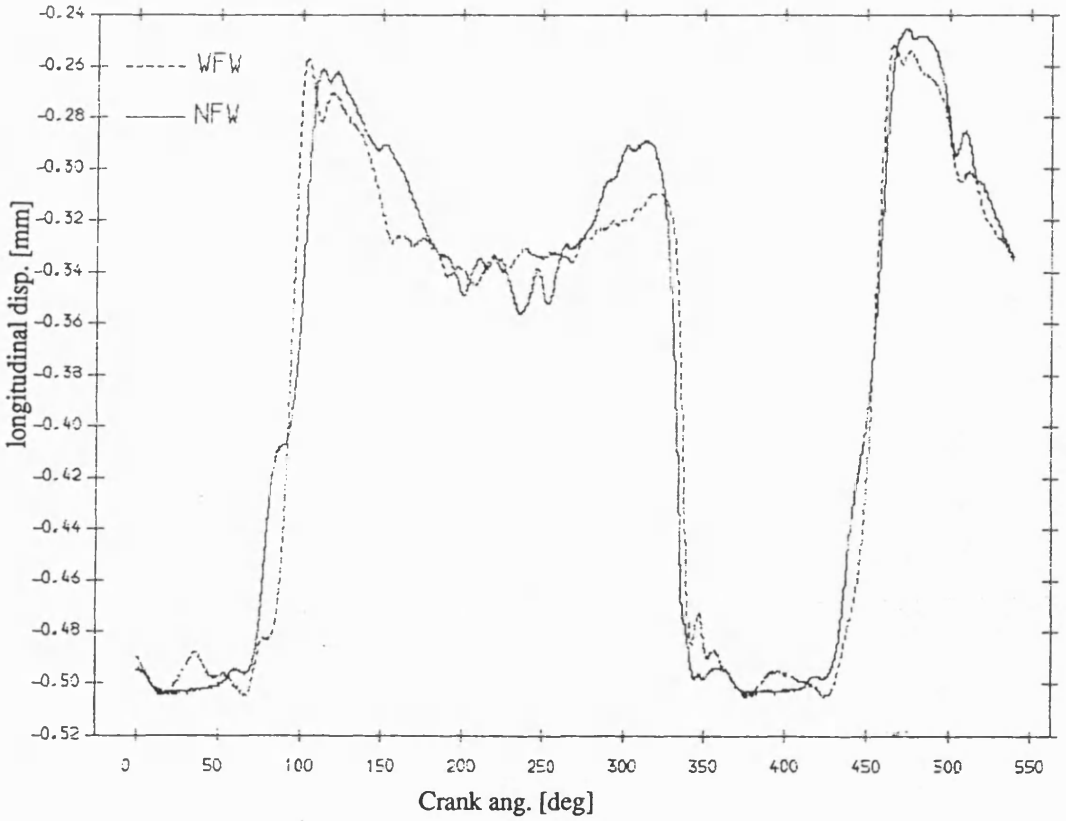

Fig 8.2.15 Exp. result longitudinal disp. of pin , normal bearing
mean speed=244 rev/min; dia. clearance=.25mm

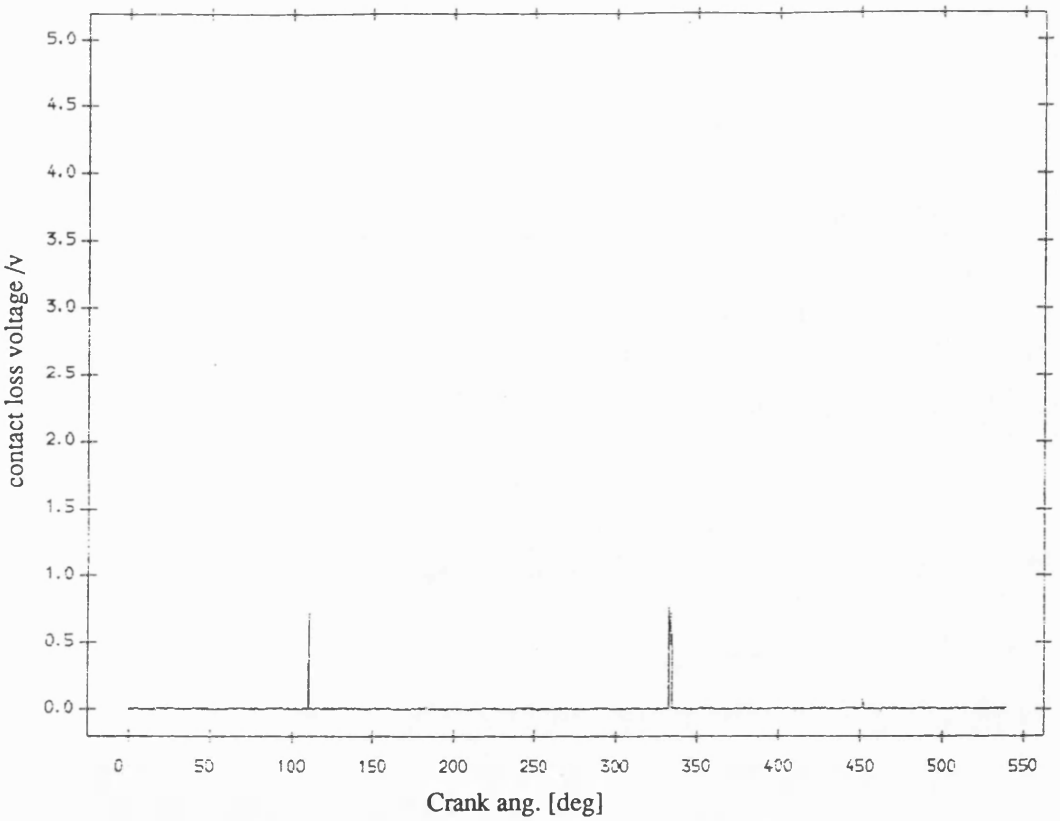

Fig 8.2.14 Exp. result contact loss of pin and normal bearing
no flywheel ;mean speed=244 rev/min ;dia. clearance=0.25mm

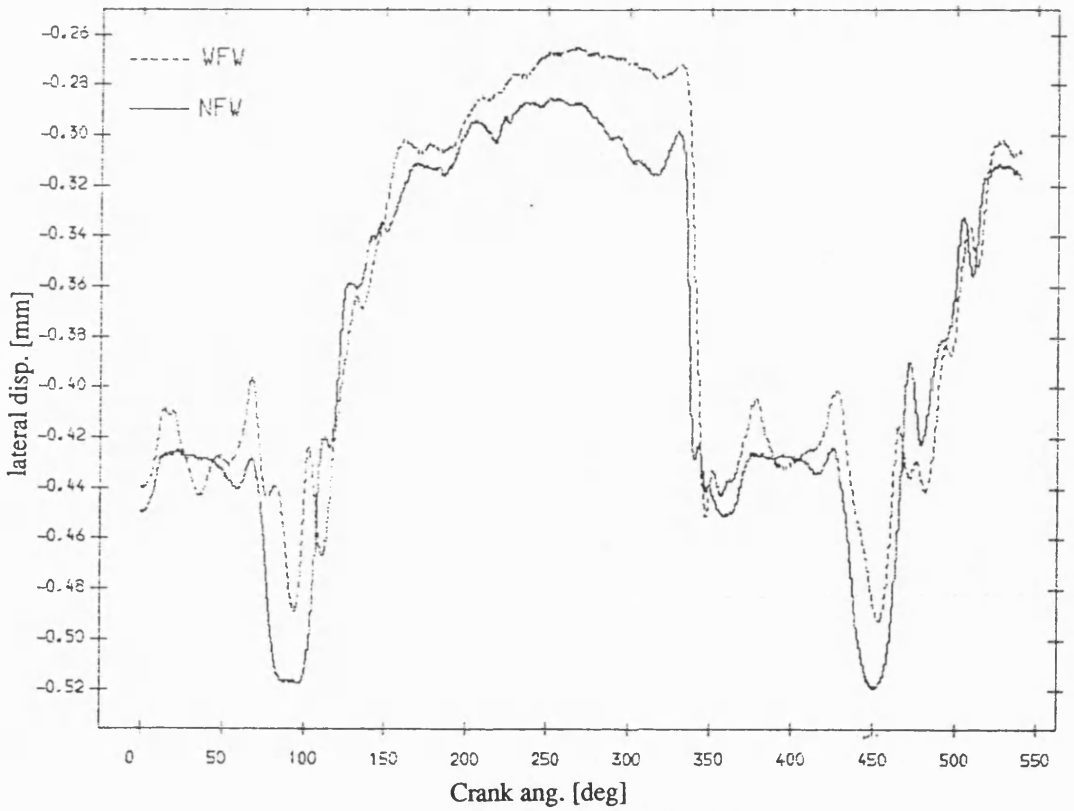

Fig 8.2.16 Exp. result lateral disp. of pin , normal bearing
mean speed=244 rev/min; dia. clearance=.25mm

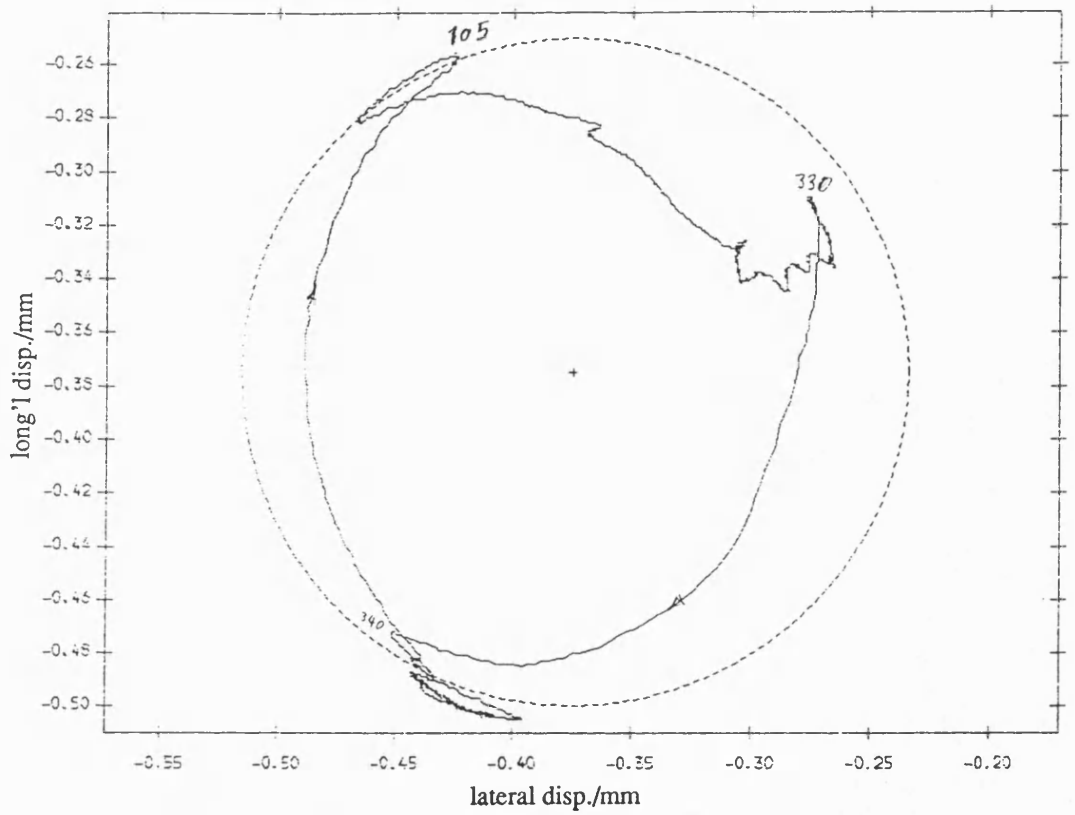

Fig 8.2.17 Exp. result polar plot of relative disp. of pin in normal bearing with fly wheel ;mean speed=244 rev/min ; dia. clearance=.25mm

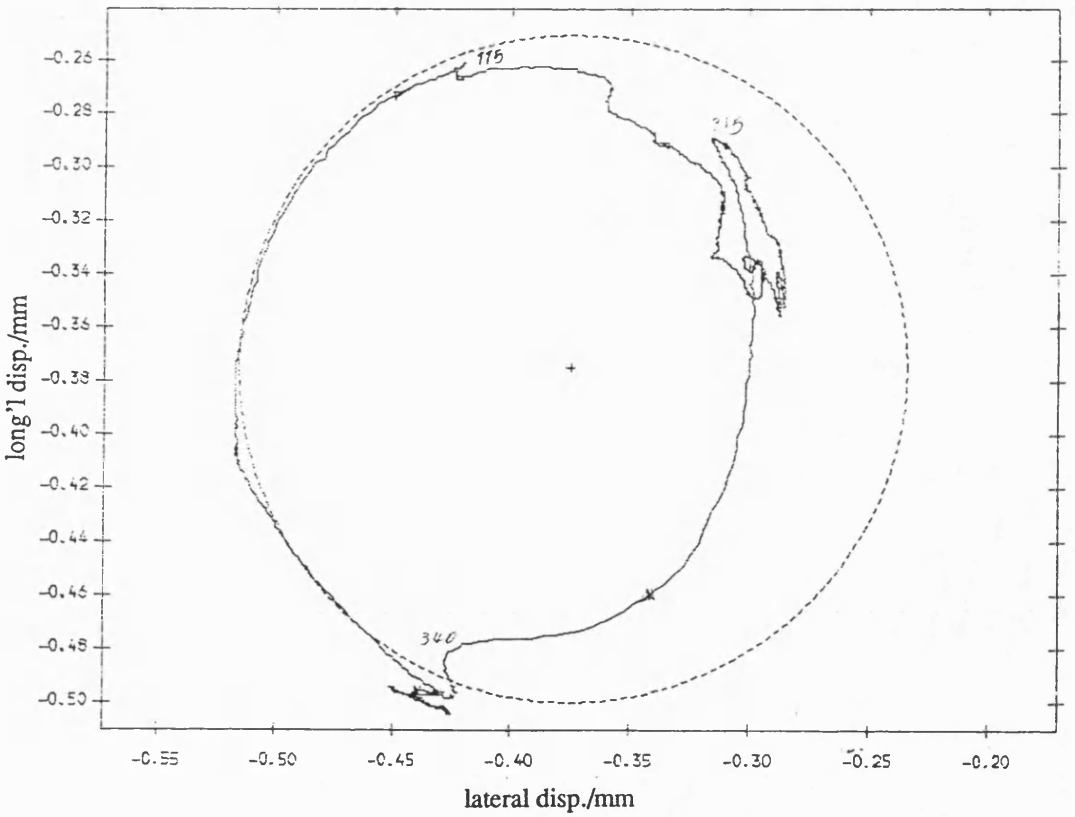

Fig 8.2.18 Exp. result polar plot of relative disp. of pin in normal bearing no fly wheel ;mean speed=244 rev/min ; dia. clearance=.25mm

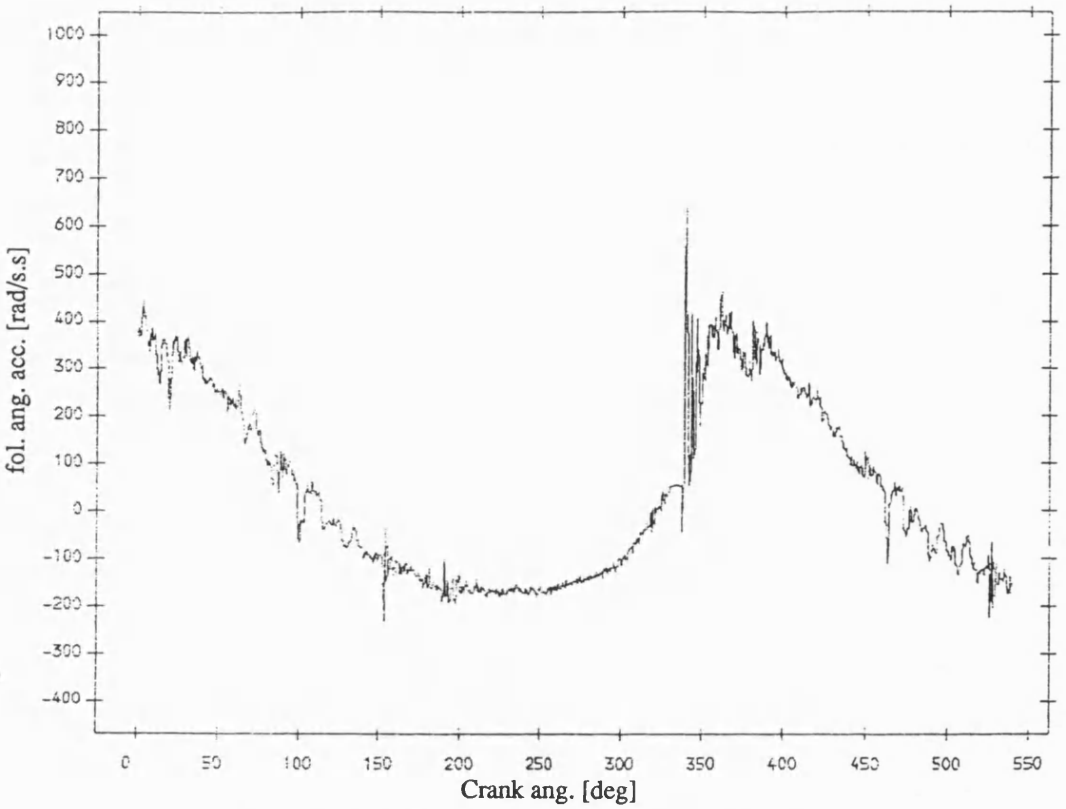

Fig 8.2.19 Exp. result follower ang. acceleration , normal bearing
with fly wheel ;mean speed=244 rev/min ; dia. clearance=.25mm

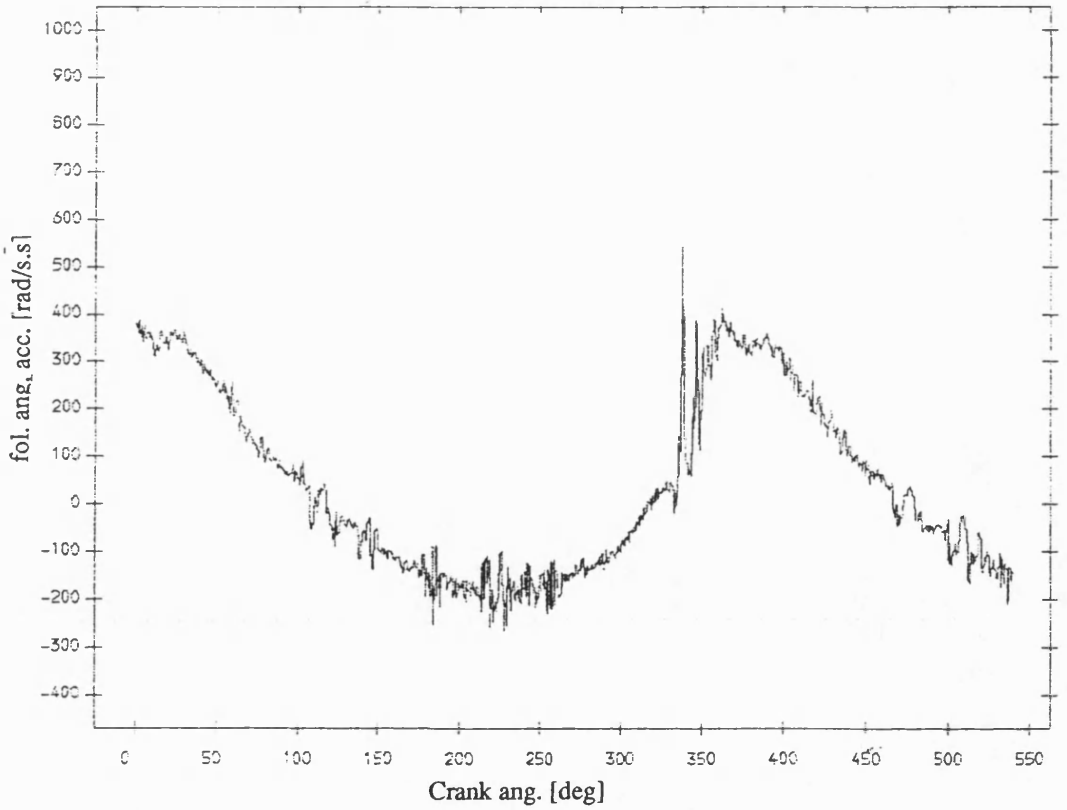

Fig 8.2.20 Exp. result follower ang. acceleration ,normal bearing
no fly wheel ;mean speed=244 rev/min ; dia. clearance=.25mm

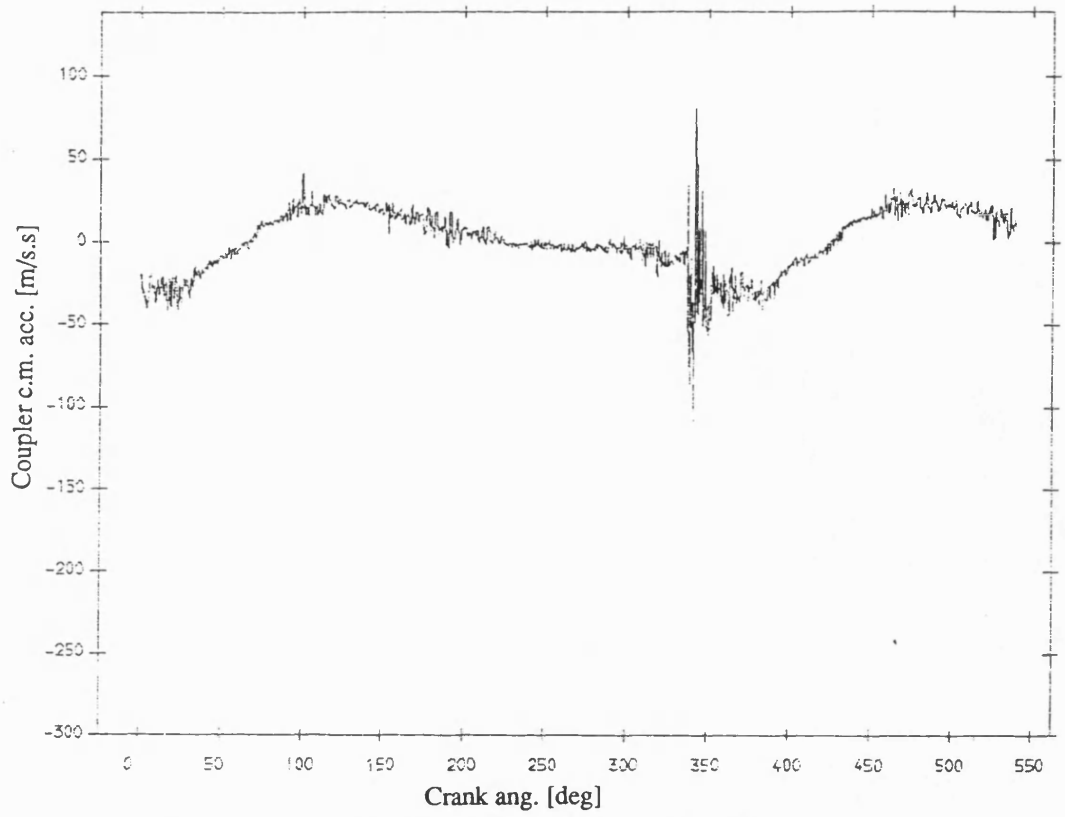

Fig 8.2.21 Exp. result coupler acceleration , normal bearing
with fly wheel ;mean speed=244 rev/min ; dia. clearance=.25mm

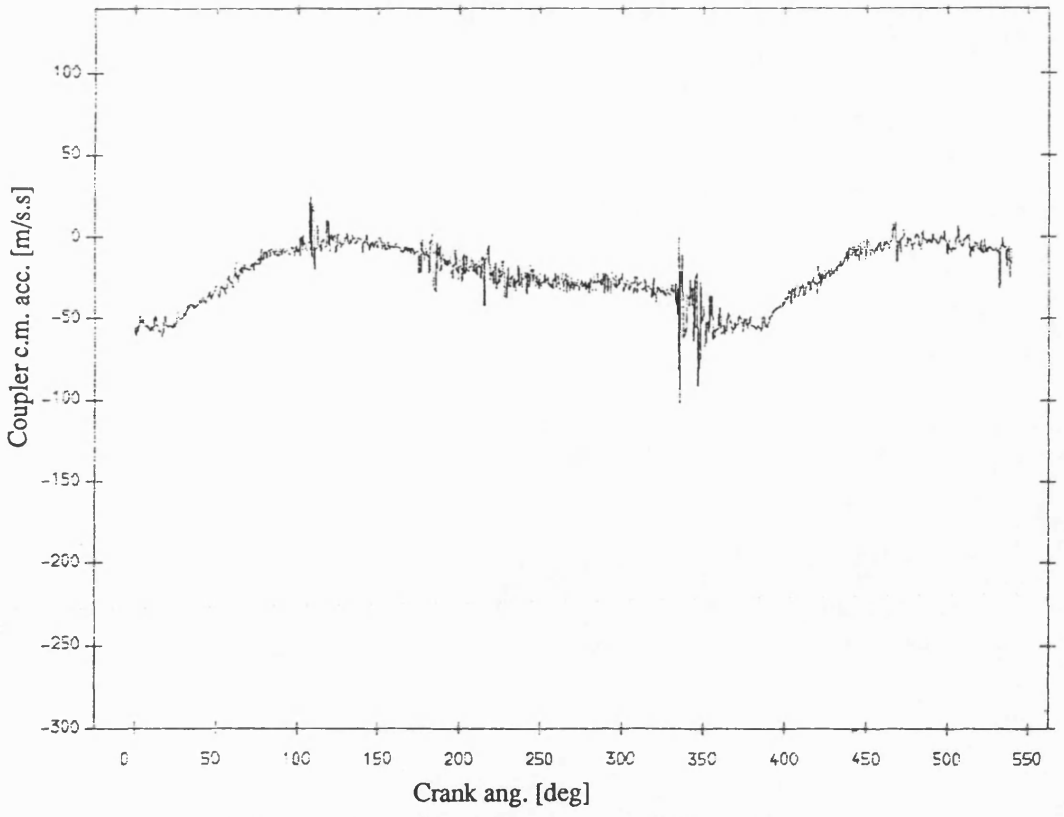

Fig 8.2.22 Exp. result coupler acceleration , normal bearing
no fly wheel ;mean speed=244 rev/min ; dia. clearance=.25mm

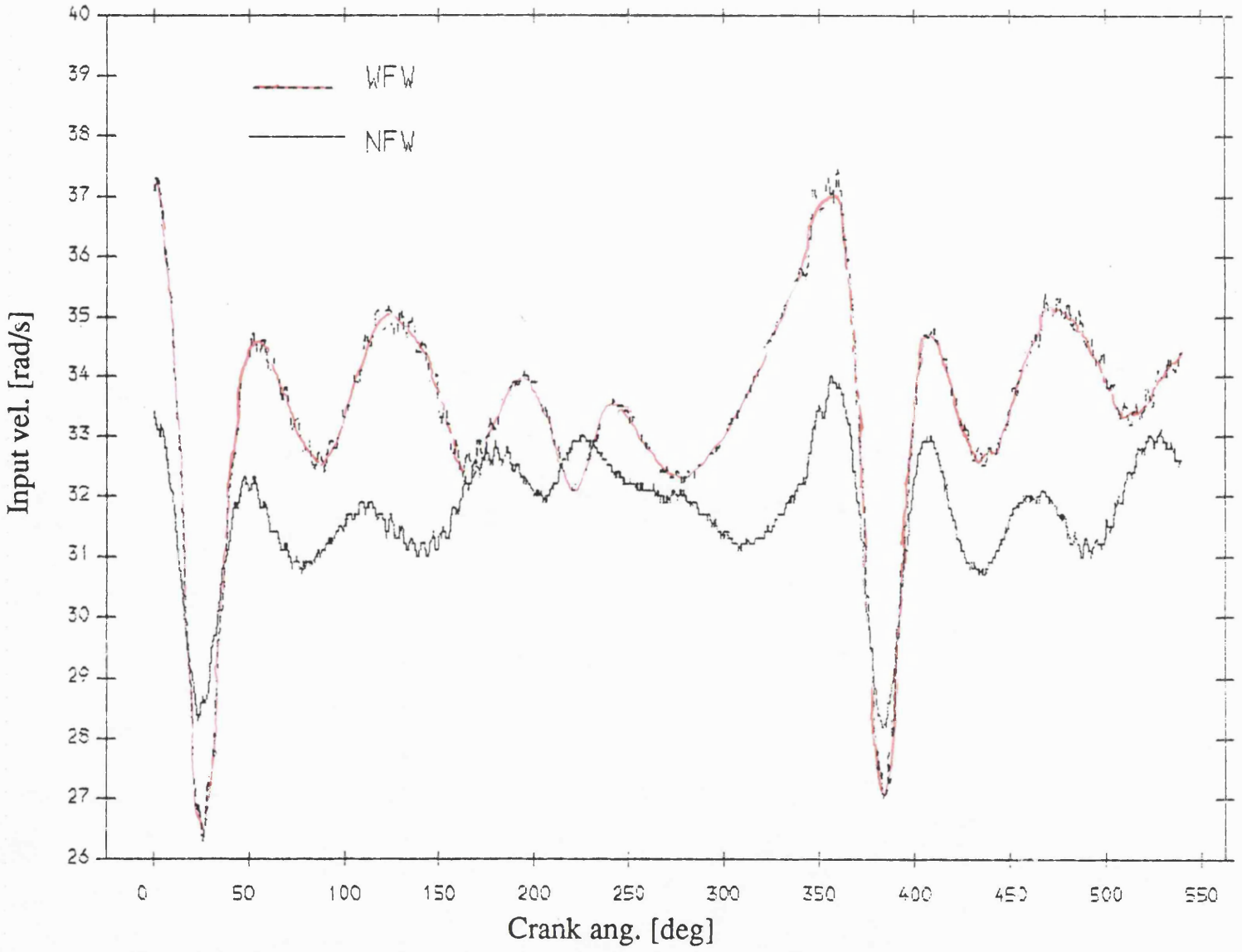

Fig 8.2.23 Exp. result input velocity , normal bearing
mean speed=327 rev/min; dia. clearance=.25mm

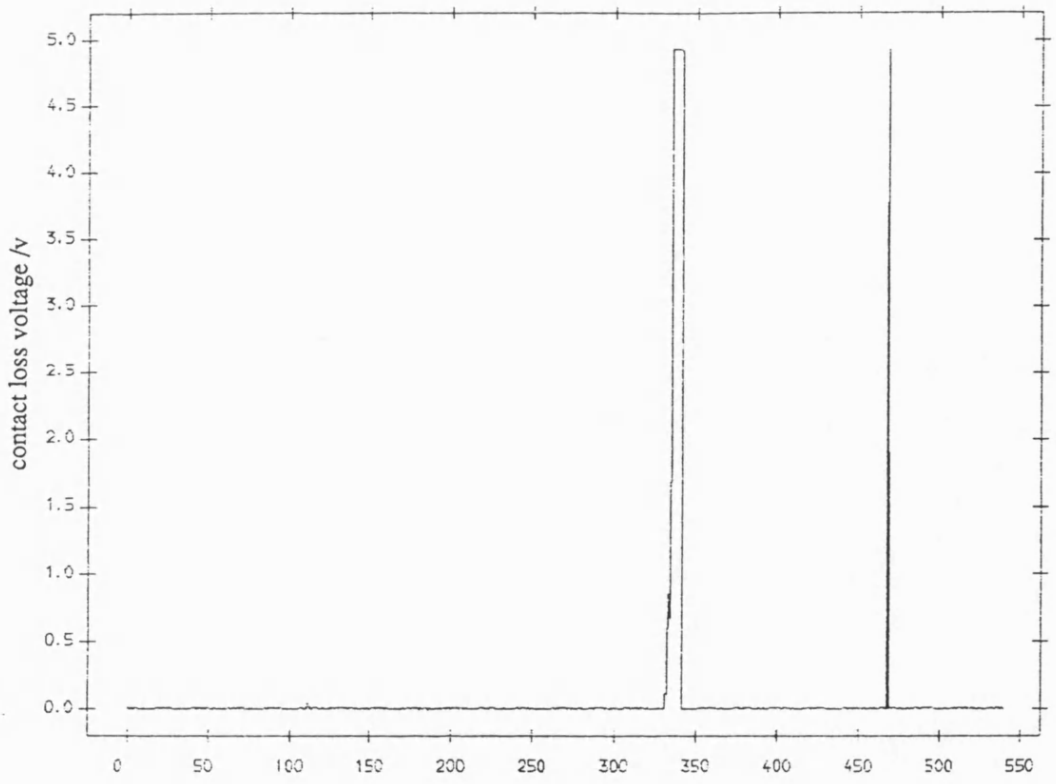

Fig 8.2.24 Exp. result contact loss of pin and normal bearing
with flywheel ;mean speed=327 rev/min ;dia. clearance=0.25mm

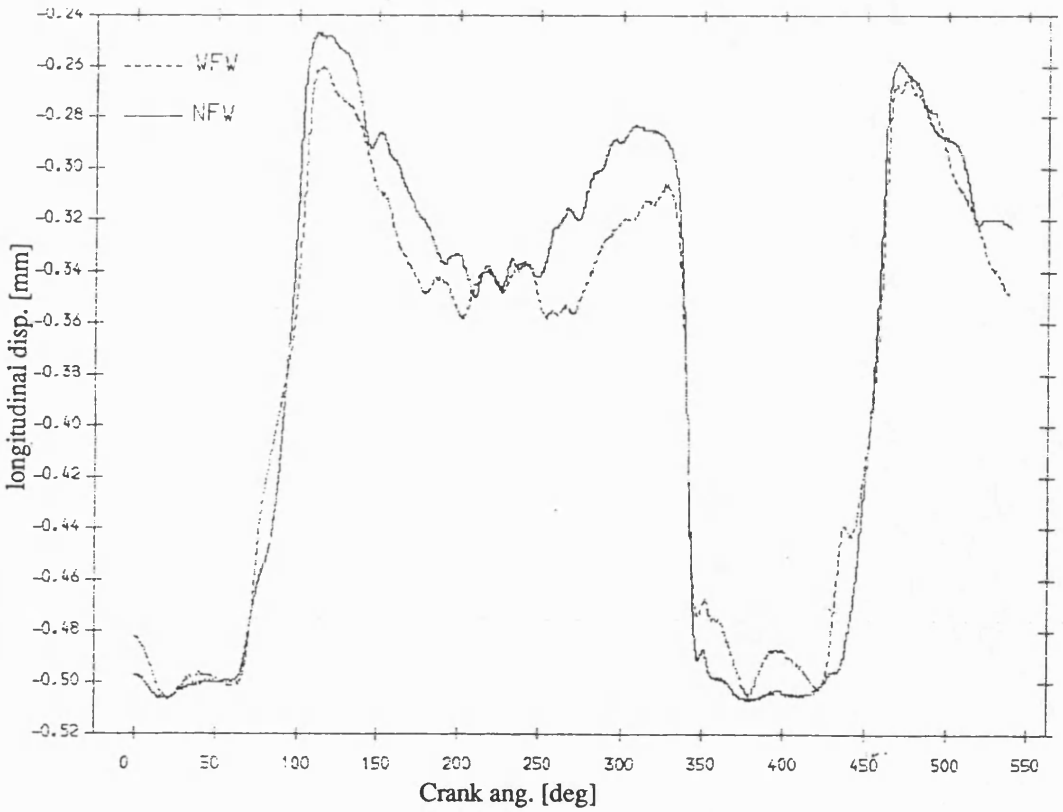

Fig 8.2.26 Exp. result longitudinal disp. of pin , normal bearing
mean speed=327 rev/min; dia. clearance=.25mm

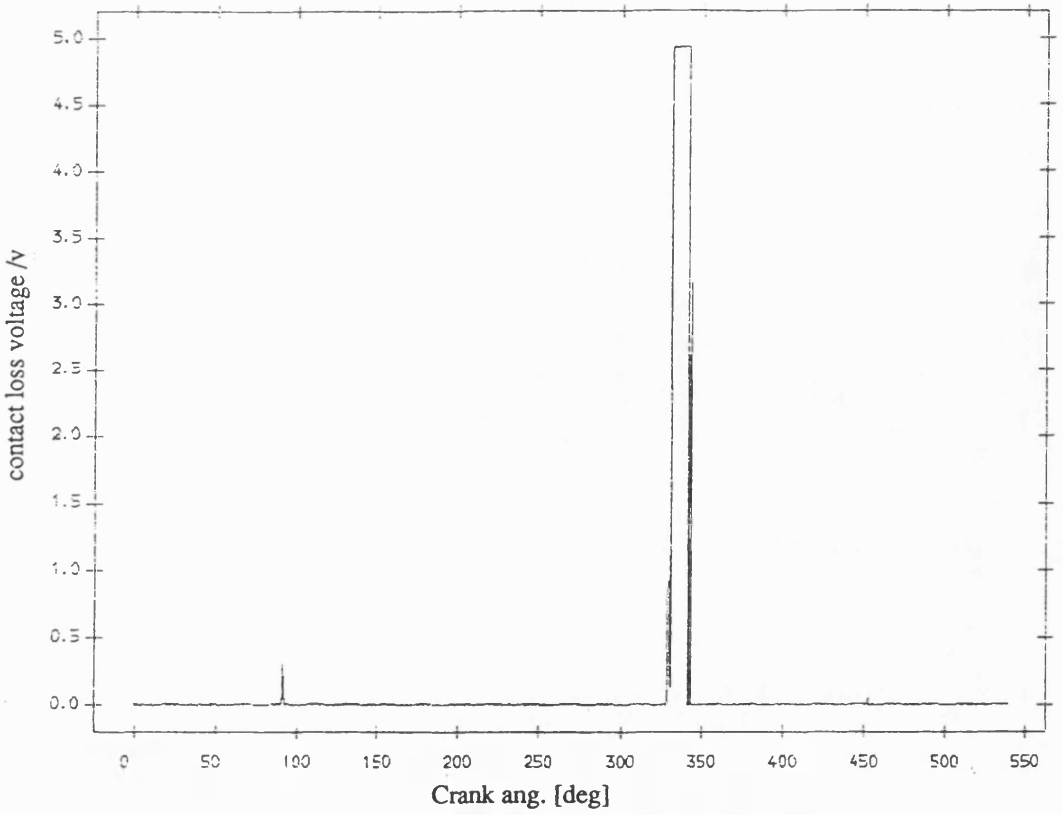

Fig 8.2.25 Exp. result contact loss of pin and normal bearing
no flywheel ;mean speed=327 rev/min ;dia. clearance=0.25mm

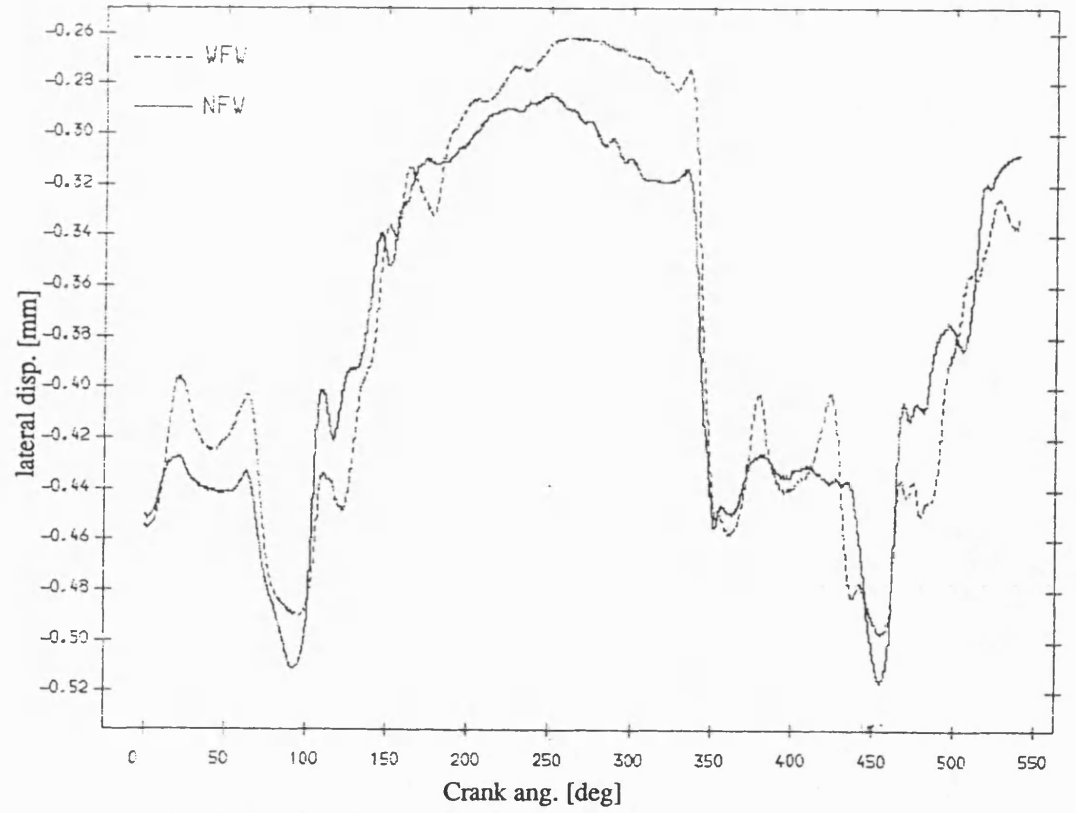

Fig 8.2.27 Exp. result lateral disp. of pin , normal bearing
mean speed=327 rev/min; dia. clearance=.25mm

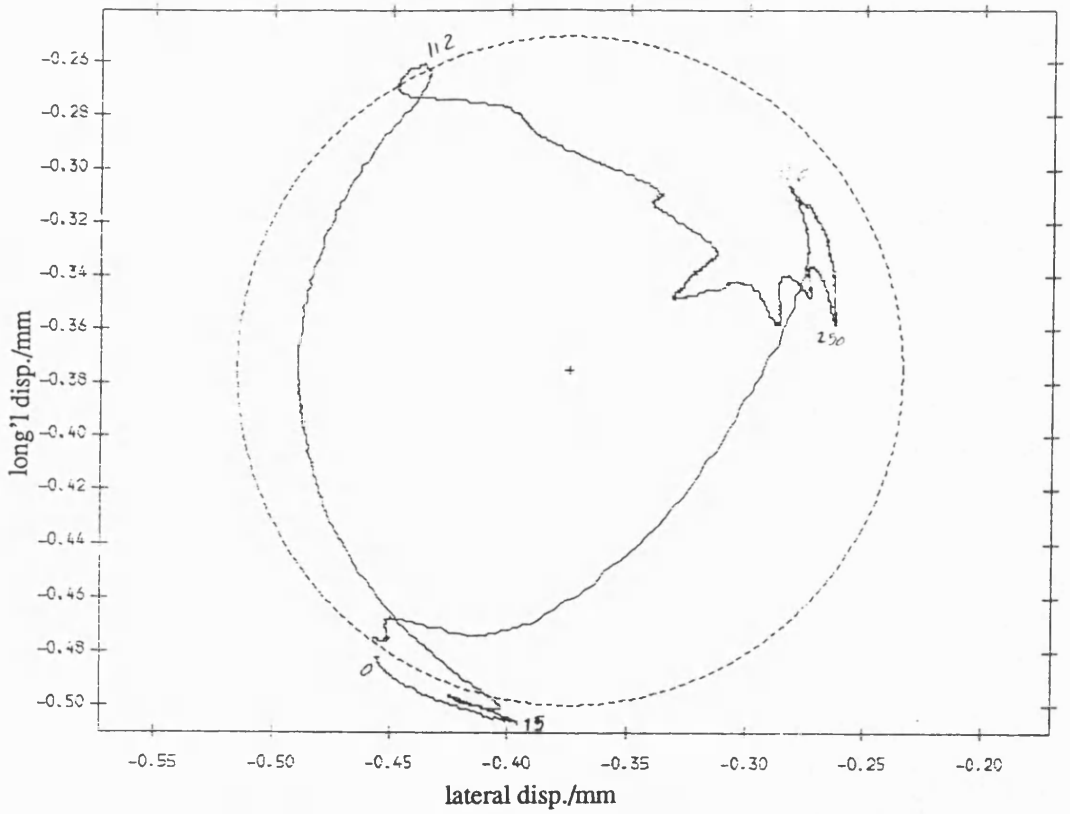

Fig 8.2.28 Exp. result polar plot of relative disp. of pin in normal bearing with fly wheel ;mean speed=327 rev/min ; dia. clearance=.25mm

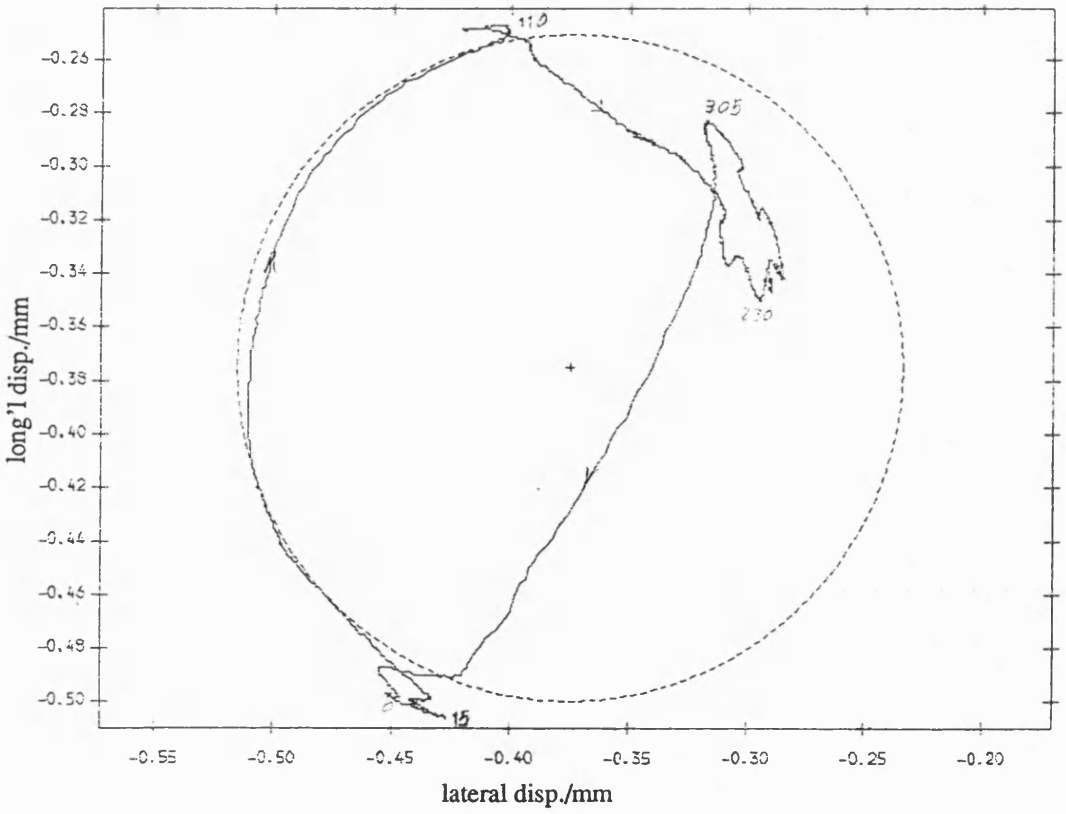

Fig 8.2.29 Exp. result polar plot of relative disp. of pin in normal bearing no fly wheel ;mean speed=327 rev/min ; dia. clearance=.25mm

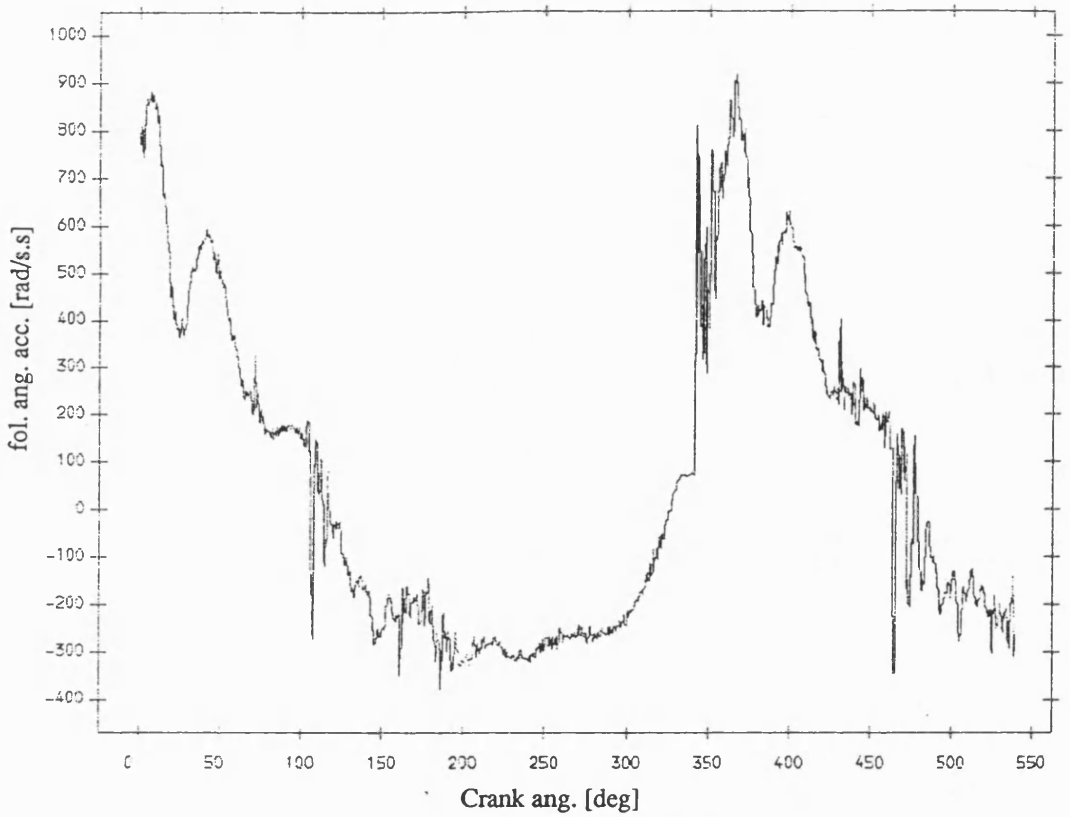

Fig 8.2.30 Exp. result follower ang. acceleration , normal bearing
with fly wheel ;mean speed=327 rev/min ; dia. clearance=.25mm

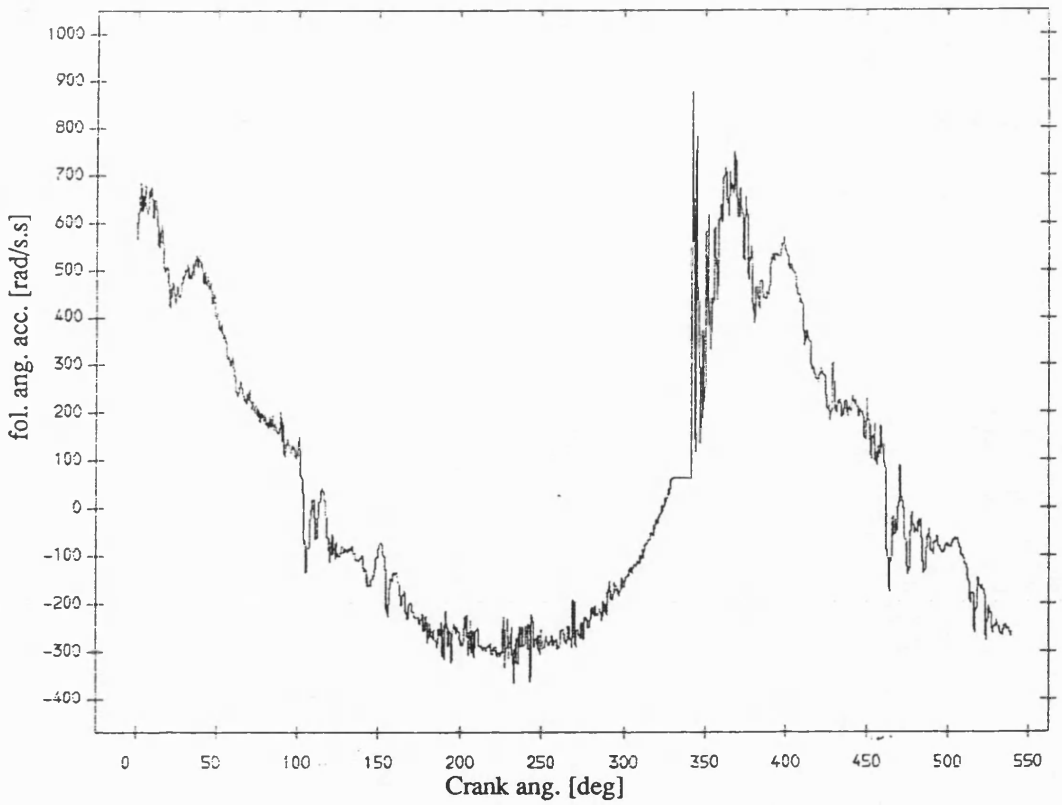

Fig 8.2.31 Exp. result follower ang. acceleration ,normal bearing
no fly wheel ;mean speed=327 rev/min ; dia. clearance=.25mm

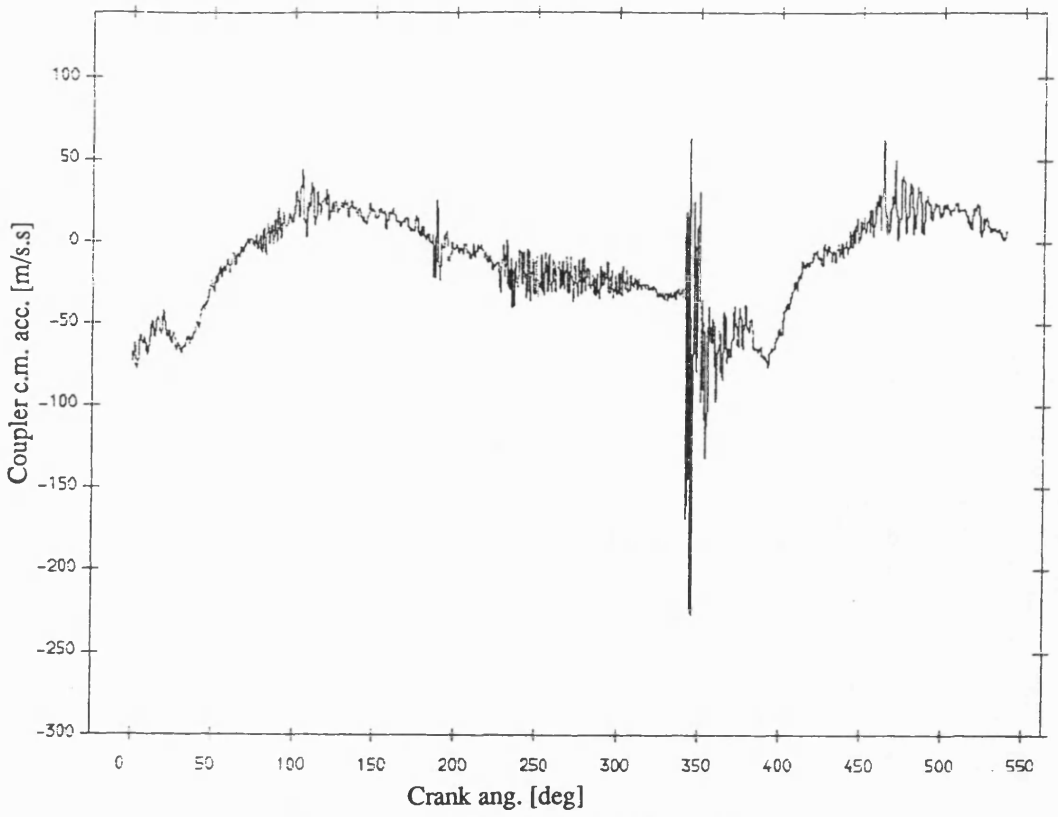

Fig 8.2.32 Exp. result coupler acceleration , normal bearing
with fly wheel ;mean speed=327 rev/min ; dia. clearance=.25mm

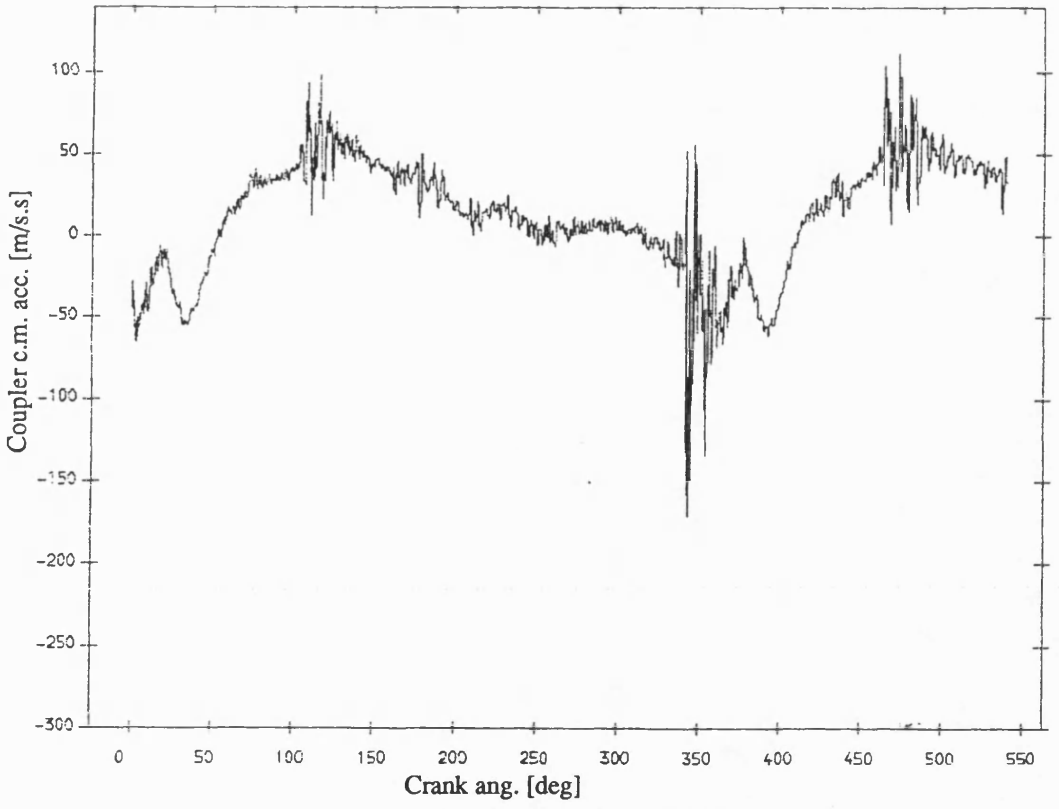

Fig 8.2.33 Exp. result coupler acceleration , normal bearing
no fly wheel ;mean speed=327 rev/min ; dia. clearance=.25mm

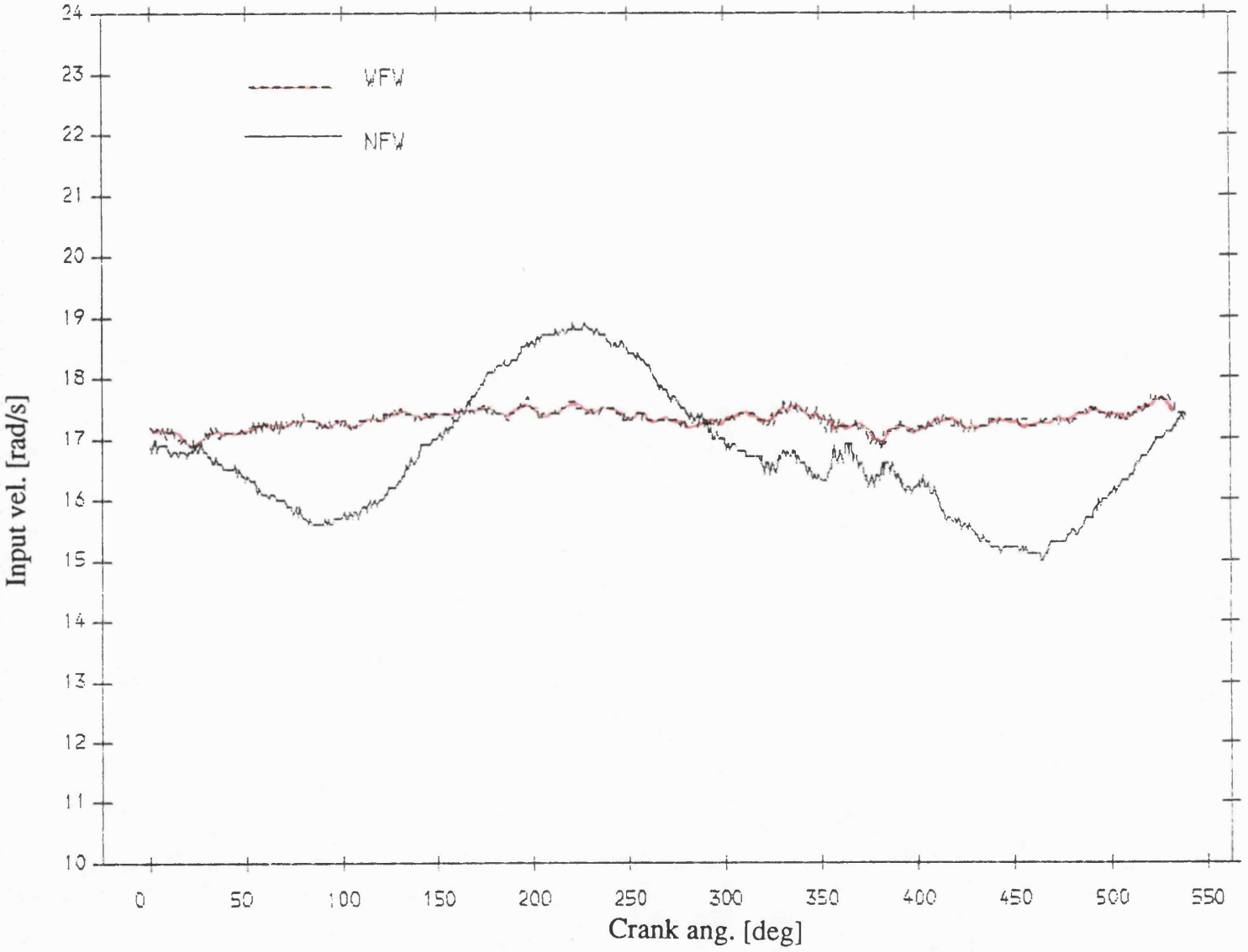

Fig 8.3.1 Exp. rePult input velocity , normal bearing
mean speed=168 rev/min; dia. clearance=.3mm

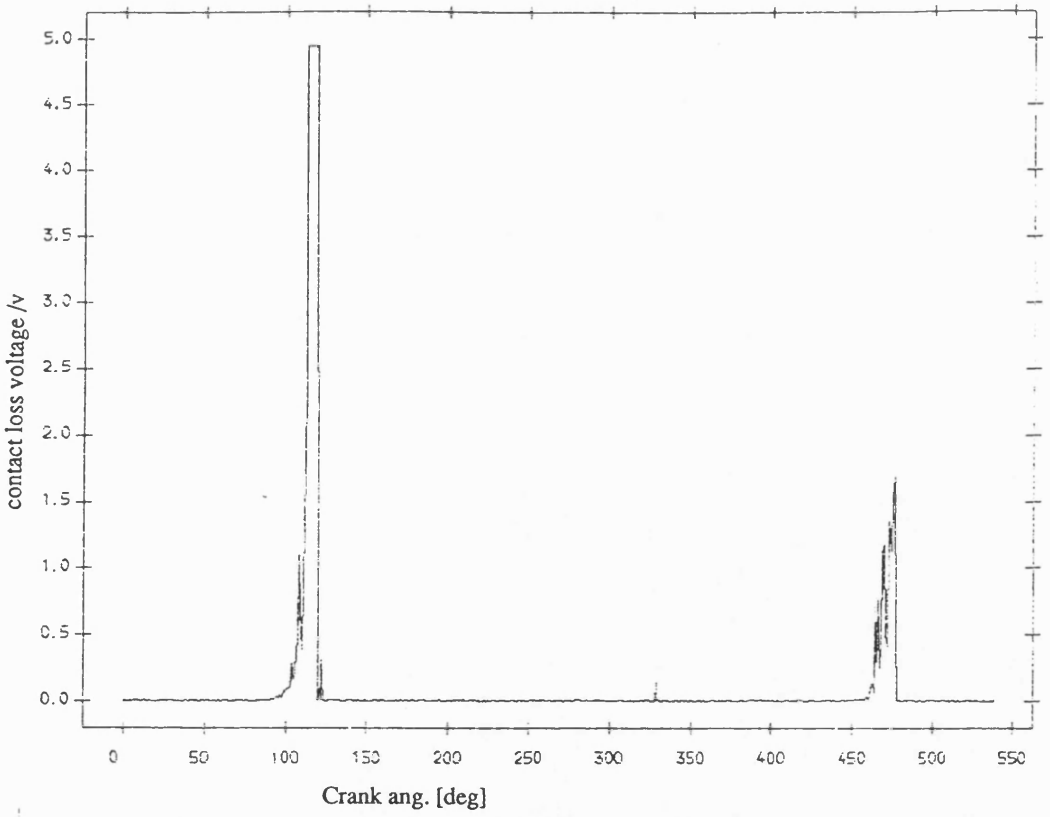

Fig 8.3.2 Exp. result contact loss of pin and normal bearing
with flywheel ;mean speed=168 rev/min ;dia. clearance=0.3mm

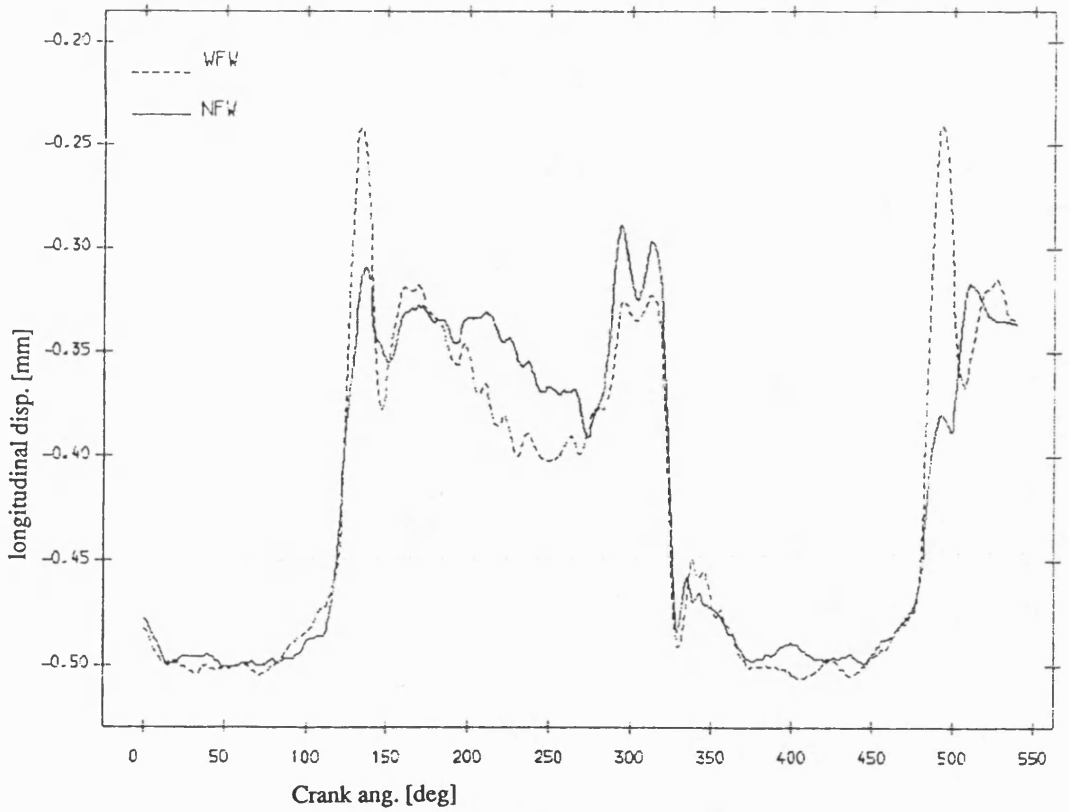

Fig 8.3.4 Exp. result longitudinal disp. of pin , normal bearing
mean speed=168 rev/min; dia. clearance=.3mm

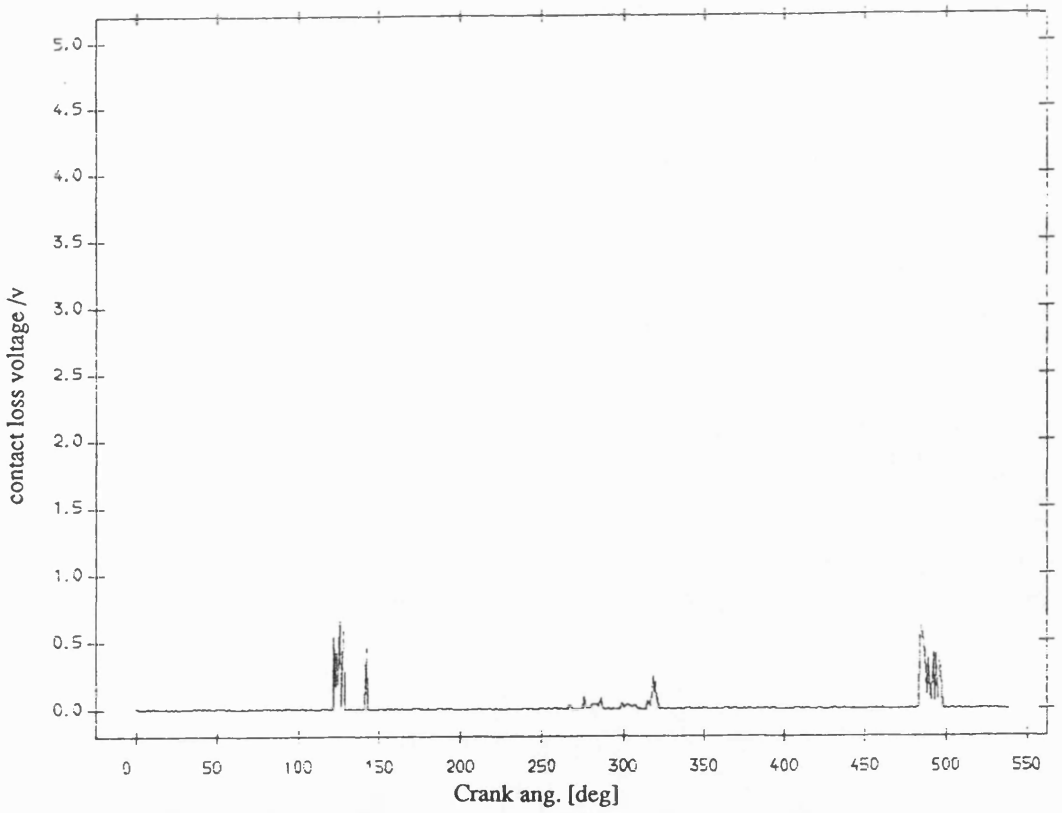

Fig 8.3.3 Exp. result contact loss of pin and normal bearing
no flywheel ;mean speed=168 rev/min ;dia. clearance=0.3mm

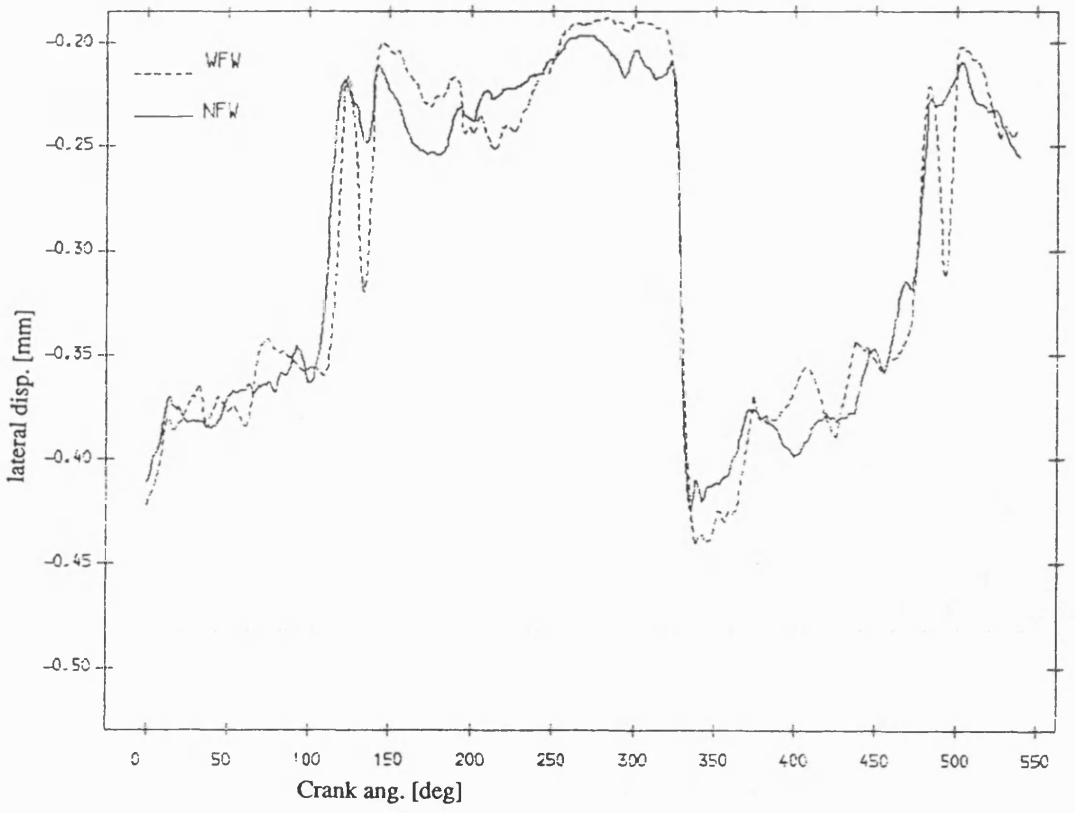

Fig 8.3.5 Exp. result lateral disp. of pin , normal bearing
mean speed=168 rev/min; dia. clearance=.3mm

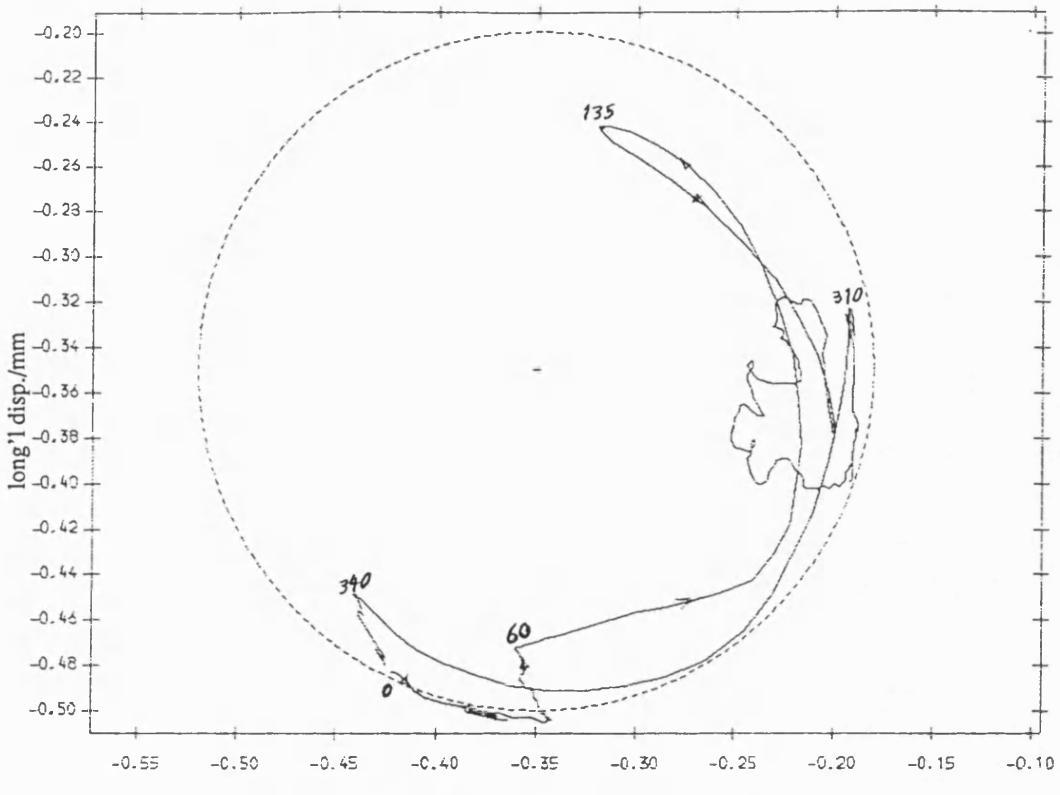

Fig 8.3.6 Exp. result polar plot of relative disp. of pin in normal bearing with fly wheel ;mean speed=168 rev/min ; dia. clearance=.3mm

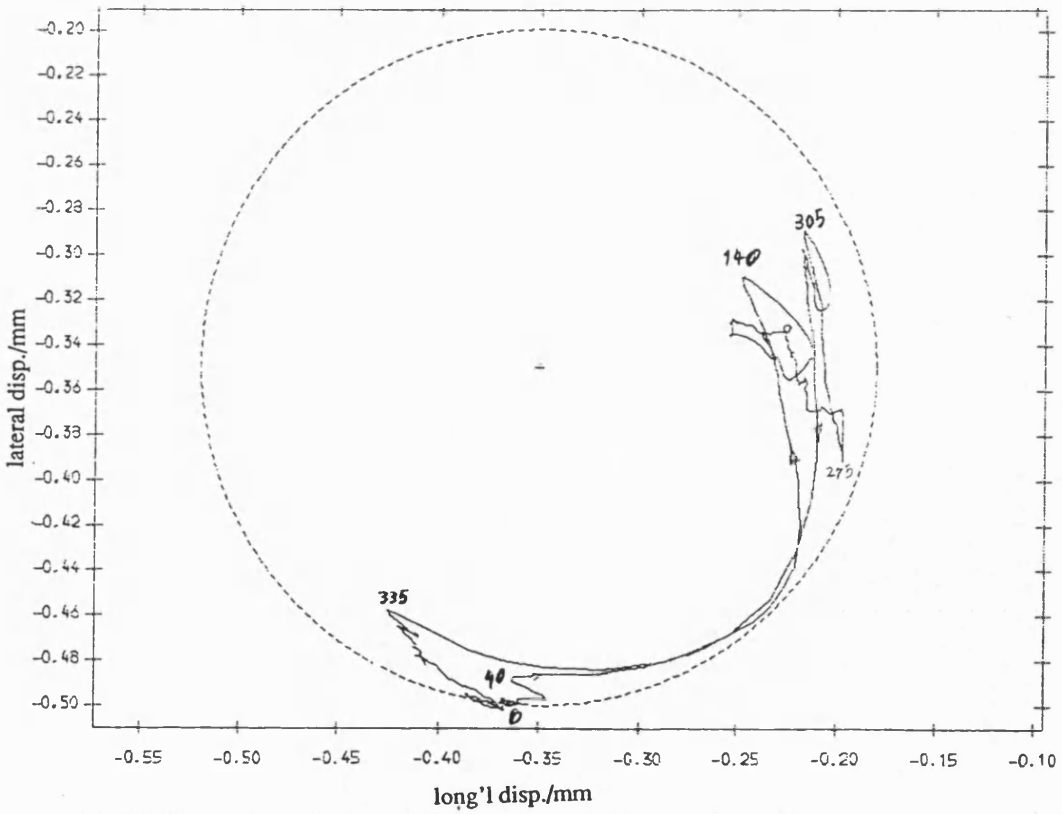

Fig 8.3.7 Exp. result polar plot of relative disp. of pin in normal bearing no fly wheel ;mean speed=168 rev/min ; dia. clearance=.3mm

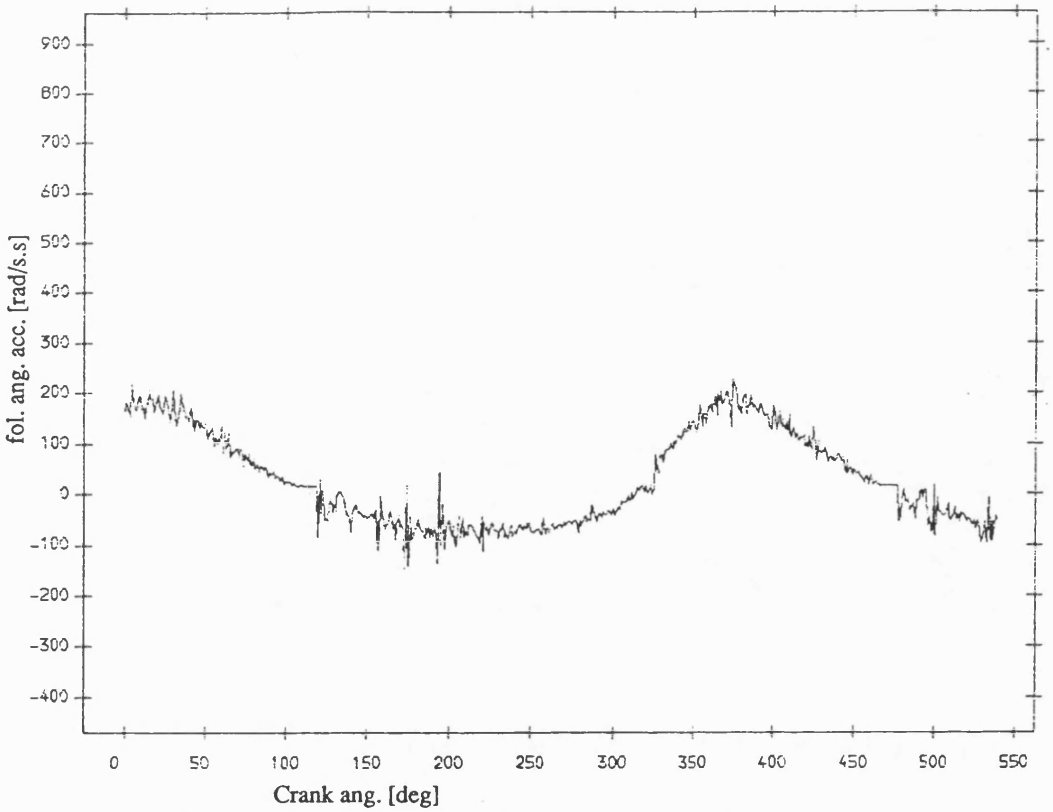

Fig 8.3.8 Exp. result follower ang. acceleration , normal bearing
with fly wheel ;mean speed=168 rev/min ; dia. clearance=.3mm

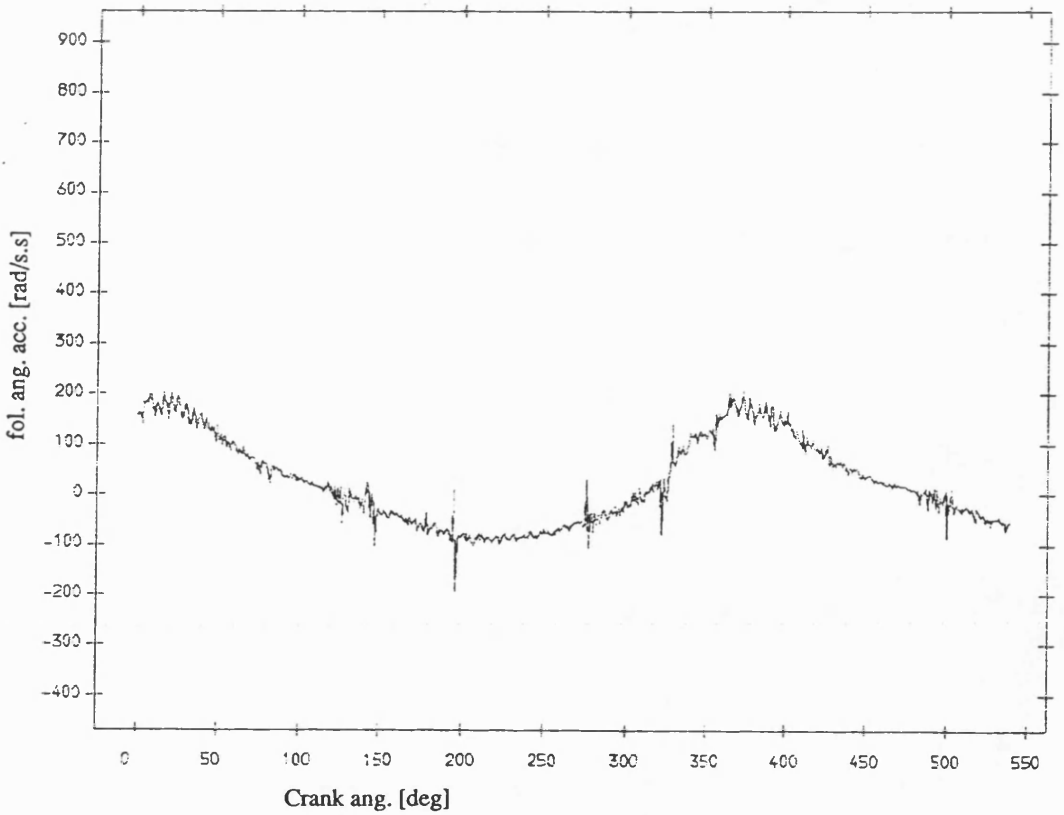

Fig 8.3.9 Exp. result follower ang. acceleration , normal bearing
no fly wheel ;mean speed=168 rev/min ; dia. clearance=.3mm

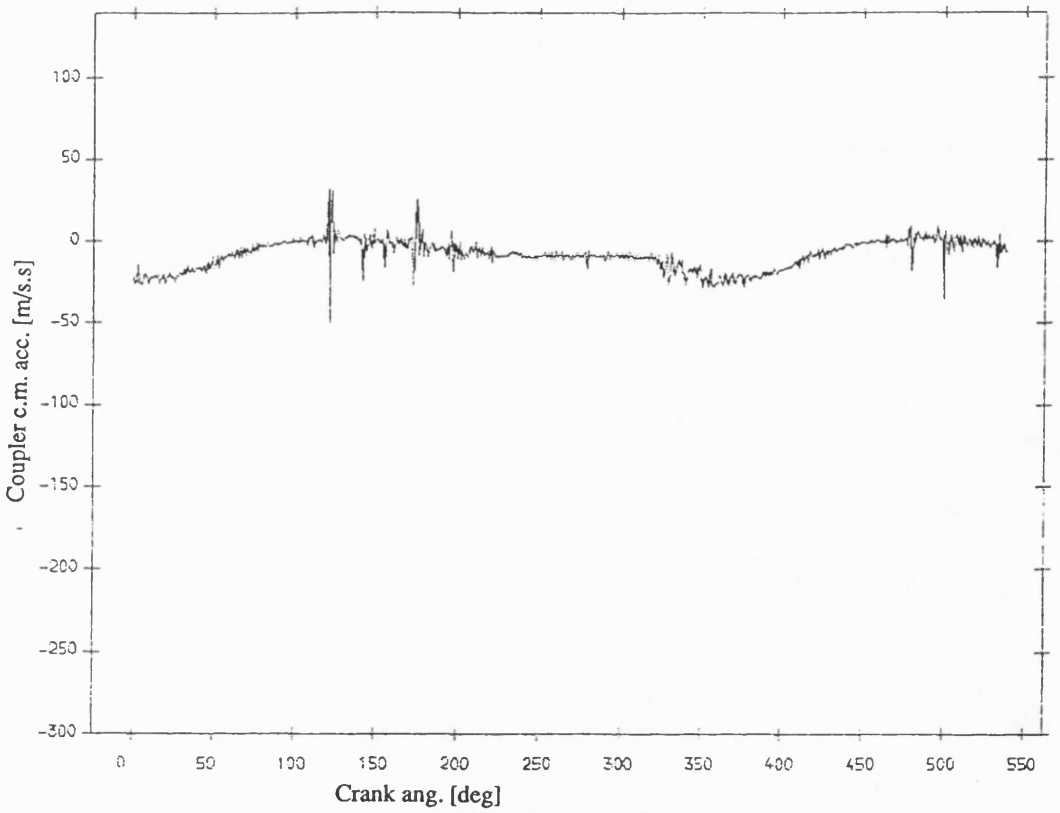

Fig 8.3.10 Exp. result coupler acceleration , normal bearing
with fly wheel ;mean speed=168 rev/min ; dia. clearance=.3mm

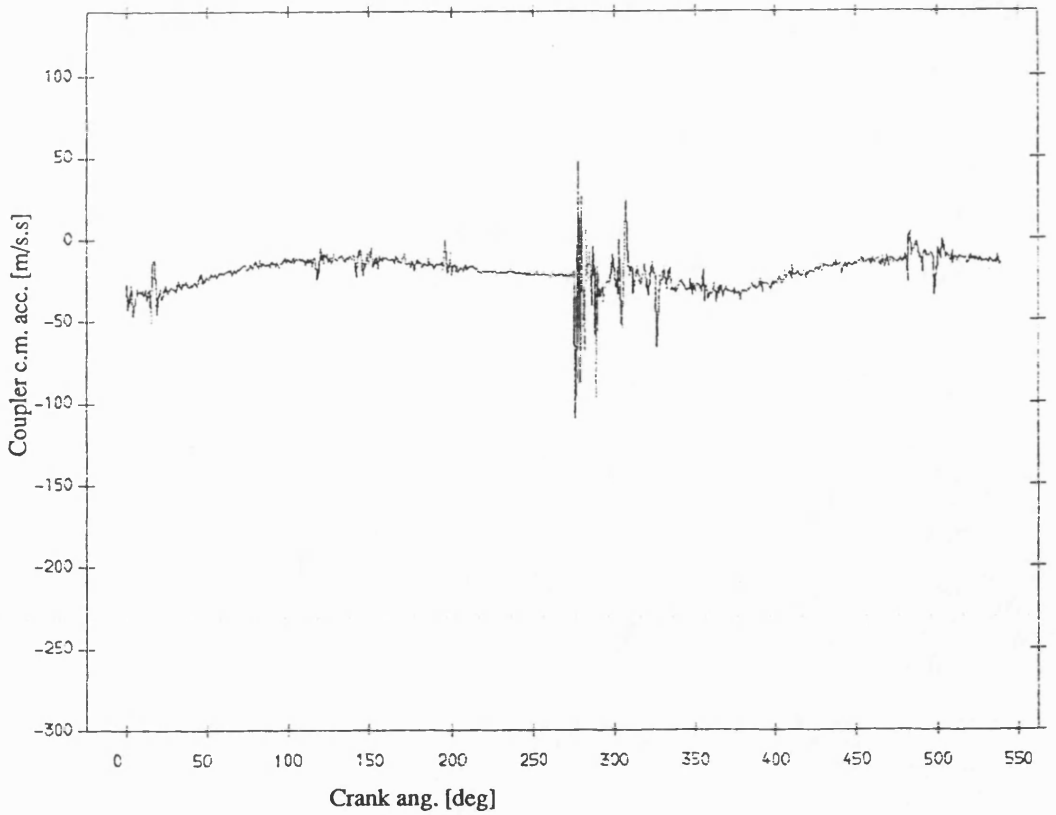

Fig 8.3.11 Exp. result coupler acceleration , normal bearing
no fly wheel ;mean speed=168 rev/min ; dia. clearance=.3mm

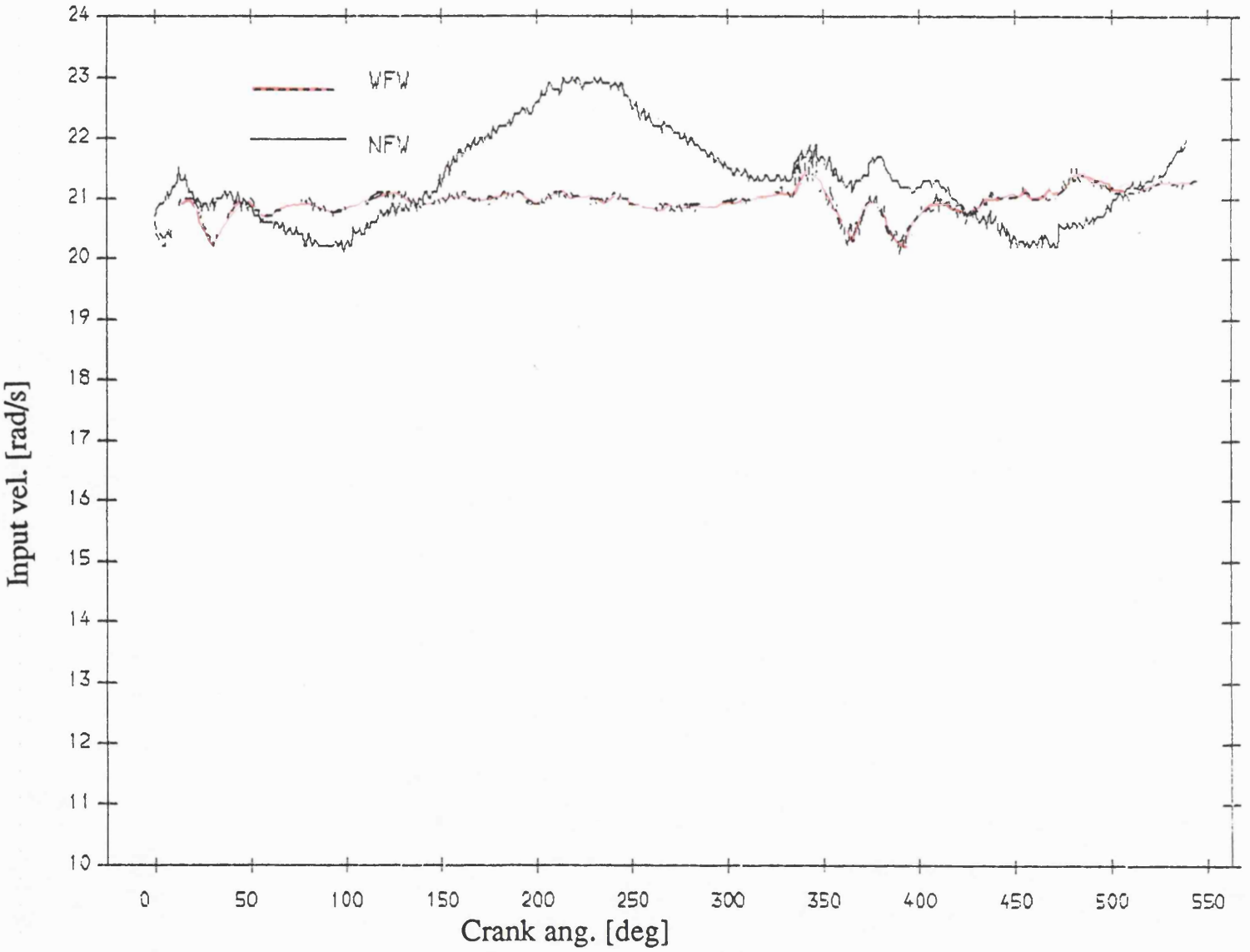

Fig 8.3.12 Exp. re ult input velocity , normal bearing
mean speed=208 rev/min; dia. clearance=.3mm

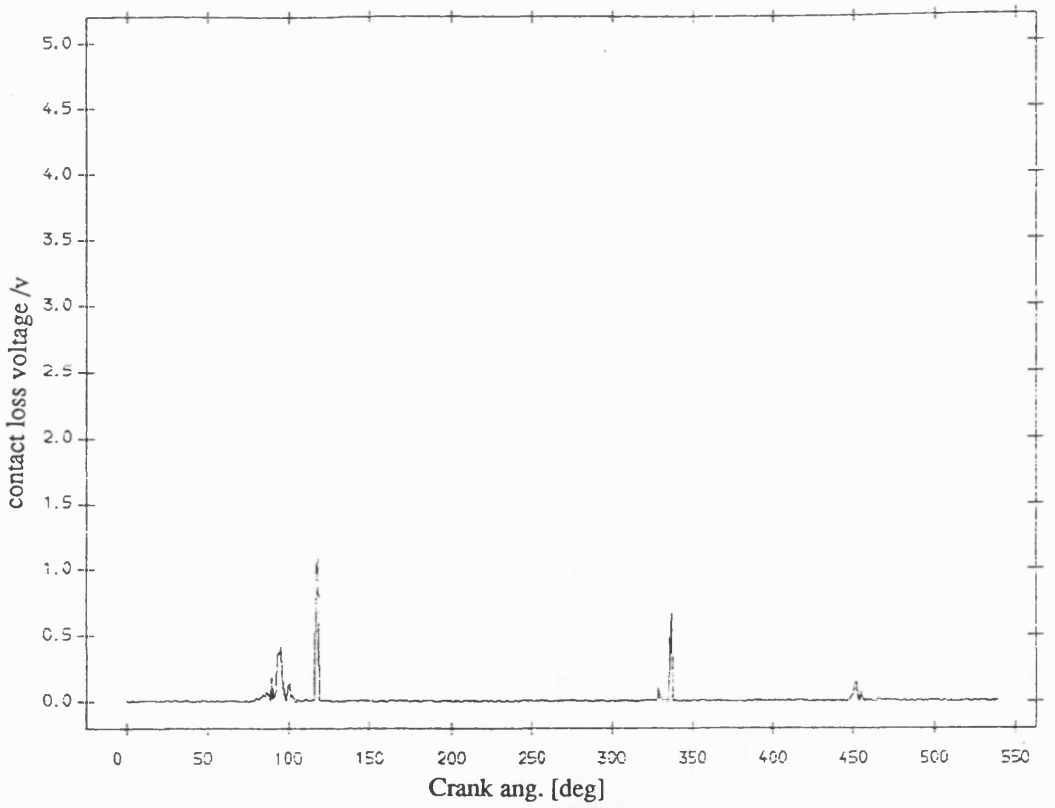

Fig 8.3.13 Exp. result contact loss of pin and normal bearing
with flywheel ;mean speed=208 rev/min ;dia. clearance=0.3mm

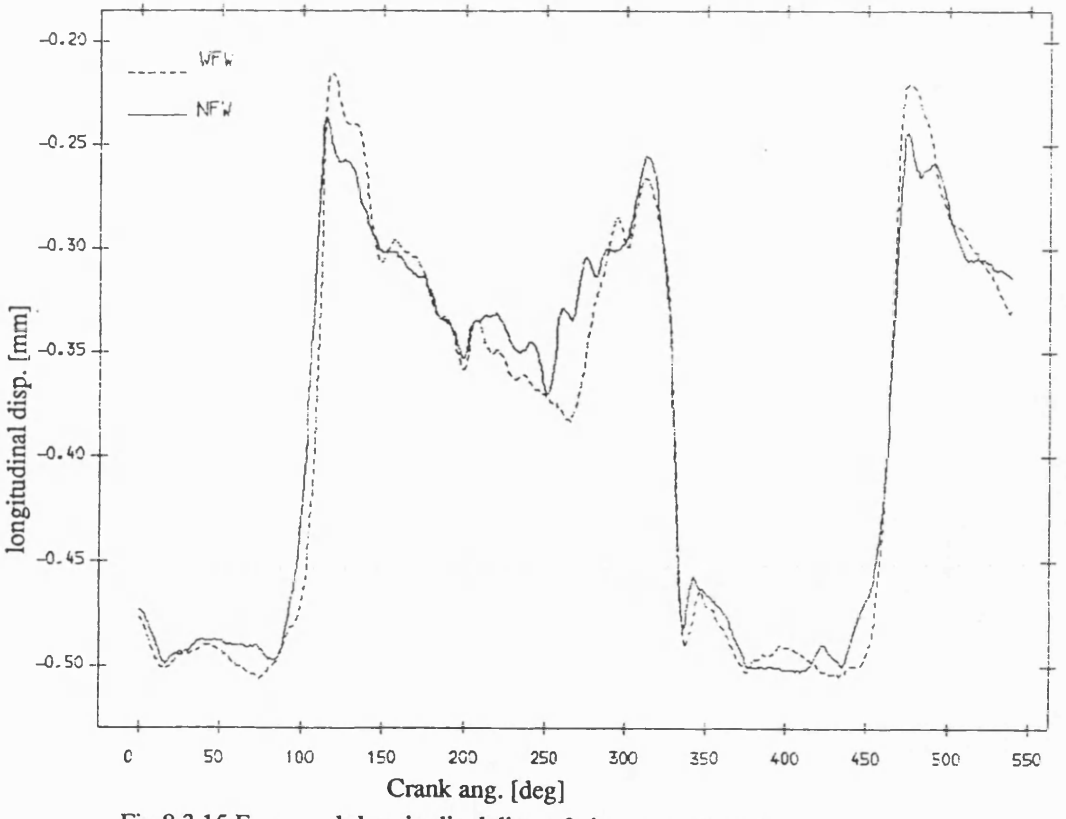

Fig 8.3.15 Exp. result longitudinal disp. of pin , normal bearing
mean speed=208 rev/min; dia. clearance=.3mm

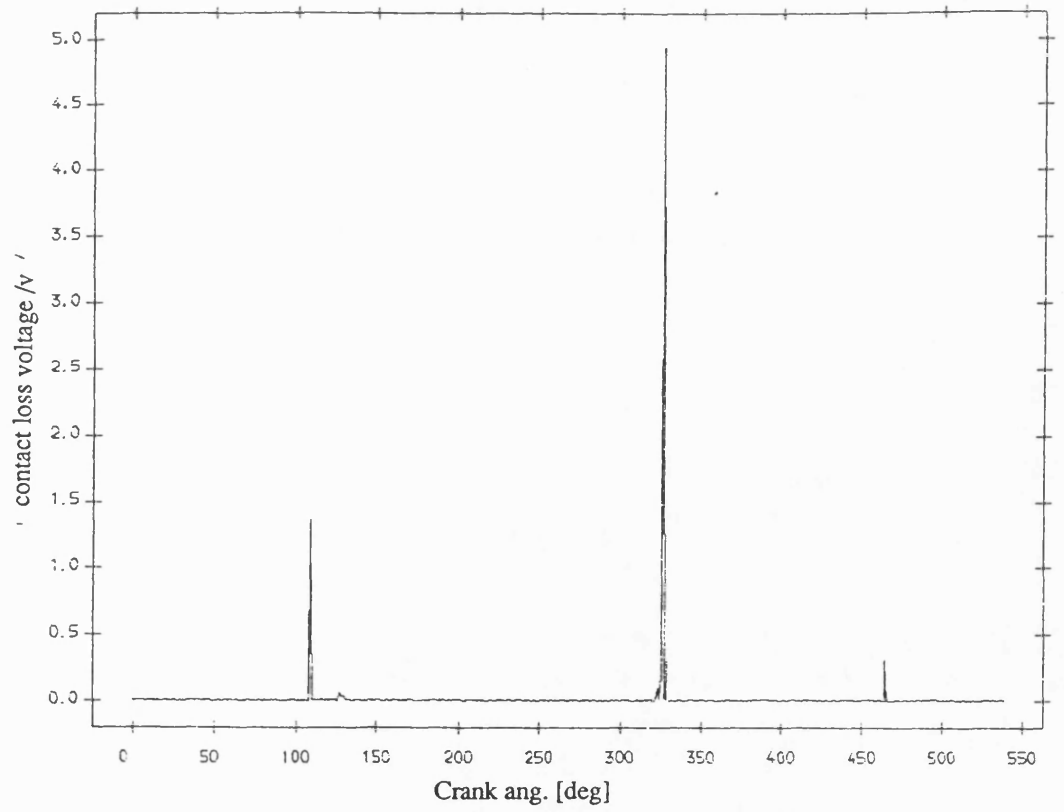

Fig 8.3.14 Exp. result contact loss of pin and normal bearing
no flywheel ;mean speed=208 rev/min ;dia. clearance=0.3mm

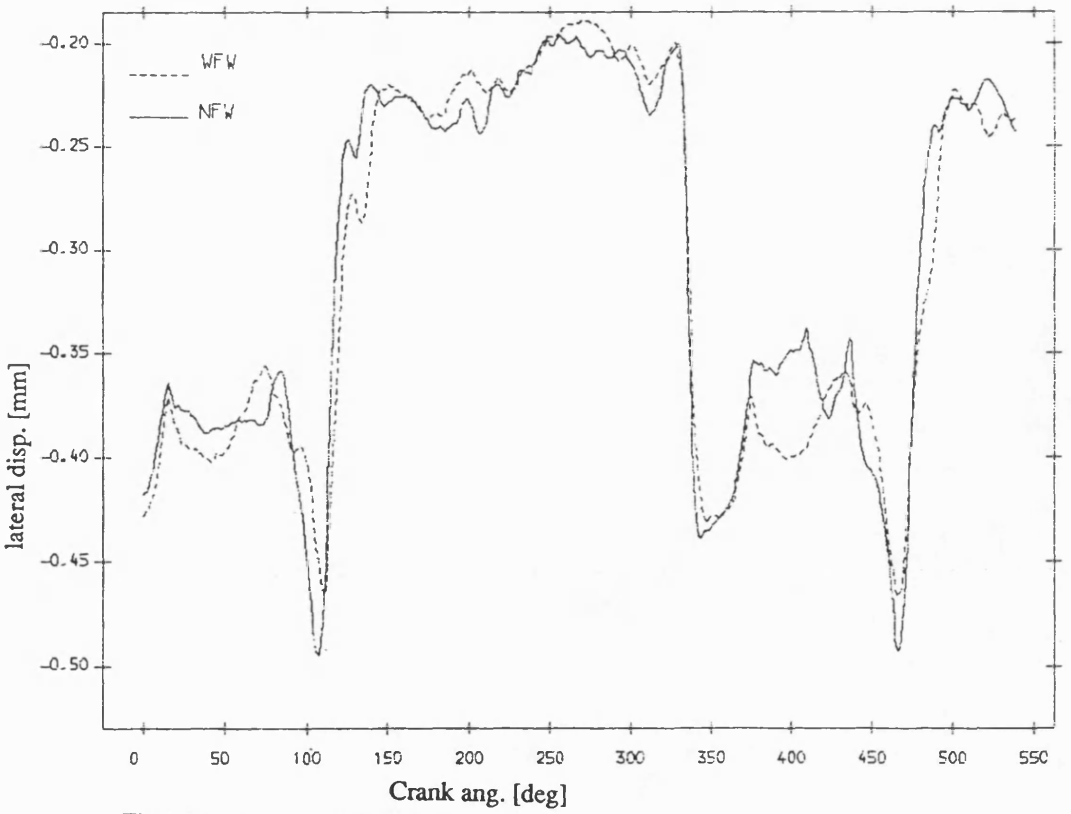

Fig 8.3.16 Exp. result lateral disp. of pin , normal bearing
mean speed=208 rev/min; dia. clearance=.3mm

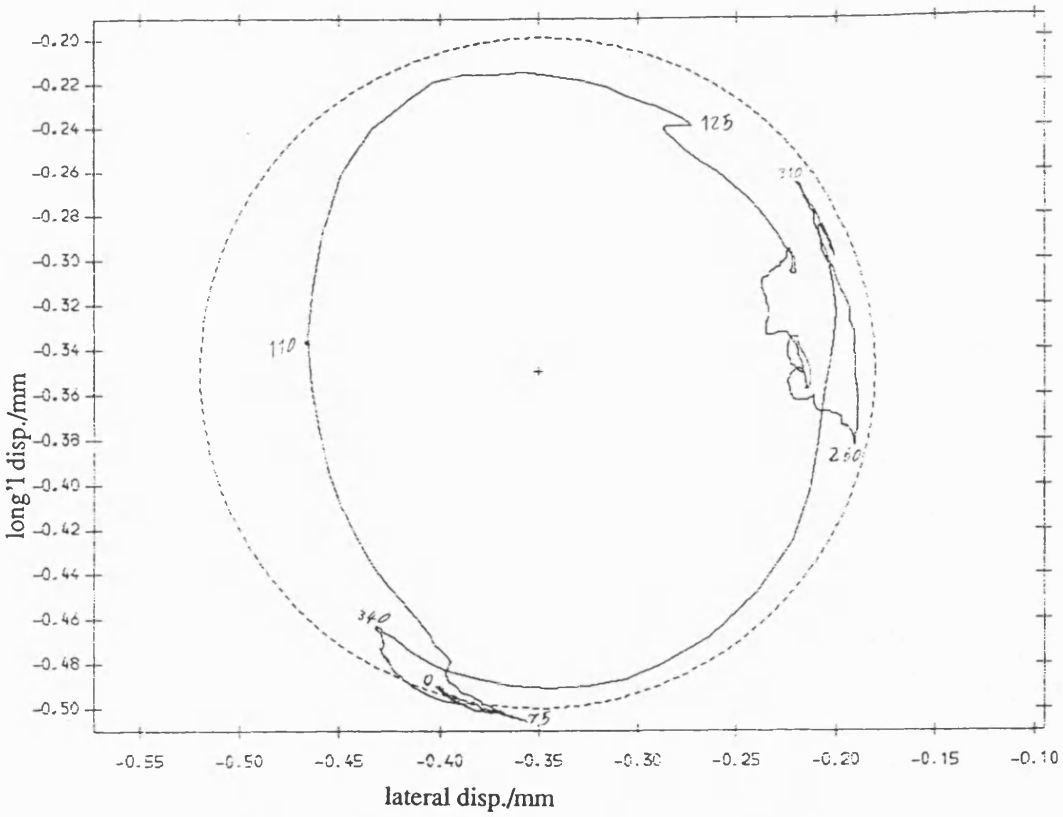

Fig 8.3.17 Exp. result polar plot of relative disp. of pin in normal bearing with fly wheel ;mean speed=208 rev/min ; dia. clearance=.3mm

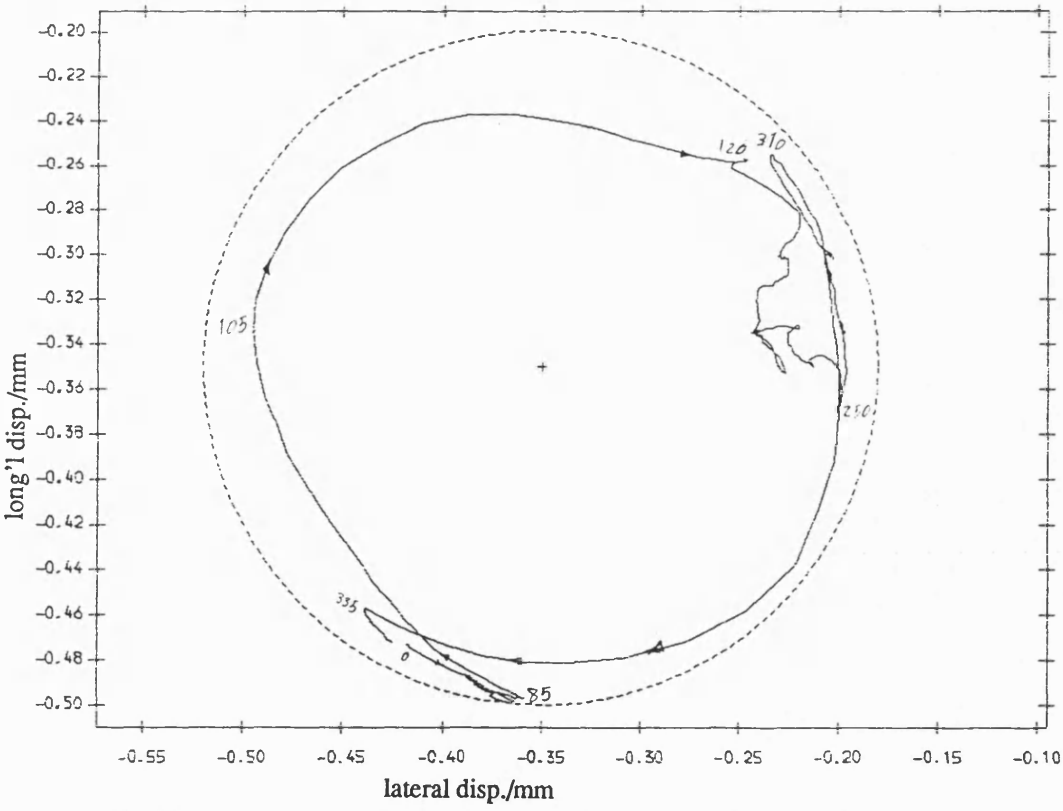

Fig 8.3.18 Exp. result polar plot of relative disp. of pin in normal bearing no fly wheel ;mean speed=208 rev/min ; dia. clearance=.3mm

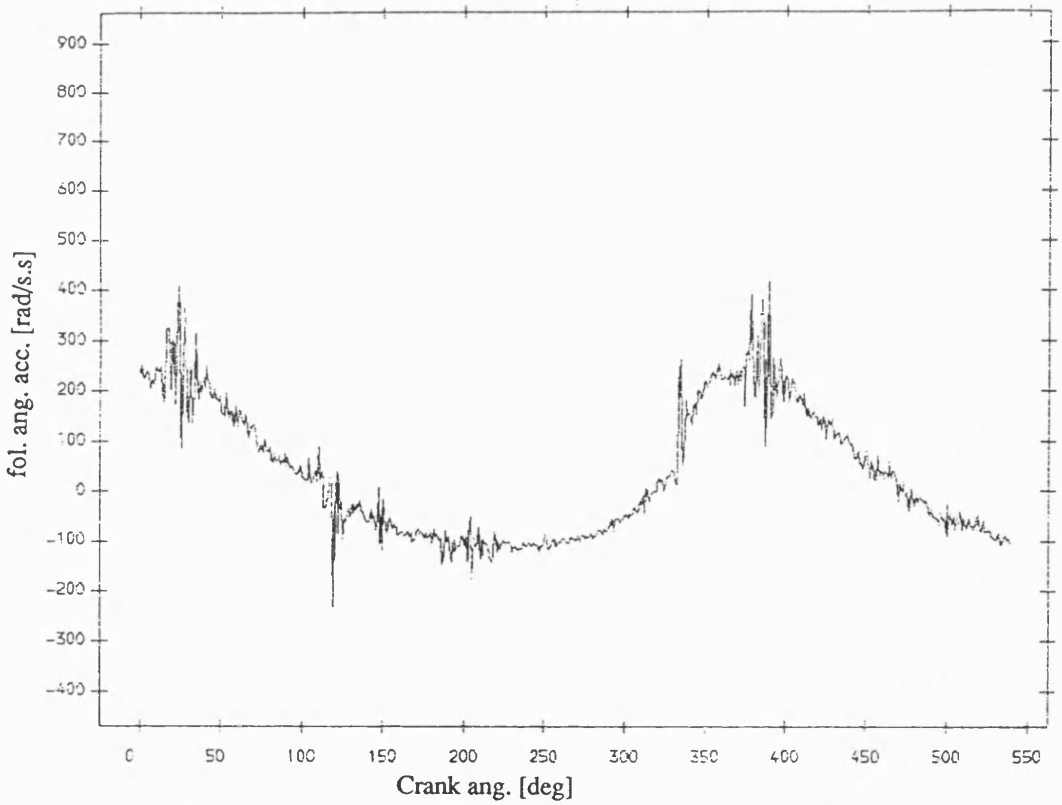

Fig 8.3.19 Exp. result follower ang. acceleration , normal bearing
with fly wheel ;mean speed=208 rev/min ; dia. clearance=.3mm

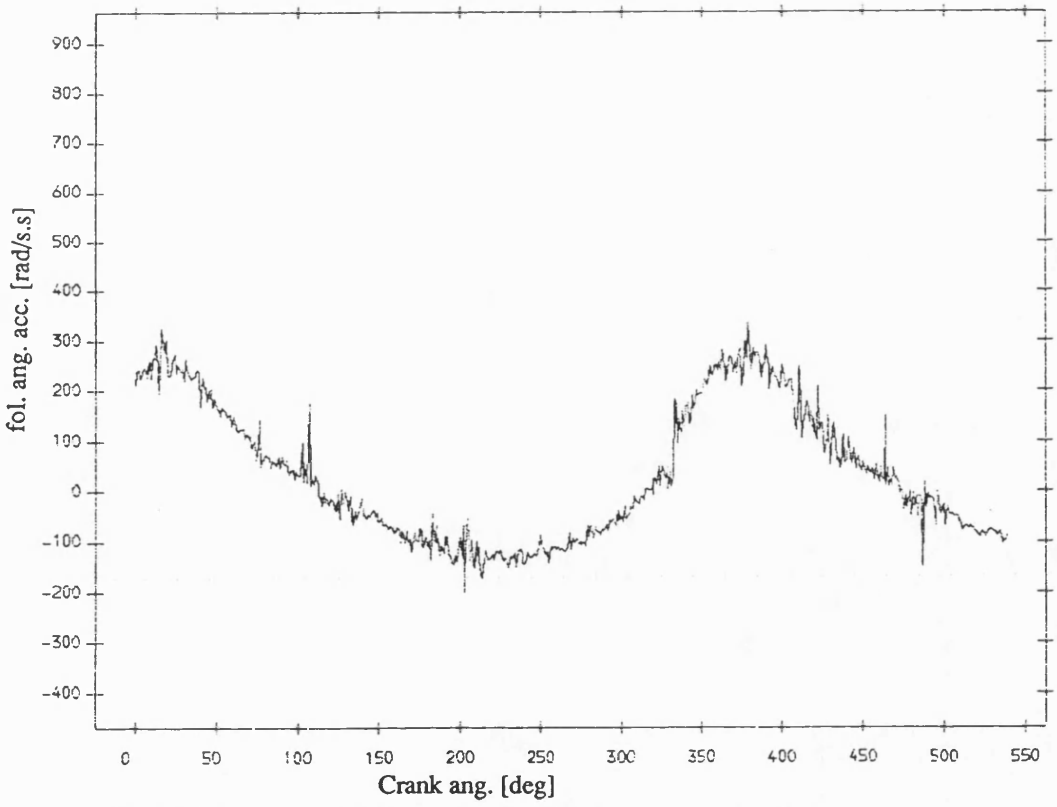

Fig 8.3.20 Exp. result follower ang. acceleration , normal bearing
no fly wheel ;mean speed=208 rev/min ; dia. clearance=.3mm

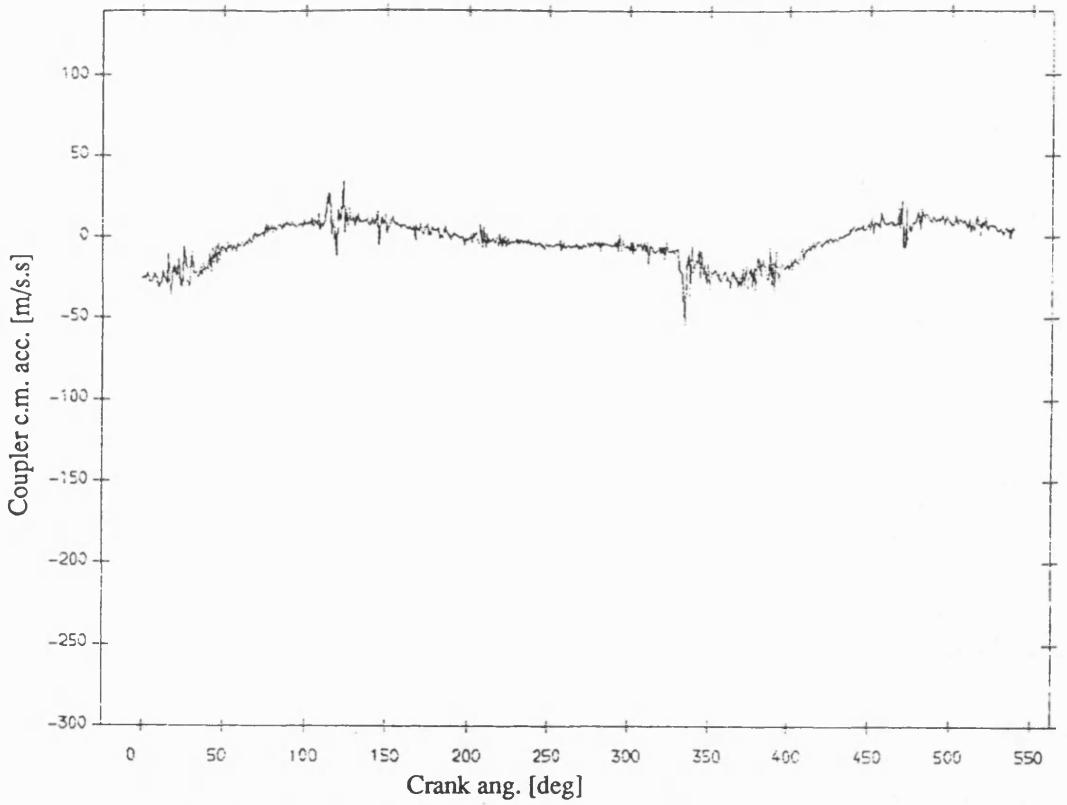

Fig 8.3.21 Exp. result coupler acceleration , normal bearing
with fly wheel ;mean speed=208 rev/min ; dia. clearance=.3mm

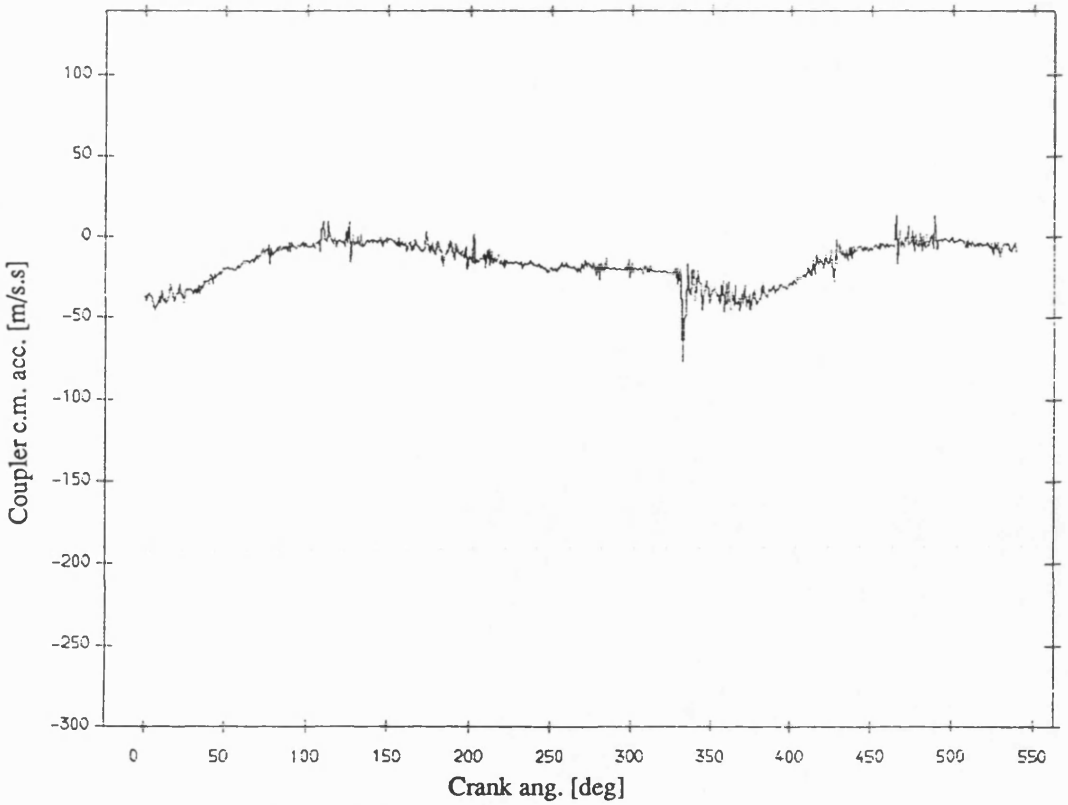

Fig 8.3.22 Exp. result coupler acceleration , normal bearing
no fly wheel ;mean speed=208 rev/min ; dia. clearance=.3mm

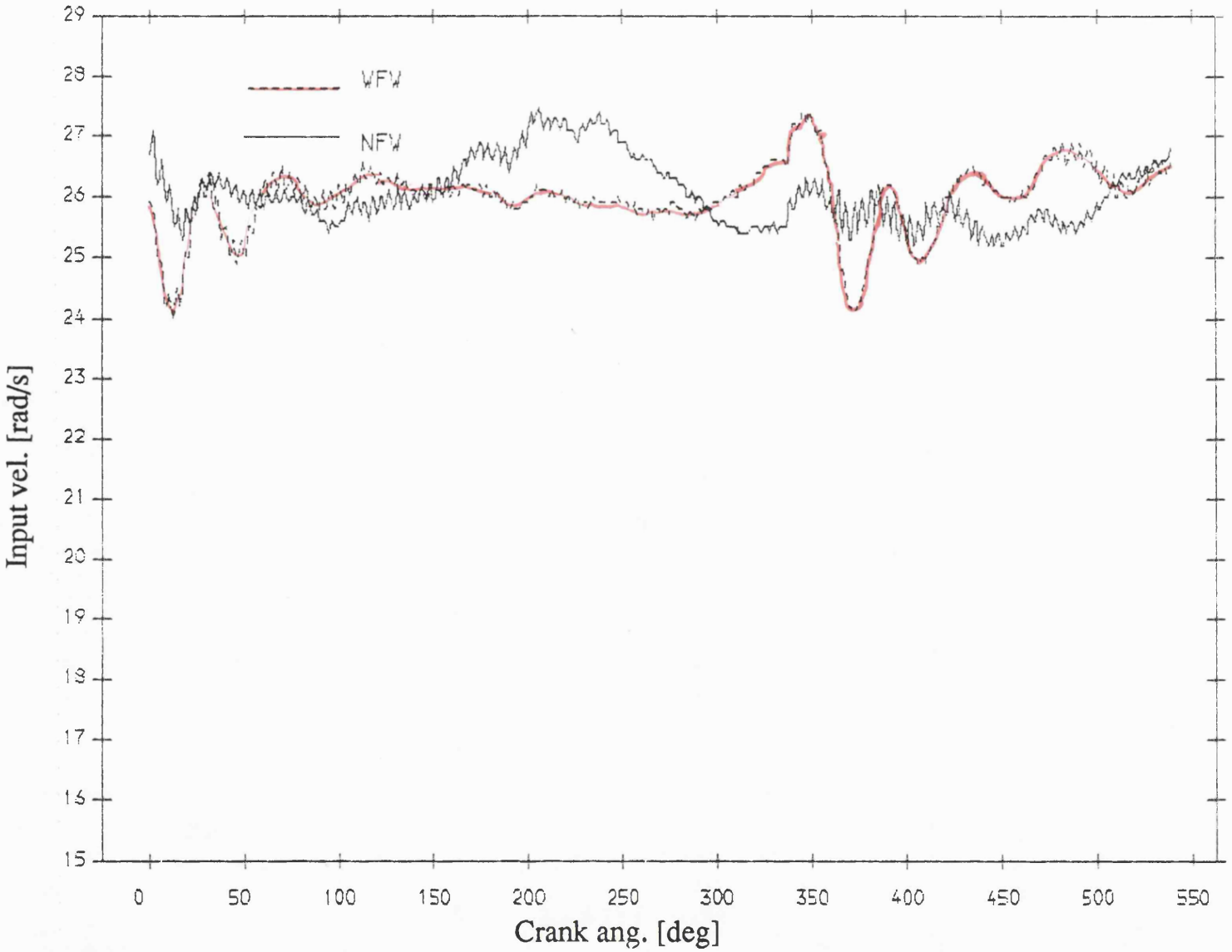

Fig 8.3.23 Exp. result input velocity , normal bearing
mean speed=244 rev/min; dia. clearance=.3mm

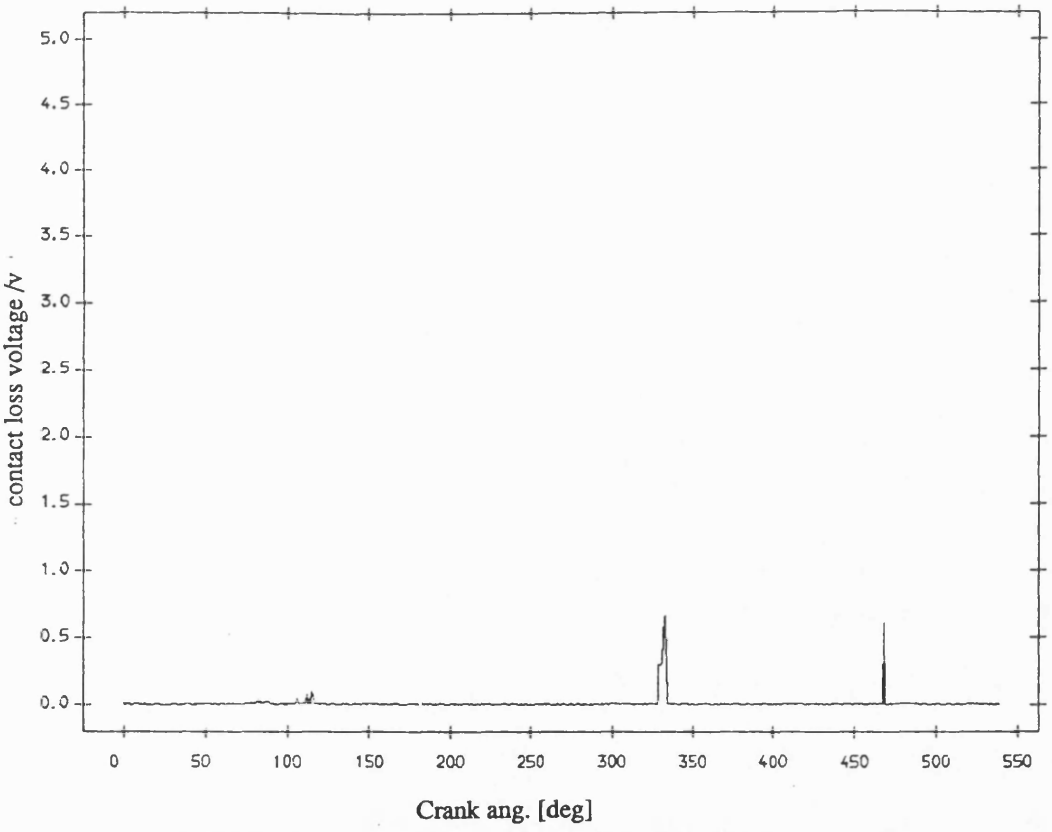

Fig 8.3.24 Exp. result contact loss of pin and normal bearing
with flywheel ;mean speed=244 rev/min ;dia. clearance=0.3mm

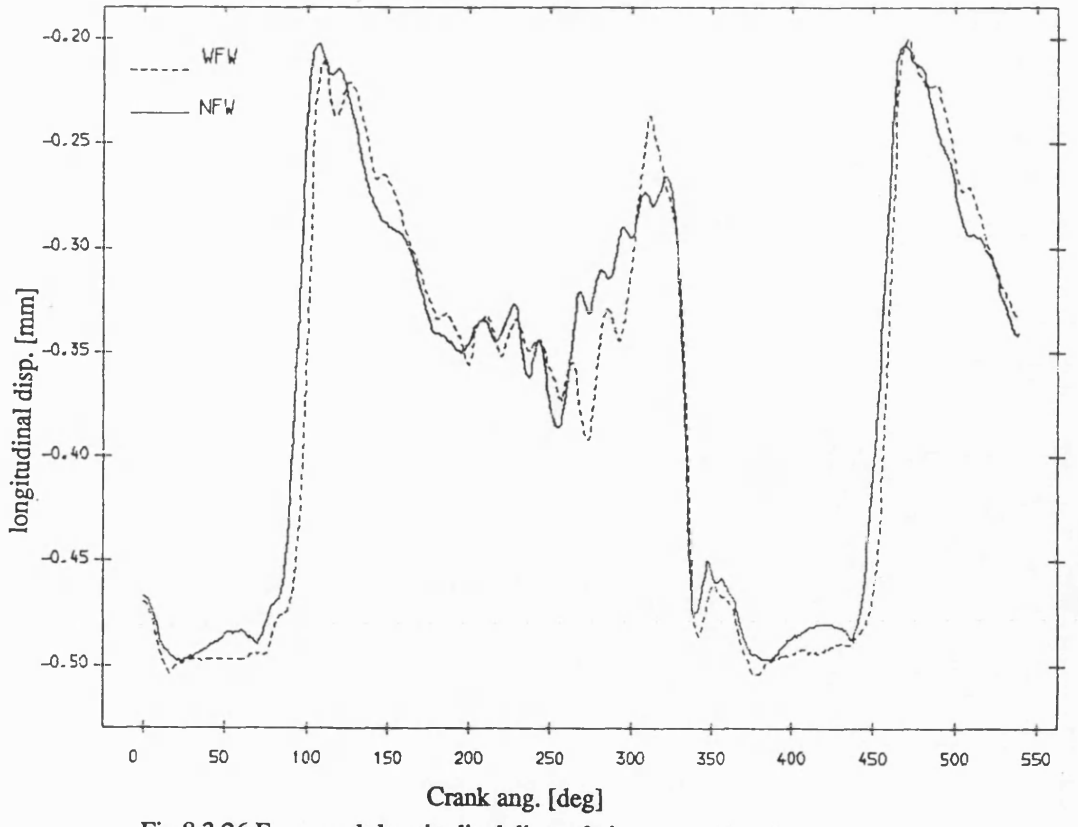

Fig 8.3.26 Exp. result longitudinal disp. of pin , normal bearing
mean speed=244 rev/min; dia. clearance=.3mm

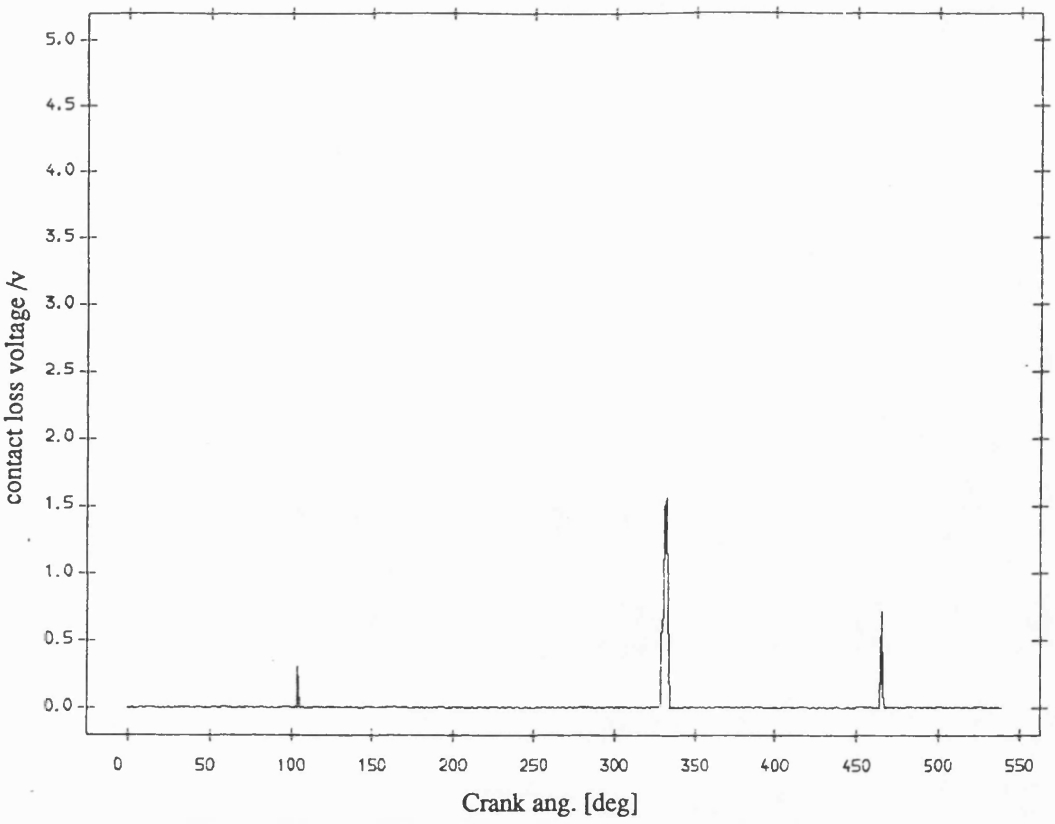

Fig 8.3.25 Exp. result contact loss of pin and normal bearing
no flywheel ;mean speed=244 rev/min ;dia. clearance=0.3mm

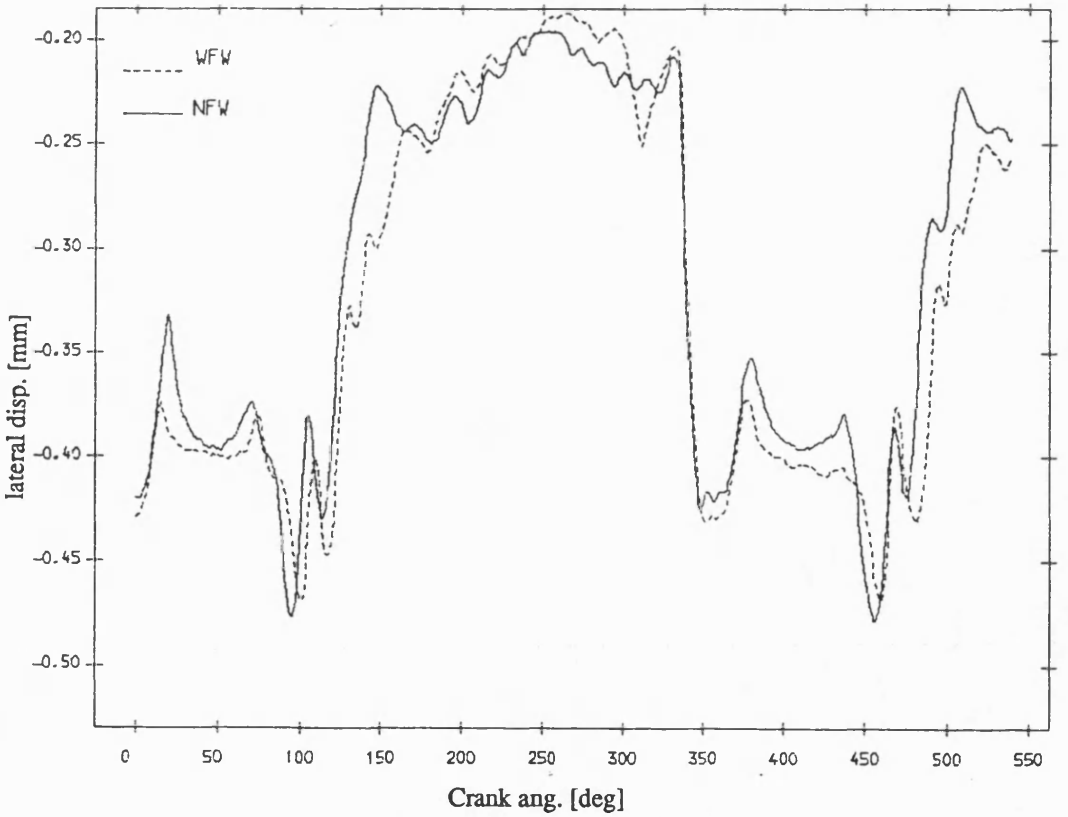

Fig 8.3.27 Exp. result lateral disp. of pin , normal bearing
mean speed=244 rev/min; dia. clearance=.3mm

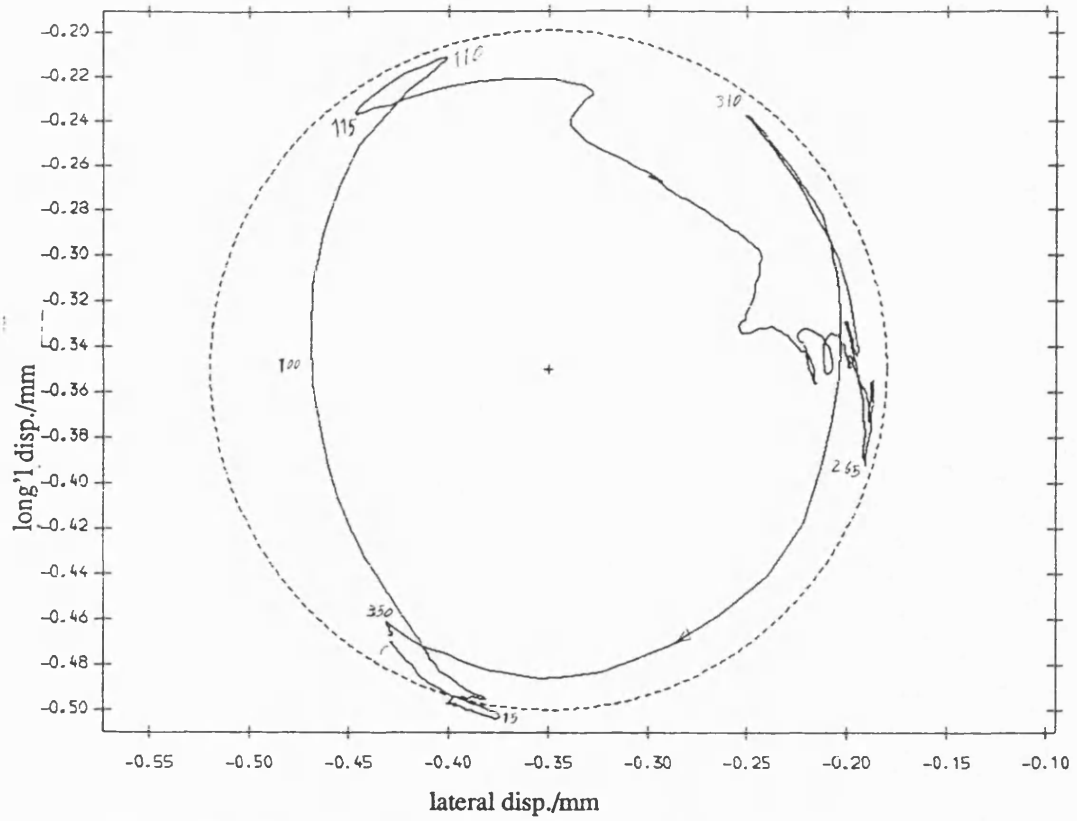

Fig 8.3.28 Exp. result polar plot of relative disp. of pin in normal bearing with fly wheel ;mean speed=244 rev/min ; dia. clearance=.3mm

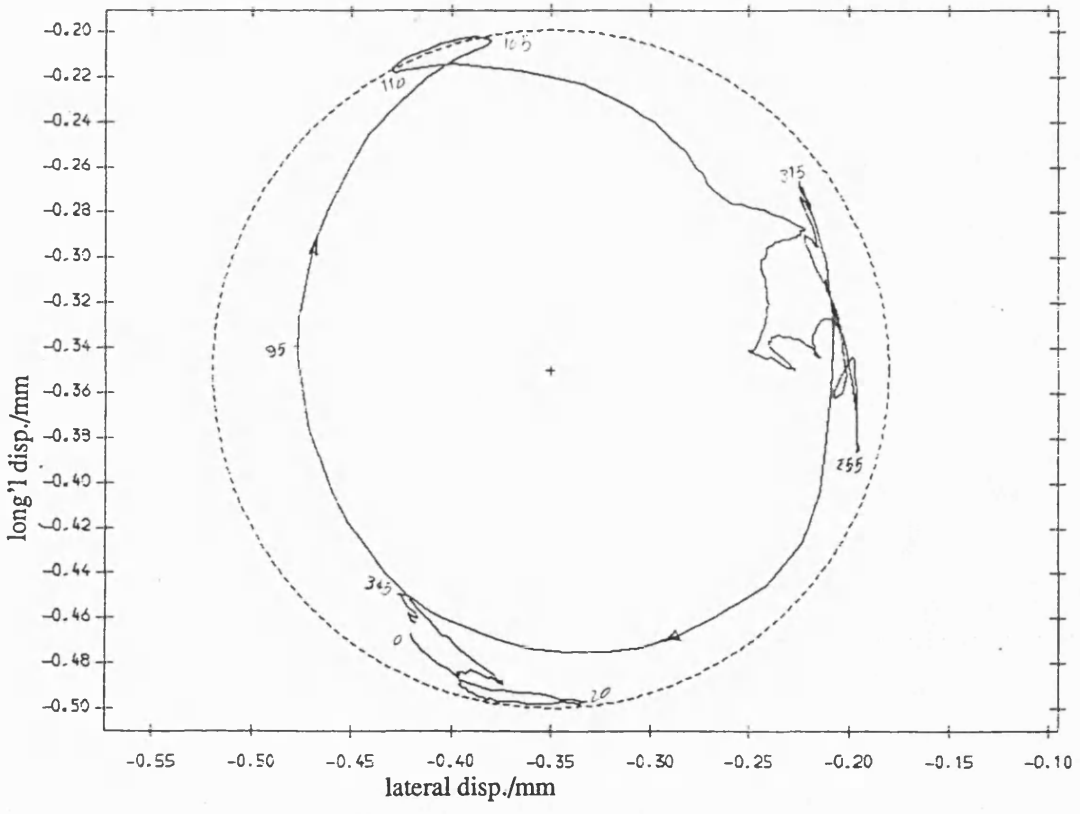

Fig 8.3.29 Exp. result polar plot of relative disp. of pin in normal bearing no fly wheel ;mean speed=244 rev/min ; dia. clearance=.3mm

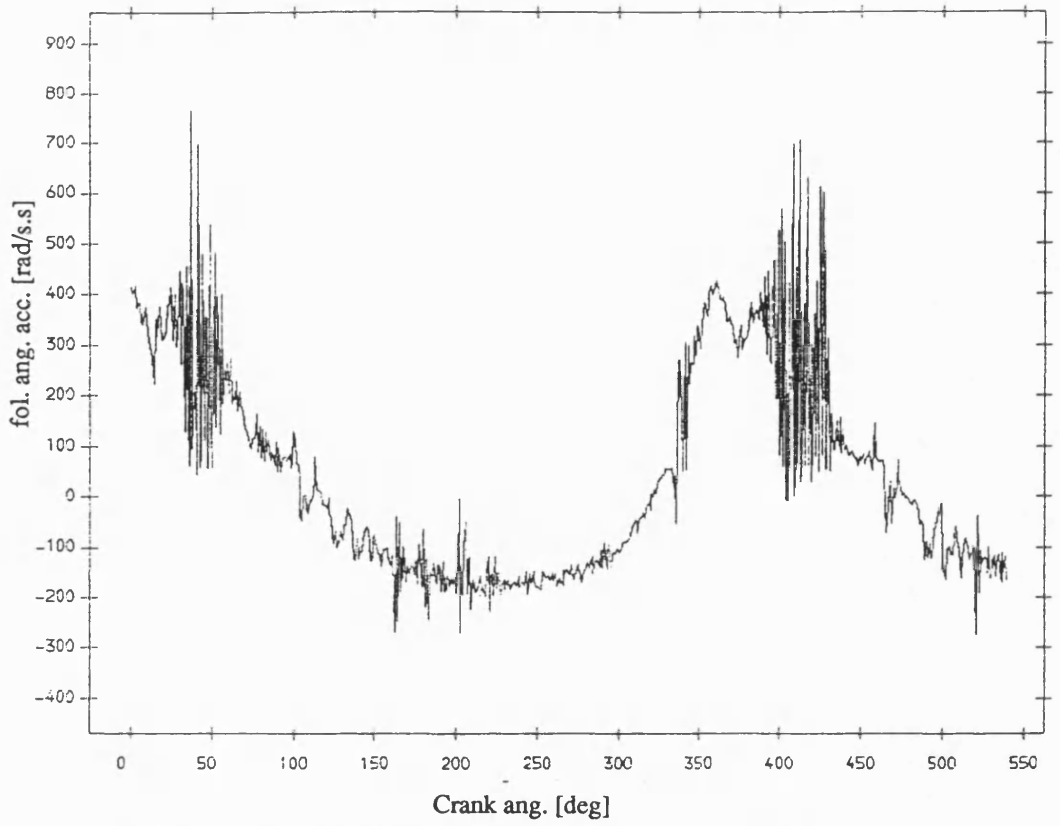

Fig 8.3.30 Exp. result follower ang. acceleration , normal bearing
with fly wheel ;mean speed=244 rev/min ; dia. clearance=.3mm

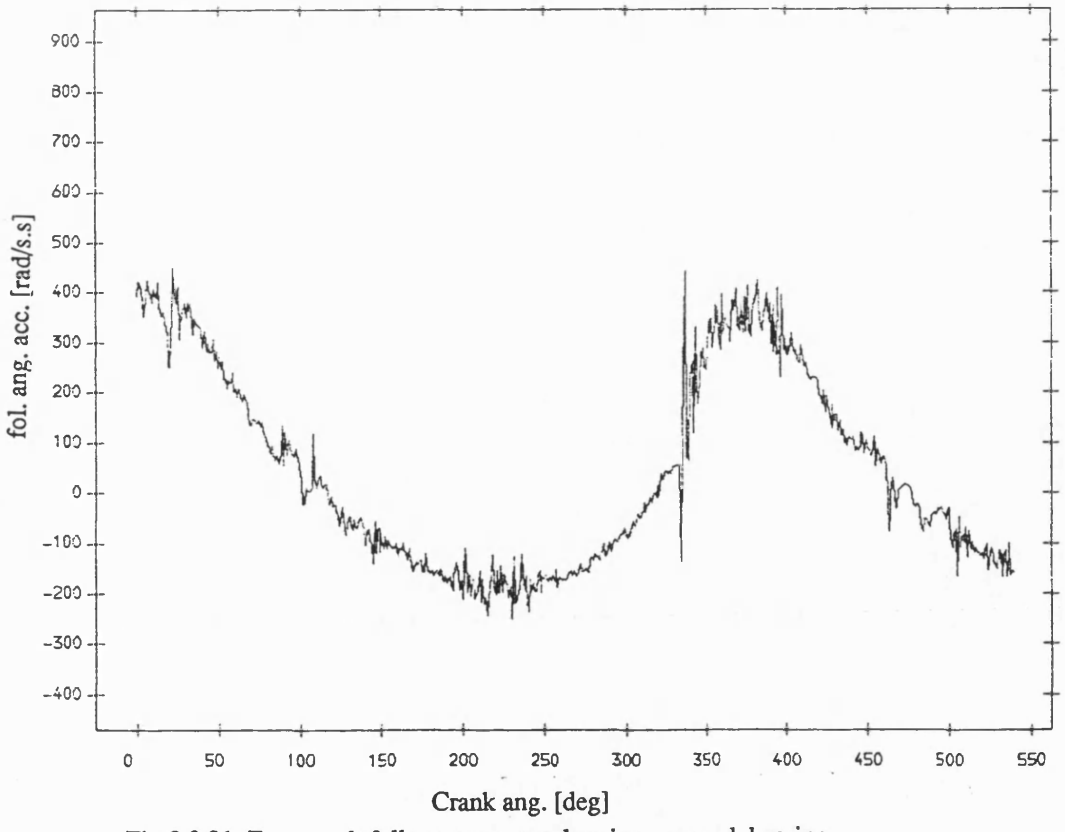

Fig 8.3.31 Exp. result follower ang. acceleration , normal bearing
no fly wheel ;mean speed=244 rev/min ; dia. clearance=.3mm

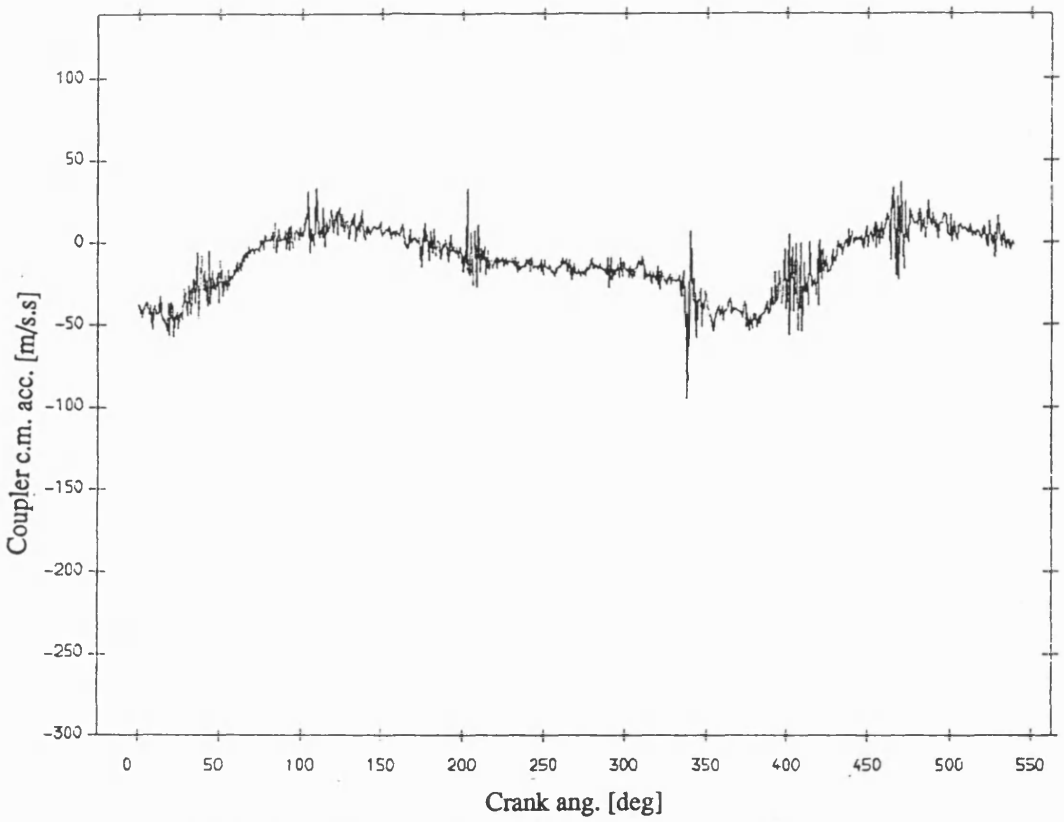

Fig 8.3.32 Exp. result coupler acceleration , normal bearing
with fly wheel ;mean speed=244 rev/min ; dia. clearance=.3mm

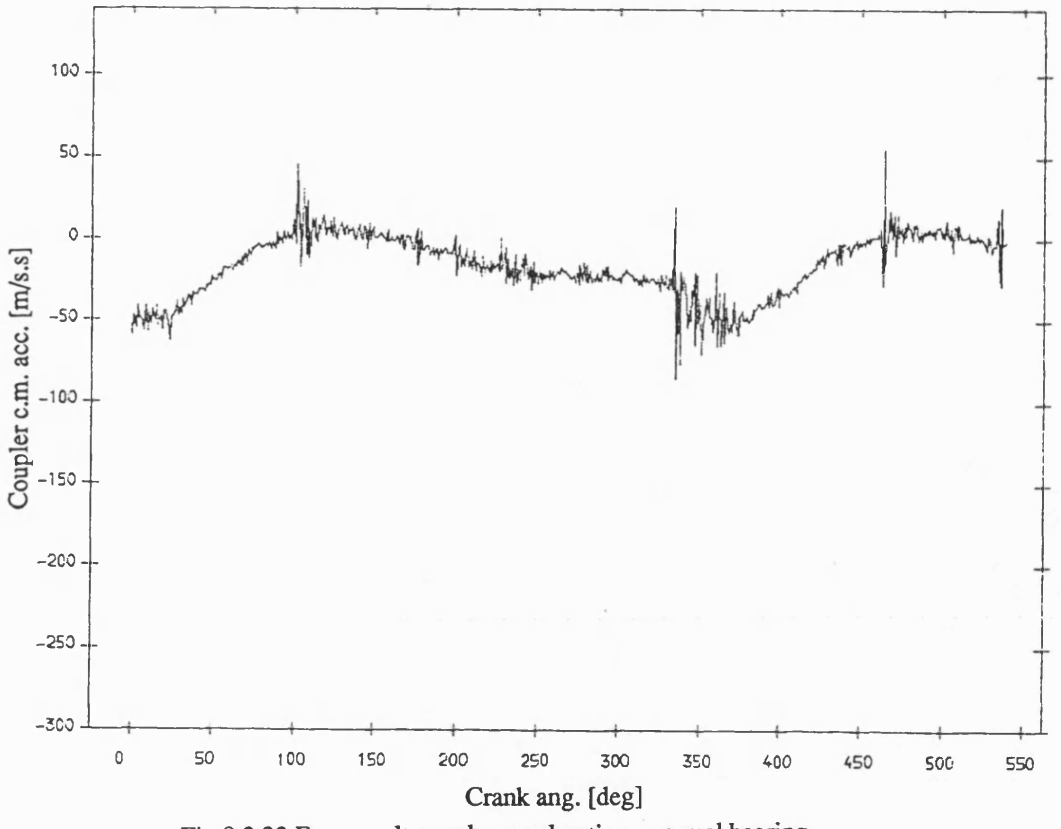

Fig 8.3.33 Exp. result coupler acceleration , normal bearing
no fly wheel ;mean speed=244 rev/min ; dia. clearance=.3mm

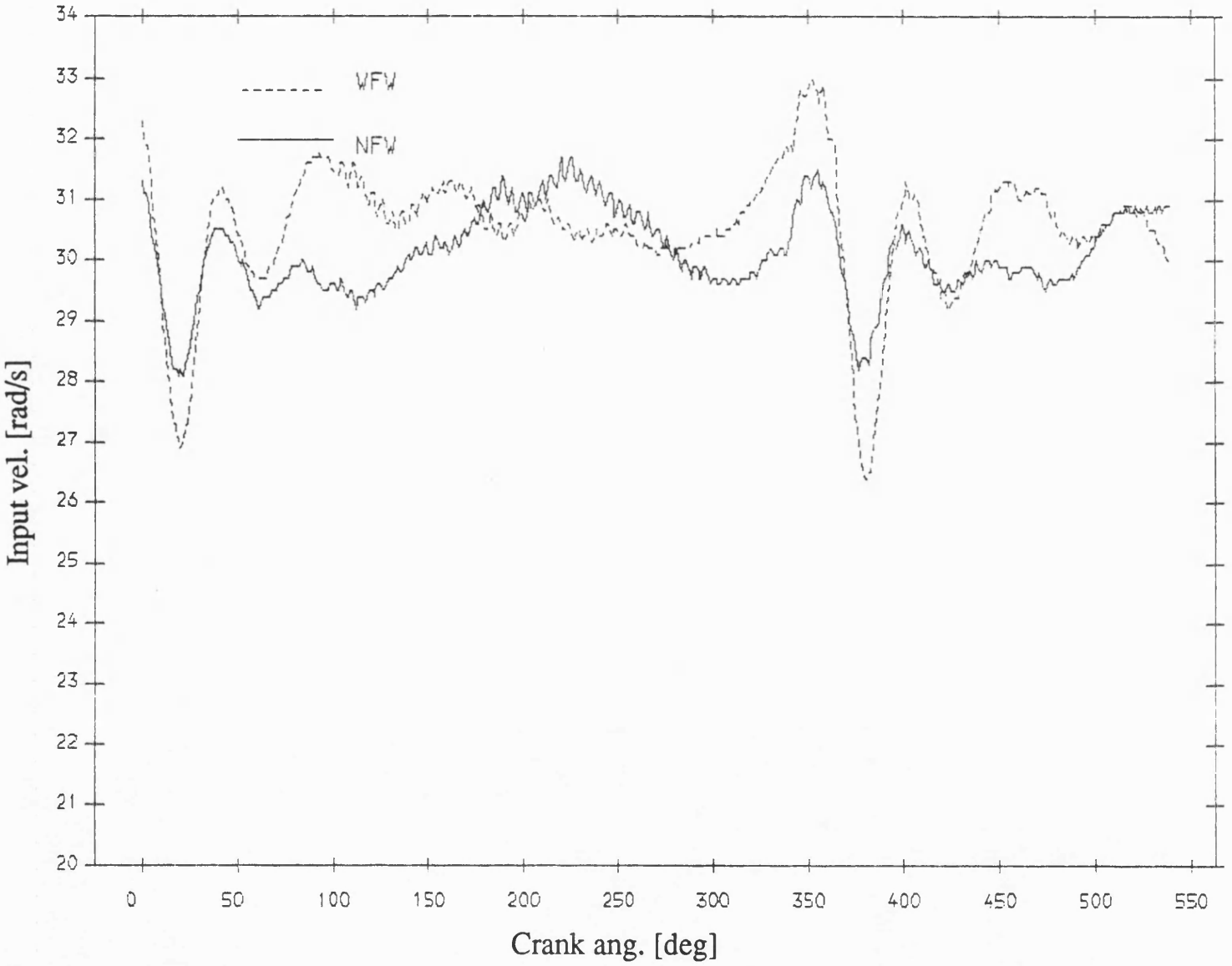

Fig 8.3.34 Exp. result input velocity , normal bearing
mean speed=290 rev/min; dia. clearance=.30mm

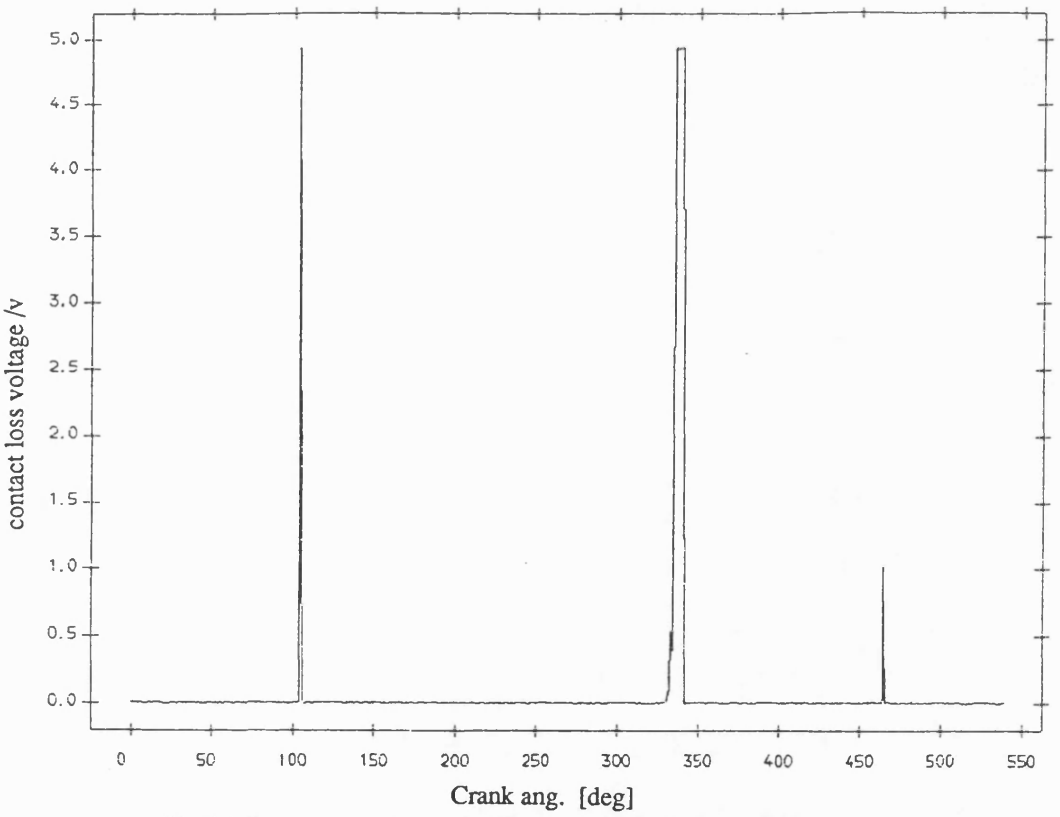

Fig 8.3.35 Exp. result contact loss of pin and normal bearing
with flywheel ;mean speed=290 rev/min ;dia. clearance=0.30mm

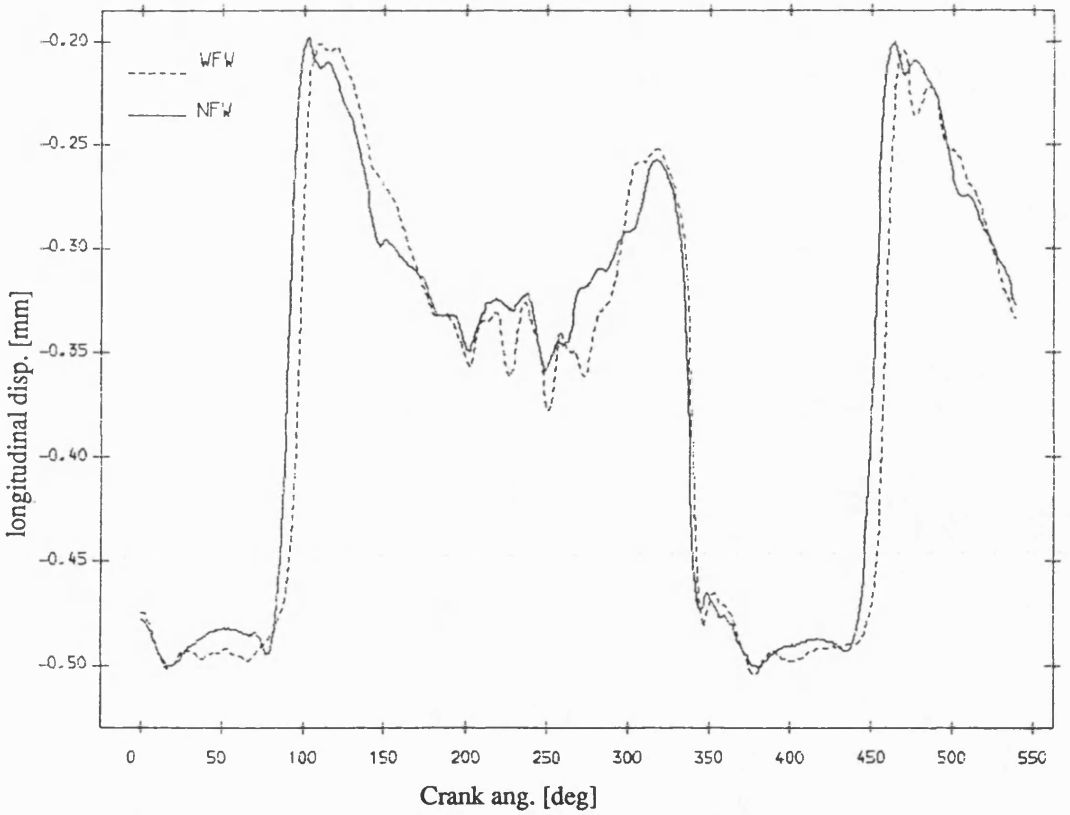

Fig 8.3.37 Exp. result longitudinal disp. of pin , normal bearing
mean speed=290 rev/min; dia. clearance=.30mm

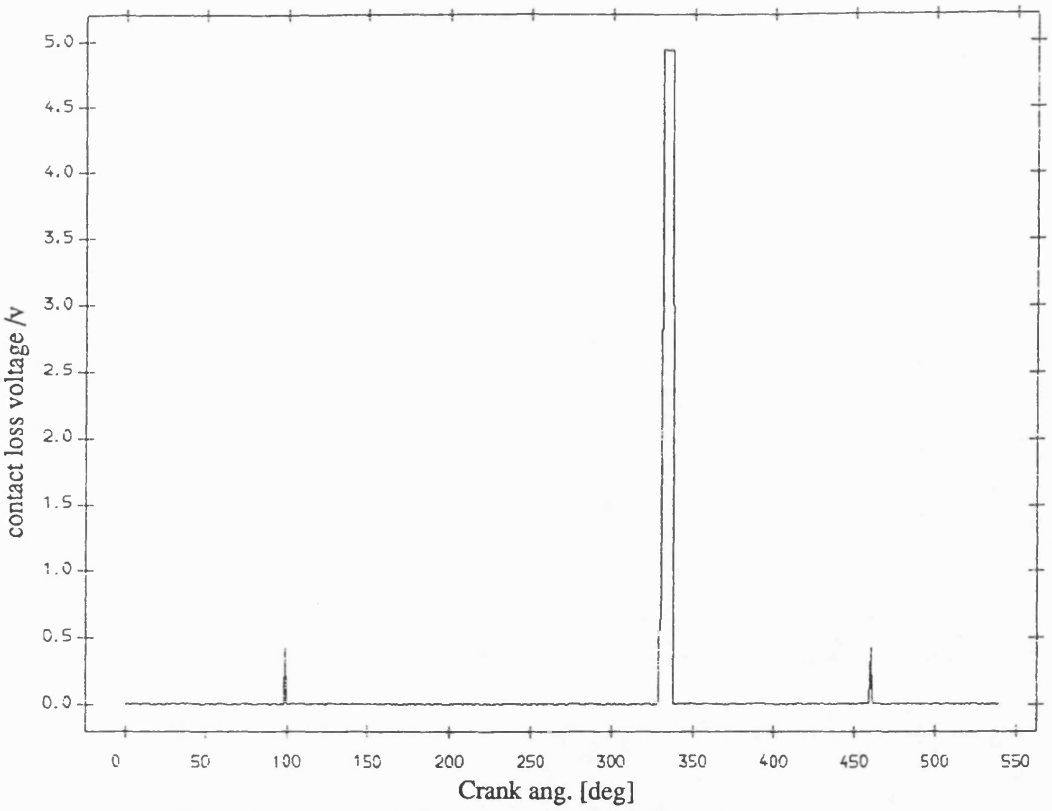

Fig 8.3.36 Exp. result contact loss of pin and normal bearing
no flywheel ;mean speed=290 rev/min ;dia. clearance=0.30mm

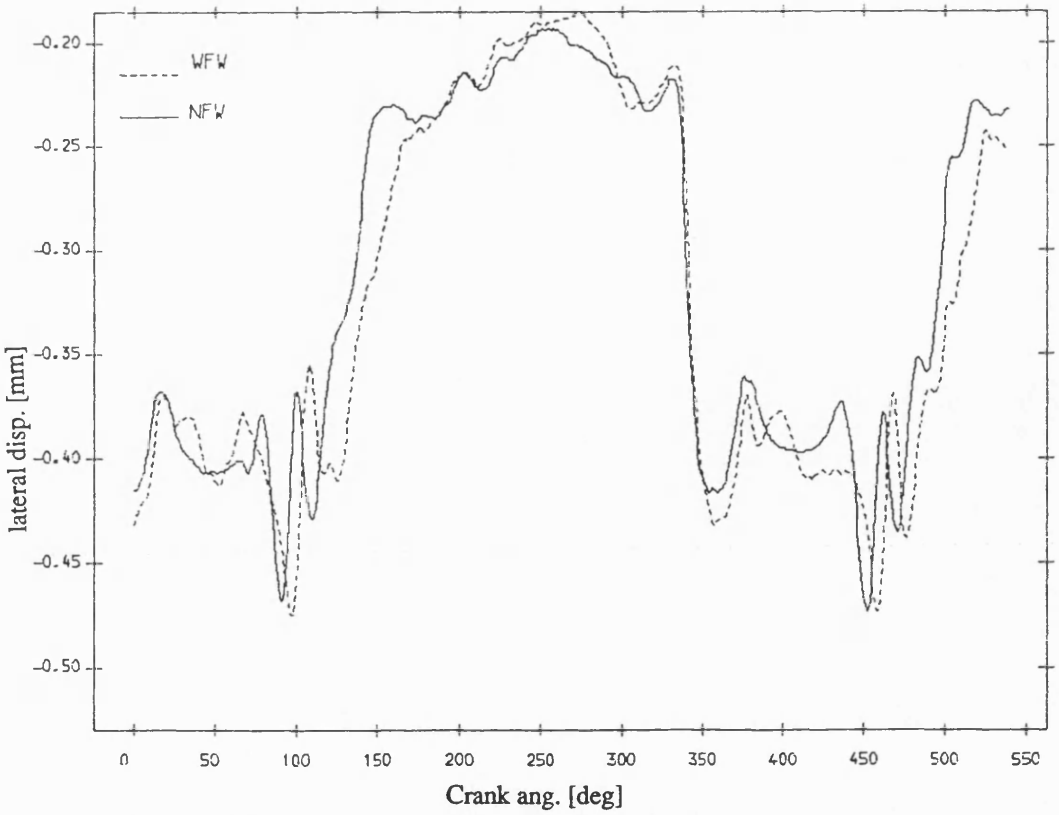

Fig 8.3.38 Exp. result lateral disp. of pin , normal bearing
mean speed=290 rev/min; dia. clearance=.30mm

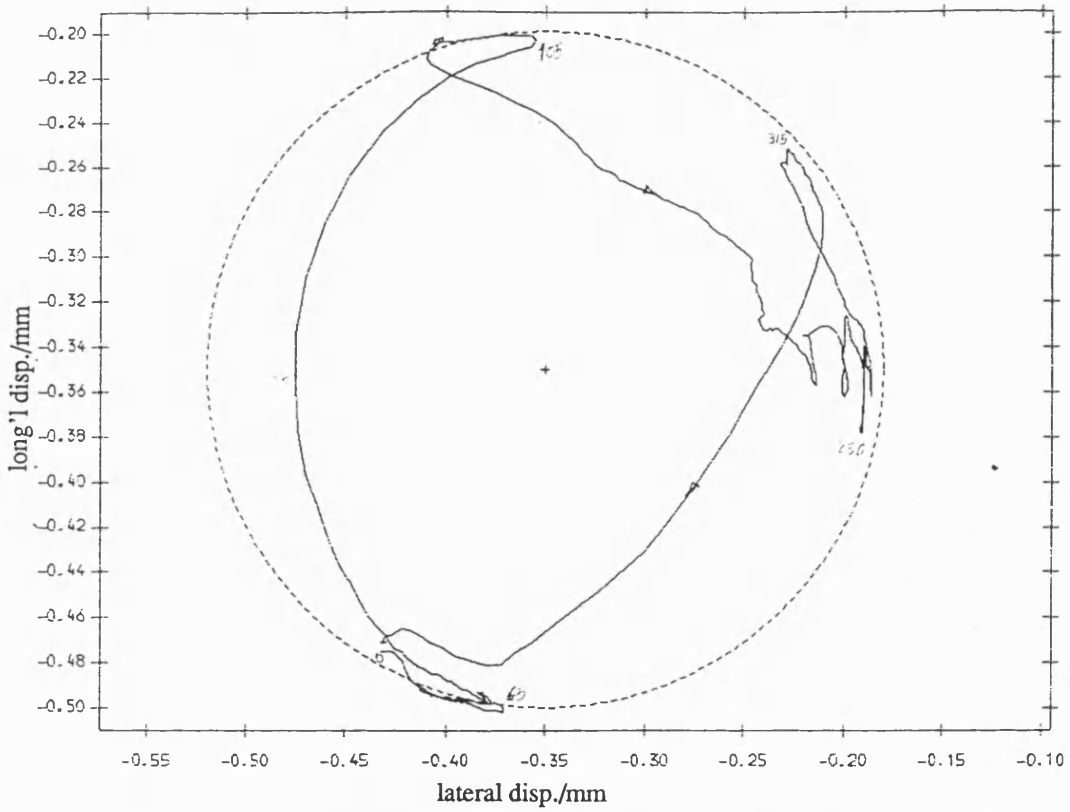

Fig 8.3.39 Exp. result polar plot of relative disp. of pin in normal bearing with fly wheel ;mean speed=290 rev/min ; dia. clearance=.30mm

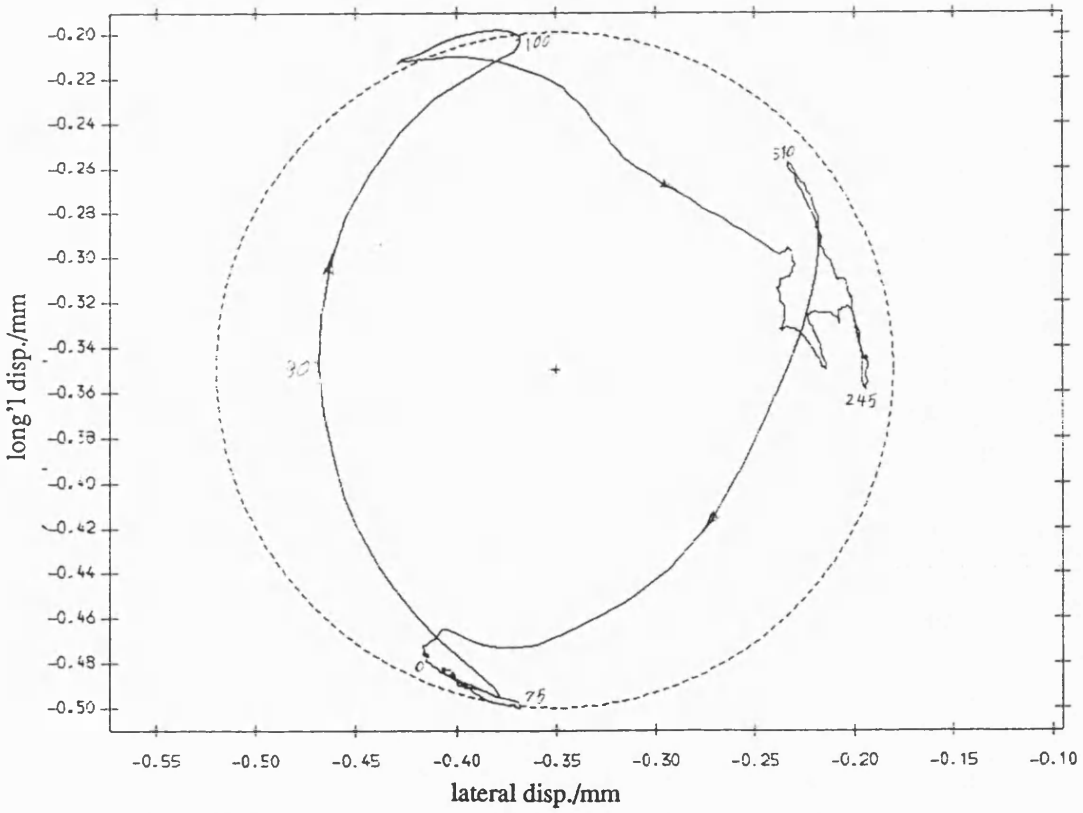

Fig 8.3.40 Exp. result polar plot of relative disp. of pin in normal bearing no fly wheel ;mean speed=290 rev/min ; dia. clearance=.30mm

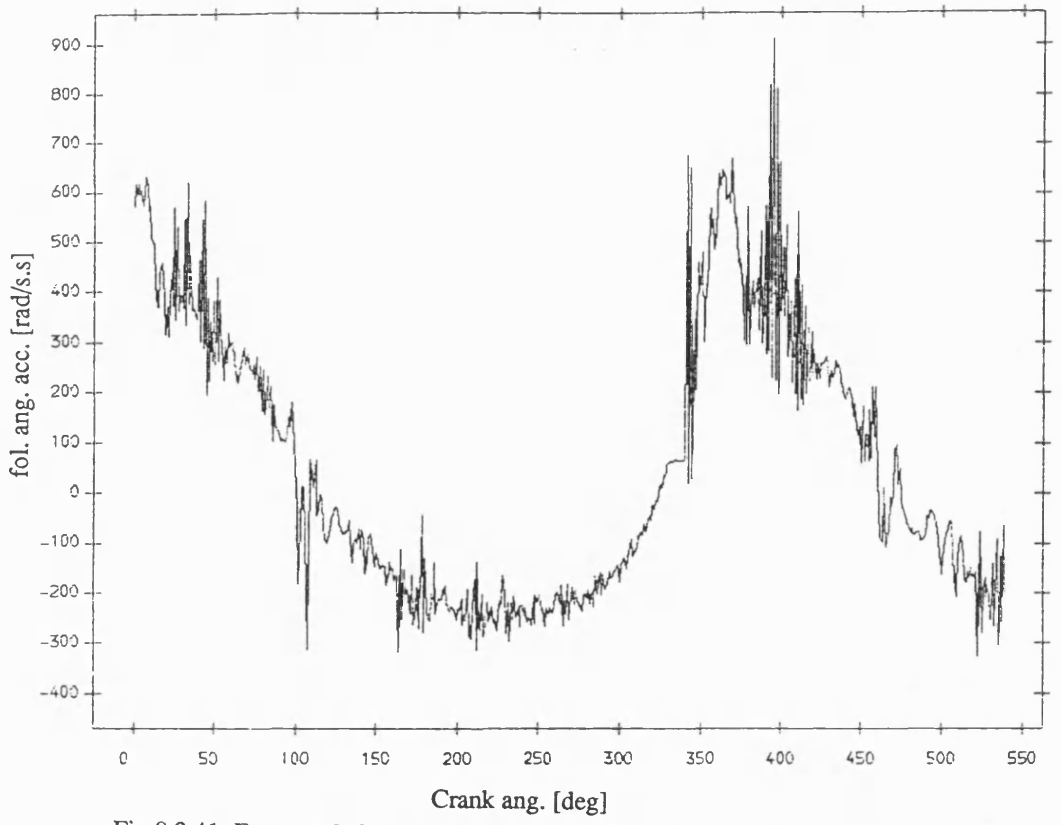

Fig 8.3.41 Exp. result follower ang. acceleration , normal bearing
with fly wheel ;mean speed=290 rev/min ; dia. clearance=.30mm

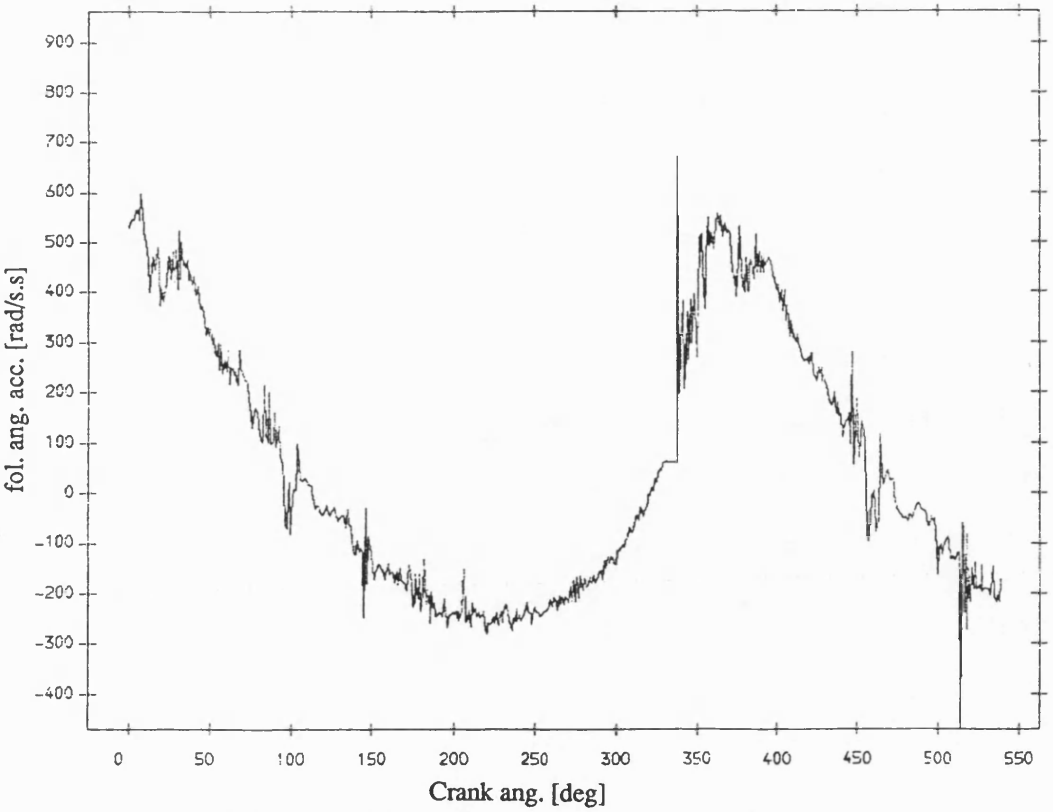

Fig 8.3.42 Exp. result follower ang. acceleration , normal bearing
no fly wheel ;mean speed=290 rev/min ; dia. clearance=.30mm

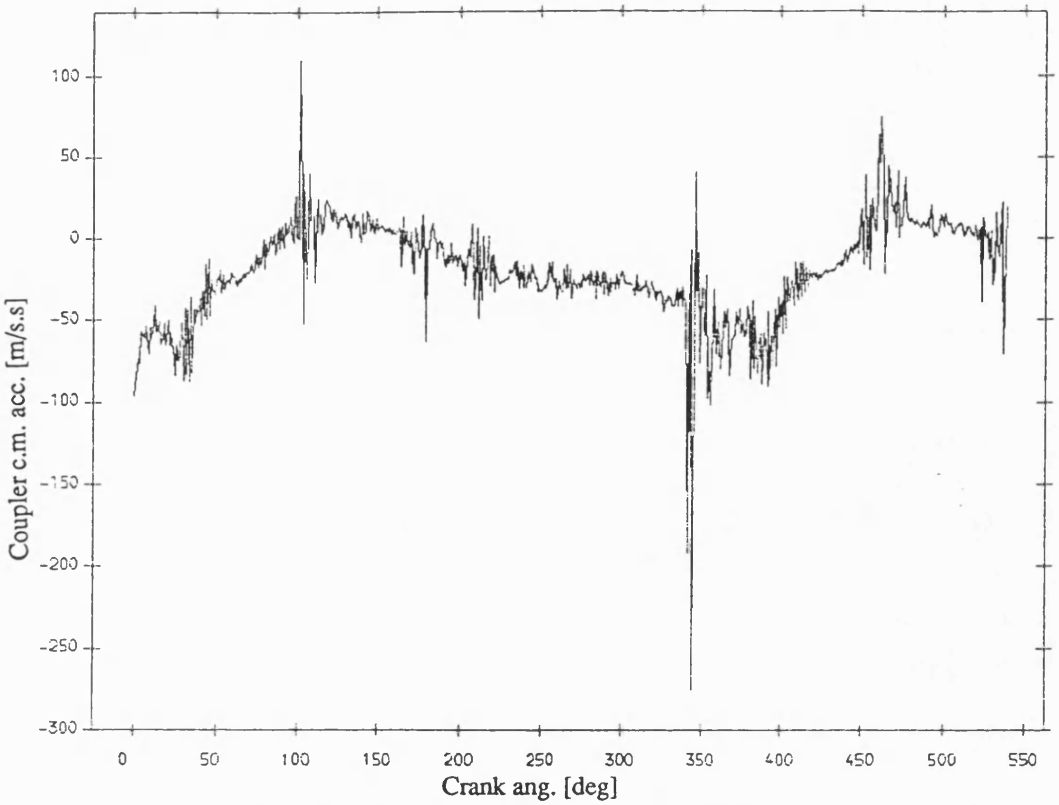

Fig 8.3.43 Exp. result coupler acceleration , normal bearing
with fly wheel ;mean speed=290 rev/min ; dia. clearance=.30mm

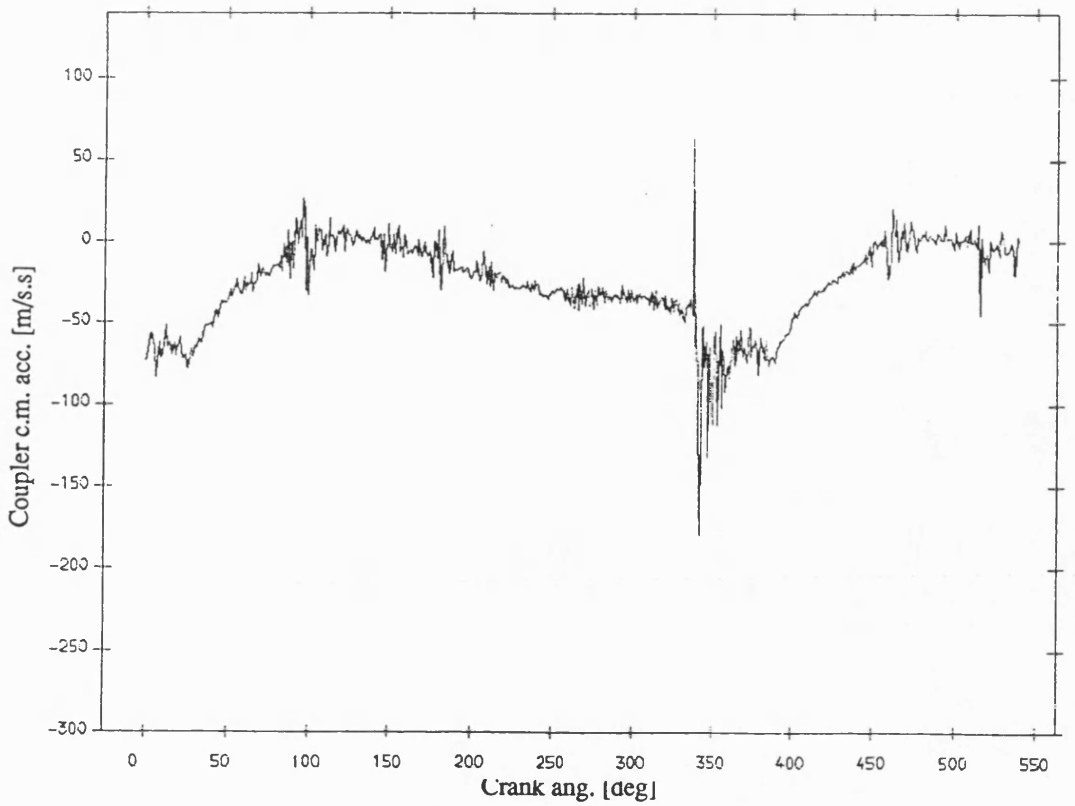

Fig 8.3.44 Exp. result coupler acceleration , normal bearing
no fly wheel ;mean speed=290 rev/min ; dia. clearance=.30mm

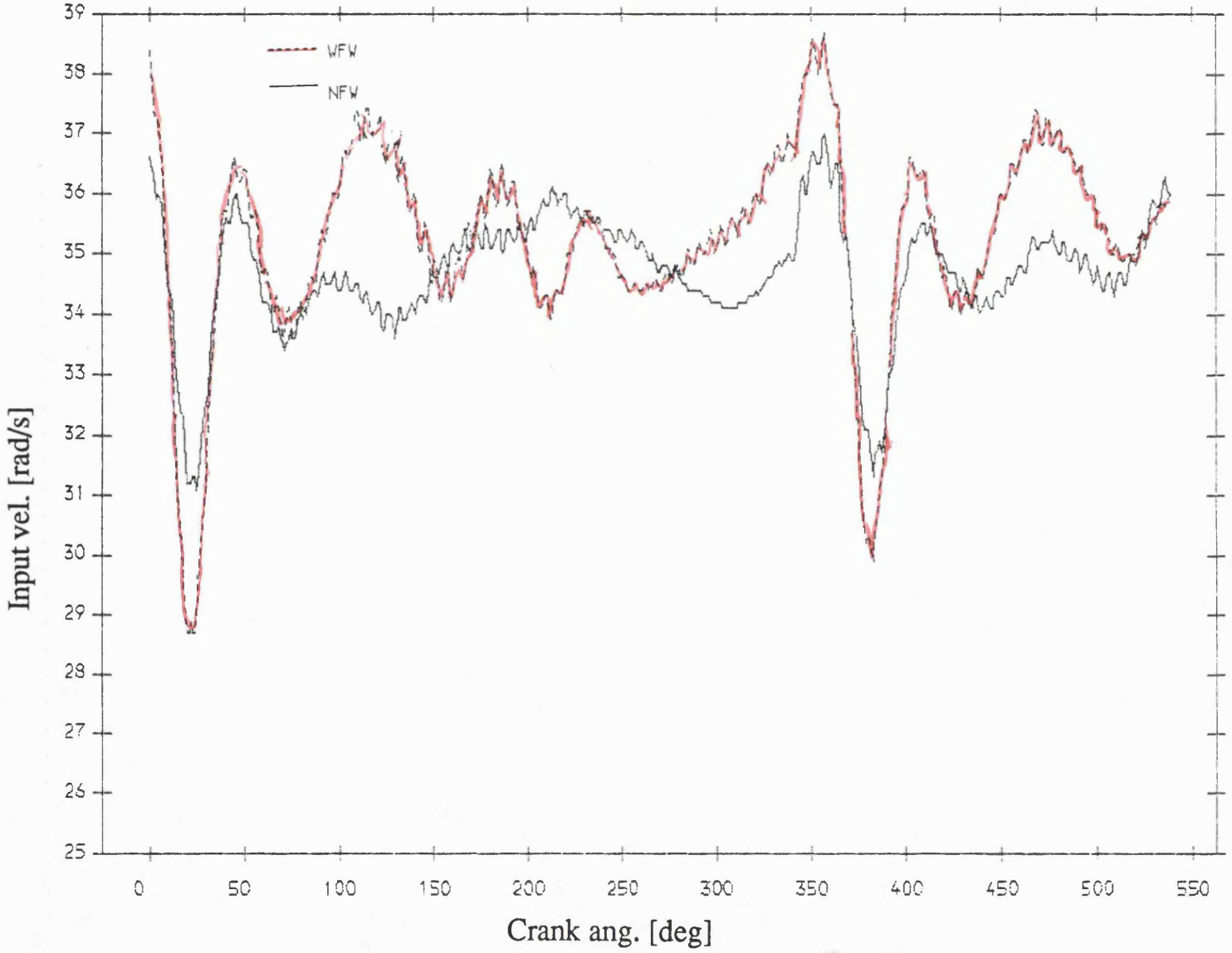

Fig 8.3.45 Exp. result input velocity , normal bearing
mean speed=327 rev/min; dia. clearance=.30mm

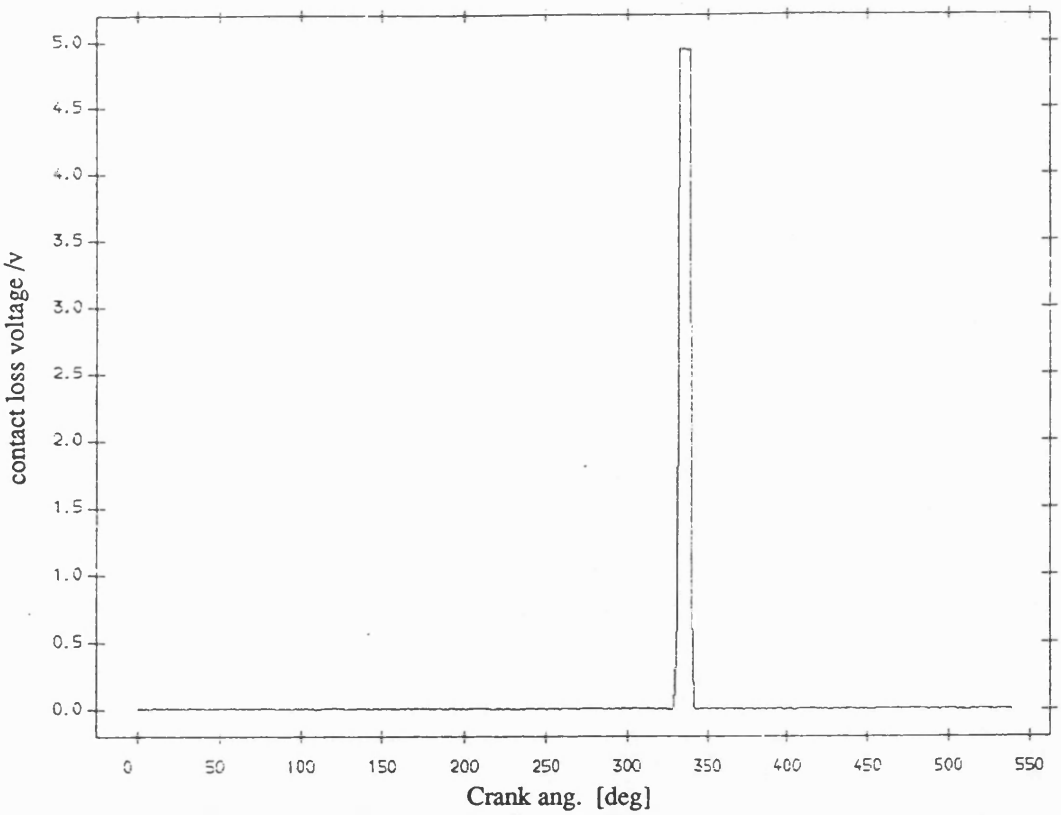

Fig 8.3.46 Exp. result contact loss of pin and normal bearing
with flywheel ;mean speed=327 rev/min ;dia. clearance=0.30mm

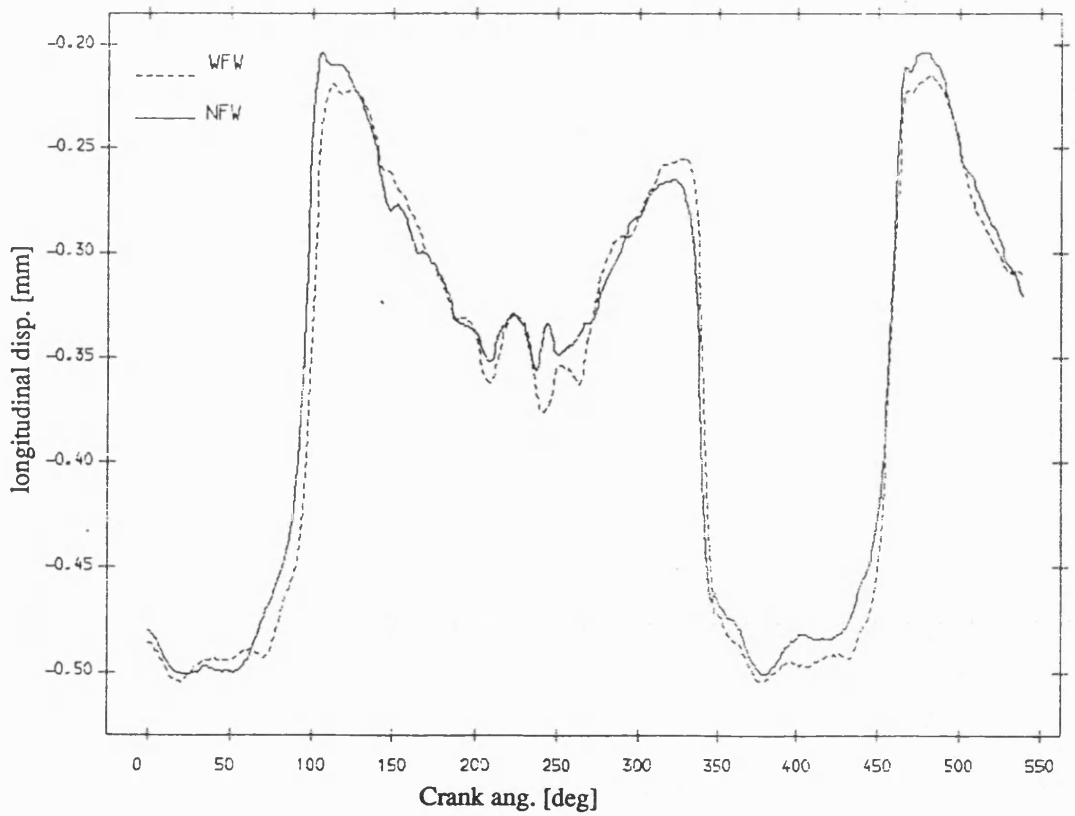

Fig 8.3.48 Exp. result longitudinal disp. of pin , normal bearing
mean speed=327 rev/min; dia. clearance=.30mm

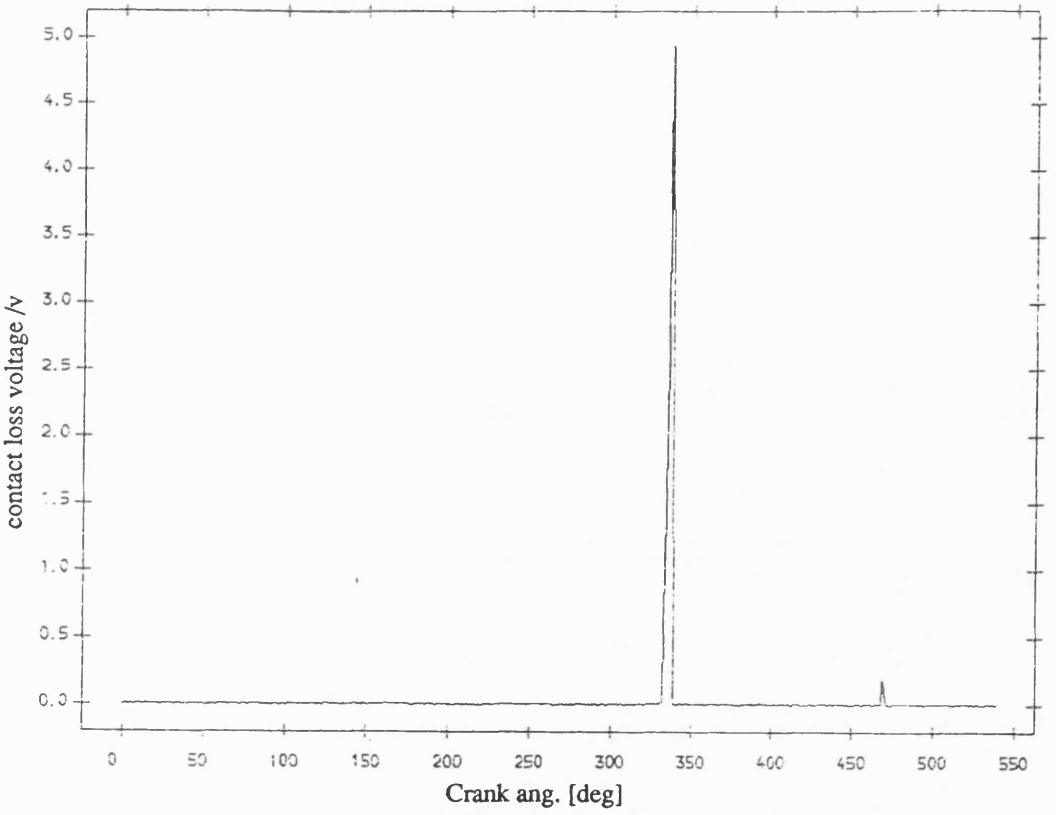

Fig 8.3.47 Exp. result contact loss of pin and normal bearing
no flywheel ;mean speed=327 rev/min ;dia. clearance=0.30mm

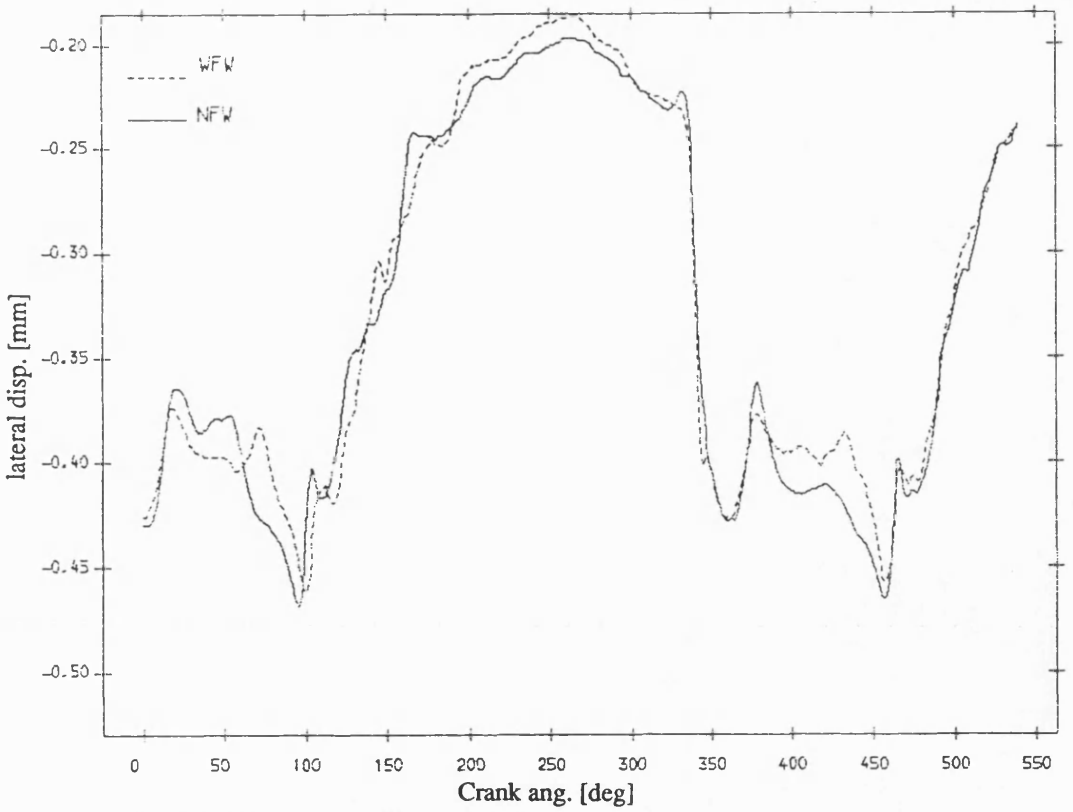

Fig 8.3.49 Exp. result lateral disp. of pin , normal bearing
mean speed=327 rev/min; dia. clearance=.30mm

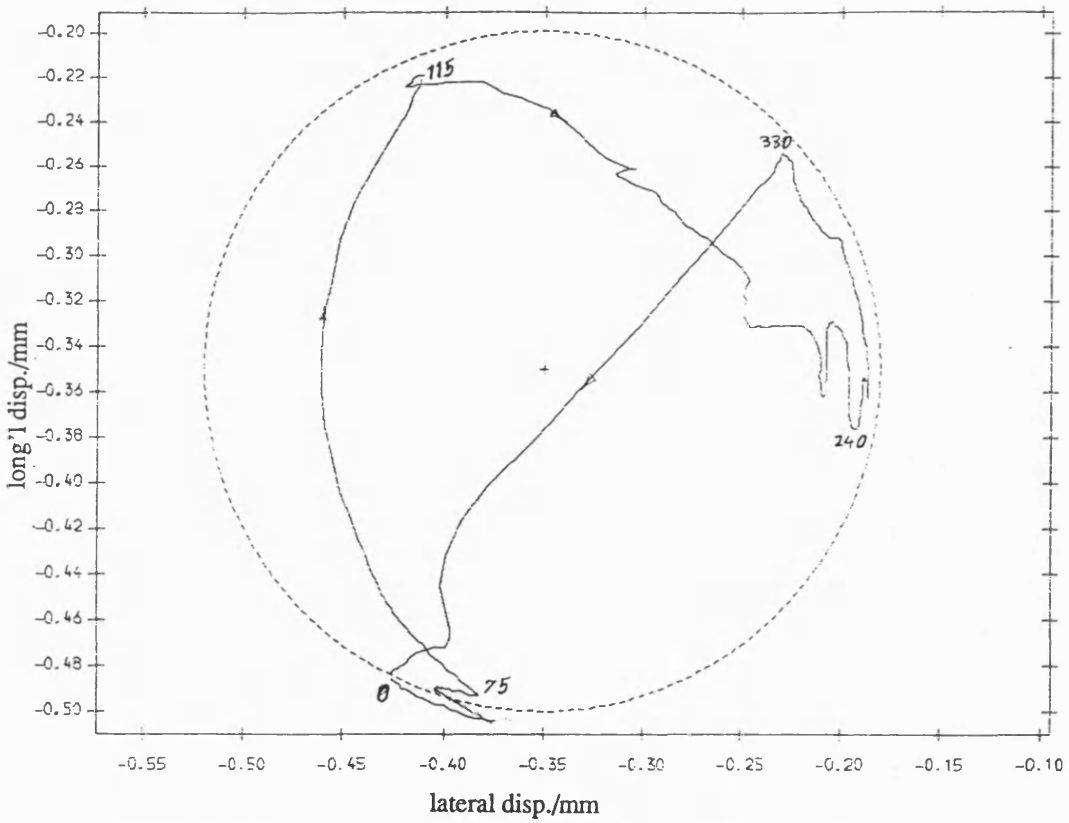

Fig 8.3.50 Exp. result polar plot of relative disp. of pin in normal bearing with fly wheel ;mean speed=327 rev/min ; dia. clearance=.30mm

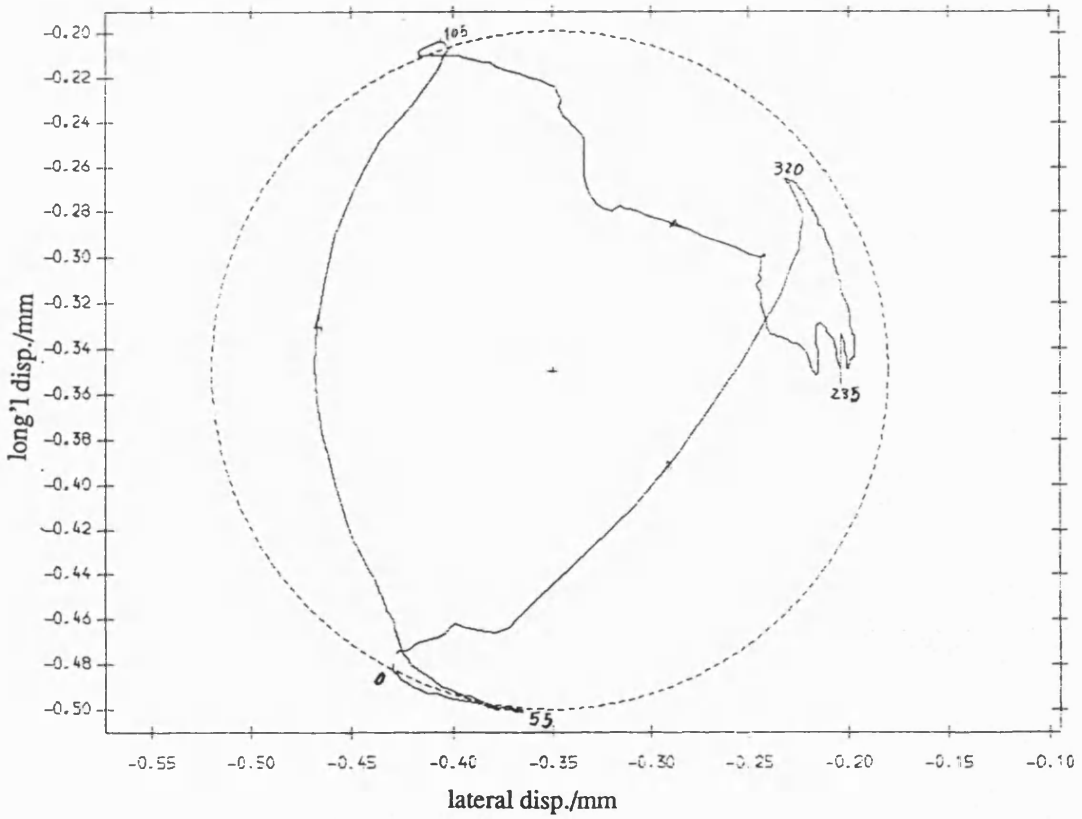

Fig 8.3.51 Exp. result polar plot of relative disp. of pin in normal bearing no fly wheel ;mean speed=327 rev/min ; dia. clearance=.30mm

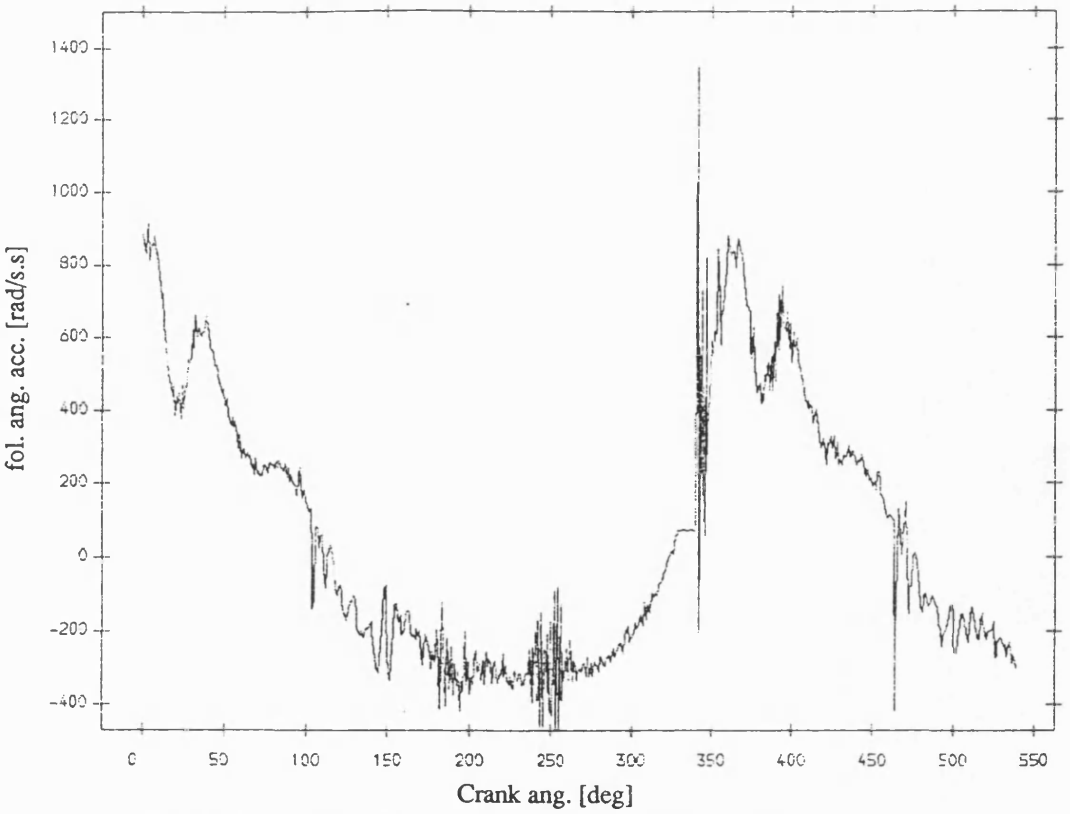

Fig 8.3.52 Exp. result follower ang. acceleration , normal bearing
with fly wheel ;mean speed=327 rev/min ; dia. clearance=.30mm

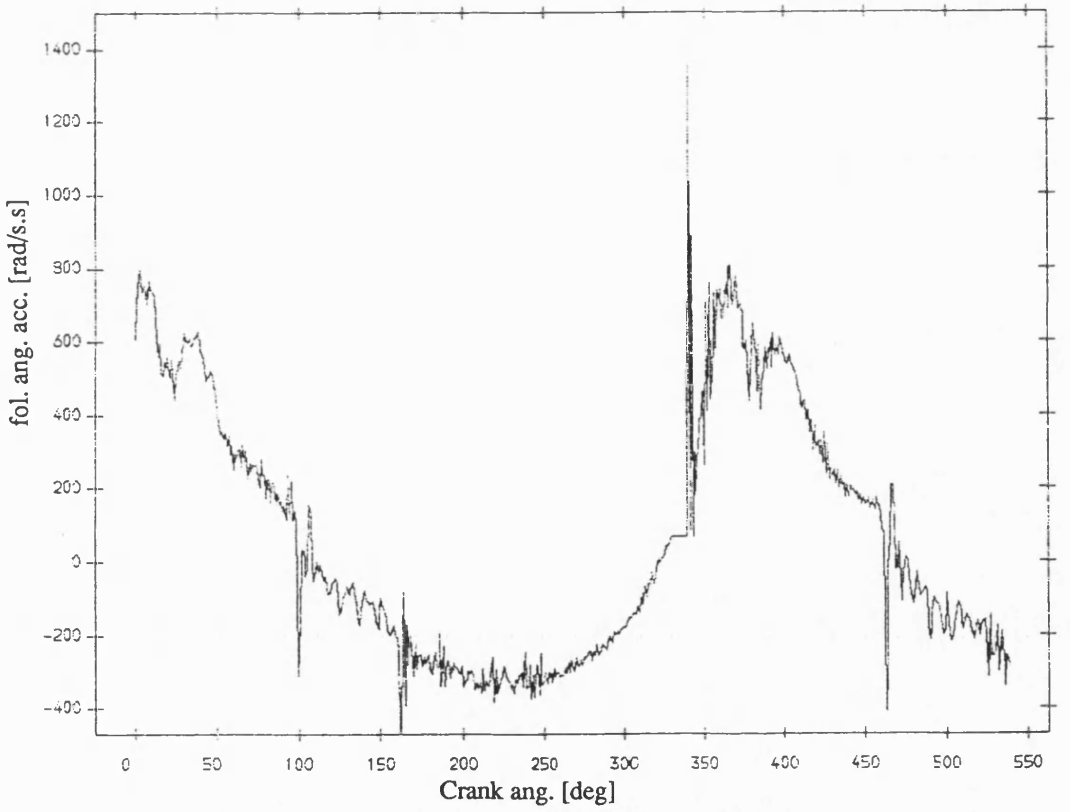

Fig 8.3.53 Exp. result follower ang. acceleration , normal bearing
no fly wheel ;mean speed=327 rev/min ; dia. clearance=.30mm

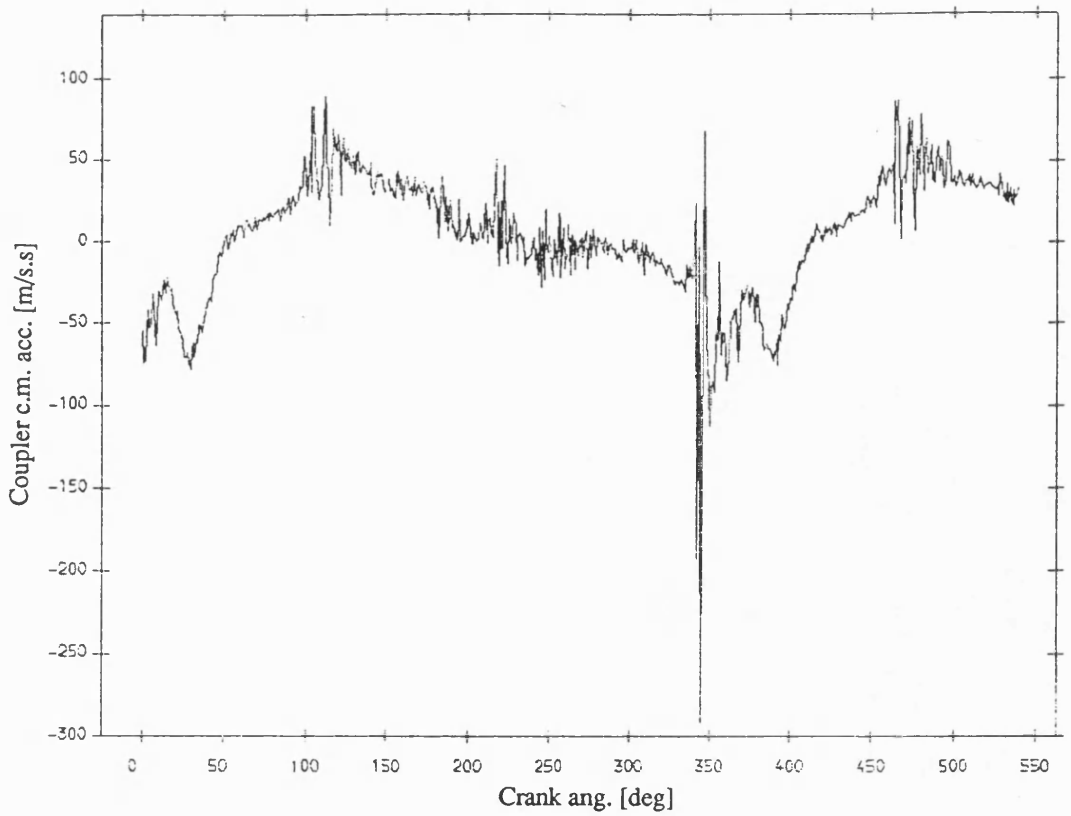

Fig 8.3.54 Exp. result coupler acceleration , normal bearing
with fly wheel ;mean speed=327 rev/min ; dia. clearance=.30mm

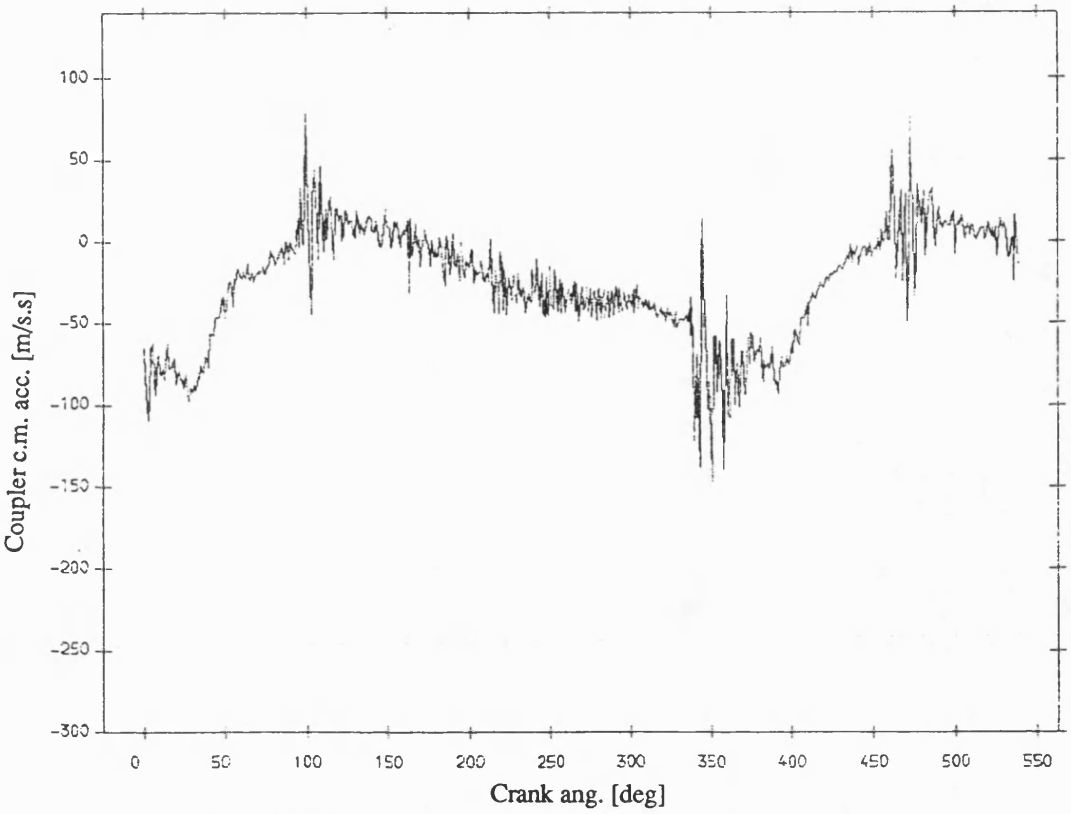

Fig 8.3.55 Exp. result coupler acceleration , normal bearing
no fly wheel ;mean speed=327 rev/min ; dia. clearance=.30mm

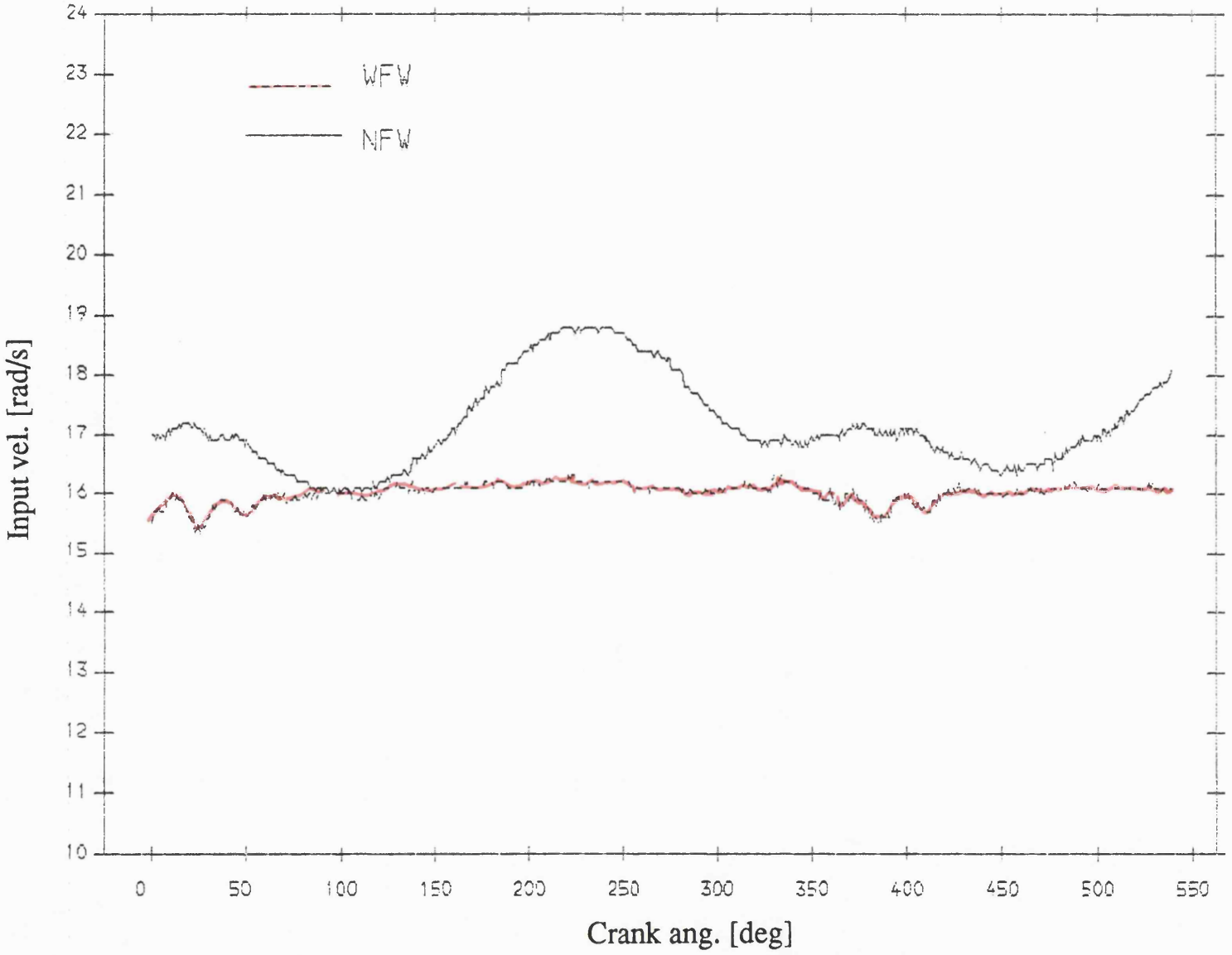

Fig 8.3.56 Exp. result input velocity , normal bearing
mean speed=168 rev/min; dia. clearance=.20mm

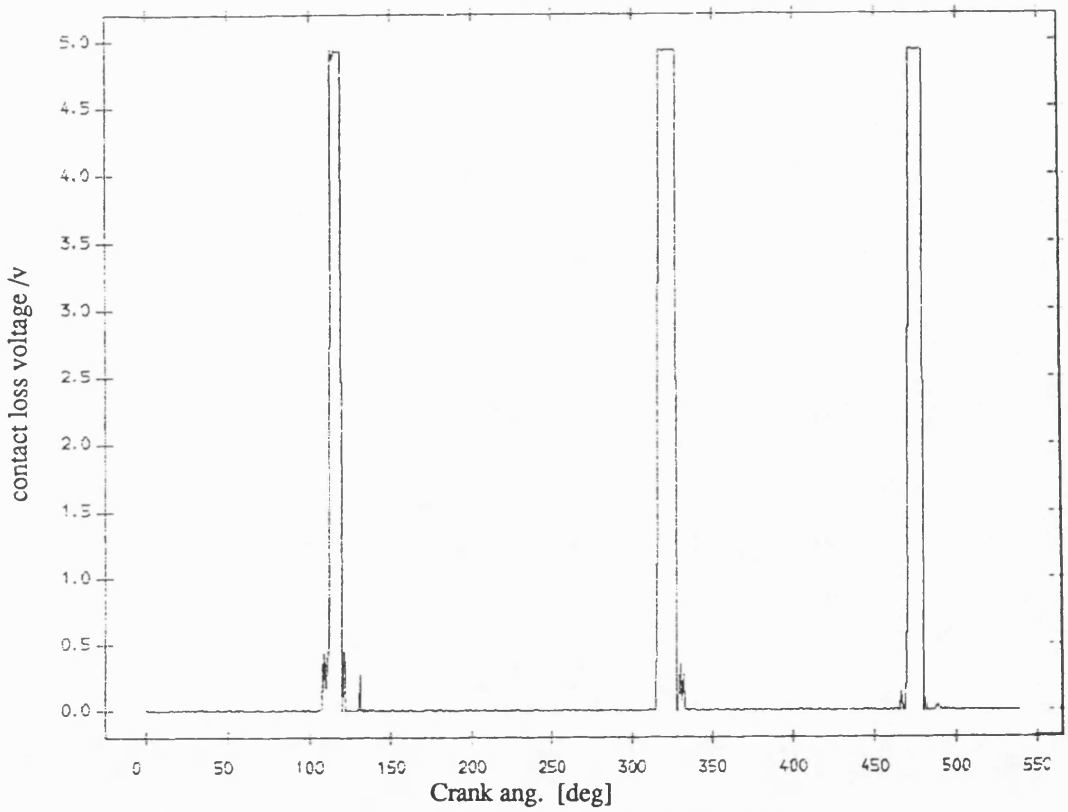

Fig 8.3.57 Exp. result contact loss of pin and normal bearing
with flywheel ;mean speed=168 rev/min ;dia. clearance=0.20mm

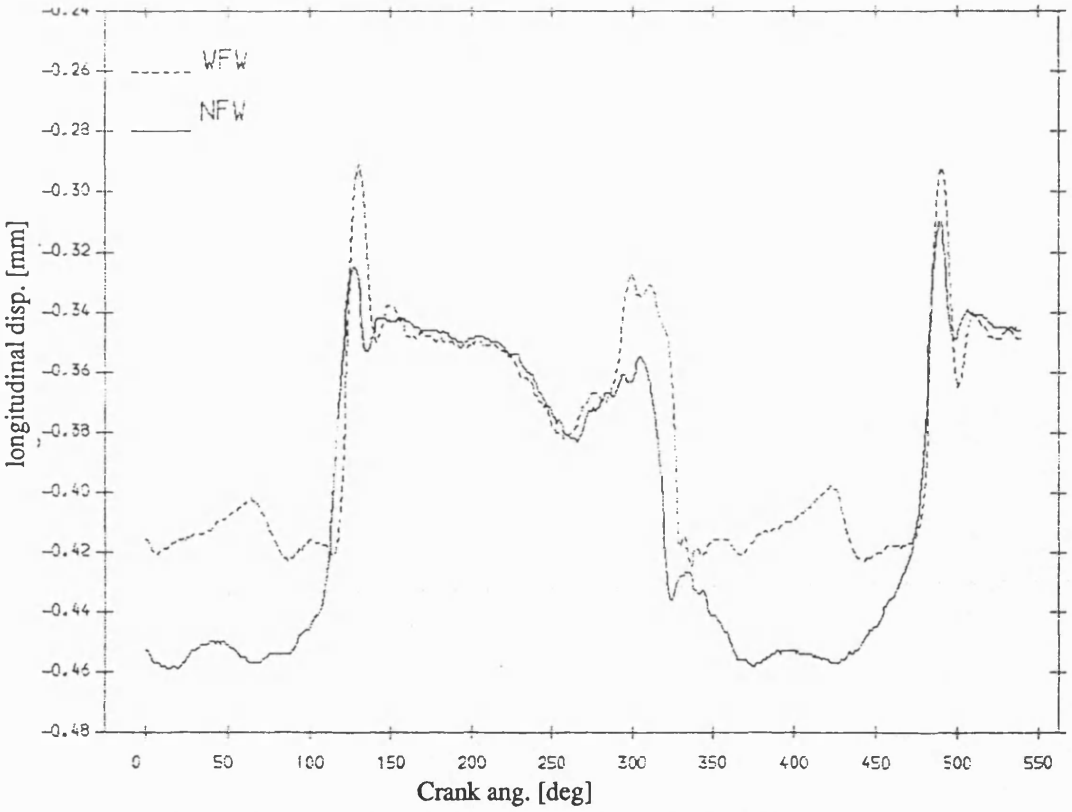

Fig 8.3.59 Exp. result longitudinal disp. of pin , normal bearing
mean speed=168 rev/min; dia. clearance=.20mm

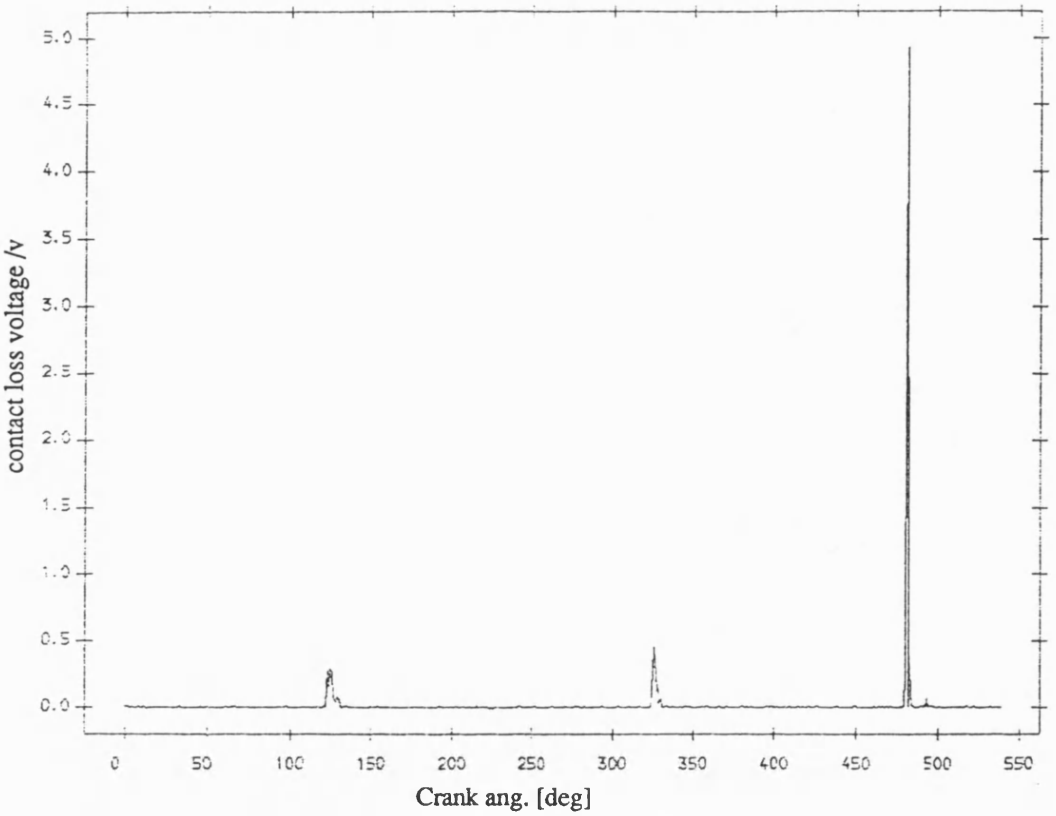

Fig 8.3.58 Exp. result contact loss of pin and normal bearing
no flywheel ;mean speed=168 rev/min ;dia. clearance=0.20mm

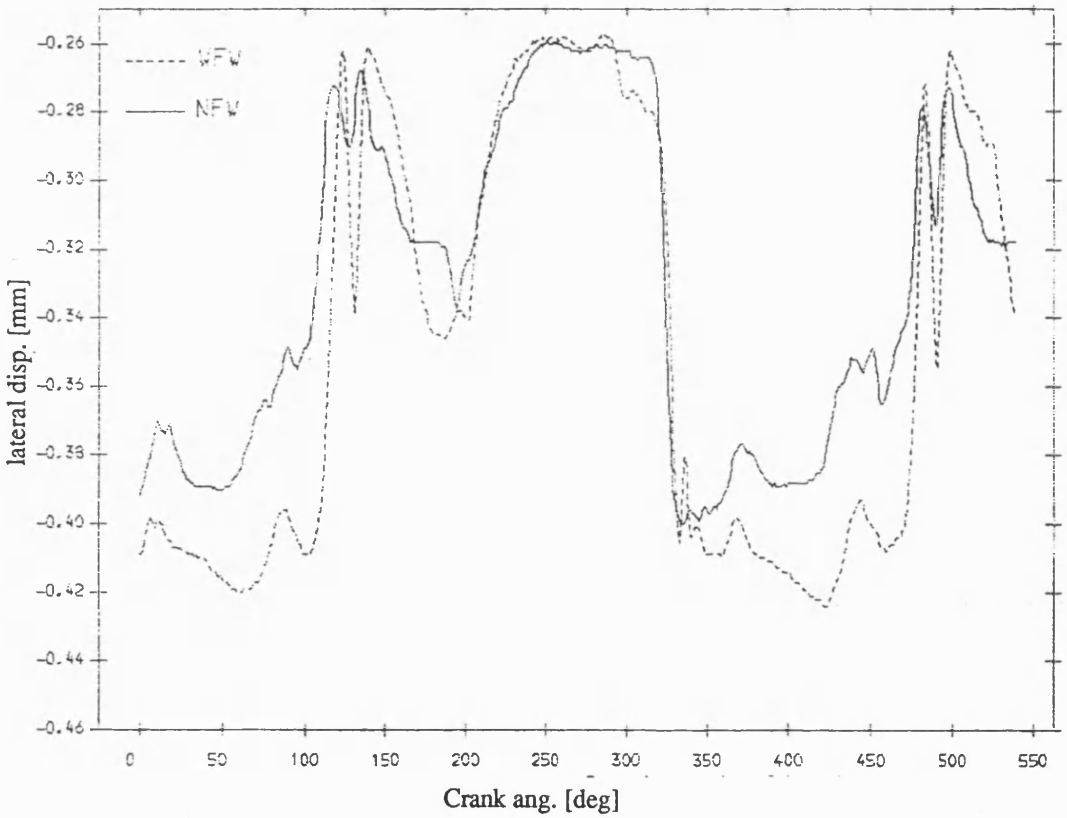

Fig 8.3.60 Exp. result lateral disp. of pin , normal bearing
mean speed=168 rev/min; dia. clearance=.20mm

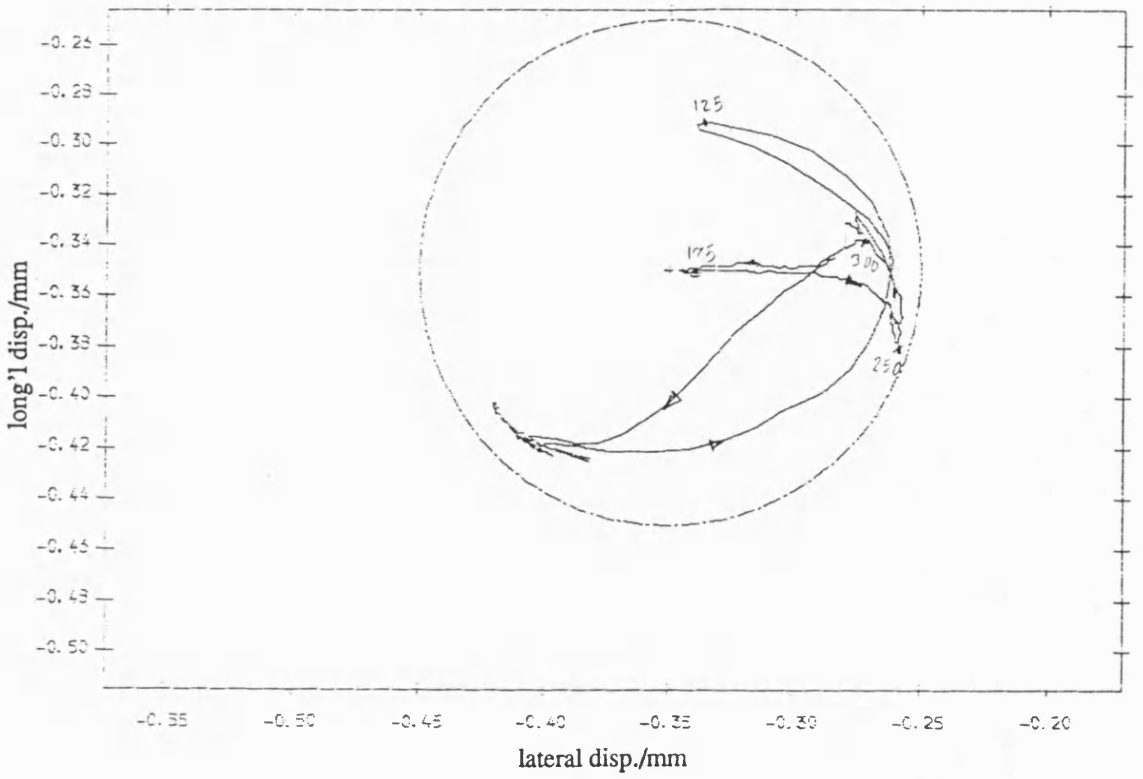

Fig 8.3.61 Exp. result polar plot of relative disp. of pin in normal bearing with fly wheel ;mean speed=168 rev/min ; dia. clearance=.20mm

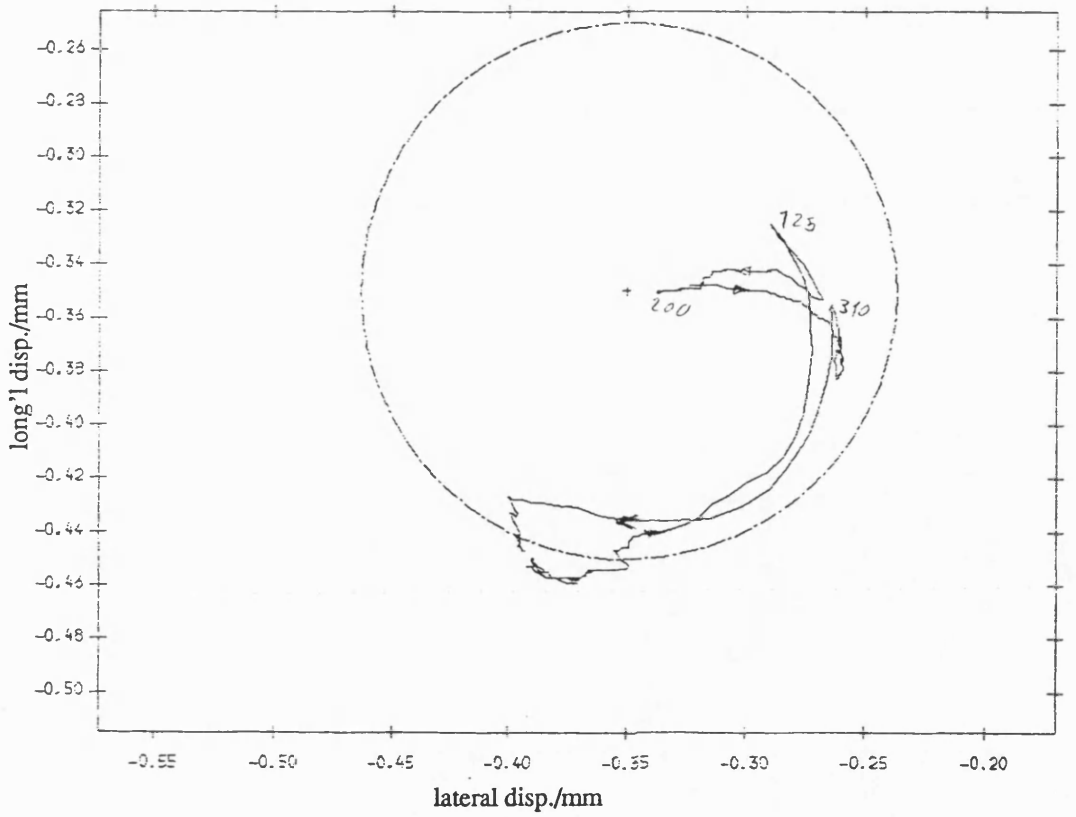

Fig 8.3.62 Exp. result polar plot of relative disp. of pin in normal bearing no fly wheel ;mean speed=168 rev/min ; dia. clearance=.20mm

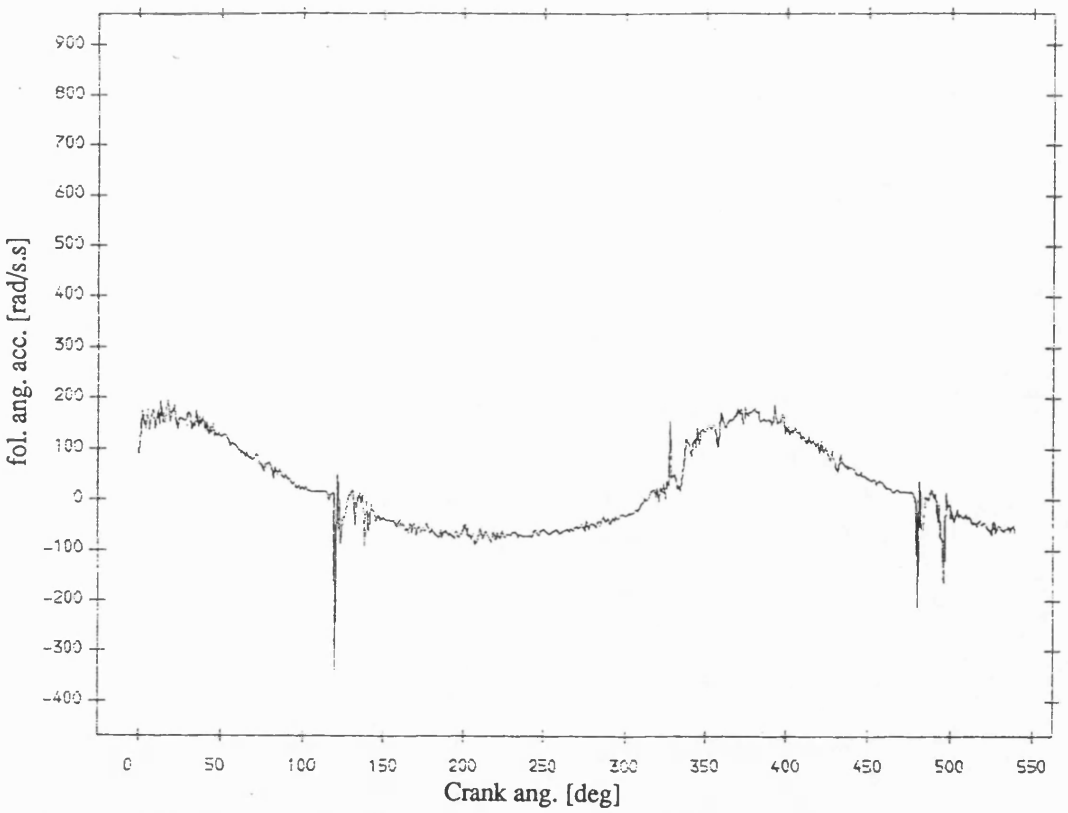

Fig 8.3.63 Exp. result follower ang. acceleration , normal bearing
with fly wheel ;mean speed=168 rev/min ; dia. clearance=.20mm

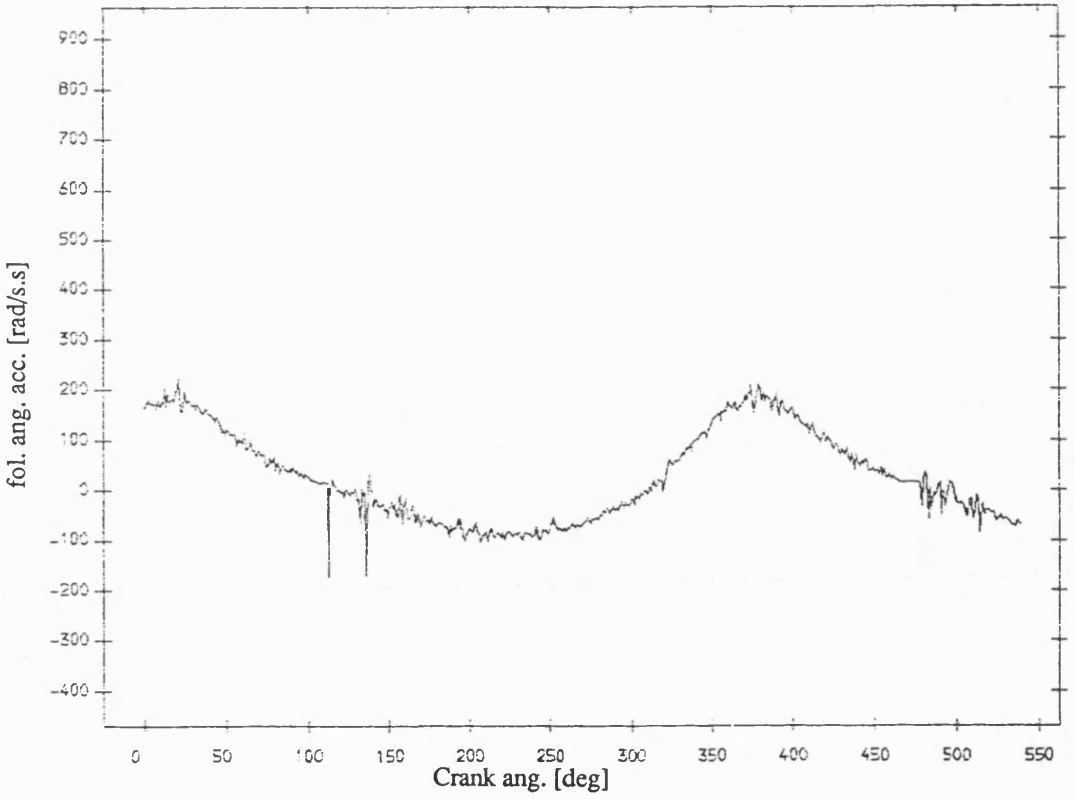

Fig 8.3.64 Exp. result follower ang. acceleration , normal bearing
no fly wheel ;mean speed=168 rev/min ; dia. clearance=.20mm

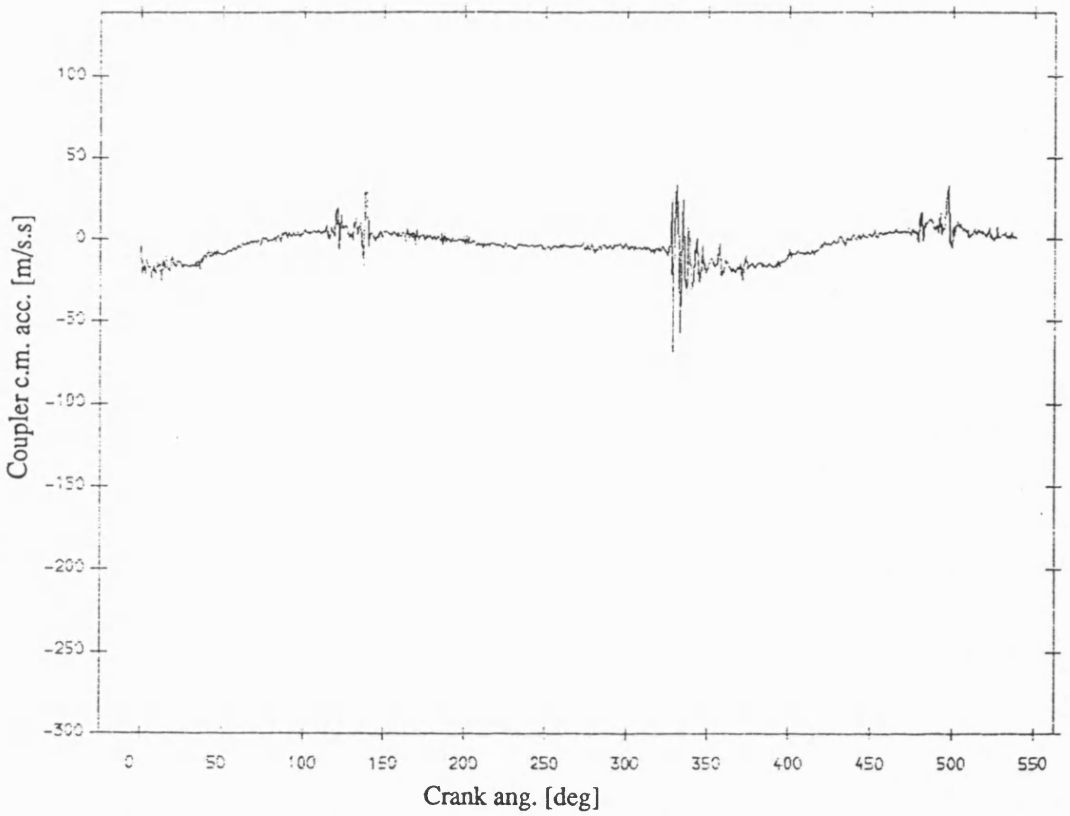

Fig 8.3.65 Exp. result coupler acceleration , normal bearing
with fly wheel ;mean speed=168 rev/min ; dia. clearance=.20mm

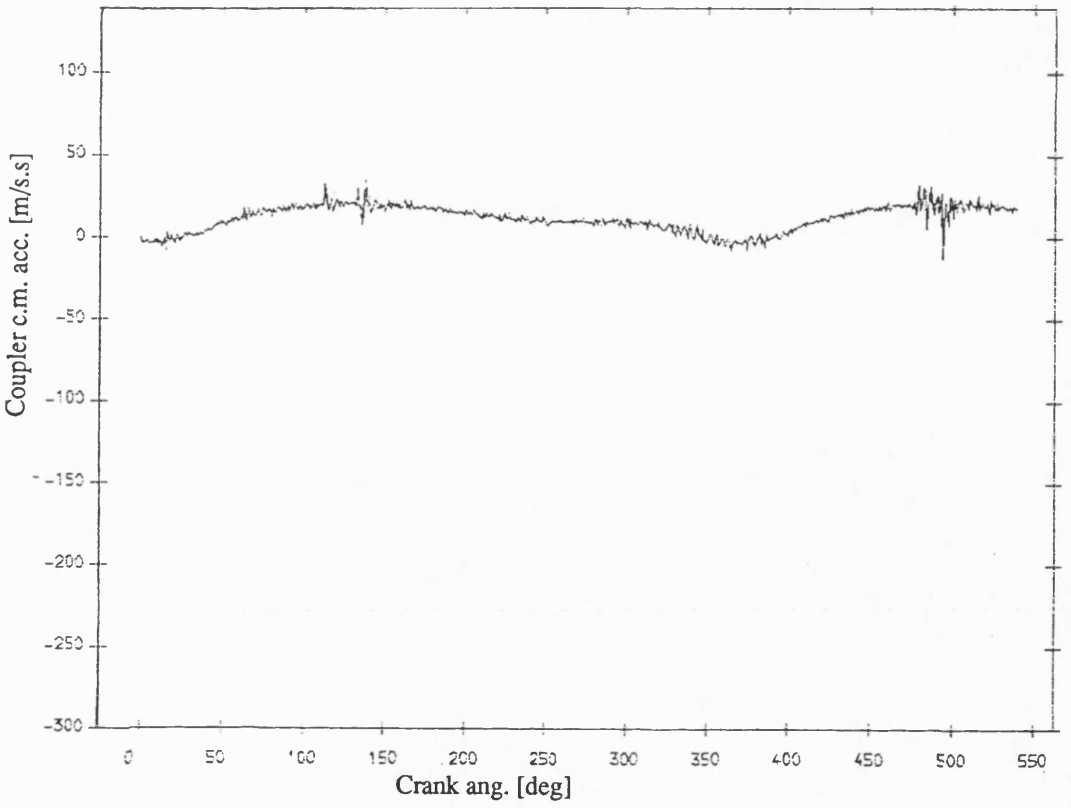

Fig 8.3.66 Exp. result coupler acceleration , normal bearing
no fly wheel ;mean speed=168 rev/min ; dia. clearance=.20mm

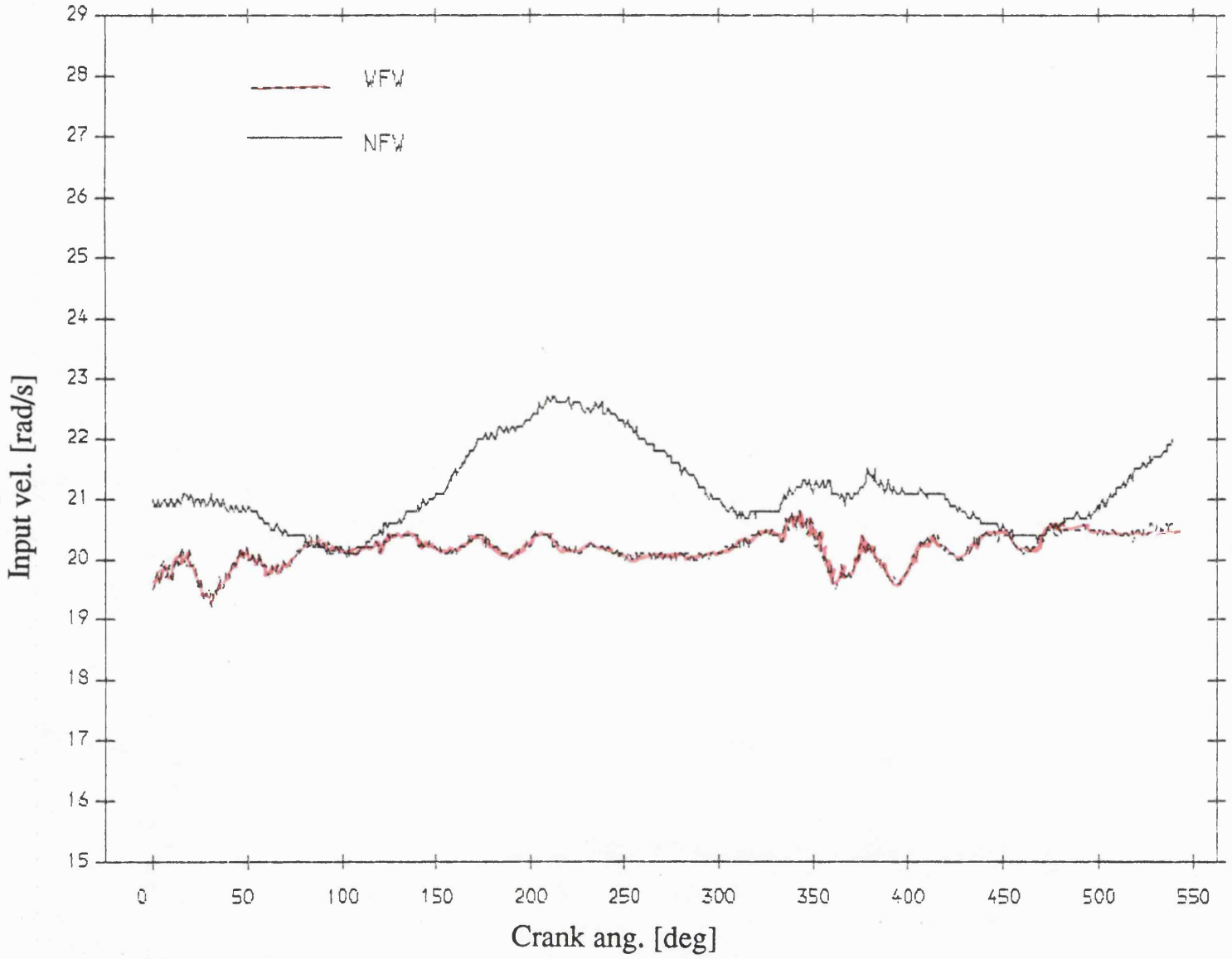

Fig 8.3.67 Exp. result input velocity , normal bearing
mean speed=208 rev/min; dia. clearance=.20mm

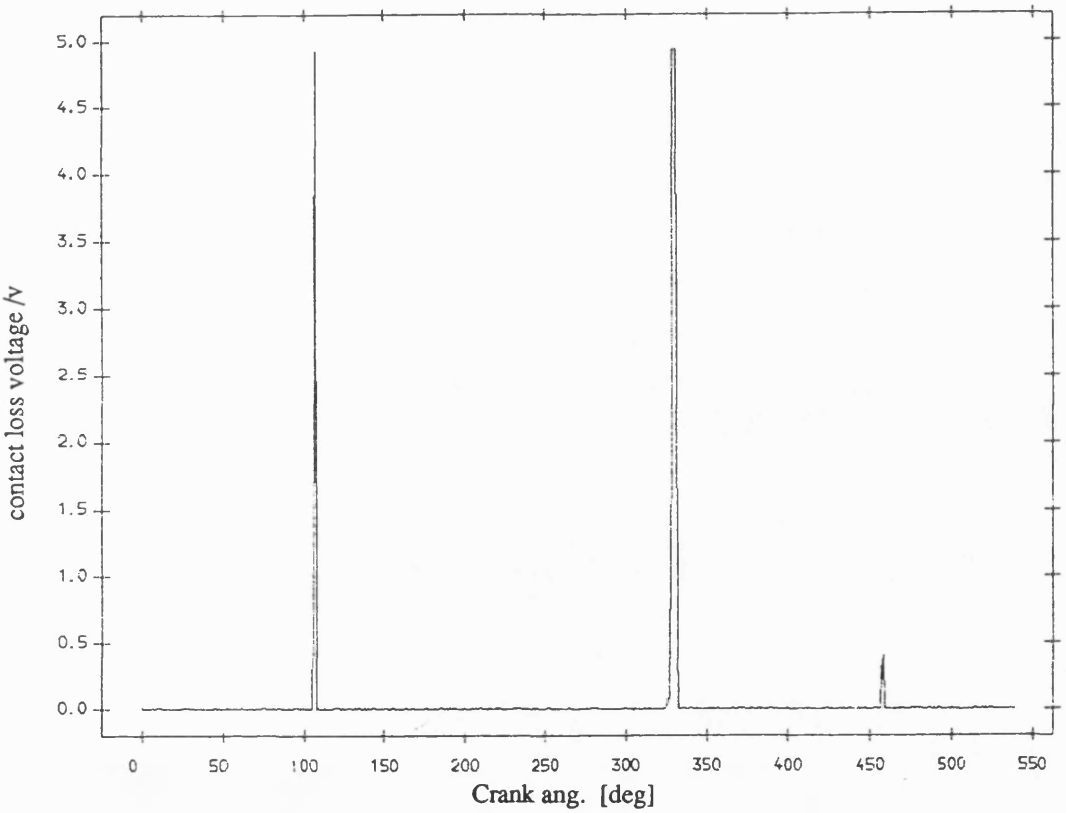

Fig 8.3.68 Exp. result contact loss of pin and normal bearing
with flywheel ;mean speed=208 rev/min ;dia. clearance=0.20mm

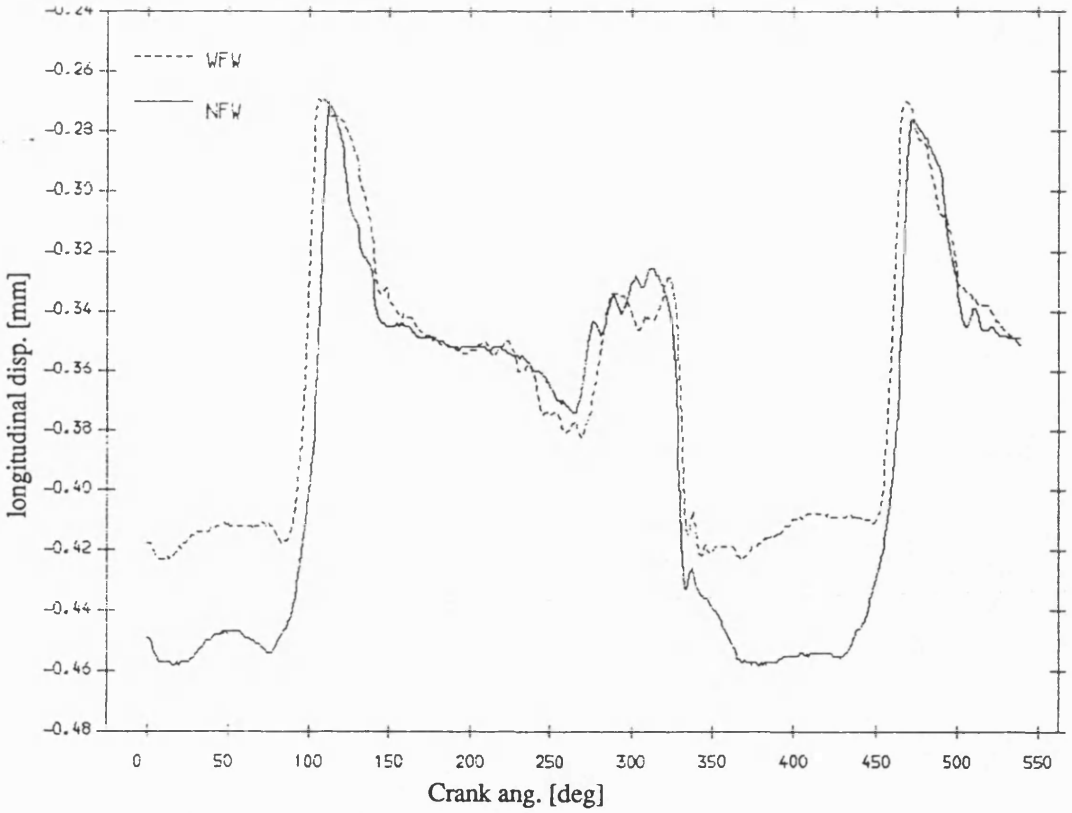

Fig 8.3.70 Exp. result longitudinal disp. of pin , normal bearing
mean speed=208 rev/min; dia. clearance=.20mm

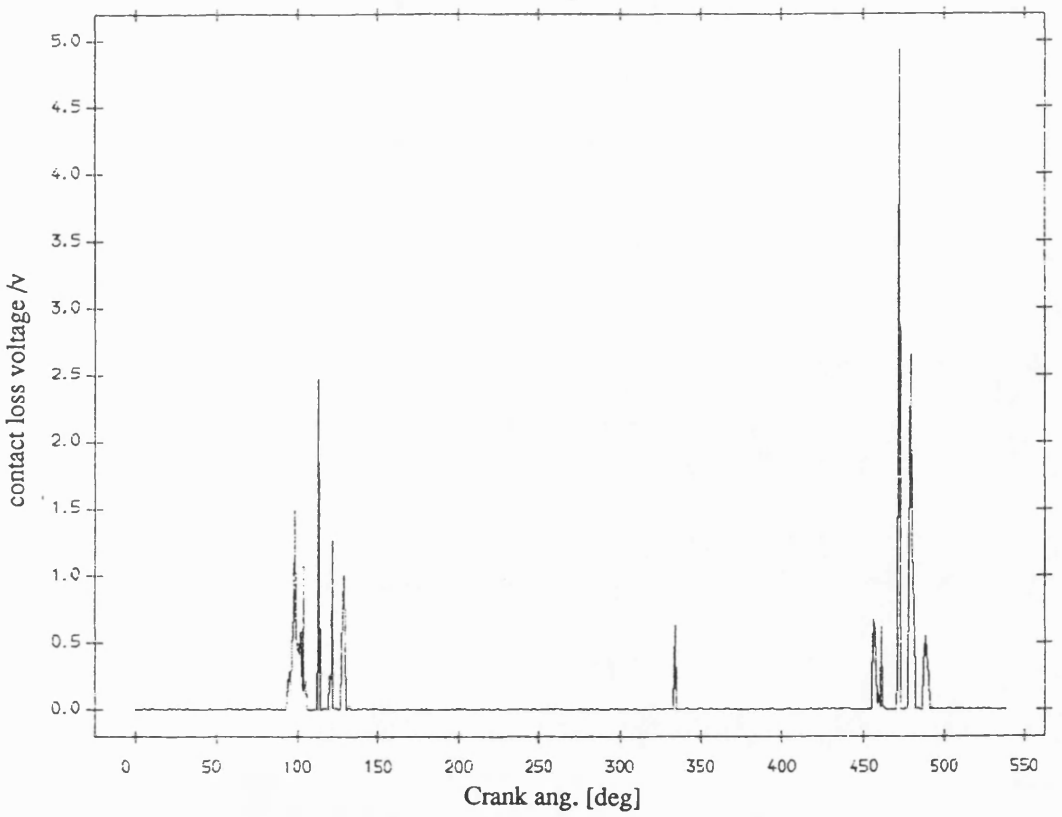

Fig 8.3.69 Exp. result contact loss of pin and normal bearing
no flywheel ;mean speed=208 rev/min ;dia. clearance=0.20mm

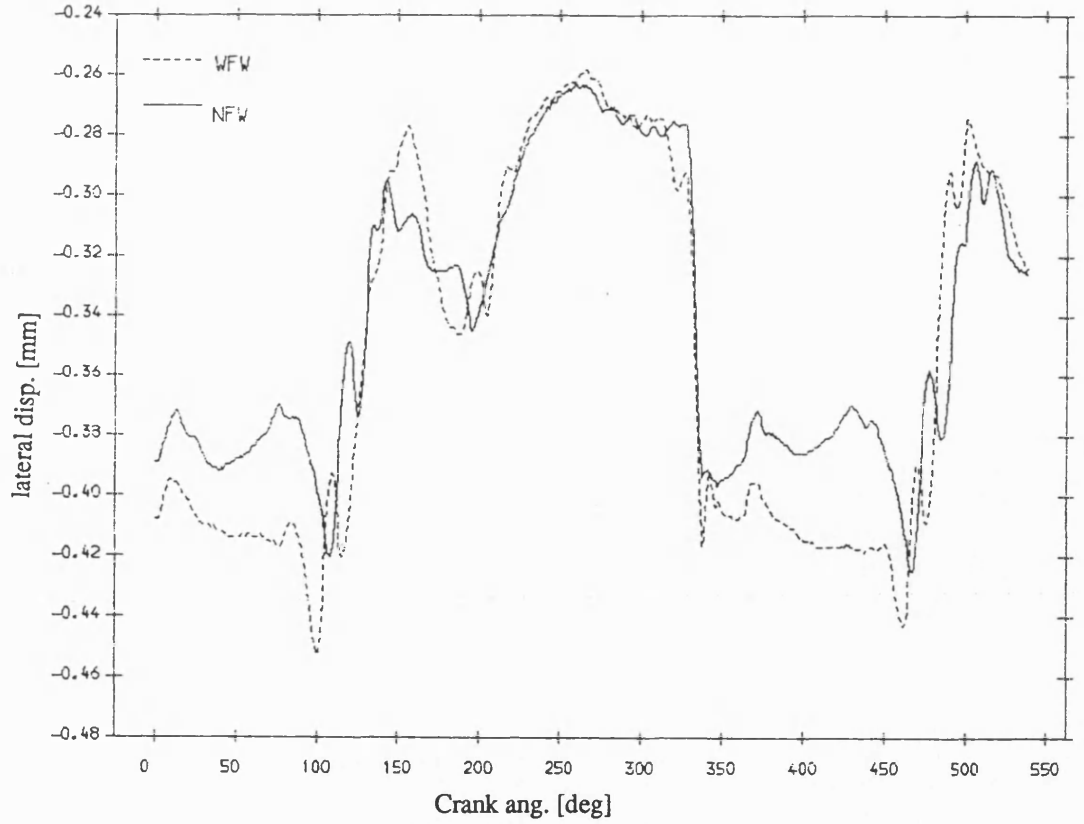

Fig 8.3.71 Exp. result lateral disp. of pin , normal bearing
mean speed=208 rev/min; dia. clearance=.20mm

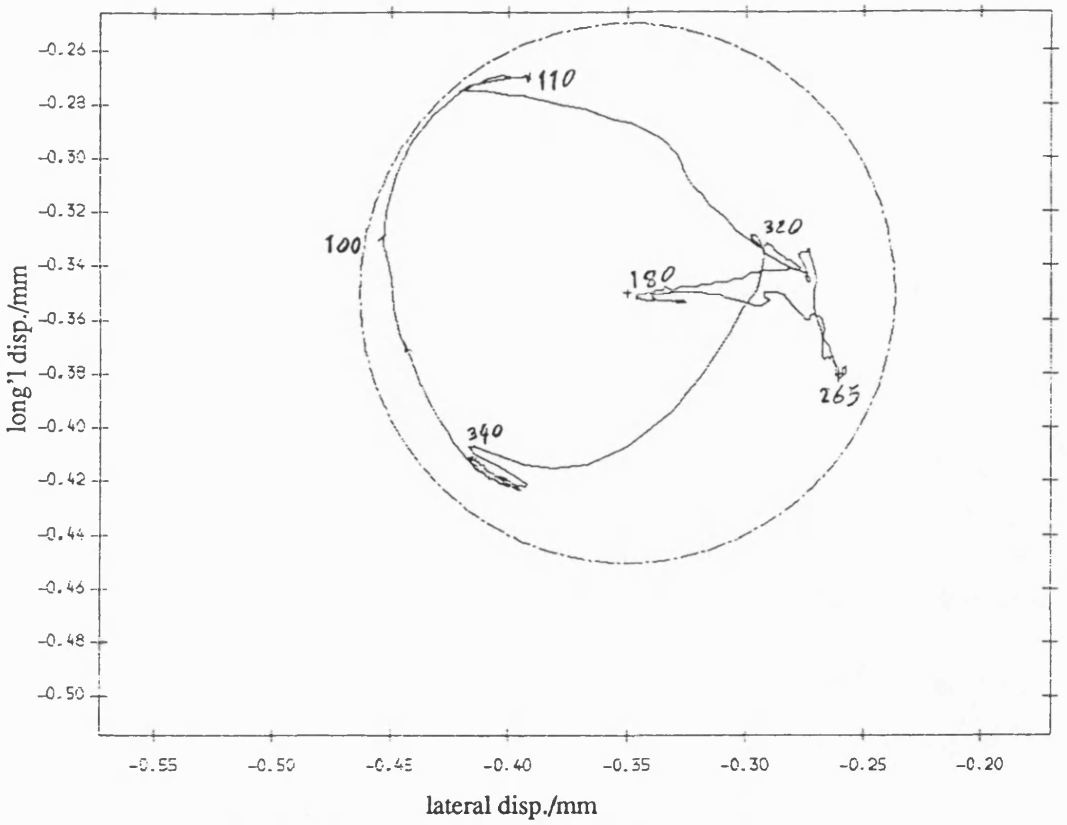

Fig 8.3.72 Exp. result polar plot of relative disp. of pin in normal bearing with fly wheel ;mean speed=208 rev/min ; dia. clearance=.20mm

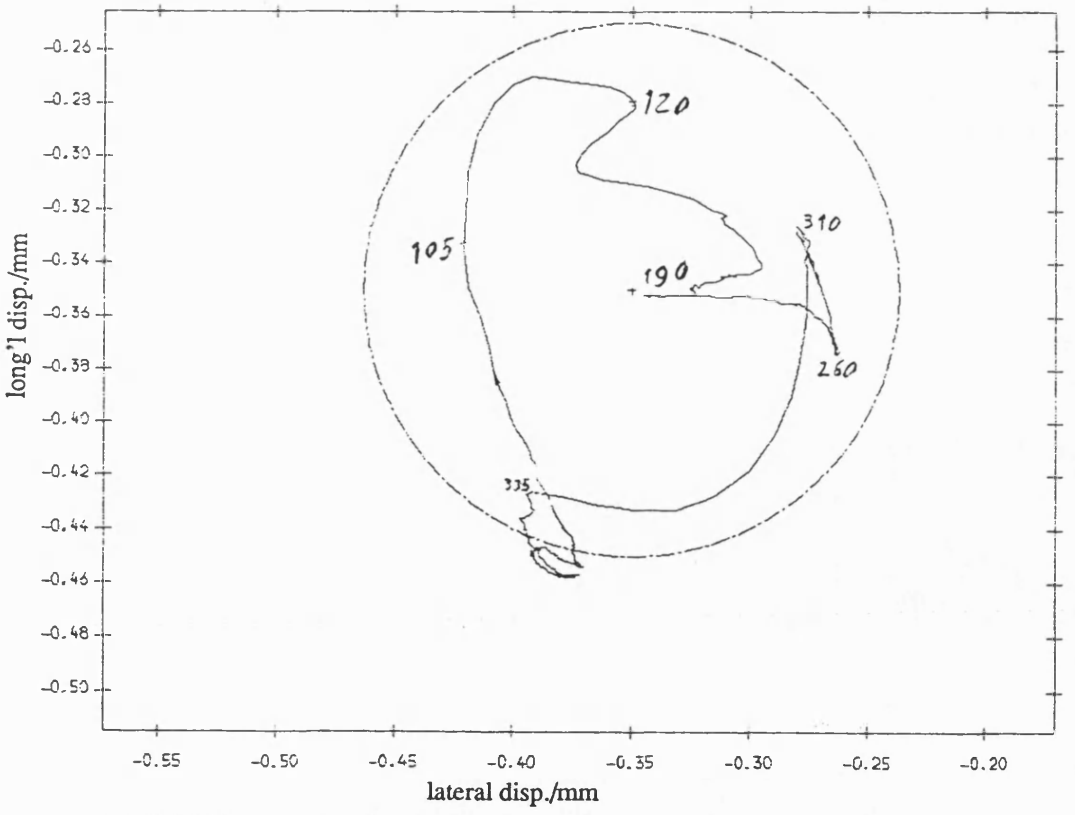

Fig 8.3.73 Exp. result polar plot of relative disp. of pin in normal bearing no fly wheel ;mean speed=208 rev/min ; dia. clearance=.20mm

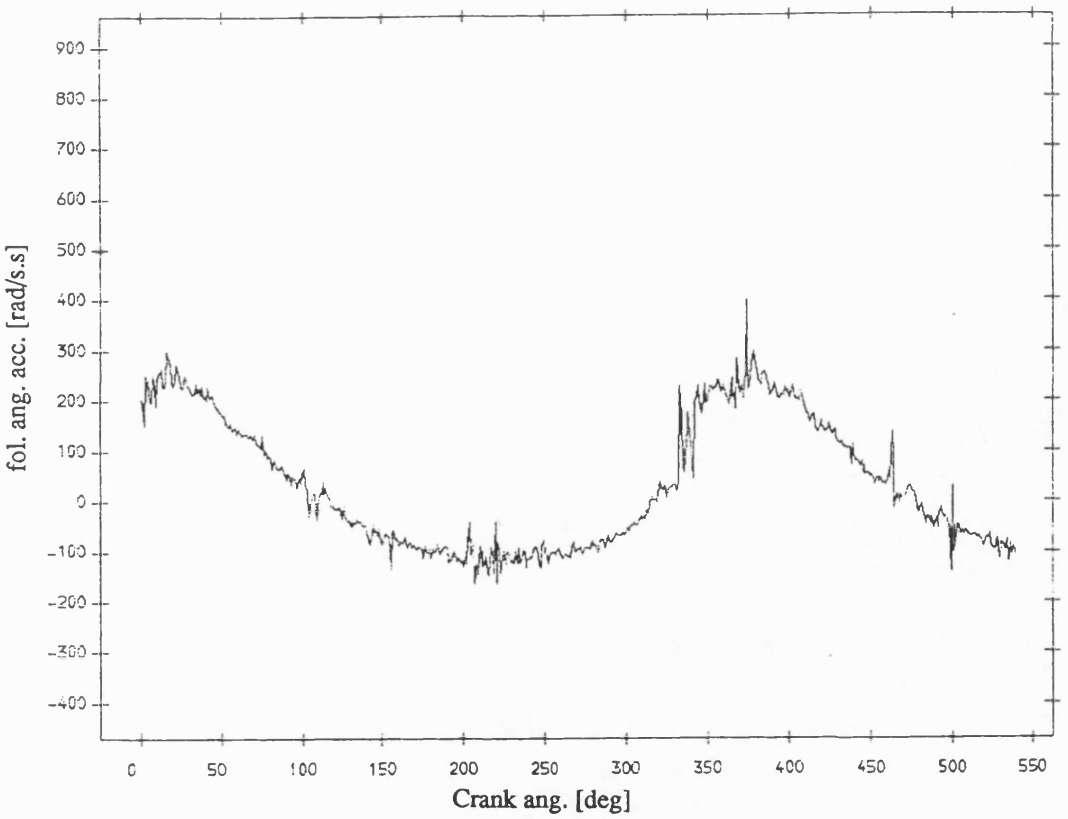

Fig 8.3.74 Exp. result follower ang. acceleration , normal bearing
with fly wheel ;mean speed=208 rev/min ; dia. clearance=.20mm

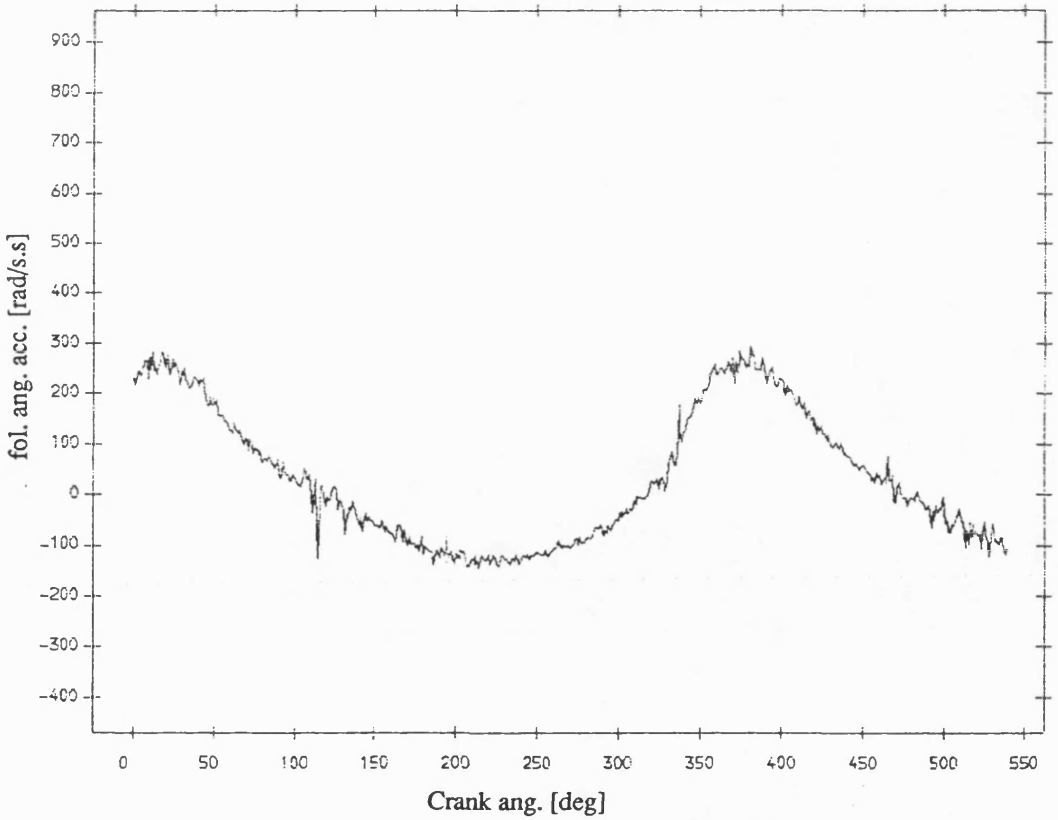

Fig 8.3.75 Exp. result follower ang. acceleration , normal bearing
no fly wheel ;mean speed=208 rev/min ; dia. clearance=.20mm

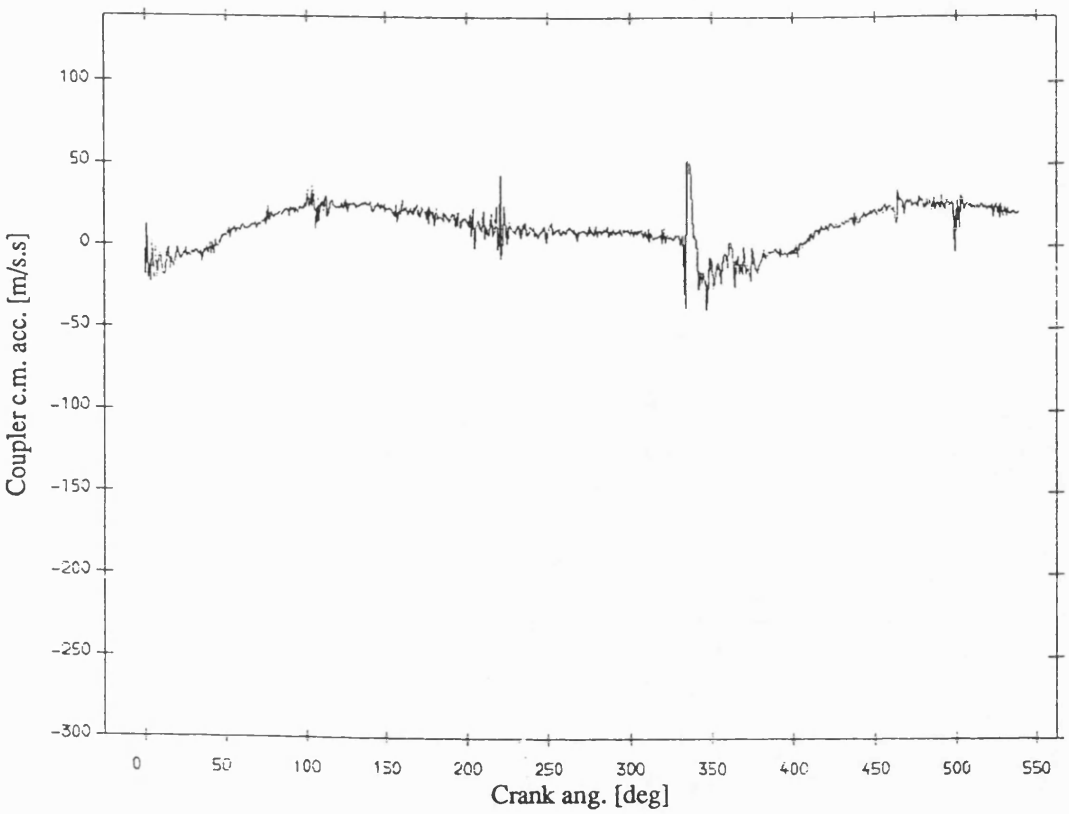

Fig 8.3.76 Exp. result coupler acceleration , normal bearing
with fly wheel ;mean speed=208 rev/min ; dia. clearance=.20mm

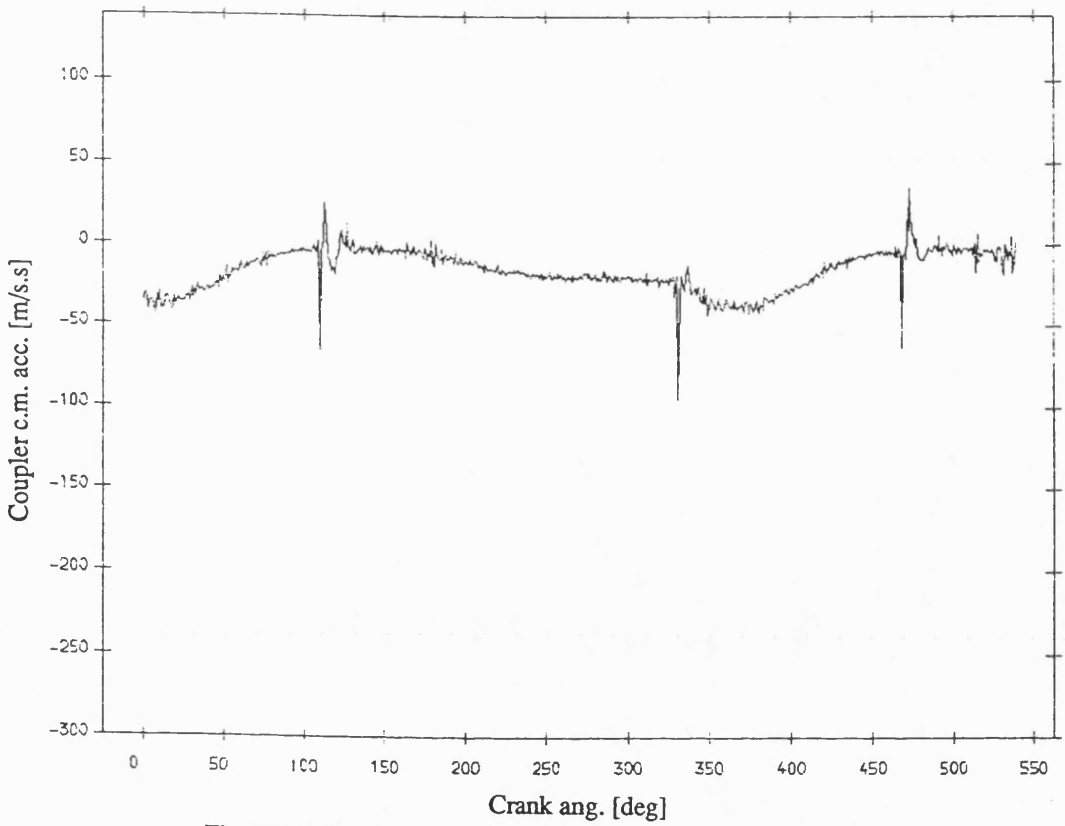

Fig 8.3.77 Exp. result coupler acceleration , normal bearing
no fly wheel ;mean speed=208 rev/min ; dia. clearance=.20mm

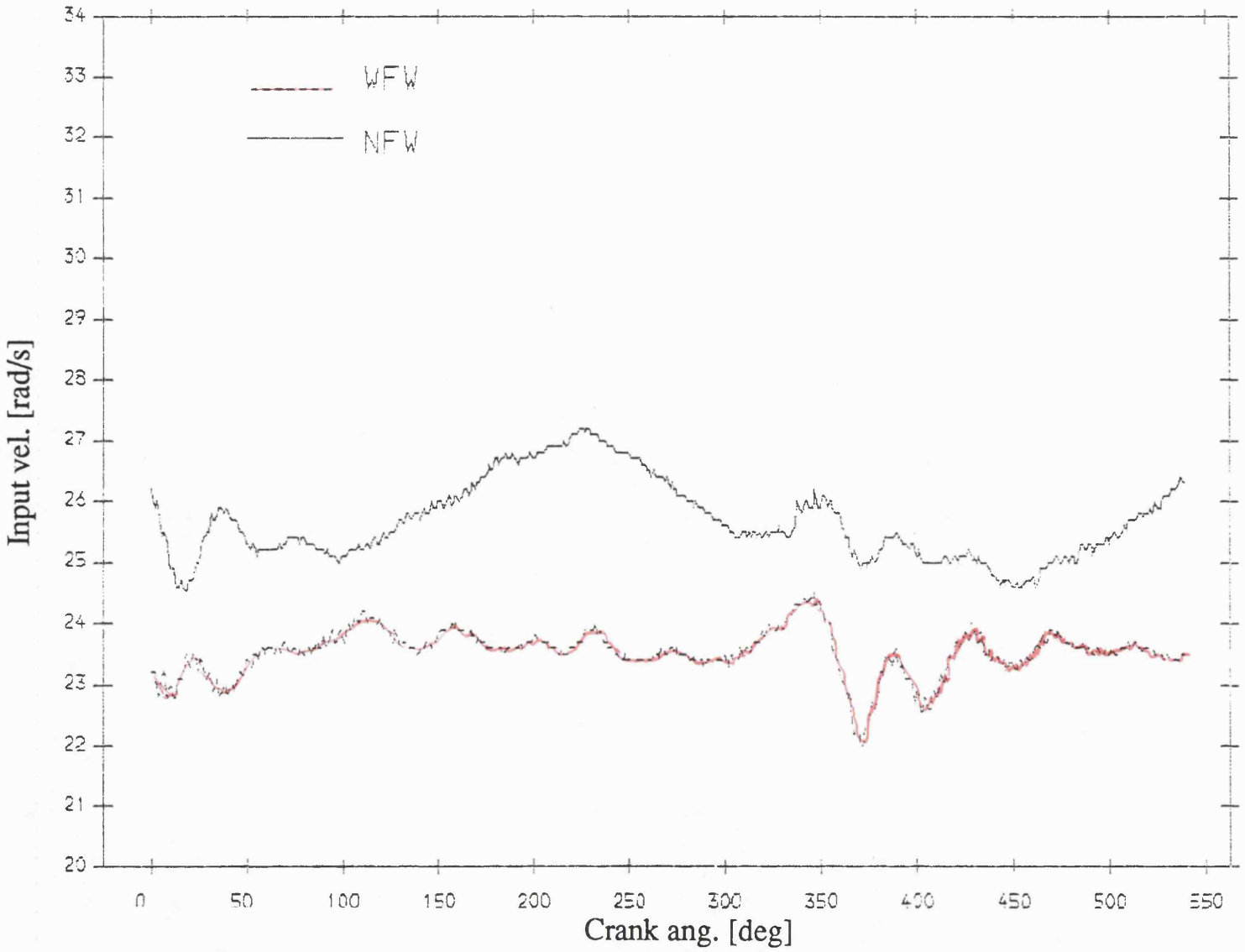

Fig 8.3.78 Exp. result input velocity , normal bearing
mean speed=244 rev/min; dia. clearance=.20mm

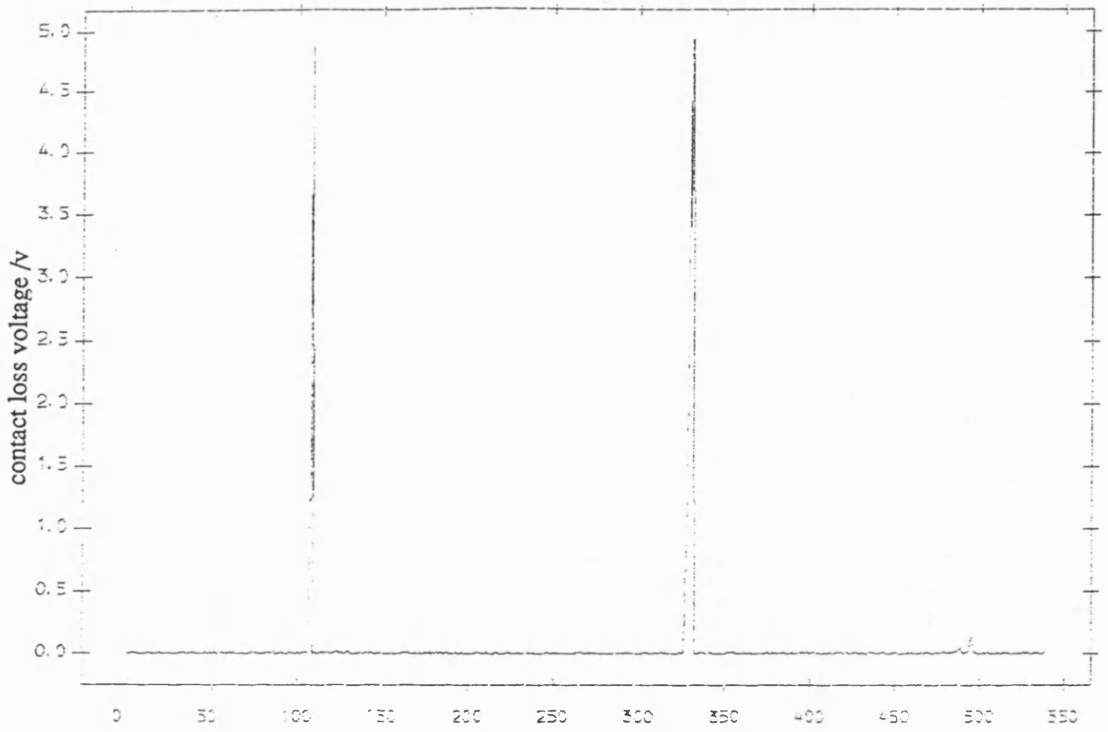

Fig 8.3.79 Exp. result contact loss of pin and normal bearing
with flywheel ;mean speed=244 rev/min ;dia. clearance=0.20mm

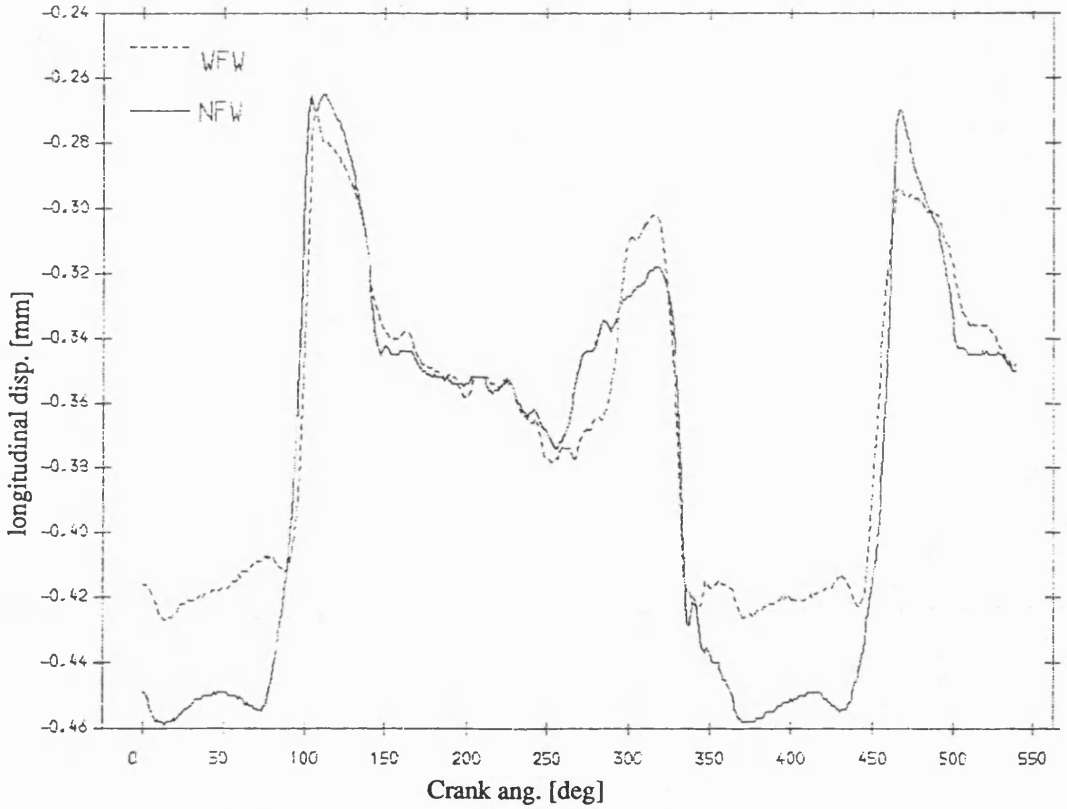

Fig 8.3.81 Exp. result longitudinal disp. of pin , normal bearing
mean speed=244 rev/min; dia. clearance=.20mm

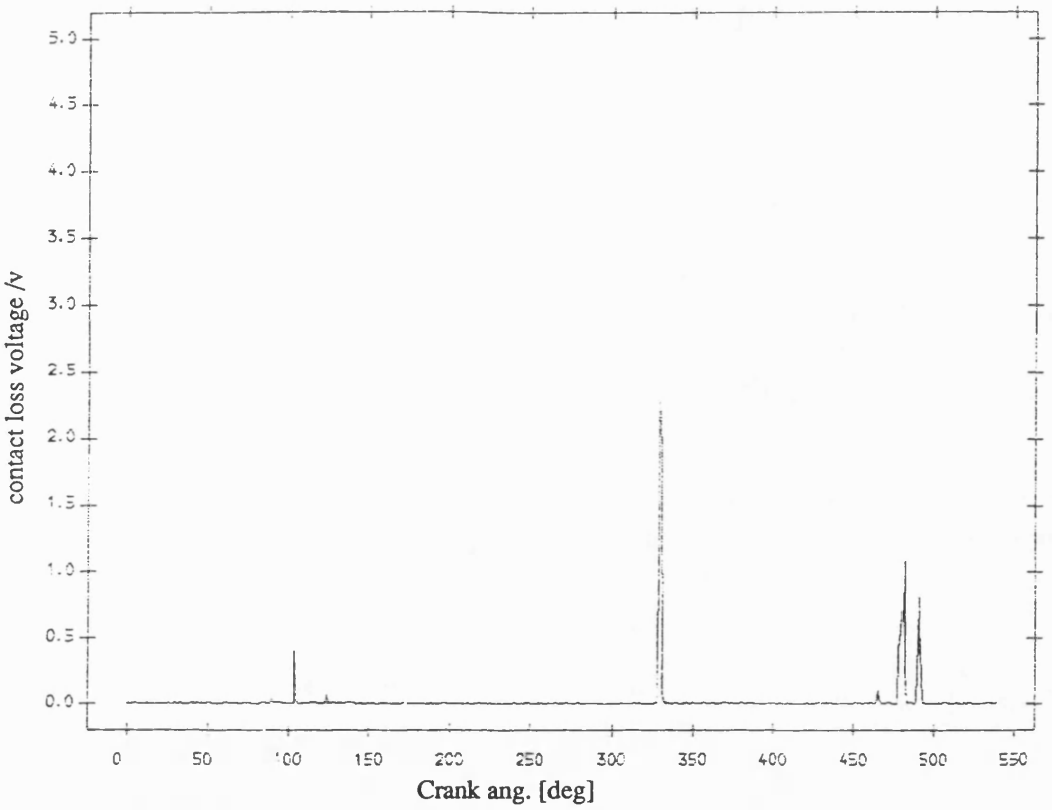

Fig 8.3.80 Exp. result contact loss of pin and normal bearing
no flywheel ;mean speed=244 rev/min ;dia. clearance=0.20mm

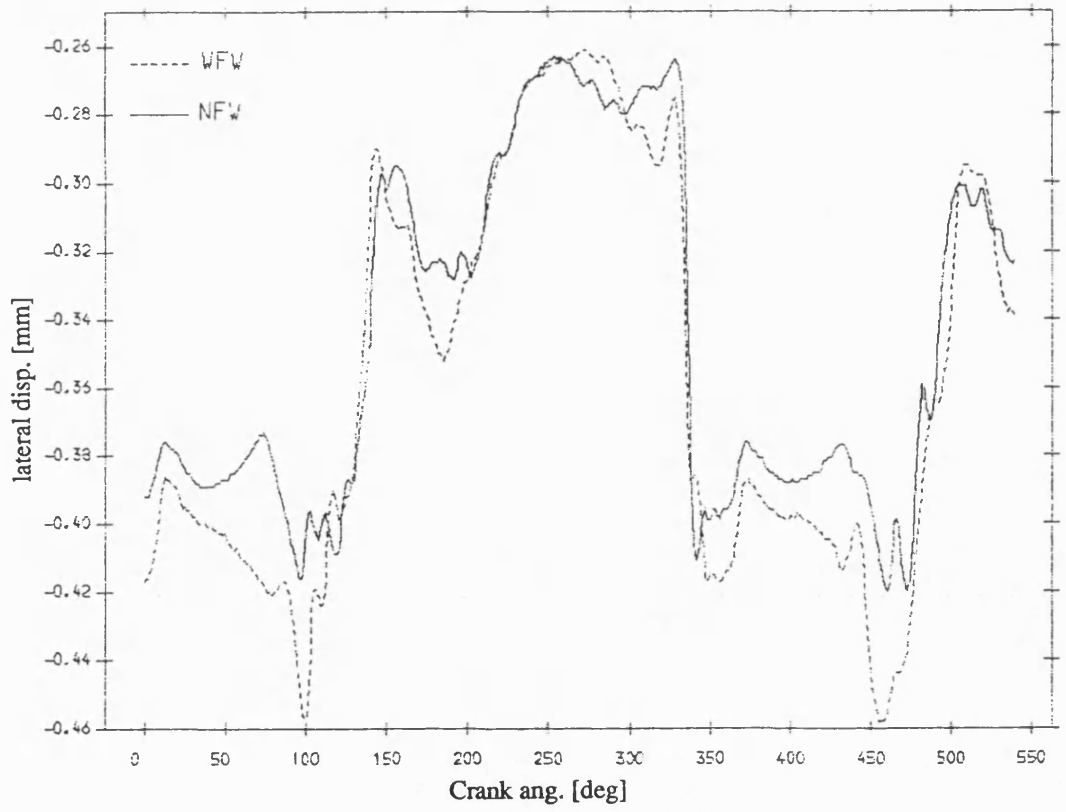

Fig 8.3.82 Exp. result lateral disp. of pin , normal bearing
mean speed=244 rev/min; dia. clearance=.20mm

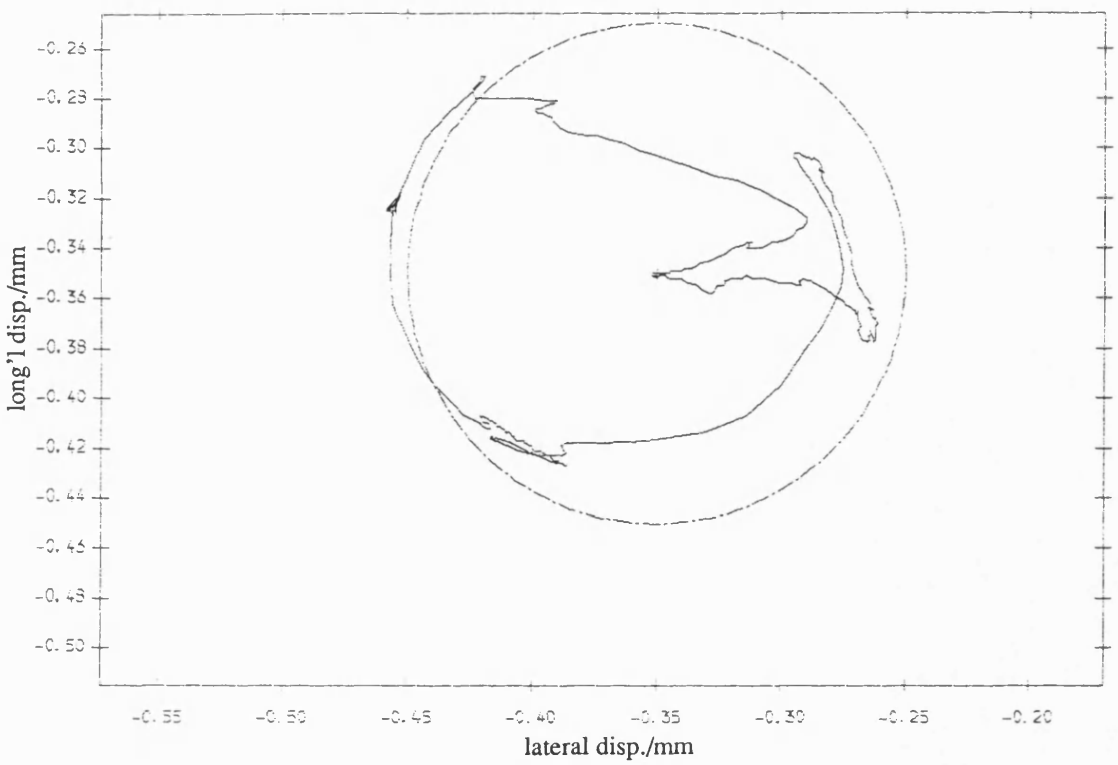

Fig 8.3.83 Exp. result polar plot of relative disp. of pin in normal bearing with fly wheel ;mean speed=244 rev/min ; dia. clearance=.20mm

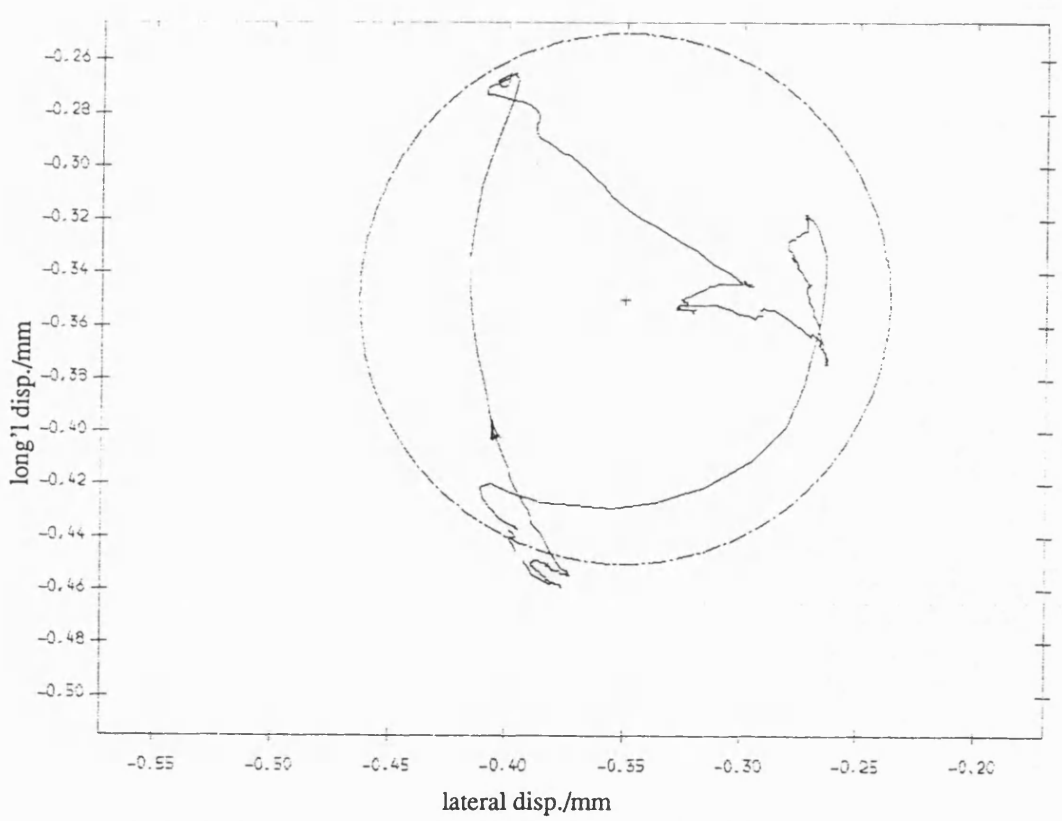

Fig 8.3.84 Exp. result polar plot of relative disp. of pin in normal bearing no fly wheel ;mean speed=244 rev/min ; dia. clearance=.20mm

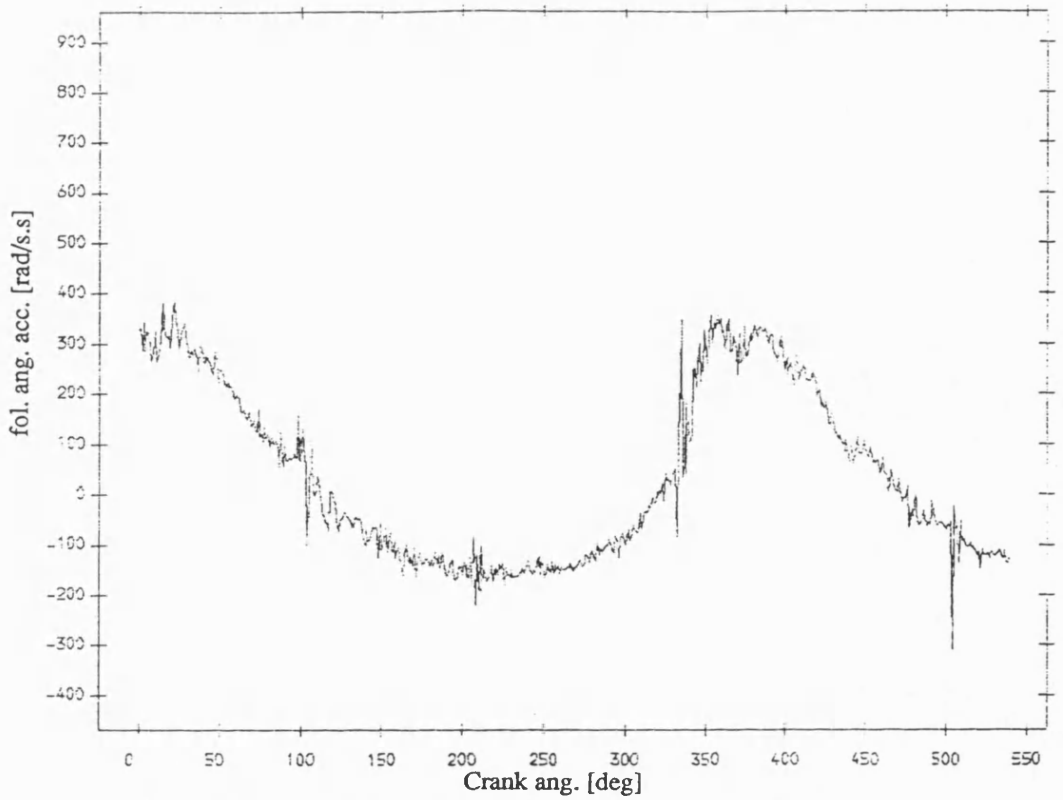

Fig 8.3.85 Exp. result follower ang. acceleration , normal bearing
with fly wheel ;mean speed=244 rev/min ; dia. clearance=.20mm

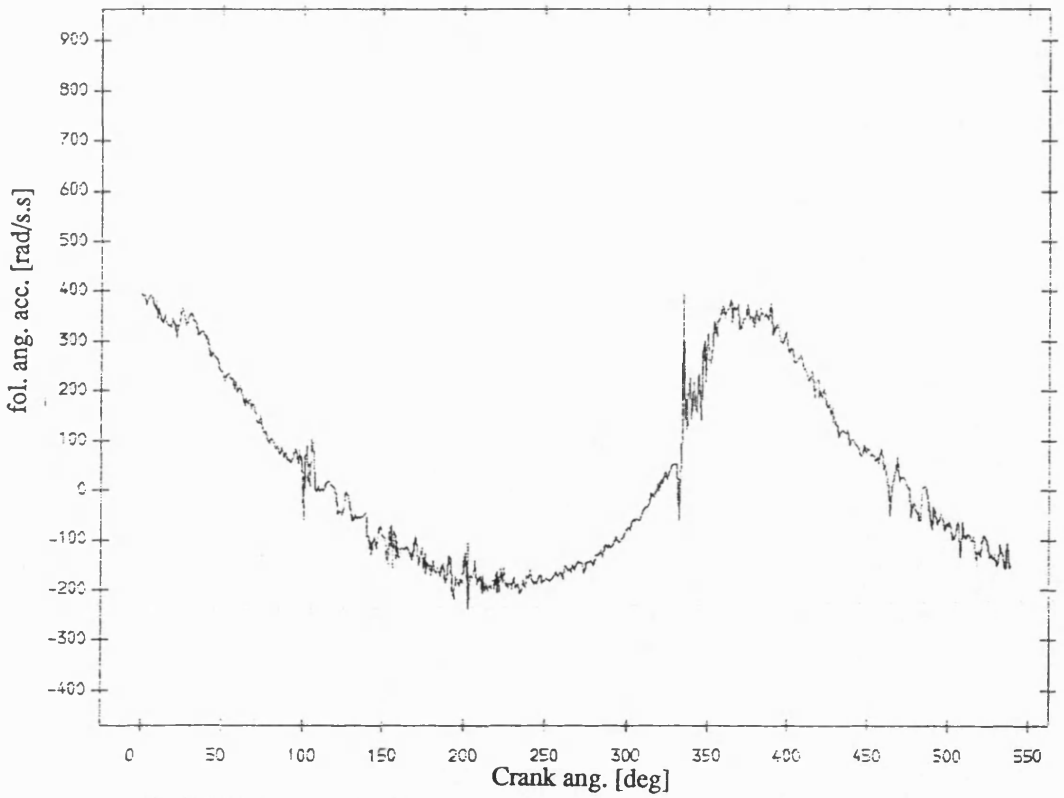

Fig 8.3.86 Exp. result follower ang. acceleration , normal bearing
no fly wheel ;mean speed=244 rev/min ; dia. clearance=.20mm

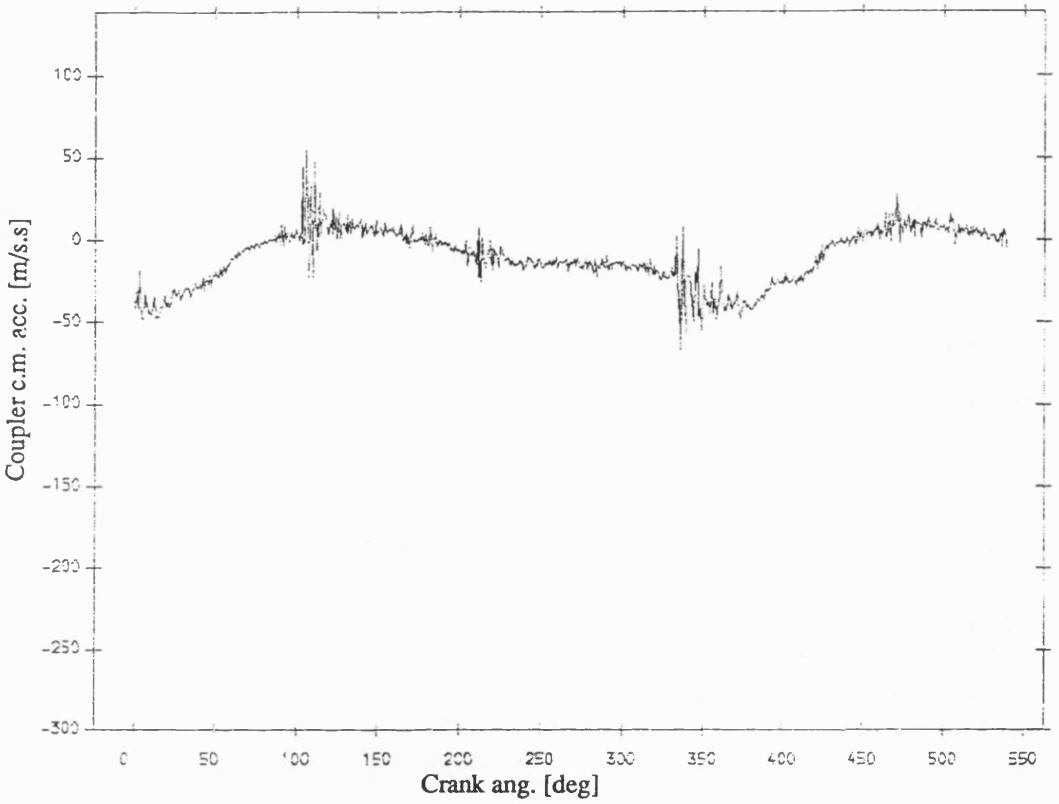

Fig 8.3.87 Exp. result coupler acceleration , normal bearing
with fly wheel ;mean speed=244 rev/min ; dia. clearance=.20mm

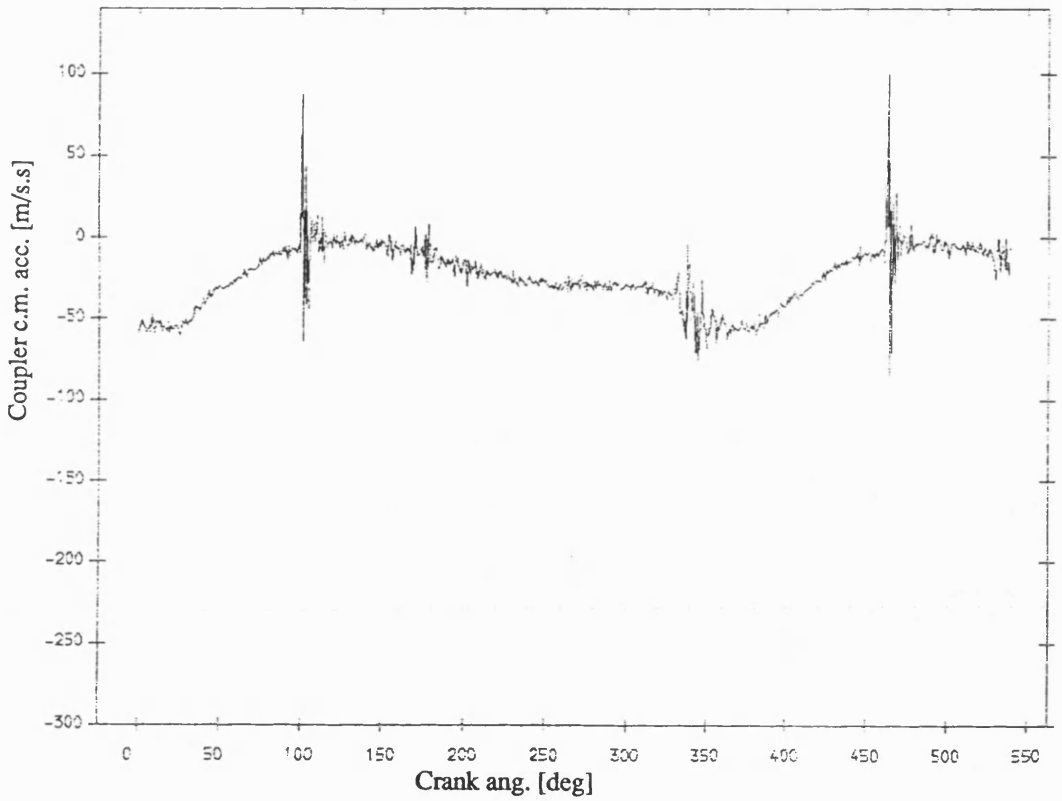

Fig 8.3.88 Exp. result coupler acceleration , normal bearing
no fly wheel ;mean speed=244 rev/min ; dia. clearance=.20mm

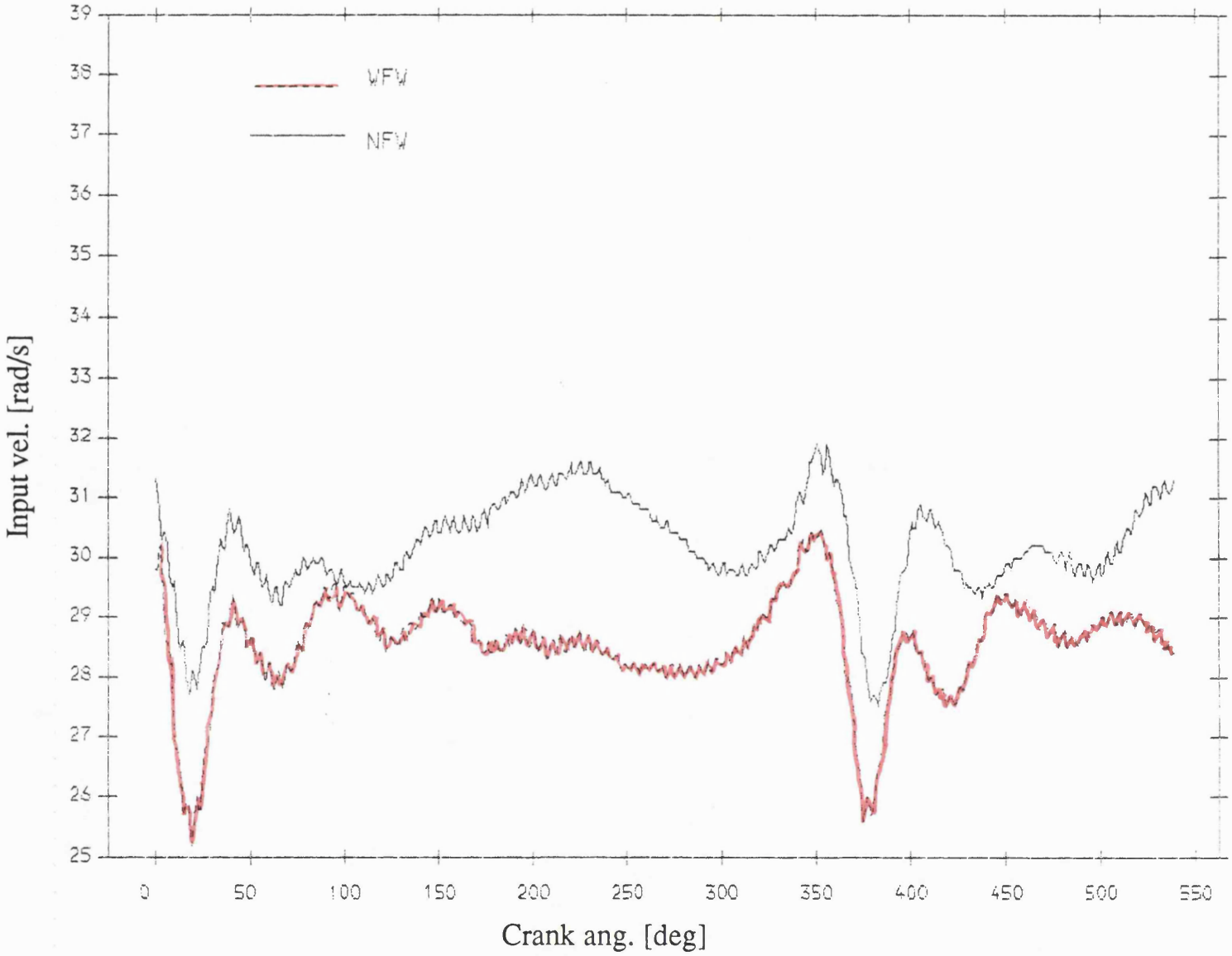

Fig 8.3.89 Exp. result input velocity , normal bearing
mean speed=290 rev/min; dia. clearance=.20mm

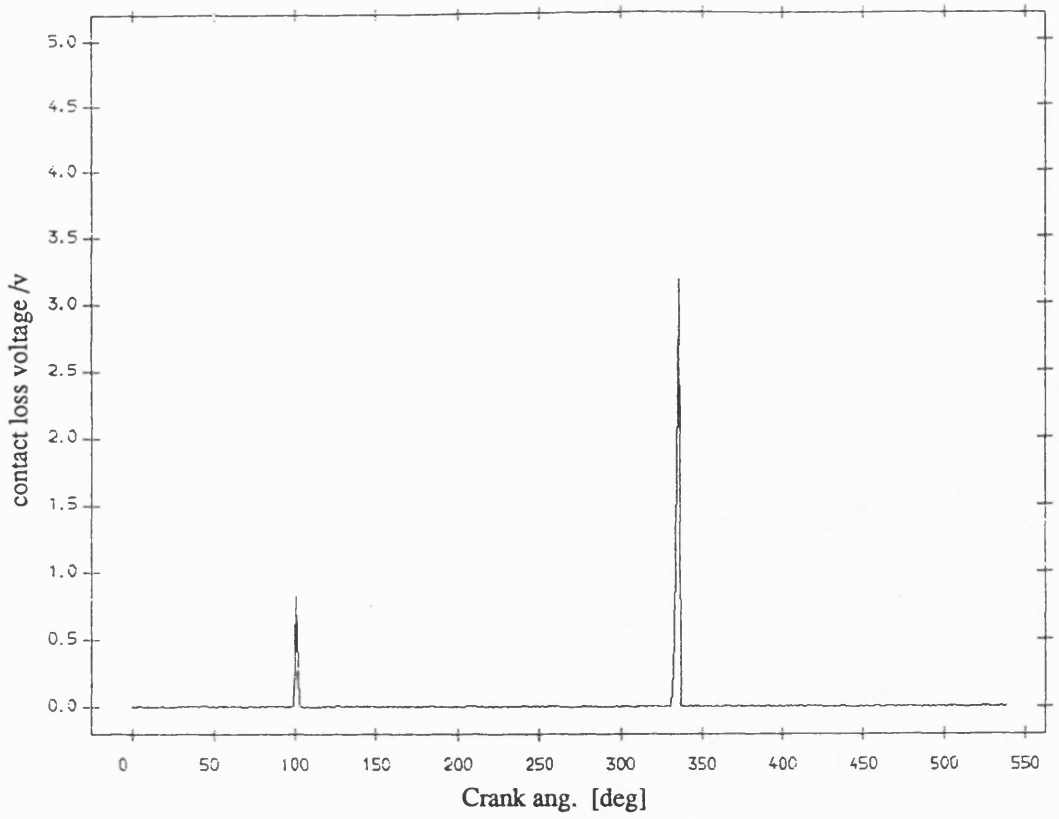

Fig 8.3.90 Exp. result contact loss of pin and normal bearing
with flywheel ;mean speed=290 rev/min ;dia. clearance=0.20mm

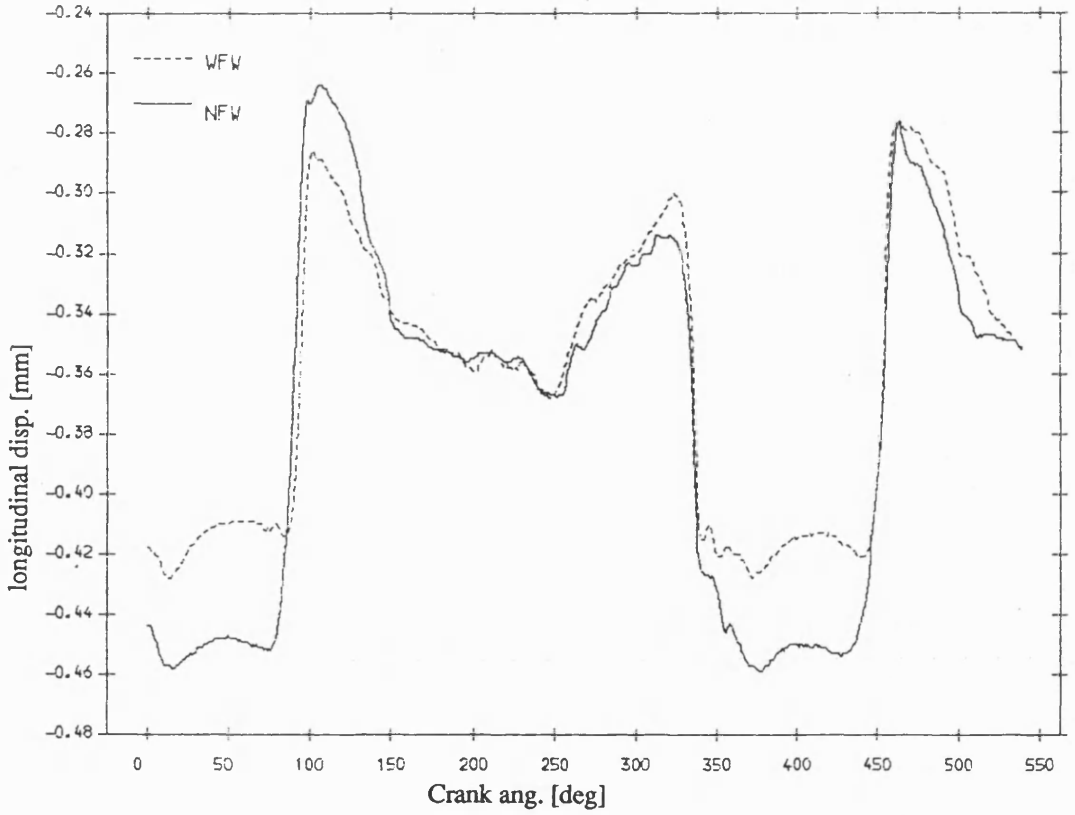

Fig 8.3.92 Exp. result longitudinal disp. of pin , normal bearing
mean speed=290 rev/min; dia. clearance=.20mm

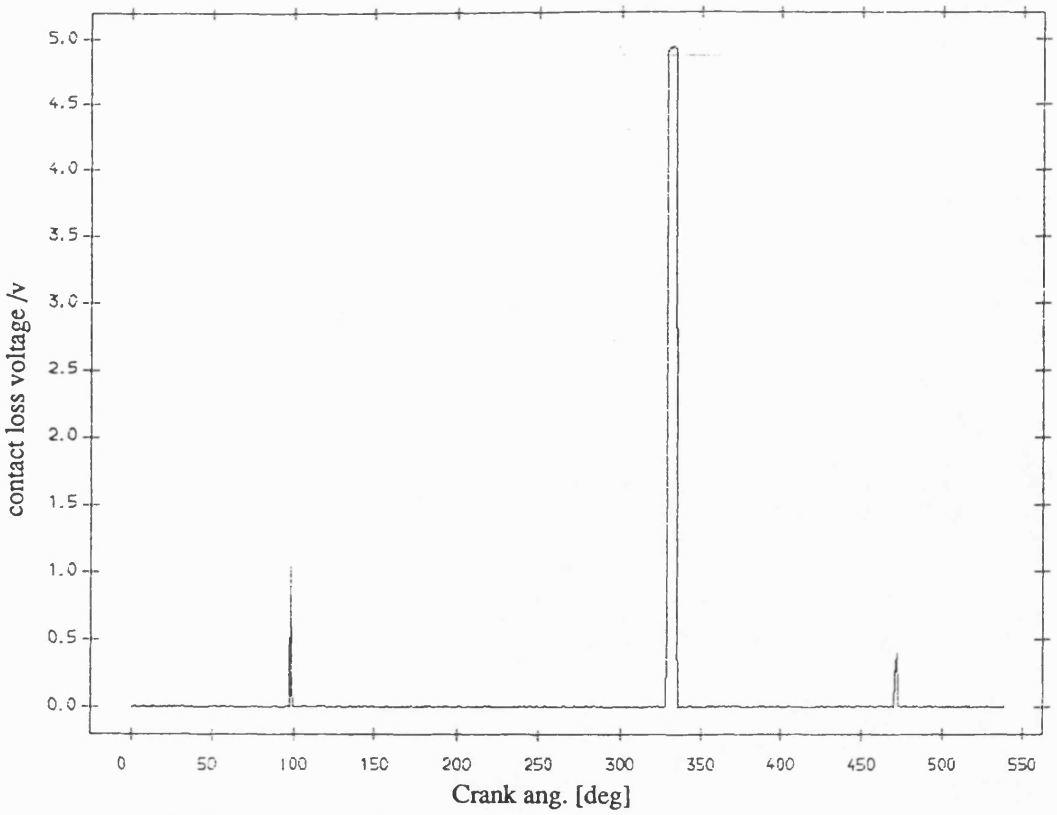

Fig 8.3.91 Exp. result contact loss of pin and normal bearing
no flywheel ;mean speed=290 rev/min ;dia. clearance=0.20mm

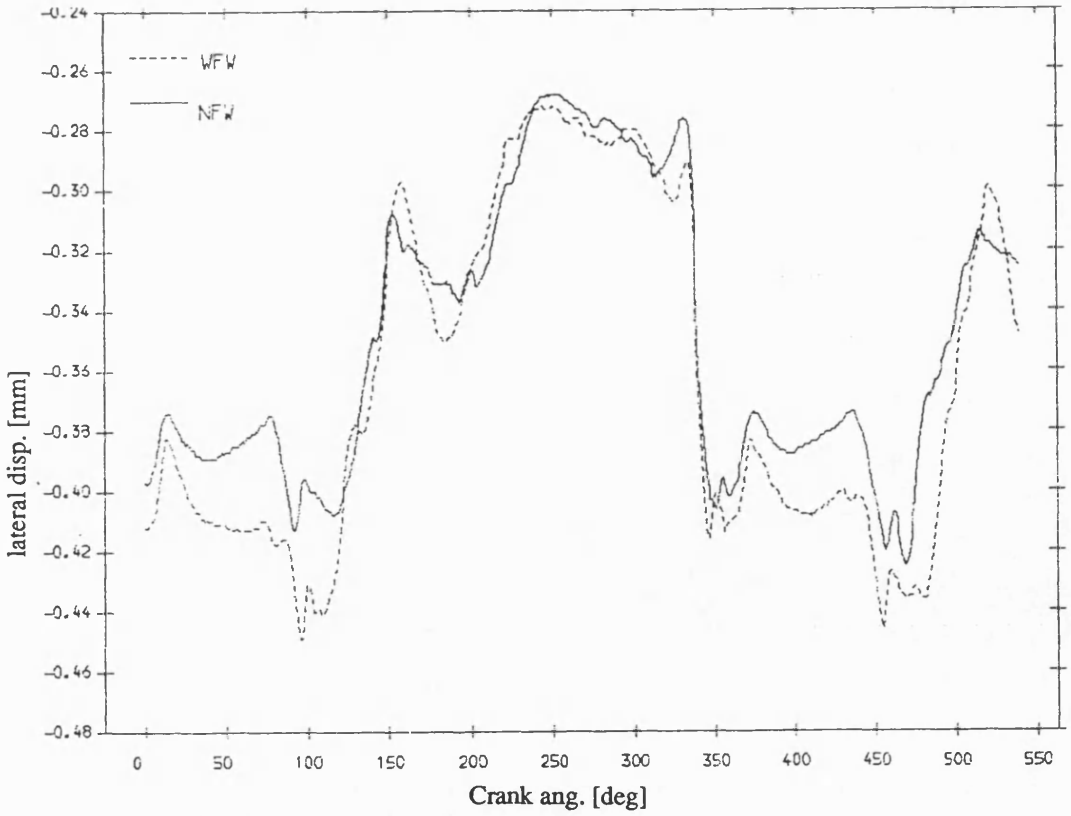

Fig 8.3.93 Exp. result lateral disp. of pin , normal bearing
mean speed=290 rev/min; dia. clearance=.20mm

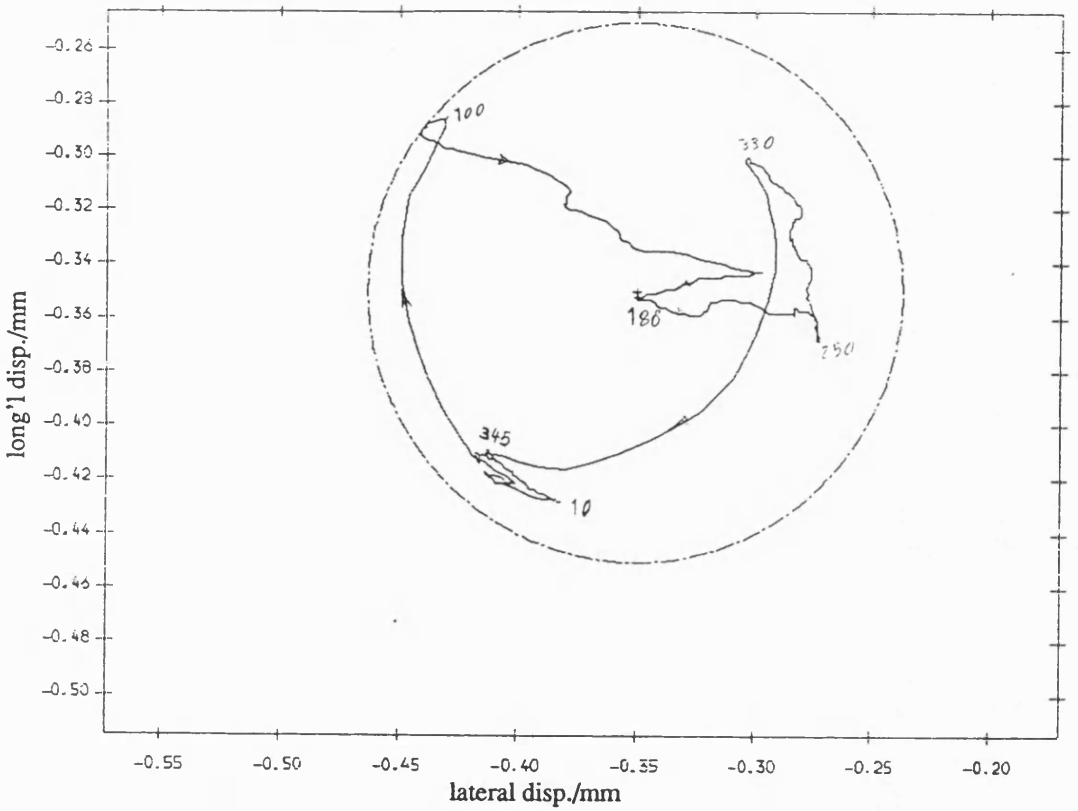

Fig 8.3.94 Exp. result polar plot of relative disp. of pin in normal bearing with fly wheel ;mean speed=290 rev/min ; dia. clearance=.20mm

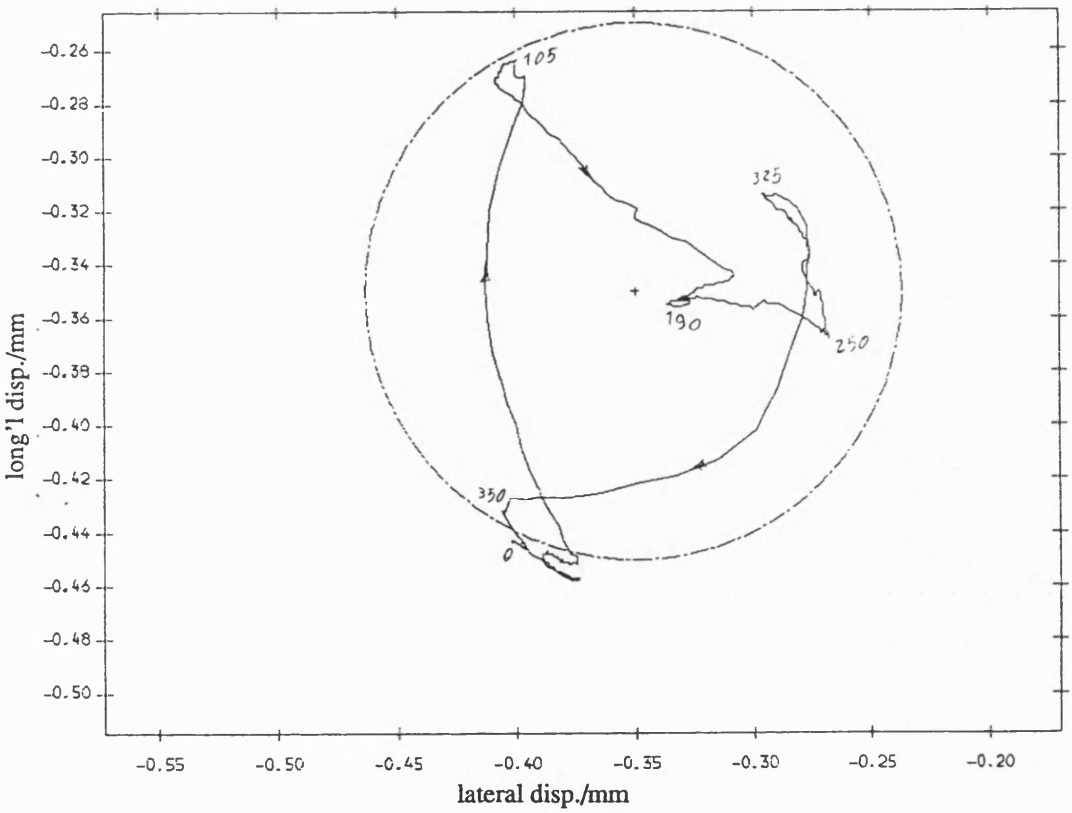

Fig 8.3.95 Exp. result polar plot of relative disp. of pin in normal bearing no fly wheel ;mean speed=290 rev/min ; dia. clearance=.20mm

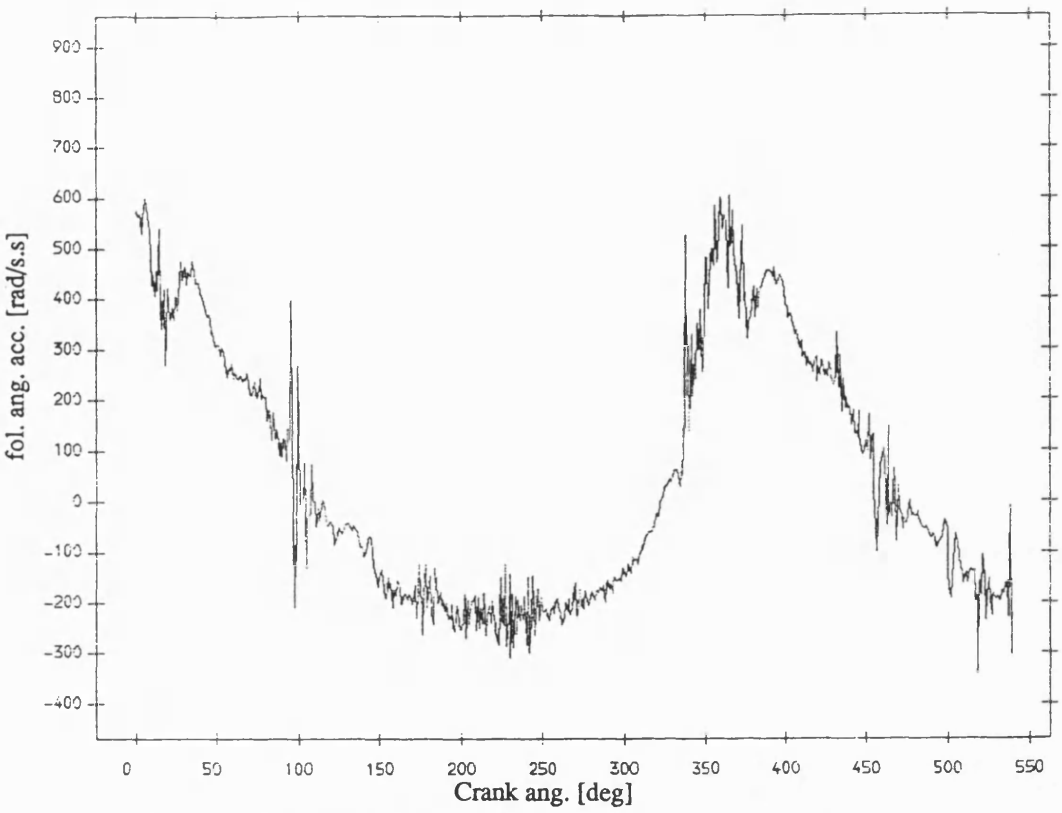

Fig 8.3.96 Exp. result follower ang. acceleration , normal bearing
with fly wheel ;mean speed=290 rev/min ; dia. clearance=.20mm

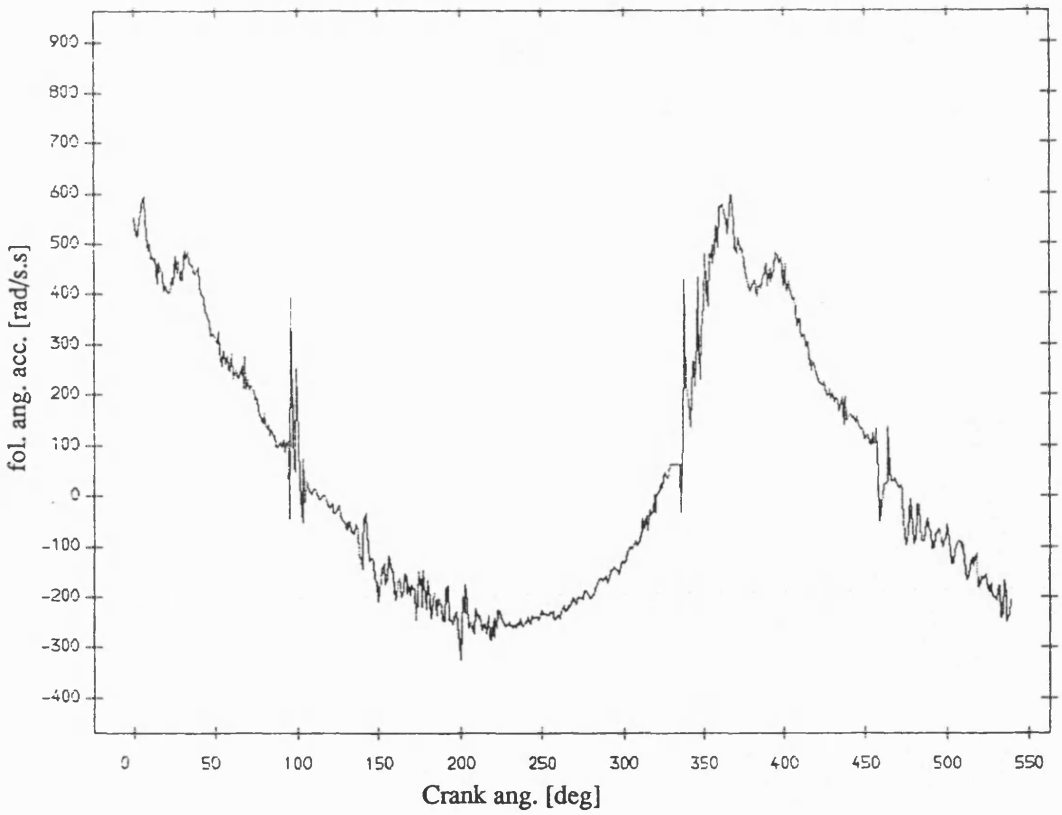

Fig 8.3.97 Exp. result follower ang. acceleration , normal bearing
no fly wheel ;mean speed=290 rev/min ; dia. clearance=.20mm

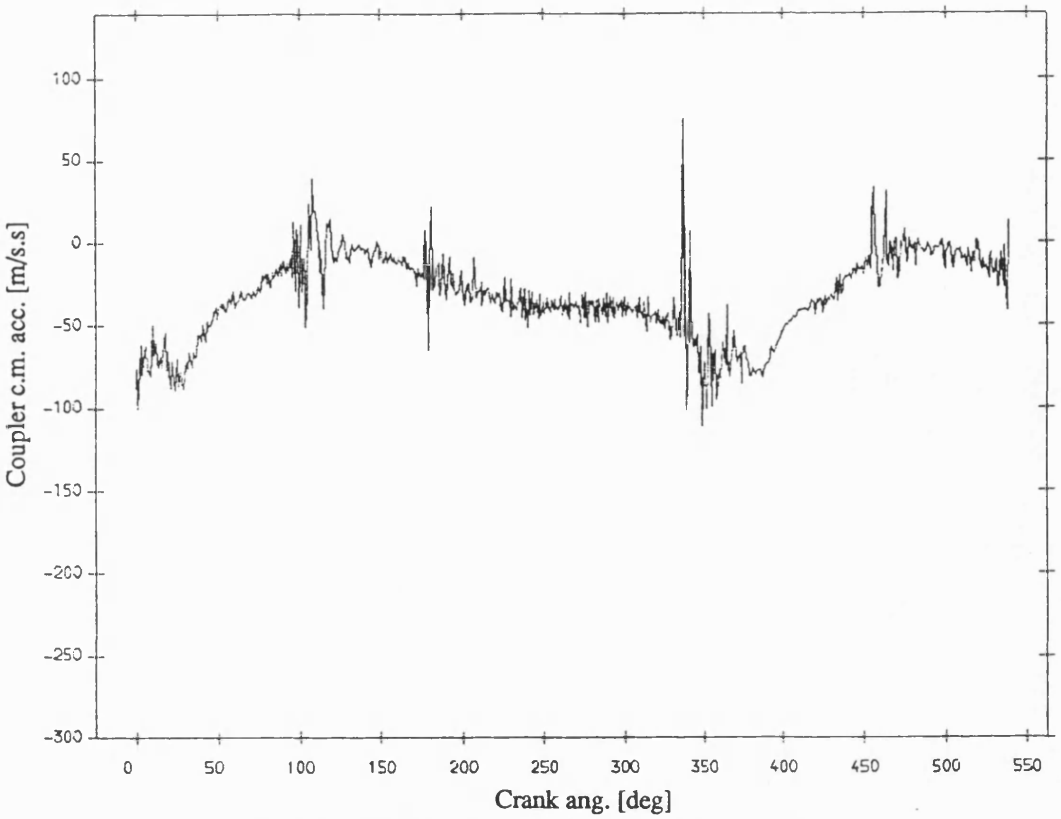

Fig 8.3.98 Exp. result coupler acceleration , normal bearing
with fly wheel ;mean speed=290 rev/min ; dia. clearance=.20mm

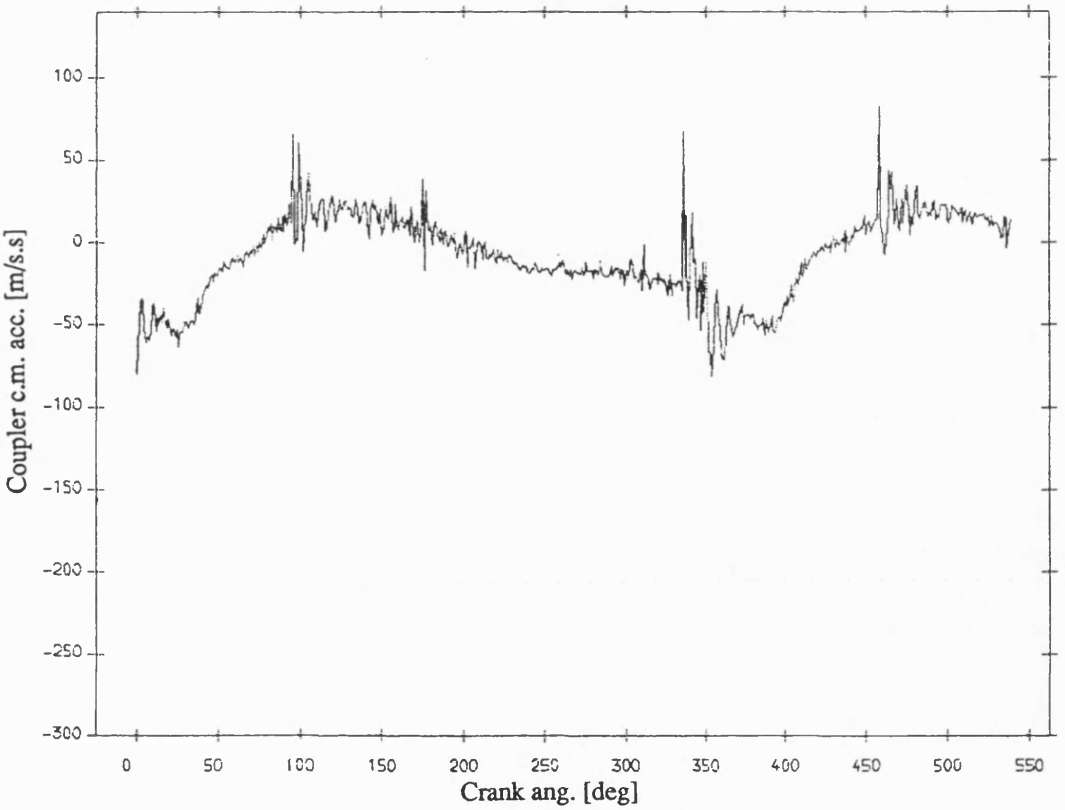

Fig 8.3.99 Exp. result coupler acceleration , normal bearing
no fly wheel ;mean speed=290 rev/min ; dia. clearance=.20mm

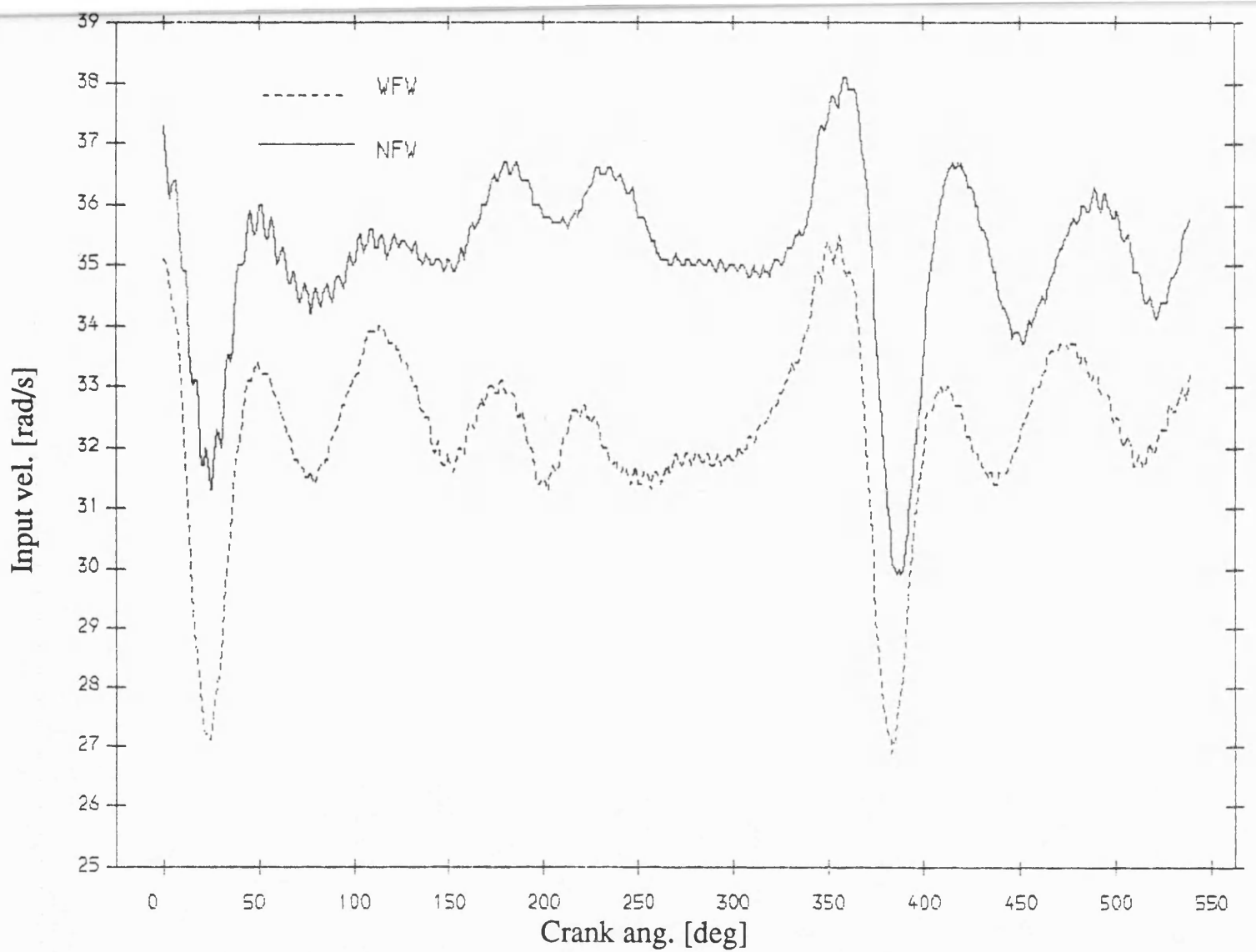

Fig 8.3.100 Exp. result input velocity , normal bearing
mean speed=327 rev/min; dia. clearance=.20mm

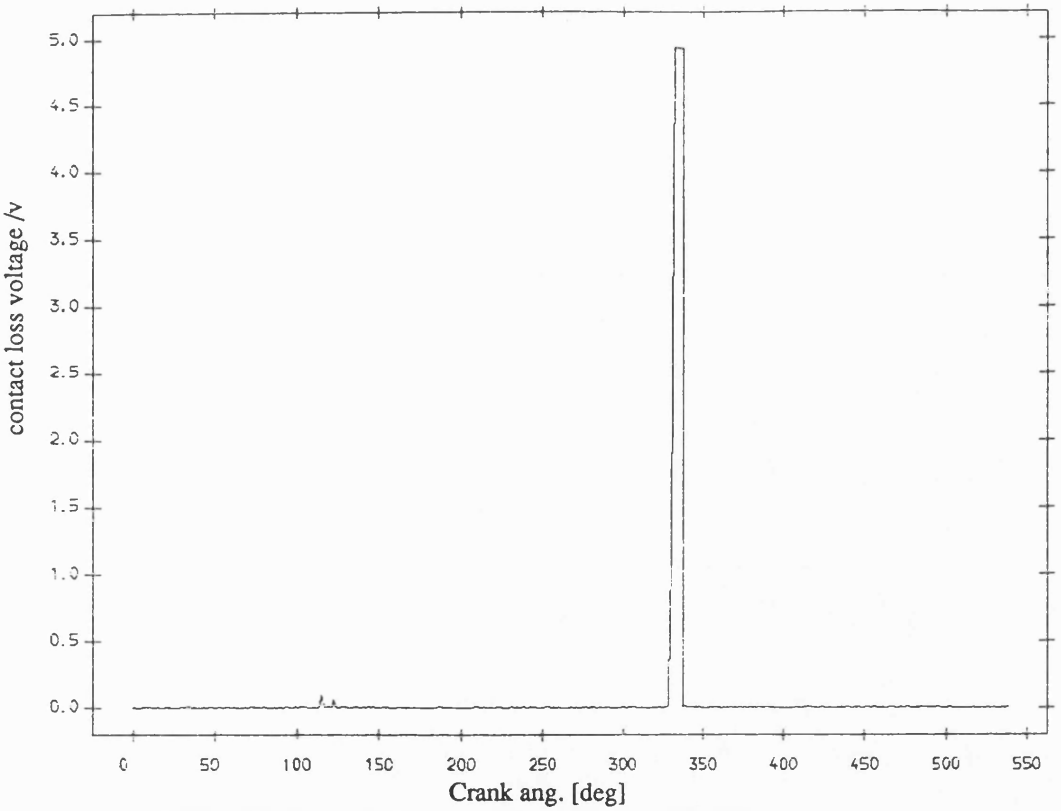

Fig 8.3.102 Exp. result contact loss of pin and normal bearing
no flywheel ;mean speed=327 rev/min ;dia. clearance=0.20mm

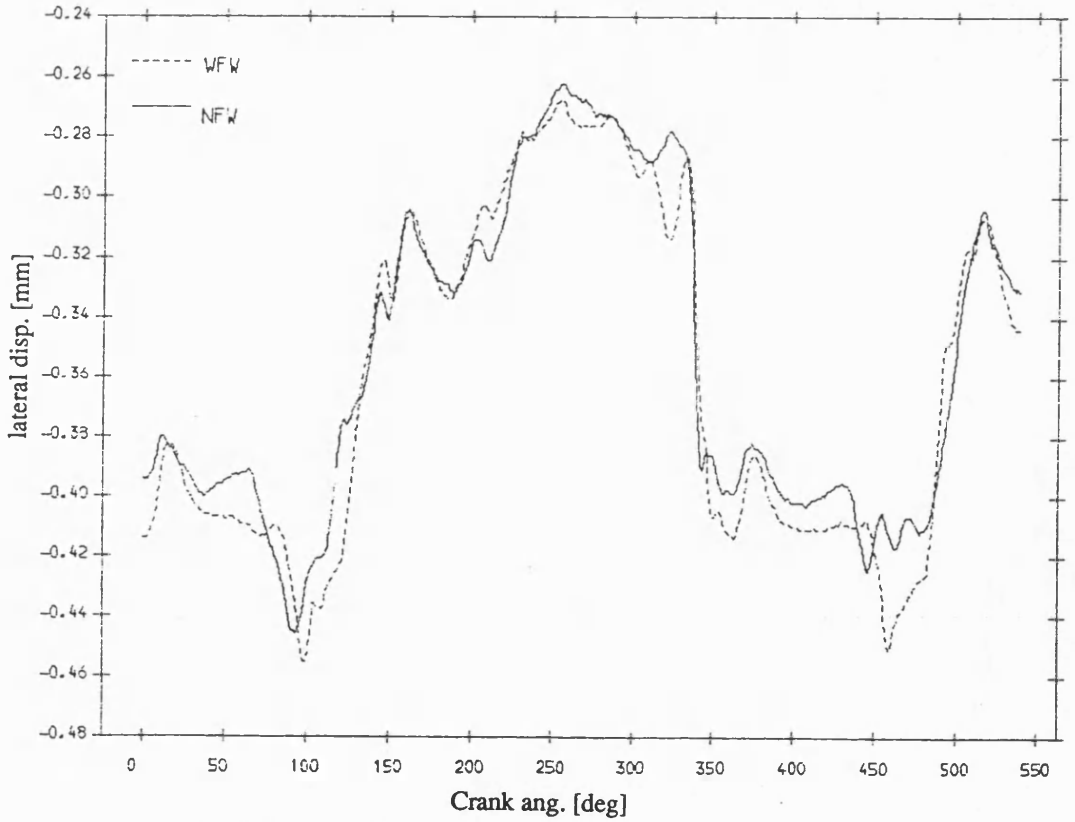

Fig 8.3.104 Exp. result lateral disp. of pin , normal bearing
mean speed=327 rev/min; dia. clearance=.20mm

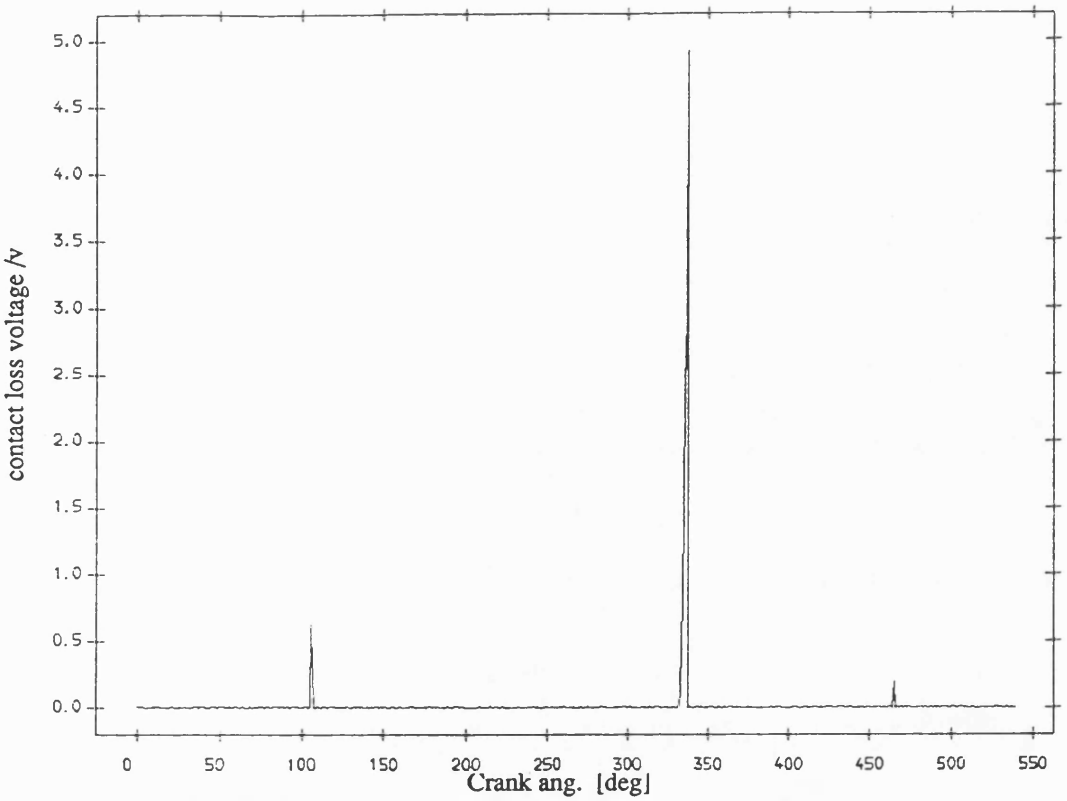

Fig 8.3.101 Exp. result contact loss of pin and normal bearing
with flywheel ;mean speed=327 rev/min ;dia. clearance=0.20mm

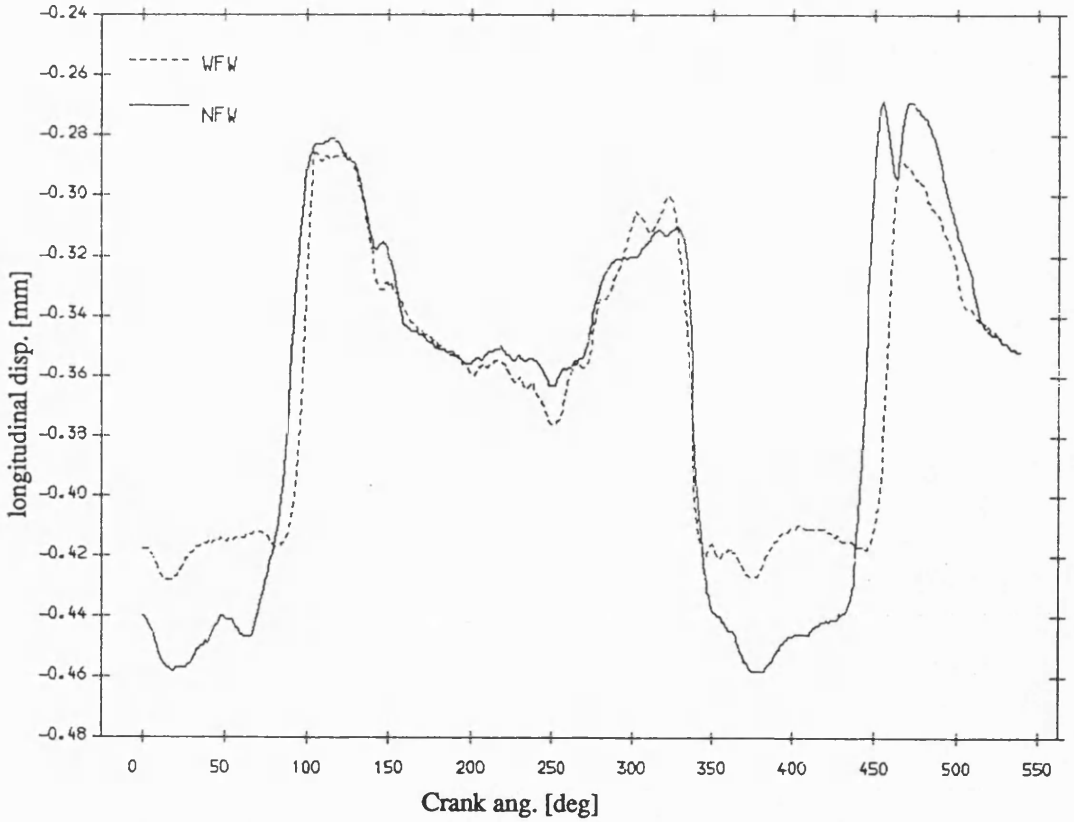

Fig 8.3.103 Exp. result longitudinal disp. of pin , normal bearing
mean speed=327 rev/min; dia. clearance=.20mm

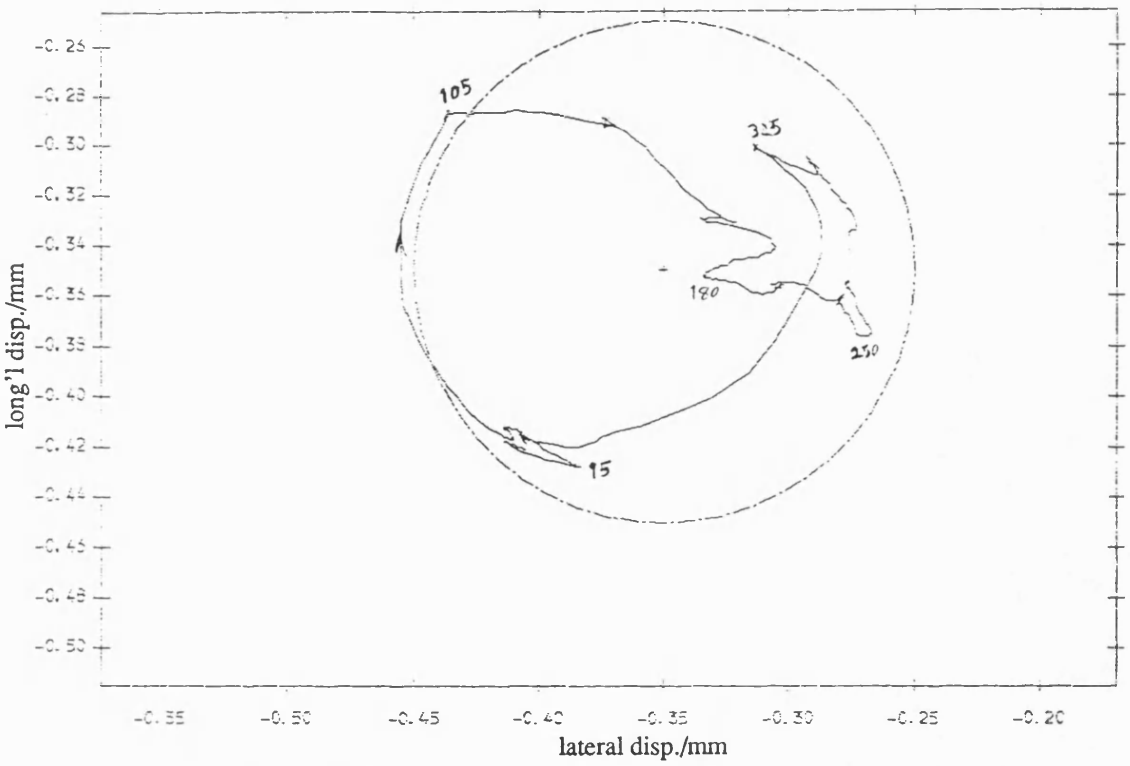

Fig 8.3.105 Exp. result polar plot of relative disp. of pin in normal bearing with fly wheel ;mean speed=327 rev/min ; dia. clearance=.20mm

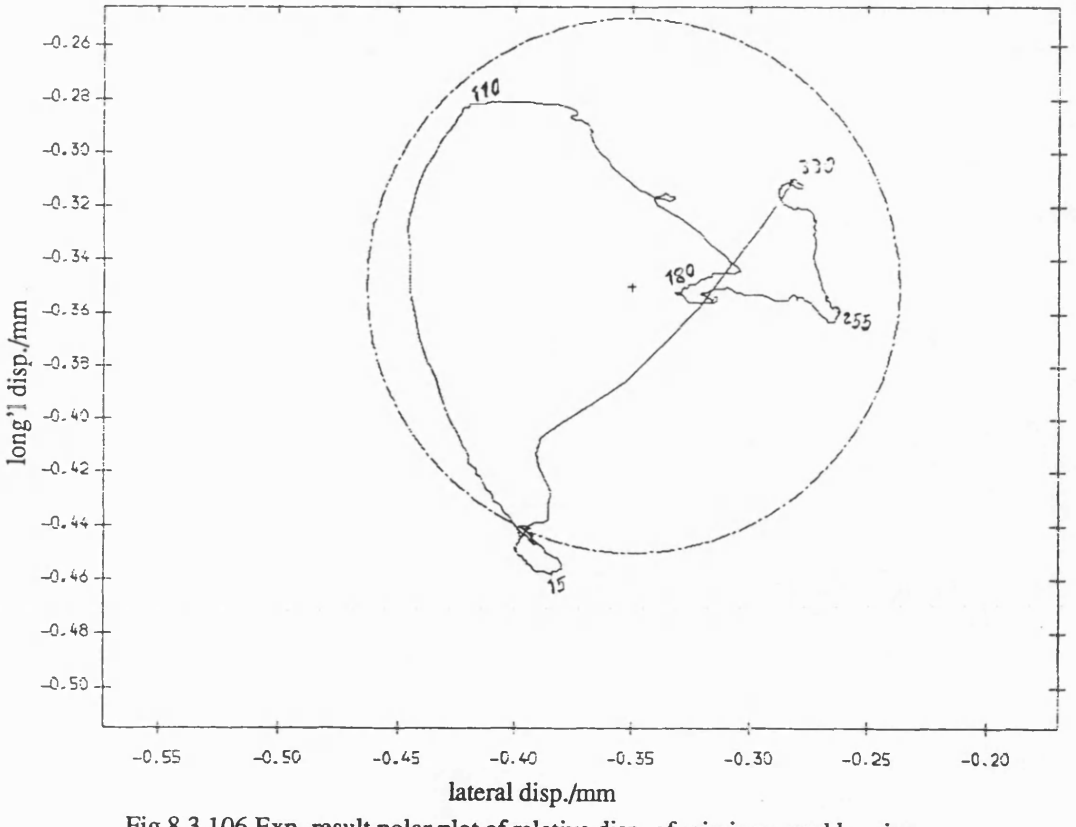

Fig 8.3.106 Exp. result polar plot of relative disp. of pin in normal bearing no fly wheel ;mean speed=327 rev/min ; dia. clearance=.20mm

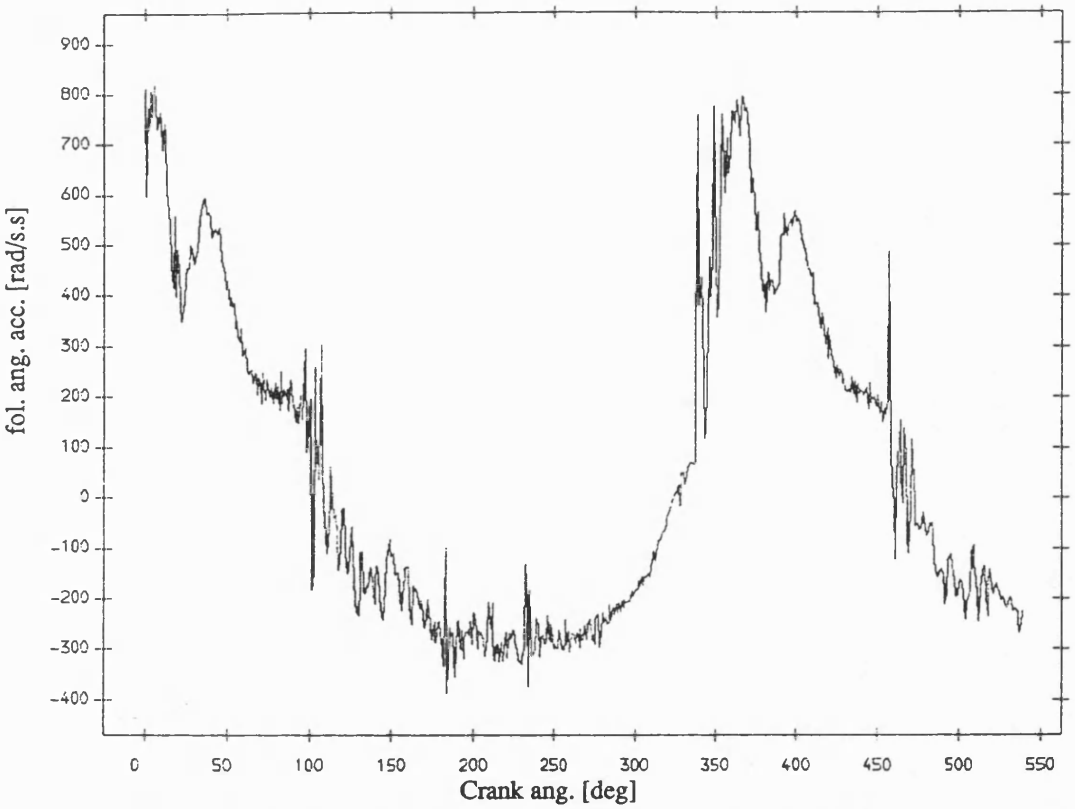

Fig 8.3.107 Exp. result follower ang. acceleration , normal bearing
with fly wheel ;mean speed=327 rev/min ; dia. clearance=.20mm

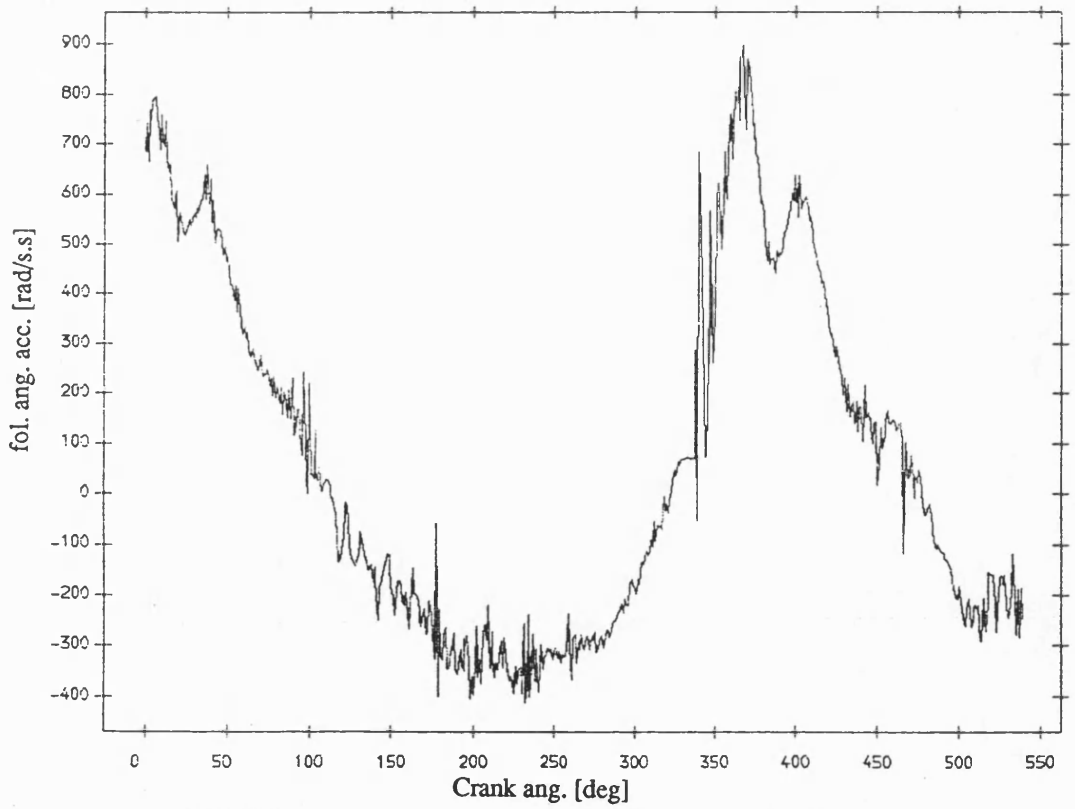

Fig 8.3.108 Exp. result follower ang. acceleration , normal bearing
no fly wheel ;mean speed=327 rev/min ; dia. clearance=.20mm

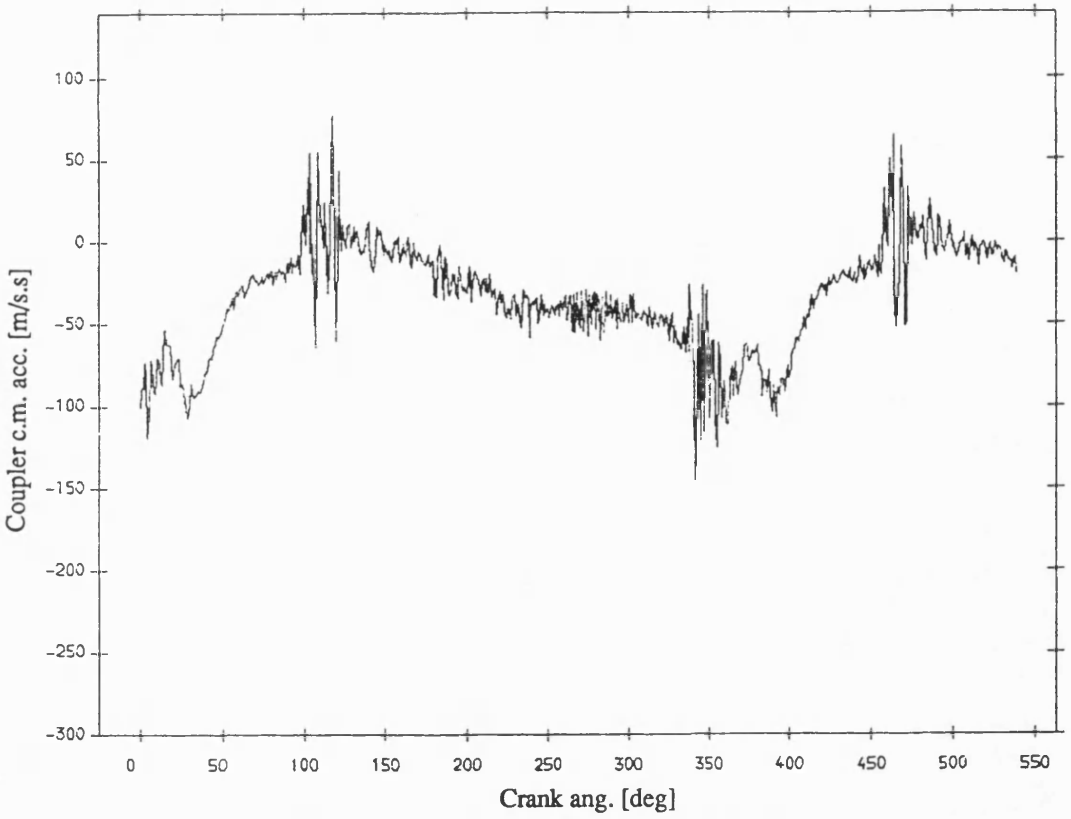

Fig 8.3.109 Exp. result coupler acceleration , normal bearing
with fly wheel ;mean speed=327 rev/min ; dia. clearance=.20mm

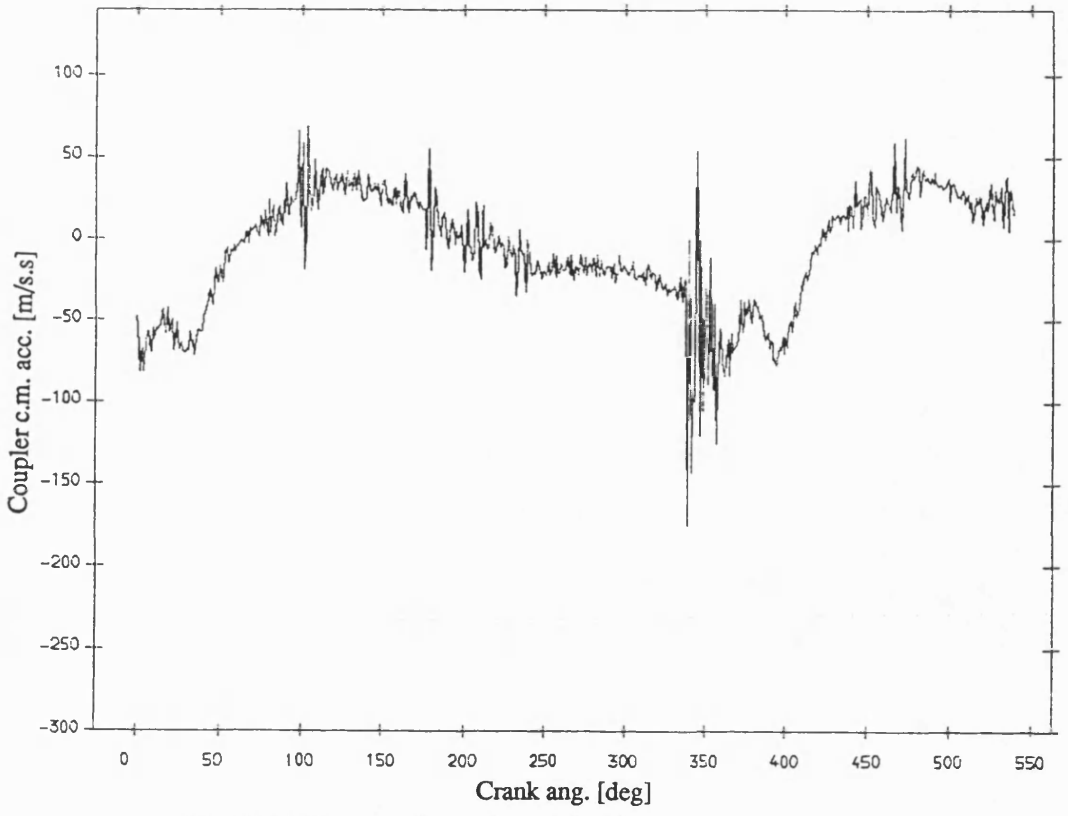

Fig 8.3.110 Exp. result coupler acceleration , normal bearing
no fly wheel ;mean speed=327 rev/min ; dia. clearance=.20mm

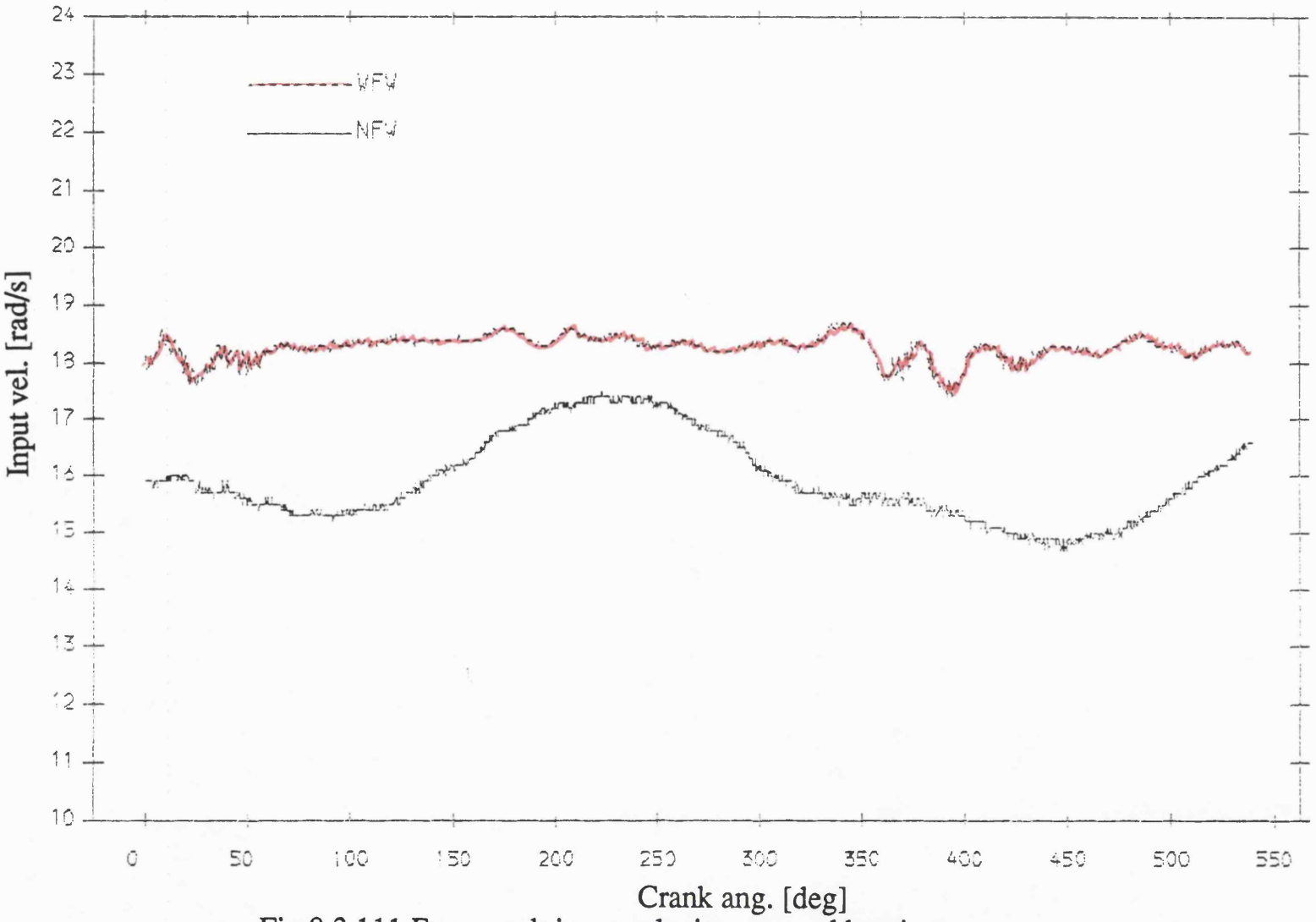

Fig 8.3.111 Exp. result input velocity , normal bearing
mean speed=168 rev/min; dia. clearance=.15mm

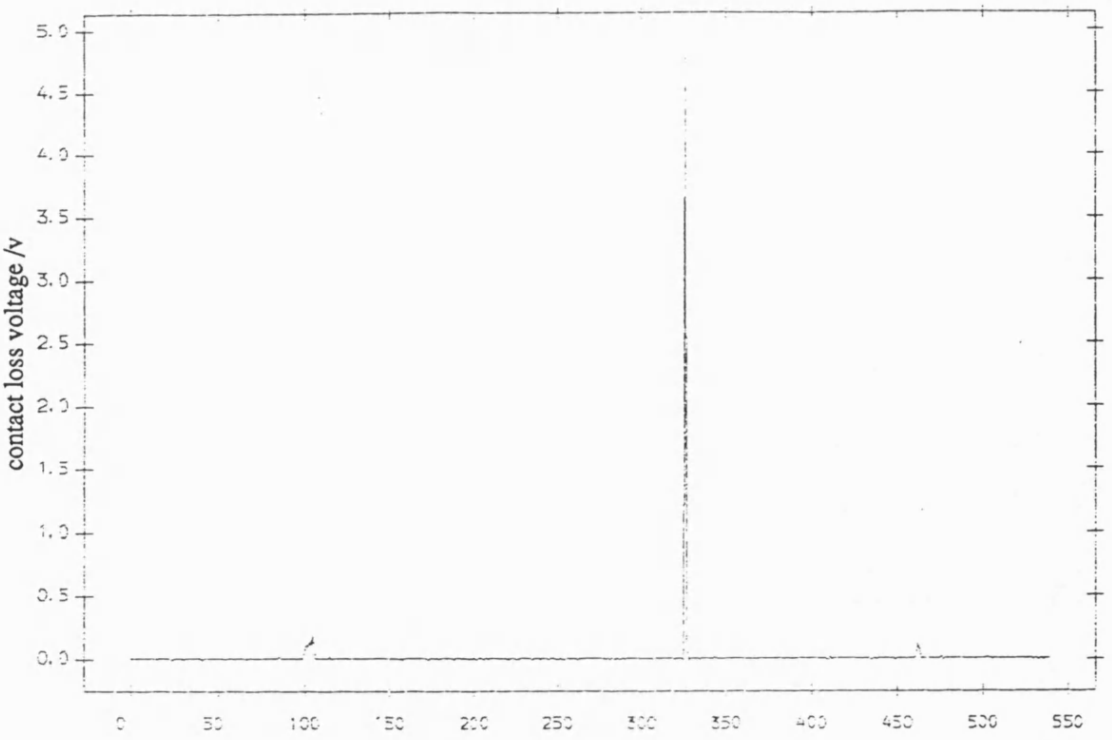

Fig 8.3.112 Exp. result contact loss of pin and normal bearing
with flywheel ;mean speed=168 rev/min ;dia. clearance=0.15mm

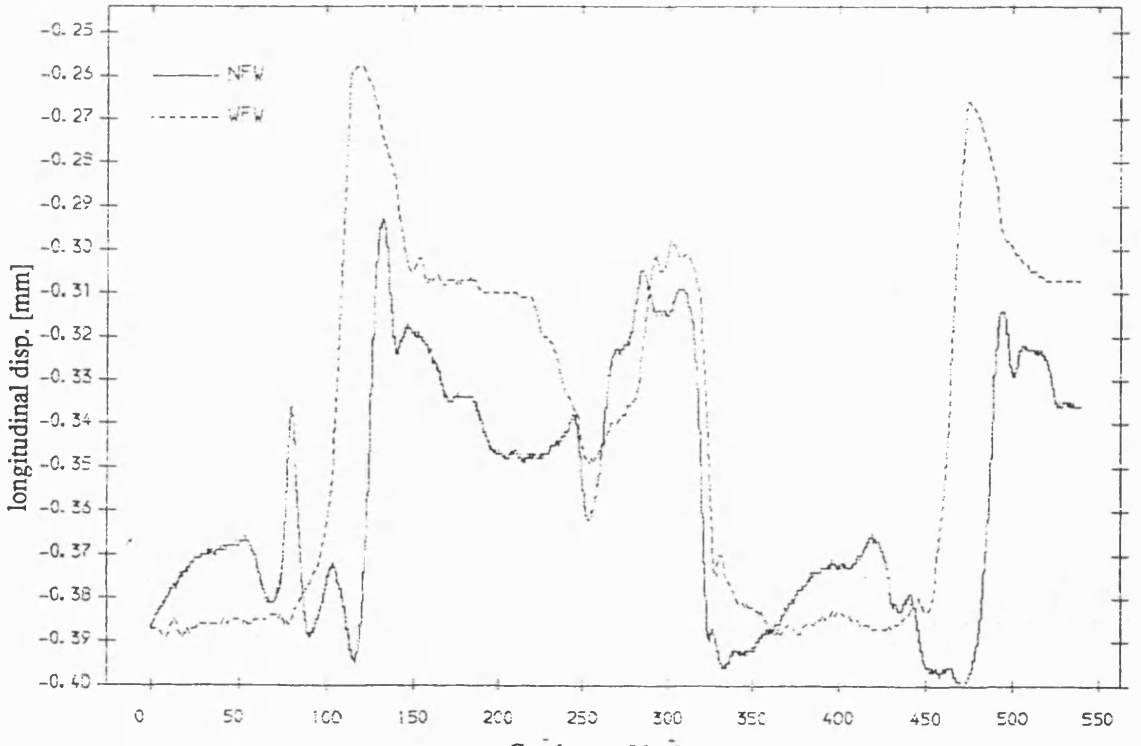

Fig 8.3.114 Exp. result longitudinal disp. of pin , normal bearing
mean speed=168 rev/min; dia. clearance=.15mm

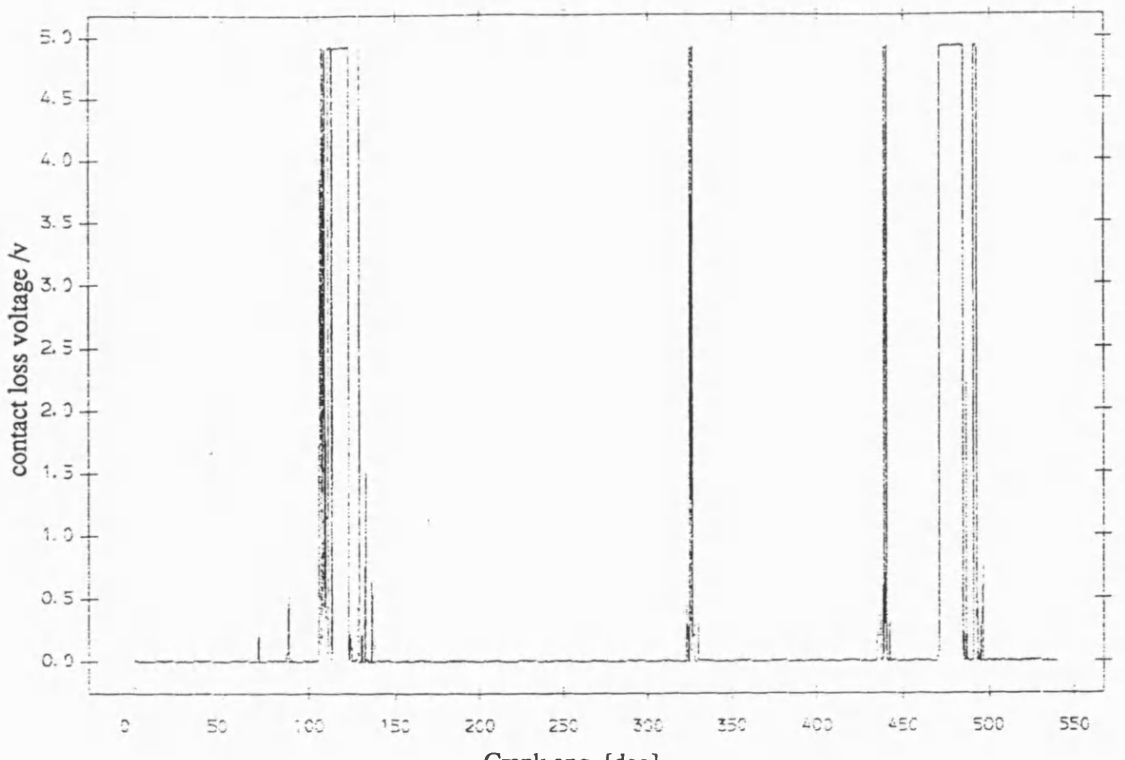

Fig 8.3.113 Exp. result contact loss of pin and normal bearing
no flywheel ;mean speed=168 rev/min ;dia. clearance=0.15mm

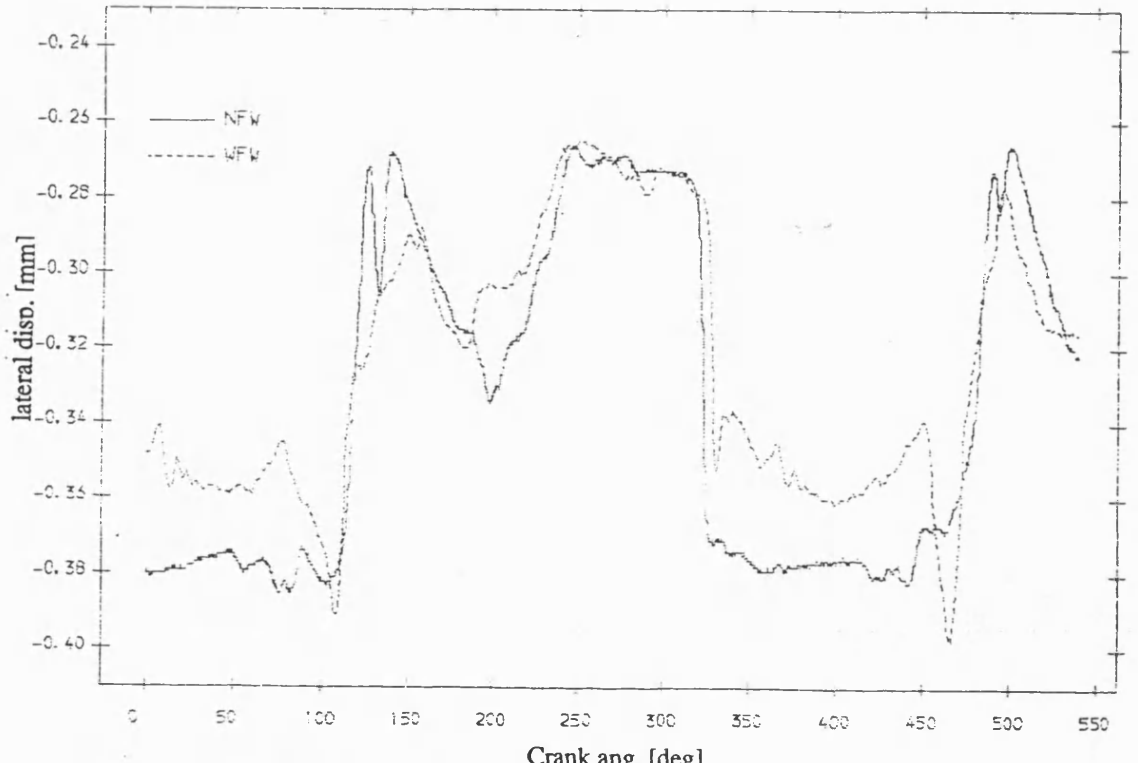

Fig 8.3.115 Exp. result lateral disp. of pin , normal bearing
mean speed=168 rev/min; dia. clearance=.15mm

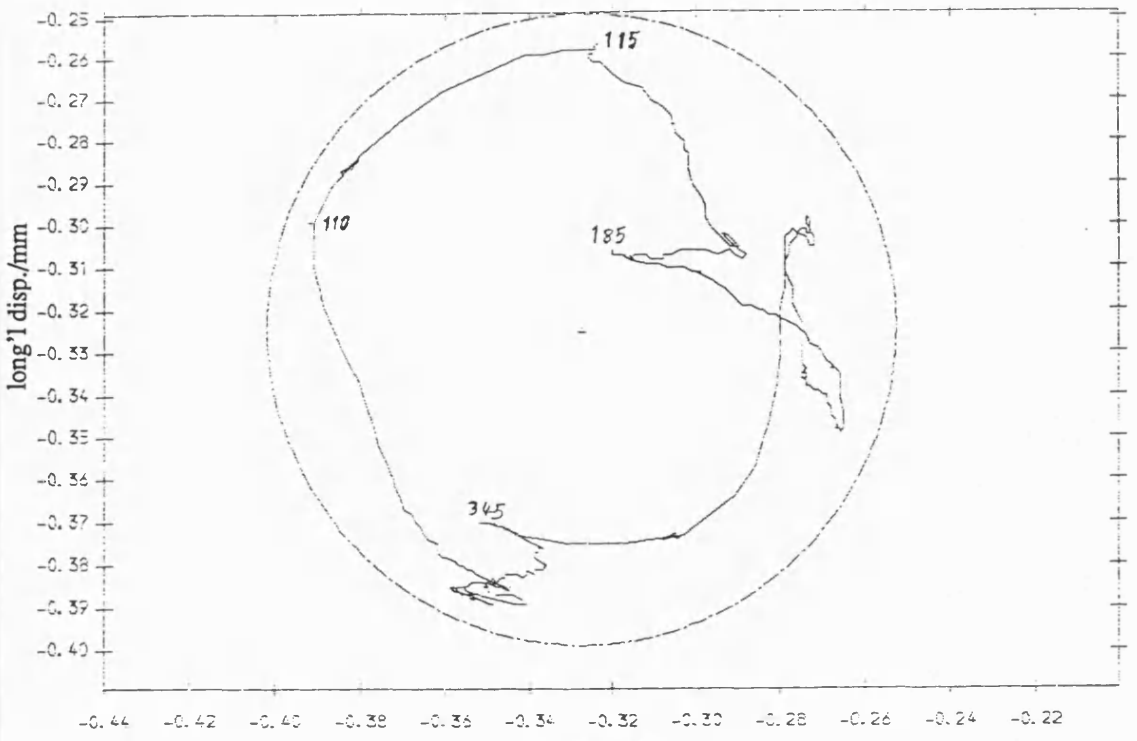

Fig 8.3.116 Exp. result polar plot of relative disp. of pin in normal bearing with fly wheel ;mean speed=168 rev/min ; dia. clearance=.15mm

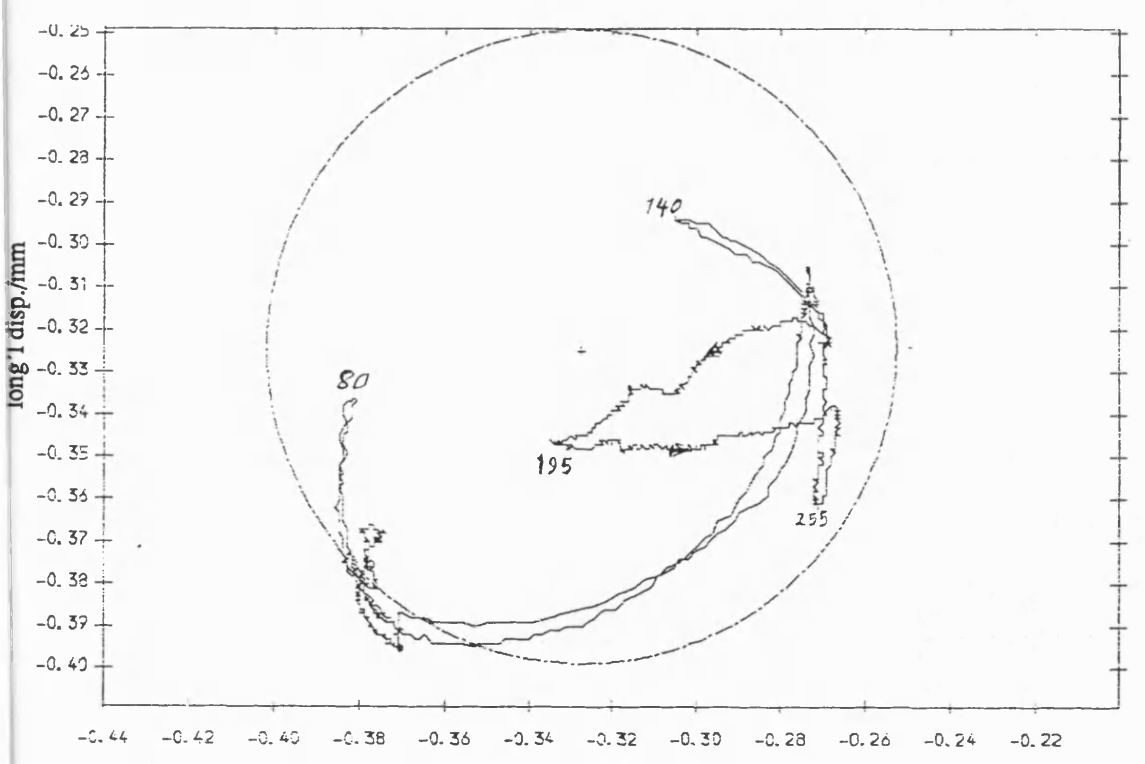

Fig 8.3.117 Exp. result polar plot of relative disp. of pin in normal bearing no fly wheel ;mean speed=168 rev/min ; dia. clearance=.15mm

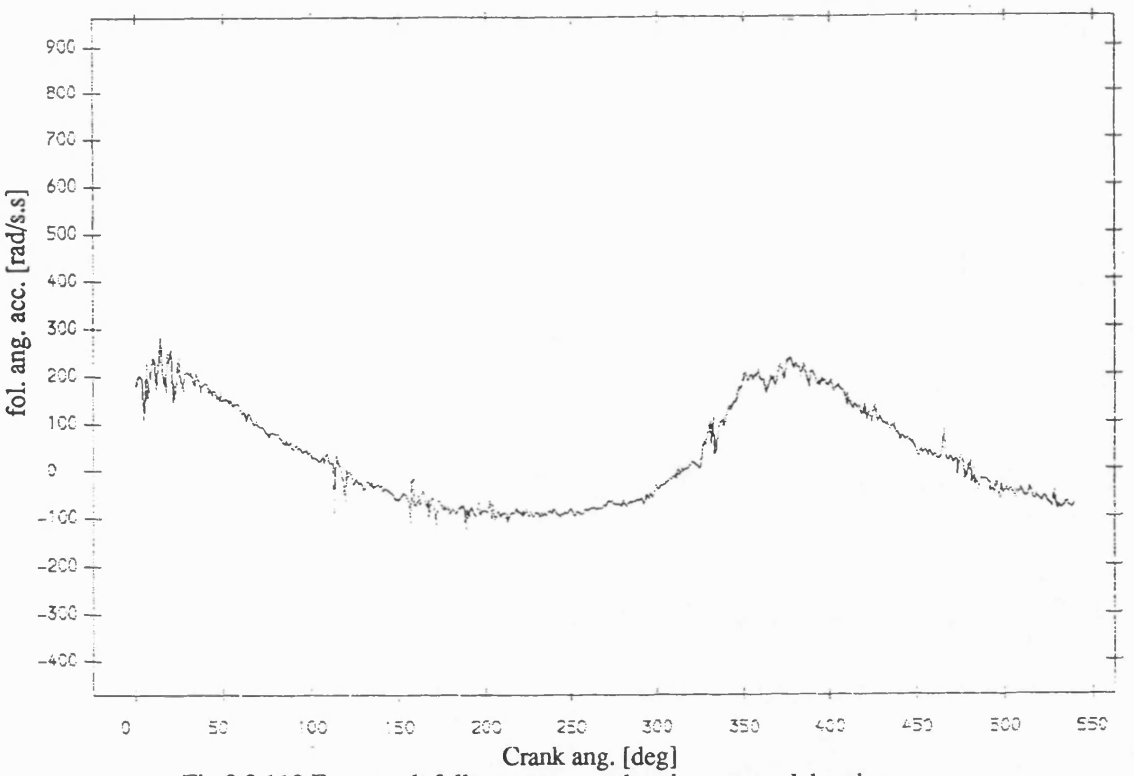

Fig 8.3.118 Exp. result follower ang. acceleration , normal bearing
with fly wheel ;mean speed=168 rev/min ; dia. clearance=.15mm

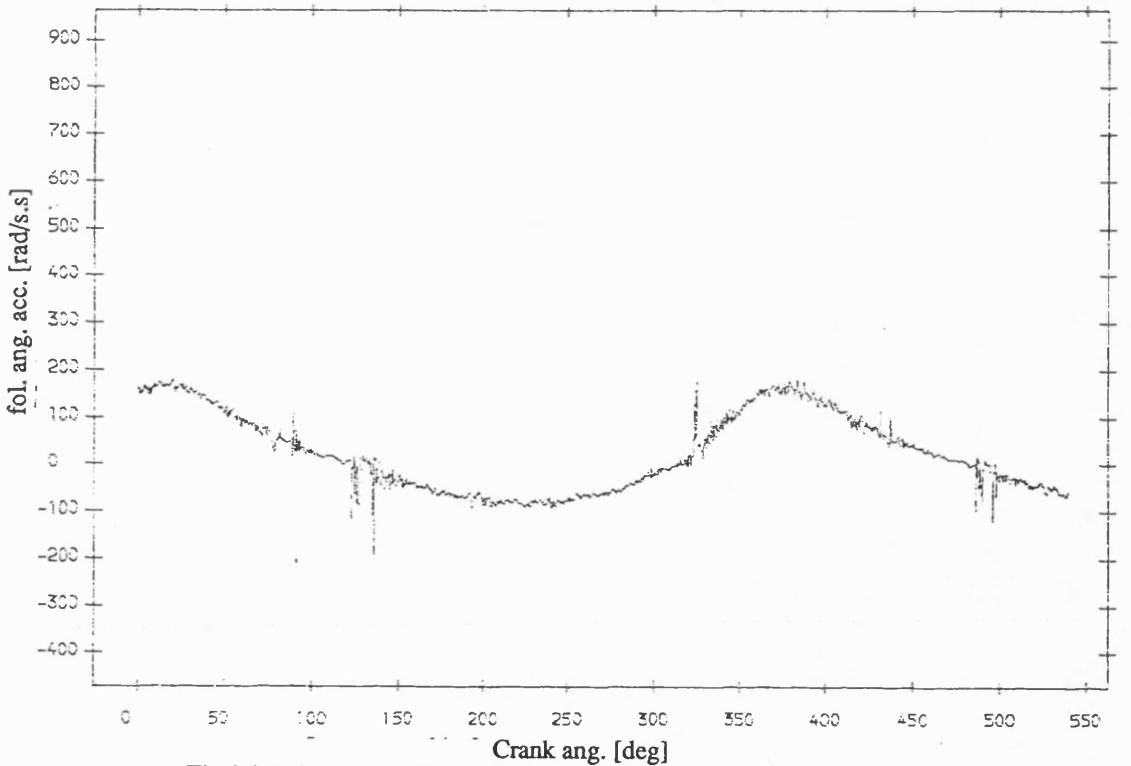

Fig 8.3.119 Exp. result follower ang. acceleration , normal bearing
no fly wheel ;mean speed=168 rev/min ; dia. clearance=.15mm

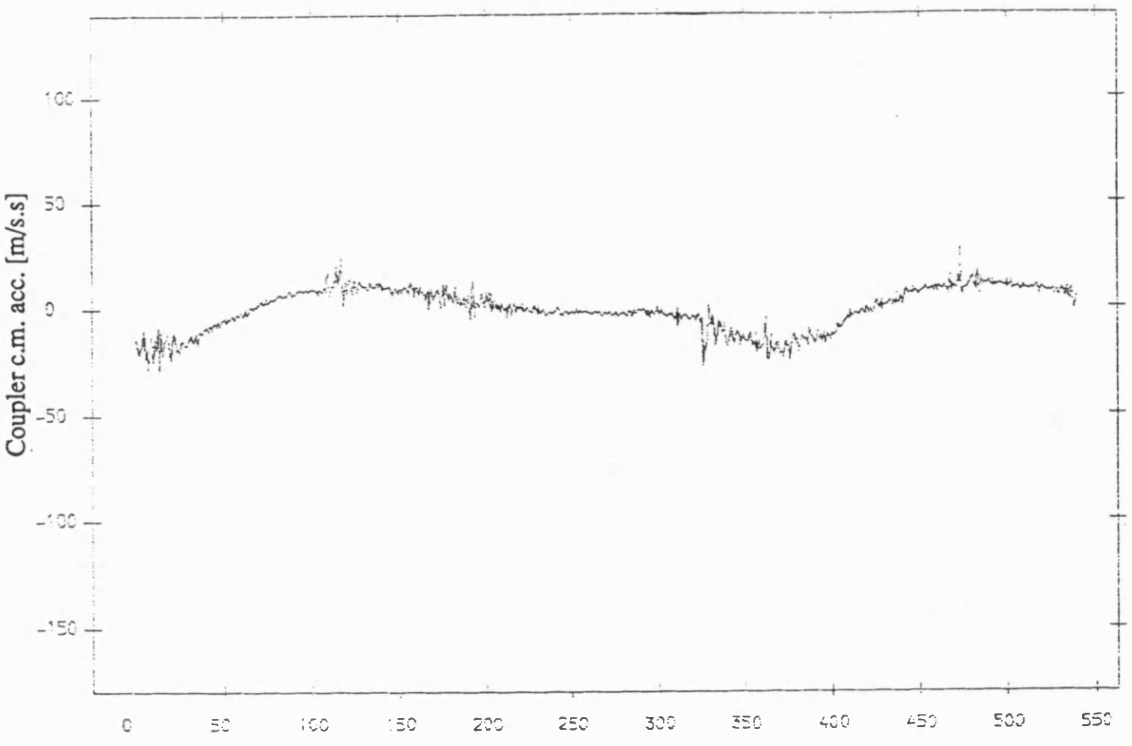

Fig 8.3.120 Exp. result coupler acceleration , normal bearing
with fly wheel ;mean speed=168 rev/min ; dia. clearance=.15mm

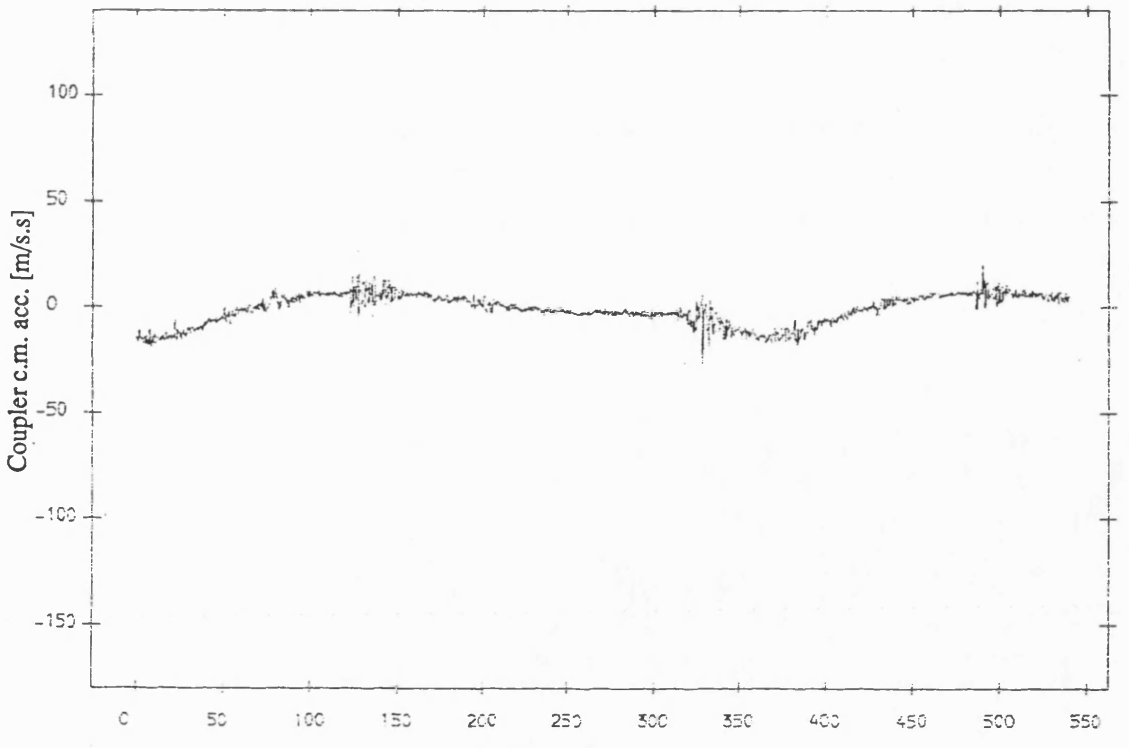

Fig 8.3.121 Exp. result coupler acceleration , normal bearing
no fly wheel ;mean speed=168 rev/min ; dia. clearance=.15mm

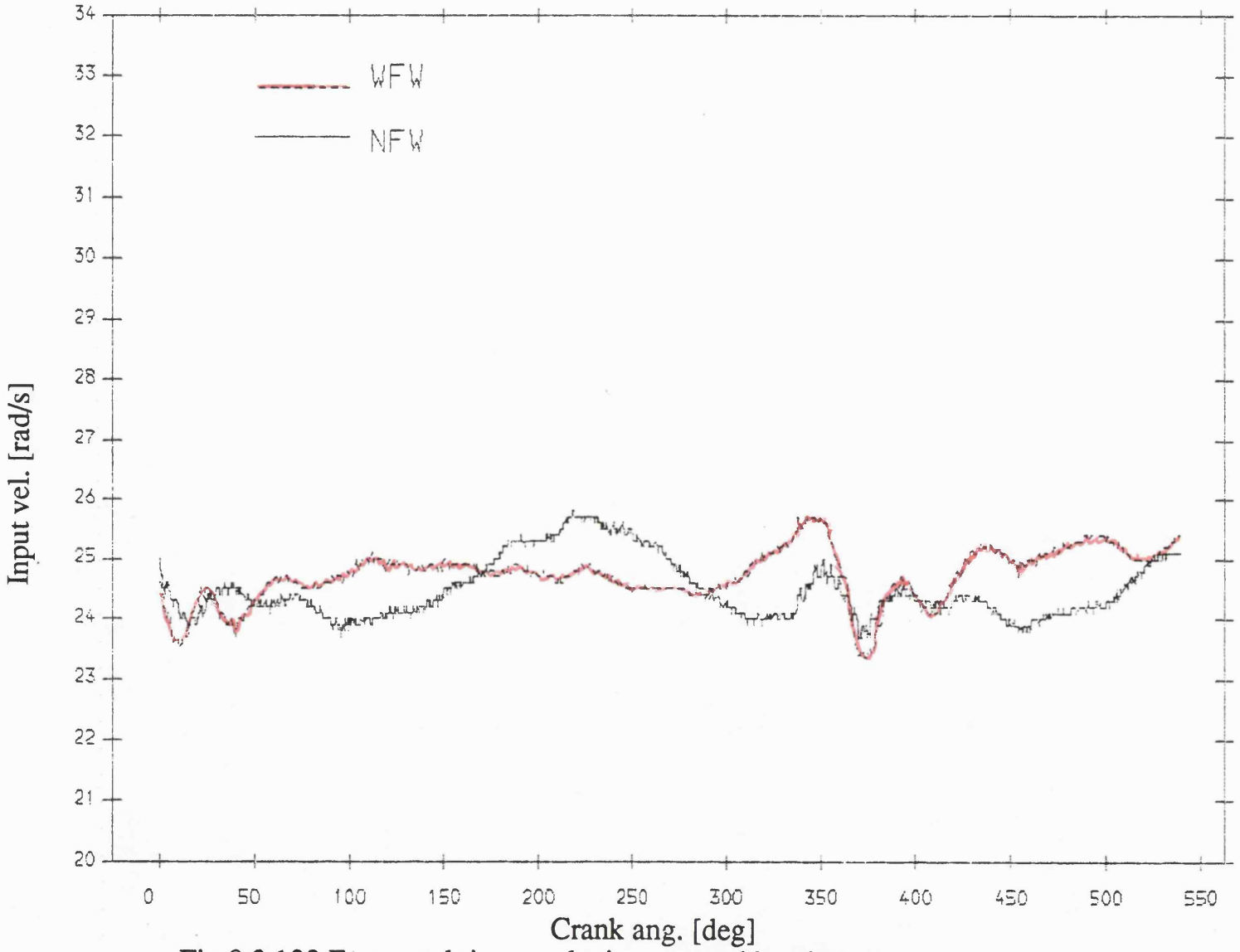

Fig 8.3.122 Exp. result input velocity , normal bearing
mean speed=244 rev/min; dia. clearance=.15mm

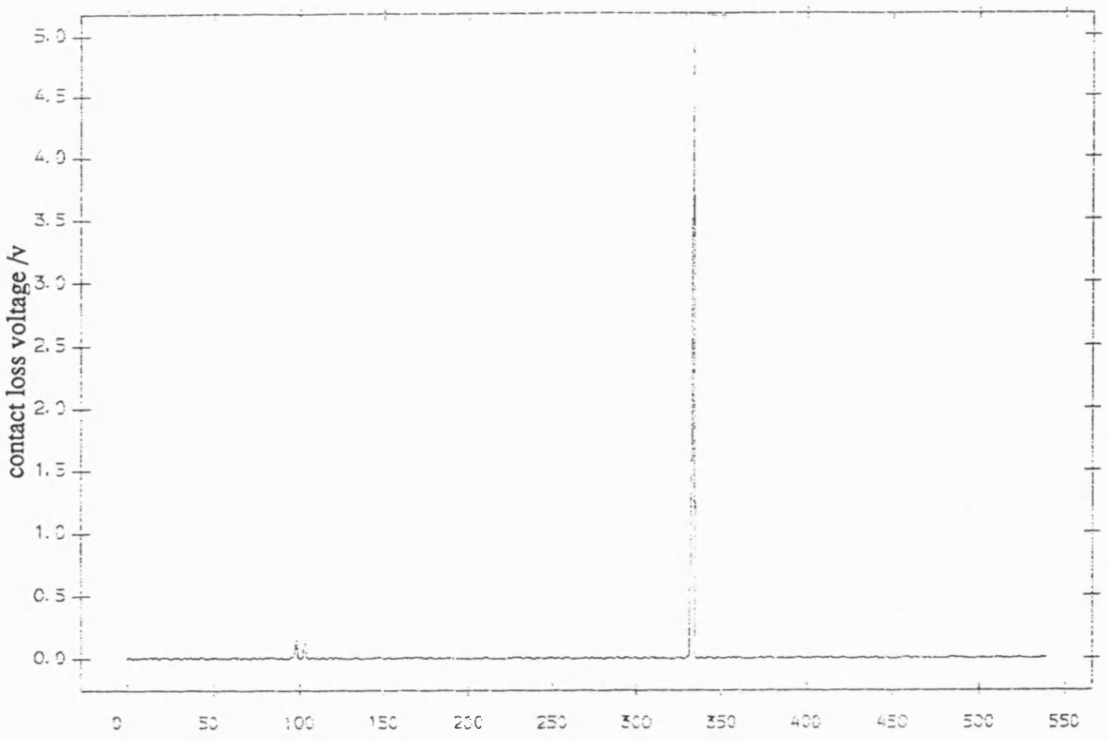

Fig 8.3.123 Exp. result contact loss of pin and normal bearing
with flywheel ;mean speed=244 rev/min ;dia. clearance=0.15mm

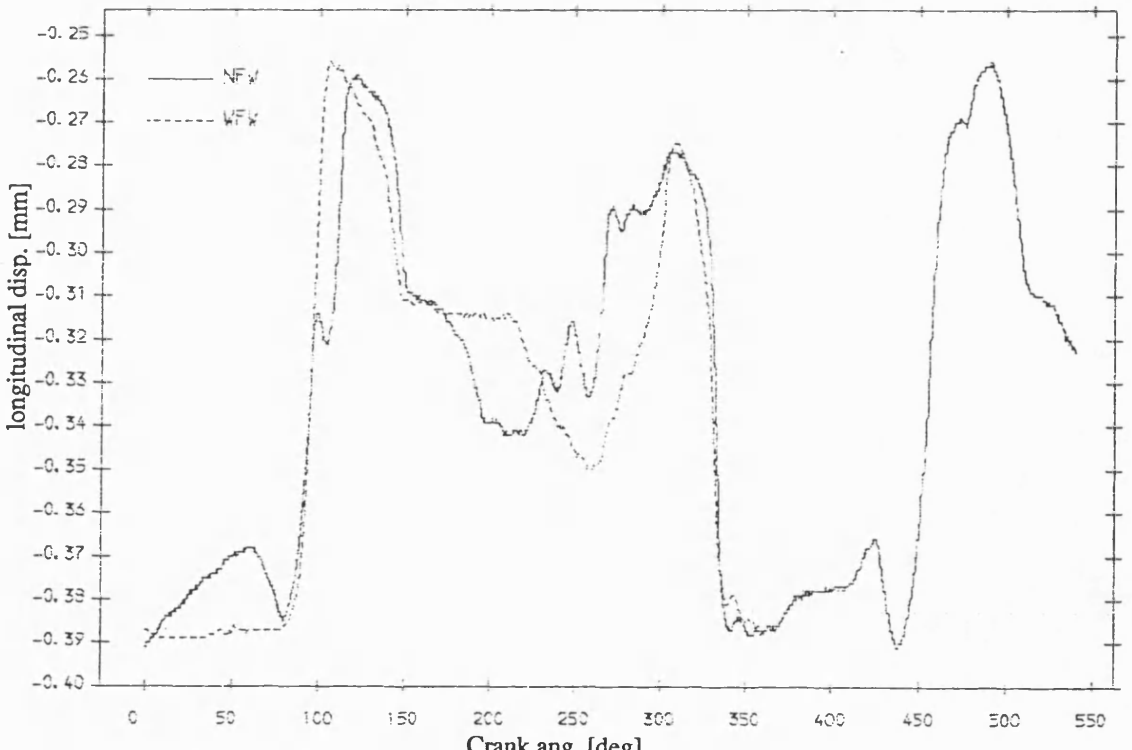

Fig 8.3.125 Exp. result longitudinal disp. of pin , normal bearing
mean speed=244 rev/min; dia. clearance=.15mm

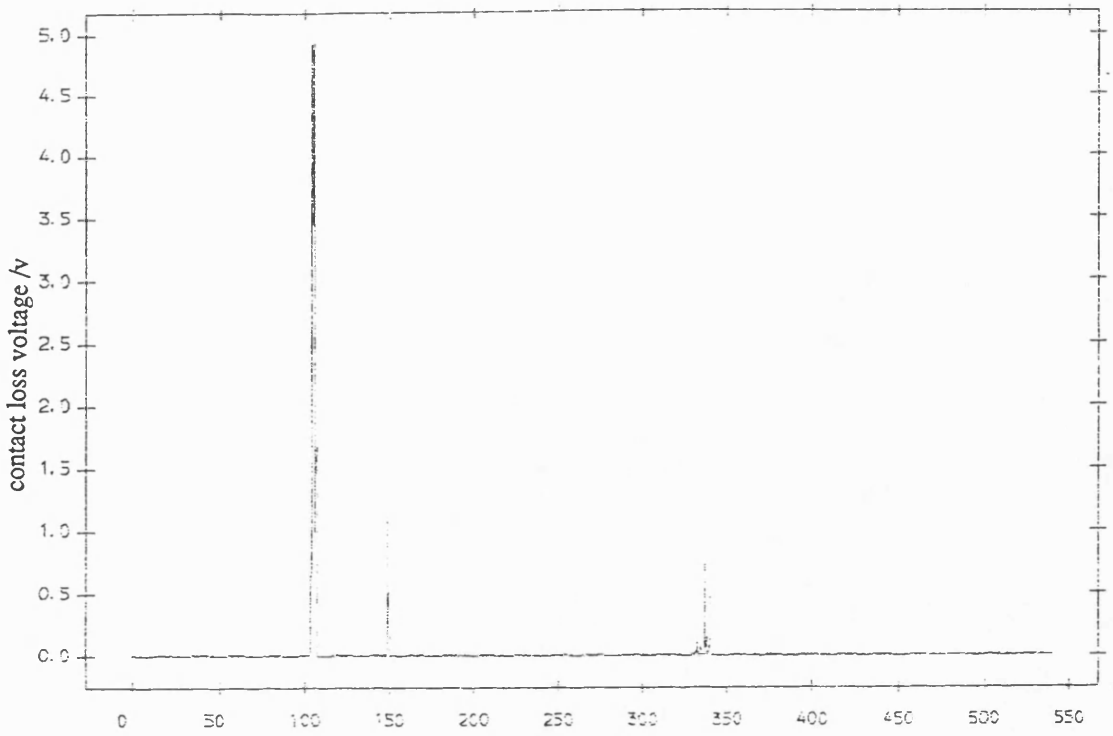

Fig 8.3.124 Exp. result contact loss of pin and normal bearing
no flywheel ;mean speed=244 rev/min ;dia. clearance=0.15mm

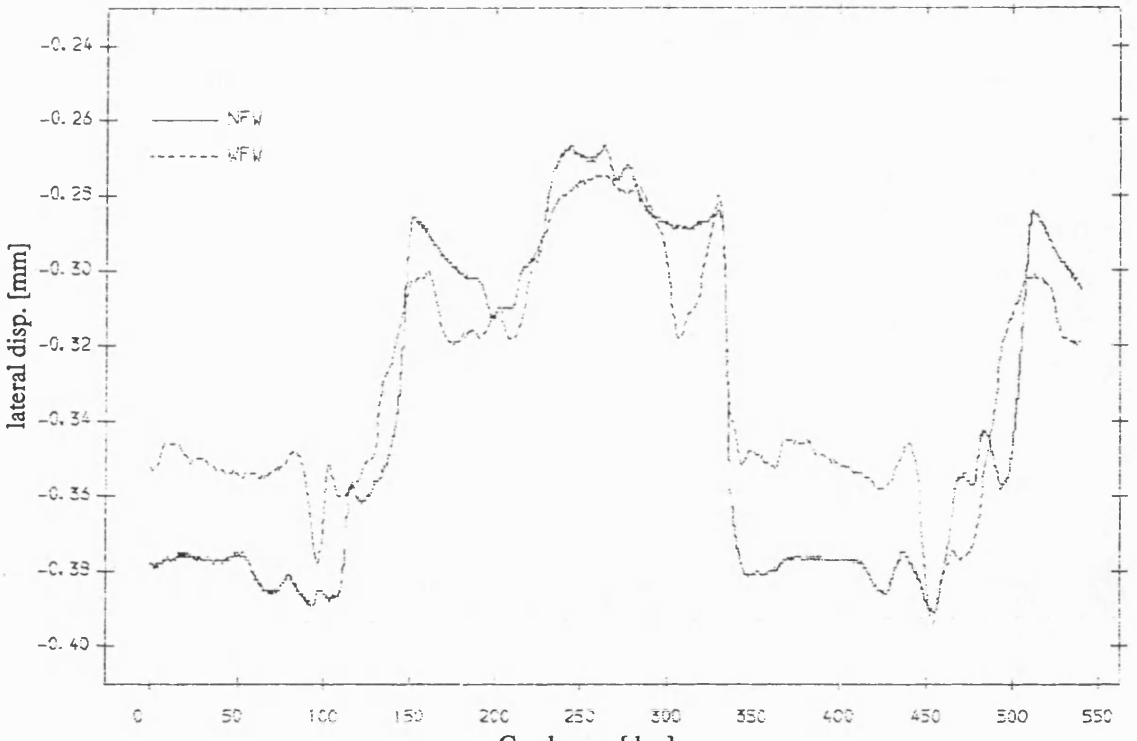

Fig 8.3.126 Exp. result lateral disp. of pin , normal bearing
mean speed=244 rev/min; dia. clearance=.15mm

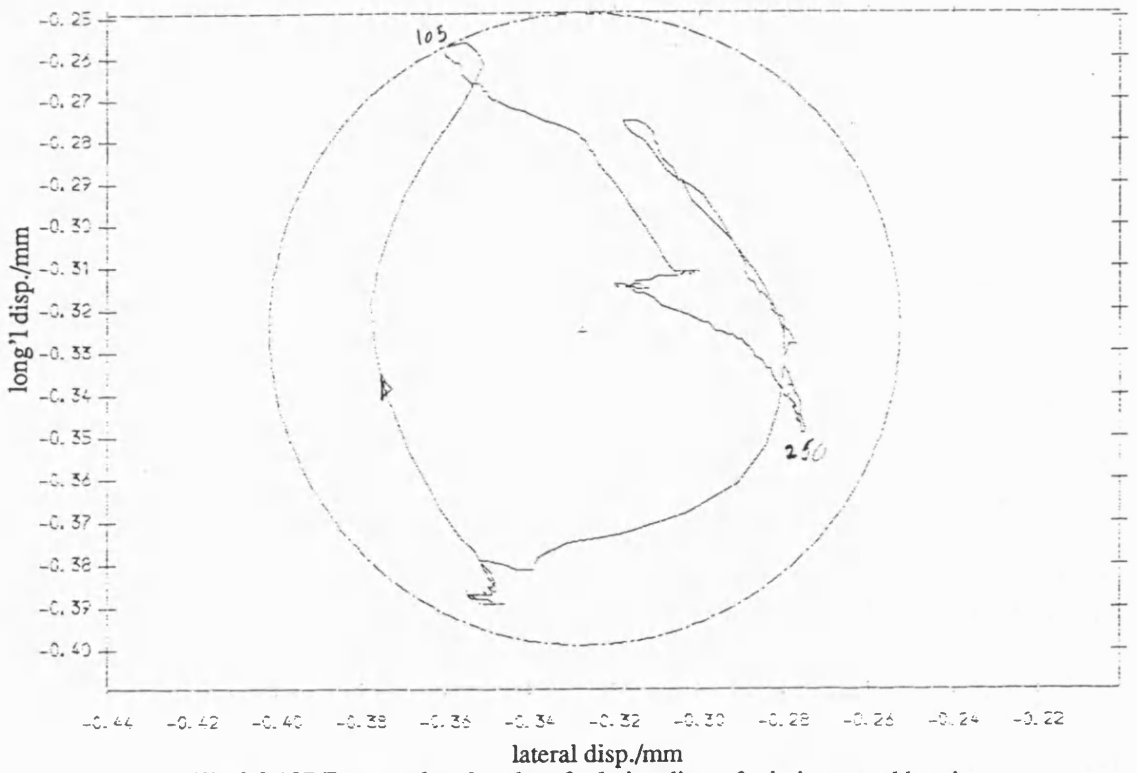

Fig 8.3.127 Exp. result polar plot of relative disp. of pin in normal bearing with fly wheel ;mean speed=244 rev/min ; dia. clearance=.15mm

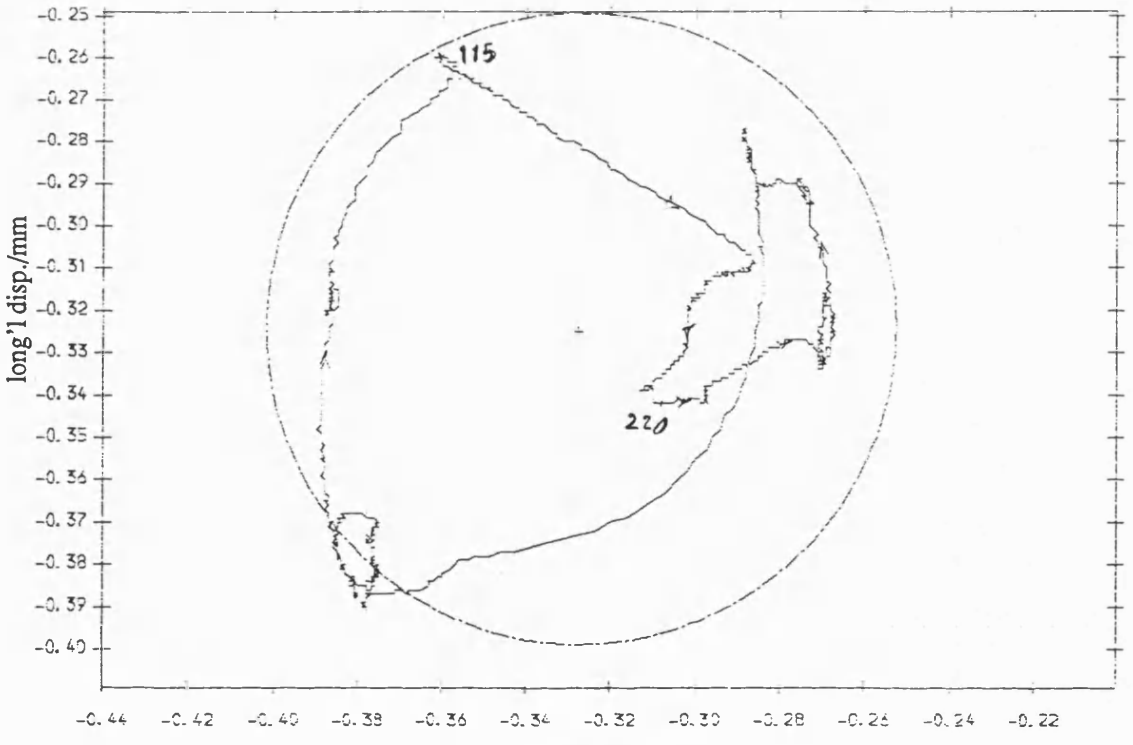

Fig 8.3.128 Exp. result polar plot of relative disp. of pin in normal bearing no fly wheel ;mean speed=244 rev/min ; dia. clearance=.15mm

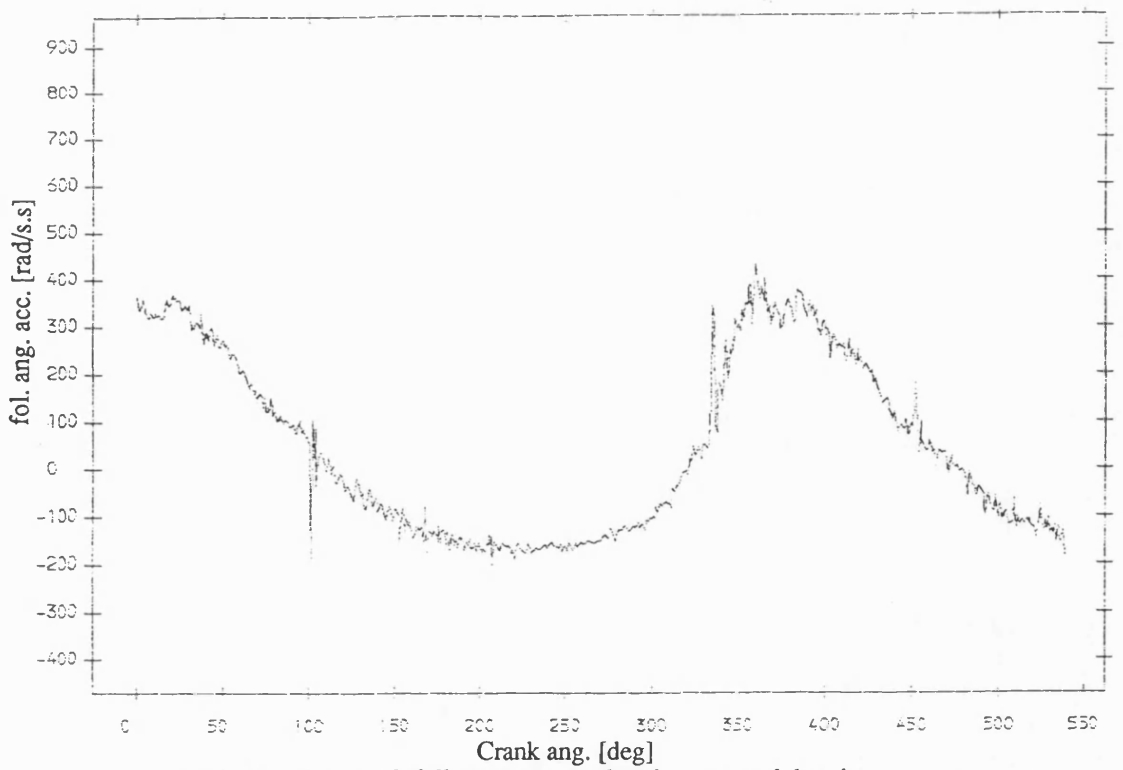

Fig 8.3.129 Exp. result follower ang. acceleration , normal bearing
with fly wheel ;mean speed=244 rev/min ; dia. clearance=.15mm

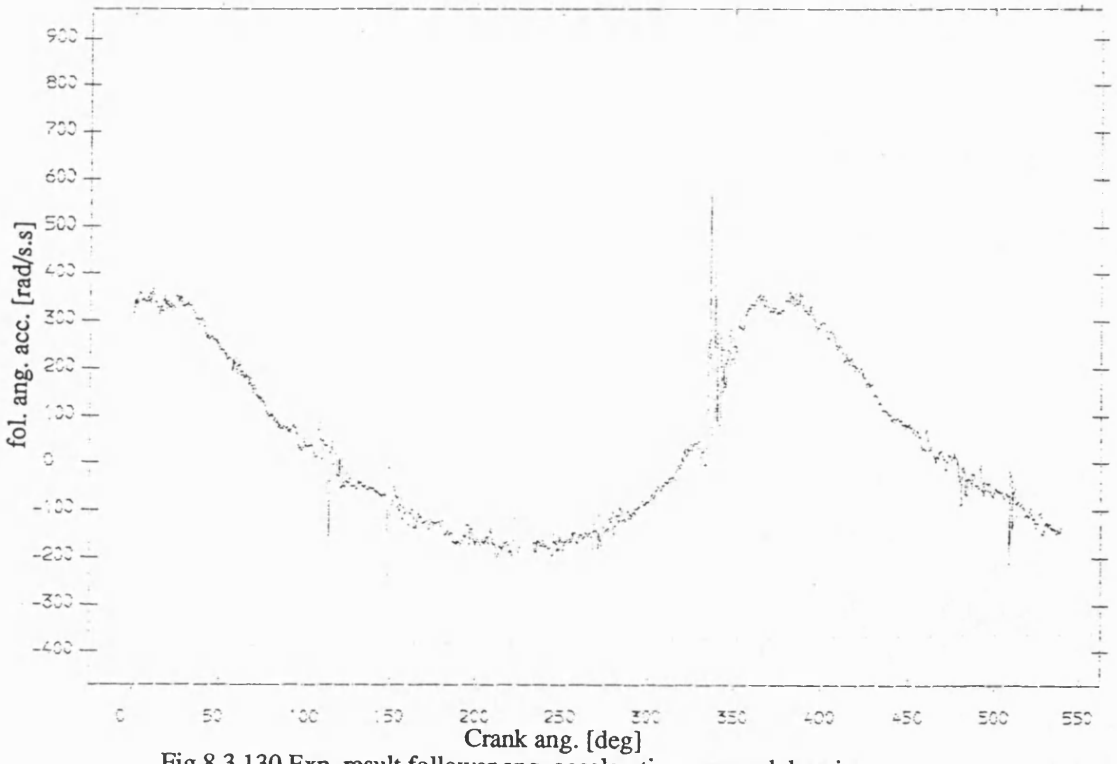

Fig 8.3.130 Exp. result follower ang. acceleration , normal bearing
no fly wheel ;mean speed=244 rev/min ; dia. clearance=.15mm

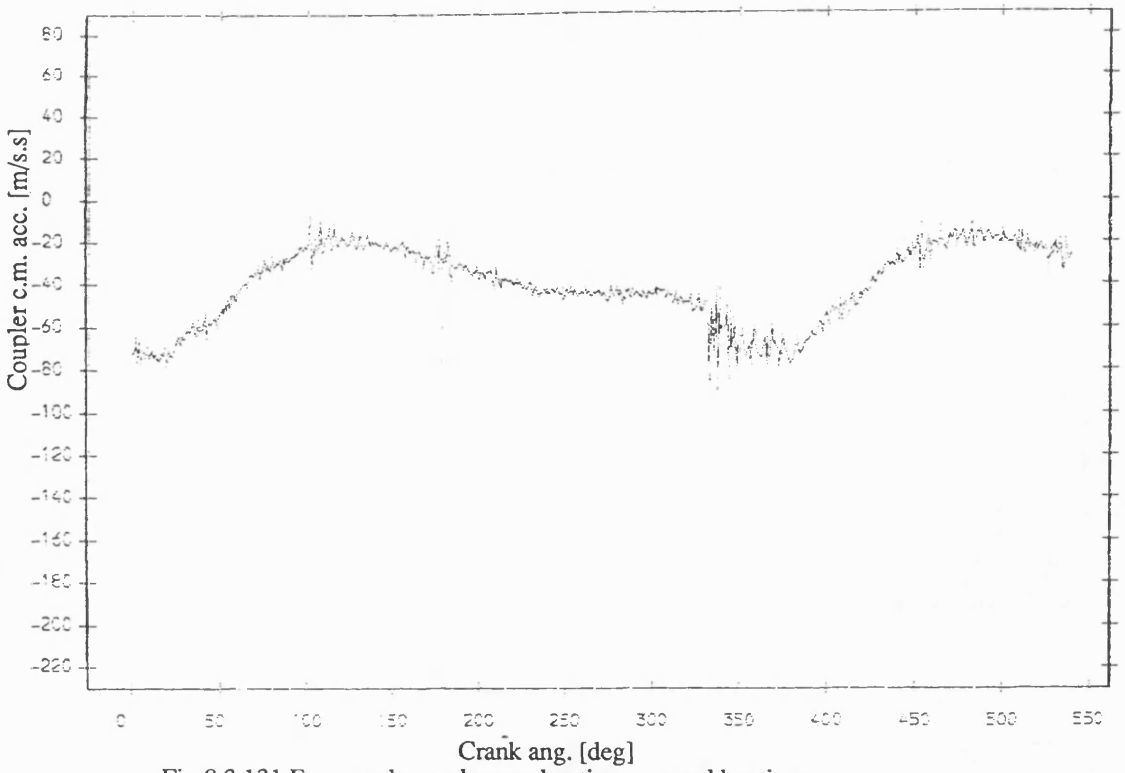

Fig 8.3.131 Exp. result coupler acceleration , normal bearing
with fly wheel ;mean speed=244 rev/min ; dia. clearance=.15mm

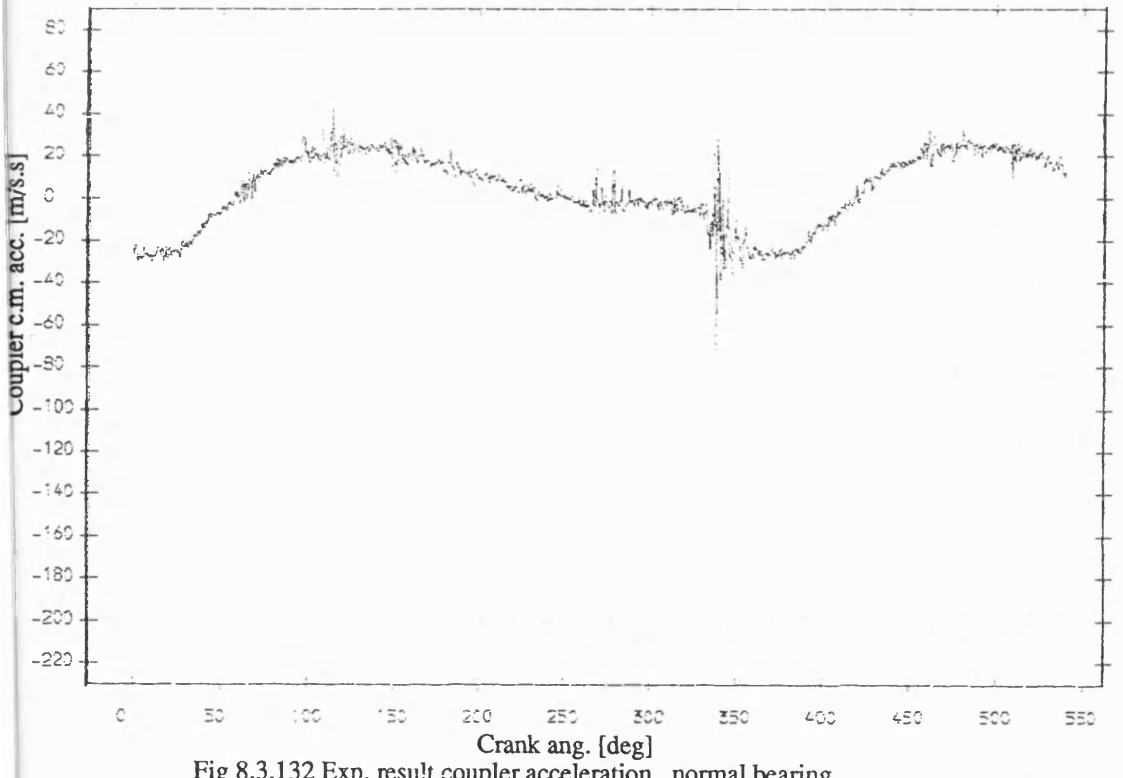

Fig 8.3.132 Exp. result coupler acceleration , normal bearing
no fly wheel ;mean speed=244 rev/min ; dia. clearance=.15mm

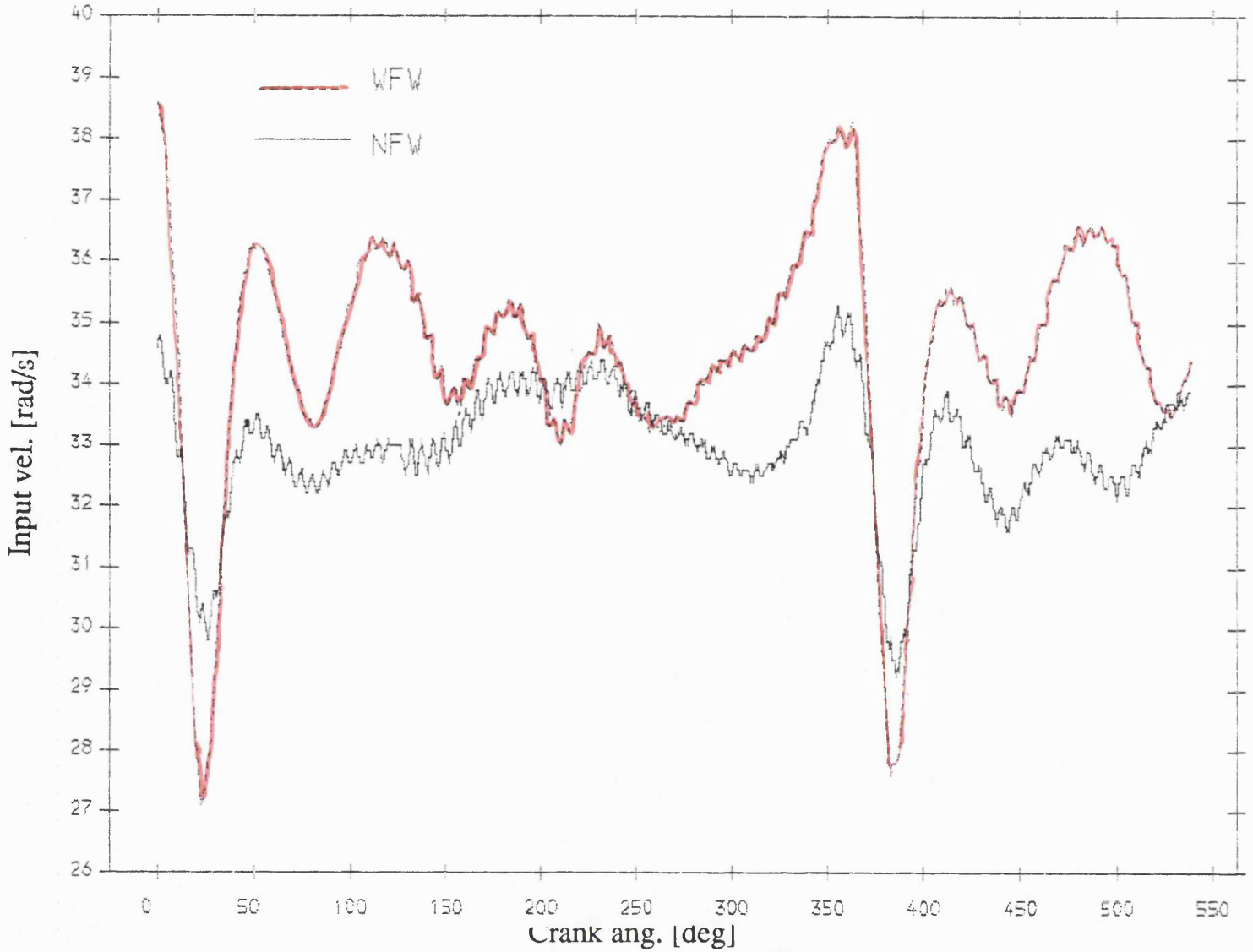

Fig 8.3.133 Exp. result input velocity , normal bearing
mean speed=327 rev/min; dia. clearance=.15mm

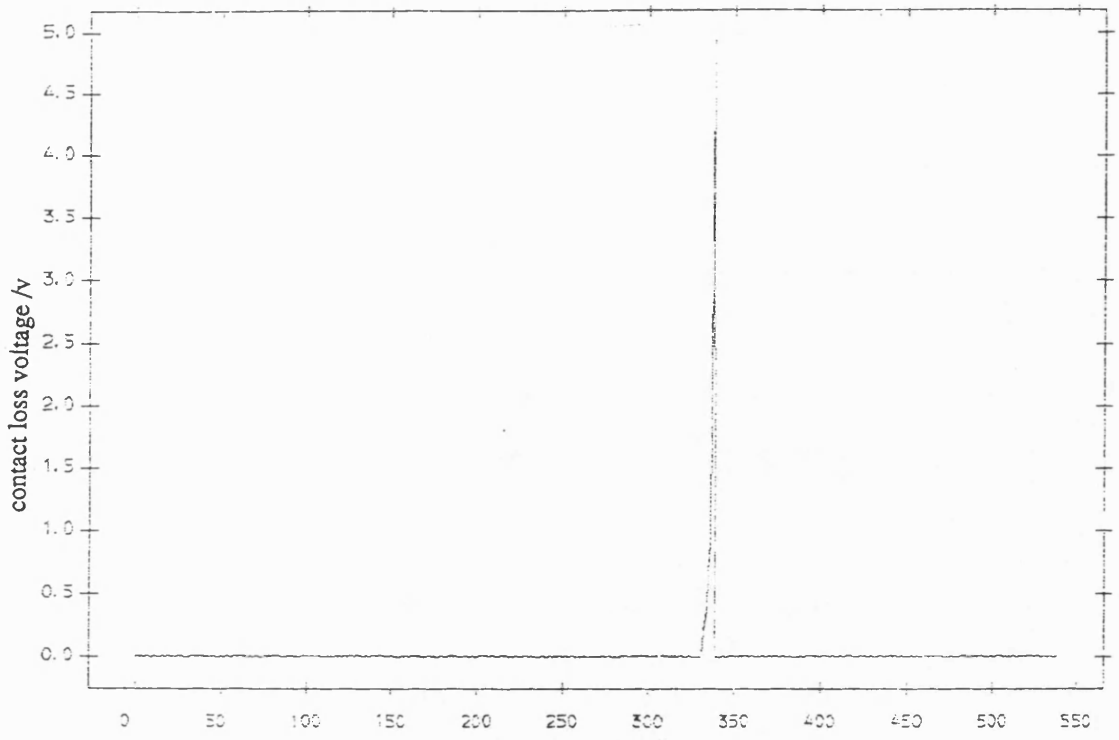

Fig 8.3.134 Exp. result contact loss of pin and normal bearing
with flywheel ;mean speed=327 rev/min ;dia. clearance=0.15mm

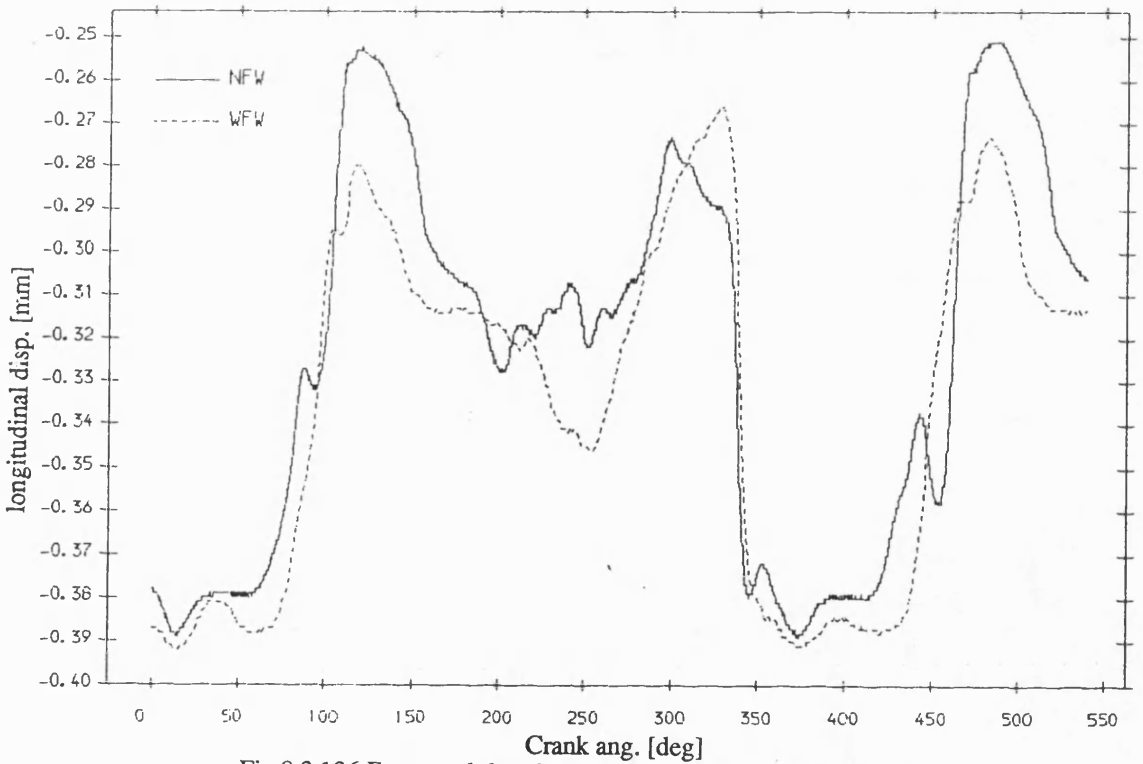

Fig 8.3.136 Exp. result longitudinal disp. of pin , normal bearing
mean speed=327 rev/min; dia. clearance=.15mm

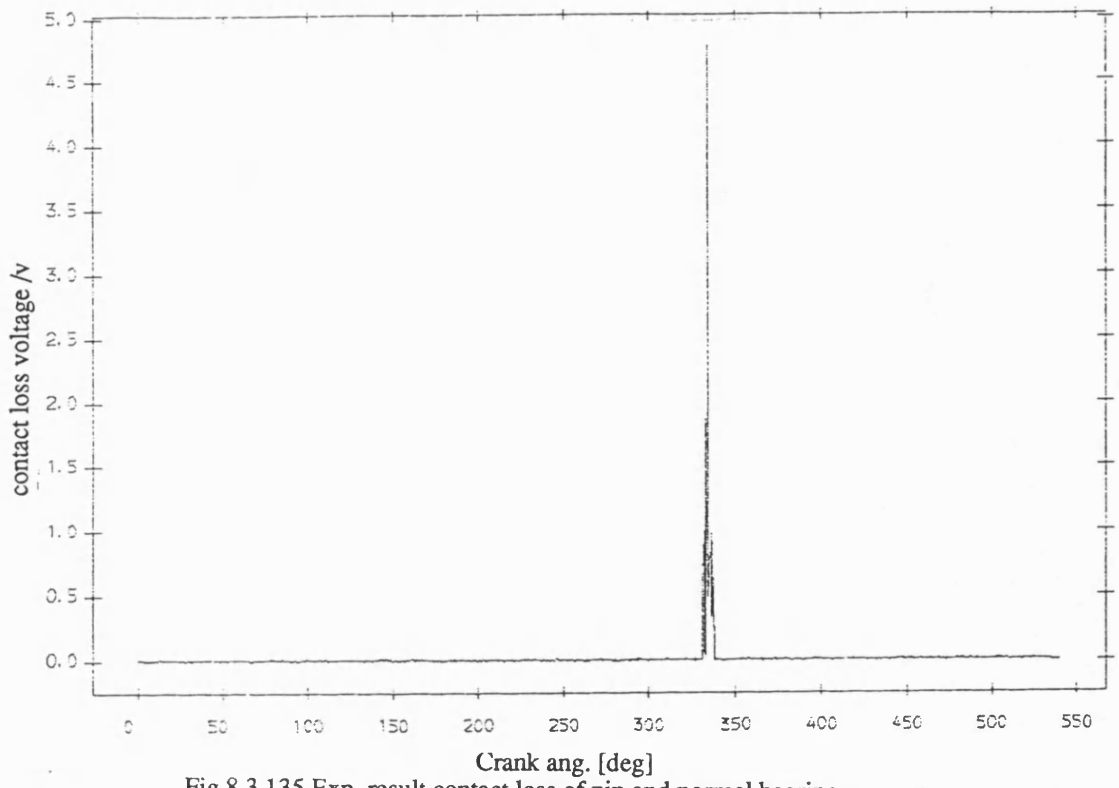

Fig 8.3.135 Exp. result contact loss of pin and normal bearing
no flywheel ;mean speed=327 rev/min ;dia. clearance=0.15mm

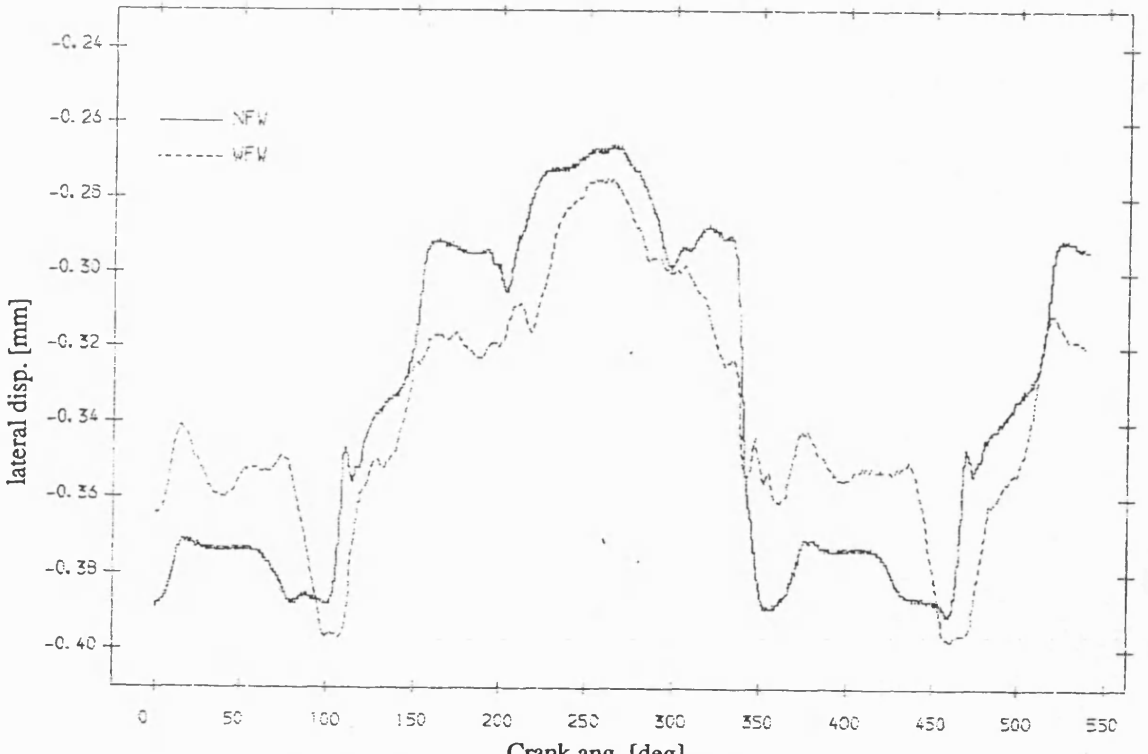

Fig 8.3.137 Exp. result lateral disp. of pin , normal bearing
mean speed=327 rev/min; dia. clearance=.15mm

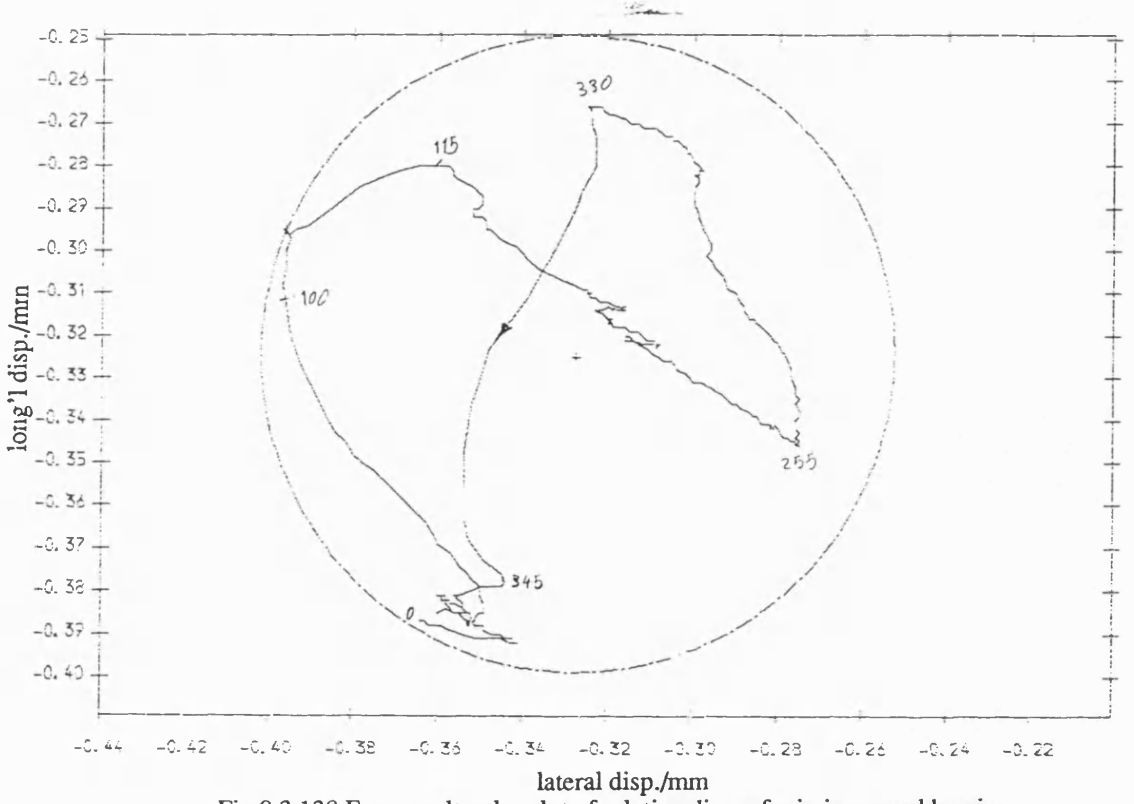

Fig 8.3.138 Exp. result polar plot of relative disp. of pin in normal bearing with fly wheel ;mean speed=327 rev/min ; dia. clearance=.15mm

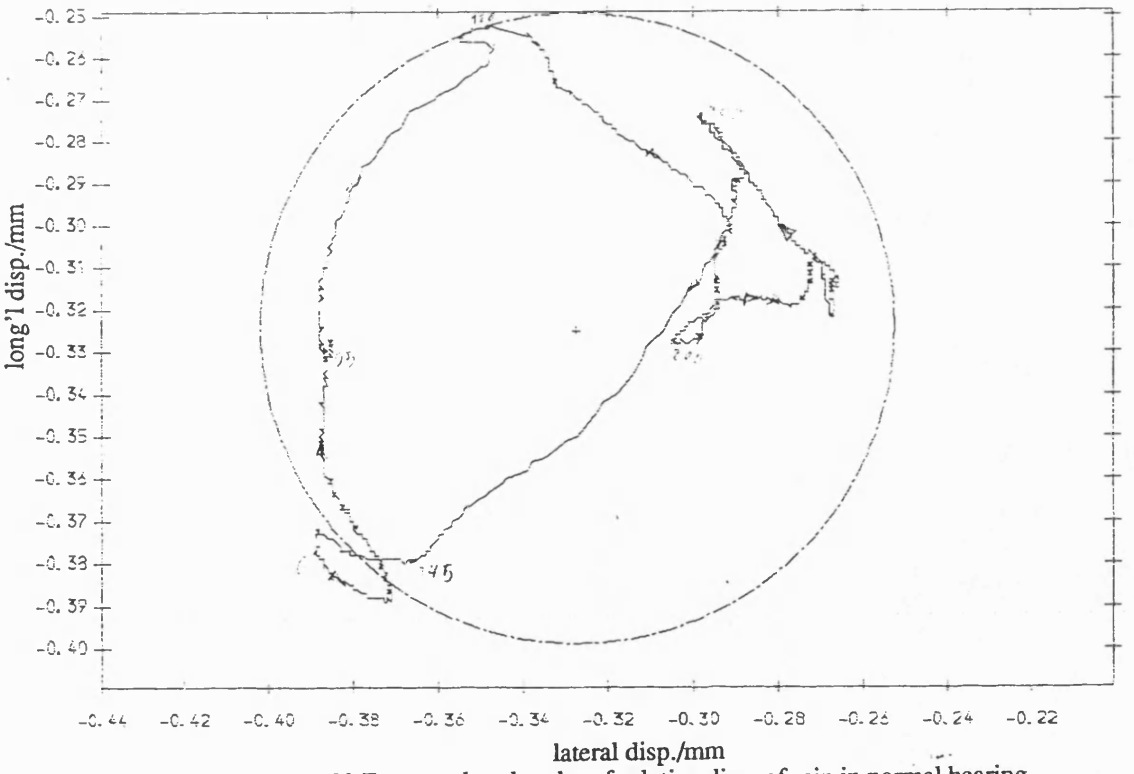

Fig 8.3.139 Exp. result polar plot of relative disp. of pin in normal bearing no fly wheel ;mean speed=327 rev/min ; dia. clearance=.15mm

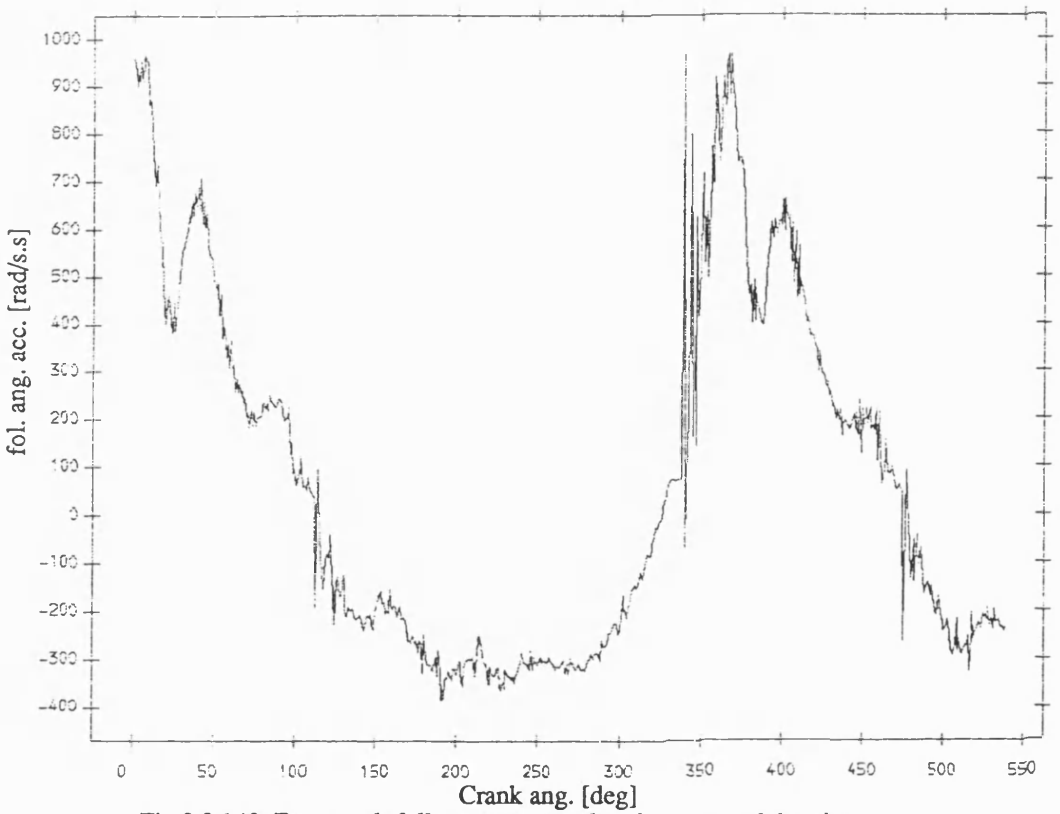

Fig 8.3.140 Exp. result follower ang. acceleration , normal bearing
with fly wheel ;mean speed=327 rev/min ; dia. clearance=.15mm

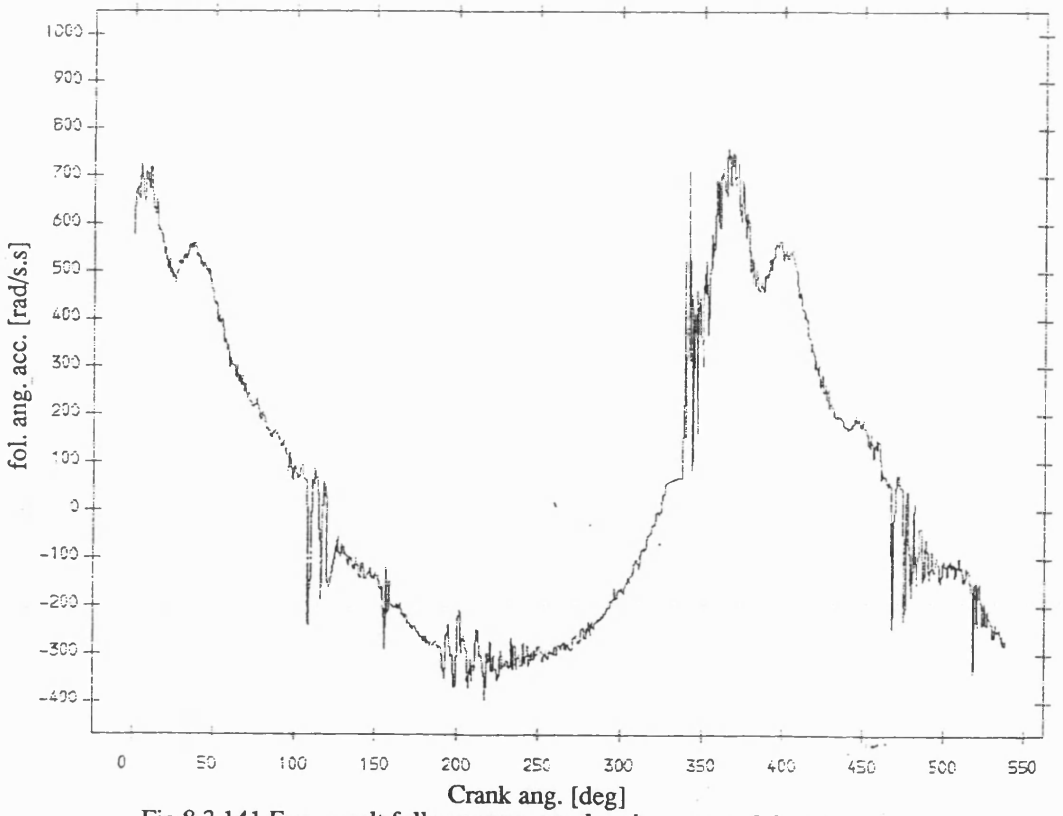

Fig 8.3.141 Exp. result follower ang. acceleration , normal bearing
no fly wheel ;mean speed=327 rev/min ; dia. clearance=.15mm

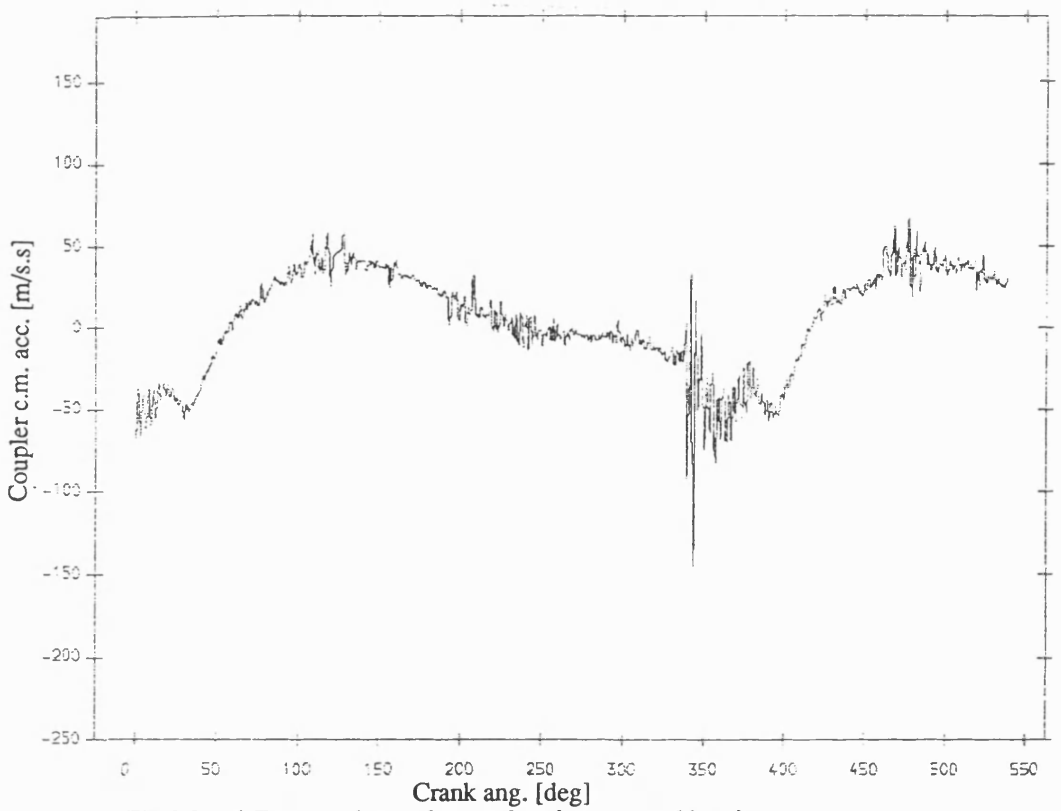

Fig 8.3.143 Exp. result coupler acceleration , normal bearing
no fly wheel ;mean speed=327 rev/min ; dia. clearance=.15mm

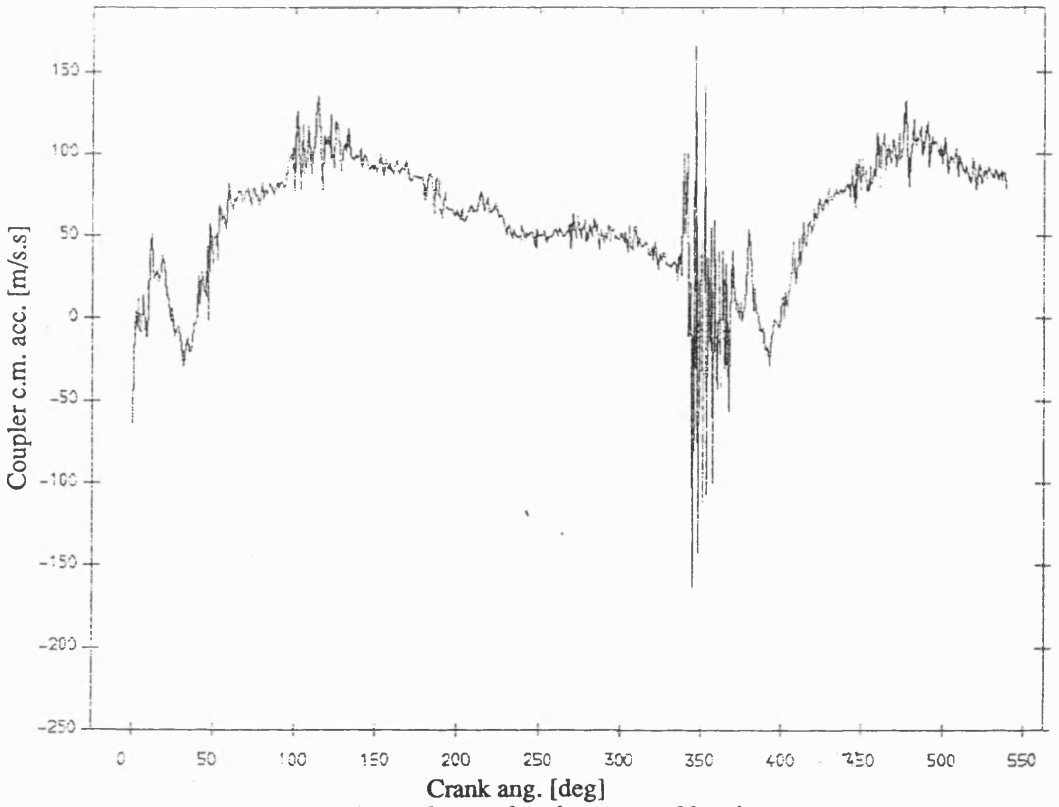

Fig 8.3.142 Exp. result coupler acceleration , normal bearing
with fly wheel ;mean speed=327 rev/min ; dia. clearance=.15mm

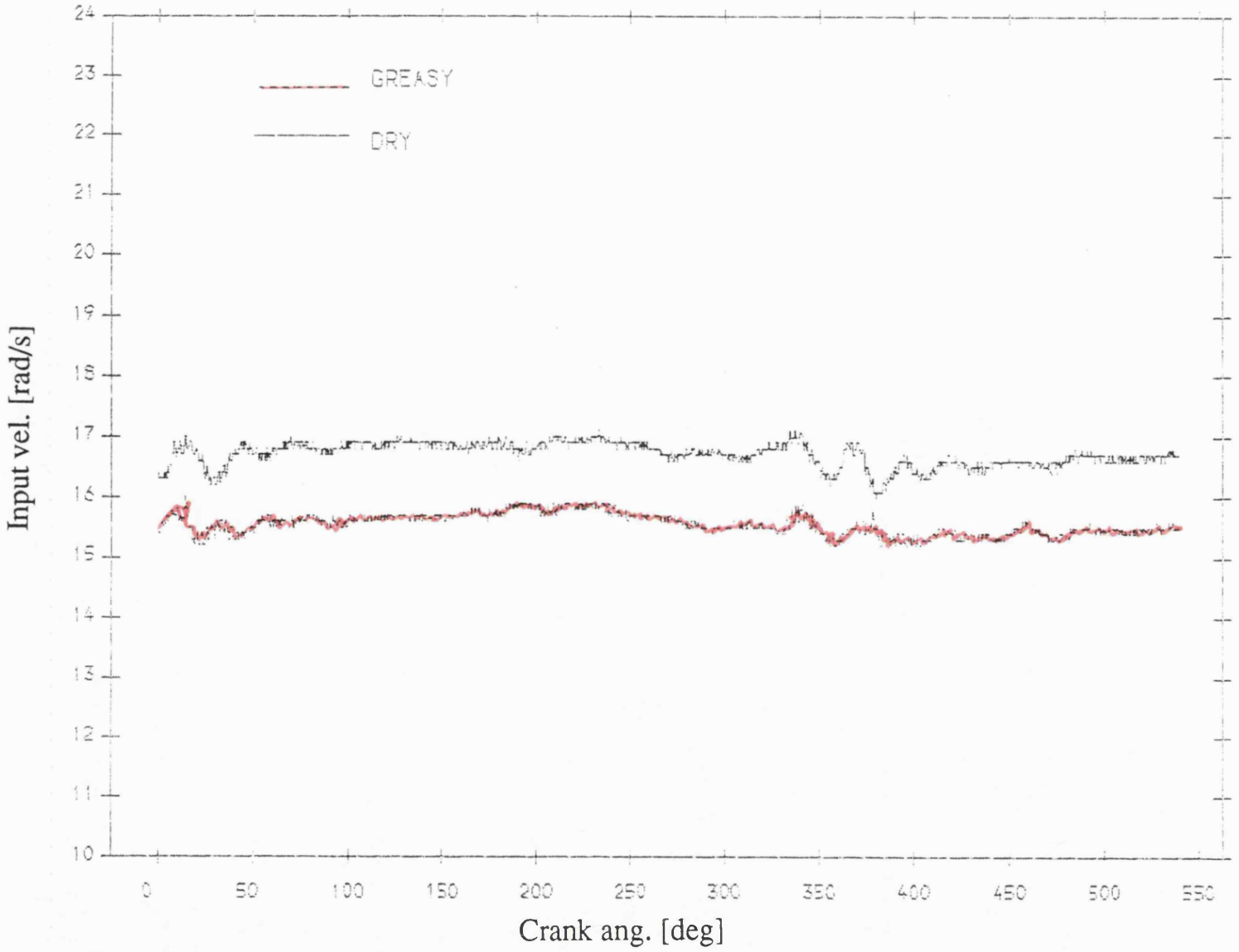

Fig 8.4.1 Exp. result input velocity , greasy v dry bearing
mean speed=168 rev/min; dia. clearance=.25mm

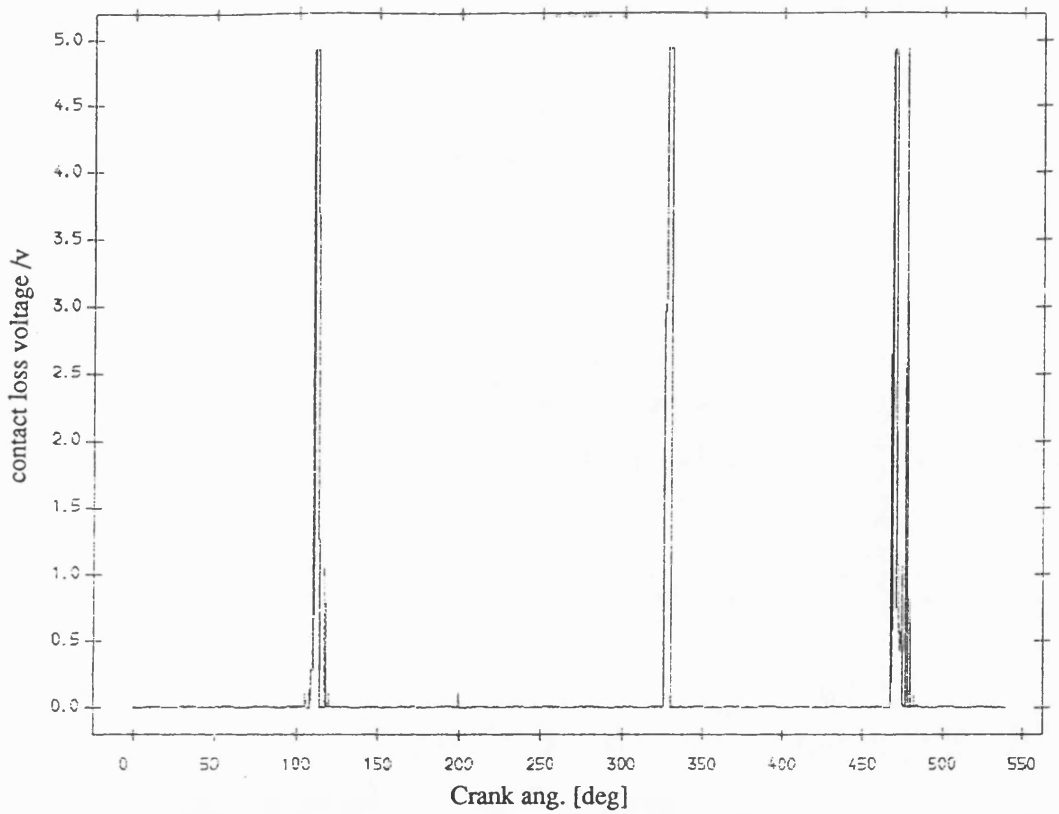

Fig 8.4.3 Exp. result contact loss of pin and dry bearing
with flywheel ;mean speed=168 rev/min ;dia. clearance=0.25mm

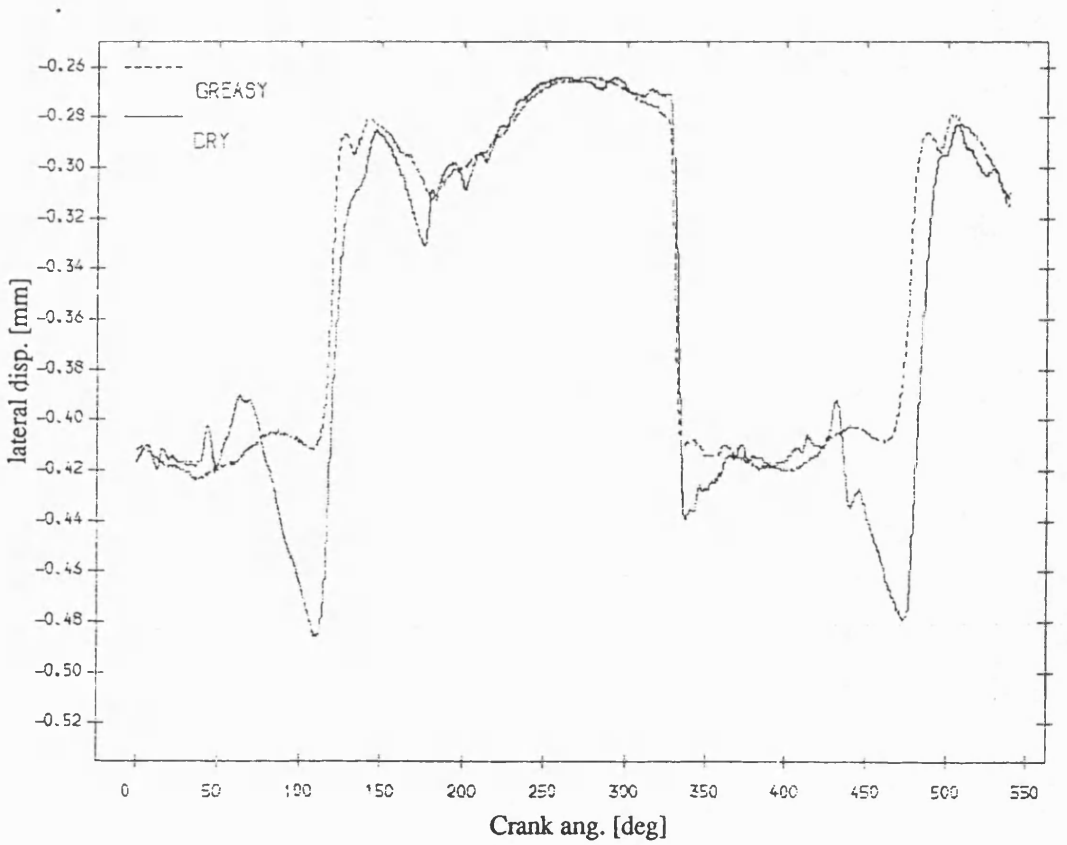

Fig 8.4.5 Exp. result lateral disp. of pin , greasy v dry bearing
mean speed=168 rev/min; dia. clearance=.25mm

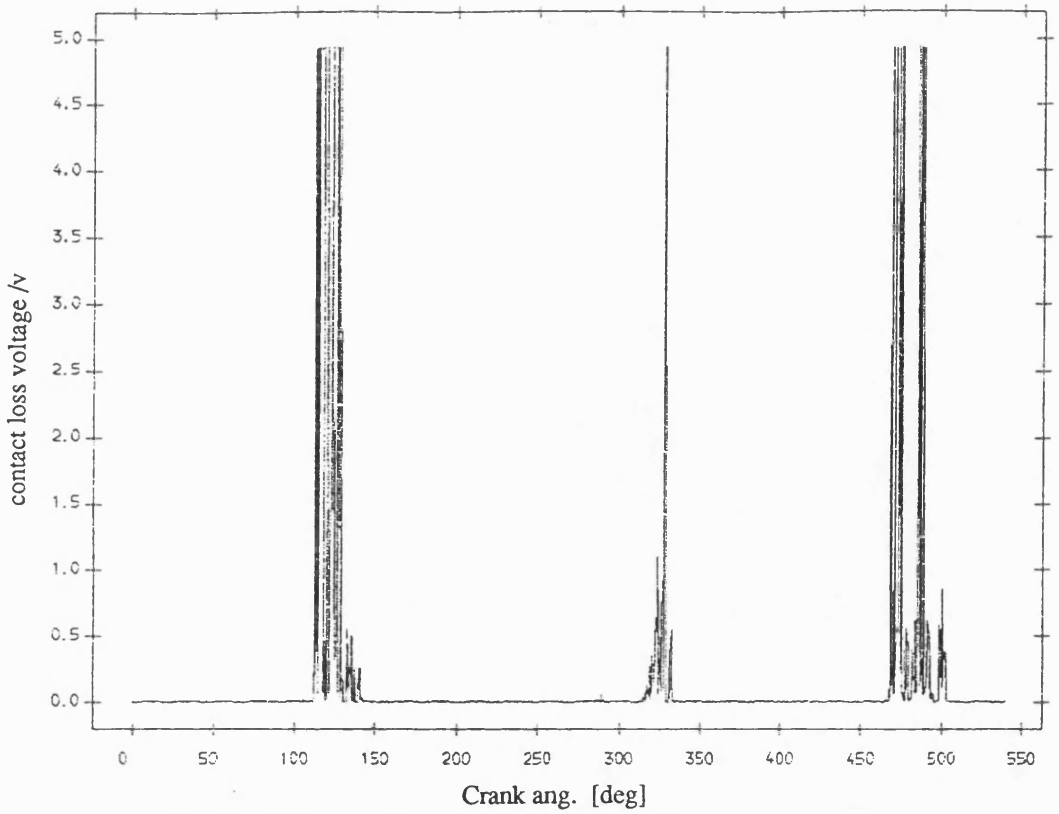

Fig 8.4.2 Exp. result contact loss of pin and greasy bearing
with flywheel ;mean speed=168 rev/min ;dia. clearance=0.25mm

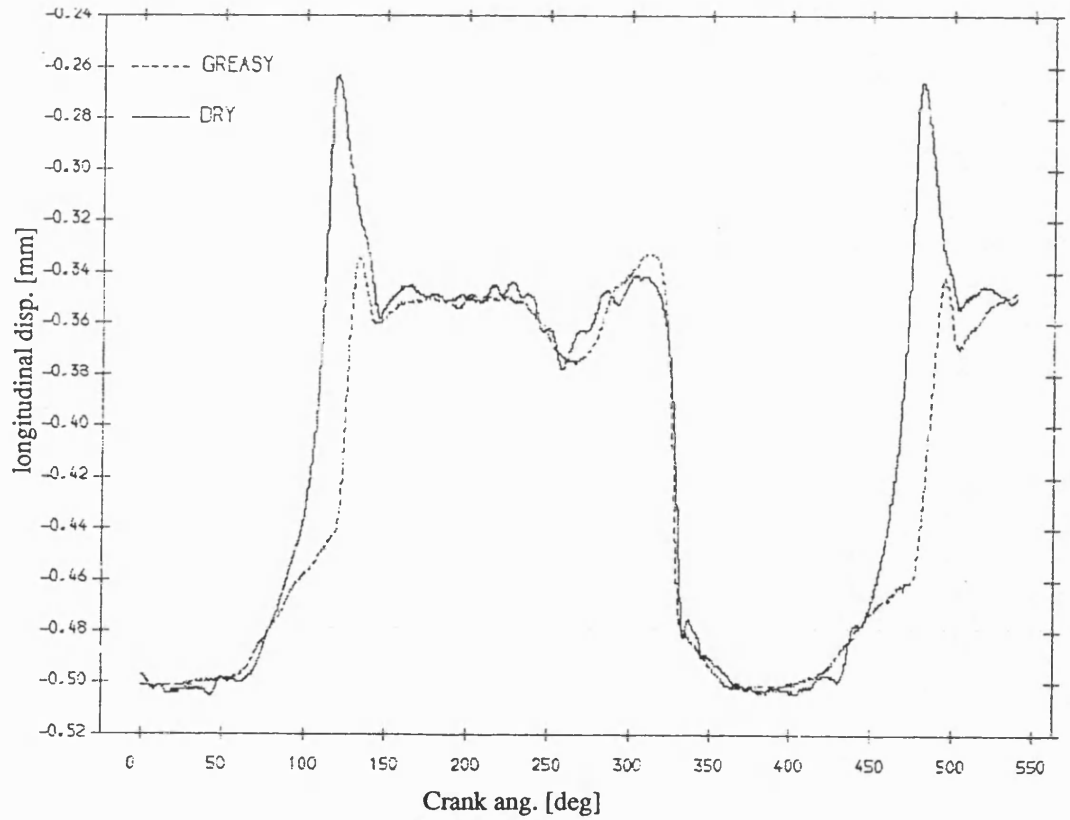

Fig 8.4.4 Exp. result longitudinal disp. of pin , greasy v dry bearing
mean speed=168 rev/min; dia. clearance=.25mm

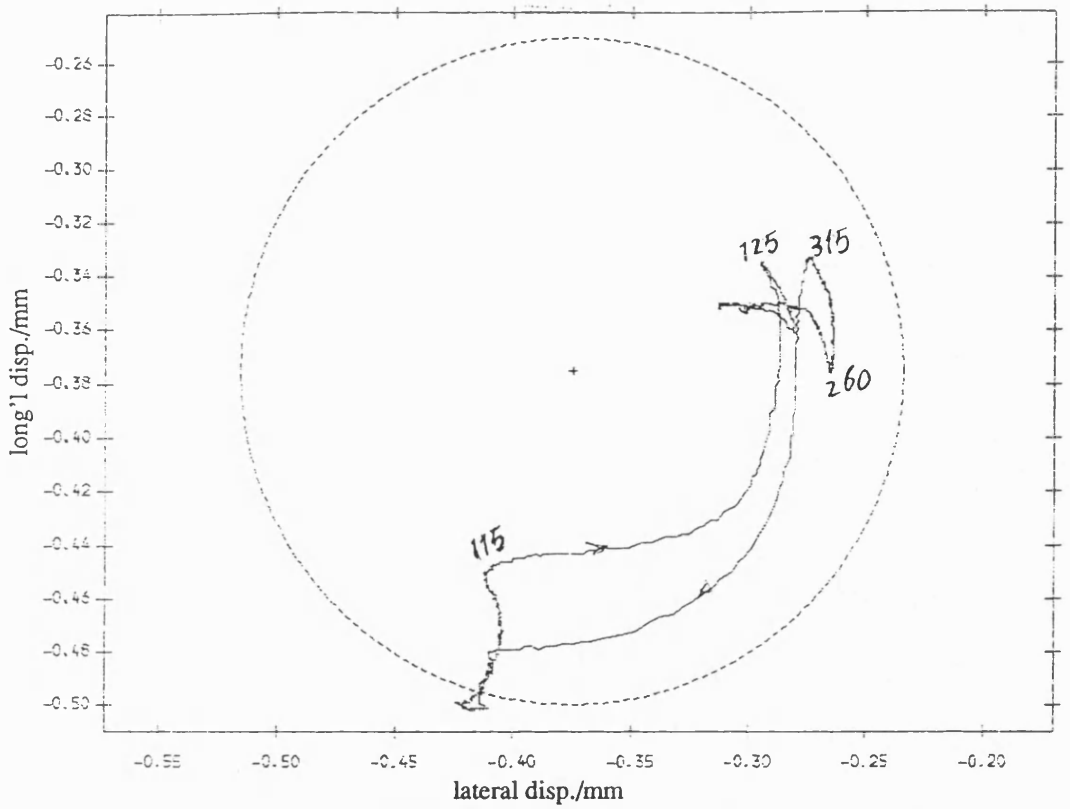

Fig 8.4.6 Exp. result polar plot of relative disp. of pin in greasy bearing with fly wheel ;mean speed=168 rev/min ; dia. clearance=.25mm

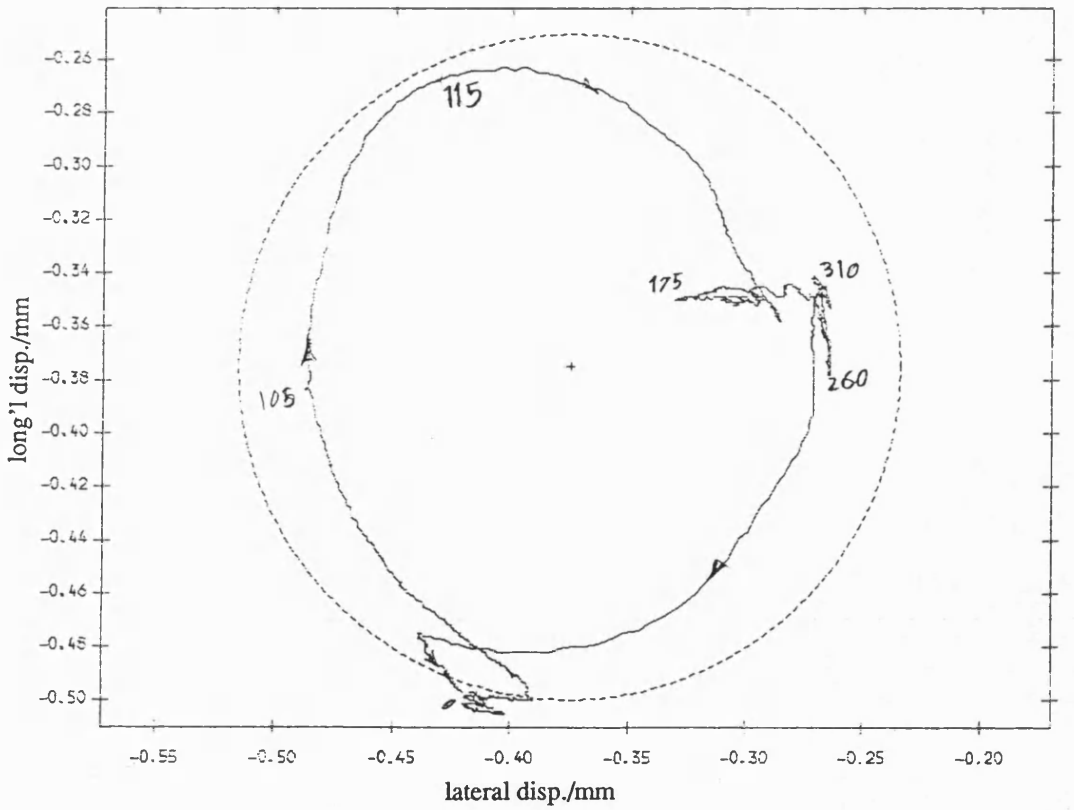

Fig 8.4.7 Exp. result polar plot of relative disp. of pin in dry bearing with fly wheel ;mean speed=168 rev/min ; dia. clearance=.25mm

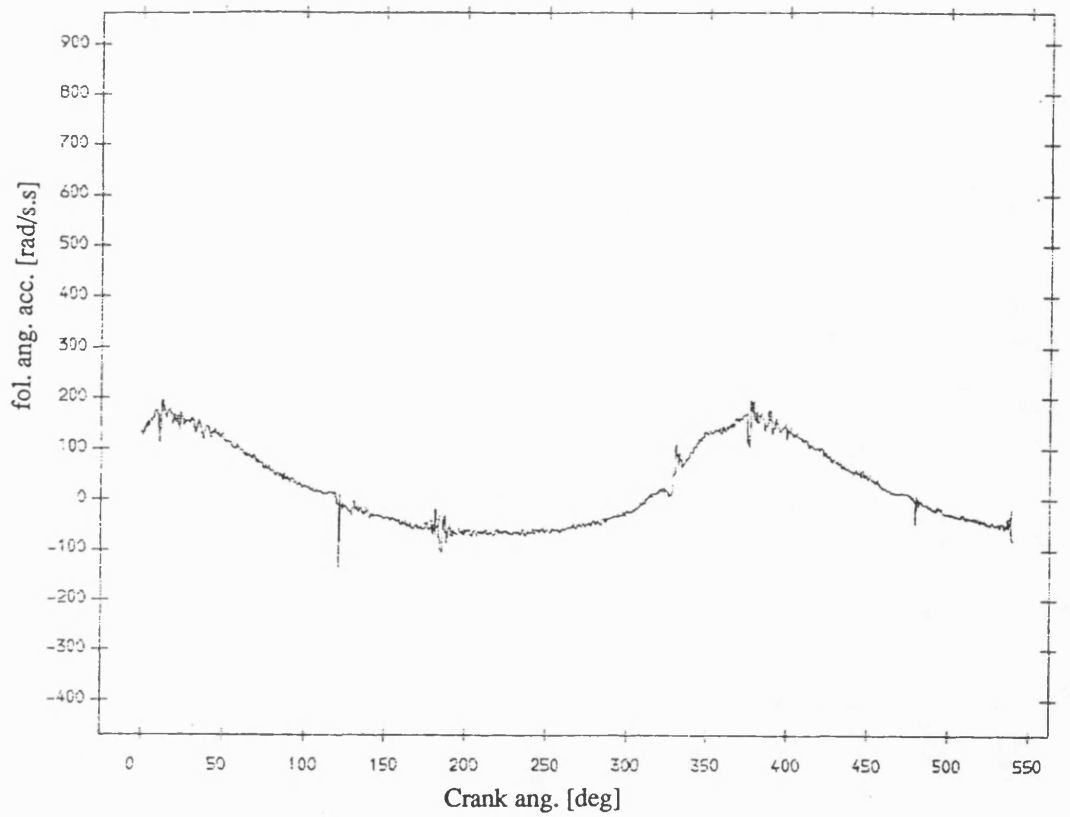

Fig 8.4.8 Exp. result follower ang. acceleration , greasy bearing
with fly wheel ;mean speed=168 rev/min ; dia. clearance=.25mm

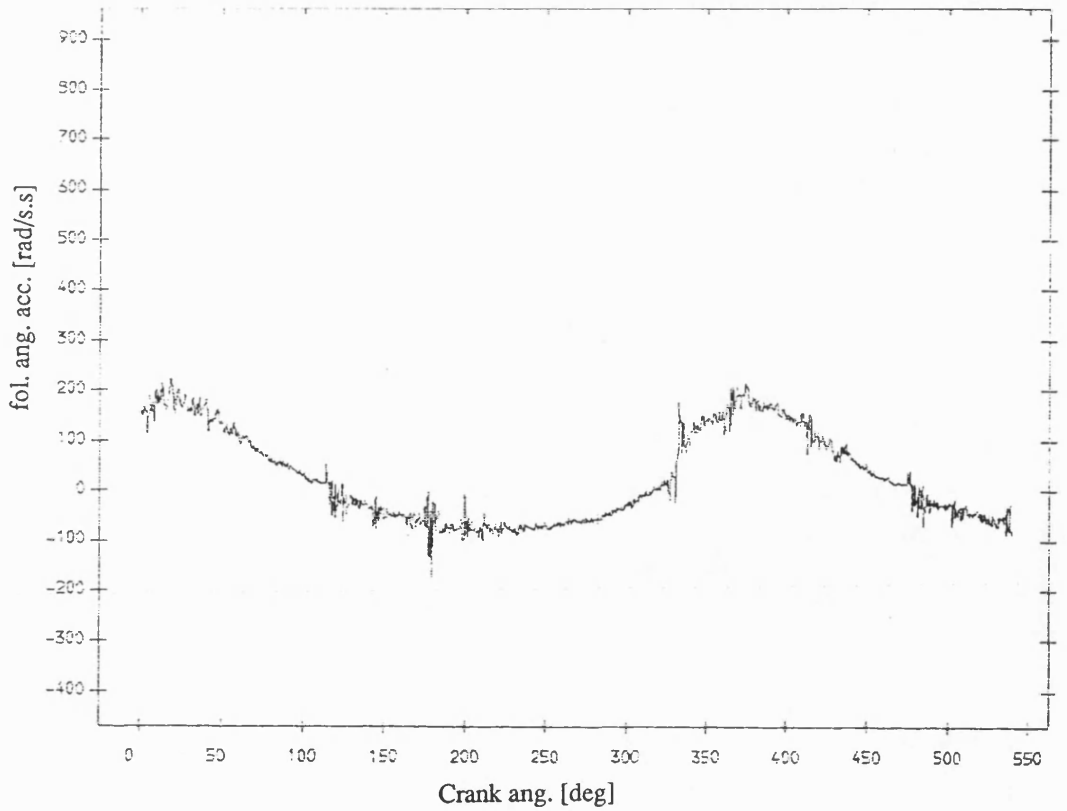

Fig 8.4.9 Exp. result follower ang. acceleration ,dry bearing
with fly wheel ;mean speed=168 rev/min ; dia. clearance=.25mm

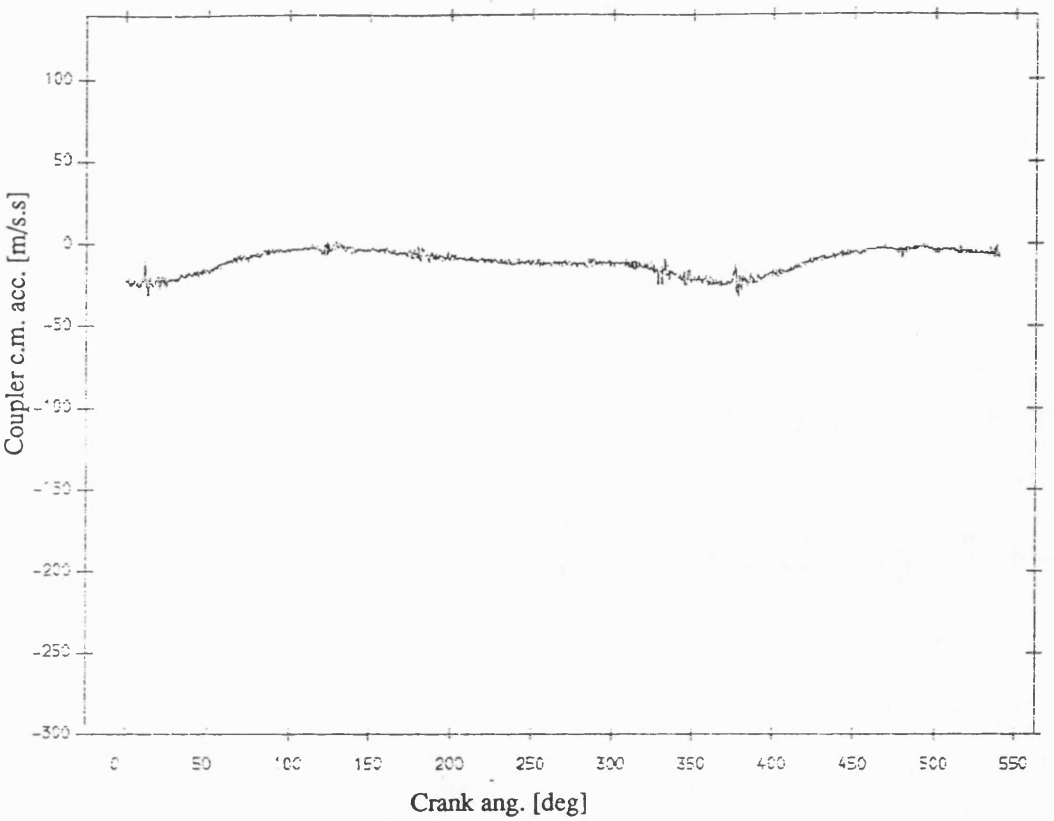

Fig 8.4.10 Exp. result coupler acceleration , greasy bearing
with fly wheel ;mean speed=168 rev/min ; dia. clearance=.25mm

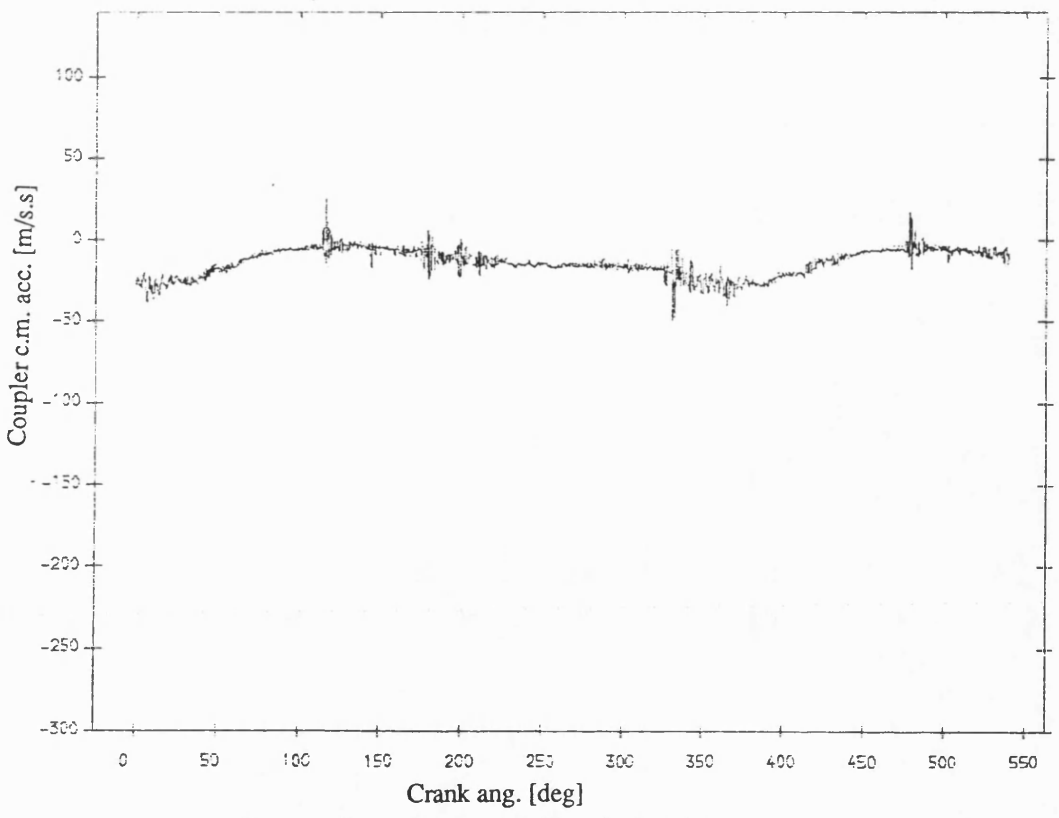

Fig 8.4.11 Exp. result coupler acceleration , dry bearing
with fly wheel ;mean speed=168 rev/min ; dia. clearance=.25mm

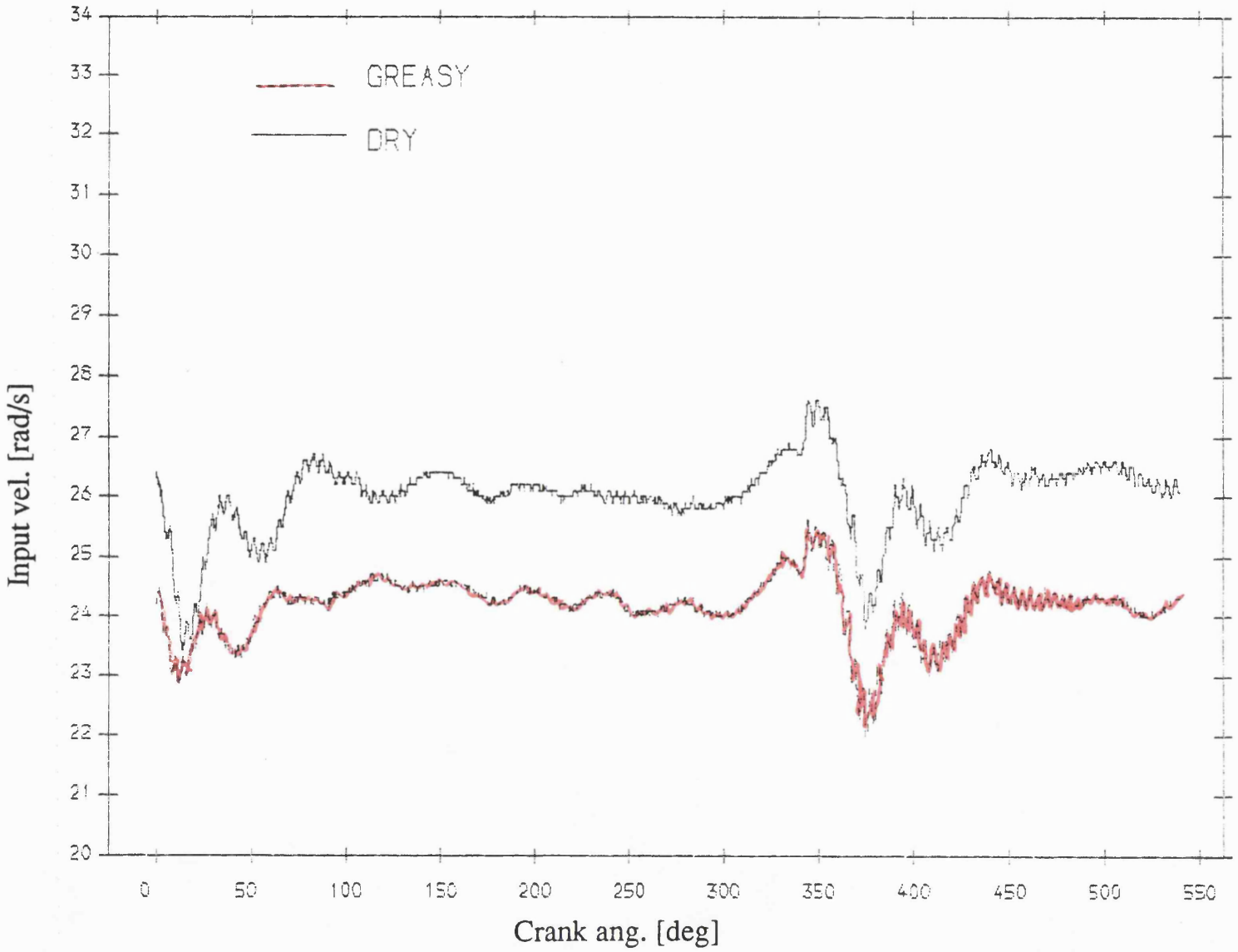

Fig 8.4.12 Exp. result input velocity , greasy v dry bearing
mean speed=244 rev/min; dia. clearance=.25mm

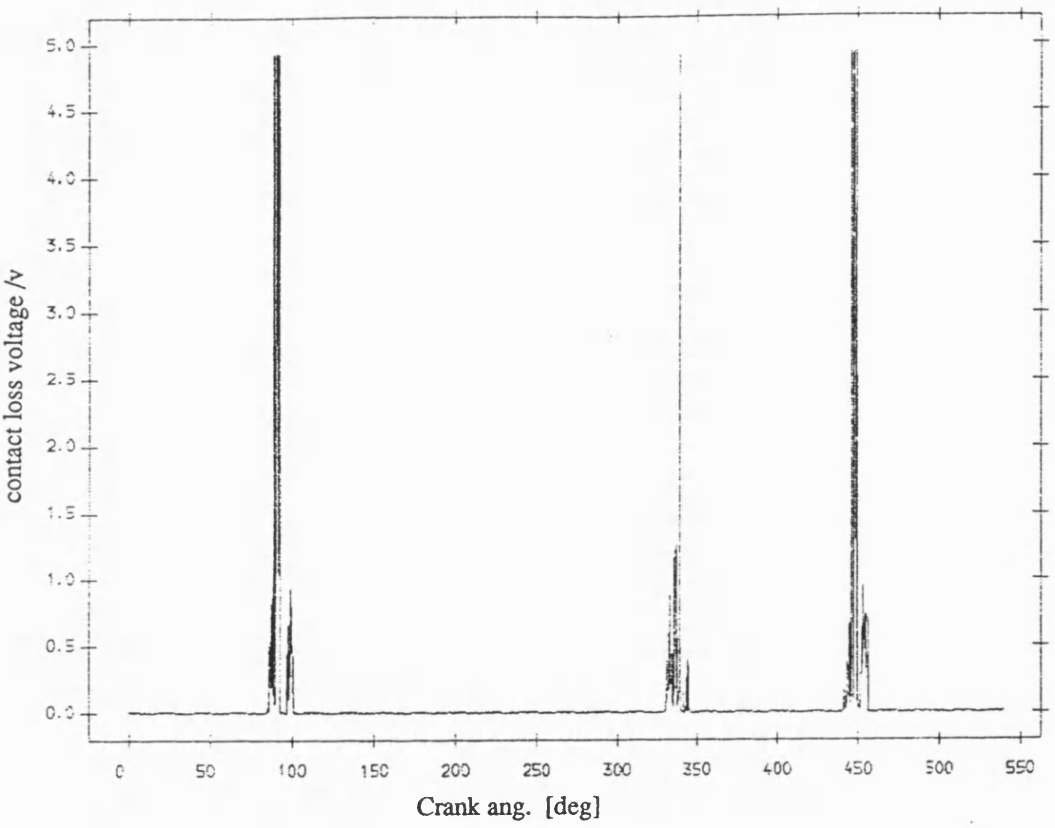

Fig 8.4.13 Exp. result contact loss of pin and greasy bearing
with flywheel ;mean speed=244 rev/min ;dia. clearance=0.25mm

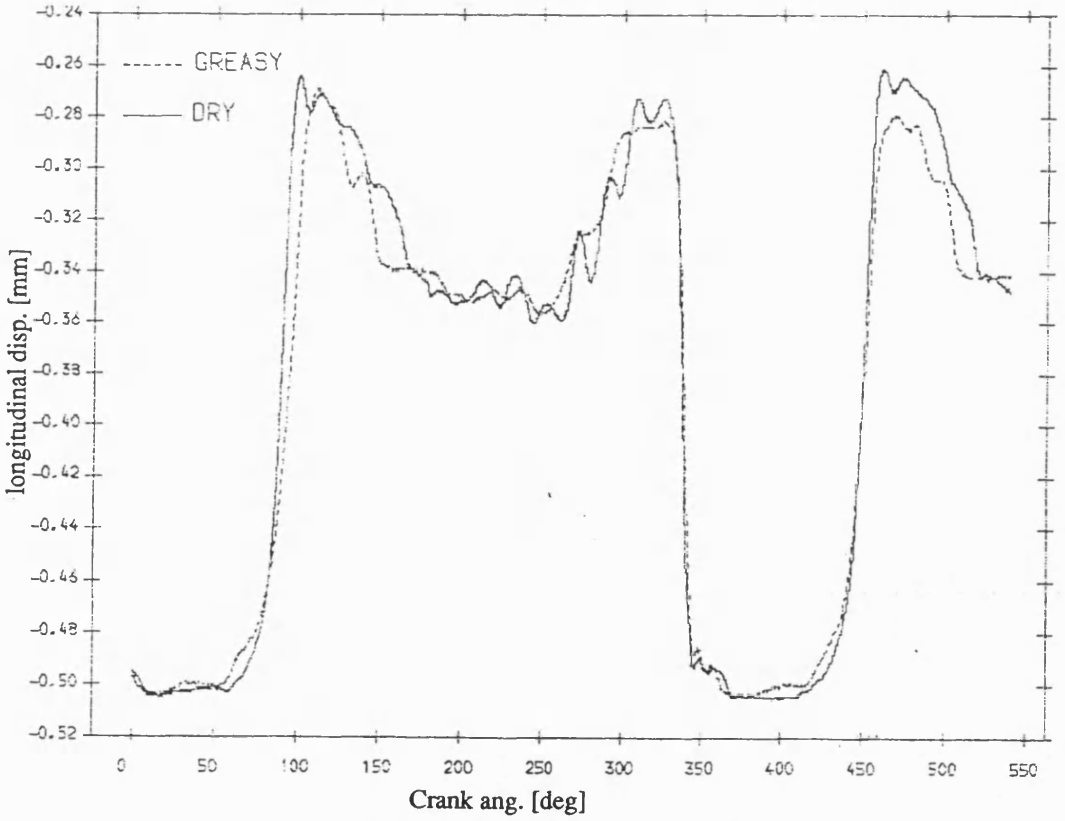

Fig 8.4.15 Exp. result longitudinal disp. of pin , greasy v dry bearing
mean speed=244 rev/min; dia. clearance=.25mm

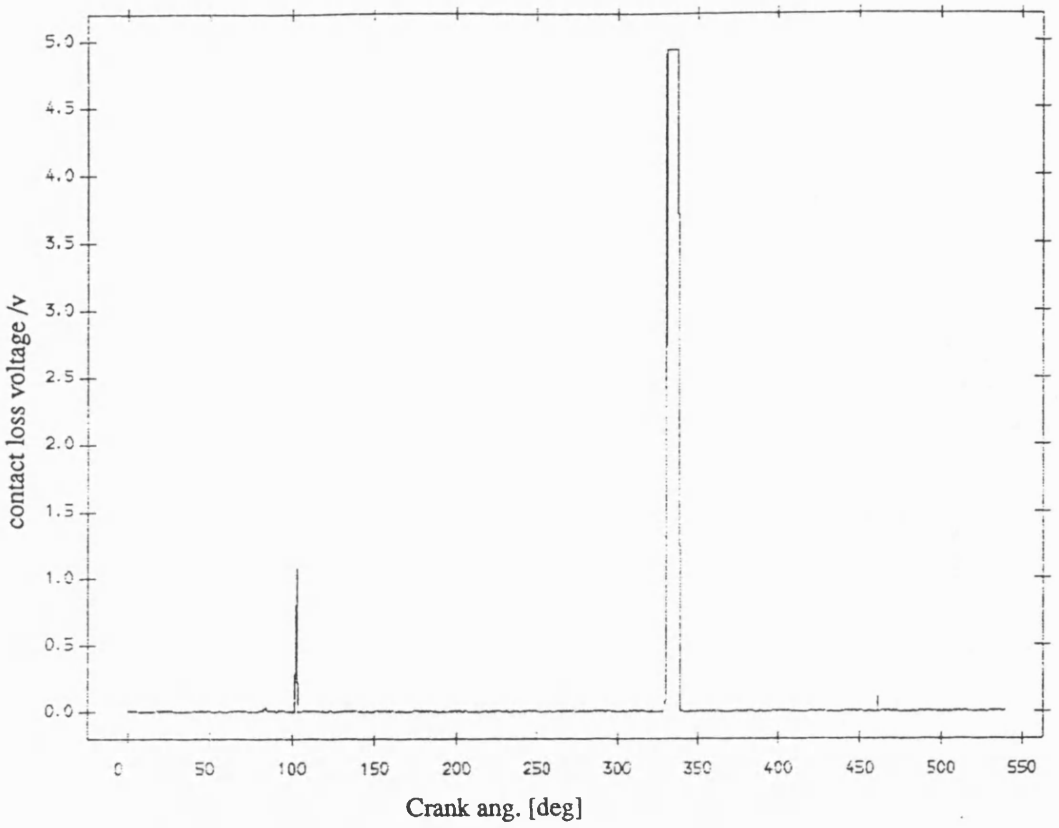

Fig 8.4.14 Exp. result contact loss of pin and dry bearing
with flywheel ;mean speed=244 rev/min ;dia. clearance=0.25mm

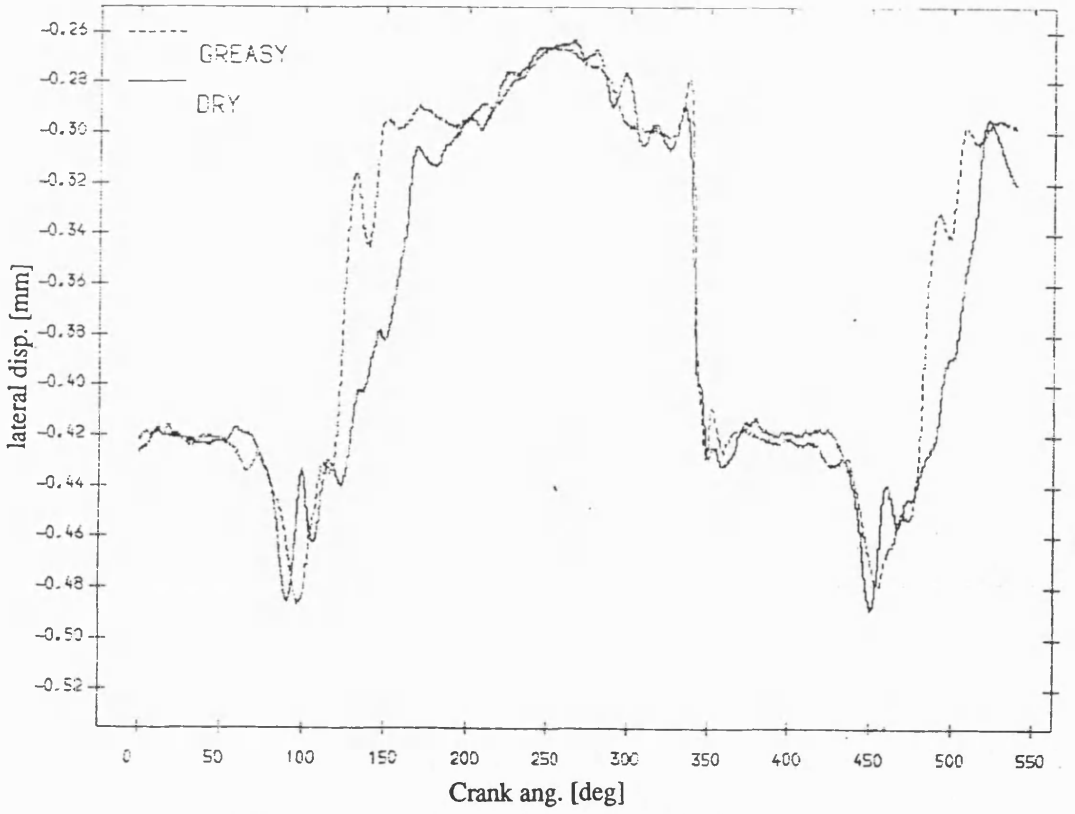

Fig 8.4.16 Exp. result lateral disp. of pin , greasy v dry bearing
mean speed=244 rev/min; dia. clearance=.25mm

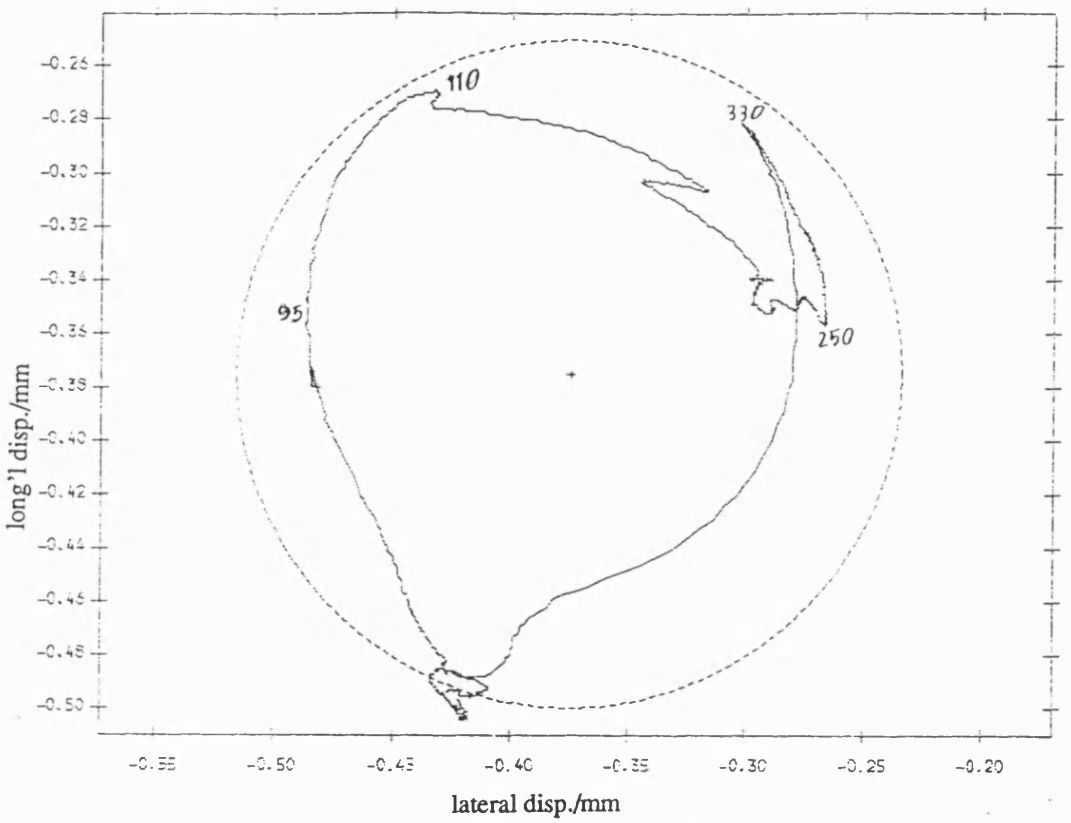

Fig 8.4.17 Exp. result polar plot of relative disp. of pin in greasy bearing with fly wheel ;mean speed=244 rev/min ; dia. clearance=.25mm

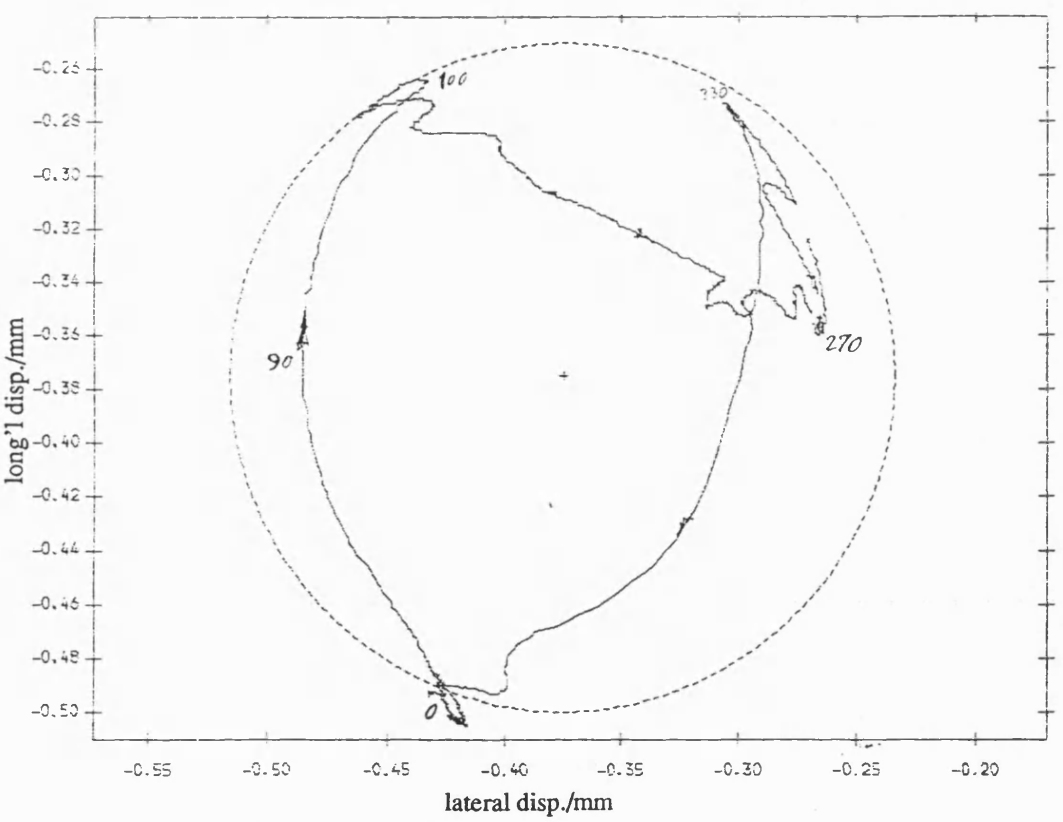

Fig 8.4.18 Exp. result polar plot of relative disp. of pin in dry bearing with fly wheel ;mean speed=244 rev/min ; dia. clearance=.25mm

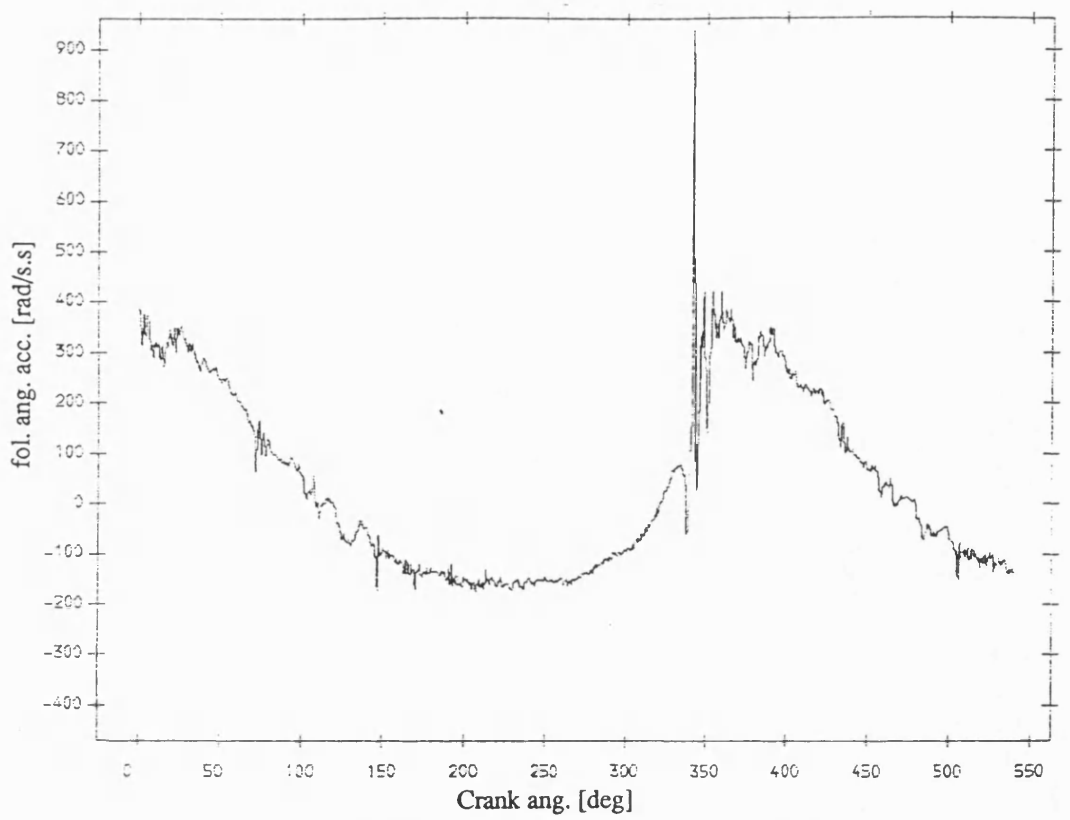

Fig 8.4.19 Exp. result follower ang. acceleration , greasy bearing
with fly wheel ;mean speed=244 rev/min ; dia. clearance=.25mm

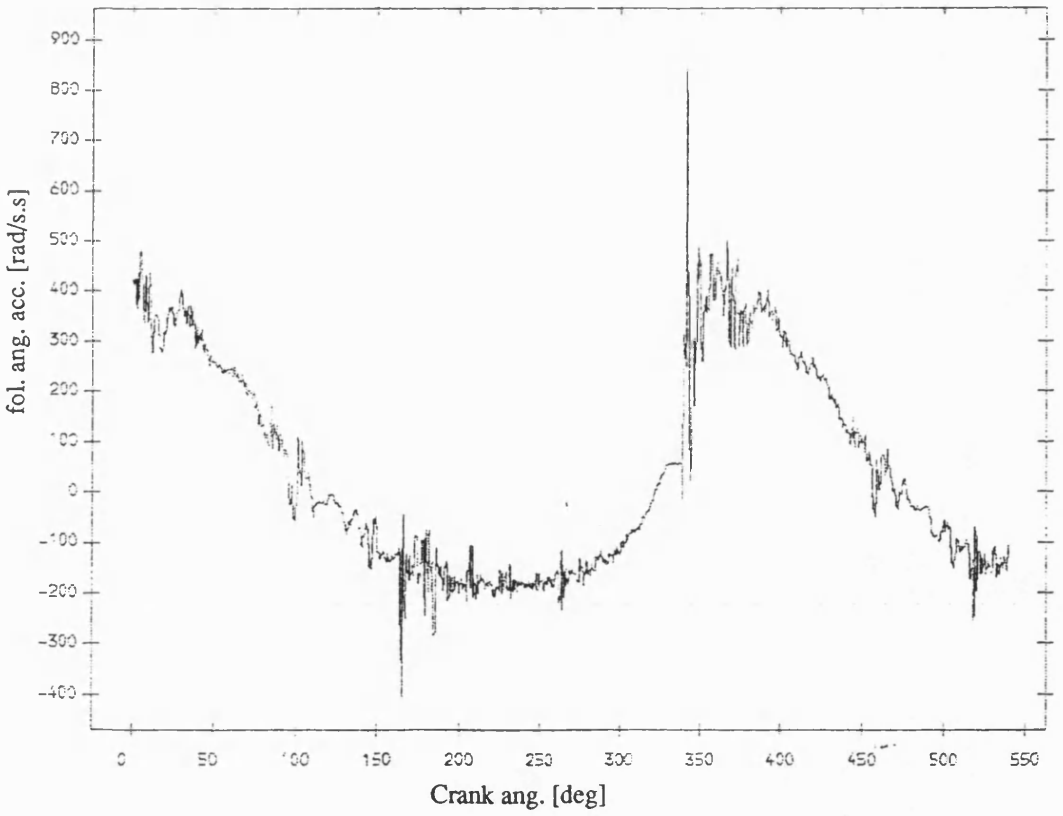

Fig 8.4.20 Exp. result follower ang. acceleration ,dry bearing
with fly wheel ;mean speed=244 rev/min ; dia. clearance=.25mm

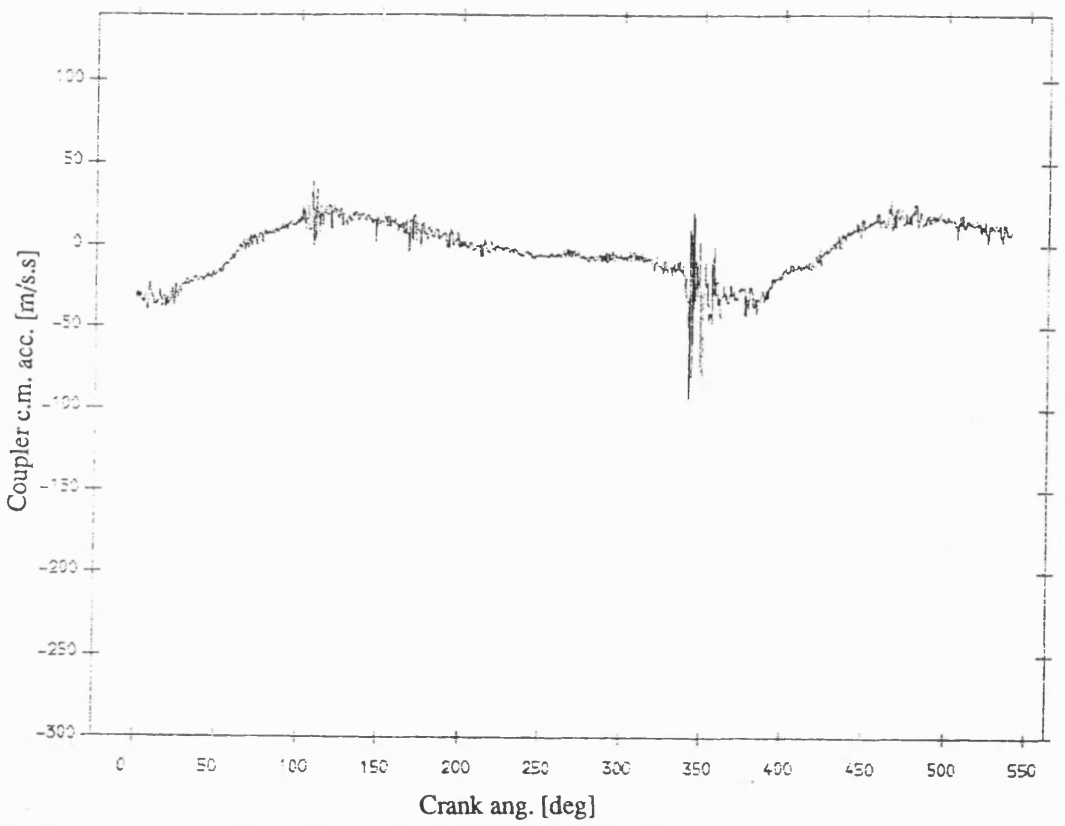

Fig 8.4.21 Exp. result coupler acceleration , greasy bearing
with fly wheel ;mean speed=244 rev/min ; dia. clearance=.25mm

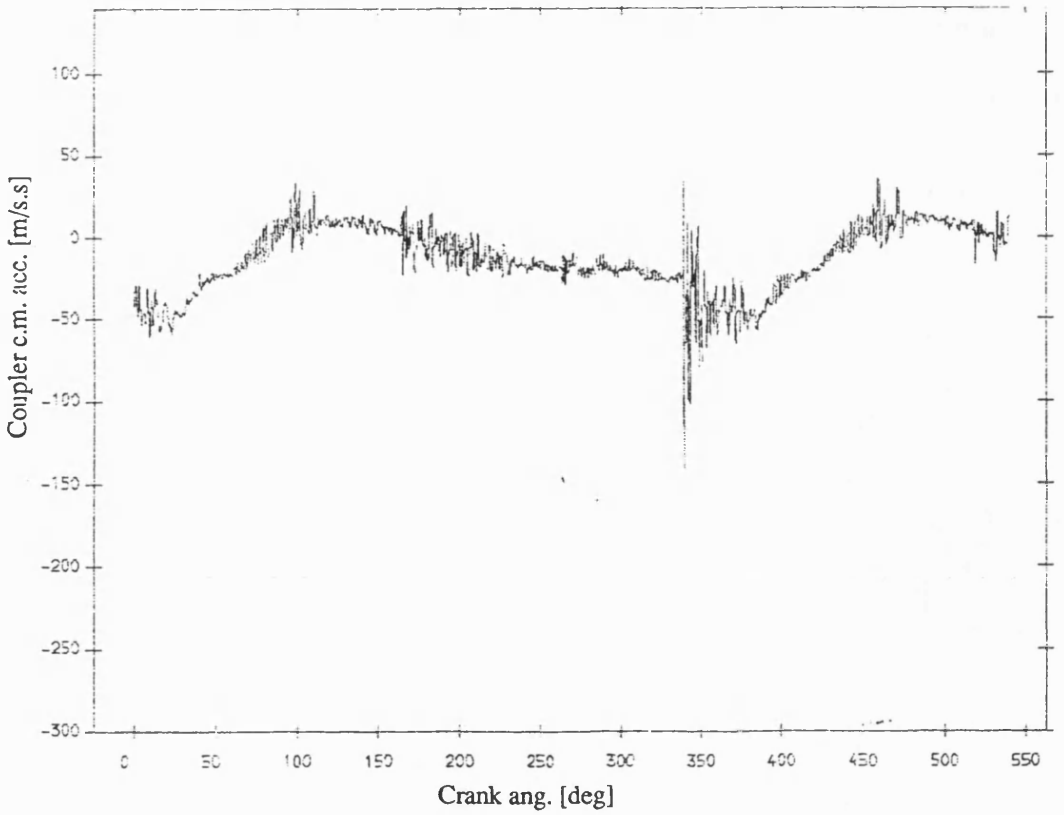

Fig 8.4.22 Exp. result coupler acceleration , dry bearing
with fly wheel ;mean speed=244 rev/min ; dia. clearance=.25mm

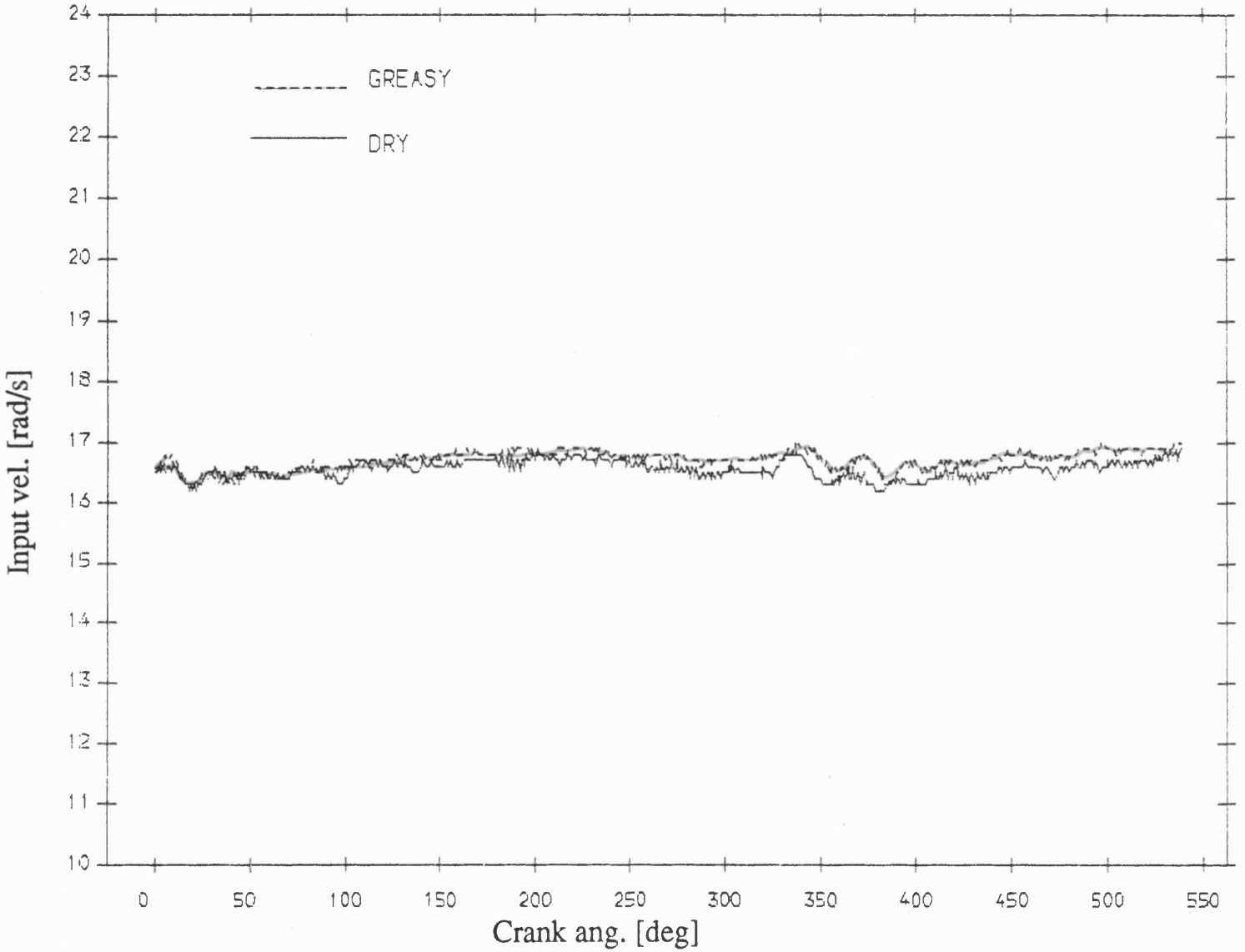

Fig 8.5.1 Exp. result input velocity , greasy v dry bearing
mean speed=168 rev/min; dia. clearance=.30mm

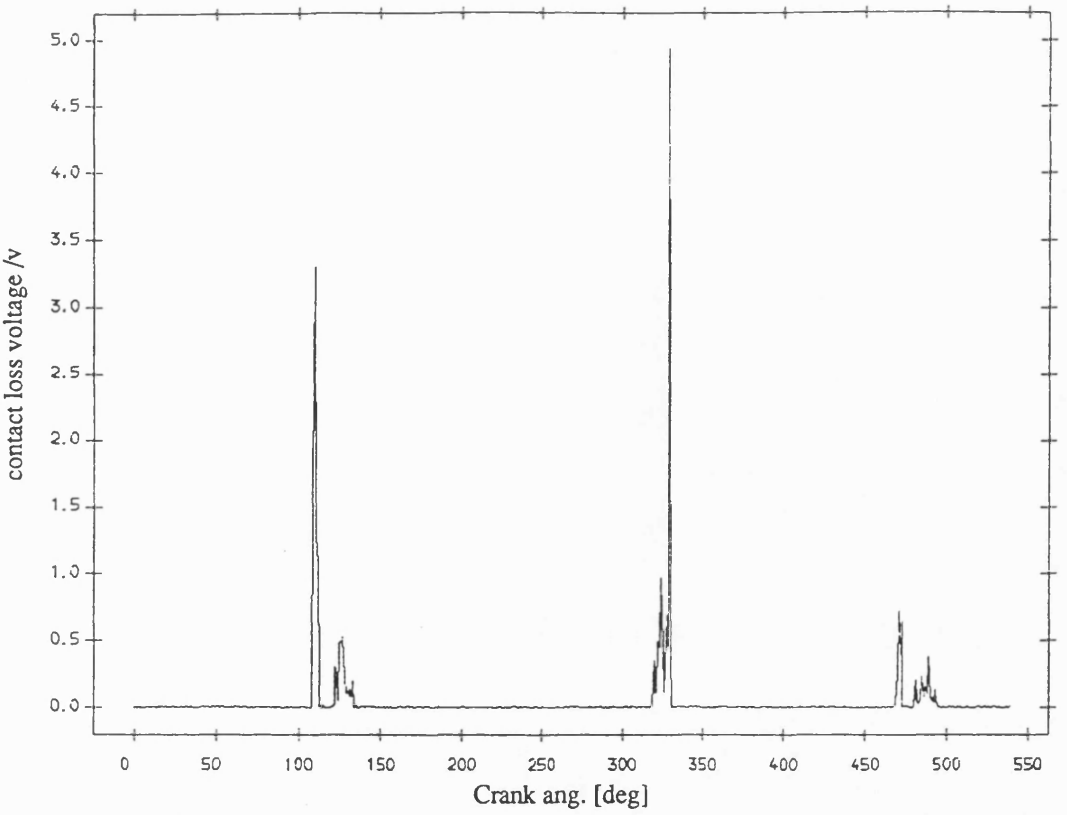

Fig 8.5.3 Exp. result contact loss of pin and dry bearing
with flywheel ;mean speed=168 rev/min ;dia. clearance=0.30mm

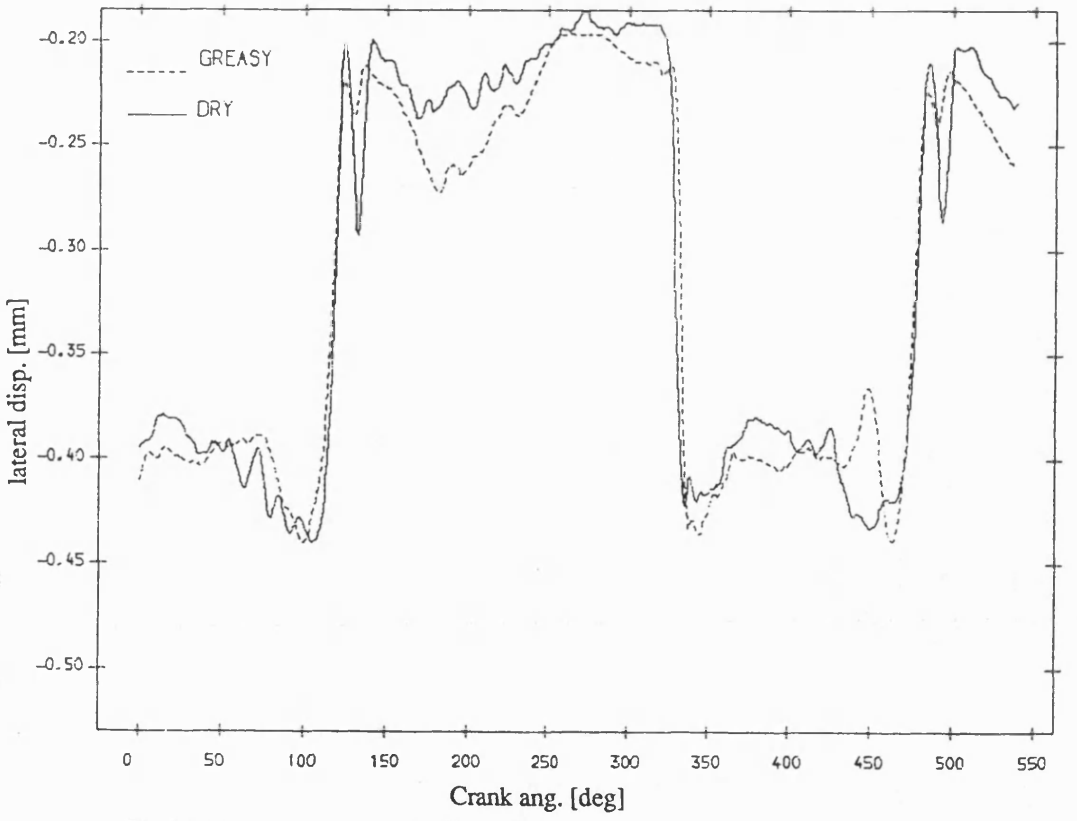

Fig 8.5.5 Exp. result lateral disp. of pin , greasy v dry bearing
mean speed=168 rev/min; dia. clearance=.30mm

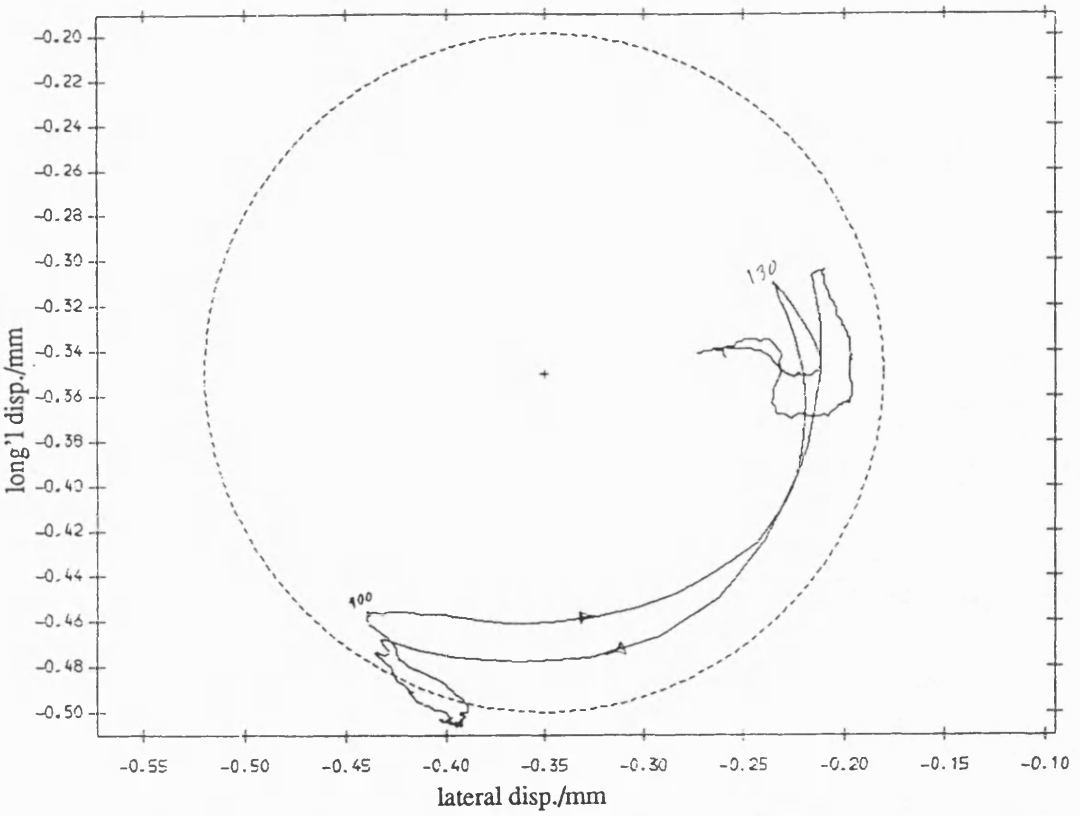

Fig 8.5.6 Exp. result polar plot of relative disp. of pin in greasy bearing with fly wheel ;mean speed=168 rev/min ; dia. clearance=.30mm

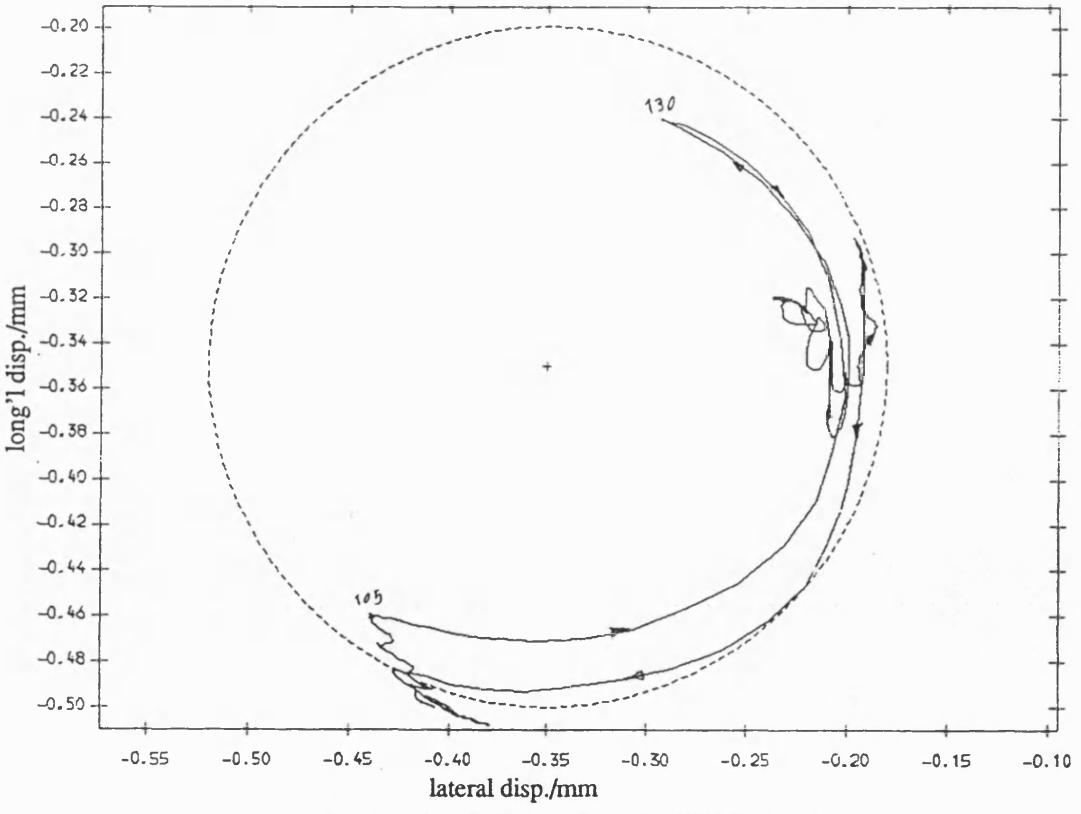

Fig 8.5.7 Exp. result polar plot of relative disp. of pin in dry bearing with fly wheel ;mean speed=168 rev/min ; dia. clearance=.30mm

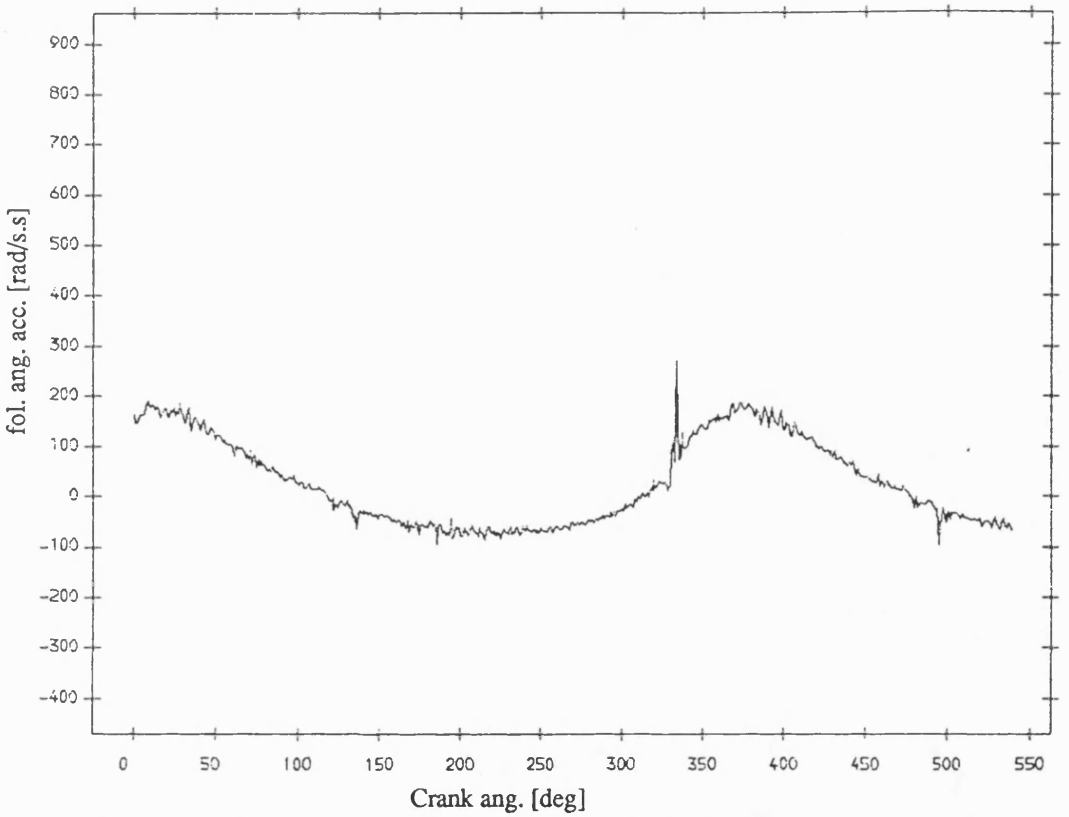

Fig 8.5.8 Exp. result follower ang. acceleration , greasy bearing
with fly wheel ;mean speed=168 rev/min ; dia. clearance=.30mm

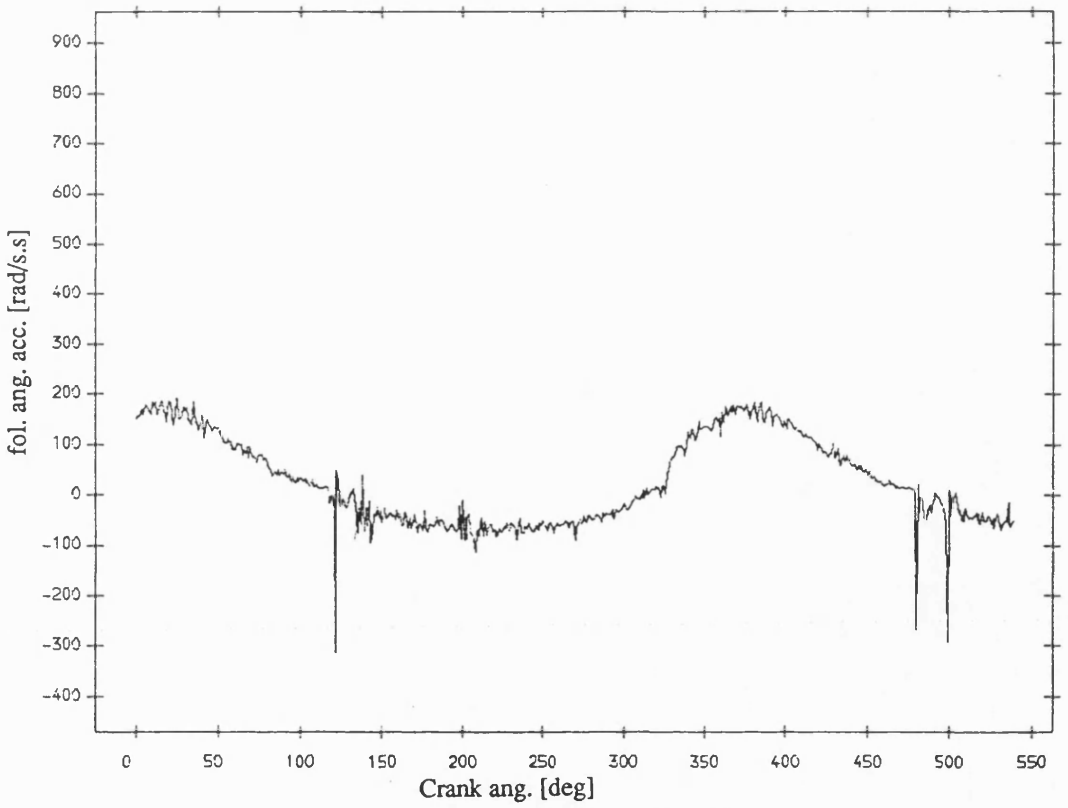

Fig 8.5.9 Exp. result follower ang. acceleration ,dry bearing
with fly wheel ;mean speed=168 rev/min ; dia. clearance=.30mm

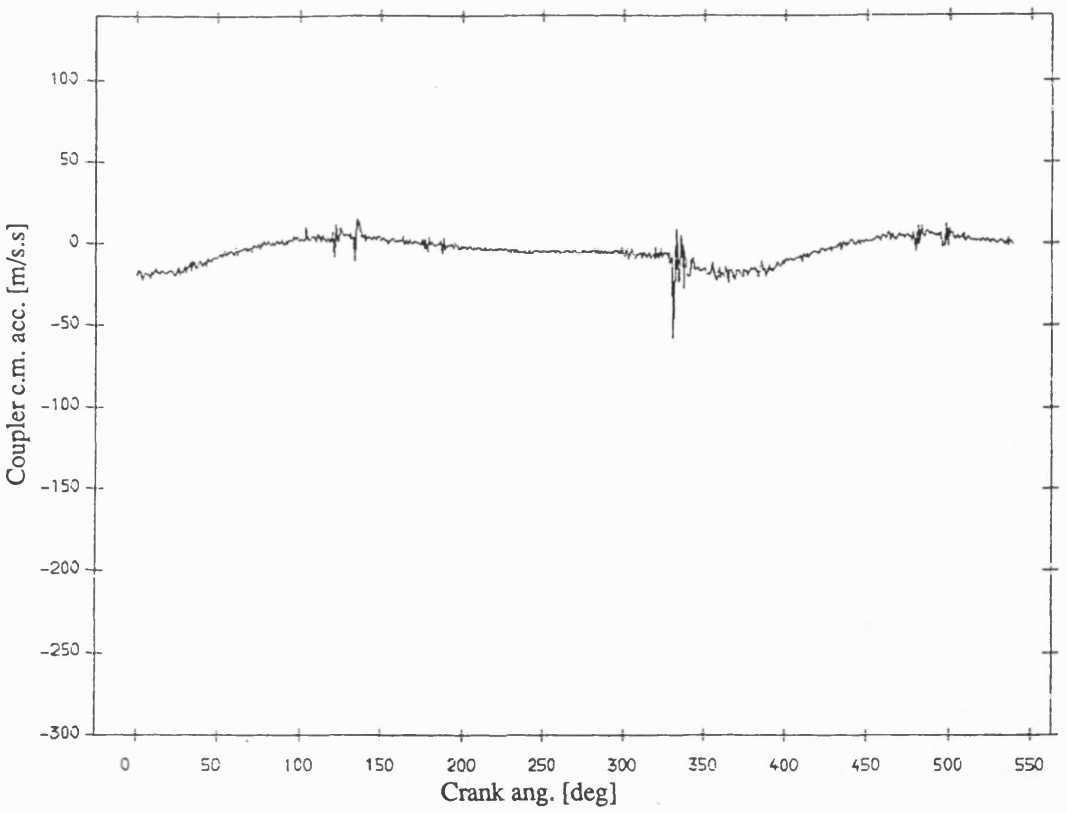

Fig 8.5.10 Exp. result coupler acceleration , greasy bearing
with fly wheel ;mean speed=168 rev/min ; dia. clearance=.30mm

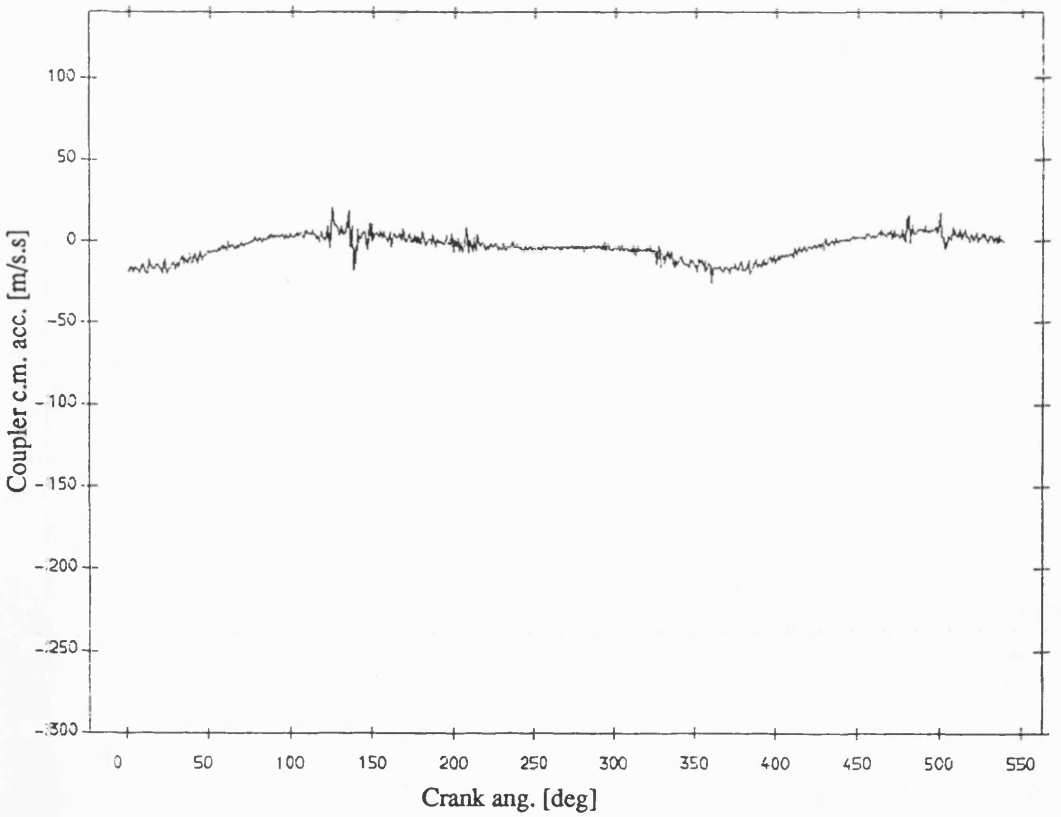

Fig 8.5.11 Exp. result coupler acceleration , dry bearing
with fly wheel ;mean speed=168 rev/min ; dia. clearance=.30mm

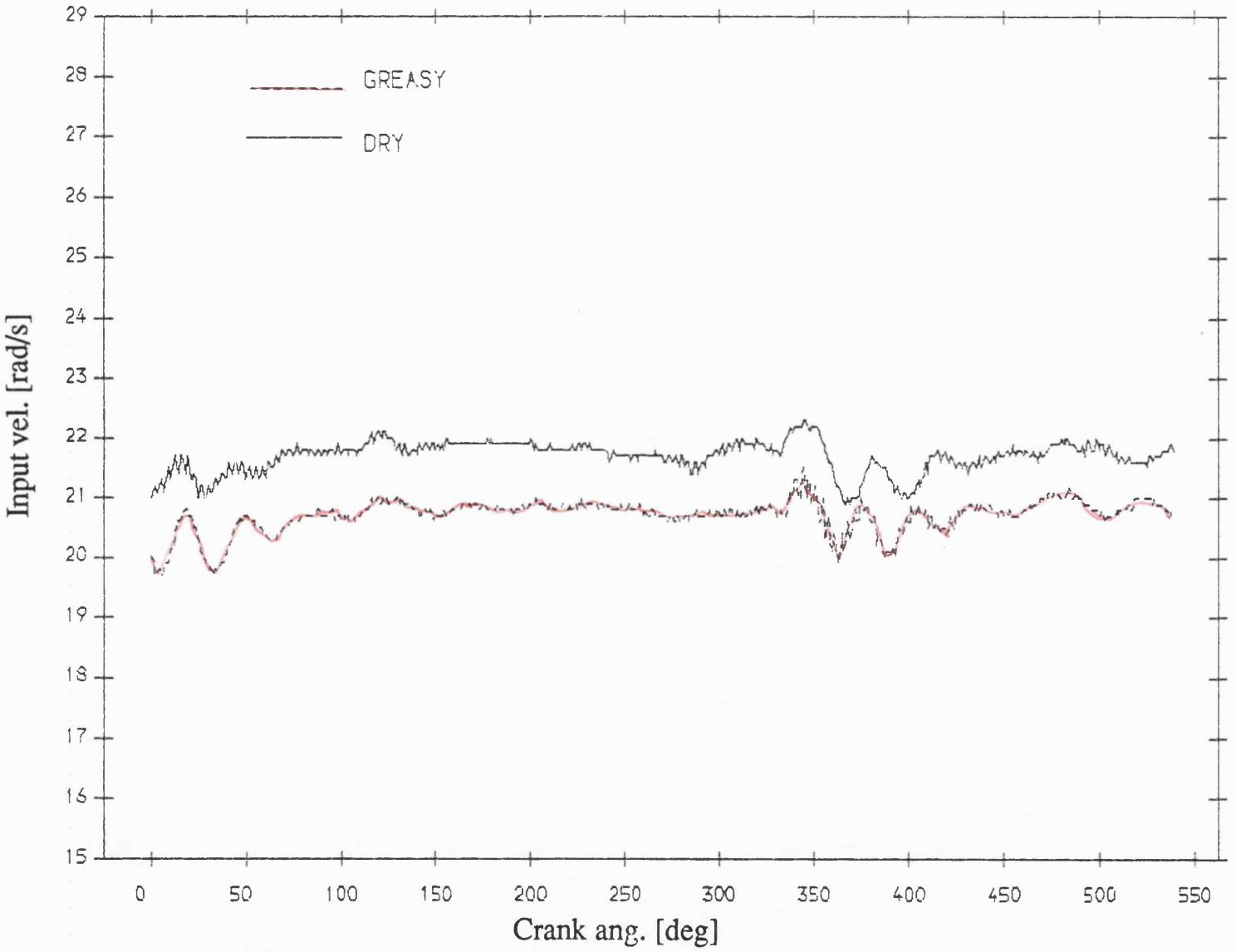

Fig 8.5.12 Exp. result input velocity , greasy v dry bearing
mean speed=208 rev/min; dia. clearance=.30mm

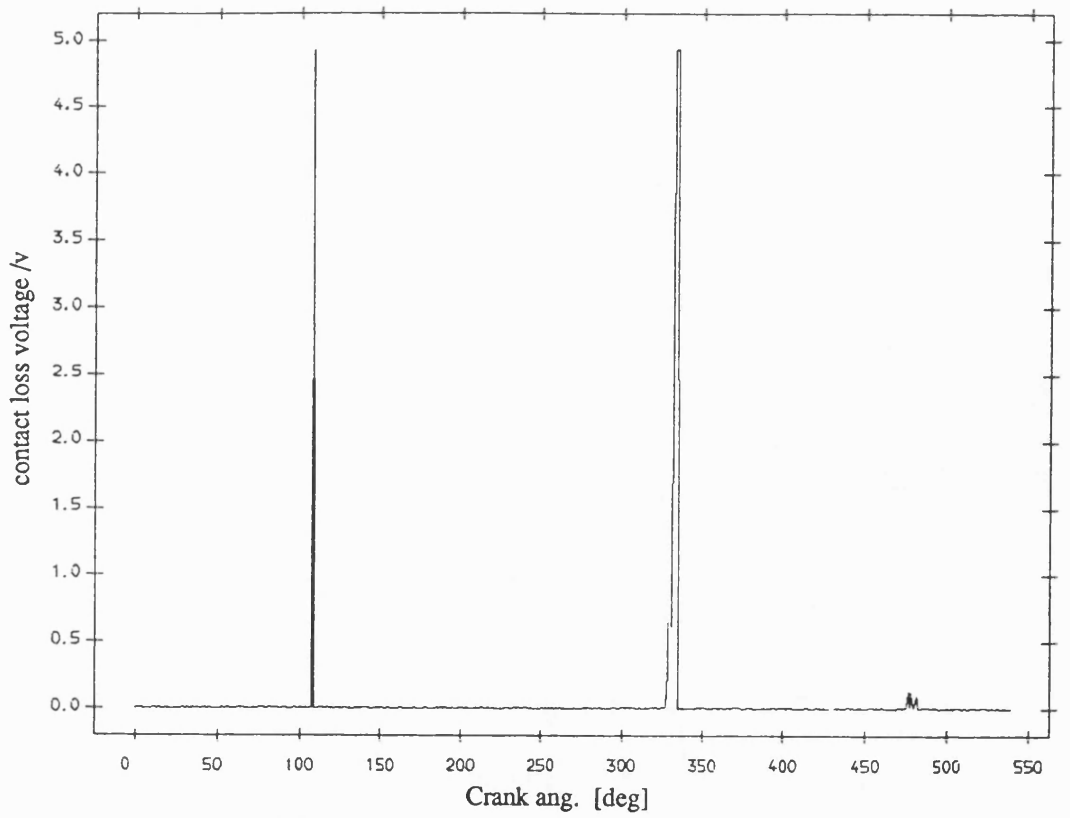

Fig 8.5.13 Exp. result contact loss of pin and greasy bearing
with flywheel ;mean speed=208 rev/min ;dia. clearance=0.30mm

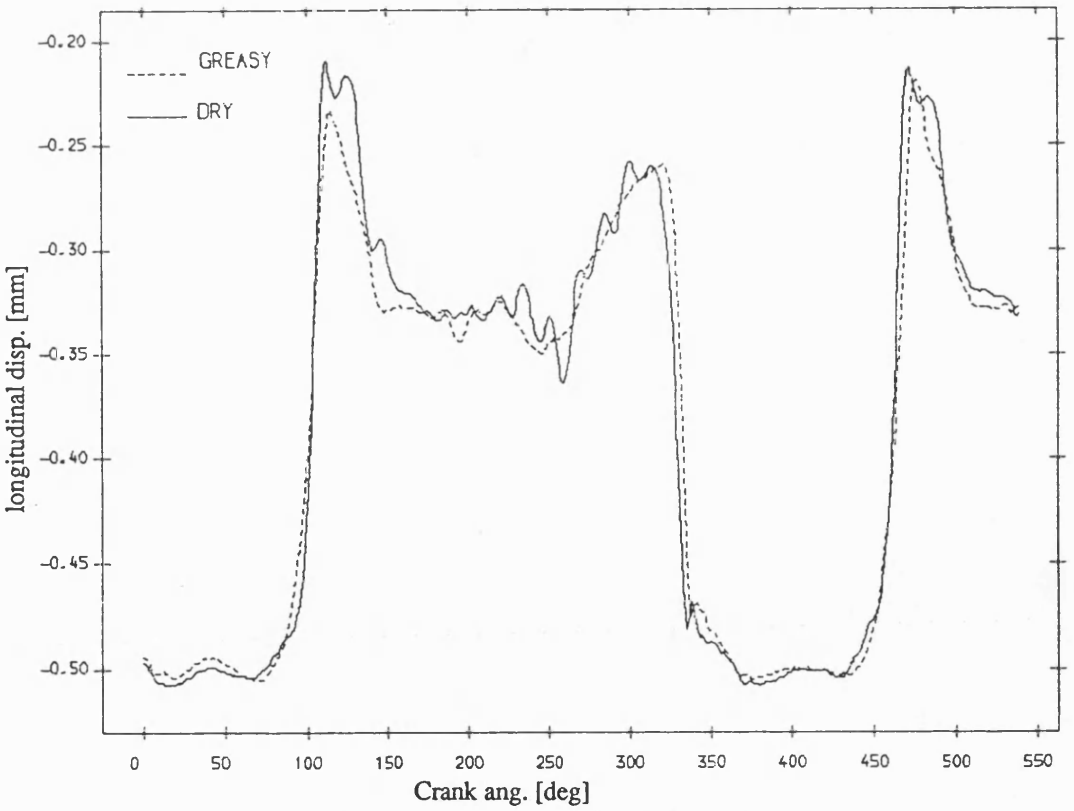

Fig 8.5.15 Exp. result longitudinal disp. of pin , greasy v dry bearing
mean speed=208 rev/min; dia. clearance=.30mm

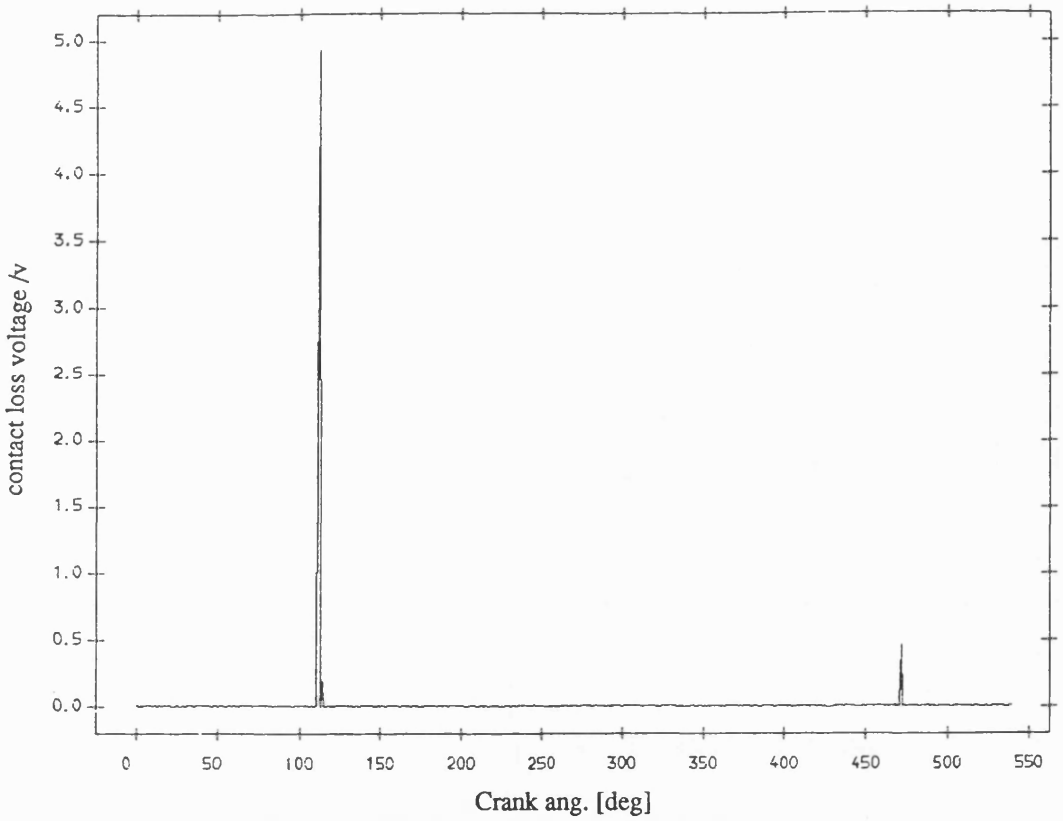

Fig 8.5.14 Exp. result contact loss of pin and dry bearing
with flywheel ;mean speed=208 rev/min ;dia. clearance=0.30mm

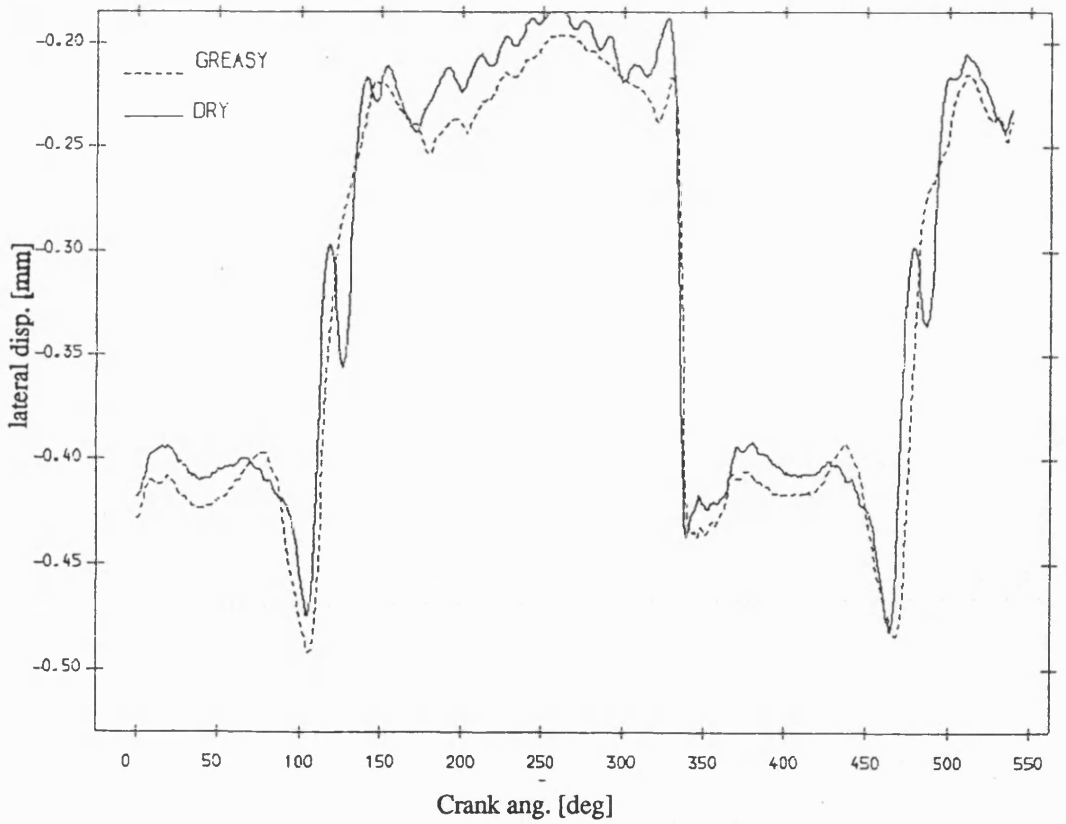

Fig 8.5.16 Exp. result lateral disp. of pin , greasy v dry bearing
mean speed=208 rev/min; dia. clearance=.30mm

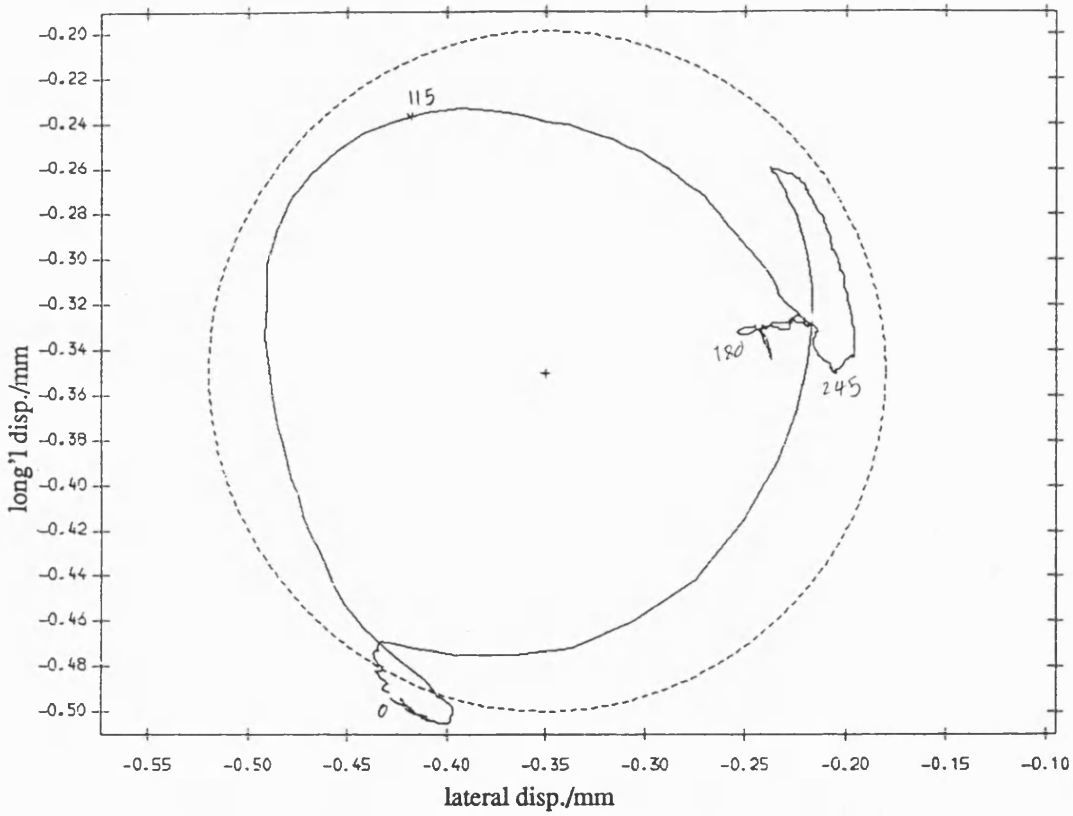

Fig 8.5.17 Exp. result polar plot of relative disp. of pin in greasy bearing with fly wheel ;mean speed=208 rev/min ; dia. clearance=.30mm

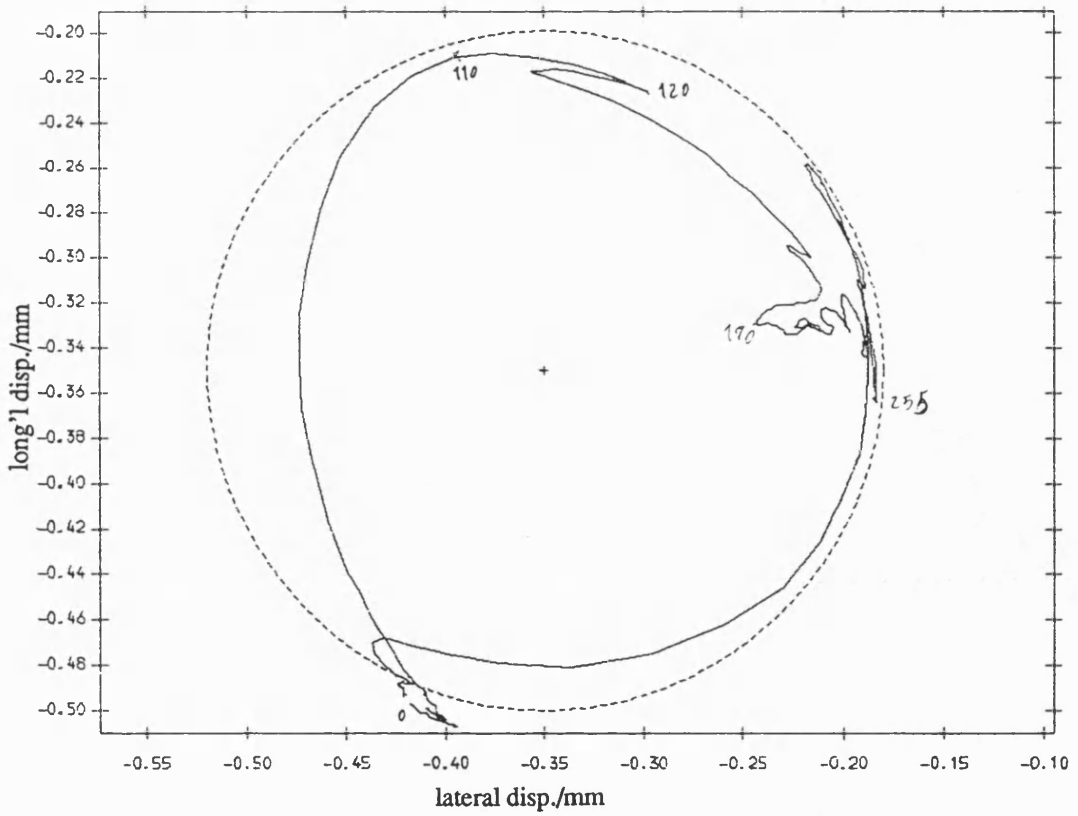

Fig 8.5.18 Exp. result polar plot of relative disp. of pin in dry bearing with fly wheel ;mean speed=208 rev/min ; dia. clearance=.30mm

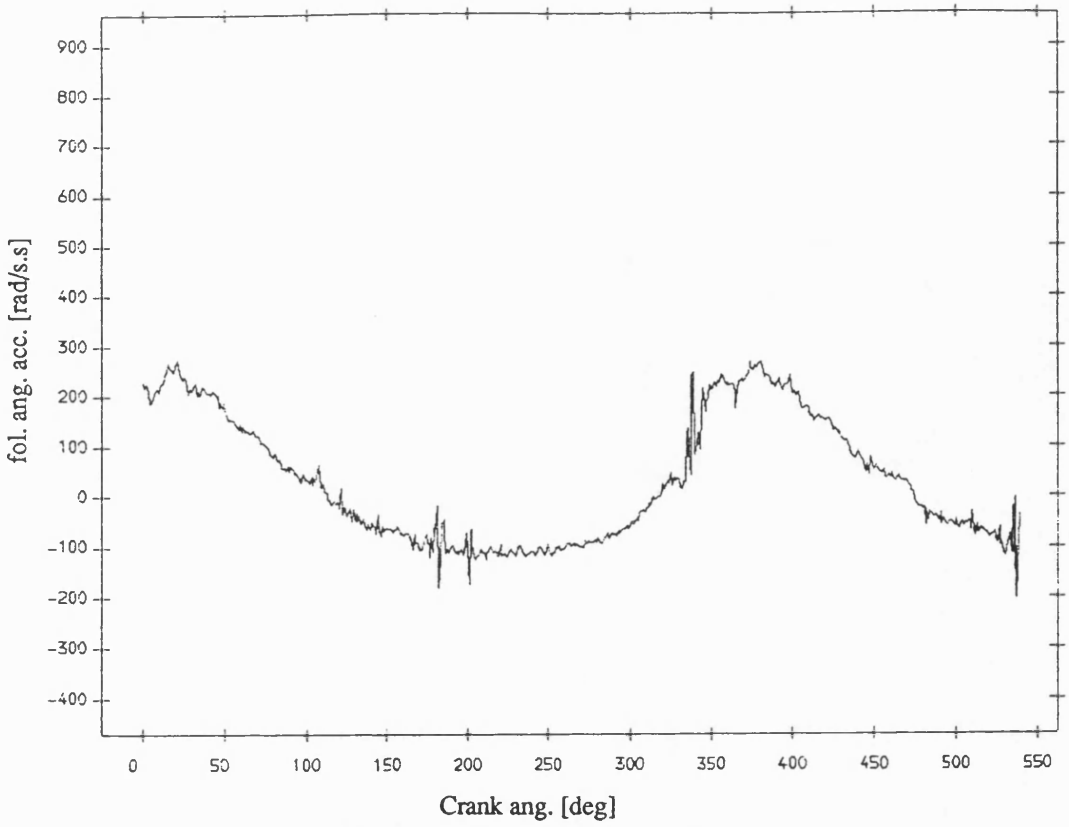

Fig 8.5.19 Exp. result follower ang. acceleration , greasy bearing
with fly wheel ;mean speed=208 rev/min ; dia. clearance=.30mm

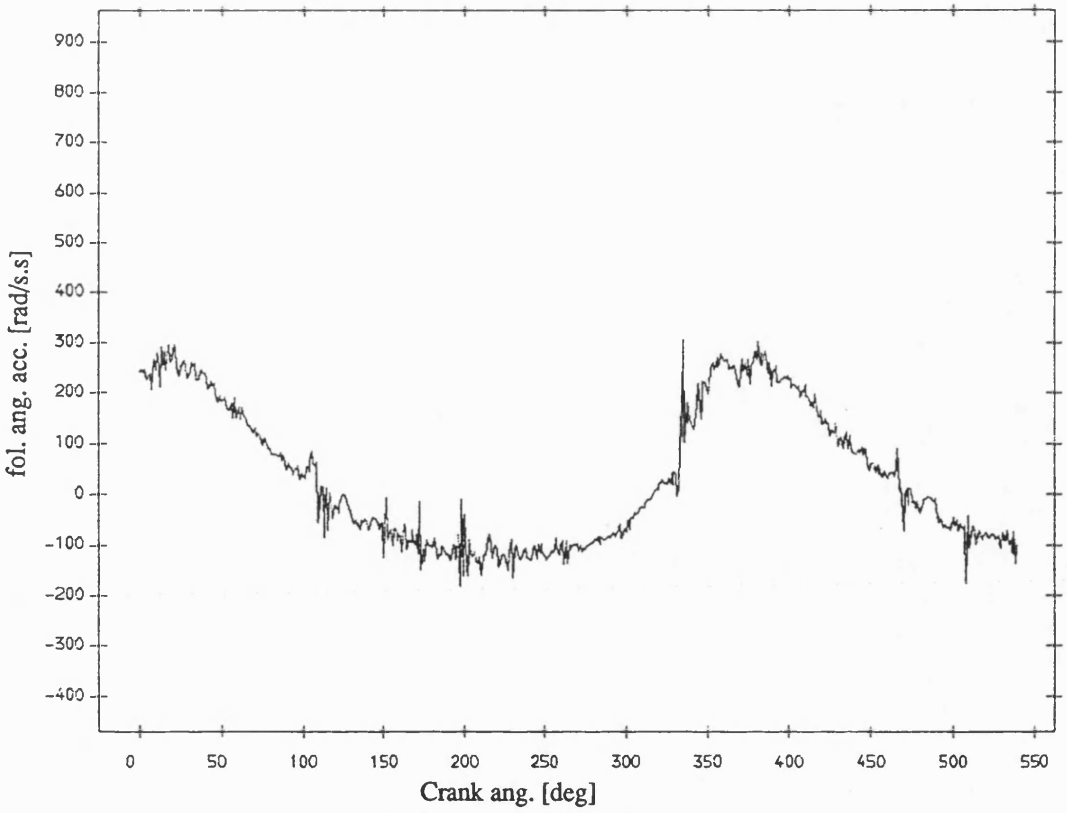

Fig 8.5.20 Exp. result follower ang. acceleration ,dry bearing
with fly wheel ;mean speed=208 rev/min ; dia. clearance=.30mm

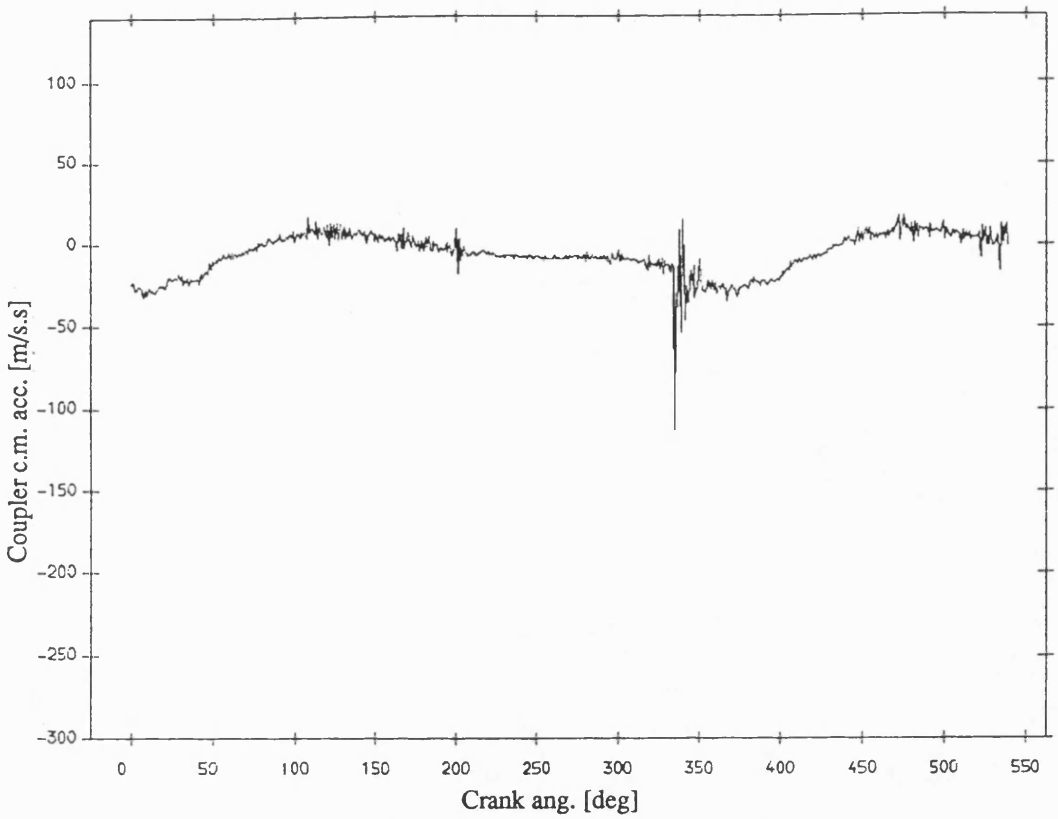

Fig 8.5.21 Exp. result coupler acceleration , greasy bearing
with fly wheel ;mean speed=208 rev/min ; dia. clearance=.30mm

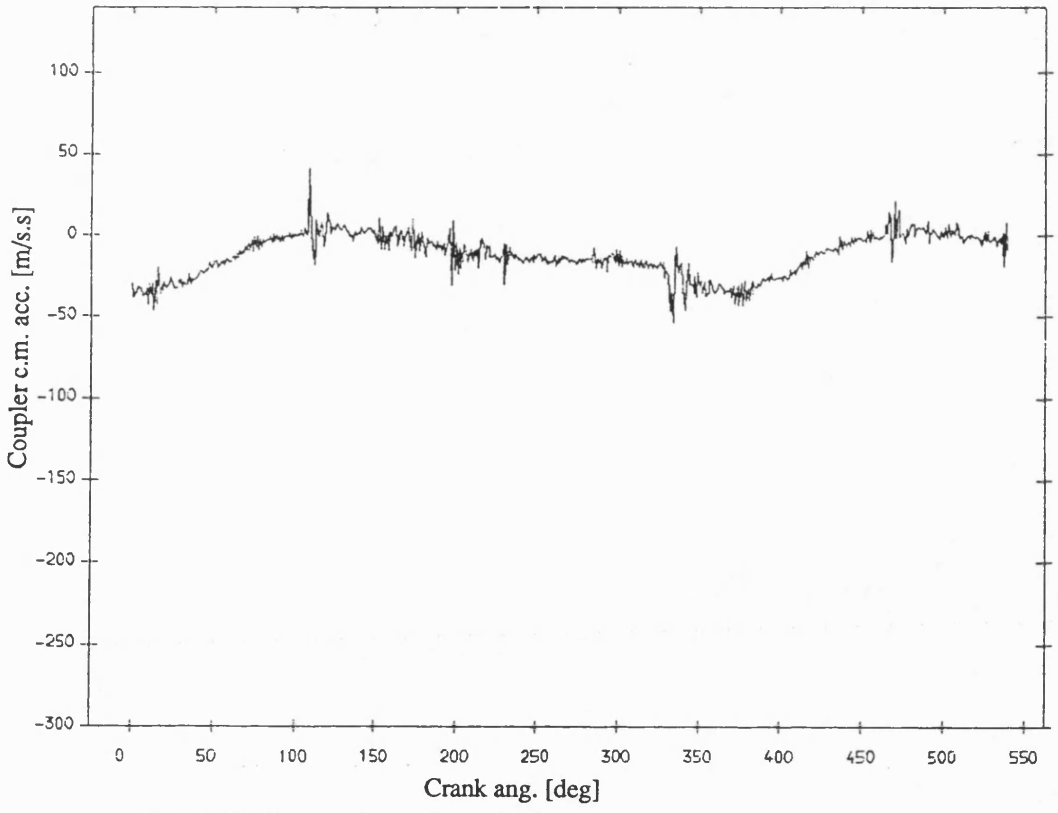

Fig 8.5.22 Exp. result coupler acceleration , dry bearing
with fly wheel ;mean speed=208 rev/min ; dia. clearance=.30mm

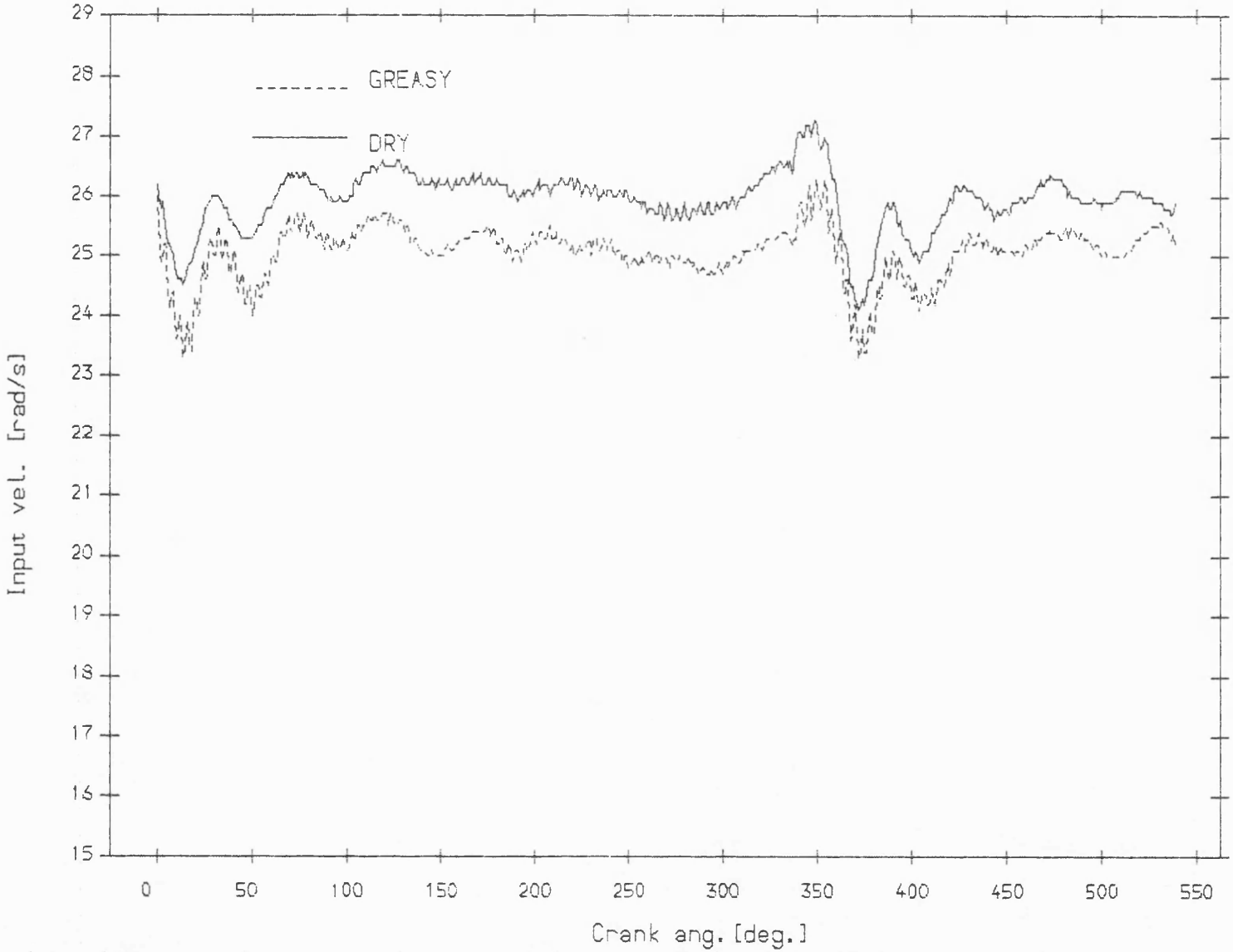

Fig( ) Exp. result input velocity rad/s greasy & dry bearing
with fly wheel mean speed=244 rev/min dia. clearance=.3mm

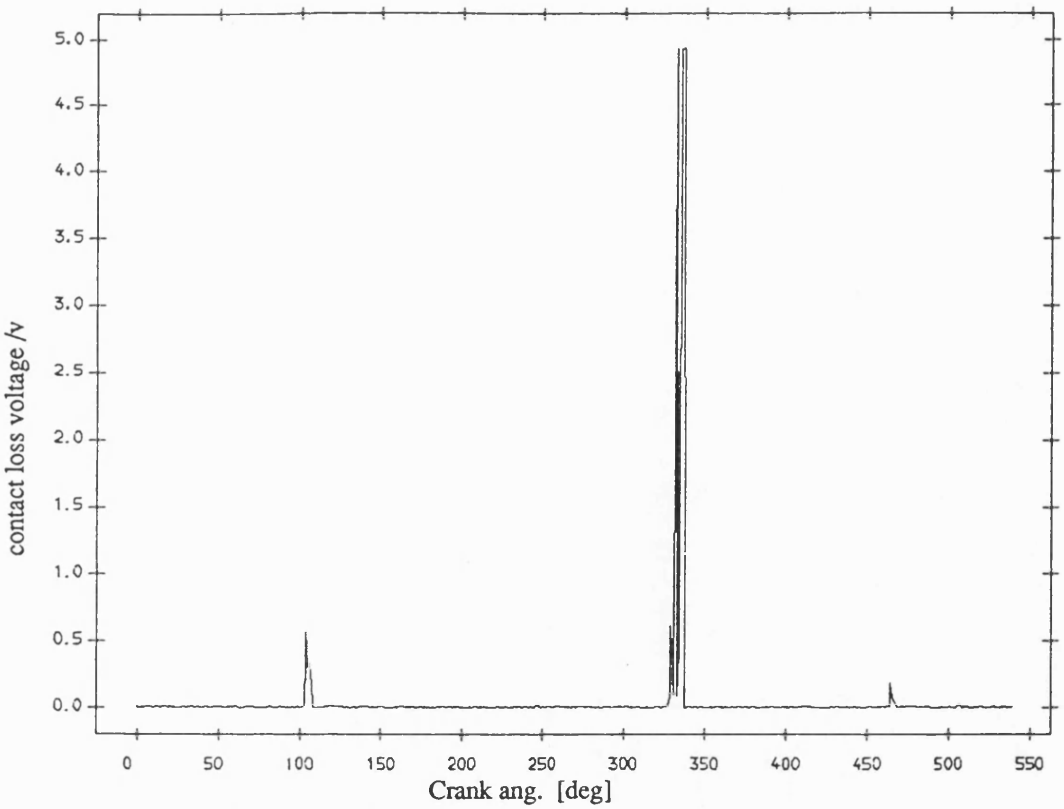

Fig 8.5.24 Exp. result contact loss of pin and greasy bearing
with flywheel ;mean speed=244 rev/min ;dia. clearance=0.30mm

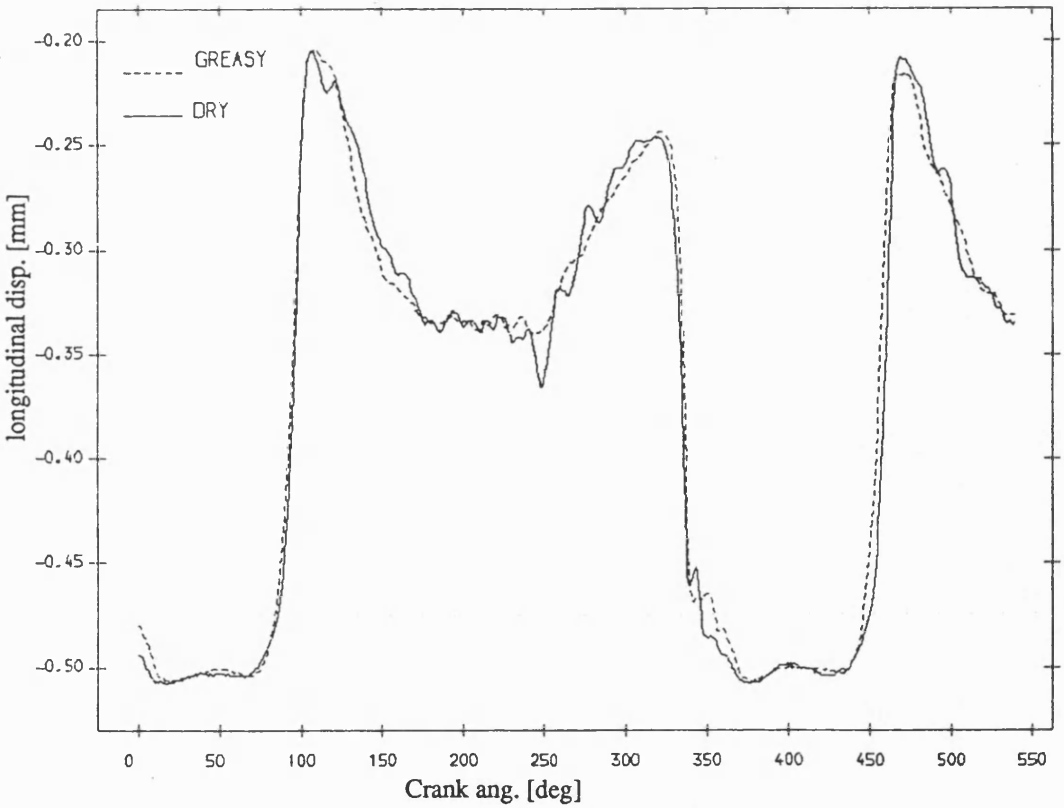

Fig 8.5.26 Exp. result longitudinal disp. of pin , greasy v dry bearing
mean speed=244 rev/min; dia. clearance=.30mm

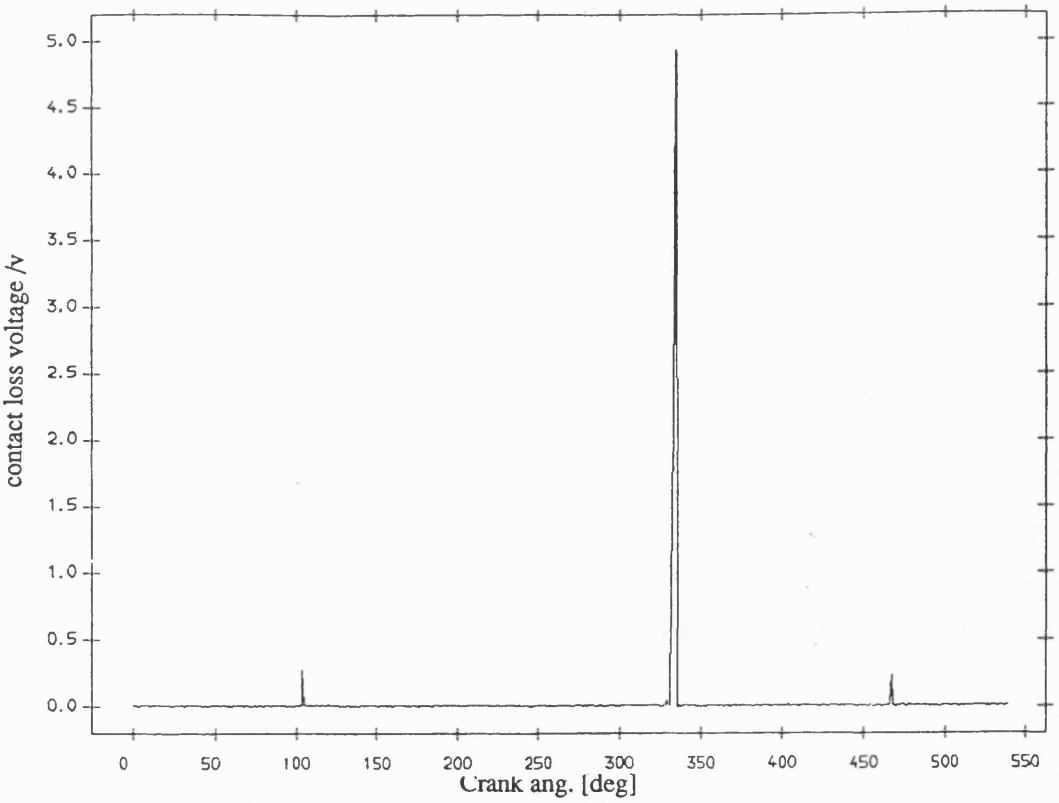

Fig 8.5.25 Exp. result contact loss of pin and dry bearing
with flywheel ;mean speed=244 rev/min ;dia. clearance=0.30mm

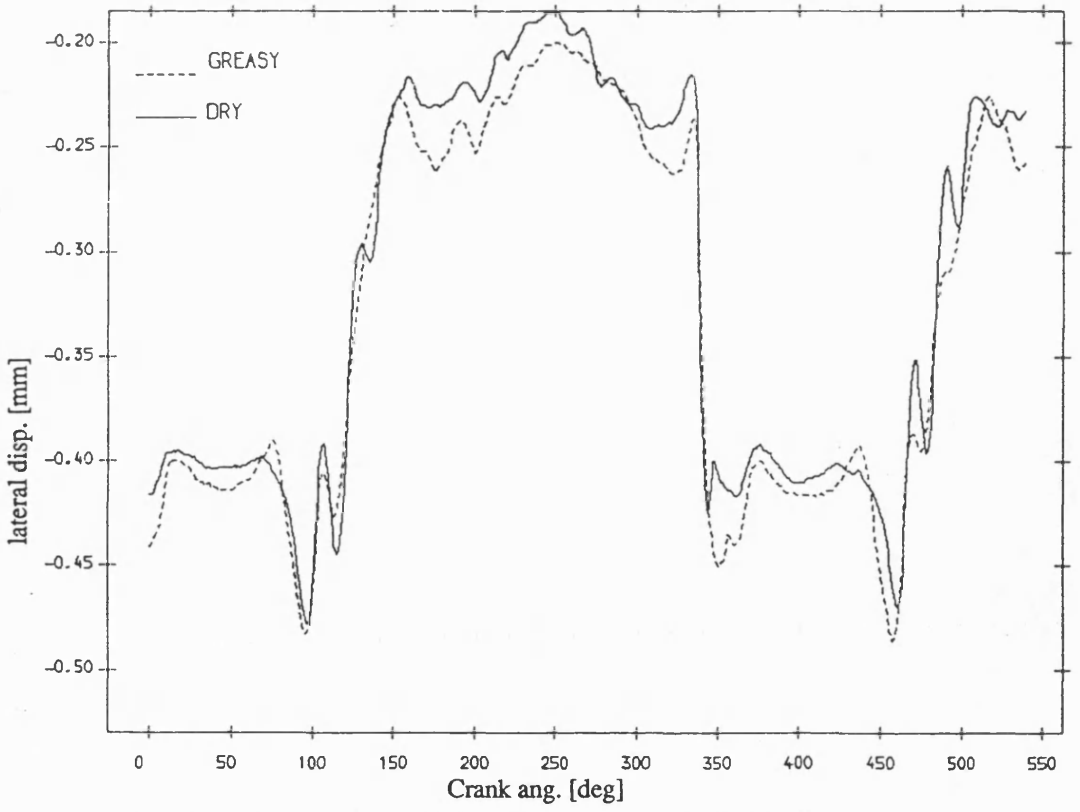

Fig 8.5.27 Exp. result lateral disp. of pin , greasy v dry bearing
mean speed=244 rev/min; dia. clearance=.30mm

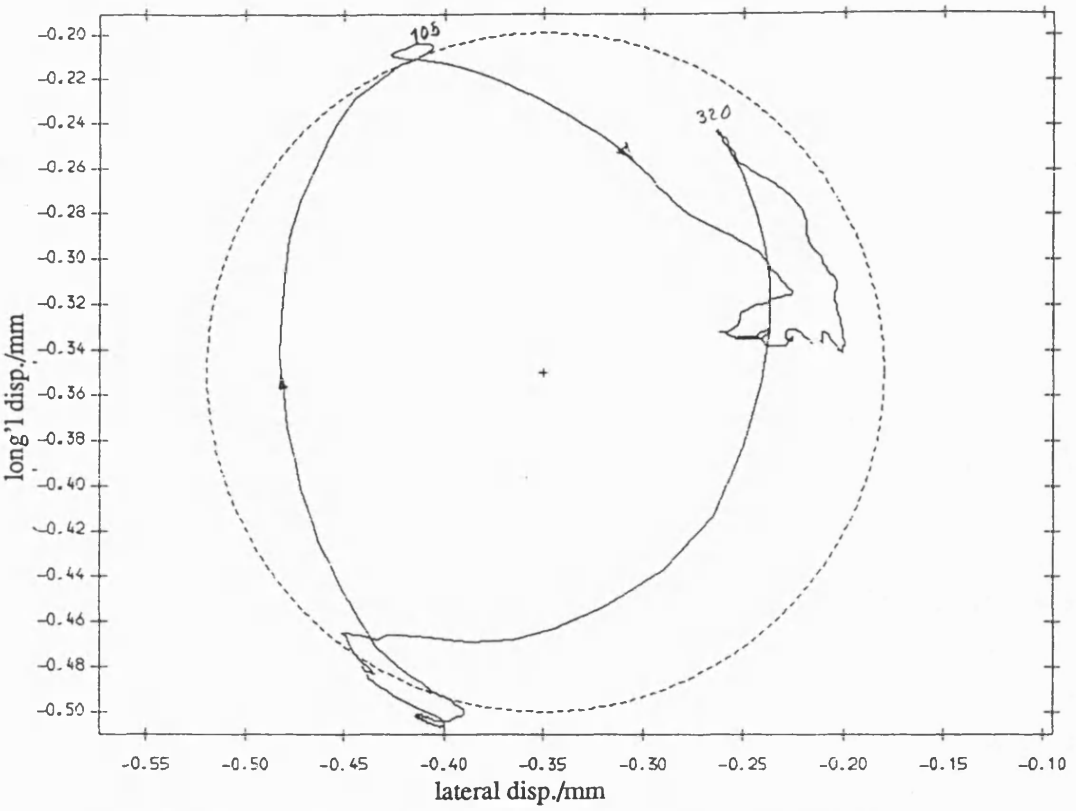

Fig 8.5.28 Exp. result polar plot of relative disp. of pin in greasy bearing with fly wheel ;mean speed=244 rev/min ; dia. clearance=.30mm

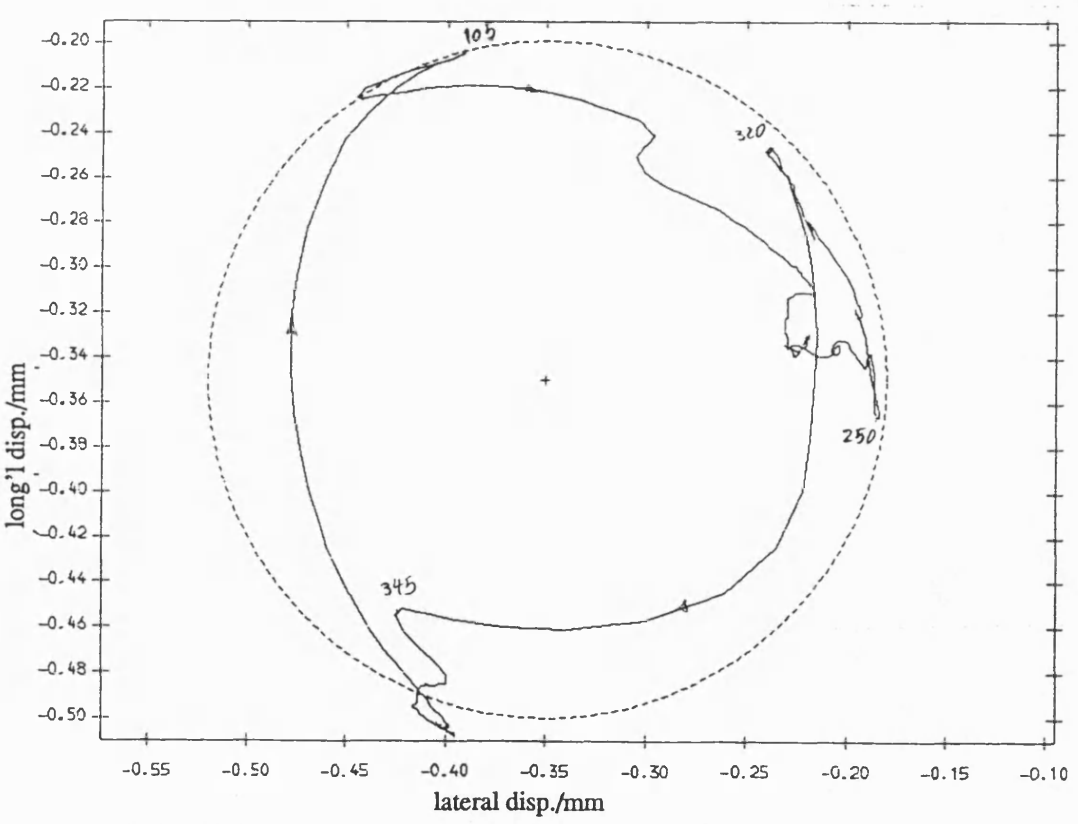

Fig 8.5.29 Exp. result polar plot of relative disp. of pin in dry bearing with fly wheel ;mean speed=244 rev/min ; dia. clearance=.30mm

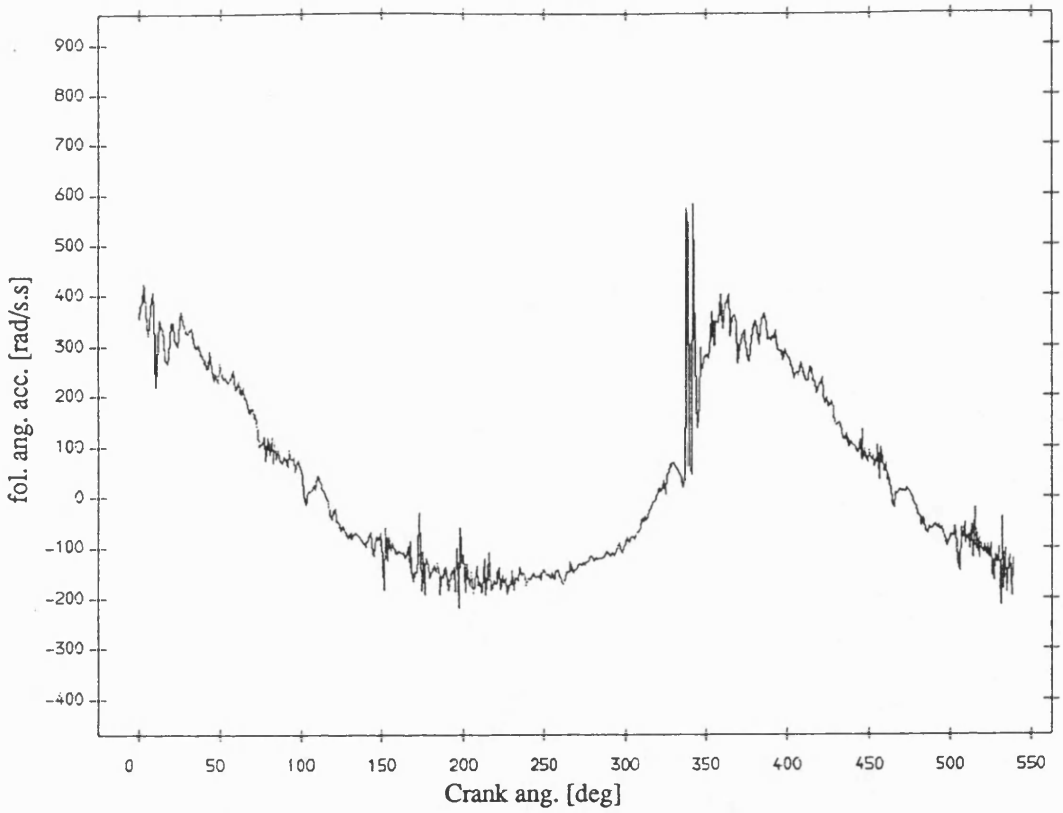

Fig 8.5.30 Exp. result follower ang. acceleration , greasy bearing
with fly wheel ;mean speed=244 rev/min ; dia. clearance=.30mm

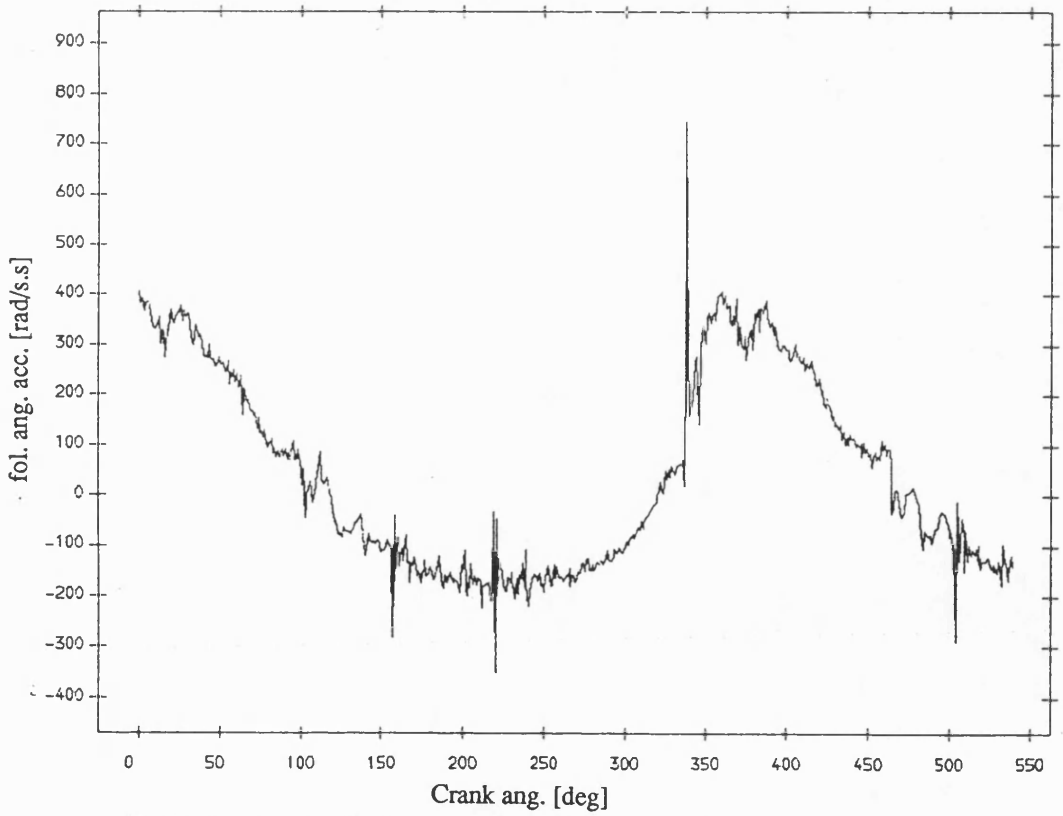

Fig 8.5.31 Exp. result follower ang. acceleration ,dry bearing
with fly wheel ;mean speed=244 rev/min ; dia. clearance=.30mm

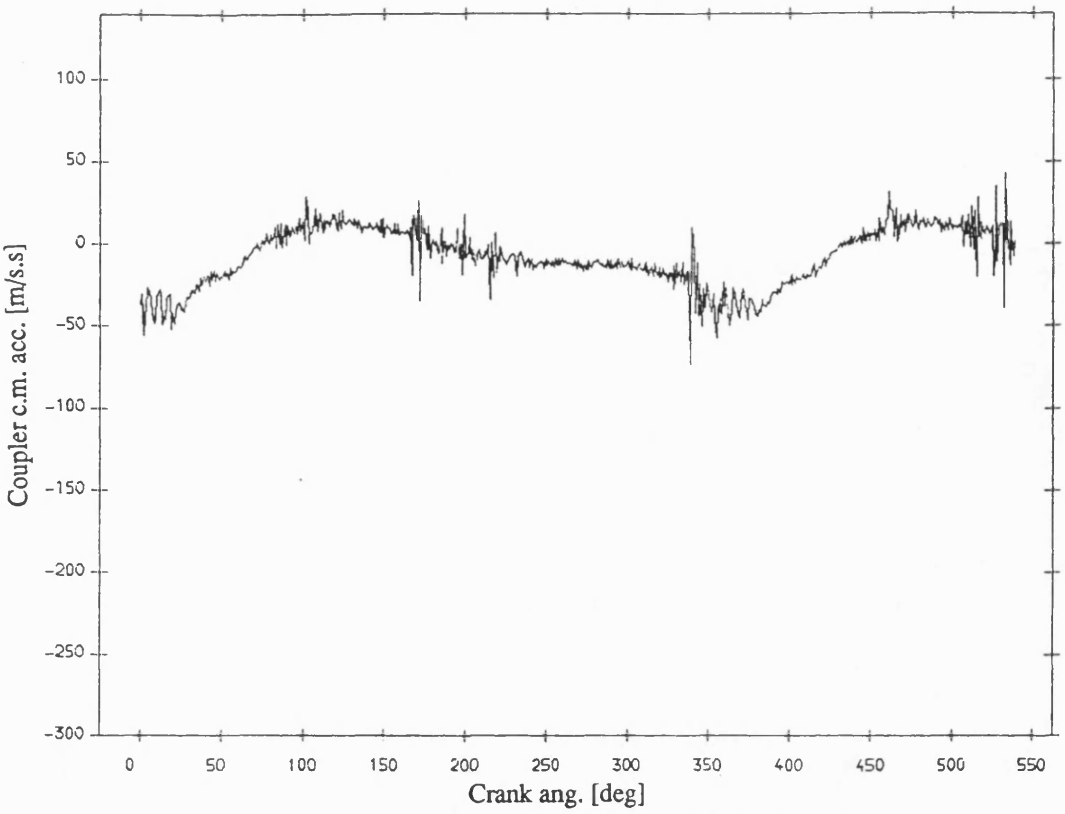

Fig 8.5.32 Exp. result coupler acceleration , greasy bearing
with fly wheel ;mean speed=244 rev/min ; dia. clearance=.30mm

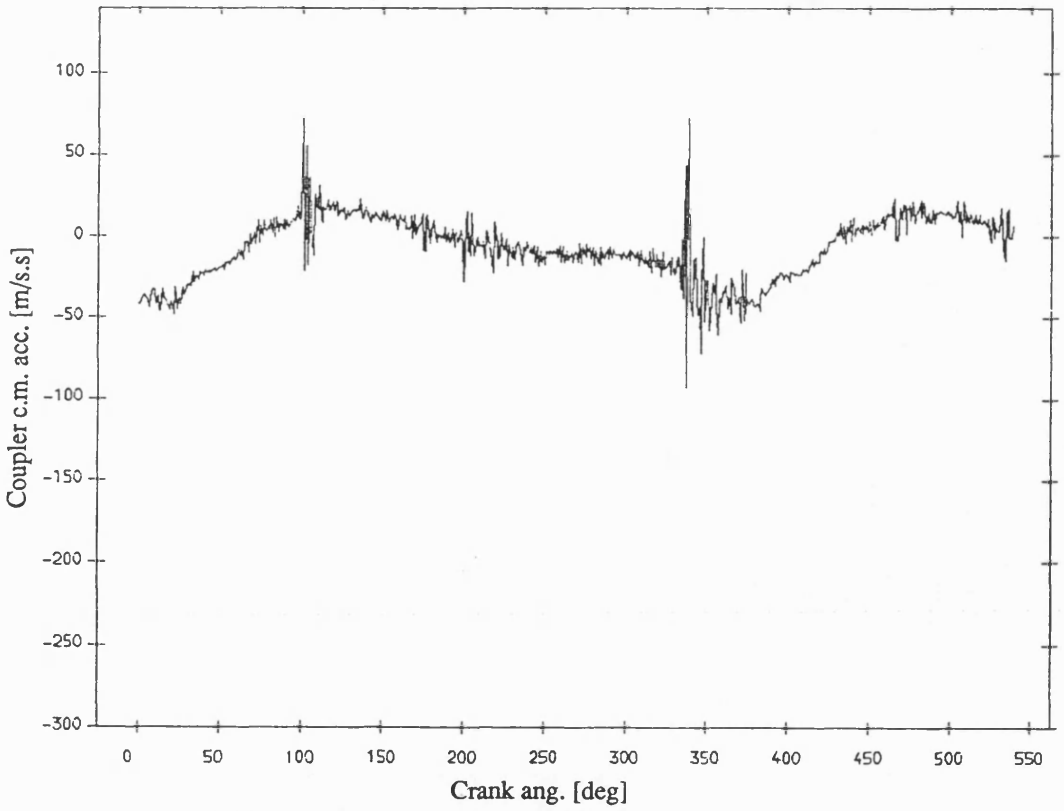

Fig 8.5.33 Exp. result coupler acceleration , dry bearing
with fly wheel ;mean speed=244 rev/min ; dia. clearance=.30mm

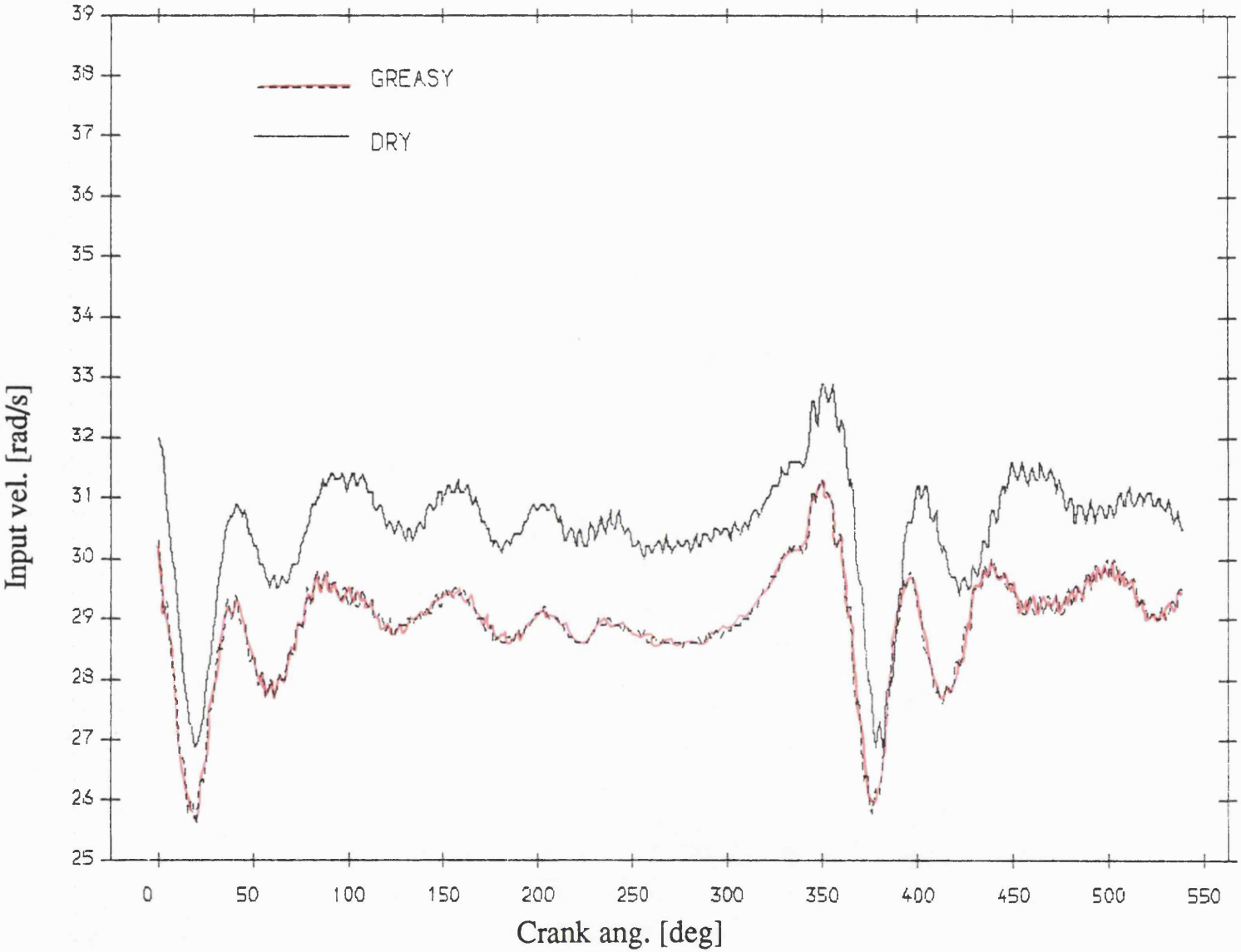

Fig 8.5.34 Exp. result input velocity , greasy v dry bearing
mean speed=290 rev/min; dia. clearance=.30mm

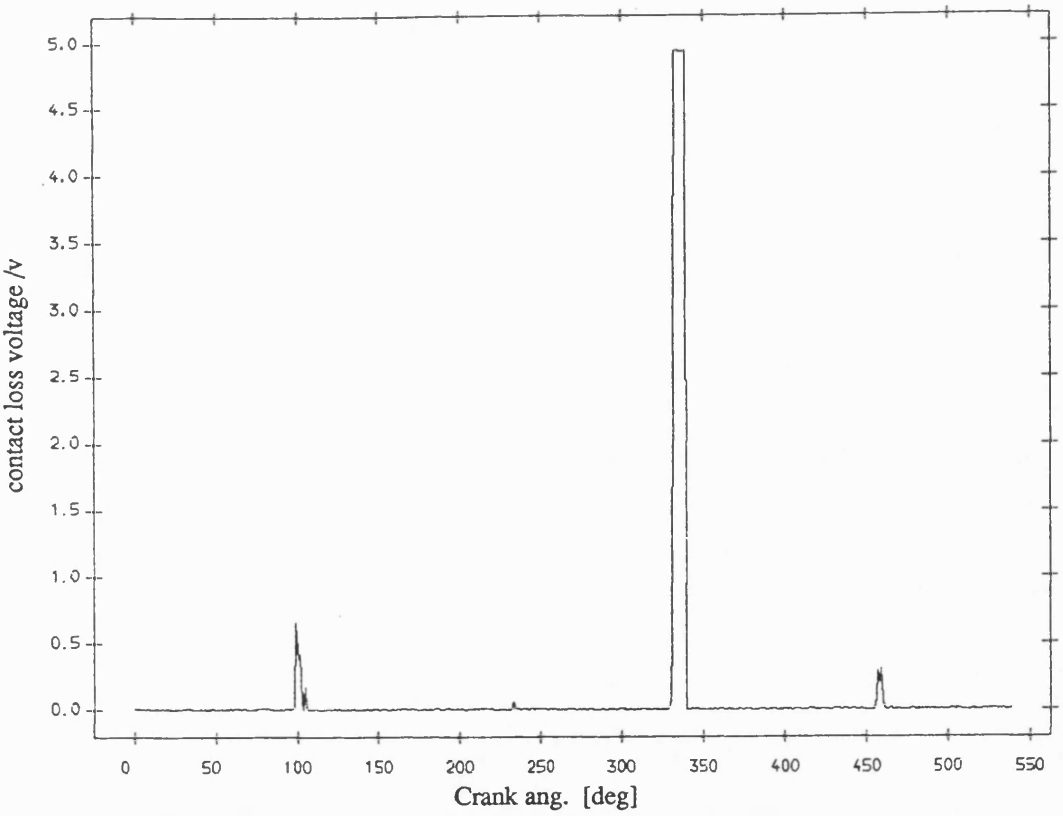

Fig 8.5.35 Exp. result contact loss of pin and greasy bearing
with flywheel ;mean speed=290 rev/min ;dia. clearance=0.30mm

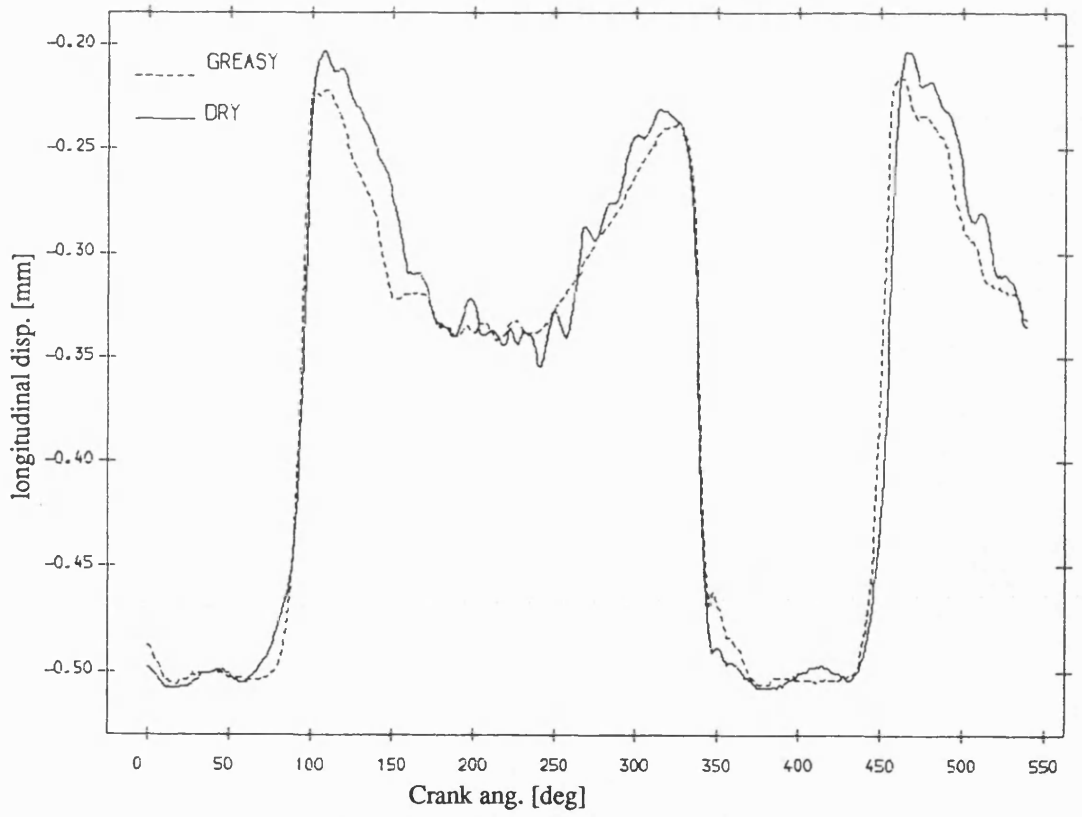

Fig 8.5.37 Exp. result longitudinal disp. of pin , greasy v dry bearing
mean speed=290 rev/min; dia. clearance=.30mm

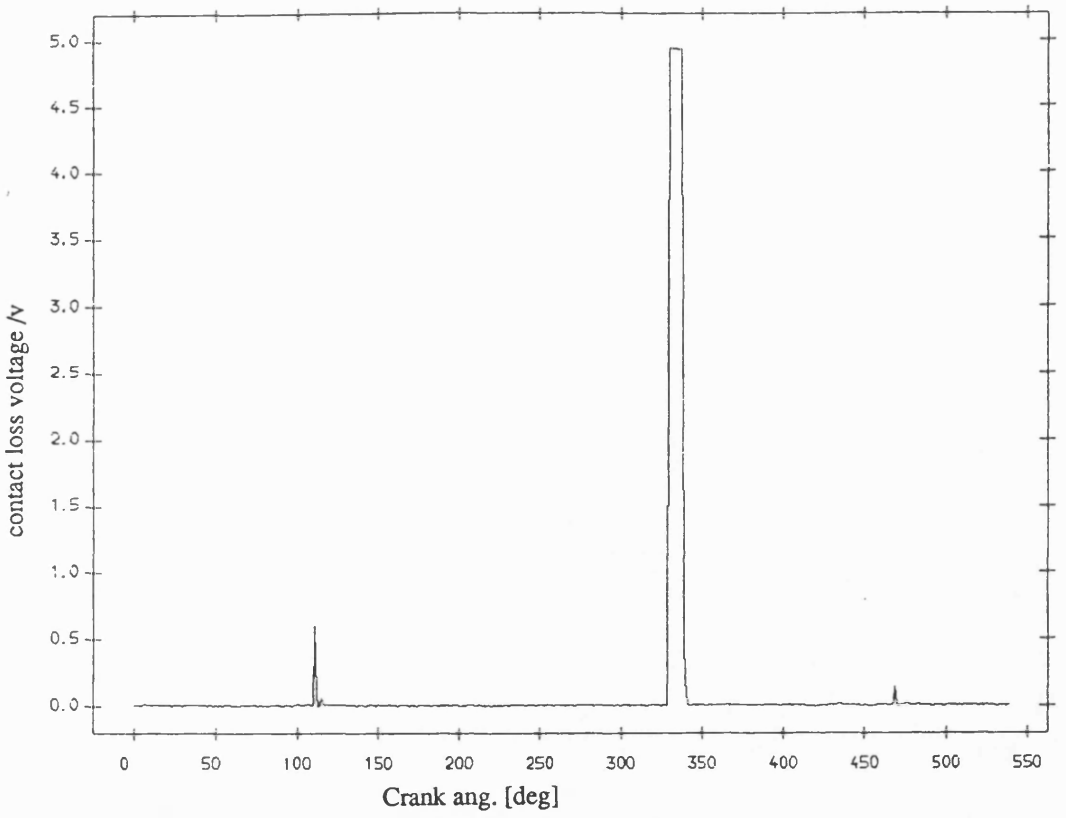

Fig 8.5.36 Exp. result contact loss of pin and dry bearing
with flywheel ;mean speed=290 rev/min ;dia. clearance=0.30mm

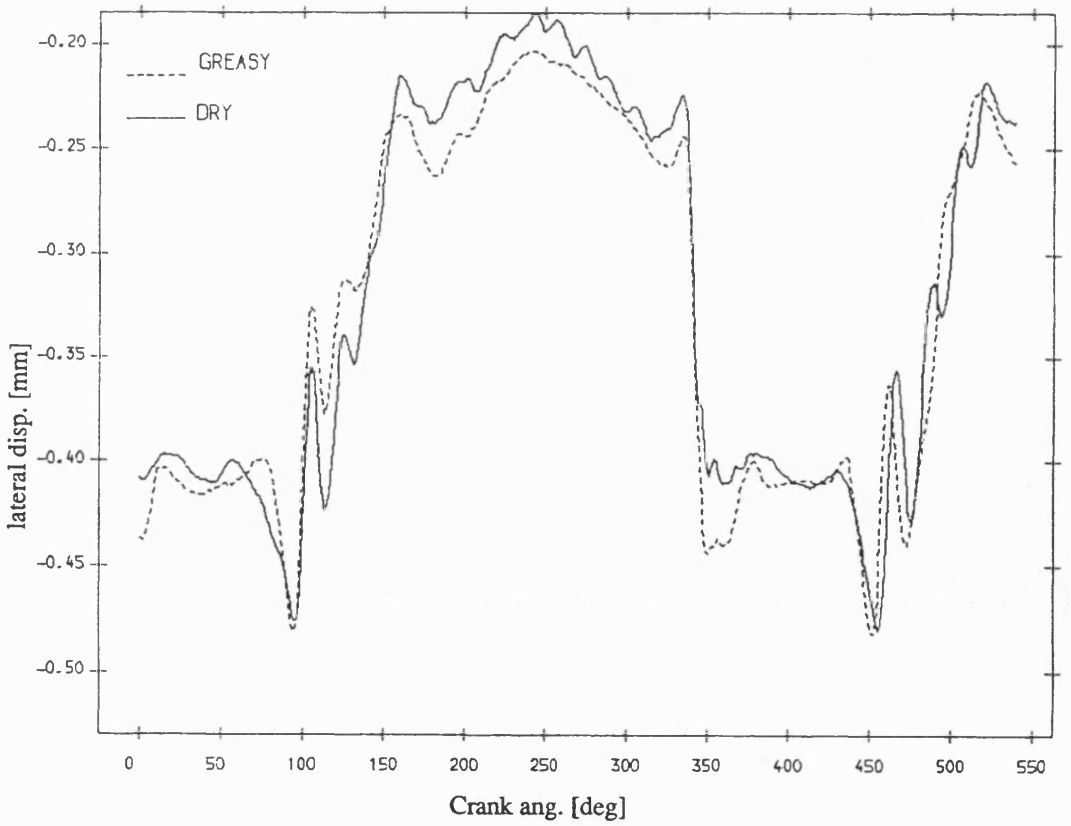

Fig 8.5.38 Exp. result lateral disp. of pin , greasy v dry bearing
mean speed=290 rev/min; dia. clearance=.30mm

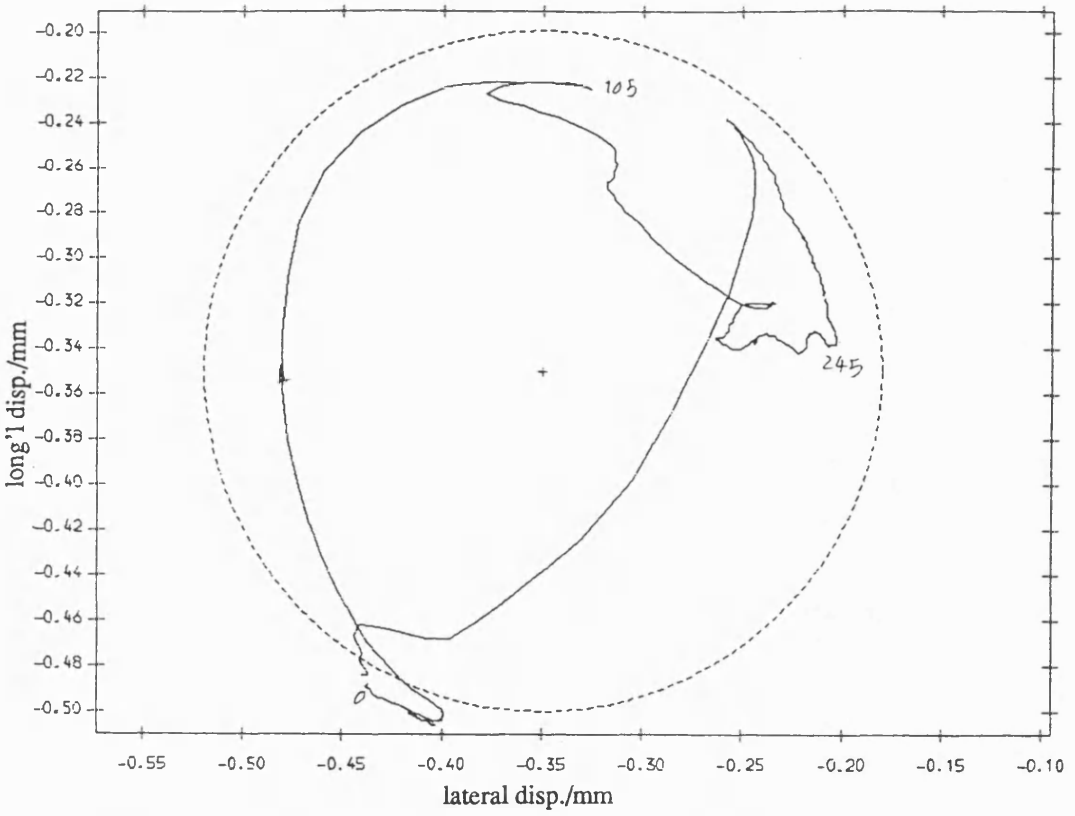

Fig 8.5.39 Exp. result polar plot of relative disp. of pin in greasy bearing with fly wheel ;mean speed=290 rev/min ; dia. clearance=.30mm

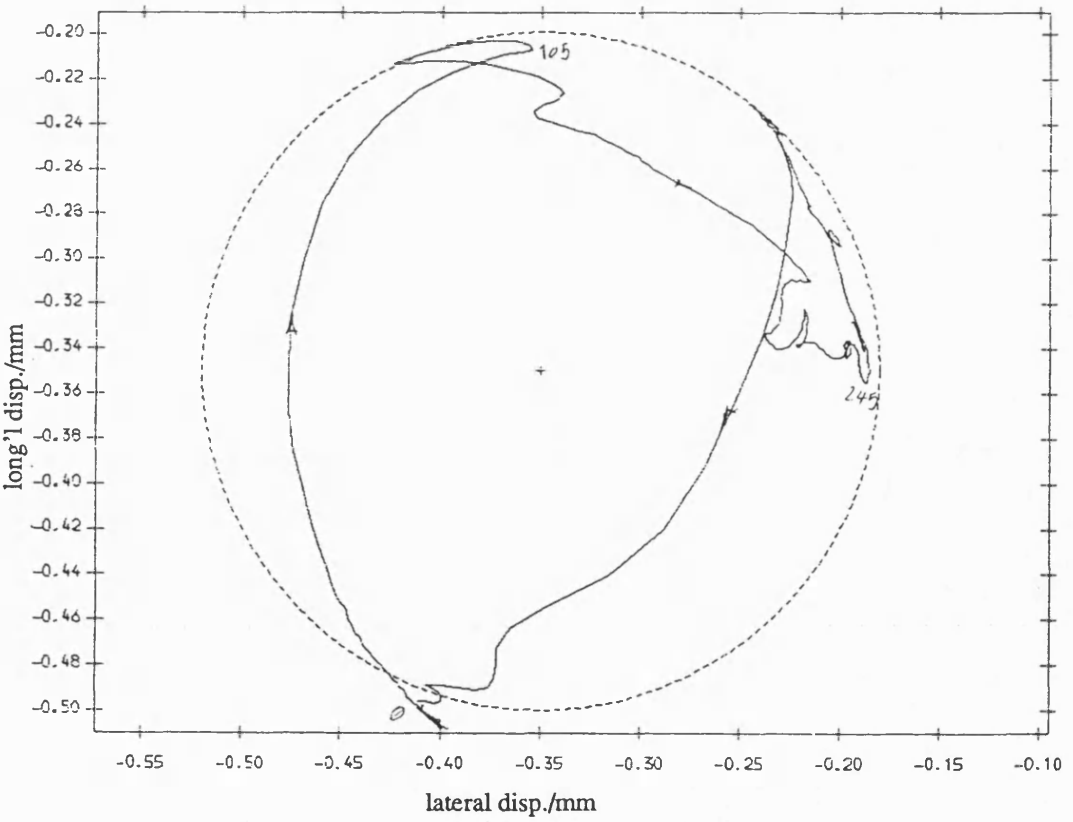

Fig 8.5.40 Exp. result polar plot of relative disp. of pin in dry bearing with fly wheel ;mean speed=290 rev/min ; dia. clearance=.30mm

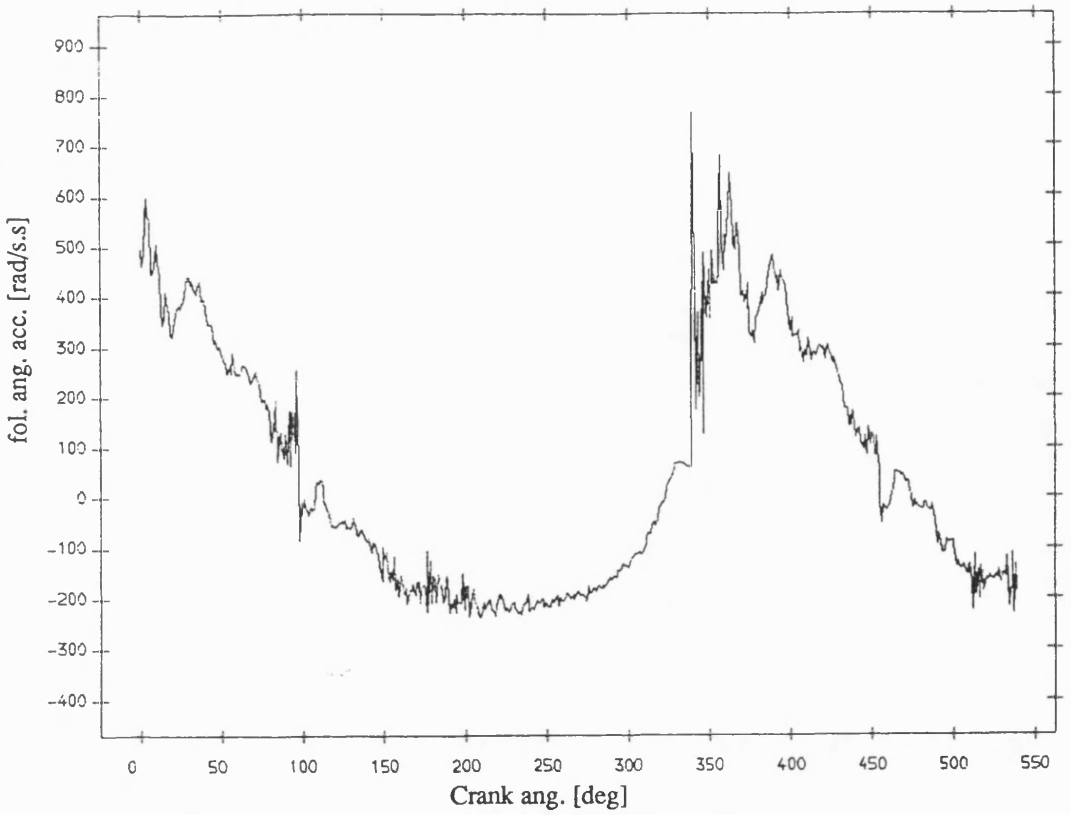

Fig 8.5.41 Exp. result follower ang. acceleration , greasy bearing
with fly wheel ;mean speed=290 rev/min ; dia. clearance=.30mm

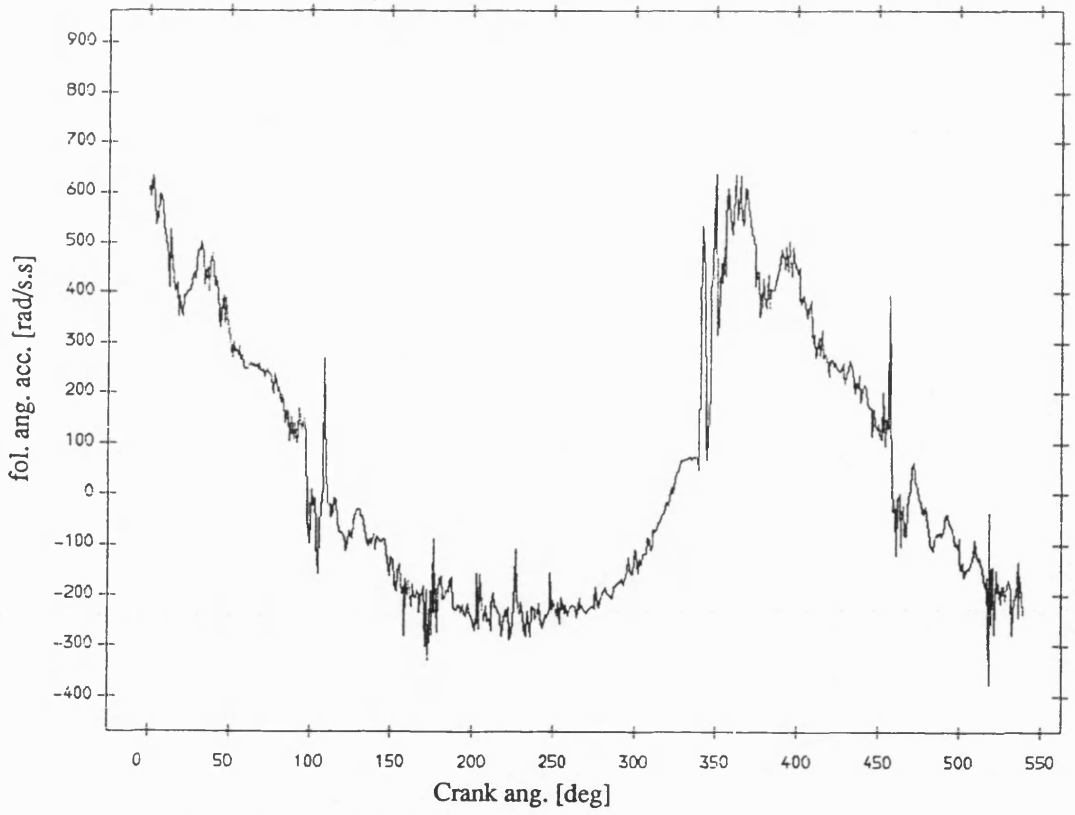

Fig 8.5.42 Exp. result follower ang. acceleration ,dry bearing
with fly wheel ;mean speed=290 rev/min ; dia. clearance=.30mm

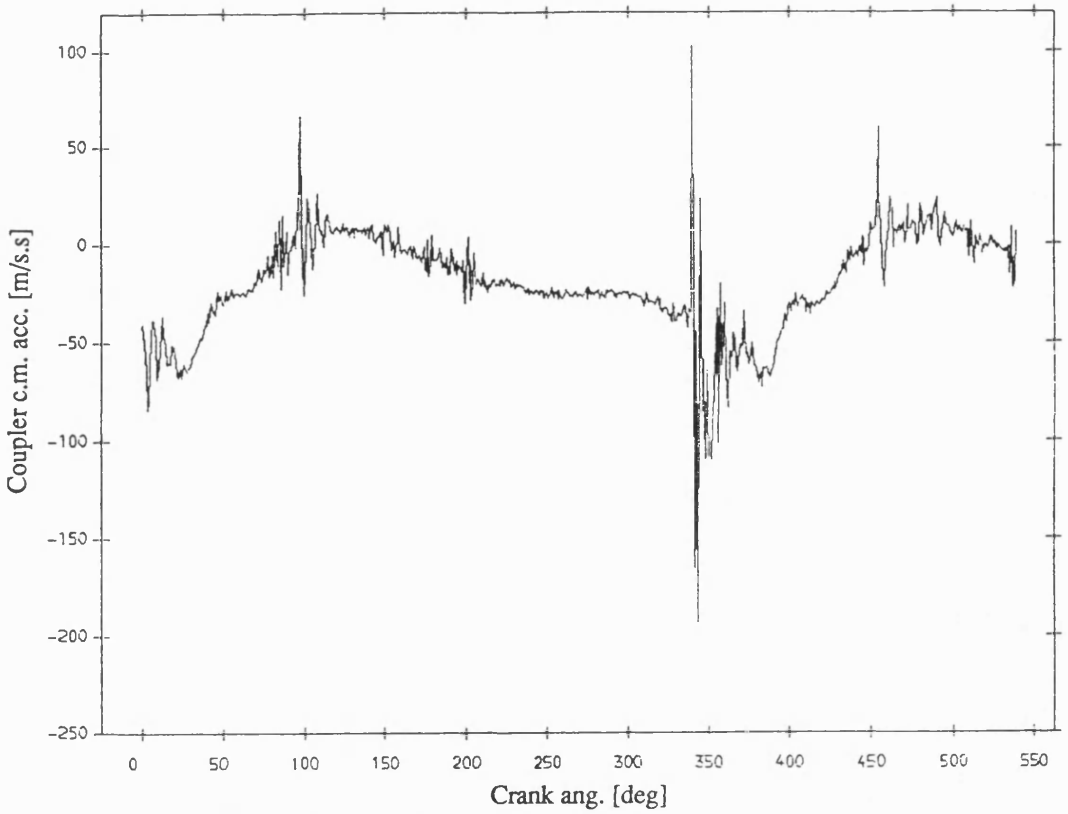

Fig 8.5.43 Exp. result coupler acceleration , greasy bearing
with fly wheel ;mean speed=290 rev/min ; dia. clearance=.30mm

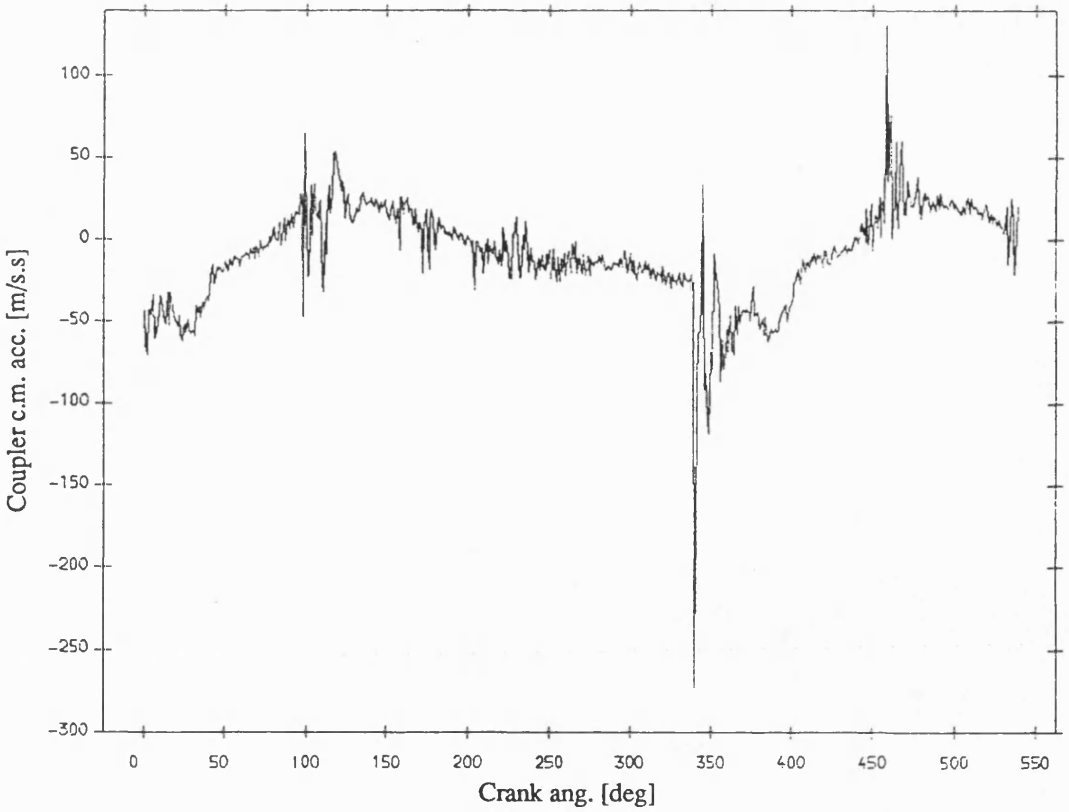

Fig 8.5.44 Exp. result coupler acceleration , dry bearing
with fly wheel ;mean speed=290 rev/min ; dia. clearance=.30mm

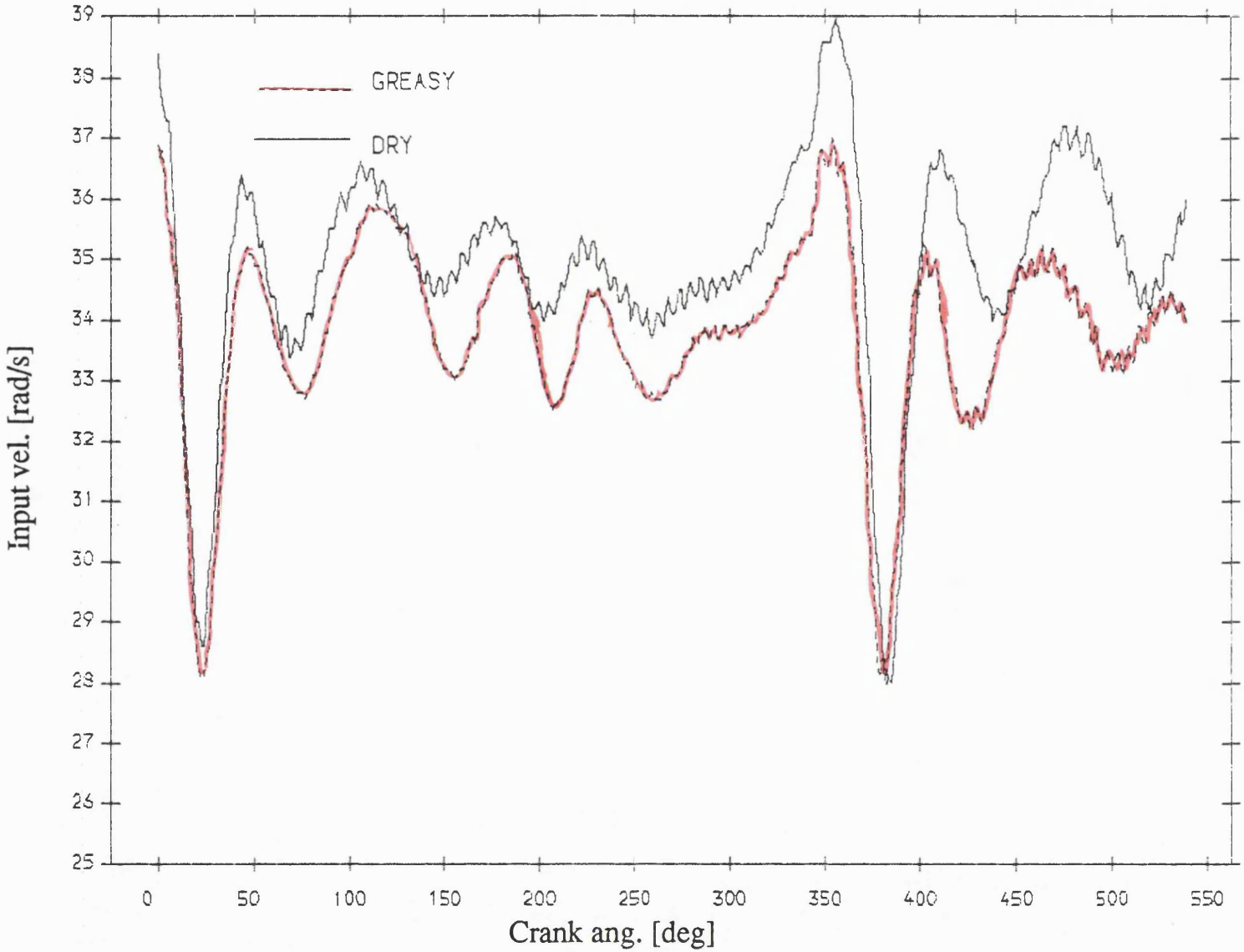

Fig 8.5.45 Exp. result input velocity , greasy v dry bearing
mean speed=327 rev/min; dia. clearance=.30mm

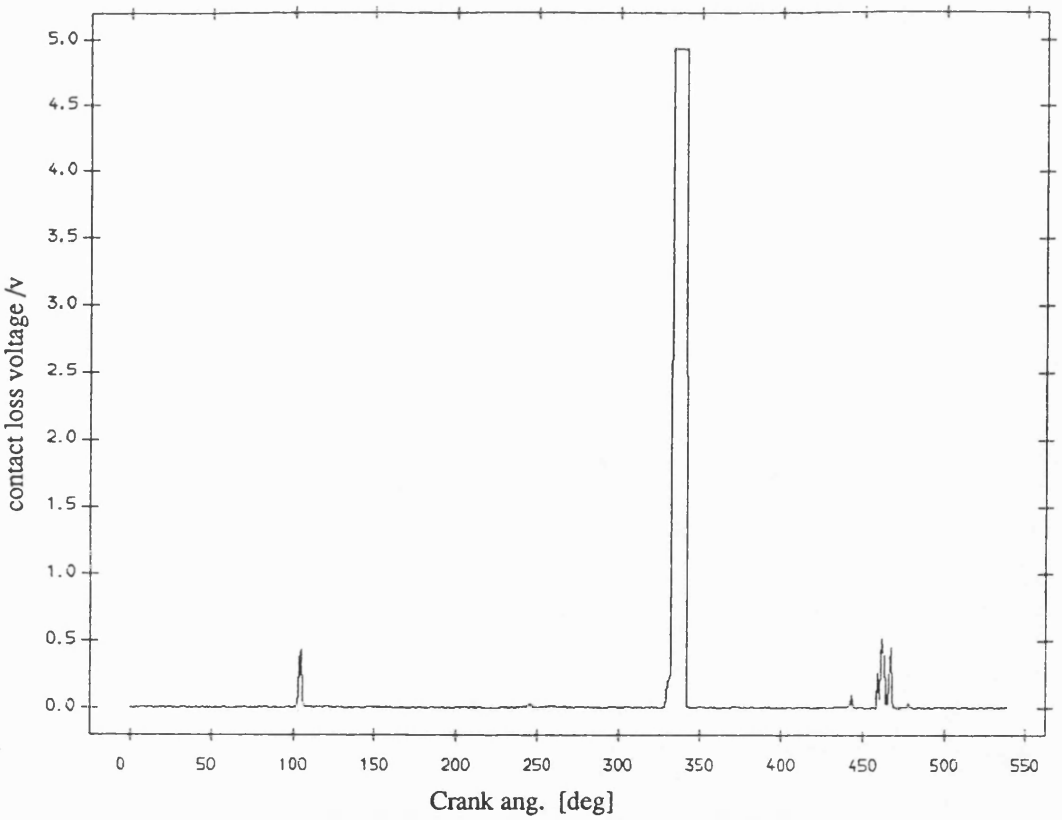

Fig 8.5.46 Exp. result contact loss of pin and greasy bearing
with flywheel ;mean speed=327 rev/min ;dia. clearance=0.30mm

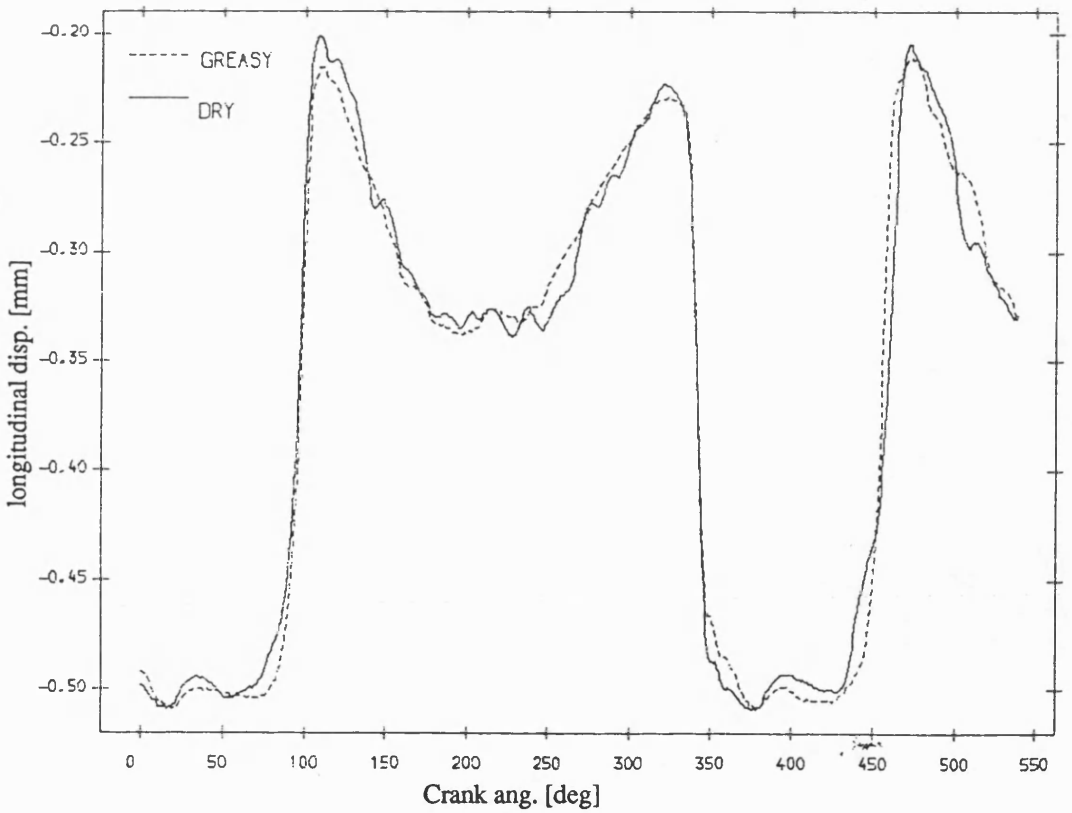

Fig 8.5.48 Exp. result longitudinal disp. of pin , greasy v dry bearing
mean speed=327 rev/min; dia. clearance=.30mm

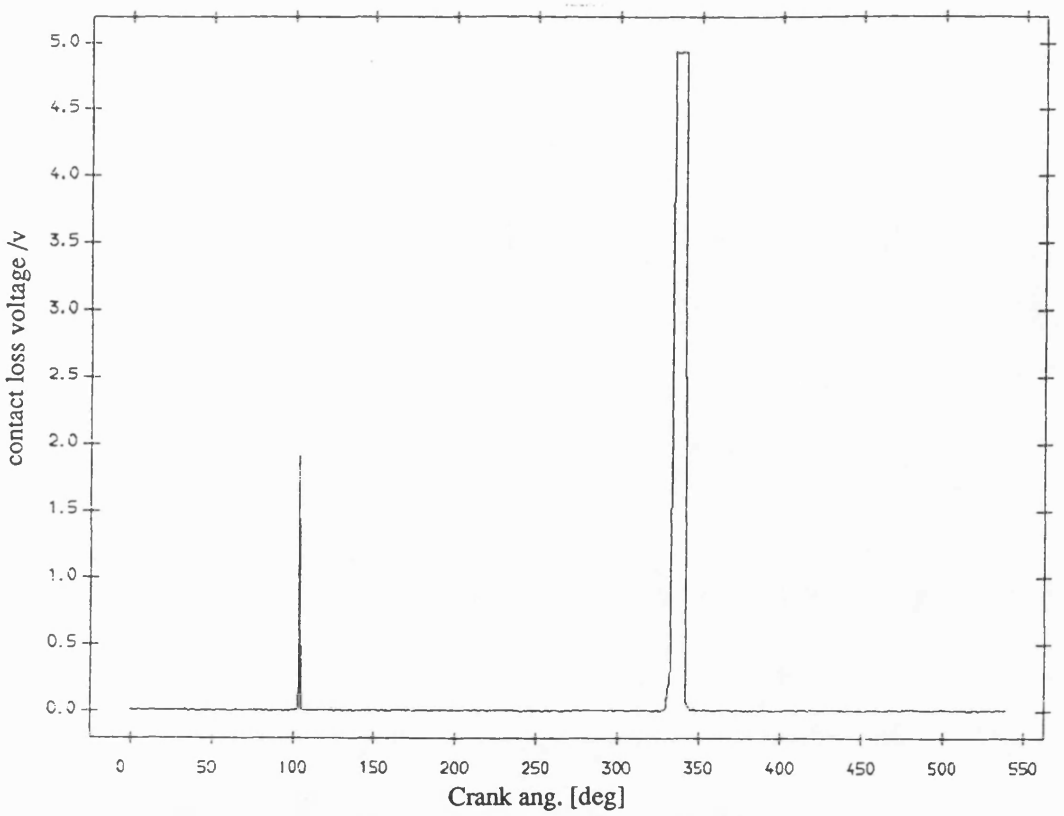

Fig 8.5.47 Exp. result contact loss of pin and dry bearing
with flywheel ;mean speed=327 rev/min ;dia. clearance=0.30mm

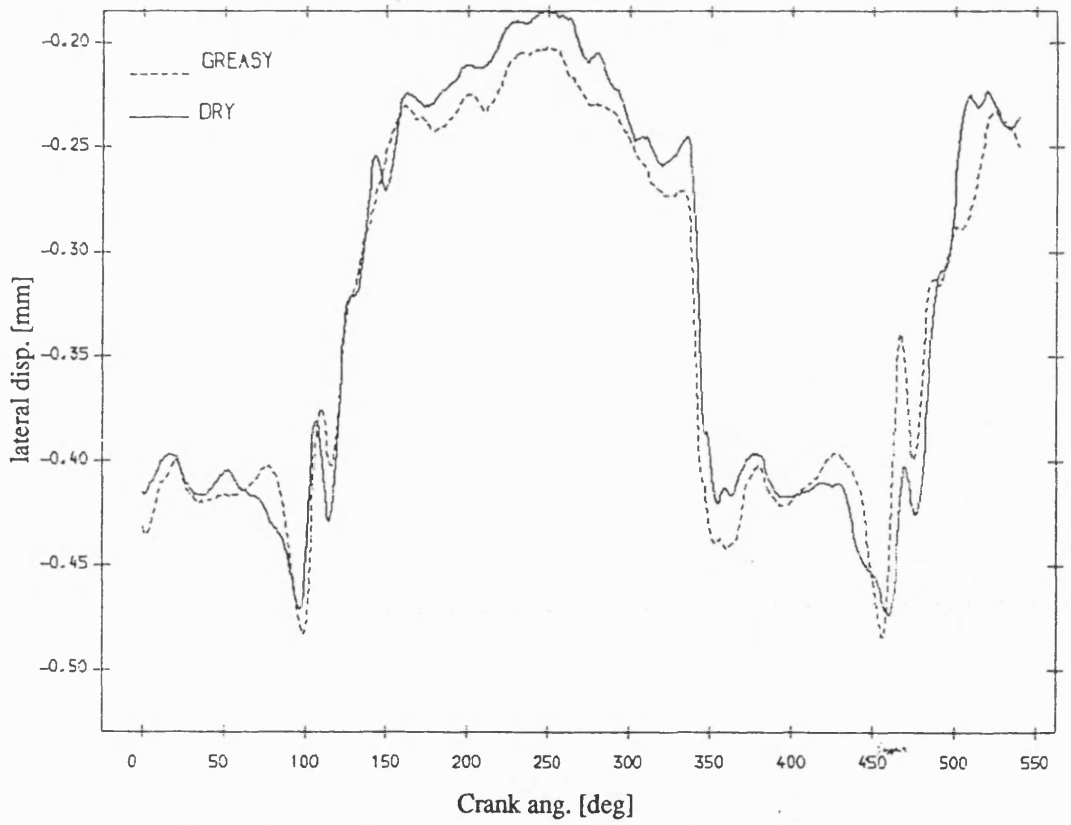

Fig 8.5.49 Exp. result lateral disp. of pin , greasy v dry bearing
mean speed=327 rev/min; dia. clearance=.30mm

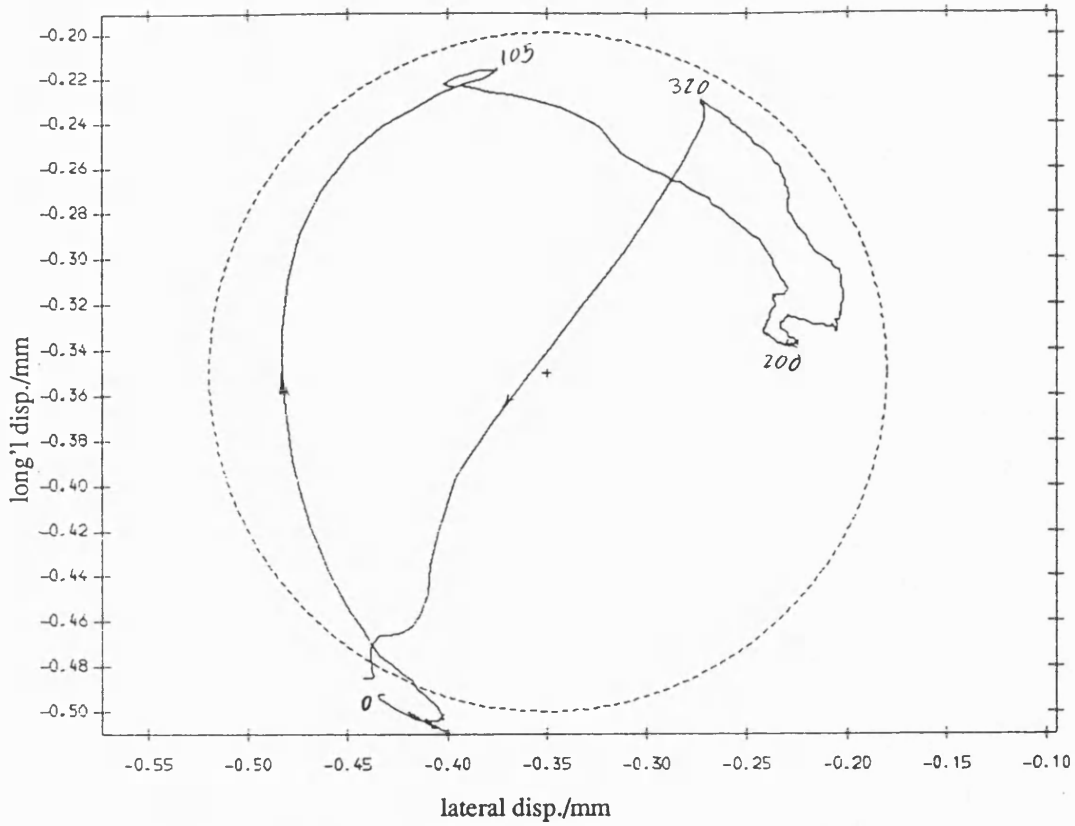

Fig 8.5.50 Exp. result polar plot of relative disp. of pin in greasy bearing with fly wheel ;mean speed=327 rev/min ; dia. clearance=.30mm

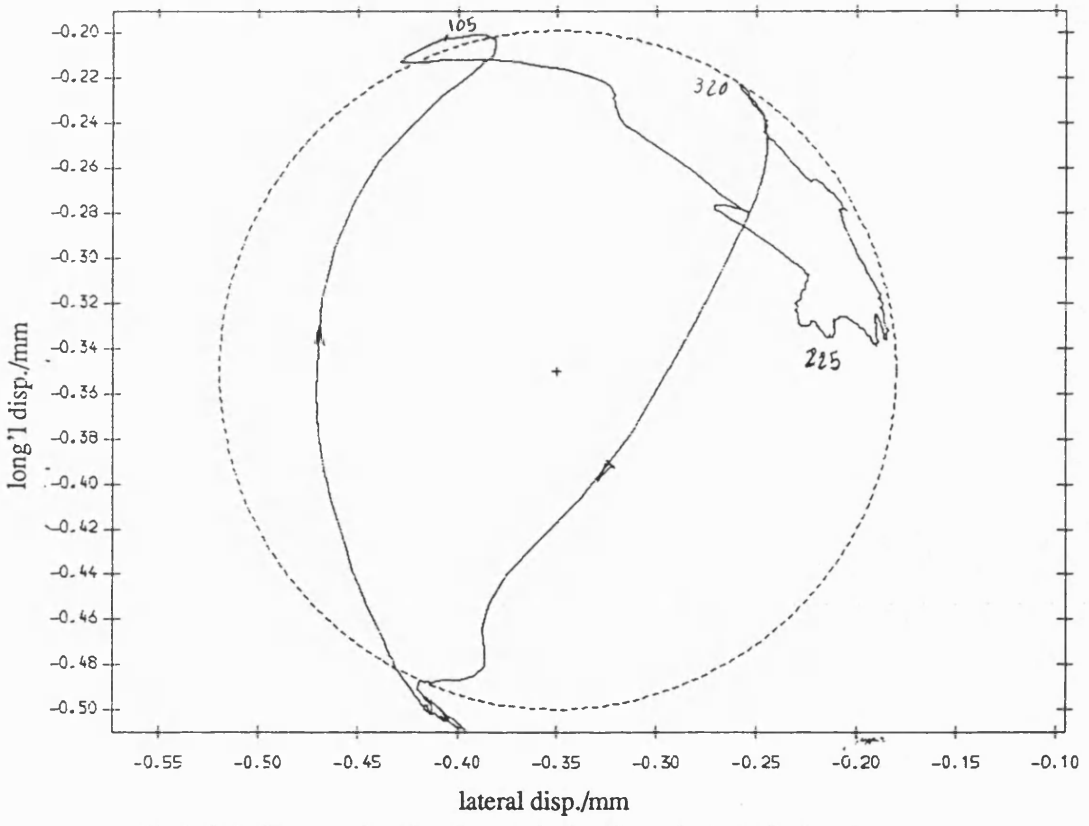

Fig 8.5.51 Exp. result polar plot of relative disp. of pin in dry bearing with fly wheel ;mean speed=327 rev/min ; dia. clearance=.30mm

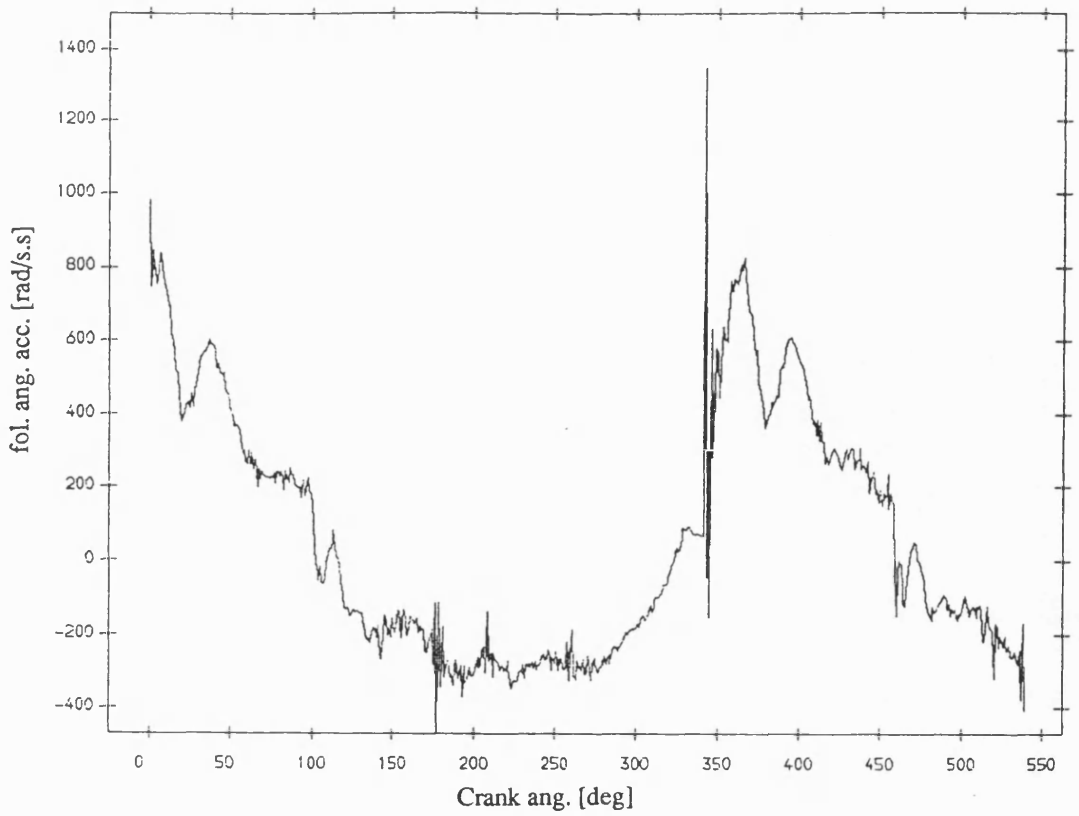

Fig 8.5.52 Exp. result follower ang. acceleration , greasy bearing
with fly wheel ;mean speed=327 rev/min ; dia. clearance=.30mm

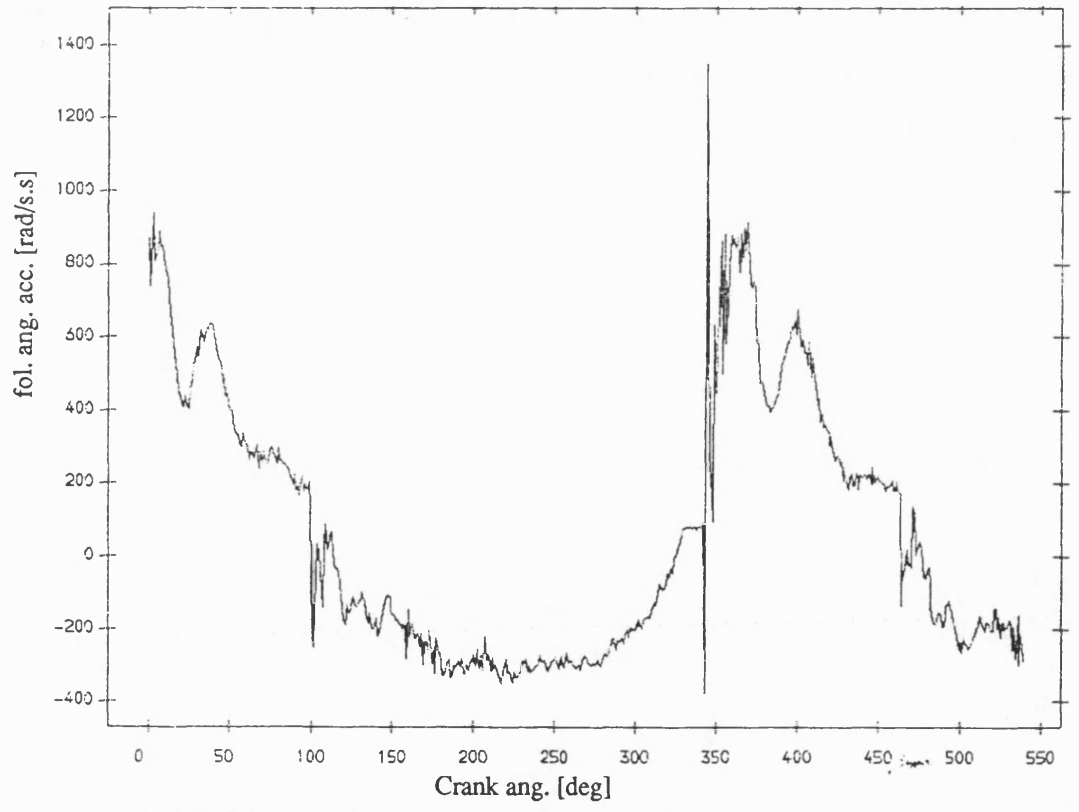

Fig 8.5.53 Exp. result follower ang. acceleration ,dry bearing
with fly wheel ;mean speed=327 rev/min ; dia. clearance=.30mm

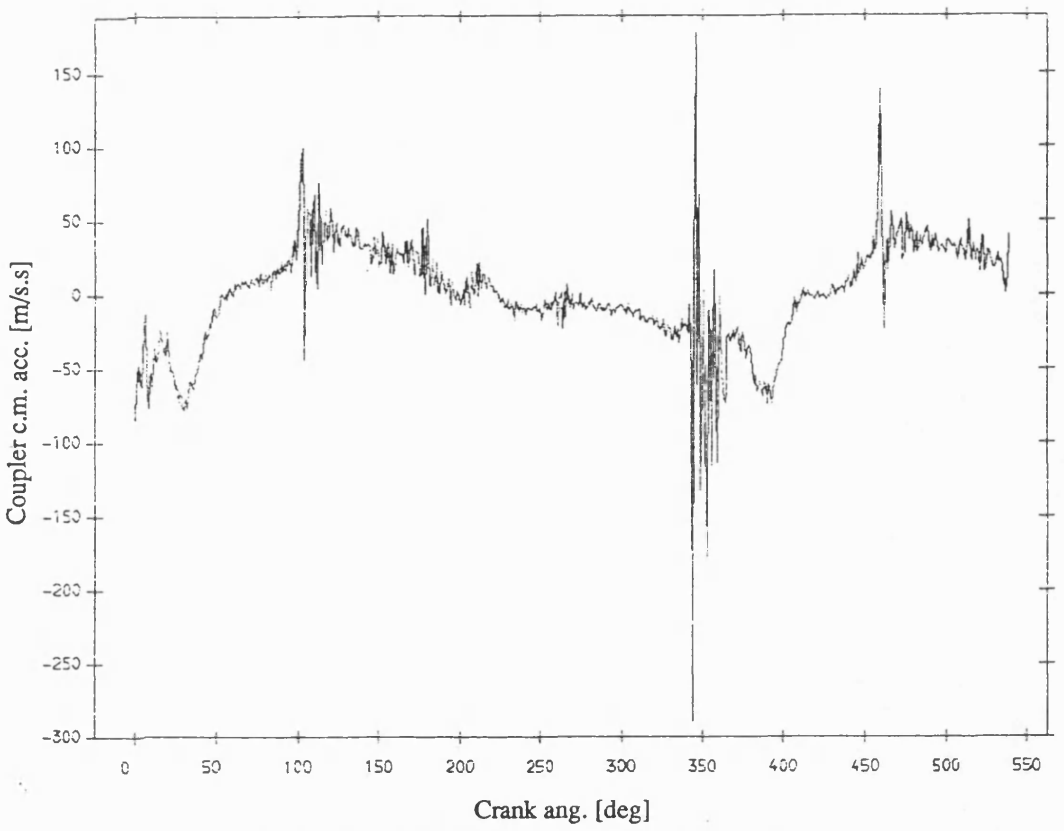

Fig 8.5.54 Exp. result coupler acceleration , greasy bearing
with fly wheel ;mean speed=327 rev/min ; dia. clearance=.30mm

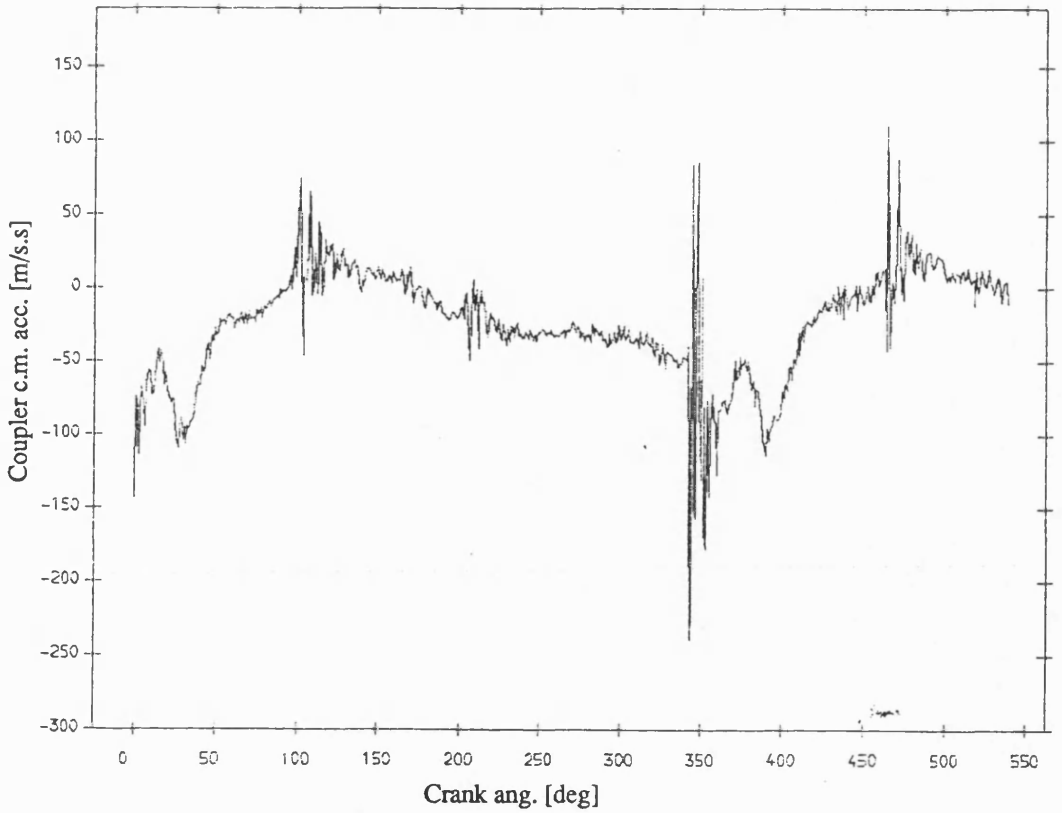

Fig 8.5.55 Exp. result coupler acceleration , dry bearing
with fly wheel ;mean speed=327 rev/min ; dia. clearance=.30mm

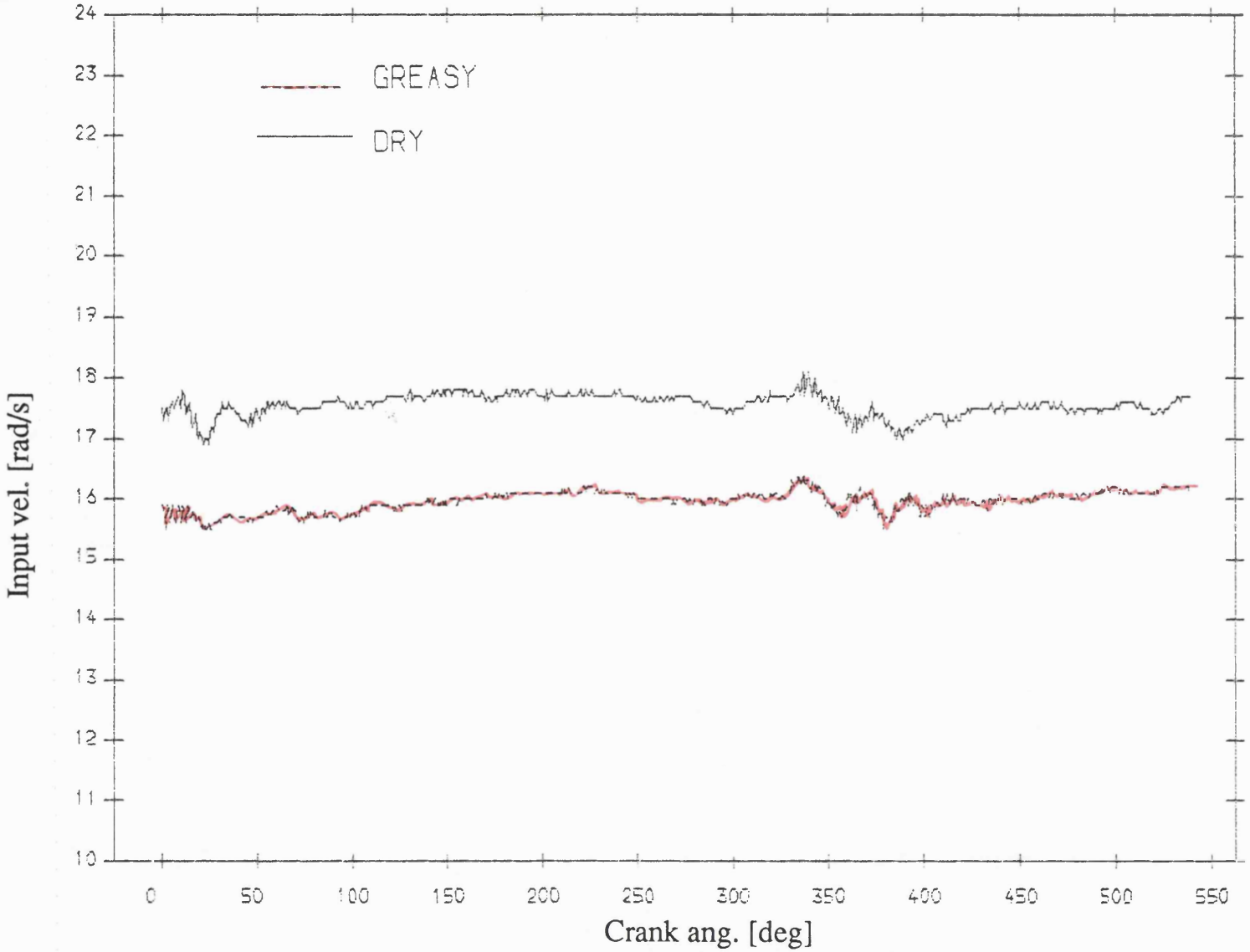

Fig 8.5.56 Exp. result input velocity , greasy v dry bearing
mean speed=168 rev/min; dia. clearance=.20mm

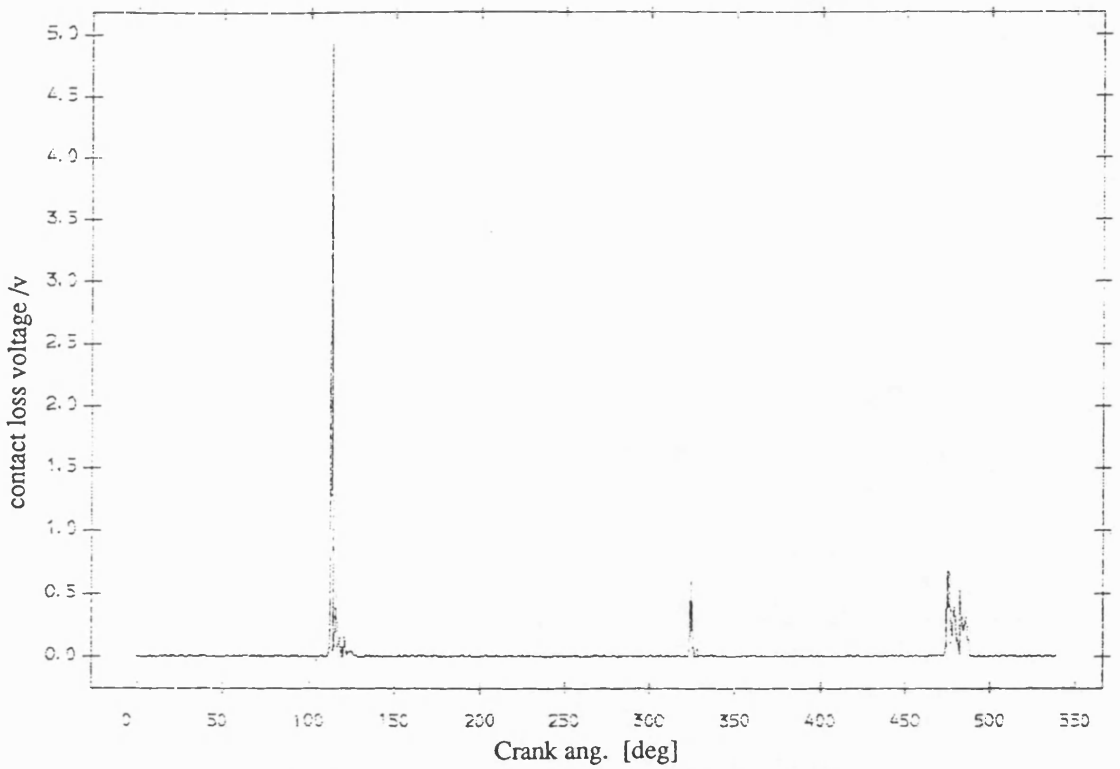

Fig 8.5.57 Exp. result contact loss of pin and greasy bearing
with flywheel ;mean speed=168 rev/min ;dia. clearance=0.20mm

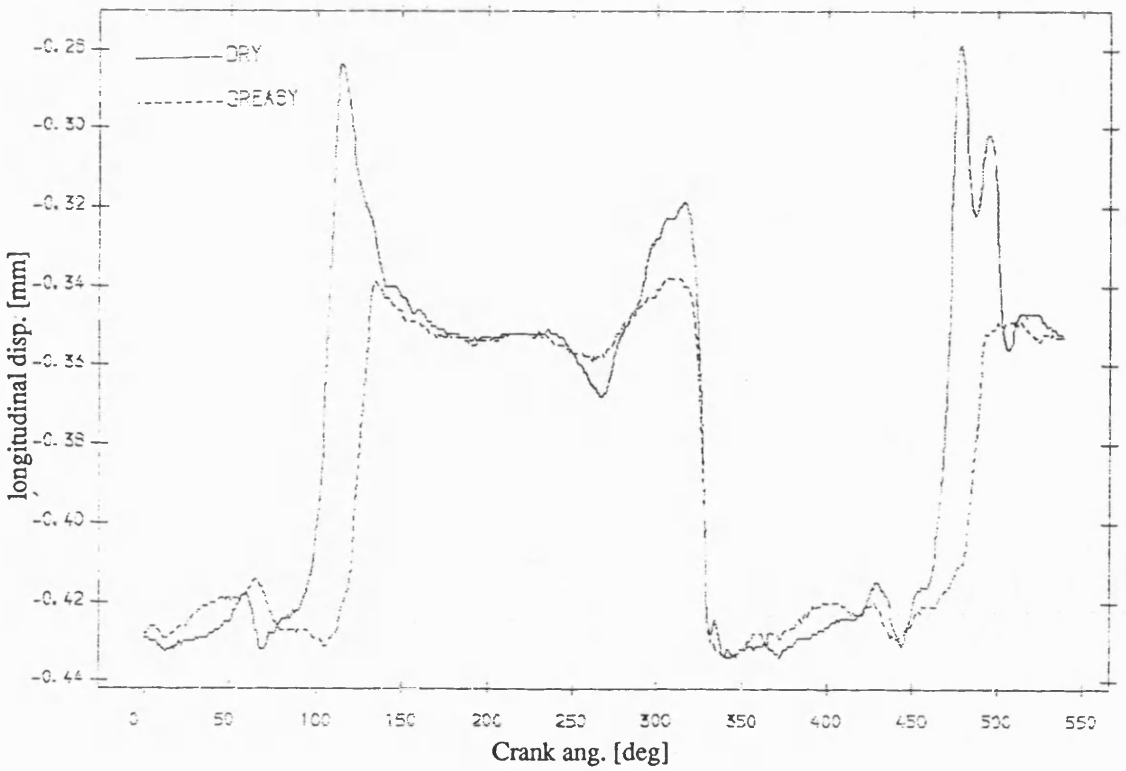

Fig 8.5.59 Exp. result longitudinal disp. of pin , greasy v dry bearing
mean speed=168 rev/min; dia. clearance=.20mm

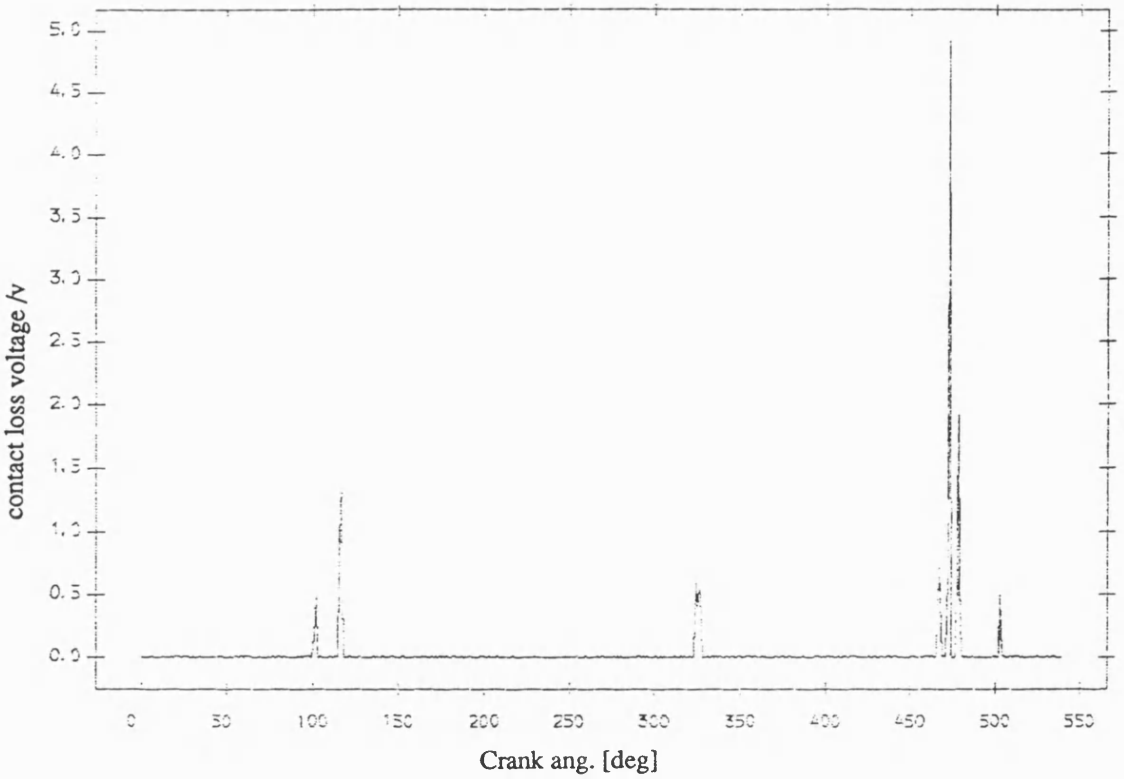

Fig 8.5.58 Exp. result contact loss of pin and dry bearing
with flywheel ;mean speed=168 rev/min ;dia. clearance=0.20mm

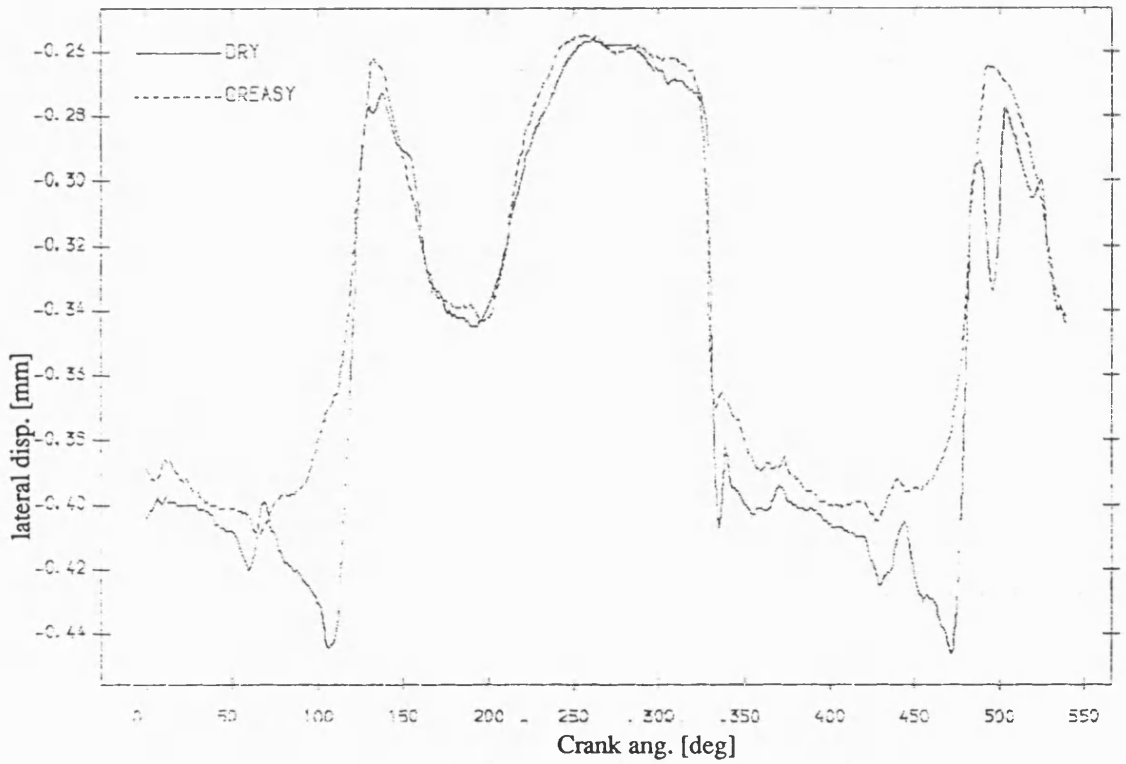

Fig 8.5.60 Exp. result lateral disp. of pin , greasy v dry bearing
mean speed=168 rev/min; dia. clearance=.20mm

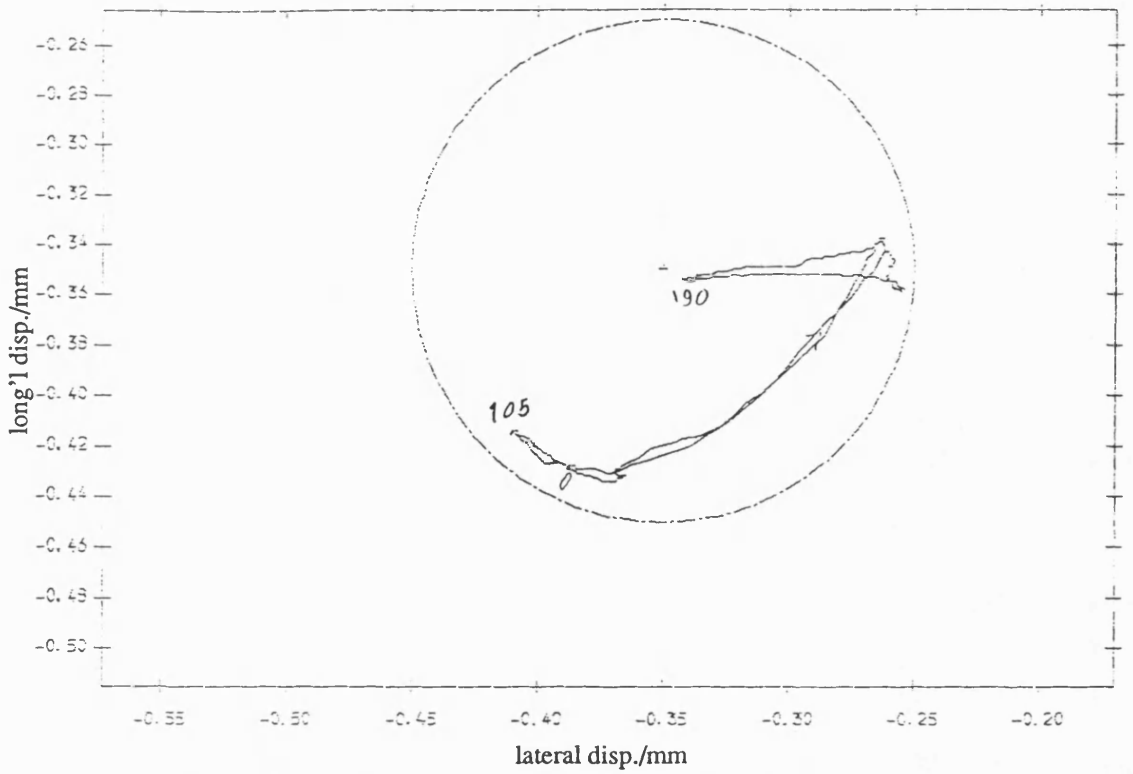

Fig 8.5.61 Exp. result polar plot of relative disp. of pin in greasy bearing with fly wheel ;mean speed=168 rev/min ; dia. clearance=.20mm

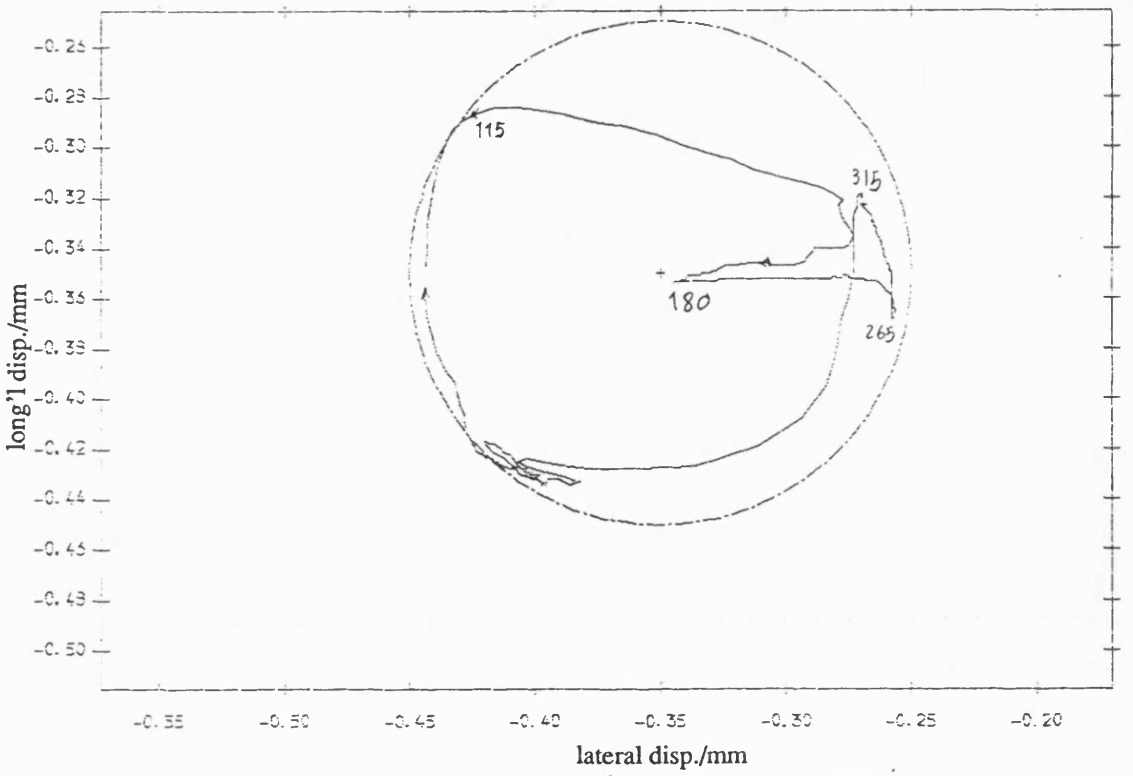

Fig 8.5.62 Exp. result polar plot of relative disp. of pin in dry bearing with fly wheel ;mean speed=168 rev/min ; dia. clearance=.20mm

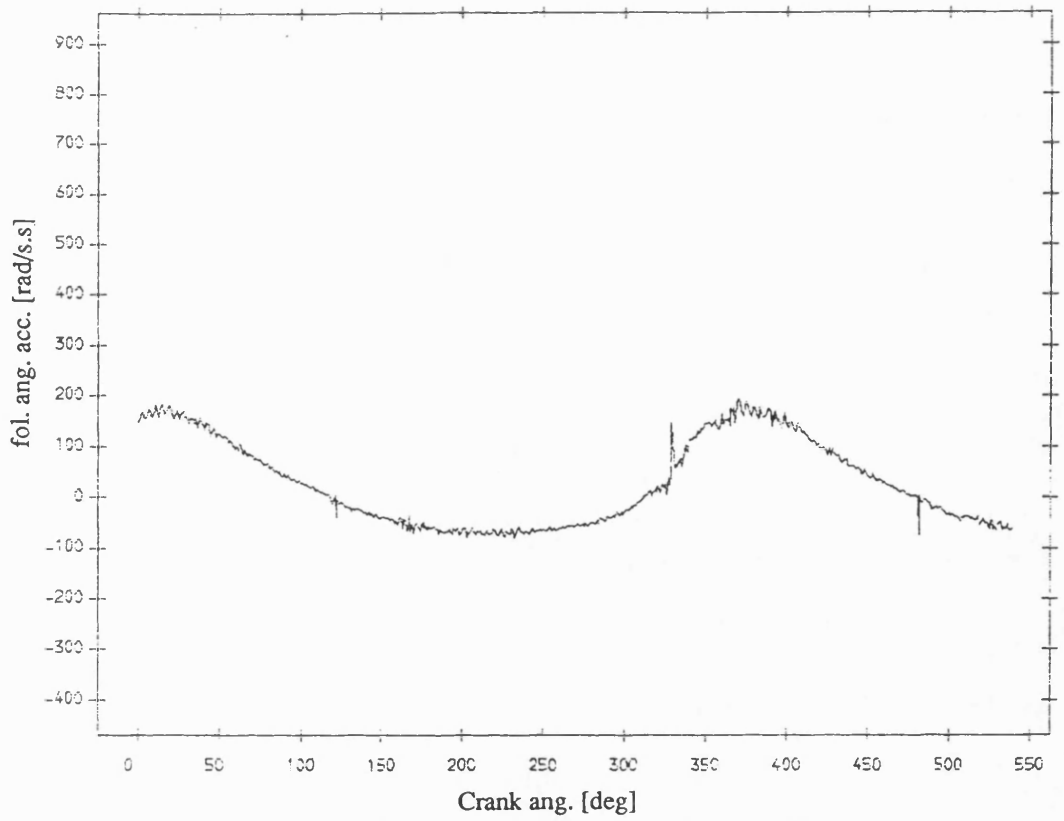

Fig 8.5.63 Exp. result follower ang. acceleration , greasy bearing
with fly wheel ;mean speed=168 rev/min ; dia. clearance=.20mm

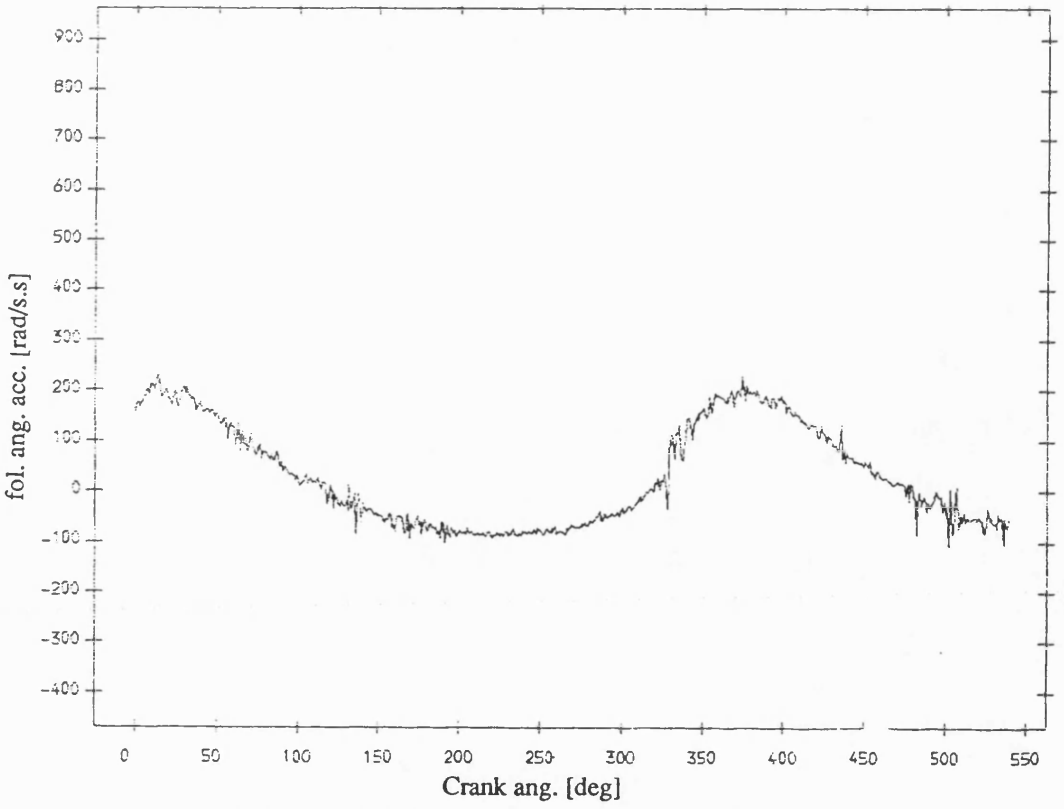

Fig 8.5.64 Exp. result follower ang. acceleration ,dry bearing
with fly wheel ;mean speed=168 rev/min ; dia. clearance=.20mm

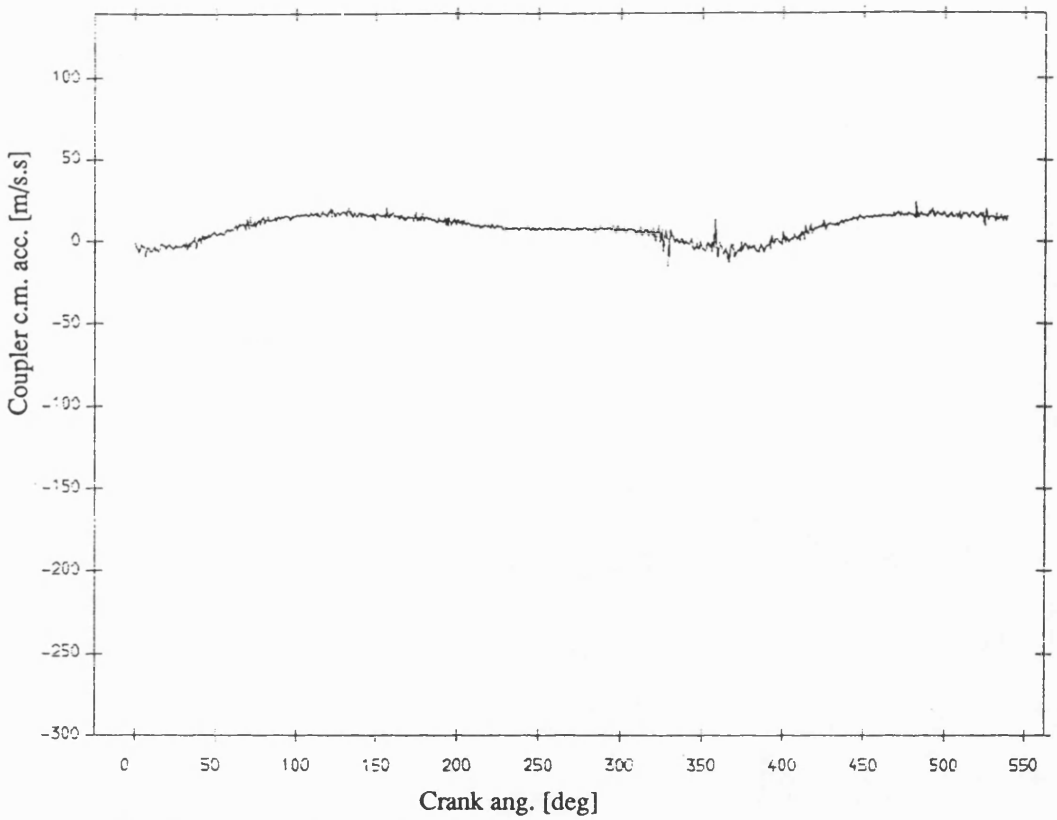

Fig 8.5.65 Exp. result coupler acceleration , greasy bearing
with fly wheel ;mean speed=168 rev/min ; dia. clearance=.20mm

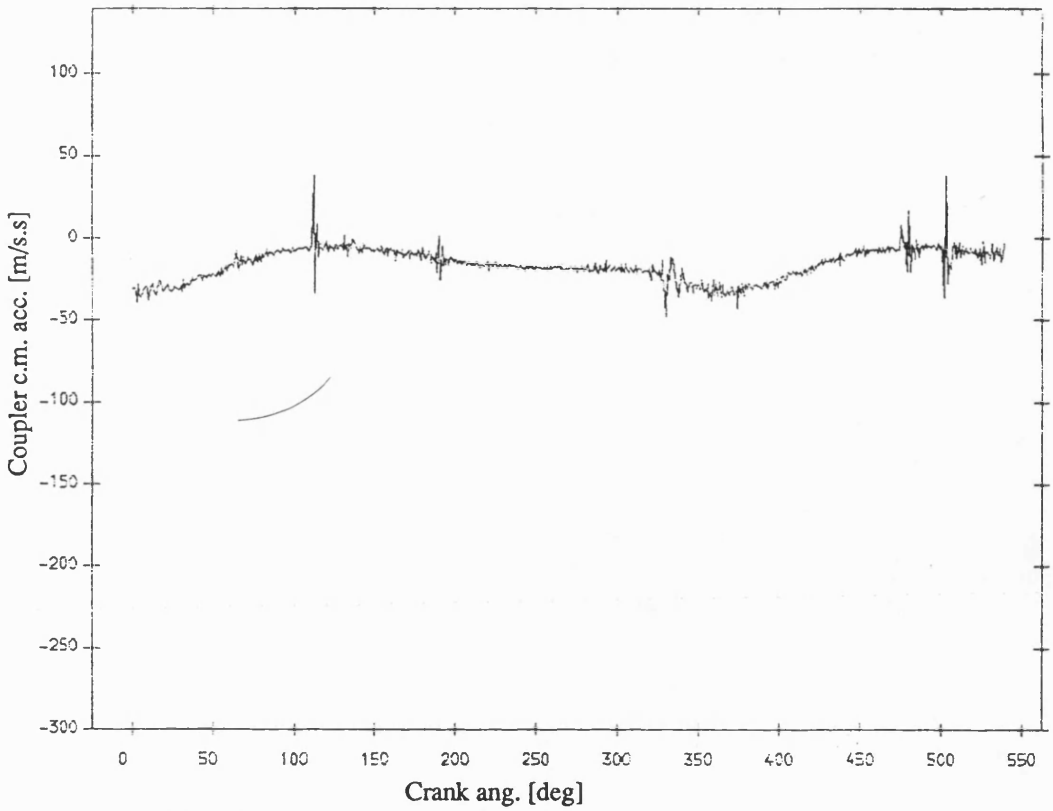

Fig 8.5.66 Exp. result coupler acceleration , dry bearing
with fly wheel ;mean speed=168 rev/min ; dia. clearance=.20mm

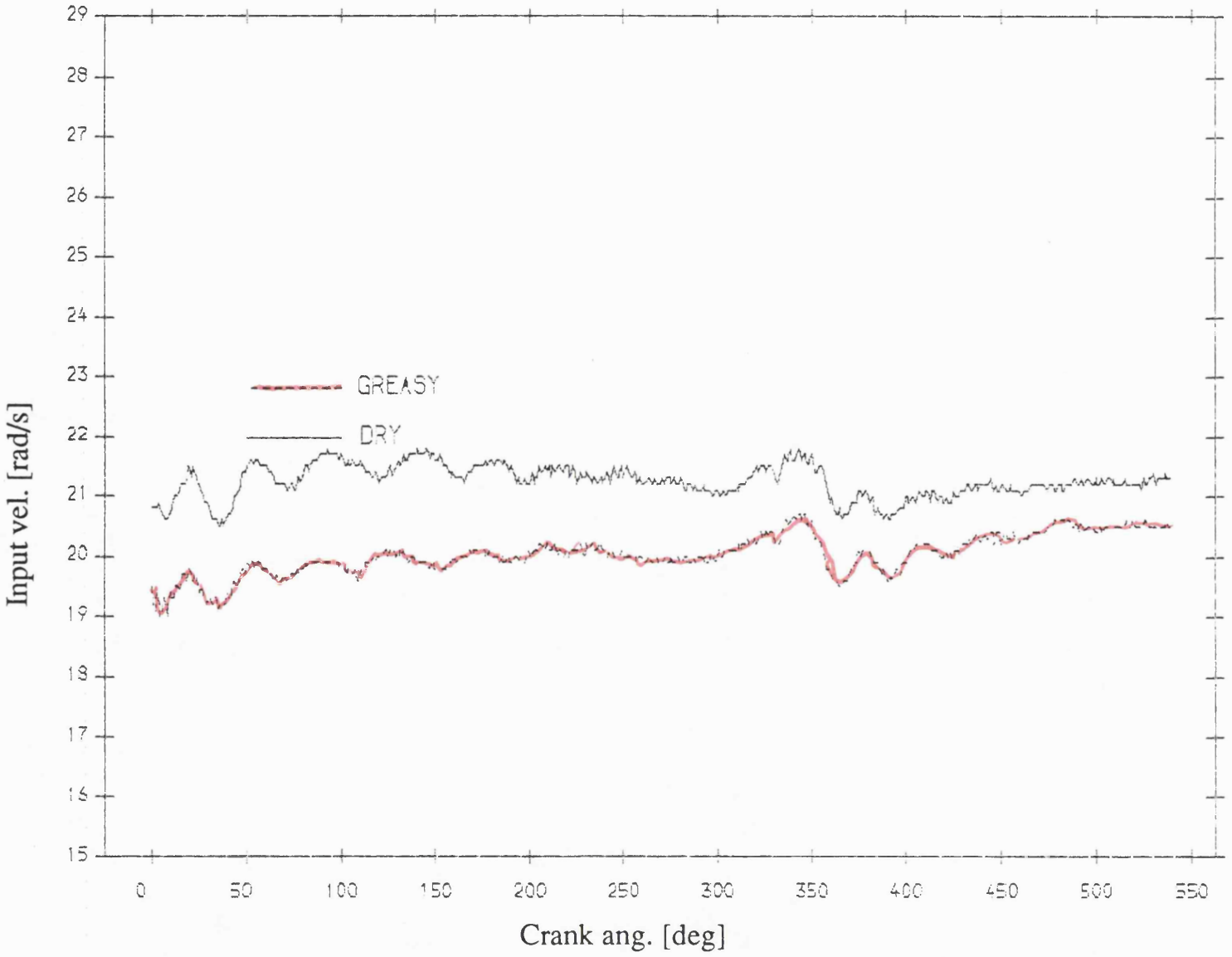

Fig 8.5.67 Exp. result input velocity , greasy v dry bearing
mean speed=208 rev/min; dia. clearance=.20mm

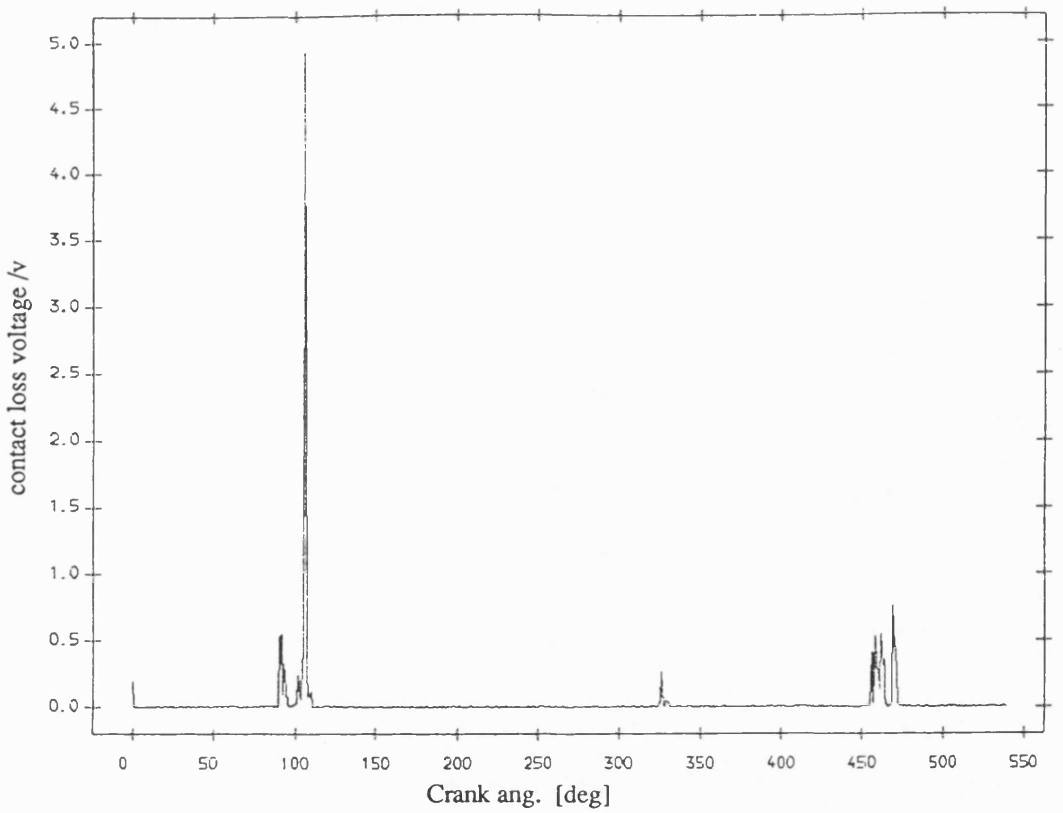

Fig 8.5.68 Exp. result contact loss of pin and greasy bearing
with flywheel ;mean speed=208 rev/min ;dia. clearance=0.20mm

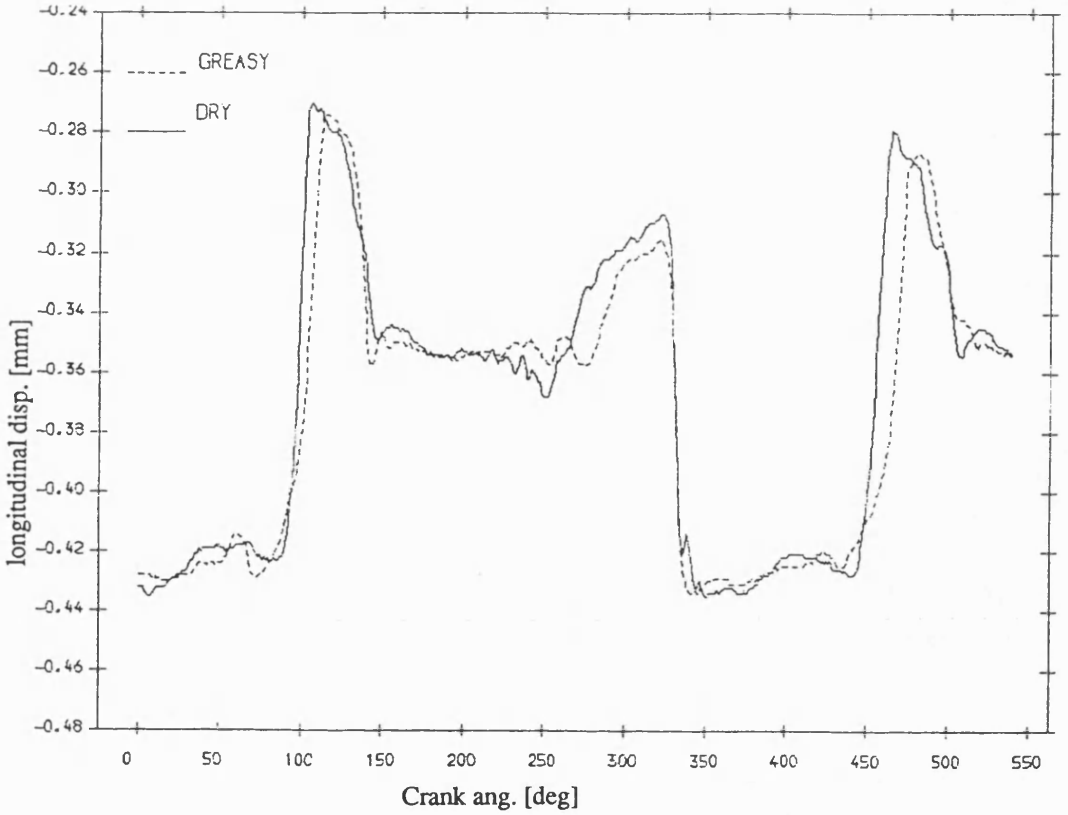

Fig 8.5.70 Exp. result longitudinal disp. of pin , greasy v dry bearing
mean speed=208 rev/min; dia. clearance=.20mm

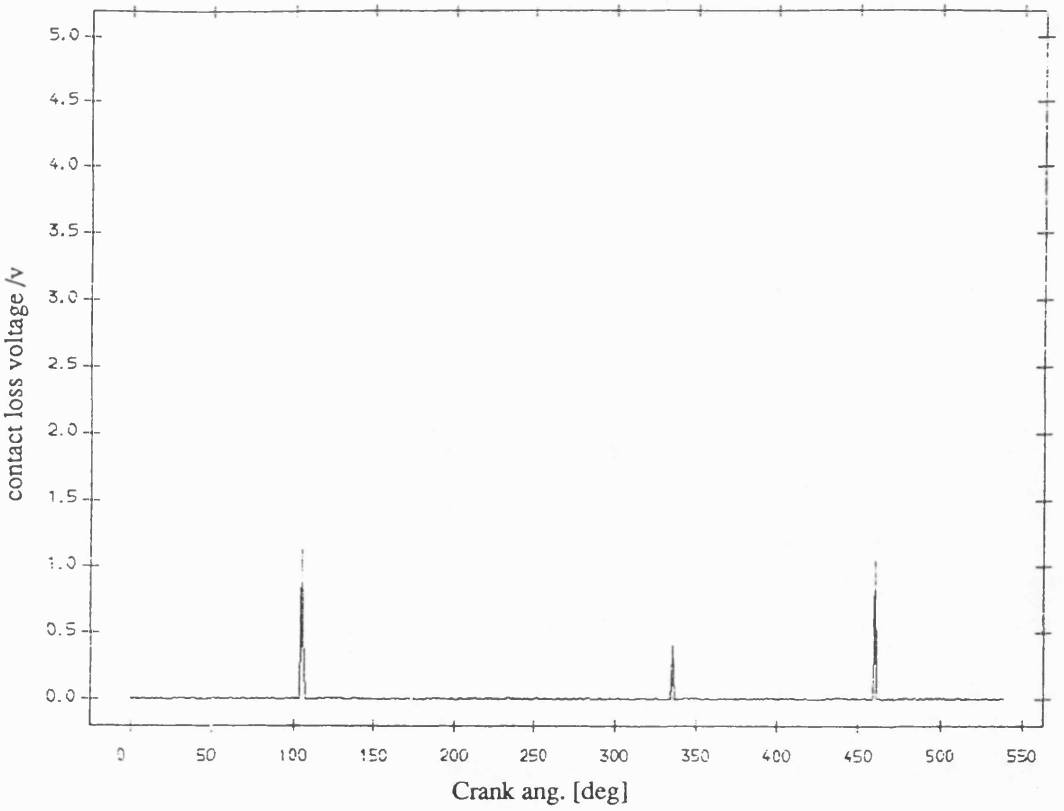

Fig 8.5.69 Exp. result contact loss of pin and dry bearing
with flywheel ;mean speed=208 rev/min ;dia. clearance=0.20mm

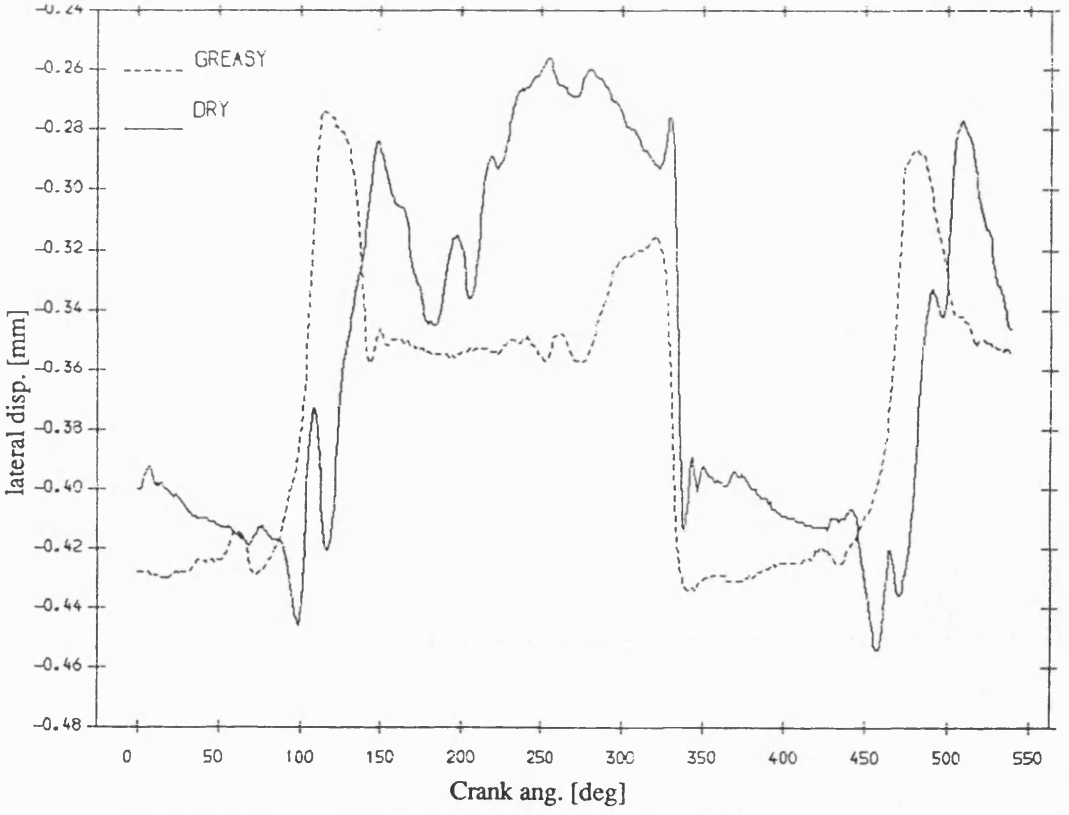

Fig 8.5.71 Exp. result lateral disp. of pin , greasy v dry bearing
mean speed=208 rev/min; dia. clearance=.20mm

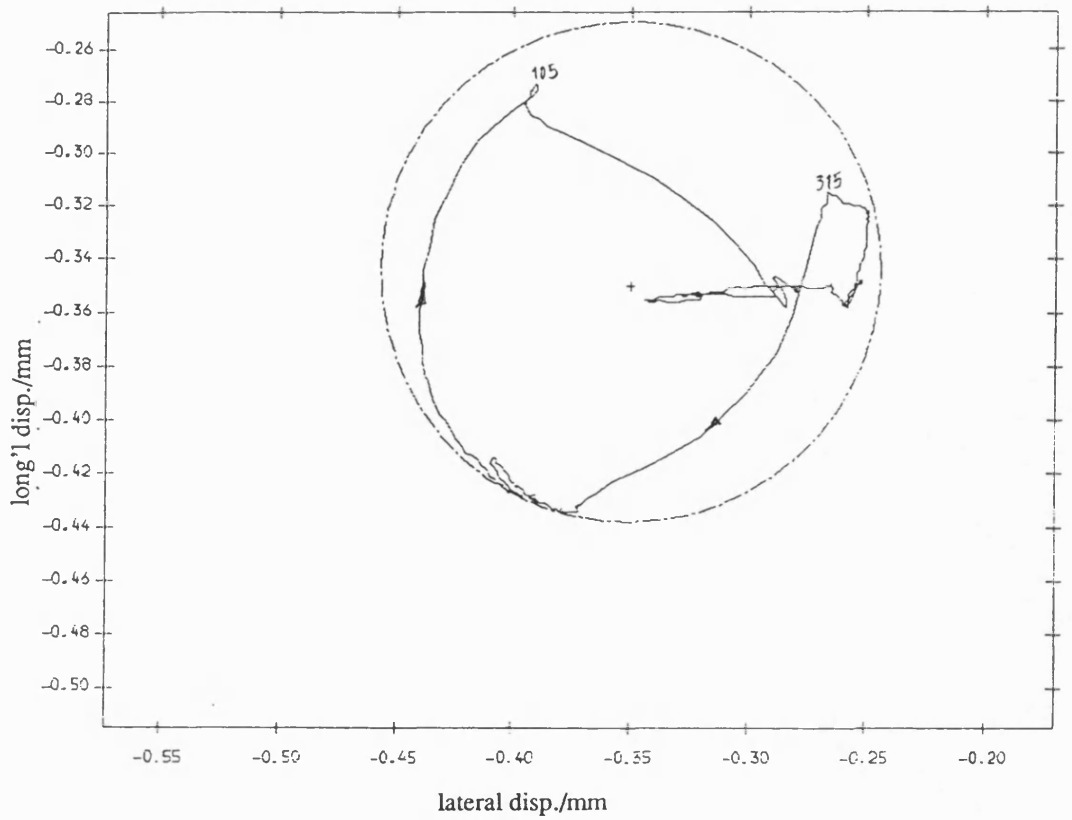

Fig 8.5.72 Exp. result polar plot of relative disp. of pin in greasy bearing with fly wheel ;mean speed=208 rev/min ; dia. clearance=.20mm

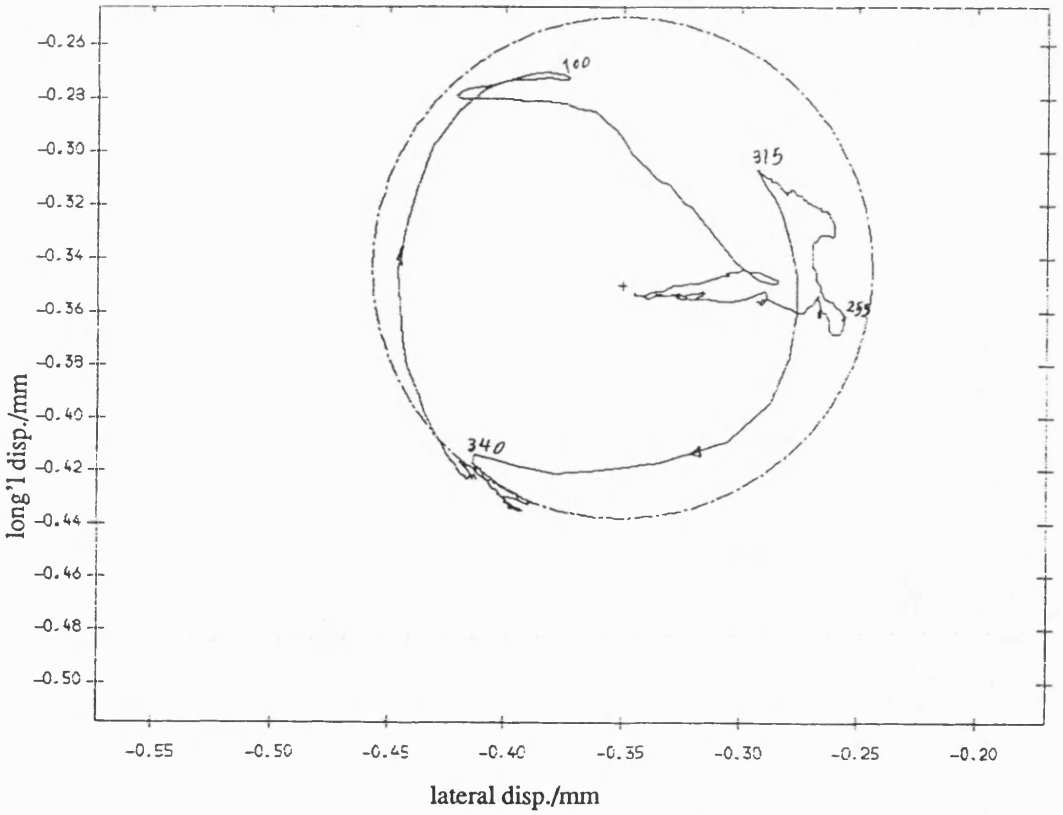

Fig 8.5.73 Exp. result polar plot of relative disp. of pin in dry bearing with fly wheel ;mean speed=208 rev/min ; dia. clearance=.20mm

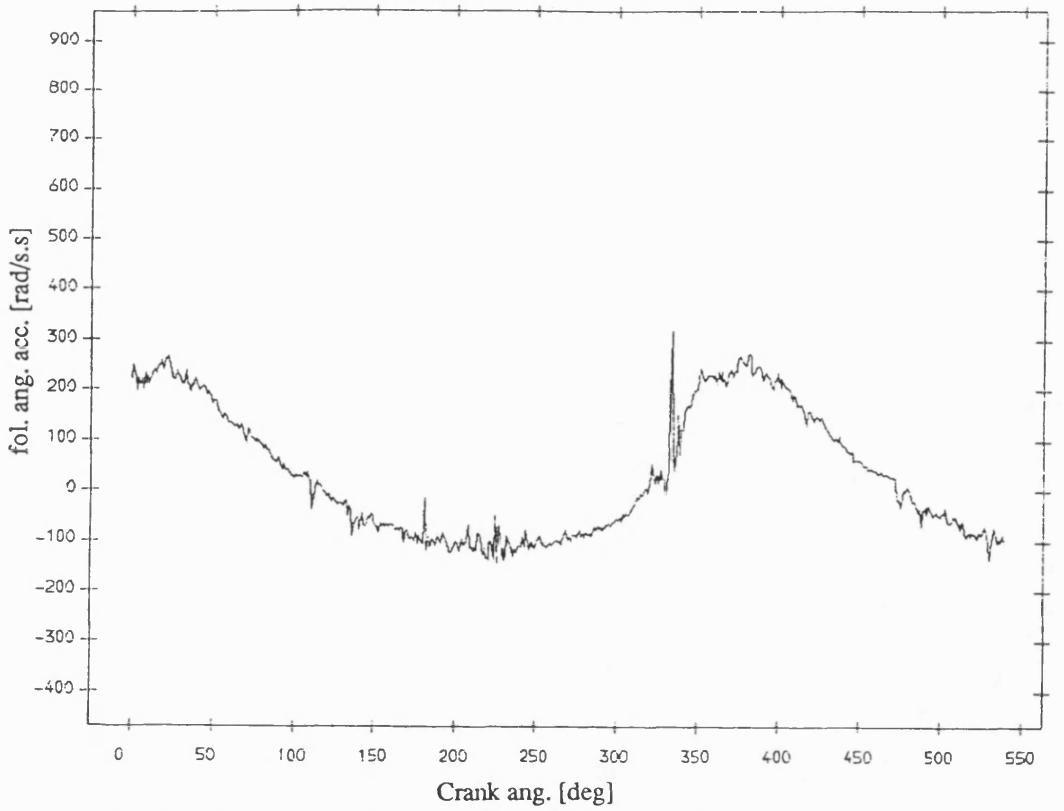

Fig 8.5.74 Exp. result follower ang. acceleration , greasy bearing
with fly wheel ;mean speed=208 rev/min ; dia. clearance=.20mm

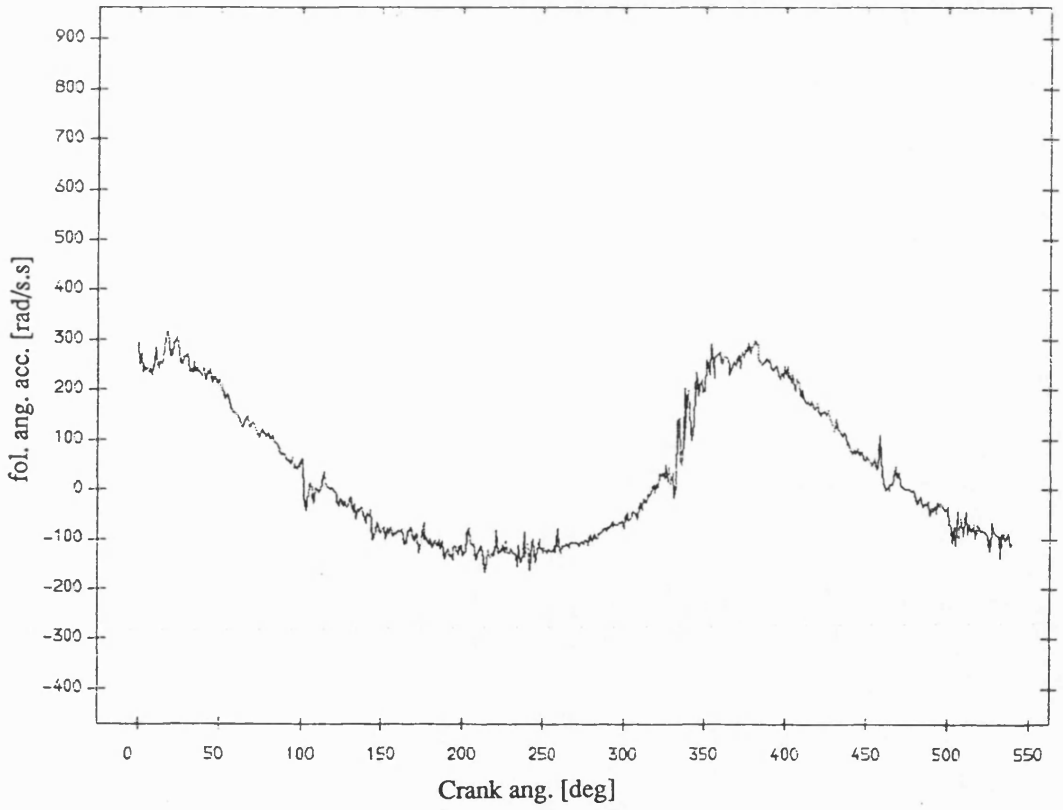

Fig 8.5.75 Exp. result follower ang. acceleration ,dry bearing
with fly wheel ;mean speed=208 rev/min ; dia. clearance=.20mm

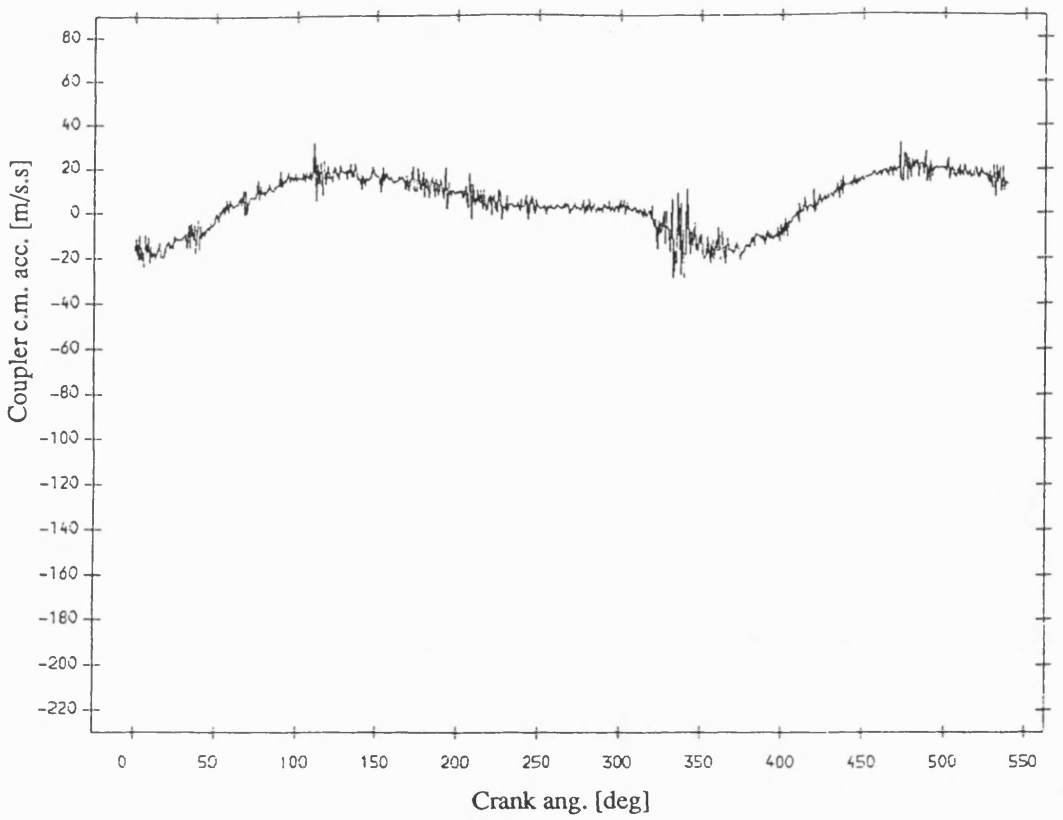

Fig 8.5.76 Exp. result coupler acceleration , greasy bearing
with fly wheel ;mean speed=208 rev/min ; dia. clearance=.20mm

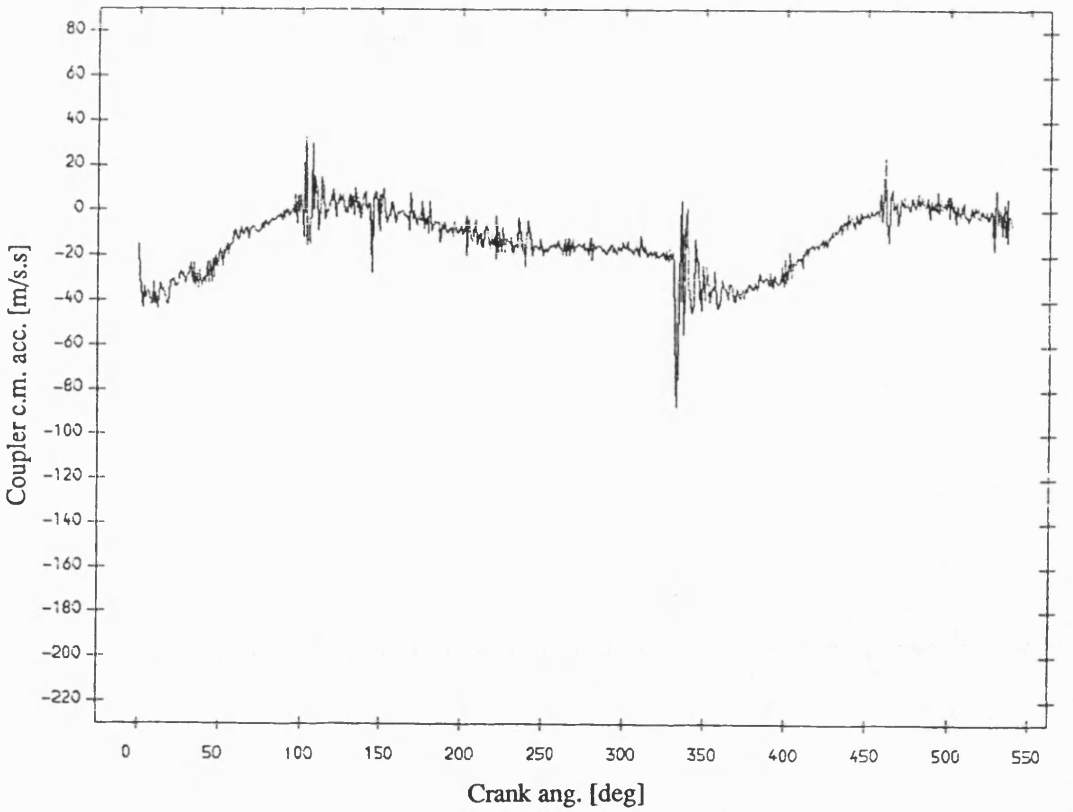

Fig 8.5.77 Exp. result coupler acceleration , dry bearing
with fly wheel ;mean speed=208 rev/min ; dia. clearance=.20mm

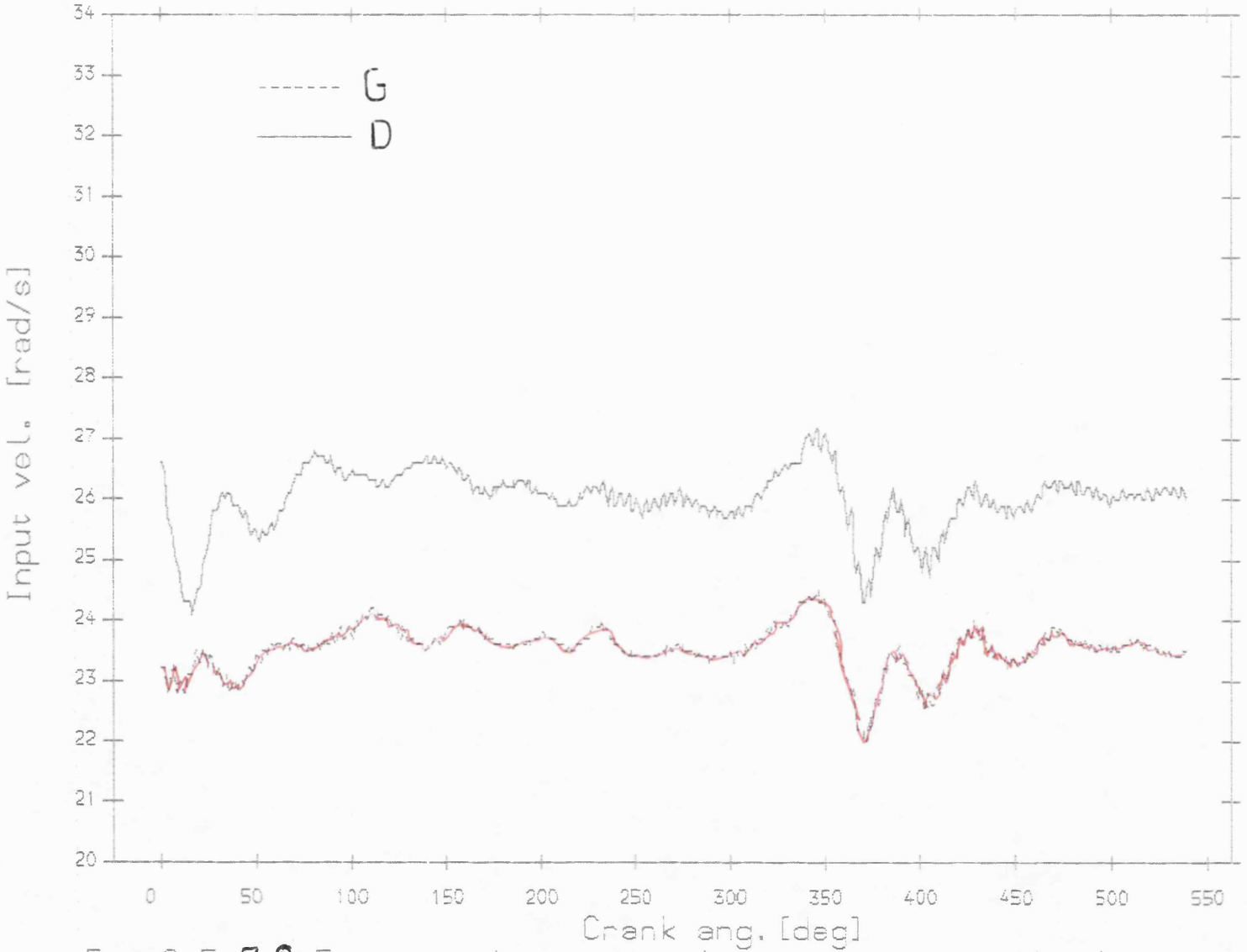

Fig 8.5.78 Exp. result input velocity „greasy v dry bearing with fly wheel mean speed=244 rev/min ; dia. clearance=0.2 mm

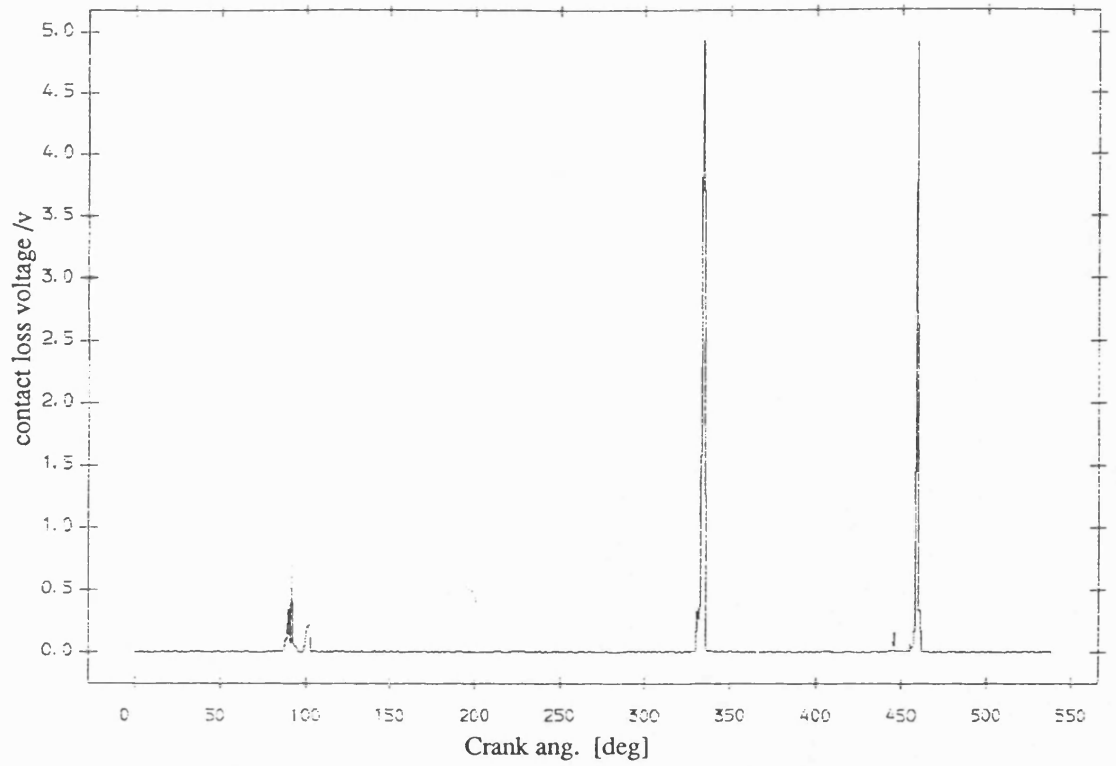

Fig 8.5.79 Exp. result contact loss of pin and greasy bearing
with flywheel ;mean speed=244 rev/min ;dia. clearance=0.20mm

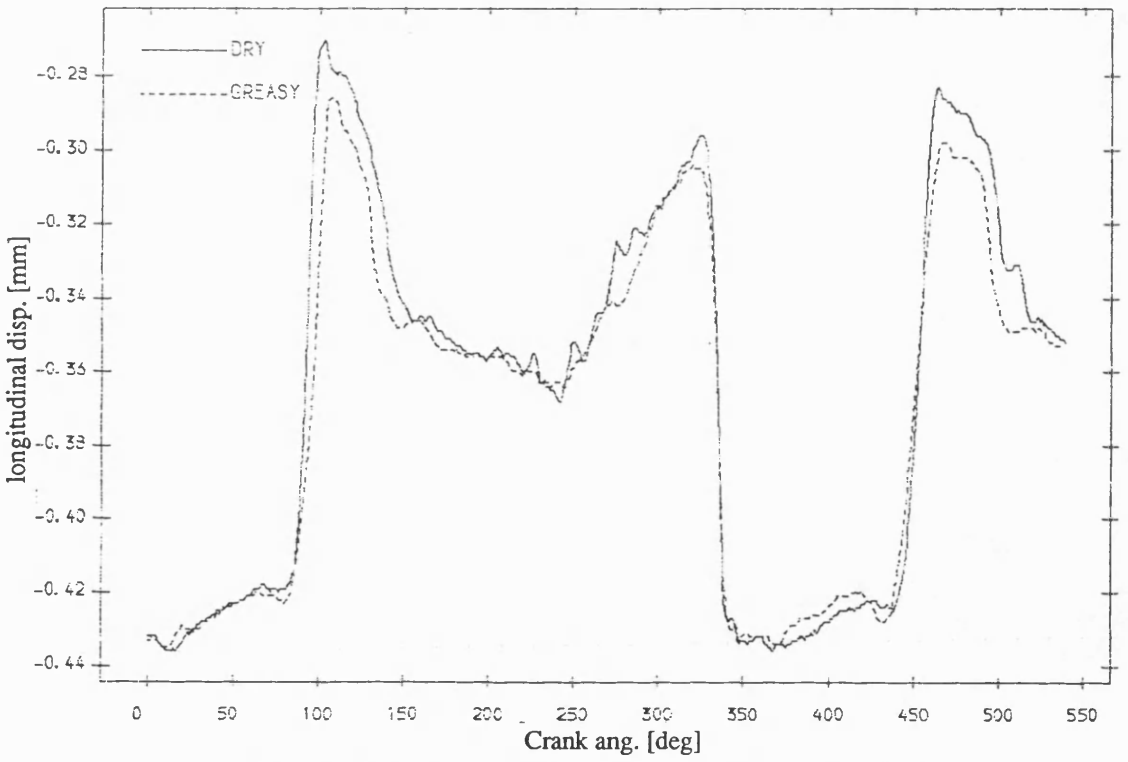

Fig 8.5.81 Exp. result longitudinal disp. of pin , greasy v dry bearing
mean speed=244 rev/min; dia. clearance=.20mm

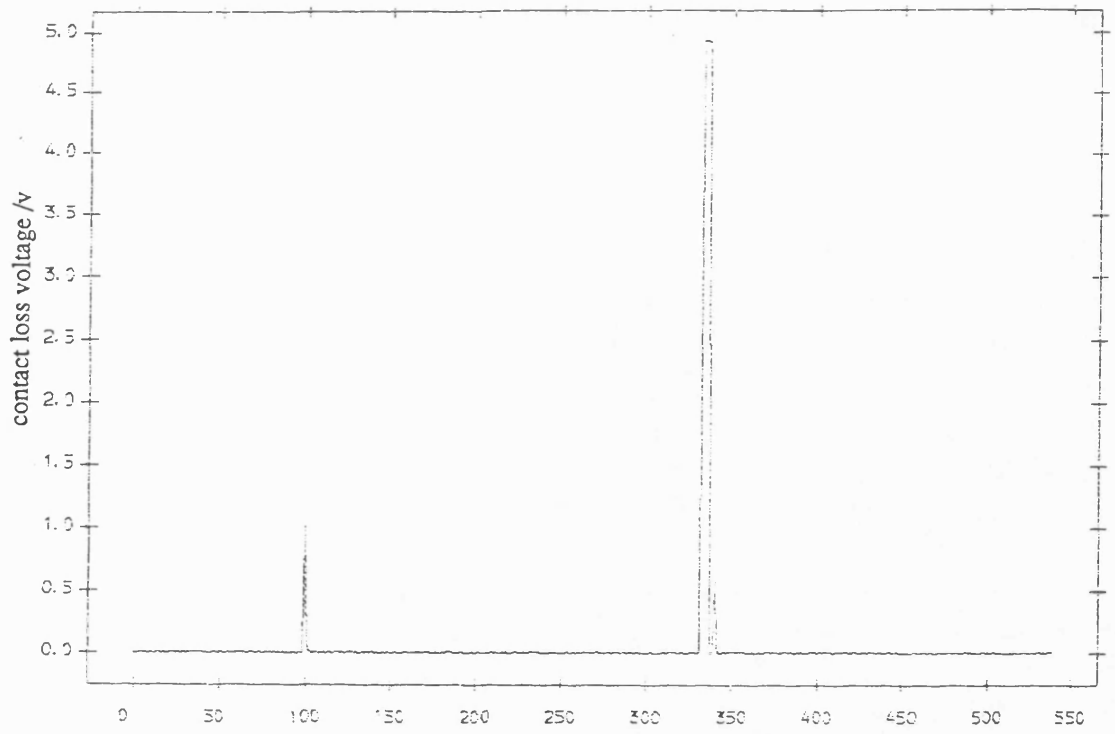

Fig 8.5.80 Exp. result contact loss of pin and dry bearing
with flywheel ;mean speed=244 rev/min ;dia. clearance=0.20mm

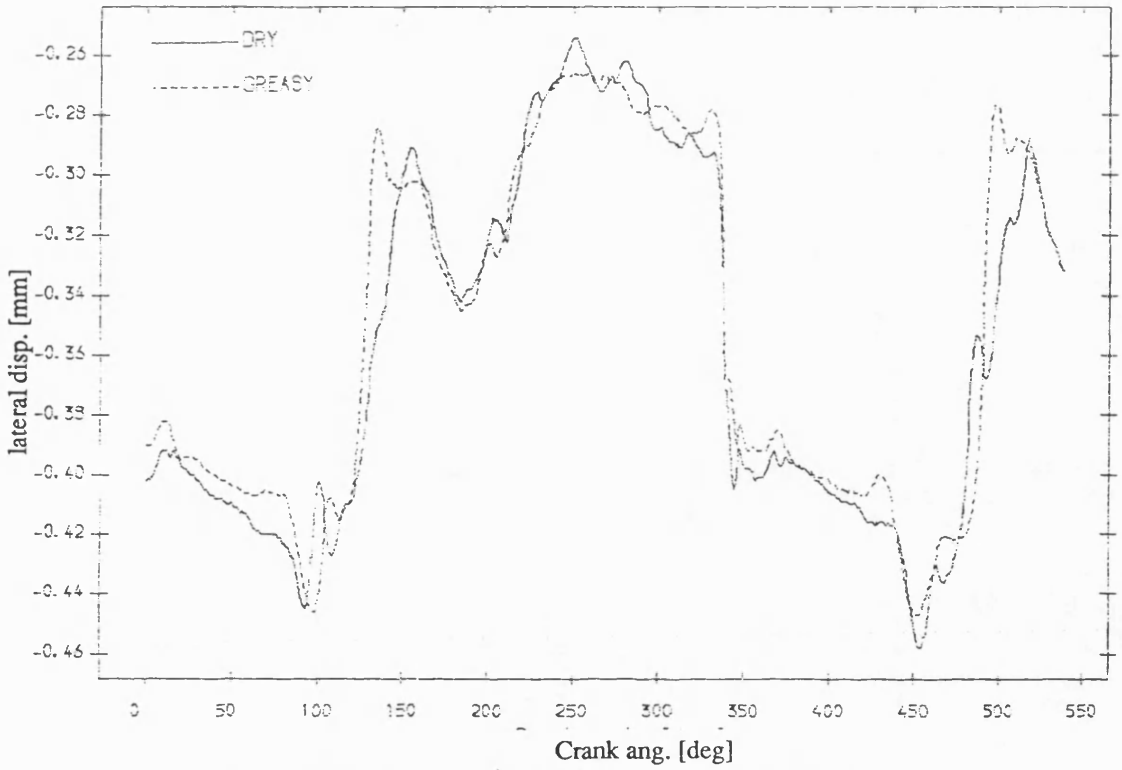

Fig 8.5.82 Exp. result lateral disp. of pin , greasy v dry bearing
mean speed=244 rev/min; dia. clearance=.20mm

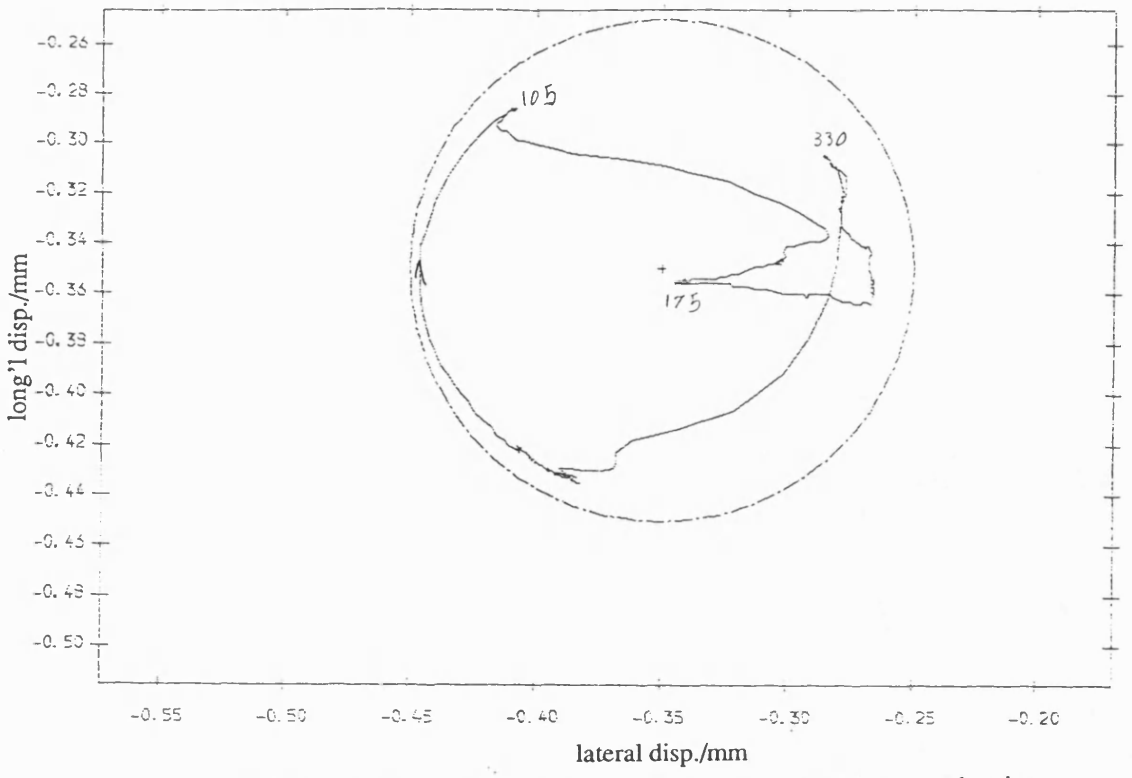

Fig 8.5.83 Exp. result polar plot of relative disp. of pin in greasy bearing with fly wheel ;mean speed=244 rev/min ; dia. clearance=.20mm

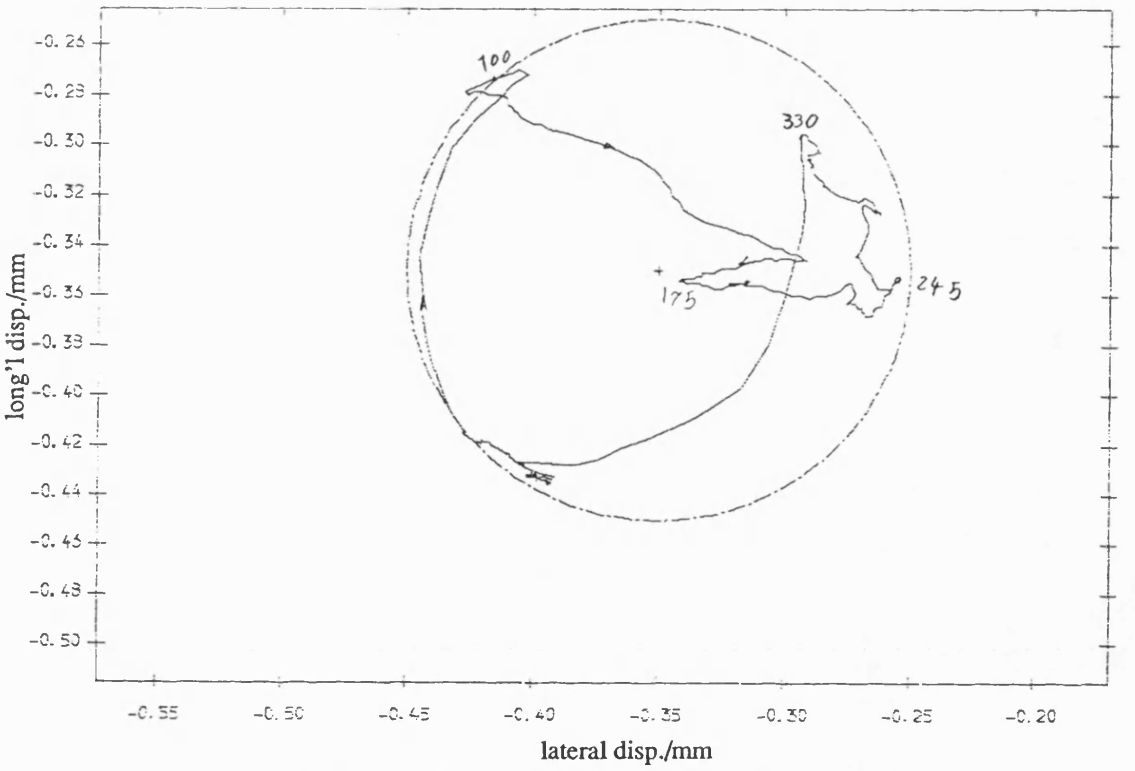

Fig 8.5.84 Exp. result polar plot of relative disp. of pin in dry bearing with fly wheel ;mean speed=244 rev/min ; dia. clearance=.20mm

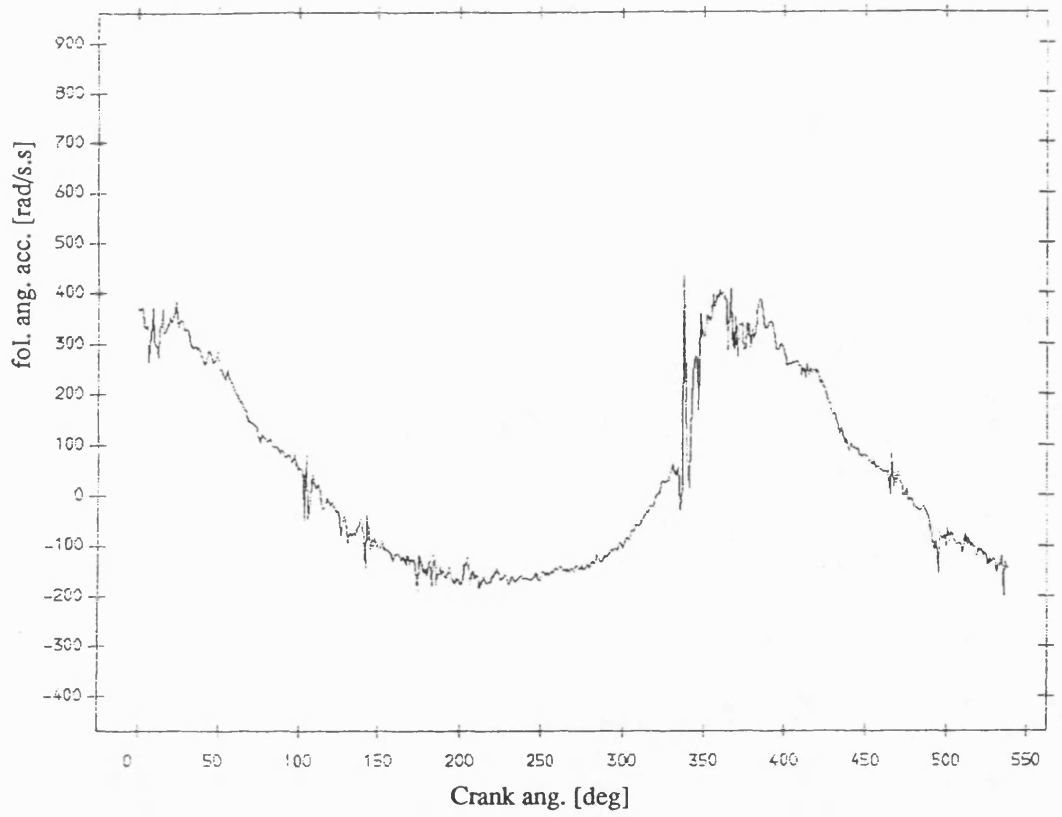

Fig 8.5.85 Exp. result follower ang. acceleration , greasy bearing
with fly wheel ;mean speed=244 rev/min ; dia. clearance=.20mm

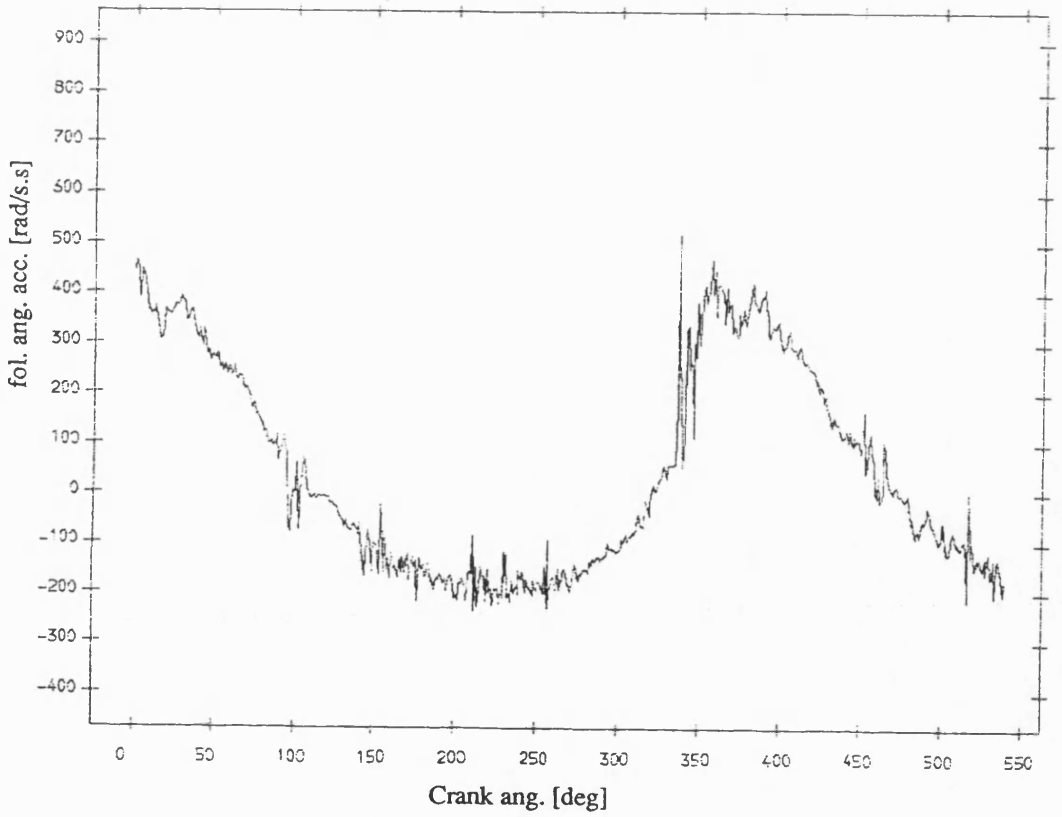

Fig 8.5.86 Exp. result follower ang. acceleration ,dry bearing
with fly wheel ;mean speed=244 rev/min ; dia. clearance=.20mm

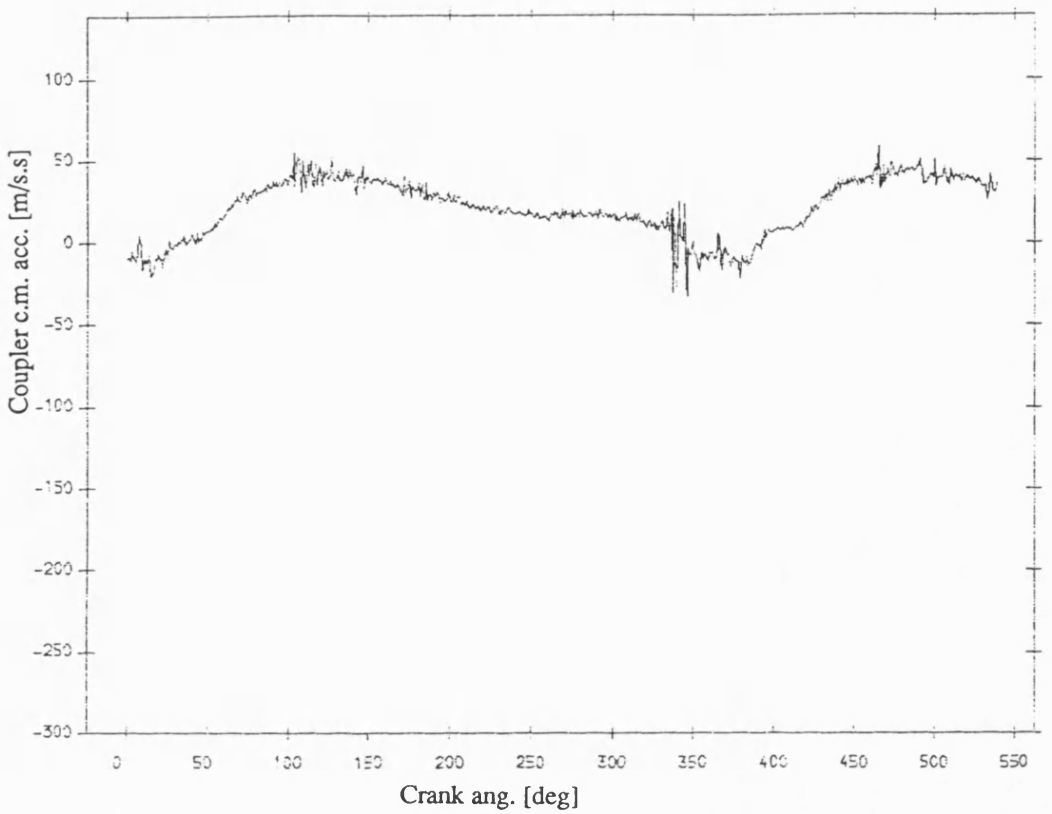

Fig 8.5.87 Exp. result coupler acceleration , greasy bearing
with fly wheel ;mean speed=244 rev/min ; dia. clearance=.20mm

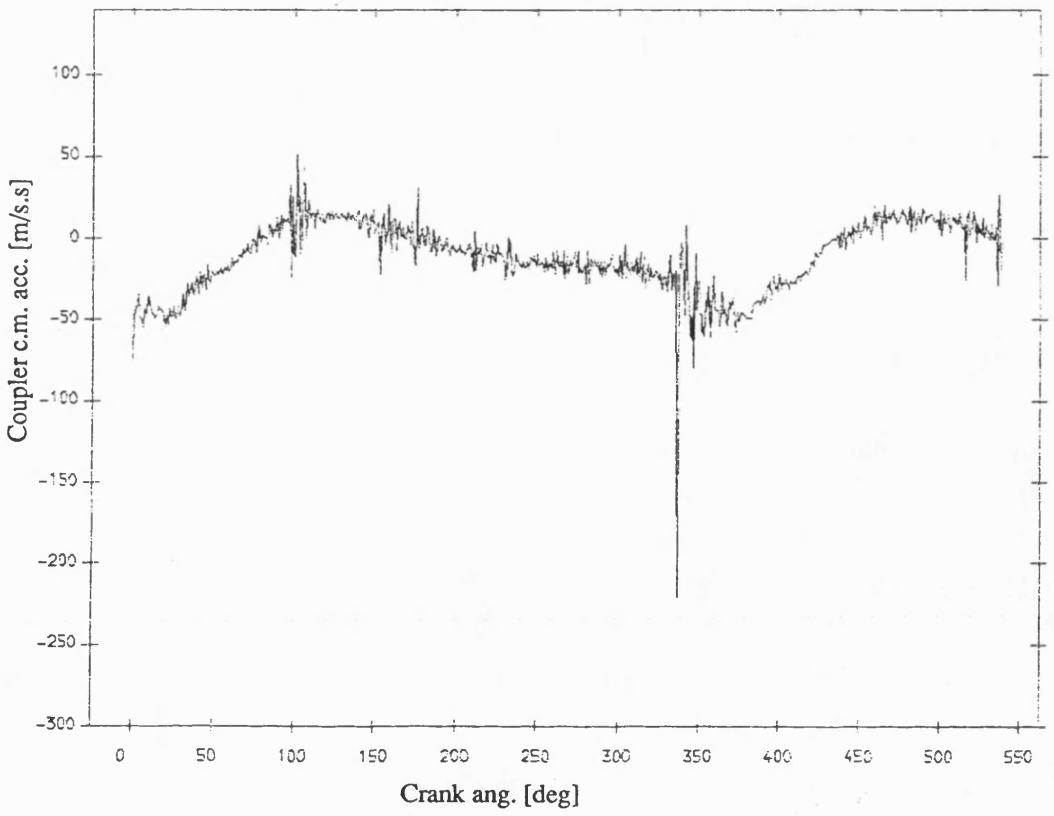

Fig 8.5.88 Exp. result coupler acceleration , dry bearing
with fly wheel ;mean speed=244 rev/min ; dia. clearance=.20mm

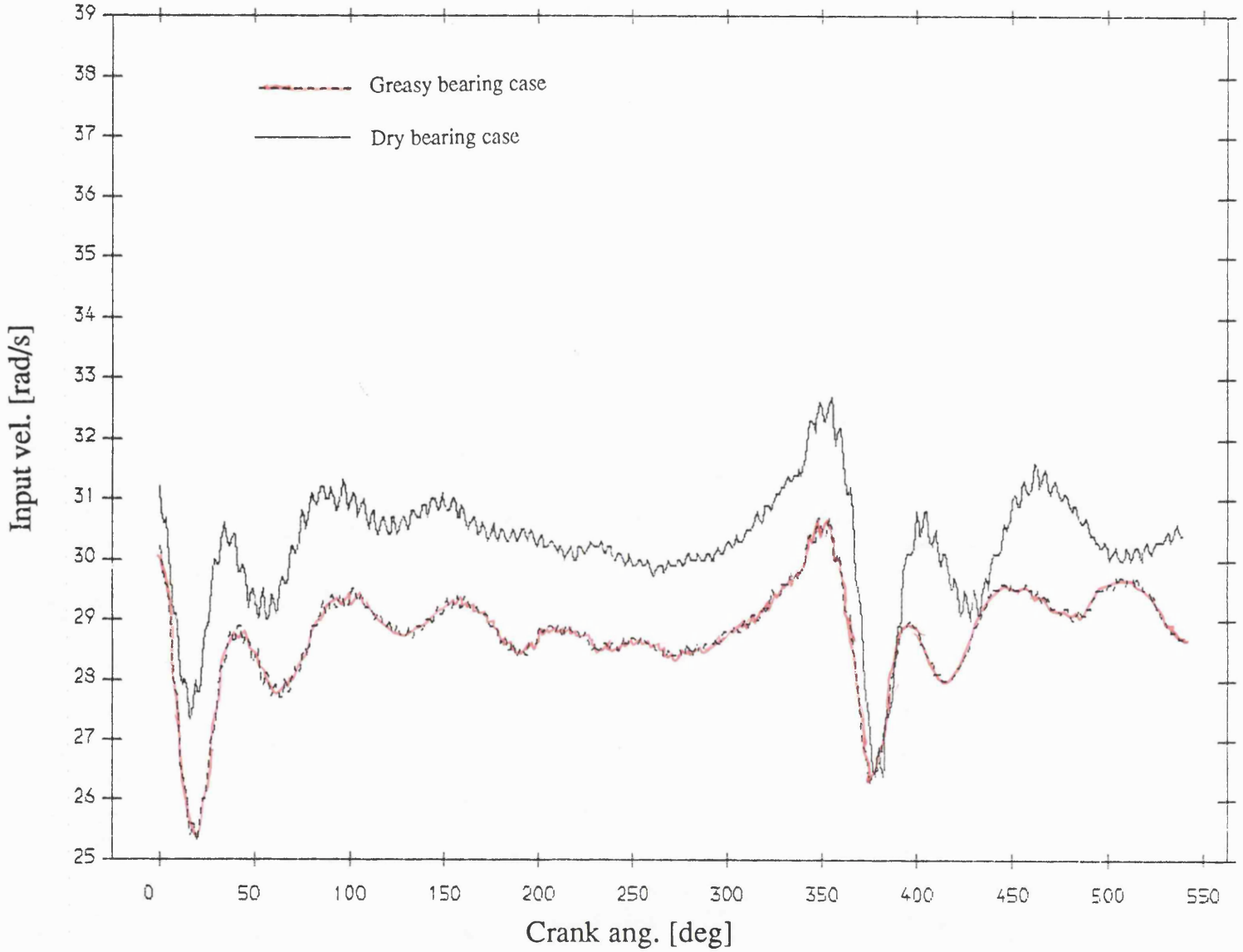

Fig 8.5.89 Exp. result input velocity , greasy v dry bearing
mean speed=290 rev/min; dia. clearance=.20mm

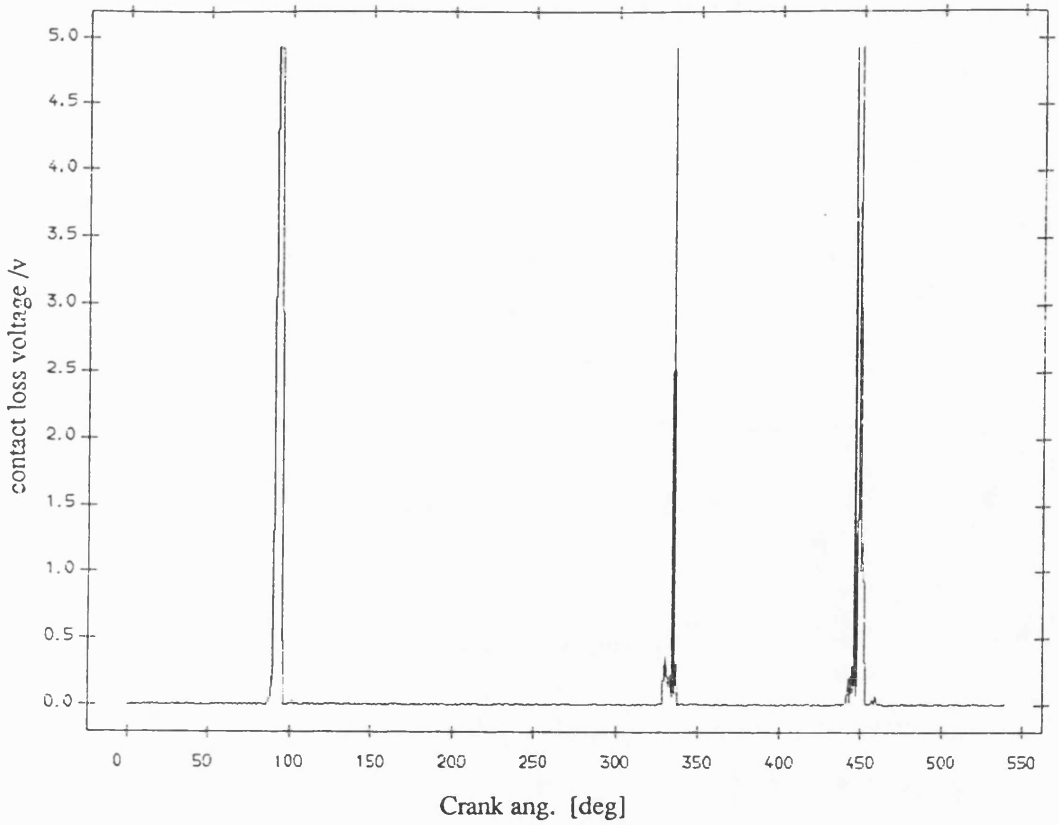

Fig 8.5.90 Exp. result contact loss of pin and greasy bearing
with flywheel ;mean speed=290 rev/min ;dia. clearance=0.20mm

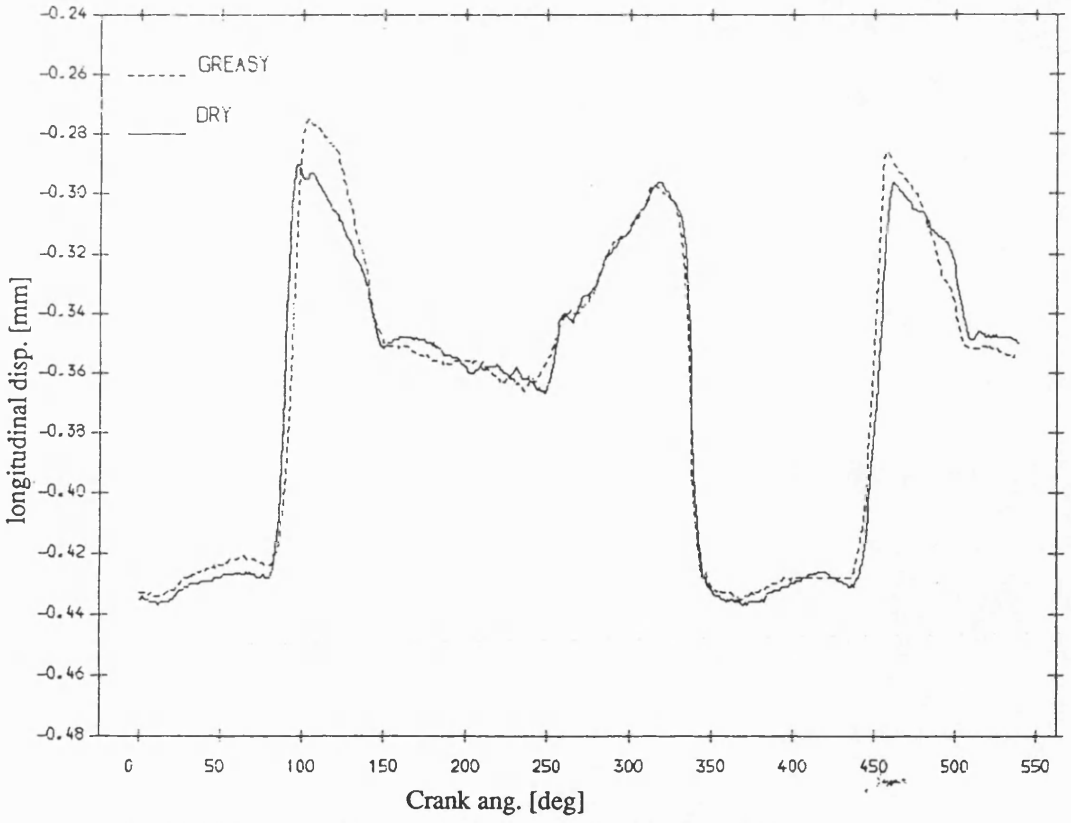

Fig 8.5.92 Exp. result longitudinal disp. of pin , greasy v dry bearing
mean speed=290 rev/min; dia. clearance=.20mm

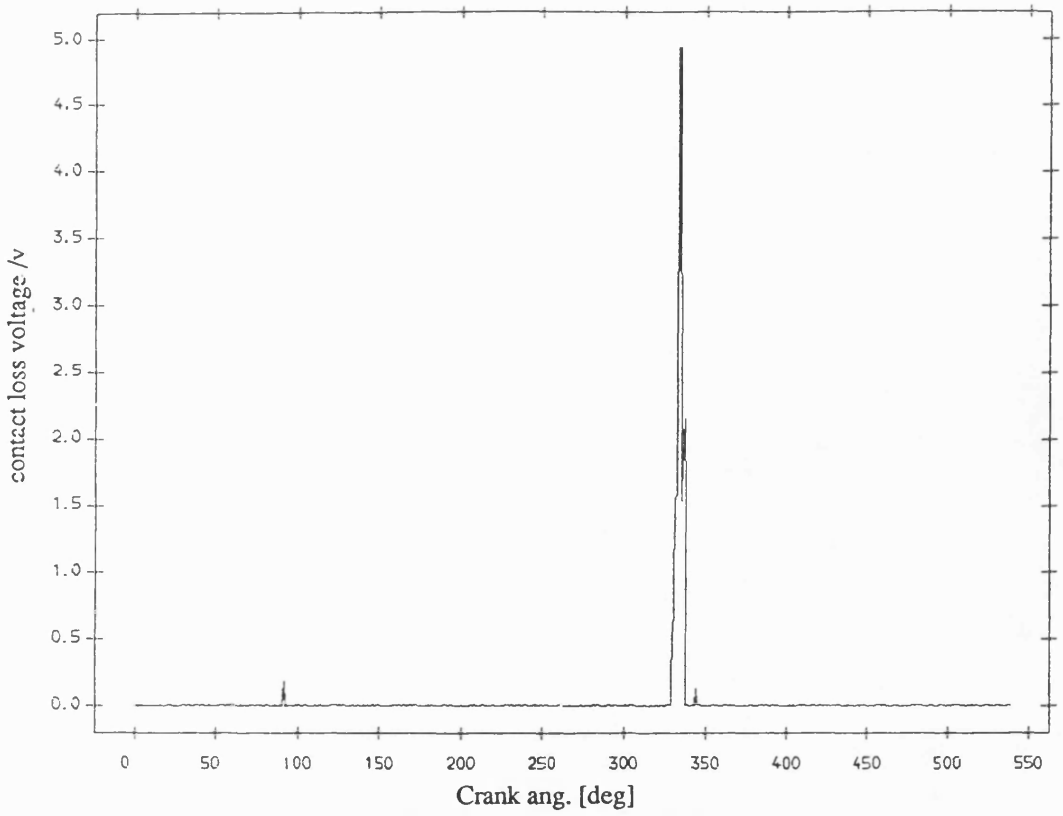

Fig 8.5.91 Exp. result contact loss of pin and dry bearing
with flywheel ;mean speed=290 rev/min ;dia. clearance=0.20mm

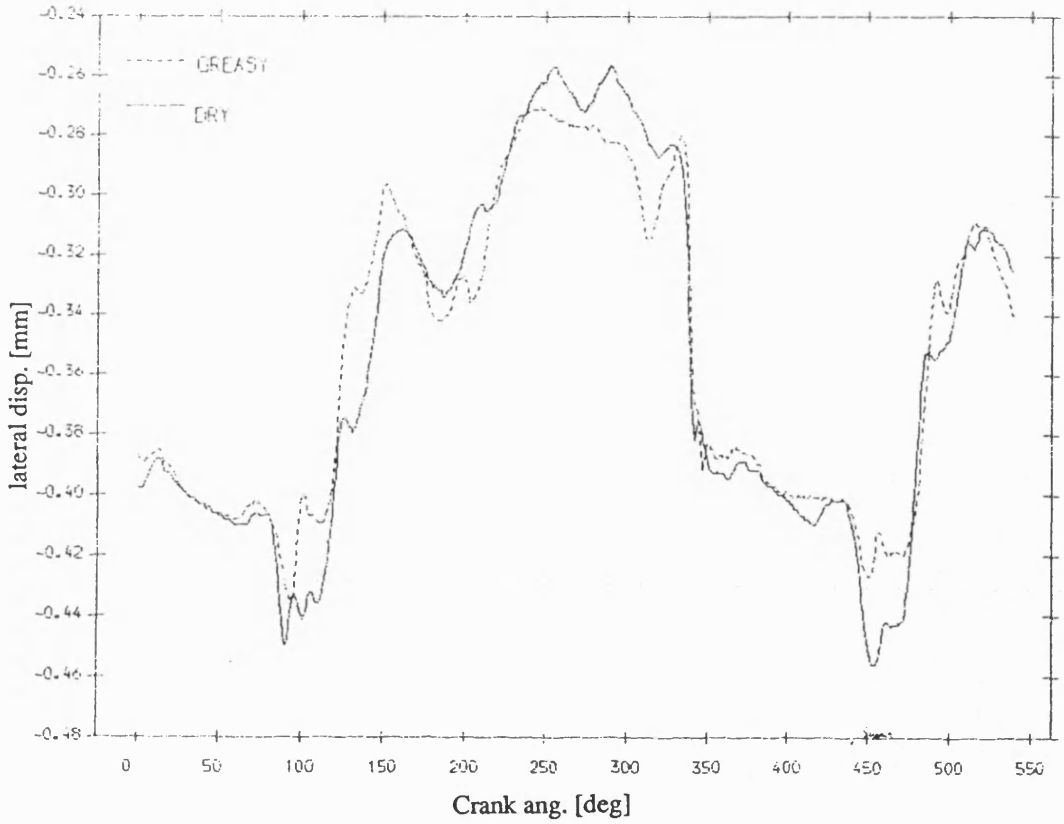

Fig 8.5.93 Exp. result lateral disp. of pin , greasy v dry bearing
mean speed=290 rev/min; dia. clearance=.20mm

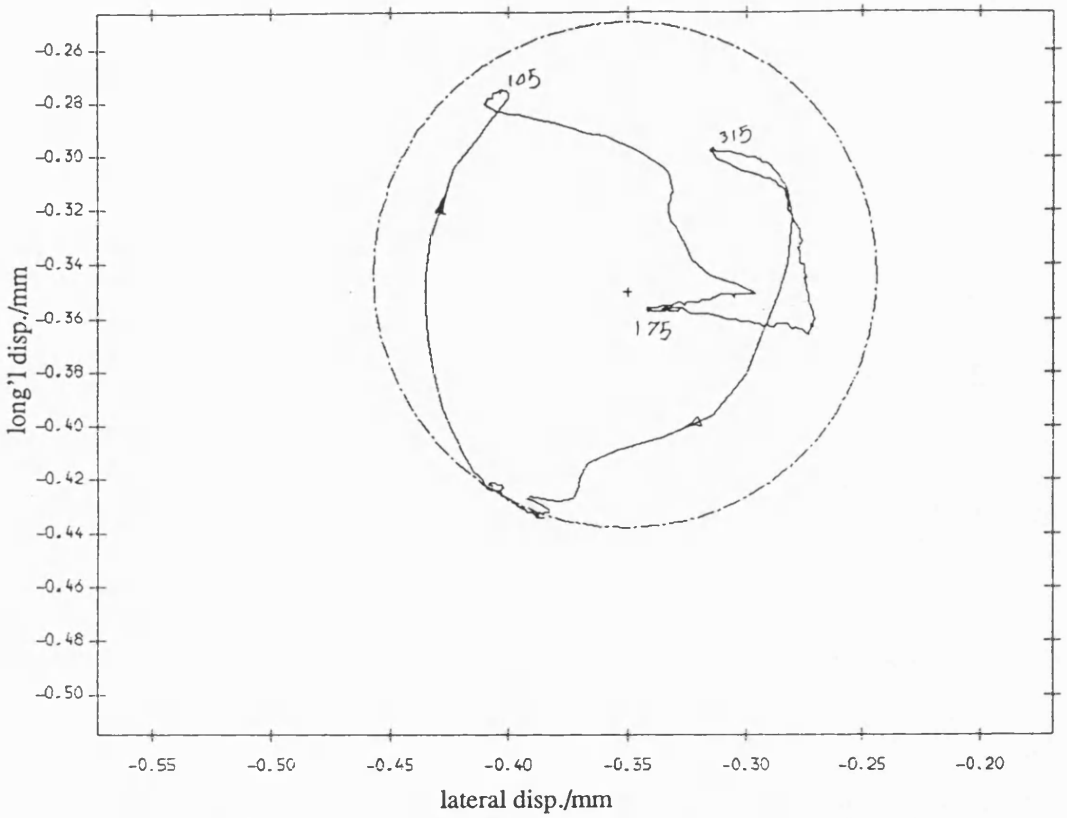

Fig 8.5.94 Exp. result polar plot of relative disp. of pin in greasy bearing with fly wheel ;mean speed=290 rev/min ; dia. clearance=.20mm

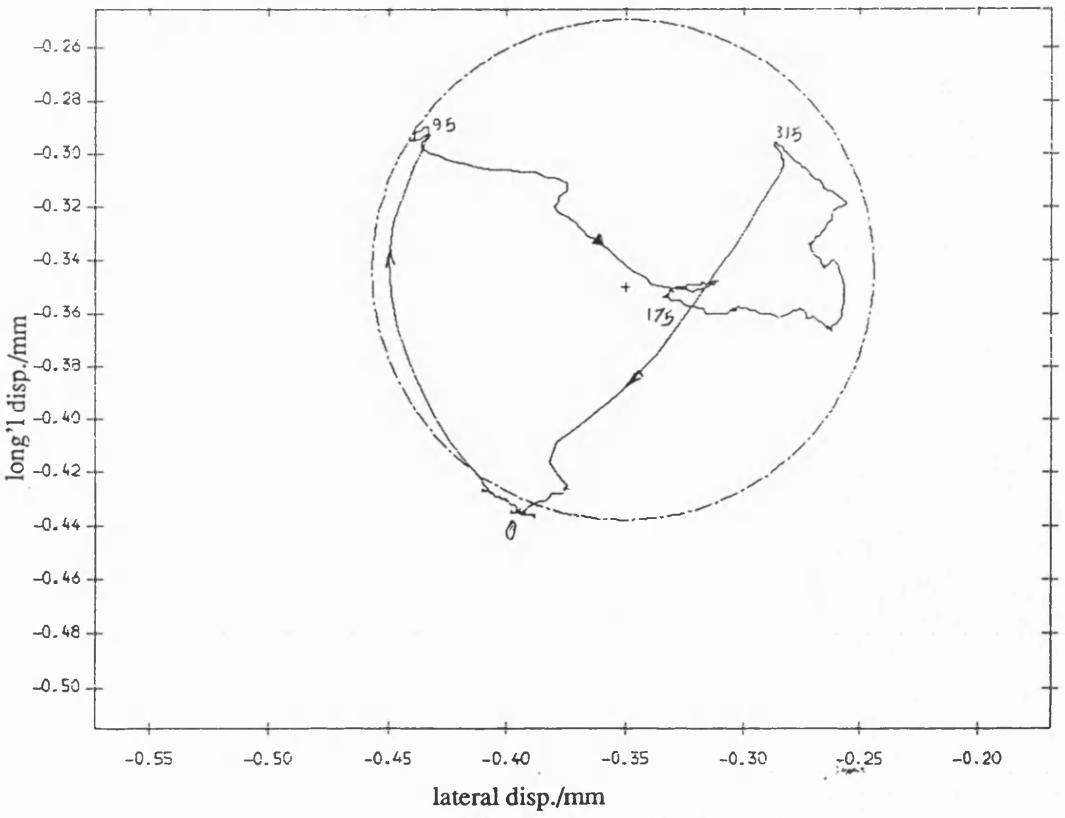

Fig 8.5.95 Exp. result polar plot of relative disp. of pin in dry bearing with fly wheel ;mean speed=290 rev/min ; dia. clearance=.20mm

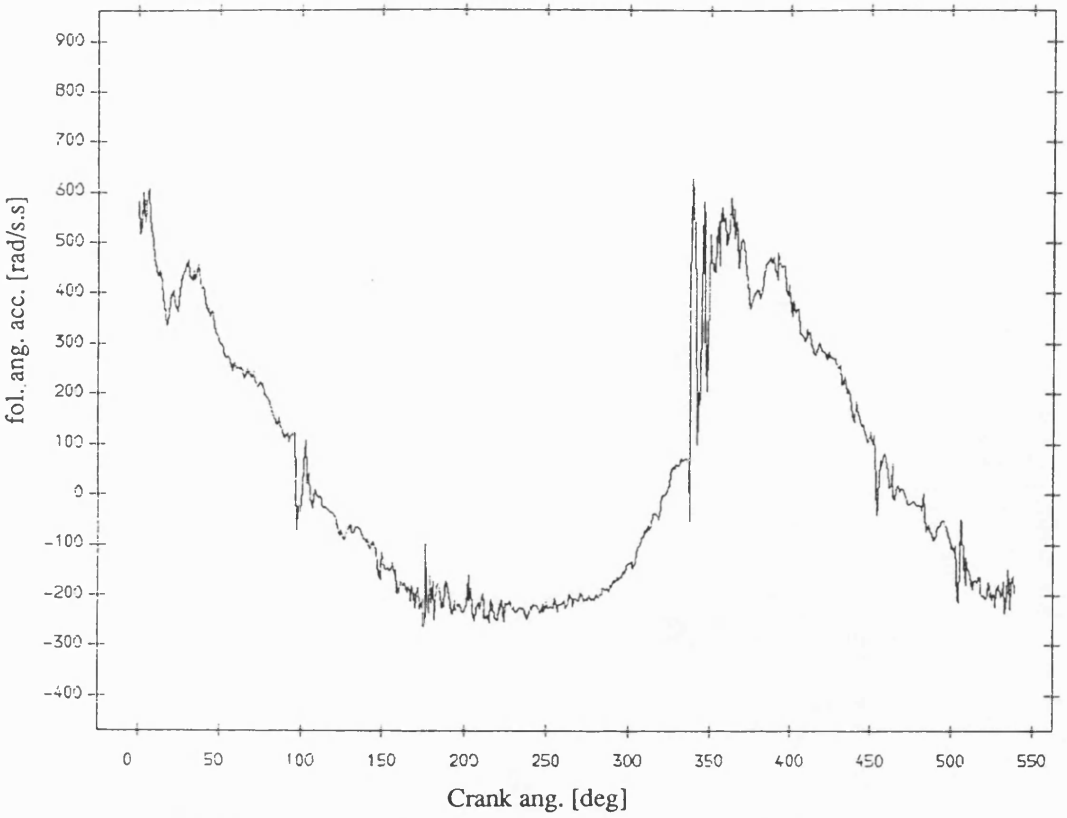

Fig 8.5.96 Exp. result follower ang. acceleration , greasy bearing
with fly wheel ;mean speed=290 rev/min ; dia. clearance=.20mm

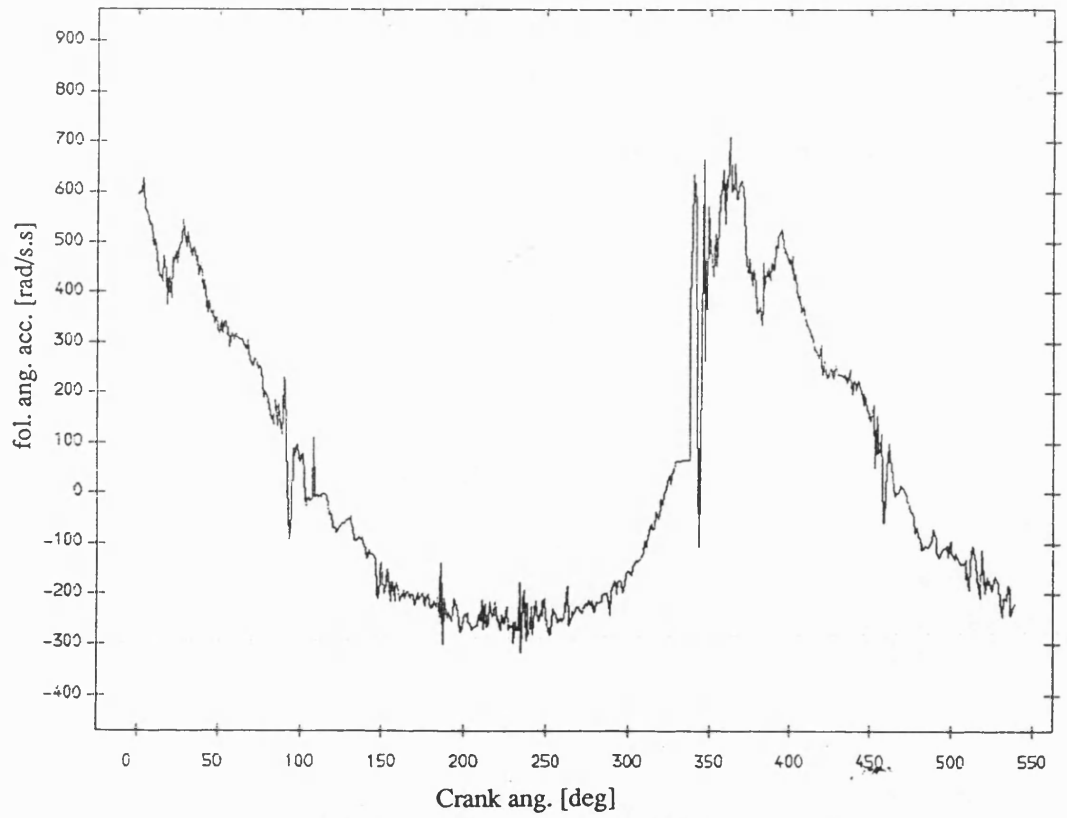

Fig 8.5.97 Exp. result follower ang. acceleration ,dry bearing
with fly wheel ;mean speed=290 rev/min ; dia. clearance=.20mm

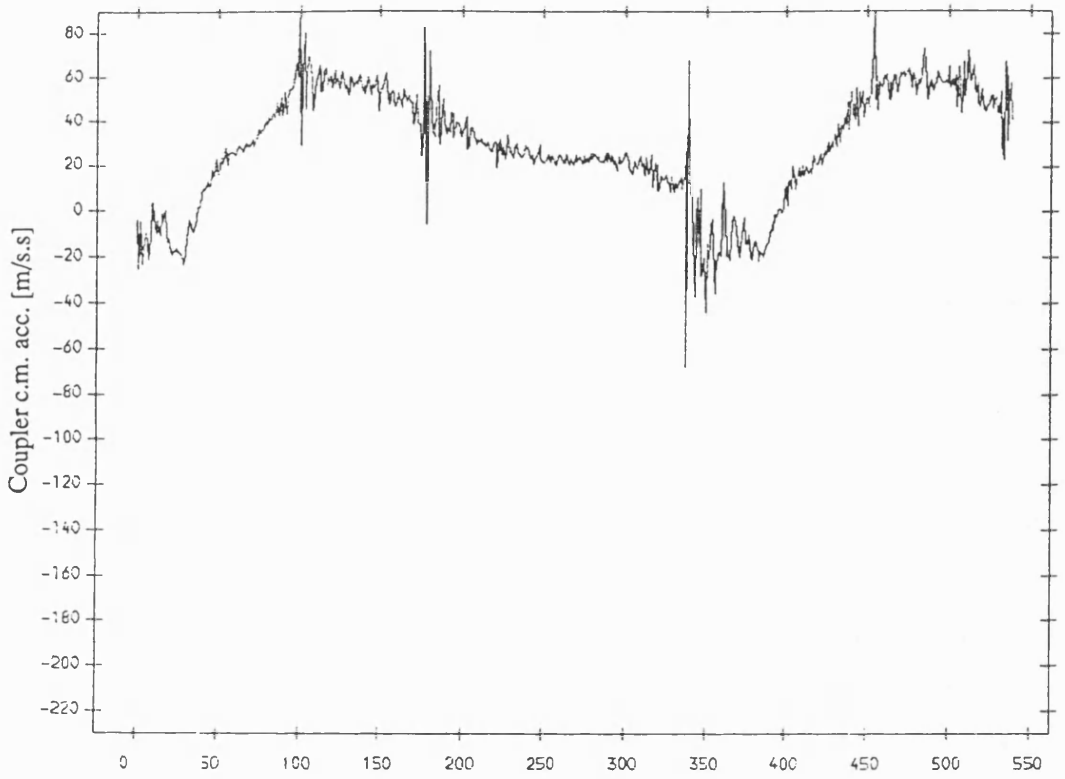

Fig 8.5.98 Exp. result coupler acceleration , greasy bearing
with fly wheel ;mean speed=290 rev/min ; dia. clearance=.20mm

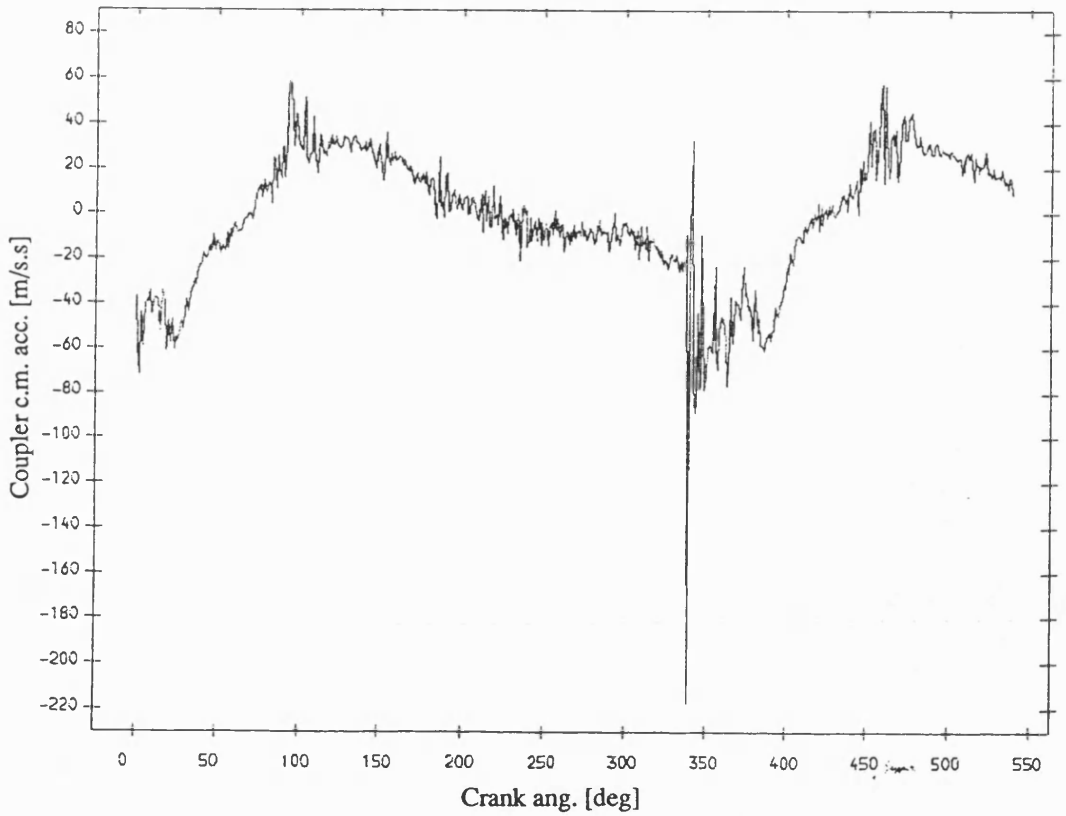

Fig 8.5.99 Exp. result coupler acceleration , dry bearing
with fly wheel ;mean speed=290 rev/min ; dia. clearance=.20mm

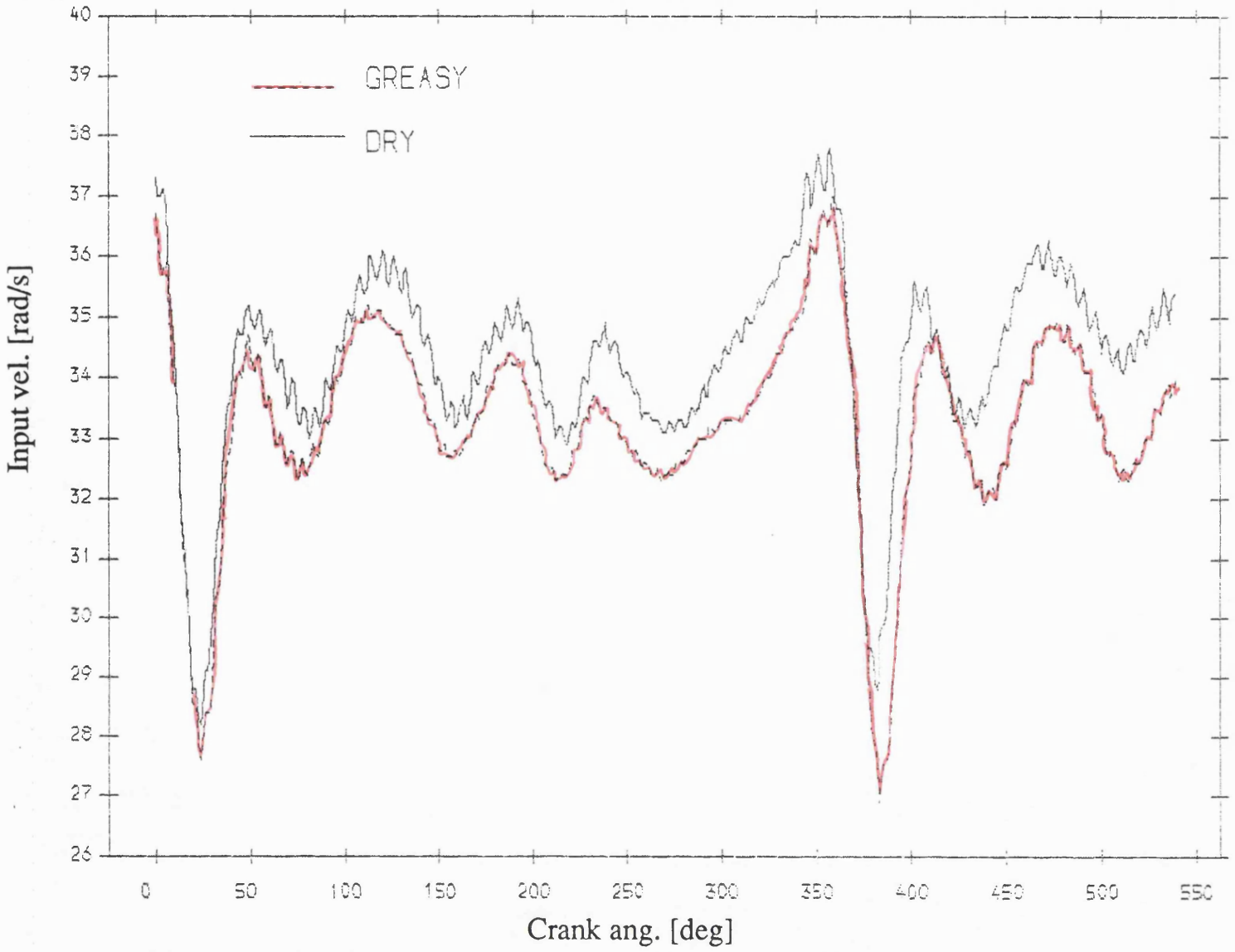

Fig 8.5.100 Exp. result input velocity , greasy v dry bearing
mean speed=327 rev/min; dia. clearance=.20mm

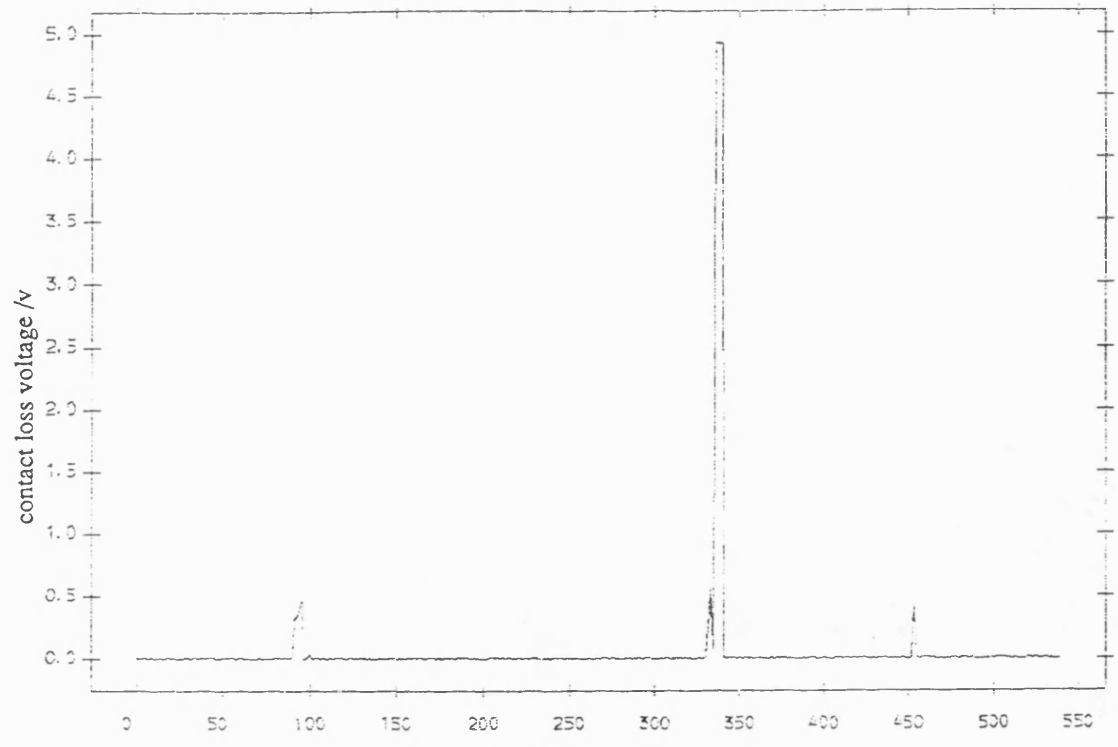

Fig 8.5.101 Exp. result contact loss of pin and greasy bearing
with flywheel ;mean speed=327 rev/min ;dia. clearance=0.20mm

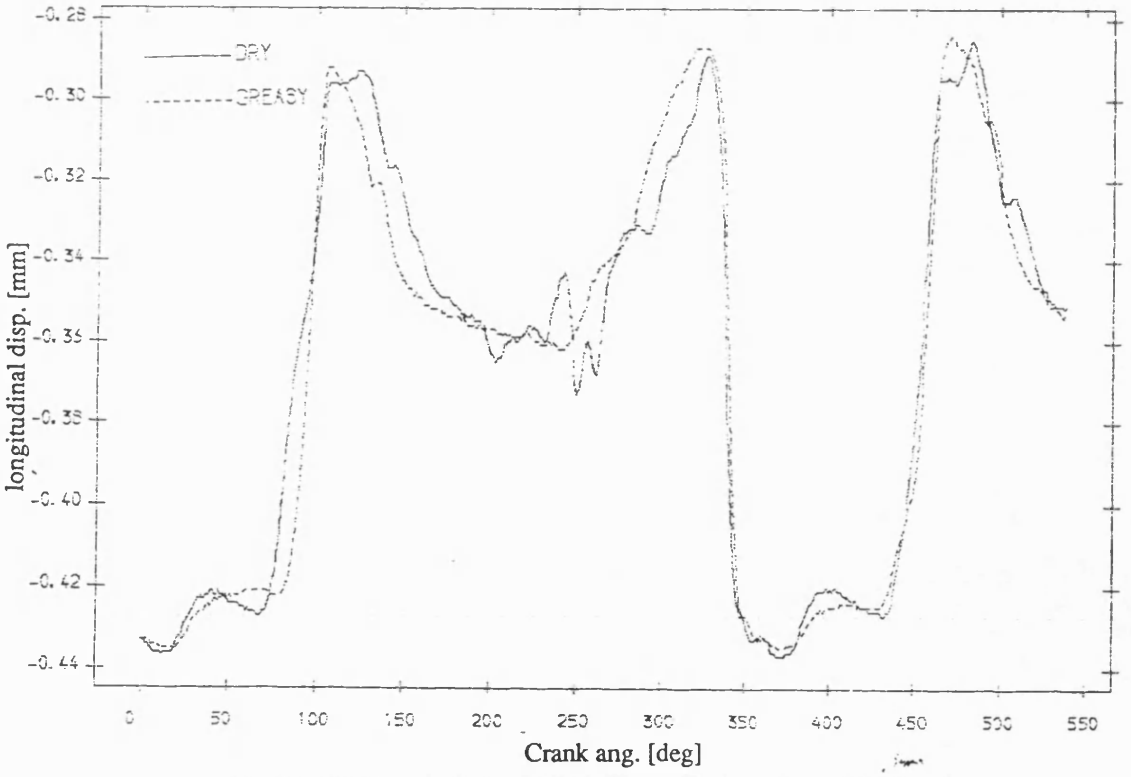

Fig 8.5.103 Exp. result longitudinal disp. of pin , greasy v dry bearing
mean speed=327 rev/min; dia. clearance=.20mm

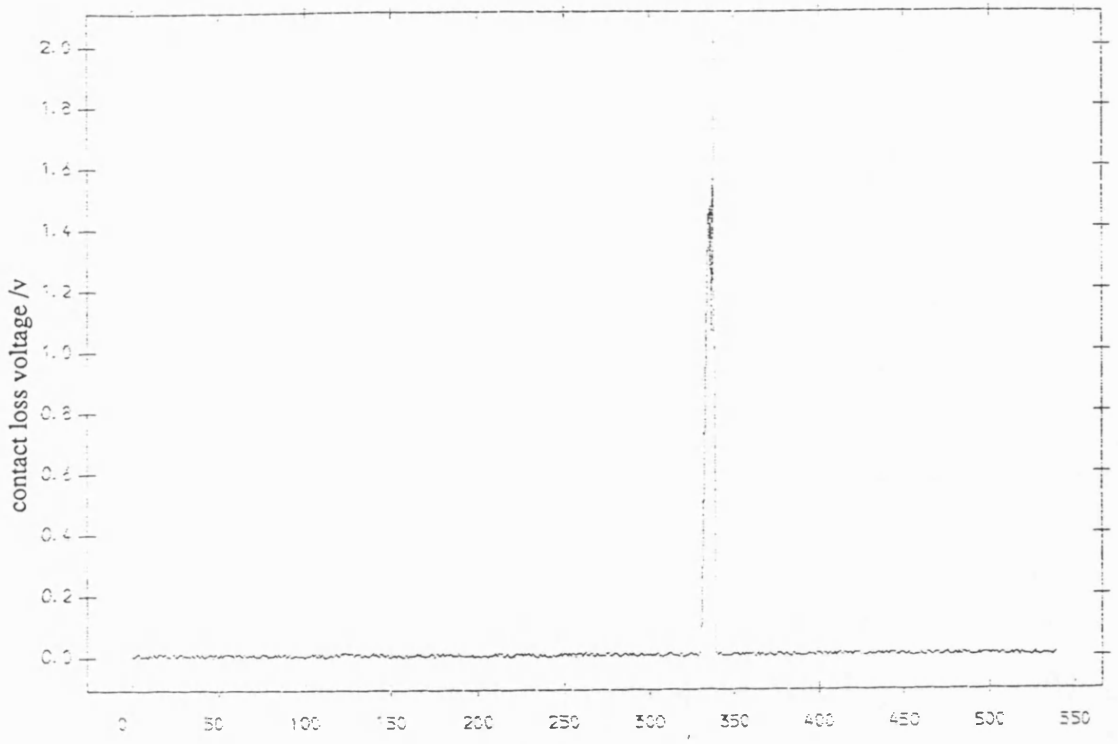

Fig 8.5.102 Exp. result contact loss of pin and dry bearing
with flywheel ;mean speed=327 rev/min ;dia. clearance=0.20mm

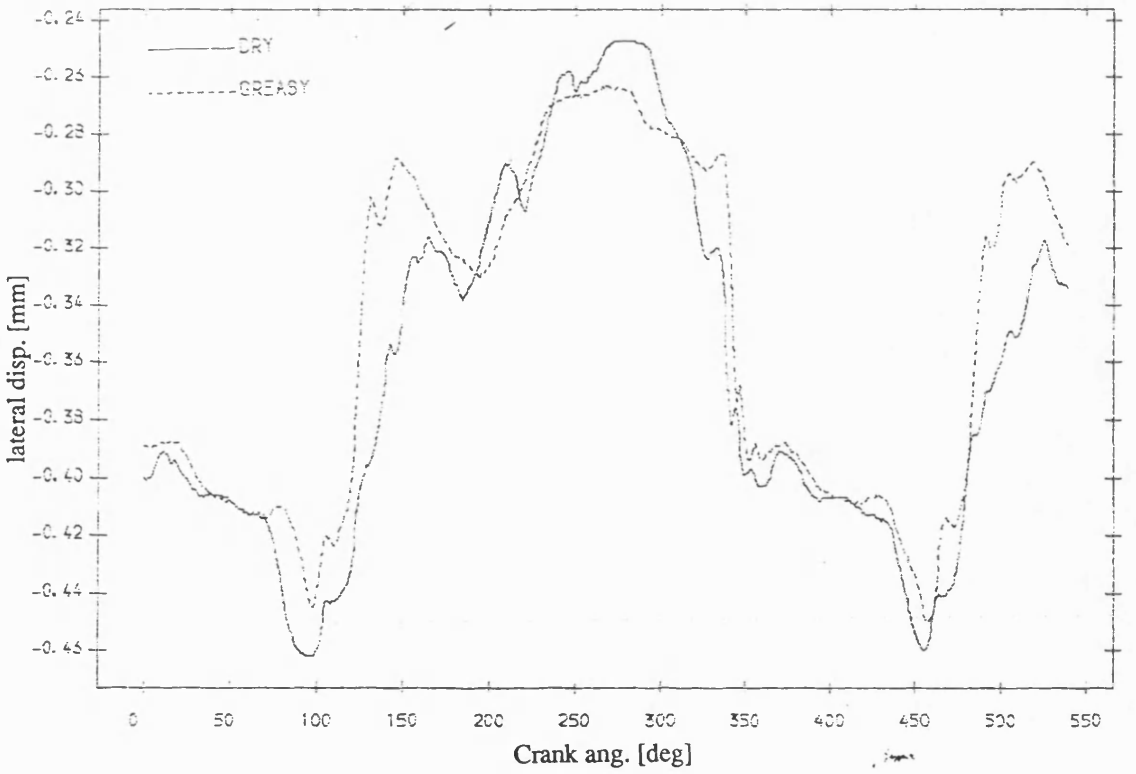

Fig 8.5.104 Exp. result lateral disp. of pin , greasy v dry bearing
mean speed=327 rev/min; dia. clearance=.20mm

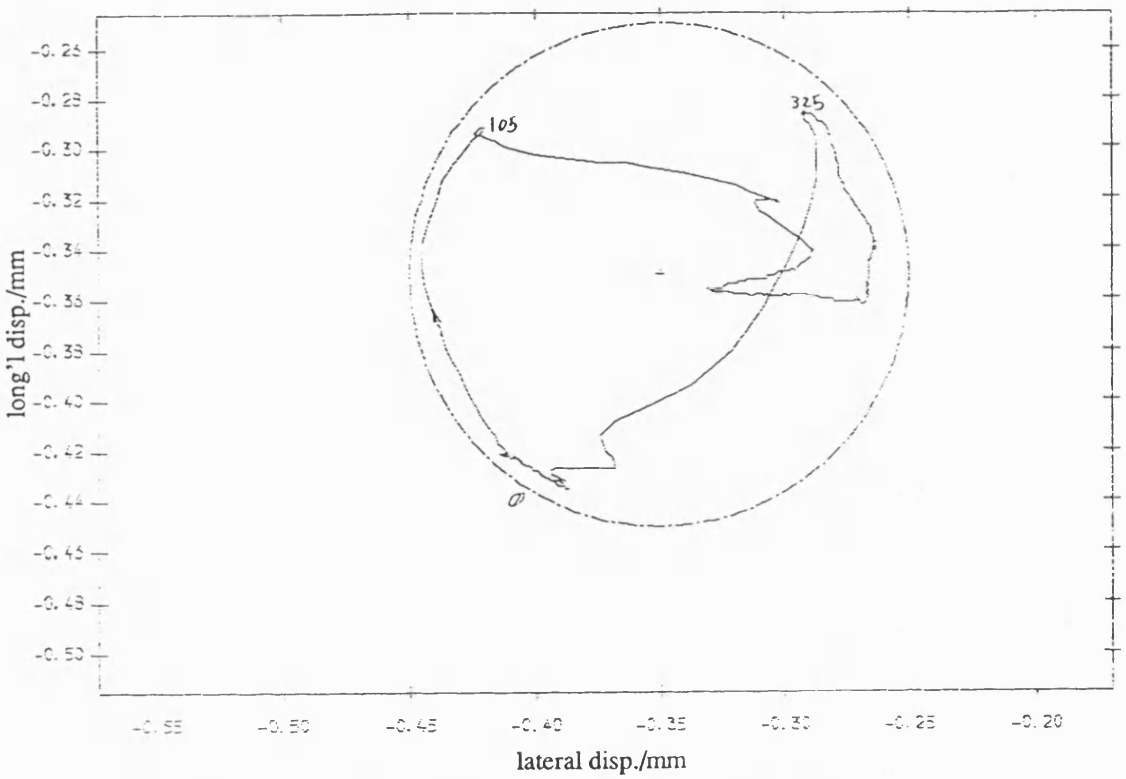

Fig 8.5.105 Exp. result polar plot of relative disp. of pin in greasy bearing with fly wheel ;mean speed=327 rev/min ; dia. clearance=.20mm

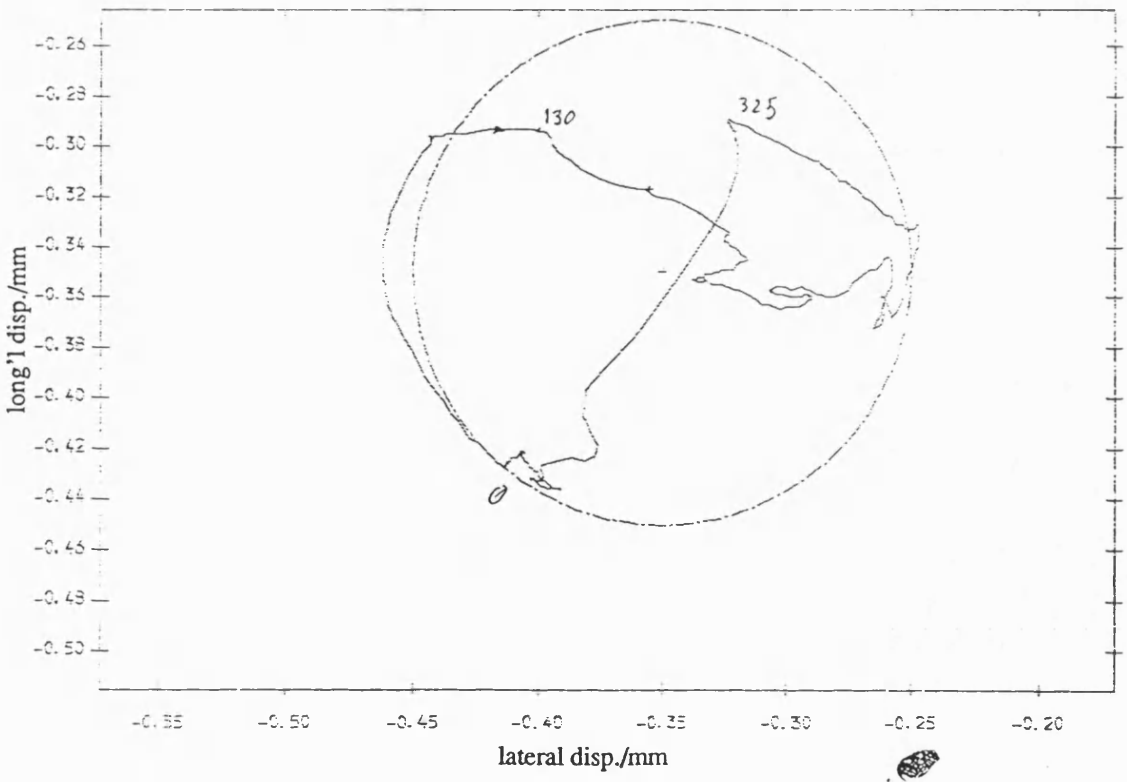

Fig 8.5.106 Exp. result polar plot of relative disp. of pin in dry bearing with fly wheel ;mean speed=327 rev/min ; dia. clearance=.20mm

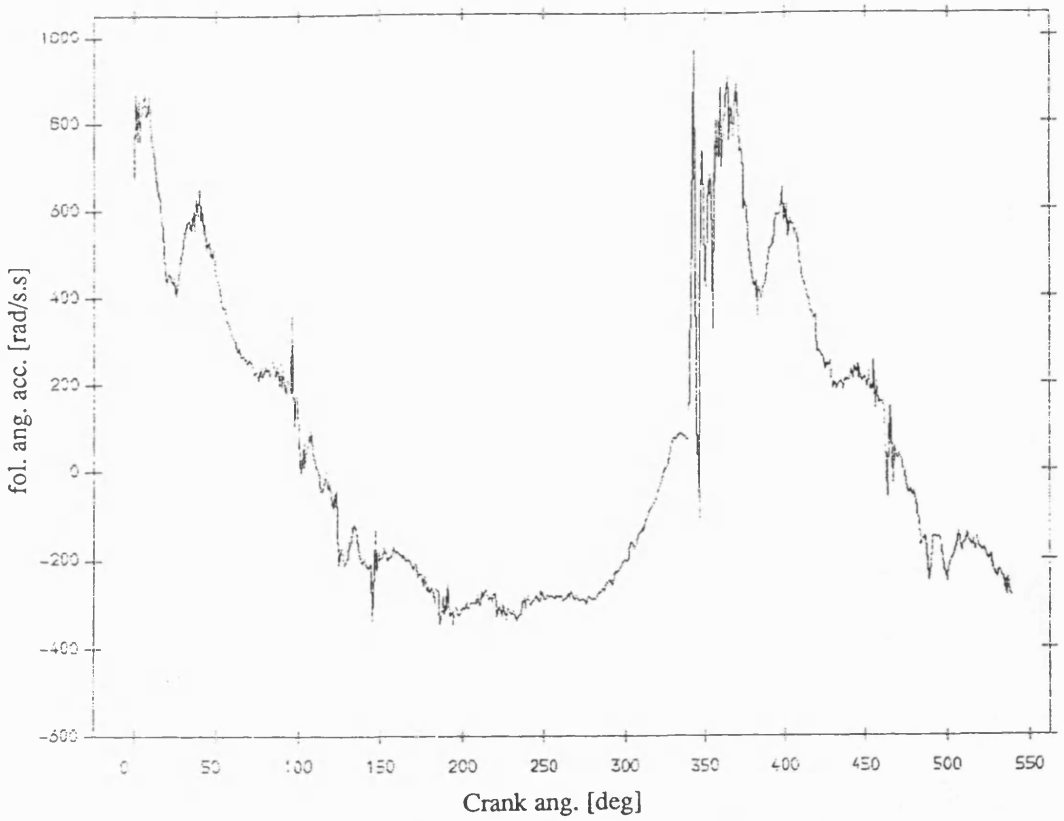

Fig 8.5.107 Exp. result follower ang. acceleration , greasy bearing
with fly wheel ;mean speed=327 rev/min ; dia. clearance=.20mm

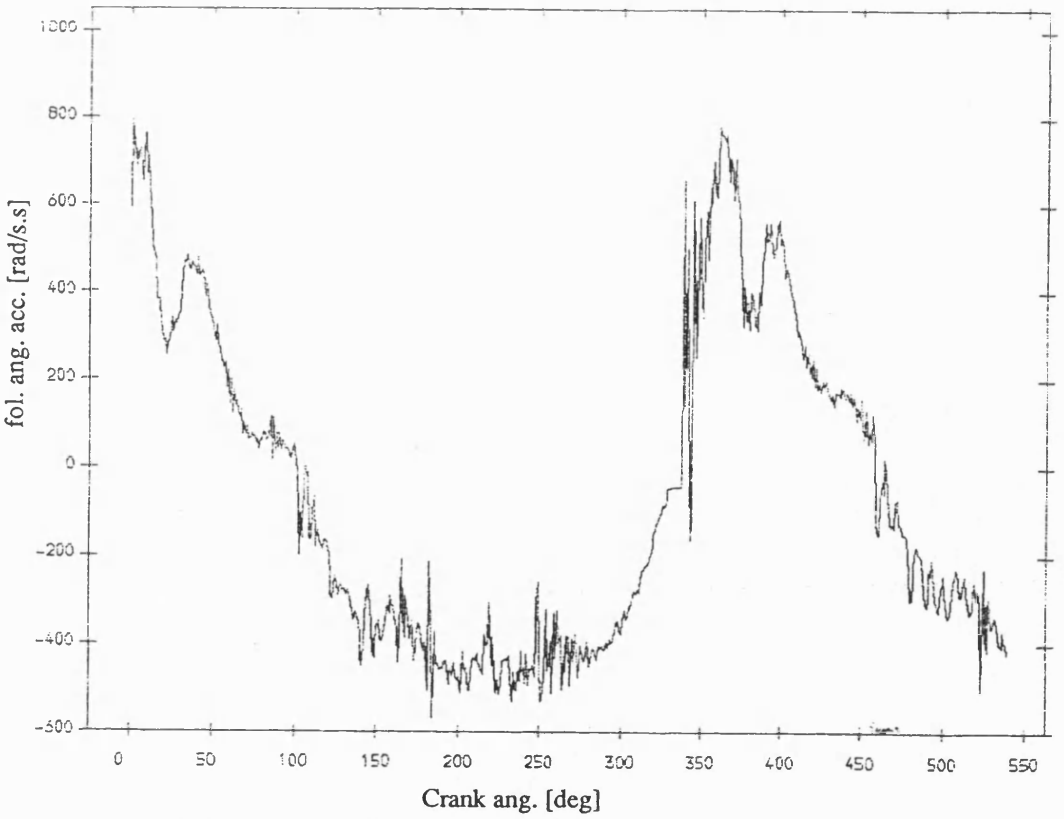

Fig 8.5.108 Exp. result follower ang. acceleration ,dry bearing
with fly wheel ;mean speed=327 rev/min ; dia. clearance=.20mm

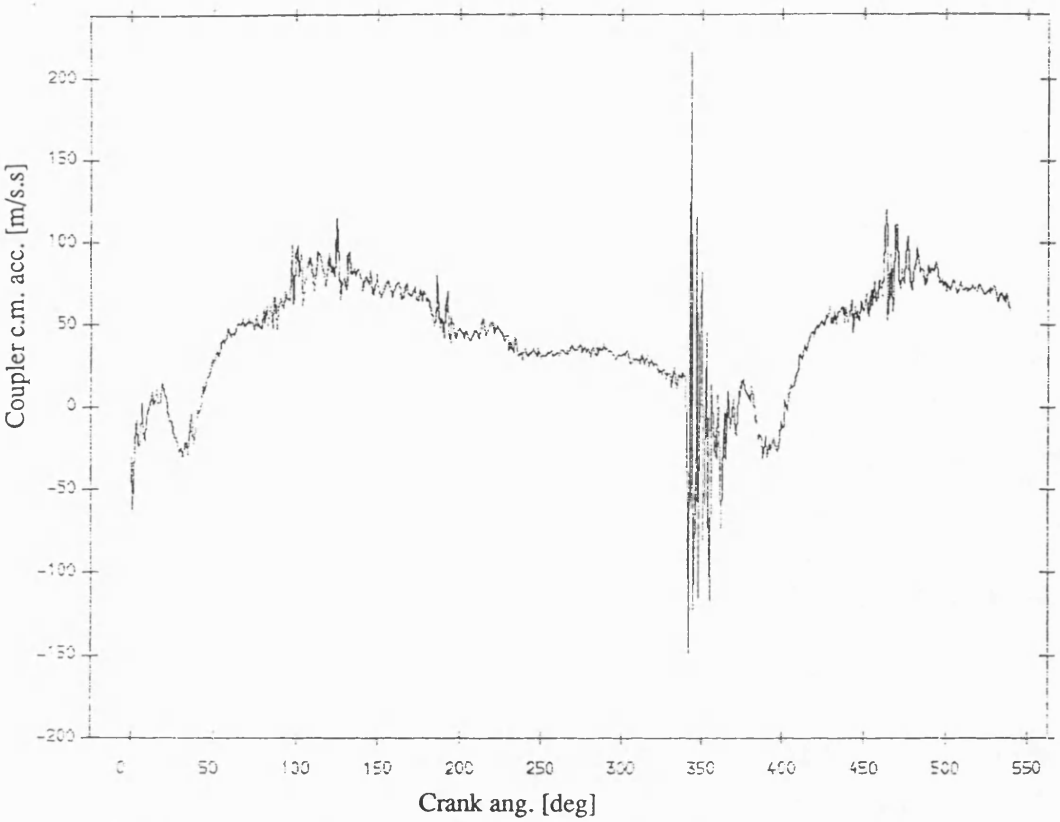

Fig 8.5.109 Exp. result coupler acceleration , greasy bearing
with fly wheel ;mean speed=327 rev/min ; dia. clearance=.20mm

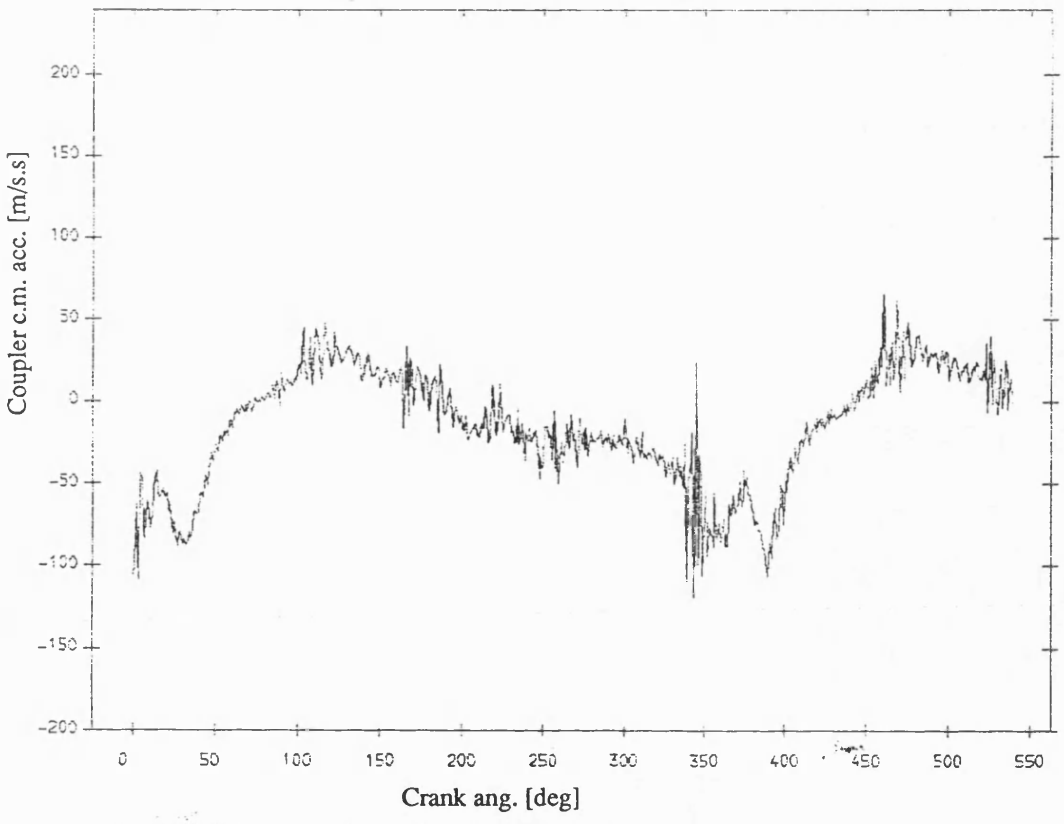

Fig 8.5.110 Exp. result coupler acceleration , dry bearing
with fly wheel ;mean speed=327 rev/min ; dia. clearance=.20mm

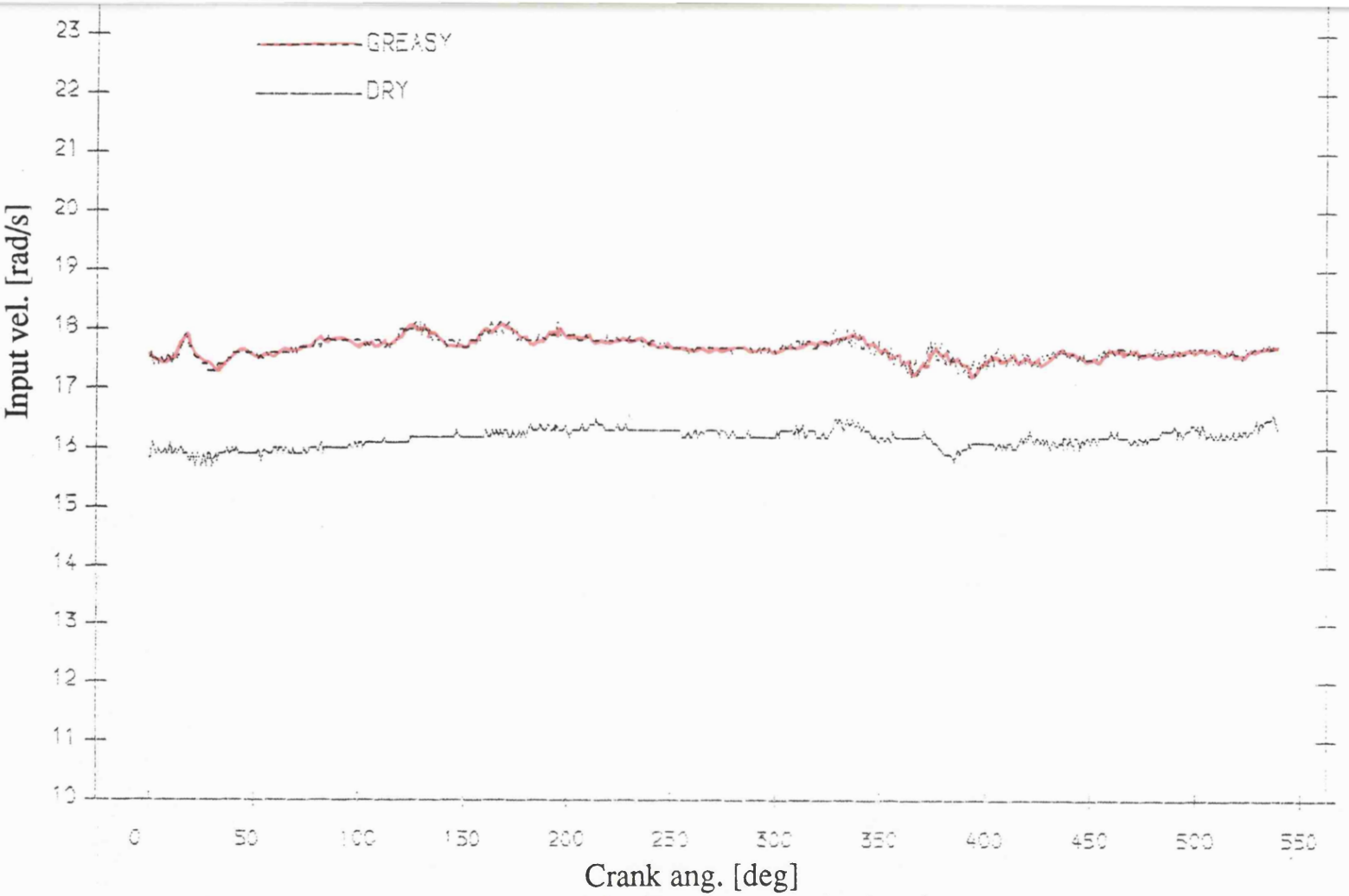

Fig 8.5.111 Exp. result input velocity , greasy v dry bearing
mean speed=168 rev/min; dia. clearance=.15mm

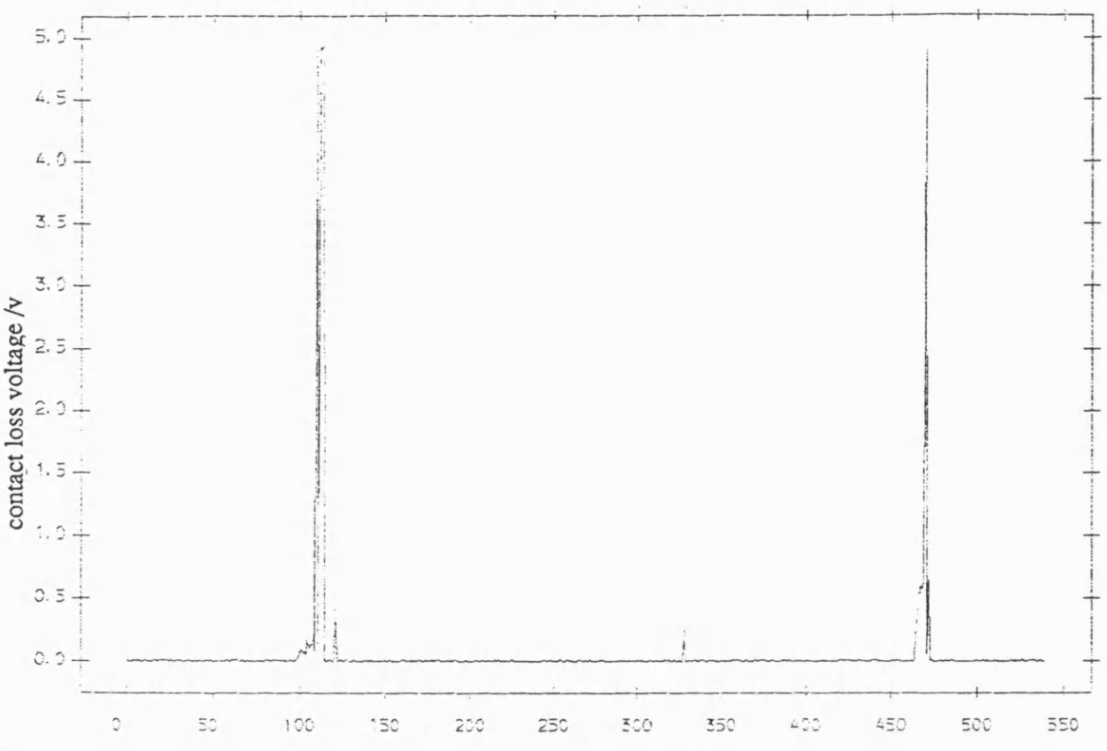

Fig 8.5.112 Exp. result contact loss of pin and ,greasy bearing
with flywheel ;mean speed=168 rev/min ;dia. clearance=0.15mm

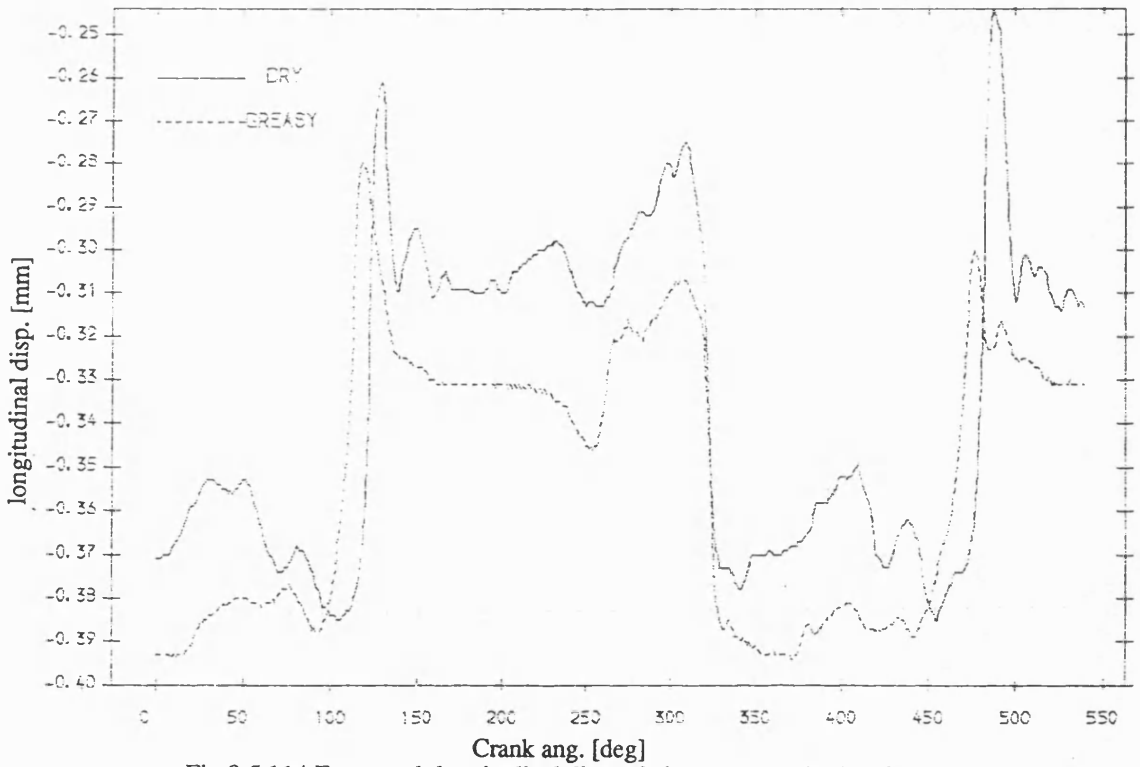

Fig 8.5.114 Exp. result longitudinal disp. of pin , greasy v dry bearing
mean speed=168 rev/min; dia. clearance=.15mm

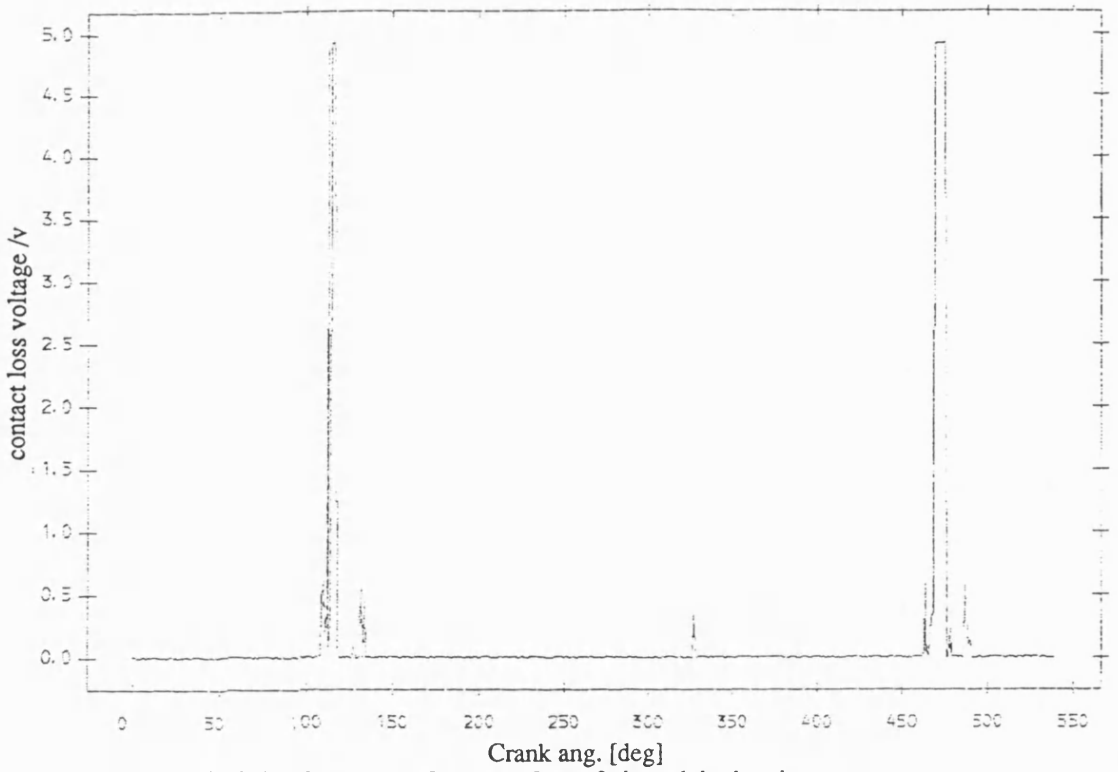

Fig 8.5.113 Exp. result contact loss of pin and dry bearing
with flywheel ;mean speed=168 rev/min ;dia. clearance=0.15mm

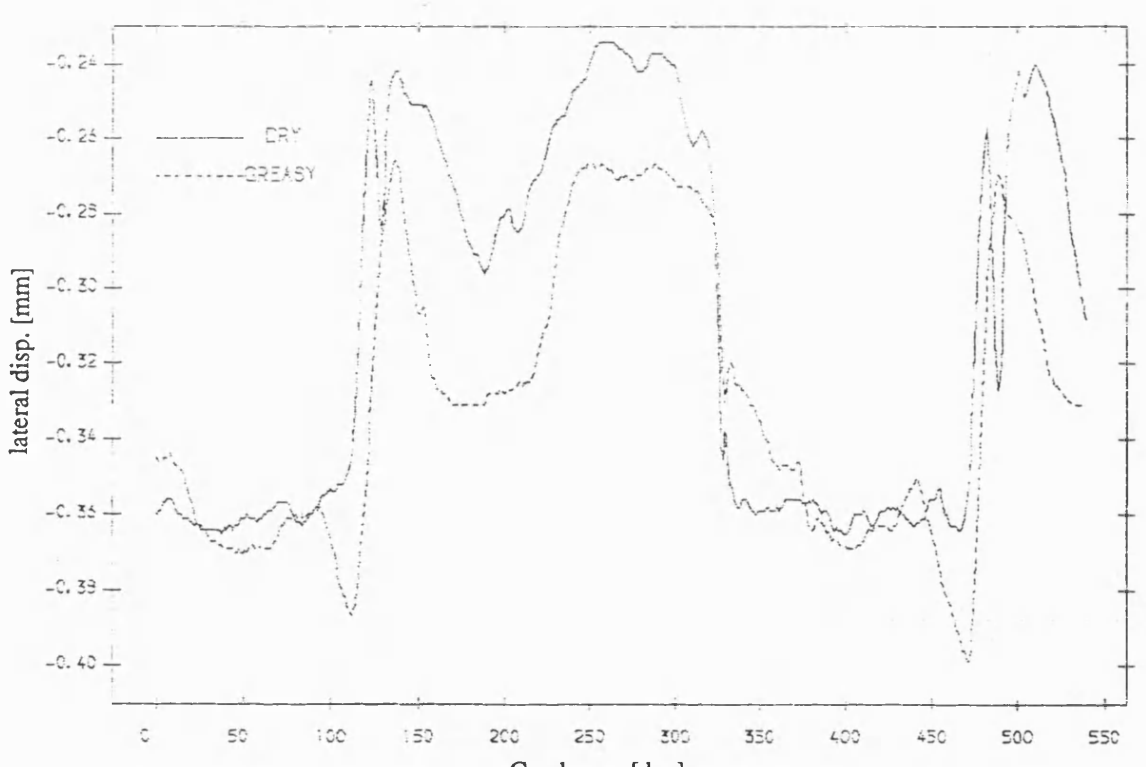

Fig 8.5.115 Exp. result lateral disp. of pin , greasy v dry bearing
mean speed=168 rev/min; dia. clearance=.15mm

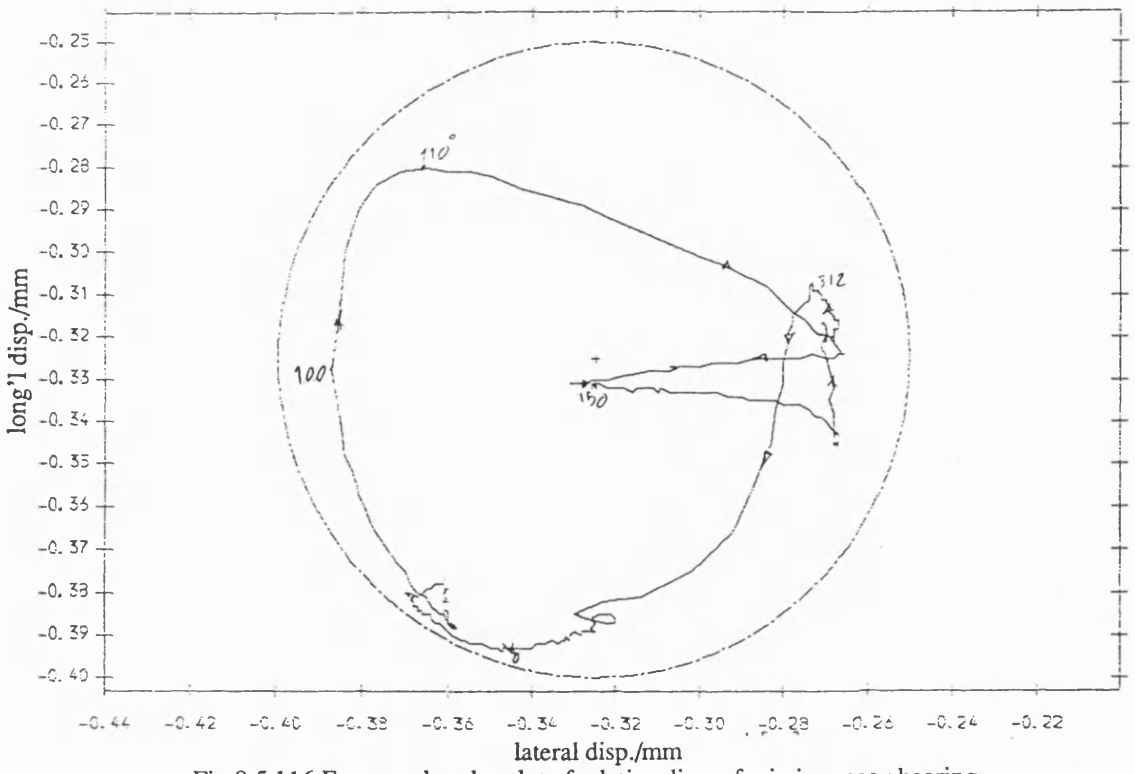

Fig 8.5.116 Exp. result polar plot of relative disp. of pin in greasy bearing with fly wheel ;mean speed=168 rev/min ; dia. clearance=.15mm

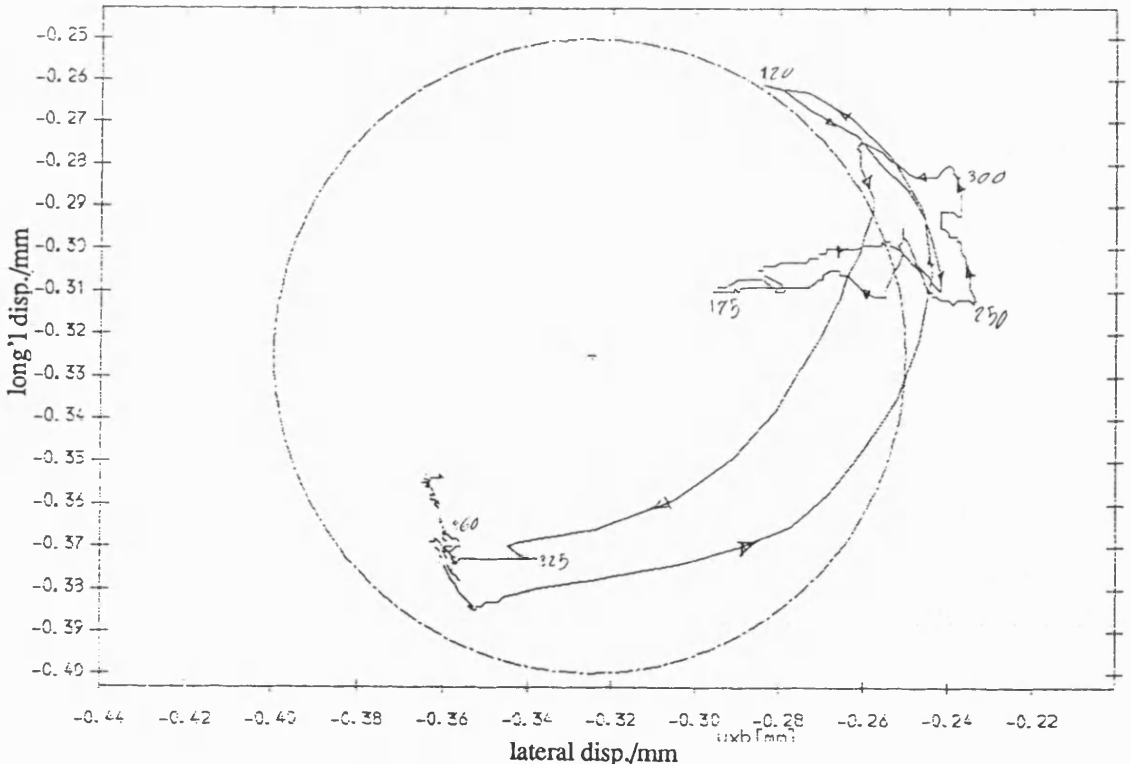

Fig 8.5.117 Exp. result polar plot of relative disp. of pin in dry bearing with fly wheel ;mean speed=168 rev/min ; dia. clearance=.15mm

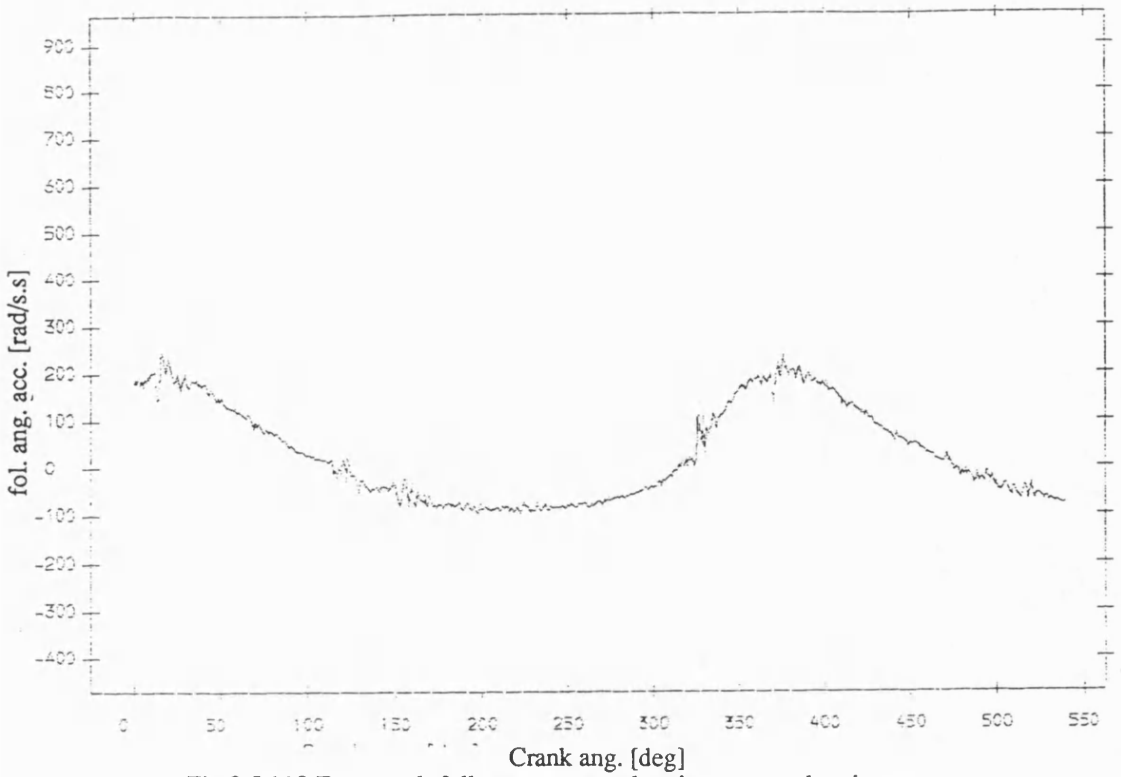

Fig 8.5.118 Exp. result follower ang. acceleration , greasy bearing
with fly wheel ;mean speed=168 rev/min ; dia. clearance=.15mm

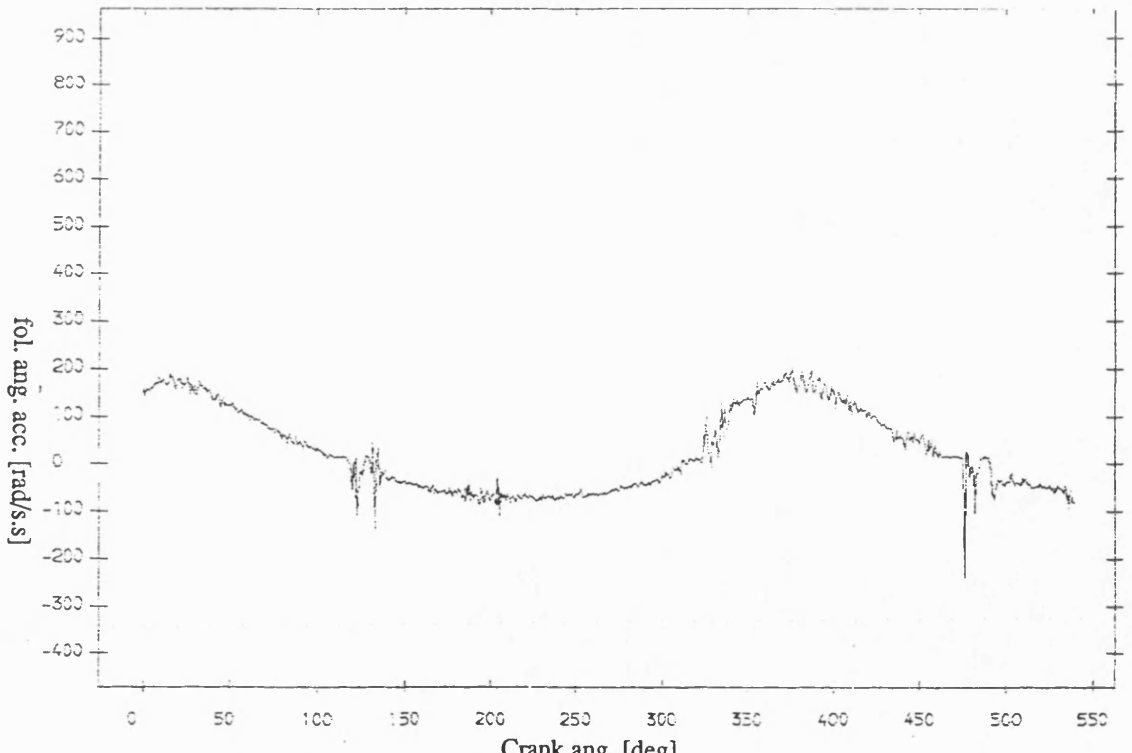

Fig 8.5.119 Exp. result follower ang. acceleration ,dry bearing
with fly wheel ;mean speed=168 rev/min ; dia. clearance=.15mm

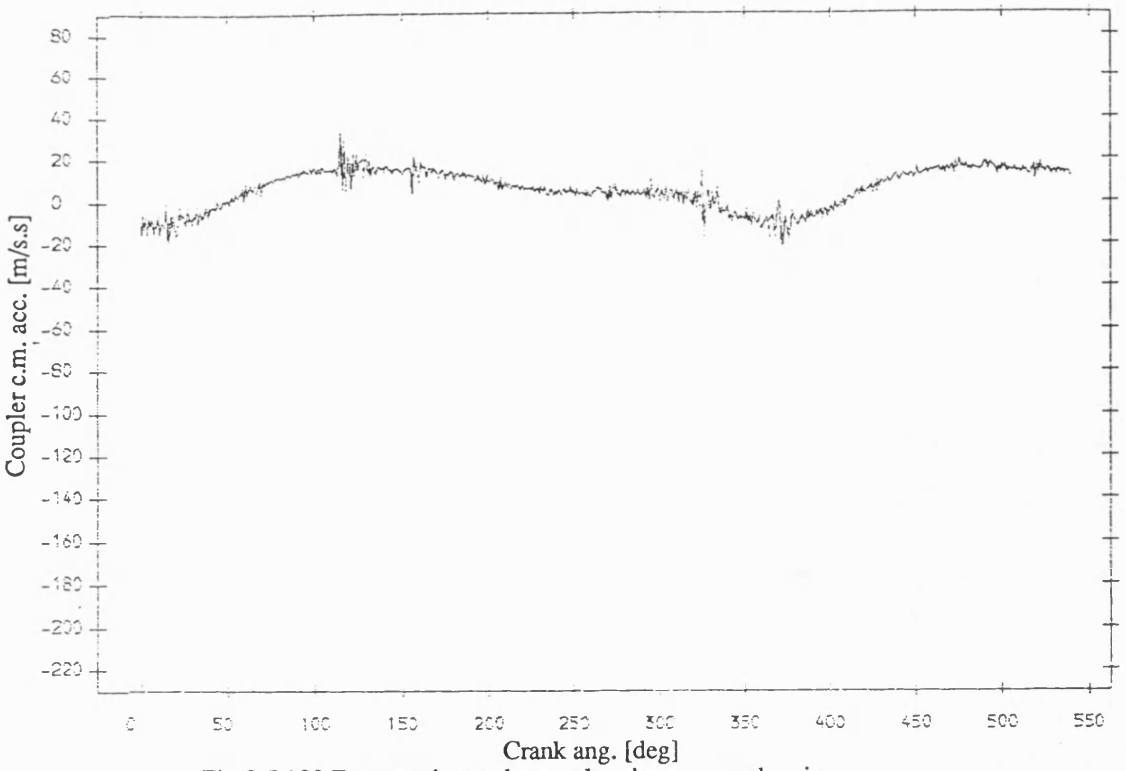

Fig 8.5.120 Exp. result coupler acceleration , greasy bearing
with fly wheel ;mean speed=168 rev/min ; dia. clearance=.15mm

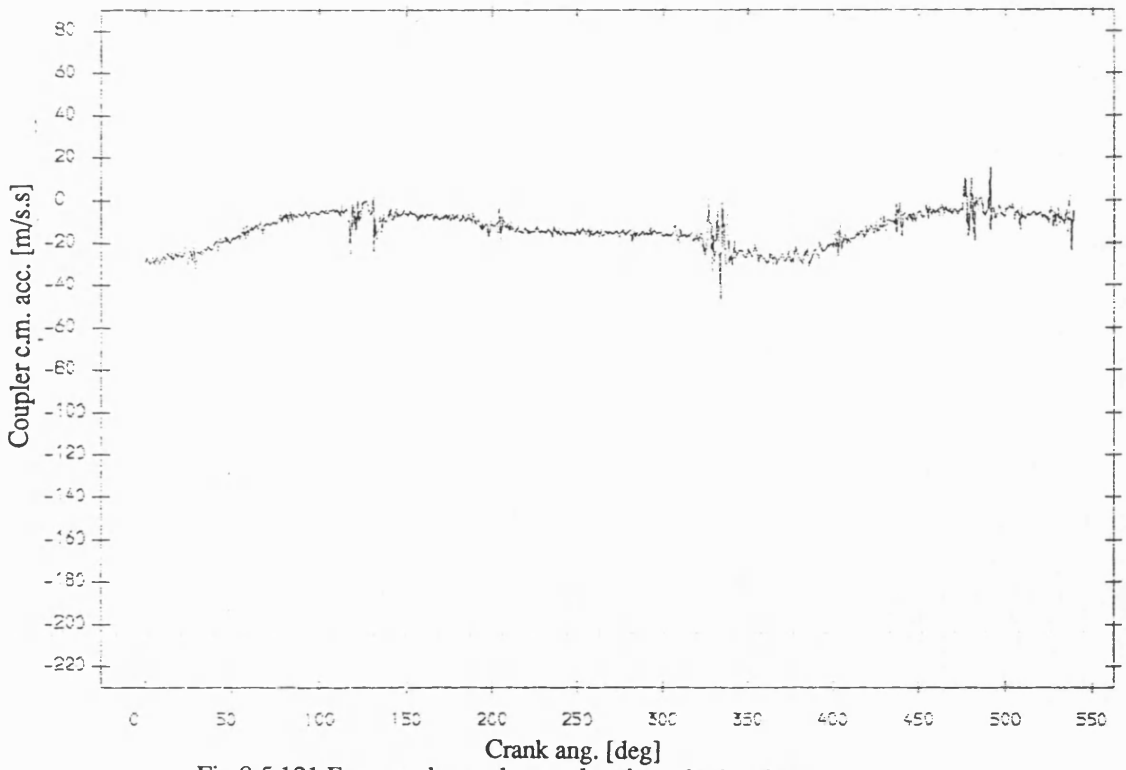

Fig 8.5.121 Exp. result coupler acceleration , dry bearing
with fly wheel ;mean speed=168 rev/min ; dia. clearance=.15mm

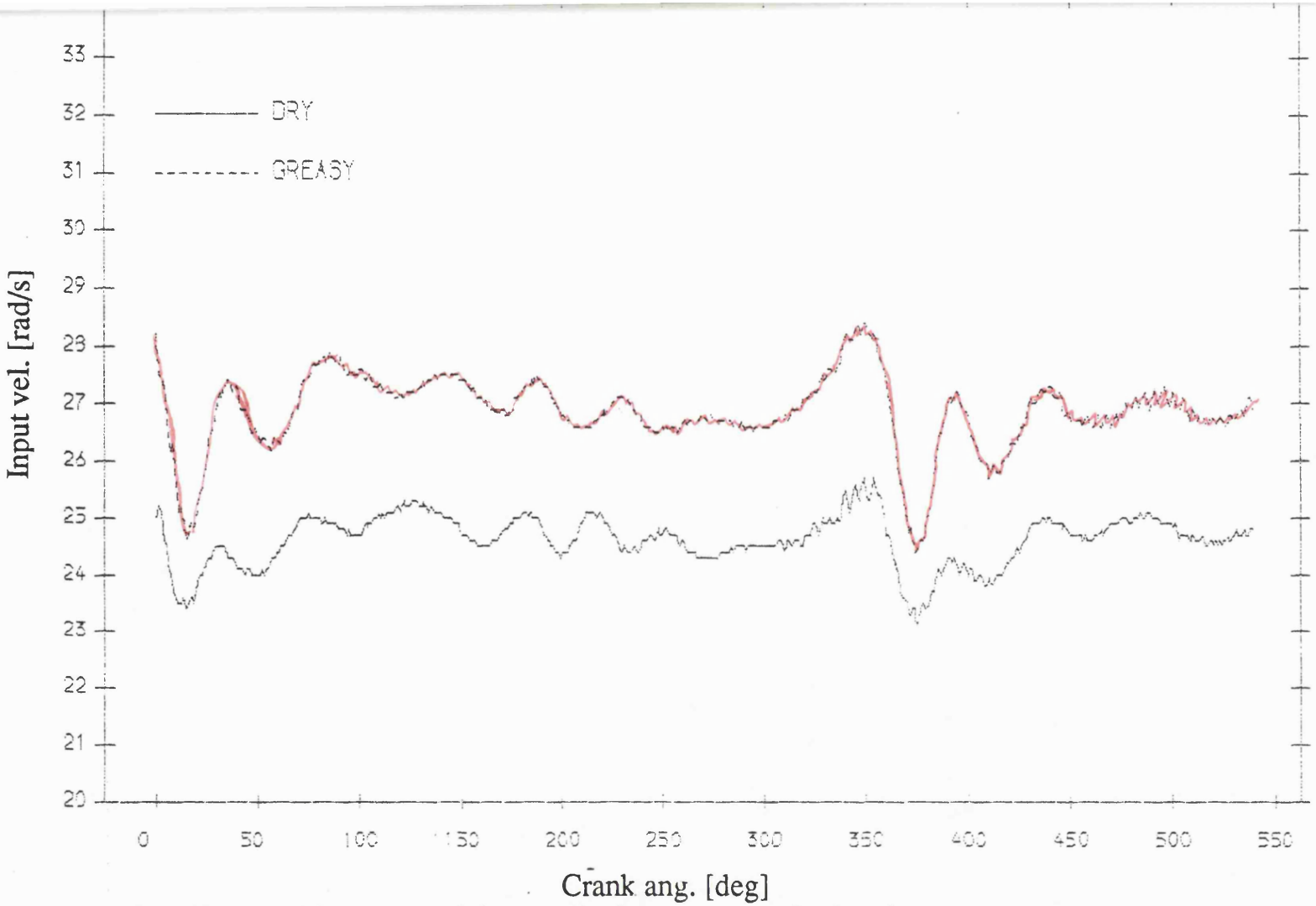

Fig 8.5.122 Exp. result input velocity , greasy v dry bearing
mean speed=244 rev/min; dia. clearance=.15mm

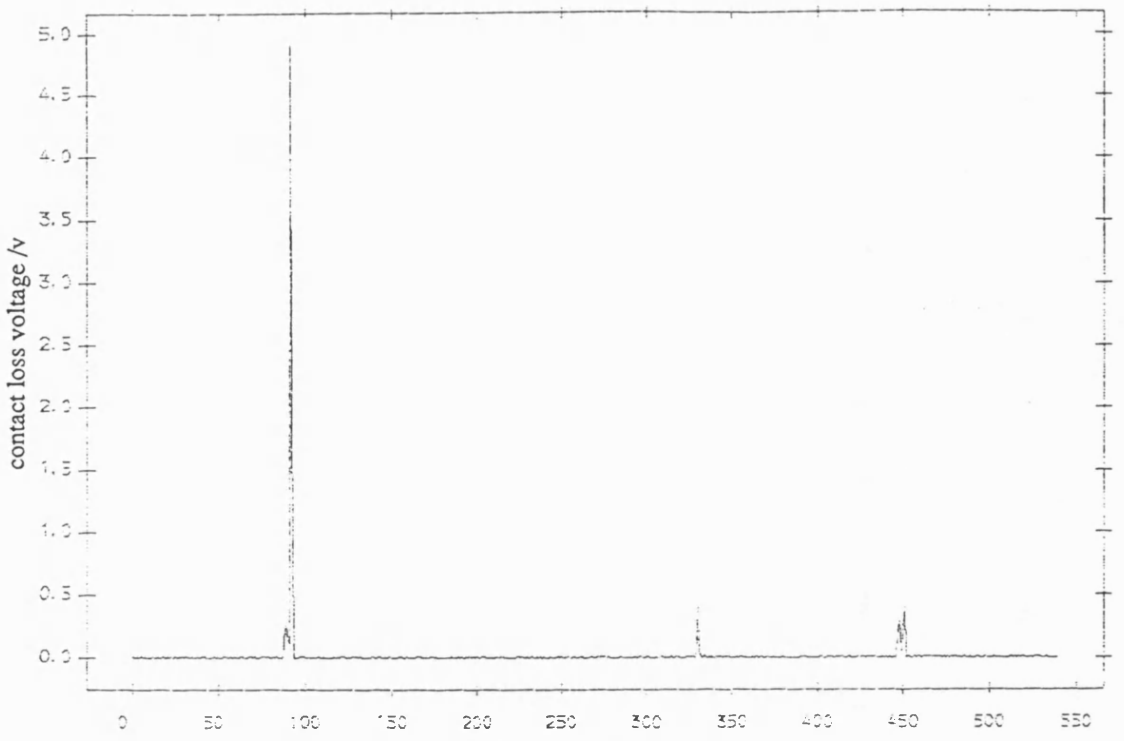

Fig 8.5.123 Exp. result contact loss of pin and ,greasy bearing
with flywheel ;mean speed=244 rev/min ;dia. clearance=0.15mm

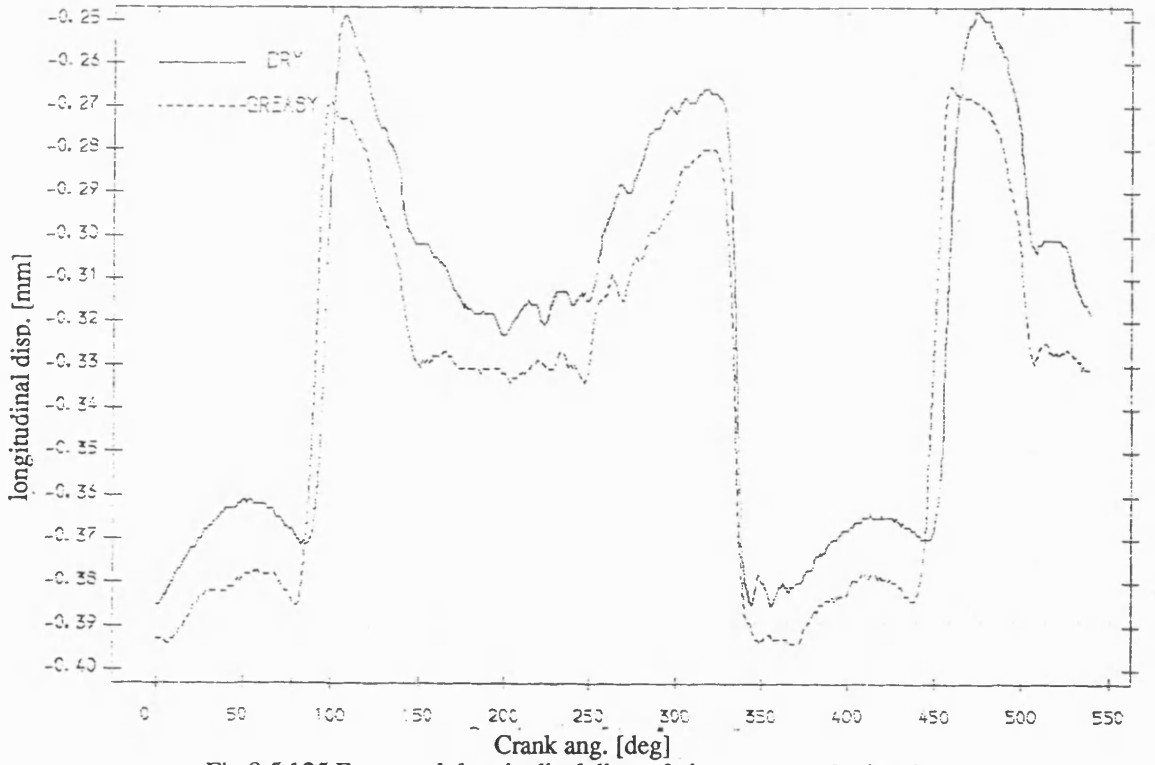

Fig 8.5.125 Exp. result longitudinal disp. of pin , greasy v dry bearing
mean speed=244 rev/min; dia. clearance=.15mm

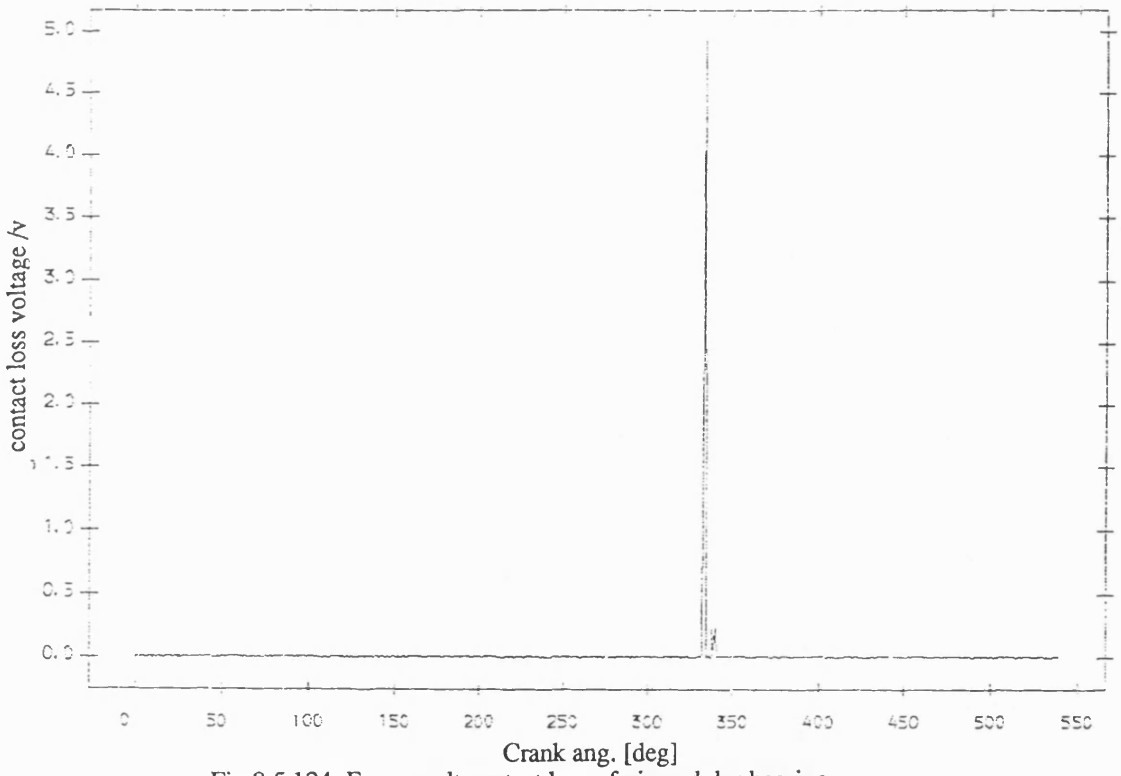

Fig 8.5.124 Exp. result contact loss of pin and dry bearing
with flywheel ;mean speed=244 rev/min ;dia. clearance=0.15mm

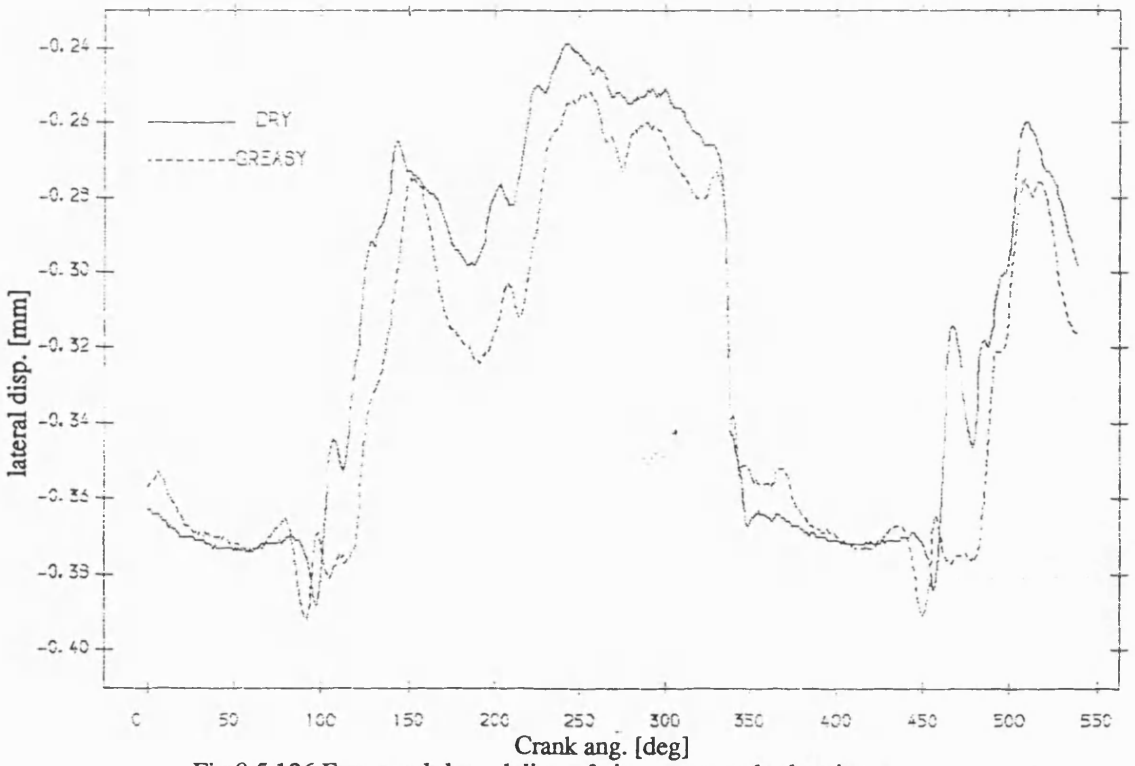

Fig 8.5.126 Exp. result lateral disp. of pin , greasy v dry bearing
mean speed=244 rev/min; dia. clearance=.15mm

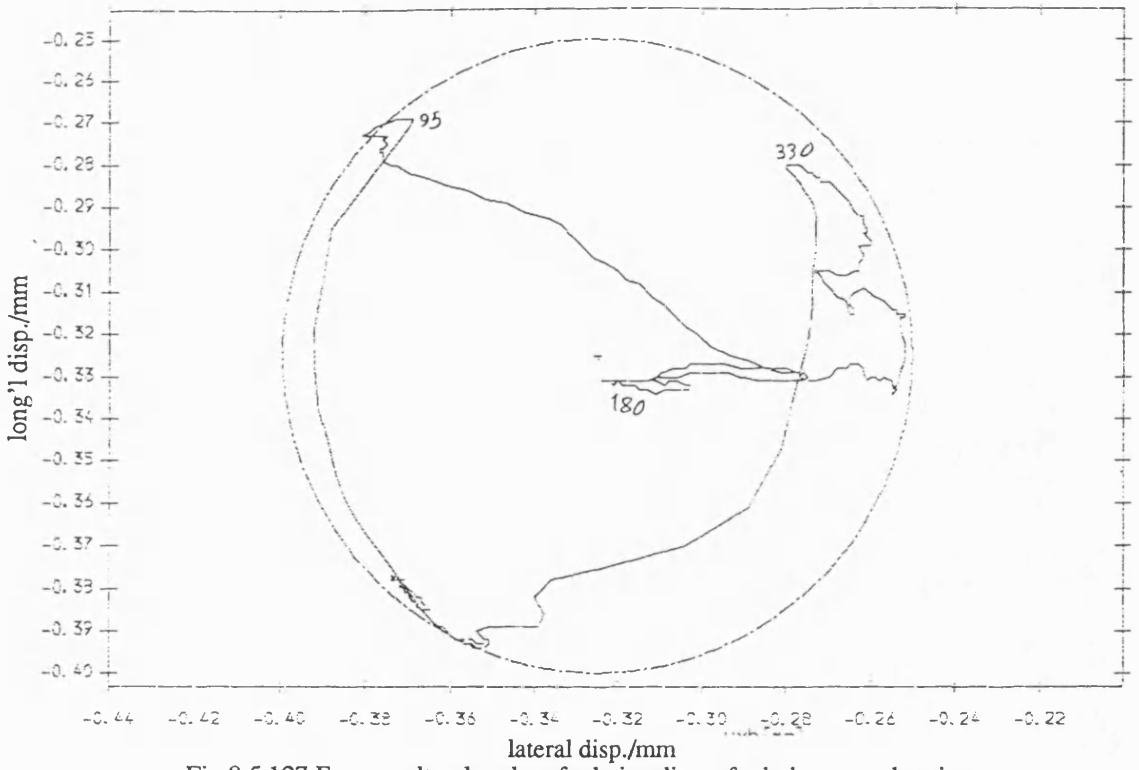

Fig 8.5.127 Exp. result polar plot of relative disp. of pin in greasy bearing with fly wheel ;mean speed=244 rev/min ; dia. clearance=.15mm

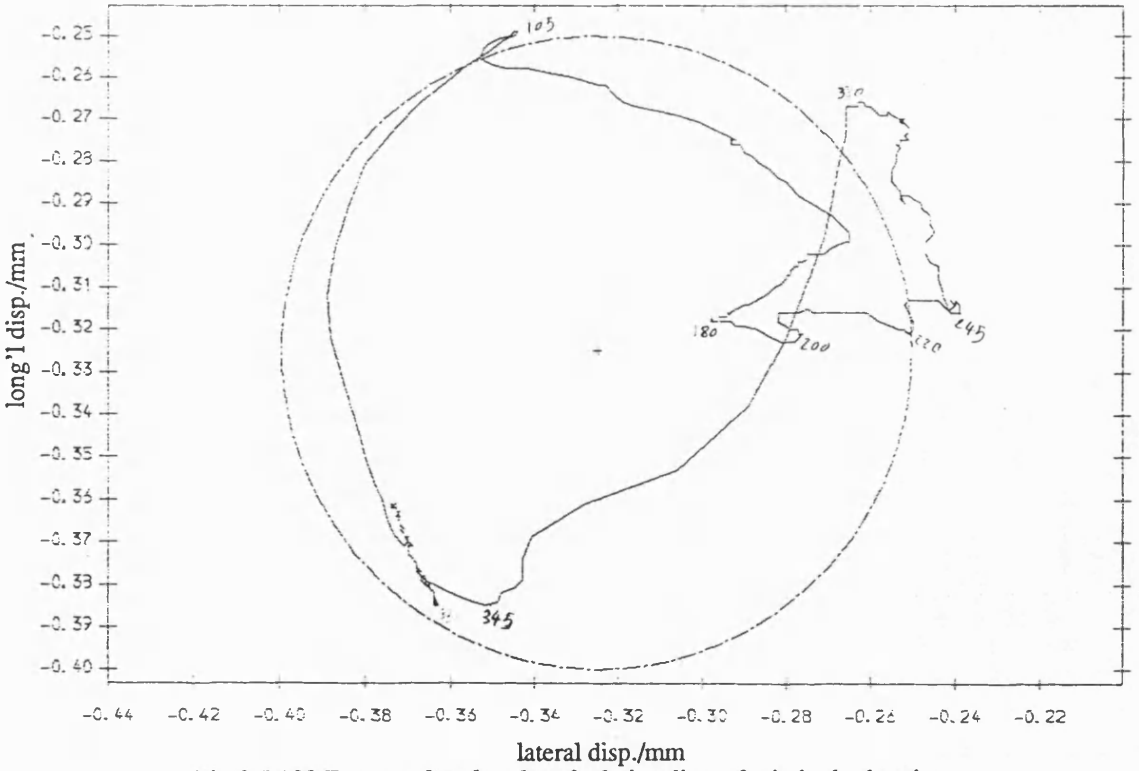

Fig 8.5.128 Exp. result polar plot of relative disp. of pin in dry bearing with fly wheel ;mean speed=244 rev/min ; dia. clearance=.15mm

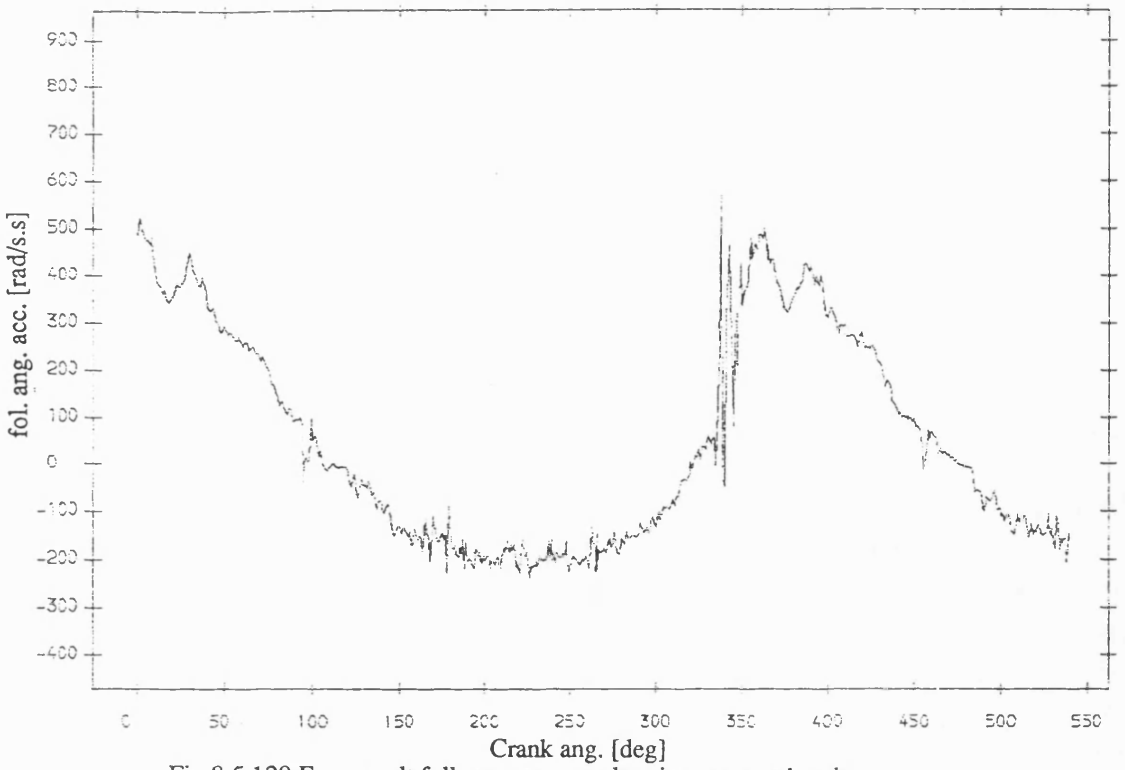

Fig 8.5.129 Exp. result follower ang. acceleration , greasy bearing
with fly wheel ;mean speed=244 rev/min ; dia. clearance=.15mm

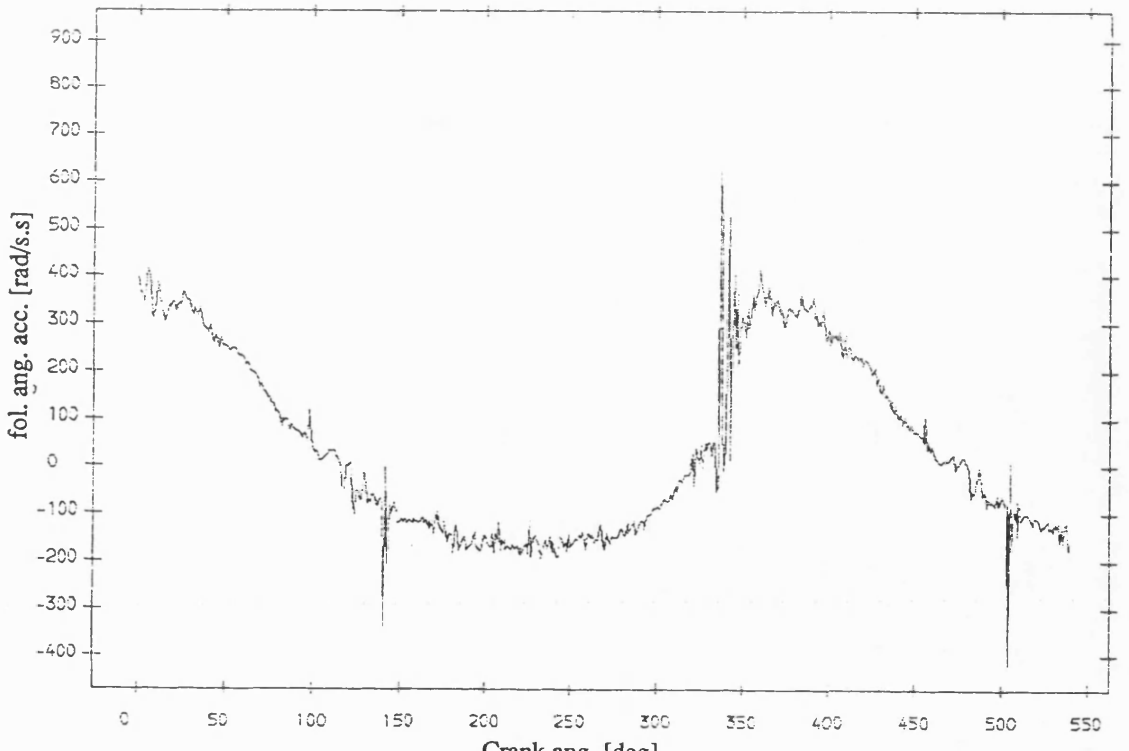

Fig 8.5.130 Exp. result follower ang. acceleration ,dry bearing
with fly wheel ;mean speed=244 rev/min ; dia. clearance=.15mm

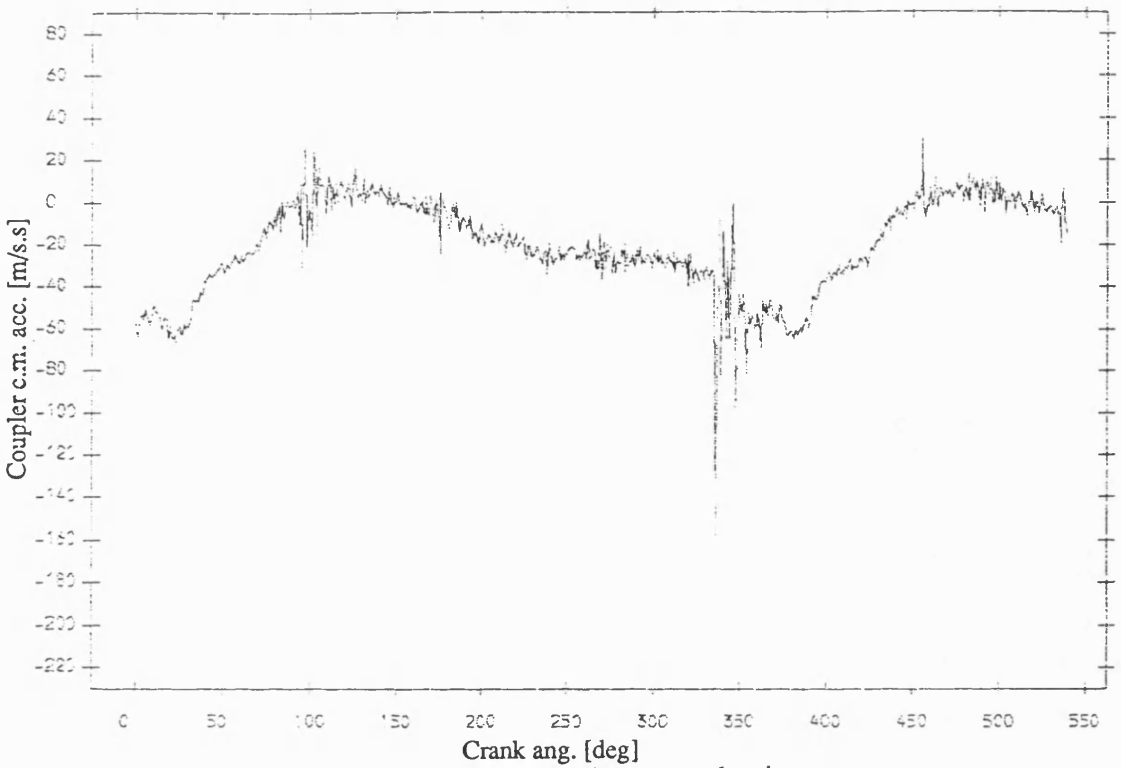

Fig 8.5.131 Exp. result coupler acceleration , greasy bearing
with fly wheel ;mean speed=244 rev/min ; dia. clearance=.15mm

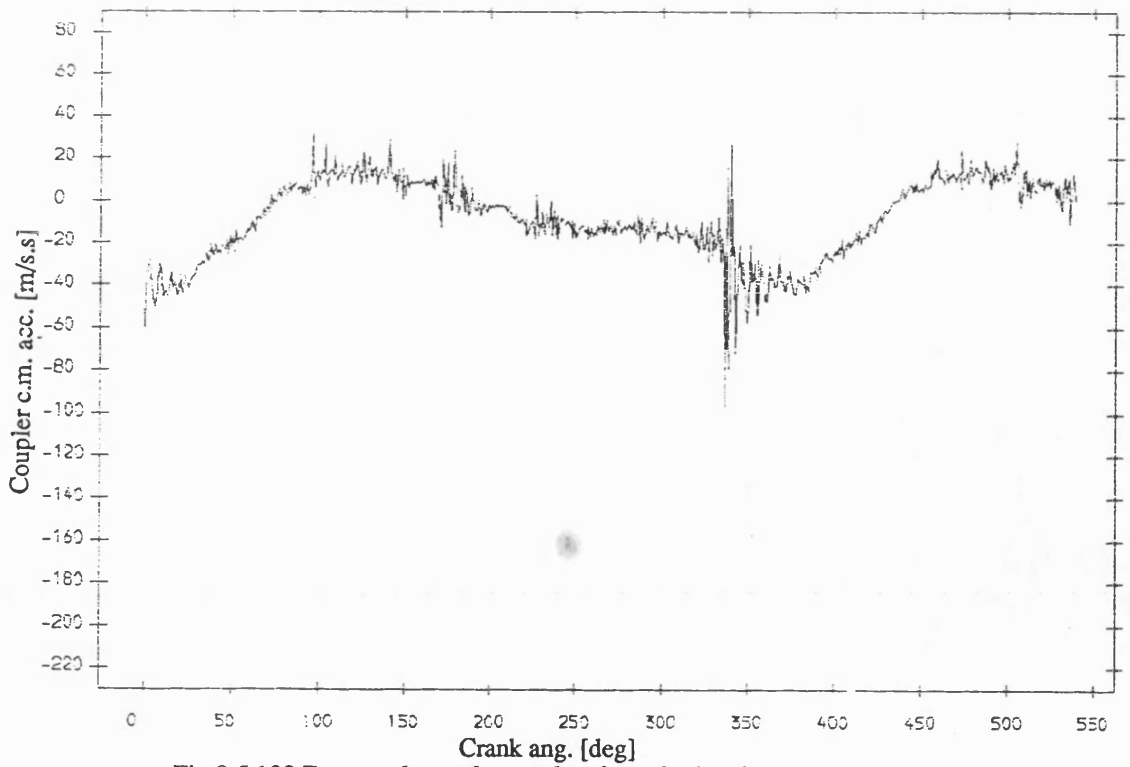

Fig 8.5.132 Exp. result coupler acceleration , dry bearing
with fly wheel ;mean speed=244 rev/min ; dia. clearance=.15mm

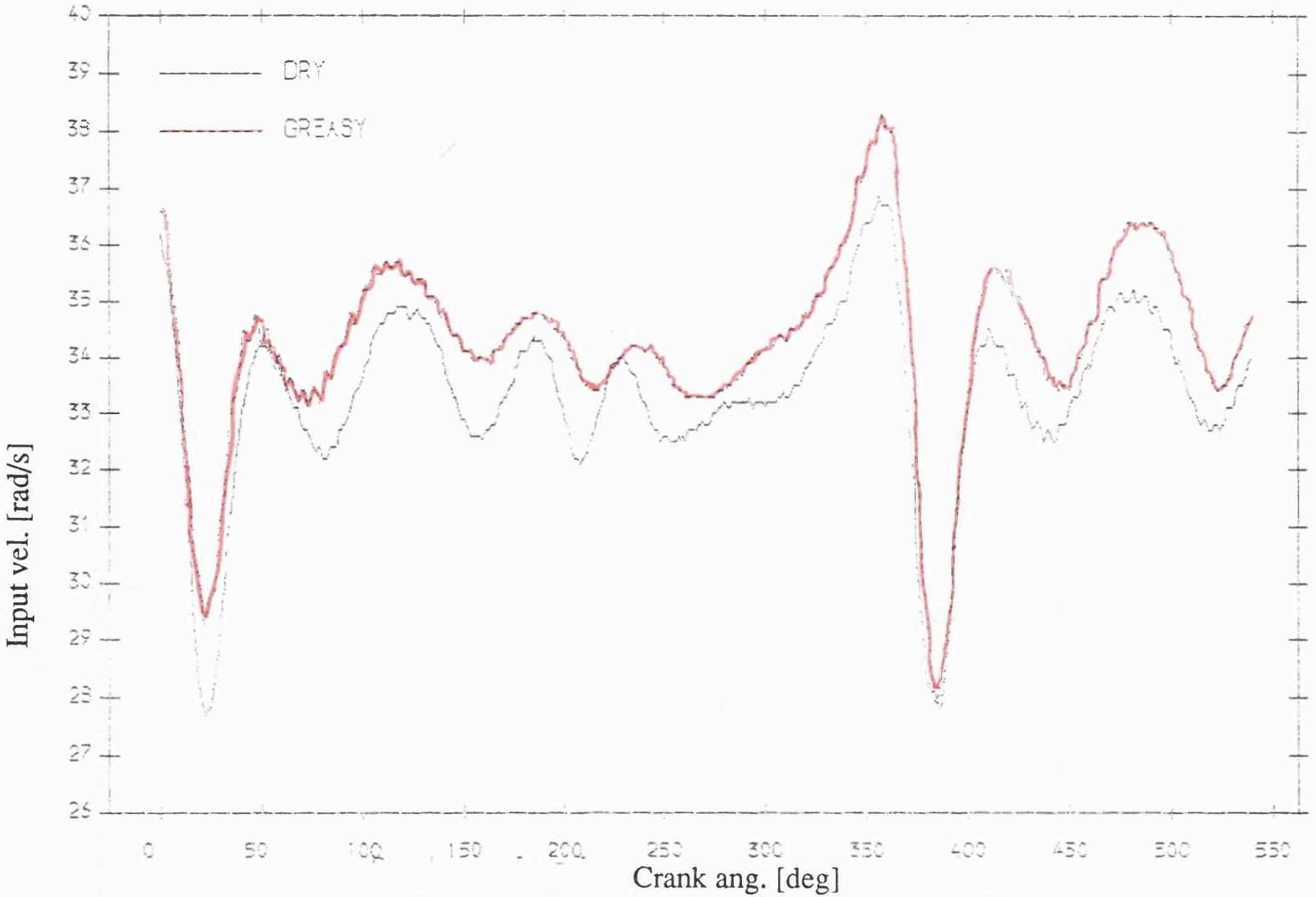

Fig 8.5.133 Exp. result input velocity , greasy v dry bearing
mean speed=327 rev/min; dia. clearance=.15mm

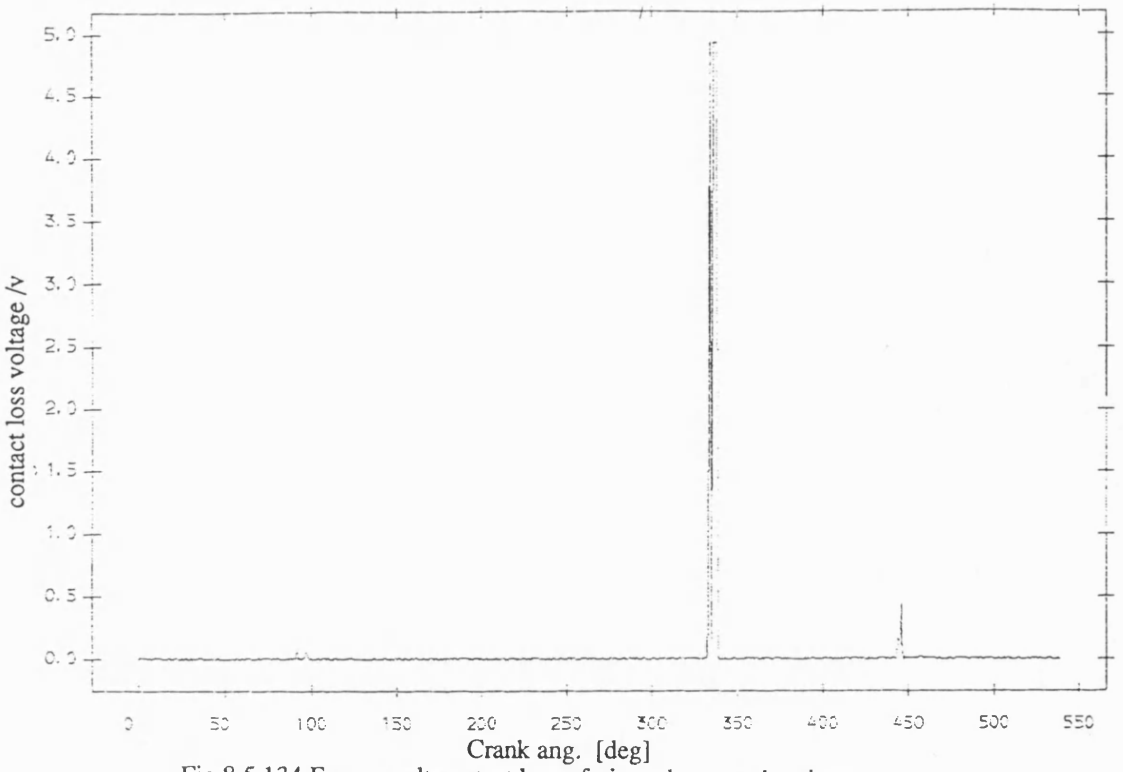

Fig 8.5.134 Exp. result contact loss of pin and ,greasy bearing
with flywheel ;mean speed=327 rev/min ;dia. clearance=0.15mm

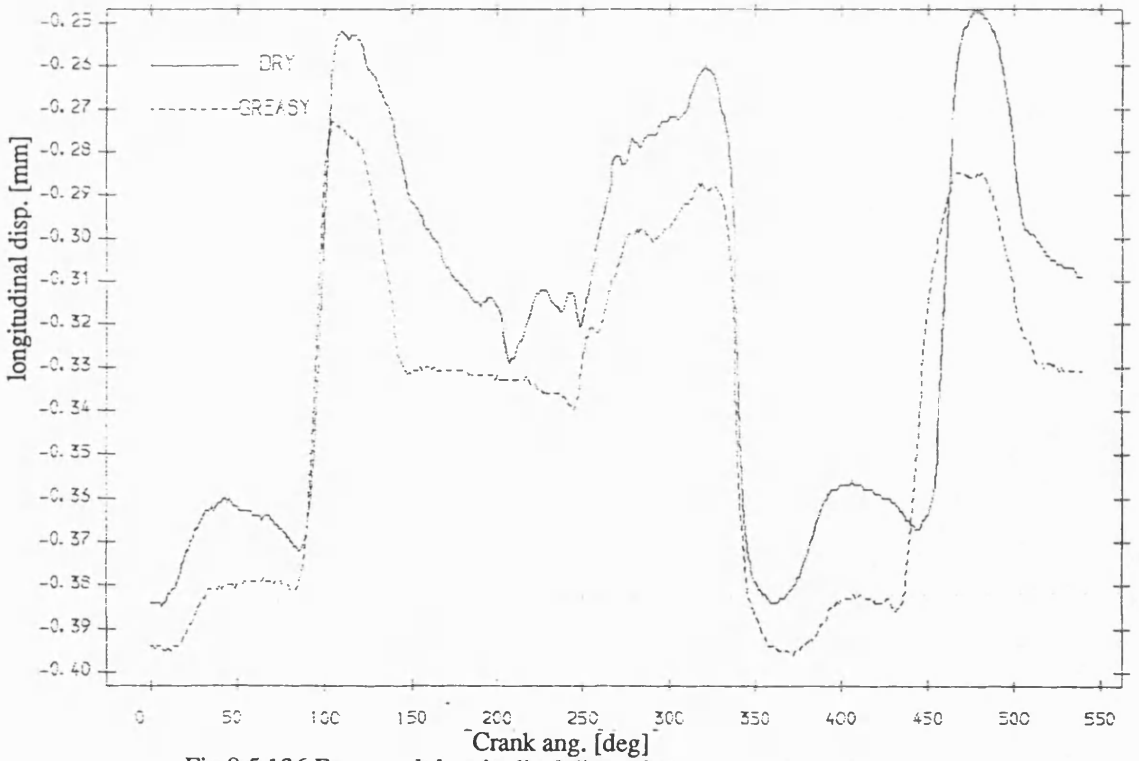

Fig 8.5.136 Exp. result longitudinal disp. of pin , greasy v dry bearing
mean speed=327 rev/min; dia. clearance=.15mm

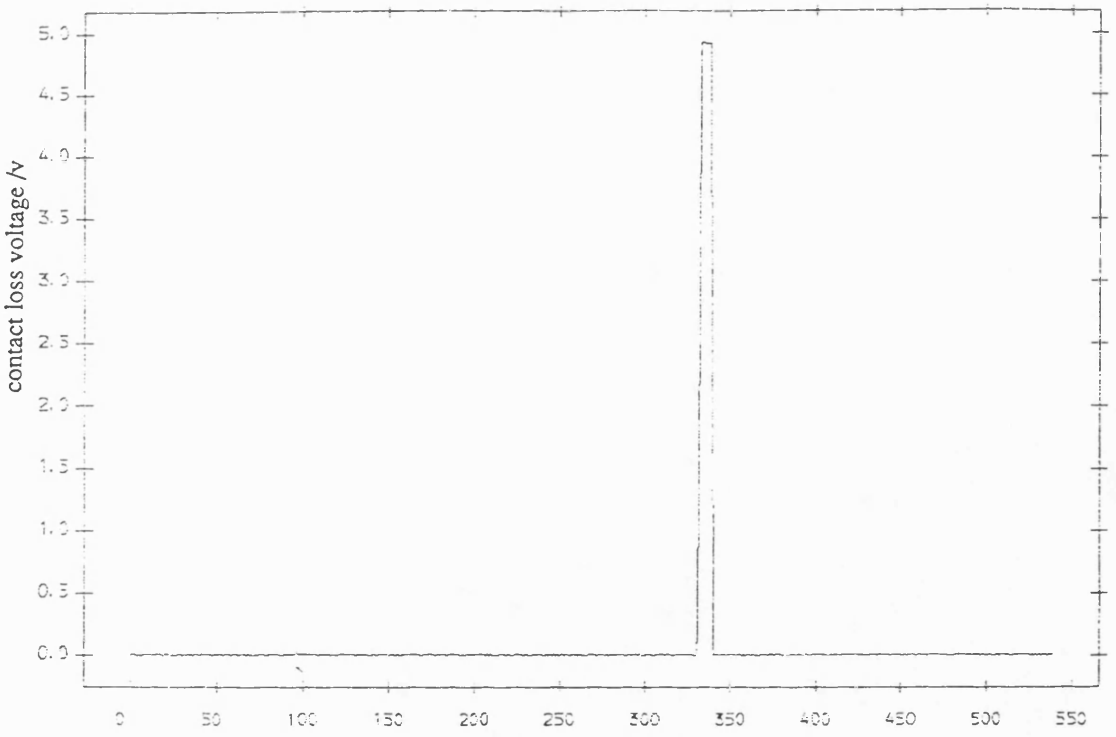

Fig 8.5.135 Exp. result contact loss of pin and dry bearing
with flywheel ;mean speed=327 rev/min ;dia. clearance=0.15mm

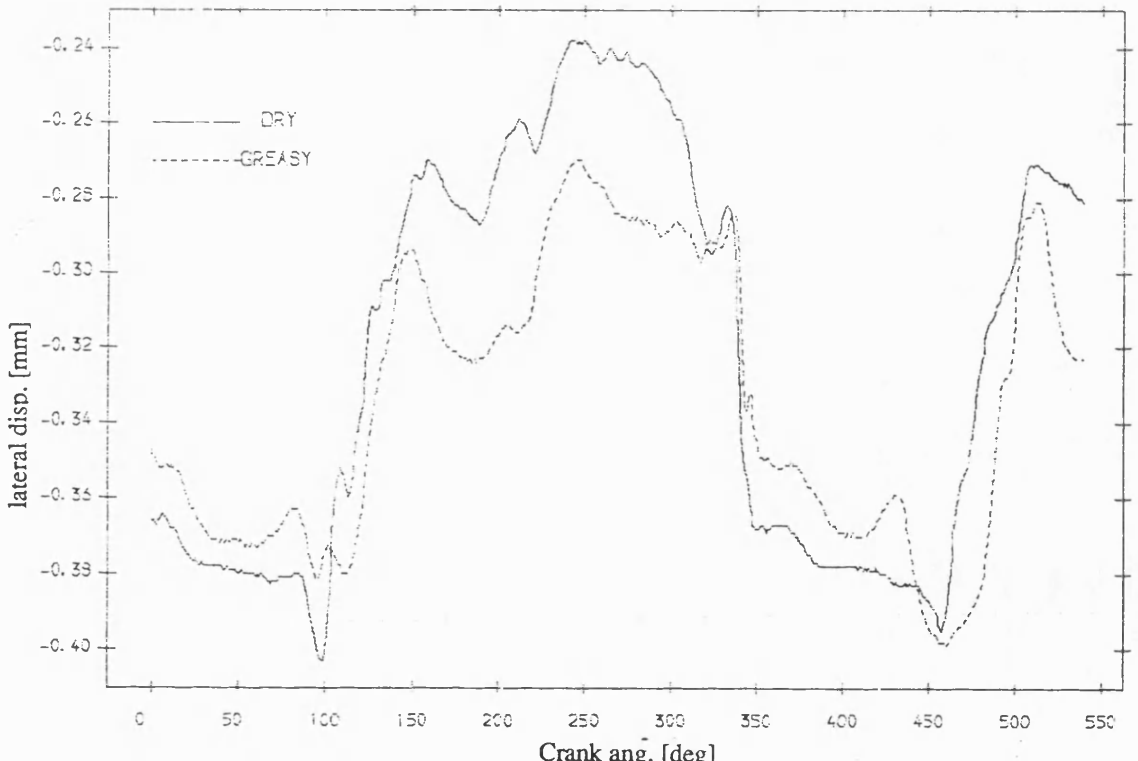

Fig 8.5.137 Exp. result lateral disp. of pin , greasy v dry bearing
mean speed=327 rev/min; dia. clearance=.15mm

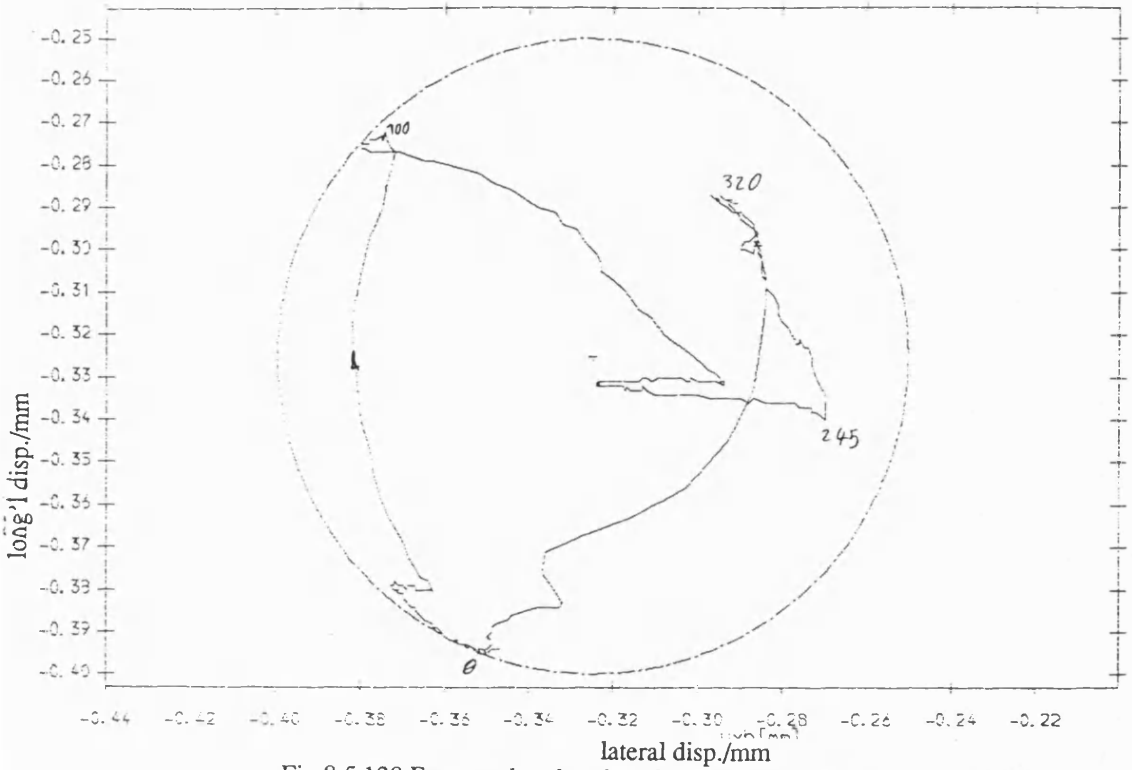

Fig 8.5.138 Exp. result polar plot of relative disp. of pin in greasy bearing with fly wheel ;mean speed=327 rev/min ; dia. clearance=.15mm

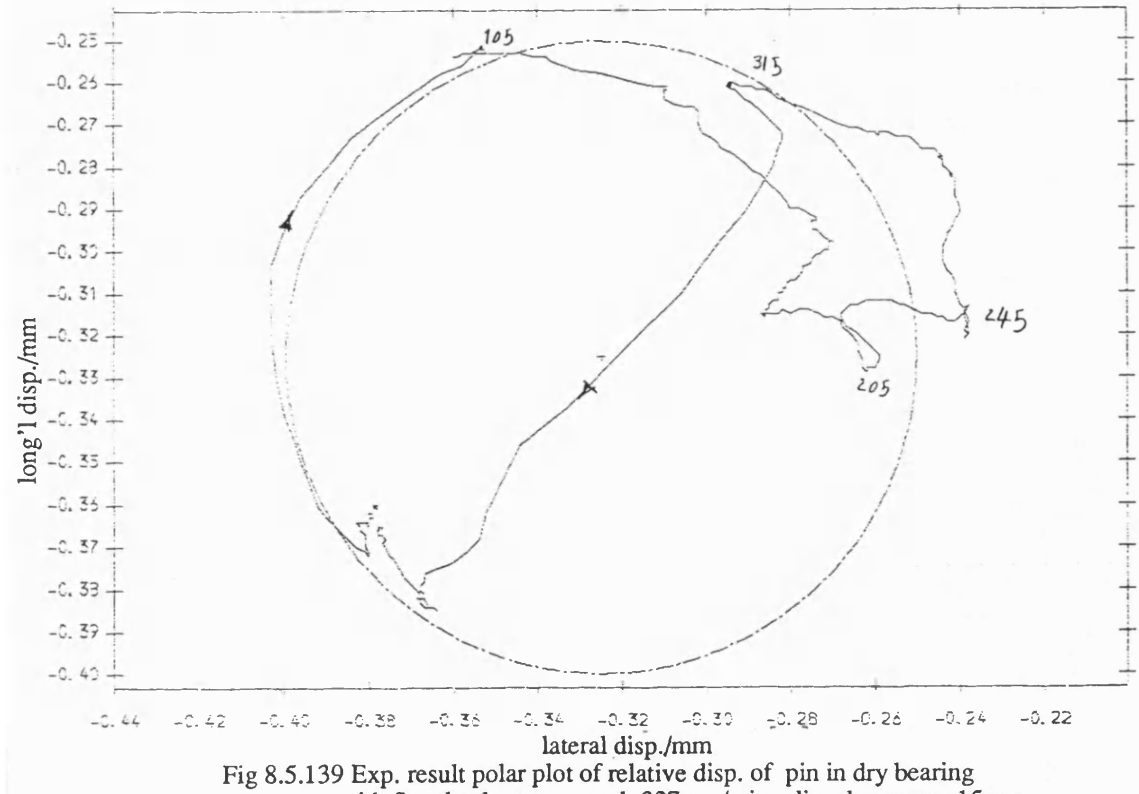

Fig 8.5.139 Exp. result polar plot of relative disp. of pin in dry bearing with fly wheel ;mean speed=327 rev/min ; dia. clearance=.15mm

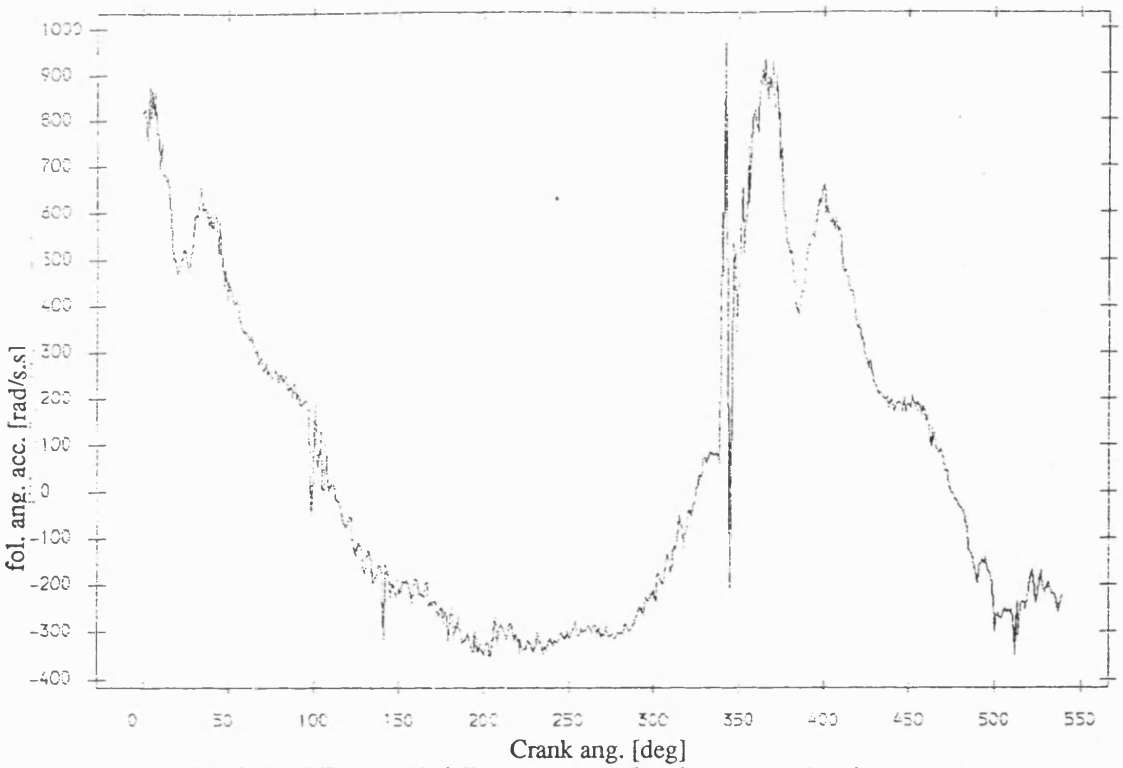

Fig 8.5.140 Exp. result follower ang. acceleration , greasy bearing
with fly wheel ;mean speed=327 rev/min ; dia. clearance=.15mm

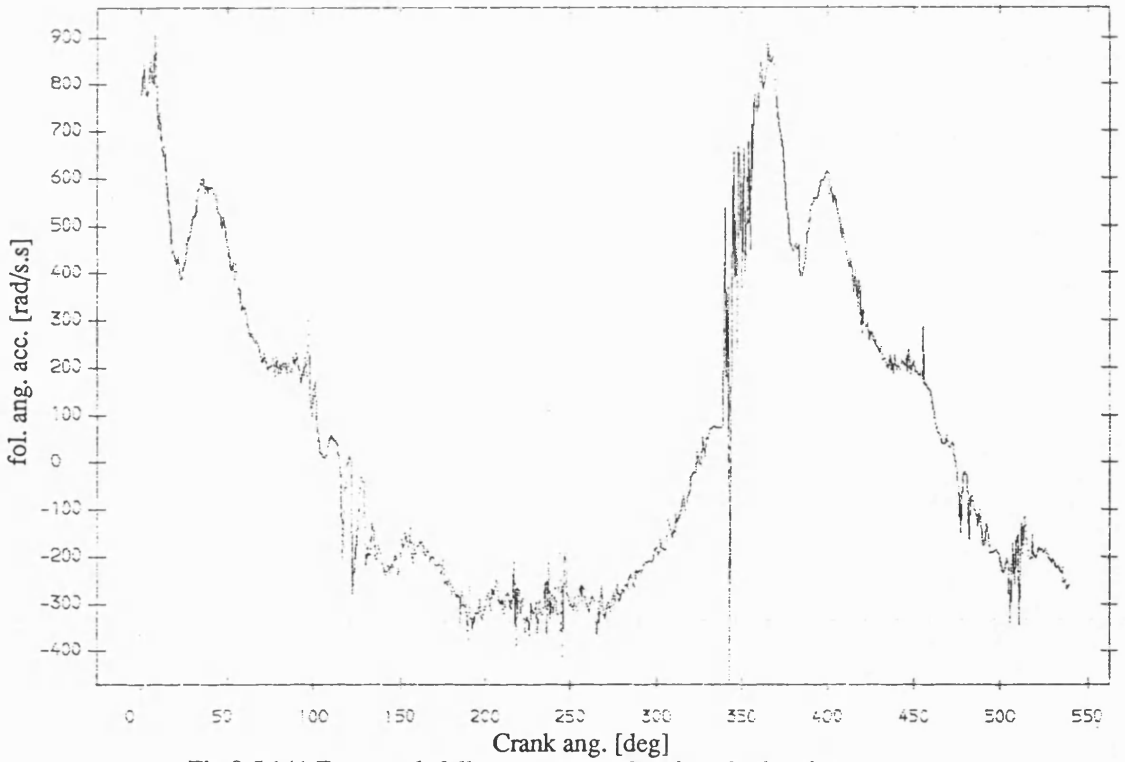

Fig 8.5.141 Exp. result follower ang. acceleration ,dry bearing
with fly wheel ;mean speed=327 rev/min ; dia. clearance=.15mm

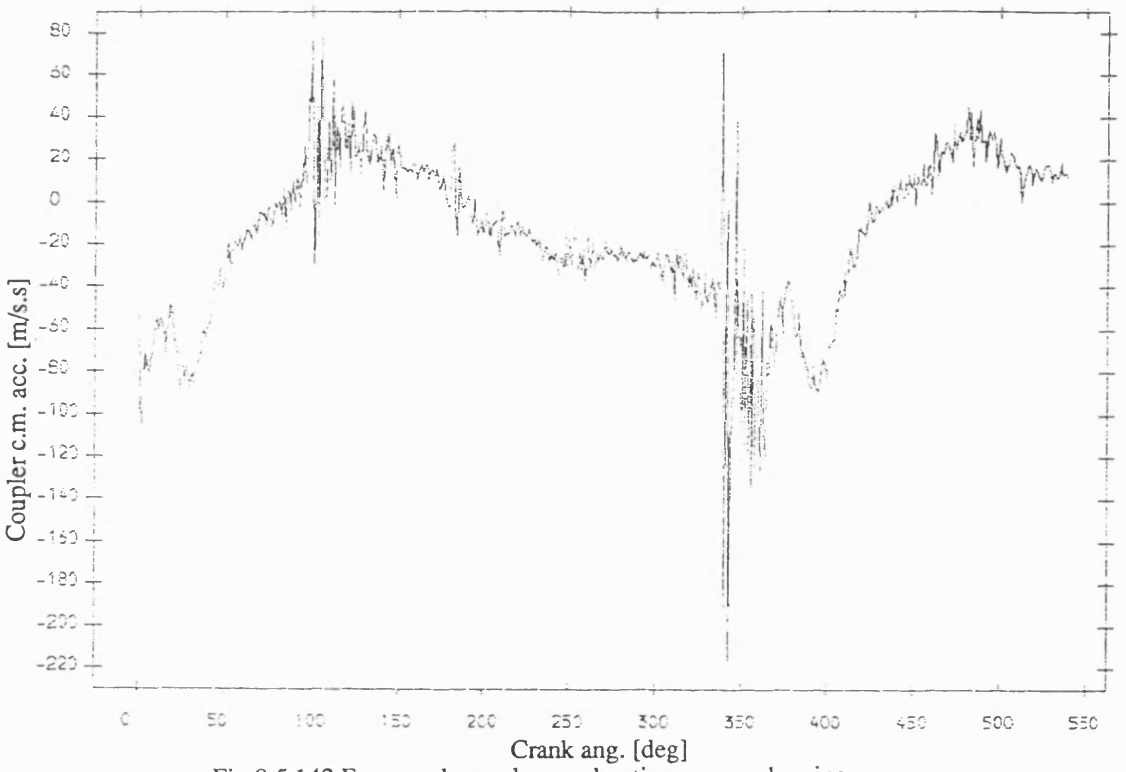

Fig 8.5.142 Exp. result coupler acceleration , greasy bearing
with fly wheel ;mean speed=327 rev/min ; dia. clearance=.15mm

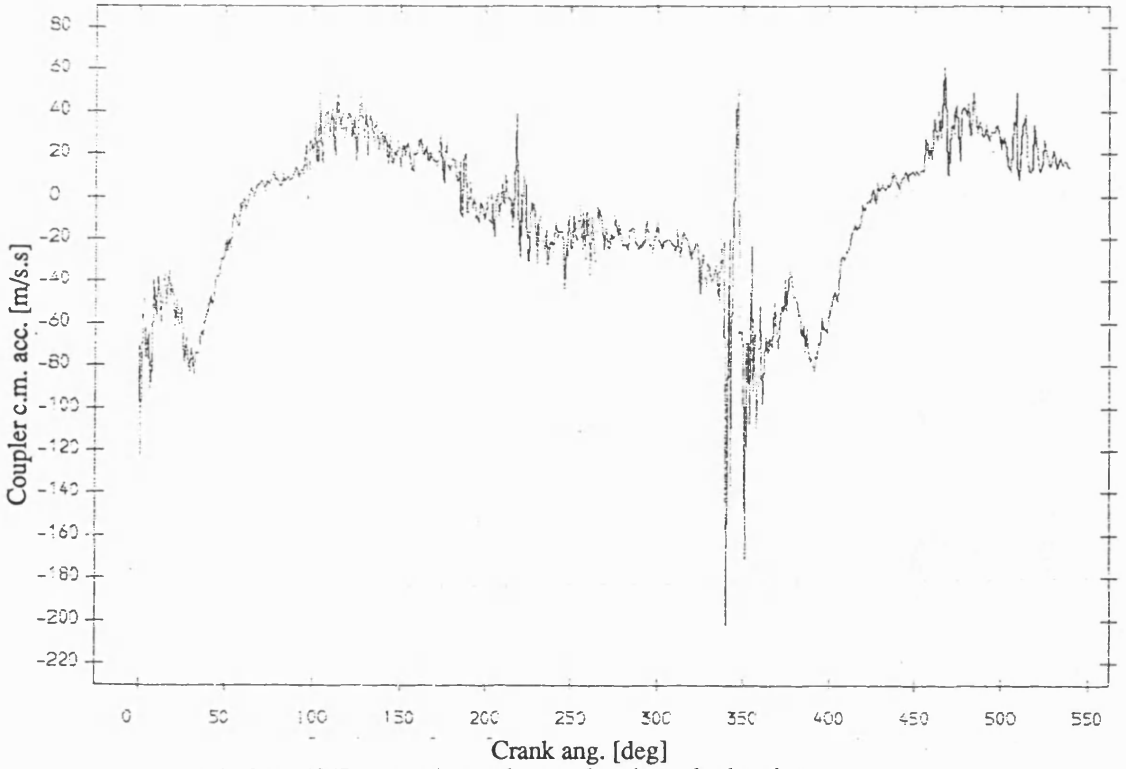

Fig 8.5.143 Exp. result coupler acceleration , dry bearing
with fly wheel ;mean speed=327 rev/min ; dia. clearance=.15mm

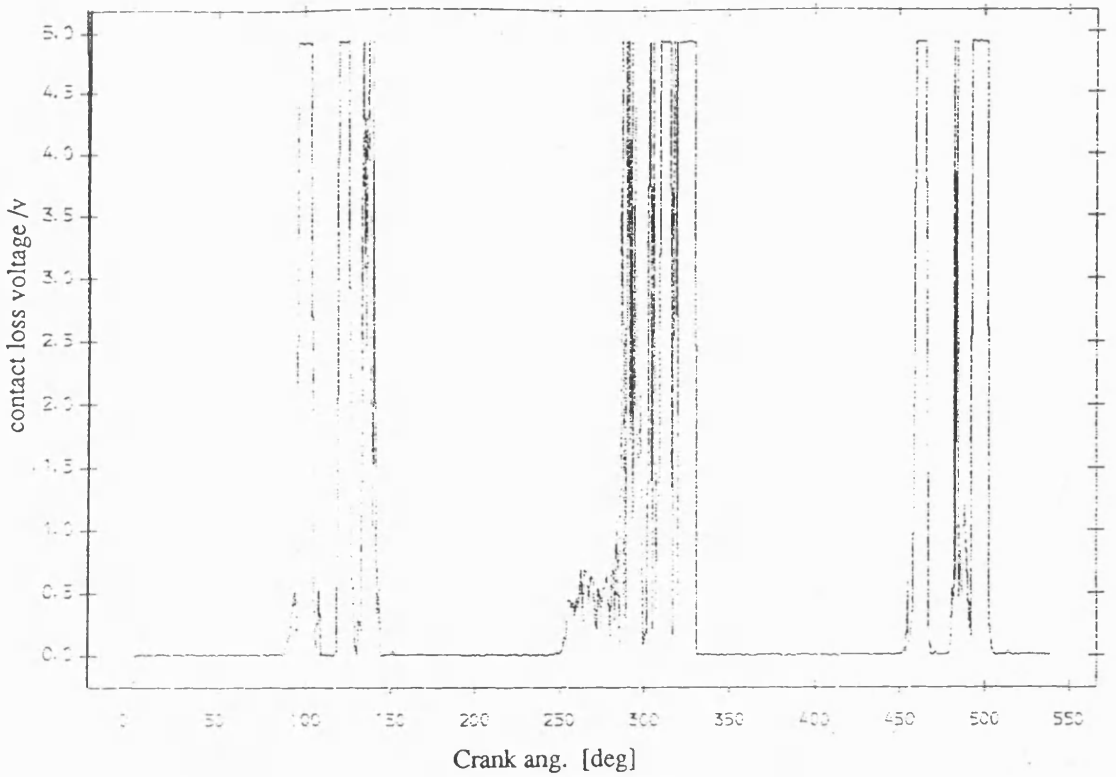

Fig 8.6.1 Exp. result contact loss , left hand pin isolated
with flywheel ;mean speed=168 rev/min ;dia. clearance=0.25mm

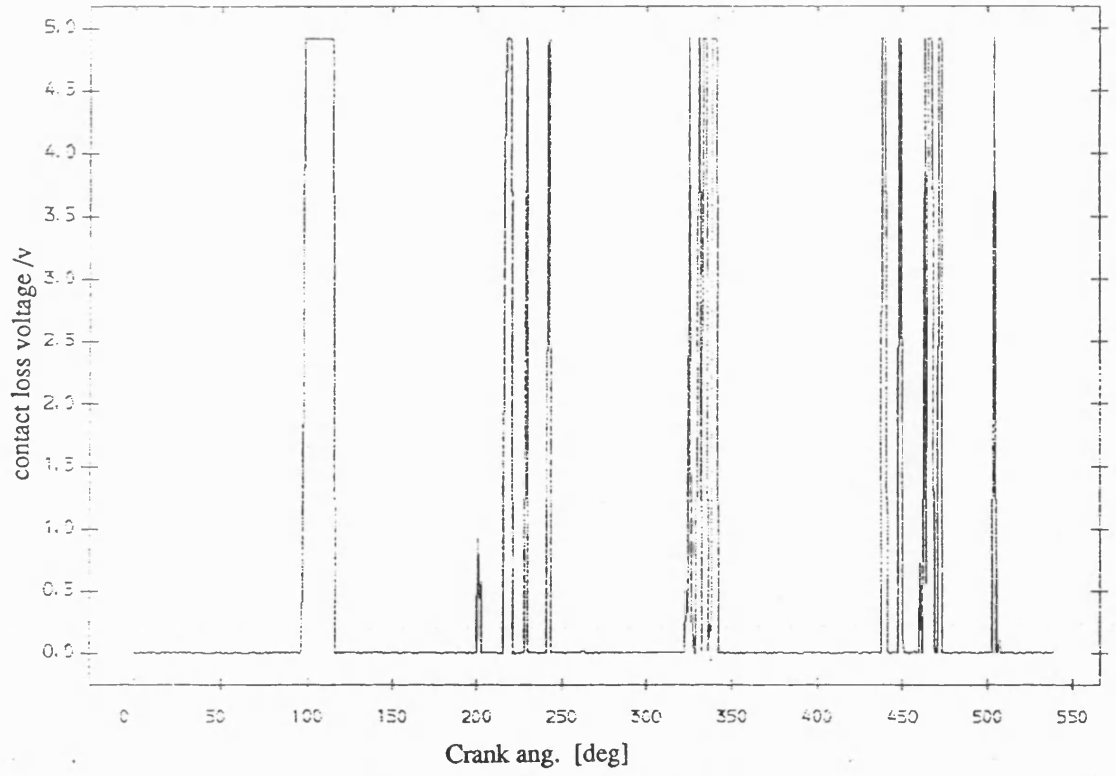

Fig 8.6.2 Exp. result contact loss , right hand pin isolated
with flywheel ;mean speed=168 rev/min ;dia. clearance=0.25mm

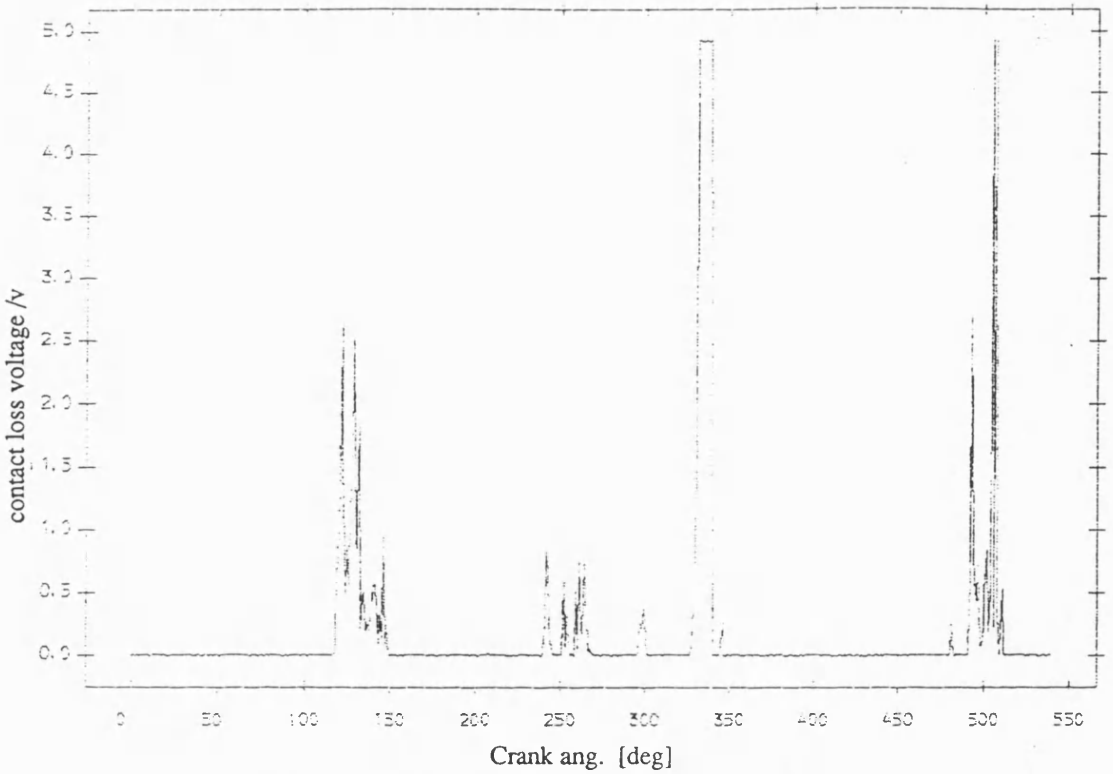

Fig 8.6.3 Exp. result contact loss › left hand pin isolated
with flywheel ;mean speed=244 rev/min ;dia. clearance=0.25mm

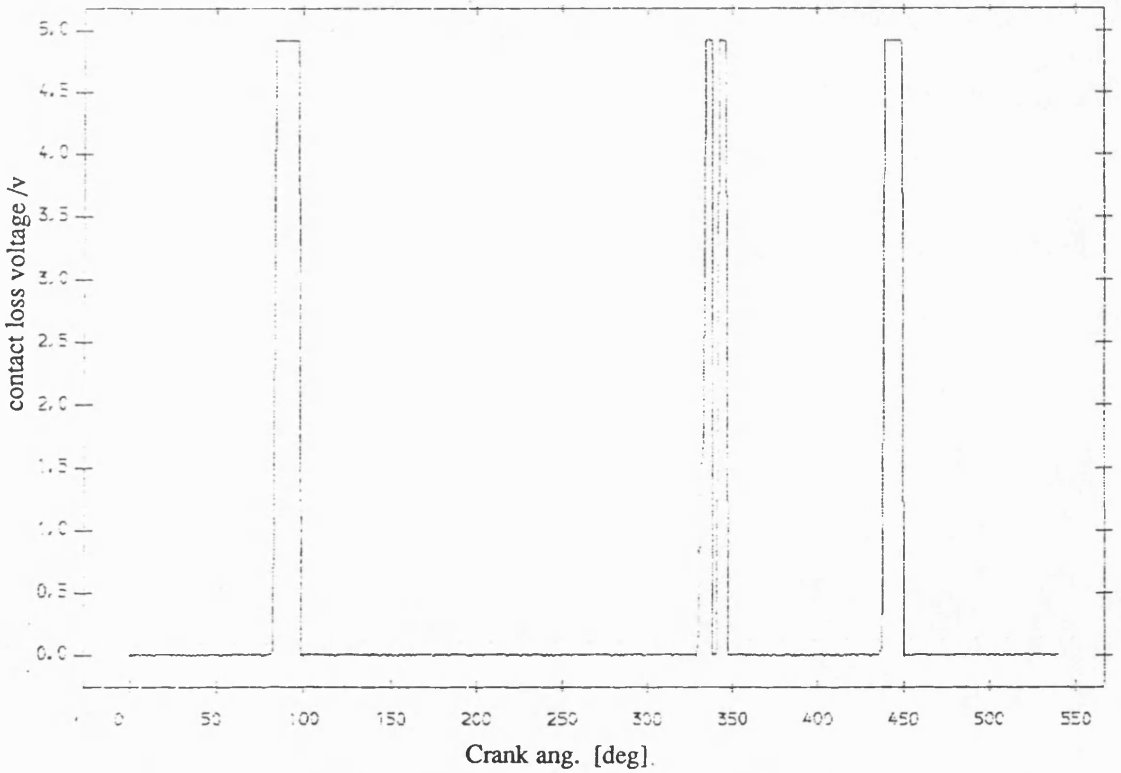

Fig 8.6.4 Exp. result contact loss ‹ right hand pin isolated
with flywheel ;mean speed=244 rev/min ;dia. clearance=0.25mm

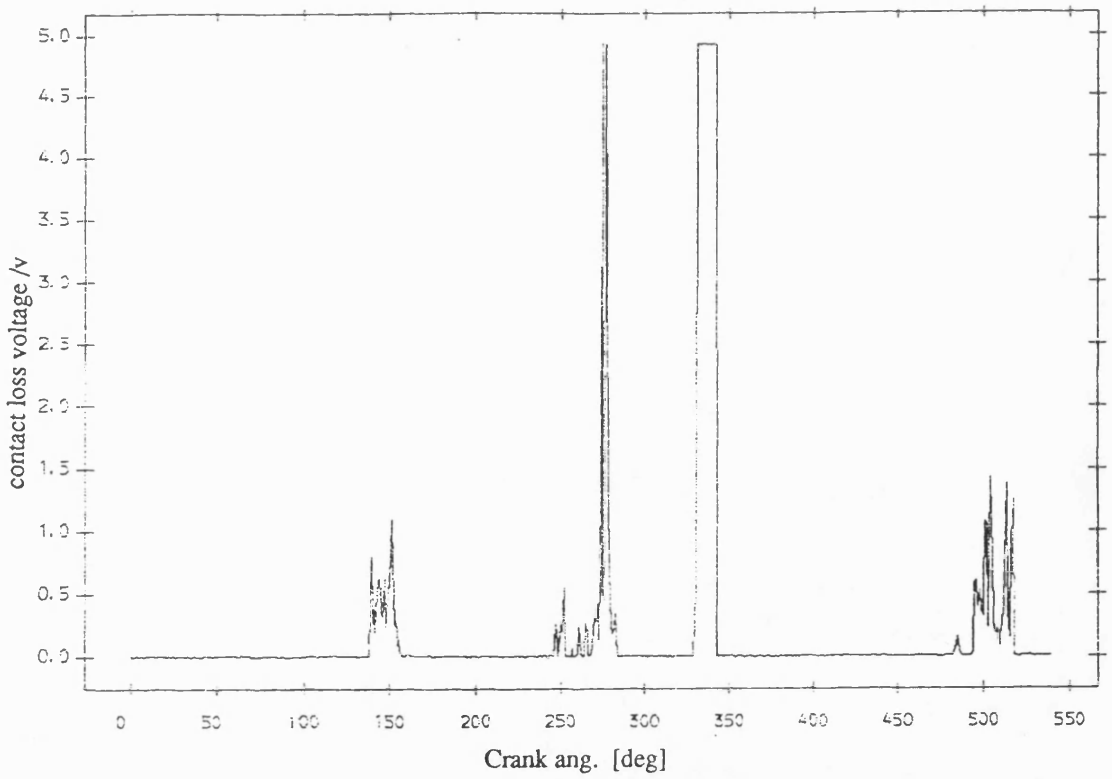

Fig 8.6.5 Exp. result contact loss , left hand pin isolated
with flywheel ;mean speed=327 rev/min ;dia. clearance=0.25mm

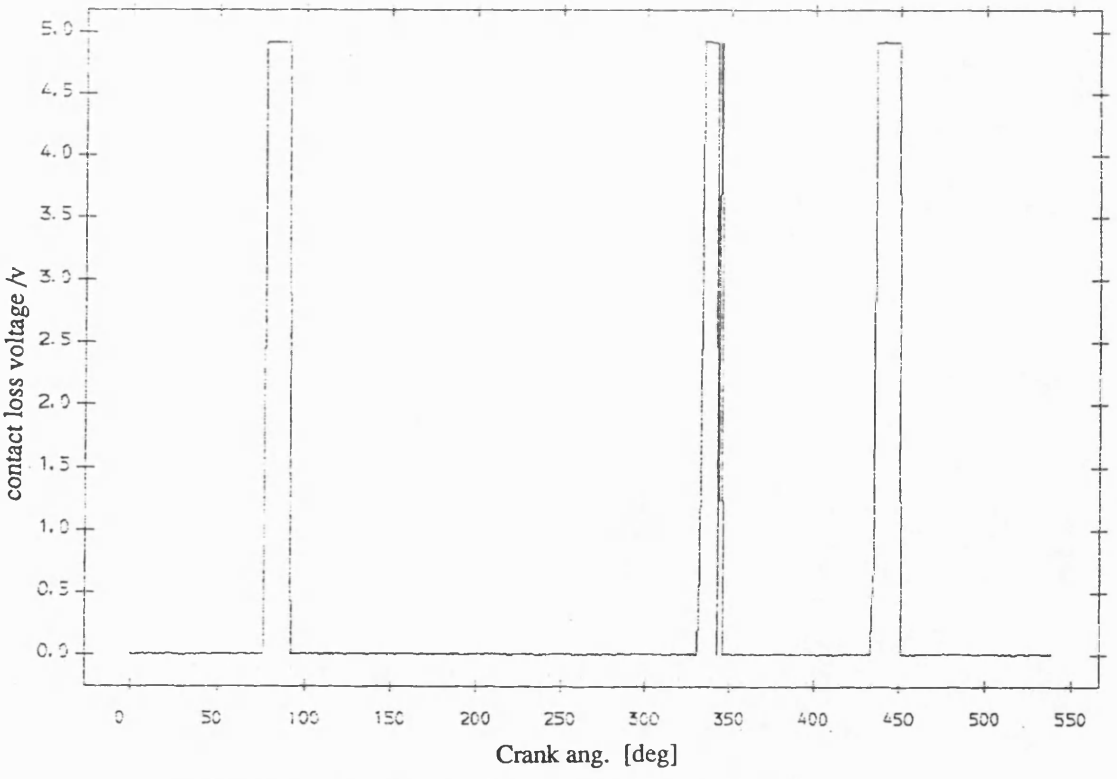

Fig 8.6.6 Exp. result contact loss , right hand pin isolated
with flywheel ;mean speed=327 rev/min ;dia. clearance=0.25mm

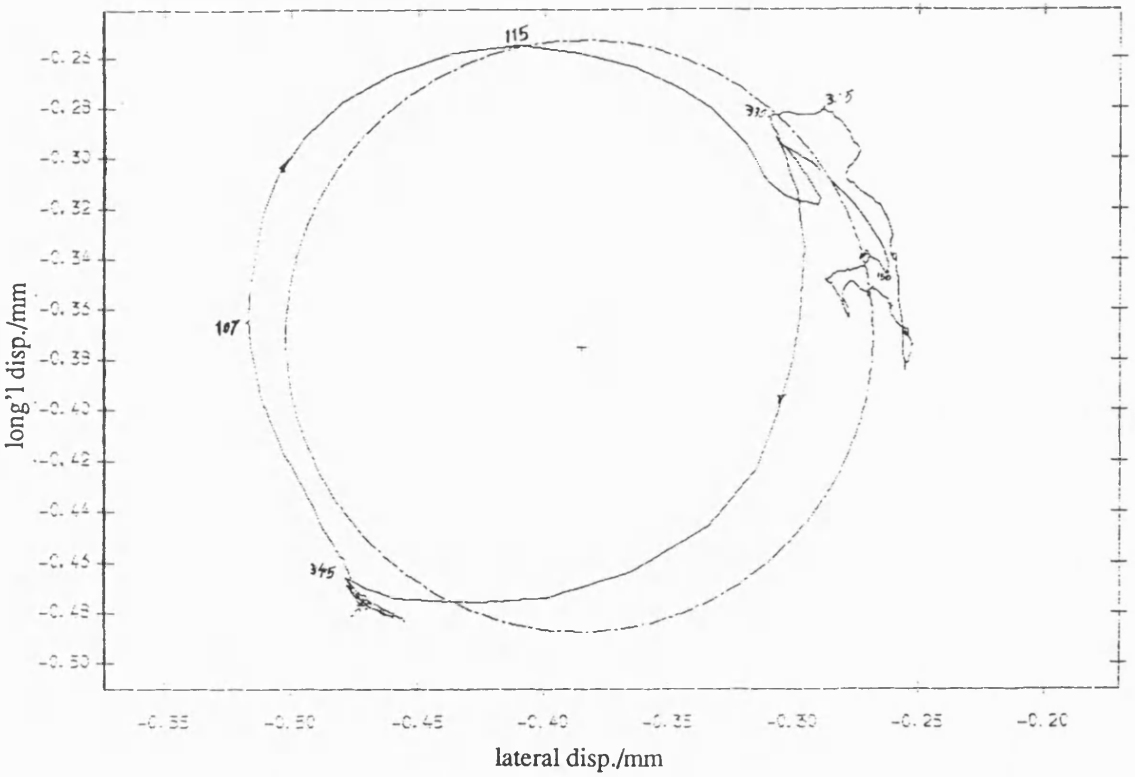

Fig 8.6.7 Exp. result polar plot of relative disp. , left hand pin isolated with fly wheel ;mean speed=168 rev/min ; dia. clearance=.25mm

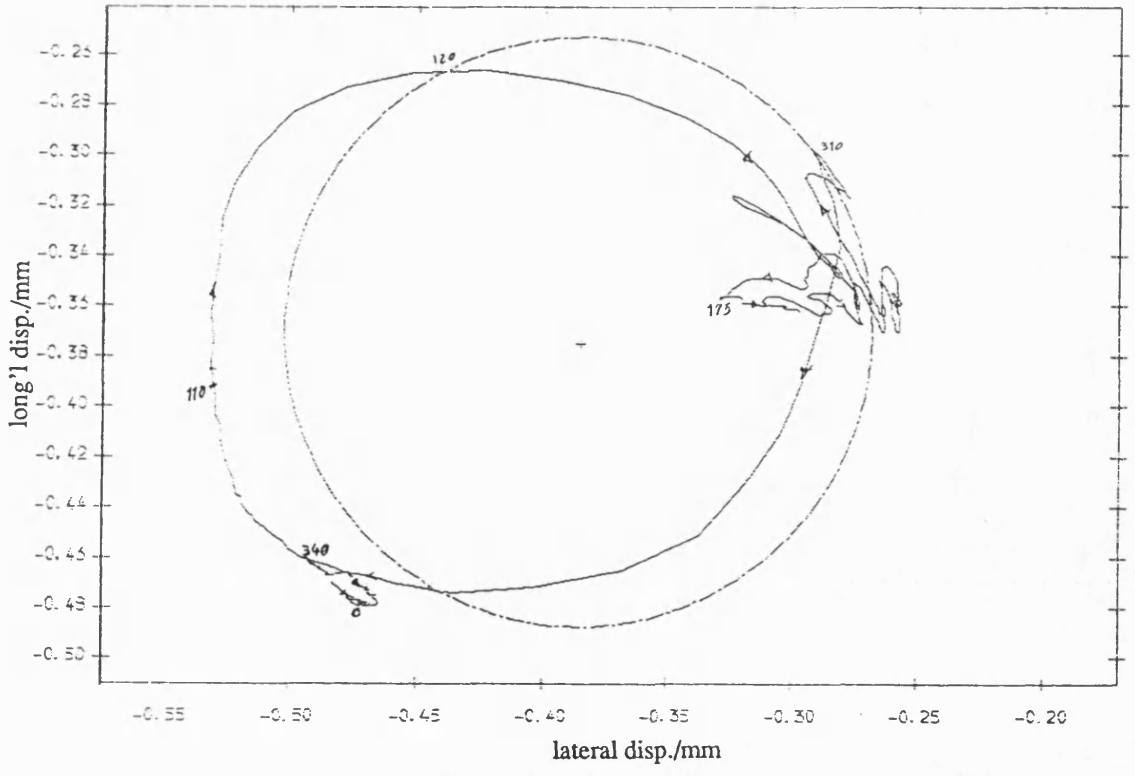

Fig 8.6.8 Exp. result polar plot of relative disp. , right hand pin isolated with fly wheel ;mean speed=168 rev/min ; dia. clearance=.25mm

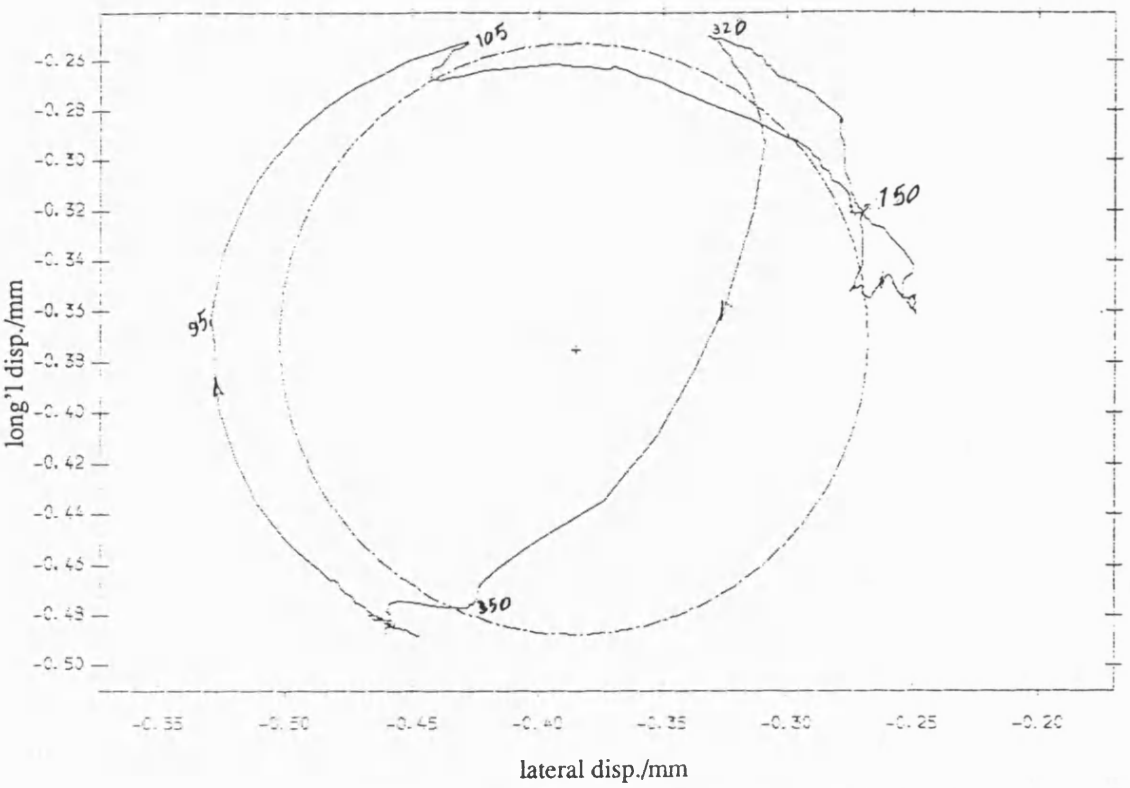

Fig 8.6.9 Exp. result polar plot of relative disp. › left hand pin isolated with fly wheel :mean speed=244 rev/min ; dia. clearance=.25mm

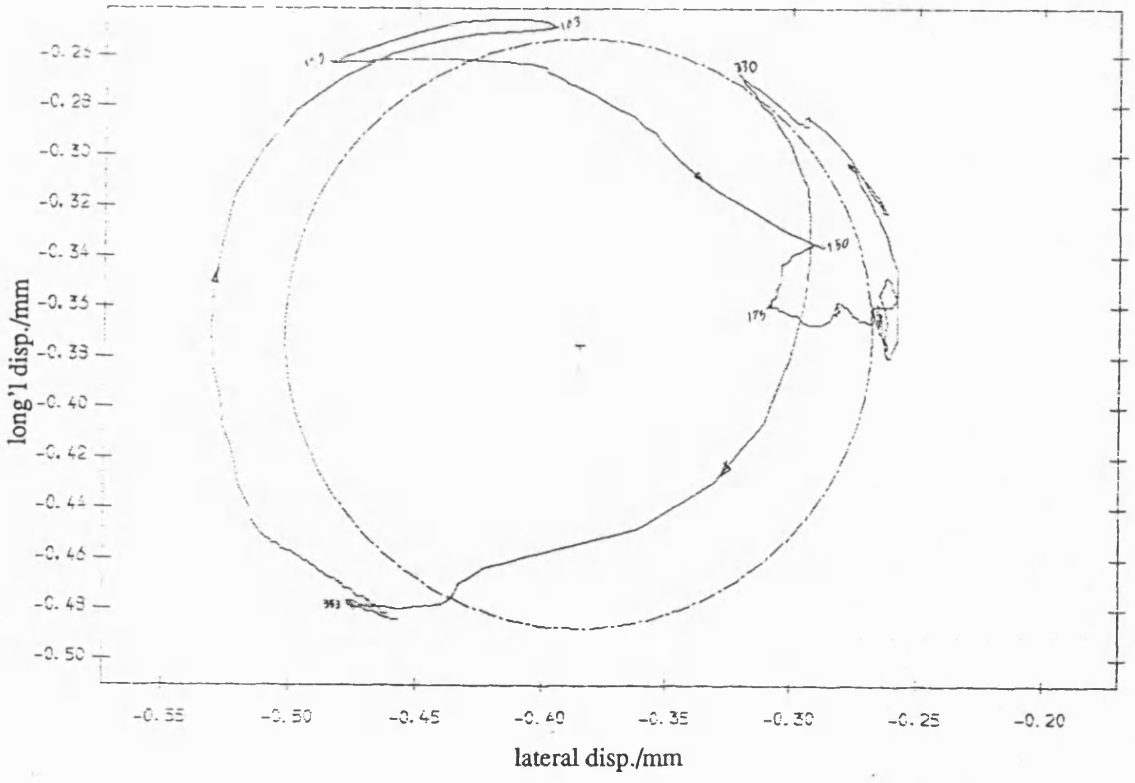

Fig 8.6.10 Exp. result polar plot of relative disp. › right hand pin isolated with fly wheel ;mean speed=244 rev/min ; dia. clearance=.25mm

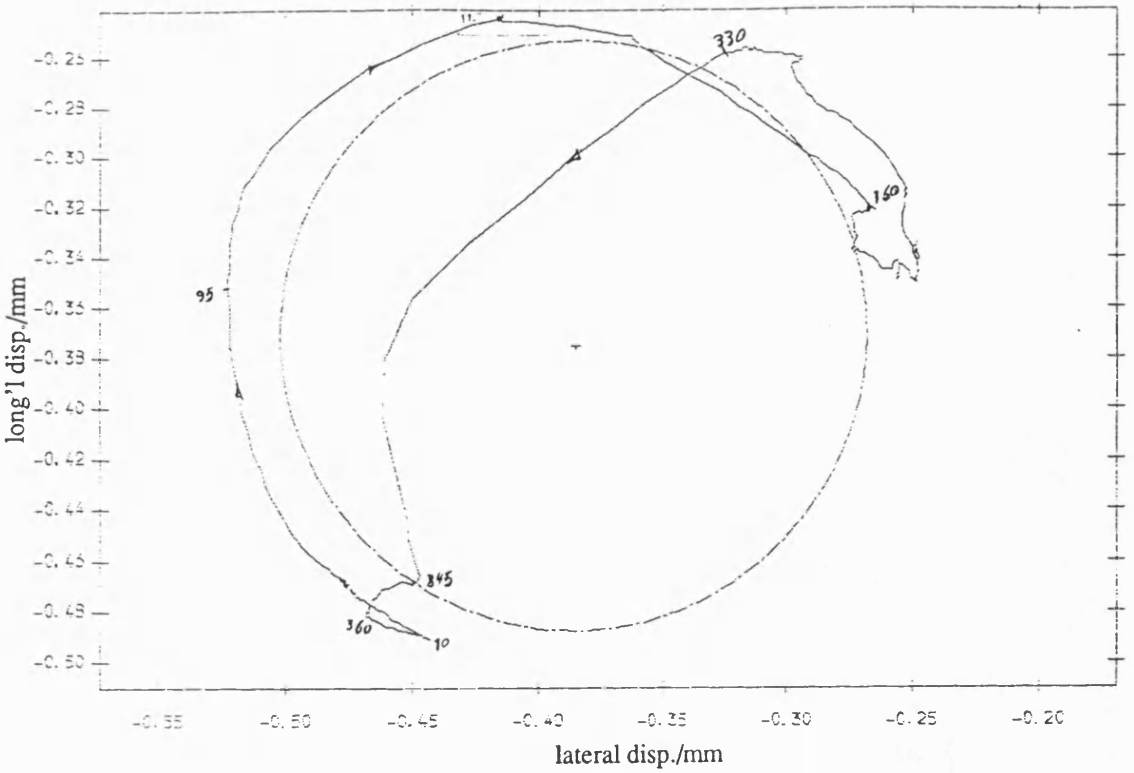

Fig 8.6.11 Exp. result polar plot of relative disp. , left hand pin isolated with fly wheel ;mean speed=327 rev/min ; dia. clearance=.25mm

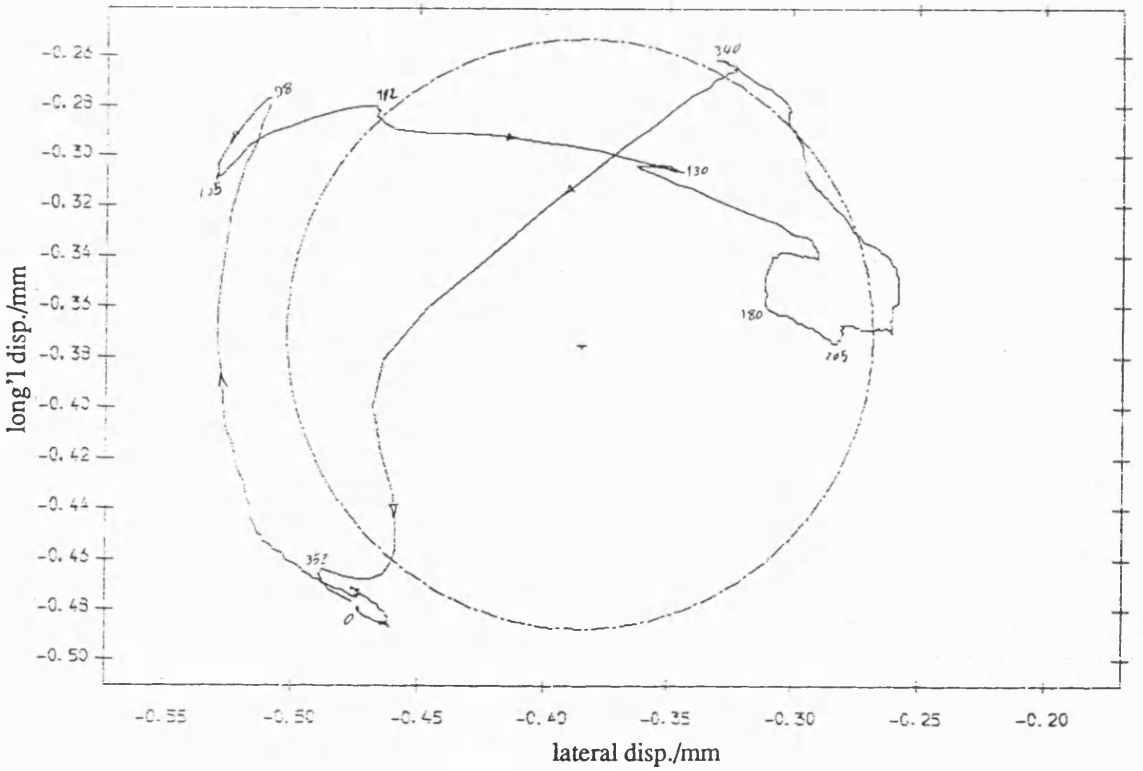

Fig 8.6.12 Exp. result polar plot of relative disp. › right hand pin isolated with fly wheel ;mean speed=327 rev/min ; dia. clearance=.25mm

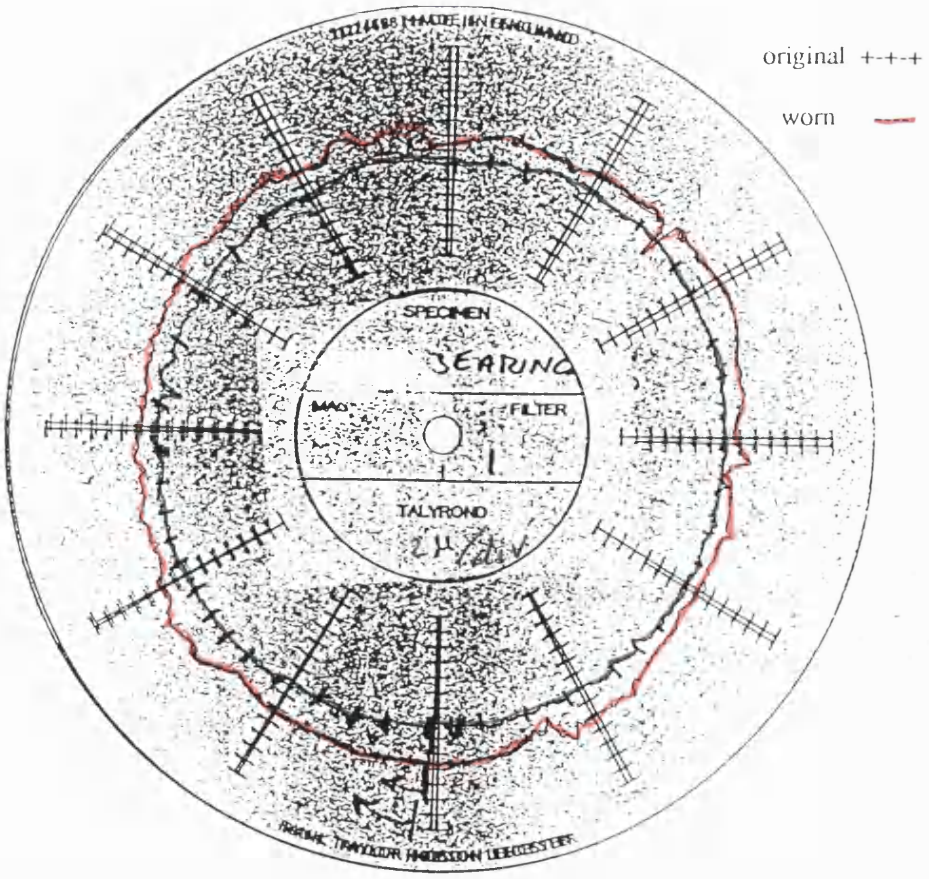

Fig 8.7.1 Bush roundness , for different speed

front(left hand)bush ; dia. clearance 0.25mm

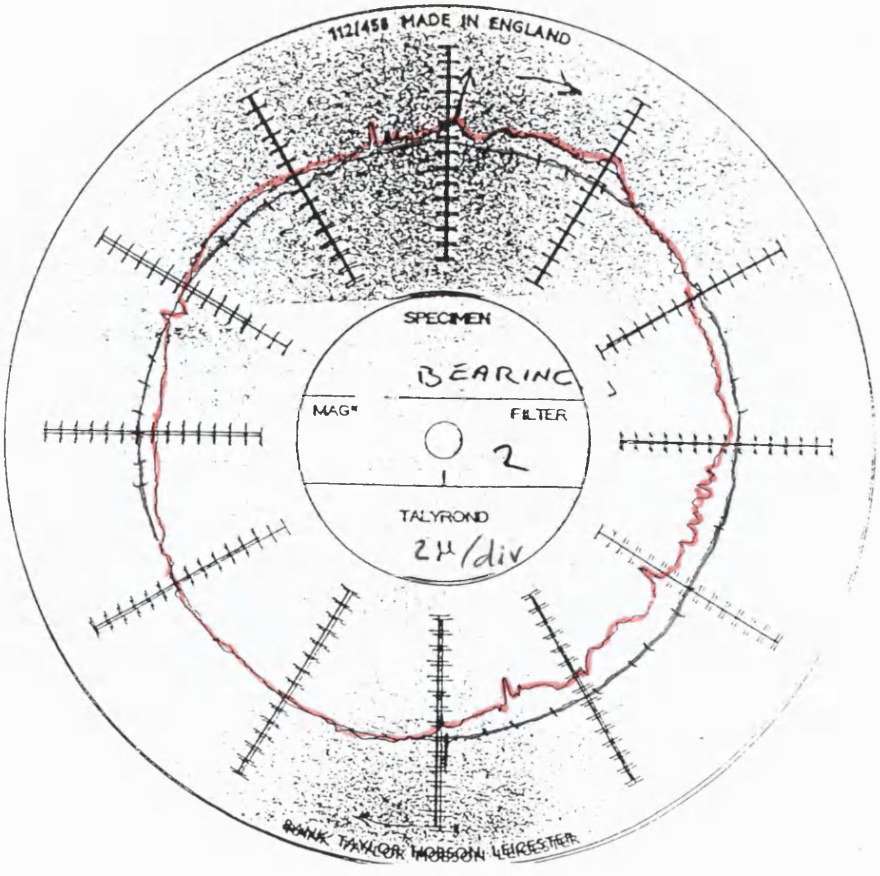

Fig 8.7.2 Bush roundness , for different speed

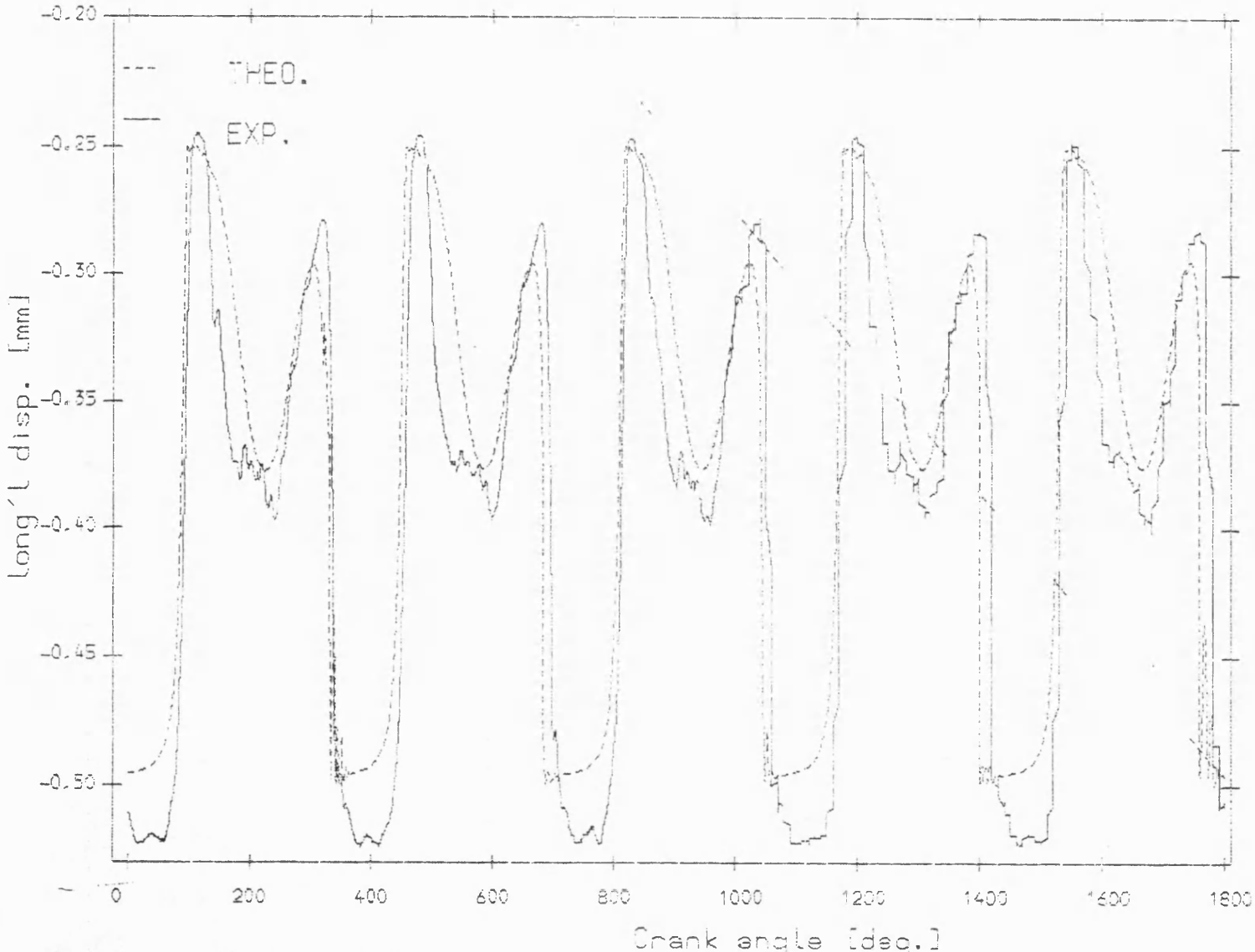

Fig 8..7.3 Long'l disp. of pin relative to greasy bush with flywheel ; mean speed=244 rev/min; dia. clearance=.25mm

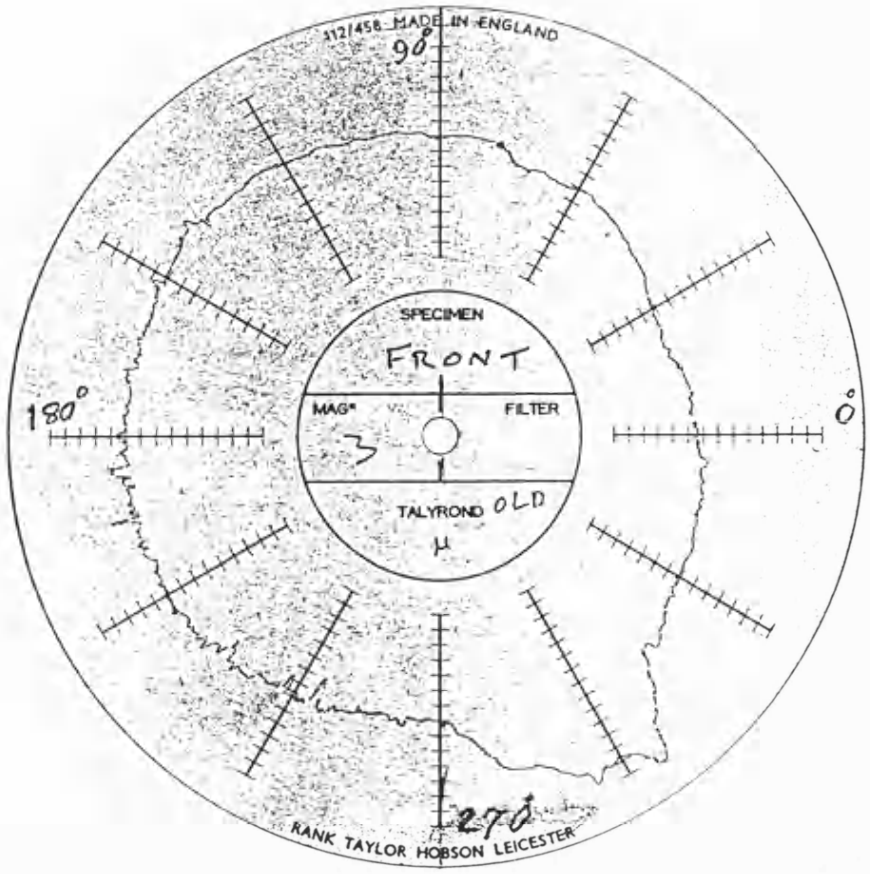

Fig 8.7.4 Bush roundness , just after getting pin motion trace

diametral clearance 0.25mm

CHAPTER 9
INFLUENCE OF SPEED, INERTIA, GREASE AND CLEARANCE

9.1 Introduction

In this chapter the effect of variable parameters such as input speed , input inertia, pin lubrication and clearance are investigated separately. The theoretical contact loss position is also studied.

The effect of input speed on different traces such as , pin displacement components,angular acceleration, polar plot and input speed is discussed in sec.(9.2).

In sec.(9.3) the effect of the fly wheel at different speeds on different traces is studied. The effect of grease on the bearing at different speeds compared with the dry bearing case is discussed in sec.(9.4). In sec.(9.5) the effect of variation of the pin clearance on different parameters is discussed.

In sec.(9.6) the contact-loss position is discussed.

9.2 Effect of speed

9.2.1 Input speed traces

There is a disturbance in input speed trace (see sec.(8.2.1a-8.2.3a)) sec(4.2)). The variation of effective inertia and friction torque during the cycle causes required input torque fluctuation of the system. The torque is controlled by the controller , but the controller response is not adequate to prevent the disturbance in input speed. The disturbance amplitude increases with speed. This may be due to frequency response of the controller, since at high speed the oscillation is more evident . The effect of

disturbance and its following oscillation may be detected in displacement and acceleration traces.

9.2.2 Contact loss traces

The first contact loss region gets narrower with speed - see tables(9.4.1 to 9.4.2). However the second region get wider. The first contact loss region starts earlier with increased speed. However the second region starts later at higher speeds - see sec.(8.2.1b to 8.2.3b).

The predicted pin force plot for zero clearance has two minima - see fig(9.2.1). The minima occur close to the angle of the first and second contact loss region. The first minimum occurs earlier with increasing input speed. However the second minimum occurs later, which correlates with contact loss when clearance exists. Both minima increase with speed. The rate of increase for the first minimum is greater than the second. i.e. the first minimum is smaller than the second at low speed. However it is greater than the second at high speed. More evidence will be present in the next sub sec.(9.2.3,9.2.4).

9.2.3 A&B (longitudinal & lateral) pin displacement components

The rising edges start earlier with increasing speed - see tables(9.4.3 to 9.4.6). However the falling edges start later. This is predicted in the theoretical results - see sec.(7.6).

The displacement range,especially at the falling edge, in the A trace increases with

speed - see sec.(8.2.1c,d to 8.2.3c,d) . However that at rising edge of B trace decreases and that at its fall increases. ie. there is a variation of flight time and also change of pin path shape with speed. This means the length of pin jump at the first region(rising edge) decreases with speed, while that at the second region(falling edge) increases. These are predicted in the theoretical traces - see sec.(7.6). There is more low frequency oscillation at low speed . There is one disturbance between the falling edge and the rising edge the amplitude of which increases with speed.

The disturbance is more detectable on the B traces. There is a small single disturbance just after the rising edge of the A traces the amplitude of which decreases with increasing the speed. This may represent flight time. This disturbance is predicted in the theoretical results - see sec.(7.6).

9.2.4 Polar plot

A general conclusion from the polar plot of the displacement trace for the wfw case is as follows :

The polar plot is roughly semicircular at low speed and the motion occurs roughly on the semicircular arc corresponding to the bottom of the bush - see sec. (8.2.1e to 8.2.3e).

With increasing speed the pin flight becomes apparent within the semicircle ; at higher speeds the polar plot becomes roughly circular. Increasing the speed again makes the polar plot roughly semicircular but at the top of the bush. The reason is that at low speed the pin is mostly governed by gravity forces. Increasing the speed will increase the inertia force and then the effect of gravity force (which is independent of input speed) and inertia force become of equal magnitude . We see

from the result this causes circularity of the polar plot . Increasing the speed will increase the inertia force further . Then the inertia force will mostly govern the pin motion. The polar plot becomes semicircular with the pin in the top half of the bush.

There is some similarity between pin force polar plot in zero clearance case and the displacement polar plot with clearance case. It is worthy of discussion that here. The above points in pin displacement polar plot are very similar to the following points in polar plot of B pin force for zero clearance see(fig(9.2.2)). Therefore the above behaviour can be justified by the following points.

1. longitudinal force is negative at low speed; this causes the motion of pin to be at the bottom of the bush.

2. With increasing speed the longitudinal force becomes positive at some range of crank angle; the pin moves toward the top of the bush therefore the displacement polar plot becomes more circular.

3. With increasing speed again , the longitudinal force becomes positive over major part of the cycle. Therefore the pin path will largely lie at the top of the bush.

4. In the region corresponding to the first region of the clearance case, the predicted zero clearance force is close to zero at low speed. The predicted minimum force increases with speed speed. However the predicted minimum force in the second region gets smaller. This may be the reason for decreasing flight time in the first region with speed and increase in the second region.

9.2.5 Follower angular acceleration traces

The first impact region starts earlier with increasing speed - see sec. (8.2.1f to 8.2.3f). However the second region starts later. This is similar to zero clearance force which discussed earlier - see sec.(9.2.2). The first impact increases slightly with speed(fig 9.3.1) . However the second one increases considerably with speed . These are predicted in the theoretical traces see sec.(7.2 , 7.3).

There is a disturbance slightly after max acceleration region . The disturbance is hardly detected at low speed. However it increases considerably with speed. This is due to disturbance in input speed see sec.(9.2.1).

9.2.6 Coupler c.m. lateral acceleration

With increasing the speed the first impact starts earlier - see table(9.4.7). However the second impact starts later. Both impacts increases with speed - see sec.(8.2.1g to 8.2.3g) . However the rate of increase for the second impact is greater. The first impact is greater than the second at low speed . However the second impact is greater than the first at high speed. These are predicted in the theoretical traces - see sec.(7.3) as discussed for other traces earlier . There is a disturbance slightly after the second impact. This is due to a disturbance in input speed at this region ,which is due to controller characteristic (9.2.1). Its amplitude will increase with increasing input speed.

9.3 Effect of input inertia

9.3.1 Input speed

There is small disturbance due to ''SCR'' speed controller characteristic (sec. 8.2.1a to 8.2.3a) . In wfw case the disturbance increases with speed at a greater rate than for the nfw case, because the controller controls the speed by changing the torque. It has a transient response when the effective inertia , friction or load torque changes. This disturbance is hardly detected in nfw and the input speed for wfw is approximately constant at low speed.

The oscillation which starts with the disturbance although damped is evident and continues throughout the cycle , which becomes more evident with increasing speed. The effect of the disturbance and its following oscillation may be detected in displacement and acceleration traces.

9.3.2 Contact loss traces

Both contact loss regions of wfw case start later than that of the nfw case(see sec.(8.2.1b-8.2.3b)). The lag of the wfw case relative to nfw increases with speed see tab(9.3.1).

9.3.3 A (longitudinal) pin displacement

The rising edge of the wfw case generally starts later than that in the nfw case(8.2.1c-8.2.3c) (see tab (9.3.3)).

The pin jump at the rising edge in the wfw case is smaller than that of nfw case. This is predicted in the theoretical traces (see sec.(7.6)). The falling edge of wfw lags that of the nfw case at low speed. The range of displacement at the falling edge in the wfw case increases with speed. This range also increases in nfw case but at a greater rate. The above range is greater than that of nfw at low speed which is the same as predicted. However it is smaller at high speed.

The effect of disturbance is more detectable in wfw case specially at high speed.

9.3.4 B (lateral) pin displacement.

The rising and falling edge in the wfw case generally start later than at the nfw case(see sec.(8.2.1d-8.2.3d)) (see tab(9.3.5).

The pin flight length in wfw case at rising edge decreases with speed at a smaller rate than nfw does. Hence at low speed the pin jump at rising edge in wfw case is greater than that at nfw. However this range is smaller at high speed in both cases.

In the wfw case at falling edge the displacement range (pin flight length) is greater than nfw case. The difference between the two increases with speed. These are predicted in the theoretical traces(see sec.(7.6)).

There is a disturbance after the falling edge in the wfw case. Its amplitude increases with increasing speed . However it is not detected in the nfw case.

The displacement of the starting point of pin flight at the rising edge in the nfw case decreases with speed. However that for the wfw does not alter. Therefor at low speed the displacement of the pin at which the rising edge occurs is greater for the

wfw case than that for nfw. However it is smaller at high speed. The former is predicted in the theoretical traces.

The displacement of the ending point of pin flight decreases with speed. The rate of decrease is greater in the wfw case. Therefor at low speed the displacement of pin at the end of the jump in rising edge is smaller than in the nfw case. However it is greater at high speed. These are predicted in the theoretical traces. The distance of the pin at which the falling edge occurs is smaller than in nfw case.

9.3.5 Polar plots

At low speed the first contact loss region of wfw is longer than at nfw - see sec.(8.2.1e to 8.2.3e). However the second region is hardly detected in wfw plot.

At high speed the distance of the pin from the bush in free flight in the first region of the wfw case is greater than that in nfw case. However at the second contact loss region the distance between pin and bush of nfw plot is greater than that at wfw trace.

There is a small loop before second region which increases in size with increasing the input speed. It is larger for nfw case. This loop is similar to a small loop in this region at polar plot force in zero clearance case(see fig(9.2.2)).

There is a small loop after 2nd contact loss region which increases with increasing the speed. It is larger in the wfw case. That may be due to the disturbance in input speed. Another possibility for the reason of this loop can be the impact itself. If so, it shows the severity of impact.

9.3.6 Follower angular acceleration

Both impact regions of the wfw case lag those of the nfw case(see sec.(8.2.1f to 8.2.3f)). The impacts of wfw case are greater than that of nfw case(see fig(9.3.1 to 9.3.3)). There is less oscillation in wfw. The effect of the input speed disturbance due to the controller in wfw case is greater(see sec.(9.3.1)) This makes the peak double which is more evident at high speed.

9.3.7 Coupler c.g lateral acceleration

The impact regions of wfw case lag those at nfw case see- sec. (8.2.1e to 8.2.3e). Both first and second impact increase with speed. The rate of increase of first impact is greater in the nfw case; however that at the second is greater in the wfw case. Therefor at low speed the first impact in the nfw case is greater than in the wfw case. However at high speed it is smaller than that in the nfw case. At high speed the second impact in the nfw case is greater than at wfw case. That is due to connection of the coupler to the crank,; when inertia is low the coupler can move fast. Since the duration of the first flight is considerable at low speed and that of the second at high speed, then the input inertia has more influence at these regions and speeds.

The oscillation amplitude at the nfw traces is slightly greater than at wfw.

9.4 Effect of grease

9.4.1 Input velocity traces

At a given controller setting, mean input velocity at all speeds that of the greasy case is slightly smaller than at the dry bearing(see sec.(8.4.1a to 8.4.3a)). That may be due to the viscous friction which increases the load torque. Looking at the velocity traces

it is evident that each time the falling part of the speed oscillation in the greasy case starts earlier than that in the dry case. This means the load torque of the greasy case is greater than at the dry case.

There is a disturbance in both the greasy and the dry case at a crank angle of about 20°. Its amplitude increases considerably at higher speed. The disturbance in the dry case lags that at the greasy bearing. The lag decreases with speed.

9.4.2 Contact loss traces

The crank angle at which the first contact loss occurs increases , however that at the second decreases with speed for both dry and greasy cases. The rate of variation with speed is greater for the greasy bearing case. At low speed both contact loss regions of the dry case start slightly earlier than that in the greasy case(see table (9.4.1b to 9.4.3b)). However at high speed it starts later than that in the greasy case. The contact loss region, particularly the first one, is wider than in the dry case at all speeds. This is due to the isolating property of the grease. It seems that in the greasy case contact remade occurs frequently within the first contact loss region.

9.4.2 A (longitudinal) pin displacement component

The crank angle at which rising edge occurs decreases with speed(see table 9.4.3,9.4.4). However that at the falling edge increases. The rate of variation is greater for the greasy case. The rising edge in the greasy case at low speed starts considerably later than in the dry case. However at high speed it leads the dry case slightly.

The first pin flight length decreases with speed in the greasy case with a greater rate

than in the dry case - see fig (8.4.2, 8.4.13, 8.4.24). The range of displacement at rising edge of the dry case(pin path length at first contact loss region) is greater than that in the greasy case. However at high speed it is slightly smaller than in the greasy case. These are due to the fact that the grease is squeezed out of the bearing and therefore viscous friction reduces. There is more oscillation in the dry traces than those at the greasy case. This is due to the damping property of the grease in the greasy case. This is predicted in the theoretical traces(see sec.(7.2)).

9.4.3 Lateral pin displacement component (trace B)

The rising edges in the dry cases and those in the greasy cases occur at much the same crank angle (see table(9.4.5 to 9.4.6)) . This may be due to the fact that the pin motion occurs mostly at the bottom and top of the bush - see sec.(9.4.5). Therefore grease is squeezed out of the bearing in these regions earlier than the other regions in the bush. As a result it produces light lubrication which reduces friction in lateral direction. The range of displacement at rising and falling edges of the greasy traces at low speed is considerably smaller than that in dry case. ie. pin path length in the contact loss region is smaller. This means the flight length is smaller and therefore the impact is less severe. At high speed there is an oscillation which starts before rising edge and is superimposed on the rising edge. That is due to a considerably high amplitude disturbance in input speed. These oscillation are more detectable in the dry case.

9.4.5 Polar plots

The pin path moves from the bush bottom to the top as the speed is increased. That in the dry bearing case occurs at a lower speed than the greasy case. At low speed (120 rev/min) the polar plot in both cases are roughly restricted to a quarter of the

clearance circle which is at the bottom right hand side - see fig(9.4.4 and 9.4.5).

By increasing the speed to 168 rev/min the polar plot in the greasy is still in a quarter of the circle(sec. 8.4.1e to 8.4.3e) . However in the dry case the pin path(polar plot) is close to the clearance circle. That may be due to viscous friction which imposes a torque against pin jump. In the greasy case the viscous friction causes slightly greater demand torque than the dry case.

At high speed the pin is slightly closer to bush in dry case. There is a loop before second region which is greater for the greasy case at low speed. However there is a loop after second region which may be due to input speed disturbance.

9.4.6 Follower angular acceleration

The crank angle at which the first impact occurs decreases with speed(see table(9.4.5)). However that at the second increases for both dry and greasy cases. The rate of increase is greater in the dry case. At low speed the first impact region of the dry trace slightly leads that at the greasy case(see sec. (8.4.1f to 8.4.3f)). However the second region starts at the same point as for the greasy case. At high speed the first impact region in the dry bearing case slightly lags that in the greasy case. However the second starts slightly earlier than in the greasy case. The viscous friction is strongly effected by normal force, because the grease film is reduced in thicknes by this force. Increasing speed therefore induces light lubrication which reduces friction rlative to low speed. On the other hand at low speed, since the forces are relatively small, the viscous friction is higher. That causes the first impact region in the greasy bearing trace to lag that in the dry case.

At high speed the viscosity reduces due to increasing speed(see above) therefore the

first impact region in the dry slightly lags that at the greasy. This may be because of the coulomb friction, which in the dry case is greater than in the greasy case. It also causes that second impact in the greasy becomes greater than that at the dry bearing case(fig 9.4.1 to 9.4.3) .

There is less oscillation in the greasy case at all the speeds particularly at low speed. This is predicted in the theoretical traces - see sec.(7.3)).

9.4.7 Coupler c.g. lateral linear acceleration

The crank angle at which the first impact occurs decreases with speed(see table(9.4.6)). The rate of decrease is smaller in the dry case. The crank angle at which the second impact occurs increases for both dry and greasy case. The rate of increase is greater in the dry case. The first impact region in the dry case starts slightly earlier than that in the greasy case (see sec.(8.2.1g to 8.2.3g). For all speeds for both dry and greasy the 2nd impact is considerably greater than the first. At low speed both first and the 2nd impact in the dry bearing case is greater than at the greasy. However at high speed the first impacts are smaller than the greasy but the 2nd impacts are greater. There is more noise in the dry case specially at low speed. At high speed 2nd impact region of the greasy case starts slightly later than that in the dry bearing case.

9.5 Effect of clearance

9.5.1 Input speed traces

There is a disturbance in all the traces the amplitude of which increases with increasing speed (see sec.(8.2.1a to 8.2.3a), fig(8.3.130 to 8.3.143 , 8.5.130 to 8.5.143)). The disturbance slightly lags that at smaller clearance.

9.5.2 Contact loss traces

The greater the clearance the wider the contact loss region and therefore the signal is clearer(see sec.(8.2.1b to 8.2.3b), fig(8.3.53 to 8.3.79 ,8.5.53 to 8.5.79)) . The first contact loss region starts earlier at lower clearance. However the second region starts later particularly at low speed.

For all clearances the first contact loss region is wider than the second at low speed. However at high speed the second contact loss region is wider.

9.5.3 A (longitudinal) displacement components

There are two local minimum in the traces between the falling and rising edge (see sec.(8.2.1c to 8.2.3c), fig(8.3.1 to 8.3.13, 8.5.1 to 8.5.13)). One is just after the rising edge and the other before the falling edge. By decreasing the clearance the distance between maximum and those local minimum relative to the clearance increases. At low speed the displacement at rising edges relative to falling edge increases with decreasing clearance. This means the pin jump at first contact loss region is greater than the second and contact loss region is wider and therefore the impact is more severe.

9.5.4 B (lateral) displacement comp.

There are two local minima; one is after the rising edge and the other is before the falling edge (see sec.(8.2.1c to 8.2.3c), fig(8.3.14 to 8.3.26, 8.5.14 to 8.5.26)). . At low speed and small clearance (0.2 ,0.15mm) the relative magnitude of the first local minimum is greater than the case with 0.25mm clearance. At high speed it becomes smaller , but the size of the second minimum is considerably greater. The ratio of

falling edge displacement to clearance considerably decreases with decreasing clearance particularly at high speed. This means at lower clearance the pin fall leads to very small impacts.

9.5.5 Polar plots

The polar plots are considerably different for lower clearance (sec. 8.2.1e-8.2.3e, fig(8.3.105 to 8.3.129, 8.5.105 to 8.5.129) . This is because by decreasing the clearance any misalignment errors become more significant.

This is more evident at low speed and low clearance. For all clearances at low speed the major part of the pin path is at the bottom right hand side of the bush. However at high speed the major part of the pin path is at the top part of the clearance circle. That is because at low speed the gravity force dominates. However at high speed the inertia forces dominate.

9.5.6 Follower angular acceleration

At low speed the first impact region starts later than at smaller clearance(see sec. (8.2.1f-8.2.3f), fig(8.3.27 to 8.3.52, 8.5.27 to 8.5.52)). . At low speed the second impact is greater than that at smaller clearance. At low speed the 1st impact is greater than the second and increasing clearance has not great effect on the impact value. However at high speed the second impact is greater than the first for all the clearances and the second impact increases considerably with the clearance - see fig (9.3.1 to 9.3.4) and fig (9.4.1 to 9.4.3).

The second impact starts later than the cases with smaller clearance. The reason can be longer duration of the free flight mode for greater clearances.

9.5.7 Coupler c.g. lateral acceleration

Both first and second impact regions start later than those at smaller clearance(see sec. (8.2.1g to 8.2.3g), fig(8.3.79 to 8.3.104 , 8.5.79 to 8.5.104)). The impacts are mostly greater than those at smaller clearance. This may be due to the fact that the greater the clearance the longer the free flight duration.

9.6 Contact loss position

Considering the follower as a separate element (fig 9.6.1) one may write the following equation for the follower angular acceleration ,which is true all the time including following modes.

$$cF_{b1}-m_3ge_3\cos\beta=I_3\ddot{\beta}$$

$$\text{then } \cos\beta=\frac{cF_{b1}-I_3\ddot{\beta}}{m_3ge_3}$$

Since F_{b1} is proportional to $\dot{\phi}^2$ and $\ddot{\beta}=\frac{DG_f}{D\phi}\dot{\phi}^2$, in zero clearance and steady running case , then increasing ϕ means increasing β.

The above equation can be written as follows:

$$\cos\beta=K(\dot{\phi}^2)$$

the following cases can be investigated.

$\beta < \frac{\pi}{2}$; K is positive and increasing $\dot{\phi}$ means increasing $\cos\beta$; that means decreasing β.

In the first half of the cycle (i.e G_f is positive - see fig 6.2.2) that means decreasing ϕ will cause decreasing β. Hence first when it occurs will occur earlier than at lower speed.

In the second half of the cycle(i.e G_f is negative - see fig 6.2.2) increasing ϕ will cause decreasing β and so the second region occurs later than at lower speed.

Table 9.3.1 Exp. crank angle position of contact loss in degrees

contact loss region for dia. clearance of 0.3mm with fly wheel(wfw)and no fly wheel(nfw)cases				
case / speed	wfw		nfw	
rev/min	region 1	region 2	region 1	region 2
168	106.9 to 120	328.9 to 330.6	121.7 to 128.3	314.1 to 324
206	115.1 to 118.4	328 to 337.2	106.9 to 110.2	324 to 327.3
244	106.9 to 108.5	328.9 to 335.5	103.6 to 106.9	328.9 to 333.9
290	103.6 to 106.9	330.6 to 340.5	98.0 to 100.3	328.9 to 337.2
327		330.6 to 340.5	106.9 to 108.6	330.9 to 338.2

Table 9.3.2 Exp. crank angle position of contact loss in degrees

contact loss region for dia. clearance of 0.25 mm for wfw and nfw cases				
case / speed	wfw		nfw	
rev/min	region 1	region 2	region 1	region 2
168	107.8 to 129.6	326.6 to 329.7	93.7 to 106.2	321.8 to 331.2
206	98.4 to 101.7	328.9 to 337.2	93.1 to 103.9	323.4 to 337.5
244	153.2 154.7	332.8 to 339.1	91.6 to 101.9	332.8 to 335.9
290	120.3 to 123.6	342.1 to 353.6	100.1 to 101.8	328.1 to 339.1
327	107.2 to 110.3	334.4 to 340.6	90.6 to 92.2	329.7 to 342.2

Table 9.3.3 Exp. crank angle position, for pin Jump at A disp. ,in degrees

crank angle position for pin Jump at A disp. comp.; dia. clearance of 0.3 mm for wfw and nfw				
case / speed	wfw		nfw	
rev/min	rising	falling	rising	falling
168	123.4	328.9	121.7	328.9
206	106.9	330.6	102	331.6
244	97	337.2	90.5	333.9
290	95.4	340.5	88.8	337.2
327	95.7	343.8	90.5	340.5

Table 9.3.4 Exp. crank angle position, for pin Jump at A disp., in degrees

crank angle position for pin Jump at A disp. comp.; dia. clearance of 0.25 mm for wfw and nfw				
case / speed	wfw		nfw	
rev/min	rising	falling	rising	falling
168	111.8	321.4	107.1	318.3
206	98.7	332.2	92	332.8
244	82.6	333.9	91.9	338.5
290	92.3	338.8	92	337.5
327	91.9	340	91.9	340.0

Table 9.3.5 Exp. crank angle position, for pin Jump at B disp., in degrees

crank angle position for pin Jump at B disp. comp.; dia. clearance of 0.3 mm for wfw and nfw				
case / speed	wfw		nfw	
rev/min	rising	falling	rising	falling
168	110.5	328.9	116.8	328.9
206	113.5	342.1	111.8	338.8
244	108.5	347	102.3	345.4
290	103.6	348.7	97.	347
327	103.6	343.8	97	345.4

Table 9.3.6 Exp. crank angle position, for pin Jump at B disp., in degrees

crank angle position for pin Jump at B disp. comp.; dia. clearance of 0.25 mm for wfw and nfw				
case / speed	wfw		nfw	
rev/min	rising	falling	rising	falling
168	121.4	330.7	118.3	327.6
208	106.9	340.5	110.9	334.4
244	104.3	343.2	108.9	340
290	105.3	343.8	103.1	342.2
327	102.5	346.3	100.9	343.2

Table 9.3.7 Exp. crank angle position in degrees for follower ang. acc. impact at B dia clea. =0.25mm

crank angle position for impact ; dia. clearance of 0.25 mm for wfw and nfw				
case / speed	wfw		nfw	
rev/min	region 1	2	region 1	2
168	121.7	327.3	126.6	327.3
208	103.6	333.9	106.9	331.6
244	102	335.5	106.9	333.9
290	100.32	340.5	90.5	337.2
327	99	342.1	97.7	338.8

Table 9.3.8 Exp. crank angle position in degrees for coupler ang. acc. impact at B dia clea. =0.25mm

crank angle position for impact ; dia. clearance of 0.25 mm for wfw and nfw				
case / speed	wfw		nfw	
rev/min	region 1	region 2	region 1	region 2
168	123.4	330.6	125.	327.3
208	123.4	335.5	123.4	332.2
244	103.6	337.2	100.3	333.9
290	100.3	340.46	97	337.2
327	100.3	340.46	97.	338.8

Table 9.4.1 Exp. crank angle position on contact loss regions

contact loss region for dia. clearance of 0.3 mm dry and greasy case				
case / speed	dry		greasy	
	1	2	1	2
168	110.2 to 123.4		106.9 to 133.2	317.4 to 330.6
206	110.2 to 115.1		106.9 to 108.6	328.9 to 335.5
244	103. to 105.3	330.6 to 337.2	103.6 to 111.2	329.9 to 337.2
290	110.9 to 113.5	328.9 to 340.5	97.7 to 106.3	330.6 to 340.5
327	102 to 103.6	332.2 to 342.1	103.6 to 106.9	332.2 to 342.1

Table 9.4.2

contact loss region for dia. clearance of 0.25mm dry and greasy case				
case / speed	dry		greasy	
	1	2	1	2
168	109.4 to 118.8	326.6 to 331.2	112.5 to 131.2	325 to 334.4
206	92.1 to 105.3		98.7 to 111.84	325.65 to 338.82
244	103.1 to 106.2	331.2 to 340.6	87.5 to 103.1	331.2 to 346.9
290	100.3 to 101.5	332.2 to 345.4	88.8 to 98.7	335.5 to 348.7
327		334.4 to 346.9	90.6 to 109.4	334.4 to 346.9

Table 9.4.3 Exp. crank angle position of pin jump in A(longitudinal)disp

pin jump position for dia. clearance of 0.3 mm dry and greasy case				
case / speed	dry		greasy	
	rising edge	falling edge	rising edge	falling edge
168	121.7	324	121.7	330.6
206	116.8	330.6	116.8	333.9
244	95.4	337.2	93.8	338.8
290	92.1	338.8	90.5	340.5
327	93.8	343.8	97	343.8

Table 9.4.4 Exp. crank angle position of pin jump in A(longitudinal)disp.

pin jump position for dia. clearance of 0.25mm dry and greasy case				
case / speed	dry		greasy	
	rising edge	falling edge	rising edge	falling edge
168	104.7	328.1	123.4	326.6
206	97	350.3	100.3	353.6
244	89.1	337.5	92.2	339.1
290	92.1	338.8	93.8	340.5
327	88.8	345.3	95.3	345.3

Table 9.4.5 Exp. crank angle position of pin jump in B(lateral)disp.

pin jump position for dia. clearance of 0.3 mm dry and greasy case				
case / speed	dry		greasy	
	rising edge	falling edge	rising edge	falling edge
168	118.8	332.8	114.1	331.3
206	106.9	335.5	110.2	338.8
244	95.3	343.8	98.4	343.8
290	100.3	343.8	100.3	347
327	98.4	345.3	98.4	345.3

Table 9.4.6 Exp. crank angle position of pin jump in B(lateral)disp.

pin jump position for dia. clearance of 0.25 mm dry and greasy case				
case / speed	dry		greasy	
	rising edge	falling edge	rising edge	falling edge
168	118.8	332.8	114.1	331.3
208	106.9	335.5	110.2	338.8
244	95.3	343.8	98.4	343.8
290	100.3	343.8	100.3	347
327	98.4	345.3	98.4	345.3

Table 9.4.7 Exp. crank angle position of the follower ang. acc. impact

impact position for dia. clearance of 0.3 mm dry and greasy case				
case / speed	dry		greasy	
	1	2	1	2
168	121.7	327.3	123.4	330.6
208	110.2	332.2	120	335.5
244	105.3	337.2	100.3	337.2
290	97.7	340.5	97	338.8
327	98.6	342.1	100.9	338.8

Table 9.4.8 Exp. crank angle position of the coupler c.g. acc. impact

impact position for dia. clearance of 0.3 mm dry and greasy case				
case / speed	dry		greasy	
	1	2	1	2
168	123.4	327.3	121.7	330.6
208	108.5	332.9	108.5	333.9
244	99.7	335.5	100.3	338.8
290	93.75	338.8	97	338.8
327	97	343.8	97	343.8

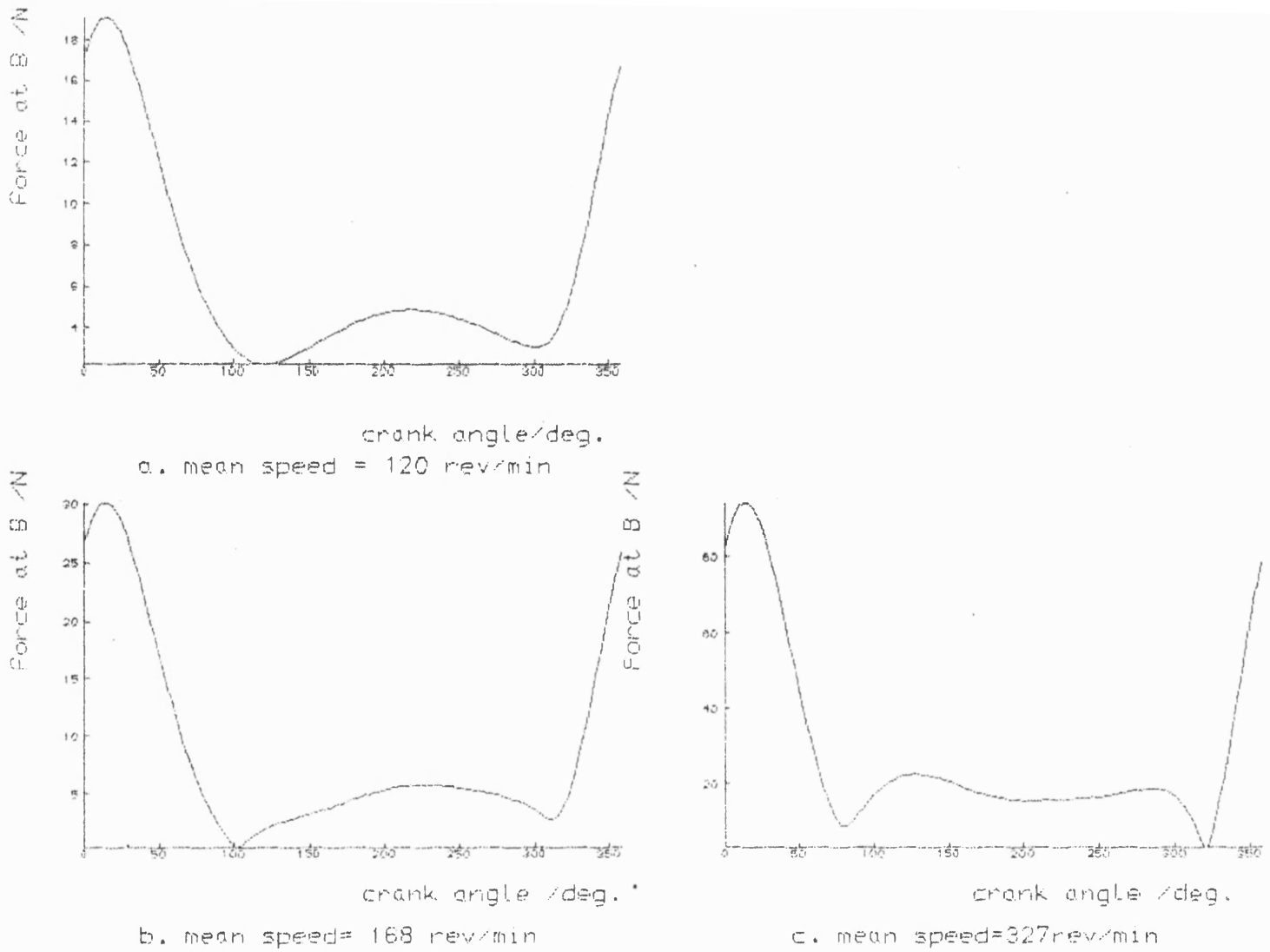

Fig 9.2.1 B pin Force For zero clearance with flywheel for different speed

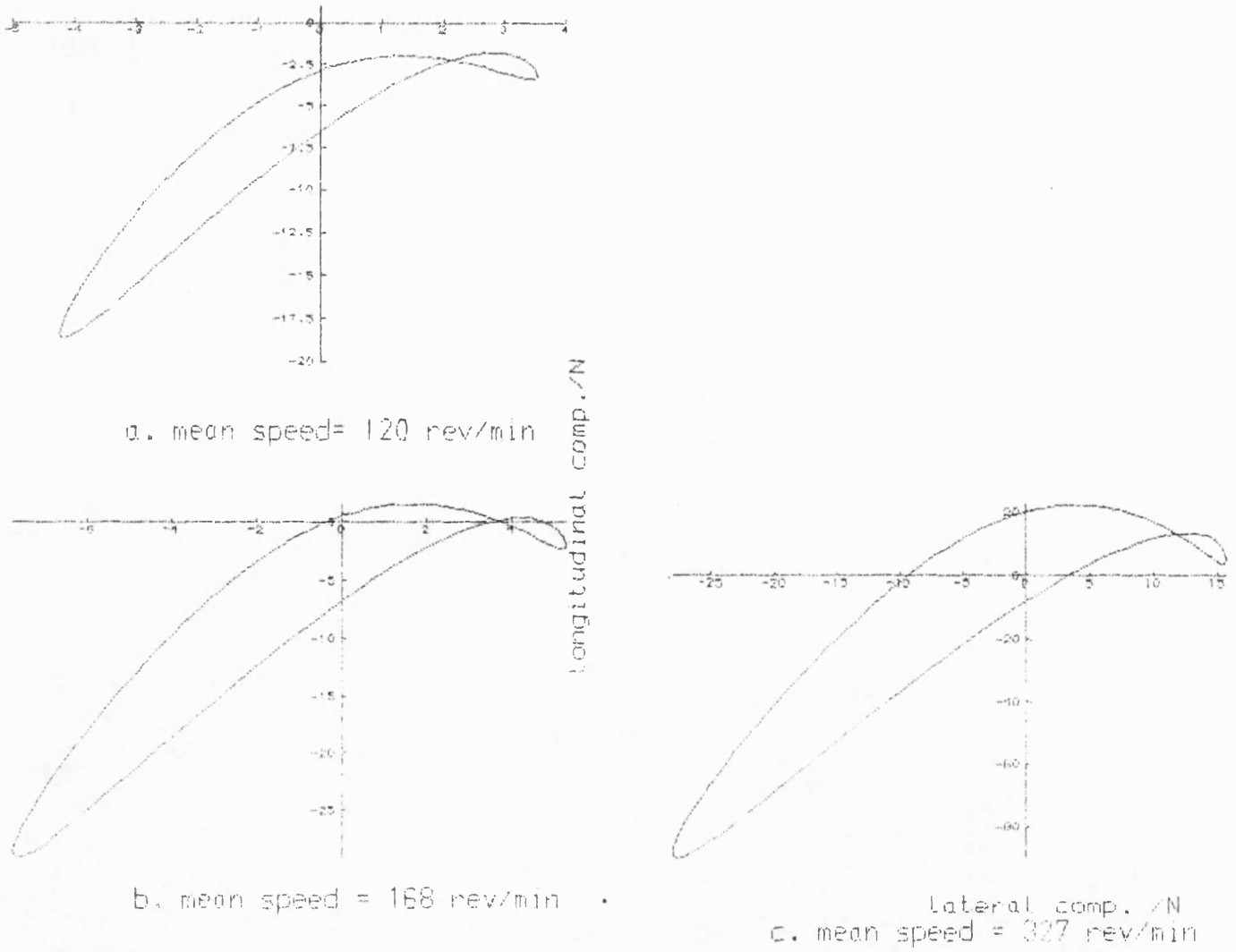

Fig 9.2.2 Polar plot of B pin Force For zero clearance with Fly wheel

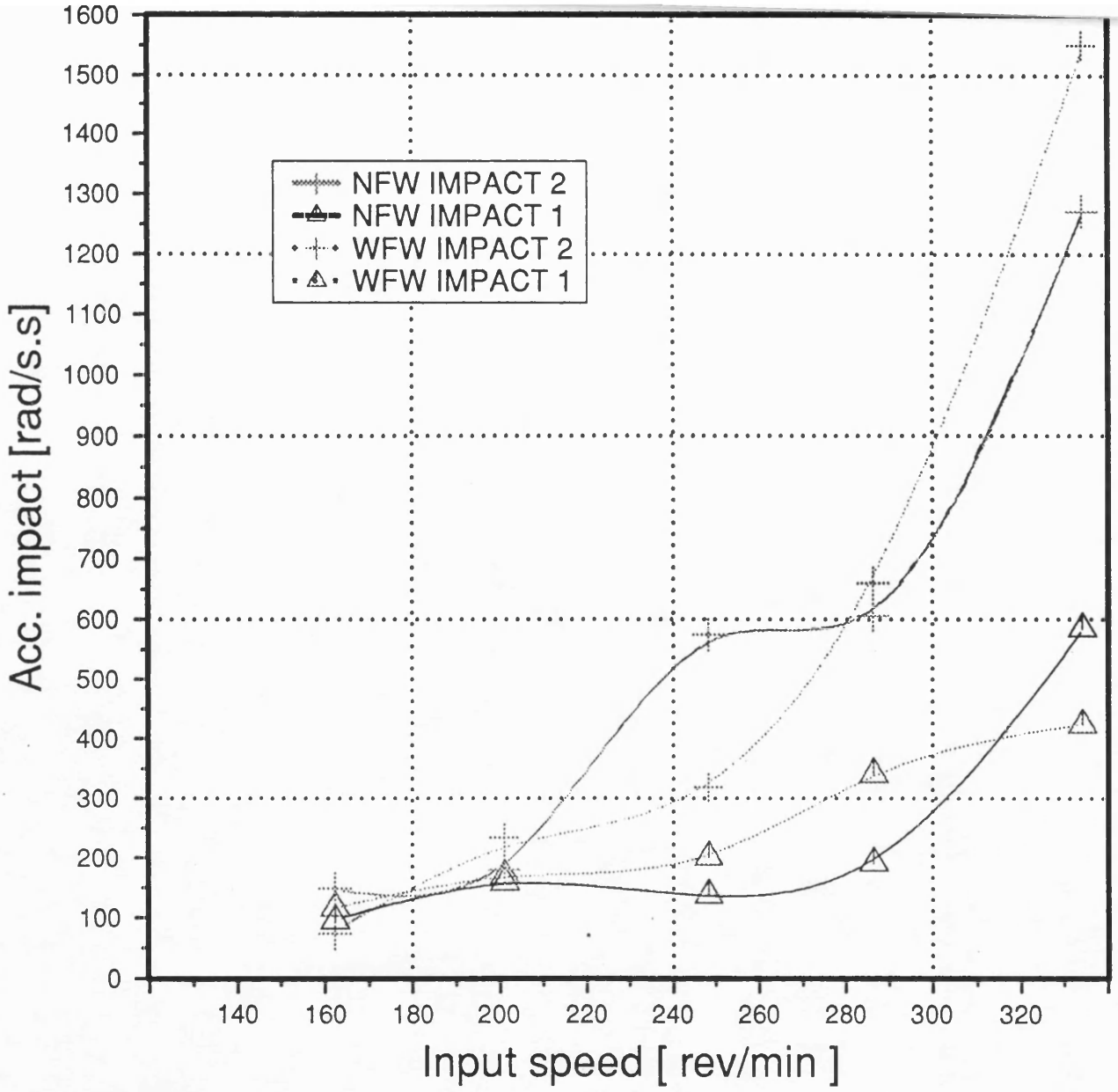

Fig 9.3.1 Experimental impact versus input speed d. clea=0 .30mm

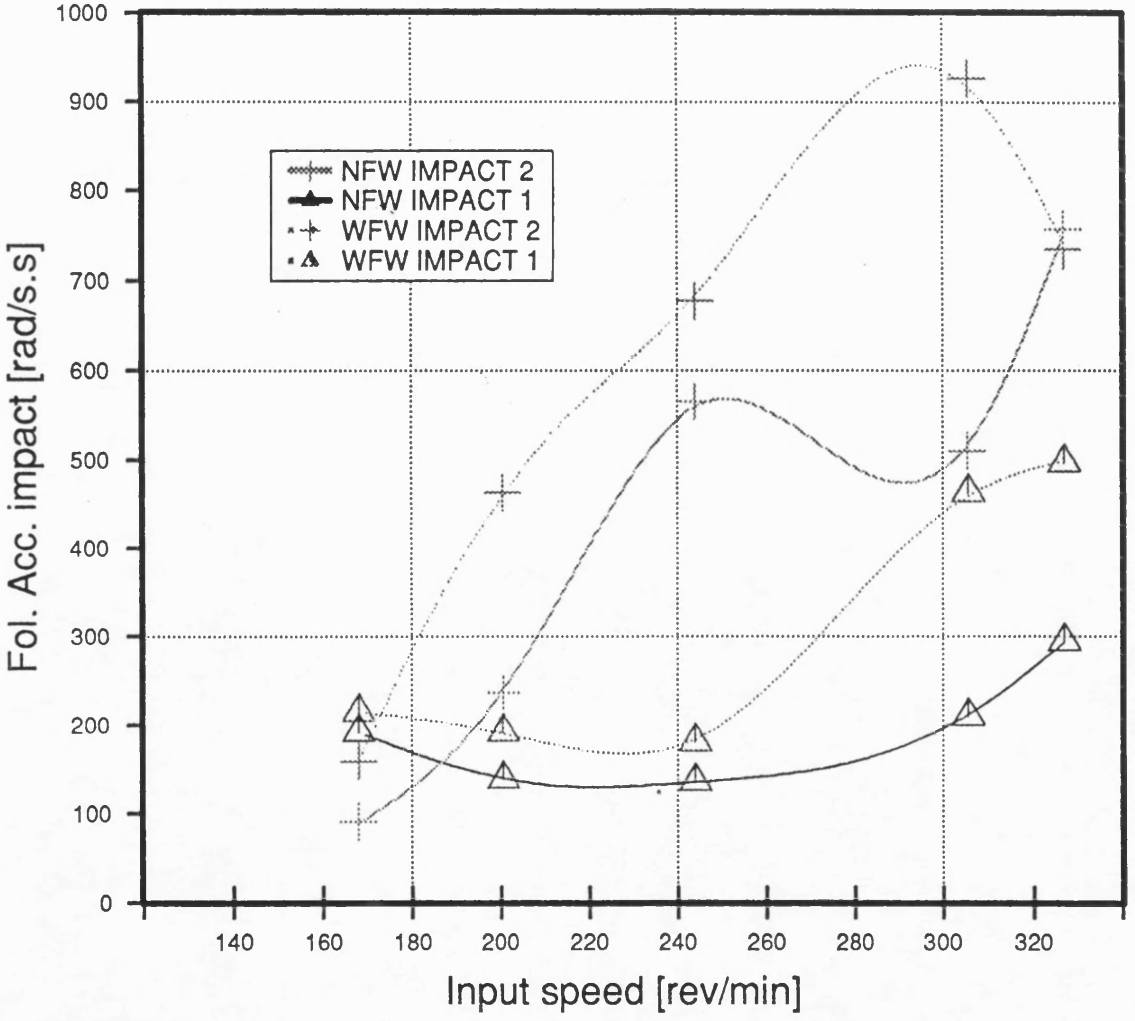

Fig 9.3.2 Experimental impact versus input speed d. clea=0. 25mm

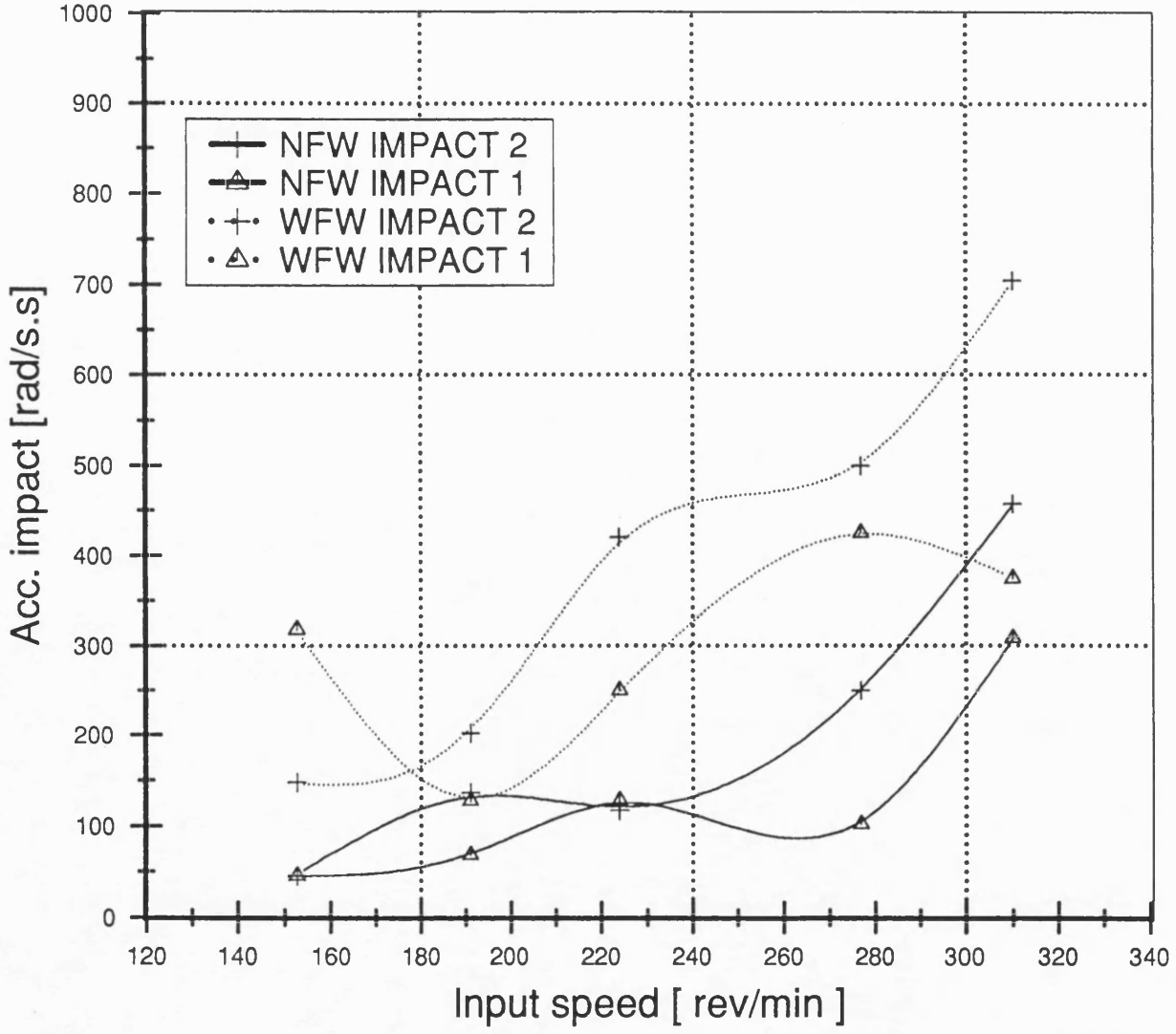

Fig 9.3.3 Experimental impact versus input speed d.clea= **0.2 mm**

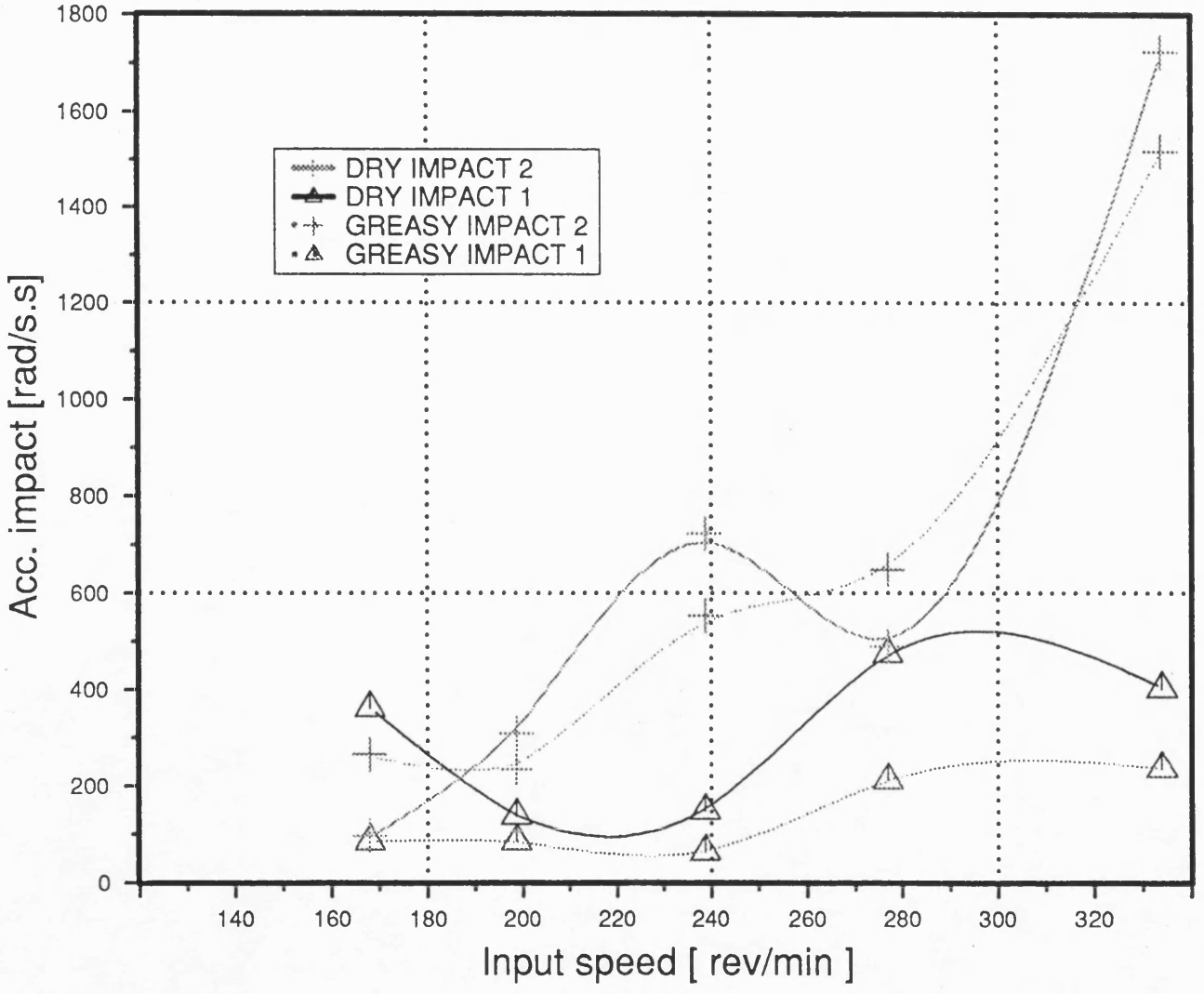

Fig 9.4.1 Experimental impact versus input speed d. clea=0.3 mm

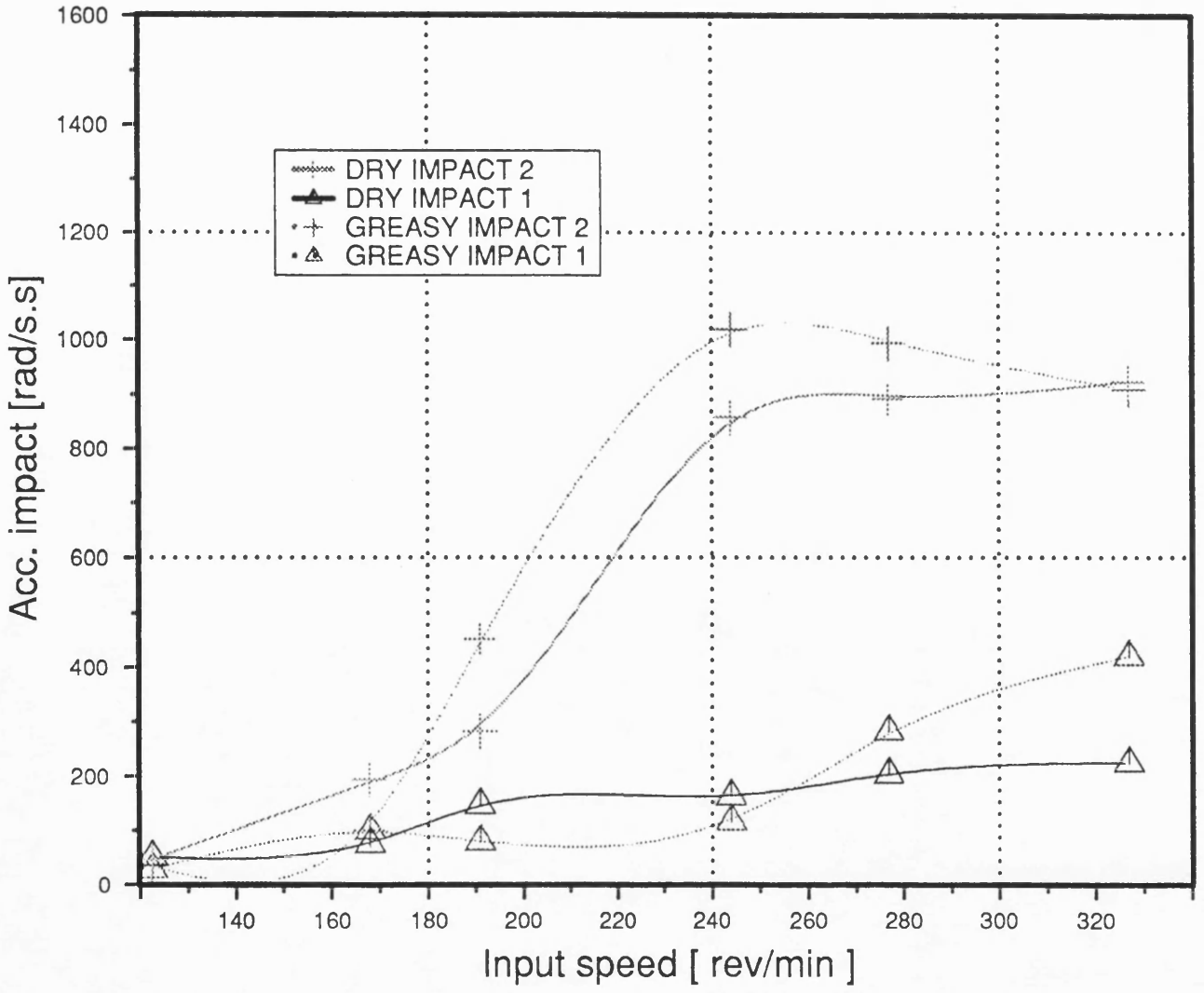

Fig 9.4.2 Experimental impact versus input speed d. clea=.2 5mm

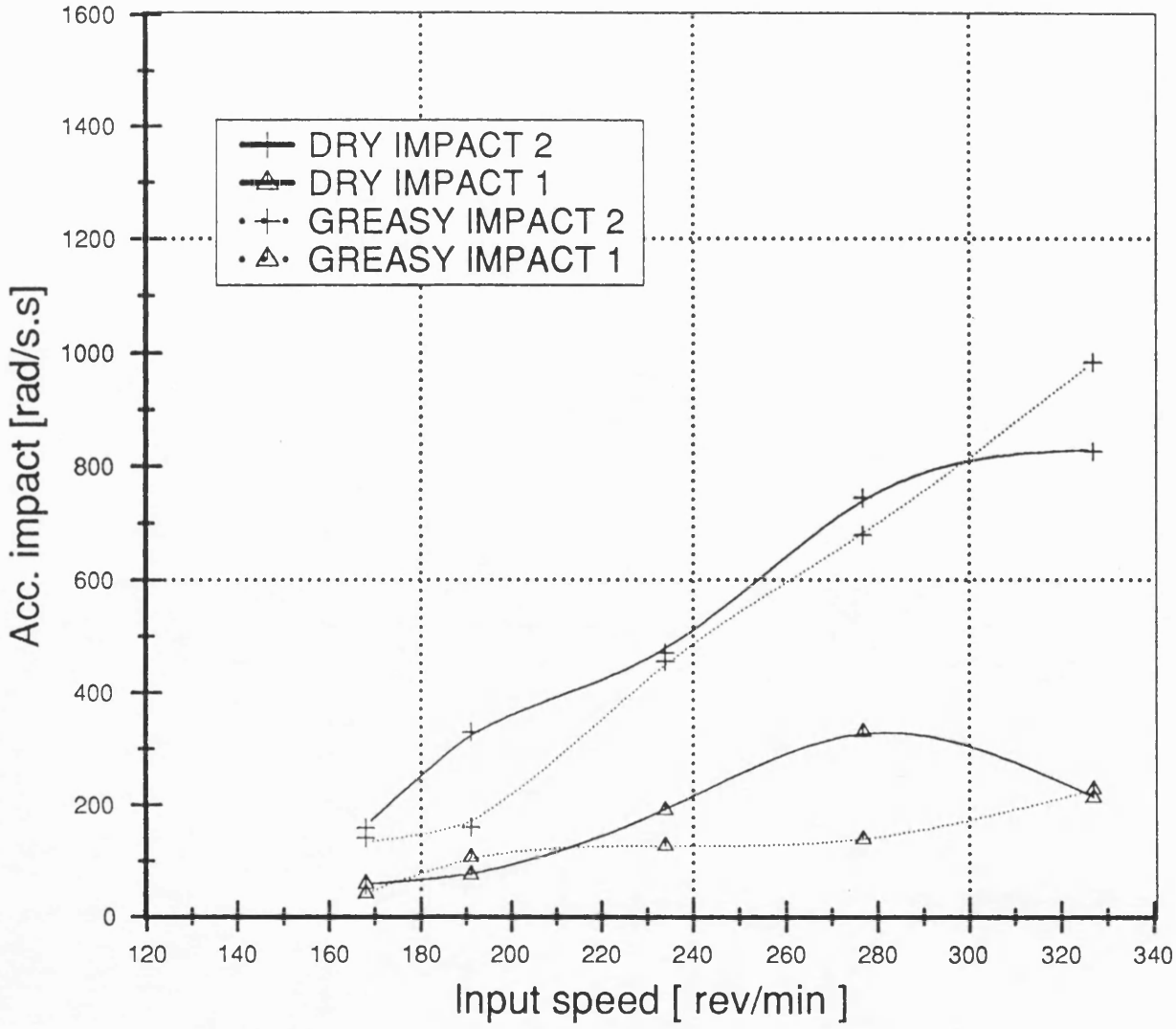

Fig 9.4.3 Experimental impact versus input speed d. clea=0. 2mm

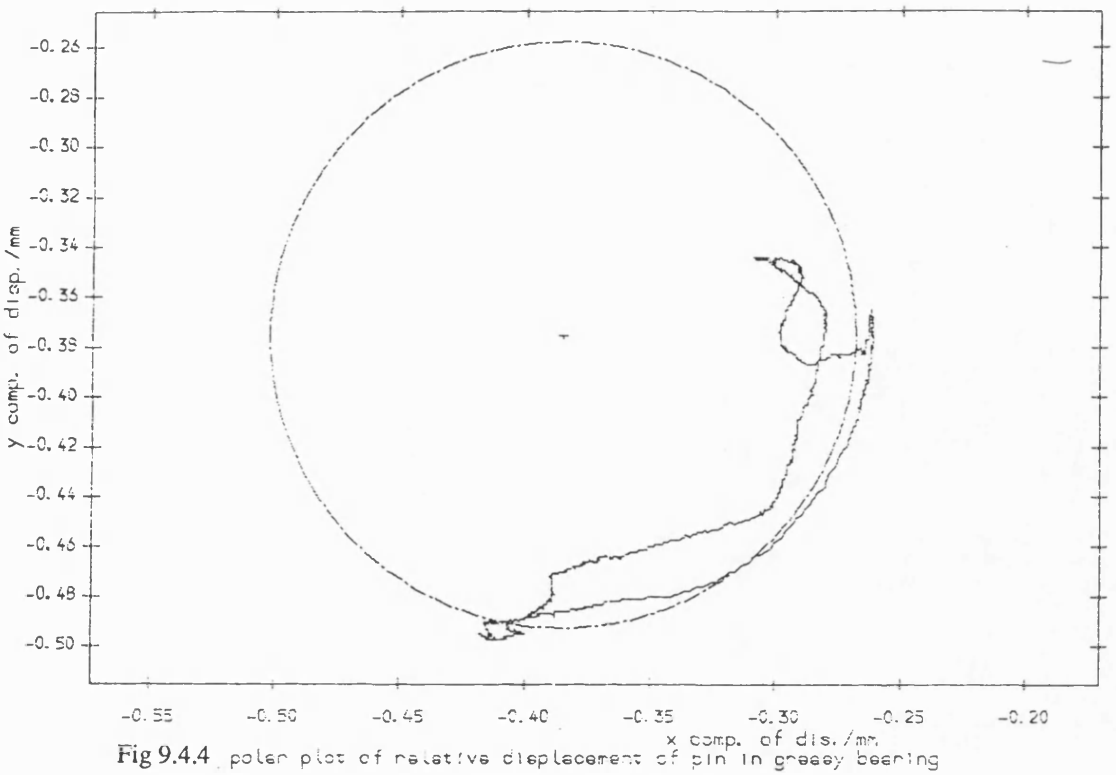

Fig 9.4.4 polar plot of relative displacement of pin in greasy bearing
With flywheel mean speed = 122.5 (rev/min) d.clea. =.25mm

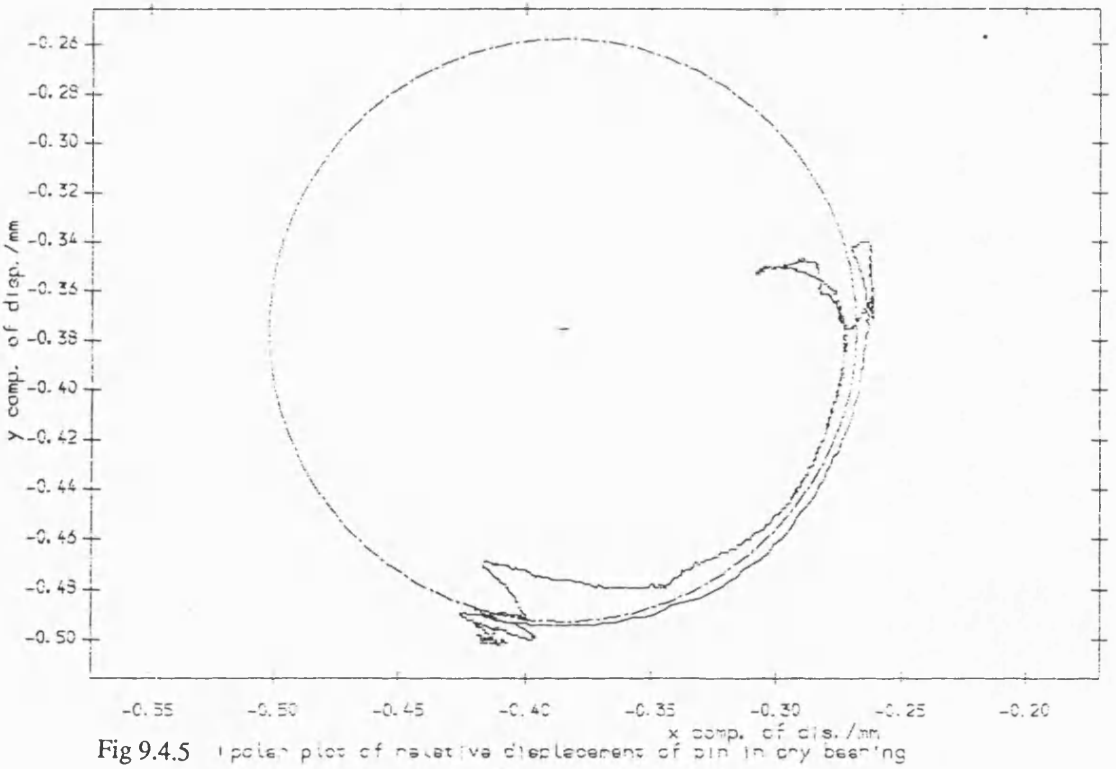

Fig 9.4.5 polar plot of relative displacement of pin in dry bearing
With flywheel mean speed = 122.5 (rev/min) d.clea. =.25mm

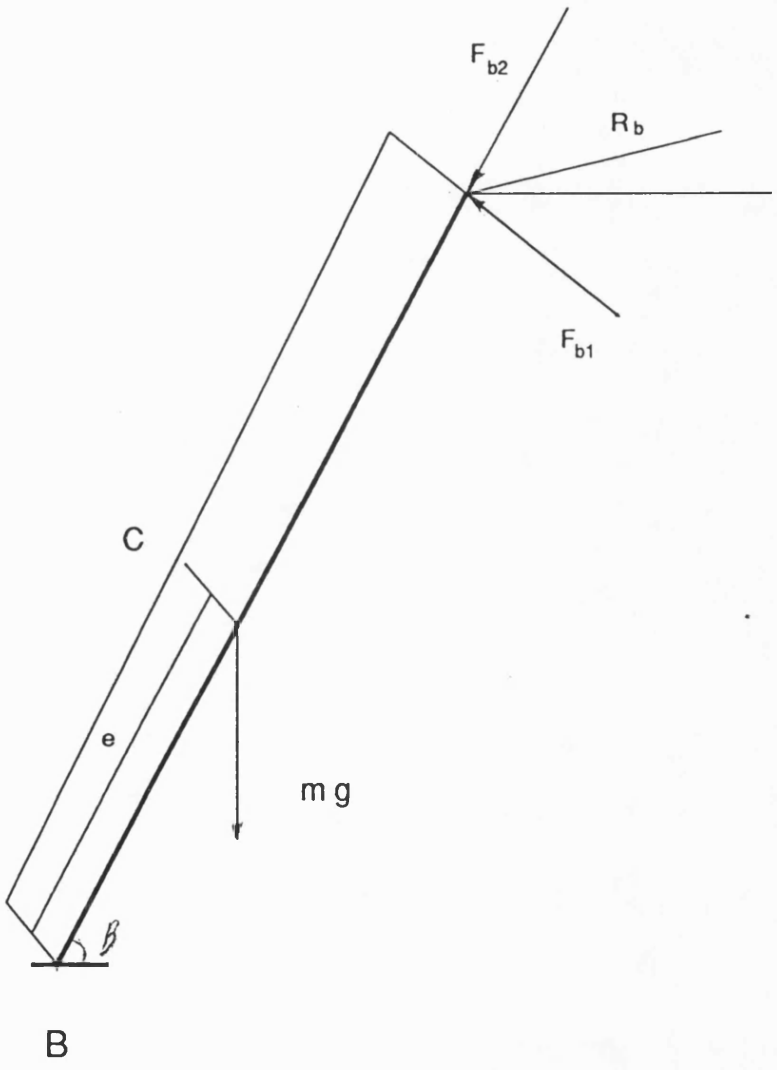

Fig 9.6.1 Follower free body diagram

CHAPTER 10
LONG TERM PIN BEHAVIOUR

This is important since wear will be governed not by a single cycle but by longer term running. Long term motion of the pin in the bearing was studied to find the extent to which motion is aperiodic, since this will affect the wear pattern.

Periodic motion would concentrate wear in a narrow region, while if the long term motion is aperiodic, or even chaotic, wear will be distributed.

10.1 Pin path and impact (5-10 cycles)

Firstly the record of the pin motion for five consecutive cycles was taken for input speed of 244 rev/min - see fig(10.1.1 and 10.1.2). Two minutes later another five cycles were recorded see fig(10.1.3 and 10.1.4).

The crank positions at which pin jump and fall occurred were similar even in cycles well separated (about 500 apart). When pin jumps and falls occur at the same crank angles for different cycles the free flight and impact follow the same pattern. The predicted pin motion were also similar for different cycles - see fig(10.1.5).However there are small differences between the oscillations after pin jumps.

Similarity of the pin jump length , starting point(separation point) and end point(landing point) on different cycles suggests that the impact over a period of running occurs at bush angles within a certain range.

The impact over 5 cycles was studied in the theoretical model for an input speed of 244 rev/min.

(1) The size of the primary impacts is much the same from cycle to cycle (see fig 10.1.6 where the value of max impact is about 0.06 Nms).

(2) Smaller secondary impacts(not plotted) are not quite so similar from cycle to cycle.

(3) The bush angle at which impact occurs is plotted versus crank angle in fig 10.1.7. The bush angle at which the impact occurs in the first region alters from cycle to cycle, but varies over a modest range of bush angle from 80° to 100°. However that in the second region varies over a larger range (-60° to -110°).

At lower speed(168 rev/min) the bush angle at which the impact in the first region occurs, varies mostly within a wider region than at 244 rev/min - see fig(10.1.8). However impacts in the second are concentrated in a 10° band around -100°.

10.2 Longer term running(impact and wear pattern)

Since wear is not evident after only a few cycles the rig was left running at 206 and 244 rev/min for an hour. For higher speed of 290 rev/min running time was decreased to half an hour to produce comparable number of cycles. The roundness chart of the bushes before and after running were recorded.

There are two bushes in the bearing which are described as front and back. If one stands in front of the rig the bush which is closer is called 'front' and the other one 'back'. The fact that the 'front' and 'back' bushes wear differently indicates pin misalignment. Predicted total impulse agrees better with measured wear on the front bush rather than that in the back one. Removing the bushes sometimes produces deformation

The result of the theoretical model for impact and bush angle was studied for a 85 cycle simulation. This simulates only about 25 seconds of real time running, but longer predictions were not possible as each 85 cycles takes ten hours or more.

Because of the very small dimensions involved , impacts were grouped into 5° bands of bush angle (this is only 0.5mm of bush circumference). It was evident that the number of predicted impacts is concentrated in one region of the bush - see fig (10.2.1 and 10.2.2). In the first region the distribution is double peaked but this might in fact be due to the small sample size(85 cycles) - the dip is caused by just one point. Longer term simulation(which is not practical) might well indicate a normal type of

distribution.

The distribution for the second region (fig 10.2.2) in the nfw case is also concentrated in a narrow range. However the wfw case indicates a double peaked distribution. This is likely to be genuine since there is a wide separation (35° bush angle, i.e 6 points) between peaks.

What matters from a wear point of view is total impulse see fig(10.2.3 to 10.2.8). The total impact distribution is also concentrated in one region of the bush. The bush angle at which the distribution peak occurs is close to the angle predicted for impact on the first few cycles - see fig(10.2.3 to 10.2.8).

(1) In the wfw case the width of the total impact peak is evidently smaller than that in the nfw case.

(2) The peak value of the distribution increases with speed particularly in the second region.

(3) The width of the peak in both cases(wfw & nfw)decreases with speed.

(4) The mean of the distribution of the number of impact is close to that of the total impact distribution - see fig(10.2.1,10.2.2 , 10.2.5a and 10.2.6a). The fact that the mean of the total impact distribution is close to that of the number of impact indicates that the larger impacts at any rate are of similar magnitude from cycle to cycle.

(5) The agreement between the predicted impact pattern and the experimental recorded roundness measurement (Talyrond) charts varies from case to case, but in several cases is reasonably close(see below) - see fig (10.2.9 to 10.2.14). The max wear region is close to the landing point of pin flight in the displacement polar plots, and to the peak of predicted total impact

(6) The total impact distribution indicates the major effect is from the primary impulse - see fig(10.2.5a to 10.2.6b). The rebounds have little effect on the distribution shape and therefore on the wear pattern.

comparison of the total impact distribution and wear pattern

For input speed of 290 rev/min fig(10.2.7 and 10.2.8) with fig (10.2.13) and 10.2.14) are compared. Predicted impacts for the two cases(wfw & nfw) are plotted on the same graph for region 1 (fig 10.2.7) and region 2 (fig 10.2.8); wfw wear is shown in fig 10.2.13. Wear in nfw case is shown in fig 10.2.14.

There are two regions of wear, the first one centred at a bush angle of 90° the second one centred at -85°. These are angles at which the predicted total impact peaks - see fig(10.2.7 and 10.2.8). Measured wear has similar pattern to the predicted total impact plot - see fig (10.2.7 and 10.2.8).

The wear pattern in region 1 is wider than the theoretical result predicted. However the wear pattern in region 2 is closer to that of the predicted total impact.

There are irregularities in the wear pattern indicating that impact wear is not a smooth process. This causes not only micro-craters due to plastic deformation but also local build up or protrusions.

In the nfw case peak total impact is predicted is less than for wfw case but has a wider distribution. The experimental wear trace (Talyrond) is in reasonable agreement - see fig (10.2.7 , 10.2.8 and 10.2.14).

For input speed of 244 rev/min the impact pattern for the second region fig(10.2.6) and wear pattern (fig 10.2.11 and 10.2.12) are more apparent than the first region. In the second region of the wfw case the predicted total impact peak is around -100°. The wear pattern peak is around -120°. In the wfw case the wear pattern peak is around -105° which is close to the peak in the predicted total impulse distribution-110°. Nevertheless the mean of the impact distribution is closer to the wear pattern peak. In the wear pattern in the wfw case(fig 10.2.12) it seems there is plastic deformation as well as wear so that the surface is not smooth.

For an input speed of 206 rev/min the wear pattern in the second region in wfw case(fig 10.2.5) is concentrated at around -90°. The peak of the predicted impact

pattern is in fact around -98 ° which is not far removed from the wear peak.

In the nfw case as predicted(fig 10.2.3 and 10.2.4) wear pattern(fig 10.2.10) is distributed over a wider range than in wfw case.

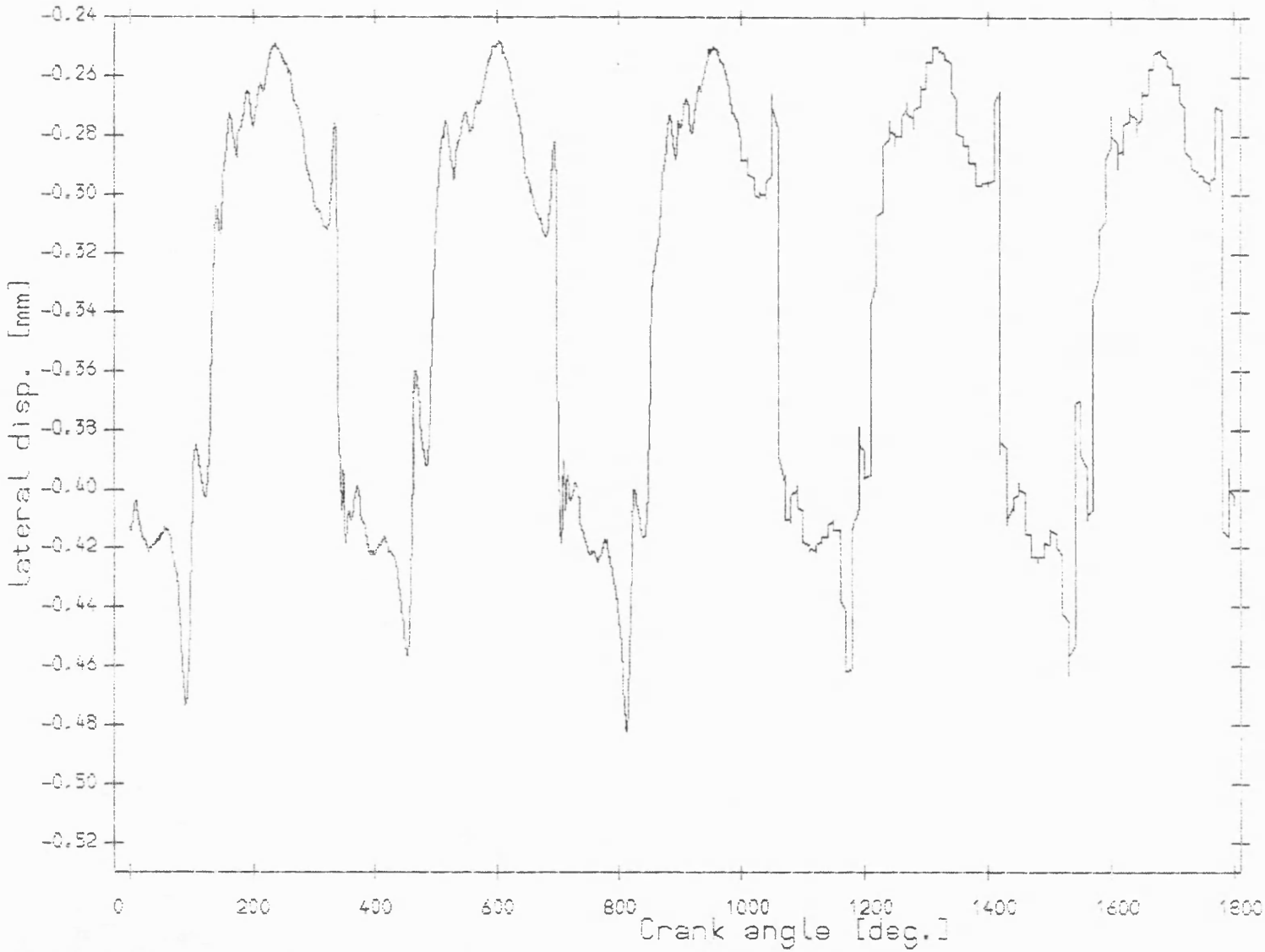

Fig 10.1.1 results lateral pin disp. relative to bush, t=0
with fly wheel, mean speed=244 rev/min, dia. clearance=.25mm

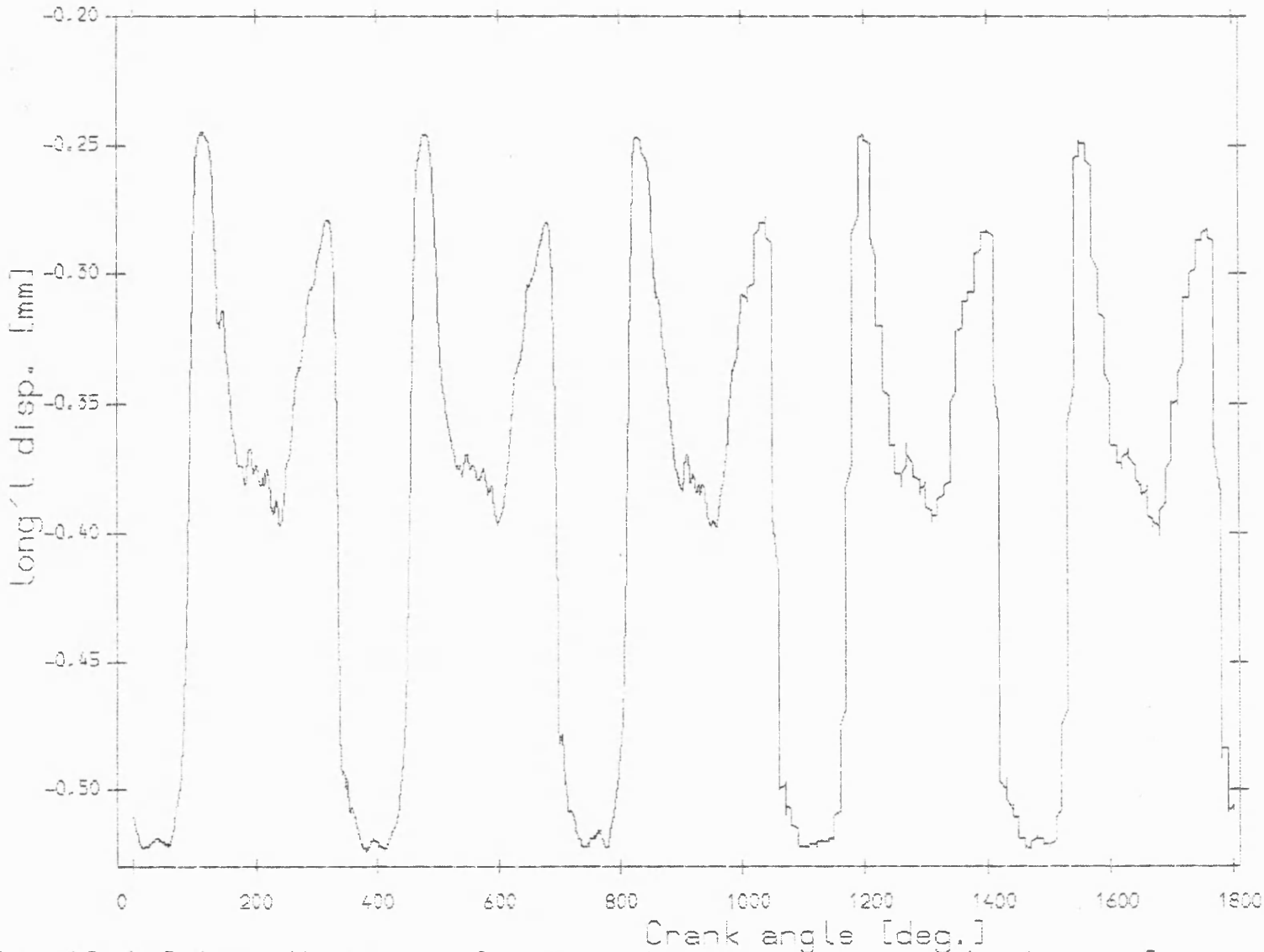

Fig 10.1.2 Long'l disp. of pin relative to greasy bush , t=0
with flywheel , mean speed=244 rev/min, dia. clearance=.25mm

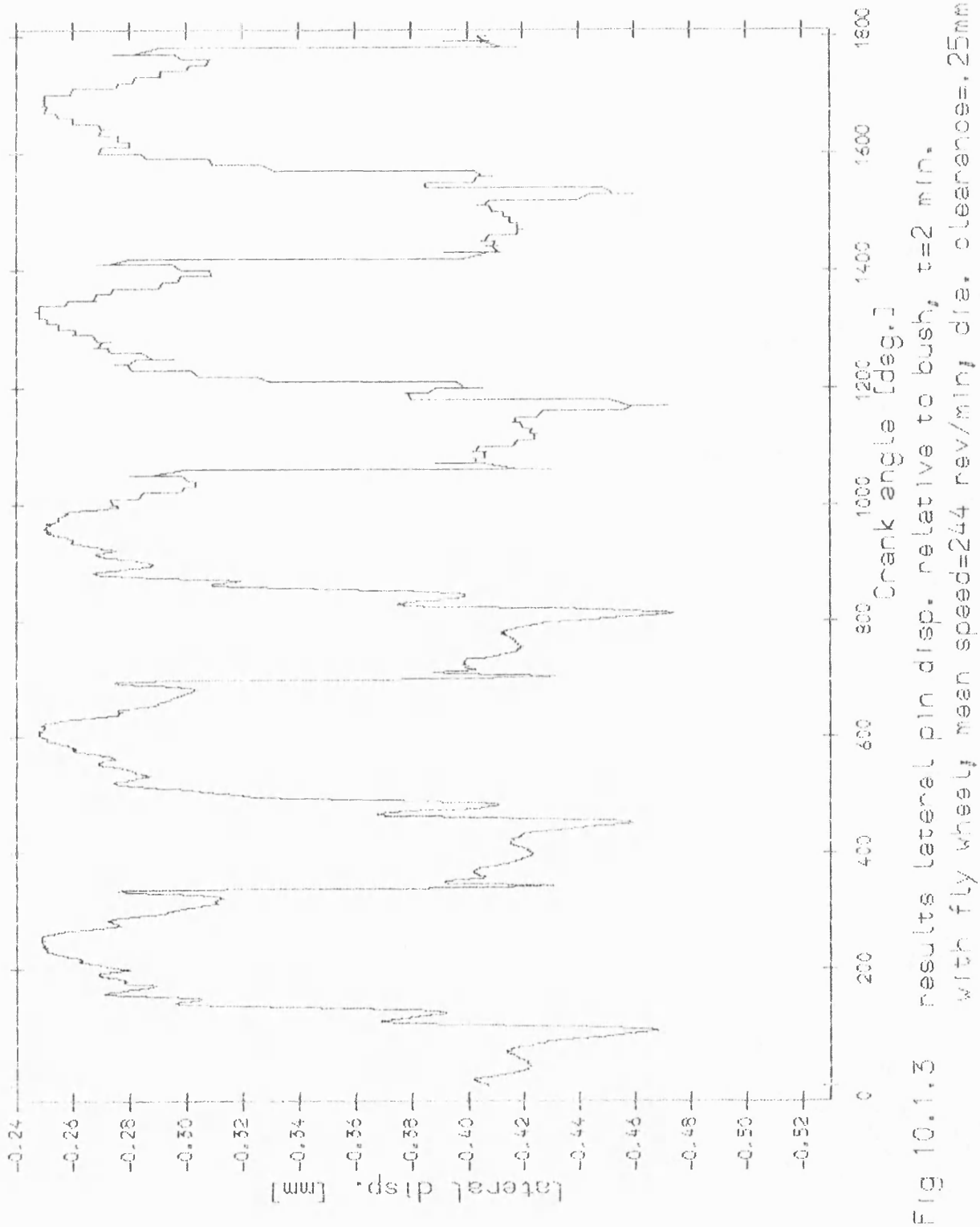

Fig 10.1.3 results lateral pin disp. relative to bush, t=2 min.
with fly wheel, mean speed=244 rev/min, dia. clearance=.25mm

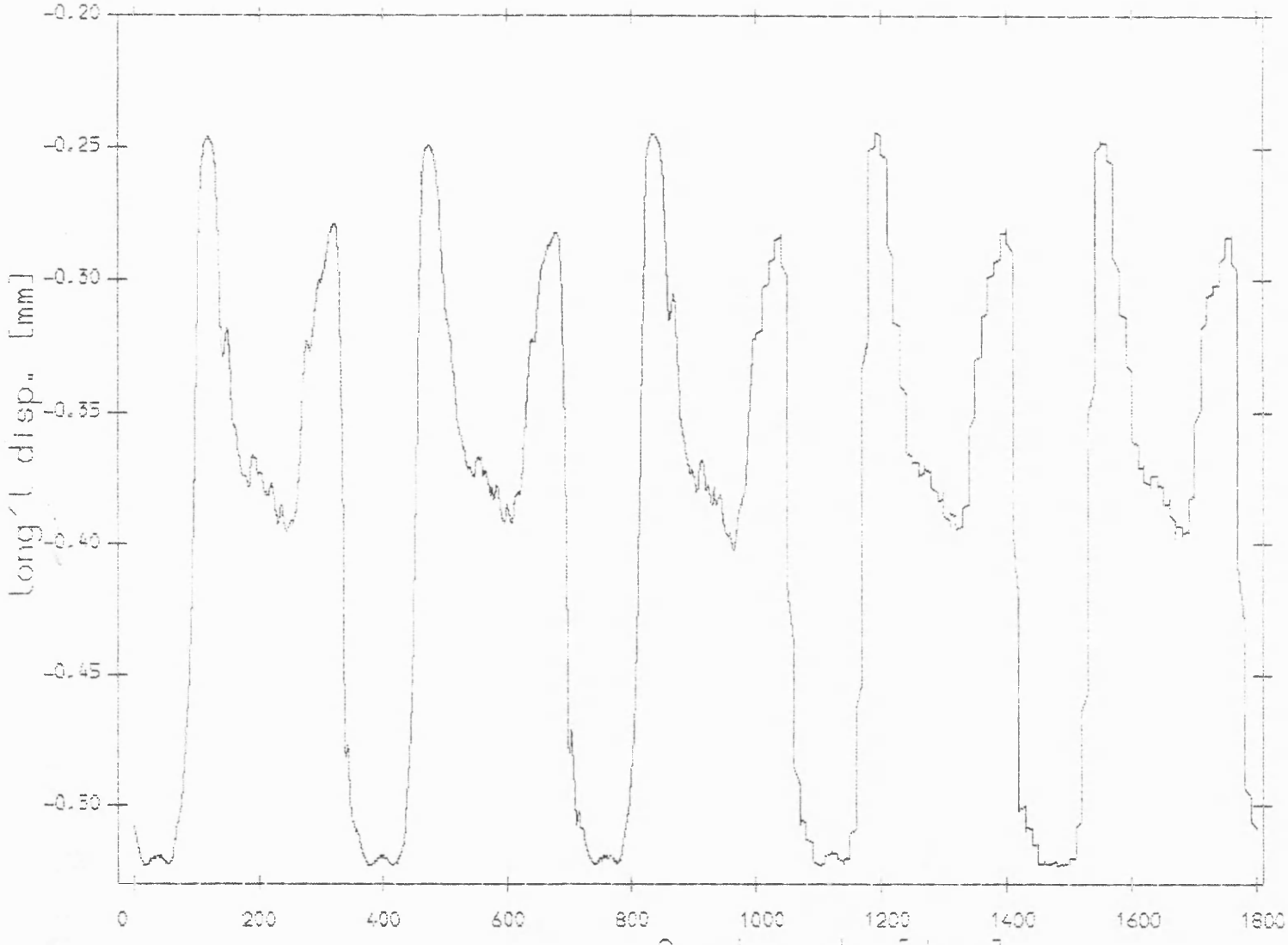

Fig 10.1.4 Long'l disp. of pin relative to greasy bush , t=2 min. with flywheel , mean speed=244 rev/min, dia. clearance=.25mm

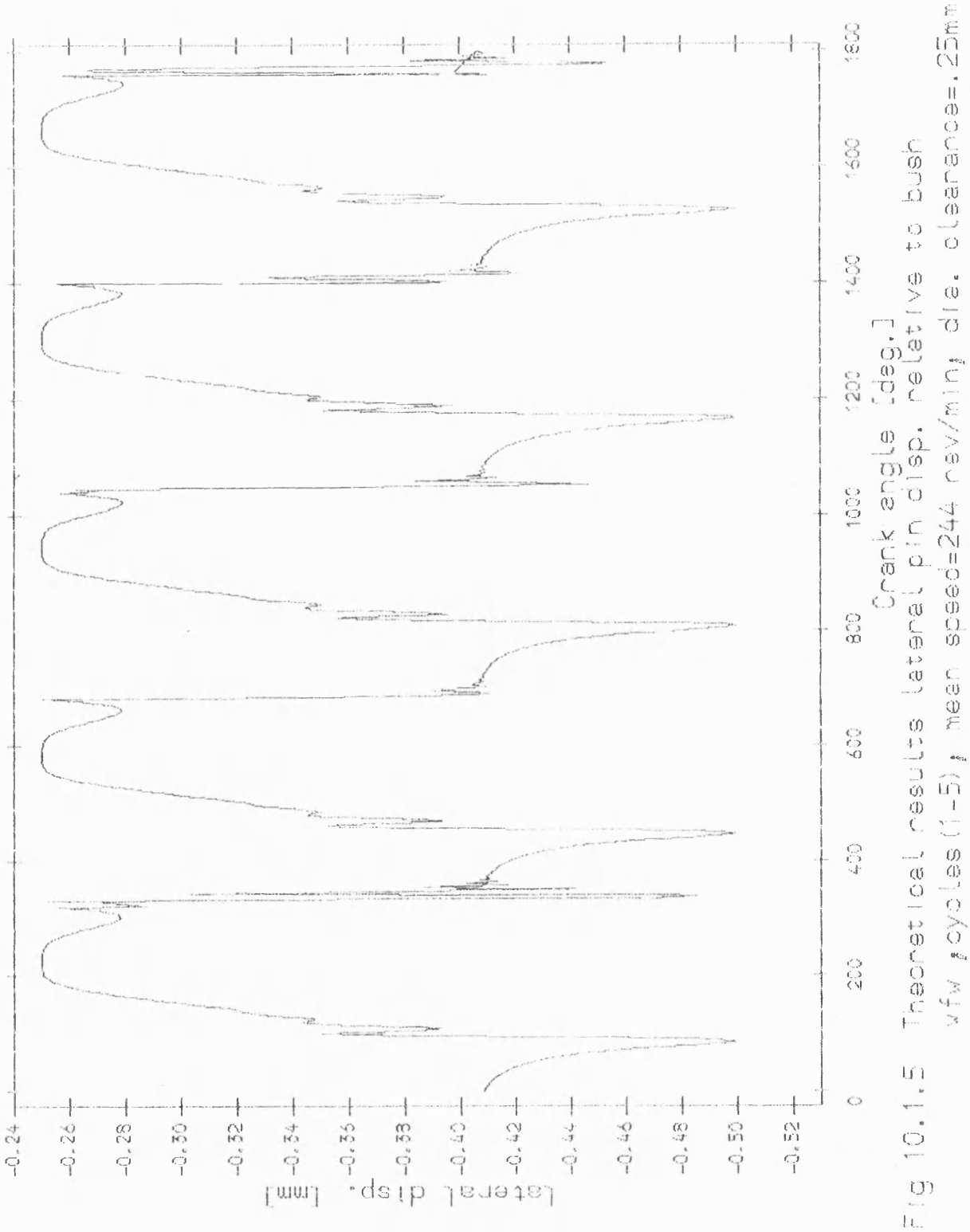

Fig 10.1.5 Theoretical results lateral pin disp. relative to bush
wfw cycles (1-5), mean speed=244 rev/min, dia. clearance=.25mm

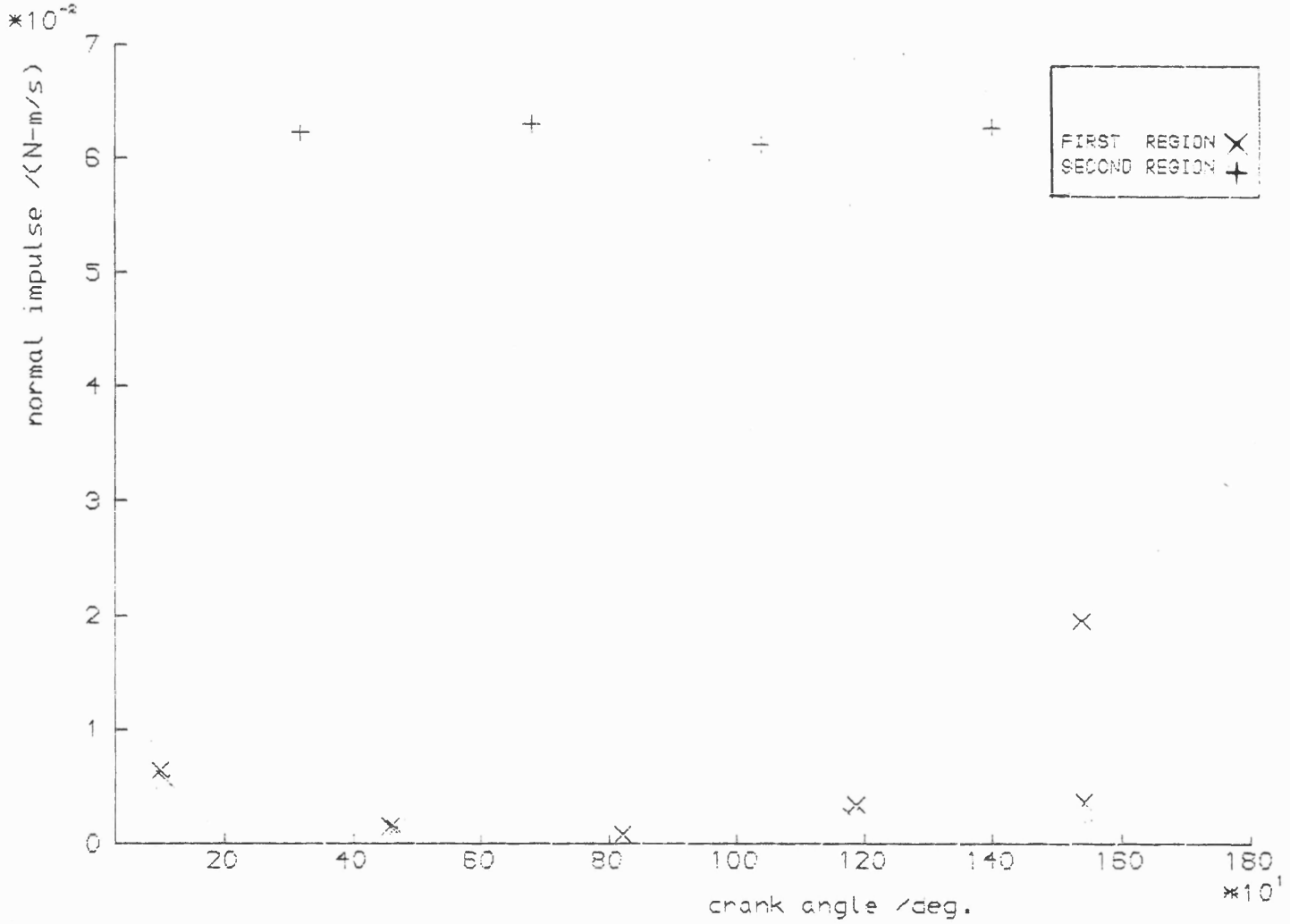

Fig 10.1.6 Impulse normal to bearing; mean speed=244 rev/min; wfw cycles 10-15

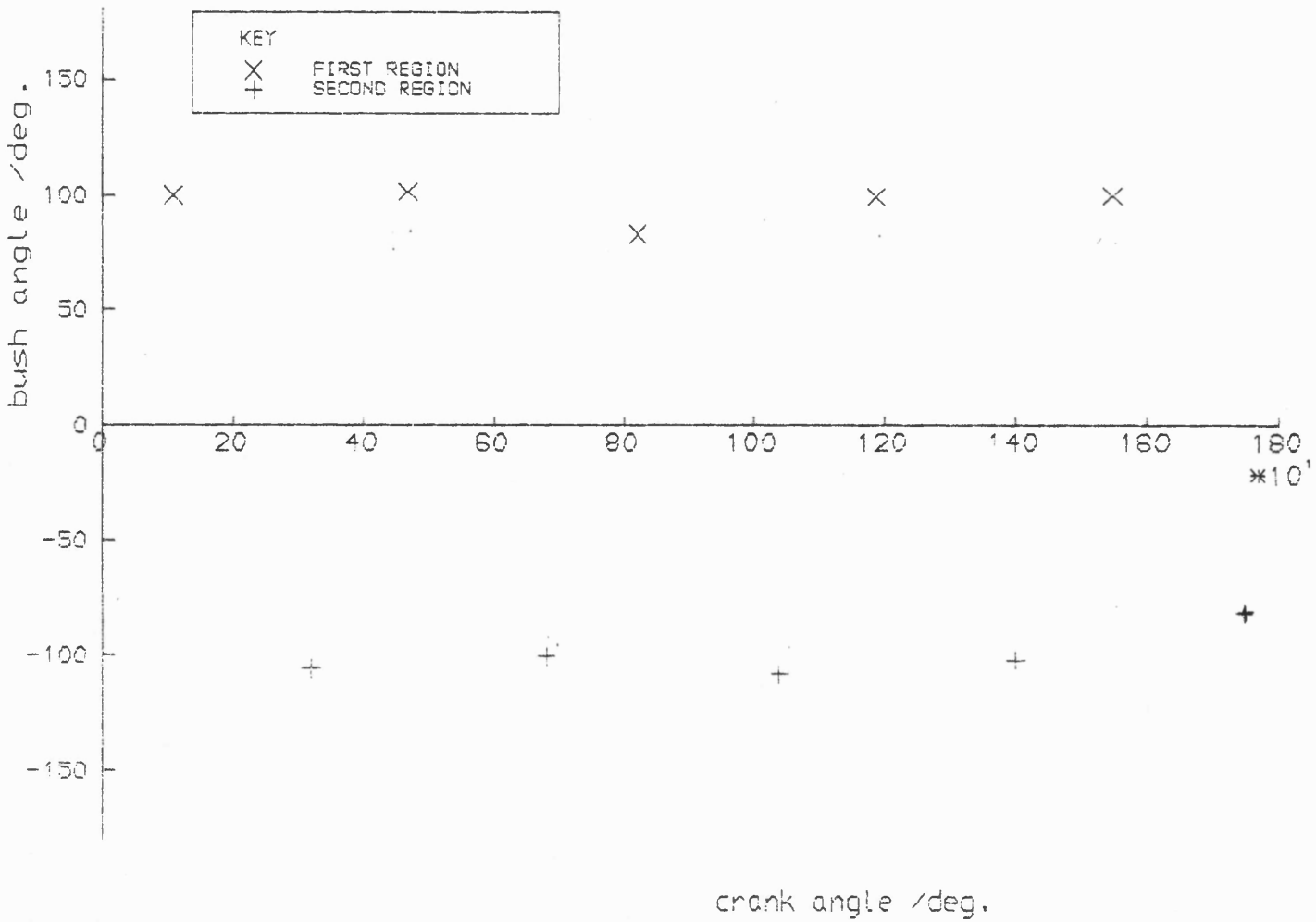

Fig 10.1.7 Angle of impulse line action , mean speed 244 rev/min ; wfw cycles 10-15

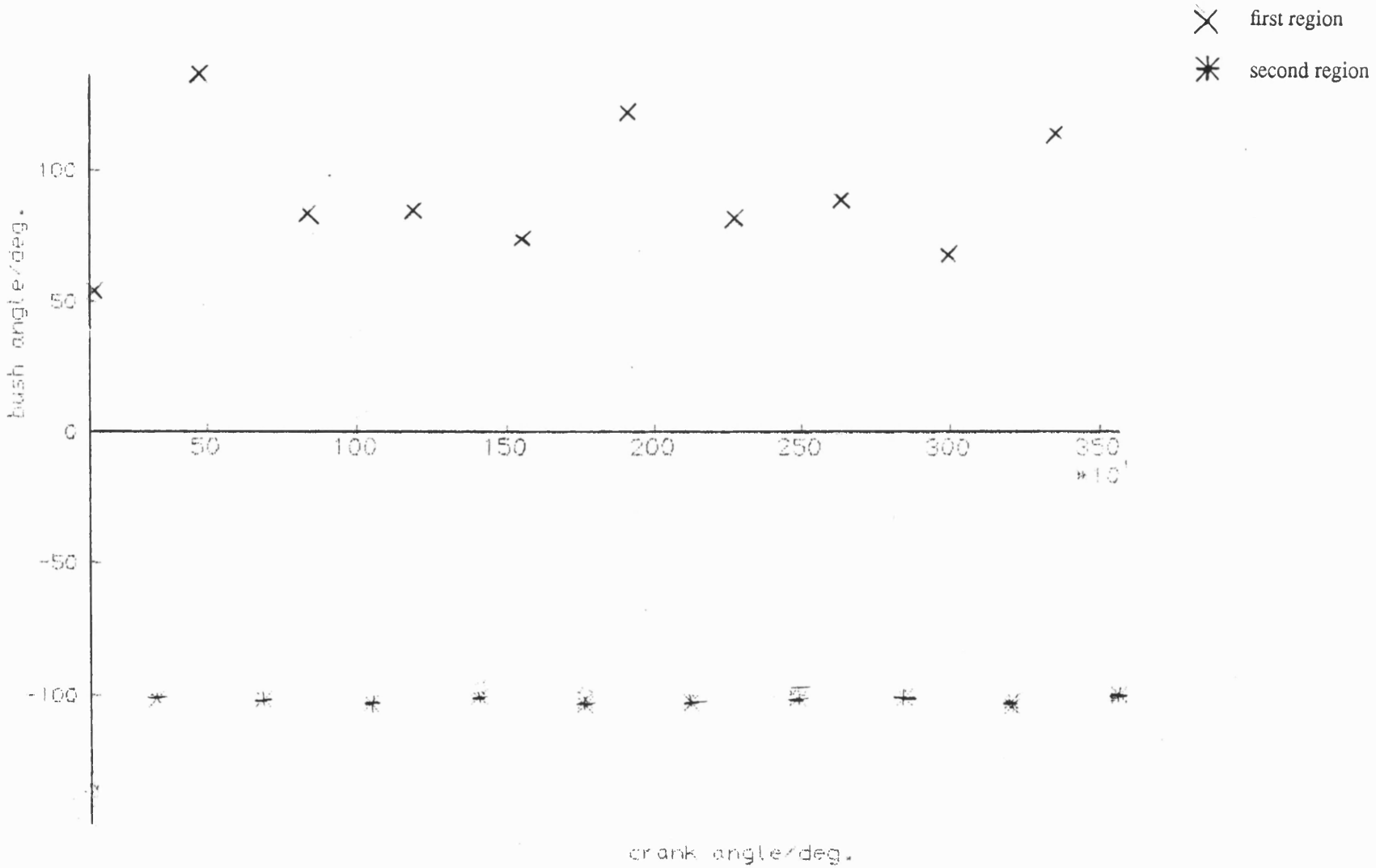

Fig 10.1.8 Impulse action line angle; n speed=168rev/min; d.clea=.25mm

Fig 10.2.1 Impulse number in first region for 85 cycles

Mean speed 244 rev/min ; dia. clearance 0.25mm

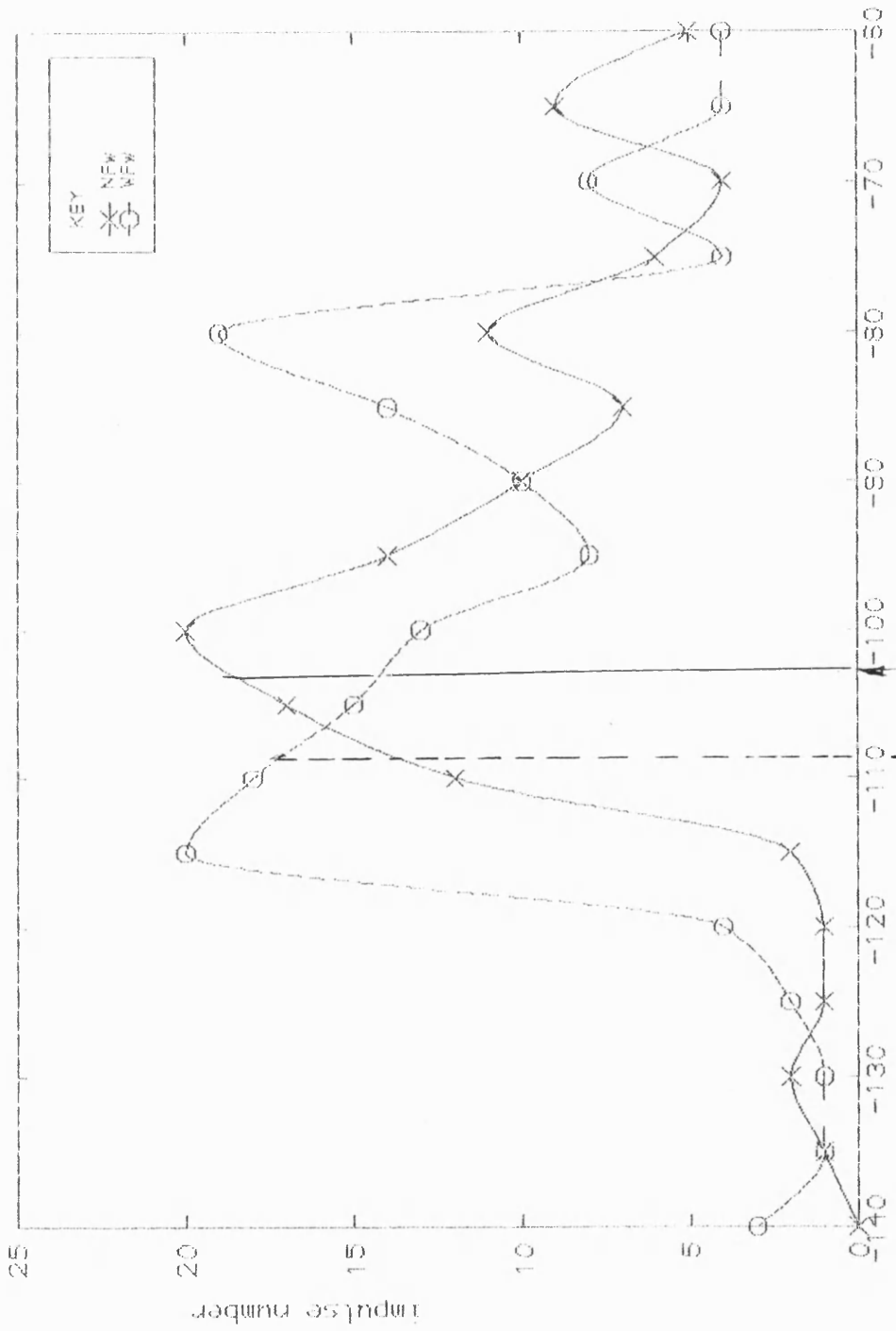

Fig 10.2.2 Impulse number in second region for 85 cycles
mean speed 244 rev/min ; dia. clearance 0.25mm

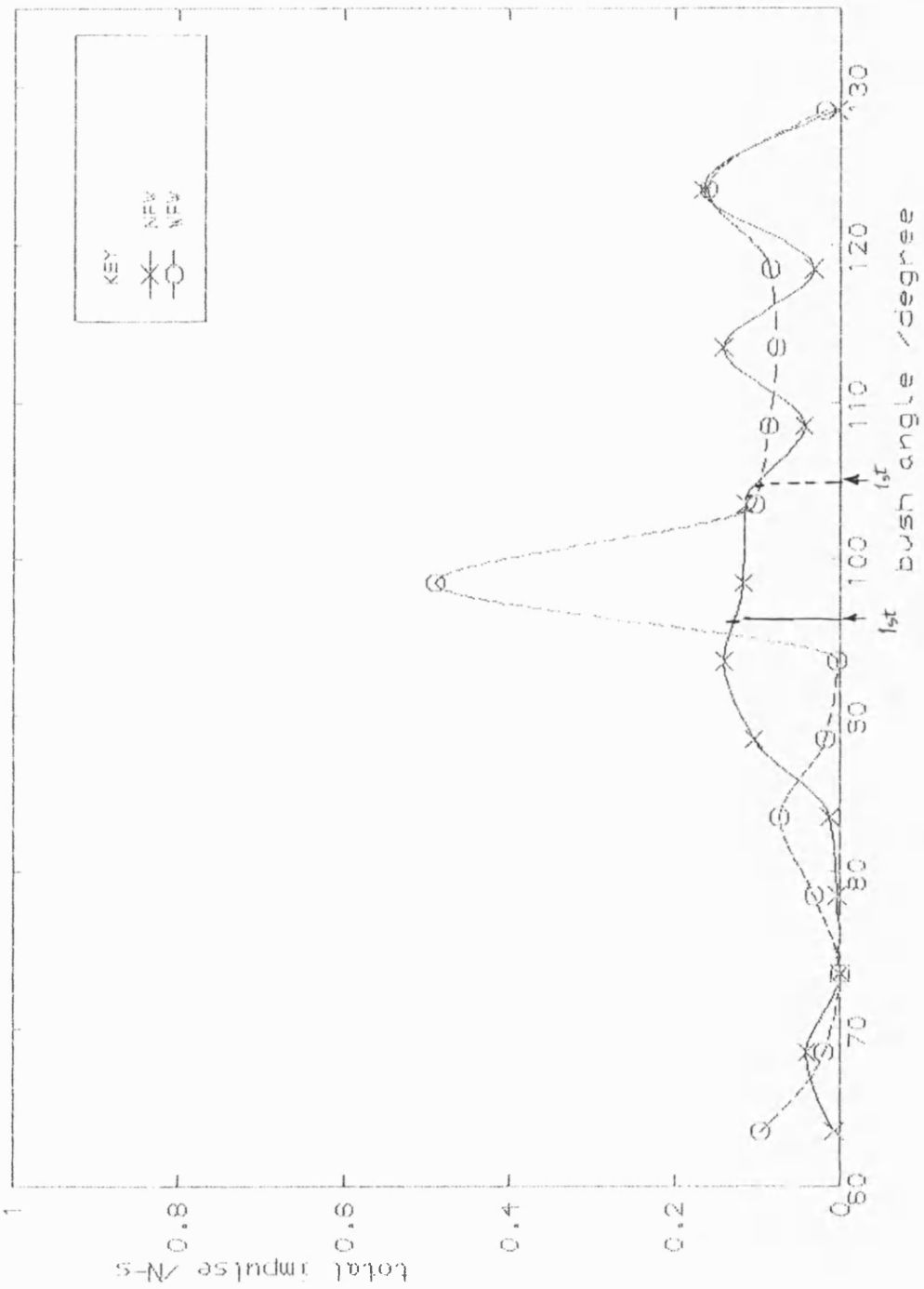

Fig 10.2.3 Predicted total impulse in first region for 25 cycles
mean speed 206 rev/min ; dia. clearance 0.25mm

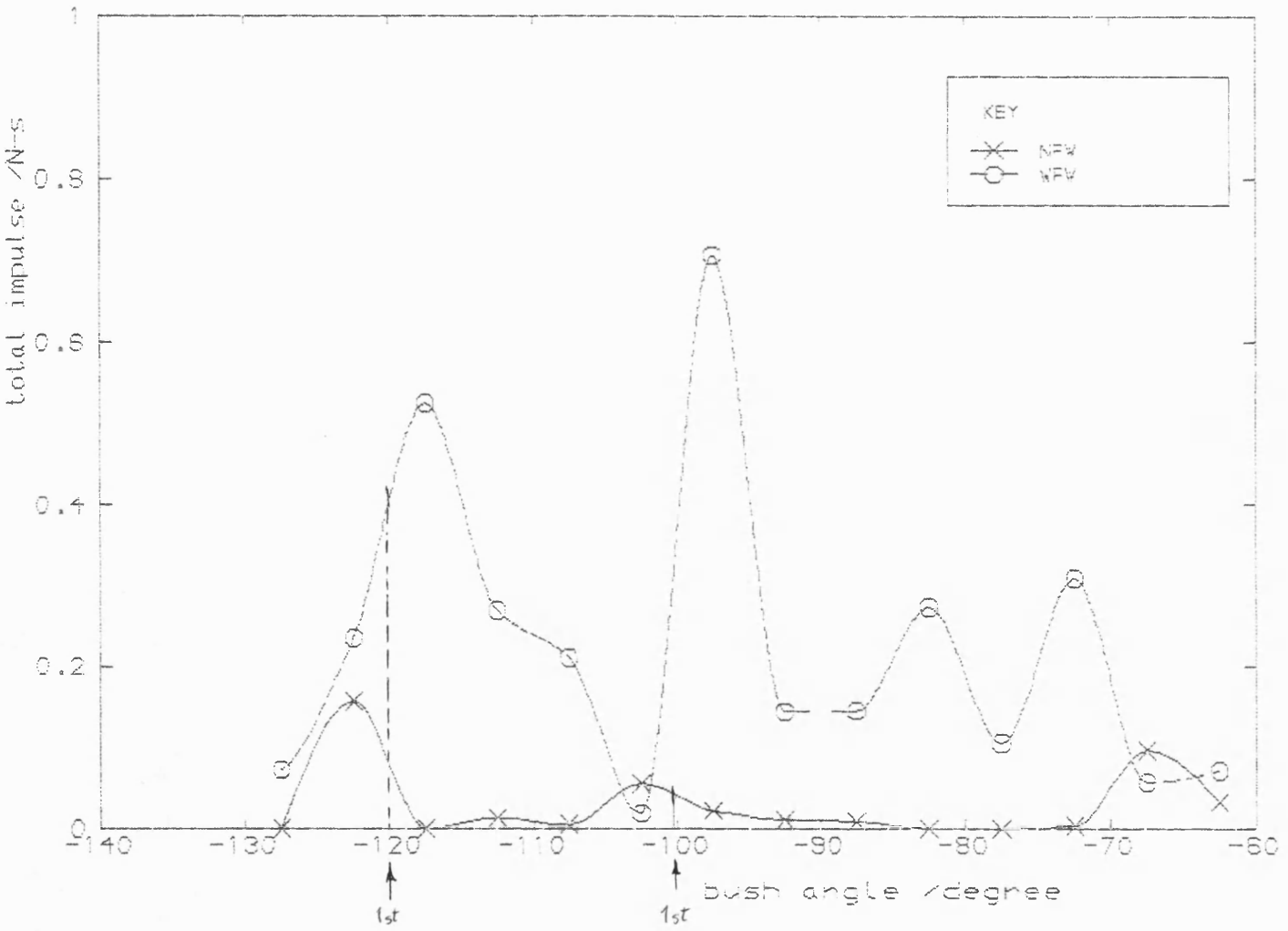

Fig 10.2.4 Predicted total impulse in second region For 25 cycles mean speed 206 rev/min ; dia. clearance 0.25mm

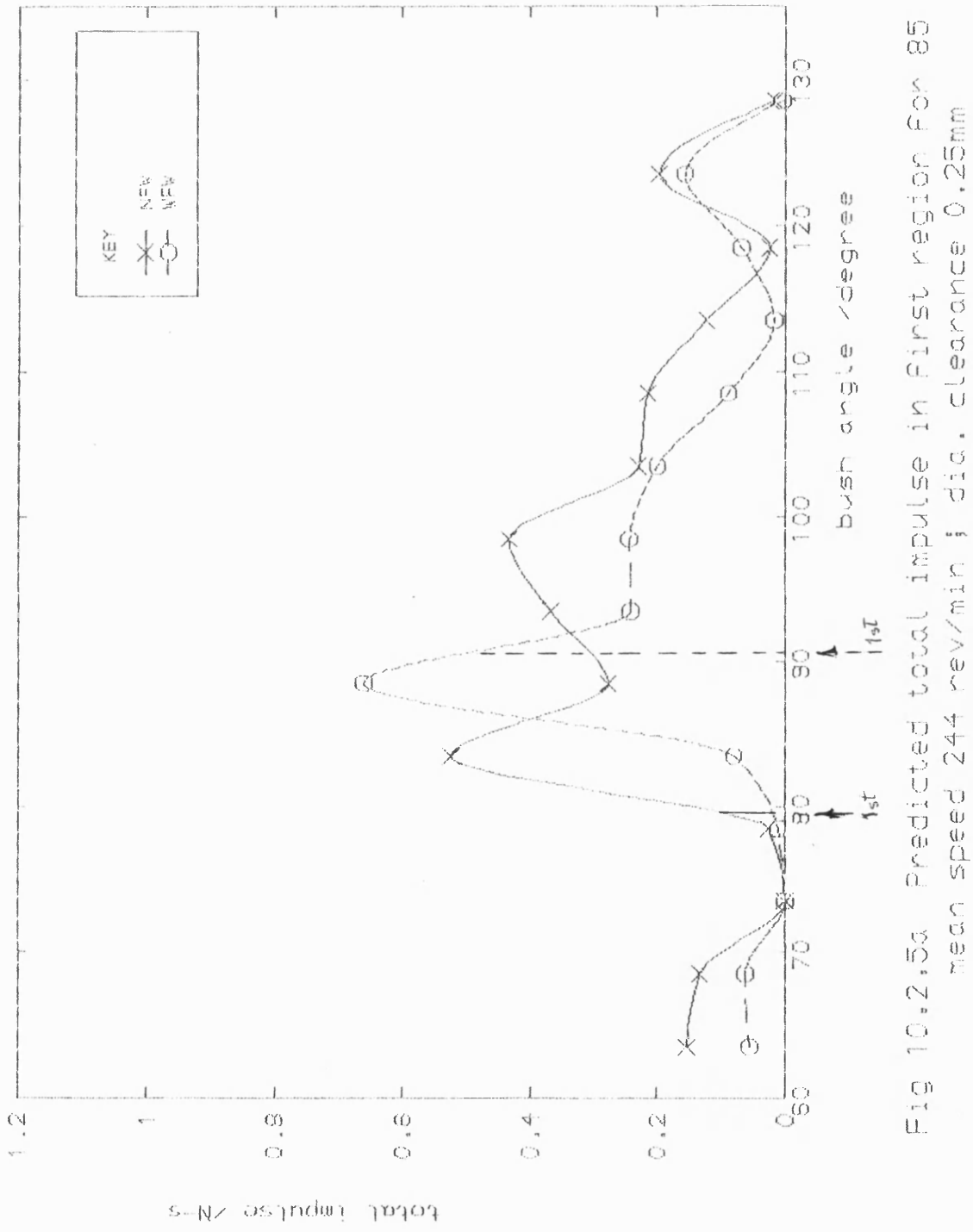

Fig 10.2.5a Predicted total impulse in first region for 85 cycles
mean speed 244 rev/min ; dia. clearance 0.25mm

Fig 10.2.5b Predicted total impulse in first region for 85 cycles
Mean speed 244 rev/min ; dia. clearance 0.25mm; no rebound

Fig 10.2.6a Predicted total impulse in second region for 85 cycles

Mean speed 247 rev/min ; dia. clearance 0.255m

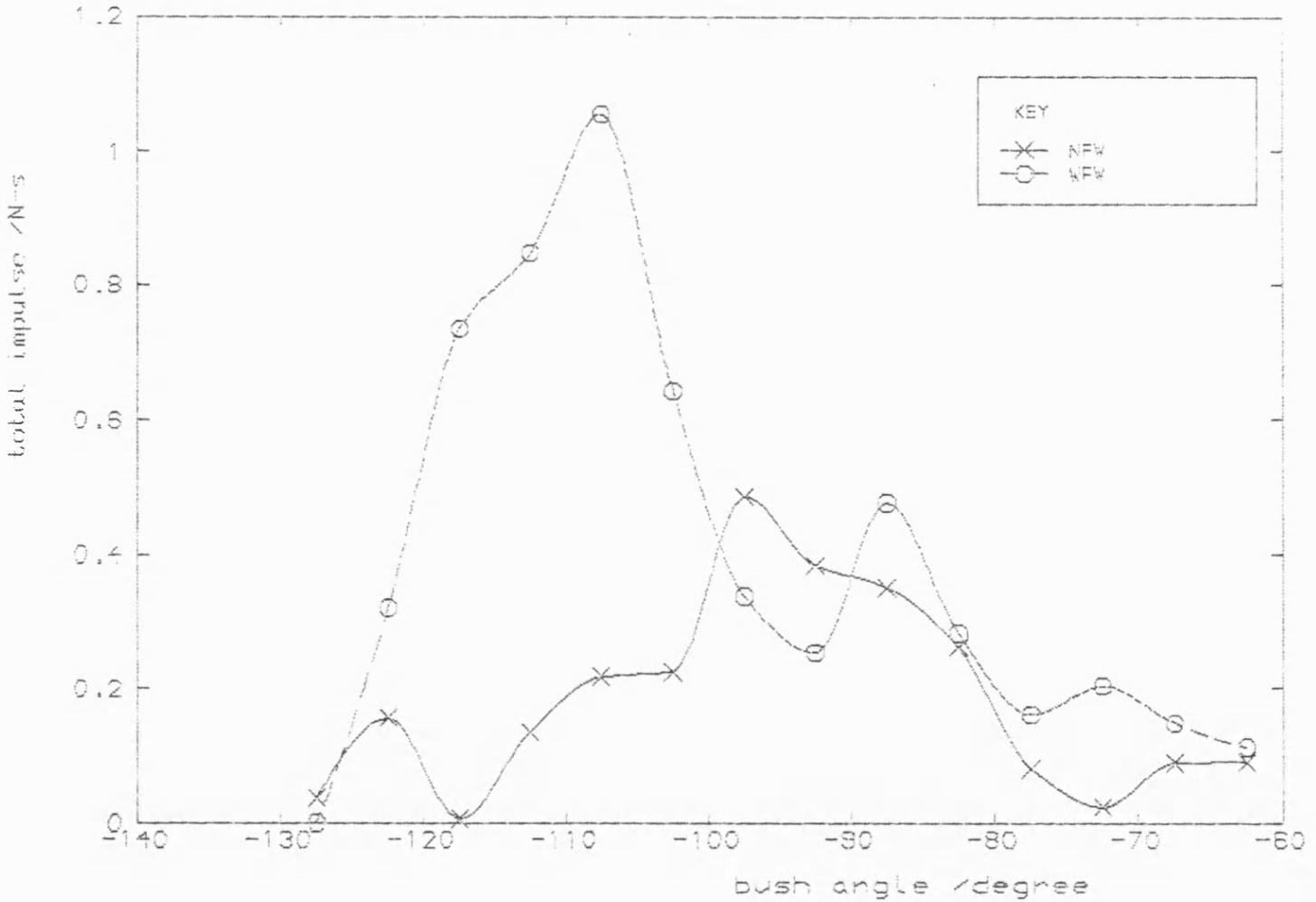

Fig 10.2.8b Predicted total impulse in second region for 85 cycles mean speed 244 rev/min ; dia. clearance 0.25mm ; no rebound

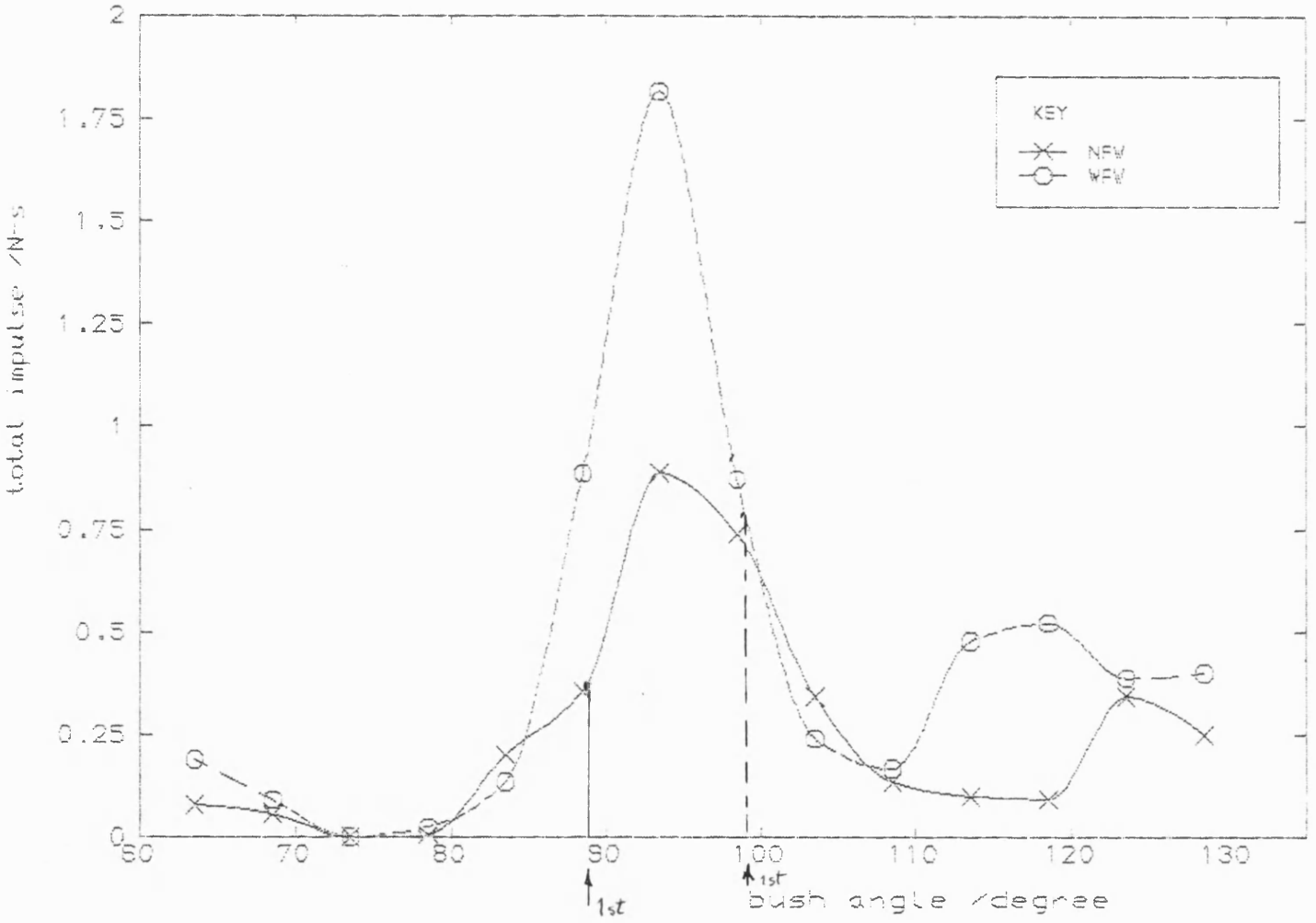

Fig 10.2.7 Predicted impulse in first region for 85 cycles mean speed 290 rev/min ; dia. clearance 0.25mm

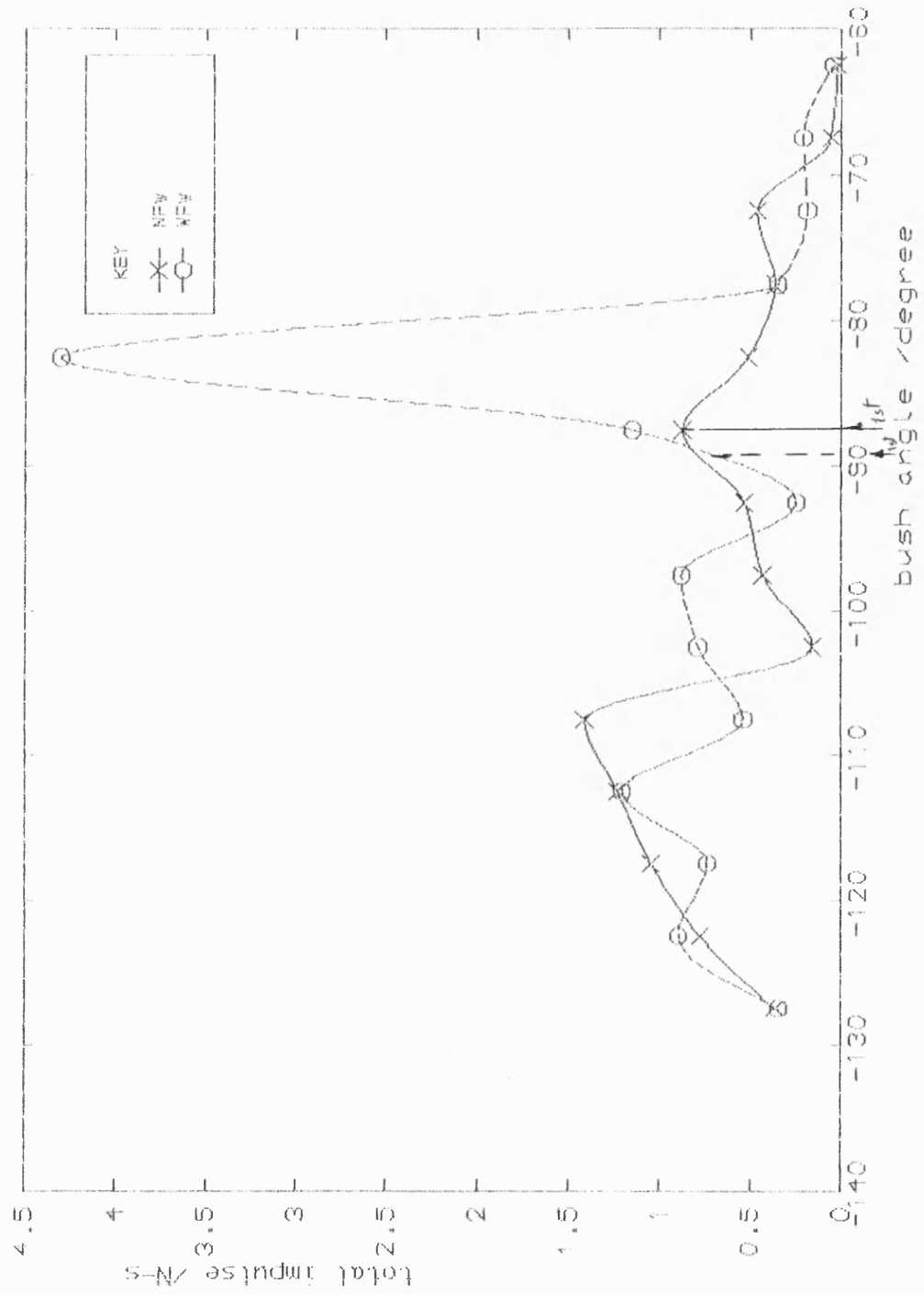

Fig 10.2.8 Predicted total impulse in second region for 85 cycles
mean speed 290 rev/min ; dia. clearance 0.25mm

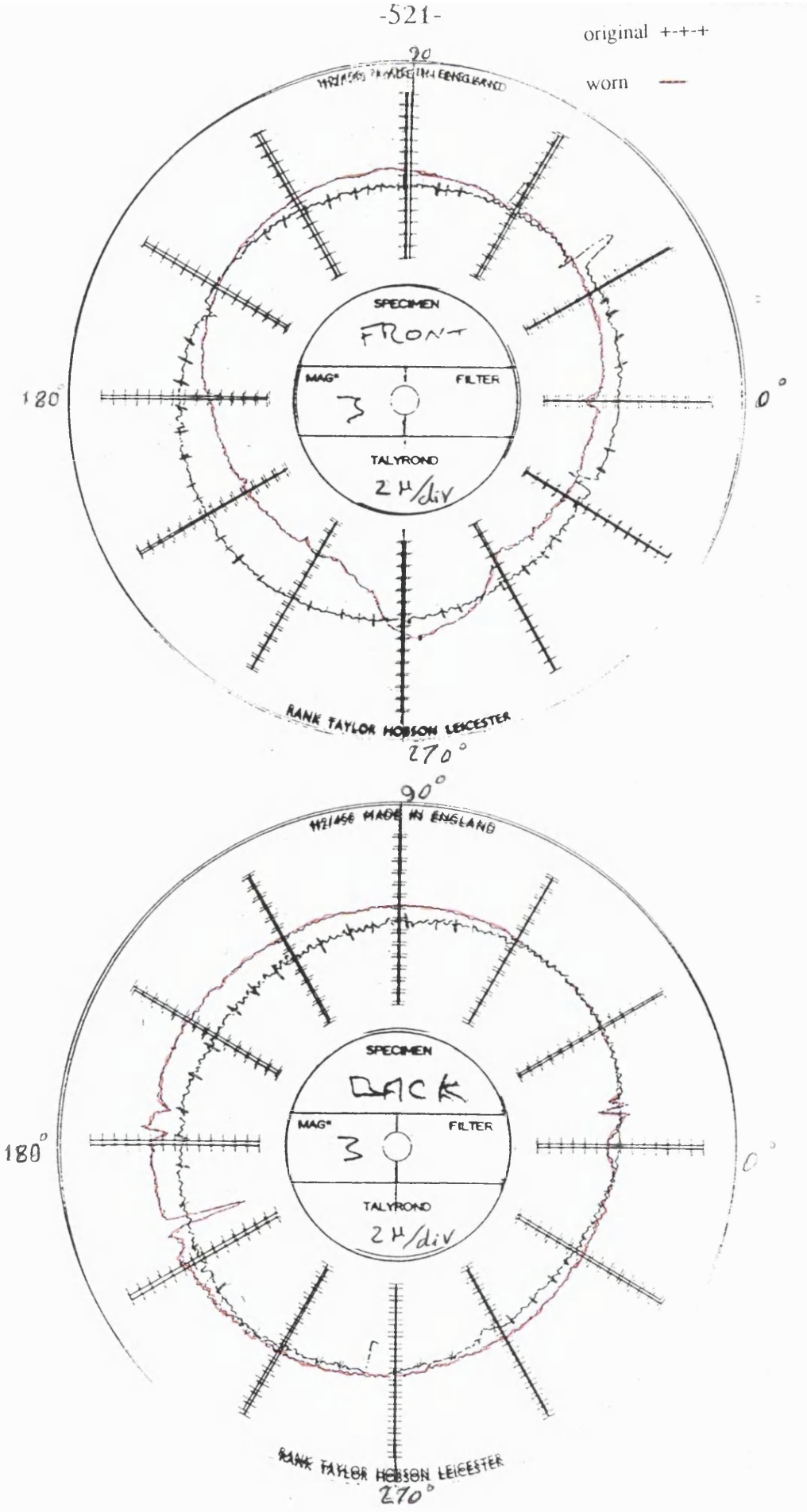

Fig 10.2.9 Bush roundness , mean speed 206 rev/min; with fly wheel

1 hr running ; dia. clearance 0.25mm

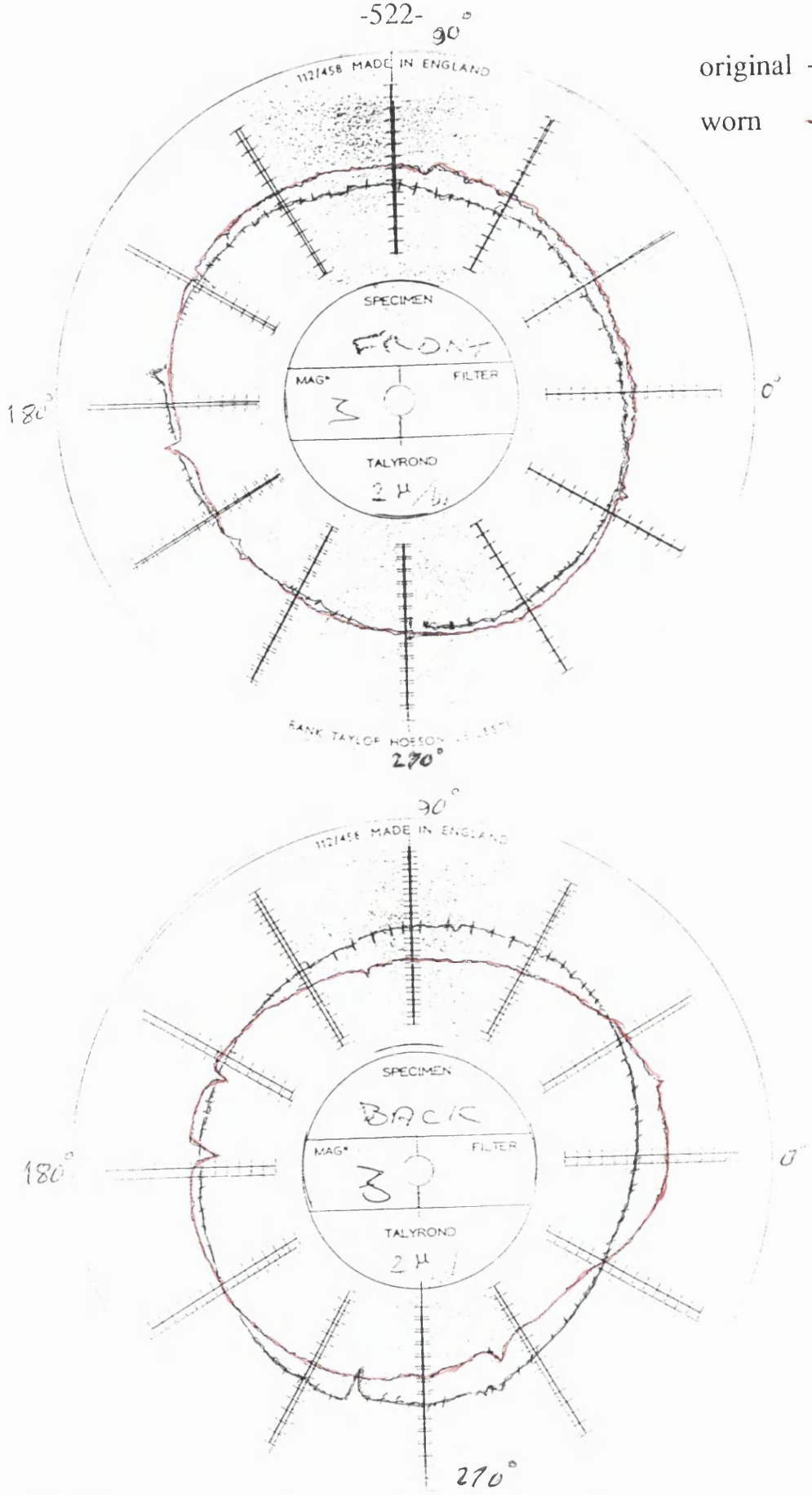

Fig 10.2.10 Bush roundness , mean speed 206 rev/min; no fly wheel
1 hr running ; dia. clearance 0.25mm

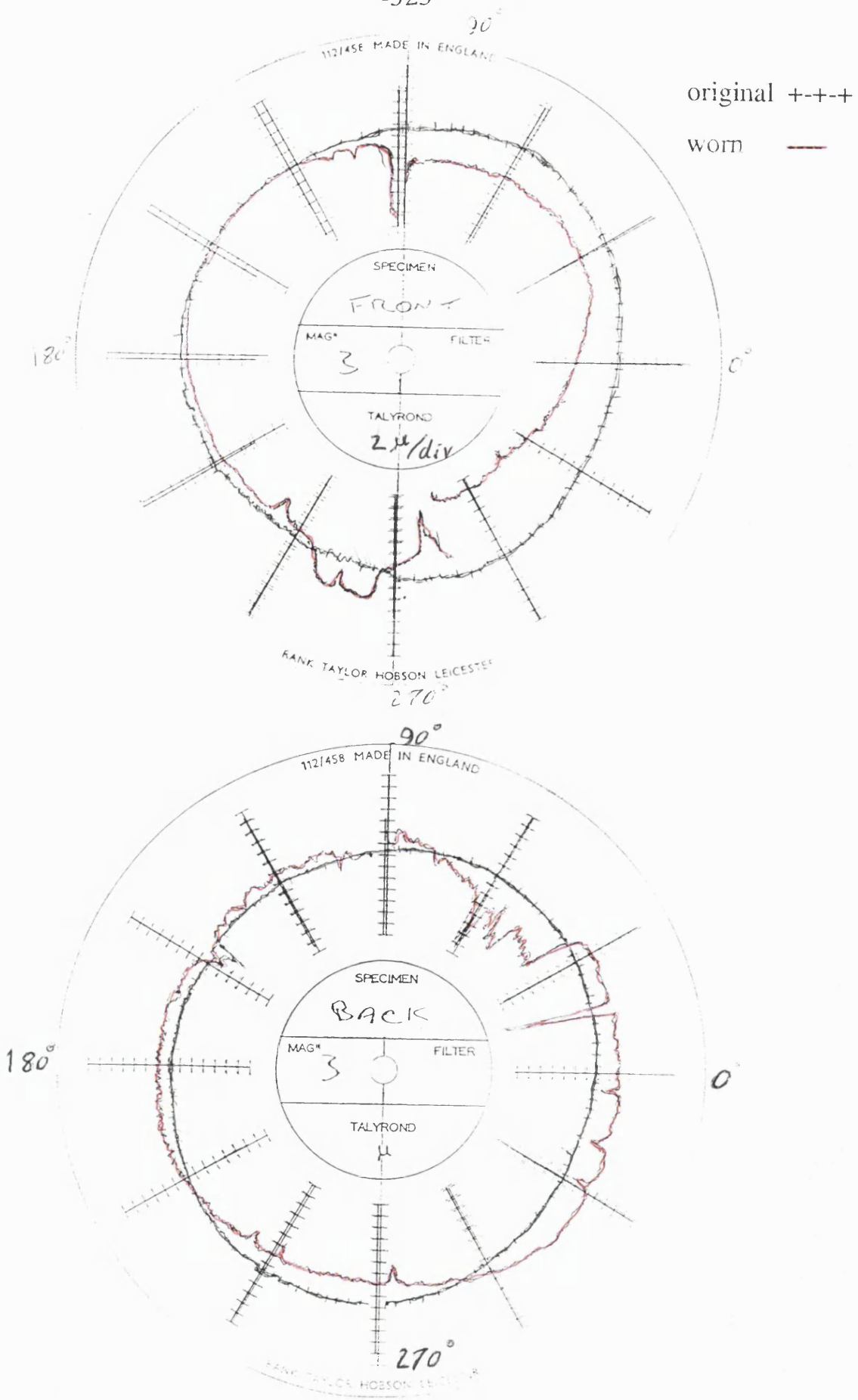

Fig 10.2.11 Bush roundness , mean speed 244 rev/min; with fly wheel

2 hr running ; dia. clearance 0.25mm

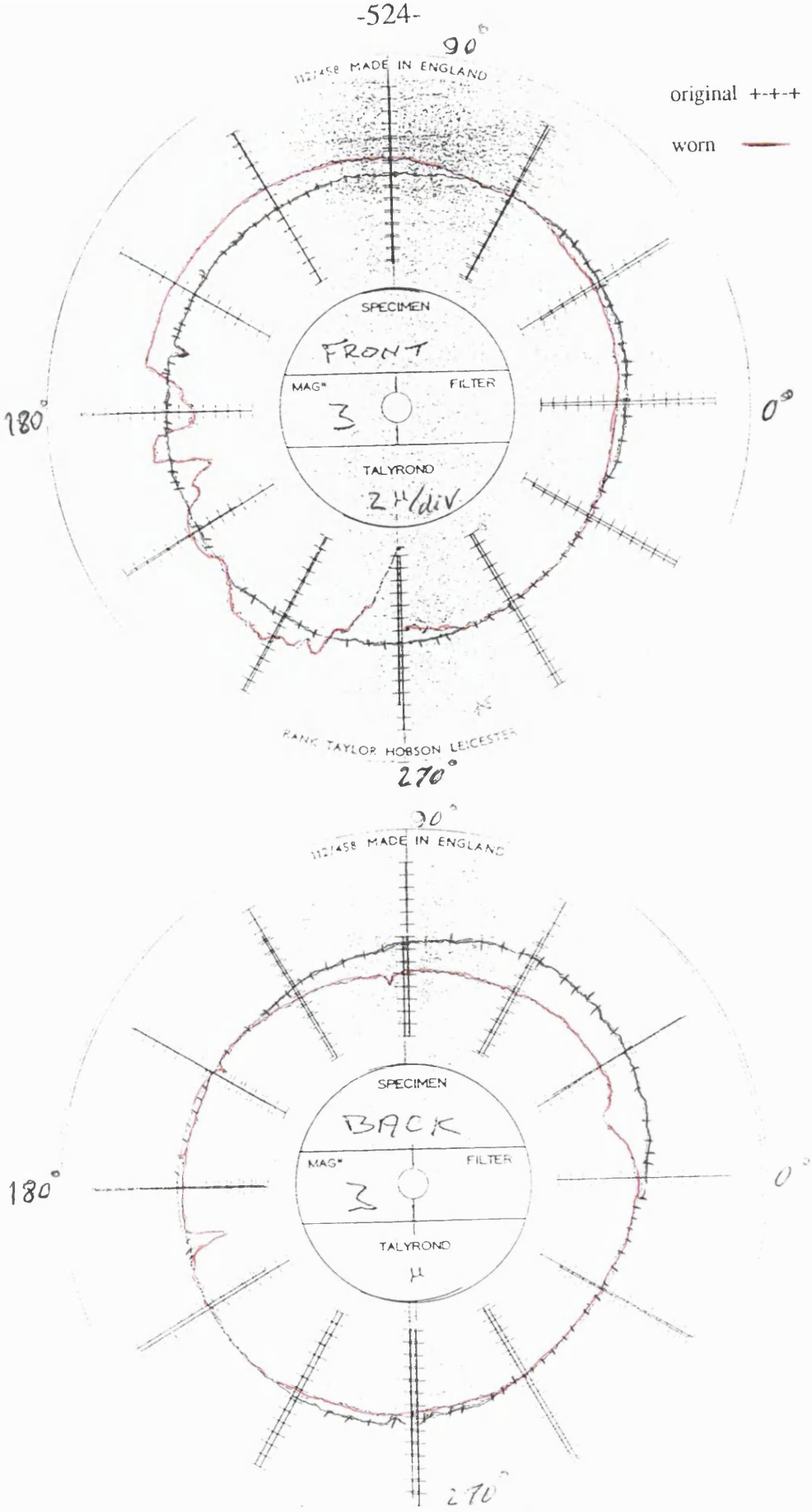

Fig 10.2.12 Bush roundness , mean speed 244 rev/min; no fly wheel
1 hr running ; dia. clearance 0.25mm

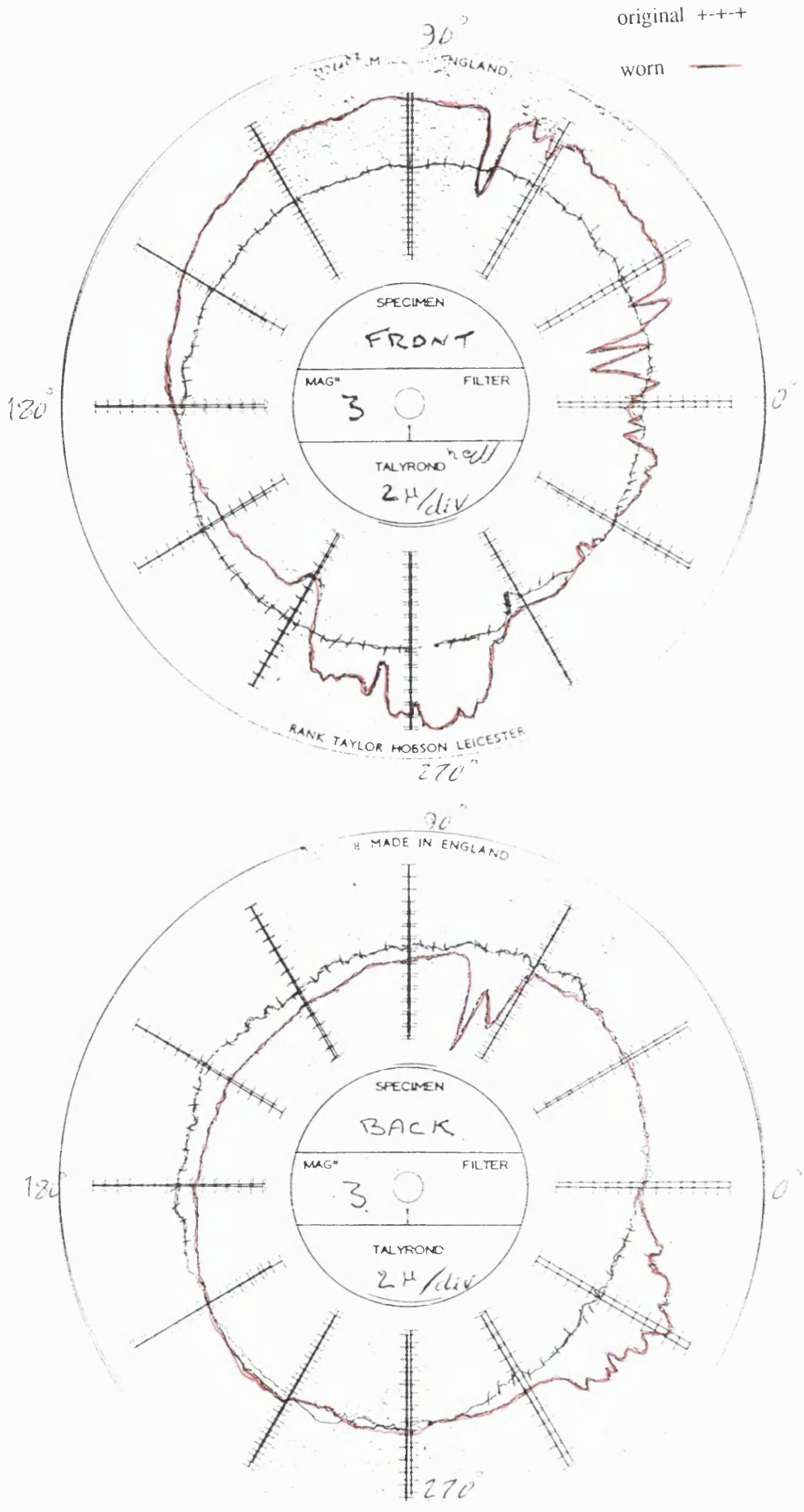

Fig 10.2.13 Bush roundness , mean speed 290 rev/min; with fly wheel

1/2 hr running ; dia. clearance 0.25mm

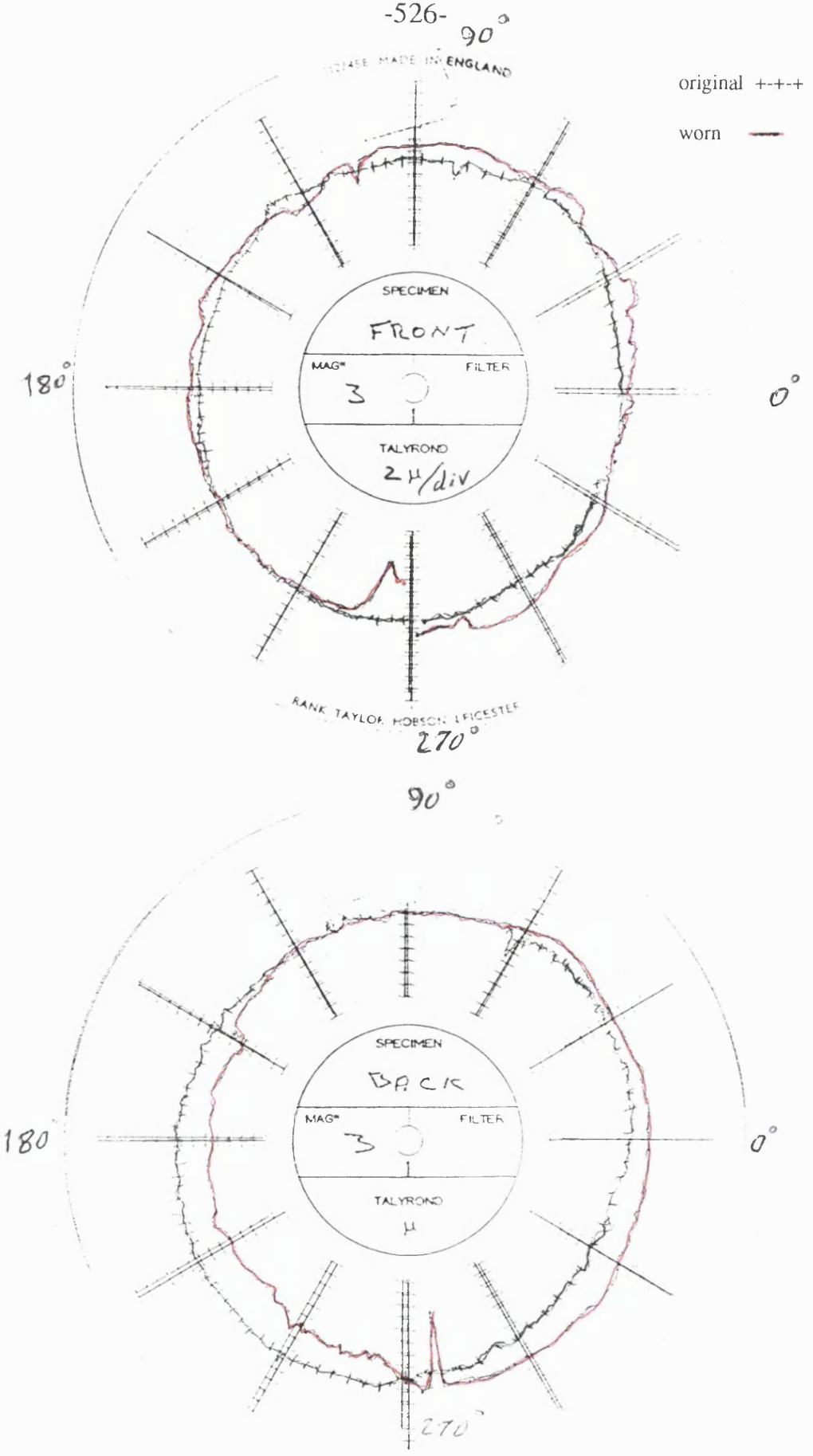

Fig 10.2.14 Bush roundness , mean speed 290 rev/min; no fly wheel
1/2 hr running ; dia. clearance 0.25mm

CHAPTER 11

CONCLUSIONS AND FURTHER WORK

11.1 Conclusions

The work indicates that a reasonably accurate prediction can be made of pin path, the magnitude of impacts and their position on the bush as a function of (a) clearance and (b) crank speed. This information provides a basis for predicting the wear experienced. It also can be used in contact-loss prevention procedures.

The three different modes of motion

(a) following mode,
(b) free flight mode
(c) impact mode

can be identified by means of a contact loss circuit, pin polar plot and accelerometers. The corresponding crank angles can be recorded by means of an optical encoder

Analysis of crank-rocker chain with zero clearance in the bearings indicates that a modest but significant reduction in wear can be achieved if speed fluctuations (due to variations in effective inertia or gravitational effects) are permitted.

A theoretical model admitting clearance and assuming continuous contact predicts rapid oscillations of pin motions , pin forces and acceleration plots in two regions during the cycle. Admitting free flight not only allows two regions of pin jump (free flight) per cycle but also predicts decreased pin oscillations (relative to continuous contact) after contact is remade particularly at low speed.

Experimental records of contact loss and pin motion exhibit rapid change of pin motion in the contact loss region. Acceleration remain approximately constant during free flight (pin jump) and is followed by impact. Agreement between

recorded and predicted pin plots is close enough to validate the theoretical model.

It is not necessary to use a contact loss criterion. In the theoretical model , the free flight condition is invoked at successive crank angles in the region of interest until pin jump(flight) actually occurs. It was observed that contact loss occurs close to the position where the pin force is minimum in the zero clearance case. It is also around that point which the angular acceleration of the follower becomes zero. This is approximately half way between the extreme positions of the follower (top and bottom dead centre).

Published theoretical contact loss criteria have been evaluated by comparison with the experimental contact loss signals.

There is a lag between predicted and recorded pin jump , believed to be due to delay(time constant) of the speed controller in supplying the required input torque to the motor.

Pin misalignment has been demonstrated by isolating one end from the bush and then the other. There is a small discrepancy in longitudinal and lateral pin displacement in the contact phase (between jump and fall) , particularly at low speed. This could be due to pin misalignment.

The bush angle at which impact occurs varies with mean speed. Hence wear is distributed around the bush if a range of speeds is employed.

With increasing speed the impact in the first region occurs earlier in the cycle, moves toward the top of the bush and increases slightly in magnitude. The crank angle at which the second impact occurs increases with speed. The impact tends to move toward the top of the bush and is increased in magnitude considerably.

Variation of the speed during the cycle has influence on the impact position and its magnitude. This is an important result since the input speed has been assumed constant by most workers. Change of flywheel will modify wear pattern.

Contact loss occurs at crank angle close to the local minima of pin forces in zero clearance case . The crank angle corresponding to the first minimum occurs earlier in the cycle as speed is increased. However that at the second occurs later.

The polar plot pin path shows the pin is at the bush bottom at low speed. It moves toward the top with increasing speed. This is similar behaviour to pin force in the zero clearance case. The longitudinal pin force in the zero clearance case is negative at low speed. It becomes positive in some portion of the cycle at greater speeds(pin force moves from bottom of the bush to top). This portion increases with speed.

When a fly wheel is added the impact occurs later and is increased in magnitude. Constant speed may be disadvantageous as far as wear is concerned.

The grease in the bearing causes impact to occur later (relative to the unlubricated case) and also reduces its magnitude, particularly at low speed.

The contact loss results indicate that generally one end of the pin leaves the bush before the other, indicating some misalignment referred to above. For this reason the circuitry was modified to indicate contact loss only when both ends leave the bush.

The worn regions of the bush are consistent with the predicted and recorded position of the impact.

A study of the long term pin motion and impact theoretically and experimentally, shows that pin motion is not exactly repetitive. However the impact region is concentrated in one area of the bush around the first predicted bush angle. The impacts are distributed over the region in a roughly normal distribution. The standard deviation of the first impact region decreases with speed. However that of the second increases.

11.2 Further work

Predicted pin motion can be used in fault monitoring with a computer on line. The

recorded pin motion can be compared with the original(unworn) pin motion which should be close to the predicted motion. When the experimental signal diverts from the predicted by more than a permitted value(wear is more than permitted) the fault monitoring system may provide a warning to the operator and if necessary stop the machinery. The proper location of the probe around the bush should be the bush angle where impact is predicted(necessarily axially removed from it).

In the absence of computer the pin motion can be recorded periodically and then compared with a p template made from predicted pin motion or the original record. When deviation exceeds a certain limit, the bush should be changed.

Pin misalignment in the bearings may affect pin response and hence impact and wear. Therefore the effect of pin misalignment in the bush is worthy of study.

This can be achieved by measurement of pin yaw and pitch via 2 longitudinal and two lateral probes in the bush. The size of transducer calls for a link larger than studied here. Because of the size of the transducers, two can only be used if larger bearings are employed.

The pin longitudinal acceleration can be measured by an accelerometer. This can be used for studying misalignment, since this should produce out of plane motion.

A probe could also be used to measure the longitudinal motion of the pin. It will give a clear signal of pin longitudinal motion(out of plane). Study of pin acceleration in this direction is also desirable.

It is desirable to insert a spring (using linear or torsional spring) to prevent impact and excessive wear. The efficiency of the method of preventing contact loss can be checked by

(1) introducing a spring into the theoretical model,
(2) by examining the experimental pin motion and contact loss traces.

REFERENCES

1 Dubowsky,S.,Young, S.C., An Experimental and Analytical study of connection Forces in High speed Mechanisms, ASME Journal of Engineering for Industry, 1975, Vol. 97B, pp. 1166-1174.

2 Earles, S. W. E. and Wu, C. L. S. Motion analysis of a rigid link mechanism with clearance at a bearing. Instn Mech. Engrs Mechanisms Conference 1972 pp 83-89

3 Earles, S. W. E. and Wu, C. L. S. Predicting the occurence of contact loss and impact at a bearing from zero_clearance analysis. Fourth World Congress on the Theory of Machines and Mechanisms, Newcastle 1975 pp 1013-1018.

4 Wu C L S and Earles S W E: A determination of contact loss at a bearing of a linkage mechanism. Trans ASME 1977, series B, 99, No 2 pp 375-380.

5 Earles, S. W. E. and Kilicay, O. A design criterion for maintaining contact at plain bearings. Proc. Instn Mech. Engrs, 1980,vol 194,pp249-258

6 Vjaters, I. J. and Earles, S. W. E. On evaluating impact interactions at bearings in a four bar mechanism. ASME Design Engineering Technical Conference, Columbia ohio 1986 86-DET-173.

7 Haines, R. S. Survey:two-dimensional motion and impact at revolute joints vol 15,1980 pp 361-370.

8 Haines, R. S. A theory of contact loss at revolute joints with clearance. J.Mech.Engng Sci.,vol 20 No 3, 1980 pp 129-136.

9 Haines, R. S. An experimental study of ludodynamics in a revolute joint. Sixth world Congress Theory of Machines and Mechanisms. New Delhi 1983 2, 725-728.

10 Haines, R. S. An experimental investigation into the dynamic behaviour of revolute joints with varying degrees of clearance. Mechanism and Machine Theory 1985, vol 20, No 3 pp 221-231.

11 Haines, R. S. Contact loss at revolute kinematic joints: A ludodynamic theory tested. Proc. Instn. Mech. Engrs 1985 vol 199, C3 , pp 173-180.

12 Fawcett, J. N., Burdess, J. S. Control of Clearance effect in linkages. Engng Materials and Design. sept 1972 pp 26-27.

13 Perera, O. , Seering, W. Prevention of Impact in bearings of four bar linkages. Trans ASME Journal of Mechanisms Sept 1983, vol 105, pp 592-508.

14 Grant, S. J. , Fawcett, J. N. Effect of clearances at the Coupler bearing of a four bar linkage. Mechanism and Machine Theory 1979, vol 14, pp 99-110

15 Osman, M. O. M., Mansour, W. M., The Proximity Perturbation Method for Kinematic Analysis of Six-Link Mechanisms. Jnl. Mechanisms 1971 Volume 6, pp.203-212

16 Bahgat,M., Osman, M.O.M., Sankar, T.S. ," On the effect of bearing clearances in the dynamic analysis of planner mechanisms" J Mech Eng Science ,Jun 1979, vol 21, pp.429-437.

17 Mansour, W. M., Townsend, M. A., Impact spectra and intensities for high-speed mechanisms. Trans ASME J Eng. Industry Feb 1975 pp 367-353.

18 Townsend, M. A. , Mansour, W. M., A pendulating model for mechanisms with clearances in the revolutes. Trans ASME J Eng Industry Feb 1975 pp 354-358.

19 Soong, K. , Thompson, B. S. A theoretical and experimental investigation of the dynamic response of planar mechanisms with radial clearance, in the revolute joints. 20th Biennial Mechanisms Conference, ASME, Kissimmee 1988 pp 47-57.

20 Kragelskii, v., Friction and Wear, Butterworths, 1958, p 118.

21 Furuhashi T., Marita, N., Matsura, M., Research on the dynamics of four bar linkage with clearances at turning pairs. 1st report, Bull JSME, vol 21, No 153, 1978 pp 518-523.

22 Furuhashi, T. et al, 2nd report ,Bull JSME, vol 21, No 153, 1978 pp 1284-1291.

23 Furuhashi, T. et al, 3nd report ,Bull JSME, vol 21, No 153, 1978 pp 1292-1298.

24 Furuhashi, T. et al, 4nd report ,Bull JSME, vol 21, No 153, 1978 pp 1299-1305.

25 Bengisu, M.T. , Hidayetoglu, T. and Akay, A. , "A Theoretical and experimental Investigation of Contact Loss in the clearance of a four bar mechanism," ASME Journal of Mechanisms, Transmissions, and Automation in Design, Vol. 108, 1986,pp. 237-244.

26 Hudson, A. J. , Baga, R., Forces and impact prediction in a four bar chain. University of Bath, School of Mechanical engineering, Report No 911, June 1988.

27 D C Motors, Speed Controls and servo-systems. Electro craft Corporation, Hopkins , Minnesota, 1973, pp 3-36

28 Perera, O.,On predicting and preventing impacts of the plain bearings of the four bar linkages. Dept of Mechanical Engineering M.I.T. S.B. thesis, feb 1982.

29 Herbert, R. G.,Mcwhannel , Shape and Frequency of Pulses from an Impact Pair. Trans ASME J Eng. Industry., Vol. 99, 1977, pp. 513-518.

30 Dubowsky, s., Norris, M., Aloni,E.,Tamir, A.,"An analytical and experimental study of the prediction of Impact in planar Mechanical systems with clearances," ASME Journal of Mechanisms, Transmissions, and Automation in Design, Vol. 106, 1984, pp. 444-451.

31 Earles, S.W.E. and Wu, C.L.S., "Motion analysis of a rigid-link mechanism with clearance at a bearing, using lagrangian mechanics and digital computation," Mechanisms, Institute of Mechanical Engineers , London, England (1973, pp. 83-89.

32 Rogers, R. J.,Andrews, G. C., Dynamic Simulation of Planar mechanical Systems with lubricated bearing clearance using vector- network methods. Trans ASME J for Ind. 1977 pp131-137.

33 Grant, S. J. and Fawcett, D. N. Control of clearance effects in mechanisms. ASME paper 77-WA/DE-2, 1977.

34 Midema, B. ,Mansour, W. M., Mechanical joints with clearance: a Three-Mode Model, ASME Journal of Engineering for Industry, 1976, vol.98B, pp. 1319-1323.

35 Funabashi H. , Ogawa K.,and Horie M., A Dynamic Analysis of Mechanisms with Clearances, Bulletin of the JSME, Vol. 21, No. 161, Nov. 1978, Paper No. 161-614.

36 Funabashi H.,et. al., A Dynamic Analysis of the Plane Crank-and-Rocker Mechanisms with Clearances, Bulletin of JSME, 1980, Vol. 23, No.177 , pp. 446-452

37 Dubowsky, S., and F. Freudenstein , Dynamic analysis of mechanical of mechanical system with clearance. ASME J. Engng. Ind. 1971 Vol. 93B. 305-316.

38 Osman, M. O. M. , Bahgat, B. M.,Sankar, T. S., On the Prediction of Journal-Bearing Separation in High Speed Mechanisms with Clearances. ,ASME Paper November 1980, No. 80-WA/DSC-36

39 Earles, S.W.E., Seneviratne, L.D., Some Kinematic Effect of Clearance in Revolute Joint of Linkage Mechanisms. Proceedings of Seventh World Congress IFTOMM,Seville,1987.

40 Earles, S.W.E., Seneviratne, L.D. , Design guidelines for predicting contact loss in revolute joints of planar linkage mechanisms. Proceeding of the Institution of Mechanical Engineers, Part C journal of mechanical,1990.

41 Grosjean,J , An Introduction to the analysis of linkages. August 1986 Stanley Thorne, pp.86-102.

42 Wilkinson, J.H. and Reinsch, C. Handbook for automatic computation. Springer-verlag,1971, volume II, linear algebra, pp.93-110.

43 Cameron,A , Principle of lubrication, Longmans,1966, pp.385-387.

44 Ralf,A. Collacott, Vibration monitoring and diagnosis, 1979, George Godwin Limited, pp. 163-164

45 Dubowsky , s. , On Predicting the Dynamic Effect of Clearances in Planar Mechanisms, ASME J. Engng Ind. 1974, Vol. 96B pp.317-323

46 Dubowsky , S. , Gardener, T. N., Dynamic Interactions of Link Elasticity and Clearance Connection in Planar Mechanical Systems, Trans. ASME,J., Engng Ind. 1977,vol 99B pp. 88-96

47 Van Valkenburg, M.E., Analog Filter Design , 1982,Holt,Rinehart and Winston, pp. 63-68

48 Grosjean, J. , private notes

49 Dubowsky, S. , Moening, M.F., An Experimental and And Analytical Study of Impact Forces in Elastic Mechanical Systems with Clearances, Mechanism and Machine Theory. 1978, Vol 13 pp.451-465

50 Dubowsky , S. , Gardener, T. N., Design and Analysis of Multilink Felexible Mechanisms With Multiple Clearance Connections, Trans. ASME,J., February 1977, pp. 88-96